THE JOURNAL OF PHYSICAL CHEMISTRY

Volume 71

MAY—AUGUST 1967

PAGES 1555—3112

EASTON, PA.
MACK PRINTING COMPANY
1967

THE JOURNAL OF

PHYSICAL CHEMISTRY

Volume 71, Number 6 May 1967

ACS Laboratory Guide

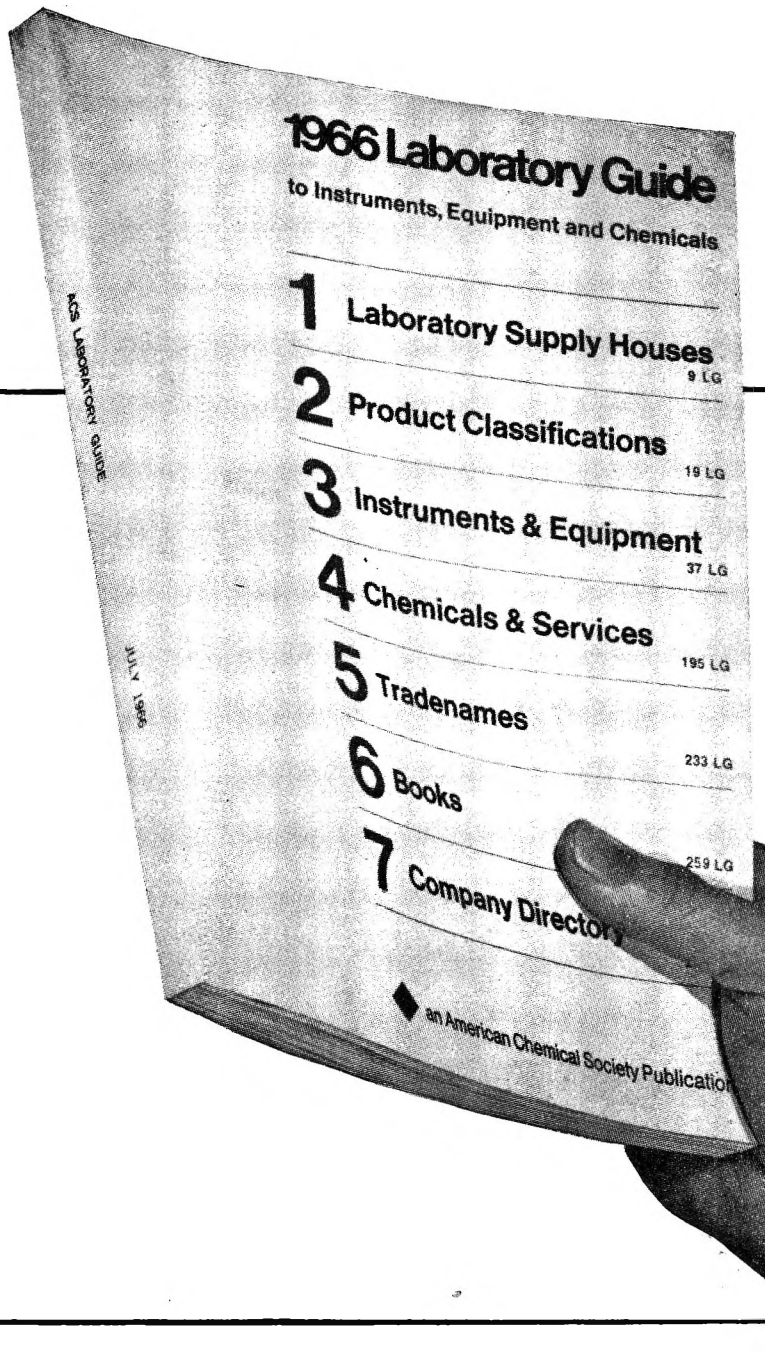

The definitive directory to research instruments, chemicals, services, books, equipment and tradenames.

Issued annually in July, used daily to...

FIND WHO SELLS WHAT

INQUIRE ABOUT PRODUCTS

LOCATE SALES OFFICES

CREATE BIDDER'S LISTS

CONTACT VENDORS

PLACE ORDERS

NOTES

COMMUNICATIONS TO THE EDITORS

AUTHOR INDEX

THE JOURNAL OF
PHYSICAL CHEMISTRY

VOLUME 71, NUMBER 6 MAY 15, 1967

The Hydrogen Resonance Spectrum of Cyclobutanone

by L. H. Sutcliffe and S. M. Walker

Donnan Chemical Laboratories, The University, Liverpool, England

Accepted and Transmitted by The Faraday Society (October 20, 1966)

The ^{1}H nmr spectra of cyclobutanone have been recorded at 40 and 56.4 Mcps and they have been analyzed on the assumption that the molecule comprises an AA′BB′B″B‴ (and not A_2B_4) spin system. All the spectral parameters derived from the analysis are unexceptional apart from the rather large H–H cross-ring coupling constants.

The ^{1}H nmr spectrum of cyclobutanone recorded at 60 Mcps has been reported recently;[1] unfortunately it was insufficiently resolved to allow proper analysis of the spectrum. In the analysis, Combs and Runnells[1] assumed that the vicinal axial–axial and axial–equatorial coupling constants are equal and calculated the spectrum from the A_2B_4 spin system for $J_{AB} = 7.9$ cps and $\delta_{AB} = 1.05$ ppm. The implication is that rapid interconversion between the two equivalent conformers of cyclobutanone causes the two coupling constants to become equal. However, a far-infrared study of cyclobutanone[2] suggests that the carbon skeleton of the molecule is planar since a ring-puckering frequency could not be found. Further evidence is that, even in asymmetrically substituted cyclobutanones, varying the temperature from −80 to +140° does not affect the spectrum;[3] also a deceptively simple spectrum is usually observed when a ring compound interconverts rapidly between two equivalent conformers.[4]

These three facts imply that the molecule is planar, and it is unlikely that the axial–axial and axial–equatorial coupling constants are equal in this situation. An A_2B_4 treatment therefore is incorrect, and this is confirmed by comparing the spectrum of Combs and Runnells[1] with the experimental spectra in Figures 1 and 2 which show the low- and high-field parts, respectively, of the spectrum obtained in this laboratory at 56.4 Mcps under frequency sweep conditions.

We have assumed planarity by analyzing the spectrum as originating from an AA′BB′B″B‴ spin system.

Experimental Section

Spectra were recorded at 40 and 56.4 Mcps using a Varian HA-60 nmr spectrometer with a TMS locking signal. Cyclobutanone was purchased from the Aldrich Chemical Co., Inc., and was degassed thoroughly.

An English Electric KDF 9 computer was used for the calculations.

Results and Discussion

The calculated spectra shown in all the figures were

(1) L. L. Combs and L. K. Runnells, *J. Chem. Phys.*, **44**, 2209 (1966).

(2) J. R. Durig and R. C. Lord, *ibid.*, **45**, 61 (1966).

(3) J. B. Lambert and J. D. Roberts, *J. Am. Chem. Soc.*, **87**, 3884 (1965).

(4) J. Feeney, L. H. Sutcliffe, and S. M. Walker, *Trans. Faraday Soc.*, **62**, 2969 (1966).

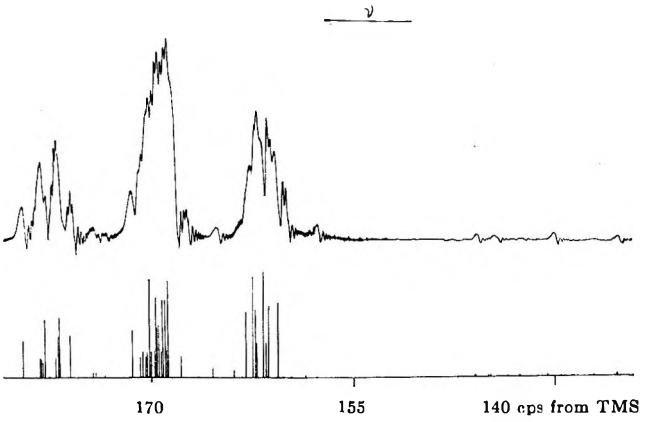

Figure 1. The low-field portion of the observed and calculated ^1H spectrum at 56.4 Mcps of neat cyclobutanone.

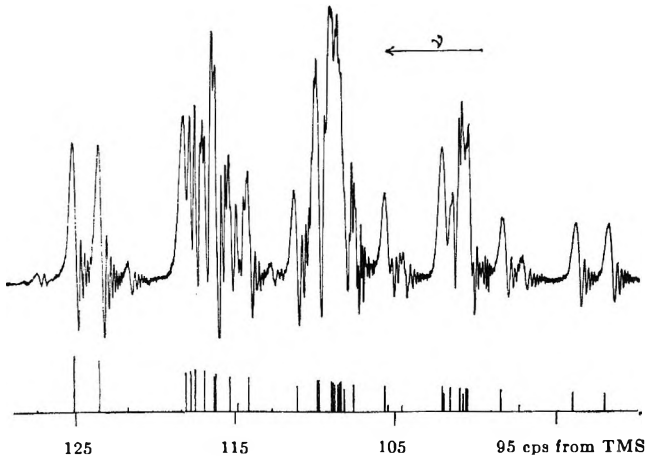

Figure 2. The high-field portion of the observed and calculated ^1H spectrum at 56.4 Mcps of neat cyclobutanone.

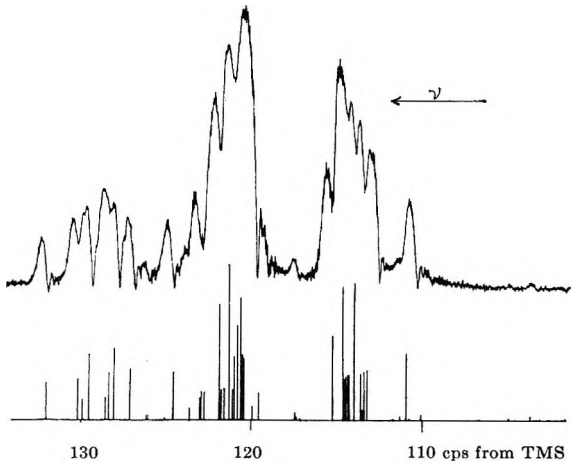

Figure 3. The low-field portion of the observed and calculated ^1H spectrum at 40 Mcps of neat cyclobutanone.

obtained using a noniterative seven-spin computer program; trial values were used until a reasonable fit was found as shown in Table I.

Table I

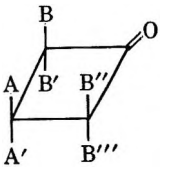

Geminal coupling constants

$J_{AA'} = -11.1$ cps

$J_{BB'} = J_{B''B'''} = -17.5$ cps

Vicinal coupling constants

cis $J_{AB} = J_{A'B'} = J_{AB''} = J_{A'B'''} = +10.0$ cps

trans $J_{AB'} = J_{A'B} = J_{AB'''} = J_{A'B''} = +6.4$ cps

Cross-ring coupling constants

cis $J_{BB''} = J_{B'B'''} = +4.6$ cps

trans $J_{BB'''} = J_{B'B''} = -2.8$ cps

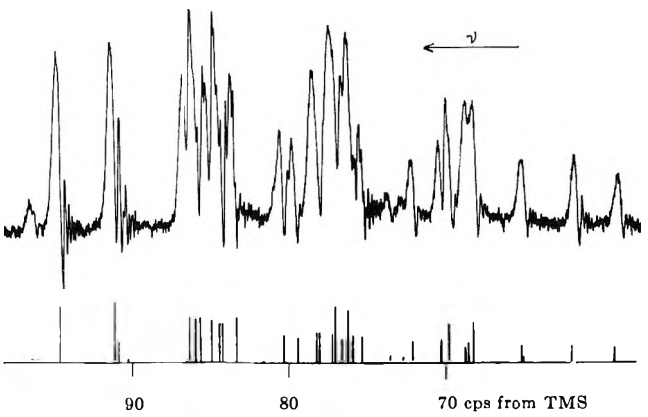

Figure 4. The high-field portion of the observed and calculated ^1H spectrum at 40 Mcps of neat cyclobutanone.

The above values are within ±0.2 cps of a perfect fit for a chemical-shift difference, $\delta_{AB} = 1.05$ ppm ($\tau_A = 8.06$ ppm and $\tau_B = 7.01$ ppm). When an iterative computer program is adopted, then a better fit should be obtained.[5] The hydrogen spectrum was recorded at 40 Mcps (see Figures 3 and 4) and computed for this radio frequency in order to check the uniqueness of the solution. In all the figures it can be seen that ringing has interfered with the experi-

(5) While this work was in progress, B. Braillon and J. Barbet, *Compt. Rend.*, 261, 1967 (1965), published a paper in which similar spectral parameters were reported. A spectrum was not reproduced, however, and we are unable to compare the accuracy of the fit with the present work.

mental spectrum, and the spurious peaks produced should not be confused with the real bands.

A notable feature of the analysis is the rather large moduli of the cross-ring coupling constants; non-interconverting tetrasubstituted cyclobutanes[6] have a modulus of about 1 cps for this type of coupling. The remaining coupling constants are normal in signs and magnitudes.

Acknowledgments. We are indebted to the Science Research Council for providing an equipment grant. Also we wish to thank Mr. D. Collens of the University Computer Laboratory for his help.

(6) C. H. Krauch, S. Farid, and G. O. Schenck, *Chem. Ber.*, 99, 625 (1966).

The Influence of Substrate Structure on Adsorption. II. Nitrogen and Benzene Adsorption on Characterized Silicas

by James W. Whalen

Research Department, Field Research Laboratory, Mobil Oil Corporation, Dallas, Texas
(Received January 26, 1966)

Precise gravimetric data extending down to 10^{-5} P/P_0 have been obtained for nitrogen and benzene on two silica surfaces previously characterized by other techniques. When subjected to a BET treatment, such data provide a needed verification of constancy of nitrogen occupancy areas on surfaces of variable chemical composition. Relatively minor apparent surface area dependence on structure was found for nitrogen. Benzene does not form complete monolayers or statistically equivalent multilayers in the region of BET applicability. Interaction energy distributions derived for the adsorption processes occurring on representative surface structural states reflect interactions with oxide and hydroxyl surface domains. Variations in the form of the distribution function and the site interaction energies are consistent with surface structures and with the specific adsorbate interaction.

The Brunauer–Emmett–Teller (BET) isotherm equation in two-constant form

$$V_a = \frac{V_m C P}{(P_0 - P)[1 + (C - 1)(P/P_0)]} \quad (1)$$

applied to the determination of surface area from nitrogen adsorption data has provided an indispensable basis for comparison of the surface properties of different substances in various states of subdivision and bulk structure. In such application the volume of adsorbed gas, V_m, equivalent to monolayer coverage, must be independent of the detailed structure of the surface. Variation in C ($\simeq \exp(E_1 - E_L)/RT$) owing to variation in average first-layer adsorbate–adsorbent interaction energy (E_1) with surface structure must be accompanied by appropriate modification in the shape of the isotherm, *i.e.*, in the $P - V_a$ dependence. In particular it is required[1] that at monolayer coverage ($V_a/V_m = 1$)

$$\left.\frac{P}{P_0}\right|_{V_m} = \frac{1}{1 + \sqrt{C}} \quad (2)$$

First-layer interaction energies for structural variations in the solid surface should be reflected both in C value variation, as obtained from the linear BET plot, and in the location of regions of linearity including the monolayer. In cases where surface structure can be modified without concomitant surface area changes, V_m should be constant if the BET method is to serve as a basis for the calculation of surface area and constant cross section is to be assigned to the adsorbate molecule.

On the basis of assumed constancy for the coverage assigned the nitrogen molecule, it is widely recognized[2] that other adsorbates reflect variable coverage on different surfaces. Various authors[3,4] have assigned real significance to apparent surface area changes of 10% or less, based on nitrogen BET treatment, in cases where the chemical nature of the adsorbent is known to be variable under the experimental conditions. The alternative explanation, that at least a part of the discrepancy may be due to variability in nitrogen coverage or effective cross-sectional area, has not been given serious consideration. The $P - V_a$ relationship for nitrogen adsorption is known to be dependent on the nature of the adsorbent surface as demonstrated by adsorption on silicas in various hydration states,[5] adsorption on presorbed layers on benzene or methyl alcohol,[6] water,[3] and on other surfaces of widely different structures.[7] There is, however, a paucity of data from which the constancy of V_m can be adequately demonstrated for variable C and fixed surface area and there are no experimental studies in the literature which demonstrate that surface areas derived from the BET treatment of nitrogen adsorption are independent of substrate structure for variable structure surfaces of constant area.

In view of the importance of surface area determination to essentially all generalization in adsorbate–adsorbent interaction studies and the rather widespread tendency to treat most adsorption systems within the BET framework, it is of interest to consider the compliance of the BET for both weakly and strongly interacting adsorbates on variable structure surfaces of constant area. The silica surface, known to contain oxide sites, both interacting and isolated hydroxyl groups, and molecular water, is particularly adaptable to such adsorbent requirements. Several structurally stable silica materials have been studied by methods which characterize the surfaces with respect to fine structure and energy.[8–10] The adsorption of nitrogen and benzene on two such materials is reported.

Experimental Section

The silica materials, supplied by Mallinckrodt Chemical Works, are precipitated gels of high purity and were used as received except for outgassing. Previous designations[9] of Silica SL for Silicic Acid Special Luminescent and Silica SB for Silicic Acid Special Bulky are used in this discussion. The samples were outgassed *in situ* at a selected temperature between 110 and 400° for 24 hr after the residual pressure in the adsorption system reached 10^{-6} torr. Immersion heat work under these conditions has established surface structure reproducibility.[9]

The adsorption measurements were carried out in the greaseless McBain-Bakr quartz spring system utilized in prior work.[11] Oil and mercury manometers were isolated from the adsorption system by a null pressure capacitance device. The oil manometer covered a pressure range equivalent to 25 mm; the mercury manometer was used at higher pressures. Quartz springs with a 250-mg load limit and sensitivities of 1.125- and 1.065-mm elongation/mg were employed. Reading accuracy was $\pm 10^{-3}$ mm in spring length. Pressure measurement accuracy was $\pm 10^{-3}$ mm in the low-pressure region and $\pm 2 \times 10^{-2}$ mm at pressures above 25 mm.

Nitrogen was purified over a copper wire screen at 450° followed by condensable trapping at 77°K. Spectroscopic grade benzene was dried over Linde 5A Molecular Sieves activated at 300° and distilled under vacuum into the adsorption reservoir.

Benzene adsorption data were obtained at 25 ± 0.05°. Nitrogen adsorption was carried out at 77°K, the liquid nitrogen temperature being monitored by oxygen gas thermometer.

Results

In light of past experience suggesting unusually restricted BET ranges for these materials, the nitrogen

(1) L. Meyer, *Z. Physik. Chem.* (Frankfurt), **16**, 331 (1958).

(2) F. Rouquerol, J. Rouquerol, and B. Imelik, *Bull. Soc. Chim. France*, 635 (1964); R. T. Davis, T. W. de Witt, and P. H. Emmett, *J. Phys. Colloid Chem.*, **51**, 1232 (1947); J. A. Singleton and G. D. Halsey, *J. Phys. Chem.*, **58**, 330 (1954).

(3) W. H. Wade, *ibid.*, **68**, 1029 (1964).

(4) A. W. Adamson, I. Ling, and S. K. Datta, Advances in Chemistry Series, No. 33, American Chemical Society, Washington, D. C., 1961, p 62.

(5) M. R. Harris and K. S. W. Sing, *Chem. Ind.* (London), 487 (1959).

(6) A. I. Sarakov, M. M. Dubinin, and Y. F. Berezkiva, *Izv. Akad. Nauk SSSR, Ser. Khim.*, 1165 (1963).

(7) P. C. Carman and F. A. Raal, *Trans. Faraday Soc.*, **49**, 1465 (1953).

(8) R. S. McDonald, *J. Phys. Chem.*, **62**, 1168 (1958).

(9) J. W. Whalen, Advances in Chemistry Series, No. 33, American Chemical Society, Washington, D. C., 1961, p 281.

(10) S. Brunauer, D. L. Kantro, and C. H. Weise, *Can. J. Chem.*, **34**, 1483 (1956).

(11) J. W. Whalen, *J. Phys. Chem.*, **65**, 1676 (1961).

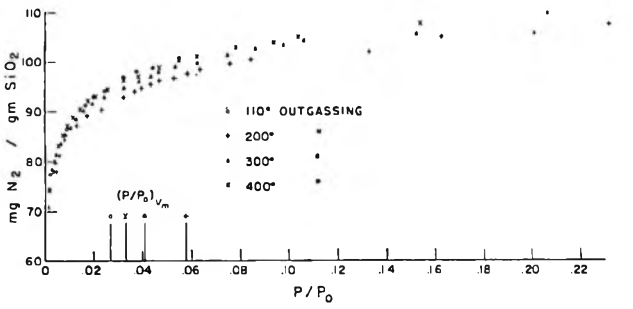

Figure 1. Nitrogen adsorption on Silica SB.

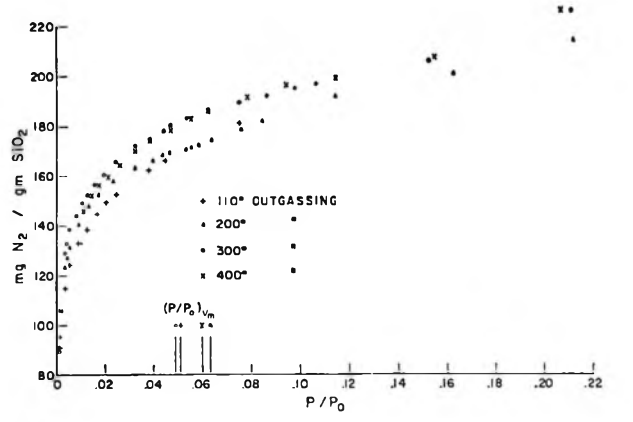

Figure 2. Nitrogen adsorption on Silica SL.

investigation was carried out over the relative pressure range $P/P_0 = 10^{-5}$ to 0.2 as a function of surface hydration for Silica SB and Silica SL. Adsorption data points are shown in Figures 1 and 2. For Silica SB (Figure 1) a significant decrease in the quantity adsorbed was obtained between 110 and 200° sample outgassing. The adsorption of nitrogen increases slightly following 300° thermal treatment and again following 400° treatment, almost coinciding in the latter case with the quantity adsorbed following 110° thermal treatment. For silica SL (Figure 2) there is no initial decrease in the quantity of adsorbed nitrogen as noted with Silica SB, but an increase over the 110–300° outgassing treatment range, corresponding to the behavior noted on the Silica SB material after removal of the molecular water. The final condensation between 300 and 400° is accompanied by an almost insignificant change in the amount of nitrogen adsorbed. Changes in shape of the adsorption isotherm are reflected as "crossing-over tendencies" for the 100–200 and 300–400° surface preparations.

The linear range in relative pressure for BET treatment was found to be quite restricted, resulting in surface area values slightly lower than those previously obtained[9,10] in the higher, generalized range. The relative pressure range for which rigorous linearity was observed in these studies for the adsorption of nitrogen on Silica SB was 0.009–0.06 P/P_0. On Silica SL the range was somewhat greater, extending from 0.005 to 0.075 P/P_0. The surface areas and average interaction energies are given in Table I. Little variation in either parameter was encountered for Silica SB. The surface area variation for Silica SL is significant, ranging from 593 to 646 m²/g with relatively constant interaction energies. The relative pressure values at which adsorbed amounts correspond to the BET indicated monolayer values (Figures 1 and 2) emphasize the variation in isotherm character with surface structure. Typical BET plots are shown in Figure 3.

Table I: BET Derived Surface Areas

Thermal treatment, °C		Nitrogen adsorption: Surface area, m²/g	Nitrogen adsorption: $E_1 = RT \ln C + E_L$, kcal/mole	Benzene adsorption: Surface area, m²/g	Benzene adsorption: $E_1 = RT \ln C + E_L$, kcal/mole
Silica SB	110	334	2.33	178	11.94
	200	341	2.31	166	10.96
	300	337	2.29		
	400	339	2.28	91	10.92
Silica SL	110	593	2.14	346	10.14
	200	611	2.19	320	10.20
	300	637	2.21		
	400	646	2.17	181	9.93

The adsorption of benzene on the same silica surfaces was carried out from relative pressures of approximately 10^{-4} to near saturation. The adsorption–desorption curves are relatively uninformative in their entirety; only the low-pressure data are shown in Figures 4 and

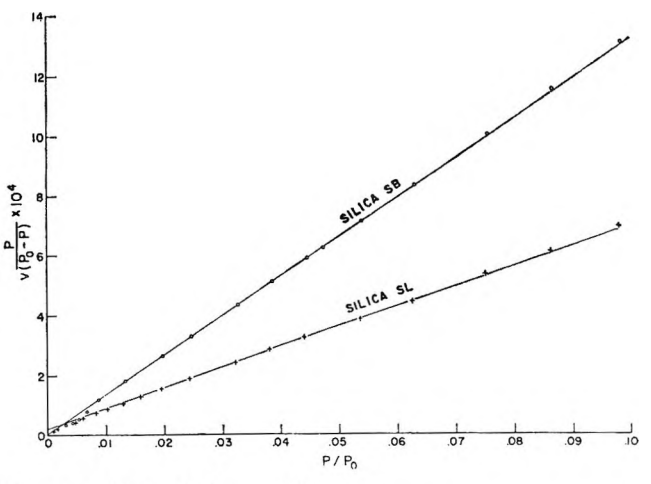

Figure 3. Typical nitrogen BET plots.

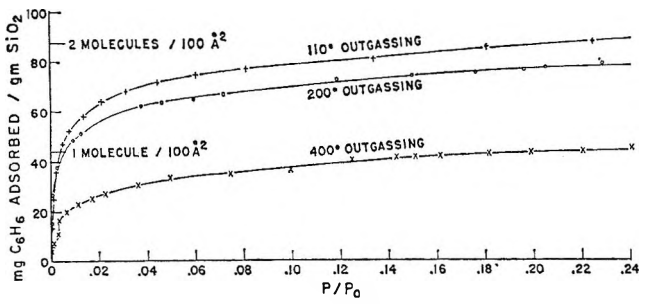

Figure 4. Adsorption of benzene vapor at low pressures on Silica SB.

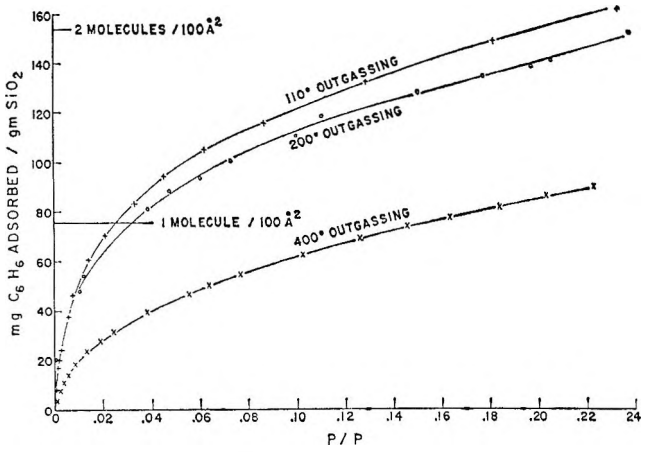

Figure 5. Adsorption of benzene vapor at low pressure on Silica SL.

5. The adsorption was reversible in this region, hysteresis being confined to relative pressures above 0.45. No significant variation in the form of the hysteresis loop was noted for the several sample preparations and direct comparison of the desorption curves for each data set showed only random point scatter well within experimental error. Utilizing a coverage of 33 A^2/molecule, as suggested by Livingston,[12] three molecules per 100 A^2 are required for monolayer coverage. On the basis of the nitrogen derived areas this coverage is not attained until the relative pressure exceeds 0.6. For Silica SB a low-pressure "limiting" adsorption value is attained at less than two adsorbed molecules per 100 A^2. The adsorption of benzene by Silica SL is a more gradual function of pressure; no "limiting" adsorption at low pressure is indicated. For both materials benzene adsorption is a strongly decreasing function of the outgassing temperature. The 110° outgassed Silica SB sample containing bound water does not exhibit oxide character as was indicated by nitrogen adsorption (Figure 1).

When the benzene adsorption data are subjected to BET treatment, linear plots are obtained within the relative pressure range 0.04–0.24 with no significant variation in the range from sample to sample. The statistical monolayer, based on the nitrogen derived area and utilizing the 33-A^2 coverage value for the benzene molecule, is not included in that range. Surface areas and average first-layer interaction energy values derived from the BET plots are summarized in Table I. The data are characterized by apparent decreases in surface area with increasing oxide surface structure and apparent surface area values which are quite low in comparison to the nitrogen derived values. Interaction energy values decrease with decreasing hydroxyl content and are, in general, two to four times the comparable values for the nitrogen–silica interaction. The relative pressure range over which BET model applicability should exist, on the basis of eq 2, is thus indicated to be even lower than that encountered for the nitrogen–silica interaction and far lower than the limits of the linear range actually encountered.

Discussion

The Silica SB surface has 2.2 water molecules and 7 hydroxyl groups per 100 A^2 following 110° outgassing. Bound water is removed under 200° outgassing and, at higher temperatures, hydroxyl sites are condensed leaving a residual 0.4 isolated hydroxyl site at 400° outgassing.[9] Silica SL has no bound water; the 5.5 hydroxyl sites present after 110° outgassing are condensed over the 200–400° temperature range leaving a residual 0.4 isolated site.[9] Nitrogen adsorption is seen from Figures 1 and 2 to show slight increases as the oxide content of the surface is increased. For Silica SB both the 110° outgassed surface containing bound water (associated in double hydrogen bonding with, and therefore shielding, hydroxyl sites) and the 400° outgassed surface exhibit maximum early stage adsorption. For Silica SL nitrogen adsorption increases throughout the range of hydroxyl group condensation.

Regions of linearity in BET plots beginning at very low relative pressures have been encountered in prior work for both nitrogen[13] and other adsorbates.[14] Meyer[1] and others[15] have demonstrated (eq 2) that such behavior is to be anticipated for high C value systems. The linear ranges encountered for nitrogen in this work (0.005–0.07 P/P_0) are in agreement with those demanded by considerations requiring applicability in the region encompassing the monolayer (Figures

(12) H. K. Livingston, *J. Colloid Sci.*, **4**, 447 (1949).

(13) D. S. McIver and P. H. Emmett, *J. Phys. Chem.*, **60**, 824 (1956).

(14) M. L. Corrin, *ibid.*, **59**, 313 (1955).

(15) G. L. Gains and P. Cannon, *ibid.*, **64**, 997 (1960).

1 and 2). Surface areas obtained in this range are slightly higher than those previously reported[9,10] based on adsorption data in the higher generalized range. The BET refinement over the Langmuir equation is superfluous at the low pressures over which the former is found to be applicable for these systems. Not surprisingly, a Langmuir treatment was found to yield comparable surface areas and a wider range data fit.

Real surface area changes, even of the order indicated by the treatment of nitrogen adsorbed on Silica SL, do not occur. The approximately 10% increase in apparent surface area for that system is, however, far outside the experimental error of these measurements. The materials are structurally stable; Silica SL has been subjected to thermal treatment above 400° in preparation prior to these studies. Both sintering, which does not occur with these materials prior to 700°, and possible pore dimension changes on dehydration[16] lead to decreases, not increases, in surface area. The apparent increase in Silica SL surface area is almost certainly due to changes in surface structure and, while negligible by routine standards, is of significance in studies related to the comparison of interaction energies (*e.g.*, heats of wetting) on various surfaces.

The adsorption of benzene on these surfaces is strongly dependent on the outgassing temperature. Although the trend toward decreasing apparent surface area appears unquestionably due to surface dehydration, the very large initial discrepancy between nitrogen and benzene derived areas could be attributed to the presence of a micropore structure of less than 7-A pore diameter. Silica structures having a majority of the pores in the 4–5 A range are known,[17] but there is no evidence that such porosity is significant in these samples. Integral energetic measurements would reflect the fractional surface involvement when expressed in energy per unit area based on total (nitrogen) area. In particular, if 50% of the surface area were unavailable to benzene, heats of wetting in benzene should be one-half those for nonporous particles of the same surface functionality. The immersion heat for quartz in benzene[18] is 115 ergs/cm^2, for Silica SB in the 200–400° surface state 100–115 ergs/cm^2, and for Silica SL from 75 to 95 ergs/cm^2.[19] In the latter case the lower immersion heats are again attributable to surface structure as evidenced by almost identical immersion heats for the two materials in cyclohexane. For the benzene–silica systems studied here it must be concluded that microporosity is not an important factor.

Hovart and Sing[20] have noted that benzene occupancy areas ranging from 31 to 50 A^2/molecule must be assigned on various silica gels and have questioned the relationship of the BET derived V_m values to true monolayer capacity. In this work benzene cross-sectional areas ranging from 62 to 119 A^2/molecule on Silica SB and from 50 to 119 A^2/molecule on Silica SL would be required to obtain data consistent with the nitrogen surface areas. It is apparent that only particular energetic fractions of the surface are included in the BET monolayer value for benzene. In addition, the relative pressure range over which BET applicability is indicated by C values from Table I is far outside the linear range actually encountered. It must be concluded that apparent compliance of the benzene data to the BET model is fortuitous.

The condensation of hydroxyl sites characteristic of these silicas can occur only between sites spaced within hydrogen-bonding distances. These spacing requirements (2.8–3.8 A) preclude the uniform distribution of such sites for all except the 400° outgassed

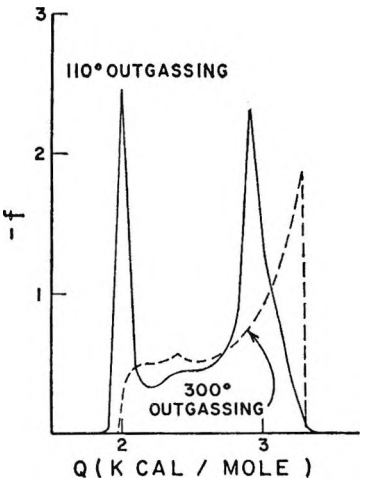

Figure 6. Site energy distribution function *vs.* site energy for nitrogen adsorbed on Silica SB. The distribution function f is defined as f = dF/dQ where F is the fraction of the surface involved in interactions having energy equal to or greater than Q. The Langmuir equation, with selected constants σ = occupancy area per molecule and τ = characteristic adsorption time, is utilized to describe local isotherms over dQ.[20] For nitrogen adsorption σ = 16.2 A^2/molecule and $\tau = 10^{-13}$ sec.

(16) J. H. deBoer and J. M. Vleeskins, *Koninkl. Ned. Akad. Wetenschap. Proc. Ser. B*, 61, 85 (1958).

(17) D. Dollimore and G. R. Heal, *Trans. Faraday Soc.*, 59, 2386 (1963).

(18) J. W. Whalen, unpublished data.

(19) J. W. Whalen, *J. Phys. Chem.*, 66, 511 (1963).

(20) D. M. Hovart and K. S. W. Sing, *J. Appl. Chem.*, 11, 313 (1961).

samples. The functional nature of the surface is that of a grouping of hydroxyl sites within the oxide matrix. This conclusion is strongly supported by site energy distribution functions derived from the adsorption isotherms by the Adamson–Ling treatment[21] and shown in Figures 6–9.

For nitrogen the site energy distribution is characterized by two peak functions which vary in accord with the established oxide–hydroxide character of the surface. The interaction energies are sharply limited between 1.9 and 3.2 kcal for all surface states. Average interaction energies obtained from the BET model (Table I) of 2.2–2.3 kcal are in reasonable agreement with the lower limit of these calculated values in accordance with expectation. The 2.9-kcal peak occurring in both Figures 6 and 7 represents nitrogen interaction with strongly hydrogen-bonded hydroxyl site groupings characteristic of the highly hydrated surface. The 3.2-kcal peak reflects nitrogen interaction with (predominantly) less strongly bonded hydrogen pair sites. Two oxide states are reflected by these data, the first at 1.9 kcal (Figure 6) associated with the strongly bound water on Silica SB and the second at 2.3 kcal characteristic of the substrate oxide surface. The entire spectrum of interaction energies is confined to a 1.3-kcal region and therefore to a correspondingly limited pressure region on the adsorption isotherm. The relative insensitivity of nitrogen as an adsorbate to distinction between these dissimilar sites, although surprising in view of the dipole–quadrupole interaction between nitrogen and hydroxyl sites, effects apparent energetic homogeneity in isotherm measurements of routine point spacing.

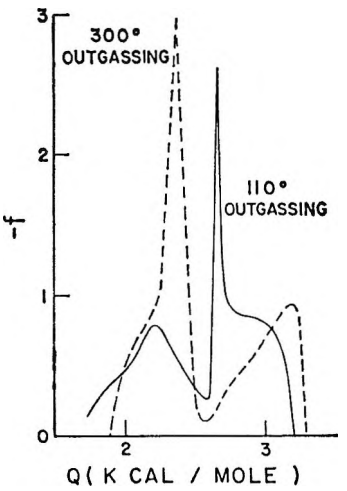

Figure 7. Site energy distribution function *vs.* site energy for nitrogen adsorbed on silica SL. σ = 16.2 A², τ = 10^{-13} sec (see Figure 6).

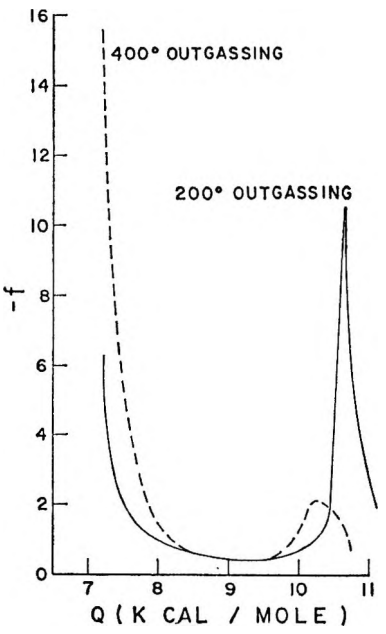

Figure 8. Site energy distribution function *vs.* site energy for benzene adsorbed on Silica SB. σ = 33 A², τ = 10^{-13} sec (see Figure 6).

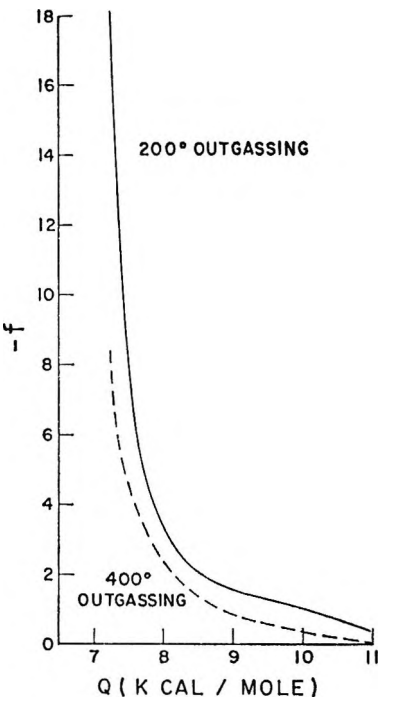

Figure 9. Site energy distribution function *vs.* site energy for benzene adsorbed on Silica SL. σ = 33 A², τ = 10^{-13} sec (see Figure 6).

(21) A. W. Adamson and J. Ling, Advances in Chemistry Series, No. 33, American Chemical Society, Washington, D. C., 1961, p 51.

In contrast to this behavior the spectrum of interaction energies for benzene with these surfaces is quite wide.[22] A resolvable high-energy peak is encountered for benzene on the Silica SB samples (Figure 8). This value of 10.2–10.8 kcal, again depending on the density of hydroxyl sites, is in close agreement with the Table I BET interaction energies of 11–12 kcal/mole for benzene–Silica SB. Clearly in view of the absence of resolved high-energy peaks in the distribution function for Silica SL (Figure 9), the spectrum of interaction energies can be quite wide depending on hydroxyl group density, distribution, and hydrogen bonding between such groups. These considerations as well as the isotherm forms offer no support for the position[23] of common isotherm character for benzene adsorption below regions of capillary condensation on silica surfaces of equal degrees of hydration.

Conclusions

The interaction of both nitrogen and benzene with the silica surface is dependent upon the substrate structure. Nitrogen interaction energies ranging from 1.9 to 2.3 kcal/mole predominate on the oxide surface. On hydroxyl surfaces, predominating interaction energies are in the 2.9–3.2-kcal/mole range. Although hydroxyl sites yielding benzene interaction energies of 10–11 kcal/mole can predominate on silica surfaces, a wider spectrum of interaction energies may result from variation in hydroxyl site distribution.

The adsorption of benzene on silica surfaces is strongly dependent on the detailed chemical nature of the surface, although no simple relationship exists between hydroxyl site content and benzene adsorption. Benzene does not form complete monolayers or statistically equivalent multilayers in the regions of BET applicability.

Surface areas derived from nitrogen adsorption data using the BET (or Langmuir) equation appear slightly dependent on surface structure for some site distributions. From the standpoint of routine surface area measurement the variations for the surfaces are not important. For the wider variation in surface structure encountered in general application and from the standpoint of the increasing importance attached to comparison of properties of surfaces of widely different nature, the 10% variation encountered in this work is disturbing.

Acknowledgment. The author expresses appreciation to Mobil Oil Corporation for permission to publish these results, to Conley Jenkins for assistance in many of the experimental measurements, and to Dr. T. W. Haas, who made a number of significant contributions.

(22) The site energy distribution treatment requires data extending over several orders of ten in pressure and includes regions of the benzene adsorption isotherm bounded by the limits $10^{-4} < P/P_0(2845) < 0.45$ and $10^{-4} < P/P_0(2846) < 0.7$.

(23) D. P. Dobychin and T. F. Tsellinskaya, *Zh. Fiz. Khim.*, **33**, 204 (1959); A. V. Kiselev, *Proc. Intern. Congr. Surface Activity, 2nd, London, 1957*, 179 (1957).

Biphenyl Radiolysis

by Michael A. Sweeney, K. Lynn Hall, and Robert O. Bolt

Chevron Research Company, Richmond, California *(Received March 3, 1966)*

Biphenyl was irradiated with Co^{60} γ rays and with 38-Mev helium ions to study its radiolysis. The major products were hydrogen, quaterphenyls, hydrogenated polyphenyls, and other polymers. For Co^{60} irradiation at 82°, $G(H_2) = (7.22 \pm 0.09) \times 10^{-3}$, $G(C_2H_2) = (0.542 \pm 0.030) \times 10^{-3}$, and $G(\rightarrow \text{residue}) = 0.226 \pm 0.009$. For He^{2+} irradiation at 82°, $G(H_2) = (18.8 \pm 0.1) \times 10^{-3}$, $G(C_2H_2) = (2.93 \pm 0.03) \times 10^{-3}$, and $G(\rightarrow \text{residue}) = 0.356 \pm 0.008$. Similar data are given for 27, 180, and 260° Co^{60} irradiations and for 180° He^{2+} irradiations. Many products were formed in low yield and the approximate G values are given. Product yields were larger at high temperatures and for more highly ionizing radiation and were lower from solid-phase irradiations. There was no apparent effect of dose or of dose rate. The distribution of products indicates the important participation of phenylcyclohexadienyl radicals and biphenylyl radicals in the radiolysis scheme.

The radiolysis of unsubstituted aromatic compounds has received considerable attention. Benzene has been exhaustively studied,[1] but biphenyl has been less thoroughly examined.[2] Since polyphenyls are used as moderators and coolants in nuclear reactors, the extent and mechanism of their radiation-induced decomposition are of practical interest.[3] The need for knowledge about this decomposition prompted the present work with biphenyl, the lowest member of the polyphenyl series.

Most previous workers measured just the major products from biphenyl radiolysis: hydrogen, acetylene, and "residue" or "polymer."[4] In the present study, we measured not only the major products, but also many products formed in very small yield. We also partially characterized the polymer and studied some effects of changes in experimental conditions (temperature, phase, dose rate, and LET[5]) on biphenyl decomposition. Relatively low radiation doses were used to permit detection of products formed early in the reaction sequence.

Experimental Section

Purification and Irradiation. Eastman Kodak White Label biphenyl was purified for the work by fractional distillation under vacuum, followed by recrystallization from methanol. Analysis was by gas chromatography (glpc), freezing point, mass spectrometry (MS), and the temperature–time slope of the freezing curve.[6] This last method indicated a purity of 99.99+ mole %, with a freezing point of 68.95° (literature values are 68.84[7] and 69.2°[8]).

Samples for irradiation were degassed and sealed

(1) J. Hoigné and T. Gaümann, *Helv. Chim. Acta*, **44**, 1337 (1961), and references cited therein.

(2) (a) W. G. Burns, W. Wild, and T. F. Williams, *Proc. U. N. Intern. Conf. Peaceful Uses At. Energy, 2nd, Geneva, 1958*, **29**, 266 (1959); (b) H. Koyama, G. Tsuchihashi, and A. Danno, *Bull. Chem. Soc. Japan*, **37**, 478 (1964); (c) W. H. Baldwin and P. S. Rudolph, *Nucl. Sci. Eng.*, **20**, 548 (1964); (d) K. L. Hall and F. A. Elder, *J. Chem. Phys.*, **31**, 1420 (1959); (e) J. M. Rayroux and P. Bartschi, *Helv. Chim. Acta*, **43**, 484 (1960); (f) J. G. Burr and J. M. Scarborough, *J. Phys. Chem.*, **64**, 1367 (1960); (g) J. M. Scarborough and J. G. Burr, *J. Chem. Phys.*, **37**, 1890 (1962); (h) W. G. Burns and C. R. V. Reed, *Trans. Faraday Soc.*, **59**, 101 (1963).

(3) R. F. Makens and Q. L. Baird, Ed., AEC Report TID-4500, National Bureau of Standards, U. S. Department of Commerce, Springfield, Va., Dec 1964.

(4) "Residue" is an operational definition, usually meaning what is left in the irradiation container after the starting material and some products have been evaporated under specified conditions. "Polymer" generally refers to substances similar in structure but of higher molecular weight than the original polyphenyl. For biphenyl, "polymer" refers to a chain made up of three or more benzene rings which may or may not be hydrogenated, alkylated, fused, etc.

(5) LET is the rate of linear energy transfer, *i.e.*, $-dE/dx$ for the radiation.

(6) A. R. Glasgow, B. J. Streiff, and F. D. Rossini, *J. Res. Natl. Bur. Std.*, **35**, 355 (1945).

(7) J. Marechal, *Bull. Soc. Chim. Belges*, **61**, 149 (1952).

(8) American Petroleum Institute Research Project 44, College Station, Texas, Vol. I, 23-2-(33.3310), Oct 31, 1963.

under vacuum in glass ampoules fitted with break-seals and thermocouple wells. Ampoules for cyclotron irradiations had thin, concave bubbles blown in the wall through which the cyclotron beam passed. Wall thickness was measured by focusing a microscope successively on the inside and outside surfaces of the bubble.

A heated vacuum system was used to sublime biphenyl into the ampoules. The ampoules, only about half full, contained 15 or 80 ml of biphenyl for γ irradiations and 60 ml for cyclotron exposures.

A 10-kcurie Co^{60} source was used for γ exposures[9] and the University of California (Berkeley) Crocker Laboratory 60-in. cyclotron for helium ion irradiations. The biphenyl temperature was controlled to $\pm 3°$ in both cases. The cyclotron samples were shaken back and forth along the beam axis during the irradiations to assure uniform temperature and prevent local accumulation of radiolysis products.

The dose rate in the Co^{60} source was measured with ferrous sulfate dosimetry[10] on eight different occasions, using the same geometry as for biphenyl irradiations. We used 5.25 years for the half-life and did a least-squares fit of 37 data points covering a 6-year period. The source strength normalized to Jan 1958 was $(2.15 \pm 0.01) \times 10^{17}$ ev g^{-1} min^{-1} in 0.8 N H_2SO_4.

The cyclotron irradiations were monitored by collecting the charge deposited by the beam.[11] Average beam currents were between 0.1 and 2.0 μa. The cyclotron beam is pulsed ($\sim 10^7$ Hz) and it is not clear whether reduction in average beam current is achieved by reducing the number of ions per pulse or the number of pulses per second.[12] Cross-sectional area of the beam was ~ 0.3 cm^2 and the original beam energy was 47.9 ± 0.1 Mev. We calculated an energy loss between the cyclotron and the biphenyl of ~ 10 Mev.[13] Beam penetration in the biphenyl was ~ 0.15 cm. Irradiation of cyclohexane confirmed that there were no gross systematic errors in cyclotron dosimetry.

Analyses. Irradiated ampoules were sealed onto a heated vacuum line where separations into three general fractions were made by condensation and distillation techniques.[14] Gaseous products were fractionated, measured in a gasometer, and collected. Products of intermediate volatility (the midfraction, *e.g.*, benzene and hydrogenated biphenyls) were similarly collected. The undecomposed biphenyl was then distilled under vacuum from the high-boiling products at 80°. The details of this general procedure have been reported.[15,16]

Gases. The separated gases were analyzed by MS. To ensure proper identification of the MS peaks, the fractions were first analyzed qualitatively by glpc. Details of the glpc procedures have been reported.[17]

Midfractions. These were collected under vacuum in small ampoules with break-seals. Three techniques were used to study them.

1. Some samples were analyzed by low-voltage mass spectrometry (LVMS) where 9.5-v electrons ionized the aromatic molecules without fragmentation. The resulting spectrum showed the molecular weight of parent molecule ions. The total ion current was related to sample size by calibration with biphenyl.

2. Some ampoules were crushed in a helium stream, which carried the contents for analysis onto a glpc column packed with poly(phenyl ethers).[17]

3. Combined glpc and MS techniques (glpc–MS) were used in some cases.[18] Samples of glpc effluent were bled into the inlet system of a high mass spectrometer. Fragmentation patterns were thus obtained for the main constituent of each glpc peak.

Residues. These were measured by weighing the material left in the irradiation ampoule. In some experiments the last traces of biphenyl were removed by sublimation at temperatures up to 200°. In others, the residue was dissolved in chloroform and the solution was analyzed for biphenyl by glpc.[17] The residue yields (biphenyl-free) determined by the two methods are in good agreement.

Results and Discussion

Control Experiments. Our analytical techniques were applied to empty irradiated ampoules and to biphenyl-containing ampoules which had been heated for long periods of time but not irradiated. Negligible amounts of product were detected, always less than 1% of the amounts produced in low-dose irradiations.

Product Yields. Gases. Hydrogen and acetylene constituted over 90% of the product gases; the re-

(9) B. Manowitz, *Nucleonics*, 9 (2), 10 (1951).

(10) J. Weiss, *ibid.*, 10 (7), 28 (1952).

(11) W. M. Garrison, H. R. Haymond, and B. M. Weeks, *Radiation Res.*, 1, 97 (1954).

(12) A. S. Newton and W. R. McDonell, *J. Am. Chem. Soc.*, 78, 4554 (1956).

(13) W. A. Aron, B. G. Hoffman, and F. C. Williams, AEC Report AECU-663, Department of Commerce, Washington 25, D. C., May 1951.

(14) R. T. Sanderson, "Vacuum Manipulation of Volatile Compounds," John Wiley and Sons, Inc., New York, N. Y., 1948, pp 86–93.

(15) K. L. Hall and W. R. Doty, *Rev. Sci. Instr.*, in press.

(16) M. A. Sweeney, AEC Report TID-19663, Department of Commerce, Washington 25, D. C., 1963, p 36.

(17) W. W. West, AEC Report TID-17508, Department of Commerce, Washington, D. C., 1962, p 35.

(18) L. P. Lindemann and J. L. Annis, *Anal. Chem.*, 32, 1742 (1960).

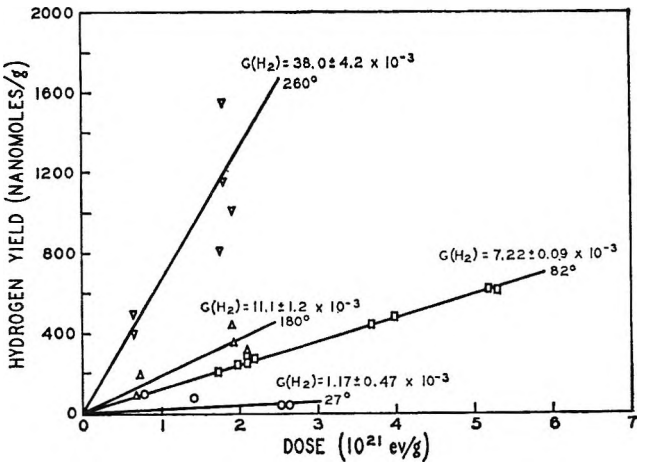

Figure 1. Hydrogen yield variations with dose and temperature in Co^{60} exposures of biphenyl.

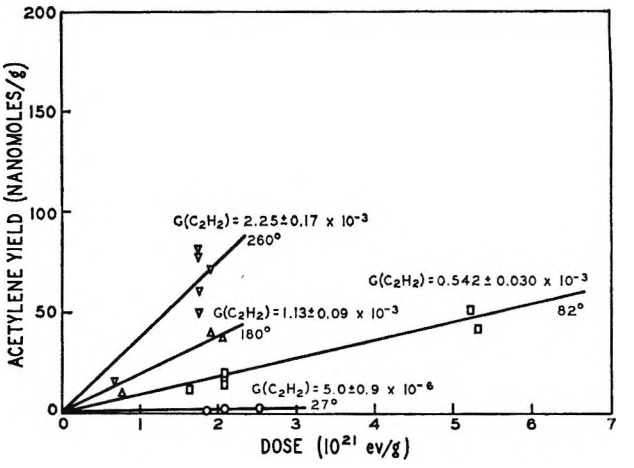

Figure 3. Acetylene yield variations with dose and temperature in Co^{60} exposures of biphenyl.

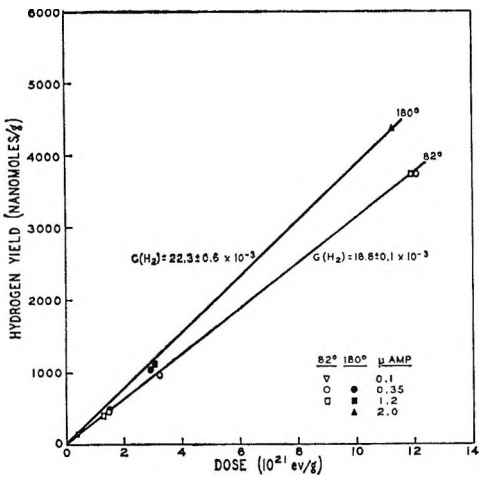

Figure 2. Hydrogen yield variations with dose, dose rate, and temperature in He^{2+} exposures of biphenyl.

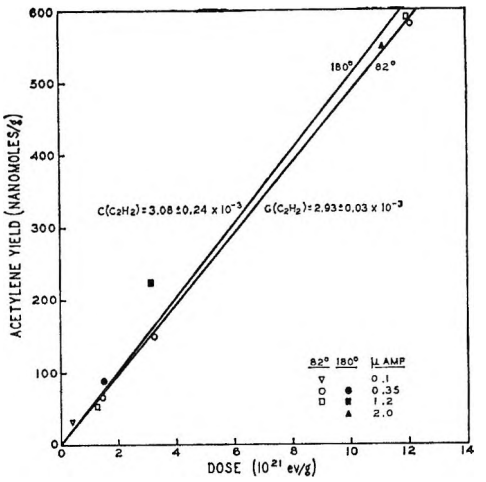

Figure 4. Acetylene yield variations with dose, dose rate, and temperature in He^{2+} exposures of biphenyl.

mainder was a mixture of low molecular weight hydrocarbons, mostly unsaturated. Yields of hydrogen and acetylene are plotted as a function of γ dose in Figure 1 and Figure 3 and of helium ion dose in Figure 2 and Figure 4. These and the other yields seem to be linear with dose. This linearity also exists with hydrogen and acetylene from benzene, both for heavy ions[19,20] and for γ rays.[2h] Some of the products, *e.g.*, butane, may be secondary products formed by hydrogenation of unsaturated primary species. The G values listed in Table I are based on the slope of the linear yield *vs.* dose curves passing through the origin. In cases where enough data were available (hydrogen, acetylene, and residue), a least-squares fit was obtained. G values for the minor gases are estimates based on MS analysis and the errors can be quite large. For instance, butane can be off by as much as 100% owing to small yield and indistinctive fragmentation pattern.

Midfractions. These were analyzed in three ways, as already described. All three methods showed appreciable yields of hydrogenated biphenyls. LVMS results from two 82° irradiations are listed in Table II according to their order-of-magnitude yield. The yields were calculated assuming all the listed products had an LVMS sensitivity equal to that of biphenyl. Since LVMS shows only the molecular weight of a parent ion, some of the compounds listed are only suggested assignments. Other compounds were, however, confirmed by glpc–MS as noted in Table II. Some of

(19) T. Gäumann and R. H. Schuler, *J. Phys. Chem.*, 65, 703 (1961).
(20) W. G. Burns, *Trans. Faraday Soc.*, 58, 961 (1962).

Table I: Biphenyl Radiolysis Yields (Milli G Values, Molecules of Product/10^5 Ev Absorbed)[a]

Gases	Co^{60} irradiations				He^{2+} irradiations	
	27°	82°	180°	260°	82°	180°
H_2	1.17 ± 0.47 (3)	7.22 ± 0.09 (11)	11.1 ± 1.2 (5)	38.0 ± 4.2 (6)	18.8 ± 0.1 (6)	23.3 ± 0.6 (4)
CH_4		<0.02			0.01	0.01
C_2H_2	0.0050 ± 0.0009 (3)	0.542 ± 0.030 (7)	1.13 ± 0.09 (3)	2.25 ± 0.17 (6)	2.93 ± 0.03 (6)	3.08 ± 0.24 (3)
C_2H_4		<0.005			0.005	0.2
C_2H_6		0.1				0.002
C_3H_4		0.005			0.06	0.07
C_3H_6		0.001			0.003	0.007
C_3H_8		0.001				
C_4H_2		0.015			0.14	0.20
C_4H_4		0.015			0.13	0.13
C_4H_6		0.003			0.013	0.013
C_4H_8		0.004			0.001	
C_4H_{10}		0.005				
Total gases (approx)	1	8	12	40	22	26
Midfraction		1-2				
Residue	128 ± 14 (3)	226 ± 9 (7)		454 ± 28 (3)	356 ± 8 (4)	

[a] Errors given are standard deviations based on the number of data points shown in parentheses. When no error is given, the G values are only approximate as discussed in the text.

Table II: Low-Voltage Mass Spectrometric Analyses of Midfractions from Biphenyl Radiolysis

Group	Compound	Milli G[b]
I	Dihydrobiphenyl[a]	>0.8
II	Tetrahydrobiphenyl[a]	>0.2
III	Methylcyclohexane, phenylacetylene, methyloctahydronaphthalene, biphenylene, phenylnaphthalene	0.04–0.2
IV	Styrene,[a] naphthalene, dihydronaphthalene, phenylpentane, hexa-[a] and octahydrobiphenyl, diphenylmethane, stilbene	0.006–0.03
V	Toluene, ethylbenzene, methylphenylacetylene, methylphenylethylene,[a] propylbenzene, tetrahydronaphthalene, phenylpentene, decahydrobiphenyl, di- and tetrahydrodiphenylmethane, diphenylethane, diphenylacetylene	0.001–0.005

[a] Identity confirmed by glpc–MS. [b] From two Co^{60} irradiations at 82°.

Table III: Glpc Analysis of Midfraction from Biphenyl Radiolysis

Compound	Milli G[a]
3-Phenyl-1,4-cyclohexadiene	~1
5-Phenyl-1,3-cyclohexadiene	~1
1-Phenylcyclohexene	0.006
3-Phenylcyclohexene	0.05
4-Phenylcyclohexene	0.0004
Phenylcyclohexane	0.004
1-Cyclohexylcyclohexene	Present
4-Cyclohexylcyclohexene	Present
Bicyclohexyl	Present

[a] From one Co^{60} irradiation at 82°.

the individual isomers of the hydrogenated biphenyls were detected with high-resolution glpc on a poly(phenyl ether) column and are listed in Table III. The yields are only approximate, owing to decomposition of some products on the glpc column and lack of individual sensitivities. LVMS shows the production of a nonaromatic tetrahydrobiphenyl not reported in Table III, causing the disparity in yields between Tables II and III.

Note that unsaturated and aromatic compounds are often accompanied by their hydrogenated derivatives, decreasing in concentration with increasing hydrogen content. This demonstrates the presence of reducing species in the irradiated liquid. Such species are also present in the radiolysis of benzene.[21-23] The small amounts observed do not require that the products be formed in low initial yield; they may participate in secondary radiation-induced reactions.

In this midfraction we also find several substituted benzenes. These most likely come from the decomposition of a biphenyl molecule or ion intensely excited by the radiation. Here a substituted benzene would be formed, together with a lower molecular weight gaseous fragment such as one of those carbon compounds in our gas fraction. Thus we find styrene and diacetylene (conjugate fragments of biphenyl) to be formed in similar yield. Other minor products, *e.g.*, the fused-ring compounds, also can come from reactive fragments of biphenyl.

Residues. The yield of this fraction is shown as a function of absorbed dose in Figure 5 for γ rays and in Figure 6 for helium ions. As with the hydrogen and acetylene, we used a least-squares analysis to calculate values for $G(\rightarrow\text{residue})$.

Table IV shows the approximate composition of several residue fractions from Co^{60} irradiations at 82°. Note that products with an even number of benzene rings predominate. This is evidence that few phenyl radicals are formed by the radiation and inter-ring C–C bond rupture is relatively unimportant.

Table IV: Yields of Polyphenyl Products from Biphenyl Radiolysis

Compound	Milli G^a
Terphenyl and hydrogenated terphenyls	4
Quaterphenyl	124
Hydrogenated quaterphenyls	82
Quinquephenyl and hydrogenated quinquephenyls	0.5
Hexaphenyl and hydrogenated hexaphenyls	4
Unidentified	8

[a] LVMS and glpc analyses from Co^{60} irradiations at 82°. Values are approximate.

The presence of reducing species in the irradiated liquid is again demonstrated by the fact that each polyphenyl product is accompanied by its hydrogenated derivatives. The occurrence of hydrogenated aromatic compounds in the residue from biphenyl radiolysis has also been reported by Baldwin and Rudolph, based on infrared spectra.[2c] Gordon, *et al.*, have found that the analogous irradiation of benzene produces not only biphenyl but also hydrogenated biphenyls in yields ~45% that of biphenyl.[21]

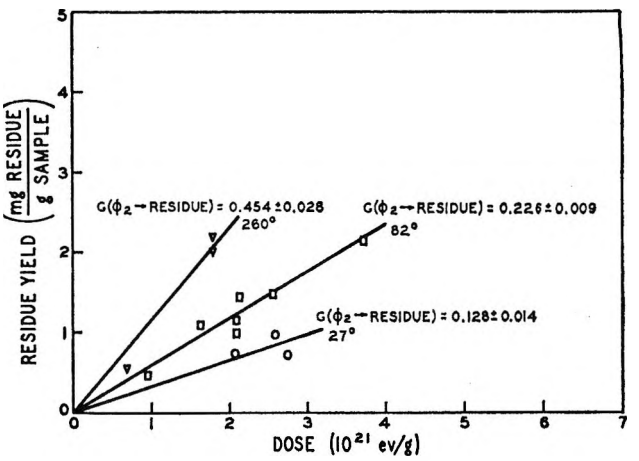

Figure 5. Residue yield variations with dose and temperature in Co^{60} exposures of biphenyl.

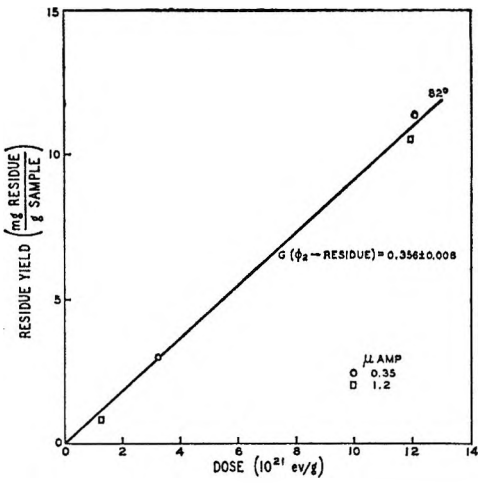

Figure 6. Residue yield variations with dose, dose rate, and temperature in He^{2+} exposures of biphenyl.

Effect of Experimental Conditions. Dose Rate. The Co^{60} irradiations were performed at only one dose rate, but helium ions were used at four average beam currents. Product yields for these different beam currents are shown in Figures 2, 4, and 6. Changing the beam current did not affect the yields within the precision of our measurements. It is not certain that the instantaneous dose rate (during the delivery of a pulse

(21) S. Gordon, A. R. Van Dyken, and T. F. Doumani, *J. Phys. Chem.*, 62, 20 (1958).

(22) M. K. Eberhardt, *ibid.*, 67, 2856 (1963).

(23) T. Gäumann, *Helv. Chim. Acta*, 46, 2873 (1963).

of ions) changed as the beam current was changed. The instantaneous dose rate was over 10^{22} ev g^{-1} sec^{-1} in the irradiation zone containing 0.05 g of biphenyl.

Temperature and Physical State. Arrhenius plots of G values for H_2, C_2H_2, and residue are given in Figures 7, 8, and 9. Points are also shown for the results of Co^{60} irradiations by other workers. The slopes of the plots correspond to apparent activation energies of 1–2.5 kcal/mole for the Co^{60} irradiations and 0.5 kcal/mole for the helium ion irradiations. Thus the yields increase only slightly as the temperature increases moderately above the melting point. The yield of hydrogen increases inordinately at high temperatures. This is consistent with other data from polyphenyl radiolysis, which generally show two activation energies, one for low temperatures and one for high temperatures.[3]

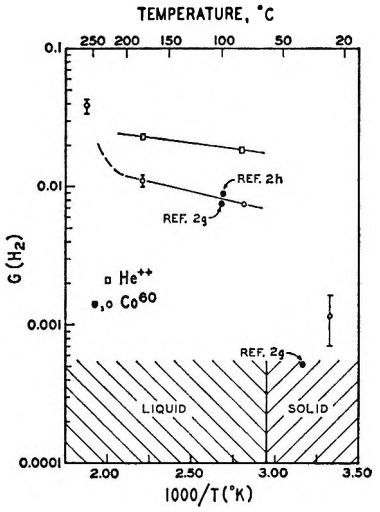

Figure 7. Hydrogen yield variations with temperature in biphenyl irradiations.

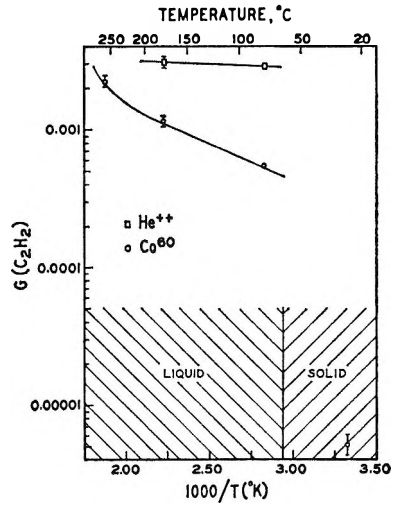

Figure 8. Acetylene yield variations with temperature in biphenyl irradiations.

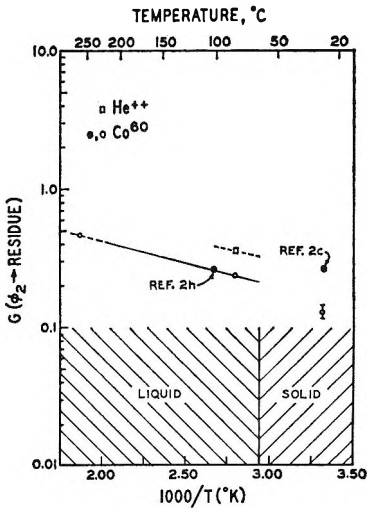

Figure 9. Residue yield variations with temperature in biphenyl irradiations.

The points corresponding to solid-phase irradiations are much lower than an extrapolation of the liquid-phase points. If reaction rates leading to product are diffusion controlled, both the low activation energies and the lower yields in the solid phase would be explained.[2g,3,24] Another explanation for the lower yields in the solid phase is energy transfer in the crystals, away from the site at which the energy is deposited.[25,26] Differences in crystallinity would then account for the extremely variable yields reported by different laboratories for solid-phase irradiations (see Figures 7 and 9).

Particle Type. The data in Table I and Figures 7, 8, and 9 show the G values to be generally higher for helium ion (2.2 ev/A initial LET in H_2O) irradiations than for γ (0.02 ev/A in H_2O) irradiations. Although the dose rates were vastly different in the two cases, there is widespread agreement that the differences in product yields from aromatics are an effect of LET.[19,27]

(24) J. Y. Chang and M. Burton, 138th National Meeting of the American Chemical Society, New York, N. Y., Sept 1960, p 17S.

(25) H. W. Fenrick, S. V. Filseth, A. L. Hanson, and J. E. Willard, *J. Am. Chem. Soc.*, 85, 3731 (1963).

(26) E. Collison, J. J. Conlay, and F. S. Dainton, *Nature*, 194, 1074 (1962).

(27) (a) J. Hoigné, W. G. Burns, W. R. Marsh, and T. Gäumann, *Helv. Chim. Acta*, 47, 247 (1964); (b) W. G. Burns and J. D. Jones, *Trans. Faraday Soc.*, 60, 2022 (1964); (c) R. H. Schuler, *ibid.*, 61, 100 (1965); (d) A. W. Boyd and H. W. J. Connor, *Can. J. Chem.*, 42, 1418 (1964); (e) J. Y. Yang, J. D. Strong, and J. G. Burr, *J. Phys. Chem.*, 69, 1157 (1965); (f) P. Huyskens, P. Claes, and F. Cracco, *Bull. Soc. Chim. Belges*, 68, 89 (1959); (g) I. V. Vereshchinskii and N. A. Bakh, *Proc. All-Union Conf. Radiation Chem., 1st, Moscow, 1957*, Part 5, 223 (1959).

Table V shows 100° G values from biphenyl (read from Figures 7 and 9) to agree well with the data of Burns and Reed.[2h] They have attributed similar increases, in the case of benzene, to the formation of products

Table V: Yields from Biphenyl Irradiations at 100°

Radiation (increasing LET)	G_{H_2}	G_{-M}[a]	Ref
Fast electrons	0.009	0.26	2h
Co^{60}	0.008	0.27	This work
38-Mev He^{2+}	0.019	0.40	This work
BEPO reactor radiation	0.059	0.69	2h
B(n, α)	0.17	1.52	2h

[a] Disappearance of starting material: molecules of biphenyl altered/100 ev absorbed.

or their precursors in the interreactions of excited molecules which are subject to deactivation.

$$M^* + M^* \longrightarrow H_2 + \text{radical or stable product} \quad (1)$$

$$M + M^* \longrightarrow 2M \quad (2)$$

In the case of benzene irradiations, the invariance with LET of $G_{H_2}/G_{C_2H_2}$ was taken as evidence for a common precursor for H_2 and C_2H_2.[19,20] In our biphenyl work, the ratios are not constant with either LET or temperature. In particular, the ratio from Co^{60} irradiations increases from ~12 at 100° to ~230 in the solid phase. Thus it is more likely that hydrogen and acetylene are produced, at least in part, by separate mechanisms. This conclusion was also reached in the fission-fragment irradiation of benzene.[27d]

Mechanism Postulations

We can deduce two significant things from the measured products. First, the high yield of quaterphenyls and the presence of hydrogenated biphenyls and hydrogenated quaterphenyls indicate the participation of biphenylyl and phenylcyclohexadienyl radicals in the radiolysis. The evidence for this is summarized in the following section. Our data do not show whether these radicals are produced initially by the radiation or only indirectly. Electron-impact studies[2d] and the low yield of products with an odd number of benzene rings indicate that few phenyl radicals are formed.

Second, some of the products—hydrogenated biphenyls and reactive fragments from the biphenyl molecule, *e.g.*, styrene, etc.—are capable of forming nonvolatile polymer during radiolysis. This explains the low yield of these products and the high yield of polymer characteristic of prolonged polyphenyl irradiations.[3]

Biphenylyl and Phenylcyclohexadienyl Radicals as Precursors. There are two reasons for believing that these radicals play an important part in biphenyl radiolysis. First, the presence of analogous radicals has been established in irradiated aromatics. Thus cyclohexadienyl radical has been confirmed in irradiated benzene by epr spectra.[28,29] Phenyl radicals have also been tentatively identified in these epr spectra.[28]

The second reason is that reactions of the biphenylyl and phenylcyclohexadienyl radicals are known and give the products that we found.

1. It is known that biphenylyl radicals add to biphenyl to give quaterphenyls,[2b,30] the principal components of our residues. Since the analogous phenyl radical adds to benzene to give the phenylcyclohexadienyl radical,[31] we may conclude that the biphenylyl radical adds to biphenyl to give a four-ring radical, which will eventually form quaterphenyl and hydrogenated quaterphenyl.

$$C_{12}H_9\cdot + C_{12}H_{10} \longrightarrow C_{24}H_{19}\cdot \quad (3)$$

$$2C_{24}H_{19}\cdot \xrightarrow{\text{disproportionation}} C_{24}H_{18} + C_{24}H_{20} \quad (4)$$

$$\longrightarrow \text{high molecular weight products}$$

2. The reactions of phenylcyclohexadienyl radicals are better known than those of biphenylyl, owing to experiments on benzoyl peroxide decomposition in benzene. Phenylcyclohexadienyl radical results from the addition of chemically generated phenyl radical to benzene. This radical undergoes combination reac-

$$C_6H_5\cdot + C_6H_6 \longrightarrow C_{12}H_{11}\cdot \quad (5)$$

tions to give hydrogenated quaterphenyls and disproportionates to give biphenyl and hydrogenated biphenyl.[31-33] Furthermore, this addition of phenyl

$$2C_{12}H_{11}\cdot \xrightarrow{\text{combination}} C_{24}H_{22} \quad (6)$$

$$\xrightarrow{\text{disproportionation}} C_{12}H_{10} + C_{12}H_{12}$$

radicals to benzene forms a high-boiling polymer,[34]

(28) R. W. Fessenden and R. H. Schuler, *J. Chem. Phys.*, **38**, 773 (1963).

(29) V. A. Tolkachev, I. N. Molin, I. I. Chkheidze, N. T. Buben, and V. V. Voevodskii, *Dokl. Akad. Nauk SSSR*, **141**, 911 (1961).

(30) W. M. Hutchison, P. S. Hudson, and R. C. Doss, *J. Am. Chem. Soc.*, **85**, 3358 (1963).

(31) D. F. DeTar and R. A. J. Long, *ibid.*, **80**, 4742 (1958).

(32) D. H. Hey, M. J. Perkins, and G. H. Williams, *J. Chem. Soc.*, 3412 (1964).

(33) G. B. Gill and G. H. Williams, *ibid.*, 995 (1965).

(34) J. M. Blair, D. Bryce-Smith, and B. W. Pengilly, *ibid.*, 3174 (1959).

presumably through the agency of the phenylcyclohexadienyl radical. We found all these products in our work.

Source of Biphenylyl and Phenylcyclohexadienyl Radicals. A likely source of these precursors is C–H bond cleavage in biphenyl to give hydrogen and biphenylyl radicals. Phenylcyclohexadienyl radicals would be formed by addition of the hydrogen atoms to biphenyl.

$$C_{12}H_{10} \longrightarrow H\cdot + C_{12}H_9\cdot \quad (7)$$

$$H\cdot + C_{12}H_{10} \longrightarrow C_{12}H_{11}\cdot \quad (8)$$

Other mechanisms are possible, *e.g.*

$$C_{12}H_{10}^{+} + C_{12}H_{10} \longrightarrow C_{12}H_{11}\cdot + C_{12}H_9^{+} \quad (9)$$
$$\qquad\qquad\qquad\qquad\qquad\qquad\qquad\qquad\qquad\qquad \downarrow$$
$$\qquad\qquad\qquad\qquad\qquad\qquad\qquad\qquad\qquad\qquad \longrightarrow C_{12}H_9$$

Two factors reinforce the plausibility of these reactions.

1. Other workers have found evidence, through isotope effects, for participation of the C–H bond in the irradiation of deuterated biphenyl.[2e,f]

2. Our detection of a series of hydrogenated biphenyls and hydrogenated quaterphenyls, diminishing in yield as they increase in molecular weight, demonstrates the existence of reducing species in the irradiated biphenyl. If these species are hydrogen atoms, they will form phenylcyclohexadienyl radical by addition to biphenyl.[35] This is shown by the fact that the same epr spectra found in irradiated benzene can be produced by reaction of hydrogen atoms with benzene.[35]

Formation of Polymer. The source of radiolytic polymer is of practical importance, for it is this polymer that changes the properties of reactor coolant. There are several possible sources of polymer. For example, it can come from radical reactions. Quaterphenyls (dimer) are produced by addition reactions of biphenylyl radicals, as already outlined. However, we have some evidence that at least part of the polymer may come from secondary decomposition of unstable radiolysis products. Several of the hydrogenated biphenyls which were detected as radiolysis products were synthesized and irradiated with Co^{60} γ rays. They polymerize readily. For example, 2-phenyl-1,3-cyclohexadiene was exposed to a total dose of $\sim 2.5 \times 10^{21}$ ev/g. $G(\rightarrow \text{polymer})$ was ~ 12 at room temperature.

Acknowledgment. The authors wish to thank the U. S. Atomic Energy Commission for support of this work under Contracts AT(11-1)-174 and AT(04-3)-248. Dr. William W. West, Dr. Merwyn L. Burrous, and Mr. Noel P. Shiells participated in many phases of the research and we are grateful for their contributions.

(35) L. I. Avramenko, N. T. Buben, R. V. Kolesnikova, V. A. Tolkachev, and I. I. Chkheidze, *Izv. Akad. Nauk SSSR, Otd. Khim. Nauk*, 2079 (1962).

Prediction of Ion-Exchange Selectivity

by J. A. Marinsky

Department of Chemistry, State University of New York at Buffalo, Buffalo, New York *(Received March 7, 1966)*

An equation introduced for the anticipation of ion-exchange selectivity by Gregor, who employed the model of an elastic matrix to describe ion-exchange equilibria, has been reexamined. The polyelectrolyte theory of Fuoss, Katchalsky, and Lifson, as adapted by Gregor and Kagawa to counterions of different sizes, has been used according to the method suggested by Feitelson to estimate their activity coefficient ratio in the exchanger. Hydration parameters obtained *via* the polyelectrolyte model appear to enhance the quantitative estimate of this ratio and of swelling pressure effects as well.

Introduction

The prediction of ion-exchange equilibria, a problem of considerable importance, has been extensively investigated for many years. The numerous attempts that have been employed to resolve this problem may be classified into two categories. In the first category, rigorous thermodynamic treatment that requires no model and no assumptions with respect to the mechanism of the phenomenon is employed. The second approach consists of the introduction of models with particular properties resembling those of the ion exchanger to permit the derivation of equations which reflect the action of various physical forces in the exchange process. A rather complete discussion of the spectrum of theoretical approaches and models has been presented by Helfferich.[1]

One of the simplest and most useful quantitative treatments of ion-exchange equilibria employs the model of an elastic matrix that was introduced by Gregor.[2] This model leads to the relation for the molal selectivity coefficient, K

$$\ln K_1^2 = \ln \frac{\bar{\gamma}_1}{\bar{\gamma}_2} + \ln \frac{\gamma_2}{\gamma_1} + \frac{(\bar{\pi} - \pi)(\bar{V}_1 - \bar{V}_2)}{RT} \quad (1)$$

where subscripts 1 and 2 refer to the counterions of uni-univalent electrolytes 1 and 2 with a common byion, the $\bar{V}$ terms are the partial molal volumes of the respective ions, and $\bar{\pi} - \pi$ is the resin-swelling pressure. Bars are placed above the appropriate symbols to designate the resin phase.

Gregor in his earliest application of the model assumed that the system behaved ideally except for solvation and attempted to correlate selectivity on the basis of swelling pressure and ionic size[3,4] alone. In anion exchange, where the selectivity could not be explained by a swelling-pressure effect, Gregor and coworkers postulated ion-pair formation.[5] Their distinction between free solvent and solvation shells and associated and free counterions was arbitrary and employment of one or both approaches is drastically deprived of thermodynamic rigor as a consequence. Qualitative rather than quantitative analysis of the ion-exchange phenomenon was the result.

The swelling-pressure term of eq 1 becomes relatively unimportant when, in an attempt for greater thermodynamic rigor, the poorly defined solvation effects are not specifically considered. The effects are instead reflected in the activity coefficients of the ions in the resin phase. Myers and Boyd[6] and Boyd, Lindenbaum, and Myers[7] avoided completely the use of empirical relations in their computation of selectivity coefficients by using exact thermodynamic equations to evaluate the three right-hand members of eq 1. The evaluation of the equations, however,

(1) F. Helfferich, "Ion-Exchange," McGraw-Hill Book Co., Inc., New York, N. Y., 1962.

(2) H. P. Gregor, *J. Am. Chem. Soc.*, **70**, 1293 (1948); **73**, 642 (1951).

(3) H. P. Gregor and J. I. Bregman, *J. Colloid Sci.*, **6**, 323 (1951).

(4) H. P. Gregor and M. Frederick, *Ann. N. Y. Acad. Sci.*, **57**, 87 (1953).

(5) H. P. Gregor, J. Belle, and R. A. Marcus, *J. Am. Chem. Soc.*, **77**, 2713 (1955).

(6) G. E. Myers and G. E. Boyd, *J. Phys. Chem.*, **60**, 521 (1956).

(7) G. E. Boyd, S. Lindenbaum, and G. E. Meyers, *ibid.*, **65**, 577 (1961).

requires a large number of measurements, and the method, although theoretically important, is not practical for predicting ion-exchange equilibria.

Glueckauf,[8] on the other hand, has been able to use the osmotic coefficient measurements of weakly cross-linked (0.5% DVB) exchangers in the pure salt forms to determine the activity coefficient ratios of the ions in the resin phase and thereby predict ion-exchange equilibria. Harned's rule[9] was employed to estimate the activity coefficients of the resinates in the mixed form.

Glueckauf's approach has been modified by Soldano, *et al.*,[10-12] who employed the Gibbs–Duhem equation to determine ion-activity coefficients. The activity coefficients of the heteroionic forms of the resin were also computed by Harned's rule.[9] The amalgamation of polyion and simple counterion interactions, implicit in their approach, leads to coefficients that are different from those that are generally observed in aqueous solutions. The Harned coefficients are much too large, and the thermodynamic requirement that their sum be a constant[13] is not obeyed.[11] The complete ion-exchange isotherm is predicted by them, however, from water vapor sorption isotherms of the pure salt forms of the resin and two equilibrium measurements with one component present in trace quantity.

The treatment by Gregor of the problem of ion-exchange selectivity appears to be most practical and it is the objective of this article to provide an appropriate modification of his approach. For this purpose we have adapted Feitelson's[14] application of the Fuoss, Katchalsky, and Lifson[15] polyelectrolyte theory as modified by Gregor and Kagawa[16] to evaluate the first term of eq 1, $\ln (\bar{\gamma}_1/\bar{\gamma}_2)$, which was neglected by Gregor and co-workers. Our employment of the third term of eq 1, $(\bar{\pi} - \pi)(\bar{V}_1 - \bar{V}_2)/RT$, is less arbitrary than Gregor's, hydration parameters for the estimate of ion volumes being derived from our interpretation[17] of the observed variation of the osmotic properties of the essentially unrestrained (<0.5% cross-linked) ion exchanger.

The ion-exchange selectivity data that are employed herein to test the unified model that is developed are from the literature and are limited to Dowex 50, the divinylbenzene copolymer of polystyrenesulfonate. The concentration of the equilibrating solutions of these various investigations was limited to 0.1 N, and the second term of eq 1 can be neglected since the ion-activity coefficients of the external electrolyte species are very nearly equal.

Evaluation of Terms in Selectivity Equation

Feitelson,[14] considering that the understanding of electrostatic interactions in ion-exchange gels should be sought to explain ion-exchange selectivity, employed the polyelectrolyte theory of Fuoss, Katchalsky, and Lifson[15] for this purpose with some success. He limited his examination to highly swollen ionized gels, however, justifying his use of polyelectrolyte theory by pointing out the similarity between the linear analog and the highly swollen cross-linked gel. We have since shown that the profitable use of polyelectrolyte theory for the interpretation of ion-exchange phenomena[18] can be extended to the more concentrated highly cross-linked ion-exchange gels. In addition we have demonstrated that the unique patterns of physical–chemical behavior that are observed with linear polyelectrolyte systems are to be expected in the highly cross-linked systems as well.[17] For example, the observation in numerous investigations of ionized polyelectrolyte–simple salt mixtures that the colligative properties of the pure components are additive[19-25] also applies to cross-linked ionized polyelectrolytes (ion-exchange resins)–simple salt mixtures.[17]

Model. The gel, in the theory of Fuoss, Katchalsky, and Lifson[15] as modified by Kagawa and Gregor,[16] is pictured to consist of a parallel arrangement of cylindrical polyion rods carrying evenly distributed fixed charges with mobile counterions of finite radius distributed in accordance with the electrostatic field in the vicinity of the polyion strands. At the midpoint,

(8) E. Glueckauf, *Proc. Roy. Soc.* (London), **A214**, 207 (1952).

(9) H. S. Harned and B. B. Owen, "The Physical Chemistry of Electrolyte Solutions," 3rd ed, Reinhold Publishing Corp., New York, N. Y., 1958, p 600 and Appendix A.

(10) B. A. Soldano and Q. V. Larson, *J. Am. Chem. Soc.*, **77**, 1331 (1955).

(11) B. A. Soldano and D. Chesnut, *ibid.*, **77**, 1334 (1955).

(12) B. A. Soldano, Q. V. Larson, and G. E. Myers, *ibid.*, **77**, 1339 (1955).

(13) E. Glueckauf, H. A. C. McKay, and A. R. Mathieson, *J. Chem. Soc.*, S299 (1948).

(14) J. Feitelson, *J. Phys. Chem.*, **66**, 1295 (1962).

(15) R. M. Fuoss, A. Katchalsky, and S. Lifson, *Proc. Natl. Acad. Sci. U. S.*, **37**, 579 (1951); S. Lifson and A. Katchalsky, *J. Polymer Sci.*, **13**, 43 (1954).

(16) I. Kagawa and H. P. Gregor, *ibid.*, **23**, 477 (1957).

(17) J. A. Marinsky, "Ion Exchange," Vol. 1, J. A. Marinsky, Ed., Marcel Dekker, Inc., New York, N. Y., 1966, Chapter 9.

(18) A. Chatterjee and J. A. Marinsky, *J. Phys. Chem.*, **67**, 41 (1963).

(19) Z. Alexandrowicz, *J. Polymer Sci.*, **56**, 115 (1962).

(20) Z. Alexandrowicz, *ibid.*, **43**, 337 (1960).

(21) M. Nagasawa, M. Izumi, and I. Kagawa, *ibid.*, **37**, 375 (1959).

(22) M. Nagasawa, M. Izumi, and I. Kagawa, *ibid.*, **38**, 213 (1959).

(23) R. A. Mock and E. A. Marshall, *ibid.*, **13**, 263 (1954).

(24) A. Katchalsky, R. Cooper, J. Upadhyay, and A. Wassermann, *J. Chem. Soc.*, 5198 (1961).

(25) F. T. Wall and M. I. Eitel, *J. Am. Chem. Soc.*, **79**, 1556 (1957).

R, between the polyelectrolyte strands $(d\psi/dr)_R = 0$; *i.e.*, the electrical force acting on an ion at the potential minimum is taken to be zero. The interaction between mobile counterions is presumed to be negligible, and at $r = R$ the counterions are considered to behave ideally, their concentration being equated with their activity. This idealized concentration, C_R, is calculable by

$$C_R = C_0 \left\{ \frac{1 + |\beta|^2}{2\lambda} - \frac{1}{\left(\frac{R}{a+b}\right)^2 - 1} \right\} \quad (2)$$

where C_0 is the average counterion concentration in the gel, a is the radial dimension of the polyion cylinder, b is the distance of nearest approach of a counterion center to the polyion cylinder surface, λ is determined by the linear charge density, and β and A are integration constants depending on λ and $R/(a + b)$.

The theroretical value of C_R/C_0, identifiable as a single-ion activity coefficient, and the experimental osmotic coefficient, φ_p, of linear polyelectrolytes have been equated to each other on a theoretical basis.[26]

We have employed eq 2 to estimate the magnitude of the charge density parameter, λ (defined by the distance between repeating charged groups along a polyion strand), at various experimental conditions.[17] In this approach C_R/C_0 is assigned a value of 0.4 (0.46 in the case of NH_4^+ ion form) to agree with the φ_p value deduced for the more concentrated (monomer basis) polyelectrolyte systems[17] encountered in this investigation. To facilitate this computation, the value of a has been taken to be 6 A rather than 3 A as was assumed by Feitelson.[14] Our radial dimension is more reasonable for the bulky polystyrenesulfonate strand on the basis of molecular model examination. The value of b has been deduced from additive combination of the bare counterion radius, and the radius of its hydration sphere was computed by assigning a volume of 30 A^3 to each attached water molecule. The method for estimating average hydration numbers for a particular counterion at various polyelectrolyte concentrations (expressed on a monomer basis) has been described in an earlier article.[17]

Activity Coefficient Ratio of Counterions in Gel. By having normalized the binding properties of the various counterion forms of the polyelectrolyte in the above manner, we are able to evaluate the interaction of a particular ion, denoted as ion 1, in the polyelectrolyte gel whose thermodynamic properties are wholly determined by ion 2. The first term of eq 1 becomes calculable by using eq 3, derived earlier by Feitelson.[14]

$$\frac{\gamma_1}{\gamma_2} = \frac{\cot|\beta|(\ln A + \ln R) - \cot|\beta|[\ln A + \ln(a + b_2)]}{\cot|\beta|(\ln A + \ln R) - \cot|\beta|[\ln A + \ln(a + b_1)]} \quad (3)$$

where parameters β, A, and R are determined by ion 2.

In this approach the relative distribution of both ions between gel and solution in the region between b_2 and R will be the same since the same electrical potential difference acts on both. The average concentration ratios of the two ions will differ, however, since only the smaller ion is able to penetrate the region between b_1 and b_2 where a particularly high electrical potential exists. Thus on a purely electrostatic basis a given gel will absorb preferentially the smaller counterions.

Pressure–Volume Effects in Gel. The method for evaluation of the third term in eq 1 has been described by Gregor.[3,4] The internal pressure π at each situation is deduced from the osmotic behavior of each counterion form of the essentially unrestrained exchanger. The water activity at a given monomer molality is defined by

$$\frac{\varphi_p m_m}{55.5} = -\ln \bar{a}_w \quad (4)$$

where

$$\ln a_w = \ln \bar{a}_w + \frac{(\bar{\pi} - \pi)\bar{V}_w}{RT} \quad (5)$$

for the cross-linked exchanger at its experimental molality. The $(\bar{\pi} - \pi)(\bar{V}_1 - \bar{V}_2)/RT$ term of eq 1 is thus made available by using the bare ion volume and a 30-A^3 volume for each molecule of bound water as described earlier.

Test of Selectivity Equation

When the terms in eq 1 are computed as described above, it is discovered that the selectivity predictions are in agreement with experimental observations in only one system (Cs^+–Na^+). The logarithm of the ratio of selectivities at different cross-linking values of the exchanger

$$\log \frac{K_1^2(\text{XDVB})}{K_1^2(\text{YDVB})}$$

is quite accurately predicted in most instances, however, to indicate that the discrepancy in each calculated value is by a constant logarithmic factor. The in-

(26) A. Katchalsky, Z. Alexandrowicz, and O. Kedem in "Chemical Physics of Ionic Solutions," B. E. Conway and R. G. Barradas, Ed., John Wiley and Sons, Inc., New York, N. Y., 1966.

Table I: Computation of Ion-Exchange Selectivity in Cross-Linked Polystyrenesulfonate Systems

System	Trace ion	% DVB	Av hydration no. ($\bar{h}$)	Log ($\bar{\gamma}_1/\bar{\gamma}_2$)	$\pi\Delta V/2.3RT$	A	K_1^2 Calcd	K_1^2 Exptl
Na–K[6]	K	2	$\bar{h}_{Na}$ = 6.0 $\bar{h}_K$ = 2.0	0.222	0.020	−0.128	1.30	1.30
		4	5.8 2.0	0.248	0.050		1.48	1.49
		8	4.7 1.8	0.292	0.075		1.74	1.71
		12	3.9 1.8	0.289	0.103		1.88	1.95
Na–K[6]	Na	2	$\bar{h}_{Na}$ = 6.0 $\bar{h}_K$ = 2.0	0.157	0.024	−0.128	1.13	1.17
		4	5.8 2.0	0.182	0.036		1.23	1.29
		8	4.7 1.8	0.252	0.060		1.53	1.37
		12	3.8 1.8	0.243	0.064		1.51	1.47
		16	3.5 1.8	0.204	0.077		1.56	1.51
Na–Cs[6]	Cs	2	$\bar{h}_{Na}$ = 6.0 $\bar{h}_{Cs}$ = 1.8	0.214	0.014	0.0	1.69	1.70
		4	5.8 1.8	0.244	0.041		1.92	1.95
		8	4.7 1.5	0.292	0.102		2.47	2.45
		12	3.9 1.5	0.315	0.154		2.94	2.95
Na–NH_4[10]	Na	2	$\bar{h}_{Na}$ = 6.0 $\bar{h}_{NH_4}$ = 4.0	0.060	0.009	−0.05	1.04	1.12
		4	5.8 3.5	0.084	0.026		1.15	1.17
		8	4.75 3.0	0.142	0.048		1.38	1.25
		12	3.9 2.6	0.124	0.050		1.33	1.39
		16	3.7 2.6	0.136	0.049		1.36	1.46
H–Na[6]	Na	2	$\bar{h}_H$ = 14 $\bar{h}_{Na}$ = 6.0	0.183	0.026	−0.197	1.03	1.02
		4	12 6.0	0.213	0.084[5]		1.26	1.10
		8	8.3 5.25	0.190	0.142		1.37	1.38
H–Na[6]	H	2	$\bar{h}_H$ = 13 $\bar{h}_{Na}$ = 6.0	0.179	0.033	−0.197	1.03	1.10
		4	10.7 5.8	0.180	0.066		1.12	1.16
		8	6.8 4.7	0.181	0.084		1.17	1.20
		12	5.2 3.9	0.178	0.081		1.15	1.13
H–Cs[10]	Cs	2	$\bar{h}_H$ = 14 $\bar{h}_{Cs}$ = 1.8	0.438	0.038	−0.197	1.90	1.92
		4	12 1.8	0.584	0.136		3.32	3.26
Na–TMA[a]	TMA	2	$\bar{h}_{Na}$ = 6.0 $\bar{h}_{TMA}$ = 7.7	−0.108	−0.017	+0.255	1.34	1.34
		4	5.8 7.7	−0.140	−0.051		1.16	1.23
		8	4.7 5.9	−0.222	−0.101		0.86	0.92
H–K[b]	H	4	$\bar{h}_H$ = 10.8 $\bar{h}_K$ = 2.0	0.342	0.084	−0.325	1.26	1.23
Na–Cs[10]	Na	2	$\bar{h}_{Cs}$ = 1.8 $\bar{h}_{Na}$ = 5.7	0.125	0.024	0	1.41	1.36

[a] A. Schwarz and G. E. Boyd, *J. Phys. Chem.*, **69**, 4268 (1965). [b] O. D. Bonner, *ibid.*, **58**, 318 (1954).

sertion of a constant term (A) to characterize each pair of counterions does indeed provide the desired correlation between computation and experiment in these cases. This parameter is independent of the monomer-based concentration of the cross-linked polyelectrolyte and remains unaffected for a given pair of ions by the identity of the potential determining counterion. There is an additive relationship between the parameter for the different systems so that, once the characteristic term for each pair of cations in the sequence of monovalent counterion species considered is known, the terms for various different combinations of pairs of counterions can be calculated.

For those systems in which the two exchanging counterions are characterized by sizable differences in hydration behavior, the concept of hydration disturbance of the trace ion needs to be introduced as well (usually only for the more highly cross-linked systems) to preserve effective correlation between computation and experimental observation. In addition, the ion-exchange behavior of Li^+ is anomalous and a second parameter, B, which is multiplied by the monomer-based concentration of the cross-linked ion-exchange resin, m_m, is needed in the selectivity computation for all Li^+–M^+ ion-exchange reactions.

The several observations with regard to the applicability of our approach for the prediction of ion-exchange selectivity that are summarized above are examined separately in the Tables I–IV. The calculated and observed ion-exchange selectivities (taken from the literature) are given in each table together with the important terms employed in the computations. Those systems in which the constant parameter provides good correlation between predicted and experimental selectivity values are cataloged in Table I. Table II lists those systems in which minor adjustment for hydration disturbance is required as well. In Table III we have presented those systems in which a

Table II: Computation of Ion-Exchange Selectivity in Cross-Linked Polystyrenesulfonate Systems (Minor Hydration Disturbance)

System	Trace ion	% DVB	Av hydration no. ($\bar{h}$)		Hydration disturbance of trace ion: Δh, mole	Hydration disturbance of trace ion: $\Delta(a+b)$, A	Log $(\bar{\gamma}_1/\bar{\gamma}_2)$	$\pi\Delta V/2.3RT$	A	K_1^2 Calcd	K_1^2 Exptl
Na–K[6]	K	16	$\bar{h}_{Na} = 3.55$	$\bar{h}_K = 1.5$	−0.3	−0.125	0.301	0.153	−0.128	2.12	2.12
		24	2.9	1.5	−0.3	−0.125	0.342	0.196		2.56	2.76
Na–K[6]	Na	24	$\bar{h}_{Na} = 2.7$	$\bar{h}_K = 1.8$	−0.2	−0.06	0.196	0.062	−0.128	1.35	1.30
Na–Cs[6]	Cs	16	$\bar{h}_{Na} = 3.55$	$\bar{h}_{Cs} = 1.3$	−0.2	−0.035	0.327	0.156	0.0	3.11	3.17
		24	2.9	1.2	−0.3	−0.06	0.356	0.184		3.46	
Na–NH_4[10]	Na	24	$\bar{h}_{Na} = 3.5$	$\bar{h}_{NH4} = 2.6$	+0.3	+0.08	0.130	0.052	−0.05	1.35	1.33
NH_4–Cs[10]	Cs	2	$\bar{h}_{NH4} = 4.0$	$\bar{h}_{Cs} = 2.0$	+0.2	+0.08	0.074	0.010	+0.05	1.36	1.36
		4	3.5	2.0	+0.2	+0.08	0.096	0.026		1.48	1.50
		8	3.0	1.8	+0.3	+0.10	0.134	0.040		1.67	1.57
		12	2.6	1.8	+0.3	+0.10	0.142	0.049		1.74	1.74
		16	2.6	1.8	+0.3	+0.10	0.142	0.050		1.74	1.78
K–Cs[10]	Cs	2	$\bar{h}_K = 2.0$	$\bar{h}_{Cs} = 2.0$	+0.2	+0.08	−0.020	−0.003	+0.128	1.27	1.14
		4	2.0	2.0	+0.2	+0.08	−0.024	−0.004		1.25	1.18
		8	1.8	1.8	+0.3	+0.10	−0.030	−0.006		1.23	1.21
		12	1.8	1.8	+0.3	+0.10	−0.051	−0.011		1.16	1.22
		16	1.8	1.8	+0.3	+0.10	−0.044	−0.014		1.17	1.31
H–Na[6]	H	16	$\bar{h}_H = 4.25$	$\bar{h}_{Na} = 3.55$	−0.3	−0.07	0.080	0.051	−0.197	0.85	0.81
		24	3.1	2.9	−0.3	−0.07	0.036	0.018		0.72	0.69

Table III: Computation of Ion-Exchange Selectivity in Cross-Linked Polystyrenesulfonate Systems (Major Hydration Disturbance)

System	Trace ion	% DVB	Av hydration no. ($\bar{h}$)		Hydration disturbance of trace ion: Δh, mole	Hydration disturbance of trace ion: $\Delta(a+b)$, A	Log $(\bar{\gamma}_1/\bar{\gamma}_2)$	$\pi\Delta V/2.3RT$	A	K_1^2 Calcd	K_1^2 Exptl
H–Na[6]	Na	12	$\bar{h}_H = 6.2$	$\bar{h}_{Na} = 3.75$	−0.6	−0.16	0.254	0.222	−0.197	1.90	1.95
		16	5.75	3.3	−0.8	−0.21	0.281	0.265		2.20	2.23
		24	4.5	1.8	−1.7	−0.56	0.498	0.467		5.85	6.38
H–Cs[10]	Cs	8	$\bar{h}_H = 8.3$	$\bar{h}_{Cs} = 1.0$	−0.5	−0.22	0.752	0.294	−0.197	7.05	6.92
		12	6.2	0.5	−1.0	−0.44	0.912	0.274		15.3	15.15
		16	5.75	0.4	−1.1	−0.55	1.053	0.470		20.2	22.6
		24	4.5	0.1	−1.4	−0.75	1.522	0.726		89.1	92.2
H–K[a]	K	4	$\bar{h}_H = 12$	$\bar{h}_K = 3.0$	+1.0	+0.34	0.421	0.123	−0.325	1.66	1.78
		8	8.3	2.5	+0.7	+0.25	0.454	0.243		2.36	2.5
		16	5.75	1.0	−0.5	−0.33	0.754	0.435		7.3	7.6
Na–TMA[b]	Na	2	$\bar{h}_{Na} = 4.0$	$\bar{h}_{TMA} = 7.66$	−2.0	−0.43	−0.20	−0.053	+0.255	1.0	0.94
		4	4.0	6.35	−0.9	−0.17	−0.272	−0.189		0.62	0.60
		8	4.0	6.0	−0.7	−0.15	−0.294	−0.216		0.54	0.48
Na–Cs[10]	Na	4	$\bar{h}_{Cs} = 1.8$	$\bar{h}_{Na} = 4.0$	−1.3	−0.31	0.108	0.023	0.0	1.35	1.33
		8	1.5	3.3	−1.0	−0.26	0.111	0.026		1.37	
		12	1.5	3.0	−0.7	−0.20	0.100	0.027		1.34	1.26
		16	1.5	2.7	−0.5	−0.17	0.131	0.022		1.42	1.37

[a] See footnote *b*, Table I. [b] See footnote *a*, Table I.

significant addition or removal of water about the trace counterion needs to be assumed in the computation of selectivity. Finally the Li^+–M^+ systems, whose selectivity behavior is predicted only after further modification of the selectivity equation by the addition of the Bm_m term, are listed in Table IV. A detailed itemization of all approximations that need to be introduced to correlate selectivity behavior with experimental observation is also included in this table.

Discussion

The fact that the effect of cross-linking on the ion-

Table IV: Computation of Ion-Exchange Selectivity in Cross-Linked Polystyrenesulfonate Systems (Li^+–M^+ Exchange Reactions)

System	Trace ion	% DVB	Av hydration no. ($\bar{h}$)	Hydration disturbance of trace ion: Δh, mole	Hydration disturbance of trace ion: $\Delta(a+b)$, A	Log $(\bar{\gamma}_1/\bar{\gamma}_2)$	$\pi\Delta V/2.3RT$	A	Bm_m (B = 0.05)	K_1^2 Calcd	K_1^2 Exptl
Li-Na[6]	Na	2	$\bar{h}_{Li}$ = 13, $\bar{h}_{Na}$ = 6	0	0	0.192	0.061	−0.284	0.09	1.12	1.12
		4	10, 5.55	0	0	0.198	0.081		0.14	1.36	1.40
		8	7.0, 4.9	0	0	0.156	0.093		0.255	1.66	1.72
		12	5.2, 4.1	0	0	0.130	0.091		0.386	2.10	2.15
		16	4.85, 3.9	0	0	0.111	0.090		0.422	2.19	2.40
		24	3.55, 3.1	0	0	0.086	0.063		0.622	3.06	3.25
Li-Na[6]	Li	2	$\bar{h}_{Li}$ = 11.2, $\bar{h}_{Na}$ = 6.0	0	0	0.144	0.040	−0.284	0.100	1.00	1.08
		4	11.6, 5.8	0	0	0.203	0.077		0.151	1.40	1.48
		8	7.0, 4.7	+0.7	+0.21	0.187	0.082		0.299	1.92	1.89
		12	4.8, 3.85	0	0	0.112	0.052		0.433	2.05	2.00
		16	3.95, 3.55	−0.25	−0.07	0.038	0.022		0.505	1.91	1.90
		24	2.7, 2.9	−0.5	−0.18	−0.096	−0.057		0.700	1.83	1.90
Li-Cs[10]	Cs	2	$\bar{h}_{Li}$ = 13, $\bar{h}_{Cs}$ = 1.8	0	0	0.494	0.087	−0.284	0.090	2.44	2.63
		4	10, 1.1	−0.7	−0.28	0.634	0.150		0.140	4.36	4.48
		8	7.0, 0.6	−0.9	−0.42	0.792	0.263		0.255	10.6	10.46
		12	5.2, 0.5	−1.0	−0.48	0.804	0.352		0.386	18.1	20.4
		16	4.85, 0.25	−1.25	−0.64	1.016	0.406		0.422	36.2	41.7
		24	3.56, 0	−1.5	−0.83	1.343	0.488		0.622	147	132
H-Li[a]	Li	4	$\bar{h}_H$ = 12, $\bar{h}_{Li}$ = 12	+0.9	0.12	0.000	0.000	+0.087	−0.120	0.925	
		8	8.3, 7.5	0.0	0.0	+0.044	+0.034		−0.229	0.86	0.76
		16	5.75, 5.25	0.0	0.0	+0.104	+0.070		−0.380	0.77	0.76

[a] See footnote *b*, Table I.

exchange selectivity behavior of most of the ion-exchange systems considered can be predicted quantitatively up to about 12% cross-linking when the selectivity behavior at one cross-linking value is known is believed to be highly significant. This result is strongly suggestive that the model that is employed to facilitate these computations is meaningful. The need to resort to the hypothesis of hydration disturbance of the trace ion at high cross-linking values of the ion-exchange resin to facilitate correlation of computed selectivity coefficients with experimental observation is therefore believed not to be a failure of the model. We feel, instead, that it may be a reasonable estimate of the situation that exists in these highly condensed systems. Valid additional insight with regard to the factors influencing selectivity may thus be derived from this manner of approach.

There is support in the literature for this type of behavior. In the qualitative analysis of ion-exchange selectivity by Diamond and Whitney,[27,28] for example, a complicated competition for macroion and solvent is considered to dominate the ion-exchange process. Our judgment with regard to hydration disturbance and hydration is thus in agreement with their qualitative diagnosis of the ion-exchange phenomenon.

The need for a constant A parameter to provide quantitative estimate of selectivity can also be rationalized. In the development of the polyelectrolyte approach for the estimate of the log $(\bar{\gamma}_1/\bar{\gamma}_2)$ term it was presumed that the relative distribution of a pair of competing counterions between b_2 and R is the same since the identical electrical potential difference acts on both in this region. The difference in the average concentration ratios of the two counterions was considered to be attributable to the fact that only the smaller hydrated counterion is able to penetrate the region between b_1 and b_2 where a particularly high potential exists.

There has been in this estimate of the situation no consideration given to the effect of counterion on water structure in the highly ordered region[29,30] of immobilized counterions where $\epsilon\psi > kT$. It is quite conceivable, for example, that the ability of an ion to fit in this highly ordered solvent region will have a noticeable effect on

(27) D. Whitney and R. Diamond, *Inorg. Chem.*, 2, 1284 (1963); *J. Inorg. Nucl. Chem.*, 27, 219 (1965).

(28) R. Diamond and D. Whitney, "Ion-Exchange," Vol. I, J. A. Marinsky, Ed., Marcel Dekker, Inc., New York, N. Y., 1966, Chapter 7.

(29) H. S. Frank and W. Y. Wen, *Discussions Faraday Soc.*, 24, 133 (1957).

(30) R. L. Kay and D. F. Evans, *J. Phys. Chem.*, 70, 2325 (1966).

its distribution in the high-potential region in the neighborhood of the polyion strand. One can also expect that hydrogen-bonding effects will be operative as well in the case of the NH_4^+ and H^+ ions to favor selective behavior.

Two opposing factors apparently operate in determining the arrangement of ion species in the ordered solvent. A large disruptive ion which effectively disturbs the solvent structure operates to oppose the preferred arrangement of a second ion which for the benefit of this argument will be considered to be weakly ordering in its interaction with solvent (*e.g.*, Cs^+ and K^+). On this basis there will be a predilection toward disorder, and the order-disturbing ion will assume a preferred distribution in the region bounded by b_2 and the radial dimension at which $\epsilon\psi = kT$. If, however, the second ion is strongly ordering (*e.g.*, H^+), it must overcome the opposing disordering effect thereby leading to its preferred distribution. The relative magnitude of A characterizing each ion is thus qualitatively explained. This type of behavior should be concentration independent as well since the highly ordered region near each polyion strand is essentially invariant.

If we examine the relative magnitude of A parameters for the various systems, we can assign a characteristic A value to each counterion species. Such an analysis results in the values listed for each ion in Table V.

Table V: Value of A Parameter Characterizing Univalent Ion

Ion	Bare ionic radius × 10^8, cm	A
K^+	1.33	0.0
NH_4^+	1.48	−0.078
Cs^+	1.69	−0.128
Na^+	0.97	−0.128
H^+	0.33	−0.325
TMA^+	2.44	−0.383
Li^+	0.60	−0.412

It seems a reasonable postulate that the A term originates as a result of the neglect in the model of counterion selectivity arising from the different characteristic assembly behavior of each ion in the highly ordered water structure that exists in the high-potential region of each polyion strand.

The anomalous behavior of Li is not easily resolved. There is no immediately obvious explanation for the observed reduction ($Bm_m = +0.05m_m$) of the preferred arrangement of Li^+ ion ($A = -0.412$) in the highly ordered zone of the polyelectrolyte as its concentration, on a monomer basis, increases.

Acknowledgment. Financial support through Contract No. AT(30-1)-2269 with the U. S. Atomic Energy Commission is gratefully acknowledged.

Vapor-Phase Absorption Characteristics of Iron(III) Bromide and Iron(III) Chloride in the Ultraviolet-Visible Region

by J. D. Christian and N. W. Gregory

Department of Chemistry, University of Washington, Seattle, Washington 98105 *(Received March 28, 1966)*

The vapor-phase absorptions of iron(III) bromide and iron(III) chloride in the interval 200–750 mμ and at temperatures between 200 and 450° have been observed. The dimers appear to be the principal absorbing species and exhibit double maxima in this interval. Absorptivities have been assigned for Fe_2Br_6 between 350 and 750 mμ.

We have been interested in using the vapor-phase absorption of light to measure the concentrations of certain species involved in vaporization equilibria and hence to determine equilibrium constants and thermodynamic properties for the associated reactions. In this paper absorption characteristics of gaseous iron(III) bromide and iron(III) chloride are reported. No previous account of the ultraviolet-visible absorption spectra for these substances has been found in the literature.

Experimental Section

Absorption measurements were made with a Beckman DU spectrophotometer. The furnace compartment and quartz cells (5-cm path length) have been described elsewhere.[1] Iron(III) bromide vapor was generated in two ways: by reaction of bromine with $FeBr_2$ and by reaction of HBr with Fe_2O_3. $FeBr_2$ is not significantly volatile in the temperature range of interest.[2] Two independent $FeBr_2$–Br_2 samples were prepared. For sample 1, Merck reagent grade iron wire (minimum 99.8% Fe) and bromine were introduced into the absorption cell. To avoid contact of bromine with stopcock grease, a sample was released by heating $CuBr_2$ in a closed Pyrex system and collected and sealed in a thin-walled Pyrex capillary tube. The capillary tube was subsequently broken (by dropping a glass encased iron weight) in an arm attached to the evacuated cell assembly. The cell, with the bromine frozen in, was sealed off; after warming to room temperature, reaction of bromine and iron was initiated by gentle flaming. For sample 2, $FeBr_2$ was formed in a reaction vessel adjacent to the cell and then a sufficient quantity vacuum sublimed into the cell. The necessary bromine was frozen in with liquid nitrogen before the cell was sealed off.

Two independent Fe_2O_3–HBr mixtures were also prepared. To obtain iron(III) oxide, $Fe(OH)_3$ was prepared by reaction of a solution of Baker's Analyzed reagent grade $FeCl_3 \cdot 6H_2O$ with NH_4OH; the precipitate was washed, dried at 120° for 24 hr, and heated in a muffle furnace around 1050° for 4 hr to form α-Fe_2O_3. Analysis gave 70.2% Fe (expected 69.64%); X-ray powder patterns confirmed the structure as that of α-Fe_2O_3. HBr (Matheson) was introduced into a dry, evacuated storage bulb. The sample was purified in several cycles in which the HBr was vacuum distilled from Dry Ice to liquid nitrogen traps. A sample of the vapor in equilibrium with the liquid at −78° vapor pressure 411 torr) was isolated in a calibrated volume at a measured pressure and transferred to an absorption cell containing Fe_2O_3.

$FeCl_3$ was prepared by treating Merck reagent grade iron wire (minimum 99.8% Fe) with chlorine (Matheson) at 300°. The chlorine was previously isolated by freezing out a sample in a liquid nitrogen cooled trap and alternately pumping (10^{-6} torr) and vacuum distilling (from Dry Ice) several times. Crystals of $FeCl_3$ were transferred in a nitrogen-filled drybox to a finger which was part of the absorption cell assembly. After evacuation, sufficient chlorine was added to prevent significant decomposition of the vapor. The desired

(1) See the Ph.D. Thesis of J. D. Christian, University of Washington, 1965. University Microfilm Pub. 66-5850, Ann Arbor, Mich.

(2) See, for example, the "JANAF Thermochemical Tables," The Dow Chemical Co., Midland, Mich.

amount of ferric chloride was vaporized into the cell by heating the isolated assembly in a drying oven to a temperature which gave the appropriate vapor pressure. The cell itself was held *ca.* 15° above the finger containing the excess solid to prevent condensation of solid in the cell. The vapor-filled cell was sealed off with an electrical heating element while the assembly was in the oven. One sample was prepared by direct reaction of a measured amount of iron with an excess of chlorine inside a sealed cell. In this case the chlorine was obtained by thermal decomposition of anhydrous cupric chloride.

The quantity of chlorine in the cells was determined from absorbance measurements at room temperature. The molar absorptivities reported by Gibson and Bayliss[3] were used to calculate the concentration of chlorine and to evaluate its contribution to the total absorbance at higher temperatures.

Results and Discussion

Earlier equilibrium studies[4] indicate that the vapor of iron(III) bromide is a mixture of $FeBr_3(g)$ and $Fe_2Br_6(g)$, with the dimer the major component in the temperature and pressure range of the present work. $K_{torr} = P_m^2/P_d$ is *ca.* 10^{-5} at 200° and increases to *ca.* 0.6 at 446°. These species are stable only in the presence of significant partial pressures of bromine. The bromine decomposition pressure above $FeBr_3(s)$ reaches 1 atm around 140°.[5] In the present study bromine pressures were small enough so that $FeBr_3(s)$ was not present above 80°; the relative pressures of Br_2 and Fe_2Br_6 were determined by the equilibrium

$$2FeBr_2(s) + Br_2(g) = Fe_2Br_6(g) \quad (1)$$

Equilibrium constants reported in the earlier study[4] led to the equation

$$\log (P_{Fe_2Br_6}/P_{Br_2}) = -4727T^{-1} - 5 \log T + 19.770 \quad (2)$$

where a value of ΔC_p° for eq 1 of -10 cal deg^{-1} has been assumed. Although the effect of ΔC_P° is small and was neglected in the earlier study, its inclusion in the present work was found to improve the correlation of the absorption data. Equation 2 indicates that the concentration of Fe_2Br_6 is only 5×10^{-4} that of Br_2 at 200°, rising to *ca.* 5×10^{-3} that of Br_2 at 300°.

Our spectrophotometric observations are consistent with the conclusions of the earlier study if we assume that the absorption in the range from 350 to 750 mμ is due to Br_2 and Fe_2Br_6, with the two spectra overlapping strongly. Although the concentrations of Fe_2Br_6 were not actually determined in the present study, an independent check of the enthalpy change for reaction 1 can be made since the bromine concentration at lower temperatures remains nearly constant and the variation of the molar absorptivity of Fe_2Br_6 with temperature is relatively small. The concentration of bromine may be closely approximated from absorbance measurements *ca.* 100°; the effect of temperature on the bromine spectrum is known from bromine absorptivity calibration data.[1,6] Hence, the bromine contribution at the various temperatures may be subtracted from the total absorbance to give the contribution to be assigned to Fe_2Br_6. The enthalpy change for reaction 1 may then be approximated from the slope of plots of log $A_{Fe_2Br_6}$, where A stands for the absorbance, *vs.* $1/T$, since for a constant bromine concentration the change in $A_{Fe_2Br_6}$ reflects the change in the concentration of Fe_2Br_6 if the temperature coefficient of the molar absorptivity of Fe_2Br_6 is neglected. For a mean temperature of 550°K, the average value of ΔH° from absorbance data at eight different wavelengths between 300 and 600 mμ for each of the samples was 15.7 ± 0.5 kcal; eq 2 gives 16.1 kcal; this agreement seems quite satisfactory.

A more detailed evaluation of the spectral data was based on the equilibrium constants predicted from eq 2 which, together with the bromine concentrations approximated by low-temperature absorbance, was used to calculate the apparent concentrations of Fe_2Br_6 and bromine at the various higher temperatures. The bromine absorbance to be expected at each of the higher temperatures, where the contribution of Fe_2Br_6 becomes significant, was then calculated and substracted from the total absorbance. Approximate molar absorptivities were subsequently assigned to Fe_2Br_6 at these higher temperatures and then used to predict the very small contribution of Fe_2Br_6 at the lowest temperatures. Subtracting this from the total absorbance led to a refined value for the initial bromine concentrations and the procedure was repeated. Two iterations were sufficient. The use of the refined values for $A_{Fe_2Br_6}$ did not change the apparent value of ΔH° for eq 1 significantly.

A further correlation was obtained between the results of the earlier equilibrium study[4] and this work. The molar absorptivities calculated as described above were averaged over the temperature intervals and used to evaluate ΔS° for reaction 1 from the absorbance

(3) G. E. Gibson and N. S. Bayliss, *Phys. Rev.*, **44**, 188 (1933).

(4) N. W. Gregory and R. O. MacLaren, *J. Phys. Chem.*, **59**, 110 (1955).

(5) N. W. Gregory and B. A. Thackrey, *J. Am. Chem. Soc.*, **72**, 3176 (1950).

(6) A. A. Passchier, J. D. Christian, and N. W. Gregory, *J. Phys. Chem.*, **71**, 937 (1967).

data and the $\Delta H°$ values obtained from the log A *vs.* T^{-1} plots

$$\Delta S° = 2.303R \log A_{Fe_2Br_6} + (\Delta H°/T) - 2.303R \log bc_{Br_2} - 2.303R \log \epsilon_{Fe_2Br_6}$$

where $\epsilon_{Fe_2Br_6}$ is the average value of the molar absorptivity for Fe_2Br_6 over the temperature range of interest; b is the cell length. Thus, for each of eight wavelengths for each sample, $\Delta S°$ was calculated; an average value of 16.9 ± 0.6 eu was found which compares favorably with 17.3 ± 0.3 eu calculated from eq 2. While this is not a completely independent determination of $\Delta S°$ for the reaction, the result indicates that the interpretations made in the two studies are consistent.

Below 100°, where the Fe_2Br_6 contribution was negligible, an extra absorbance remained which was quite marked at 200 mμ and which fell off at an exponential rate to nothing at 380 mμ. This extra absorbance was also observed at room temperature. Its magnitude at a given wavelength appeared to increase with temperature but remained constant at temperatures above 100°. The extra absorbance did not follow the HBr spectrum,[1,7] nor did it vary systematically with the concentration of bromine. Its contribution was relatively small and was subtracted from the total absorbance. Since this extra absorbance was observed at temperatures lower than those at which the existence of appreciable amounts of any volatile compound of iron could reasonably be expected, it was assumed to be due to a minor impurity, possibly a bromide of an impurity in the iron wire. No similar contribution was observed in studies of Fe_2O_3–HBr samples.

The molar absorptivities of Fe_2Br_6 derived are shown for some representative temperatures in Figure 1. Two maxima of nearly equal intensity, centered around 285 and 450 mμ, respectively, are observed. Both maxima decrease as the temperature is increased and hence they appear to be associated with the same species. If one peak were associated with the monomer and the other the dimer, the monomer peak, if incorrectly attributed to the dimer, should increase as the temperature is increased because of the associated increase in the degree of dissociation of the dimer. The molar absorptivities evaluated for Fe_2Br_6 show good consistency for the various samples at wavelengths between 350 and 750 mμ, see Table I. Values (Figure 1) near the maxima are rather large, suggestive of a charge-transfer process. The apparent variation with temperature in the region of the maximum around 285 mμ is appreciably larger than that near 450 mμ.

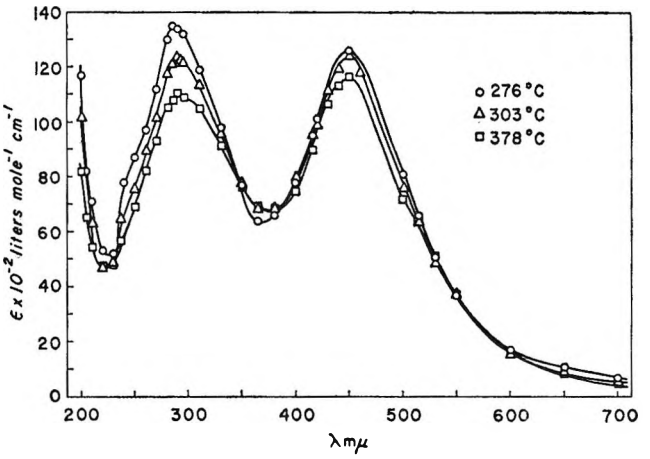

Figure 1. Apparent molar absorptivities at various wavelengths for Fe_2Br_6 at three temperatures. Sample 1, $FeBr_2$–Br_2 system.

In addition, for a given temperature the calculated absorptivities in the short-wavelength region depend somewhat on the Fe_2Br_6 concentration; *i.e.*, an apparent deviation (10–20%) from Beer's law is observed. This suggests that some other species may contribute to the absorption in this region, although from the marked variation with temperature Fe_2Br_6 still appears to be the major contributor. We have not included numerical values of the apparent absorptivities of Fe_2Br_6 at the shorter wavelengths in Table I because of doubt as to the correct assignment. They may be found, along with the original absorbance data, in ref 1. Attempts to resolve the total absorbance into contributions from species such as $FeBr_3$, Fe_3Br_8, Fe_3Br_9, FeOBr, etc., paired singly with Fe_2Br_6 in an equilibrium relationship, were unsuccessful.

Between 200 and 446° the reaction of Fe_2O_3 and HBr is essentially

$$Fe_2O_3(s) + 6HBr(g) = 2FeBr_2(s) + 3H_2O(g) + Br_2(g) \quad (3)$$

Equilibrium constants for eq 3 were determined from absorbance data in the range 200–325°.[8] In this temperature interval, for the small amounts of HBr introduced, the bromine pressure is small and the concentration of Fe_2Br_6, formed concomitantly, is so small that error in corrections for its absorbance does not introduce significant error in the determination of Br_2 and HBr concentrations. This is not true at higher

(7) J. R. Bates, J. O. Halford, and L. C. Anderson, *J. Chem. Phys.*, **3**, 531 (1935); C. F. Goodeve and A. W. C. Taylor, *Proc. Roy. Soc.* (London), **A152**, 221 (1935); J. Romand, *Ann. Phys.*, **4**, 527 (1948).

(8) J. D. Christian and N. W. Gregory, *J. Phys. Chem.*, **71**, 1583 (1967).

Table I: Molar Absorptivities for $Fe_2Br_6(g)$ ($\epsilon \times 10^{-2}$ l. mole^{-1} cm^{-1})[a]

$FeBr_2(s) + Br_2$ System

	Sample 1				Sample 2			
P_B = 30.0	P_D = 0.289		P_m = 0.043		P_B = 48.9	P_D = 0.47		P_m = 0.054
λ, mμ	276°	303°	332°	378°	254°	289°	324°	361°
700.0	7	6	5	5	0.1	3	4	4
650.0	11	9	8	9	8	8	8	9
600.0	17	16	16	16	13	14	15	16
550.0	37	37	36	37	29	31	34	35
530.0	51	49	50	51	38	45	47	48
514.0	66	64	63	64	65	62	61	61
500.0	81	76	77	72	79	75	74	71
450.0	126	124	118	117	...	113	108	99
420.0	101	99	96	...	95	88	86	...
416.0	95	95	...	90	83	85	...	...
400.0	78	80	73	75	72	69	69	69
380.0	66	68	65	68	59	64	61	61
365.0	64	68	68	69	52	61	63	78
350.0	77	78	75	77	69	72	72	71

	Sample 1			Sample 2				
P_B = 29.8	P_D = 0.286		P_m = 0.042	P_B = 15.6		P_D = 0.15	P_m = 0.03	
λ, mμ	323°	359°	398°	324°	357°	397°	411°	446°
750.0	2.2	2.3	2.4	2.2	2.3	2.7	2.7	2.9
700.0	4.0	4.0	4.1	3.5	5.0	4.1	4.1	4.8
650.0	6.8	7.0	7.2	6.3	7.2	7.6	7.2	8.1
600.0	13	14	15	13	13	14	15	17
570.0	23	24	24	22	22	23	24	26
550.0	32	34	33	32	32	33	34	36
530.0	45	46	46	45	44	45	46	50
513.7	57	59	58	55	56	57	58	63
500.0	71	73	70	70	68	70	71	77
416.0	98	94	85	89	85	85	87	90
380.5	69	68	63	63	60	61	63	68
370.0	...	...	...	65	61	62	64	68

[a] The partial pressures (torr) of Br_2 (P_B), Fe_2Br_6 (P_D), and $FeBr_3$ (P_m) are indicated for each sample at 325°.

temperatures, however, and for evaluation of molar absorptivities of Fe_2Br_6 between 325 and 446°, Br_2 and HBr pressures were calculated from equilibrium constants for eq 3 extrapolated into this range. Their predicted contributions to the total absorbance were subtracted and the remainder attributed to Fe_2Br_6. From this, the Br_2 pressure and the known equilibrium constants for the Fe_2Br_6–Br_2–$FeBr_2$ system, molar absorptivities were assigned to Fe_2Br_6. These values are compared with those from the $FeBr_2$–Br_2 study in Table I.

Iron(III) chloride also shows two absorption bands, centered around 243 and 361 mμ, respectively. A representative total absorbance spectrum (at 245°) is presented in Figure 2. In view of the similarities to Fe_2Br_6 and because of the similar temperature dependences of the two maxima, both bands are believed to arise from the species Fe_2Cl_6. The concentration of the monomer in the chloride system is expected to

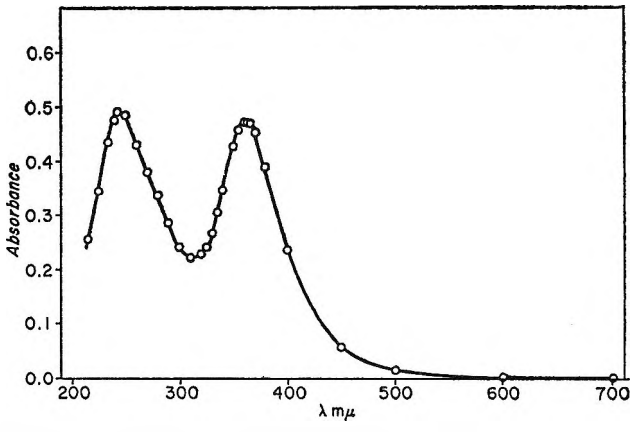

Figure 2. Absorption spectrum of gaseous iron(III) chloride. Sample 1 at 245°; estimated pressure of Fe_2Cl_6, 0.35 torr. The absorption of added chlorine, present at *ca.* 2.5 torr, has been subtracted.

be only of the order of 1% or less than that of the dimer.[9,10] Unreasonably high molar absorptivities

would be required of the monomer for it to give absorbances of the magnitude observed. Furthermore, after exhaustion of the solid phase the absorbance did not increase rapidly with temperature, contrary to what would be expected if the monomer were the principal absorbing species.

The two peaks are very nearly equal in intensity. The structure of the dimer is reported to be bridgelike.[11]

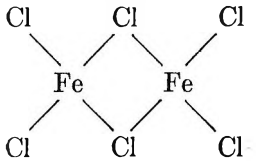

Possibly the two peaks may result from electron-transfer processes involving halogen atoms in the two different environments.

Only these general characteristics of the iron(III) chloride spectrum can be reported at this time. Three independent samples were studied with results in qualitative agreement; however, the quantities of material in the cells were not established with the certainty needed to permit a meaningful evaluation of absorptivities.

Acknowledgment. This work was supported by a grant from the National Science Foundation (GP 3775) which we are pleased to acknowledge.

(9) H. Schäfer, *Z. Anorg. Chem.*, **259**, 53 (1949).

(10) W. Kangro and H. Bernstorff, *Z. Anorg. Allgem. Chem.*, **263**, 316 (1950).

(11) E. Z. Azsorin, N. G. Rambidi, P. A. Akishin, *Zh. Strukt. Khim.*, **4**, 910 (1963).

Equilibrium between Iron(III) Oxide and Hydrogen Bromide

by J. D. Christian and N. W. Gregory

Department of Chemistry, University of Washington, Seattle, Washington 98105 *(Received March 28, 1966)*

A spectrophotometric study of the equilibrium between hydrogen bromide and ferric oxide has been made. The standard enthalpy of formation, -59.6 kcal mole^{-1}, and entropy, 33.3 cal mole^{-1} deg^{-1}, of $FeBr_2$ at 25° have been evaluated from the results.

Some time ago, a study was made in these laboratories of the interaction of hydrogen bromide and iron(III) oxide. The reaction

$$Fe_2O_3(s) + 6HBr(g) = 2FeBr_2(s) + 3H_2O(g) + Br_2(g) \quad (1)$$

appeared suitable for study as a means of determining the thermodynamic properties of iron(II) bromide.[1] Measured quantities of hydrogen bromide were introduced into a Pyrex diaphragm gauge which contained an excess of iron(III) oxide. The gauge was sealed and total pressures were measured at various temperatures. Equilibrium constants for eq 1 were evaluated from $P°$, the pressure equivalent at a particular temperature to the initial quantity of hydrogen bromide added, and P_t, the measured total pressure at that temperature.

$$K_1 = P^3_{H_2O}P_{Br_2}/P^6_{HBr} = 27P^4_{Br_2}/(P° - 6P_{Br_2})^6 = (27/16)(P° - P_t)^4/(3P_t - 2P°)^6 \quad (2)$$

However, data from four independent series of measurements, with different values of $P°$, did not give mutually consistent values of the equilibrium constant; *i.e.*, the value of K calculated from any one series was not

(1) R. O. MacLaren, Ph.D. Thesis, University of Washington, 1954. University Microfilms No. A-54-1690, Ann Arbor, Mich.

the same (at a given temperature) as that from any one of the other series. However, in each series independently, the total pressures were reproducible on increasing and decreasing temperature sides of repeated heating cycles. This suggested that products other than those expected from reaction 1 might be formed, but no postulated set of reactions could be found which would correlate the data satisfactorily.

We now report results of a spectrophotometric study of this system. The absorption of light by the equilibrium vapor phase at various frequencies in the ultraviolet-visible range has been used to evaluate bromine and hydrogen bromide pressures. The evidence supports the assumption that reaction 1 is the one of principal importance in the temperature range 200–325° and mutually consistent values of the equilibrium constant have been obtained in two series of experiments with different $P°$ values. Thermodynamic properties of iron(II) bromide have been evaluated from the results and an explanation for the behavior observed in the earlier diaphragm study is suggested.

Experimental Section

Ferric hydroxide was prepared by reaction of a solution of Baker's Analyzed reagent grade $FeCl_3 \cdot 6H_2O$ with NH_4OH; the precipitate was washed, dried at 120° for 24 hr, and heated in a muffle furnace around 1050° for 4 hr to form α-Fe_2O_3. Analysis gave 70.2% Fe (theoretical 69.64%); X-ray powder patterns confirmed the structure as that of α-Fe_2O_3. Hydrogen bromide (Matheson) was purified by fractional distillation and introduced into an evacuated absorption cell containing *ca.* 0.5 g of finely divided ferric oxide. The quartz cells (path lengths 4.986 and 4.699 ± 0.01 cm, respectively) were sealed off with a flame while the HBr was frozen in with liquid nitrogen. Two independent samples were studied over the temperature interval 147–446° with a Beckman DU spectrophotometer with high-temperature furnace attachment.[2]

A prior spectrophotometric study of bromine and hydrogen bromide has been made in this laboratory, as well as by others, and molar absorptivities established at temperatures between 20 and 450°.[2-4] Total absorbances of the vapor phase in the Fe_2O_3–HBr-filled cell were measured at *ca.* 5-mμ intervals between 200 and 750 mμ at various temperatures. Below 150–195°, the particular temperature depending on the amount of HBr introduced, an unidentified condensed phase is formed. This phase is believed to be a hydrate of iron(III) bromide; no attempt was made to determine equilibrium constants when it was present. The temperature at which it disappeared could easily be found from the associated marked change in the pressure–temperature coefficient of bromine. At higher temperatures, absorbance by Fe_2Br_6, expected in the reaction

$$2FeBr_2(s) + Br_2(g) = Fe_2Br_6(g) \qquad (3)$$

was detected.[5] Molar absorptivities have been assigned to Fe_2Br_6 at wavelengths between 500 and 750 mμ.[5] It also absorbs strongly at shorter wavelengths, but some deviation from Beer's law results below 500 mμ if Fe_2Br_6 is assumed to be the only iron bromide absorbing species.

For the study of reaction 1, absorbance data between 195 and 325° were used. In this temperature interval the contribution of Fe_2Br_6 to the total absorbance at wavelengths suitable for determination of the concentrations of Br_2 and HBr, respectively, was sufficiently small (generally <10%) that the effect of error in estimating its contribution at wavelengths below 500 mμ was insignificant. Data at temperatures above 325° and in the longer wavelength interval (500–750 mμ) were discussed in another paper and used to confirm assigned molar absorptivities to Fe_2Br_6.[5]

The partial pressures of Br_2 and of HBr were evaluated as follows. HBr does not absorb light at wavelengths between 300 and 750 mμ. Hence in this range the principal absorbance below 325° is due to bromine, although the small contribution of Fe_2Br_6 must be considered. By the Beer–Lambert law, $A = A_B + A_F = \epsilon_B b C_B + \epsilon_F b C_F = b C_B(\epsilon_B + \epsilon_F K_3)$ where the subscripts B and F, respectively, denote Br_2 and Fe_2Br_6, b is the path length, the C's are molar concentrations, $K_3 = C_F/C_B$, and the absorbances A and molar absorptivities ϵ are functions of wavelength. From values of K_3,[6] ϵ_B,[2,3] and of ϵ_F,[2,5] values of C_B and C_F, based on an average of results at various wavelengths between 380 and 530 mμ, were found for each sample at each temperature. In all cases $\epsilon_F K_3$ was small compared with ϵ_B.

Once the concentrations of both bromine and Fe_2Br_6 were established, their contributions to the total absorbance in the interval 200–250 mμ were evaluated

(2) For details see the Ph.D. thesis of J. D. Christian, University of Washington, 1965. University Microfilms Publication No. 66-5850, Ann Arbor, Mich.

(3) See, for example, R. G. Acton and N. S. Bayliss, *Trans. Faraday Soc.*, **34**, 1371 (1938); D. J. Seery and D. Britton, *J. Phys. Chem.*, **68**, 2263 (1964).

(4) J. R. Bates, J. O. Halford, and L. C. Anderson, *J. Chem. Phys.*, **3**, 531 (1931); C. F. Goodeve and A. W. C. Taylor, *Proc. Roy. Soc.* (London), **A152**, 221 (1935); J. Romand, *Ann. Phys.* (Paris), **4**, 566 (1949).

(5) J. D. Christian and N. W. Gregory, *J. Phys. Chem.*, **71**, 1579 (1967).

(6) N. W. Gregory and R. O. MacLaren, *ibid.*, **59**, 110 (1955).

from calibration data reported earlier[2,5] and subtracted from the total absorbance. In this wavelength interval their combined contribution was small compared with the total absorbance. The difference was attributed to HBr and its concentration evaluated from its molar absorptivity.[4,5] Partial pressures were then calculated from the concentrations, cell volumes, and temperatures.

At temperatures below 195°, where the HBr pressure is small, evidence was observed in the 200–250-mμ wavelength region to suggest absorption by an additional species. The extra absorption disappeared as the temperature increased, which suggested that it was due to some relatively unstable intermediate. The possibility of hydrate formation between Br_2 and H_2O may be ruled out on the basis of an independent study of that system.[2] Results were quite satisfactory when the absorbance in this wavelength range was attributed solely to HBr, Br_2, and Fe_2Br_6 in the temperature interval 195–325°. At these temperatures water pressures were assumed to be three times those of bromine, according to the stoichiometry of reaction 1. This can be justified only by the consistency of the results.

Table I: Equilibrium Pressures (torr) for Reaction 1 from Spectrophotometric Data

°K	P_{Br_2}	P'_{HBr}	P° (apparent) at 298°K	K_1, torr^{-2}
		Sample 1		
448.5	24.50	7.77	102.9	...
468.0	26.02	8.17	104.7	41.5
490.6	27.54	13.53	106.2	6.28
513.0	28.15	15.39	107.1	1.28
537.8	28.87	21.42	107.9	1.94×10^{-1}
565.8	30.17	27.65	109.9	5.01×10^{-2}
595.8	30.22	36.28	108.9	9.87×10^{-3}
		Sample 2		
420.7	12.89	3.44	57.26	...
443.5	13.90	4.53	59.12	...
477.6	14.79	7.33	59.98	8.30
509.0	15.15	11.34	59.88	6.70×10^{-1}
545.0	15.26	17.60	59.71	4.93×10^{-2}
569.4	15.54	20.91	59.76	1.88×10^{-2}
597.4	15.35	25.94	58.90	4.91×10^{-3}

Results and Discussion

Partial pressures of HBr and Br_2, evaluated from absorbance measurements, and corresponding equilibrium constants for reaction 1 are shown in Table I. Data from the two samples, considered independently, gave the same van't Hoff slope, although the lines were slightly displaced from each other. The displacement corresponded to a difference in the entropy to be assigned to the reaction of about 0.6 eu. The average of the two for the temperature interval 468–598°K gave the equation

$$-RT \ln K_1 = \Delta G^\circ = -35{,}800 + 43.8T \qquad (4)$$

with the standard states for the gases taken as the ideal gas at 1 atm pressure. Use of published heat capacity data[7,8] leads to values of −36.4 kcal mole^{-1} and −45.0 cal deg^{-1} mole^{-1} for ΔH°_{298} and ΔS°_{298}, respectively, for reaction 1. With thermodynamic constants for the other substances involved,[9,10] we obtain −59.6 ± 1 kcal mole^{-1} and 33.3 ± 1 cal mole^{-1} deg^{-1} for the standard enthalpy of formation (relative to liquid bromine) and standard entropy of $FeBr_2$(s) at 298.2°K. These values are in good agreement with enthalpy of formation data based on heat of solution measurements,[11] −58.7, and that reported by National Bureau of Standards Circular 500,[12] −60.0 kcal mole^{-1}, and the value of $S^\circ_{298} = 33.6$ eu found by Westrum[13] from heat capacity measurements from 5 to 303°K. The close correspondence of the entropies indicates the absence of significant entropy contributions below the range of the heat capacity measurements.

If reaction 1 is the only significant process occurring in the equilibrium system, the sum $P_{HBr} + 6P_{Br_2}$ should equal P° and should correspond to the fixed quantity of HBr initially introduced. The experimentally determined sum does correspond (within experimental error) to a fixed quantity in the higher temperature range of the measurements, as can be seen in Table I. Average values of P°, reduced to 25°, for samples 1 and 2 are 109.4 and 59.8 torr, respectively. However, the apparent values of P° fall off noticeably, particularly for sample 1, as the temperature is decreased. We suggest this apparent loss of HBr may be due to the adsorption of significant amounts of gas on the oxide surface at the lower temperatures. The

(7) N. W. Gregory and H. E. O'Neal, *J. Am. Chem. Soc.*, 81, 2649 (1959).

(8) K. K. Kelley, U. S. Bureau of Mines Bulletin No. 584, U. S. Government Printing Office, Washington, D. C., 1960.

(9) K. K. Kelley and E. G. King, U. S. Bureau of Mines Bulletin No. 592, U. S. Government Printing Office, Washington, D. C., 1961.

(10) G. N. Lewis, M. Randall, K. S. Pitzer, and L. Brewer, "Thermodynamics," 2nd ed, McGraw-Hill Book Co., Inc., New York, N. Y., 1961.

(11) J. C. M. Li and N. W. Gregory, *J. Am. Chem. Soc.*, 74, 4670 (1952).

(12) F. D. Rossini, *et al.*, "Selected Values of Chemical Thermodynamic Properties," National Bureau of Standards Circular 500, U. S. Government Printing Office, Washington, D. C. 1952.

(13) E. F. Westrum, Jr., University of Michigan, private communication.

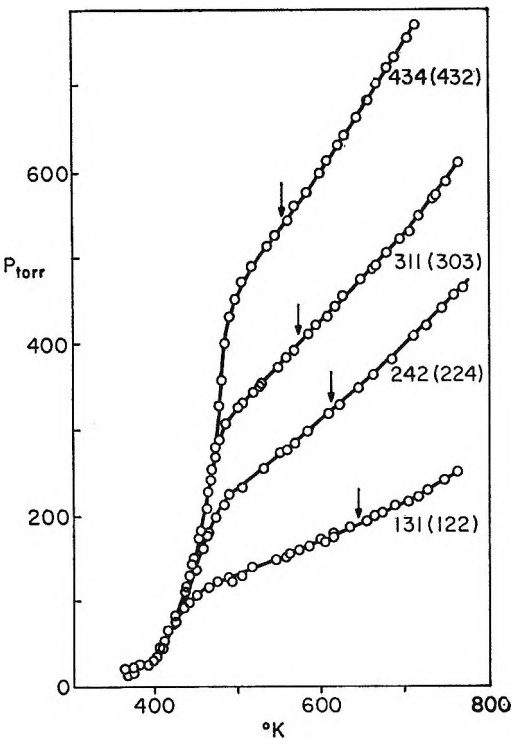

Figure 1. Equilibrium pressures (diaphragm gauge) for the Fe_2O_3–HBr system. $P°$ values at 25°, based on quantity measured in calibrated volume and the adjusted values (in parentheses), are indicated for each curve.

magnitude of the quantity adsorbed depends on the pressure. This effect appears to be an important key to interpretation of the diaphragm gauge data obtained earlier.[1]

If it is assumed that an amount of gas, proportional to the pressure of HBr in the diaphragm gauge, is effectively removed by adsorption on the oxide surface at lower temperatures, values of the equilibrium constant consistent with the spectrophotometric study can be obtained. The apparent amount adsorbed gradually diminishes as the temperature is increased. Such an effect offers a plausible explanation for the difficulty encountered in earlier attempts to correlate the diaphragm gauge data; as the temperature increased, the total gas pressure increased, not only because of a shift in the equilibrium constant according to reaction 1 but also by desorption of gas from the solid surface. The data of MacLaren will be discussed briefly as the effect observed may have general importance in diaphragm gauge work on other similar systems.

The original diaphragm gauge results are shown graphically in Figure 1. The exponentially rising portion, where the total pressure is independent of the amount of HBr initially added to the gauge, is believed to correspond to the decomposition of a solid hydrate of $FeBr_3$. The principal species in the gas phase in this region are bromine and water, with only minor amounts of HBr. When the hydrate is exhausted, equilibrium gas pressures are largely determined by reaction 1. The four curves correspond to the four different initial amounts of HBr placed in the gauge; an excess of Fe_2O_3, *ca.* 1 g, was present in each case.

If equilibrium constants are calculated from eq 2 (measured P_t values were corrected for the small contribution of vapors of iron(III) bromide), the values from the four independent experiments do not agree with each other. Part of the difficulty may be attributed to small errors in values of $P°$. The pressure of the HBr sample was measured in a calibrated volume; it was frozen into the gauge by cooling with liquid oxygen. The gauge assembly was subjected to high vacuum (10^{-6} torr) for some time and then sealed off. A small amount of HBr may have been lost during this period. However, even if the value of $P°$ is "adjusted" to give equilibrium constants in agreement with eq 4 at the highest temperature in each case (the adjusted value of $P°$ needed, shown in parentheses on Figure 1, was only at most a few per cent less than the "measured" value), the apparent constants at lower temperatures still diverge from each other and from those predicted by eq 4. Furthermore, the interpretation is seen to be invalid because at temperatures below the points indicated by the arrows on Figure 1, the total pressure measured in the gauge is less than two-thirds the amount of HBr initially introduced, which is impossible according to reaction 1.

If eq 4 is assumed to give correct values of the equilibrium constant, the procedure can be reversed and the predicted value of $P°$ at lower temperatures calculated from K_1 and P_t. This treatment was applied to all four sets of data. $P°$(calcd) was always less than

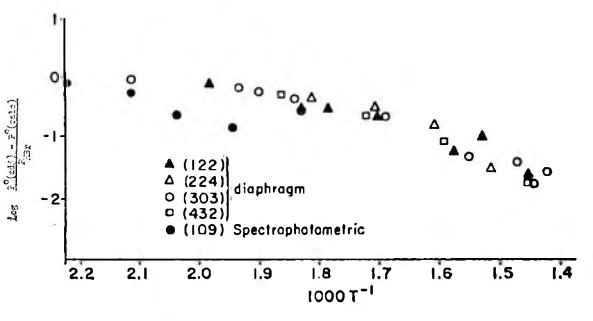

Figure 2. Comparison of the ratio apparent quantity of HBr adsorbed (expressed as a pressure equivalent at each temperature) over the HBr pressure for the different samples at various temperatures. The various series of points are identified by their associated $P°$ values shown in Figure 1 or in Table I.

$P°$(adjusted), and the difference increased as the temperature decreased. The ratio $[P°(\text{adj}) - P°(\text{calcd})]/P_{HBr}$ was found to be roughly the same (at corresponding temperatures) for the four experiments and also close to the similar ratio indicated by the present spectrophotometric study. Results are compared in Figure 2. If the surface area of the oxide is taken as 1 m^2/g, the maximum quantity of HBr assumed adsorbed in these calculations is found to be of the order of a monolayer. Although the experimental data are not suitable for a good quantitative measure of the amount adsorbed (the surface areas were not measured), the approximate results as well as the interaction energy indicated by a van't Hoff interpretation of the mean slope of Figure 2, 9 kcal $mole^{-1}$, seem to be of reasonable magnitude for such a phenomenon.

We conclude that diaphragm gauge measurements on systems similar to the one currently under study may be significantly affected by adsorption; to ensure that adsorption does not introduce serious errors, equilibrium constants must be evaluated from data at widely varying total pressures.

Acknowledgment. This work was supported by grants from the National Science Foundation and the U. S. Army Research Office (Durham), which we acknowledge with thanks.

Rate Constants for Deuterium Exchange of Trimethylammonium Ion in Heavy Water

by Robert J. Day and Charles N. Reilley

Department of Chemistry, University of North Carolina, Chapel Hill, North Carolina 27514
(Received June 27, 1966)

Rate constants for deuterium transfer in D_2O solutions of trimethylammonium ion at 33° have been measured by proton magnetic resonance from the collapse of proton–deuterium coupling. The mechanisms advanced by earlier workers to describe the corresponding proton-transfer rates are also adequate for deuterium exchange. The rate of the direct reaction with solvent, $BD^+ + D_2O \xrightarrow{k_4} B + D_3O^+$, extrapolated to infinite dilution is $k_4 = 1.08\ sec^{-1}$ while, for the symmetric reaction $BD^+ + OD_2 + B \xrightarrow{k_7} B + DOD + DB^+$, $k_7 = 1.12 \times 10^8\ M^{-1}\ sec^{-1}$. The decrease of k_4 at high D^+ concentrations interpreted by the mechanism $B\cdots(DOD)_m \xrightarrow{k_{DB}} B + mDOD$ gives $k_{DB} = 8.5 \times 10^9\ sec^{-1}$. The direction and magnitudes of the isotope effects on the rate parameters are consistent with the postulated mechanisms.

Introduction

The kinetics of NH proton exchange of the methylamines have been extensively studied in aqueous solution using proton magnetic resonance by following the collapse of the CH_3–NH proton coupling and from the line broadening of the H_2O proton resonance.[1-7]

The significant mechanisms of proton exchange for aqueous methylamine–hydrochloride salts at HCl concentrations in the range $1\text{–}10^{-5}\ M$ are

$$R_3N^+H + H_2O \xrightarrow{k_1} R_3N + H_3O^+ \quad (1)$$

$$R_3N^+H + NR_3 \xrightarrow{k_2} R_3N + HN^+R_3 \quad (2)$$

$$R_3N^+H + \underset{\displaystyle H}{\underset{|}{O}}\text{–}H + NR_3 \xrightarrow{k_7} R_3N + \underset{\displaystyle H}{\underset{|}{H\text{–}O}} + HNR_3 \quad (3)$$

Reaction 1 is further delineated by the reactions[7]

$$R_3N^+H\cdots(H_2O)_m + H_2O \underset{k_-}{\overset{k_+}{\rightleftharpoons}} R_3N\cdots(H_2O)_m + H_3O^+ \quad (4)$$

$$R_3N\cdots(H_2O)_m \xrightarrow{k_H} R_3N + (H_2O)_m$$

where k_H is represented as the rate of "breaking of the $R_3N\cdots(H_2O)_m$ hydrogen bond," $k_+/k_- = K_A$, the acid dissociation constant, and

$$k_4 = k_+/\{1 + k_-[H^+]/k_H\} \quad (5)$$

Because the isotope effects upon the processes involved in the proton exchange not only should be of interest in themselves but also provide an additional qualitative check on the mechanisms used to describe the proton exchange, this study of the corresponding deuterium-exchange kinetics was undertaken using the exchange collapse of deuterium–proton coupling by proton nmr in a manner similar to the way that proton–proton coupling is used for the study of proton exchange. While as a result of the interaction of the quadrupole moment of deuterium with rapidly fluctuating electric field

(1) E. Grunwald, A. Loewenstein, and S. Meiboom, *J. Chem. Phys.*, **27**, 630 (1957).

(2) A. Loewenstein and S. Meiboom, *ibid.*, **27**, 1067 (1957).

(3) E. Grunwald, P. J. Karabatsos, R. A. Kromhout, and E. L. Purlee, *ibid.*, **33**, 556 (1960).

(4) M. T. Emerson, E. Grunwald, M. L. Kaplan, and R. A. Kromhout, *J. Am. Chem. Soc.*, **82**, 6307 (1960).

(5) T. M. Connor and A. Loewenstein, *ibid.*, **83**, 560 (1961).

(6) Z. Luz and S. Meiboom, *J. Chem. Phys.*, **39**, 366 (1963).

(7) E. Grunwald, *J. Phys. Chem.*, **67**, 2208, 2211 (1963).

gradients, the deuterium T_1 in many chemical species is frequently so short that any coupling of the deuterium with other nuclei is relaxed, the quadrupole relaxation of deuterium in $(CH_3)_3N^+D$ is slow enough so that there is an observable coupling between deuterium and the CH_3 protons[4,8] which allows deuterium-exchange rates to be measured by proton nmr for $(CH_3)_3N^+D$ in D_2O.

In the proton-exchange studies, k_4 and $k_6 + k_7$ were measured using the CH_3 proton resonance and k_7 separately from the H_2O proton resonance. Studies of the analogous deuterium-exchange reactions for $(CH_3)_3N \cdot DCl$ in D_2O by proton nmr are more limited because only the CH_3 proton spectrum may be used. While kinetic information may be obtained from the residual HOD proton resonance, the measured rate corresponds to the reaction

$$(CH_3)_3N^+\overset{D}{\underset{|}{D}} + \overset{|}{O}\text{–}H + N(CH_3)_3 \xrightarrow{k_7'} (CH_3)_3N + \overset{D}{\underset{|}{D}}\text{–}O + HN^+(CH_3)_3 \quad (6)$$

which will proceed at a somewhat greater rate than the reaction involving D_2O. In the case of $(CH_3)_3NHCl$, it was found that as a result of steric effects, k_6 was too small with respect to k_7 to be measurable, and it would be expected that this would also be the case in D_2O.

Experimental Section

Reagents and Solutions. D_2O was obtained from Columbia Organic Chemicals Co., Inc., and was of 99.7% isotopic purity. Other reagents were of the highest purity commercially available and were used without further purification. Solutions of DCl in D_2O were prepared by a method similar to that described by Herber[9] in which SO_3 polymer is distilled into D_2O to produce D_2SO_4 after which NaCl is added, and the resulting DCl is passed into D_2O. NaOD in D_2O was prepared by adding reagent grade NaOH to D_2O. $(CH_3)_3NDCl$ was prepared by distilling anhydrous $(CH_3)_3N$ into a solution of DCl in D_2O until most of the HCl was neutralized, with the concentration of $(CH_3)_3NDCl$ being determined potentiometrically by $AgNO_3$ titration, correcting for the excess DCl which was determined by pH titration. The solutions for the kinetic measurements were prepared by a method similar to that used by Loewenstein and Meiboom[2] in which two solutions of the same $(CH_3)_3NDCl$ content, one acidic (~0.01 *F* DCl) and the other basic (~0.01 *F* NaOD), were mixed to give the desired $[D^+]$ with the pD being monitored by a glass electrode standardized with the acidic solution, using a Leeds and Northrup expanded-scale pH meter, while solutions with [DCl] greater than 0.01 *M* were prepared volumetrically. Dissolved air was not removed from the solutions because of the probable loss of $(CH_3)_3N$ from samples of low [DCl] during the deaeration. The concentration of residual H in the solutions was measured from the ratios of the integrals of the HOD and $(CH_3)_3N^+D$ proton resonances by comparison with standard samples. The concentration of HOD varied somewhat for different solutions, but the variation did not appear to have any adverse influence. The HOD concentration was approximately 0.5 *M* in most cases although a few solutions which required somewhat longer periods of time than usual for preparation and were more exposed to H_2O contamination from the laboratory atmosphere contained up to 1 *M* HOD.

Effective K_A values ($K_A = [(CH_3)_3N][D^-]/[(CH_3)_3N^+D]$) were determined by the differential potentiometric method.[10] Activity coefficient corrections were not made because, except for solutions used to determine k_4 at high acidities, the solution conditions other than D^+ concentration were the same for the p*K* measurements as those for the rate measurements. To prevent H_2O contamination from the reference electrode, the electrode was filled with a 1 *M* KCl solution in D_2O. For best results, it was necessary to correct for loss of $(CH_3)_3N$ after addition of the NaOD titrant by extrapolating the pD readings back to the time of addition. This correction was minor, normally being about 0.01 pD unit. The precision of the p*K* measurements is about 0.005 p*K* unit, but because of possible junction potential errors and other instrumental errors, the accuracy of the effective pK_a values is thought to be approximately 0.02 p*K* unit.

Instrumental Work. The proton nmr spectra were recorded with a Varian A-60 high-resolution instrument at the ambient temperature of the probe which was found to be 33.2°. To increase the stability of the instrument, the magnetic cooling system was made a part of a constant-temperature circulating system; the Fenwall regulator and three-way valve originally used in the coolant regulating system were found to be the major sources of short-term stability problems. This instrumental modification increased the precision of line-width measurements from 0.1 to 0.02 cps. Peak heights and widths were measured directly from precalibrated chart paper, for which the sweep-width

(8) D. E. Leyden and C. N. Reilley, *Anal. Chem.*, **37**, 1333 (1965).
(9) R. H. Herber, *Inorg. Syn.*, **7**, 155 (1963).
(10) A. L. Bacarella, E. Grunwald, H. P. Marshall, and E. L. Purlee, *J. Org. Chem.*, **20**, 747 (1955).

calibration was checked with a side-band oscillator and a frequency counter. Peak integrals were measured with the A-60 electronic integrator. Because the slowest sweep rate available was 0.1 cps/sec and the minimum useful radiofrequency field was 0.04 mgauss, slow passage and unsaturated conditions could not be strictly achieved. Therefore, the spectra were recorded at radiofrequency fields of 0.04–0.16 mgauss and sweep rates of 0.1–0.5 cps/sec, and the measured parameters (peak to valley ratios, peak to peak ratios, and peak widths at half-height) were then extrapolated to zero radiofrequency field and zero sweep rate. In the case of a singlet, the excess line width caused by saturation for slow passage should be linearly dependent upon the radiofrequency field (H_1) at the values used even in the presence of an inhomogeneous main magnetic field (H_0).[11] The theoretical treatment of Jacobsohn and Wangsness[12] indicates that the broadening resulting from rapid passage is linearly dependent upon the sweep rate for nonsaturation conditions and a homogeneous H_0. However, because of the presence of inhomogeneities in H_0 and both sweep rate and saturation broadening, the correct form of the extrapolations to zero H_1 and sweep rate are uncertain. It was found that plots of the line width, $W_{1/2}$, against H_1 for a given sweep rate were linear within measurement error (0.02 cps) and that a plot of these $W_{1/2}$ values (extrapolated to zero H_1) against sweep rate was also linear. In the case of a triplet, the dependencies of peak to peak and peak to valley ratios and peak to peak separations (apparent coupling constants) upon H_1 and sweep rate are also uncertain, but it was found that, within the precision of the measurements, the same type of extrapolations to zero H_1 and then zero sweep rate could be used. The exact values of H_1 are uncertain because a radiofrequency voltmeter with a sufficient band pass (60 Mc) to measure H_1 was not available so that the H_1 values had to be taken from the dial calibration of the A-60 radiofrequency field attenuator. While the values of dial calibration are only approximate, the relative values should be sufficiently accurate so that the extrapolation will, in fact, be to zero H_1. The only available method for checking this was the use of a spectrum which had several measurable parameters, each exhibiting different dependencies upon H_1 to see if the corrections agreed. For the CH_3 proton triplet, the two pairs of center-peak to outer-peak ratios and outer-peak to valley ratios are affected differently by H_1 because, during the course of sweeping through the triplet, the portion occurring earlier in the sweep is saturated less than that later in the sweep. Hence, if the extrapolation to zero radiofrequency field is not correct, the two values will not agree. It was found in most cases, however, that within the precision of the extrapolation, the two values agreed for both pairs.

Kinetic Measurements

Of the several available theoretical treatments upon which the calculation of the shape of the CH_3 proton resonance as a function of the deuterium exchange rate may be based, the most convenient is the equation derived by Sack[13] for a symmetric triplet

$$I(\omega) \sim \frac{p(\delta^2 + 9p^2 + 18pp'' + \omega^2) + 2p''\omega^2}{\omega^2(\delta^2 - \omega^2)^2 + 4p^2\delta^4 + \omega^2\delta^2p(4p'' - 10p) + \omega^2p^2(3p + 6p'')^2 + \omega^4(10p^2 + 4pp'' + 4p''^2)} \quad (7)$$

where $I(\omega)$ is the intensity, ω is the frequency (sec^{-1}) measured from the center of the triplet, δ is the deuterium–proton coupling constant (sec^{-1}), p is the spin transition probability of deuterium for $I = 0 \rightleftarrows I = \pm 1$, and p'' is the deuterium spin transition probability, $I = 1 \rightleftarrows I = -1$. For chemical exchange, the probabilities of the incoming deuterium being in any given spin state are equal so that $p = p''$ and the contribution of chemical exchange to p and p'' is equal to $^2/_3R$, where R is the rate constant for deuterium exchange, $\{1/[(CH_3)_3N^+D]\}\{d[(CH_3)_3N^+D]/dt\}$. The factor of $^2/_3$ arises because, in one-third of the exchanges, the incoming deuterium will be in the same spin state as the previous deuterium so that there will be no effect on the spectrum. For quadrupole relaxation, $p'' = 2p$,[14] so that the complete transition probabilities are

$$p = \frac{2}{3}R + \frac{1}{\tau_Q}; \quad p'' = \frac{2}{3}R + \frac{2}{\tau_Q} \quad (8)$$

where $1/\tau_Q$ represents the quadrupole transition probability. The relationship p and p'' to the deuterium T_1 is given by:[14] $[1/T_1] = p + 2p''$.

Sack's equation is not completely adequate to describe real spectra because it involves only the spin interchange of the deuterium nuclei and does not take into account magnetic field inhomogeneities or relaxation effects of the CH_3 protons. In addition, the treatment is valid only when the deuterium–proton coupling constant and the transition probabilities are small compared to the difference in the resonance frequencies of deuterium and the CH_3 protons. Obviously, these

(11) A. L. Van Geet and D. N. Hume, *Anal. Chem.*, **37**, 979 (1965).

(12) B. A. Jacobsohn and R. K. Wangsness, *Phys. Rev.*, **73**, 942 (1948).

(13) R. A. Sack, *Mol. Phys.*, **1**, 163 (1958).

(14) J. A. Pople, W. G. Schneider, and H. J. Bernstein, "High Resolution Nuclear Magnetic Resonance," McGraw-Hill Book Co., Inc., New York, N. Y., 1959.

criteria are satisfied in the present case even for rates much larger than those required to collapse completely the coupling within the resolution of the nmr spectrometer.

The usual method of including the additional broadening by relaxation and inhomogeneity effects in the GMS[15] and similar theories is to insert a phenomenological factor, $1/T_2'$, into the theoretical equations, T_2' representing an effective transverse relaxation time in the absence of exchange so that field inhomogeneity is treated as if it were a relaxation process. The treatment of Sack could be modified in a similar manner by inserting a $1/T_2'$ factor into the original matrix equation and rederiving the above equation or using the matrix equation directly. However, in the present case, the transverse relaxation time for the CH_3 proton resonance is long (>10 sec) compared to the resolution of the nmr instrument (0.24 cps or 1.3 sec). The resolution is determined by inhomogeneity broadening which arises because there is a distribution of magnetic fields in the volume of the sample and, hence, a distribution of resonant frequencies. Therefore, because the major portion of the nonkinetic broadening of the CH_3 proton spectrum is caused by this distribution, it should be possible to account phenomenologically for these effects by taking a theoretical spectrum calculated from Sack's equation and then applying a shaping procedure that will reproduce the distribution of frequencies in the actual spectrum. The major defect of this method is that the shape of the field inhomogeneity distribution must be known accurately, and it is difficult to measure this distribution because with any spectrum in which the line shape is determined chiefly by the field inhomogeneity, the spectrum is so distorted by sweep rate effects that the line shape cannot be determined. While the lorentzian-shape function is normally used for field inhomogeneity, the shape of the magnetic field distribution will not necessarily follow any specific function and may vary from magnet to magnet. In addition, the field shape for a given magnet will depend upon the adjustments of the homogeneity controls of the magnet. This is demonstrated for the instrument used in this study by the fact that when one or more of the homogeneity controls are deliberately changed from the most homogeneous settings, the shape of a sharp line becomes very distorted and does not fit any simple distribution function.

Tiers[16] used the ratios of observed peak widths to the theoretical lorentzian peak widths at various fractions of the peak height as a function of sweep rate as the basis of an argument that the lorentzian shape was adequate for A-60 spectra, but a lorentzian peak with additional gaussian broadening or a similar shape will also exhibit a similar effect, and the differences in the actual ratio values are not enough greater than the precision of the measurements to provide a sensitive test between different shapes.

For the present case, the most sensitive test of the shaping distribution is provided by the peak to valley and peak to peak ratios (corrected to zero radiofrequency field and sweep rate) of the CH_3 proton spectrum of $(CH_3)_3N^+D$ at slow deuterium exchange rates. After proper adjustment of the various parameters, a gaussian shaping distribution gives calculated ratios which agree with the measured ratios within the precision of the ratio measurements at all DCl concentrations for which accurate measurements can be made, while with a lorentzian shaping function, a satisfactory fit cannot be obtained for solutions with a DCl concentration greater than 0.4 M.

It is difficult to estimate the error introduced in the rate measurements by an incorrect shaping function. The error will be small at relatively large deuterium-exchange rates and will increase with increasing DCl concentration. A relatively poor choice of shaping function will not give a satisfactory fit at high concentrations, but a somewhat better choice will give a fit although the calculated rate constants will be in error. This error if significant would be apparent in the values of k_-/k_{DB} because of the fact that the increase of the error with increasing DCl concentration will lead to a dependence of the rate ratio upon the DCl concentration, while there will be no dependence if the rate constants are not in error. Since the k_-/k_{DB} values obtained in this study are not dependent upon the DCl concentration within the accuracy of the rate measurements, a gaussian shaping distribution is apparently adequate to describe the field inhomogeneity of the instrument used in this study.

The σ of the gaussian distribution is chosen so that the half-width of the calculated spectrum at very rapid rates of exchange will equal the corrected experimental half-width of an actual spectrum. This has the effect of including the proton relaxation broadening in the inhomogeneity broadening, but this does not cause significant error because the relaxation broadening is estimated to be only about 0.03 cps, and the error in treating it in this manner is less than this value and, therefore, less than the precision of the measurement which is 0.02 cps. Another possible source of broadening would be coupling of the CH_3 protons with the

(15) H. S. Gutowsky, D. W. McColl, and C. P. Slichter, *J. Chem. Phys.*, 21, 279 (1953).

(16) G. V. D. Tiers, *J. Phys. Chem.*, 65, 1916 (1961).

nitrogen nucleus, but the N–H coupling constant is small for methylamine CH_3 protons, and the quadrupole relaxation of the nitrogen is rapid compared to the N–CH_3 proton coupling constant for trimethylammonium ion in H_2O so that the coupling is almost entirely collapsed.

Therefore, the parameters required for the calculation of the theoretical spectra are the rate, the deuterium quadrupole relaxation time, the deuterium–proton coupling constant, and the σ of the gaussian shaping distribution.

Each series of solutions has a fixed formal concentration of $(CH_3)_3N^+D$, D^+ concentrations which vary from approximately 0.08 to 5×10^{-5} M, and one solution with approximately 10^{-9} M D^+. The σ of the shaping distribution is determined from the line width of the CH_3 resonance of the 10^{-9} M D^+ solution, the kinetic measurements using the CH_3 resonance are made from the solutions with D^+ concentrations greater than 5×10^{-4} M, and the HOD proton resonance measurements were made from solutions with D^+ concentrations from 10^{-3} to 5×10^{-5} M. The H–D coupling constant is determined from solutions with the higher concentrations of D^+ where the CH_3 proton resonance has a triplet shape. It was necessary to fit the coupling constant in the calculations because the triplet is partially collapsed even at slow exchange rates because of the deuterium quadrupole relaxation. Once the coupling constant was determined from several spectra, it was not redetermined for the rest of the measurements. After the coupling constant and the shaping σ have been determined, outer-peak to valley and peak to peak ratios for the triplets are calculated as a function of exchange rate for various τ_Q values. The two ratios are affected somewhat differently by τ_Q and R because exchange tends to broaden all three peaks by the same amount while quadrupole relaxation broadens the outer peaks more than the inner peak. Therefore, there is only a small range of τ_Q and R values that will correctly give both ratios. The D^+ concentrations were chosen such that two solutions in each series gave rise to a triplet line shape, and the average of the two τ_Q values was used in the calculation of the line widths of the broadened singlets as a function of exchange rate. There is a possibility that τ_Q might change as the D^+ concentration is lowered, but this would only be a small source of error for the singlets because R is significantly greater than $1/\tau_Q$ at these concentrations.

In the case of solutions with DCl concentrations greater than 0.1 M, the determination of the shaping σ is not as straightforward as for the other solutions because of the large change in solution conditions in going to a similar solution with a 10^{-9} M D^+ concentration. However, the line width of the residual HOD proton resonance is unaffected by the increasing DCl concentration over the range 0.02–1.5 M and, therefore, may be used as a check on the instrumental broadening.

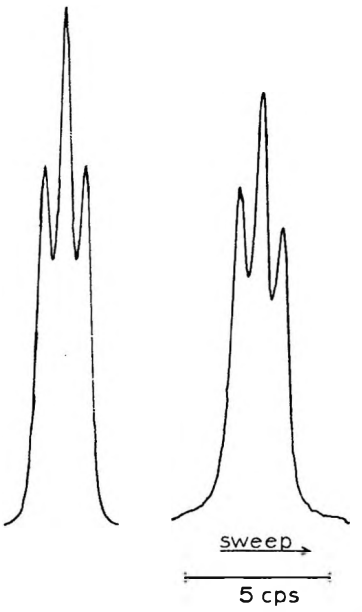

Figure 1. Left: calculated spectrum of $(CH_3)_3N^+D$ for J = 0.79 cps, τ_Q = 4.7 sec, R = 0.45 sec^{-1}, and shaping width = 0.25 cps. Right: proton nmr spectrum of 1.76 F $(CH_3)_3NDCl$ and 0.22 F DCl, recorded at a sweep rate of 0.1 cps/sec and a radiofrequency field of 0.04 mgauss.

Examples of a calculated and an actual spectrum are shown in Figure 1. The parameters for the calculated spectrum correspond to the actual spectrum after correcting to zero radiofrequency field and sweep rate, with the calculated spectrum being normalized for equal areas. The differences in the two spectra illustrate the influence of sweep rate effects and partial saturation. The actual spectrum was taken at the slowest available sweep rate and the smallest useful radiofrequency field.

The rate, R, measured from the CH_3 proton resonance in terms of reactions 1–3 is given by

$$R = k_4 + (k_6 + k_7)K_A[(CH_3)_3N^+D]/[D^+] \quad (9)$$

so that k_4 is a pseudo-first-order rate constant, and k_7 is a pseudo-second-order rate constant. By plotting R against $1/[D^+]$, the intercept gives k_4, and the slope gives $k_6 + k_7$; k_{DB}, the rate of "breaking the $R_3N\cdots(D_2O)_m$ deuterium bond," which is equivalent to Grunwald's[7] k_H is determined by the decrease of k_4 at higher concentrations of DCl.

The accuracy of R is limited at slow rates because quadrupole relaxation and inhomogeneity broadening are more important than exchange in determining the shape of the triplet while at rapid rates the line width is controlled largely by the inhomogeneity broadening. As a result of the small value of the deuterium–proton coupling constant, the collapse of the triplet into a singlet occurs over a relatively small range of exchange rates compared to the proton-exchange case because the NH–CH_3 proton coupling constant is 5.15 cps[7] or about 6.5 times the deuterium–proton coupling constant. As a result, the accuracy of the rates reported in this communication is not as good as the accuracy of the proton-exchange rates although somewhat lower rates may be measured.

The rate of reaction 6 can be measured from the line broadening of the HOD resonance. Using the slow-exchange approximation (where the exchange broadening is small compared to the frequency difference between the HOD and N–H proton resonances) $\pi W_{1/2} = 1/T_{2_e} + 1/\tau_{HOD}$ where $W_{1/2}$ is the line width in cps, T_{2_e} the effective line width of the HOD resonance in the absence of exchange but including field inhomogeneities, and τ_{HOD} the average lifetime of a proton in HOD before being transferred to a nitrogen. The third-order rate constant k_7' is given by

$$k_7' = \rho[D^+]/[(CH_3)_3N^+D]^2K_A\tau_{HOD} \qquad (10)$$

The statistical factor ρ arises because a portion of the exchanges involving HOD transfers a deuterium to $(CH_3)_3N$ rather than a proton so that the factor ρ must be applied to obtain a rate constant which will be comparable to k_7 for D_2O or H_2O. An effective pseudo-second-order rate constant, k_{7HOD}, for comparison with the k_7 measured from the CH_3 proton resonance, is obtained by multiplying k_7' by the concentration of D_2O, 55 M. The accuracy of the HOD line-width measurements is limited because the signal to noise ratio is poor for the broadened resonance, so that the precision is approximately 10–15%. The $[D^+]$ values are also not as accurate as those of the solutions in which the CH_3 proton resonance is studied because the $[D^+]$ must be lower to get a measurable broadening, and in this concentration range, the solution is poorly buffered; hence, the $[D^+]$ is sensitive to acidic or basic impurities adsorbed on the nmr sample tubes and to the possible loss of $(CH_3)_3N$ from the solution.

Results and Discussion

Values of the experimental rate constant, R, determined from the CH_3 proton resonance were plotted against the reciprocal of the deuterium ion concentration for various $(CH_3)_3N^+D$ concentrations, and the results are shown in Figure 2. The experimental points at higher D^+ concentrations have been corrected for the decrease of k_4 *via* reaction 4 using eq 5, after k_+ and k_-/k_{DB} have been determined by successive approximations. A portion of the plots at low R values has been expanded in the inset for increased clarity. These plots are linear within experimental error, and the rate constants evaluated therefrom are given in Table I. The agreement of the k_7 values, which are not expected to have a significant salt effect, is well within experimental error, the average deviation being only 3%, while the estimated error is 10% for k_4 and k_7. A plot of log k_4 against total concentration is linear with a slope of -0.09_0 and intercept which gives a k_4^0 value of 1.0_8 sec^{-1}. Log K_A is linearly

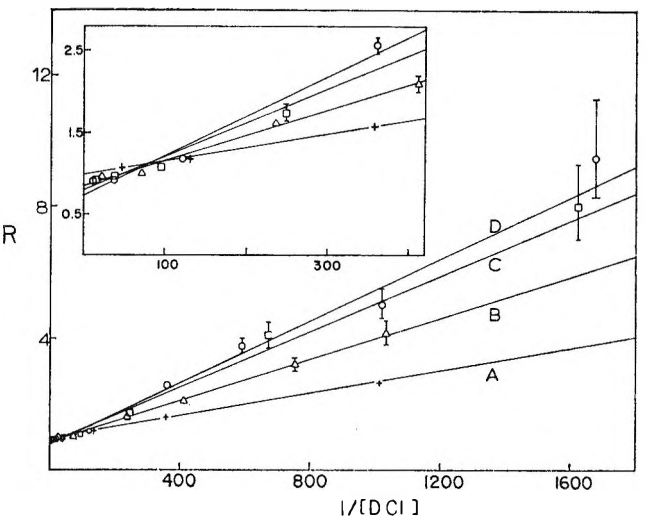

Figure 2. Plots of the experimental exchange rate constant R as a function of the reciprocal of the D^+ concentration for different concentrations of $(CH_3)_3N^+D$: A, 0.439 F; B, 0.878 F; C, 1.32 F; D, 1.76 F. The inset is a magnification of the portion of the plots at small R.

Table I: N–D Deuterium-Exchange Rates for Trimethylammonium Ion in D_2O at 33.2°

$[(CH_3)_3N^+D]$, M	k_4, sec^{-1}	$(k_6 + k_7)K_A$, sec^{-1} × 10^2	K_A, $M \times 10^{11}$	k_7,[a] M^{-1} sec^{-1} × 10^{-8}	T_{1Q},[b] sec
0.439	1.00	3.85	3.46	1.11	4.0
0.878	0.85	3.56	3.04	1.17	2.2
1.32	0.80	3.17	2.80	1.13	1.8
1.76	0.74	2.68	2.55	1.05	1.6

[a] Assuming $k_6 \ll k_7$. [b] T_{1Q} is the contribution of deuterium quadrupole relaxation to the N–D deuterium T_1 ($T_{1Q} = \tau_Q/5$).

dependent upon $[(CH_3)_3N^+D]^{1/2}$ with the intercept giving K_A^0 to be 4.76×10^{-11}; therefore, taking $k_+^0 = k_4^0$, $k_-^0 = 2.3 \times 10^{10}\ M^{-1}\ sec^{-1}$.

Table II gives the effect of higher D^+ concentrations on k_4. The ratio k_-/k_{DB} was calculated from eq 5 assuming, as did Grunwald,[7] that there is no salt effect upon the ratio and that the salt effect of D^+ upon k_+ is the same as that of $(CH_3)_3NDCl$. The agreement of the ratios is satisfactory in view of the accuracy of k_4 in this range which is only 15–25%. The average ratio is 2.7 so that k_{DB} is $8.5 \times 10^9\ sec^{-1}$. The contribution of quadrupole relaxation to the deuterium T_1 of $(CH_3)_3N^+D$ is not a simple function of concentration. This arises because changes in concentration of the various species in solution can affect T_{1Q} ($T_{1Q} = \tau_Q/5$) by two different mechanisms, one involving the correlation time for molecular rotation, τ_C, and the other involving the electrical field gradient about the deuterium nucleus. The effect of concentration changes of τ_C can be considered as a viscosity effect, and a plot of log T_{1Q} against concentration should be approximately linear with the effect of changes in $(CH_3)_3N^+D$ concentration being much greater than changes in D^+ concentration. However, plots of log T_{1Q} against concentration are not linear; furthermore, the effect of DCl is greater than that of $(CH_3)_3NDCl$ or LiCl. The greater influence of DCl *vs.* LiCl indicates that this is not a simple anion effect leading to increased ion pairing. Therefore, at the relatively large concentrations required for this study, there is apparently a change in ion pairing or some other factor, leading to a significant alteration of the microscopic structure of the solution about a $(CH_3)_3N^+D$ molecule as the concentrations of the various species are changed, leading to changes in the electric field gradient about the deuterium nucleus.

Table II: Rate Constants for Deuterium Exchange at Higher Acidities

$[(CH_3)_3N^+D]$, *M*	[DCl], *M*	k_4, sec^{-1}	k_-/k_{DB}, M^{-1}	T_{1Q}, sec
0.44	1.10	0.22	2.5	0.8
0.44	0.88	0.26	2.4	0.8
0.44	0.66	0.29	3.0	0.8
0.44	0.44	0.44	2.4	1.0
0.50	0.22	0.57	2.9	1.3
0.50[a]	0.22	0.45	3.1	1.1
1.76	0.22	0.45	2.7	0.9

[a] Also contains 1.0 *F* LiCl.

The kinetic parameters determined from the CH_3 proton resonance, extrapolated to infinite dilution, are summarized in Table III along with the corresponding proton-exchange rates and isotope effects calculated at 33.2° from the empirical rate equations for proton exchange given in ref 7. These isotope effects are in agreement with mechanisms used to describe the exchange processes. The large isotope effect on k_4 is consistent with the hypothesis[7] that the position of the transition state of reaction 1 along the reaction coordinate is not very far from the products so that there would be a significant difference in the zero-point energies between transition state and the reactants. In the case of k_7, the rapidity of the symmetrical reaction indicates that the transition state is not very different from the reactants (or the products); thus, the difference in zero-point energies would be smaller; hence, the isotope effect on k_7 should be smaller than that on k_4. Because k_- is considered to be diffusion controlled, the isotope effect should be determined by the differences in diffusion between H_2O and D_2O so that the ratio of rates should be given approximately by the mobility ratio of H^+/D^+ which is 1.4,[17] within experimental error of the measured value of 1.3. The calculation of the theoretical isotope effect on k_H, the rate of "hydrogen bond breakage," may be based on the treatment of Conway, Bockris, and Linton,[17] who considered the rate-determining step in proton conductance in H_2O to be the reorientation of the hydrogen-bonded H_2O molecules. In the mechanism suggested by Grunwald, the rate step should also be the reorientation of H_2O molecules so that the theoretical ratio of k_H/k_{DB} would also be 1.4, in agreement with the experimental value of 1.4.

Table III: Isotope Effects for Exchange of Trimethylammonium Ion at 33.2° at Infinite Dilution

Rate parameter	k_{H_2O}[a]	k_{D_2O}	k_{H_2O}/k_{D_2O}
k_4^0, sec^{-1}	7.2	1.08	6.7
k_7^0, $M^{-1}\ sec^{-1}$	3.8×10^8	1.12×10^8	3.4
K_A^0, *M*	2.40×10^{-10}	4.76×10^{-11}	5.0
k_-^0, $M^{-1}\ sec^{-1}$	3.0×10^{10}	2.3×10^{10}	1.3
k_H^0, sec^{-1}	1.2×10^{10}	8.5×10^9	1.4

[a] Calculated from ref 7.

The results from the line broadening of the HOD proton resonance using eq 10 are given in Table IV,

(17) B. E. Conway, J. O'M. Bockris, and H. Linton, *J. Chem. Phys.*, 24, 834 (1956).

taking 1.45 as the value for the statistical factor ρ. This value was determined by assuming that k_7 for deuterium transfer from HOD has the same value as k_7 for deuterium transfer from D_2O so that ρ is given by $[k_{7HOD} + k_{7D_2O}]/k_{7HOD}$ (k_{7HOD} refers to proton transfer from HOD). This assumption should be valid within the experimental error. The average deviation of the k_{7HOD} values is 12%, which is within the estimated experimental error of 20%. The isotope ratio k_{7H_2O}/k_{7HOD} is 1.6, approximately half that of k_{7H_2O}/k_{7D_2O} in D_2O; this is in agreement with a concerted reaction.

Table IV: Proton-Exchange Rates Measured from the HOD Proton Resonance

$[(CH_3)_3N^+D]$, M	$k_7'K_A$, M^{-1} sec^{-1} $\times 10^4$	k_7', M^{-2} sec^{-1} $\times 10^{-6}$	k_{7HOD}, M^{-1} sec^{-1} $\times 10^{-8}$
0.439	1.7	5.2	2.9
0.878	1.0	3.4	1.9
1.32	1.2	4.2	2.3
1.76	1.2	4.6	2.6

The rate parameters were not measured at other temperatures because the reproducibility of the instrumental broadening was not sufficient to permit accurate rate measurements; this is caused primarily by poor temperature control of the variable-temperature probe. In addition, the triplet shape is collapsed at higher temperatures for D^+ concentrations below 0.1 M so that the determination of T_{1Q} values becomes difficult.

Acknowledgment. The authors are indebted to Drs. L. B. Anderson and D. E. Leyden for their assistance in the preparation of the computer program for the calculation of the theoretical spectra. Research was supported in part by National Institutes of Health Grant GM-12598-01 and by the Advanced Research Projects Agency.

Dicarboxylic Acid–Urea Complexes

by Jack Radell,[1] B. W. Brodman, and J. J. Domanski, Jr.

Pitman-Dunn Research Laboratories, Chemistry Research Laboratory, Frankford Arsenal, Philadelphia, Pennsylvania 19137, and Philadelphia College of Textiles and Science, Philadelphia, Pennsylvania 19144
(Received June 30, 1966)

A study of the reaction of several acids with urea resulted in a series of compounds of varying stoichiometry and structure. The acids having the structure $HO_2C(CH_2)_nCO_2H$ produced saltlike compounds with urea when $n = 0$ and 1 and H-bonded complexes for $n = 2$–5. The stoichiometry of all the complexes was $2H_2NCONH_2 \cdot HOOC(CH_2)_nCOOH$, except for $n = 1$ which had a 1:1 ratio of urea to acid. None of the products was an inclusion compound. From our general observations, we concluded that urea and the dicarboxylic acids are unlikely to form inclusion compounds, and reports of such molecular compounds should be verified by X-ray powder diffraction measurement as well as analysis.

Introduction

In order to obtain urea inclusion compounds of exceptionally high stability, an investigation of molecules with two terminal polar groups on a straight chain was undertaken. It was known from earlier work[2] that the presence of one polar end group enhanced the stability of a urea inclusion compound. The introduction of a second polar group at the opposite end was expected to give the added stability without increasing either the cross-sectional diameter or the chain length significantly. This effect of polar groups has recently been verified for alkyl halides.[3]

The carboxyl group was chosen because of its polarity and because the *n*-aliphatic monobasic acids were known to form highly stable urea inclusion compounds. We were specifically interested in obtaining urea inclusion compounds with dissociation temperatures above 133° (mp of urea) about which little is known.[4]

Discussion

No urea inclusion compounds[5] of the α,ω-dicarboxylic acids studied were obtained. This was demonstrated[5b] by the X-ray data in Table I. None of the values corresponded to that of a typical urea inclusion compound, as, *e.g.*, dodecane with major spacing in order of decreasing intensity at 4.12, 3.56, 7.10, and 3.39 A. Instead, molecular compounds were obtained in which the acid and urea were present in whole number molar ratios. The name *stoichiometric compound* is used to describe these compounds irrespective of whether they are simple salts or hydrogen-bonded complexes of the acid and urea.

Oxalic Acid

The earliest reference to compounds of 2-urea–oxalic acid appear in Beilstein[6] and Gmelin.[7] Although the structure of the oxalic acid–2-urea was not shown by these earlier workers, Gottlieb[6] reported that one part of oxalic acid–2-urea dissolved at 16° in 23 parts of water, 62.5 parts of alcohol, and 50,000 parts of ether, respectively, at room temperature. This would support the formation of a urea oxalate salt structure. In addition, Marchand[6] described a compound of 2-urea–oxalic acid–2-water. Ljubawin[6] in 1872 de-

(1) Reprint requests should be addressed to this author at the Pitman-Dunn Research Laboratories.

(2) (a) W. Schlenk, Jr., *Ann.*, **565**, 204 (1949); (b) L. C. Fetterly, "Non-Stoichiometric Compounds," John Wiley and Sons, Inc., New York, N. Y., 1961, Chapter 8; (c) C. Asseline and J. Asseline, *Ann. Chim.* (Paris), **9**, 460 (1964).

(3) H. G. McAdie, *Can. J. Chem.*, **41**, 2144 (1963); J. Radell, B. W. Brodman, and E. D. Bergmann, *ibid.*, **42**, 1069 (1964).

(4) I. R. Krichevskiy, G. D. Efremova, and G. G. Leontyeva, *Rept. USSR Acad. Sci.*, **113**, 817 (1957).

(5) (a) Urea inclusion compounds refer to the channel compounds discovered by Bengen. These compounds have been variously referred to as occlusion compounds, complexes, adducts, clathrates, canal, and channel compounds. (b) The urea channel compounds may be characterized by their X-ray powder diffraction patterns: J. Radell and J. W. Connolly, *Advan. X-Ray Anal.*, **4**, 140 (1961).

(6) F. K. Beilstein, "Handbuch der organischen Chemie," Vol. III, Julius Springer, Publisher, Berlin, 1921, p 55.

(7) L. Gmelin, "Handbuch der Organischen Chemie," Vol. IV, C. Friedheim and F. Peters, Publishers, Heidelberg, Germany, 1870, p 869.

Table I: Interplanar X-Ray Data

Oxalic acid–2-urea	*d*, A[c]	3.11	4.07	6.43	4.74	2.81	3.66								
	I[a]	100	4	4	3	3	2								
Oxalic acid	*d*, A	3.07	2.43	4.73	5.96	3.28	2.93	2.37	2.25	3.44	2.94	5.79	2.66	2.57	2.63	2.90
	I	100	55	50	50	30	25	25	25	25	20	15	11	9	3	3
Malonic acid–1-urea	*d*, A	3.23	2.49	4.50	3.45	2.92										
	I	100	2	1	1	1										
Malonic acid	*d*, A	3.74	3.53	2.69	4.95	4.72	4.13	3.29	2.53	2.36	2.25	3.15	2.98	2.86		
	I	100	70	70	60	50	30	30	30	30	20	14	14	14		
Succinic acid–2-urea	*d*, A	5.98	6.07	3.60	4.82	3.95	3.23	4.14	3.40	4.07						
	I	100	86	40	18	15	9	9	5	4						
Succinic acid	*d*, A	4.46	3.42	2.86	2.17	4.07	3.30									
	I	100	26	18	6	5	4									
Glutaric acid–2-urea	*d*, A	3.48	5.68	3.80	4.82	3.02	3.90	3.72								
	I	100	6	5	3	3	2	2								
Glutaric acid	*d*, A	3.71	3.27	6.44	4.06	4.53	2.41	2.26								
	I	100	15	11	10	6	5	5								
Adipic acid–2-urea	*d*, A	3.98	3.22	3.30	5.84	5.03	2.53	3.15	3.50	2.84	4.21	4.42	4.65			
	I	100	52	46	21	9	9	8	6	6	5	3	3			
Adipic acid	*d*, A	4.13	3.45	2.87	3.32	6.86	3.53	2.41	2.15							
	I	100	25	14	8	8	6	3	3							
Pimelic acid–2-urea	*d*, A	3.39	5.53	4.31	4.35	3.56	2.36	2.91	1.98	4.64	3.22	2.67	4.69	2.72	2.77	
	I	100	60	19	17	16	9	5	5	4	4	4	3	3	3	
Pimelic acid	*d*, A	3.85	3.75	7.62	3.20	4.62	3.34	4.04	4.82	3.06	8.55	2.60				
	I	100	100	41	21	18	8	8	6	6	5	5				
Suberic acid–*x*-urea[b]	*d*, A	3.24	3.58	4.14	4.72	3.97	3.53									
	I	100	3	3	2	2	2									
Suberic acid	*d*, A	4.14	3.59	2.93	3.42	2.39	2.17									
	I	100	83	27	13	10	8									
Azelaic acid–*x*-urea	*d*, A	3.48	4.69	5.25	7.76	4.04	3.56	3.06								
	I	100	20	18	15	13	13	8								
Azelaic acid	*d*, A	3.93	4.69	3.31	4.19	4.86	3.67	3.20								
	I	100	53	29	22	21	15	15								
Sebacic acid–*x*-urea	*d*, A	3.23	3.46	6.93	4.73	4.13	3.80	3.40	2.30	4.03	3.13					
	I	100	14	9	9	9	9	9	7	5	5					
Sebacic acid	*d*, A	4.15	3.60	2.96	4.41	3.44	3.42	2.41	2.33	2.17						
	I	100	50	17	13	13	13	13	13	13						
Undecanedioic acid–*x*-urea	*d*, A	3.90	4.11	4.21	3.59	3.24	1.94	2.34	4.69	3.42	2.55	3.37	2.17	2.60	2.63	2.71
	I	100	33	16	16	16	14	12	10	8	7	5	5	3	3	3
Dodecanedioic acid–*x*-urea	*d*, A	2.34	3.44	3.25	4.79	3.93	3.87	3.60	4.14	2.58	3.55	2.76	2.70	4.37	2.72	2.39
	I	100	91	75	63	42	47	41	39	38	31	25	25	22	19	17
Tridecanedioic acid–*x*-urea	*d*, A	4.20	3.62	3.93	2.34	3.31	4.41	2.58	2.18	2.64	1.96	3.03	3.21	3.16		
	I	100	88	34	32	24	17	17	17	12	12	10	5	5		

[a] *I* is for relative intensity, 100 representing the strongest. [b] *x* indicates an uncertain ratio of urea to acid. [c] Interplanar spacing, *d*, in angstroms.

scribed a compound of oxalic acid–urea–water which he proposed as an intermediate structure between oxalic acid–2-urea and the oxalic acid dihydrate. Schlenk,[2a] reporting on urea inclusion compounds, described oxalic as being one of several acids capable of forming a compound with 2 moles of urea and as being different from the urea inclusion compounds discovered by Bengen.[8]

Merritt and Sturdivant[9] reported in a preliminary account with no details that oxalic acid and urea, the components in crystalline oxalic acid–2-urea, are held together by strong H bonds to form layers with an O–O distance of 2.50 A and are also held together by van der Waals forces.

Kutzelnigg and Mecke,[10] using infrared spectroscopy, concluded that the structure of oxalic acid–2-urea was

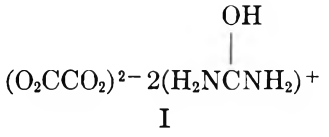

I

I, with the proton attached to the oxygen of urea. This protonation site would be consistent with the fact that the hydrogen is attached to the more electronegative oxygen rather than nitrogen and the resonance stabilization of structure II would be considerably greater than III because of both the greater number and greater equivalence of the contributing forms to II. Our oxalic acid–2-urea had the same infrared pattern as reported by Kutzelnigg and Mecke.[10] We confirmed

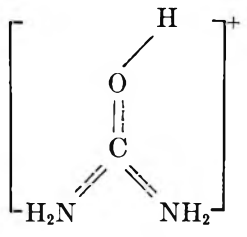

II

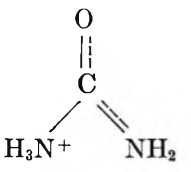

III

the saltlike structure of I in solution by molar conductance measurements. A 0.00524 *M* aqueous solution of urea cation oxalate had a molar conductance of 281.98 cm^2 ohm^{-1} $mole^{-1}$ (see Table II). Using an average of 60[11] for the equivalent conductance of all ions, then an ordinary univalent cation, $(urea\ H)^+$, and a divalent anion, $(OOC\text{–}COO)^{2-}$, would be 240 cm^2 ohm^{-1} $mole^{-1}$ at a corresponding concentration. Our measured value of 280 cm^2 ohm^{-1} $mole^{-1}$ would be in agreement with the $2(urea\ H)^+$ $(oxalate)^{2-}$ ionized structure. Although these measurements do not indicate the site at which the proton was attached to urea, they do eliminate the possibility that only one carboxyl group formed a salt while the second was involved in some type of H-bond formation with urea. When I was acidified and extracted with ether, the oxalic acid was recovered.

Table II: Specific Conductivity and Molar Conductance at 25°

Compound	R_x[a]	$10^{-3}L$[b]	$10^{-3}C$[c]	Λ_m[d]
Oxalic acid–2-urea	680	1.473	5.224	281.98
Malonic acid–1-urea	943	1.062	9.980	106.41
Succinic acid–2-urea	4070	0.2461	8.950	27.50
Glutaric acid–2-urea	4360	0.2297	9.554	24.04
Adipic acid–2-urea	8230	0.1217	4.875	24.96
Pimelic acid–2-urea	7030	0.1425	6.207	22.96

[a] Measured resistance in ohms. [b] Specific conductivity (L) in ohm^{-1} cm^{-1} = conductivity × cell constant (1.0018 cm^{-1}). [c] Concentration in moles per liter. [d] Molar conductance (Λ_m) in cm^2 $mole^{-1}$ ohm^{-1} = $1000L/C$.

The main peaks are reported for the differential thermal analysis data in Table III. The incipient temperatures preceding the peaks were omitted because the selection of a point of deviation from base line was arbitrary. The observed melting point was usually lower than the main peak value and closer to the incipient temperature.

Malonic Acid

A malonic acid–urea complex having a 1:1 molar ratio was prepared with difficulty. Attempts to repeat the preparation met with sporadic success. A search of the literature revealed a reference to a malonic acid–2-urea stoichiometric complex in a review article by Schlenk.[2a] He reported without reference or experimental detail that malonic acid, as well as other dibasic acids, combines with two molecules of urea. We have been unable to obtain a malonic acid–urea complex with any ratio other than 1:1. In an earlier reference to Matignon,[6] malonic acid–urea was reported briefly and described as being slightly soluble in water.

Structure IV is proposed for malonic acid–urea. The saltlike character of IV is dictated by the molar conductance of the urea–malonic acid compound which was 106.41 cm^2 ohm^{-1} $mole^{-1}$ (Table II) in agreement with the predicted[11] value of 120 cm^2 ohm^{-1} $mole^{-1}$ for a salt of a univalent cation and a univalent anion.

(8) M. F. Bengen, *Experientia*, **5**, 200 (1949).

(9) L. L. Merritt and J. H. Sturdivant, *Struct. Rept.*, **13**, 477 (1950).

(10) W. Kutzelnig and R. Mecke, *Chem. Ber.*, **94**, 1706 (1961).

(11) S. Glasstone, "An Introduction to Electrochemistry," D. Van Nostrand Co., Inc., Princeton, N. J., 1942, p 71.

Table III: Thermal Data

Compound	Temp (°C) of peaks in differential thermal analysis						Mp, °C	
							Obsd[c]	Lit.
Oxalic acid–2-urea	122[a]	154[g]	166[b]	207			140–151[e]	170–171[f]
Oxalic acid	99[g]	156	187				190[e]	189[d]
Malonic acid–1-urea	93[g]	178					60–93	
Malonic acid	90	130[g]	184	259[b]			131	135.6[d]
Succinic acid–2-urea	116	141[g]	164	290			134–140	
Succinic acid	177[g]	220	240	258			190	185, 189–190[d]
Glutaric acid–2-urea	113	127[g]	290				120–130	
Glutaric acid	80	96[g]					94	95–96[d]
Adipic acid–2-urea	72	106[g]	190	202	326		102–110	
Adipic acid	146[g]	324					150	151–153[d]
Pimelic acid–2-urea	116	127[g]	234	331			124–130	
Pimelic acid	86	93	101[g]	343	349	362	103	103[d]
Urea	113	132[g]	183	245	396		132	132.7[d]

[a] All values are endotherms unless indicated. [b] Exotherm. [c] Uncorrected melting points were determined on a Fisher-Johns melting point block. [d] Reported in the "Handbook of Chemistry and Physics," 43rd ed. [e] Decomposition. [f] Reported in "Langes Handbook of Chemistry," 6th ed. A value of 173° dec was reported in the "Handbook of Chemistry and Physics," 45th ed. [g] Strongest peak below 200°.

The protonation of urea on oxygen is supported by our agreement with the infrared evidence as reported by Mecke and Kutzelnigg[10] for I. The structure of the anion shown is based upon the reaction of the most acidic hydrogen atoms of malonic acid with urea before solution.

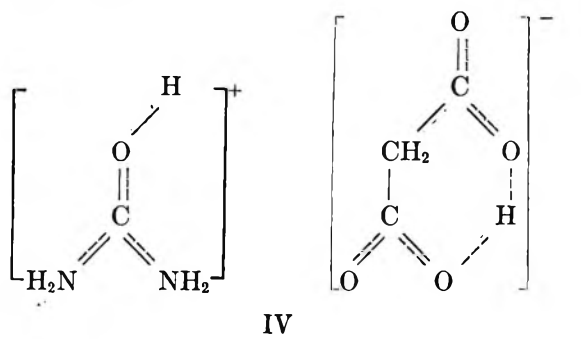

IV

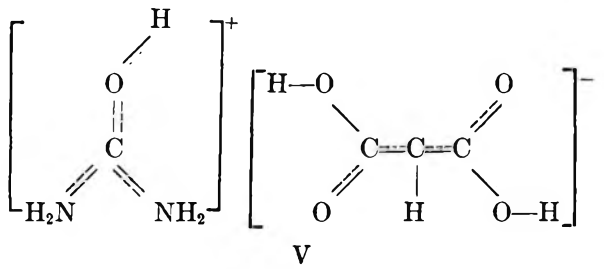

V

Succinic Acid

The first report of a succinic acid–2-urea compound was made by Loschmidt.[6] A Spanish article,[12] in 1961, gave the X-ray powder diffraction data and cell constants of a compound of urea and succinic acid but no information on the structure or analysis of the compound. Our measurements of the X-ray powder diffraction pattern were not in good agreement with the above data. The synthesis of the succinic acid–2-urea compound was reported by Holzl.[13] Schlenk[2a] mentioned, without reference, the formation of a succinic acid–2-urea molecular compound. A study of the Raman spectrum of 2-urea–succinic acid was reported by Schrader, Nerdel, and Kresze.[14] Griffith and Kwiram[15] reported the synthesis of 2-urea–fumaric acid and compared it with the crystals of succinic acid–2-urea. They concluded from the esr and Laue X-ray data that succinic acid and fumaric acid, in their respective molecular compounds with urea, had the same orientation. We believe these conclusions are supported by the similarity in both the geometry and the pK_a values of fumaric and succinic acids as described in a recent publication.[16]

The molar conductance of 27.50 cm^2 ohm^{-1} $mole^{-1}$ (Table II) measured at 0.00895 M precludes the possibility[11] that this compound is a salt in aqueous solution. Instead it appears to form a complex in which each carboxyl is independently H bonded to a molecule of urea in solution.

(12) J. J. Amoros and M. L. Palomar, *Bol. Real Soc. Esp. Hist. Nat., Secc. Geol.*, 59, 25 (1961).

(13) See ref 6, 2nd supplement to Vol. III, p 48.

(14) B. Schrader, F. Nerdel, and G. Kresze, *Z. Anal. Chem.*, 170, 43 (1959).

(15) O. H. Griffith and A. L. Kwiram, *J. Am. Chem. Soc.*, 86, 3937 (1964).

(16) J. Radell, B. W. Brodman, A. Hirshfeld, and E. D. Bergmann, *J. Phys. Chem.*, 69, 928 (1965).

Table IV: Analysis and Yield of Complexes

Compound	% C		% H		% N		% yield
	Obsd	Calcd	Obsd	Calcd	Obsd	Calcd	
Oxalic acid–2-urea	22.7	22.86	5.0	4.80	26.9	26.66	42.92
Malonic acid–urea	29.4	29.27	4.8	4.91	17.0	17.07	6.86
Succinic acid–2-urea	30.3	30.25	6.2	5.92	23.5	23.52	57.50
Glutaric acid–2-urea	33.3	33.33	6.4	6.39	22.2	22.21	36.98
Adipic acid–2-urea	35.6	36.09	6.8	6.81	24.4	21.04	29.28
Pimelic acid- 2-urea	38.7	38.56	7.1	7.19	20.1	19.99	17.82

Glutaric Acid

A reference to "urea glutarate"[17] appeared in the patent literature. Although the stoichiometry and analysis were not reported, one could deduce that the compound may have had the composition of 2-urea–glutaric acid since the compound was described as containing approximately 50% by weight of glutaric acid. Our preparation, in analytically pure form, had a composition of 2-urea–glutaric acid (Table IV). The saltlike structure implied by the name "urea glutarate" was refuted by the molar conductance value of 24.04 cm^2 ohm^{-1} $mole^{-1}$. For the same reasons given for succinic acid, we propose that 2-urea–glutaric acid is an H-bonded complex in solution.

Adipic Acid

Molecular compounds obtained from adipic acid and urea have been reported in the literature[2a] with the composition 2-urea–adipic acid which we confirmed (Table IV). Redlich, *et al.*,[18] reported a molar ratio of 5.3:1. Since no X-ray data for this compound were reported, it is not certain that this compound is a urea inclusion compound. From the reported[18] heat of formation and our experimental results, we do not believe this is a urea inclusion compound. Alsberg and Jeffers[17] refer to a compound of urea and adipic acid with insufficient detail to characterize the product. Barlow and Corish[19], prepared the adipic acid–2-urea complex and correctly noted that it had a different infrared spectrum from the urea inclusion compounds but incorrectly concluded that this change was due to a change in the conformation of the adipic acid rather than in the type of complex. Amoros and Palomar[12] reported on the cell constants and X-ray powder patterns of a complex of adipic acid and urea of unreported purity. Our X-ray data were in only fair agreement. Griffith and Kwiram[15] found in their esr studies that adipic acid–2-urea has a structure which is similar to succinic acid–2-urea and fumaric acid–2-urea. Our molar conductance measurements (Table II) confirm the similarity of adipic acid–2-urea and succinic acid–2-urea with a molar conductance of 24.96 and 27.50 cm^2 ohm^{-1} $mole^{-1}$, respectively. A nonionic H-bonded structure is also proposed for adipic–2-urea in solution.

Pimelic Acid

A complex of pimelic acid and urea was reported[15] as something other than a urea inclusion compound, although the stoichiometry was not given. Amoros and Palomar[12] report that a urea–pimelic acid complex was easy to obtain but was of "anomalous form." It was our experience that pimelic acid was the most difficult molecular compound to prepare after malonic acid–urea. The complex was nonionic and had a molar conductance of 22.96 cm^2 ohm^{-1} $mole^{-1}$ at 0.006207 *M*. An H-bonded structure is also proposed for pimelic acid–2 urea in solution.

Higher Acids

Higher dicarboxylic acid homologs were investigated to determine the possibility of obtaining a urea channel compound of any α,ω-dicarboxylic acid. Since the stability and ease of formation of a urea channel inclusion compound is proportional to the chain length, it was anticipated that an inclusion compound would be more likely to form for the longer dibasic acids. This would be especially true since the stability and ease of formation of the stoichiometric complexes is inversely proportional to the chain length. These facts, coupled with the literature citations[2a,18] of urea inclusion compound formation of some dicarboxylic acids, lead to the investigation of the reaction of urea and the acids $HOOC(CH_2)_nCOOH$ for n = 6–11, inclusive. Although products were obtained containing urea and acid, the composition was both nonstoichiometric and nonreproducible. The crossover from stable stoichiometric complexes to stable inclusion compounds, which we hoped to observe with increasing chain length of the acid, never occurred. The X-ray

(17) F. R. Alsberg and F. G. Jeffers, British Patent 805,507 (1958).

(18) O. Redlich, C. M. Gable, A. K. Dunlop, and R. W. Miller, *J. Am. Chem. Soc.*, 72, 4153 (1950).

(19) G. B. Barlow and P. J. Corish, *J. Chem. Soc.*, 1706 (1959).

powder patterns of the products obtained confirmed the absence of urea inclusion compound formation for any of the acids studied.

Conclusions

The ability of the dibasic acids to form a complex with one or two molecules of urea appears to be a function of the acidity of the carboxyl group and its related stereochemistry. The oxalic acid with a reported pK_{a_1} of 1.10 readily forms an ionic complex with two molecules of urea. The reported pK_{a_2} of 4.21 for oxalic acid might not be applicable for complex formation if the urea is partially associated with the carboxylate ion, thus reducing the field effect on the second carboxyl group. This would result in a lower pK_{a_2} than 4.21 with the resultant observed salt formation between urea and the second carboxyl group as well. In malonic acid, the pK_{a_1} of 2.85 is sufficiently low for salt formation. However, owing to the much higher pK_{a_2} (6.10) and the geometric factor of ring formation (IV), the second carboxyl does not react or coordinate with urea at all. Succinic acid is the longest homolog with distinguishable acidity of the two carboxyls: $pK_{a_1} = 4.17$ and $pK_{a_2} = 5.57$. The pK_{a_1} is too high for salt formation and both carboxyl groups are sufficiently acidic and available for H-bond formation with urea. All of the higher acids have pK_{a_1} and pK_{a_2} values of about 4.35 and are capable for forming H-bonded complexes only with both carboxyl groups. However, as the molecule gets longer, the constant stabilizing effect of the complexed carboxyl groups represents a smaller and smaller percentage of the molecule. Consequently, pimelic acid is the longest dibasic acid to form a stoichiometric complex sufficiently stable for us to isolate and analyze.

Experimental Section

Preparation of Complexes. All of the complexes, except malonic acid–1-urea, were prepared by the following method. To 1 g of acid dissolved in 7 ml of methanol was added 16 ml of a urea–methanol solution (0.15 g of urea/ml of methanol). After cooling for a specified period of time, a white mass of crystalline solid precipitated. Oxalic and succinic acids formed complexes immediately at room temperature, while the following acids formed complexes at 25° but not instantaneously: glutaric acid (3 hr), adipic acid (48 hr), and pimelic acid (48 hr). The remaining compounds formed on cooling at 5°: adipic acid (10 hr) and pimelic acid (144 hr). The crystals were filtered with suction on a Hirsh funnel and dried in an Abderhalden at 56° (1 mm) for 8 hr over P_2O_5.

Preparation of Malonic Acid–Urea Complex. To 5 ml of a urea–methanol solution (0.15 g of urea/ml of methanol) was added 5 ml of a malonic acid solution (0.42 g of malonic acid/ml of methanol). The resulting solution was cooled to −25° for 30 days. The resulting precipitate was filtered cold and dried in the Abderhalden, as above.

Measurements. The uncorrected melting points reported in Table III were obtained using a Fisher-Johns melting point apparatus.

The differential thermal analysis data were corrected by running standards in the temperature range covered by this work. The measurements were all made at 20°/min and under an N_2 atmosphere. A Du Pont Model DTA was used.

The X-ray powder diffraction apparatus and procedures have been previously described.[3]

A description of the conductivity apparatus has previously been reported.[20]

Acknowledgment. The authors gratefully acknowledge the assistance of Dr. J. Varimbi in making the conductance measurements.

(20) D. Edelson and R. M. Fuoss, *J. Chem. Educ.*, **27**, 610 (1950)

The Chemiluminescent Reactions of Atomic Oxygen with Carbonyl Sulfide and Hydrogen Sulfide[1]

by A. Sharma, J. P. Padur, and P. Warneck

GCA Corporation, Bedford, Massachusetts 01730 *(Received July 15, 1966)*

The chemiluminescence intensity in the reactions O + COS and O + H_2S was studied in a flow system as a function of reaction time and reactant concentrations. In the initial stage of the reactions, the intensity increases linearly with time, the slope being proportional to the concentration of COS or H_2S and to the square of atomic oxygen concentration. A kinetic analysis shows that these results are consistent with the notion that the reaction responsible for the emission in both cases is reaction 7, O + SO → SO_2 + $h\nu$. From the relative intensities, the rate of SO formation in the H_2S reaction was found to be 1.85 times greater than that in the COS reaction. In the 400–800-μ pressure region studied here, reaction 7 was found to be pressure dependent. The associated emission rate was determined at 800 μ by comparison with the air–afterglow reactions as $k_7 = 5.7 \times 10^{-15}$ cc/molecule sec. The consumption of SO radicals by reactions other than reaction 7 is discussed together with intensity–time profiles for the later stages of the O + COS reaction.

Introduction

Mass spectrometric investigations by Liuti, Dondes, and Harteck[2a] and in this laboratory[2b] have shown that the first step in the reaction of oxygen atoms with carbonyl sulfide is the formation of SO radicals

$$O + COS \longrightarrow CO + SO \qquad (1)$$

The rate constant for this process has been determined.[2b] The reaction of oxygen atoms with hydrogen sulfide has also been found to produce SO radicals,[3] but the mechanism for this reaction is more complex than the first one. From mass spectrometer observations, Liuti, Dondes, and Harteck[3] suggest

$$O + H_2S \longrightarrow OH + SH \qquad (2)$$

$$O + OH \longrightarrow O_2 + H \qquad (3)$$

$$H + H_2S \longrightarrow H_2 + SH \qquad (4)$$

$$O + SH \longrightarrow SO + H \qquad (5)$$

where the last two reactions constitute a chain. The chain cannot be long since the ratio of SO production to H_2S consumption is only about 0.5. The reactant consumption ratio, O:H_2S, is only slightly greater than unity and a bimolecular rate law is obeyed. Liuti, *et al.*, have also considered the step

$$O + H_2S \longrightarrow H_2 + SO \qquad (6)$$

but ruled it out as a major contributing reaction on the basis of the isotope scrambling observed in the products when atomic oxygen was treated with a mixture of H_2S and D_2S.

The chemiluminescence associated with these reactions has also been investigated.[4-8] A comparative

(1) Supported by the National Aeronautics and Space Administration.

(2) (a) G. Liuti, S. Dondes, and P. Harteck, presented at the 152nd National Meeting of the American Chemical Society, New York, N. Y., 1963; (b) J. O. Sullivan and P. Warneck, *Ber. Bunsenges. Physik. Chem.*, **69**, 7 (1965).

(3) G. Luiti, S. Dondes, and P. Harteck, *J. Am. Chem. Soc.*, **88**, 3212 (1966).

(4) A. Sharma, J. P. Padur, and P. Warneck, *J. Chem. Phys.*, **43**, 2155 (1965).

(5) A. G. Gaydon, "The Spectroscopy of Flames," Chapman and Hall, Ltd., London, 1957.

(6) L. Hermann, J. Skrich, and M. Grenat, *J. Quant. Spectry. Radiative Transfer*, **2**, 215 (1962).

(7) C. J. Halstead and B. A. Thrush, *Nature*, **204**, 992 (1964).

(8) T. R. Rolfes, R. R. Reeves, and P. Harteck, *J. Phys. Chem.*, **69**, 849 (1965).

study[4] has shown that the emission spectra from the reactions of oxygen atoms with carbonyl sulfide, hydrogen sulfide, and carbon disulfide and the SO_2 afterglow spectrum are nearly identical, featuring similar intensity distributions. These observations suggest that the emitter and the process leading to the formation of the emitter are the same in all four cases of chemiluminescence. Evidence is mounting that the reaction responsible for the emission is

$$O + SO \longrightarrow SO_2 + h\nu \qquad (7)$$

as was originally suggested by Gaydon.[5] Hermann, *et al.*,[6] observed that the short-wavelength cutoff of the SO_2 afterglow near 2400 A coincides with the onset of the dissociation continuum in the SO_2 absorption spectrum. Halstead and Thrush[7] found that the SO_2 afterglow intensity is directly proportional to the product of oxygen atom and SO radical concentrations. Most recently, Rolfes, Reeves, and Harteck[8] studied the light emission from the reaction of O atoms with COS at low total pressures and compared it with the $O + NO_2$ reaction resulting in the air–afterglow emission involving radiative combination of atomic oxygen with nitric oxide. Their results indicate that at low pressures, the two reactions are analogous and that reaction 7 proceeds *via* a simple two-body combination mechanism.

The present work set out to derive additional evidence for the occurrence of reaction 7 by studying the time dependence of the chemiluminescent intensity in the reactions of atomic oxygen with COS and H_2S for various initial reactant concentrations. From such experiments, the rate of SO production associated with reactions 1 and 2 could be determined. The rate for reaction 7 was also determined. In addition, intensity profiles were obtained for the later stage of the reaction of oxygen atoms with COS to explore the possibilities of SO loss reactions.

Experimental Section

The conventional fast-flow system employed a cylindrical reactor of 1.9-cm i.d. Atomic oxygen was produced by microwave discharge. Either a 99:1 argon–oxygen mixture or pure oxygen was discharged. The second reactant entered the reactor *via* an inlet provided with several radially oriented holes. The inlet could be moved along the reactor axis by means of a friction drive. Observations were made downstream of the mixing point using a 1P28 photomultiplier tube connected to a Victoreen microammeter. The chemiluminescent emission was viewed through a quartz window mounted on the side of the reactor. A collimating slit system was interposed so that a spatial resolution of about 7 mm was obtained. The corresponding time resolution was 0.7 msec for linear flow rates around 10 m/sec.

Capillary flowmeters were used to measure volume flow rates of the individual gaseous components: argon, oxygen, carbonyl sulfide, and hydrogen sulfide. The concentrations of these constituents at the mixing point were determined from the fraction of the total flow rate and the prevailing total pressure measured with a McLeod gauge. The total pressure was held at 800 μ unless stated otherwise. Atomic oxygen concentrations were determined by gas titration, using the procedure described by Harteck, *et al.*[9] This is a two-step method. Oxygen atoms are first titrated with NO_2 to determine the maximum intensity corresponding to the titration half-point. The NO_2 is then replaced by NO to determine the NO flow corresponding to the same intensity value. The accuracy of this method is not as good as the direct titration with NO_2, but the complications due to the $2NO_2 \rightleftharpoons N_2O_4$ equilibrium in measuring NO_2 flow rates are avoided.

Results and Discussion

Dependence of Intensity on Time and Concentration. To investigate the time dependence of the chemiluminescence intensity, the photomultiplier currents were recorded as a function of the reactant inlet position and the reaction time was calculated from the distance between inlet position and observation point and the prevailing linear flow rate of the gas mixture in the reactor. The introduction of both COS and H_2S gave emission intensities whose increase with time was linear so long as the reaction times were reasonably short and the employed concentrations were moderate. Figure 1 demonstrates this observation for the reaction of oxygen atoms with COS in a plot of intensities *vs.* time for three initial COS concentrations. Only the highest COS concentration produces a nonlinear intensity–time dependence at reaction times greater than 8 msec. Figure 1 also shows that the intensities extrapolate to zero at a common origin beyond the point of reactant introduction. This is primarily due to the limited spatial resolution of the collimating slit system, although back diffusion can also contribute to the effect.

The linearity of intensity with time for short reaction times permits the use of the initial slope of the intensity–time profile as a measure of the reaction rate. The variation of the initial slope with oxygen atom concen-

(9) P. Harteck, R. R. Reeves, and G. G. Manella, *J. Chem. Phys.*, 32, 632 (1960).

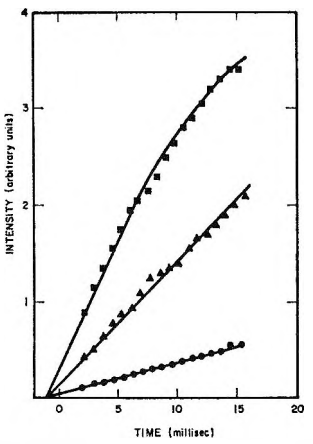

Figure 1. Chemiluminescence intensity *vs.* reaction time in the system O + COS for three initial COS pressures: ●, 7.6 μ; ▲, 20.6 μ; ■, 35 μ; the average O atomic pressure was 9.5 μ.

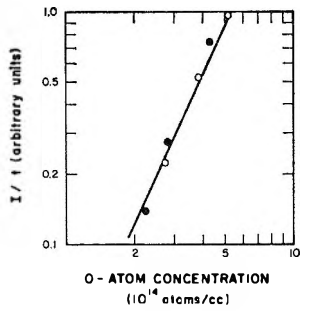

Figure 2. Initial slope of intensity–time profile as a function of O atom concentration for the systems: ●, O + COS; ○, O + H_2S.

tration for the reactions with either COS or H_2S is shown in Figure 2 using a logarithmic plot presentation. The concentrations of COS and H_2S, respectively, were held constant in these experiments. The intensities for the H_2S reaction actually were brighter than those shown in Figure 2 by about a factor of 2, but these data points were adjusted to fall onto the same line as the COS data, so that the equivalence of the dependence on oxygen atom concentration in both cases is more clearly demonstrated. The slope of the straight line in Figure 2 is $S = 2.08$, indicating that the chemiluminescence intensity is proportional to the square of the oxygen atom concentration.

Figure 3 shows, in a similar fashion, the variation of the initial slope of the intensity–time profile with COS concentration and H_2S concentration, respectively. Data from several runs performed on different days were used in this plot and corrected for the observed oxygen atom concentration, making use of the $(O)^2$ law. Here again, the data indicate a brighter chemi-

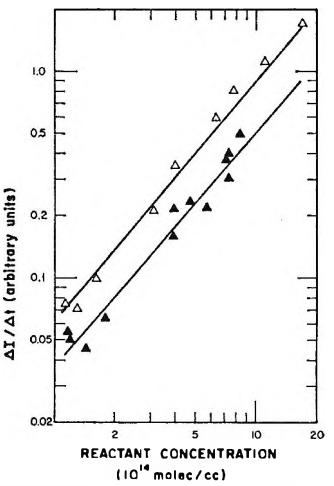

Figure 3. Initial slope of intensity–time profile as a function of COS (▲) and H_2S (△) concentrations.

luminescence for the H_2S reaction when compared with the emission from the reaction with COS. However, both plots yield straight lines with nearly identical slopes. The averaged value for the two slopes, $S = 1.1$, indicates a first-order concentration dependence for carbonyl sulfide and hydrogen sulfide.

In addition to these experiments in which the total pressure was 800 μ, a set of experiments was carried out for the O + COS reaction at a total pressure of only 330 μ. It was established that, at the lower pressure, the intensity dependence on reaction time and initial reactant concentrations was the same as that at 800 μ, but the over-all intensity was found to be about three times smaller. While this result indicates a pressure dependence of reaction 7 (in contrast to the observation by Rolfes, *et al.*[8]), it has not been possible to study this effect in detail because the flow rate could not be adequately controlled in the present apparatus. However, the measured rate of reaction 7 reported below also indicates a pressure effect and the discussion of this point will be deferred.

The results summarized in Figures 1–3 can be interpreted in terms of reaction 7 if it is taken into account that, for sufficiently short reaction times, the consumption of the initial reactants is still negligible. With this condition, the SO concentration is a linear function of reaction time, at least in the initial stage of the reaction where the destruction of SO radicals by reaction 7 or other follow-up reactions is not yet significant. For the reaction of atomic oxygen with carbonyl sulfide, the initial rate of SO radical production is

$$\frac{\Delta[SO]}{\Delta t} = k_1[O][COS]$$

and the increase of intensity, ΔI, produced by reaction 7 in the time interval, Δt, is correspondingly

$$\frac{\Delta I_1}{\Delta t} = k_7[O]\frac{\Delta[SO]}{\Delta t} = k_7k_1[O]^2[COS] \qquad (A)$$

The right-hand side of this equation represents the initial slope of the intensity–time profile. A similar expression is derived also for the reaction of oxygen atoms with hydrogen sulfide

$$\frac{\Delta I_2}{\Delta t} = k_7[O]\frac{\Delta[SO]}{\Delta t} = k_7k_x[O]^2[H_2S] \qquad (B)$$

where k_x denotes the rate constant for SO production in the over-all mechanism of the O + H_2S reaction. k_x is not to be identified with the rate constant for reaction 5, even though this reaction may be the principal generator of SO radicals. Instead, k_x is proportional to k_2 by a factor which depends on the number of chains involving reactions 4 and 5.

Equations A and B predict a linear relationship with initial COS or H_2S concentration and a quadratic one for the atomic oxygen concentration. This is in agreement with the relationship found in the present experiments. Alternatively, the present results can be used to demonstrate that the chemiluminescence intensity is proportional to the product of the concentrations of atomic oxygen and SO radicals, as required if reaction 7 is the predominant light-emitting process. These results, therefore, are in good agreement with the data reported by Halstead and Thrush[7] and by Rolfes, *et al.*[8] It is also significant that the analysis of the present data refers to the very early stage in the reactions because mechanisms can be suggested which lead to the observed concentration dependence but feature different chemiluminescent reactions. However, such mechanisms would require the buildup of an intermediate concentration (such as SO), so that initially the chemiluminescence intensity could not be a linear function of time. The observed concentration dependences and linearity with time taken together constitute strong evidence in favor of assigning reaction 7 as the principal chemiluminescent reaction.

Determination of the Rate Constant k_x. It has been noted above that the reaction of atomic oxygen with H_2S produces a brighter chemiluminescence than the reaction with COS under similar conditions. This fact can now be explained by the difference of the associated rates for SO formation. As eq A and B show, the ratio of the initial slopes obtained for the intensity–time profiles in the two reactions is given by

$$\frac{\Delta I_2/\Delta t}{\Delta I_1/\Delta t} = \frac{k_x}{k_1}\frac{[H_2S]}{[COS]}\frac{[O]_2^2}{[O]_1^2} \qquad (C)$$

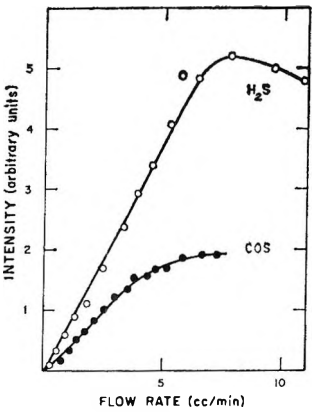

Figure 4. Intensity *vs* flow rate of COS (●) and H_2S (○) at constant O atom concentration.

where $[O]_1$ and $[O]_2$ refer to the initial oxygen atom concentrations prevailing in the COS and H_2S experiments, respectively. According to eq C, the ratio of the rate constants, k_x/k_1, can be obtained directly from Figure 2, where the data are corrected for the varying initial oxygen atom concentrations. Since the logarithmic plot in Figure 2 yields parallel lines, k_x/k_1 is represented simply by the ratio of the $\Delta I/\Delta t$ values for identical COS and H_2S concentrations. The averaged ratio of rate constants obtained from these data is $k_x/k_1 = 1.85$.

In the region where the dependence of intensity on reaction time is still linear, the right-hand side of eq C also represents the ratios of intensities at any time, t. An experiment was performed in which the chemiluminescence intensity close to the mixing point (at $t \approx 1$ msec) was recorded as a function of the COS and H_2S flow rates. The results, shown in Figure 4, are appropriately corrected for the difference of oxygen atom concentration in the two cases. Since for small reactant flows the reactant concentrations are proportional to the measured flow rates, the observed linear increase of intensities for moderate flow rates again verifies the first-order concentration dependence discussed above. The ratio of the slopes in Figure 4 is

$$\frac{\Delta I_2/\Delta[H_2S]}{\Delta I_1/\Delta[COS]} = \frac{k_x}{k_1} = 1.85$$

in excellent agreement with the average value found above. Applying the previously determined value for the rate constant of the O + COS reaction, $k_1 = 0.91 \times 10^{-14}$ cc/molecule sec,[2b] one obtains the absolute value $k_x = 1.70 \times 10^{-14}$ cc/molecule sec. It should be emphasized again that this rate constant refers only to that portion of the O + H_2S reaction which leads to the formation of the SO radicals.

The present value for k_x is smaller by a factor of 6 than that inferred from the mass spectrometric data reported by Liuti, *et al.*:[3] $k_x = 1 \times 10^{-13}$ cc/molecule sec. The resulting discrepancy is not easily explained, since the experimental conditions concerning flow rates, reactant concentrations, etc., in both investigations are rather similar. Thus, one would expect the same reaction mechanism to hold in both cases. One possibility for the disagreement may be due to a difference in the wall conditions. In the mechanism indicated in the Introduction, the production of SO proceeds rapidly only if the HS radicals are not easily removed at the wall. The enhancement of HS consumption at the wall by adverse conditions in the present experiments therefore may have reduced the SO production to the observed level.

Determination of the Rate Constant k_7. The rate constant associated with the reaction 7 was determined by comparing the light emission from the O + COS reaction with that produced in the air–afterglow reaction

$$O + NO \longrightarrow NO_2 + h\nu \qquad (8)$$

The relative spectral intensity distribution for reaction 7 was previously determined in this laboratory.[4] The emission lies mainly in the violet and ultraviolet portion of the spectrum. Fontijn, Meyer, and Schiff[10] have determined the spectral intensity distribution for reaction 8 and have shown that it is centered in the red and near infrared. Both emissions overlap in the 3800–5200-A wavelength region. An interference filter was therefore employed in the comparison experiment to limit the radiation seen by the photomultiplier to the region of overlap. The filter featured a transmission maximum near 4100 A and a band width of 75 A. The fraction of radiation registered by the photomultiplier–filter combination compared to the total integrated emission from each reaction was determined from the known spectral response of the phototube, the transmission characteristics of the filter, and the relative spectral intensity distributions for both reactions. The evaluation of the comparison experiment requires only the ratio of the two fractions, which was found to be $f_8/f_7 = 0.029$, where the subscripts refer to reactions 8 and 7, respectively.

The introduction of nitric oxide to the gas flow containing oxygen atoms results in an emission intensity which is time independent, whereas it has been shown above that the introduction of carbonyl sulfide produces an intensity which increases linearly with time. In the first case, the intensity is given by

$$I_8 = k_8[O][NO]$$

and in the second case by eq A. With the provision that the oxygen atom concentration remains constant the combination of both equations yields

$$k_7 = \frac{k_8[NO]\Delta I_1/\Delta t}{k_1[O][COS]I_8} \qquad (D)$$

or when the total intensities, I_1 and I_8, are replaced by the equivalent photomultiplier currents, i_1 and i_8

$$k_7 = \frac{f_8 k_8[NO]\Delta i_1/\Delta t}{f_7 k_1[O][COS]i_8}$$

The following individual rate constants were employed in the evaluation of eq D: $k_1 = 0.91 \times 10^{-14}$ cc/molecule sec, given by Sullivan and Warneck,[2b] and $k_4 = 6.4 \times 10^{-17}$ cc/molecule sec, determined by Fontijn, Meyer, and Schiff.[10]

Figure 5 shows the results of the comparison experiments. The photomultiplier currents registered upon admixture of either NO or COS to a discharged argon–oxygen mixture are plotted as a function of reaction time. From the slope of the current–time profile for the O–COS reaction, one obtains $\Delta i_1/\Delta t = 330 \times 10^{-7}$ A/sec, whereas $i_8 = 0.085 \times 10^{-7}$ A. The prevalent concentrations of nitric oxide, carbonyl sulfide, and atomic oxygen are given in the legend. With these data, eq D yields the rate constant associated with reaction 7: $k_7 = 5.7 \times 10^{-15}$ cc/molecule sec. This value is about 8 times greater than the rate constant estimate of Rolfes, Reeves, and Harteck[8] for pressures around 10 μ. The discrepancy is greater than the combined experimental error in both determinations. The fact that the present result, obtained at a higher pressure, is much larger indicates again a pres-

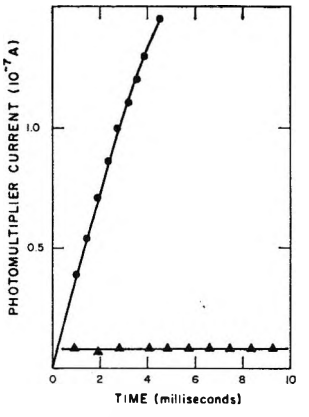

Figure 5. Intensity–time profile for O + COS (●) and O + NO (▲). Concentrations in molecules per cubic centimeter are $[COS]_0 = 4.2 \times 10^{14}$, $[NO]_0 = 5 \times 10^{14}$, and $[O]_0 = 1.65 \times 10^{14}$.

(10) A. Fontijn, C. B. Meyer, and H. I. Schiff, *J. Chem. Phys.*, **40**, 64 (1964).

sure effect, thereby substantiating the data presented earlier in this paper. However, the increase in the emission rate is insufficient for a reaction that occurs solely by third-body association. Apparently, reaction 7 can proceed both as a two-body and as a three-body association reaction, with the former being predominant at lower pressures and the latter becoming important as the pressure is increased. This interpretation is consistent with the results by Rolfes, *et al.*,[8] Halstead and Thrush,[9,11] and the present data. Thus, reaction 7 should proceed mainly as a two-body reaction at pressures below 100 μ, whereas at 800 μ pressure, the predominant reaction would be

$$O + SO + M \longrightarrow M + SO_2 + h\nu \qquad (7M)$$

From the above data, one obtains the corresponding third-body rate constant: $k_{7M} = k_7/[M] = 2.2 \times 10^{-31}$ cc²/molecule² sec. This value is only one-fourth as large as the over-all third-body association rate constant found by Halstead and Thrush[11] for the reaction

$$O + SO + M \longrightarrow SO_2 + M \qquad (9)$$

which presumably includes reaction 7M and was studied in SO_2 afterglow experiments. Most significant for the O + COS reaction is the result that, under the present experimental conditions, reactions 7 and 9 combined are as rapid as the precursor reaction 1, so that these reactions are effective SO loss processes. This aspect of the reaction will now be discussed.

SO Radical Consumption. The importance of the SO losses in the O + COS reaction has been recognized previously. Rolfes, *et al.*,[8] considered the reactions

$$SO + SO \longrightarrow SO_2 + S \qquad (10)$$

$$SO + O_2 \longrightarrow SO_2 + O \qquad (11)$$

and the occurrence of reaction 10 was suggested also by the mass spectrometer observations of Sullivan and Warneck.[2b] On the other hand, Halstead and Thrush[11] argued for an alternative explanation of these results in terms of reaction 9 in combination with a reaction of SO with COS. While the present experiments could provide no detailed information on the individual SO loss reactions, it was of interest to investigate the intensity–time profiles in the later stage of the O + COS reaction for comparison with profiles calculated on the basis that reaction 9 is the major SO loss reaction. The rate coefficient $k_9 = 8.3 \times 10^{-31}$ cc/molecule sec given by Halstead and Thrush was used in the calculations.

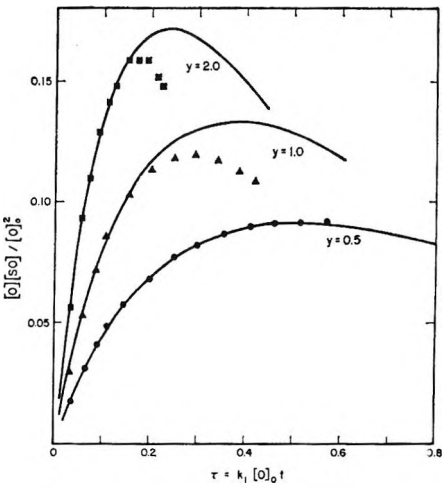

Figure 6. Intensity–time profile for the system O + COS for different initial concentration ratios $y = [COS]_0/[O]_0$. Experimental data: ●, 0.57; ▲, 0.93; ■, 1.9. Calculated results are shown by solid lines.

The results of this experiment are shown in Figure 6. Intensities were calculated by numerical integration of the pertinent differential equations and are plotted in the form $[SO][O]/[O]_0^2$ *vs.* the reaction parameter $\tau = k_1[O]_0 t$ for several initial reactant concentration ratios $y = [COS]_0/[O]_0$. The experimental data points were obtained with 650 μ of pure oxygen instead of the argon–oxygen mixtures, so that a higher initial oxygen–atom concentration could be realized. A common scaling factor was applied to the experimental intensity data to facilitate the comparison.

Figure 6 demonstrates a fairly good agreement between the calculated and observed intensity profile for $y = 0.5$. Marked deviations occur in the later stage of the reaction for the higher initial [COS]/[O] concentration ratios, thus indicating the consumption of SO by reactions occurring in addition to reaction 9. The observed increase in the deviations with increasing COS concentration points to the importance of either reaction 10 or the reaction of SO with COS as suggested by Halstead and Thrush.[11] Reaction 11 would not explain the observed behavior. These results, therefore, lead to the conclusion that, despite its comparatively fast rate, reaction 9 alone is insufficient to explain the observed intensity profiles. It should be noted, however, that the fast rate deduced previously[2b] for reaction 10 cannot be upheld.

(11) C. J. Halstead and B. A. Thrush, *Photochem. Photobiol.*, **4**, 1009 (1965).

The Position of Protonation of 1,1,3,3-Tetramethyl-2-nitroguanidine in Strong Acids

by E. Price, R. D. Barefoot, A. S. Tompa, and J. U. Lowe, Jr.

Research and Development Department, Naval Ordnance Station, Indian Head, Maryland
(Received July 18, 1966)

Evidence is presented to establish that protonation of 1,1,3,3-tetramethyl-2-nitroguanidine in strong acids occurs primarily at the dimethylamino site. This conclusion is based on the following nmr data: (1) in 37.5% HCl and at temperatures above −15°, one singlet is observed for the methyl groups; (2) for the same solutions and at temperatures below −15°, a doublet is observed for the methyl protons; (3) in 38% DCl in D_2O and at −20 and −35°, no doublet is observed for the methyl protons; (4) the addition of H_2O to tetramethylnitroguanidine in 38% DCl in D_2O at these temperatures causes the methyl protons to split into a doublet. The splitting of the N–CH_3 resonance into a doublet is attributed to spin–spin coupling of the adjacent N–H proton with the methyl protons due to protonation at the dimethylamino site.

The structure of certain nitroguanidines (I) and their conjugate acids has been discussed and ultraviolet absorption spectra data have been presented to support protonation at the nitrimino site, a[1] (R = methyl or

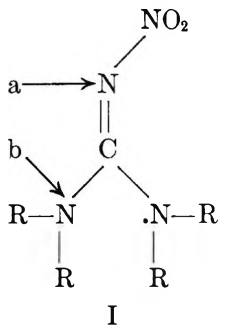

I

hydrogen). This conclusion was drawn from the following facts: (1) in all the nitroguanidines studied the presence of a strong absorption band at 2600–2700 A has been observed, the exact position and intensity of which depends on the substituent groups; (2) the absorption spectrum of nitramide (H_2NNO_2) is quite different with a broad band at 2250 A (ε 5900 in water);[2] (3) the absorption band characteristic of nitramide appears in the spectra of nitroguanidines in strong acidic solutions and reaches maximum intensity in 40–50% sulfuric acid corresponding to complete conversion of the nitroguanidine into its conjugate acid. It has been reported that the change is accompanied by the disappearance of the absorption band characteristic of the free base, nitroguanidine.[1] In our laboratories, preliminary studies of the absorption spectra of 1,1,3,3-tetramethyl-2-nitroguanidine (TMNG) in various nitric acid solutions are in agreement with the latter fact. However, we offer evidence to show that protonation of nitroguanidines does not occur primarily at the nitrimino site, a, but rather at the amino site, b.

From nuclear magnetic resonance (nmr) measurements, the following observations have been obtained: (1) for 1,1,3,3-tetramethyl-2-nitroguanidine in 30.5% HNO_3 or 37.5% HCl and at temperatures above −15°, a singlet is observed for the methyl groups; (2) for the same solutions and at temperatures below −15°, a doublet is observed for the methyl protons. It is recognized that these facts may be interpreted in terms of one of the following explanations. The existence of the doublet below −15° may indicate (1) that hindered rotation produces nonequivalent methyl

(1) T. G. Bonner and J. C. Lockhart, *J. Chem. Soc.*, 3858 (1958).
(2) R. N. Jones and G. D. Thorn, *Can. J. Res.*, B27, 828 (1949).

groups, (2) that the methyl groups are spin–spin coupled with the proton that adds to the amino site, b, and that proton exchange is rapid at temperatures above −15°, or (3) that protonation is occurring at both the nitrimino and amino sites. We believe that the second explanation is more in agreement with all the facts.

From our knowledge of the base-strengthening effects of methyl groups in guanidines[3] and the base-weakening effect of a nitro group, one would expect protonation of 1,1,3,3-tetramethyl-2-nitroguanidine to occur at the dimethylamino site, b, rather than the nitrimino site, a.

Once protonation occurs at the dimethylamino site, this group $[(CH_3)_2\overset{+}{N}H-]$ acts inductively as an electron-withdrawing group and would also make the nitrimino site, a, even less basic.[4]

It has been observed that the character of the N–CH_3 resonances of aqueous solutions of methyl derivatives of nitroguanidine is dependent on the acidity of the medium (Table I). For 1,1,3,3-tetramethyl-2-nitroguanidine the methyl resonance shifts approximately 16 cps downfield in going from 0 to 70 wt % nitric acid. The chemical shifts observed for the methyl protons in these media are largely attributed to deshielding caused by the positive charge developed at the amino nitrogen.

A more substantial demonstration of protonation at the amino site is indicated as follows. For TMNG one singlet resonance at 183.9 cps is observed for the methyl protons in water, while in 37.5% by weight hydrochloric acid one singlet is observed at 196.6 cps (reference, internal sodium 2,2-dimethyl-2-silapentane-5-sulfonate).[5] In the latter solution, it has been observed that the N–CH_3 resonance splits into a doublet in the temperature range 8 to −30°. This doublet is partially resolved with a separation ranging from 1.7 to 3.0 cps at 8 to −30°, respectively. A partially resolved doublet is also observed in 23% hydrochloric acid and in 30–70% nitric acid solutions at temperatures below −15°. The splitting of the N–CH_3 resonance into a doublet is attributed to spin–spin coupling of the adjacent N–H proton with methyl protons owing to protonation at the dimethylamino site. This is confirmed (Figure 1) by the absence of the doublet in 38% DCl in D_2O solutions of TMNG at −20 and −35°.[6] The addition of H_2O to TMNG in 38% DCl in D_2O at these temperatures causes the methyl protons to split into a doublet. The formation of a singlet for the N–CH_3 resonance at temperatures above −15° is attributed to rapid proton exchange between the amino sites and the solvent.

We believe that protonation of 1,1-dimethyl-2-nitroguanidine (DMNG) occurs mainly at the primary amino site rather than the tertiary amino site because the former is a more basic site.[7] No doublet for the methyl resonance for the dimethylamino group in DMNG in 70% HNO_3 was observed at temperatures as low as −35°. Under no conditions in aqueous media could the N–H protons of methylnitroguanidines

Table I: Nmr Chemical Shifts at 60 Mc/sec for Methylnitroguanidines in Aqueous Acids at Room Temperature

Wt % of HNO_3	CH_3 resonance[a]		
	TMNG[b]	DMNG[c]	MNG[d]
70.0	199.8	204.1	194.8
56.9	197.0	201.1	192.4
46.7	...	...	189.2
45.2	196.5	198.8	...
39.4	195.9	...	...
37.9	195.4	...	188.0
36.6	...	195.8	...
30.5	194.5	...	183.4
23.1	193.0	191.3	182.1
12.6	...	188.3	179.0
10.5	188.5	...	...
6.4	186.1	...	...
5.2	...	177.7	...
4.9	...	...	177.7
3.2	184.8	...	...
1.4	183.9	...	...
37.5% HCl	196.6	200	188.2
CH_3COOH	183.9	...	177.0
H_2O	183.9	...	...

[a] Cyclies per second downfield from sodium 2,2-dimethyl-2-silapentane-5-sulfonate used as internal standard. The concentration of the nitroguanidines was ~0.04 *m*. [b] 1,1,3,3-Tetramethyl-2-nitroguanidine. [c] 1,1-Dimethyl-2-nitroguanidine. [d] 1-Methyl-2-nitroguanidine.

(3) S. J. Angyal and W. K. Warburton, *J. Chem. Soc.*, 2492 (1951).

(4) The presence of any diprotonated form of TMNG in strong acids is unlikely in our experiments. It follows from the order of magnitude of the pK_a for the guanidinium cation (pK_a ~−11) that guanidine does not form a doubly charged cation to any considerable extent in acids weaker than 99% H_2SO_4. By analogy the weakly basic TMNG is not expected to become doubly charged; *cf.*, G. Williams and M. L. Hardy, *ibid.*, 2560 (1953).

(5) Two doublets (J = 5.00 cps) at 179 and 188.5 cps have been observed for N,N′-dimethylacetamidinium chloride solutions in 14% H_2SO_4 and in 60% D_2SO_4 at 184.0 and 194.0 cps, respectively: R. C. Neuman, Jr., and A. S. Hammond, *J. Phys. Chem.*, 67, 1659 (1963).

(6) The effect of the deuterium atom on the methyl proton spectra is to cause the methyl proton line to split into three lines by spin–spin coupling to the deuterium nuclei. Since the coupling is small, the observed effect is to broaden the methyl proton resonance line into an unresolved multiplet.

(7) H. C. Brown, *J. Am. Chem. Soc.*, 67, 378 (1945). For the behavior of DMNG in 70–90% H_2SO_4, see J. C. Lockhart, *J. Chem. Soc.*, 1174 (1966).

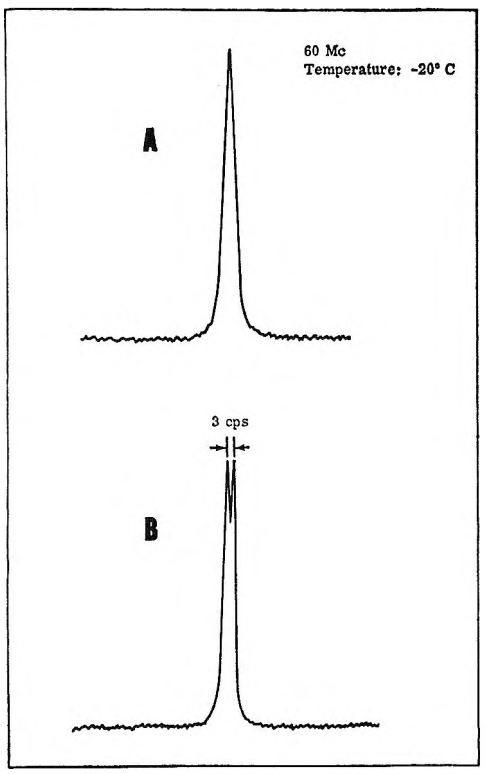

Figure 1. Nuclear magnetic resonance spectra of N-methyl protons in TMNQ; A, 38% DCl in D_2O; B, 26.7% DCl–HCl in D_2O–H_2O.

be observed because the solvent resonance obscures the N–H signal.

Experimental Section

DCl (38%) (99% isotopic purity) in D_2O (99.5% purity) was obtained from Volk Radiochemical Co.

1,1,3,3-Tetramethyl-2-nitroguanidine (TMNQ). TMNQ was prepared by the mixed acid nitration of 1,1,3,3-tetramethylguanidine (Eastman White Label) by the procedure of Kirkwood and Wright.[8] Several recrystallizations from absolute ethanol–ethyl acetate gave a sample whose melting point was 84.5°.[9] *Anal.* Calcd for $C_5H_{12}N_4O_2$: C, 37.49; H, 7.55; N, 34.99. Found: C, 38.02; H, 7.73; N, 34.05. TMNQ was dried for 20 hr at 56° in an Abderhalden just before the solutions were prepared for deuterium experiments.

Methylnitroguanidine (mp 161.8–162°; lit.[10] 160–161°) and 1,1-dimethyl-2-nitroguanidine (mp 197–198°; lit.[10] 193.5–195°) were conveniently prepared from ethanolic solutions of 2-methyl-1-nitro-2-thiopseudourea with methyl- and dimethylamines, respectively. Analytically pure samples were obtained by repeated crystallization of newly synthesized methylnitroguanidines from absolute ethanol–ethyl acetate.

1,1,3,3-Tetramethyl-2-nitroguanidine was dissolved in 38% DCl in D_2O to give a 1.92 *M* solution. The nmr spectrum of this solution was then taken immediately at −35 and −20°. Afterward, the 1.92 *M* solution was diluted with water to give a 1.28 *M* solution of 1,1,3,3-tetramethyl-2-nitroguanidine in 26.7% DCl HCl in D_2O–H_2O mixture. The nmr spectrum of this solution was also recorded immediately.

The nmr measurements were performed with a Varian DA-60-El spectrometer equipped with a superstabilizer. The chemical shifts were measured with a precision of 0.05 cps by placing side bands on both sides of the signal. The side-band frequency was measured with a Hewlett-Packard Model 522-B electronic frequency counter. The temperature was kept constant to within ±0.2° by the use of a Leeds and Northrup Azar H recorder–controller. The temperature was varied with dry nitrogen gas and the use of a Varian 4340 variable-temperature probe assembly and a Model V-4331-THR spinning sample dewar probe insert.

Acknowledgment. We gratefully acknowledge support of this work by the Foundational Research Program of the Naval Ordnance Systems Command.

(8) M. W. Kirkwood and G. F. Wright, *Can. J. Chem.*, **35**, 527 (1957).

(9) All melting points were taken on a micro Kofler hot stage.

(10) T. G. Bonner and J. C. Lockhart, *J. Chem. Soc.*, 3852 (1958).

Analysis of the High-Pressure Region of Certain Sorption Isotherms

by Akira Takizawa

Faculty of Textile Technology, Tokyo Institute of Technology, Tokyo, Japan *(Received May 9, 1966)*

In order to describe the high vapor pressure region of the sorption isotherm of polar polymer–polar small molecule systems, theoretical investigations of the statistical thermodynamics of solution accompanied by adsorption were made. The result was applied to the experimental isotherms of protein–water and cellulose nitrate–acetone systems. The theory of solution accompanied by adsorption seems to be adequate for the polymer–solvent systems, because it not only gives a constant interaction parameter, χ_1, for the polymer–solvent systems over the whole relative pressure range, but it also yields an interaction parameter which agrees with that obtained by another method.

I. Introduction

In order to develop a new concept that will be able to describe the high-pressure region of the sorption isotherm of a polar polymer–polar small molecule system, several possibilities were first examined for protein–water systems.

Brunauer, Emmett, and Teller's theory[1] can describe the experimental isotherm of an insulin–water system at 25°[2] with the aid of a restricted number (five to eight) of adsorbed layers. It is, however, only one among several possible descriptions and lacks concrete physical meaning.

The generalized adsorption equation that is obtained from a fundamental statistical treatment is expressed as[3,4]

$$A/A_m = x\phi'/\phi$$

where $\phi = 1 + C_1x + C_1C_2x^2 + C_1C_2C_3x^3 + \ldots$ and C_i is the ratio of partition function for the ith layer to that for the liquid state. By setting up the experimental equation that might describe the equilibrium sorption isotherm of an insulin–water system over the whole pressure range and comparing it with the above theoretical equation C_i values are determined. The result shows that some of the C_i values are negative. Because partition functions cannot be negative, the result means that the "adsorption" theory cannot explain the isotherm over the whole range of relative vapor pressure.

Rowen and Simha's treatment[5] based on the Flory–Huggins' "solution" theory was examined for insulin–water (25°) and egg albumin–water (26.5°) systems.[6] The interaction parameter, χ_1, increased with the relative pressure or volume fraction of water and the initial stage of the sorption showed a large affinity (low χ_1) between protein and water. This tendency means that a high interaction energy by adsorption is evolved at the initial stage of mixing and this exothermic tendency gradually diminishes as the adsorption mechanism decreases. Because of the strong interactions between polar sites of the polymer and small polar molecules, small molecules adsorbed at the initial stage of sorption must be far from a randomly mixed state even at high vapor pressures.

Therefore, it is most desirable to develop the statistical thermodynamics of solution accompanied by adsorption for the description of these systems.

The results of the theoretical investigation will be examined by the experimental isotherms of protein–water and cellulose nitrate–acetone systems.

II. Theory

In the following, we shall assume that small molecules are sorbed to polymer molecules in two different ways: one is the Langmuir-type adsorption with strong inter-

(1) S. Brunauer, "Adsorption of Gases and Vapors," Princeton University Press, Princeton, N. J., 1943, p 154.

(2) W. Heller and A. Takizawa, unpublished work.

(3) T. L. Hill, *J. Chem. Phys.*, **14**, 263, 272 (1946).

(4) M. Dole, *ibid.*, **16**, 25 (1948).

(5) J. W. Rowen and R. Simha, *J. Phys. Colloid Chem.*, **53**, 921 (1949).

(6) W. Heller and A. Fogiel, *J. Phys. Chem.*, **70**, 2039 (1966).

action and the other is the Flory–Huggins type of random mixing of small molecules with polymer segments.

As has been customarily done with the statistical mechanical treatment of adsorption,[3,7,8] the sorption isotherm in the present paper is derived by setting up the partition function of the two-component system, assuming that adsorption is accompanied by solution. Furthermore, since the present case is essentially the two-component theory, the result was examined by applying the Gibbs–Duhem equation to the derived chemical potentials of vapor and polymer.

We suppose that there are PB polar sites per P polymer molecule, that X of these sites are occupied by adsorbed molecules, and that $(A - X)$ small molecules are mixed randomly with polymer segments PM. P is the number of polymer molecules and M is the number of segments per molecule.

(1) Theory I. The Case Where $B \ll M$ or $X \ll PM + (A - X)$. There are $(PB)!/(PB - X)!X!$ distinguishable ways that X identical molecules may be distributed among PB sites. When adsorbed molecules are characterized by a potential energy, $-E_s$, the partition function for an adsorbed molecule is expressed as $q_s \exp(E_s/kT)$, where q_s is related to the internal degrees of freedom. Furthermore, we designate q_m and q_n as the partition functions for the perturbed and unperturbed adsorption sites, respectively. The partition function of the surface phase including X molecules adsorbed on the PB sites is then

$$Q_s = \frac{(PB)!}{(PB - X)!X!}[q_s \exp(E_s/kT)]^X q_m^{(PB-X)} q_n^X \quad (1)$$

The partition function of polymer solution including $(A - X)$ small molecules and PM polymer segments is[9]

$$Q_L = (q_1 e^{-Cw_{11}/2kT})^{A-X}(q_p e^{-Cw_{22}/2kT})^{PM} \times \prod_{i=0}^{P-1}(A - X + PM - Mi)^M \times \frac{[(C - 1)/(A - X + PM)]^{M-1}}{P!} e^{C(A-X+PM)v_1v_2w/2kT} \quad (2)$$

where q_1 is the internal partition function of mixed small molecule, q_p is the internal partition function of mixed polymer segment, $w = w_{11} + w_{22} - 2w_{12}$, w_{12} is the interaction potential energy of 1 (small molecule)–2 (polymer segment) interaction; w_{11} is the interaction potential energy of 1–1 interaction, w_{22} is the interaction potential energy of 2–2 interaction, C is the coordination number, v_1 is the volume fraction of small molecule $= (A - X)/(A - X + PM)$, and v_2 is the volume fraction of polymer $= PM/(A - X + PM)$.

The complete partition function of the system is then

$$Q = \sum_{X=1}^{PB} Q_s Q_L \quad (3)$$

where Q_s and Q_L are given by eq 1 and 2, respectively. Using the maximum-term method,[10] the X value that gives the maximum term in the sum of eq 3 is given by

$$\ln [(PB - X)/] + \ln K + \ln v_1 + (1 - (1/M))v_2 - (Cw/2kT)v_2^2 = 0 \quad (4)$$

where

$$K = \frac{q_s \exp(E_s/kT)}{q_1 \exp(-Cw_1/2kT)} \frac{q_n}{q_m}$$

The chemical potential of the small molecule in the system is

$$\mu_A/kT = -\partial \ln Q_s Q_L/\partial A = -\ln q_1 e^{-Cw_{11}/2kT} + \ln v_1 + v_2(1 - (1/M)) - (Cw/2kT)v_2^2 \quad (5)$$

where X in v_1 and v_2 is to be determined by eq 4.

For the gas phase, the chemical potential is given as

$$\mu_G/kT = (\alpha/kT) + \ln p \quad (6)$$

where α is a constant and p is the vapor pressure.

Equating μ_A and μ_G and putting $p = p_0$, $v_1 = 1$, and $v_2 = 0$ for the pure liquid, we have

$$\ln x = \ln v_1 + v_2(1 - (1/M)) - (Cw/2kT)v_2^2 \quad (7)$$

where x is the relative vapor pressure p/p_0. When we put $-Cw/2kT = \chi_1$, the next Flory–Huggins equation is obtained.

$$\ln x = \ln v_1 + v_2(1 - (1/M)) + \chi_1 v_2^2 \quad (7')$$

Substituting eq 7 or 7′ into eq 4

$$\ln [(PB - X)/X] + \ln K + \ln x = 0$$

or

$$X = PBKx/(1 + Kx) \quad (8)$$

Equation 8 is the usual Langmuir isotherm.

Substituting eq 8 into eq 7′ and eliminating X

$$\ln x = \ln \frac{A - \{PBKx/(1 + Kx)\}}{A + PM - \{PBKx/(1 + Kx)\}} + \frac{PM}{A + PM - \{PBKx/(1 + Kx)\}} + \chi_1\left[\frac{PM}{A + PM - \{PBKx/(1 + Kx)\}}\right]^2 \quad (9)$$

(7) A. B. D. Cassie, *Trans. Faraday Soc.*, **41**, 450 (1945).

(8) W. L. Peticolas, *J. Chem. Phys.*, **27**, 436 (1957).

Equation 9 gives the relationship between A (sorbed small molecules per P polymer molecules) and relative vapor pressure, x.

The chemical potential of the polymer is calculated as

$$\mu_P/kT = -\partial \ln Q_s Q_L/\partial P$$

$$= B \ln \frac{PB - X}{PB} + \ln v_2 - (M - 1)v_1 + \chi_1 M v_1^2 - \ln K' \quad (10)$$

where

$$K' = q_m{}^B (q_p e^{-Cw_{22}/2kT})^M M \left(\frac{C - 1}{e}\right)^{M-1}$$

and X in v_1 and v_2 is to be obtained by eq 4.

It can be seen that eq 5 and 10 satisfy the Gibbs-Duhem equation

$$A d\mu_A + P d\mu_P = 0 \quad (11)$$

by using eq 8 for the first term of eq 10 and by expressing μ_A and μ_P as functions of v_2.

(2) Theory II. The Case Where B or X Is of Comparable Order with M or PM + (A − X), Respectively. In this case we cannot neglect the effect of combined X molecules on the dimension of the polymer molecule. In the following, we assume that X molecules adsorbed to strong polar sites of polymer molecules participate as parts of polymer segments. Thus the volume fractions are defined as v_1', volume fraction of small molecule = $(A - X)/(A + PM)$, and v_2', volume fraction of polymer segment (including adsorbed small molecules) = $(X + PM)/(A + PM)$.

The partition function for the X molecules is the same as eq 1. The partition function of the polymer solution in this case is

$$Q_L = (q_s e^{(E_s/kT) - (Cw_{11}/2kT)})^X (q_1 e^{-Cw_{11}/2kT})^{A-X} \times (q_p e^{-Cw_{22}/2kT})^{PM} \times \prod_{i=0}^{P-1} [A + PM - ((X/P) + M)i]^{(X/P)+M} \times \frac{\left(\frac{C - 1}{A + PM}\right)^{(X/P)+M-1}}{P!} \times e^{(Cw/2kT)[APM/(A+PM)]} \quad (12)^{11}$$

The X value which corresponds to the maximum term in the complete partition function of the system eq 3, where Q_s and Q_L are given by eq 1 and 12, respectively, is

$$\ln [(PB - X)/X] + \ln v_1' + \ln K = 0 \quad (13)$$

where

$$K = [q_s \exp(E_s/kT)]^2 (C - 1) q_n/(q_1 q_m)$$

The chemical potential, μ_A, of the small molecules in the system can be calculated by the same procedure as eq 5. Equating μ_A and μ_G of eq 6

$$-\ln (q_1 e^{-Cw_{11}/2kT}) + \ln v_1' + v_2' - [v_2' - (X/(A + PM))]/M - (Cw/2kT)[v_2' - (X/(A + PM))]^2 = (\alpha/kT) + \ln p \quad (14)$$

For the pure liquid, v_1', v_2', and A become 1, 0, and ∞, respectively.

Hence

$$\ln x = \ln v_1' + v_2' - \left(v_2' - \frac{X}{A + PM}\right)\frac{1}{M} - \frac{Cw}{2kT}\left(v_2' - \frac{X}{A + PM}\right)^2 \equiv \ln v_1' + v_2' - (v_{20}'/M) + \chi_1 v_{20}'^2 \quad (15)$$

where $v_{20}' = v_2' - (X/(A + PM))$ is the true volume fraction of polymer (excluding the adsorbed small molecules) of the entire system.

From eq 13 and 15

$$\frac{PB - X}{X} Kx = e^{v_2' - (v_{20}'/M) + \chi_1 v_{20}'^2} \quad (16)$$

In the region of relatively low x, v_2' and v_{20}' of the right-hand side of eq 16 approach unity. Then, neglecting the effect of the v_{20}'/M term and putting $K/e^{1+\chi_1} = K'$

$$\lim_{p \to 0} X = \frac{PBK'x}{1 + K'x} \quad (17)$$

Equation 17 has the same form as the Langmuir equation.

For the whole pressure range, we have to calculate an x *vs.* A relationship by eliminating X using eq 15 and 16.

(9) T. L. Hill, "An Introduction to Statistical Thermodynamics," Addison-Wesley Publishing Co., Inc., Reading, Mass., 1960, pp 372, 405.

(10) T. L. Hill, see ref 9, p 478

(11) In the derivation of eq 12, average interaction potential energies are assumed as

$$w_{12'} = \frac{w_{12}PM + w_{11}X}{PM + X}$$

$$w_{2'2'} = \frac{w_{22}(PM)^2 + w_{12}2PM + w_{11}X^2}{(PM + X)^2}$$

where subscript 2′ means polymer segment including adsorbed small molecules.

The chemical potential of the polymer in this case is calculated as

$$\mu_P/kT = -\partial \ln Q_s Q_L/\partial P$$
$$= B \ln \frac{PB - X}{PB} + \ln v_2' - (M - 1) + Mv_2' - v_{20}' - \ln (v_2'/v_{20}') + \chi_1 M(1 - v_{20}')^2 - \ln K' \quad (18)$$

where K' is equal to that of eq 10 and X in v_1', v_2', and v_{20}' is to be obtained by eq 13.

In this case, too, it may be seen that the μ_A (left-hand side of eq 14) and the μ_P of eq 18 satisfy the Gibbs–Duhem equation (eq 11) by using eq 16 for the first term of eq 18 and by expressing both μ_A and μ_P as functions of v_2'.[12]

III. Application of the Present Theory to Experimental Isotherms

(*1*) *Insulin–Water System.* The experimental isotherm at 25°[2] (A moles sorbed/100 g of insulin *vs.* relative vapor pressure x relation) is shown in Figure 1 by open circles. (Experimental details were given in a former paper.[6])

For the determination of the Langmuir-type isotherm of eq 8, we assume X (adsorbed) is nearly equal to A in the low-pressure region because of the large adsorption energy. Applying the least-square method to the six points up to $x = 0.05136$ of the x/X *vs.* x relation

$$x/X = 0.1579 + 0.4835x$$

X values calculated by this equation correspond to the Langmuir-type adsorption. Subtraction of the X value from A to each x gives the water molecules that are randomly mixed with polymer segments according to eq 7. Transforming the unit of $(A - X)$ from moles per 100 g of insulin to centimeters per g of insulin and using the specific volume of insulin, 0.73513 cc/g,[13] one can calculate the volume fraction of freely mixed water molecules, v_1.

Then, by using eq 7′ and neglecting the term $1/M$, values of χ_1 at various x value are obtained.

The result of calculation is shown in Figure 1 by closed circles. χ_1 values obtained by this theory show constancy over the wide range of x. The average value of χ_1 is 1.063. Using this value, the calculated adsorption isotherm is also included in Figure 1. The theoretical curve explains the experimental data quite satisfactorily.

(*2*) *Egg Albumin–Water System.* The experimental isotherm at 26.5°[6] is shown in Figure 2 by open circles. By the same procedure as in the case of insulin, χ_1 values at various x values are calculated and are shown in Figure 2 by closed circles. In this case, too, the result shows almost constant χ_1 values (average 1.087) over the wide range of x.

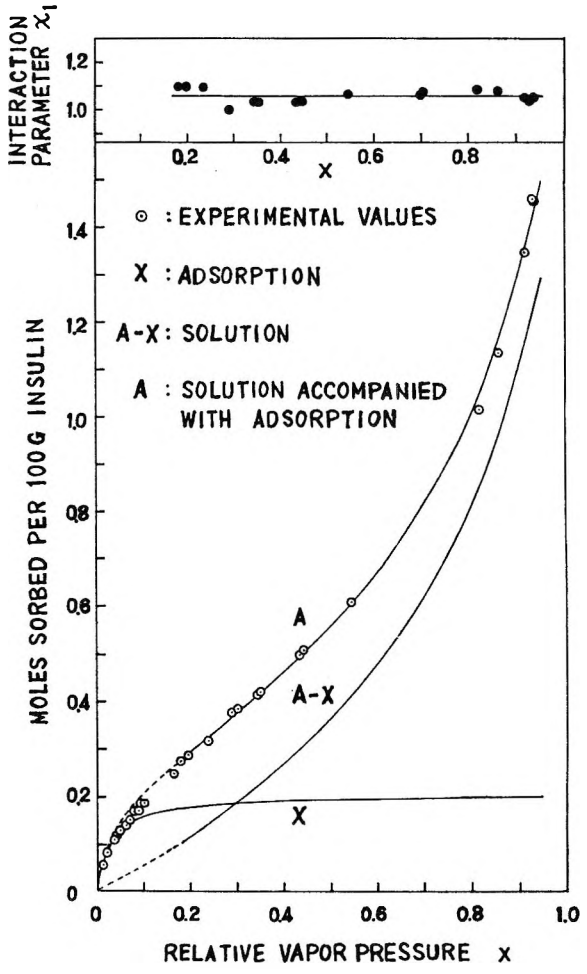

Figure 1. Interaction parameter (●), χ_1, and, theoretical isotherm (—), calculated by theory I for insulin–water system (25°); ○, experimental isotherm.

(*3*) *Cellulose Nitrate–Acetone System.* Using Campbell and Johnson's isotherm[14] of nitrocellulose of nitrogen content 11.2% plus acetone system (reproduced in Figure 3), Rowen and Simha's treatment[5] and the analysis by the present theory I were made. Though the present theory I gives more uniform χ_1 values (-0.093 at $x = 0.2$ to -0.016 at $x = 0.9$) than those (-1.41 at $x = 0.2$ to -0.18 at $x = 0.9$) of Rowen and Simha's treatment, the difference between χ_1 values of the osmotic pressure determination and the present

(12) The terms relating to v_{20}' are expressed by using the relation $dv_{20}' = (dv_{20}'/dv_2')dv_2'$.

(13) J. D. Edsall, "The Proteins," Academic Press Inc., New York, N. Y., 1953, p 562.

(14) H. Campbell and P. Johnson, *J. Polymer Sci.*, **4**, 247 (1947).

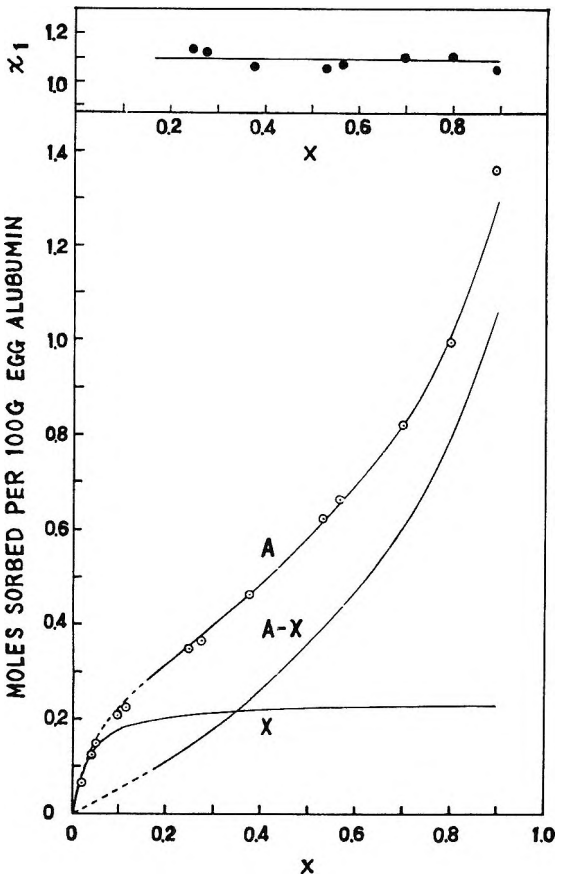

Figure 2. Interaction parameter (●), χ_1, and theoretical isotherm (—) calculated by theory I for egg albumin–water system (26.5°); O, experimental isotherm.

theory I still cannot be neglected. (For nitrocellulose of nitrogen content 11.45% and acetone system at 22°, χ_1 was given as 0.265 by osmotic pressure determination.)[15]

In the case of the protein–water system, X was small compared with PM. In other words, the volume fraction of water molecule, v_1, was given by $(A - X)/(A - X + PM)$ with an error of less than 5%. In the nitrocellulose–acetone system, the corresponding volume fraction of acetone is smaller than $(A - X)/(A - X + PM)$ with an error of more than 10%. We have to use as the volume fraction $(A - X)/(A + PM)$ instead of $(A - X)/(A - X + PM)$ in this case. This means that theory II of the preceding section is a better description of this system.

The practical procedure of applying theory II is somewhat intricate. At first, applying eq 17 to the experimental A *vs.* x relation in the low-pressure region and neglecting the minor decrease of v_2' and v_{20}', we can obtain the values of B and $K' = K/\exp(1 + \chi_1)$. Then eq 13 is rewritten as

$$\frac{B - X}{X} K' \exp(1 + \chi_1) v_1' = 1 \qquad (13')$$

Using eq 13′ and 15, we can determine values of both χ_1 and X at each x by a trial-and-error method as follows. Putting an arbitrary value of χ_1 into eq 13′, the X value at that x is determined noting that $v_1' = (A - X)/(A + PM)$. (A and PM are known from the experiment.) Then, substituting this X value into eq 15 and neglecting the term v_{20}'/M, χ_1 corresponding to the former arbitrary χ_1 is obtained. If both χ_1 values agree with each other, this consistent value is the correct χ_1 value at that x. From this χ_1, $K = K' \exp(1 + \chi_1)$ can also be calculated. We can examine the applicability of theory II to a system by checking the constancy of χ_1 and K over the whole range of relative vapor pressure.

For the present nitrocellulose–acetone system, according to the Langmuir adsorption isotherm $x/X = 0.382 + 3.58X$ obtained by applying the least-square method to the x/X values at $x = 0.02$, 0.03, and 0.05, $B = 0.279$ (3), and $K' = 0.937$ (0). The results of cal-

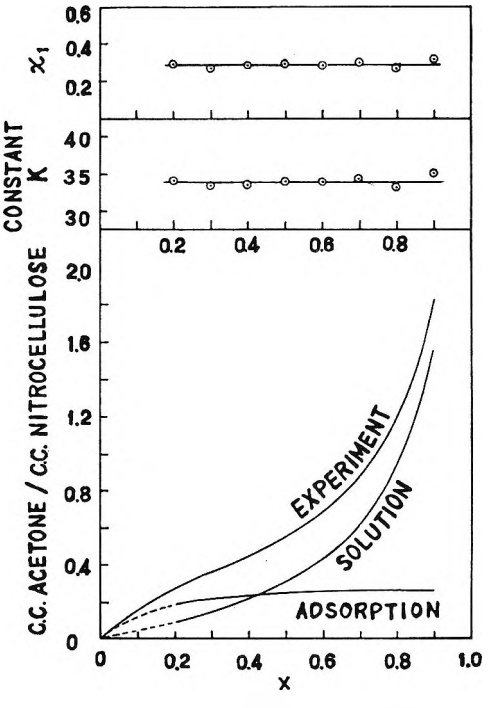

Figure 3. Interaction parameter, χ_1, and constant K calculated by theory II *vs.* relative pressure relations and separation of experimental isotherm into "adsorption" and "polymer solution" by the theory (cellulose nitrate–acetone system, 20°[12]).

(15) H. A. Stuart, "Die Physik der Hochpolymeren, Zweiter Band: Das Makromolekül in Lösungen," Springer-Verlag, Berlin, 1953, p 152.

culations of χ_1 and K at various x values are shown in Figure 3. From Figure 3, it is seen that χ_1 and K show almost constant values over the whole range of pressure and the average value of χ_1 (0.290) is almost equal to that (0.265) obtained from osmotic pressure measurement, in spite of the several assumptions involved in the theory. Thus, as it is clear that theory II is adequate to describe the experimental sorption isotherm of the nitrocellulose–acetone system, we can divide the isotherm into an "adsorption" part and a "polymer solution" part as is shown in Figure 3.

Acknowledgment. Part of this work was done during the stay of the author in Wayne State University, Detroit, Mich., and the author expresses his gratitude to Professor W. Heller of the university for continuous encouragement and fruitful discussions about the problem.

The Oxidation of Molybdenum(V) by Iodine and Oxygen[1]

by E. P. Guymon[2] and J. T. Spence

Chemistry Department, Utah State University, Logan, Utah *(Received August 4, 1966)*

The oxidation of Mo^{V}_2 by I_3^- and O_2 has been studied over the pH range 1.65–7.20 in phosphate buffer. In all cases the reaction is first order in Mo^{V}_2 and zero order in oxidant. From pH 1.65 to 3.92 the rate of the reaction is dependent on H^+, while above pH 5.50, the rate is pH independent. The activation energy and the entropy of activation for the reaction have been measured, and three possible mechanisms have been considered. The epr studies have eliminated Mo^{V} monomer as an intermediate in the reaction.

As part of a study of reactions of molybdenum(V) as possible models for molybdenum enzymes, the oxidation of Mo^{V}_2 by NO_2^- and NO_3^- has recently been reported.[3,4] To obtain more information about the mechanisms of molybdenum(V) reactions, this study has been extended to other oxidants and the reaction of Mo^{V}_2 with I_3^- and O_2 is reported here.

Aqueous solutions of Mo^{V}_2, unless stabilized by strong acid or certain chelating agents,[5] are easily oxidized by atmospheric O_2 and must be handled under anaerobic conditions. No quantitative studies of the oxidation have been reported, however.

Experimental Section

Stock solutions of Mo^{V}_2 were prepared by quantitative reduction of Na_2MoO_4 by shaking over Hg in 3 *M* HCl; they were allowed to stand over Hg in 3 *M* HCl 1 week before use. The Na_2MoO_4 was standardized as previously described.[6] Standard solutions of I_3^- were prepared by the method of Kolthoff and Sandell.[7] $K_3Mo(CN)_8$ was prepared by oxidation of $K_4Mo(CN)_8$ with Ce(IV) in 1 *M* H_2SO_4. $K_4Mo(CN)_8$ was prepared and standardized as described by Audrieth.[8] All buffers were made from reagent grade chemicals, using H_2O that had been passed through a mixed-bed ion exchanger to remove any metal ions. Helium,

(1) Journal Paper No. 603, Utah State Agricultural Experiment Station.

(2) Abstracted from the Ph.D. thesis of E. P. Guymon, Utah State University, 1966.

(3) J. A. Frank and J. T. Spence, *J. Phys. Chem.*, **68**, 2131 (1964).

(4) E. P. Guymon and J. T. Spence, *ibid.*, **70**, 1964 (1966).

(5) J. T. Spence and E. R. Peterson, *Inorg. Chem.*, **1**, 277 (1962).

(6) J. T. Spence and G. Kallos, *ibid.*, **2**, 710 (1963).

(7) I. M. Kolthoff and E. B. Sandell, "Textbook of Quantitative Inorganic Analysis," The Macmillan Co., New York, N. Y., 1952, p 592.

(8) L. F. Audrieth, *Inorg. Syn.*, **3**, 160 (1950).

99.99% pure, used for deaeration, was purchased from Matheson Co.

Molybdenum(V) was determined by measuring its absorbance at 298 mμ in the reaction with O_2. In the reaction with I_3^-, both Mo^V_2 and I_3^- absorb at this wavelength. This difficulty was overcome by measuring the absorbance at 298 and 350 mμ, since I_3^- has an absorption maximum at both wavelengths, but Mo^V_2 does not absorb at 350 mμ. Thus, both I_3^- and Mo^V_2 were determined simultaneously by measuring the absorbance at 350 and 298 mμ and subtracting the contribution of I_3^- at 298 mμ to obtain Mo^V_2 concentration. The molar absorptivities for both Mo^V_2 and I_3^- were determined from standard solutions of the reagents. Both Mo^V_2 and I_3^- obey Beer's law in the concentration range used.

For the I_3^- reaction a vessel was constructed, to which a quartz spectrophotometric cell which could be evacauated was joined. The proper amount of deaerated Mo^V_2 or I_3^- stock solution was added to the deaerated buffer in the reaction vessel under He. The other deaerated solution (I_3^- or Mo^V_2) was then added to the vessel through a rubber diaphragm with a gastight syringe, and the solution was mixed vigorously with the He stream. The moment of mixing was taken as zero time. A stopcock was then opened and the solution was allowed to flow into the evacuated spectrophotometer cell. This cell was closed, either by a stopcock for short time periods or by sealing with an oxygen torch for long reaction times. Then the cell was removed from the vessel and placed in a constant-temperature bath. For spectrophotometric measurements the cell was placed in a specially constructed cell compartment in the Beckman DU spectrophotometer which maintained a temperature of ±0.2°. For short-time reactions, the cell was left in this compartment.

For the O_2 reactions, the same technique was used. The closed cell was placed in the spectrophotometer compartment and the initial Mo^V_2 absorbance recorded. The cell was then opened and O_2 bubbled through the cell using a capillary tube. The absorbance was followed with time. For stoichiometric measurements of the Mo^V_2–O_2 reaction a Gilson Respirometer was used to measure the uptake of O_2.

In order to keep μ and total phosphate concentration constant with changes in pH, the following concentrations of total phosphate were used, and μ was adjusted with Na_2SO_4: μ 0.51, 0.50 *M* buffer; μ 0.75, 0.30 *M* buffer; μ 0.09, 0.10 *M* buffer.

For measuring the rate of formation and dimerization of Mo(V) monomer, the buffer solution was placed in a water-jacketed vessel and deaerated with He. The proper amount of Mo^V_2 in 3 *M* HCl (for monomer formation) or Mo^V in 10 *M* HCl (for dimerization) was then added with a syringe through a rubber diaphragm and the solution was mixed with a magnetic stirrer. Samples were withdrawn with a gastight syringe and transferred anaerobically to quartz epr tubes, which were frozen immediately in liquid nitrogen, and the signal heights (g = 1.92) were measured on a Varian V-4500 epr spectrometer using 100-kc modulation. The epr signals were calibrated by comparison of the double-integrated curves with the double-integrated curves obtained from a standard solution of $K_3Mo(CN)_8$. The concentration of Mo^V_2 was obtained by withdrawing a sample and measuring its absorbance at 298 mμ.

Rate constants and activation parameters were obtained from the proper plots by the method of least squares.

Results

Oxidation by I_3^-. Because of the effect of pH and ionic strength on the reaction rate, several different temperatures and ionic strengths had to be used in order to cover a wide pH range. A 100-fold excess of KI was used in all reactions so that essentially all the I_2 would be present as I_3^-.

Stoichiometry. The concentrations of I_3^- and Mo^V_2 with time were determined simultaneously at pH 2.0 and 6.1 and it was found that the rates of disappearance are essentially identical (Figure 1). Thus the stoichiometric reaction may be written

$$Mo^V_2 + I_3^- \longrightarrow 3I^- + 2Mo^{VI}$$

Molybdenum(V) is most likely a dimer at the pH used,[9] and both Mo^V_2 and Mo^{VI} are undoubtedly complexed with the buffer, but the structures of the complexes are not known. Furthermore, H^+ is involved in the reaction at pH below 5.5.

Kinetics. Because of the pH dependence of the rate, data were obtained at three temperatures: pH 1.65–2.00, 30°; pH 2.00–3.92, 20°; pH 5.50–7.20, 2.5°. In addition, the rates at four temperatures at pH 2.00 were measured in order to obtain the activation parameters.

The over-all order of the reaction was determined by trial and error plots for different orders and by measuring the half-life as a function of total concentration for runs equimolar in Mo^V_2 and I_3^-. The half-life was found to be independent of initial concentration and the data gave good first-order plots when either

(9) C. R. Hare, I. Bernal, and H. B. Gray, *Inorg. Chem.*, 1, 831 (1962).

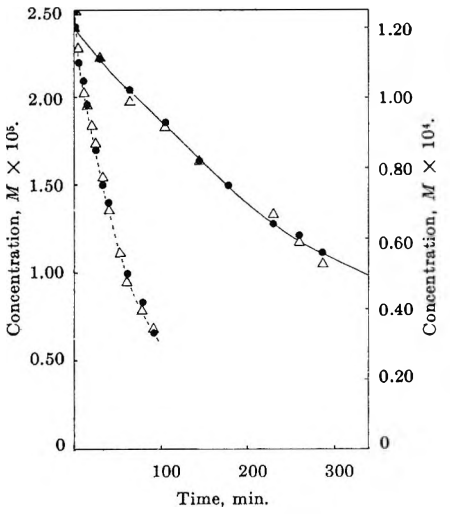

Figure 1. Reaction of I_3^- with Mo^V_2: ———, pH 2.00, μ 0.51, 20°, right ordinate; – – – –, pH 6.10, μ 0.75, 2.5°, left ordinate; ●, $[I_3^-]$; △, $[Mo^V_2]$.

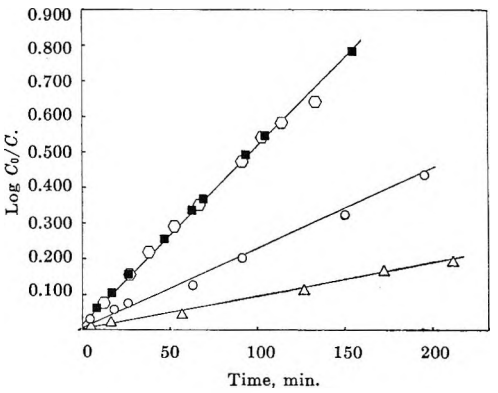

Figure 2. First-order plots of reaction of Mo^V_2 with I_3^- and O_2: △, $[I_3^-]_0 = [Mo^V_2]_0 = 2.50 \times 10^{-5}$ M, pH 1.65, 30°, μ 0.51; ○, $[I_3^-]_0 = [Mo^V_2]_0 = 1.58 \times 10^{-5}$ M, pH 2.61, 20°, μ 0.51; ■, $[I_3^-]_0 = [Mo^V_2]_0 = 1.17 \times 10^{-4}$ M, pH 6.10, 2.5°, μ 0.75; ○, $[Mo^V_2] = 1.19 \times 10^{-4}$ M, excess O_2, pH 6.10, 2.5°, μ 0.75. C_0 = initial concentration of I_3^- or Mo^V_2; C = concentration of I_3^- or Mo^V_2 with time.

the disappearance of Mo^V_2 or I_3^- was used. Therefore, the over-all order of the reaction was concluded to be one. When an eightfold excess of Mo^V_2 was used, the rate of disappearance of I_3^- was zero order. Furthermore, when Mo^V_2 concentration was kept constant and I_3^- concentration changed, no effect on the rate was found. These results indicate the rate-controlling step involves only Mo^V_2. The rate expression may therefore be written

$$\text{rate} = \frac{-d[Mo^V_2]}{dt} = \frac{-d[I_3^-]}{dt} = k_1[Mo^V_2]$$

This gives the standard first-order equation upon integration. Representative plots of the data are found in Figure 2.

The effect of pH on the reaction was studied by measuring the rate between pH 1.65 and 7.20. The changes in temperature were necessary because of the large increase in rate with increasing pH. No measurements were made between pH 3.92 and 5.50 because of the lack of buffering capacity of phosphate in this region.

The order of the reaction with respect to H^+ was determined from the slope of the line obtained from the equation: $\log k_1 = -n(\text{pH})$, assuming $-\log [H^+] = \text{pH}$. These results are found in Figure 3. In the regions pH 2.00–3.92 and 1.65–2.00 the slope of the lines is 0.85, indicating n is very likely -1. From pH 5.50 to 7.20 the slope is almost zero, and the rate is essentially independent of pH. Unfortunately the three sets of points cannot be drawn on the same curve because of the difference in temperature. The rate constants obtained in the pH regions 1.65–2.00

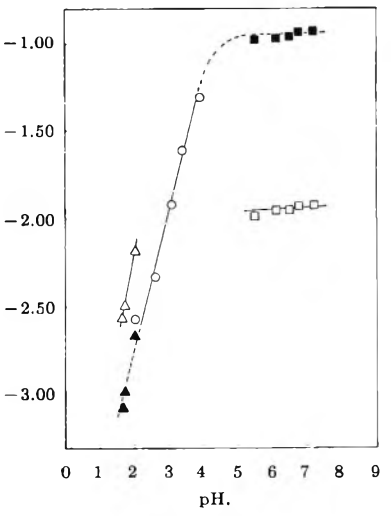

Figure 3. Effect of pH on k_1: ○, 20°; △, 30°; ▲, same values calculated for 20°; □, 2.5°; ■, same values calculated for 20°; ———, experimental; – – – –, calculated.

(30°) and 5.50–7.20 (2.5°) were converted to 20° by using $\Delta F^{\pm}$ for the reaction (see below) and the relationship

$$\log k_{20°} = \frac{\Delta F^{\pm}}{2.30R}\left(\frac{1}{275.5 \text{ (or } 303)} - \frac{1}{293}\right) + \log k_{2.5° \text{ or } 30°}$$

Considering the fact that the different phosphate species are present at different pH and that $\Delta F^{\pm}$ was obtained at pH 2.00, the agreement is very good.

The rate at pH 2.00 was measured at four temperatures—15, 25, 35, and 40°— and the activation energy

and entropy were obtained from the Arrhenius plot, giving E_a = 24.3 kcal and $\Delta S^{\pm}$ = 13.6 eu at 35°. $\Delta F^{\pm}$ was calculated to be 20.1 kcal at 35°. The effect of ionic strength on the rate was determined by adding 1 *M* Na_2SO_4. As can be seen by comparing runs 22 and 23 (Table I) this decreased the rate by a large factor.

Table I: Rate Constants for Oxidation by I_2

Run	pH	$10^4[I_3^-]_0$, *M*	$10^4[Mo^V_2]_0$, *M*	Temp, °C	10^2k_1, min^{-1}	μ, *M*
1	1.65	0.240	0.240	30	2.72	0.51
2	1.72	1.20	1.20	30	3.26	0.51
3	2.00	0.282	0.282	30	6.71	0.51
4	2.00	1.20	1.20	30	6.68	0.51
5	2.02	0.240	0.240	20	2.69	0.51
6	2.02	1.20	1.20	20	2.69	0.51
7	2.61	0.319	0.159	20	4.71	0.51
8	2.61	0.158	0.158	20	4.62	0.51
9	2.61	0.193	0.193	20	4.82	0.51
10	2.61	1.59	0.788	20	4.62	0.51
11	2.61	1.15	1.15	20	4.58	0.51
12	3.08	0.240	0.240	20	12.8	0.51
13	3.08	1.20	1.20	20	11.4	0.51
14	3.38	1.20	1.20	20	24.7	0.51
15	3.92	1.20	1.20	20	49.5	0.51
16	5.50	1.16	1.16	2.5	9.79	0.75
17	6.10	1.22	1.22	2.5	11.2	0.75
18	6.50	0.242	0.242	2.5	10.9	0.75
19	6.50	1.21	1.21	2.5	11.7	0.75
20	6.75	1.21	1.21	2.5	12.0	0.75
21	7.20	0.242	0.242	2.5	12.8	0.75
22	2.18	1.24	1.24	30	7.88	0.19
23[a]	2.18	1.19	1.19	30	0.509	3.19
24	2.00	1.25	1.25	15	2.85	0.09
25	2.00	1.25	1.25	25	9.69	0.09
26	2.00	1.25	1.25	35	38.9	0.09
27	2.00	1.25	1.25	40	78.7	0.09
28	6.10		1.20	2.5	11.6	0.75
29	6.10		10.0	2.5	10.9	0.75
30	6.10		1.07	2.5	18.5	0.07
31	2.00		3.18	20	2.24	0.51

[a] Run 23 contained 1 *M* Na_2SO_4.

Oxidation by O_2. Stoichiometry. The stoichiometry for the reaction of Mo^V_2 with O_2 was determined by measuring the O_2 uptake in a Gilson Respirometer. Table II gives the results. It is clear that 0.5 mole of O_2 is used for every mole of Mo^V_2 and the over-all reaction may be written

$$4H^+ + O_2 + 2Mo^V_2 \longrightarrow 4Mo^{VI} + 2H_2O$$

Kinetics. Because of the difficulty of accurately measuring O_2 concentration in solution, initial experiments were run with excess O_2 (saturated solutions). When the rate of oxidation of Mo^V_2 was compared with the rate of oxidation by I_3^- at the same pH and temperature, it was found to be identical within experimental error (Table I). Furthermore, when a trace of O_2 was added to a deaerated solution of Mo^V_2, the oxidation was found to proceed at the same rate as the comparable I_3^- oxidation until the O_2 was used. Clearly then, the reaction is first order in Mo^V_2 and zero order in O_2, identical with the I_3^- oxidation.

Table II: Oxygen Uptake by Mo^V_2 at pH 6.2, μ 0.75, and 2.5°

Run	$[Mo^V_2]$, m*M*	$[O_2]$, m*M*
1	0.00463	0.00220
2	0.00463	0.00234
3	0.00463	0.00246
4	0.00463	0.00238
	Av	0.00238

Discussion and Mechanism

The results indicate the oxidations of Mo^V_2 by I_3^- and O_2 proceed by the same mechanism, with the rate-controlling step involving only Mo^V_2.

In the reduction of NO_3^- by Mo^V_2, the rate-controlling step is apparently the reaction of Mo^V monomer, formed from the dimer, with NO_3^-.[4] This suggests that a possible mechanism for the reaction of Mo^V_2 with I_3^- and O_2 might involve the dissociation of the dimer into monomer as the rate-controlling step. This would then be followed by a fast reaction of the monomer with I_3^- or O_2.

$$Mo^V_2 \xrightarrow{k_1'} 2Mo^V \quad \text{slow} \quad (1)$$

$$2Mo^V \xrightarrow{k_2} Mo^V_2 \quad \text{slow} \quad (2)$$

$$Mo^V + I_3^- \xrightarrow{k_3} Mo^{VI} + I_2^- + I^- \quad \text{fast} \quad (3)$$

$$2I_2^- \xrightarrow{k_4} I_3^- + I^- \quad \text{fast} \quad (4)$$

By applying the steady-state condition to Mo^V and I_2^- and making the assumption that $k_3[I_3^-] >> 2k_2 \cdot [Mo^V]$, this leads directly to the experimental rate law and is therefore consistent with the kinetics. In order to obtain evidence for this mechanism, the rate of formation of monomer from dimer (step 1) was investigated. This was possible because Mo^V monomer is paramagnetic (d_1 ion) and small concentrations can be detected by epr. It was found that there is a small equilibrium concentration of Mo^V monomer in

phosphate buffer at pH 2.00, but not at pH 6.00. Fortunately, this equilibrium concentration is considerably larger than in 3 M HCl so that, when a small amount of Mo^{V}_2 in 3 M HCl is added to deaerated buffer, the epr signal due to Mo^{V} increases with time, allowing the kinetics of its formation to be followed, as seen in Figure 4. The reaction is pseudo first order since the Mo^{V}_2 concentration is effectively constant and the plot of Mo^{V} monomer concentration *vs.* time is linear until equilibrium is approached. By adding a solution of Mo^{V} in 10 M HCl, in which the molybdenum(V) is 100% monomer, the equilibrium can be approached from the other direction (dimerization). This reaction is second order until equilibrium is approached. In both cases, the complete rate expression taking into account the reverse reaction may be integrated directly, allowing the evaluation of k_1 by two methods. For monomer formation

$$Mo^{V}_2 \underset{k_2}{\overset{k_1'}{\rightleftharpoons}} 2Mo^{V}$$

$$\frac{d[Mo^{V}]}{dt} = 2k_1'[Mo^{V}_2] - 2k_2[Mo^{V}]^2$$

Since $[Mo^{V}_2]$ is effectively constant and $[Mo^{V}]$ at equilibrium can be measured

$$k_2 = \frac{k_1'[Mo^{V}_2]}{[Mo^{V}]_e^2}$$

$$\frac{d[Mo^{V}]}{dt} = 2k_1'[Mo^{V}_2] - 2k_1'\frac{[Mo^{V}_2][Mo^{V}]^2}{[Mo^{V}]_e^2}$$

This is of the form, $dx/(a + bx^2) = 2k_1'c\,dt$, which gives on integration

$$\frac{1}{2\sqrt{-ab}} \ln \frac{a + x\sqrt{-ab}}{a - x\sqrt{-ab}} = 2k_1'ct$$

Making the appropriate substitutions for a, b, and c

$$\log \frac{1 + \frac{[Mo^{V}]}{[Mo^{V}]_e}}{1 - \frac{[Mo^{V}]}{[Mo^{V}]_e}} = \frac{4k_1'[Mo^{V}_2]}{2.30[Mo^{V}]_e}\,t$$

This is plotted in Figure 4 for a representative run, and k_1' was obtained from the slope of this plot.

For dimerization the same treatment can be applied. In this case, owing to the time necessary for sample withdrawal (~30 sec) and the difficulty of obtaining instantaneous mixing, the Mo^{V} monomer concentration has fallen to approximately 10% of total Mo^{V} in the first sample. Therefore the Mo^{V}_2 concentration is almost constant and the compete rate equation can be integrated readily, giving an expression of the same

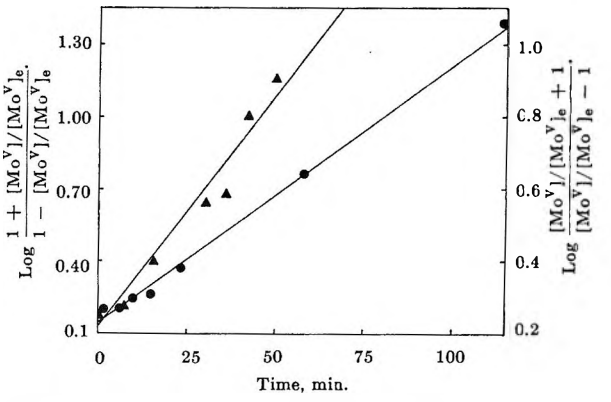

Figure 4. Formation and dimerization of Mo^{V} monomer. Mo^{V} monomer concentration determined from epr signals (g = 1.92) at −195°. ▲, left ordinate: formation of monomer, $[Mo^{V}_2]$ = 2.47 × 10^{-4} M, pH 2.00, μ 0.51, 20°; ●, right ordinate: dimerization, $[Mo^{V}_2]$ = 1.68 × 10^{-4} M, pH 2.00, μ 0.51, 20°.

form as for monomer formation. This is also plotted in Figure 4, and k_1' is obtained from the slope as before. Both methods gave results in agreement within the experimental error and the combined result with standard deviation is: k_1' = (4.0 ± 1.2) × 10^{-4} min^{-1}, at pH 2.00, μ 0.51, and 20°.

If the mechanism is correct, the value of k_1' for monomer formation should be identical with the value of k_1 found in the oxidation because this is the rate-controlling step. Since the value of k_1 for the oxidation under these conditions (Table I) is approximately 7 times larger, it is clear this mechanism must be rejected.

A second possible mechanism involves the conversion of the Mo^{V}_2, which is most likely $Mo_2OCl_{10}^{2-}$ in 3 M HCl, to a phosphate complex by a ligand-exchange reaction as the slow step. The phosphate complex would then have to react with I_3^- or O_2 in a fast step. This mechanism also must be excluded, however, since solutions of Mo^{V}_2 aged in phosphate buffer for 2 days were oxidized by I_3^- at exactly the same rate as freshly prepared solutions. Also, the rate of oxidation was found to be the same, regardless of the order in which the reactants were added, thus eliminating the possibility of a slow oxidation of a molybdenum(V)–chloride complex and a faster oxidation of a Mo^{V}–buffer species which might have formed in the interval between addition of reactants. If an exchange reaction occurs, it must be fast relative to both oxidation and monomer formation or else the rates of these reactions are unaffected by the ligands in the coordination sphere.

A third mechanism involves the disproportionation of Mo^{V}_2 into Mo^{VI} and Mo^{VI} as the slow step, followed by a fast reaction of Mo^{IV} with I_3^- or O_2

$$Mo^{V}_{2} \xrightarrow{k_1''} Mo^{IV} + Mo^{VI} \qquad \text{slow}$$

$$Mo^{VI} + Mo^{IV} \xrightarrow{k_2} Mo^{V}_{2} \qquad \text{slow}$$

$$Mo^{IV} + I_3^- \xrightarrow{k_3} 3I^- + Mo^{VI} \qquad \text{fast}$$

Applying the steady-state condition to Mo^{IV} and assuming $k_3[I_3^-] >> k_2[Mo^{VI}]$, the experimental rate law is readily obtained. Unfortunately, no positive evidence for the existence of Mo^{IV} in phosphate buffer has been found. If the Mo^{IV} existed in a high-spin complex it should give a triplet epr signal, but none was observed (such a signal can be detected for a molybdenum(IV)–gluconic acid complex). If the complex is low spin, however, no signal would be seen. Polarographic reduction of Mo^{VI} in phosphate likewise gave no evidence for the existence of a Mo^{IV} species, as contrasted with reduction in gluconate.[6] This does not eliminate this mechanism, since only a low concentration of Mo^{IV} would be necessary if its rate of reaction with I_3^- and O_2 is very fast. It should be pointed out that there is evidence Mo^{IV} is an intermediate in other reactions involving molybdenum ions.[10,11] At present, however, this mechanism, although reasonable, can only be regarded as possible.

Acknowledgment. Thanks are expressed by the authors to the National Science Foundation for a predoctoral fellowship for E. P. G. and to the U. S. Public Health Service (Grant GM-08347-04, National Institute of General Medical Science) for financial support.

(10) A. A. Bergh and G. P. Haight, Jr., *Inorg. Chem.*, 1, 688 (1962).
(11) G. P. Haight, Jr., and A. Katz, *Acta Chem. Scand.*, 16, 659 (1962).

Equilibrium and Water Uptake in Barium–Hydrogen and Related Ion-Exchange Systems

by Imelda Gamalinda, Lois A. Schloemer, Howard S. Sherry, and Harold F. Walton

University of Colorado, Boulder, Colorado 80302 *(Received August 8, 1966)*

Equilibrium selectivity measurements have been made for the barium–hydrogen and barium–sodium exchanges in a sulfonated polystyrene resin and values have been calculated for the free energy, enthalpy, and entropy of the reactions. The entropy changes can be explained qualitatively by ion hydration in the aqueous phase, but the difference in the entropies of the two reactions is larger than expected. The swelling and water uptake were measured for different cation ratios in the systems Ba^{2+}–H^+, Ca^{2+}–H^+, La^{3+}–H^+, Cs^+–H^+, Ba^{2+}–Na^+, and Na^+–H^+. Both the water uptakes and the ion-exchange equilibria point to significant ion pairing between divalent ions and the fixed ions of the exchanger.

In 1961, we published selectivity data for the Ba–H exchange in a sulfonated polystyrene resin and reported that the selectivity for barium increased with with the proportion of barium ions in the exchanger.[1] We also noted that the absorption of water by the barium-loaded resin was substantially less than that by the hydrogen-loaded resin. Qualitatively the results indicated that the activity of the ions in the exchanger depended on the proportion of ions to water in the exchanger, that is, on the molality of the internal solution rather than on the proportion of the cations to the fixed ionic groups. The selectivity quotients were calculated with resin concentrations expressed as equivalent fractions. For exchanges of ions of unequal charge, the concentration units must be clearly specified.

The selectivity of the exchanger for barium ions is large, and to find distribution quotients one must measure very small concentrations of dissolved barium ions. The method we had used was to add dilute sulfuric acid, evaporate the solution and precipitate together in a weighed platinum dish without filtering, and weigh the product. This method assumes that no nonvolatile substance is present other than barium sulfate. Even a small amount of nonvolatile impurity leached from the resin would invalidate the result, and apparently this happened.

The investigation here reported had two parts. One was to measure distribution quotients for the barium–hydrogen and barium–sodium exchanges, using radioactive tracer Ba-133 (half-life 7.2 years). The second was to measure water uptake as a function of resin composition for resins containing barium and hydrogen ions, barium and sodium ions, and for certain other pairs of ions.

Experimental Section

(*a*) *Materials.* The *cation-exchange resin* was the sulfonated styrene–divinylbenzene copolymer, Dowex 50-W, with 8% cross-linking, obtainined in purified form from the Bio-Rad Corp. Two batches were used, one a 20–50 mesh material out of which was wet-screened a 20–24 mesh fraction for the water uptake experiments, and the other a 50–100 mesh material which was used for the selectivity measurements. Both were used in the hydrogen form, except for one series of measurements where the sodium form was used. One set of water uptake measurements was made with a third batch of resin, as will appear below. The *barium tracer* was obtained as a barium chloride solution of specific activity 2 curies/g of Ba from the

(1) H. F. Walton, D. E. Jordan, S. R. Samedy, and W. N. McKay, *J. Phys. Chem.*, 65, 1477 (1961).

Nuclear Science and Engineering Corp. Its radiochemical purity was confirmed using a 512-channel γ-ray spectrometer.

(*b*) *Equilibrium Measurements.* In each series of experiments, quantities of air-dried resin as nearly equal as possible were weighed into dry 50-ml polyethylene bottles; then measured amounts of aqueous perchloric acid and barium perchlorate (or aqueous sodium chloride and barium chloride) were added, and water was added to give a predetermined volume. About 5 mequiv of resin and 12 ml of 0.5 *N* solution were used in most experiments. Finally, the tracer was added as a 50, 100, or 500-μl volume of a stock solution. The bottles were stoppered and shaken for at least 16 hr in a water bath at constant temperature. (The experiments at 6° were done in a cold room.) The attainment of equilibrium was virtually complete in 1 hr except at the lowest barium concentrations. Equilibrium was verified by shaking for extended periods with repeated analysis and also by raising the temperature, thus shifting the equilibrium, then bringing the temperature back to its original value and checking that the solution had the same composition as before.

Counting was done with a crystal scintillation counter and pulse-height analyzer, using the 0.355-Mev γ rays. Care was taken to avoid getting specks of resin into the test tubes used for counting. With the runs at 60°, portions of about 2.5 ml were withdrawn from the bottles while they were in the bath; then the 2.00-ml samples for counting were taken from these portions after they had cooled.

In a number of the Ba^{2+}–H^+ experiments the acid in the solution was determined by titration, and so was the hydrogen-ion content of the resin. This checking was important at the higher barium loadings, but it confirmed the radiochemical analyses very well. Also at the higher loadings the barium concentration of the solution was checked by conventional gravimetric analysis.

The radiochemical analysis was further checked by scanning the γ-ray spectrum of the solution after equilibration. At low loadings, less than 1% of the added tracer remained in the solution, so that a small amount of a weakly absorbed radioactive impurity could have caused a large error in the distribution measurement. Fortunately, the γ-ray spectrum of the solution was identical with that of a barium-133 standard.

(*c*) *Microscopic Measurements.* The method was that of Freeman and Scatchard.[2] Sets of six beads, about 0.5 mm in diameter, were selected from batches of Dowex 50-X8 resin prepared beforehand with different proportions of barium ions and hydrogen ions and stored in the wet condition. The beads were transferred to a small cell on a microscope slide, immersed in pure water, and observed with a monocular Leitz microscope with 10× apochromatic objective and ocular micrometer. Illumination was with light of 550 mμ, obtained with an interference filter and ortho-illuminator. Each bead was measured in four directions at 45° to one another. Then the beads were dried under vacuum over magnesium perchlorate for 5 days. Their diameters in the dry condition were measured after immersion in *n*-hexane, freshly distilled from sodium wire. The percentage volume shrinkage on drying was determined.

To find the ionic composition of the resins, samples of the batches from which the beads had been taken were air dried and portions titrated with sodium hydroxide to determine the hydrogen-ion content. Other portions were wet-ashed by digestion with perchloric and periodic acids,[3] after which the barium was titrated with EDTA. The digestion was very tedious, however, and later the barium contents were found by titrating the barium remaining in the solution after stirring the pure hydrogen-form resin with aqueous barium chloride and subtracting from the barium added to find the amount of barium that had entered the resin.

(*d*) *Centrifuge Measurements of Water Uptake.* These were based on the work of Pepper, Reichenberg, and Hale[4] as modified by Scatchard and Anderson.[5] Quantities of 20–24 mesh resin were placed in stainless steel cylinders 13 mm i.d. and 75 mm long, closed at one end with fine-mesh stainless steel gauze. This was cut into circles and fixed in position in the tube by crimping the end of the latter around it; no solder was used. For weighing, each steel cylinder was placed in a stoppered glass vial. It was weighed empty, then with air-dried resin of known moisture content, then with the swollen resin after centrifuging.

Before centrifuging, the resin was backwashed several times with distilled water using the arrangement shown in Figure 1a. Water was passed upward to drive the resin into the long vertical glass tube; then the flow was stoppered to let the resin settle. The water was drained down through the tube, then passed upward again. This was done with the aid of a funnel and rubber tube connection (not shown). The object of this treatment was to classify the resin beads according to size so that the packing would be

(2) D. H. Freeman and G. Scatchard, *J. Phys. Chem.*, 69, 70 (1965).

(3) G. F. Smith and H. Diehl, *Talanta*, 4, 185 (1960).

(4) K. W. Pepper, D. Reichenberg, and D. K. Hale, *J. Chem. Soc.*, 3129 (1952).

(5) G. Scatchard and N. J. Anderson, *J. Phys. Chem.*, 65, 1536 (1961).

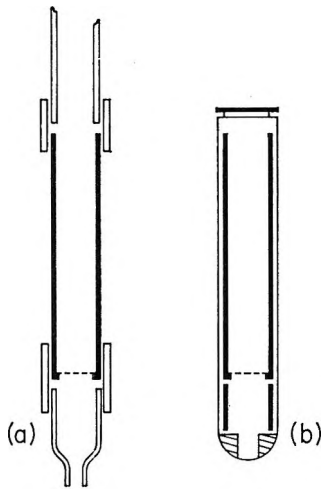

Figure 1. Steel cylinders used for centrifuge studies: (a) cylinder in place for filling and backwashing; (b) cylinder in centrifuge tube.

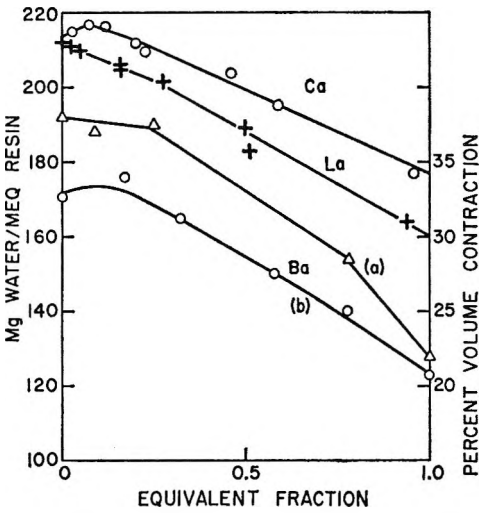

Figure 2. Water uptake by 8% cross-linked resins loaded with H^+ and Ba^{2+}, La^{3+}, or Ca^{2+}. Curve a was obtained by microscope measurements; read ordinate at right; see text. Curve b was obtained by centrifuge experiments. For this and the other two curves, read ordinate at left. Abscissas are fractions of ions other than H^+. The barium curves in this figure refer to a different batch of resin than that used in other tests.

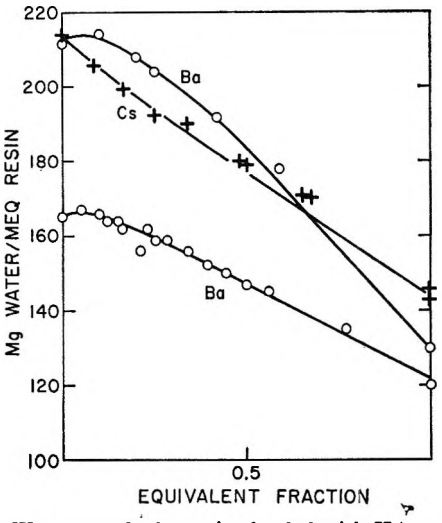

Figure 3. Water uptake by resins loaded with H^+ and Cs^+ or Ba^{2+}. Lower curve, 12% cross-linking; two upper curves, 8% cross-linking. Centrifuge data. Abscissas are fractions of Cs^+ or Ba^{2+}.

as near as possible to the close packing of uniform spheres and the number of contacts between spheres reproducible. Finally, the water was drained out of the resin and any particles of resin sticking to the inside of the upper glass tube were washed down with a water jet from a wash bottle. The steel cylinder was removed from the holder and allowed to stand and drain on absorbent tissue paper for a few minutes. It was then placed in the nylon centrifuge tube shown in Figure 1b. This carried a small rubber or plastic pad in the bottom, then a stainless steel ring about 15 mm high. Thus space was provided to hold the water which was spun out of the resin. The centrifuge tube was closed with a plastic cap, as shown.

Centrifuging was done in a Servall refrigerated angle centrifuge. An estimate of the water retained between the resin spheres was made by spinning beads of styrene–divinylbenzene copolymer, lightly sulfonated on the surface by stirring in fuming sulfuric acid for 1–2 min at 80°. The beads were 28 mesh, smaller than those of the ion-exchange resins, but we only needed a rough estimate as we were interested in the change in water uptake with ionic composition rather than in absolute values for the water uptake. At 5000g, the interstitial water retained by a tubeful of polystyrene beads was about 40 mg, corresponding to 4–5 mg/mequiv of ion-exchange resin. In constructing the curves shown in Figures 2, 3, and 4, this correction was not applied except for the Ba–H curve (b) of Figure 2, where a centrifugal force of 1100g was used and the water retained between the beads was about 20 mg/mequiv.

The effects of centrifugal force and temperature of centrifugation were studied with hydrogen-form, 8% cross-linked resin. With 30 min spinning time, the results with the two tubes of resin, corrected for retention between beads, were the following (given as grams of water in swollen resin)

(a) 8.27 mequiv of resin: 0°, 3020g, 1.761; 4900g, 1.737; 9750g, 1.722. 20°, 4900g, 1.732

Table I: Representative Centrifuge Data. H Resin Plus Cesium Hydroxide

No.[a]	Mequiv R⁻	Mequiv H⁻	Mequiv Cs⁺	Dry wt, mg R⁻	Dry wt, mg H⁺	Dry wt, mg Cs⁺	Total	Wt. of swollen resin	Wt. of inhibited water	Mg of H_2O per mequiv	Equiv fraction of Cs⁺
1	8.270	8.27	0	1606	8	0	1614	3386	1772	214	0
2	8.270	7.58	0.69	1606	8	92	1706	3409	1703	206	0.08
3	8.270	6.89	1.38	1606	7	183	1796	3445	1649	200	0.17
4	8.270	6.20	2.07	1606	6	275	1887	3478	1591	192	0.25
5	8.268	5.48	2.79	1604	5	371	1980	3548	1568	190	0.34
6	8.268	4.09	4.18	1604	4	556	2164	3647	1483	179	0.505
7	8.268	2.69	5.58	1604	3	742	2349	3754	1405	170	0.575
8	8.36	0	8.36	1623	0	1111	2734	3993	1219	146	1.00
9	8.22	0	8.22	1596	0	1092	2688	3901	1173	143	1.00

[a] No. 1–4 were obtained on the same filling of resin; so were 5–7. No allowance is made for superficial water between the resin beads.

(b) 8.84 mequiv of resin: 0°, 3020*g*, 1.797; 4900*g*, 1.791; 9750*g*, 1.788. 20°, 4900*g*, 1.784

In most runs the temperature was 15°, the speed 8000 rpm, or 7600*g* at the bottom of the tube, and the spinning time 45–60 min.

After a centrifuge run with hydrogen-form resin, the resin from each cylinder was washed into a plastic bottle and a measured amount of standard base solution, $Ba(OH)_2$, $Ca(OH)_2$, or CsOH, was slowly added with shaking. (Solutions of $BaCl_2$ and $La(NO_3)_3$ were also used, since we knew that virtually all the added metal ions were taken up by the resin.) The resins were shaken with the solutions for 30 min, then transferred back to the centrifuge tubes, backwashed, and centrifuged as previously described. A representative set of data is given in Table I.

Results and Discussion

(*a*) *Equilibrium.* Figures 5 and 6 show the distribution quotients, K_c, defined as

$$K_c = \frac{\left[\begin{array}{c}(\text{equivalents of Ba in resin}) \times \\ (\text{equivalents of H in resin})^2\end{array}\right]}{\left[\begin{array}{c}(\text{equivalents of H in solution})^2 \times \\ (\text{equivalents of Ba in solution})\end{array}\right]} \times \left[\frac{(\text{equivalents of resin})}{(\text{liters of solution})}\right] \quad (1)$$

The units of solution concentration were normalities; those of resin concentration were equivalent fractions.

Clearly the distribution quotients do *not* increase steeply with loading as we reported in 1961, but are essentially independent of the barium content of the resin. This confirms the recent work of Krylova, Soldatov, and Starobinets.[6] One concludes that the activity of the ions in the exchanger is more nearly proportional to their equivalent fraction, that is, to the ratio of counterions to fixed ions, than it is to the ratio of counterions to imbibed water (see Figures 2 and 3). One may not, in other words, consider the solution inside the resin as in any way analogous to an ideal dilute solution. The ion-pair model of Rice and Harris[7] is more appropriate, though it is not the only possibility.

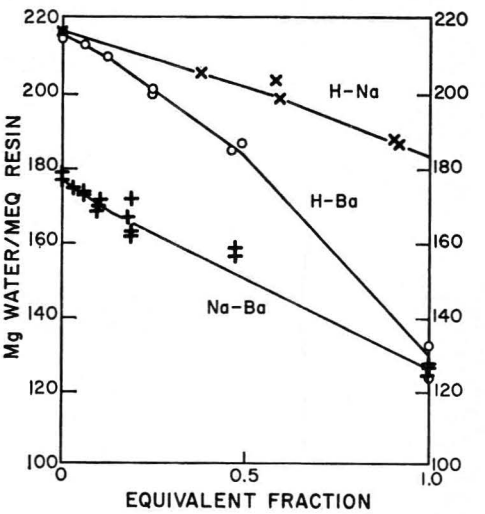

Figure 4. Water uptake by 8% cross-linked resins loaded with H^+ and Na^+ (top curve), H^+ and Ba^{2+} (middle curve), Na^+ and Ba^{2+} (lower curve). Abscissas, fraction Na^+ (top curve), Ba^{2+} (two lower curves). Centrifuge data.

To take account of the nonideality of the external solution one may define an "activity quotient" by eq 2.

(6) A. A. Krylova, V. S. Soldatov, and G. L. Starobinets, *Zh. Fiz. Khim.*, **39**, 2989 (1965).

(7) S. A. Rice and F. E. Harris, *Z. Physik. Chem.* (Frankfurt), **8**, 207 (1956).

$$K_a = K_c \frac{f^3_{BaX_2}}{f^4_{HX}} \qquad (2)$$

where X is the external anion, here the perchlorate ion. No activity coefficients are available for mixed barium perchlorate–perchloric acid solutions, but we can use as a guide the coefficients determined in mixed barium chloride–hydrochloric acid solutions by Harned and Gary[8] and by Lietzke and Stoughton.[9] From the latter, at ionic strength 0.5 and at 25°, log $\gamma_{HCl} = -0.12$ and log $\gamma_{BaCl_2} = -0.30$; at ionic strength 1.0, the numbers are -0.10 and -0.32. Therefore one would expect an increase of 36% in K_c in going from ionic strength 1.0 to 0.5. (The difference between the molal activity coefficients cited in ref 9 and the molar coefficients in eq 2 is too small to be significant.) We found an increase of 16% in going from ionic strength 1.0 to 0.4. Krylova, *et al.*,[6] found a considerable effect of ionic strength below $\mu = 0.5$, and this is to be expected.

Our barium–hydrogen equilibria were measured at a constant total normality of 0.38; the ionic strength was not constant, yet the equilibrium is so one-sided that the barium ions in the solution have little effect on the ionic strength except at high resin loadings; see Figure 6. No attempt was made, therefore, to adjust the equilibrium quotients to constant ionic strength.

Our temperature effect was in the same direction as that of Krylova, *et al.*, that is, the affinity of barium ions for the hydrogen-form resin decreased with rising temperature, but our value of ΔH was 2.5 times their value. They used resins with 6.5, 10.5, and 25% divinylbenzene and temperatures of 0, 20, and 60°. The three K values for 6.5% cross-linking give a uniform ΔH of -1600 cal/mole of Ba, as do the values for 10.5% cross-linking at 20 and 60°; the 0 and 20° curves give $\Delta H = -2600$ cal. Our value is -4200 cal/mole of Ba; see below. We have no explanation for this difference except to note that their equilibrations were done by flowing solutions of known compositions through resin columns, a doubtful technique in view of the one-sided distribution. For the barium–sodium exchange, we found the opposite temperature effect; the selectivity for barium increased slightly with rising temperature.

To treat the data thermodynamically, we used the simplified equation of Gaines and Thomas[10]

$$\Delta F^\circ = RT(Z_2 - Z_1) - RT\int_0^1 \ln K_a' dN \qquad (3)$$

where Z_2 and Z_1 are the charges of the entering and leaving ions (2 and 1 in this case), N is the equivalent fraction of one of the exchanging ions in the resin, and K_a' is *twice* the K_a defined in eq 2. In K_a' the solution concentrations are expressed in molalities, whereas in K_a of eq 2 they are given in normalities. Resin compositions are expressed as equivalent fractions in both quotients. The free energy calculated by eq 3 is that necessary to transfer 1 mole of barium ions from

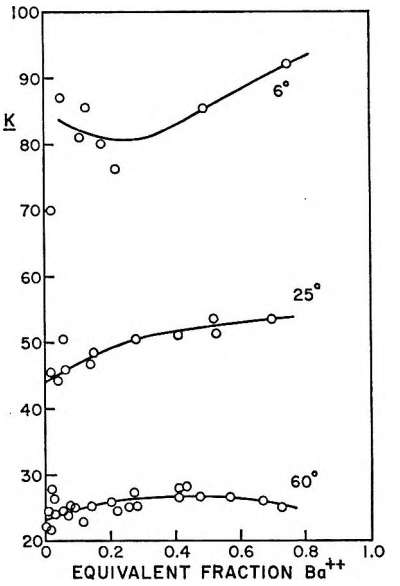

Figure 5. Equilibrium quotients for 8% cross-linked resin, Ba^{2+}–H^+ exchange. The ordinates are values of k_c (eq 1) uncorrected for solution activities. Solutions were 0.38 N.

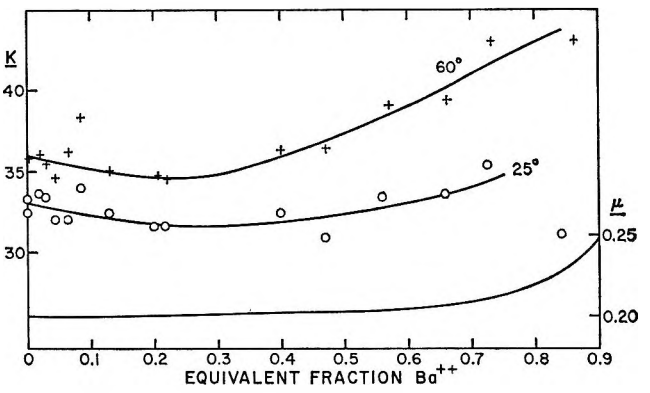

Figure 6. Equilibrium quotients for 8% cross-linked resin, Ba^{2+}–Na^+ exchange. The ordinates are values of K_c (eq 1) uncorrected for solution activities. The lower curve shows the ionic strength of the equilibrium solutions; see ordinate scale on right. Solutions were 0.20 N.

(8) H. S. Harned and R. Gary, *J. Am. Chem. Soc.*, 76, 5924 (1954).

(9) M. H. Lietzke and R. W. Stoughton, *J. Phys. Chem.*, 70, 756 (1966).

(10) G. L. Gaines and H. C. Thomas, *J. Chem. Phys.*, 21, 714 (1953).

a pure ideal 1 m barium salt solution into the resin, converting the resin entirely from the hydrogen form into the barium form, and receiving the liberated hydrogen ions in an ideal 1 m solution of the pure acid. The complete equation of Gaines and Thomas includes terms for the change in water activity and the energy and transfer of water between the exchanger and solution. Using our data for the water uptake (see the next section) and published values of osmotic coefficients we can make an estimate of the errors introduced by neglecting these solvent terms. They amount to about 50 cal/mole of barium perchlorate.

Rewritten for the Ba^{2+}–H^+ or Ba^{2+}–Na^+ exchange in terms of our K_a, eq 3 reads

$$\Delta F^\circ = RT(1 - \ln 2) - RT\int_0^1 \ln K_a dN \quad (3a)$$

For the activity coefficient quotient in eq 2 we have arbitrarily selected a value of 0.40 for ionic strength 0.4 and 0.50 for ionic strength 0.2. The former value is extrapolated from the data of Lietzke and Stoughton[9] for chloride solutions; see above. It also agrees very well with that estimated *a priori* from the approximate Debye–Hückel equation

$$\log f_i = -\frac{0.5Z_i^2\sqrt{\mu}}{1 + \sqrt{\mu}} \quad (4)$$

and this equation was used to estimate the activity coefficients at ionic strength 0.2.

From the data in Figures 5 and 6 we calculate the following energy quantities, expressed per mole of barium ions at 25°; Ba^{2+}–H^+ exchange: $K_c = 52$, $K_a = 21$; $\Delta F^\circ = -1620$ cal, $\Delta H^\circ = -4200$ cal, $\Delta S^\circ = -8.6$ cal deg^{-1}; Ba^{2+}–Na^+ exchange: $K_c = 32.5$, $K_a = 16.5$; $\Delta F^\circ = -1480$ cal, $\Delta H^\circ = 920$ cal, $\Delta S^\circ = 8.1$ cal deg^{-1}.

The most striking feature of these data is the great difference in the entropy of these two exchanges. Qualitatively, this difference is as expected; the hydrogen ion is more hydrated in aqueous solution than the sodium ion and the more negative value obtained for ΔS° in the exchange with hydrogen reflects the greater organization of the water structure produced by the strongly hydrated H^+. Quantitatively, the difference of nearly 17 entropy units is much larger than expected from the entropies of hydration of ions given by Powell and Latimer.[11] They quote these entropies of hydration in calories per degree per mole at 25°: H^+ −26, Na^+ −21, and Ba^{2+} −38. From these figures we expect the entropy difference to be no more than ten units and two factors would make the difference smaller; first, the presumption that the ions are hydrated to some extent in the resin, with hydrogen more so than sodium, and second, the configurational entropy of the resin, which increases when the polymer network contracts; this contraction is greater in the H^+–Ba^{2+} exchange (see next section) and might account for two to three entropy units in this case.[12] Of course, if our value of ΔH for the Ba^{2+}–H^+ exchange were too great[6] the anomaly would disappear.

One can avoid uncertainties in configurational entropy by studying ion exchange in rigid aluminosilicate frameworks and data obtained in our laboratory by Sherry and Walton on the Molecular Sieve Linde A give for Ba^{2+}–Na^+, $\Delta S^\circ = +8$, for Ca^{2+}–Na^+, $\Delta S^\circ = +23$ cal deg^{-1}/mole of divalent ions. The first value is surprisingly and fortuitously close to that found in Dowex 50-X8 resin. The difference of 15 units is somewhat larger than the 12 units expected from the compilation of Powell and Latimer.[11]

(*b*) *Water Uptake.* The data are shown in Figures 2, 3, and 4. Figure 2 shows the microscopic data (curve a) and centrifuge data obtained with the same batch of resin (curve b). The other data were obtained with another batch of resin which was the same in all cases except for the 12% cross-linked resin shown in Figure 3. The standard deviation of the several microscope measurements taken on each sample was about ±1% in the volume; that of any one series of centrifuge measurements, made on the same resin in the same centrifuge tube, was about ±1 mg/mequiv. Points from different fillings of resin are not distinguished by different symbols, but are plotted to indicate the degree of reproducibility.

The microscope measurements give a different quantity to that given by the centrifuge data. Their interpretation requires a knowledge of the partial molal volumes of the ions and the water. Qualitatively, they confirm the results of the centrifuge measurements and since the centrifuge data are more complete, we shall address our discussion to these.

There is evidence of "bowing" or convexity in the curves for barium–hydrogen and calcium–hydrogen mixed resins and possibly even of a slight maximum at low divalent-ion loadings. This was especially evident in the calcium–hydrogen exchange, where the shape of the curve was confirmed by repeated tests. The water contents of resins with 10–20% of divalent ions are greater than would be the case if each resin species bound water independently of the other.

(11) R. E. Powell and W. M. Latimer, *J. Chem. Phys.*, **19**, 1139 (1951).

(12) B. R. Sundheim, M. H. Waxman, and H. P. Gregor, *J. Phys. Chem.*, **57**, 974 (1953).

This did not happen with the mixed sodium–barium resins, and it seems that the bowing is associated with the combination of hydrogen ions and divalent ions. We hope to obtain more experimental data before offering explanations of this effect.

One conclusion can be drawn from our data; introduction of divalent ions causes the resin to shrink much more than it would if these ions remained fully hydrated in the resin. Estimates of hydration from partial molal volumes, ionic conductances, and Debye–Hückel interaction parameters show the barium ion to be at least twice as strongly hydrated in solution as the sodium ion, yet Figure 4 shows that the water content of barium resin is considerably less than that of sodium resin. Ion pairing and perhaps bridging of polyelectrolyte chains must surely be important with divalent ions. As we have already noted, the fact that the activities of the ion–resin combinations are proportional to the equivalent fraction of the resin, rather than to the ratio of ions to water in the resin, strongly supports the view that ion pairing predominates, or at any rate an association of unhydrated ions as visualized by Eisenman.[13]

Acknowledgments. This work was supported by the U. S. Atomic Energy Commission under Contract No. At(11-1)-499. It is a pleasure to acknowledge the help of David H. Freeman of the National Bureau of Standards, who personally supervised the microscopic measurements, and also the technical assistance of Ellen Sheets and Kazuko Shimomura.

(13) G. Eisenman, *Biophys. J.*, 2, 259 (1962).

Pulse Radiolysis of Aqueous Eosin[1a]

by J. Chrysochoos, J. Ovadia, and L. I. Grossweiner[1b]

Department of Radiation Therapy, Michael Reese Hospital and Medical Center, Chicago, Illinois
(Received August 10, 1966)

A pulse radiolysis investigation of aqueous eosin (S) has shown that the initial products are semireduced eosin (R) [$e_{aq}^- + S \rightarrow R$ ($k \geq 5 \times 10^9 M^{-1}$ sec^{-1})], semioxidized eosin (X) [$OH + S \rightarrow OH^- + X$ ($k = (1.4 \pm 0.4) \times 10^{10} M^{-1}$ sec^{-1})], and a long-lived "red product" attributed to the H and OH ring-addition products. In deaerated solutions the dye radicals decay predominantly by the back reaction $R + X \rightarrow 2S$ ($k \cong 8 \times 10^8 M^{-1}$ sec^{-1}), with permanent bleaching due to $R + R \rightarrow S +$ leuco base ($k = (4.2 \pm 0.9) \times 10^6 M^{-1}$ sec^{-1}) and $X + X \rightarrow$ products ($k = (2.0 \pm 0.5) \times 10^8 M^{-1}$ sec^{-1}). Measurements made in the presence of H_2O_2, to convert e_{aq}^- to OH, and OH scavengers led to the results $S + CH_3\dot{C}HOH \rightarrow R + CH_3CHO$ ($k = (1.1 \pm 0.2) \times 10^9 M^{-1}$ sec^{-1}) and $S + CO_2^- \rightarrow R + CO_2$ ($k = (2.5 \pm 0.5) \times 10^8 M^{-1}$ sec^{-1}). The results are compared with previous flash photolysis measurements and predictions of the Debye equation for encounter-limited reactions.

Introduction

Eosin Y (the dianion of 2′,4′,5′,7′-tetrabromofluorescein) is a dye whose properties as a photochemical sensitizer have been studied in some detail. Investigations with conventional light sources have shown that light absorption in the longest wavelength band (λ_{max} 516 mμ) excites a triplet that can oxidize many organic molecules, thereby reducing the dye to a semiquinone intermediate.[2-4] Flash photolysis measurements led to spectral data on the triplet and semireduced eosin (R)[5,6] and also on a semioxidized form of the dye (X) produced by triplet–triplet and triplet–dye reactions and by the reaction of the triplet with certain oxidants.[7,8]

It was reported in a preliminary note[9] that electron pulse radiolysis of deaerated, aqueous eosin gave the spectra associated with R and X plus a broad absorption in the red region that was attributed to triplet eosin, based on its spectrum, rapid formation (<1 μsec), decay, and ability to sensitize the oxidation of *p*-cresol in the presence of hydroxyl scavenger. More recent work, however, has shown that the absorption formerly identified as the triplet is due to a longer lived "red product" of unknown structure, produced by the attack of H or OH on eosin. This paper extends the previous report with new results on the formation and disappearance of the eosin radiolysis products in deaerated and aerated solutions, and in the presence of e_{aq}^- and OH scavengers.

Experimental Details

The irradiation source was a linear accelerator providing 1-μsec pulses of 30-Mev electrons, at 1175 rads/pulse as determined with the modified Fricke dosimeter.[10] The flash spectra were taken at a minimum time delay of 5 μsec by synchronizing an E.G.&G.

(1) (a) This work was supported by U. S. Public Health Service Grant No. GM-12716 from the National Institute of General Medical Sciences; (b) Department of Physics, Illinois Institute of Technology, Chicago, Ill. 60616.

(2) (a) G. Oster and A. H. Adelman, *J. Am. Chem. Soc.*, **78**, 913 (1956); (b) M. Imamura, *J. Inst. Polytech. Osaka City Univ., Ser. C*, **5**, 85 (1956).

(3) M. Imamura and M. Koizumi, *Bull. Chem. Soc. Japan*, **29**, 899, 914 (1956).

(4) M. Imamura, *ibid.*, **30**, 249 (1957).

(5) L. I. Grossweiner and E. F. Zwicker, *J. Chem. Phys.*, **34**, 1411 (1961).

(6) E. F. Zwicker and L. I. Grossweiner, *J. Phys. Chem.*, **67**, 549 (1963).

(7) V. Kasche and L. Lindqvist, *Photochem. Photobiol.*, **4**, 923 (1965).

(8) T. Ohno, S. Kato, and M. Koizumi, *Bull. Chem. Soc. Japan*, **39**, 232 (1966).

(9) L. I. Grossweiner, A. F. Rodde, Jr., G. Sandberg, and J. Chrysochoos, *Nature*, **210**, 1154 (1966).

(10) L. M. Dorfman and M. S. Matheson, *Progr. Reaction Kinetics*, **3**, 237 (1965).

FX-33 flashtube (50 w-sec input) with the electron pulse. A Hilger E498 quartz prism spectrograph was used with Kodak I-N plates. The kinetic studies were made with an Osram XBO-450 xenon arc as the monitoring light and a Hilger E720 scanning unit on the spectrograph. The photomultipliers used were an RCA 1P28 below 650 mμ and a Hamamatasu R136 from 500 to 800 mμ. The photomultiplier anode was directly coupled to a Tektronix Type 535 oscilloscope with Type M preamplifier by means of 60 ft of Columbia HH 2000 delay cable terminated at both ends by 2200 ohms. This introduced a 7.5-μsec delay in the transmission of the actual photomultiplier signal to the oscilloscope, which permitted the transient interference from the accelerator to decay and made it possible to follow the growth of the species during the pulse with a rise time of 0.2 μsec. Slow transient changes were monitored simultaneously with an Esterline-Angus Type E1101S recorder. Photolysis of the dye samples by the strong monitoring light was minimized by introducing a Corning C.S. No. 0-52 filter between the lamp and cell.

The irradiations were performed in 5 cm long cylindrical cells of Amersil "Supersil" fused quartz, which were evacuated to below 2×10^{-6} mm by vigorous shaking under pumping. A two-pass optical system was used, with the monitoring light confined to a 1-cm diameter, within the spread of the electron beam whose profile had been determined in separate experiments. Eosin was purified chromatographically to give ϵ(516 mμ) $9.4 \times 10^4\ M^{-1}\ cm^{-1}$. The other chemicals were CP grade. The solutions were made with triply distilled water and were buffered with dilute KH_2PO_4 or $Na_2B_4O_7$.

Results

Figure 1 shows transient spectra of deaerated (solid line) and air-saturated (dashed line) eosin solutions taken 5 μsec after pulse irradiation. (The absorption of unexcited eosin (dotted line) shown for comparison is not to scale.) The broad band at 405 mμ has been assigned to the dianion of R previously identified in flash photolysis.[5] The suppression of this band by oxygen indicates that eosin is reduced by e_{aq}^- (and possibly H), because the reaction of R with oxygen is too slow to account for the result (see below). The identification was confirmed by irradiating at pH 5.5, in which case the 405-mμ band decreased and the absorption of the R monoanion at 369 mμ appeared.[6] The band near 450 mμ has been identified with X.[7,8] It was not formed when OH scavengers were present (such as $HCOO^-$, 2-propanol, *p*-cresol, aniline) which indicates that X is formed by the attack of OH on

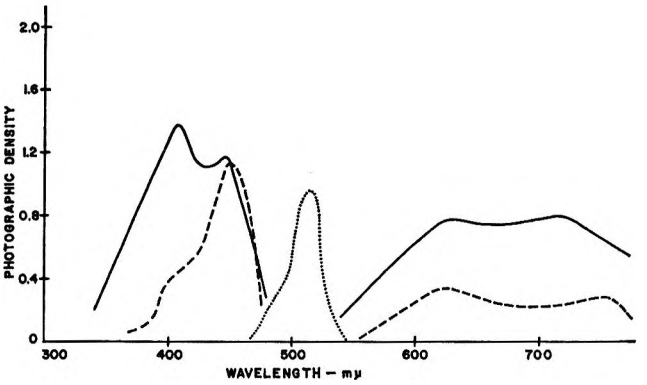

Figure 1. Flash spectra from the pulse radiolysis of aqueous eosin: solid line, deaerated 10 μ*M* (pH 8.5); dashed line, air saturated 20 μ*M* (pH 11) (Kodak I-N spectroscopic plates, uncorrected); dotted line, unexcited eosin (not to scale).

eosin. The diffuse absorption in the red region is attributed to e_{aq}^- in deaerated solutions and to at least two products from the dye with different decays, of which only the shorter lived one is suppressed by oxygen (see below). With the exception of the triplet, species absorbing in this region have not been observed in the flash photolysis of aqueous eosin. The major part of this paper is concerned with kinetic studies that relate to the production, fate, and identification of the species evident in Figure 1.

Table I: Initial *G* Values from the Pulse Radiolysis of Aqueous Eosin at pH 8.5

[Eosin], μ*M*	G(R)[a]	G_a(R)[b]	G(X)[c]	G_a(X)[b]
10	1.60	0.30	0.39	0.30
20	1.96	0.50	0.93	0.80
30	2.18	0.60	1.25	1.47
40	2.20	0.86	...	1.72
50	...	...	...	2.12
60	2.45	1.00	...	...

[a] Based on ϵ(R) $3.8 \times 10^4\ M^{-1}\ cm^{-1}$ at 405 mμ from ref 6. The estimated error in G(R) is ±10%. [b] Obtained with air-saturated solutions. [c] Based on ϵ(X) $5 \times 10^4\ M^{-1}\ cm^{-1}$ at 450 mμ from ref 7. The estimated error in G(X) is ±20%.

(*1*) *Semireduced Eosin.* The maximum growth of R was attained within 3 μsec after the electron pulse. Initial G values for deaerated and air-saturated solutions at different eosin concentrations are given in Table I. The approach of the maximum yield toward the G value for the hydrated electron supports the reaction

$$S + e_{aq}^- \xrightarrow{H^+} R \qquad (1)$$

In alkaline conditions the reaction of e_{aq}^- with H_3O^+ is insignificant. A lower limit for k_1 was determined from the competition between reaction 1 and the bimolecular e_{aq}^- decay

$$e_{aq}^- + e_{aq}^- \longrightarrow 2OH^- + H_2 \qquad (2)$$

because OH is effectively scavenged by eosin at the concentrations employed (see section 2).

The solution to the pertinent rate equation during the buildup period is

$$[R]_{max} = (k_1[S]/2k_2) \ln (1 + 2k_2e_0^-/k_1[S]) \qquad (I)$$

where e_0^- is the hydrated electron yield from pure water under equivalent conditions. The above result can be expanded at suitably high eosin concentrations ($2k_2e_0^-/k_1[S] < 1$) to give

$$[R]_{max} \simeq e_0^-[1 - {}^1/_2(2k_2e_0^-/k_1)[S]^{-1}] \qquad (II)$$

A graph of $[R]_{max}$ *vs.* $[S]^{-1}$ for data taken at pH 8.5 and 10.5 is shown in Figure 2. The intercept gives $e_0^- = 3.0 \times 10^{-6}\ M$, in good agreement with the value calculated from the dose and with $G_e = 2.6$.[10] The slope gives $k_1 = 5 \times 10^9\ M^{-1}\ sec^{-1}$, based on $2k_2 = (1.0 \pm 0.2) \times 10^{10}\ M^{-1}\ sec^{-1}$,[10] which is taken as a lower limit because the scavenging of e_{aq}^- by impurities has not been considered.

The initial yield of R in air-saturated solutions is limited by a competition between reaction 1 and

$$e_{aq}^- + O_2 \longrightarrow O_2^- \qquad (3)$$

The buildup kinetics lead to

$$[G_e/G_a(R)] = 1 + (k_3[O_2]/k_1[S]) \qquad (III)$$

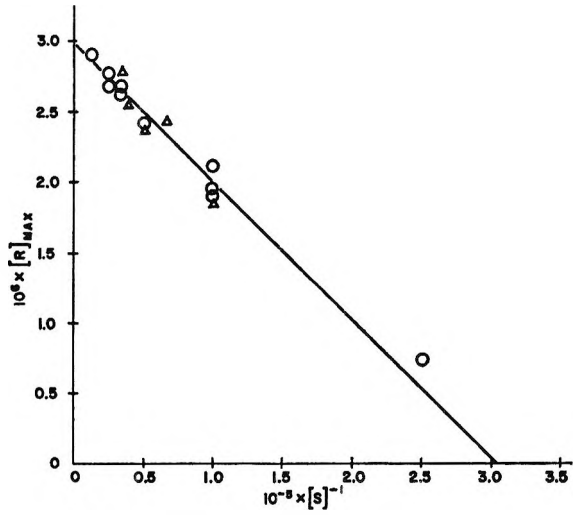

Figure 2. Maximum yield of semireduced eosin (measured at 405 mμ) *vs.* initial eosin concentration, plotted according to eq II: ○, pH 8.5; △, pH 10.5.

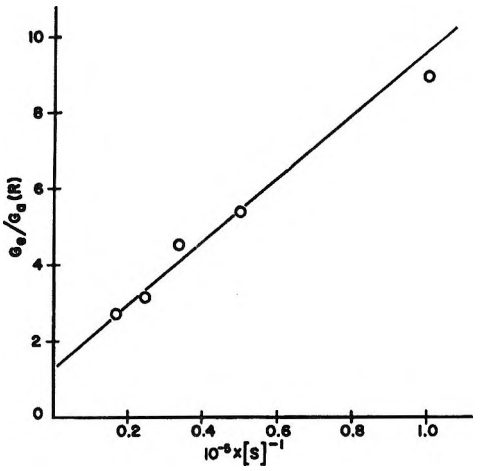

Figure 3. *G* value of semireduced eosin in air-saturated solutions *vs.* eosin concentration, plotted according to eq III.

The data taken at different dye concentrations (Figure 3) show that the functional dependence of eq III is obeyed and give $k_1 = 6 \times 10^{10}\ M^{-1}\ sec^{-1}$, based on $k_3 = 1.9 \times 10^{10}\ M^{-1}\ sec^{-1}$.[10] (The reduction of eosin by H atoms would lower k_1 to $5 \times 10^{10}\ M^{-1}\ sec^{-1}$.) This result is higher than both the encounter-limited value (see below) and the rate constant for the reaction of e_{aq}^- with cationic methylene blue[11] of $2.5 \times 10^{10}\ M^{-1}\ sec^{-1}$ and is taken as an upper limit: $5 \times 10^9 < k_1 < 6 \times 10^{10}\ M^{-1}\ sec^{-1}$.

(*2*) *Semioxidized Eosin.* Initial *G* values for X formation are given in Table I. In contrast to the case of R, where $\epsilon(405)$ values reported in ref 6 and 7 agree to within 5%, the values of $\epsilon(450)$ for X reported in ref 7 and 8 differ by severalfold. The value used in this work is based on ref 7 with a possible 20% error that has been included in the rate constants derived from this quantity. The formation of X is attributed to

$$S + OH\cdot \longrightarrow X + OH^- \qquad (4)$$

The rate of reaction 4 was measured by the competition method[12] using carbonate ion as the reference system

$$CO_3^{2-} + OH\cdot \longrightarrow CO_3^- + OH^- \qquad (5)$$

Air-saturated solutions were used to suppress the e_{aq}^- absorption, and the dye concentration was kept below 10 μM to minimize the overlapping "red product" absorption. The measurements were made at pH 10.5

(11) J. P. Keene, E. J. Land and A. J. Swallow, "Pulse Radiolysis," M. Ebert, J. P. Keene, A. J. Swallow, and J. H. Baxendale, Ed., Academic Press Inc., New York, N. Y., 1965, pp 227–245.

(12) G. E. Adams, J. W. Boag, and B. D. Michael, *Trans. Faraday Soc.*, 61, 1417 (1965).

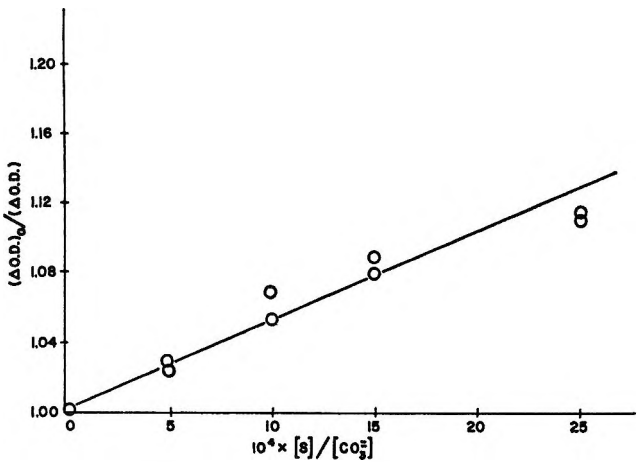

Figure 4. Optical density of CO_3^- (measured at 600 mμ) *vs.* eosin:total carbonate concentration ratio; 0.002 *M* Na_2CO_3 at pH 10.5.

to suppress the dissociation of OH (pK_a = 11.8[13]) although this led to the presence of HCO_3^- (pK_a = 10.20) and necessitated a correction for the actual CO_3^{2-} concentration. (The rate constant for the reaction of HCO_3^- with OH is 10^7 M^{-1} sec^{-1}.[14] The data are plotted in Figure 4 according to

$$(\Delta OD)_0/(\Delta OD) = 1 + (k_4/k_5)([S]/[CO_3^{2-}]) \quad (IV)$$

and give $k_4 = (1.4 \pm 0.4) \times 10^{10}$ M^{-1} sec^{-1}, based on $k_5 = 4.1 \times 10^8$ M^{-1} sec^{-1}.[15]

(3) *Eosin Radical Decay.* In deaerated solutions the eosin radicals can disappear by the simultaneous processes

$$R + X \longrightarrow 2S \quad (6)$$

$$X + X \longrightarrow \text{products} \quad (7)$$

$$R + R \longrightarrow S + L \quad (8)$$

where L is leuco eosin. The rate constant of reaction 8 was obtained by irradiating in the presence of 1 m*M* formate to suppress X formation. The decay of R at 405 mμ was measured after a 50-μsec delay to permit the completion of eosin reduction by oxidized formate (see reaction 12 below) to give $2k_8 = (4.2 \pm 0.9) \times 10^6$ M^{-1} sec^{-1} (Figure 5). The rate constant of reaction 7 was measured by irradiating 20 μM eosin (pH 7.9) with 1 m*M* H_2O_2 present, which led to an initial yield of X ($G(X) \simeq 1.1$) approximately 2 times larger than the initial yield of R ($G(R) \simeq 0.5$). The decay of X, as measured at 450 mμ, followed a two-stage process as shown in Figure 6. The initial rapid phase is attributed to reaction 6, while the slower stage is attributed to reaction 7 with a second-order rate constant $2k_7 = (2.0 \pm 0.5) \times 10^8$ M^{-1} sec^{-1}.

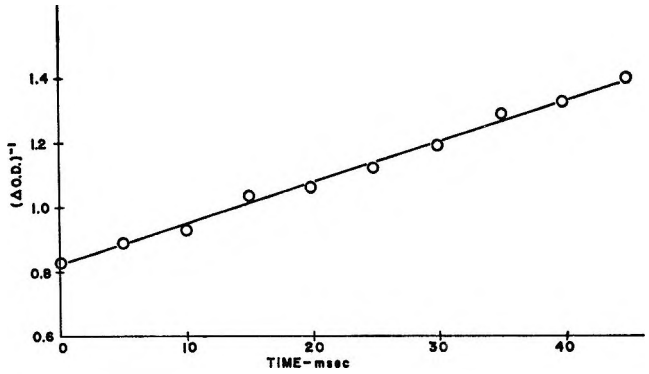

Figure 5. Decay of semireduced eosin (measured at 405 mμ) after pulse radiolysis of 10 μM deaerated eosin in the presence of 1 m*M* formate (pH 8.7).

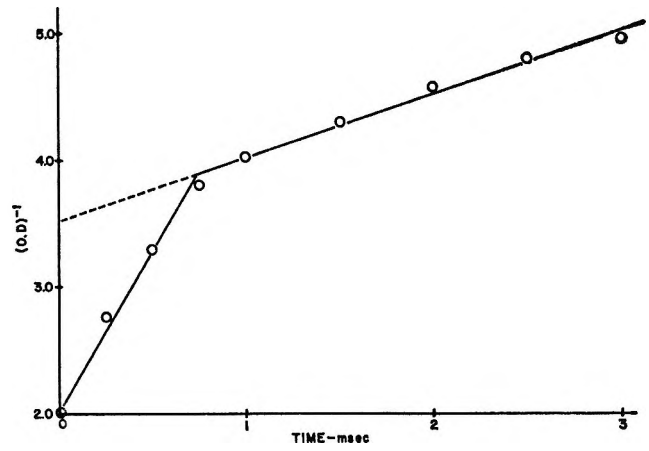

Figure 6. Decay of semioxidized eosin (measured at 450 mμ) after pulse radiolysis of 20 μM deaerated eosin in the presence of 1 m*M* H_2O_2 (pH 7.9).

The data for the decay of R and X in the absence of scavengers cannot be solved in closed form by the usual procedures. An approximate value for k_6 was obtained on the assumption that reaction 6 predominates, in which case the observed decays correspond to the reaction of two species present in different initial concentrations and should follow

$$\ln [A_0(B_0 - A_0 + A)/B_0A] = (B_0 - A_0)k_6t \quad (V)$$

where $A \equiv [X]$ and $B \equiv [R]$ for the case of X decay and *vice versa* for R decay. The reasonably good fit of the data to eq V is shown in Figures 7 and 8, and the rate constant calculation is summarized in Table II.

(13) J. Rabani and M. S. Matheson, *J. Am. Chem. Soc.*, **86**, 3175 (1964).

(14) J. P. Keene, Y. Raef, and A. J. Swallow, ref 11, pp 99–106.

(15) (a) J. L. Weeks and J. Rabani, *J. Phys. Chem.*, **70**, 2100 (1966). (b) Recent work has shown that approximately 50% of the OH reacts to give the "red product," so that R_4 should be considered as the total rate constant for APP OH attack processes.

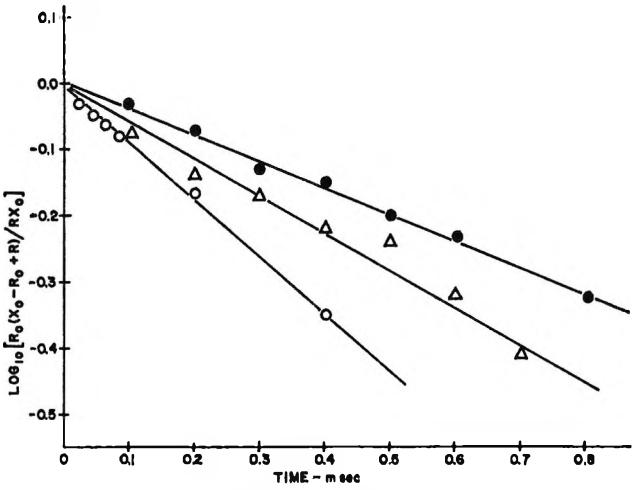

Figure 7. Decay of semireduced eosin (measured at 405 mμ) plotted according to eq V: ○, 10 μ*M* eosin; △, 20 μ*M* eosin; ●, 30 μ*M* eosin (pH 8.5).

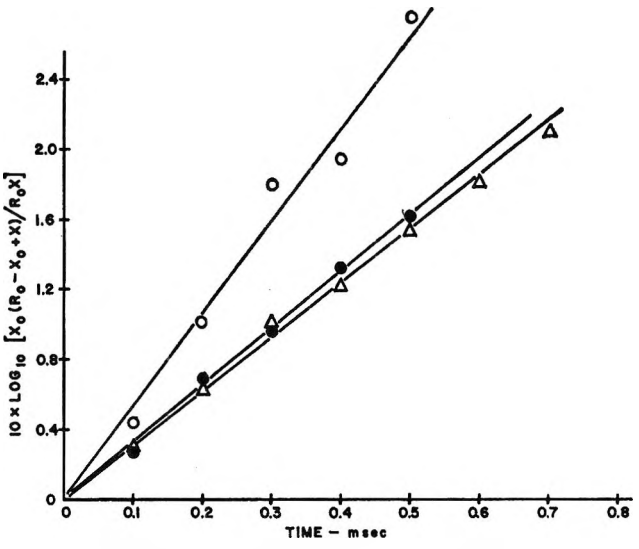

Figure 8. Decay of semioxidized eosin (measured at 450 mμ) plotted according to eq V: ○, 10 μ*M* eosin; △, 20 μ*M* eosin; ●, 30 μ*M* eosin (pH 8.5).

The approximately constant value of k_6 obtained from independent measurements of R and X decay support the validity of this approximation, which is favored also by the higher initial yields of R compared to X.

The actual decay rates of R and X in air-saturated solutions were more rapid and fit pseudo-first-order kinetics. Figure 9 shows data for X disappearance which give a half-time of 110 μsec. A similar analysis gives a 700-μsec half-time for the R decay. The reactions in each case are believed to be

$$X + O_2 \longrightarrow \text{product} \qquad (9)$$

$$R + O_2 \longrightarrow S + HO_2 \qquad (10)$$

Table II: The Disappearance of Semireduced and Semioxidized Eosin *via* Bimolecular Back Reaction

[Eosin], μ*M*	$[X]_0$, μ*M*	$[R]_0$, μ*M*	$10^8 k_6$ From R decay[a]	$10^8 k_6$ From X decay[b]
10	0.41	1.95	12.8	7.8
20	1.18	2.40	10.4	5.9
30	1.33	2.56	7.5	6.1

$k_6 \cong 8 \times 10^8\ M^{-1}\ \text{sec}^{-1}$

[a] Taken from Figure 7. [b] Taken from Figure 8.

Other evidence to support the occurrence of reactions 9 and 10 is discussed below.

(4) *"Red Product."* The "red product" was best studied in the presence of H_2O_2 to suppress the overlapping e_{aq}^- absorption. Figure 10 shows the spectrum obtained by photoelectric monitoring from 525 to 800 mμ. Although the broad absorption with a maximum at 600 mμ is quite similar to that of a triplet spectrum,[6-8] the decay characteristics differ. As shown in Figure 11, there is a rapid exponential decay of $(3.6 \pm 0.2) \times 10^3\ \text{sec}^{-1}$ which is quenched by oxygen and a slower exponential decay of $(3.5 \pm 0.4) \times 10^2\ \text{sec}^{-1}$ which is not. Careful measurements of the buildup with 50 μ*M* deaerated eosin in the presence of 5 m*M* H_2O_2 showed that there is a rapid initial rise, completed within 1 μsec, followed by a slower stage requiring less than 10 μsec. In air-saturated solutions the slower stage extended for approximately 200 μsec. The initial rapid rise requires a rate constant $>2 \times 10^{10}\ M^{-1}\ \text{sec}^{-1}$, which almost certainly limits the reaction to one between eosin and either H or OH. The addition of 10 m*M* formate entirely suppressed the "red product," which supports a reaction with H or OH but does not distinguish between the two pos-

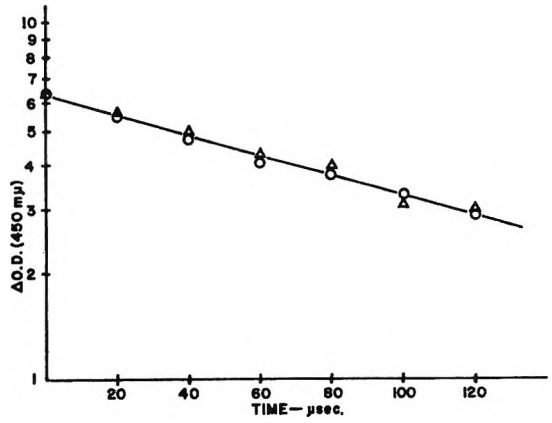

Figure 9. Decay of semioxidized eosin (measured at 450 mμ) in air-saturated 30 μ*M* eosin solutions: ○, pH 8.8; △, pH 6.8.

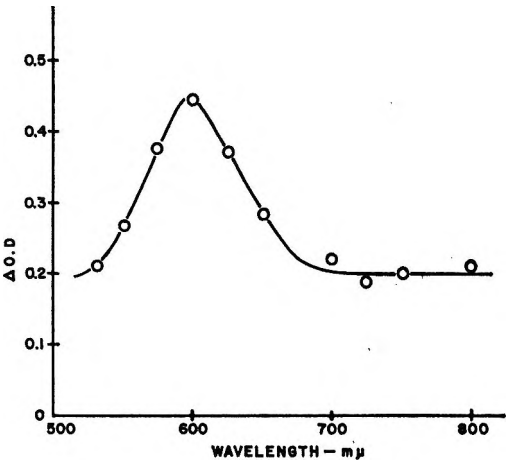

Figure 10. Spectrum of the "red product" in the pulse radiolysis of 50 μM deaerated eosin in the presence of 1 mM H_2O_2 (pH 8.0); obtained by photoelectric detection.

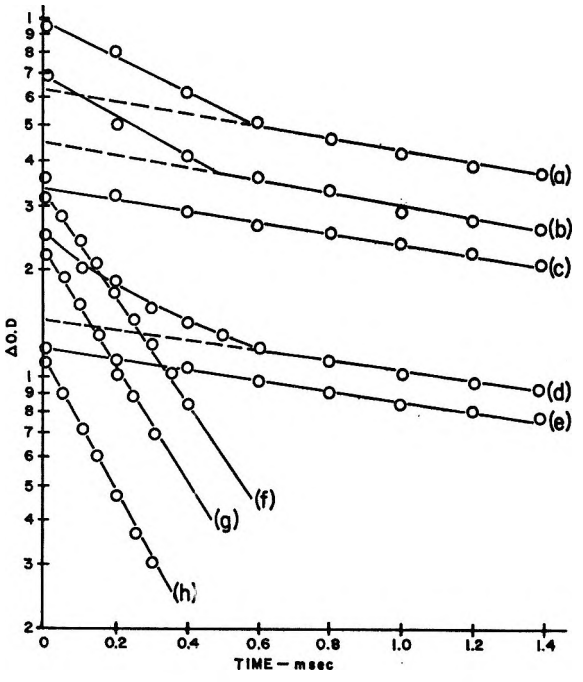

Figure 11. Decay of the "red product": (a) 300 μM deaerated eosin (pH 8.5), measured at 600 mμ; (b) 100 μM deaerated eosin (pH 8.5), measured at 600 mμ; (c) 1 mM air-saturated eosin (pH 8.5), measured at 700 mμ; (d) 60 μM deaerated eosin (pH 8.5) measured at 700 mμ; (e) 40 μM air-saturated eosin (pH 9.1), measured at 800 mμ; (f) fast component of curve a; (g) fast component of curve b; (h) fast component of curve d.

sibilities. On the other hand, a debromination reaction can be ruled out, because the irradiation of fluorescein under similar conditions gave an analogous "red product" with the absorption maximum shifted to 525 mμ.

(5) *Eosin Radiolysis in the Presence of Radical Scavengers.* In these experiments the initial products of water radiolysis were scavenged by additives, so that the observed dye products were due mostly to the reaction of the reacted scavenger with eosin.

(a) *Eosin–H_2O_2–C_2H_5OH Reaction.* The measurements were made on deaerated eosin in the presence of 1 mM H_2O_2 and 10 mM C_2H_5OH, so that e_{aq}^- was converted to OH while OH was effectively converted to $CH_3\dot{C}HOH$.[16] The only transient product of significance was found to be R, which attained its maximum yield after approximately 10 μsec. A rapid initial rise, completed within 2 μsec, was observed in each run which accounted for approximately 20% of the total yield. It is probably due to the reduction of eosin by H which would not have been scavenged as effectively as OH and e_{aq}^-. The slower growth of R is attributed to the attack of α-ethanol radical

$$CH_3\dot{C}HOH + S \longrightarrow R + CH_3CHO \qquad (11)$$

which competes with the decay of $CH_3\dot{C}HOH$ by association and disproportionation.[10,16] The rate constant was determined from the buildup of R in the period from 5 to 30 μsec after the pulse, when the very fast initial phase was complete and before the competing reactions of α-ethanol radical cause any significant depletion

$$(d[R]/dt)_0 = k_{11}[S][CH_3\dot{C}HOH]_0 \qquad (VI)$$

The data in Figure 12 lead to $k_{11} = (1.1 = 0.2) \times 10^9\ M^{-1}\ sec^{-1}$, where $[CH_3\dot{C}HOH]_0$ was calculated from the pulse dose and the assumption that $G(CH_3\dot{C}HOH) = G_e + G_{OH}$.

(b) *Eosin–H_2O_2–$HCOO^-$ Reaction.* The pulse radiolysis of deaerated eosin in the presence of 1 mM H_2O_2 to scavenge e_{aq}^- and 10 mM formate to scavenge both OH and H showed a slow rise of R as the only transient intermediary. In this case, the reaction is attributed to competition between the reduction of eosin by CO_2^-

$$CO_2^- + S \xrightarrow{H^+} CO_2 + R \qquad (12)$$

and its dimerization to give oxalic acid.[14] The data for the initial rise of R at 405 mμ (Figure 12) give $k_{12} = (2.5 \pm 0.5) \times 10^8\ M^{-1}\ sec^{-1}$, where $G(CO_2^-)$ was taken as equal to $G_e + G_H + G_{OH}$ in this case.

Discussion

The principal initial reactions in the radiolysis of deaerated, aqueous eosin are the oxidative and reduc-

(16) I. A. Taub and L. M. Dorfman, *J. Am. Chem. Soc.*, 84, 4053 (1962).

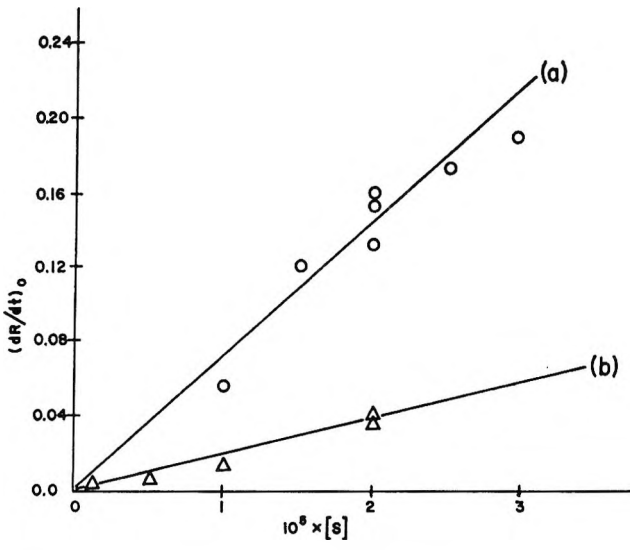

Figure 12. Initial growth of semireduced eosin (measured at 405 mμ) *vs.* eosin concentration: (a) 1 m*M* H_2O_2 and 10 m*M* C_2H_5OH; (b) 1 m*M* H_2O_2 and 10 m*M* HCOONa (deaerated solutions, pH 8.5–9.0).

tive attack of OH and e_{aq}^-, respectively. A semiquinone structure has been postulated for R with the unpaired electron on carbon-9.[17] It exists as the monoanion in acidic solution and the dianion in basic solution.[6] The oxidation product X has been attributed to the monoanion formed by splitting at the 3′-position OH bond.[7] The "red product" is a new intermediate that has not been reported in flash photolysis results. There appear to be two components with different growth and decay rates. The longer lived species was not significant below 30 μ*M* eosin and is attributed to the addition of OH in a reaction at least a factor of 10 slower than reaction 4. The faster growing and shorter lived species not observed with oxygen is attributed to H atom addition. Since the addition of 1 m*M* H_2O_2 as e_{aq}^- scavenger did not entirely suppress the rapid growth of R (see paragraphs 3 and 5a), it is believed that H also reduces eosin by a reaction similar to reaction 1. The very slow growth of "red product" observed only in air-saturated solutions may be due to the addition of HO_2. The addition of OH and HO_2 would be expected to be slower than that of H because of steric hindrance by the halogens.

The rate constants for the dye–dye reactions obtained in this work can be compared to flash photolysis information. The only reported measurement of the eosin (R + X) rate constant appears to be the estimate made by Ohno, *et al.*,[8] of 9×10^8 M^{-1} sec^{-1}, which is in good agreement with this work. In addition, Lindqvist[18] obtained evidence for the occurrence of this reaction in the case of fluorescein, with an estimated rate constant of 10^9 M^{-1} sec^{-1}. Furthermore, he proposed that reaction 7 (for fluorescein) is actually the dimerization: X + X → X_2. Somewhat more information is available on the R + R reaction. For the case of fluorescein, Lindqvist[18] noted that the decay of R became very slow after X had disappeared and also that S reappeared at the same slow rate. The complex reaction: 2R + X_2 → 4S was proposed to explain the latter. On the other hand, Zwicker and Grossweiner[6] proposed that R decays by dismutation and obtained 1.4×10^{10} as the product of the rate constant for the monoanion (R + R) decay and the rate constant for the bimolecular disappearance of phenoxyl. Taking 5.6×10^9 M^{-1} sec^{-1} for the latter[19] gives $2k_8 = 3 \times 10^6$ M^{-1} sec^{-1}, which is in satisfactory agreement with this work if the ionic charge is not a major factor.

The occurrence of reaction 10 for the case of fluorescein has been proposed by Kasche and Lindqvist,[20] with an estimated rate constant of 10^8–10^9 M^{-1} sec^{-1}.

Table III: Summary of Rate Constants and Comparison with Encounter-Limited Values from the Debye Equation

	Reaction	z_1z_2	$10^{-9}k$ (calcd)[a]	$10^{-9}k$ (exptl)
(1)	$S + e_{aq}^- \xrightarrow{H^+} R$	2	11[b,c]	⩾5
(4)	$S + OH\cdot \rightarrow X + OH^-$	0	13[d]	14 ± 4[h]
(6)	$R + X \rightarrow 2S$	2	4.6	≅0.8
(7)	$X + X \rightarrow$ product	1	5.2	0.10 ± 0.03[e]
(8)	$R + R \rightarrow L + S$	4	1.4	0.0021 ± 0.0004[e]
(11)	$S + CH_3\dot{C}HOH \rightarrow R + CH_3CHO$	0	8.2[f]	1.1 ± 0.2
(12)	$S + CO_2^- \rightarrow R + CO_2$	2	2.9[g]	0.25 ± 0.05

[a] Based on a dielectric constant of 80 for water and diffusion constants derived from Stokes' law. [b] The diffusion constant of e_{aq}^- was taken from K. H. Schmidt and W. L. Buck, *Science*, **151**, 70 (1966), and the radius was taken as 2.7 A. [c] The molecular radii of S, R, and X were all taken as 5.0 A, based on a sphere of density 1.3 and the fluorescein molecular weight corrected by substituting four bromine volumes for hydrogen atoms. [d] The OH· radius was taken as 1.1 A. [e] The value listed is the encounter rate, not $2k$. [f] The α-ethanol radical radius was taken as 2.6 A from a sphere of appropriate density and molecular weight reduced by an H atomic volume. [g] The CO_2^- radius was taken as 1.8 A from a sphere of appropriate density and molecular weight reduced by two H atomic volumes. [h] See ref 12.

(17) N. N. Bubnov, L. A. Kibalko, V. F. Tsepalov, and V. Ya. Shliapintokhh, *Opt. i Spektroskopiya*, **7**, 117 (1959).

(18) L. Lindqvist, *Arkiv Kemi*, **16**, 79 (1960).

(19) G. Dobson and L. I. Grossweiner, *Trans. Faraday Soc.*, **61**, 708 (1965).

(20) V. Kasche and L. Lindqvist, *J. Phys. Chem.*, **68**, 817 (1964).

Although this quantity has not been measured previously for eosin, there is little doubt that it takes place in eosin-sensitized photooxidations under aerobic conditions, where the reduced dye is restored for further sensitization. Additional support for this reaction comes from the recent work of Usui, *et al.*,[21] in which it was reported that the photolysis of aerobic, aqueous eosin leads to an uptake of oxygen and the production of H_2O_2. There does not appear to be any previous information about reaction 9, although the change of the X decay from second order in deaerated solutions to first order with air present is considered to be good evidence for the process. The measured rate constants are summarized in Table III and are compared to the encounter-limited values obtained with the Debye equation.[22] The results indicate that the reactions of eosin with e_{aq}^- and OH are encounter limited. The dye–dye reactions are 5–700 times slower, probably due to steric factors. The reaction rate of eosin dianion with CO_2^- is some 20 times slower than the comparable reaction with methylene blue cation (5.6×10^9 M^{-1} sec^{-1} [11]), while the coulombic effect predicts only a factor of 5. However, the experimental rate constant for reaction of the neutral α-ethanol radical with eosin is also lower than the calculated value by ~ 10, so that the difference between k_{12} measured in this work and the corresponding methylene blue result is probably real and not due to a large error in either determination.

Acknowledgment. The authors wish to acknowledge the valuable assistance of Mr. G. Sandberg with the design and operation of the pulse radiolysis system and to thank Dr. P. Cordier for making available his work on fluorescein pulse radiolysis. In particular, we are indebted to Dr. E. J. Hart of the Chemistry Division, Argonne National Laboratory, for informing us of his unpublished results on eosin radiolysis.

(21) Y. Usui, K. Itoh, and M. Koizumi, *Bull. Chem. Soc. Japan*, **38**, 1015 (1965).

(22) P. Debye, *Trans. Electrochem. Soc.*, **82**, 265 (1942).

Constant-Potential Reactions Simultaneously Controlled by Charge-Transfer and Mass-Transfer Polarization at Planar, Spherical, and Cylindrical Electrodes

by Charles A. Johnson and Sidney Barnartt

Edgar C. Bain Laboratory for Fundamental Research, United States Steel Corporation Research Center, Monroeville, Pennsylvania *(Received August 11, 1966)*

The theory of constant-potential electrode reactions for first-order charge-transfer mechanisms is extended. For planar electrodes, new analytical procedures are described for extracting the mechanistic parameters of the charge-transfer process from potentiostatic current–time curves. The solution to the boundary value problem for spherical electrodes is given in closed form. For the corresponding cylindrical electrode problem, an approximate solution, valid at short times, is derived, and a numerical method is outlined for obtaining the entire current–time curve for any given case. It is shown that the small spherical electrode remains under partial charge-transfer control at all times and that long-time current measurements are useful for determining the charge-transfer parameters.

In general, the rate of an electrode reaction will be determined by both charge-transfer and mass-transfer polarization, even in the case of slow reactions if the concentration of one reactant is small. The purpose of this paper is to examine the theoretical time behavior of the reaction rate at constant potential for electrodes having planar, spherical, or cylindrical symmetry. The electrochemical systems considered will be limited to first-order charge-transfer mechanisms. The current–time relation for planar electrodes at constant potential is known. This will be examined in greater detail, particularly from the standpoint of rapid reactions. Then a general solution will be given in closed form for spherical electrodes. Finally, an approximate solution will be developed for cylindrical electrodes, and a numerical method for the general solution will be outlined.

Current–Potential Relations

The current–potential relation for a reaction of the type $R^{(z-n)+} = O^{z+} + ne^-$ was derived by Gerischer.[1]

$$i/i_0 = \frac{a_R}{a_R^0} \exp[(1 - \beta)n\epsilon\eta] - \frac{a_O}{a_O^0} \exp[-\beta n\epsilon\eta] \quad (1)$$

Here i is the net anodic current density at overpotential η, i_0 is the exchange current density, β is the transfer coefficient, and $\epsilon \equiv F/RT$. The activities of R and O are designated a_R and a_O at the electrode–solution interface at time t; these differ from the bulk values a_R^0 and a_O^0 as a result of mass transfer effects. Equation 1 is limited to those charge-transfer mechanisms in which all of the electrical work involved occurs during the rate-determining step, and which are first order (defined at constant potential) with respect to the activities a_R and a_O.[2,3]

For rapid reactions, the following approximation to eq 1, also due to Gerischer,[4] is generally used.[5–7]

$$i/i_0 = n\epsilon\eta + \frac{a_R}{a_R^0} - \frac{a_O}{a_O^0} = n\epsilon\eta + \frac{\Delta a_R}{a_R^0} - \frac{\Delta a_O}{a_O^0} \quad (2)$$

where $\Delta a_R = a_R - a_R^0$ and $\Delta a_O = a_O - a_O^0$. Equation 2 was derived on the assumption that η, Δa_R, and Δa_O are all small, a set of limitations too confining for rapid

(1) H. Gerischer, *Z. Elektrochem.*, **54**, 362 (1950).
(2) R. Parsons, *Trans. Faraday Soc.*, **47**, 1332 (1951).
(3) S. Barnartt, *Electrochim. Acta*, **11**, 1531 (1966).
(4) H. Gerischer, *Z. Elektrochem.*, **55**, 98 (1951).
(5) W. Vielstich and P. Delahay, *J. Am. Chem. Soc.*, **79**, 1874 (1957).
(6) P. Delahay, *Advan. Electrochem. Electrochem. Eng.*, **1**, 233 (1961).
(7) P. Delahay, "Double Layer and Electrode Kinetics," Interscience Publishers, Inc., New York, N. Y., 1965.

reactions where activity changes develop rapidly. We propose, instead, a more basic relation for rapid reactions, valid at all values of Δa_R and Δa_O. This is obtained from eq 1 by use of $\exp(k\eta) \simeq 1 + k\eta$

$$(i/i_0)_{\eta \to 0} = n\epsilon\eta \frac{a_R}{a_R^0} + (1 - \beta n\epsilon\eta)\left[\frac{a_R}{a_R^0} - \frac{a_O}{a_O^0}\right] \quad (3)$$

where $[(\Delta a_R/a_R^0) - (\Delta a_O/a_O^0)]$ may be substituted for the last factor. Equation 3 reduces to eq 2 only if the assumption is made that Δa_R and Δa_O are small. This assumption is valid only during a very short interval after a rapid reaction is initiated; at longer times, eq 2 will exhibit greater deviations from the true relation (eq 1) than will eq 3. An illustration of these deviations will be given below for the case of linear diffusion.

Planar Electrodes

Potentiostatic Current–Time Relations. Gerischer and Vielstich[8] have derived the solution, in closed form, for a first-order reaction described by eq 1, with semi-infinite linear diffusion as the sole mass-transfer process. The electrolyte is assumed to contain excess neutral salt, so that concentration ratios may replace the activity ratios in eq 1 with little error. The solution will be reproduced here and applied numerically to a typical fast reaction to illustrate the range of validity for eq 2 and 3. The solutions for the concentrations and current density at the electrode surface are

$$c_R = c_R^0 - (A/\lambda\kappa^{1/2})[1 - \exp(\lambda^2 t)\ \mathrm{erfc}(\lambda t^{1/2})] \quad (4)$$

$$c_O = c_O^0 + (A/\lambda)[1 - \exp(\lambda^2 t)\ \mathrm{erfc}(\lambda t^{1/2})] \quad (5)$$

$$i = i_{(t=0)} \exp(\lambda^2 t)\ \mathrm{erfc}(\lambda t^{1/2}) \quad (6)$$

where the desired charge-transfer current corresponding to overpotential η is

$$i_{(t=0)} = i_0[\exp(1 - \beta)n\epsilon\eta - \exp(-\beta n\epsilon\eta)] \quad (7)$$

Here the quantities λ and A are defined by

$$\lambda = \frac{i_0 \exp[(1 - \beta)n\epsilon\eta]}{nFc_R^0 D_R^{1/2}} + \frac{i_0 \exp(-\beta n\epsilon\eta)}{nFc_O^0 D_O^{1/2}} \quad (8)$$

$$A = \frac{\kappa^{1/2} i_0 \exp[(1 - \beta)n\epsilon\eta]}{nFD_R^{1/2}} - \frac{i_0 \exp(-\beta n\epsilon\eta)}{nFD_O^{1/2}} \quad (9)$$

where $\kappa \equiv D_R/D_O$, the ratio of the diffusion coefficients. It should be noted that the equations as given in the Gerischer–Vielstich paper[8] contained two errors (no post-publication correction found): (1) omission of $\kappa^{1/2}$ from the first term of A; (2) the quantity $(\kappa^{-1/2}A/\lambda)$ in eq 4 was given as $(\kappa^{1/2}A/\lambda)$. The quantity A may be written in terms of the charge-transfer current as

$$A = i_{(t=0)}[nFD_O^{1/2}]^{-1} \quad (9a)$$

Substituting for A in eq 4 and 5, one obtains the concentrations in terms of the charge-transfer current

$$c_R = c_R^0 - i_{(t=0)}[nFD_R^{1/2}\lambda]^{-1} \times [1 - \exp(\lambda^2 t)\ \mathrm{erfc}(\lambda t^{1/2})] \quad (4a)$$

$$c_O = c_O^0 + i_{(t=0)}[nFD_O^{1/2}\lambda]^{-1} \times [1 - \exp(\lambda^2 t)\ \mathrm{erfc}(\lambda t^{1/2})] \quad (5a)$$

If the electrode reaction is rapid (η small), the current–time relation is still given by eq 6, but the parameters $i_{(t=0)}$, λ, and A may be simplified to

$$i_{(t=0)} = i_0 n\epsilon\eta \quad (10)$$

$$\lambda = \frac{i_0}{F}\left[\frac{\epsilon\eta}{c_R^0 D_R^{1/2}} + \left(\frac{1}{n} - \beta\epsilon\eta\right)\left(\frac{1}{c_R^0 D_R^{1/2}} + \frac{1}{c_O^0 D_O^{1/2}}\right)\right] \quad (11)$$

$$A = i_0\eta/RTD_O^{1/2} \quad (12)$$

The current–time relation (eq 6) is obtainable from eq 1 by substitution for c_R and c_O from eq 4 and 5. Similarly, substitution for these concentrations in eq 2 and 3 yields the corresponding approximate current–time curves. The following numerical case was selected to illustrate the deviations of the approximate curves from the rigorous one: $i_0 = 5 \times 10^{-3}$ A/cm² at 25°, $\beta = 0.5$, $n = 1$, $c_O^0 = 5 \times 10^{-2}$, and $c_R^0 = 10^{-2}$ mole/l.; $D_O = 2 \times 10^{-5}$ and $D_R = 10^{-5}$ cm²/sec. With these values, the reaction rates should be roughly equivalent to those reported[9] for the ferrous–ferric reaction on bright platinum. Figure 1 shows the calculated current–time curves for an applied overpotential of 10 mv. At the longest time shown ($t = 0.21$ sec), c_O has changed by 2.4% and c_R by 17%. These changes are sufficient to cause considerable deviation of eq 2 from the true curve, but eq 3 remains extremely close. Thus eq 3 should be used as the basic rapid-reaction equation, while the former is an approximation useful only for very short reaction times.

It may be noted from eq 4a and 5a that the maximum change in concentration, which occurs at $t \to \infty$ (and $i \to 0$), is given for each of the diffusing substances by $i_{(t=0)}[nFD^{1/2}\lambda]^{-1}$. At any given time t, the same fraction $[1 - \exp(\lambda^2 t)\ \mathrm{erfc}(\lambda t^{1/2})]$ of the maximum change has taken place for each substance. In the present example, this fraction is 0.572 at the longest time considered (0.21 sec).

(8) H. Gerischer and W. Vielstich, *Z. Physik. Chem.* (Frankfurt), **3**, 16 (1955).

(9) H. Gerischer, *Z. Elektrochem.*, **54**, 366 (1950).

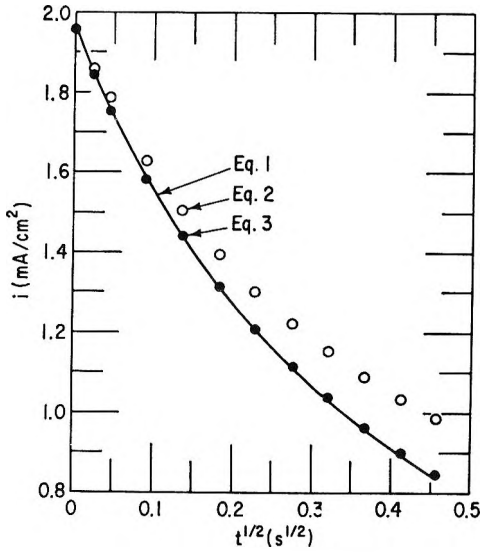

Figure 1. Calculated constant-potential current–time relations, planar electrodes: ———, eq 1; O, eq 2; ●, eq 3.

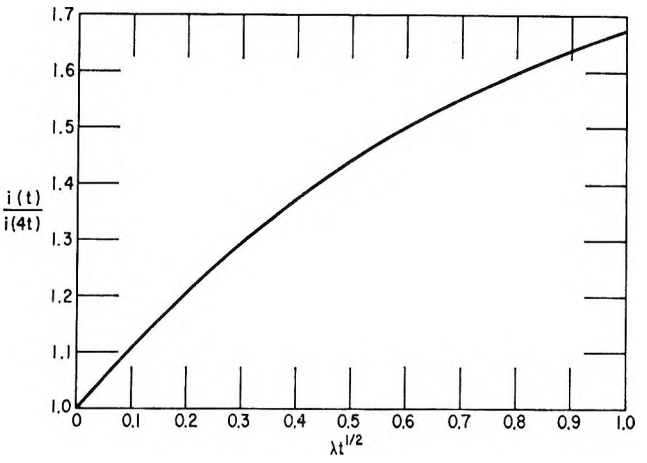

Figure 2. Variation of current ratio $i_{(t)}/i_{(4t)}$ with $\lambda t^{1/2}$, planar electrodes.

Evaluation of $i_{(t=0)}$ *and* λ. If the argument $\lambda t^{1/2}$ is small, eq 6 may be approximated by

$$i = i_{(t=0)}[1 - (2/\pi^{1/2})\lambda t^{1/2} + \lambda^2 t] \qquad (13)$$

For a very short period, up to the time the last term in brackets ceases to be negligible, the initial region of the i–$t^{1/2}$ curve is linear (*e.g.*, $t < 10$ msec in Figure 1). From this line $i_{(t=0)}$ may be obtained by extrapolation, and the slope of the line yields λ. Experimentally, however, this linear region will often be inaccessible for moderately rapid reactions with present-day potentiostatic circuitry. An appreciable time is required to attain the control potential within a small fraction of a millivolt (η being small), primarily because it is necessary to incorporate automatic compensation for the *IR* drop between the controlled electrode and the capillary tip of the reference electrode.[10]

To permit analysis of experimental current–time curves which exclude the initial linear region, we present here another simple procedure for evaluating $i_{(t=0)}$ and λ. In this method, one selects an arbitrary time, t, and reads the current from the experimental curve at times t and $4t$. The ratio of these currents is

$$\frac{i_{(t)}}{i_{(4t)}} = \frac{\exp(\lambda^2 t)\ \mathrm{erfc}(\lambda t^{1/2})}{\exp(4\lambda^2 t)\ \mathrm{erfc}(2\lambda t^{1/2})} \qquad (14)$$

This ratio is readily calculated for all values of $\lambda t^{1/2}$ from tables[11] of the function $\exp(y^2)\ \mathrm{erfc}(y)$, and is shown in Figure 2 for $\lambda t^{1/2} = 0$ to 1. The experimental value of the current ratio for a specific time t_1 has a corresponding value of $\lambda t_1^{1/2}$ which is obtained from the master curve, Figure 2, and this value yields λ. The procedure may be repeated for times t_2, t_3, t_4 ... to obtain a mean value of λ. Utilizing the mean λ, each measured current at t_1, t_2, t_3 ... yields $i_{(t=0)}$ from eq 6. If the deviations of the individual values of λ or of $i_{(t=0)}$ about the mean value are found to be small and randomly distributed, one has support for the *a priori* assumption of a first-order charge-transfer mechanism. As $\lambda t^{1/2}$ increases, the slope of the curve in Figure 2 decreases; hence the precision with which λ can be evaluated decreases with increasing time in the intermediate-time range ($0.85 \gtrsim i_{(t)}/i_{(t=0)} \gtrsim 0.45$).[12]

Evaluation of Charge-Transfer Parameters.[6,7] For slow electrode reactions (η relatively large), it is sufficient to determine $i_{(t=0)}$ from potentiostatic current–time curves as a function of η, either for anodic (η positive) or cathodic (η negative) polarization. The well-known Tafel plot then yields both i_0 and β. For rapid reactions (small η), measurement of $i_{(t=0)}$ in a given solution yields i_0 from eq 10; since i_0 is given by

$$i_0 = i_{0,s}\ (a_R{}^0)^{\beta}(a_O{}^0)^{1-\beta} \qquad (15)$$

where $i_{0,s}$ is the standard exchange current density,[13] and β is obtained from determinations of i_0 with solutions in which $a_R{}^0$ is varied at constant $a_O{}^0$ *or* $a_O{}^0$ varied at constant $a_R{}^0$.

(10) S. Barnartt, submitted for publication.

(11) H. S. Carslaw and J. C. Jaeger, "Conduction of Heat in Solids," 2nd ed, Clarendon Press, Oxford, 1959.

(12) As pointed out by a referee, a quantitative treatment of this decrease in precision with time was given recently by K. B. Oldham and R. A. Osteryoung, *J. Electroanal. Chem.*, **11**, 397 (1966). These authors also present a novel method of evaluating λ and $i_{(t=0)}$ from current measurements in the intermediate time range. Their method differs significantly from ours in that it involves current measurements from tangents drawn to the experimental current–time curve.

(13) S. Barnartt, *J. Phys. Chem.*, **70**, 412 (1966).

Evaluation of D_R or D_O. The ratio $i_{(t=0)}/\lambda$ from eq 7 and 8 is given by

$$\frac{i_{(t=0)}}{\lambda} = nF[\exp(n\epsilon\eta) - 1] \times \left[\frac{\exp(n\epsilon\eta)}{c_R^0\sqrt{D_R}} + \frac{1}{c_O^0\sqrt{D_O}}\right]^{-1} \quad (16)$$

and is seen to be independent of i_0 and β. Thus the values of $i_{(t=0)}$ and λ obtained from a single potentiostatic current–time curve permit estimation of one of the diffusion coefficients if the other is known. This is so even though $i_{(t=0)}$ and λ are obtained from the current–time curve at short times, where the reaction is partly controlled by the charge-transfer kinetics.

The current at long times ($\lambda t^{1/2} >> 1$) is under complete mass-transfer control, and a plot of i *vs.* $t^{-1/2}$ is linear with a slope proportional to the ratio $i_{(t=0)}/\lambda$, as was shown by Gerischer and Vielstich.[8] Hence, the long-time currents permit evaluation of the diffusion coefficient somewhat more directly.

Spherical Electrodes

The problem is solved here in closed form for an electrode reaction at constant potential involving a first-order charge-transfer mechanism (eq 1), with diffusion in a system of spherical symmetry as the sole mode of mass transfer. The mathematical formulation of the problem comprises differential equations

$$D_R \frac{1}{r^2}\frac{\partial}{\partial r}\left(r^2\frac{\partial c_R}{\partial r}\right) = \frac{\partial c_R}{\partial t}; \quad D_O \frac{1}{r^2}\frac{\partial}{\partial r}\left(r^2\frac{\partial c_O}{\partial r}\right) = \frac{\partial c_O}{\partial t}$$

with initial conditions ($t = 0$, $r \geq a$): $c_R = c_R^0$, $c_O = c_O^0$ and boundary conditions (all t)

$$r \longrightarrow \infty: \quad c_R \longrightarrow c_R^0; \quad c_O \longrightarrow c_O^0$$

$$r = a: \quad i = nFD_R\frac{\partial c_R}{\partial r} = -nFD_O\frac{\partial c_O}{\partial r}$$

Here a is the electrode radius, and i is the current density given by eq 1 with concentrations substituted for activities.

General Solution. The general solution of this problem, derived by the Laplace transform method, is presented in the Appendix. Equations A17 and A18 give the concentration changes at the electrode, and eq A19 gives the current density. Two regions of the current–time curve are of particular interest for extracting the charge-transfer parameters, namely the initial short-time section and the final long-time section.

(*a*) *Short-Time Solution.* This is obtained by use of the approximation, $\exp x^2 \operatorname{erfc} x \simeq 1 - (2/\pi^{1/2})x + x^2$, which is valid for small values of x. Equations A17–19 convert to eq 17–19.

$$c_R = c_R^0 - \frac{i_{(t=0)}}{nFD_R^{1/2}}\left[\frac{2}{\pi^{1/2}}t^{1/2} - \left(1 + \frac{D_R^{1/2}}{a\lambda}\right)\lambda t\right] \quad (17)$$

$$c_O = c_O^0 + \frac{i_{(t=0)}}{nFD_O^{1/2}}\left[\frac{2}{\pi^{1/2}}t^{1/2} - \left(1 + \frac{D_O^{1/2}}{a\lambda}\right)\lambda t\right] \quad (18)$$

$$i = i_{(t=0)}\left[1 - \frac{2}{\pi^{1/2}}\lambda t^{1/2} + \left(1 + \frac{\lambda_R D_R + \lambda_O D_O}{a\lambda^2}\right)\lambda^2 t\right] \quad (19)$$

where

$$\lambda_R = \frac{i_0\exp(1-\beta)n\epsilon\eta}{nFD_R c_R^0}; \quad \lambda_O = \frac{i_0\exp(-\beta n\epsilon\eta)}{nFD_O c_O^0} \quad (20)$$

and also $\lambda = \lambda_R D_R^{1/2} + \lambda_O D_O^{1/2}$ and $i_{(t=0)} = nF\cdot(\lambda_R D_R c_R^0 - \lambda_O D_O c_O^0)$ as for planar geometry. A comparison of eq 19 with the corresponding eq 13 for the planar case shows that, over sufficiently short times such that the term in t is negligible, the sphere and plate electrodes yield the same linear i–$t^{1/2}$ relation. The linear behavior terminates sooner for the small sphere, however, since the term in t is larger in eq 19 than in eq 13.

If this linear portion of the curve is experimentally accessible, the values of λ and $i_{(t=0)}$ obtained from it can be used to determine the charge-transfer parameters and one of the diffusion coefficients, as described above for planar electrodes. For moderately rapid reactions, if the initial portion is inaccessible, charge-transfer parameters can be determined from the long-time portion of the curve as shown below.

(*b*) *Long-Time Solution.* Use is made of the approximation, $\exp x^2 \operatorname{erfc} x = \pi^{-1/2}x^{-1}$, valid for large values of x. Equations A17–A19 become

$$c_R = c_R^0 - \frac{i_{(t=0)}}{nF}\frac{a}{D_R(1 + a\lambda_R + a\lambda_O)} \times \left[1 + \frac{a\lambda_O(\kappa^{1/2} - 1) - 1}{1 + a\lambda_R + a\lambda_O}\frac{a}{(D_R\pi t)^{1/2}}\right] \quad (21)$$

$$c_O = c_O^0 + \frac{i_{(t=0)}}{nF}\frac{a}{D_O(1 + a\lambda_R + a\lambda_O)} \times \left[1 + \frac{a\lambda_R(\kappa^{-1/2} - 1) - 1}{1 + a\lambda_R + a\lambda_O}\frac{a}{(D_O\pi t)^{1/2}}\right] \quad (22)$$

$$i = \frac{i_{(t=0)}}{1 + a\lambda_R + a\lambda_O} \times \left[1 + \frac{a^2(\lambda_R/D_R^{1/2} + \lambda_O/D_O^{1/2})}{1 + a\lambda_R + a\lambda_O}\frac{1}{(\pi t)^{1/2}}\right] \quad (23)$$

A plot of i against $t^{-1/2}$ is a straight line, of form

$$i = i_{(t\to\infty)} + \sigma t^{-1/2} \quad (23a)$$

with intercept

$$i_{(t\to\infty)} = \frac{i_{(t=0)}}{1 + a\lambda_R + a\lambda_O} \quad (23b)$$

and slope

$$\sigma = \frac{a^2(\lambda_R/D_R^{1/2} + \lambda_O/D_O^{1/2})\, i_{(t=0)}}{\pi^{1/2}(1 + a\lambda_R + a\lambda_O)^2} \quad (23c)$$

It may be recalled[14] that reversible reactions at spherical electrodes also exhibit a linear i–$t^{1/2}$ curve at long times, but the intercept and slope are then quite different from the corresponding expressions for irreversible reactions (eq 23b,c).

At long times, the current at a spherical electrode goes toward the finite value given by eq 23b, whereas at a plane electrode, the corresponding current goes to zero. In the latter case, the reaction becomes essentially diffusion controlled[8] at $\lambda t^{1/2} > 1$ (or at $i/i_{(t=0)} < 0.43$), so that current measurements at long times give no information about the charge-transfer mechanism. With small spherical electrodes, however, the reaction remains under partial charge-transfer control at all times. Provided the diffusion coefficients are known, the charge-transfer parameters may be derived as follows. We define the quantity

$$\rho \equiv \frac{\lambda_R}{\lambda_O} = \frac{c_O^0 D_O}{c_R^0 D_R} \exp(n\epsilon\eta) \quad (24)$$

The combination of eq 23b, 23c, and 24 yields

$$\frac{1}{\lambda_O} = a\left[\frac{a i_{(t\to\infty)}}{\sigma\pi^{1/2}}\left(\frac{\rho}{D_R^{1/2}} + \frac{1}{D_O^{1/2}}\right) - \rho - 1\right] \quad (25)$$

This permits evaluation of λ_O corresponding to the value of η which establishes the current–time curve. After measuring current–time curves at several values of η, we may plot $\log \lambda_O$ against η, since from eq 20

$$\log \lambda_O = \log (i_0/nFD_O c_O^0) - (\beta n\epsilon/2.3)\eta \quad (20a)$$

to obtain β from the slope and i_0 from the intercept at $\eta = 0$.

Particular Case: $D_R = D_O$. It is of interest to examine the special case of $D_R = D_O = D$ which was treated by Shain, Martin, and Ross.[15] The time variations of current density and concentrations at the electrode surface become, from eq A17–A19

$$c_R = c_R^0 - \frac{i_{t=0}}{nFD^{1/2}\lambda(1 + \delta)} \times [1 - \exp((1 + \delta)^2\lambda^2 t)\ \mathrm{erfc}((1 + \delta)\lambda t^{1/2})] \quad (26)$$

$$c_O = c_O^0 + \frac{i_{(t=0)}}{nFD^{1/2}\lambda(1 + \delta)} \times [1 - \exp((1 + \delta)^2\lambda^2 t)\ \mathrm{erfc}((1 + \delta)\lambda t^{1/2})] \quad (27)$$

$$\frac{i}{i_{(t=0)}} = \frac{\delta}{1 + \delta} + \frac{1}{1 + \delta} \times [\exp((1 + \delta)^2\lambda^2 t)\ \mathrm{erfc}((1 + \delta)\lambda t^{1/2})] \quad (28)$$

where $\delta = D^{1/2}/a\lambda$. Equation 28 is equivalent to the solution for the current previously given.[15]

The short-time current at $\lambda t^{1/2} << 1$ now becomes

$$i = i_{(t=0)}\,[1 - 2\pi^{-1/2}\lambda t^{1/2} + (1 + \delta)\lambda^2 t] \quad (29)$$

Thus from a single potentiostatic current–time curve, the initial linear i–$t^{1/2}$ portion yields λ and $i_{(t=0)}$, from which the charge-transfer quantities β and i_0 are evaluated, and the ratio $i_{(t=0)}/\lambda$ gives the diffusion coefficient (eq 16).

If the initial portion of the curve is experimentally inaccessible, it is possible to derive the charge-transfer parameters from the currents at longer times provided the diffusion coefficient is known. Shain, *et al.*,[15] described a treatment of the longer-time currents involving trial-and-error curve fitting; this treatment is restricted to slow reactions at relatively high η. We note here that the long-time current is given by eq 23, which when simplified for $D_R = D_O = D$ yields

$$\frac{i}{i_{(t=0)}} = \frac{\delta}{1 + \delta} + \left(\frac{1}{1 + \delta}\right)^2 \frac{1}{\pi^{1/2}\lambda t^{1/2}} \quad (30)$$

This provides a more direct method, and one which is applicable to rapid reactions. The slope σ and intercept $i_{(t\to\infty)}$ of this linear $i/t^{-1/2}$ relation yields λ in the form

$$\lambda = \sigma D\pi^{1/2}(a^2 i_{(t\to\infty)} - a\sigma\pi^{1/2}D^{1/2})^{-1} \quad (31)$$

From λ the quantity $\delta = \sqrt{D}/a\lambda$ is calculated, whence $i_{(t=0)}$ is obtained from the intercept $i_{(t\to\infty)} = i_{(t=0)}\,\delta(1 + \delta)^{-1}$. We may determine $i_{(t=0)}$ in this way at several values of η, using a single solution and either anodic *or* cathodic polarization. Thus for anodic polarization the charge-transfer current is given by eq 7, which may be rearranged to

$$\log\left(\frac{i_{(t=0)}}{\exp(n\epsilon\eta) - 1}\right) = \log i_0 - \left(\frac{\beta n\epsilon}{2.3}\right)\eta \quad (32)$$

A plot of the left side against η yields i_0 (intercept) and β (slope).

Cylindrical Electrodes

Here the problem comprises a first-order charge-transfer mechanism (eq 1) combined with diffusion to

(14) P. Delahay, "New Instrumental Methods in Electrochemistry," Interscience Publishers, Inc., New York, N. Y., 1954.

(15) I. Shain, K. J. Martin, and J. W. Ross, *J. Phys. Chem.*, 65, 259 (1961).

a cylindrical electrode of radius a as the sole mass-transfer process. As before, the time variations of current and concentrations at the electrode surface are to be determined for a reaction at constant potential. The mathematical description consists of differential equations

$$\frac{\partial c_R}{\partial t} = D_R\left[\frac{\partial^2 c_R}{\partial r^2} + \frac{1}{r}\frac{\partial c_R}{\partial r}\right]; \quad \frac{\partial c_O}{\partial t} = D_O\left[\frac{\partial^2 c_O}{\partial r^2} + \frac{1}{r}\frac{\partial c_O}{\partial r}\right]$$

with initial conditions ($t = 0$, $r \geq a$): $c_R = c_R^0$, $c_O = c_O^0$, and boundary conditions (all t)

$$r \longrightarrow \infty: \quad c_R \longrightarrow c_R^0; \quad c_O \longrightarrow c_O^0$$

$$r = a: \quad i = nFD_R\frac{\partial c_R}{\partial r} = -nFD_O\frac{\partial c_O}{\partial r}$$

A solution of this problem, based on the use of Laplace transforms, is described in the Appendix. The method does not lead to a general solution in closed form, but the entire current–time curve may be determined numerically for any specific case. An approximate solution, valid at sufficiently short times, is derived with the use of asymptotic expansions. The current and the concentrations at the electrode surface are given by eq A33–A35 of the Appendix. For the special case $D_R = D_O = D$, these equations convert to

$$i/i_{(t=0)} = 1 - 2\pi^{-1/2}\lambda t^{1/2} + (1 + \delta/2)\lambda^2 t \quad (33)$$

$$c_R = c_R^0 - \frac{i_{(t=0)}}{nFD^{1/2}}(2\pi^{-1/2}t^{1/2} - \bar{\lambda}t) \quad (34)$$

$$c_O = c_O^0 + \frac{i_{(t=0)}}{nFD^{1/2}}(2\pi^{-1/2}t^{1/2} - \bar{\lambda}t) \quad (35)$$

where $\bar{\lambda} = \lambda(1 + \delta/2)$; quantities λ and δ are the same as defined above for planar and spherical symmetry. The equations reduce to the corresponding ones for planar electrodes if the cylinder is large ($a >> D^{1/2}/\lambda$). It is seen from eq 33 that there will be a short period of time during which a cylindrical electrode of any radius will yield the same linear i–$t^{1/2}$ relation as does the plane electrode. Deviation from this line, represented by the term in $\lambda^2 t$, will develop somewhat faster at a small cylindrical electrode than at a plate, but not so fast as at a spherical electrode of the same radius.

Comparison of Planar, Spherical, and Cylindrical Electrodes

A numerical solution was carried out[16] (see Appendix) for the current–time curve at a small cylinder of radius $a = \sqrt{D}/\lambda$ (hence $\delta = 1$) for the special case of $D_R = D_O = D$. This is compared in Figure 3 with the corresponding curve for a sphere of the same radius, obtained from eq 28. Also shown is the curve for a large sphere or large cylinder ($a >> \sqrt{D}/\lambda$), which is the same as eq 6 for the plane. At $\lambda t^{1/2} = 5$, the current ratio for this small sphere is close to the value $\delta/(1 + \delta) = 1/2$ for $t \to \infty$ (see eq 28). The current ratio for the planar electrode goes to zero as $t \to \infty$. The curve for the cylinder is positioned about midway between the other two.

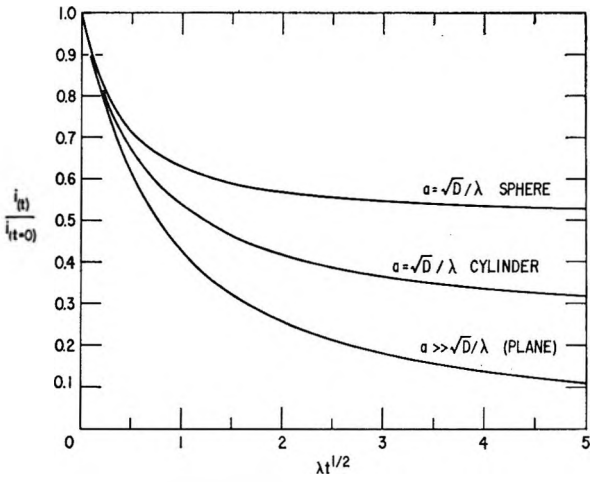

Figure 3. Constant-potential current–time relations for spherical and cylindrical electrodes.

Figure 4 presents the short-time approximations to these curves, as given by eq 13, 29, and 33 for the planar, spherical, and cylindrical cases, respectively. These approximate curves lie somewhat above the corresponding curves in Figure 3, but for the range $\lambda t^{1/2} = 0$ to 0.25 the deviation is small. At $\lambda t^{1/2} = 0.25$, the currents given in Figure 4 are 1.4% high for the planar electrode, 2.6% high for the cylindrical electrode and 4.3% high for the spherical electrode. As the electrode radius is increased above the value $\sqrt{D}/\lambda$, the upper two curves in Figures 3 and 4 will move gradually closer to the planar-electrode curve.

Summary

1. A current–potential relation for rapid reactions, applicable to first-order charge-transfer mechanisms, is proposed and illustrated by a numerical example. This equation (eq 3) has a much wider range of validity than the form previously used (eq 2).

2. The analysis of potentiostatic current–time curves for planar electrodes, for reactions controlled simultaneously by charge-transfer and mass-transfer polarization, has been extended. This analysis is based upon measurements of the ratio of current at

(16) A. Papoulis, *Quart. Appl. Math.*, **14**, 405 (1957).

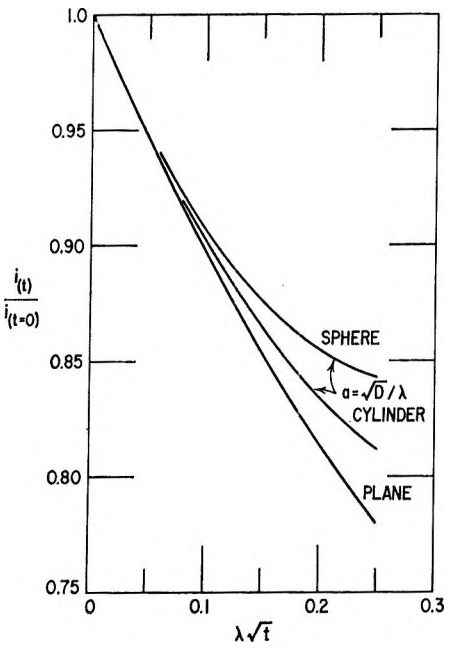

Figure 4. Current–time relations at short times.

some time t to that at $4t$, and permits extraction of the charge-transfer parameters β and i_0 from the experimentally more accessible part of the curve following the linear i–$t^{1/2}$ portion.

3. Closed-form solutions to the general boundary value problem for spherical electrodes are derived.

4. The boundary-value problem for cylindrical electrodes has been treated, and a general method for obtaining numerical solutions has been outlined. Also, approximate analytical solutions valid for short times are derived.

5. Current–time curves for a particular small radius of sphere and cylinder are compared with the corresponding planar-electrode curves. The small sphere yields higher currents at a given time than does the plate. The curve for the cylinder lies between the other two.

6. The current at a small sphere approaches a constant value, different from zero, as $t \rightarrow \infty$. The long-time current permits determination of the charge-transfer parameters because the reaction remains under partial charge-transfer control at all times.

Appendix

Solution of the Diffusion Problem for Spherical Electrodes. The diffusion equation for a system having full spherical symmetry is

$$D\frac{1}{r^2}\frac{\partial}{\partial r}\left(r^2\frac{\partial c}{\partial r}\right) = \frac{\partial c}{\partial t}$$

where $c = c(r,t)$ is the concentration at time t and radial distance r. On making the substitution[11]

$$U(r,t) = rc(r,t)$$

the diffusion equation becomes

$$D\frac{\partial^2 U}{\partial r^2} = \frac{\partial U}{\partial t}$$

and in terms of the new variable $U = rc$ can now be treated in much the same fashion as diffusion in a linear system. Thus in the present problem we define

$$U_R(r,t) = rc_R(r,t); \quad U_O(r,t) = rc_O(r,t) \qquad \text{(A1)}$$

which satisfy the differential equations

$$D_R\frac{\partial^2 U_R}{\partial r^2} = \frac{\partial U_R}{\partial t}; \quad D_O\frac{\partial^2 U_O}{\partial r^2} = \frac{\partial U_O}{\partial t} \qquad \text{(A2)}$$

with initial conditions, for a spherical electrode of radius a

$$r \geq a: \quad U_R(r,t=0) = c_R^0 r; \quad U_O(r,t=0) = c_O^0 r \qquad \text{(A3)}$$

and boundary conditions

$$r \longrightarrow \infty: \quad U_R(r,t) \longrightarrow c_R^0 r; \quad U_O(r,t) \longrightarrow c_O^0 r \qquad \text{(A4)}$$

The remaining condition is that for the electrode current. The current density is given (in terms of the electrode reaction) by eq 1, which in the present notation is

$$\frac{i(t)}{i_0} = \frac{\exp[(1-\beta)n\epsilon\eta]}{c_R^0 a}U_R(r=a,t) - \frac{\exp[-\beta n\epsilon\eta]}{c_O^0 a}U_O(r=a,t) \qquad \text{(A5)}$$

and (in terms of the diffusion currents) by

$$i(t) = +nFD_R\left(\frac{\partial c_R}{\partial r}\right)_{r=a} = nFD_R\left[\frac{1}{a}\left(\frac{\partial U_R}{\partial r}\right)_{r=a} - \frac{1}{a^2}U_R(a,t)\right] \qquad \text{(A6)}$$

and

$$i(t) = -nFD_O\left(\frac{\partial c_O}{\partial r}\right)_{r=a} = -nFD_O\left[\frac{1}{a}\left(\frac{\partial U_O}{\partial r}\right)_{r=a} - \frac{1}{a^2}U_O(a,t)\right] \qquad \text{(A7)}$$

On combining eq A5–A7, we find the conditions which must be satisfied on the electrode surface $r = a$.

$$\left(\frac{\partial U_O}{\partial r}\right)_{r=a} = -U_O(a,t)\left[\lambda_O + \frac{1}{a}\right] - U_R(a,t)\lambda_R\kappa \quad \text{(A8)}$$

$$\left(\frac{\partial U_R}{\partial r}\right)_{r=a} = -U_O(a,t)\frac{\lambda_O}{\kappa} + U_R(a,t)\left[\lambda_R + \frac{1}{a}\right]$$

with $\kappa = D_R/D_O$ and

$$\lambda_R = \frac{i_0 \exp[(1-\beta)n\epsilon\eta]}{nFD_R c_R^0}; \quad \lambda_O = \frac{i_0 \exp[-\beta n\epsilon\eta]}{nFD_O c_O^0} \quad \text{(A9)}$$

as in the Gerischer–Vielstich notation.[8] In terms of the Laplace transforms

$$Y_O(r,s) = \int_0^\infty e^{-st}U_O(r,t)dt$$

$$Y_R(r,s) = \int_0^\infty e^{-st}U_R(r,t)dt$$

the differential equations A2 and initial conditions A3 become

$$D_R\frac{\partial^2 Y_R}{\partial r^2} = sY_R - c_R^0 r;$$

$$D_O\frac{\partial^2 Y_O}{\partial r^2} = sY_O - c_O^0 r \quad \text{(A10)}$$

The solution which satisfies the boundary conditions A4 is

$$Y_O(r,s) = \alpha(s)\exp[-\sqrt{s/D_O}r] + c_O^0 r/s \quad \text{(A11)}$$

$$Y_R(r,s) = \beta(s)\exp[-\sqrt{s/D_R}r] + c_R^0 r/s$$

where $\alpha(s)$ and $\beta(s)$ are determined by the simultaneous solution of eq A8

$$\alpha(s) = \frac{[\lambda_R\kappa c_R^0 - \lambda_O c_O^0][a\sqrt{sD_O} + \sqrt{D_O D_R}]\exp[a\sqrt{s/D_O}]}{s[s + \gamma'\sqrt{s} + \delta']} \quad \text{(A12)}$$

$$\beta(s) = \frac{[\lambda_O c_O^0/\kappa - \lambda_R c_R^0][a\sqrt{sD_R} + \sqrt{D_O D_R}]\exp[a\sqrt{s/D_R}]}{s[s + \gamma'\sqrt{s} + \delta']}$$

with

$$\gamma' = \lambda_R\sqrt{D_R} + \lambda_O\sqrt{D_O} + (\sqrt{D_O} + \sqrt{D_R})/a \quad \text{(A13)}$$

$$\delta' = \sqrt{D_O D_R}[1 + a(\lambda_R + \lambda_O)]/a^2 \quad \text{(A14)}$$

Equations A11, with the values of $\alpha(s)$, $\beta(s)$ from eq A12, determine the Laplace transforms of the variables $U_O(r,t)$, $U_R(r,t)$ and hence the concentrations $c_O(r,t)$, $c_R(r,t)$.

We require the values of the concentrations at the phase boundary $r = a$ and the current as functions of the time. The current is most easily obtained by taking the Laplace transform of eq A7

$$J(s) = -nFD_O\left[\frac{1}{a}\left(\frac{\partial Y_O}{\partial r}\right)_{r=a} - \frac{1}{a^2}Y_O(a,s)\right] \quad \text{(A15)}$$

with $Y_O(r,s)$ given by eq A11 and

$$J(s) = \int_0^\infty i(t)e^{-st}dt$$

The current and concentrations are now readily obtained by inversion of eq A15 and A11. To accomplish this we must first factor the common denominator of $\alpha(s)$, $\beta(s)$

$$(s + \gamma'\sqrt{s} + \delta') = (\sqrt{s} + \xi)(\sqrt{s} + \mu)$$

$$\xi = {}^1/_2\Big\{\lambda + (\sqrt{D_O} + \sqrt{D_R})/a + \left[\lambda^2 + \left(\frac{\sqrt{D_O} - \sqrt{D_R}}{a}\right)^2 + \frac{2}{a}(\lambda_R\sqrt{D_R} - \lambda_O\sqrt{D_O})(\sqrt{D_R} - \sqrt{D_O}\right]^{1/2}\Big\} \quad \text{(A16)}$$

$$\mu = {}^1/_2\Big\{\lambda + (\sqrt{D_O} + \sqrt{D_R})/a - \left[\lambda^2 + \left(\frac{\sqrt{D_O} - \sqrt{D_R}}{a}\right)^2 + \frac{2}{a}(\lambda_R\sqrt{D_R} - \lambda_O\sqrt{D_O})(\sqrt{D_R} - \sqrt{D_O}\right]^{1/2}\Big\}$$

with $\lambda = \lambda_O\sqrt{D_O} + \lambda_R\sqrt{D_R}$. These relations yield[11]

$$c_R = c_R^0 - \frac{A}{\sqrt{\kappa}(\xi - \mu)}\left[\frac{\sqrt{D_O}}{a}\left(\frac{1}{\mu} - \frac{1}{\xi}\right) + \left(1 - \frac{\sqrt{D_O}}{a\mu}\right)\exp(\mu^2 t)\,\mathrm{erfc}(\mu\sqrt{t}) - \left(1 - \frac{\sqrt{D_O}}{a\xi}\right)\exp(\xi^2 t)\,\mathrm{erfc}(\xi\sqrt{t})\right] \quad \text{(A17)}$$

$$c_O = c_O^0 + \frac{A}{\xi - \mu}\left[\frac{\sqrt{D_R}}{a}\left(\frac{1}{\mu} - \frac{1}{\xi}\right) + \left(1 - \frac{\sqrt{D_R}}{a\mu}\right)\exp(\mu^2 t)\,\mathrm{erfc}(\mu\sqrt{t}) - \left(1 - \frac{\sqrt{D_R}}{a\xi}\right)\exp(\xi^2 t)\,\mathrm{erfc}(\xi\sqrt{t})\right] \quad \text{(A18)}$$

$$\frac{i_{(t)}}{i_{(t=0)}} = \frac{1}{1 + a\lambda_R + a\lambda_O} + \frac{1}{\xi - \mu}\left[\frac{(\sqrt{D_R} - a\xi)(\sqrt{D_O} - a\xi)}{a^2\xi}\exp(\xi^2 t)\,\mathrm{erfc}(\xi\sqrt{t}) - \frac{(\sqrt{D_R} - a\mu)(\sqrt{D_O} - a\mu)}{a^2\mu}\exp(\mu^2 t)\,\mathrm{erfc}(\mu\sqrt{t})\right] \quad \text{(A19)}$$

where A is given by eq 9a. These equations reduce to the corresponding results for planar electrodes if a is large; *i.e.*, $a >> (\lambda_R + \lambda_O)^{-1}$.

Approximate Solution of the Diffusion Problem for Cylindrical Electrodes. The diffusion equations for the species O and R in a system having full cylindrical symmetry are

$$D_O\left[\frac{\partial^2 c_O}{\partial r^2} + \frac{1}{r}\frac{\partial c_O}{\partial r}\right] = \frac{\partial c_O}{\partial t} \quad \text{(A20)}$$

$$D_R\left[\frac{\partial^2 c_R}{\partial r^2} + \frac{1}{r}\frac{\partial c_R}{\partial r}\right] = \frac{\partial c_R}{\partial t} \quad \text{(A21)}$$

and are to be solved subject to the initial conditions

$$r \geq a: \quad c_R(r,t=0) = c_R^0,\ c_O(r,t=0) = c_O^0 \quad \text{(A22)}$$

and the boundary conditions

$$r \longrightarrow \infty: \quad c_R(r,t) \longrightarrow c_R^0,\ c_O(r,t) \longrightarrow c_O^0 \quad \text{(A23)}$$

$$i(t) = nFD_R\left(\frac{\partial c_R}{\partial r}\right)_{r=a} = -nFD_O\left(\frac{\partial c_O}{\partial r}\right)_{r=a} \quad \text{(A24)}$$

The combination of eq 1 and A24 yields the conditions which must be satisfied on the electrode surface $r = a$

$$\left(\frac{\partial c_O}{\partial r}\right)_{r=a} = \lambda_O c_O(a,t) - \lambda_R\kappa c_R(a,t)$$
$$\left(\frac{\partial c_R}{\partial r}\right)_{r=a} = -\frac{\lambda_O}{\kappa}c_O(a,t) + \lambda_R c_R(a,t) \quad \text{(A25)}$$

In terms of the Laplace transforms

$$U_O(r,s) = \int_0^\infty c_O(r,t)e^{-st}\,dt$$
$$U_R(r,s) = \int_0^\infty c_R(r,t)e^{-st}\,dt \quad \text{(A26)}$$

the differential equations A20 and A21 and initial conditions A22 become

$$D_O\left[\frac{\partial^2 U_O}{\partial r^2} + \frac{1}{r}\frac{\partial U_O}{\partial r}\right] = sU_O - c_O^0$$
$$D_R\left[\frac{\partial^2 U_R}{\partial r^2} + \frac{1}{r}\frac{\partial U_R}{\partial r}\right] = sU_R - c_R^0 \quad \text{(A27)}$$

The solution which satisfies the boundary conditions A23 is[11]

$$U_O(r,s) = \frac{c_O^0}{s} + \alpha(s)K_O\left(\sqrt{\frac{s}{D_O}}r\right)$$
$$U_R(r,s) = \frac{c_R^0}{s} + \beta(s)K_O\left(\sqrt{\frac{s}{D_O}}r\right) \quad \text{(A28)}$$

where $K_O(x)$ is the modified Bessel function of the second kind of order zero. $\alpha(s)$ and $\beta(s)$ are determined by the simultaneous solution of eq A25

$$\alpha(s) = \frac{K_1\left(\sqrt{\frac{s}{D_R}}a\right)\sqrt{D_O}[\lambda_R\kappa c_R^0 - \lambda_O c_O^0]}{s\left[\sqrt{s}K_1\left(\sqrt{\frac{s}{D_O}}a\right)K_1\left(\sqrt{\frac{s}{D_R}}a\right) + \lambda_O\sqrt{D_O}K_O\left(\sqrt{\frac{s}{D_O}}a\right)K_1\left(\sqrt{\frac{s}{D_R}}a\right) + \lambda_R\sqrt{D_R}K_O\left(\sqrt{\frac{s}{D_R}}a\right)K_1\left(\sqrt{\frac{s}{D_O}}a\right)\right]}$$

$$\beta(s) = \frac{K_1\left(\sqrt{\frac{s}{D_O}}a\right)\sqrt{D_R}[\lambda_O c_O^0/\kappa - \lambda_R c_R^0]}{s\left[\sqrt{s}K_1\left(\sqrt{\frac{s}{D_O}}a\right)K_1\left(\sqrt{\frac{s}{D_R}}a\right) + \lambda_O\sqrt{D_O}K_O\left(\sqrt{\frac{s}{D_O}}a\right)K_1\left(\sqrt{\frac{s}{D_R}}a\right) + \lambda_R\sqrt{D_R}K_O\left(\sqrt{\frac{s}{D_R}}a\right)K_1\left(\sqrt{\frac{s}{D_O}}a\right)\right]} \quad \text{(A29)}$$

where $K_1(x) = -dK_O(x)/dx$ is the modified Bessel function of the second kind and of order 1.

Equations A28, together with the values of $\alpha(s)$ and $\beta(s)$ from eq A29, determine $U_O(r,s)$ and $U_R(r,s)$, the Laplace transforms of the concentrations $c_O(r,t)$ $c_R(r,t)$. From either of these expressions, together with eq A24, we obtain the Laplace transform, $J(s)$, of the current $i(t)$

$$J(s) = \frac{i_{(t=0)}}{\sqrt{s}\left\{\sqrt{s} + \lambda_O\sqrt{D_O}\left[K_O\left(\sqrt{\frac{s}{D_O}}a\right)\Big/K_1\left(\sqrt{\frac{s}{D_O}}a\right)\right] + \lambda_R\sqrt{D_R}\left[K_O\left(\sqrt{\frac{s}{D_R}}a\right)\Big/K_1\left(\sqrt{\frac{s}{D_R}}a\right)\right]\right\}} \quad \text{(A30)}$$

Unfortunately, the expressions for U_O, U_R, and J cannot be inverted analytically to give c_O, c_R, and i. A complete solution may be obtained, however, by numerical inversion of the Laplace transforms, follow-

ing the method described by Papoulis.[16] We used this procedure for the specific cases discussed in the text. In addition, an approximate analytical solution has been derived. This is valid for times much shorter than the smallest of a^2/D_O, a^2/D_R, $a/\lambda\sqrt{D_R}$, $a/\lambda\sqrt{D_O}$ (*i.e.*, times sufficiently short that the diffusion distance is small in comparison with the radius of the electrode). The approximate short-time solution for the current, $i(t)$, will be sketched; short-time approximate solutions for the concentrations are found in much the same way, and only the final expressions will be given.

The approximate solution for $i(t)$ is based on the fact that the behavior of $i(t)$ for small t is determined by the behavior of $J(s)$ for large s. For large s we have[11]

$$\frac{K_O\left(\sqrt{\frac{s}{D_O}}\,a\right)}{K_1\left(\sqrt{\frac{s}{D_O}}\,a\right)} \longrightarrow 1 - \frac{\sqrt{D_O}}{2a\sqrt{s}} + \frac{3D_O}{8a^2 s} + O(s^{-3/2})$$

so that, as $s \to \infty$

$$J(s) \longrightarrow \frac{i_{(t=0)}}{s + \lambda\sqrt{s} - (\lambda_O D_O + \lambda_R D_R)/2a} \qquad \text{(A31)}$$

On factoring the denominator of this equation, as in the above treatment of the spherical electrode, we obtain eq A32.

$$\frac{i_{(t)}}{i_{(t=0)}} = \frac{1+\bar{\delta}}{2\bar{\delta}} \exp\left[\left(\frac{1+\bar{\delta}}{2}\right)^2 \lambda^2 t\right] \times \operatorname{erfc}\left[\frac{1+\bar{\delta}}{2}\,\lambda\sqrt{t}\right] - \frac{1-\bar{\delta}}{2\bar{\delta}} \exp\left[\left(\frac{1-\bar{\delta}}{2}\right)^2 \lambda^2 t\right] \times \operatorname{erfc}\left[\frac{1-\bar{\delta}}{2}\,\lambda\sqrt{t}\right] \qquad \text{(A32)}$$

where

$$\bar{\delta} = \left[1 + \frac{2(\lambda_R D_R + \lambda_O D_O)}{a\lambda^2}\right]^{1/2}$$

This result may be simplified by introducing the approximation $\exp x^2 \operatorname{erfc} x \simeq 1 - 2\pi^{-1/2}x + x^2$, valid for $x \ll 1$, to obtain

$$\frac{i_{(t)}}{i_{(t=0)}} \simeq 1 - \frac{2}{\sqrt{\pi}}\lambda\sqrt{t} + \left(1 + \frac{\lambda_R D_R + \lambda_O D_O}{2a\lambda^2}\right)\lambda^2 t \qquad \text{(A33)}$$

Similarly, the concentrations at the electrode surface, for small t, are given by

$$c_R(a,t) \simeq c_R^0 - \frac{i_{(t=0)}}{nF\sqrt{D_R}}\left[\frac{2}{\sqrt{\pi}}\sqrt{t} - \left(1 + \frac{\sqrt{D_R}}{2a\lambda}\right)\lambda t\right] \qquad \text{(A34)}$$

$$c_O(a,t) \simeq c_O^0 + \frac{i_{(t=0)}}{nF\sqrt{D_O}}\left[\frac{2}{\sqrt{\pi}}\sqrt{t} - \left(1 + \frac{\sqrt{D_O}}{2a\lambda}\right)\lambda t\right] \qquad \text{(A35)}$$

For large cylindrical electrodes, such that $a \gg (\lambda_R + \lambda_O)^{-1}$, these equations reduce to the corresponding results for planar electrodes.

Mass Spectrometry of Some Polyphenyls

by E. J. Gallegos

Chevron Research Company, Richmond, California *(Received August 17, 1966)*

The mass spectra, including metastable transitions and appearance potentials for the principal positive ions, were measured for several polyphenyls by a high-resolution mass spectrometer. The parent molecule-ion beam gave the most intense peak in the spectra for all of the polyphenyls. The doubly charged parent is generally second in intensity in the spectra of the *m*- and *p*-polyphenyls studied. The *o*-polyphenyls show that the doubly charged molecular ion makes a minor contribution to the mass spectra. The doubly charged parent increased in abundance, whereas their appearance potentials decreased with an increasing total number of π electrons. Resonance effects in ionization and dissociation of the polyphenyls are discussed in light of this study. The measured values for the parent ions are: *m*-octaphenyl, 8.28 ev; *p*-hexaphenyl, 7.67 ev; *m*- and *p*-quinquephenyl, 8.45 and 8.18 ev; *o*-, *m*-, and *p*-quarterphenyl, 8.52, 8.51, and 8.08 ev; *o*-, *m*-, and *p*-terphenyl, 8.64, 8.80, and 8.78 ev; and biphenyl, 8.95 ev.

Introduction

Systematic electron-impact studies have recently been made on a number of polynuclear aromatic hydrocarbons.[1,2] However, little information[3] is found in the literature on the mass spectra and energetics of polyphenyls other than biphenyl.[2] The lack of information of this kind on the higher molecular weight conjugated molecules provided an incentive to undertake this study.

Two unique features of the mass spectra of higher molecular weight, highly conjugated compounds are the low abundance of fragment ions and the relatively high abundance of multiply charged ions. The purpose of this paper is to present data for a series of polyphenyls.

Experimental Section

The data were obtained with an AEI MS-9 high-resolution mass spectrometer equipped with an automatic voltage scanner which decreases the electron accelerating voltage in increments of 0.05 or 0.2 v in the range of 80–3 v. This system has been described elsewhere.[4] Partial mass spectra reported here were obtained at 70 ev with a 100-μa ionizing current using a rhenium filament. Source temperature was 240°. Appearance potentials were obtained using a 20-μa ionizing current.

In the polyphenyl nomenclature, *o*, *m*, or *p* refers to the type of linkage throughout the molecule. Unsubstituted polyphenyls do not exhibit stereoisomerism. The polyphenyls were obtained from K & K Laboratories. *o*-, *m*-, and *p*-terphenyls showed no impurities in the gas chromatogram. Of the polyphenyls of higher molecular weight, *p*-hexaphenyl and *m*-octaphenyl showed impurities. These were further purified by microsublimation[5] under nitrogen. Ultraviolet spectra of the purified polyphenyls show only one absorption maximum each. Infrared spectra obtained also show no trace of impurities. Mass spectra of the polyphenyls, as purified or as received, show only negligible impurities of higher molecular weight in the mass spectrum.

Appearance potentials of 1,4-bis(trifluoromethyl)-benzene parent and selected fragments of perfluorotributylamine were determined using noble gases as a standard and these fragments were subsequently used as secondary standards for ionization potential de-

(1) M. E. Wacks, 13th Annual Conference on Mass Spectrometry and Allied Topics, St. Louis, Mo., May 16–21, 1965.

(2) P. Natalis and J. L. Franklin, *J. Phys. Chem.*, **69**, 2935 (1965).

(3) P. Bradt and F. L. Mohler, *J. Res. Natl. Bur. Std.*, **60**, 143 (1958).

(4) E. J. Gallegos and R. F. Klaver, presented at the 14th Annual Conference on Mass Spectrometry and Allied Topics, Dallas, Texas, May 22–27, 1966.

(5) W. H. Melhuish, *Nature*, **184**, 1933 (1959).

Table I: Partial Mass Spectra of Several Polyphenyls (Source Temperature 240°, Pressure 2×10^{-7} Torr)

m/e	Type of ion[a]	Relative abundances at 70 ev									
		o-Ph3	m-Ph3	p-Ph3	o-Ph4	m-Ph4	p-Ph4	m-Ph5	p-Ph5	p-Ph6	m-Ph6
29									1.4		2.7
36											2.4
39		2.2	2.9	1.2					1.3		
43		1.0							1.3		
50		1.4	2.1								3.6
51		2.8	4.7	1.9	2.0				1.4		
55											2.0
57		1.3									2.0
63		2.4	3.2	1.5	1.3						
75		2.2	2.5	1.4							
76		2.3	3.0	2.3							
77		1.7	3.1	1.6	1.8				2.1		
88		4.2	2.6	2.3							
89		1.7	2.2	2.0							
91					2.8				2.2		
94.5	d		1.2	1.2							
99		1.0									
100		4.3	1.7	1.6							
101		12.7	5.2	5.3							
101.5	d	3.8	1.0	1.1							
102		1.4	2.6	1.7							
106.5	d	1.9									
107.5	d	8.0	1.1								
112		2.6									
112.5	d	1.9									
113		13.2	3.1	3.8	1.9	1.2					
113.5	d	4.3		1.2							
114		14.4	1.9	2.1							
229		4.6									
115		1.0	1.7	4.0	1.1				1.4		
115	d	3.0	6.9	9.5							
115.5	d	0.6	1.4	1.9							
119.5	d				1.2						
125					2.3						
126		1.1	1.7		2.0	1.5					
128			3.0	2.4			1.2		1.4		
130.5	d				1.0						
131.5	d				3.6	1.2					
137					2.3						
138					7.3	2.4	1.0				
138.5	d				2.3						
139			1.3		2.7	1.1					
143.5	d				3.4						
144					2.4						
144.5	d				10.6	2.3					
145					13.0	1.3	1.2				
145.5	d				4.2						
150		1.5	1.6	1.0	4.9	1.8			1.2		
150.5	d				1.7						
151		1.9	3.4	2.5	6.5	3.2	2.3	1.4	2.4		
151.5	d				2.2						
152		2.5	6.9	4.8	3.6	3.6	3.7	2.3	4.1	1.9	
153			2.5	2.2				1.0	1.4	1.0	
153.0	d				2.2	16.6	13.6				
307						4.2	3.3				
165		2.8	1.4		3.0				1.6		
168.9	m				<0.1	<0.1	<0.1				
171.4	m				<0.1	<0.1	<0.1				
178		2.3			2.0				1.2		

[a] Symbols: P, parent peak; i, isotope peak; m, metastable ion; d, doubly charged ion.

m/e	Type of ion[a]	Relative abundances at 70 ev									
		o-Ph3	m-Ph2	p-Ph3	o-Ph4	m-Ph4	p-Ph4	m-Ph5	p-Ph5	p-Ph6	m-Ph8
189		2.4	2.3	1.5	1.3			1.4	1.9	1.0	
190.5	d							1.1			
191.0	d							22.4	12.7		
191.5	d							7.3	3.9		
200		2.7	1.7	1.1	1.6						
200.9	m	0.2	0.1	<0.1							
201		2.4	1.4		1.2						
202		10.2	6.4	4.6	4.5	1.8	2.3	1.4	2.6		
203		3.9	2.3	1.7	1.8						
213		2.0	1.0								
215		28.7	3.8	3.3	14.5						
216		5.4			2.7						
225	m	0.2	0.1	0.1							
226		14.5	6.1	5.9	8.6	3.5	3.9	2.3	4.0	2.8	
226	m	0.3	0.2	0.2	0.1	0.1	0.1				
227		10.5	4.7	4.8	4.9	1.9	2.3	1.2	2.0	2.1	
227	m	0.4	0.3	0.3							
228		29.9	12.4	12.2	18.3	3.5	3.9	2.1	3.2	4.0	
228	m	0.5	0.4	0.4							
229		58.2	9.7	8.8	22.3	1.7	1.8				
229	m	7.0	0.7	0.7							
229.0	d									21.2	
229.5	d									8.5	
230					4.1					1.9	
230	m	0.2	0.1	0.1							
230	P	100.0	100.0	100.0							
231	i	19.3	19.1	19.7							
232	i	1.7	1.8	1.8							
252					2.2				1.3		
265					4.0						
275	m				0.1	<0.1	<0.1	<0.1			
276					5.0	1.7			1.6	1.1	
276	m				0.4	0.3	0.3				
277					3.0		2.0				
278					2.6		1.2				
288	m				0.5	0.3	0.3				
289					16.5	5.5		1.7	2.4	1.6	
290					9.2	2.2	5.4				
291					10.0	1.3	2.2				
292					2.3		1.3				
300					2.9	1.2	1.5		1.3		
301	m				0.4	0.3	0.3				
302					8.1	3.4	3.7	1.8	2.8	2.1	
303					7.3	2.9	3.0	1.2	1.9	1.4	
304					5.4	2.5	2.7		1.7	1.1	
305					18.2	1.6	1.5				
305	m				0.8	0.6	0.6				
305.0	d										38.6
305.1	d										19.3
306.0	d										4.8
306	P				100.0	100.0	100.0	1.7			
307	i				25.7	25.8	26.1				
308	i				3.2	3.3	3.3				
382	P							100.0	100.0		
383	i							32.2	32.2		
384	i							5.3	5.2		
458	P									100.0	
459	i									38.1	
460	i									7.4	
610	P										100.0
611	i										46.8
612	i										11.5
613	i										2.0

terminations of some of the higher molecular weight polyphenyls. Fragment ions from perfluorotributylamine were chosen on the basis of their ease of introduction into the mass spectrometer and relatively low appearance potentials and the similarity of the ionization efficiency curve to that of a polyphenyl molecular ion. Secondary calibrants were necessary because the peak-matching facilities of the MS-9 requires that the ratio of the low to high mass be no greater than 2.

Ionization potential data have been determined by comparison with a reference curve using the semilogarithmic,[6] vanishing current and extrapolated voltage difference[7] methods. The average of the three methods and triplicate runs gave a reproducibility of ±0.05 v. Appearance potentials of doubly charged parent ions and of fragment ions were generally treated in the same way, except in some cases where semilogarithmic curves became excessively divergent. Reproducibility of appearance potential values of these ions is usually 0.1–0.4 v. Absolute error, however, can be several times that shown.

General Features of the Mass Spectra

The partial mass spectra of the polyphenyls are given in Table I. Ions accounting for less than 1% of the base peak have been deleted. Metastable transitions with relative abundances much less than 0.1% are not included. Ions appearing at a given nominal mass are not corrected for any contribution owing to doubly charged fragments. Corrections in this table, however, are made for contributions from doubly charged parent ions. All odd doubly charged ions appear at one-half nominal mass and are reported as such. Corrections for possible C^{13} isotope contributions to the ion intensity at one-half nominal mass were not made, except for doubly charged parent ions.

Metastable transitions indicate consecutive loss of hydrogens. The relative abundance of metastable transitions decreases with increased molecular weight of the polyphenyl. Also, the relative abundance of the metastables is shown to decrease in the order from *o*- to *m*- to *p*-polyphenyl.

Table II shows the sum of the per cent of total ionization of the parent singly and doubly charged species and the ratio of the parent to the doubly charged parent ion.

Significant contribution of fragment ions to the M^{2+} is observed for the lower molecular weight polyphenyls (see Table III). As a result, all appearance potential measurements of the doubly charged parent ion were made from the C^{13} isotope peak.

The values presented for per cent M^{2+} and per cent $^1/_2M^+$ were calculated on the basis of the C^{13}/C^{12} isotope ratio measured for the parent. Sensitivity reproducibility is approximately 3%.

Table II: Per Cent of Total Ionization of Parent Singly and Doubly Charged Ions and the Ratio of M^{2+} to M^+

Mol wt	Molecule	% of total ionization of $M^{2+} + M^+$	Ratio M^{2+}/M^+
230	*p*-Terphenyl	50.9	0.14
306	*p*-Quaterphenyl	61.0	0.16
382	*p*-Quinquephenyl	67.0	0.18
458	*p*-Hexaphenyl	70.0	0.21
230	*m*-Terphenyl	44.2	0.09
306	*m*-Quaterphenyl	56.8	0.17
382	*m*-Quinquephenyl	62.5	0.22
610	*m*-Hexaphenyl	85.2	0.35
230	*o*-Terphenyl	25.8	0.05
306	o-Quaterphenyl	26.0	0.03

Table III: Contribution of Fragment Ions to One-Half Parent Mass

Compd	Measd $(M + 1)^{2+}/M^{2+} + {}^1/_2M^+$	% M^{2+}	% $^1/_2M^+$	$(M + 1)^+/M^+$ Measd	$(M + 1)^+/M^+$ Calcd
o-Terphenyl	0.16	80	20	0.20	0.20
m-Terphenyl	0.14	70	30	0.20	0.20
p-Terphenyl	0.17	81	19	0.21	0.20
o-Quaterphenyl	0.23	85	15	0.27	0.26
m-Quaterphenyl	0.26	96	4	0.27	0.26
p-Quaterphenyl	0.26	96	4	0.27	0.26
m-Quinquephenyl	0.33	99	1	0.33	0.33
p-Quinquephenyl	0.33	99	1	0.33	0.33
p-Hexaphenyl	0.40	100	..	0.40	0.39
m-Octaphenyl	0.57	100	..	0.57	...

The *p*-polyphenyls show the singly and doubly charged parent as the most intense peaks in the mass spectra. Additional benzene rings in the *p* position result in a decreasing amount of fragmentation and a lowering of the appearance potentials.

The *m*-polyphenyls also generally show the parent ion as the largest peak in the spectrum followed by the doubly charged parent. One exception is the *m*-terphenyl, where $(M - H)^+$ and $(M - 2H)^+$ are slightly more intense than M^{2+}. The per cent of total ionization of the parent$^+$ and parent^{2+} is less than that for the corresponding *p*-polyphenyls, as shown in Table II.

o-Terphenyl and *o*-quaterphenyl show by far the greatest fragmentation, with the parent accounting

(6) F. P. Lossing, A. W. Tickner, and W. A. Brice, *J. Chem. Phys.*, 19, 1254 (1951).

(7) J. W. Warren, *Nature*, 165, 810 (1960).

for less than one-third of total ionization. The parent^{2+} becomes a minor peak in these mass spectra. $(M - H)^+$ and $(M - 2H)^+$ for these molecules increase greatly in intensity along with the corresponding doubly charged species compared to similar ions of the *p*- and *m*-polyphenyls. The *o*-polyphenyls show considerable numbers of ions representing the loss of methyl groups.

Appearance Potentials. The ionization potentials of the polyphenyl molecular ions and the appearance potentials of their corresponding doubly charged parents are given in Table IV. Some appearance potentials of fragment ions were measured and are listed in Table V.

Table IV: Ionization Potentials (ev) of Several Polyphenyls at 240° and 2×10^{-7} Torr

	This work		I.P., lit.
	I.P.[a]	A.P.(M^{2+})[a]	
m-Octaphenyl	8.28 ± 0.05	20.3 ± 0.4	...
p-Hexaphenyl	7.67 ± 0.05	19.5 ± 0.4	...
m-Quinquephenyl	8.45 ± 0.05	20.0 ± 0.4	...
p-Quinquephenyl	8.18 ± 0.05	19.6 ± 0.4	...
o-Quaterphenyl	8.52 ± 0.05	20.5 ± 0.4	...
m-Quaterphenyl	8.51 ± 0.05	20.5 ± 0.4	...
p-Quaterphenyl	8.08 ± 0.05	20.2 ± 0.4	...
o-Terphenyl	8.64 ± 0.05	21.5 ± 0.4	...
m-Terphenyl	8.80 ± 0.05	21.5 ± 0.4	...
p-Terphenyl	8.78 ± 0.05	21.5 ± 0.4	...
Biphenyl	8.95 ± 0.05	...	8.96[b]

[a] The potential data shown represent an average of several determinations. Ionization potentials are reproducible to ±0.05 v. Reproducibility of doubly charged ions are usually ±0.4 v. Absolute error can be five to ten times that shown. [b] See Ref 2.

Discussion

Generally, as the number of π electrons increases in the *p* and *m* series, there is observed a decrease in the ionization potential and an increase in the formation of doubly ionized parent ions. Also, the ionization potentials for the *p* series are generally less than those of the corresponding *o* or *m* series. However, the ionization potential given for *o*-terphenyl is lower than expected and the ionization potential values given for *p*-quinquephenyl and *p*-quaterphenyl are reversed from that expected.

The reasons for this are not clear. These values may reflect real resonance structure differences or may merely be a measure of the absolute error involved in obtaining ionization potentials by conventional methods.

Table V: Appearance Potentials of Selected Fragment Ions of Some Polyphenyls at 240° and 2×10^{-7} Torr

m/e		A.P., ev
229	*o*-Terphenyl	11.7 ± 0.1
228	*o*-Terphenyl	11.7 ± 0.1
215	*o*-Terphenyl	12.0 ± 0.1
454	*p*-Hexaphenyl	15.6 ± 0.2
229	*p*-Hexaphenyl	19.5 ± 0.3
228	*p*-Hexaphenyl	18.5 ± 0.3
228	*m*-Quaterphenyl	16.7 ± 0.3
226	*m*-Quaterphenyl	18.3 ± 0.3
305	*o*-Quaterphenyl	11.7 ± 0.1
291	*o*-Quaterphenyl	12.7 ± 0.1
289	*o*-Quaterphenyl	15.5 ± 0.2
229	*o*-Quaterphenyl	12.8 ± 0.1
228	*o*-Quaterphenyl	13.0 ± 0.1
226	*o*-Qnaterphenyl	19.0 ± 0.4
215	*o*-Quaterphenyl	13.0 ± 0.2

The *p*-polyphenyls should and do exhibit the greatest resonance stabilization. Indeed, from ultraviolet data by Gillman and Hey[8] and work done here, the *p* series shows that the wavelength λ_{max} of the most intense absorption increases almost regularly with the number of benzene rings.

Values of λ_{max} for the *m*-polyphenyls show a small but very definite increase from 2468 ± 10 A for *m*-terphenyl to 2530 ± 10 A for *m*-octaphenyl. This increase, however, is considerably smaller than would be expected on the basis of energetics.

o-Terphenyl and *o*-quaterphenyl show a lower λ_{max} of 2310 ± 10 and 2225 ± 10 A, respectively. This is expected. The *o*-polyphenyls from steric considerations should exhibit little if any interphenyl resonance. A decrease in resonance stabilization is reflected in the abundance of fragment ions. Mass spectra of the *o*-polyphenyls do show a high degree of fragmentation compared to the *m*- and *p*-polyphenyls. The per cent of total ionization of $M^{2+} + M^+$ remains nearly constant for *o*-terphenyl and *o*-quaterphenyl, respectively.

(8) A. E. Gilman and D. H. Hey, *J. Chem. Soc.*, 1170 (1939).

Thermal Electron Attachment to Some Aliphatic and Aromatic Chloro, Bromo, and Iodo Derivatives

by W. E. Wentworth, Ralph S. Becker, and Roberta Tung

Department of Chemistry, University of Houston, Houston, Texas 77004 *(Received August 18, 1966)*

Thermal electron attachment to some aliphatic and aromatic halogen derivatives was investigated by the pulse-sampling technique as a function of temperature (≈30–200°). In contrast to stable negative ion formation, the electron attachment increased with increasing temperature, indicating an energy of activation for the process despite the fact that the over-all process is exothermic. Two mechanisms are proposed to explain the observed results: (1) electron attachment to a thermally excited molecule followed by direct dissociation into a halide ion and a radical; (2) electron attachment to form a stable negative ion of the molecule which in turn becomes thermally activated to undergo dissociation into the halide ion and radical. Except for special cases, assignment between the two mechanisms is based upon comparison of the carbon–halogen bond dissociation energies with energies of activation along with estimated or known electron affinities of the aromatic derivatives and the aromatic radical. The aliphatic halides (CH_2Cl_2, $CHCl_3$, CCl_4, n-C_3H_7Br, and C_2H_5I) apparently undergo dissociative electron attachment by the former mechanism, whereas the aromatic derivatives (bromobenzene, *o*-dichlorobenzene, *m*-dichlorobenzene, 1-chloronaphthalene, and 1-bromonaphthalene), which are expected to have a reasonable electron affinity, apparently follow the latter mechanism.

Introduction

It is generally considered that electron attachment to molecules occurs by either of two processes represented by the chemical equations[1–6]

$$AB + e^- \longrightarrow AB^-$$

$$AB + e^- \longrightarrow A + B^-$$

The latter process, called dissociative electron capture or attachment, in contrast to the nondissociative process, will be the primary concern of this paper. Thus far, most research on dissociative electron attachment has been concerned with the rate or cross section for the process as a function of the electron energy. Generally, the work has been carried out at ambient or near ambient temperatures on relatively small compounds. In contrast, the work described in this paper is restricted to thermal or near-thermal electron energies, and the temperature dependence of the dissociative electron-attachment process has been investigated where possible over the range 30–200°. Chloro, bromo, and iodo organic derivatives have been studied, and in extreme cases the electron attachment can vary 1000-fold over this temperature range.

Within the past 10 years or so, techniques for obtaining monoenergetic electrons have been developed and applied toward the study of dissociative electron attachment. Fox[7] observed a maximum cross section

(1) No attempt will be made to cite all the original references on this subject. Only more general sources will be cited which within themselves contain most of the important original references.

(2) R. H. Healy and J. W. Reed, "The Behavior of Slow Electrons in Gases," Amalgamated Wireless Press (Australasia) Ltd., Sydney, 1941.

(3) (a) H. S. W. Massey, "Negative Ions," Cambridge University Press, New York, N. Y., 1950; (b) H. S. W. Massey and E. H. S. Burhop, "Electronic and Ionic Impact Phenomena," Oxford University Press, New York, N. Y., 1952.

(4) F. H. Field and J. L. Franklin, "Electron Impact Phenomena," Academic Press Inc., New York, N. Y., 1957.

(5) L. B. Loeb, "Basic Processes of Gaseous Electronics," University of California Press, Berkeley, Calif., 1961.

(6) E. W. McDaniel, "Collision Phenomena in Ionized Gases," John Wiley and Sons, Inc., New York, N. Y., 1964.

(7) R. E. Fox, *J. Chem. Phys.*, 26, 1281 (1957).

for HCl at 0.66 ev. Frost and McDowell[8] investigated the remaining hydrogen halides and found a correlation between the electron energy at the maximum cross section and the difference between electron affinity of the halide and bond dissociation energy. In general, a rough correlation of this type would be expected; however, a rigorously perfect correlation would not be necessary. Hickam and Berg[9] studied a series of fluoro and chloro derivatives of methane and ethane and generally found one or more maxima at or above thermal energies. The only compound in their study common to those considered in this paper was CCl_4. Some other compounds are similar to ours and these will be commented on later in the paper. In the case of CCl_4, Hickam and Berg reported a slight temperature dependence for the electron-attachment cross section. After taking into account the change in gas density, their variations are on the same order of magnitude as our measurements. Later, Fox and Curran[10] reinvestigated the electron attachment of CCl_4 as a function of source temperature in addition to electron energy and found no significant change in the shape of the curves. However, no mention was made concerning any change in magnitude of capture. Stockdale and Hurst,[11] using a swarm technique, found maximum cross section for electron attachment at electron energies of 0.76 and 0.70 ev for chlorobenzene and bromobenzene, respectively. Dissociative electron attachment was confirmed by observing Cl^- and Br^- in a negative-ion time-of-flight mass spectrometer. Bromobenzene was included in the present studies and the results relative to the above values will be discussed later. An attempt was made in this work to study chlorobenzene; however, the gas chromatographic columns employed did not give sufficient separation from the impurities to give reliable results.

Dissociative electron capture can also occur in rigid media by γ radiation of organic halides in hydrocarbons.[12] Presumably, thermal electrons are produced by the γ radiation of the solvent or other species present, followed by dissociative electron capture by the organic halide. Many of the radical products have been identified by their visible–ultraviolet absorption spectra and more recently by paramagnetic resonance.[13] To the best of our knowledge, there has not been an extensive study of dissociative electron attachment in the gas phase using thermal electrons.

In our work, the "pulse-sampling technique" was employed which has been described previously.[14,15] The details of the operational parameters have been reported recently[16] along with justification for electron–molecule interaction under a zero potential field. In a gas of argon–10% methane, presumably thermal or near-thermal electron energies are obtained within the relatively long 1000-μsec pulse intervals. The kinetics of the process have been presented for the nondissociative electron-attachment process.[16] A similar investigation of the kinetic processes for dissociative capture will be presented in this paper.

Further indirect support for thermal or near-thermal electrons exists from previous correlations of these measurements with other experimental and theoretical results. Wentworth and Becker first suggested that the electron-capture results could be used to calculate molecular electron affinities and applied the method to some polycyclic aromatic hydrocarbons.[17] They showed a positive correlation between the experimental electron affinities from electron-capture coefficients and polarographic half-wave reduction potentials. Also, good agreement with theoretical estimates of electron affinities was obtained. Later, Becker and Wentworth[18] showed that the sum of the electron affinity and ionization potential for the polycyclic aromatic hydrocarbon was essentially constant as predicted by theory. Recent experimental electron affinities of the five-ring polycyclic aromatic hydrocarbons,[19] along with the the more recent values for the three- and four-ring compounds,[16] also show good agreement with recent theoretical considerations and predictions.[19] Finally, experimental electron affinities for some aromatic aldehydes and ketones correlate well with polarographic half-wave reduction potentials.[20] These electron affinities, along with a more recent investigation of fluoro-, methyl-, and trifluoromethyl-substituted derivatives of these compounds, agree reasonably well with molecular orbital calculations based on Hückel approximations.[21] In total, 33 compounds which apparently undergo nondissociative

(8) D. C. Frost and C. A. McDowell, *J. Chem. Phys.*, 29, 503 (1958).

(9) W. H. Hickam and D. Berg, *ibid.*, 29, 517 (1958).

(10) R. E. Fox and R. K. Curran, *ibid.*, 34, 1595 (1961).

(11) J. A. Stockdale and G. S. Hurst, *ibid.*, 41, 255 (1964).

(12) E. P. Bertin and W. H. Hamill, *J. Am. Chem. Soc.*, 86, 1301 (1964).

(13) D. W. Skelly, R. G. Hayes, and W. H. Hamill, *J. Chem. Phys.*, 43, 2795 (1965).

(14) J. E. Lovelock, *Nature*, 189, 729 (1961).

(15) J. E. Lovelock and N. L. Gregory, "Gas Chromatography," N. Brenner, Ed., Academic Press Inc., New York, N. Y., 1962, p 219.

(16) W. E. Wentworth, E. Chen, and J. E. Lovelock, *J. Phys. Chem.*, 70, 445 (1966).

(17) W. E. Wentworth and R. S. Becker, *J. Am. Chem. Soc.*, 84, 4263 (1962).

(18) R. S. Becker and W. E. Wentworth, *ibid.*, 85, 2210 (1963).

(19) R. S. Becker and E. Chen, *J. Chem. Phys.*, 45, 2403 (1966).

(20) W. E. Wentworth and E. Chen, *J. Phys. Chem.*, 71, 1929 (1967).

(21) R. S. Becker, W. E. Wentworth, and L. Wang, in preparation.

electron attachment have been studied by the pulse-sampling technique in our laboratories to date. In all cases, the experimental electron affinities appear reasonable with respect to other experimental and theoretical estimates of the electron affinities as well as by correlation with other parameters.

The pulse-sampling technique, in addition to its simplicity in operation and design, has another distinct advantage since it can be used in conjunction with a gas chromatograph. At present, gas chromatography is probably the most effective technique to separate and/or purify organic compounds. For this reason, with a relatively impure sample, a satisfactory separation of the major constituent from its impurities can frequently be made with proper gas chromatographic procedures. The use of a gas chromatograph is extremely important when very weakly capturing species are being studied, as will become evident later.

Kinetic Model

In the electron-capture detector,[14,15] argon atoms are either ionized or excited to metastable states upon collisions with β particles emitted from a tritium foil. The electrons ejected from the argon atoms will then gradually lose their kinetic energy through numerous collisions with other particles in the cell. Since an argon atom does not have the vibrational and/or rotational levels which a polyatomic molecule possesses, it is not very effective in removing energy from an electron through mutual collisions. When a small amount of methane is mixed with the argon, however, the electrons can soon lose their excess energy to the low-lying excited vibrational and/or rotational levels of methane molecules and come to thermal equilibrium with the gas.[16] A constant supply of thermal electrons can thus be obtained. The gas being added to the argon to permit "cooling" of the electrons to thermal energies will be called the moderating gas. Furthermore, the moderating gas (at $\approx 10\%$ concentration by volume) is effective in quenching the metastable argon atoms produced.

If now a thermal electron is captured by a molecule, AB, which can undergo dissociative capture, two processes may occur. In one process, an unstable negative ion, AB^-, is first formed which then either dissociates to give a free radical A· and a negative ion B^- or releases the electron through collision with a third particle. In the other case, the molecule, after capturing the electron, is promoted to a repulsive dissociative state and dissociation proceeds immediately. Since various radicals and positive ions resulting from ionization and dissociation are present in the cell, it is also possible that electrons and negative ions may react with these species. In a general model, all of these possible reactions will be considered. Different situations may arise for different types of compounds and lead to cancellation of certain reactions, but the general model should still be applicable.

Before proceeding to the reactions, it is appropriate to define some terms and names that are to be used: e^- is the thermal electron; AB is the capturing molecule; AB^- is a negative ion; A and B^- are products of dissociation; P^+ is a symbol to designate any of the positive ions in the cell, *e.g.*, Ar^+, ArH^+, $ArCH^+$, $ArCH_2^+$, $ArCH_3^+$, $ArCH_4^+$, CH_4^+, CH_3^+, CH_2^+, H^+, etc.; R· is a symbol to designate any of the radicals in the cell, *e.g.*, H·, CH_3·, CH_2·, etc. The concentration of each species is represented by brackets containing the name of the species, for example, $[AB^-]$.

The possible reactions are listed below, with reaction rate constants attached to the corresponding reactions.

$$\beta^- + Ar + CH_4 \xrightarrow{k_p R\beta} P^+ + e^- + \beta^- \qquad (1)$$

(This reaction also includes cooling of the electrons.)

$$AB + e^- \xrightarrow{k_{12}} A\cdot + B^- \qquad (2)$$

$$AB + e^- \xrightarrow{k_1} AB^- \qquad (3)$$

$$AB^- + M \xrightarrow{k_{-1}'} AB + e^- + M \qquad (4)$$

$$AB^- + M \xrightarrow{k_2'} A\cdot + B^- + M \qquad (5)$$

$$e^- + P^+ \xrightarrow{k_N'} R\cdot \qquad (6)$$

$$e^- + R\cdot \xrightarrow{k_R'} R^- \qquad (7)$$

$$AB^- + P^+ \xrightarrow{k_{N_1}'} \begin{cases} \rightarrow AB + R\cdot \\ \rightarrow A\cdot + B\cdot + R\cdot \end{cases} \qquad (8)$$

$$AB^- + R\cdot \xrightarrow{k_{R_1}'} \begin{cases} \rightarrow ABR^- \\ \rightarrow AB + R^- \xrightarrow{+P^+} \text{neutrals} \\ \rightarrow AR + B^- \end{cases} \qquad (9)$$

$$B^- + P^+ \xrightarrow{k_{N_2}'} \begin{cases} \rightarrow BP \\ \rightarrow B\cdot + R\cdot \end{cases} \qquad (10)$$

$$B^- + R\cdot \xrightarrow{k_{R_2}'} BR + e^- \qquad (11)$$

$$A\cdot + e^- \xrightarrow{k_3} A^- \qquad (12)$$

$$A^- + P^+ \xrightarrow{k_{N_4}'} AP \text{ or } A\cdot + R\cdot \qquad (13)$$

$$A^- + R\cdot \xrightarrow{k_{R_4}'} AR + e^- \qquad (14)$$

$$A^{\cdot} + AB^{-} \xrightarrow{k_{E_4}} AB + A^{-} \quad (15)$$

The following assumptions are made in this model: (a) the electrons are produced by the β particles at a constant rate; (b) the diffusion loss of electrons can be neglected; (c) the concentration of the negative ions is negligible compared to the capturing species; (d) the positive species and radicals are present in large excess compared to the negative ion concentration; (e) a steady state is reached by the intermediate negative species e^-, AB^-, and B^- during the time when the pulse is off; (f) essentially no reaction occurs during the application of the pulse necessary to collect electrons.

At this point, certain arguments will be given so that some of the reactions listed can be neglected. First of all, comparing reactions 2, 3, 6, 7, and 12 and using the assumptions made in (c) and (d) above, it can be seen that since $[A^{\cdot}]$ is probably much smaller than either $[R^{\cdot}]$ or [AB], eq 12 can be neglected. Since reactions 13, 14, and 15 are dependent on (12), elimination of (12) also eliminates these reactions. Therefore, only reactions 1–11 will be involved in the kinetic expressions.

The steady-state equations of the negative species are

$$\frac{d[e^-]}{dt} = 0 = k_p R_\beta - (k_1 + k_{12})[AB][e^-] - (k_N'[P^+] + k_R'[R^{\cdot}])[e^-] + k'_{-1}[AB^-][M] + k_{R2}'[B^-][R^{\cdot}] \quad (16)$$

$$\frac{d[AB^-]}{dt} = 0 = k_1[AB][e^-] - (k_{-1}' + k_2')[M][AB^-] - (k_{N1}'[P^+] + k_{R1}'[R^{\cdot}])[AB^-] \quad (17)$$

$$\frac{d[B^-]}{dt} = 0 = k_2'[AB^-][M] + k_{12}[AB][e^-] - (k_{N2}'[P^+] + k_{R2}'[R^{\cdot}])[B^-] \quad (18)$$

According to assumption d above, [M], $[R^{\cdot}]$, and $[P^+]$ are large and can be considered constant. Thus, some of the reactions involving these particles can be considered as pseudo-first-order reactions. The primed second-order rate constant times the corresponding concentration can be replaced by an unprimed pseudo-first-order rate constant; e.g., $k_{-1}'[M] = k_{-1}$ and $k_N'[P^+] = k_N$.

Based on assumption c, $[AB^-]$ is negligible compared to [AB]. Therefore, a, the initial concentration of AB, can be used in these equations instead of [AB]. Equations 16, 17, and 18 can be simplified to give

$$k_p R_\beta - (k_1 + k_{12})a[e^-] - (k_N + k_R)[e^-] + k_{-1}[AB^-] + k_{R2}[B^-] = 0 \quad (19)$$

$$k_1 a[e^-] - (k_{-1} + k_2)[AB^-] - k_{N1}[AB^-] - k_{R1}[AB^-] = 0 \quad (20)$$

$$k_2[AB^-] + k_{12}a[e^-] - k_{N2}[B^-] - k_{R2}[B^-] = 0 \quad (21)$$

respectively. An expression for $[AB^-]$ in terms of $[e^-]$ can be obtained from eq 20 and an expression for $[B^-]$ in terms of $[AB^-]$ and $[e^-]$ can be obtained from eq 21. Thus from eq 20 and 21, $[AB^-]$ and $[B^-]$ can be expressed in terms of $[e^-]$ and substituted into eq 19 giving

$$k_p R_\beta - (k_1 + k_{12})a[e^-] - (k_N + k_R)[e^-] + \frac{k_{-1}k_1 a[e^-]}{\sum k} + \frac{k_{R2}a[e^-]}{k_{N2} + k_{R2}}\left(k_{12} + \frac{k_2 k_1}{\sum k}\right) = 0 \quad (22)$$

where $\sum k = k_{-1} + k_2 + k_{N1} + k_{R1}$.

In the absence of a capturing species, $a = 0$, $[e^-] = [e^-]_{a=0}$, and eq 22 becomes

$$[e^-]_{a=0} = b = \frac{k_p R_\beta}{k_N + k_R} \quad (23)$$

Equations 22 and 23 can be combined to eliminate $k_p R_\beta$, giving the single expression

$$\frac{b - [e^-]}{[e^-]} = \left[\frac{k_{N2}}{k_{N2} + k_{R2}}\frac{k_{12}}{k_N + k_R} + \frac{k_{N2}}{k_{N2} + k_{R2}}\frac{k_1 k_2}{(k_N + k_R)\sum k} + \frac{k_1(k_{N1} + k_{R1})}{(k_N + k_R)\sum k}\right]a = Ka \quad (24)$$

This general equation shows that the quantity $(b - [e^-])/[e^-]$ is a linear function of a, the concentration of the capturing species, the slope, K, being a combination of rate constants of reactions 2 to 11.

Experimental Section

The construction of an electron-capture detector as well as the flow diagram of the equipment used along with the detector has been described in satisfactory detail previously.[14,15] The electron-capture cell used for this work was much the same and will not be described again. A tritium-imbedded titanium foil with an activity of $\approx$0.1 curie was used in the cell. A square-wave potential of 40 v was applied across the cell by means of a Datapulse generator, Model 102. The pulse width, depending on the moderating gas used, ranged from 0.5 μsec for methane to 4.0 μsec for pure argon (Table I). The pulse interval was 1000 μsec.

During the applied pulse, free electrons were collected

on the grid, and the current was detected and magnified by a Cary 31 vibrating-reed electrometer.

Preceding the electron-capture detector was a short section of tubing allowing scavenger gas and moderating gas to mix with the column effluent. Most of the columns used in this work were made of 0.25-in. packed columns 2–6 ft in length. The solid support for all packed columns was Analabs ABS 70–80 mesh. CCl_4, $CHCl_3$, CH_2Cl_2, C_2H_5I, C_3H_7Br-1, and C_4H_9Cl-1 were run on a 20% C-16 column at room temperature. Iodobenzene, bromobenzene, and *o*- and *m*-dichlorobenzenes were run on a Carbowax 20M column at 85–120°. 1-Bromonaphthalene was chromatographed on a 3% C-60 column, whereas a 250-ft, 0.03-in. i.d. (polyphenyl ether) column was required to obtain sufficient purity.

Table I: Pulse Widths Required for Various Gas Mixtures (Pulse Interval 1000 μsec, Pulse Voltage 40 v)

Gas mixture	Pulse width, μsec
Ar–10% CH_4	0.5
Ar–1.5% CO_2	2.0
Ar–2.0% H_2	2.5
Ar	4.0

Argon from the Big Three Welding Equipment Co. (purity >99.99%) was used without further purification but was passed through a molecular sieve (Type 5A) trap, the Illinois Institute Dri-pak, to remove traces of moisture in the gas. Methane (Matheson, 99.9%) was also passed through the Dri-pak before mixing with the scavenger argon. Flow rate was measured at the outlet of the electron-capture detector with a soap bubble flowmeter and a stopwatch. The flow rate was measured at room temperature while the temperature in the cell was usually higher. In order to obtain the true flow rate in the cell, a correction factor was needed. Assuming ideal gas behavior, in this temperature and pressure range, the true flow rate in the cell was obtained by multiplying the measured flow rate with the factor $T/298$. A random error of about 10% may be involved in the measurement of flow rate.

The temperature of both the column and detector was controlled with Variacs and read with thermometers inserted into the ovens. For this work, the accuracy of column temperature is not very critical. On the other hand, an accurate cell or detector temperature reading is very important. Since the thermometer bulb was in the air instead of being directly in contact with the cell, a possible error was involved in cell temperature reading. The resulting bias error could be 1°.

Solutions of the tested compounds were prepared to give suitable peak sizes (about 60% capture) and linearity of response in the concentration ranges used. The solutions were prepared by volume measurements. Concentrations in moles per liter were then calculated with known densities and molecular weights. The concentration of a solution thus prepared has been checked by weighing the solute also. The error proved to be small. Especially when the amount of solute is as small as a few microliters, weights may not be any more accurate than volumes. When the compound was very high capture and a very dilute solution was needed, a second dilution of a diluted solution of the compound was made. The solvents used were all low-capture compounds like benzene and toluene.

All samples were injected with a Hamilton 10-μl syringe. The injector was heated to a temperature comparable to column temperature so that the sample would not condense in the injector.

Since the electron-capture ability has a very selective response to certain compounds, sometimes it became necessary to identify the major peak among several peaks in a sample. This is especially true for the low-capture compounds. A detector developed in this laboratory was used for this purpose[22] which shows roughly the same sensitivity for all compounds.

Toward the end of this work, a 50-ft packed SE 30 column was available (HiPak purchased from F & M Scientific). This column was capable of giving much better resolution than the other columns used, so it was utilized to check some of the compounds that were suspected to have high-capture impurities. Chlorobenzene and chlorobutane were run at a column temperature of 100° and were found to have impurities very close to the major peak. For this reason, these compounds were not included in this study. A benzene solution of propyl bromide run at the same column temperature shows only the benzene peak and the sample peak. Bromobenzene was run at 105°. The nearest impurity was 6.5 min after bromobenzene, while the latter has a retention time of 17 min. It was thus concluded that the impurity would also be resolved, if the column given earlier was used. The *o*- and *m*-dichlorobenzenes were both run at 150°. Benzene, which was the solvent, was the only other peak seen besides the sample peak. For all these compounds, the column flow rate was approximately 30 ml/min.

In eq 24, a is the concentration of the tested com-

(22) W. E. Wentworth and W. Ristau, in preparation.

pound in moles of compound per liter of gas. Since a is not available directly in this experiment, an integration is carried out on both sides of eq 24 to give

$$\int_0^v \frac{b - [e^-]}{[e^-]} dv = K \int_0^v a dv \qquad (25)$$

where v is the volume of gas flowing through the detector during the peak. The integral on the right-hand side readily gives n, the number of moles of the compound. To obtain the integral on the left-hand side, a transformation needs to be carried out; v can be expressed in terms of some measurable quantities as

$$v = \frac{F_r}{C_s} w \qquad (26)$$

where F_r is the gas flow rate in the detector in liters per minute, C_s is the chart speed in inches per minute, and w is the peak width in inches. Taking the differential of eq 26 and substituting into the left-hand side of eq 25, we have

$$\frac{F_r}{C_s} \int_0^w \frac{b - [e^-]}{[e^-]} dw = \frac{F_r}{C_s} A = Kn \qquad (27)$$

or

$$K = \frac{A}{n} \frac{F_r}{C_s}$$

where A is the transformed peak area. In an actual experiment, however, n is a product of two other quantities, namely, the microliters of solution injected and concentration of the solution in moles per microliter. Using S and C for these two quantities, respectively, we have

$$K = \frac{A}{SC} \frac{F_r}{C_s} = \frac{A/S}{C} \frac{F_r}{C_s} \qquad (28)$$

The peak areas are calculated with a digital computer program written for this purpose.[23] A series of straight lines are drawn approximating the curve as closely as possible, and the coordinates of each point joining adjacent lines are taken with reference to the origin as the start of the peak. On the basis of this, the computer calculates the transformed response $(b - [e^-])/[e^-]$ for each given point and then calculates the peak area with the transformed coordinates. For some compounds a Leeds and Northrup analog computer was used. This instrument converts the output signal of the electrometer to $(b - [e^-])/[e^-]$ and integrates over the gas chromatographic peak.

From five to ten samples were injected at each temperature. The areas obtained were plotted against the corresponding sample sizes S. A straight line

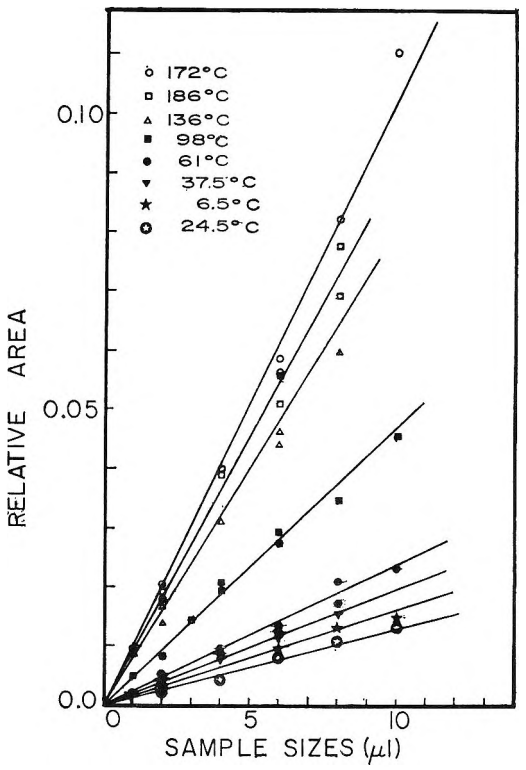

Figure 1. Integrated converted electron-capture response, $\int(b - [e^-])/[e^-]\, dw$, for $CHCl_3$ as a function of concentration at various temperatures. The slope at 24.5° is lower than at 6.5°; however, correction for the span, b, makes the true K value at 6.5° lower than at 24.5°.

through the origin was drawn that would best fit the data points. As an example, Figure 1 shows the plotted data of chloroform at several temperatures. It is to be noted that the integrated response $\int_0^v (b - [e^-])/[e^-]\, dw$ does appear to be a linear function of the sample size—consistent with eq 27 and 28, derived earlier. The slope of the straight line, A/S, multiplied by the factor $(F_r/C_s)/C$, gives the constant K at this temperature.

Resulting from bleed of the gas chromatographic column and/or a slowly emerging peak of a high boiler, the span b may not stay constant. This problem has been mentioned in an earlier publication and a correction factor of b_0/b is applicable under certain conditions;[16] b_0 is the span when pure carrier gas (no column bleed or impurity) is passed through the cell, and b is the measured span when the column is used. As mentioned earlier,[16] this problem is under study, and, at present, data are taken only where b_0/b is relatively close to unity. In this work, the correction factor ranges from $^{100}/_{40}$ to $^{100}/_{150}$, which is not actually

(23) W. Hirsch, M.S. Thesis, University of Houston, 1965.

large when one considers that the change in capture coefficient may be 1000 or so over a 200° range.

Wentworth, *et al.*,[16,17] have shown that, for a nondissociative electron-capture reaction, the statistical thermodynamic expression of the equilibrium constant can be employed. This gives

$$K = ZT^{-3/2}e^{-\Delta E/kT} \tag{29}$$

where K is the electron-capture coefficient, Z is a preexponential factor independent of temperature, ΔE is the electron affinity, k is the Boltzmann constant, and T is the cell temperature.

Equation 29 was rearranged to give

$$\ln KT^{3/2} = \ln Z - \frac{\Delta E}{kT} \tag{30}$$

In general, a temperature region was observed where a graph of $\ln KT^{3/2}$ *vs.* $1/T$ was linear with the expected *positive* slope.[16]

A brief survey of reactions 1 through 11 reveals that there are several types of reactions, each involving very different charged or uncharged species. No satisfactory theoretical treatment as to the role of temperature in the preexponential factor has been known for these reactions. It is thus impossible at the present time to derive an expression similar to eq 30 for the dissociative model suggested here. However, in order to simplify the comparison of the results of this study with those previously published, all data obtained for dissociative capture are plotted as $\ln KT^{3/2}$ *vs.* $1/T$. As can be seen in Figure 2, a linear relation is obtained for all the compounds studied. The slopes are related to the activation energies for the operative mechanism, as will be discussed later.

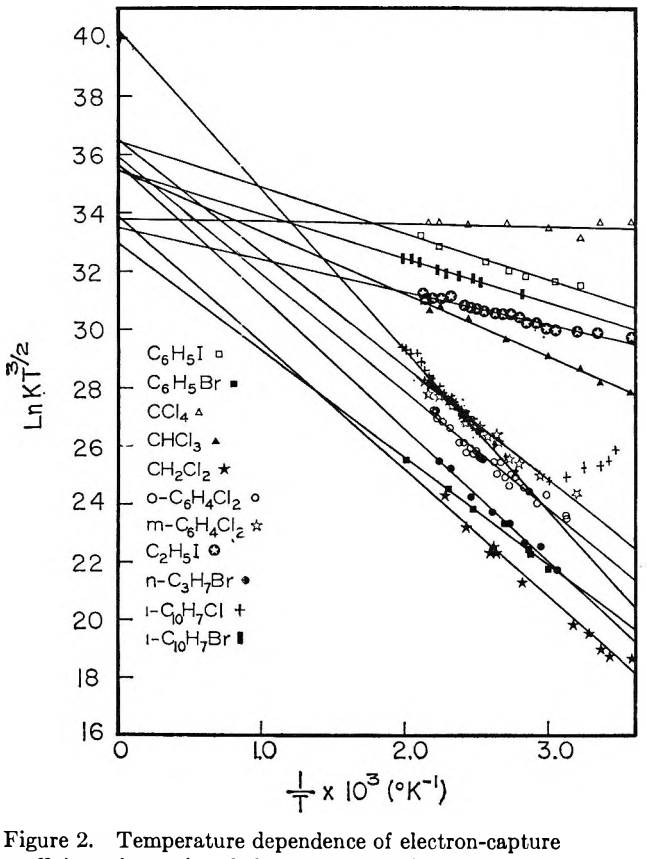

Figure 2. Temperature dependence of electron-capture coefficients for various halogenated organic compounds.

A weighted least-squares adjustment of data to eq 30 was carried out.[24] The solid lines drawn in Figure 2 are the least-squares estimate of the function. The errors involved in measuring the parameters were estimated as follows. The value of K, as expressed in eq 28, is calculated from five independent measurements, and its error will be a function of the errors in these measurements. The error in chart speed can be assumed to be negligible. Thus the error in K is expressed in terms of the other four parameters as

$$\sigma_K^2 = \left[\frac{\partial K}{\partial (A/S)}\right]^2 \sigma_{A/S}^2 + \left[\frac{\partial K}{\partial F_r}\right]^2 \sigma_{F_r}^2 + \left[\frac{\partial K}{\partial C}\right]^2 \sigma_C^2$$

$$= \left[\frac{F_r/C_s}{C}\right]^2 \sigma_{A/S}^2 + \left[\frac{A/S}{CC_s}\right]^2 \sigma_{F_r}^2 + \left[\frac{A(F_r/C_s)}{SC^2}\right]^2 \sigma_C^2$$

$$= \left[\frac{K}{A/S}\right]^2 \sigma_{A/S}^2 + \left[\frac{K}{F_r}\right]^2 \sigma_{F_r}^2 + \left[\frac{K}{C}\right]^2 \sigma_C^2 \tag{31}$$

It follows that

$$\left[\frac{\sigma_K}{K}\right]^2 = \left[\frac{\sigma_{A/S}}{A/S}\right]^2 + \left[\frac{\sigma_{F_r}}{F_r}\right]^2 + \left[\frac{\sigma_C}{C}\right]^2 \tag{32}$$

Assuming a 10% error is involved in flow rate measurement and in solution preparation, eq 32 becomes

$$\left[\frac{\sigma_K}{K}\right]^2 = \left[\frac{\sigma_{A/S}}{A/S}\right]^2 + (0.1)^2 + (0.1)^2 = \left[\frac{\sigma_{A/S}}{A/S}\right]^2 + 0.02 \tag{33}$$

As was described earlier, A/S is the slope obtained from the plot of peak areas *vs.* sample sizes at a certain temperature. A weighted least-squares adjustment of the linear relationship between A and S gives the error in this slope.

The parameters resulting from the least-squares adjustment of $\ln KT^{3/2}$ *vs.* $1/T$ are given in Table II. The column E^* is the energy of activation one would

(24) W. E. Deming, "Statistical Adjustment of Data," Dover Publications, New York, N. Y., 1964.

Table II: Least-Squares Adjustment of the Temperature Dependency of Electron-Capture Coefficients

Compound	Intercept	$\Delta E = -\text{slope} \times R$, kcal/mole	E^*, kcal/mole	$\sigma_{ext}^2/\sigma_0^2$
Carbon tetrachloride	33.82 ± 0.31	0.19 ± 0.22	−0.05	1.14
Ethyl iodide	33.50 ± 0.26	2.18 ± 0.19	1.07	0.38
Iodobenzene	36.45 ± 0.43	3.14 ± 0.32	1.55	0.35
1-Bromonaphthalene	35.47 ± 0.51	3.00 ± 0.43	1.74	0.09
Chloroform	35.49 ± 0.35	4.25 ± 0.255	3.09	0.35
m-Dichlorobenzene	36.41 ± 0.35	7.70 ± 0.29	6.54	0.48
Bromobenzene	32.97 ± 0.43	7.32 ± 0.33	5.91	1.82
o-Dichlorobenzene	35.95 ± 0.37	8.05 ± 0.29	6.91	0.76
Methylene chloride	33.90 ± 0.35	8.68 ± 0.24	7.53	2.15
n-Propyl bromide	35.67 ± 0.71	9.03 ± 0.55	7.88	0.50
1-Chloronaphthalene	40.55 ± 0.33	11.01 ± 0.29	9.87	0.74

have obtained if ln K *vs.* $1/T$ had been plotted. Without knowing the preexponential temperature-dependence term, one cannot precisely establish the energy of activation. E^* would be the activation energy if the preexponential term were constant. The σ_{ext}^2 in Table II should be compared to σ_0^2 which was assigned a value of unity.[24] In general, the σ_{ext}^2 are of the same order of magnitude, indicating the data can be adjusted to this function within the expected experimental error. If anything, the σ_{ext}^2 are probably less than σ_0^2, suggesting that our error estimates in eq 33 were pessimistic. In that case, the quoted errors in the parameters are likewise pessimistic.

The gas mixture used for the previous work was argon plus 10% methane. In order to study the importance of radical reactions, iodobenzene and bromobenzene were run using mixtures of argon and moderating gases other than methane. Hydrogen and carbon dioxide were used. The percentage of each moderating gas was such that additional moderating gas does not result in an appreciable increase in standing current. Different pulse widths were used in each case, as stated before, and are listed in Table I. The electron-capture data obtained were treated as discussed previously except that least-squares adjustment was not carried out. The data were graphed as ln $KT^{3/2}$ *vs.* $1/T$ as before. No obvious difference in slope was observed; however, there was some increase in magnitude with CO_2 and H_2 for bromobenzene. Since the differences in slopes were not considered significant, the effect of different radicals as in eq 7, 9, and 11 apparently does not alter the energy of activation.

The relative orders of magnitude of the capture coefficient of some of these compounds have been obtained before by Lovelock.[14,15,25] These seem to be in general agreement with the present work. Some differences occur (*e.g.*, *o*- and *m*-dichlorobenzenes) probably owing to the fact that he used short pulse intervals. Furthermore, he did not specify the cell temperature, and for compounds such as bromobenzene this can be most important.

Lee,[26] using nitrogen as carrier gas in the swarm method, investigated electron attachment to a number of aliphatic halides as a function of electron energy. The energy range in this work was 0.02–1.2 ev. A comparison of Lee's values at E/p 0.2 and ~0.032 with the present work shows general agreement on relative magnitudes. In the case of CH_2Cl_2, Lee's sample would have to be extremely pure in order for his results to be meaningful. For example, our value for CCl_4 is approximately 10^4 greater than CH_2Cl_2 and hence a 0.01% impurity of CCl_4 in CH_2Cl_2 would result in a 100% error. Other weaker capturing impurities, however, would be less critical.

Discussion

A very striking feature about the data presented in Figure 2 is the completely different temperature dependence compared to the nondissociative cases. The capture coefficients either increase with increasing temperature (decreasing $1/T$) or remain constant. This is probably characteristic of the dissociative compounds in general. Analogous to the nondissociative case, however, the extrapolation of the slopes in Figure 2 to infinite temperature ($1/T = 0$) shows that several compounds seem to have a common intercept. Thus iodobenzene, chloroform, *o*- and *m*-dichlorobenzene, 1-bromonaphthalene, and *n*-propyl bromide all extrapolate to an intercept in the region of 35.9. Carbon tetrachloride, methylene chloride, and ethyl iodide extrapolate to approximately 33.5. Bromo-

(25) J. E. Lovelock, *Anal. Chem.*, **35**, 474 (1962).

(26) T. G. Lee, *J. Phys. Chem.*, **67**, 360 (1963).

benzene alone seems to have a lower intercept, whereas 1-chloronaphthalene is exceedingly high at 40.5. However, the least-squares adjustment does indicate that the errors in some intercepts seem to overlap the standard-error estimate of others. Off hand, it is difficult to assign any significance to the different intercepts. A conclusion as to whether there is a common intercept may be premature at the present stage. It is, however, proper to examine the fit of the proposed model in view of the observed temperature dependence.

From eq 24 it can be seen that K is a sum of three terms representing three processes. The first term represents the spontaneous dissociative process, eq 2; the second term, the intermediate negative ion process, eq 3–5; and the third, the stable negative ion case, eq 3 and 4. Since k_{12} appears only in the first term, it can be considered separately when the first term is assumed to predominate. For the $\sum k$ in the second and third terms of eq 24, we can consider two limiting situations: (1) when $k_{-1} >> (k_2 + k_{N1} + k_{R1})$; and (2) when $k_2 >> (k_1 + k_{N1} + k_{R1})$. The situation when $(k_{N1} + k_{R1}) >> (k_2 + k_{-1})$ will not be considered here since this has been shown to correspond to the temperature-independent region of the stable negative ion case.[16] Before considering the validity of each limiting case, a simplifying assumption will be made that $k_{N2}/(k_{N2} + k_{R2})$ is very close to unity. This is not an unreasonable assumption based on the two following reasons. First, the attraction between two unlike charged particles should be much larger than the attraction between an uncharged and a charged particle; hence, k_{N2} should be much larger than k_{R2}. Second, the experiments done with different moderating gases have shown that radical reactions apparently are relatively unimportant from the standpoint of regenerating neutral molecules and free electrons. The term $k_{N2}/(k_{N2} + k_{R2})$ arises only when free electrons are assumed to be formed in the radical reaction with a B^- ion, eq 11. For this reason, we will eliminate this term in the subsequent simplified expressions for K. This does not mean that radical reactions as shown in eq 11 do not occur and that they are not important in themselves. In particular, only in the interpretation of the results in this work they should not play an important role.

Considering first the situation when the first term in eq 24 predominates, *i.e.*, $k_{12} >> (k_1k_2/\sum k) + [k_1(k_{N1} + k_{R1})/\sum k]$. The expression for K is thus

$$K = \frac{k_{12}}{k_N + k_R} \qquad (34)$$

Figure 3 contains various potential energy diagrams

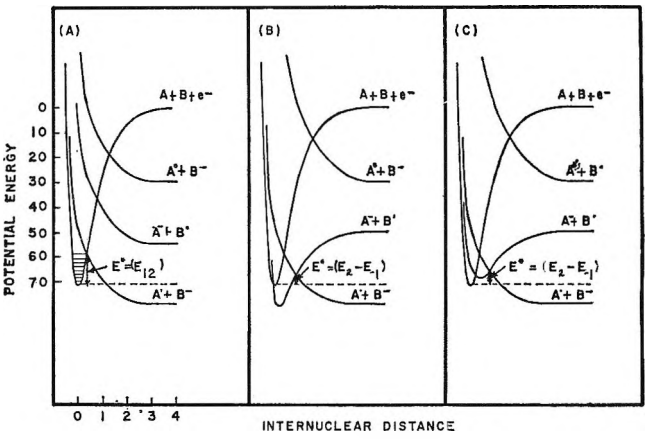

Figure 3. Representative potential energy curves for dissociative electron attachment: A, k_{12} mechanism; B, k_1k_2/k_{-1} mechanism (with a positive electron affinity, *i.e.*, energy release); C, k_1k_2/k_{-1} mechanism (with a negative electron affinity).

which may represent the mechanisms proposed for dissociative electron attachment. The spontaneous dissociative process represented by eq 2 is shown in Figure 3A. The energy of activation would be that required to populate thermally the neutral molecule in the ground electronic state to some higher vibrational mode at an energy where the dissociative curve crosses the ground-state potential energy curve. Electron attachment to such a vibrationally excited state should result in spontaneous dissociation. The experimentally observed negative slope of $\ln KT^{3/2}$ *vs.* $1/T$ (Figure 2) can thus be explained by this mechanism. Two higher energy dissociative potential energy curves are included in Figure 3A for completeness to represent, in general, transitions which may be observed by other experimental techniques.

When the latter two terms in eq 24 predominate, *i.e.*, $(k_1k_2/\sum k) + [k_1(k_{N1} + k_{R1})/\sum k] >> k_{12}$, the two possible limiting situations in the $\sum k$ can be considered. First, if $k_{-1} >> k_2$ then the expression for K becomes

$$K = \frac{k_1k_2}{(k_N + k_R)k_{-1}} + \frac{(k_{N1} + k_{R1})}{(k_N + k_R)}\frac{k_1}{k_{-1}} \qquad (35)$$

The second term in eq 35 is the stable negative ion case,[16] and is certainly not applicable to the data obtained in this study. The first term is the mechanism for dissociative electron attachment which involves the formation of an intermediate stable negative ion. Typical potential energy diagrams for this case are shown in Figures 3B and 3C. The mechanistic path followed is the formation of a stable negative ion followed by thermal activation of the negative ion to

a vibrational mode which crosses the lowest energy dissociation curve. We refer to this dissociative process as the k_1k_2/k_{-1} mechanism. The over-all energy of activation is shown as $E^* = (E_2 - E_{-1})$ where the E_2 and E_{-1} are the corresponding energies of activation for the rate constants k_2 and k_{-1}. Figure 3B is the more general case where the electron affinity of the molecule is positive (*i.e.*, exothermic in going from the neutral molecule to the stable negative ion). There is the possibility, depicted in Figure 3C, where a molecule has a negative electron affinity. However, this situation is probably unlikely, but may explain the data for some of the halogen-substituted benzenes. This will be discussed later in detail.

If $(k_{N1} + k_{R1})$ in eq 35 is not negligible compared to k_2, we have a sum of two terms, one for the intermediate negative ion, the other for the stable negative ion. It is possible to observe a transition region for such a case. The first term would appear at higher temperatures and decrease with decreasing temperatures. As the temperature gets low enough, the second term should predominate and K starts to increase with decreasing temperature. The only compound investigated in this study that does this is 1-chloronaphthalene.

The situation where $k_2 >> k_{-1}$ does not really add much to the explanation of the temperature dependency for dissociative electron attachment. Under these assumptions, eq 24 will reduce to

$$K = \frac{k_1}{k_N + k_R} + \frac{k_{N1} + k_{R1}}{k_N + k_R}\frac{k_1}{k_2} \qquad (36)$$

The first term has to be very large compared to the second term, the former term being the maximum value for the intermediate negative ion term.[16] Since the second term has k_2 in the denominator and $k_2 >> (k_{N1} + k_{R1})$, it is necessarily smaller than the first term where there is a high-capture coefficient k_1 with little or no temperature dependence. Of the compounds investigated, only carbon tetrachloride could fit this model. However, one could also explain carbon tetrachloride by the k_{12} mechanism if there was no energy of activation; *i.e.*, $E_{12} = 0$.

One should also consider the situation where k_2 gets larger and becomes comparable to k_{-1}. One may think that a curvature will be observed owing to the factor $k_2/(k_2 + k_{-1})$ in the first term of eq 35 which can be expressed as $A_2e^{-E_2/kT}/(A_2e^{-E_2/kT} + A_{-1}e^{-E_{-1}/kT})$. However, actual calculation of the factor $k_2/(k_2 + k_{-1})$ using different values for E_2 and E_{-1} shows that the curvature is hardly perceivable even if the preexponential factors are different by a factor of 10 in either sense. In short, if this is the case, the temperature dependence will appear to be the same as the case when k_{-1} is much greater than k_2. The only difference is that the former case, $k_{-1} >> k_2$, probably has a steeper slope.

Finally, there is the possibility that the first two terms of eq 24 are both of comparable magnitude. However, this is probably unlikely since it would be coincidental that the potential energy curves would cross with approximately the same energy of activation for both the k_{12} and the k_1k_2/k_{-1} mechanisms.

In conclusion, there are two possible mechanisms which can explain the temperature dependence of K observed experimentally and shown in Figure 2. These are the k_{12} mechanism as given by eq 34 and the k_1k_2/k_{-1} mechanism as given by eq 35. On simply the information of the temperature dependence, it is impossible to decide which mechanism is operative. However, as will be discussed shortly, comparison of results for different compounds is suggestive that the k_1k_2/k_{-1} mechanism is operative in some compounds.

Possible potential energy curves for bromobenzene are shown in Figure 4. The available data for the bond dissociation energy, the electron affinity of the bromine atom, and the electron affinity of the phenyl radical[27] are used and drawn to scale. A potential

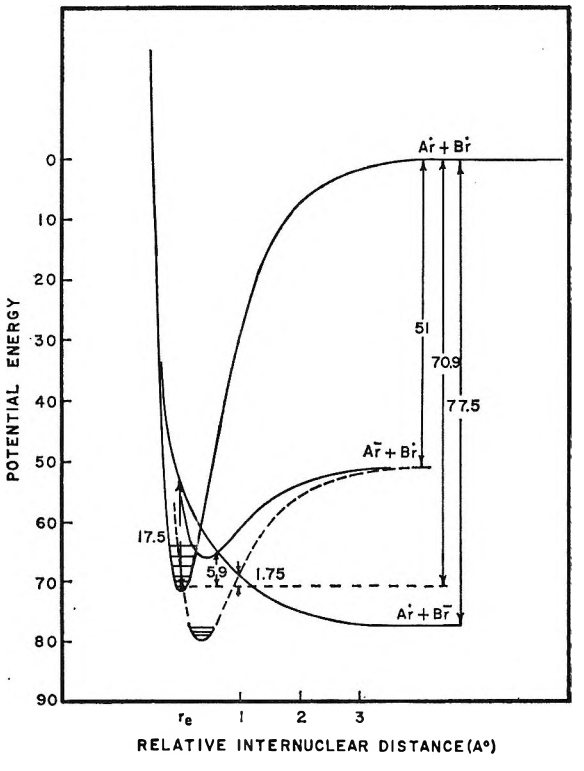

Figure 4. Possible potential energy curves for bromobenzene and bromonaphthalene: Ar·, aromatic radical; – – – –, stable negative ion potential energy curve for bromonaphthalene.

energy curve resulting in dissociation to $Ph^- + Br^\cdot$ is shown. It represents a stable negative ion formation, but with a negative electron affinity. As mentioned previously, in general this is probably a very unlikely situation, but it appears to be a reasonable possibility for bromobenzene. This will become more convincing after comparison with propyl bromide and 1-bromonaphthalene. The experimentally observed 5.9 kcal/mole energy of activation is shown for the k_1k_2/k_{-1} mechanism.

Stockdale and Hurst[11] measured the electron-capture cross section of bromobenzene and chlorobenzene with a swarm method. Using argon, nitrogen, and ethylene as carrier gases, they were able to measure the cross section with a distribution at thermal electron energies to distributions with maxima at about 10 ev. The maximum cross section occurs at 0.76 ev (17.5 kcal/mole) and 0.7 ev for bromobenzene and chlorobenzene, respectively. The present data give 5.9 kcal/mole for the energy required for the over-all process for bromobenzene. The discrepancy is apparently due to the different modes of electron attachment. In the swarm method, a high-energy electron collides with a ground-state molecule; hence, a vertical transition from the neutral molecule to the dissociative state can occur.[28] However, in the electron-capture cell, the molecules are heated and, thereby, low-lying vibrational levels become occupied to the point where the potential energy curve for the neutral molecule crosses with the dissociative state. In Figure 4, the vertical transition is represented by 17.5 kcal/mole. It is obvious from this figure that a higher value for the energy of the over-all process will be obtained if the swarm method is used. Because of the difficulty in resolving the impurity in our work, no data on chlorobenzene are available for comparison.

As stated earlier although we cannot distinguish between the k_{12} and k_1k_2/k_{-1} mechanism in all cases, evidence can be given which suggests the k_1k_2/k_{-1} mechanism is the primary process for some compounds. In comparing bromobenzene and 1-bromonaphthalene, the C–Br bond-dissociation energy in the two compounds is quoted as the same value, 70.9 kcal/mole.[29] Therefore, since the electron affinity for the halide atom is identical in both cases, the dissociative state giving Ar + Br^- for 1-bromonaphthalene should be similar to that for bromobenzene as given in Figure 4. However, since naphthalene itself has a measurable electron affinity of 0.15 ev[16] and benzene is expected to have a negligible or, more likely, a negative electron affinity,[18,19] the potential energy curve for the stable negative ion should be much lower for 1-bromonaphthalene compared to bromobenzene. Furthermore, the naphthyl radical would be expected to have a comparable electron affinity to that of the phenyl radical. In Figure 4, the electron affinities for the aromatic radicals have been assumed to be identical. The electron affinity for 1-bromonaphthalene has been estimated by adding the effect of a Br substituent to the electron affinity of naphthalene. From half-wave reduction potentials and charge-transfer spectra, the effect of bromo substituent on quinone increased the electron affinity by 0.2 ev.[30] This value of 0.2 ev was added to the electron affinity of naphthalene to give an estimated electron affinity of 0.35 ev for 1-bromonaphthalene. This estimate of electron affinity was used to draw the potential energy curve for the stable negative ion of 1-bromonaphthalene in Figure 4 (dashed curve). These curves in Figure 4 suggests that 1-bromonaphthalene may go through the k_1k_2/k_{-1} mechanism with a lower energy of activation and a higher capture of electrons compared to bromobenzene. This interpretation is supported by the observations shown in Figure 2 and Table III. In bromobenzene, the k_1k_2/k_{-1} or the k_{12} mechanism or both may be important. Shortly, it will be shown why we favor the former mechanism.

Table III: Bond Energies for Some Bromobenzenes

Compound	D(C–Br), kcal/mole
Bromobenzene	71,[a] 70.9[b]
p-ClC_6H_4Br	70.3[c]
m-ClC_6H_4Br	69.9[c]
o-ClC_6H_4Br	69.7[c]
p-$CH_3C_6H_4Br$	70.7[c]
m-$CH_3C_6H_4Br$	70.7[c]
o-$CH_3C_6H_4Br$	70.1[c]

[a] P. Smith, *J. Chem. Phys.*, **29**, 681 (1958). [b] M. Szwarc, *ibid.*, **20**, 1170 (1952). [c] M. Szwarc and D. Williams, *Proc. Roy. Soc.* (London), **A219**, 353 (1953).

(27) A. F. Gaines and F. M. Page, *Trans. Faraday Soc.*, 59, 1266 (1963).

(28) In a more recent paper, Christophorou, *et al.* (L. G. Christophorou, R. N. Compton, G. S. Hurst, and P. W. Reinhardt, *J. Chem. Phys.*, 43, 4273 (1965)), describe a procedure which combines electron-swarm data with electron-beam measurements to obtain absolute cross sections for electron attachment as a function of electron energy. The maximum for *o*-chlorotoluene differs from the maximum obtained from electron-swarm or electron beam measurements. A similar investigation of bromobenzene should be made and the energy of the true maximum should be used in place of the 0.76 ev (17.5 kcal/mole) quoted above.

(29) T. L. Cottrell, "The Strength of Chemical Bonds," Academic Press Inc., New York, N. Y., 1958.

(30) K. M. C. Davis, P. R. Hammond, and M. E. Peover, *Trans. Faraday Soc.*, 61, 1560 (1965).

Table IV: Activation Energy for Dissociative Electron Attachment Related to Energy Change for the Process (kcal/mole)[a]

Compound	Formula	E^*	D_{A-B}	EA_B[h]	$D_{AB} - EA_B$
Carbon tetrachloride	CCl_4	-0.05 ± 0.22	67.9 ± 3[g]	83.16	-15.3 ± 3
Chloroform	$CHCl_3$	3.10 ± 0.26	71.4 ± 2[c]	83.16	-11.8 ± 2
Methylene chloride	CH_2Cl_2	7.54 ± 0.24	75 ± 2[c]	83.16	-8.2 ± 2
m-Dichlorobenzene	*m*-$Cl_2C_6H_4$	6.54 ± 0.29	87[i]	83.16	+3.8
o-Dichlorobenzene	*o*-$Cl_2C_6H_4$	6.91 ± 0.29	87[i]	83.16	+3.8
1-Chloronaphthalene	1-$ClC_{10}H_7$	9.87 ± 0.29	87[i]	83.16	+3.8
n-Propyl bromide	C_3H_7Br	7.89 ± 0.55	64 ± 3[b]	77.55	-13.6 ± 3
Bromobenzene	C_6H_5Br	5.92 ± 0.33	70.9 ± 1.5[d]	77.55	-6.6 ± 1.5
1-Bromonaphthalene	1-$BrC_{10}H_7$	1.75 ± 0.43	70.9[d]	77.55	−6.6
Ethyl iodide	C_2H_5I	1.07 ± 0.20	52.9 ± 1.0[f]	70.63	-17.7 ± 1.0
Iodobenzene	C_6H_5I	1.55 ± 0.31	57 ± 2.5[d,e]	70.63	-13.6 ± 2.5

[a] The literature values quoted in this paper are, in the author's opinion, the best presently available. No attempt has been made to give recognition of possibly earlier or more recent estimates with similar or less reliability. [b] Bond dissociation energies for CH_3–Br and C_2H_5–Br are 67 and 65 kcal/mole, respectively, according to T. L. Cottrell.[29] This difference is in line with the change from CH_3–I to C_2H_5–I. On this basis, we have estimated the value for propyl bromide. [c] P. Goldfinger and G. Martens, *Trans. Faraday Soc.*, **57**, 2220 (1961). [d] M. Szwarc and D. Williams, *J. Chem. Phys.*, **20**, 1171 (1952). [e] M. Szwarc, *Chem. Rev.*, **47**, 75 (1950). [f] D. B. Hartley and S. W. Benson, *J. Chem. Phys.*, **39**, 132 (1963). [g] J. B. Farmer, *et al.*, *ibid.*, **24**, 348 (1956). [h] R. S. Berry and C. W. Riemann, *ibid.*, **38**, 1540 (1963). [i] C–Cl bond dissociation energy is taken to be that of chlorobenzene on the basis of previous discussion of the data in Table III. Chlorobenzene bond dissociation from S. W. Benson, "Foundations of Chemical Kinetics."

If the upper limit for the electron-capture coefficient of chlorobenzene is correct, then the data for the disubstituted *o*- and *m*-dichlorobenzenes also suggest that the intermediate stable negative ion mechanism is operative. The C–Cl bond dissociation energy for chlorobenzene is probably close to that of the C–Cl bond for the *o*- and *m*-dichlorosubstituted benzenes. Support for this supposition exists in the comparison of C–Br bond dissociation energies for several substituted bromobenzenes with that for unsubstituted bromobenzene as shown in Table III.

The electron-capture coefficient for the disubstituted compounds is well above even any upper limit estimate for the chlorobenzene, and again according to the proposed mechanisms one must assume that the intermediate stable negative ion plays an important role in the dichlorobenzenes. Apparently, the presence of two chloro substituents increases the electron affinity sufficiently to be effective in determining the mechanism of the over-all dissociative electron-attachment process.

A similar situation occurs with 1-chloronaphthalene, where it is expected to have an electron affinity greater than that of naphthalene. In fact, the positive slope at lower temperatures for this compound offers positive proof that a negative molecule ion forms.

Since there are no low-lying vacant π orbitals in the aliphatic halides, the electron affinities for these compounds should be negligible, and dissociative electron attachment probably goes by the k_{12} mechanism. In contrast to the previously mentioned differences between the monosubstituted benzenes and the monosubstituted naphthalenes or disubstituted benzenes, comparison of iodobenzene with ethyl iodide and bromobenzene with *n*-propyl bromide reveals a much smaller difference in activation energy for dissociative electron attachment. However, in making these comparisons in activation energies, one must also consider the differences in bond dissociation energy. As can be seen from the data in Table IV relative to the activation energies, the bond energies for the aromatic halides are significantly larger than the corresponding aliphatic halides. Taking this into consideration, bromo- and iodobenzenes probably undergo dissociative electron attachment by the k_1k_2/k_{-1} mechanism. The electron affinities of bromo- and iodobenzenes are small and possibly even negative as illustrated in Figure 4. Mass spectrometric analysis of the negative ions would be required to confirm the existence of the intermediate molecular negative ion. The concentration of the molecular negative ion would probably be very low considering the expected low electron affinity. The potential energy curves in Figure 4 are drawn so that the k_1k_2/k_{-1} mechanism for bromobenzene requires the 5.9-kcal/mole energy of activation. The k_{12} mechanism according to Figure 4 would have a higher energy of activation. If bromobenzene dissociates according to the k_1k_2/k_{-1} mechanism, then most certainly bromonaphthalene with a greater electron affinity would go by the same mechanism.

As mentioned earlier, Frost and McDowell[8] found a correlation between the electron energy at the maxi-

mum cross section for hydrogen halides and the difference between the electron affinity of the halogen atom and the bond dissociation energy. Their mechanism for dissociative electron attachment is the same as our k_{12} mechanism; however, they apparently measure the vertical transition to the dissociative potential energy curve. We interpret our energies of activation as the difference in energy between the crossing point of this potential energy curve with the ground-state potential energy curve for the neutral molecule and the zero-point vibrational level of the ground state for the neutral molecule (E_{12} in Figure 3A). In a similar manner, we would expect a rough correlation between our energies of activation and the difference between the electron affinity of the halogen atom and the bond dissociation energy for those molecules which we expect go through the k_{12} mechanism. The correlation would not be expected to be perfect even in the absence of experimental errors. Such data are tabulated in Table IV along with similar data for compounds which apparently go by the k_1k_2/k_{-1} mechanism.

Hickam and Berg have investigated the dissociative electron attachment to CCl_4, CCl_3F, CCl_2F_2, $CHCl_2F$, and $CClF_3$ as a function of energy, observing Cl^- appearance on the mass spectrometer. The appearance of SF_6^- from electron attachment to SF_6 was also run as a reference along with each compound. SF_6 apparently captures electrons over a very narrow energy band with the maximum at very low energies. The difference in electron-accelerating voltage at the peak maximum from that for SF_6^- for these compounds is as follows: CCl_4, 0.1 v; CCl_3F, 0.2 v; CCl_2F_2, 0.8 v; $CHCl_2F$, 0.8 v. We have not investigated these same compounds, except for CCl_4. However, we have studied some of the series with F replaced by H and one will note with reference to Table IV that the above order is identical with that of the activation energies for CCl_4, CCl_3H, and CCl_2H_2. Again, it appears that we are probably measuring the same transition to a dissociative state, except that we are promoting the transition by thermal means. In Hickam and Berg's work, and others using this technique, the transition occurs by increasing the electron energy only.

A more recent paper by Christophorou, *et al.*,[31] describes dissociative electron attachment by some chloro-, bromo-, and nitrobenzene derivatives. It is stated[31] that the results contradict a previously reported interpretation by Wentworth and Becker[17] that this group of molecules captures low-energy electrons through a nondissociative resonance process. However, Wentworth and Becker[17] make no mention or inference that halogenated benzenes form stable negative ions. In a more recent publication,[16] it was suggested that dissociative and nondissociative electron attachment can be differentiated by the temperature dependence of the electron-attachment process at thermal energies. It was stated that chloro, bromo, and iodo compounds probably dissociate upon electron attachment. The interpretation in the present investigation is in full accord with not only our previous publications,[16,17] but also with the work of Christophorou, *et al.*[31]

Conclusions

1. The electron-attachment coefficients with thermal electrons increase with increasing temperature (except for CCl_4) for some aliphatic and aromatic chloro, bromo, iodo compounds. Apparently, in these compounds the molecular negative ion is not stable with respect to dissociation into another ion and radical. This temperature dependency is opposite to that previously observed for compounds which are expected to form stable negative ions. It is suggested that the temperature dependency can be used to distinguish between electron attachment forming a stable negative ion and dissociative electron attachment in most cases.

2. Two possible mechanisms are proposed for dissociative electron attachment, both of which can require an energy of activation which can be observed experimentally. One mechanism is the direct dissociation of the molecule upon electron attachment in which the molecule and electron possess the necessary activation energy for dissociation. The energy of activation in this case is the energy above the zero-point energy of the molecule at which the potential energy of a dissociative state crosses that of the ground state of the molecule. This mechanism has been proposed before by other investigators. The other mechanism involves the formation of an intermediate stable negative ion which in turn can either lose the electron or undergo dissociation into the halide and ion and a radical. In this latter case, the energy of activation is the energy above the zero-point energy of the molecule at which the potential energy curve of a dissociative state crosses that of the ground state of the intermediate negative ion.

3. Comparison of results suggests that the aliphatic chloro, bromo, and iodo derivatives probably undergo dissociative electron attachment by the direct mechanism whereas the 1-chloro- and 1-bromonaphthalenes and *o*- and *m*-dichlorobenzenes probably go by the intermediate negative ion mechanism. Bromo- and iodobenzenes appear to undergo dissociative electron attach-

(31) L. G. Christophorou, R. N. Compton, G. S. Hurst, and P. W. Reinhardt, *J. Chem. Phys.*, **45**, 536 (1966).

ment by the latter mechanism, but the electron affinity of the molecule is most likely quite small and probably negative.

Acknowledgments. The authors wish to express their gratitude to the Robert A. Welch Foundation for financial assistance, to Dr. Edward Chen for assistance in the experimental work and specifically for the data on 1-bromonaphthalene, to Miss Elsie Bryan for assistance in preparing the manuscript, and to Mr. Joe Steelhammer for the data on 1-chloronaphthalene.

The Kinetics of Ion Exchange Accompanied by Irreversible Reaction. I. Film Diffusion Controlled Neutralization of a Strong Acid Exchanger by Strong Bases

by R. A. Blickenstaff, J. D. Wagner, and J. S. Dranoff

Department of Chemical Engineering, Northwestern University, Evanston, Illinois *(Received August 31, 1966)*

An experimental study has been made of the neutralization of a strong-acid ion exchanger by strong-base solutions. The kinetic data obtained in a well-stirred batch reactor were found to be self-consistent and to agree closely with the model proposed by Helfferich for the conditions of film diffusion controlled reaction.

Introduction

The rates of ion exchange coupled with reaction have recently been explored in depth by Helfferich.[1] He has developed the first detailed theoretical analysis of four different exchange-reaction systems and has presented a collection of rate laws for each system under conditions of intraparticle and external film diffusion rate control. Helfferich's analysis rests on the customary simplifying assumptions used in describing the ion-exchange process, including the coupled effects of concentration and electrical potential gradients on the diffusion of ionic species.

The present work was undertaken to provide an experimental test of the first of the processes enumerated by Helfferich, the irreversible consumption by chemical reaction of counterions released from the solid exchanger during the exchange process. The results presented below indicate the analysis to be valid and furnish numerical values for the model parameters.

Theory

The basic reaction scheme under consideration is illustrated by

$$\overline{H}^+ + M^+ + OH^- \longrightarrow \overline{M}^+ + H_2O \qquad (1)$$

where the barred quantities represent species in the resin phase. It is assumed that both the acid-form resin and the neutralizing base are completely dissociated, while the water produced by the reaction is dissociated only to its usual slight extent. It is also assumed that the resin particles are uniform spheres, that the system remains isothermal, and that physical properties of the various species remain constant.

The observable rate of the process which occurs when acid-form resin particles and basic solution are contacted in a batch reaction vessel will be controlled by diffusion of the various reactant species, *i.e.*, dif-

(1) F. Helfferich, *J. Phys. Chem.*, 69, 1178 (1965).

fusion of base in the solution outside the particle and/or interdiffusion of H^+ and M^+ ions within the particle. For the case at hand the rate-controlling process is taken to be diffusion of reacting species in the solution surrounding the particles. This, in effect, means that diffusion within the particle is fast enough to eliminate any concentration gradients in the resin phase. The external diffusion process may be conveniently idealized as taking place across a thin region of thickness δ located at the particle–solution interface, with no concentration gradients existing in the solution outside this film. In the case of neutralization, the only ionic species existing in the solution are the M^+ and OH^- ions. These diffuse together across the film to the particle surface where the M^+ ions enter the resin phase and are replaced in solution by H^+ ions. The latter immediately react with the OH^- ions of the solution to produce inert water. The conditions for film diffusion control of the over-all exchange rate are well known and comprise mainly small particle size and low solution concentrations.

Following Helfferich,[1] one may derive rate laws for this process. It should be noted that these laws follow two related but distinct forms, dependent upon the relative ionic capacity of the solution and resin phases. Thus, when $CV < \overline{CV}$, the fractional approach to equilibrium $F(t)$ is given by

$$F(t) = 1 - \exp\left(-\frac{3D_{MOH}\bar{V}}{r_0 V\delta}t\right) \quad (2)$$

However, when $CV > \overline{CV}$

$$F(t) = \frac{CV}{\overline{CV}}\left[1 - \exp\left(-\frac{3D_{MOH}\bar{V}}{r_0 V\delta}t\right)\right] \quad (3)$$

for $0 \leq t \leq t_c$, where

$$t_c = \frac{r_0 V\delta}{3D_{MOH}\bar{V}} \ln\left(\frac{CV}{CV - \overline{CV}}\right) \quad (4)$$

and

$$F(t) = 1 \quad (5)$$

for $t \geq t_c$. It should be noted that for very small ratios of $\bar{V}$ to V, eq 3 becomes linear, as shown in

$$F(t) = \frac{3D_{MOH}C}{r_0\delta\bar{C}}t \quad (6)$$

for $0 \leq t \leq t_c$. This corresponds to the case of infinite solution capacity in which the exchange produces negligible changes in the solution composition. Full details of the derivation of these equations are given elsewhere.[1-3]

Experimental Section

The goal of the experimental program was to test the applicability of the rate laws described above. The apparatus consisted of a well-stirred vessel in which solutions of strong base could be contacted with the acid-form resin. Reaction was initiated by the rapid injection of resin into the basic solution and monitored continuously thereafter by measurement of the electrical conductivity of the solution.

The cylindrical reactor was made of glass and Plexiglas and was surrounded by a constant-temperature bath. The solution conductivity was measured with a commercial cell mounted centrally in the reactor base. This cell was excited by high-frequency alternating current and its response was continuously recorded. (The presence of resin particles in the solution was found to have a negligible effect on the measured conductivities in this work.) Solution conductivities were later reduced to extents of reaction by suitable calibrations.

The resin employed was Dowex 50W-X8. Two particle-size fractions were obtained by wet screening of sodium-form resin. The actual sizes used were 20–25 mesh (0.0388-cm average radius) and 40–50 mesh (0.0179-cm average radius). Measured exchange capacities of these fractions were 1.77 and 1.76 mequiv/ml, respectively. The bases used were sodium and potassium hydroxide. Several experiments were also made to compare the kinetics of ordinary ion exchange with the neutralization reaction and sodium nitrate solutions were used for this purpose.

All experiments were carried out at 25° with 600 ml of 0.005 N reactant solution in order to ensure film diffusion rate control.[3] Experiments were made with resin samples of both size ranges in amounts of 5, 1, and approximately 0.03 ml (to cover the range of conditions corresponding to eq 2–6). The samples were injected into the reactor from specially constructed syringes to initiate reaction. Previous attempts to start reaction by injection of concentrated solution were less successful in approximating initial film diffusion control because of the high-concentration regions which persisted in the solution for 1 or 2 sec prior to complete dispersion within the vessel. Most of the experiments were duplicated in order to check experimental reproducibility. Further details of the experimental apparatus and techniques are presented elsewhere.[2,3]

(2) R. A. Blickenstaff, M.S. Thesis, Northwestern University, Evanston, Ill., 1965.

(3) J. D. Wagner, M.S. Thesis, Northwestern University, Evanston, Ill., 1966.

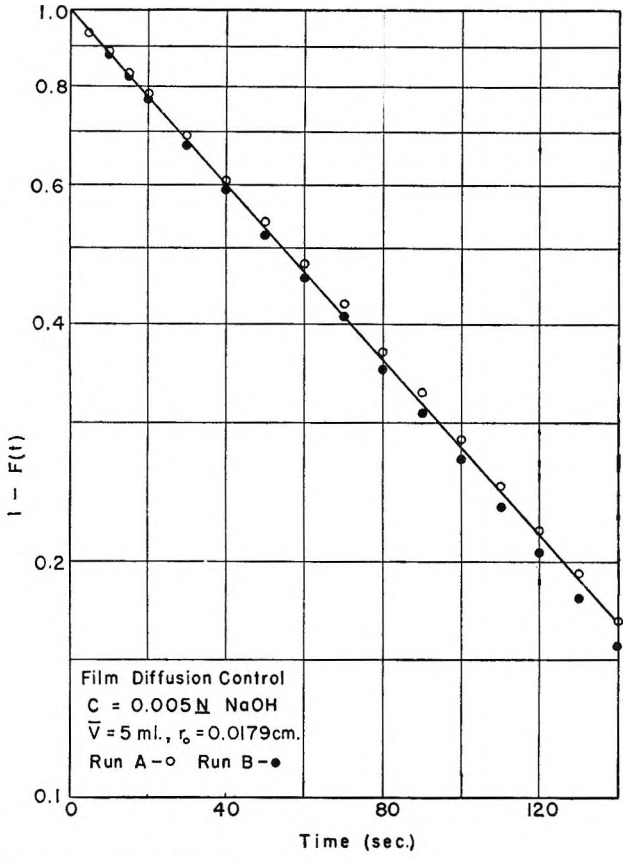

Figure 1. Experimental test of eq 2.

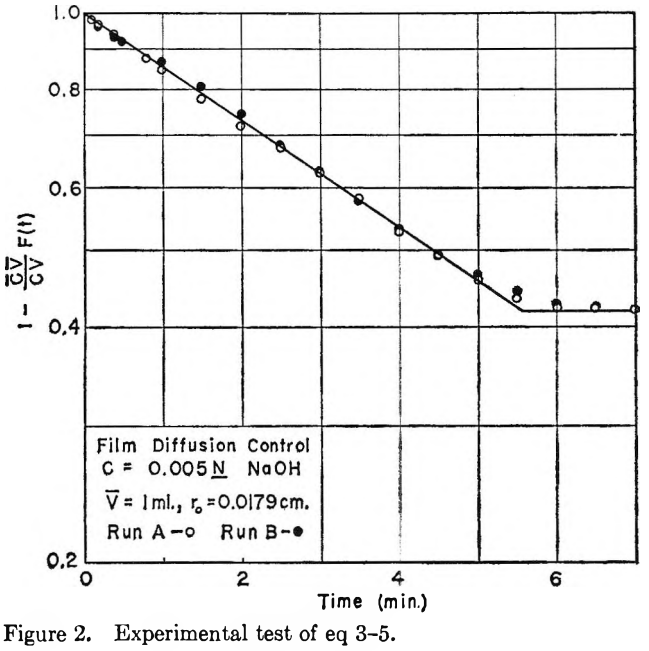

Figure 2. Experimental test of eq 3–5.

Results and Discussion

An experimental test of eq 2 was made first, using 5 ml of resin. According to eq 2, a semilog plot of

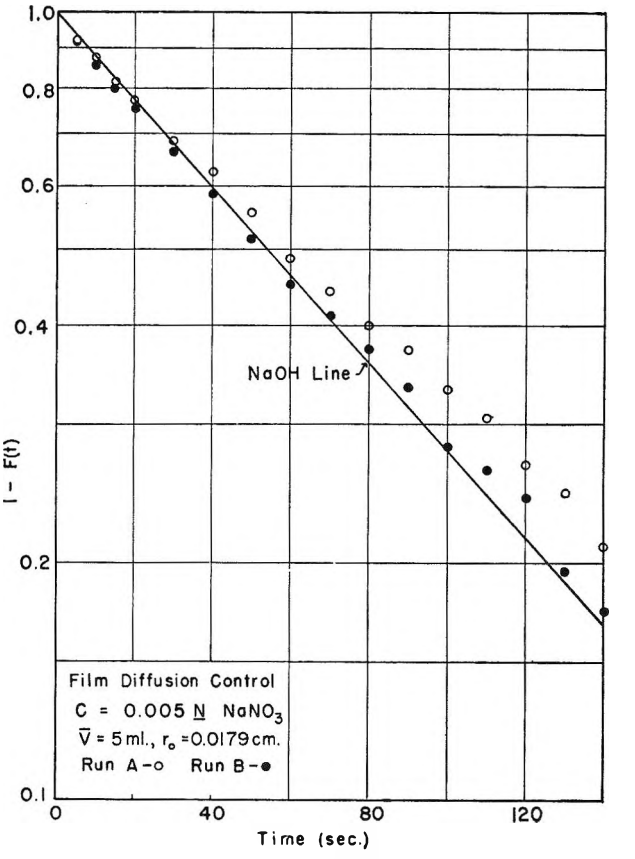

Figure 3. Comparison of ordinary exchange and exchange with reaction.

$[1 - F(t)]$ *vs.* time should be linear. Data obtained with NaOH and the smaller particles are shown in Figure 1, which indicates excellent agreement with the required form as well as excellent reproducibility. The points shown are selected values taken from the continuous experimental record.

Experiments were subsequently made with 1 ml of resin to test eq 3–5. In this case a semilog plot of $[1 - \frac{\overline{CV}}{CV} F(t)]$ *vs.* time should be linear up to a critical time, t_c, and should remain constant thereafter. Data for NaOH are shown in Figure 2. Once again the fit and reproducibility are seen to be excellent. The results do not quite match the abrupt change in the theoretical curve, but do come acceptably close.

Similar results were obtained for the larger particle size and with KOH solutions as well.

Experiments were also made with $NaNO_3$ solution to demonstrate the differences between ordinary ion exchange and the neutralization reaction. The results are shown in Figures 3 and 4 for 5 and 1 ml of resin, respectively. Also shown are the lines corresponding to the NaOH data. These plots indicate

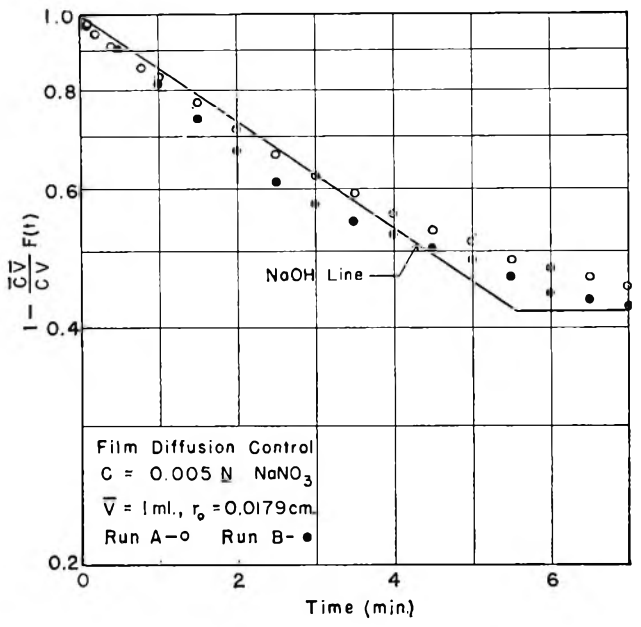

Figure 4. Comparison of ordinary exchange and exchange with reaction.

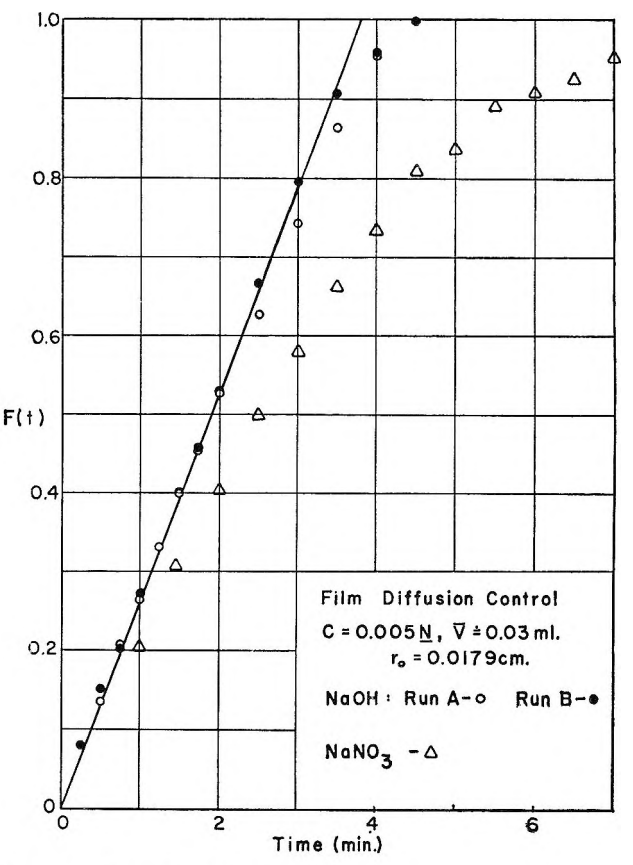

Figure 5. Experimental test of eq 6.

that ordinary ion exchange does not conform to the exponential solutions presented for the neutralization. (It should be realized that $F(t) = 1.0$ for ordinary exchange corresponds to incomplete conversion of the resin owing to a finite equilibrium constant, as compared with complete resin conversion when irreversible neutralizations are considered.)

Finally, a partial test of eq 6 was made by reaction of an extremely small (imprecisely measured) resin sample. Note that for very small $\bar{V}$, $F(t)$ is independent of $\bar{V}$. This should yield a linear plot, or at least a plot with a linear portion for small times. The experimental data are shown in Figure 5, along with similar results for $NaNO_3$. The straight line which has been drawn through the early NaOH points can be seen to provide a good fit for $F(t)$ up to at least 0.8. The $NaNO_3$ data deviate considerably from linear behavior, again showing the difference between ordinary ion exchange and exchange coupled with reaction. In this case the ordinary ion exchange should also proceed to complete exhaustion of the resin because of the small amount of resin present.

Thus far it has been shown that the experimental kinetic data for the neutralization reaction are in excellent agreement with the form of the proposed theoretical model and differ significantly from data for ordinary equilibrium-limited exchange. The model may be evaluated further by consideration of the values of the unknown parameter—D_{MOH}/δ. These can be found from the measured slopes of graphs such as Figures 1, 2, and 5, and the known values of other experimental parameters. The results are summarized in Table I.

Table I: Film Diffusion Control Rate Parameter

r_0, cm	$\bar{V}$, ml	D_{NaOH}/δ, cm/sec	D_{KOH}/δ, cm/sec
0.0179	~0.03	0.0151	0.0193
0.0179	1.00	0.0154	0.0180
0.0179	5.00	0.0151	0.0187
0.0388	~0.03	0.0169	
0.0388	1.00	0.0157	
0.0388	5.00	0.0148	
		Av 0.0155	0.0187

These data provide further support for the theory, since the values found for each base with different amounts of resin are in close agreement. Furthermore, the fact that results for two significantly different particle sizes agree closely is strong verification for the model. It indicates that a particle-diffusion mechanism can hardly be expected to describe the

process, since particle-size effects in that case are usually dependent on the square of the particle radius, rather than the first power as in film diffusion.

Finally, it is of interest to compare the value of the model parameter for the two different bases studied. The data of Table I indicate

$$\frac{D_{NaOH}/\delta}{D_{KOH}/\delta} = 0.83$$

Although one might expect this ratio to agree with the ratio D_{NaOH}/D_{KOH}, literature data[4] indicate the latter to be 0.74 at infinite dilution. However, film mass-transfer coefficients have been found[5] to vary with diffusivity to powers ranging from 0.5 to 1. Since the square root of 0.74 is 0.86, it is clear that the present results behave essentially as expected for mass-transfer coefficient. More definitive comparisons cannot be made with the present limited data. It is clear, however, that the parameter δ cannot be safely handled alone, but rather only in combination with diffusivity, as a mass-transfer coefficient.

Conclusions

The experimental data obtained in this study provide strong verification of Helfferich's model for ion exchange coupled with irreversible reaction in the film diffusion controlled region. The data follow the theoretical equations very closely, while differing significantly from data for ordinary ion exchange, and the model parameter is consistent with other mass-transfer studies.

Notation

C, mequiv/ml	Initial solution concentration
$\bar{C}$, mequiv/ml	Concentration of fixed ionic groups in the solid exchanger
D_i, cm²/sec	Diffusion coefficient for species i
F	Fractional attainment of equilibrium
r_0, cm	Radius of exchanger particle
t, sec	Time
t_c, sec	Time for complete reaction
V, ml	Solution volume
$\bar{V}$, ml	Resin volume
δ, cm	Film thickness

Acknowledgment. This work has been supported by Grant GP-2725 from the National Science Foundation.

(4) H. S. Harned and B. B. Owen, "The Physical Chemistry of Electrolytic Solutions," Reinhold Publishing Corp., New York, N. Y., 1958.

(5) P. Harriott, *A.I.Ch.E. J.*, 8, 93 (1962).

The Kinetics of Ion Exchange Accompanied by Irreversible Reaction. II. Intraparticle Diffusion Controlled Neutralization of a Strong Acid Exchanger by Strong Bases

by R. A. Blickenstaff, J. D. Wagner, and J. S. Dranoff

Department of Chemical Engineering, Northwestern University, Evanston, Illinois *(Received September 20, 1966)*

An experimental study has been made of the neutralization of a strong-acid ion exchanger by strong-base solutions in the intraparticle diffusion controlled region. Data obtained in a well-stirred batch reactor were consistent with the theory of Helfferich and yielded reasonable values for intraparticle diffusivities. However, the results have also shown that the model fails to account properly for the effects of different co-ions.

Introduction

This paper presents the results of an experimental study of the rate of neutralization of a strong-acid ion exchanger by strong-base solutions. Part I[1] presented a verification of theoretical models for this process under conditions of film diffusion control of the observable rate. Part II is concerned with the regime of intraparticle diffusion control. Results to be exhibited below indicate the theory of Helfferich[2] to be essentially valid, with one exception, in this range as well. The data to be reported were obtained as outlined in part I and by an additional technique involving a specially constructed cage reactor.

Theory

As before, the basic reaction under consideration is the neutralization illustrated in eq 1

$$\overline{H}^+ + M^+ + OH^- \longrightarrow \overline{M}^+ + H_2O \qquad (1)$$

where barred quantities represent species in the resin phase. The reaction is considered to take place in a well-stirred batch reactor under conditions of intraparticle diffusion control, *i.e.*, high solution concentrations, large particle size, and vigorous solution agitation. Thus, there are no concentration gradients in the solution phase, while the presence of OH^- ions there keeps the concentration of H^+ ions essentially equal to zero everywhere outside the particle. (The OH^- ions are virtually excluded from the interior of the resin beads by the Donnan effect.)

Therefore, the situation within the exchanger particles is exactly the same during neutralization as under conditions of ordinary ion exchange. The only difference is in the boundary condition at the particle surface. For neutralization, the concentration of H^+ ions at the surface remains negligible. However, this is true for ordinary exchange only in the case of "infinite solution volume."

Solutions for the infinite volume case have been previously obtained and reported by Helfferich and others.[3,4] The tabulated solutions numerically relate the fractional attainment of equilibrium, $G(t)$, to time for a binary exchange in terms of the ionic diffusivities of the two components. More specifically, the solution involves the ratio of the two diffusivities as well as the absolute value of one of them.

Now the rate law for the intraparticle diffusion controlled neutralization can be formulated in terms of the known $G(t)$.[2] If $\overline{CV} < CV$

$$F(t) = G(t) \qquad (2)$$

If $\overline{CV} > CV$

$$F(t) = \frac{\overline{CV}}{CV} G(t) \qquad (3)$$

(1) R. A. Blickenstaff, J. D. Wagner, and J. S. Dranoff, *J. Phys. Chem.*, **71**, 1665 (1967).

(2) F. Helfferich, *ibid.*, **69**, 1178 (1965).

(3) M. S. Plesset, F. Helfferich, and J. N. Franklin, *J. Chem. Phys.*, **29**, 1064 (1958).

(4) F. Helfferich, *ibid.*, **38**, 1688 (1963).

for $0 \leq t \leq t_c$, and

$$F(t) = 1 \tag{4}$$

for $t \geq t_c$, where $F(t)$ is the fractional conversion of the resin during neutralization and t_c represents the time for complete reaction.

The goal of this study was to test eq 2–4 by experimental measurement of $F(t)$ and comparison with the theoretical solution. This requires selection of appropriate values for $\bar{D}_H$ and the ratio of $\bar{D}_H/\bar{D}_M$.

The ratio may be determined after certain assumptions. One assumes first that the ratio of diffusivities of the two ions within the solid exchanger is the same as in liquid solution

$$\bar{D}_H/\bar{D}_M = D_H/D_M \tag{5}$$

It is then assumed that the Nernst–Einstein equation can be used to relate ionic mobility at infinite dilution to diffusivity

$$u_i = D_i F/RT \tag{6}$$

This leads to an expression for the diffusivity ratio (given in eq 7) in terms of existing ionic mobility data.[5]

$$\bar{D}_H/\bar{D}_M = u_H/u_M \tag{7}$$

A suitable value for $\bar{D}_H$ may be found by best fit of the experimental data to the theoretical model. Validity of the model can then be assessed in terms of the goodness of fit of experimental to calculated curves, as well as the magnitude of the $\bar{D}_H$ values so determined. Some deviations between model and experiment are probably to be expected in view of assumptions made.

Experimental Section

The experimental apparatus, materials, and procedure used in the bulk of this work are the same as described earlier,[1] the main difference being in the solution concentration and resin volumes used. All experiments were performed at 25° with 600 ml of 0.4 *N* reactant in order to ensure intraparticle diffusion control.[6]

An attempt was also made to determine the $G(t)$ curve experimentally by the infinite solution volume technique. For this purpose, a special cage-type reactor device was constructed, which was a modification of a similar device used some time ago by Kressman and Kitchener.[7] It consisted of a cylindrical cage of 60-mesh stainless steel screen, 1.5 in. in diameter and 1 in. long, with Plexiglas supporting pieces. The cage was attached to a stainless steel telescoping shaft, by which it could be rotated and easily lowered or raised. Rotation of this device in solution produced a continuous flow of liquid over the particles retained within the cage as well as vigorous mixing of the external solution.

Reaction could be quickly initiated by lowering this device into reactant solution and terminated as quickly by lifting it out of solution again. The extent of reaction achieved was measured by displacing and then titrating the unreacted H^+ ions from the resin sample. Displacement was accomplished by immersion of the entire cage in concentrated $NaNO_3$. Regeneration was similarly achieved with acid solution.

Results and Discussion

The applicability of eq 2 was first tested using two different bases, two volumes of resin, and two resin particle sizes. Fractional approach to equilibrium was determined directly at various time intervals from the continuous traces of solution conductivity *vs.* time generated by the apparatus. The experimental data points were then compared graphically with the theoretical $G(t)$ curve for each system. The diffusivity ratios used in determining the latter were: $\bar{D}_H/\bar{D}_{Na} = 6.98$ and $\bar{D}_H/\bar{D}_K = 4.76$. $G(t)$ curves for

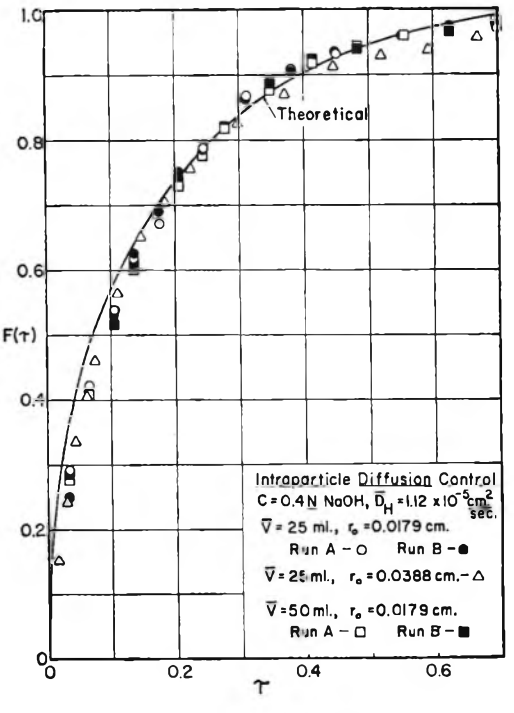

Figure 1. Experimental test of eq 2 with NaOH.

(5) H. S. Harned and B. B. Owen, "The Physical Chemistry of Electrolytic Solutions," Reinhold Publishing Corp., New York, N. Y., 1958.

(6) J. D. Wagner, M.S. Thesis, Northwestern University, Evanston, Ill., 1966.

(7) T. R. E. Kressman and J. A. Kitchener, *Discussions Faraday Soc.*, **7**, 90 (1949).

these ratios were interpolated from existing tabulated results.[4] The appropriate values of $\bar{D}_H$ were found for each set of data by a graphical matching technique.[6] The conditions and values of $\bar{D}_H$ for each experiment are presented in Table I. An average $\bar{D}_H$ value was then calculated for each system. With this parameter known, a single graph may be constructed for all of the data for each base by plotting $F(\tau)$ *vs.* τ, where $\tau = \bar{D}_H t/r_0^2$. Such plots are shown in Figures 1 and 2 for NaOH and KOH, respectively. Also shown on each figure is the theoretical line.

Table I: Experimental Values of $\bar{D}_H$

Counter-ion	$\bar{V}$, ml	r_0, cm	$\bar{D}_H \times 10^6$, cm²/sec
Na	25	0.0179	1.12
Na	50	0.0179	1.16
Na	25	0.0388	1.07
K	25	0.0179	1.35
K	50	0.0179	1.25
K	25	0.0388	1.41

These figures indicate that reproducibility of the experiments was good and that the theoretical model agrees quite closely with the experimental results for each system. The magnitude of the $\bar{D}_H$ values also seems appropriate. There are some deviations exhibited between the theoretical line and the points, which are probably due to experimental errors (especially at the very beginning of the reactions where imperfect dispersion of the resin particles may have influenced the data) and the failure of the approximations of eq 5 and 6 to apply exactly.

In the last connection, the difference in the magnitude of $\bar{D}_H$ as measured in the NaOH and KOH experiments must be due to such a failure, since one would otherwise expect the diffusivity to be the same in both cases. Further experimental evidence will be necessary before a complete picture of the influence of the exchanging ion on this parameter can be explained.

It should be noted that Hering and Bliss[8] have previously reported similar difficulty in applying the theoretical model for intraparticle diffusion (based on the Nernst–Planck flux equations) to data for several different exchanging systems. They did not use eq 7 to determine the diffusivity ratio but rather chose the values of the two diffusivities to give the best fit to data from exchanges run in both directions. They found the values determined in this way to depend strongly on the ion pair involved. It thus appears that this effect is a general one and that further modification of the Nernst–Planck model may be necessary to account for it.

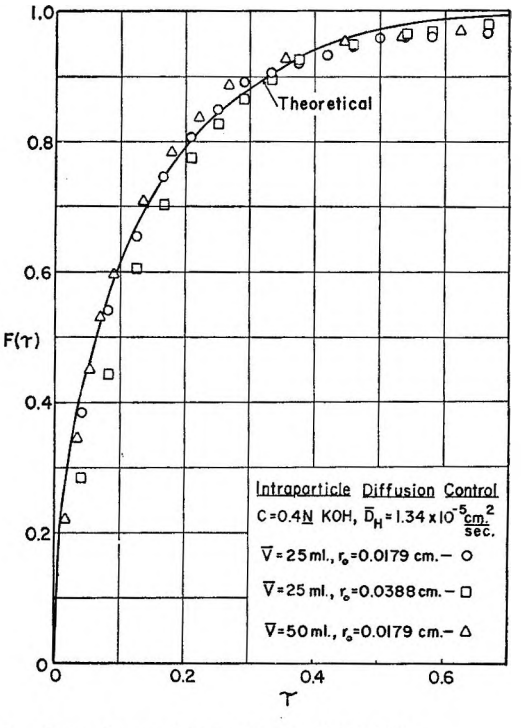

Figure 2. Experimental test of eq 2 with KOH.

Some experiments were made under similar conditions with $NaNO_3$ solution in order to demonstrate experimentally the difference between ordinary ion exchange and that coupled with reaction. The resultant data for the smaller particles are shown as $F(t)$ *vs.* actual time in Figure 3 along with some of the NaOH data and the theoretical curve from Figure 1. With $NaNO_3$, $F(t) = 1.0$ does not correspond to complete exchange of the resin as long as $\bar{V}$ is significant because of the equilibrium limitations. Figure 3 shows that these two processes follow somewhat different rate laws, with ordinary exchange being surprisingly faster until $F(t)$ exceeds about 0.8. It was not possible to estimate $\bar{D}_H$ from the $NaNO_3$ data because a suitable rate law does not yet exist for the finite solution volume case studied here.

Finally, experiments were made to determine experimentally the $G(t)$ *vs.* t plot for the H^+–Na^+ exchange by means of the infinite solution technique described earlier. This was done as a check on the basic applicability of the model to the experimental data obtained in this work. Results obtained for the larger particle size with 0.4 *N* $NaNO_3$ are shown in Figure 4. Determination of these points was found to

(8) B. Hering and H. Bliss, *A.I.Ch.E. J.*, 9, 495 (1963).

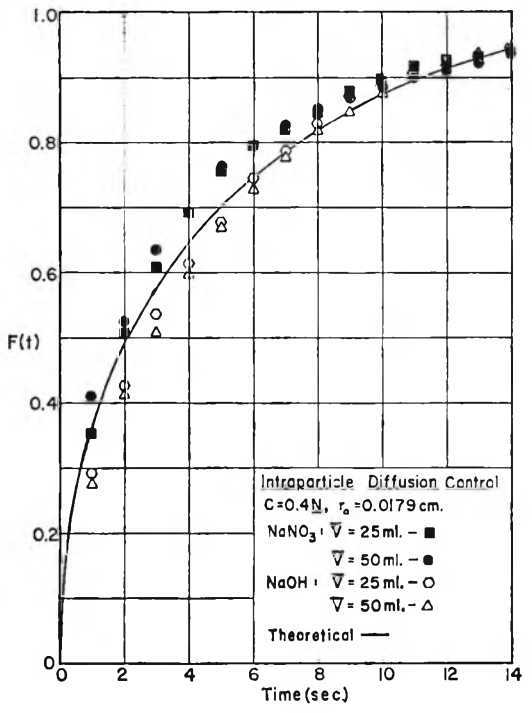

Figure 3. Comparison of ordinary ion exchange and neutralization.

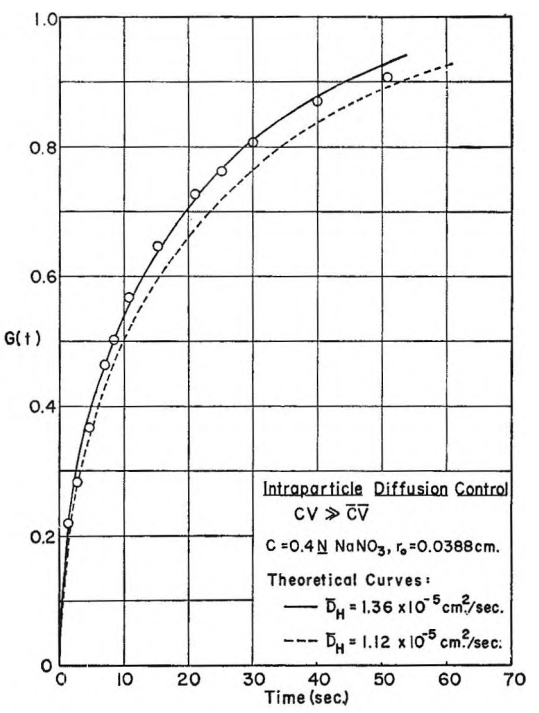

Figure 4. Experimental determination of $G(t)$.

be more difficult than originally anticipated because of repeated resin bead fracture in the apparatus. Earlier experiments showed considerable scatter and subsequent microscopic examination of the resin particles showed that they had been severely fractured during repeated use because of the violent motion within the cage reactor and the great concentration changes to which the particles were necessarily subjected. The stirring rate was diminished somewhat and the data shown in Figure 4 were obtained. Examination of the particles used in this case revealed little breakage of the spherical beads, although they did develop a large number of cracks. It is felt that these cracks provide a relatively easy path for diffusing ions into the bead interior and hence should result in a faster rate of reaction than might otherwise be expected. Comparison of the experimental data and the theoretical curves shown in Figure 4 confirm this expectation. The two curves correspond to $\bar{D}_H = 1.12 \times 10^{-5}$ cm²/sec (from the NaOH data shown earlier) and $\bar{D}_H = 1.36 \times 10^{-5}$ cm²/sec (best fit to the $NaNO_3$ data). It is clear that the latter provides an excellent fit to the data, confirming the essential validity of the theoretical model. The fact that the apparent diffusivity in this case is higher than that found for the neutralization reaction can be ascribed to the previously mentioned cracks and the resulting more open structure of the resin beads used. Additional experiments under less violent conditions of agitation and/or with more stable resin particles will be necessary for further verification of this conclusion.

Some attempts were also made to verify the validity of eq 3 and 4 for the case where the resin capacity exceeds that of the solution. No satisfactory data have been obtained in this region and further consideration of the basic equations seems to preclude their application. In this case, reaction should proceed until the solution is completely exhausted. However, as this condition is approached, solution concentrations will fall into the range where film diffusion can be expected to play a significant, if not controlling, role. Therefore, one might expect the initial stages of reaction to follow the intraparticle diffusion equations, but this model should cease to be effective as reaction proceeds. Further study of this phenomenon will be necessary in order to provide a suitable quantitative description.

Conclusions

The experimental data obtained in this work indicate that the Helfferich's model for intraparticle diffusion controlled neutralization of acid-form resins by strong bases is essentially correct as long as exhaustion of the solution is avoided. The data are consistent with curves based on this model (differing

significantly from data for ordinary ion exchange) and yield reasonable values for intraparticle diffusivities. However, additional work is necessary to understand the effects of various co-ions on the measured diffusivities, as well as to uncover a model suitable for the case of low solution ionic capacity ($CV < \overline{CV}$).

Notation

C, mequiv/ml	Initial solution concentration
$\overline{C}$, mequiv/ml	Concentrations of fixed ionic groups in the solid exchanger
D_i, cm²/sec	Solution phase diffusion coefficient for species i
$\overline{D}_i$, cm²/sec	Intraparticle diffusion coefficient for species i
F, coulombs/mole	Faraday's constant
$F(t)$	Fractional attainment of equilibrium during neutralization
$G(t)$	Fractional exhaustion of resin during ordinary exchange with infinite solution boundary condition
r_0, cm	Radius of exchanger particle
R, ergs/mole °K	Gas constant
t, sec	Time
t_0, sec	Time for complete reaction
T, °K	Absolute temperature
u_i, cm²/sec v	Mobility of species i
V, ml	Solution volume
$\overline{V}$, ml	Resin volume
τ	Dimensionless time

Acknowledgment. The authors wish to acknowledge with thanks support of this work by the National Science Foundation under Grant GP-2725.

The Photolysis of Fluoroacetone and the Elimination of Hydrogen Fluoride from "Hot" Fluoroethanes[1]

by G. O. Pritchard and R. L. Thommarson

Department of Chemistry, University of California, Santa Barbara, California 93106
(Received August 31, 1966)

Fluoroacetone was photolyzed in the region of 3130 A, and the rates of collisional stabilization *vs.* HF elimination of the "hot" fluoroethanes $C_2H_5F^*$ and $C_2H_4F_2^*$ produced in the system were examined as functions of the temperature and the pressure. The classical Rice–Ramsperger–Kassel theory of unimolecular reactions is shown to give a quantitative description of the decomposition of the "hot" molecules, as was demonstrated recently by Benson and Haugen[2] for $C_2H_4F_2^*$. The reduction in the number of effective oscillators in $C_2H_5F^*$, as opposed to $C_2H_4F_2^*$, results in the predicted enhancement of the rate of HF elimination from $C_2H_5F^*$. The values of the activation energies for H atom abstraction from the ketone are 4.6 and 6.7 kcal mole^{-1} for CH_3 and CH_2F radicals, respectively.

Introduction

There has been much recent interest in the elimination of HF from vibrationally excited fluoroethanes, formed by methyl radical recombination,[3-6] and the observed rates have been correlated with the decreasing number of effective oscillators in the molecules with decreasing fluorine atom content.[2] On this basis $C_2H_5F^*$ should show the greatest rate of HF elimination for a given set of experimental conditions.[2] This

(1) This work was supported by a grant from the National Science Foundation.

(2) S. W. Benson and G. Haugen, *J. Phys. Chem.*, **69**, 3898 (1965).

(3) G. O. Pritchard, M. Venugopalan, and T. F. Graham, *ibid.*, **68**, 1786 (1964).

work describes experiments with this "hot" molecule and also with $CH_2FCH_2F^*$, which is formed in the system.

Experimental Section

The apparatus and procedure have been described.[3] The ketone was obtained from City Chemical Corp. and it was purified by vpc. Its mass spectrum is given in Table I. The base peak is due to CH_3CO^+, as is the case in the mass spectrum of CH_3COCF_3.[7] A similar observation[8] was made with $C_2H_5COC_3F_7$, although the base peak was $C_2H_5^+$ rather than $C_2H_5CO^+$. The photolysis pattern of unsymmetrical fluoro ketones shows the same preferred dissociative mode; *e.g.*

$$CH_3COCF_3 + h\nu \longrightarrow CH_3CO + CF_3$$

and

$$C_2H_5COC_2F_5 + h\nu \longrightarrow C_2H_5CO + C_2F_5$$

have been established as the primary acts in the respective photodecompositions at 3130 A.[9,10] It is therefore probable that

$$CH_2FCOCH_3 + h\nu \longrightarrow CH_2F + COCH_3 \quad (1)$$

is the primary photolytic decomposition step at 3130 A in the photolysis of fluoroacetone.

Table I: Mass Spectrum of Fluoroacetone

m/e	Probable positive ion	Relative abundance[a]
12	C	2.0
13	CH	4.3
14	CH_2	15.4
15	CH_3	46.8
25	C_2H	1.9
26	C_2H_2	5.8
27	C_2H_3	10.7
28	CO	2.3
29	CHO	5.8
31	CF	3.4
32	CHF	2.3
33	CH_2F	21.6
37	C_3H	2.0
38	C_3H_2	1.7
39	C_3H_3	1.6
40	C_2O	1.2
41	C_2HO	1.5
42	C_2H_2O	8.3
43	C_2H_3O	100.0
45	C_2H_2F	1.9
47	C_2H_4F	2.0
58	C_3H_3F	2.0
61	C_2H_2FO	5.7
76	C_3H_5FO	6.1

[a] *m/e* less than 1% of the 43 ion peak have been omitted; no isotope corrections have been made and isotope peaks have been omitted.

Some quantum yield data are reported; in these experiments the 3130-A line was isolated with an interference filter supplied by Farrand Optical Co.; the peak wavelength was at 3135 A, with a half band width of 90 A. The incident intensity was 9.4×10^{13} quanta cc^{-1} sec^{-1}. The extinction coefficient of the ketone at 3130 A is 4.9 l. $mole^{-1}$ cm^{-1}, where $\log (I_0/I) = \epsilon cl$.

CO and CH_4 were collected at $-210°$ and analyzed by vpc on an activated charcoal column. C_2H_6, C_2H_4, CH_3F, C_2H_3F, and C_2H_5F were collected at $-145°$ and analyzed on a 2-m 3% squalane-on-alumina column. The $C_2H_4F_2$, plus some ketone, was collected at $-80°$ and analyzed on a short (0.5-m) 3% squalane-on-alumina column, on which the ketone was retained. The separation was conducted in this manner to reduce the retention time for the $C_2H_4F_2$. The columns were calibrated with pure samples of each of the compounds. No search was made for any of the high-boiling products.

A series of experiments at 382°K was conducted with various added pressures of perfluorocyclohexane. This contained a very small impurity which showed up as a peak similar in area and very close to the C_2H_5F peak on the chromatograms. To remove any ambiguity in our determination of C_2H_5F, some further experiments were carried out with n-C_6F_{14}, which did not show any evidence of such an impurity.

Results

Quantum Yields and H Atom Abstractions. The data on 14 experiments over the temperature range 329–585°K are reported in Table II. In these experiments the ketone pressure varied between 4 and 7 cm, although most of the runs were carried at 6 ± 0.2 cm. Those marked with a Φ indicate that quantum yield determinations were made and these are given in Table III. In some quantum yield experiments carried out at room temperature very little CO and no C_2H_6 was obtained, although some ethylene and fluorine-containing products were formed. At 56° the

(4) G. O. Pritchard and J. T. Bryant, *J. Phys. Chem.*, 69, 1085 (1965); 70, 1441 (1966).

(5) R. D. Giles and E. Whittle, *Trans. Faraday Soc.*, 61, 1425 (1965).

(6) W. G. Alcock and E. Whittle, *ibid.*, 61, 244 (1965).

(7) J. R. Majer, *Advan. Fluorine Chem.*, 2, 55 (1961).

(8) G. O. Pritchard and R. L. Thommarson, *J. Phys. Chem.*, 69, 1001 (1965).

(9) E. A. Dawidowicz and C. R. Patrick, *J. Chem. Soc.*, 4250 (1964).

(10) R. L. Thommarson and G. O. Pritchard, *J. Phys. Chem.*, 70, 2307 (1966).

Table II: Data on CH_2FCOCH_3 Photolysis[a]

Run	Temp, °K	Time, sec	[Ketone] × 10^6, moles cc^{-1}	[Product] × 10^6, moles							
				CO	CH_4	C_2H_6	C_2H_4	CH_3F	C_2H_3F	C_2H_5F	$C_2H_4F_2$
1Φ	329	7200	2.90	1.23	1.09	0.008	0.138	0.361	0.343	0.024	0.284
2	362	1800	2.65	15.5	11.3	0.158	1.66	1.04	1.85	0.389	1.48
3Φ	382	7200	1.68	10.6	7.30	0.150	1.29	0.656	1.12	...	...
4Φ	406	7200	2.32	13.6	9.36	0.145	1.04	1.49	1.12	0.223	0.838
5	417	1500	2.26	28.0	17.0	0.390	2.71	1.73	2.28	0.497	1.82
6Φ	420	5400	2.57	14.5	8.46	0.186	1.28	1.31	0.930	0.218	...
7	450	1200	2.00	23.1	13.3	0.433	2.49	1.61	2.10	0.336	1.37
8Φ	464	7200	2.01	15.2	11.2	0.092	0.651	2.57	0.937	0.118	0.555
9	480	900	1.97	18.0	10.8	0.293	1.82	1.66	1.42	0.252	0.935
10	505	900	1.81	18.9	12.3	0.283	1.69	2.44	1.67	0.192	0.802
11Φ	525	5400	1.87	15.5	11.9	0.066	0.407	3.11	0.620	0.062	...
12Φ	552	5400	1.69	12.7	9.29	0.044	0.312	4.63	0.474	0.045	0.111
13	571	600	1.66	13.4	9.66	0.094	0.699	3.15	0.880	0.096	0.262
14Φ	585	3600	1.65	9.73	7.88	0.025	0.225	4.61	2.79	...	...

[a] The mass balance ratio = $(\frac{1}{2}CH_4 + C_2H_6 + C_2H_4 + \frac{1}{2}CH_3F + C_2H_3F + C_2H_5F + C_2H_4F_2)/CO = 0.63 \pm 0.3$, except for run 1 where it is 1.24, owing to the nondissociative fate of CH_3CO below 100°; see text.

Table III: Quantum Yields of the Products of the Photolysis of CH_2FCOCH_3 at 3130 A

Temp, °K	CO	CH_4	C_2H_6	C_2H_4	CH_3F	C_2H_3F	C_2H_5F	$C_2H_4F_2$
329	0.065	0.057	0.0004	0.007	0.019	0.002	0.001	0.001
382	1.04	0.711	0.015	0.125	0.064	0.109	...	...
406	0.995	0.684	0.010	0.096	0.109	0.082	0.016	0.061
420	1.08	0.629	0.013	0.095	0.097	0.069	0.021	...
464	0.939	0.690	0.006	0.040	0.158	0.058	0.007	0.034
525	1.21	0.925	0.005	0.031	0.243	0.048	0.004	...
552	0.899	0.659	0.003	0.022	0.328	0.034	0.003	0.008
585	0.948	0.767	0.002	0.022	0.449	0.027	...	...

ethane quantum yield was approximately 4×10^{-4}, although $\Phi_{CO} \cong \Phi_{CH_4}$ (Table III). This substantiates that reaction 1 represents the primary split and that below 100° ($\Phi_{CO} \approx 1$ at 109°) the acetyl radicals play a role in the mechanism. Consequently hydrogen abstraction data on the reactions

$$CH_3 + CH_2FCOCH_3 \longrightarrow CH_4 + CHFCOCH_3 \text{ or } CH_2FCOCH_2 \quad (2)$$

and

$$CH_2F + CH_2FCOCH_3 \longrightarrow CH_3F + CHFCOCH_3 \text{ or } CH_2FCOCH_2 \quad (3)$$

vs. radical recombination data

$$2CH_3 \longrightarrow C_2H_6 \quad (4)$$

and

$$2CH_2F \longrightarrow C_2H_4F_2 \text{ or } C_2H_3F + HF \quad (5)$$

will be complicated by the reactions

$$CH_3 + CH_3CO \longrightarrow CH_4 + CH_2CO$$

$$CH_2F + CH_3CO \longrightarrow CH_3F + CH_2CO$$

That this is so is evident in the Arrhenius plots given in Figure 1. Least-squares lines of the functions (above 100°)

$$k_2/k_4^{1/2} = R_{CH_4}/R_{C_2H_6}^{1/2}[\text{ket}]$$

and

$$k_3/k_5^{1/2} = R_{CH_3F}/R_{(C_2H_4F_2+C_2H_3F)}^{1/2}[\text{ket}]$$

yield

$$k_2/k_4^{1/2} = 2.9 \times 10^3 e^{-4600/RT} \text{ mole}^{-1/2} \text{ cc}^{1/2} \text{ sec}^{-1/2}$$

and

$$k_3/k_5^{1/2} = 1.9 \times 10^3 e^{-6700/RT} \text{ mole}^{-1/2} \text{ cc}^{1/2} \text{ sec}^{-1/2}$$

Limits of error on the activation energies are 0.5 kcal

mole^{-1} for reaction 2 and 0.2 kcal mole^{-1} for reaction 3. The latter result fits the general picture for these abstractions,[3,4] but E_2 appears to be exceptionally low. However, we have also obtained[11] a low activation energy, 4.3 kcal mole^{-1}, for the reaction

$$CH_3 + CHF_2COCHF_2 \longrightarrow CH_4 + CF_2COCHF_2$$

The frequency factor ratios for all of these reactions tend to be low, which would imply[11] that the activation energies should each be raised by about 1 kcal mole^{-1}.

Radical–Radical Interactions. The cross-combination ratio for CH_3 and CH_2F is given by

$$k_6/k_4^{1/2}k_5^{1/2} = R_{(C_2H_5F+C_2H_4)}/R_{C_2H_6}{}^{1/2}R_{(C_2H_4F_2+C_2H_3F)}{}^{1/2}$$

where

$$CH_3 + CH_2F \longrightarrow C_2H_5F \text{ or } C_2H_4 + HF \qquad (6)$$

The average value for the ten experiments in Table II, where $C_2H_4F_2$ analyses were obtained, is 2.4. Collision theory predicts a value of 2.3, using collision diameters σ_{CH_3} = 3.5 A and σ_{CH_2F} = 4.0 A and assuming that the reactions have identical activation energies and steric factors, usually taken to be zero and unity, respectively.

The elimination of HF can occur from the vibrationally excited fluoroethanes originally produced by radical combination in reaction sequences 5 and 6.

$$2CH_2F \longrightarrow CH_2FCH_2F^* \xrightarrow[M]{k_{5a}} CH_2FCH_2F \qquad CH_2F^* \xrightarrow{k_{5b}} CH_2{=}CHF + HF \qquad (5)$$

and

$$CH_3 + CH_2F \longrightarrow CH_3CH_2F^* \xrightarrow[M]{k_{6a}} CH_3CH_2F \qquad CH_3CH_2F^* \xrightarrow{k_{6b}} CH_2{=}CH_2 + HF \qquad (6)$$

where M represents a third body necessary for collisional deactivation processes.

The temperature dependencies for $k_{5a}/k_{5b} = R_{C_2H_4F_2}/R_{C_2H_3F}[M]$, and $k_{6a}/k_{6b} = R_{C_2H_5F}/R_{C_2H_4}[M]$ are given in Figure 2, where [M] is the pressure of the reacting ketone. The data in Figure 2 is taken from the ten experiments in Table II for which complete analyses are given.

The pressure dependencies for the stabilization/elimination ratios at 406°K are given in Figure 3, showing the expected trend with increasing pressure.[3,5]

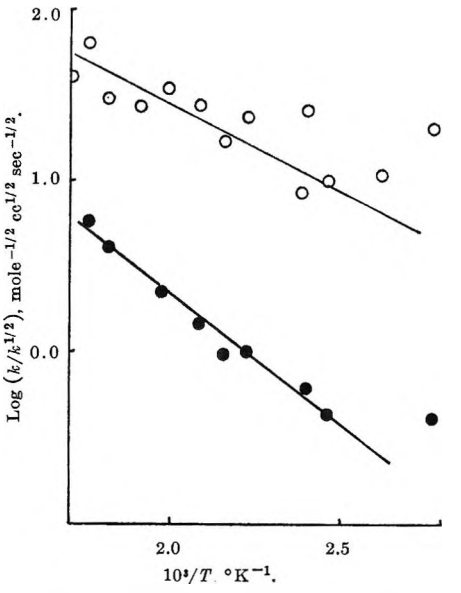

Figure 1. Arrhenius plots for H atom abstraction from CH_2FCOCH_3: ○, log $(k_2/k_4^{1/2})$; ●, log $(k_3/k_5^{1/2})$.

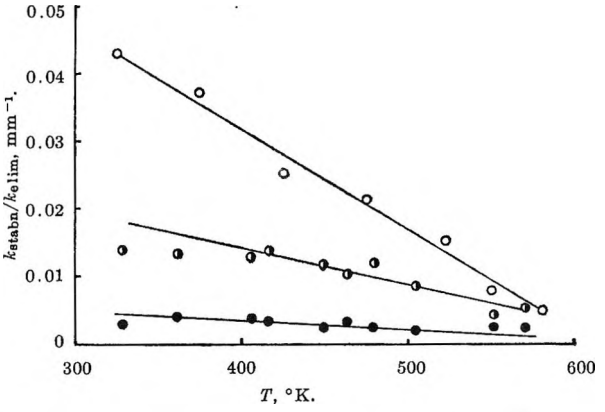

Figure 2. Temperature dependence of $k_{stabilization}/k_{elimination}$: ●, k_{6a}/k_{6b}; ◑, k_{5a}/k_{5b}; ○, k_{5a}/k_{5b}, $(CH_2F)_2CO$ photolysis.[3]

(The points in Figure 2 at 406°K correspond arbitrarily to the high-pressure points, >50 mm, in Figure 3, as the slopes of the lines are not constant.) In Figure 4 the ratio $R_{C_2H_5F}/R_{C_2H_4}$ is shown as a function of the pressure of an added gas (perfluorocyclohexane and perfluorohexane) at constant ketone pressure (4 cm) at 382°K.

Discussion

The rate of HF elimination from a vibrationally excited fluoroethane molecule will depend upon (a) the vibrational energy content of the "hot" molecule, (b) the F atom content and distribution in the molecule,

(11) J. T. Bryant and G. O. Pritchard, to be published.

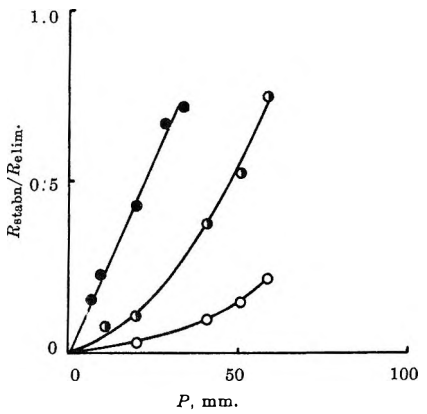

Figure 3. Pressure dependence of the stabilization/elimination rate ratios for $C_2H_5F^*$ and $C_2H_4F_2^*$. P represents the initial pressure (mm) of ketone: ○, $R_{C_2H_5F}/R_{C_2H_4}$ (405°K); ◑, $R_{C_2H_4F_2}/R_{C_2H_3F}$ (405°K); ●, $R_{C_2H_4F_2}/R_{C_2H_3F}$ (475°K), $(CH_2F)_2CO$ photolysis.[3]

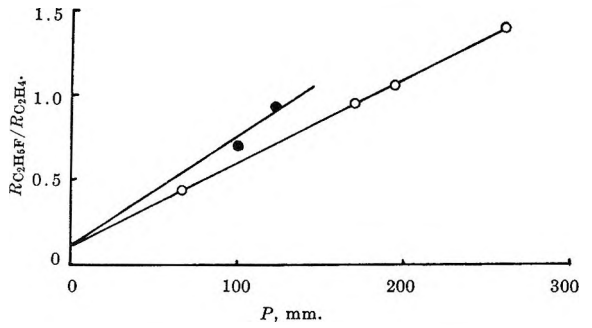

Figure 4. Pressure dependence of $R_{C_2H_5F}/R_{C_2H_4}$ in the presence of an added gas. P represents the pressure (mm) added to 40 mm of CH_2FCOCH_3 at 382°K: ○, c-C_6F_{12}; ●, n-C_6F_{14}.

and (c) the nature of the environment with respect to collisional quenching.

(a) The initial vibrational energy content of the "hot" molecule is primarily a function of the strength of the C–C bond which is formed on radical combination and the temperature of the system. Based on a number of factors, including the uncertainty in $D(CF_3–CF_3)$ and the weakening of the C–C bond in ethane with increasing chlorination, we have suggested[10] that fluorination may tend to weaken C–C bonds, so that, with increasing fluorination, the energy content of the "hot" fluoroethane, formed by radical combination, will be lowered, tending to a reduced rate of HF elimination. Alternatively, other investigations would suggest that fluorination of ethane increases the C–C bond strength,[12] leading to an enhancement in the rate of HF elimination. The vibrational heat capacity of the molecule will also rise with increasing F atom content.

(b) Assuming equal C–C bond energies in the "hot" molecules $C_2H_5F^*$, $C_2H_4F_2^*$, $C_2H_3F_3^*$, and $C_2H_2F_4^*$, BH[2] estimated relative rates of HF elimination to stabilization from these molecules at 298°K of approximately 400:50:7:1 based on the increasing number of effective oscillators with increasing F atom content of the molecules. This approach gives the best description of the experimental results and there is no doubt that the number of effective oscillators in the "hot" molecule is the predominant factor in determining its fate. However, it should be remembered that the activation energy for HF elimination probably decreases with increasing fluorination, so that the decrease in HF elimination will not be so marked as would be expected. Maccoll[13] has tabulated the activation energies for the unimolecular dehydrohalogenations in the pyrolyses of the haloethanes C_2H_5Cl, $C_2H_4Cl_2$, and $C_2H_3Cl_3$, and C_2H_5Br and $C_2H_4Br_2$; there is a distinct decrease in activation energy with increasing halogenation. Further, the elimination from $CH_2FCH_2F^*$ will not necessarily be identical with that for $CH_3CHF_2^*$, as α halogenation tends to promote the rate of dehydrohalogenation relative to β halogenation.[13] We are currently investigating[11] these effects through the interactions of the radical pairs $CH_3 + CHF_2$ and $CH_2F + CHF_2$.

(c) For a given temperature and a given collision frequency the deactivation rate of a particular "hot" molecule will also be a function of the nature of the deactivating species in the system. For example, Giles and Whittle[5] in their investigation of the hot molecule $CH_3CF_3^*$ find values of $R_{CH_3CF_3}/R_{CH_2=CF_2}$ varying by a factor of 20 at 150° by changing the nature and the pressure of the quenching molecules present in the system.

Treatment of the Data. Based on the treatment of BH[2] for $CH_2FCH_2F^*$ produced in $(CH_2F)_2CO$ photolysis,[3] we may make a kinetic analysis of the present data on $C_2H_5F^*$ and $C_2H_4F_2^*$ in terms of the RRK theory of unimolecular reactions[2] and relate the rate constant k_{5b} (or k_{6b}) to the internal energy content, E, of the molecule. That is

$$k_{5b} \text{ (or } k_{6b}) = A(1 - E^*/E)^{n-1} \qquad (7)$$

where E^* represents the critical energy necessary for decomposition, n is the number of effective oscillators, and A is the frequency factor for the unimolecular

(12) Although estimates of $D(CF_3–CF_3)$ vary from 65 to 95 kcal mole^{-1} (E. Tschuikow-Roux, *J. Phys. Chem.*, **69**, 1075 (1965)), most recent evidence (E. Tschuikow-Roux, *J. Chem. Phys.*, **43**, 2251 (1965), and H. O. Pritchard, private communication) favors the extreme upper value. W. C. Steele and F. G. A. Stone, *J. Am. Chem. Soc.*, **84**, 3450 (1962), calculate $D(CF_3–CH_3)$ as 88 kcal mole^{-1}.

(13) A. Maccoll, *Advan. Phys. Org. Chem.*, **3**, 91 (1965).

elimination. Following BH[2] we assume that deactivation occurs on a single collision and the rate of collisional deactivation can be written as

$$k_{5a} \text{ (or } k_{6a}) = QZ \tag{8}$$

where Z is the number of collisions per second per millimeter and Q represents the probability of complete deactivation on collision. From a cascade (see later) point of view $1/Q$ represents the average number of collisions required for deactivation below the threshold energy for elimination. From eq 7 and 8 we have

$$\frac{k_{5a}}{k_{5b}} = \frac{1}{P}\frac{R_{C_2H_4F_2}}{R_{C_2H_3F}} = \frac{QZ_{5a}}{A_{5b}}\left[\frac{E}{E - E^*}\right]^{n-1} \tag{9}$$

where P is the third-body pressure in millimeters. A similar equation represents k_{6a}/k_{6b}. The temperature dependence of the ratio k_{5a}/k_{5b} is assumed[2] to be due to the temperature dependence of E and the temperature dependencies of the collision terms QZ are neglected.[14]

$E(T)$ for $C_2H_4F_2$* has been estimated by BH[2] and the function for C_2H_5F* may be estimated in a similar manner and is given in Table IV, where ΔC_v^{vib} is defined as the difference in vibrational specific heat of the two radicals and the hot molecule and

$$E = E_0 + \Delta C_v^{vib}(T - 298)$$

where E_0 is the energy change on combination, taken to be 85.4 kcal mole^{-1}.

The experimental data and some representative theoretical curves computed from eq 9 are given as a function of temperature in Figures 5 and 6 for k_{5a}/k_{5b} and Figures 7 and 8 for k_{6a}/k_{6b}. The curve fitting was performed by choosing a suitable value for log (QZ/A), which shifts the curve vertically. The choice of values of n and E^* to obtain a fit is somewhat arbitrary.[2] The curves have been fitted to the experimental data in Figures 5 and 7 in the temperature range 400–500°K as we consider that the analysis for the products in question, particularly C_2H_5F, is the most accurate in this range (see Table II). An exact fit is not, in any case, to be expected, owing to the neglect of the influence of temperature on n, Q, and Z. Except for the experiments at the lowest and highest temperatures, where the C_2H_5F yields were low, the correlation in Figure 7

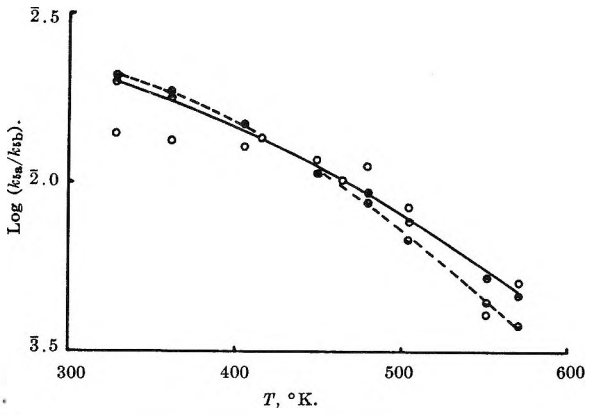

Figure 5. Comparison of the theoretical and observed temperature dependence of k_{5a}/k_{5b} for n = 11: O, experimental points; ◓, E^* = 59 kcal mole^{-1}, log (QZ/A) = −6.75; ◒, E^* = 62 kcal mole^{-1}, log (QZ/A) = −7.24.

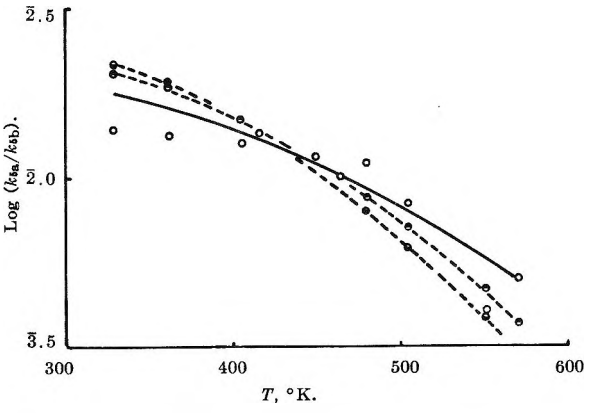

Figure 6. Comparison of the theoretical and observed temperature dependence of k_{5a}/k_{5b} for n = 12: O, experimental points (solid line); ◓, E^* = 59 kcal mole^{-1}, log (QZ/A) = −7.24; ◒, E^* = 62 kcal mole^{-1}, log (QZ/A) = −7.77.

Table IV: Internal Energy of CH_3CH_2F*

T, °K	Thermal energy,[a] $\Delta C_v^{vib}(T - 298)$, kcal mole^{-1}	E, kcal mole^{-1}
298	0	85.4
329	0.5	85.9
362	1.1	86.5
406	2.1	87.5
417	2.3	87.7
450	3.1	88.5
464	3.5	88.9
480	4.0	89.4
505	4.7	90.1
552	6.3	91.7
570	7.0	92.4

[a] The change in the internal energy with temperature was calculated from $\Delta C_v^{vib}(T - 298) = 3R(T - 298) + [C_{v,CH_3}^{vib}(T) + C_{v,CFH_2}^{vib}(T)]T - [C_{v,CH_3}^{vib}(298) + C_{v,CFH_2}^{vib}(298)]298$. Vibrational contributions to the heat capacities of CH_3 and CFH_2 were estimated from the heat capacities of CH_4 and CFH_3, respectively.

(14) These are expected[2] to be much smaller than $E(T)$ and are also compensatory, as values of Q decrease with increasing temperature; see J. R. Dacey, R. F. Mann, and G. O. Pritchard, *Can. J. Chem.*, **43**, 3215 (1965), and D. H. Shaw and H. O. Pritchard, *J. Phys. Chem.*, **70**, 1230 (1966).

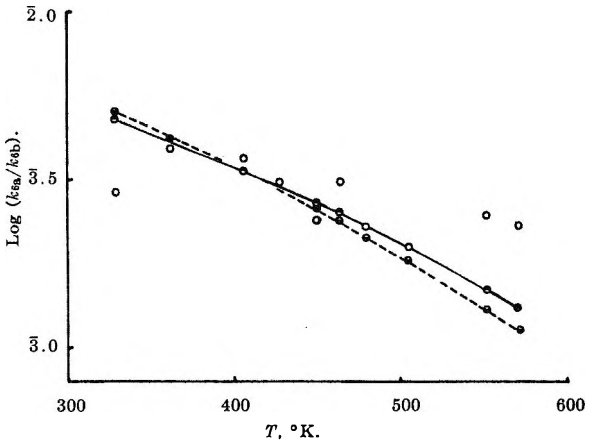

Figure 7. Comparison of the theoretical and observed temperature dependence of k_{6a}/k_{6b} for n = 10: O, experimental points; ◓, E^* = 59 kcal mole^{-1}, log (QZ/A) = −6.86; ◒, E^* = 62 kcal mole^{-1}, log (QZ/A) = −7.29.

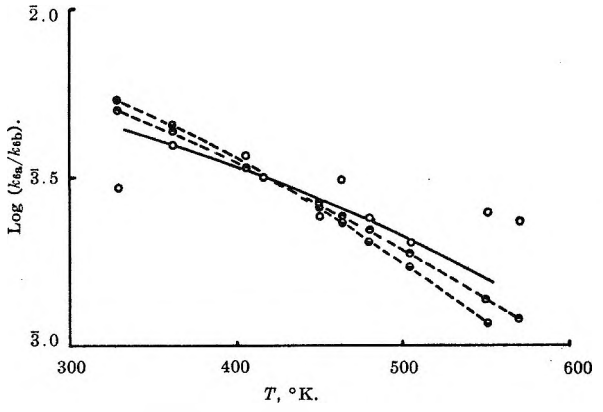

Figure 8. Comparison of the theoretical and observed temperature dependence of k_{6a}/k_{6b} for n = 11: O, experimental points (solid line); ◓, E^* = 59 kcal mole^{-1}, log (QZ/A) = −7.34; ◒, E^* = 62 kcal mole^{-1}, log (QZ/A) = −7.83.

for $C_2H_5F^*$ with values of n = 10 and E^* = 59 kcal mole^{-1} appears to be satisfactory. We have tended to ignore the two low-temperature points in Figure 5. Flatter curves may be obtained by lowering E^* for a particular n or lowering n for a particular E^*, but in view of the expected values of these parameters[2] for $C_2H_4F_2^*$ we have adopted n = 11 and E^* = 59 kcal mole^{-1}.

Assuming collision diameters of 5.0 A for the two fluoroethanes and a collision diameter of 5.5 A for monofluoroacetone, the collisions frequencies are Z_{5a} = $10^{7.07}$ and Z_{6a} = $10^{7.11}$ mm^{-1} sec^{-1} at 298°K. Taking[2,13] A_{5b} = A_{6b} = $10^{13.5}$ sec^{-1}, we may calculate values of Q from Figures 5, 6, 7, and 8. These are given in Table V. The values of Q obtained with n = 11 and E^* = 59 kcal mole^{-1} for k_{5a}/k_{5b} and with n = 10 and E^* = 59 kcal mole^{-1} for k_{6a}/k_{6b} are 0.47 and 0.34, respectively.

Table V: Variation of Q with Different Choices of n and E^*

	E^*, kcal mole^{-1}	n		n^a	
		11	12	11	12
k_{5a}/k_{5b}	59	0.47	0.15	1.3	0.41
	62	0.15	0.046	0.43	0.13
		n			
		10	11		
k_{6a}/k_{6b}	59	0.34	0.11		
	62	0.14	0.036		

[a] Data of BH[2] with $(CH_2F)_2CO$ as the quenching molecule.

The "hot" fluoroethane molecules formed in these systems must lose about 25 kcal mole^{-1} of excess vibrational energy by collision, before they fall below the threshold for HF elimination. Rabinovitch and his co-workers[15] have made extensive studies of the quenching of "chemically activated" species, finding that on the average the amount of vibrational energy transferred on collision may vary between 2 and >15 kcal mole^{-1}, depending mainly on the complexity of the quenching molecules. From the variation in the values of Q given in Table V, no exact assessment of the magnitude of the vibrational energy transferred on collision in these systems can be made. The uncertaintity in the Q values is evidenced by the physically meaningless value of 1.3 given for $C_2F_4H_2^*$, for n = 11, and E^* = 59 kcal mole^{-1} in the $(CH_2F)_2CO$ system.[2] However, these values of the parameters do not represent the best fit for the "hot" molecule; BH[2] suggest n = 12 and E^* = 62 kcal mole^{-1}, with a value of Q = 0.13, as a good representation of the system. Taken in conjunction with the present data on $C_2H_4F_2^*$, it would seem that values of n between 11 and 12 and E^* between 59 and 62 kcal mole^{-1} give an adequate description of the "hot" molecule, formed by CH_2F recombination. Once n and E^* are chosen, identical values of Q are not to be expected for the two systems, owing to the differing deactivation efficiencies of the two molecules $(CH_2F)_2CO$ and CH_2FCOCH_3.

From the slopes and the intercepts in Figure 4 it is possible to show that (see eq 11, given later) the perfluorocyclohexanes are two to three times more efficient deactivators than the ketone, indicating that Q < 0.5 for the ketones; BH[2] recommend a value of 0.1–0.2, which seems to be justifiable.

In Figure 2 it is seen that the rate of HF elimination from $C_2H_5F^*$ exceeds that from $C_2H_4F_2^*$ in accord with the increase in effective oscillators in the latter

(15) See F. Fletcher, B. Rabionvitch, K. Watkins, and D. Locker, *J. Phys. Chem.*, **70**, 2823 (1966), for a recent summary.

molecule. At 298°K the experimental value of $(k_{6a}/k_{6b})/(k_{5a}/k_{5b})$ is about 0.25 in Figure 2. Using the values that we have recommended we see that

$$\frac{(k_{6a}/k_{6b})_{298°K}}{(k_{5a}/k_{5b})_{298°K}} = \frac{10^{-6.86}\left(\frac{85.4}{85.4-59}\right)^{9}}{10^{-6.75}\left(\frac{85.4}{85.4-59}\right)^{10}} = 0.24$$

In their analysis BH[2] suggest a value of 0.14 for this ratio. The agreement is satisfactory, as it should be noted that provided values of QZ/A and E^* are reasonable and not markedly different, such ratios are dependent mainly on the choice of the change in n, Δn, when a C–H oscillator is replaced by a more effective (lower frequency) C–F oscillator. Ratios of about 0.2 are readily computed assuming Δn = 1–1.5 for the replacement of an H atom by an F atom in the "hot" molecule.

The two sets of data in Figure 2 on $C_2H_4F_2^*$ are best interpreted by assuming that $(CH_2F)_2CO$ is a more efficient energy acceptor than is CH_2FCOCH_3, so that stabilization is relatively more favored with the heavier ketone. In Table V, for a particular choice of n and E^*, it is seen that $Q_{(CH_2F)_2CO}$ exceeds $Q_{CH_2FCOCH_3}$ by a factor of about 3.[16] As Q decreases and the energy content of the molecules increases, with increasing temperature, this difference becomes less important at higher temperatures, as the rate of deactivation below the threshold energy for HF elimination becomes slower; eventually a stage may be reached in either system where most of the "hot" molecules have time to eliminate HF from some level on the vibrational cascade. At extremely high temperatures this is seen to be the case. For example, although very little HF elimination occurs from $C_2H_2F_4^*$[17] and $C_2HF_5^*$ at normal temperatures,[4] primarily owing to the increase in the effective oscillators in these molecules,[2] at 1200–1600°K Tschuikow-Roux[18] finds $R_{C_2HF_5}/R_{C_2F_4} < 0.02$ for $C_2HF_5^*$.

Pressure Effects. In the presence of an added third body, M, we have eq 10 and 11 for the two stabilization/elimination ratios, as the deactivating efficiency

$$R_{C_2H_4F_2}/R_{C_2H_3F} = (k_{5a}[CH_2FCOCH_3] + k_{5a}'[M])/k_{5b} \quad (10)$$

$$R_{C_2H_5F}/R_{C_2H_4} = (k_{6a}[CH_2FCOCH_3] + k_{6a}'[M])/k_{6b} \quad (11)$$

of M is not necessarily the same as for the ketone.[5] The linearity predicted by eq 11 for constant ketone concentration and varying [M] is shown in Figure 4 and the intercepts are in agreement with the expected value of $R_{C_2H_4F}/R_{C_2H_4}$ at [M] = 0 and 4-cm pressure of ketone at 382°K.

When ketone only is present, *i.e.*, [M] = 0, eq 10 and 11 predict that the stabilization/elimination ratios are linear functions of the ketone concentration passing through the origin. In Figure 3 it is seen that the data on $C_2H_4F_2^*$ in the difluoroacetone system[3] at 478°K are in accord with this simple mechanism,[2] *i.e.*, reaction 5 where M is $(CH_2F)_2CO$. However, in the same figure, it is seen that the data on $C_2H_4F_2^*$ and $C_2H_5F^*$, obtained in the present work, tend to show curvature, which is not completely in accord with the simple mechanism as depicted by reactions 5 and 6. Adopting a cascade mechanism for deactivation, we may consider the simplest case of a two-step deactivation process to a molecule $C_2H_4F_2^{***}$ which has insufficient energy to eliminate HF

$$CH_2F + CH_2F \underset{k_{-5}}{\overset{k_5}{\rightleftharpoons}} C_2H_4F_2^* \xrightarrow{k_{5b}} C_2H_3F + HF$$

$$C_2H_4F_2^* \xrightarrow{M,\ k_{5c}} C_2H_4F_2^{**} \xrightarrow{k_{5d}} C_2H_4F_2^*$$

$$C_2H_4F_2^{**} \xrightarrow{M,\ k_{5e}} C_2H_4F_2^{***} \xrightarrow{M} C_2H_4F_2$$

Now $R_{C_2H_4F_2} = k_{5e}[M][C_2H_4F_2^{**}]$ and $R_{C_2H_3F} = k_{5b}[C_2H_4F_2^*] + k_{5d}[C_2H_4F_2^{**}]$. Assuming a steady state for $C_2H_4F_2^{**}$, we have

$$d[C_2H_4F_2^{**}]/dt = 0 = k_{5c}[M][C_2H_4F_2^*] - k_{5d}[C_2H_4F_2^{**}] - k_{5e}[M][C_2H_4F_2^{**}]$$

and

$$\frac{R_{C_2H_4F_2}}{R_{C_2H_3F}} = \frac{k_{5c}k_{5e}[M]^2}{k_{5b}k_{5d} + [M](k_{5b}k_{5e} + k_{5c}k_{5d})} \quad (12)$$

The term in $[M]^2$ would cause upward curvature, as seen in Figure 3, and when [M] = 0, the ratio $R_{C_2H_4F_2}/R_{C_2H_3F} = 0$. In the region of high pressure the term $k_{5b}k_{5d}$ becomes less important with respect to $[M]\cdot(k_{5b}k_{5e} + k_{5c}k_{5d})$, leading to a linear relationship between $R_{C_2H_4F_2}/R_{C_2H_3F}$ and [M], which our results tend to do.

(16) This factor appears to be too large; Giles and Whittle[5] find a factor of 2 in the deactivating efficiencies of $(CF_3)_2CO$ and $(CH_3)_2CO$ for the "hot" molecule $CH_3CF_3^*$. However, our discussion is presumably qualitatively correct.

(17) At 464°K, $R_{C_2H_2F_4}/R_{C_2HF_3}$ = 38 at 0.72 cm pressure of $(CHF_2)_2CO$.[11]

(18) E. Tschuikow-Roux, *J. Chem. Phys.*, **42**, 3639 (1965).

The extent of the curvature is dependent upon the magnitude of the first term in the denominator in eq 12. At 405°K, we may take $k_{5c} = k_{5e} = 10^{7.14}$ mm^{-1} sec^{-1} and $k_{5b} = 10^{13.5}\left(\frac{87.4 - 59}{87.4}\right)^{10} = 4.15 \times 10^{8}$ sec^{-1} and express [M] in millimeters. Assuming $k_{5d} = k_{5b}$, the ratio in eq 12 reduces to $[M]^2/(980 + 60[M])$, which almost exactly represents the experimental curve for $C_2H_4F_2$* for the present system in Figure 3. As the internal energy of $C_2H_4F_2$** is reduced below that of $C_2H_4F_2$*, we should take a value of $k_{5d} < k_{5b}$. Assuming $k_{5d} = 0.1k_{5b}$, the ratio in eq 12 leads to a line of lesser curvature and to values of $R_{C_2H_4F_2}/R_{C_2H_3F}$ that are too big, *e.g.*, 0.23 at 10 mm and 1.4 at 50 mm, both at 405°K. Taking $k_{5d} = 0.1k_{5b}$ leads to an internal energy for $C_2H_4F_2$** of 79.5 kcal mole^{-1} at 405°K, based on $E^* = 59$ kcal mole^{-1} and $n = 11$, for the hot molecule. This is a decrease of 8 kcal mole^{-1} below the internal energy for $C_2H_4F_2$* at 405°K. A better correlation is obtained by assuming a "weaker" deactivating collision, *e.g.*, $k_{5d} = 0.5k_{5b}$, which corresponds to a drop of about 3 kcal mole^{-1} in the internal energy. ($R_{C_2H_4F_2}/R_{C_2H_3F}$ is 0.11 at 10 mm and 0.93 at 50 mm.) If this amount of energy is transferred per collision by a "hot" molecule while it is on the vibrational cascade, it would take about eight collisions before it falls below the limit for HF elimination, which we may equate with a value of $Q = 0.13$.

Several other more complicated cascade schemes were tried,[19] in particular for cases where there were more than two levels on the cascade from which elimination could occur and where there was competition between a one-step and a two-step deactivation process below the threshold from a particular level on the cascade. Application of the steady-state treatment leads to more involved expressions than eq 12, which predict upward curvature for $R_{C_2H_4F_2}/R_{C_2H_3F}$ with increasing [M] and reduce to zero at [M] = 0.

In the case where M is a very efficient quenching molecule, $C_2H_4F_2$** may be close to or below the threshold for elimination so that $k_{5d} \simeq 0$ and we revert to the simple mechanism, reaction 5, where $k_{5c} = k_{5a}$. From Figure 3, it would therefore appear that $(CH_2F)_2CO$ is an efficient deactivator of $C_2H_4F_2$*. The efficiency of the perfluorohexanes as deactivators for C_2H_5F* is exemplified in Figure 4. It should be pointed out that this linearity does not mean complete deactivation below the threshold energy on the first collision, *i.e.*, $Q = 1$. However, if a "hot" molecule is sufficiently deactivated by the first collision, its energy level may be such that rate of HF elimination is not significant when compared to the rate from the "hot" molecule before collision; note above that $k_{5d} = 0.1k_{5b}$ corresponds to a decrease of 8 kcal mole^{-1} in internal energy. Our result that $Q_{(CH_2F)_2CO} = 3Q_{CH_2FCOCH_3}$ for $C_2H_4F_2$* (Figure 2 and Table V) would also seem to be justified (Figure 3).

Summary

It should be noted that our description and that of BH[2] are in good accord. From the known experimental and calculated activation energies for dehydrohalogenation of haloethanes,[2,13] it seems that values for $C_2H_4F_2$ and C_2H_5F are in the range 59–62 kcal mole^{-1}. Once E^* is chosen, it is seen that the value of Q obtained is very sensitive to the value of n. Within the allowable margin of variation for these parameters, there is reasonable agreement between the theoretical model and the experimental systems. In the systems discussed here, C_2H_5F* and $C_2H_4F_2$* with the ketones as quenching molecules, we may estimate that somewhere between 3 and 8 kcal mole^{-1} of excess vibrational energy is transferred on collision.

Acknowledgment. G. O. P. wishes to thank Professor J. R. Dacey for his generous hospitality and several helpful discussions during the completion of the manuscript for this article.

(19) R. L. Thommarson, Ph.D. Thesis, University of California, Santa Barbara, Calif., 1966.

Pulse Radiolysis Studies in Oxygenated Alkaline Solutions[1]

by Gideon Czapski[2]

Chemistry Department, Brookhaven National Laboratory, Upton, New York *(Received September 6, 1966)*

The reaction kinetics of transient species in aqueous oxygenated solutions have been investigated by pulse radiolysis techniques. The decay of O_3^- was followed at 4300 A. The dependence of the yield and the decay rate was measured over the pH range 12.7–14 as a function of concentrations of oxygen, N_2O, and H_2O_2. The decay was first order under all conditions and the O_3^- was stabilized by oxygen; $\tau_{1/2} = 11.4 \times [O_2]$ sec. The decay of the absorption at 2400 A was found to be much slower than at 4300 A, indicating that at these wavelengths different species are the absorbing intermediates. The possible identity of the species and the mechanism are discussed.

Introduction

The identity and kinetics of intermediates occurring in oxygenated aqueous solutions have been investigated using several techniques.[3–10] In neutral and acid solutions the final radiolysis products are H_2 and H_2O_2. The free radicals in this system are the OH, HO_2, and O_2^- radicals. In addition it was shown that H_2O_3 is formed in acid solution from the recombination of HO_2 and OH radicals.[5]

The absorption spectrum of the hydroperoxy radical was determined, the acid form (HO_2) and the neutral form (O_2^-) having their maximum absorptions at 2400 and 2300 A, respectively.[4b,6,8] The pK of the radical was found to be 4.4 ± 0.2[5,6,11,12] and the recombination kinetics were studied.[3b–8a]

The radiation chemistry of alkaline solutions has received less attention, but recently this region was studied by pulse radiolysis techniques.[6,7,8a,10] As the pK of HO_2 is 4.4[5,6,11] and that of the OH is 11.9[12] and H_2O_2 has a pK of 11.8,[13] we expect to find the following species in strongly alkaline solutions: O_2^-, O^-, and HO_2^-. It was shown that a new species, believed to be O_3^-, is formed[6,7,10]

$$O_2 + O^- \longrightarrow O_3^- \qquad (1)$$

The O_3^- radical was shown to have a maximum at 4300 A using flash photolysis[10] and pulse radiolysis techniques,[6,7] in agreement with the spectrum of O_3^- in its stable solution in liquid ammonia.[14]

Adams, Boag, and Michael claimed that the O_3^- has two absorption peaks,[7,8] one at 4300 A and the other in the ultraviolet region at about 2600 A. The decay of O_3^- was found to be pH dependent at pH 10–12 and to be first order in oxygenated solutions.[6] Adams, *et al.*,[7,8] showed it to be second order in N_2O–O_2 solution and claimed the absorption at 2600 and 4300 A has the same decay mode, while Czapski and Dorfman[6] found different decay kinetics at 2400 and 4300 A, attributing the two absorptions to two different intermediates.

In this work the pulse radiolysis technique was used

(1) Research performed under the auspices of the U. S. Atomic Energy Commission.

(2) To whom all correspondence should be addressed at the Department of Physical Chemistry, The Hebrew University, Jerusalem, Israel.

(3) (a) B. H. J. Bielski and E. Saito, *J. Phys. Chem.*, **66**, 2266 (1962); (b) E. Saito and B. H. J. Bielski, *J. Am. Chem. Soc.*, **83**, 4467 (1961).

(4) (a) K. Schmidt, *Z. Naturforsch.*, **166**, 206 (1961); (b) J. H. Baxendale, *Radiation Res.*, **17**, 312 (1962).

(5) G. Czapski and B. H. J. Bielski, *J. Phys. Chem.*, **67**, 2180 (1963).

(6) G. Czapski and L. M. Dorfman, *ibid.*, **68**, 1169 (1964).

(7) G. E. Adams, J. W. Boag, and B. D. Michael, *Nature*, **205**, 898 (1965).

(8) (a) G. Adams, submitted for publication; (b) J. Rolfe, F. R. Lipsett, and W. J. King, *Phys. Rev.*, **123**, 447 (1961).

(9) G. Adams, private communication.

(10) L. J. Heidt and V. R. Landi, *J. Chem. Phys.*, **41**, 176 (1964).

(11) J. Rabani, W. A. Mulac, and M. S. Matheson, *J. Phys. Chem.*, **69**, 53 (1965).

(12) J. Rabani and M. S. Matheson, *J. Am. Chem. Soc.*, **86**, 3175 (1964).

(13) F. R. Duke and T. W. Haas, *J. Phys. Chem.*, **65**, 304 (1961).

(14) A. J. Kacmareck, J. M. McDonough, and I. J. Solomon, *Inorg. Chem.*, **1**, 659 (1962)

to learn more about the decay of the absorption assumed to be due to the O_3^-.

Experimental Section

Materials. Barium hydroxide and sodium hydroxide were of analytical grade. Barium hydroxide was recrystallized once from N_2-saturated triply distilled water.

All the solutions were prepared with triply distilled water. Matheson's helium, oxygen, and N_2O were used without further purification, except passing them through two washing bottles with triply distilled water.

Sample Preparation. All the solutions were saturated with the gases by bubbling them through the solution for 1 hr.

Stock solutions of barium hydroxide, sodium hydroxide, and triply distilled water saturated with He, O_2, and N_2O were prepared. The different concentrations of the irradiated solutions were prepared by mixing the stock solutions in syringes. Solutions of $Ba(OH)_2$ were used up to 0.5 *N;* for higher alkalinity, mixtures of NaOH and $Ba(OH)_2$ had to be used owing to the limited solubility of $Ba(OH)_2$. The irradiation cell was flushed with helium, then several times with the solution to be irradiated.

Pulse Irradiation and Apparatus. A 2-Mev electron beam from a Van de Graaff accelerator was used throughout this work. Beam currents of 5–20 ma were used. The pulse duration ranged from 5 μsec up to about 1 msec. The dose per pulse was varied by both beam current and pulse duration. The pulse was monitored with a current integrator which was calibrated against a Fricke dosimeter.

The irradiation cell was made of quartz having dimensions of about 2 × 2 × 0.8 cm. The electron beam entered the cell through a 2- × 2-cm quartz window which was ground down to a thickness of about 0.5 mm in order to reduce the energy loss in the window.

The intermediates were followed spectrophotometrically. The light crossed the cell three times along a 2-cm axis. Three different light sources were used: a 300-w xenon arc, a 30-w deuterium arc, and a 150-w tungsten–iodine lamp. The last two were used for most of the work as their stability over longer time intervals is superior, although their intensity is lower. The light sources were inside the irradiation room. The light was passed out of the irradiation room, then through a Bausch and Lomb grating monochromator (f/3.5) to the photomultiplier. The signal was detected and photographed on a 555 Textronix oscilloscope.

Results

Formation of Initial Absorption. The absorption at 4300 A is formed within 5–50 μsec depending on the oxygen concentration. The present measurements confirm the value of $2.5 \times 10^9\ M^{-1}\ \text{sec}^{-1}$ [7] for the rate constant of reaction 1.

The initial optical density (before appreciable decay occurs) depends on the pH, as shown before,[6] reaching the maximum at pH 12. No absorption at 4300 A could be found below pH 10. The absorption magnitude does not depend on pH or O_2 concentration above pH 12 as long as $O_2 \geq 10^{-5}\ M$. We found, as Adams[7] has shown, that in the presence of sufficient N_2O the absorption is about doubled. In O_2–He and O_2–N_2O mixtures, the initial optical density depends on the concentration ratios, as shown in Figure 1.

Addition of H_2O_2 to oxygenated solutions increases the initial absorption in a similar fashion to N_2O.

In the absence of O_2 the initial absorption at both 4300 and 2400 A was very small but increased with repetitive pulses.

In neutral solutions containing about 1 mM O_3 and 1 mM O_2 no absorption at 4300 A was observed.

The decay of the absorption was followed at 4300 A and was found to be first order over the whole range of pH, and O_2 and N_2O concentrations studied. Figures 2 and 3 show first-order plots in O_2 and N_2O–O_2 solutions. It can be seen that while the initial concentration is

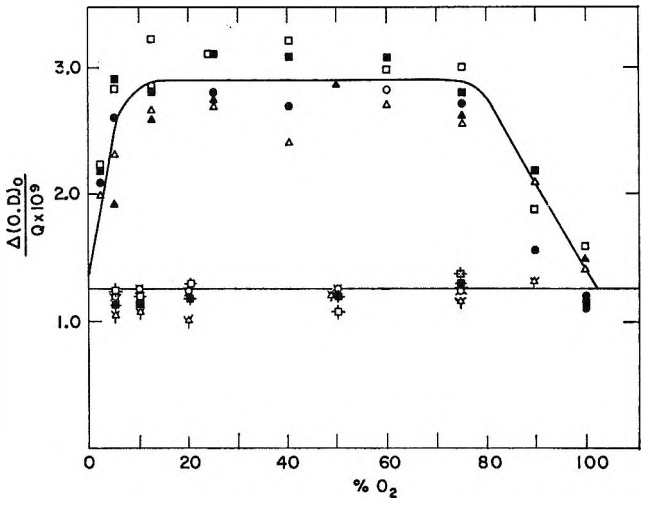

Figure 1. Dependence of initial o.d. at 4300 A in oxygen concentration (Q is the energy of pulse in coulombs) in solutions saturated with 1 atm of gas at 23°. Flagged points (lower curve) are He–O_2 mixtures; unflagged points (upper curve) are N_2O–O_2 mixtures: ●, ×, −0.105 N $Ba(OH)_2$; ○, ⊠, −0.14 N $Ba(OH)_2$; ■, ⊕, −0.19 N $Ba(OH)_2$; □, ⊕, −0.3 N $Ba(OH)_2$; △, ☆, −0.5 N $Ba(OH)_2$; ▲, ★, −0.3 N $Ba(OH)_2$ + 1.1 N $NaOH$.

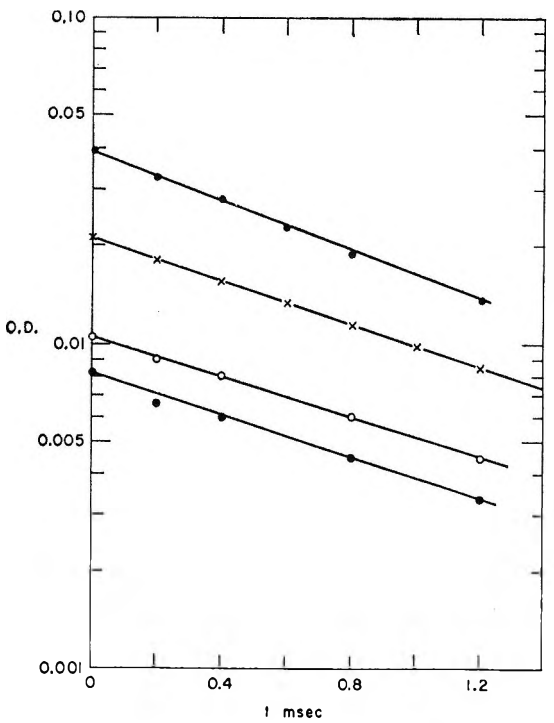

Figure 2. Decay of the ozonide ion at 4300 A produced in 0.1 *N* $Ba(OH)_2$ saturated with 4% oxygen–96% N_2O mixture. (The four curves are with different doses.)

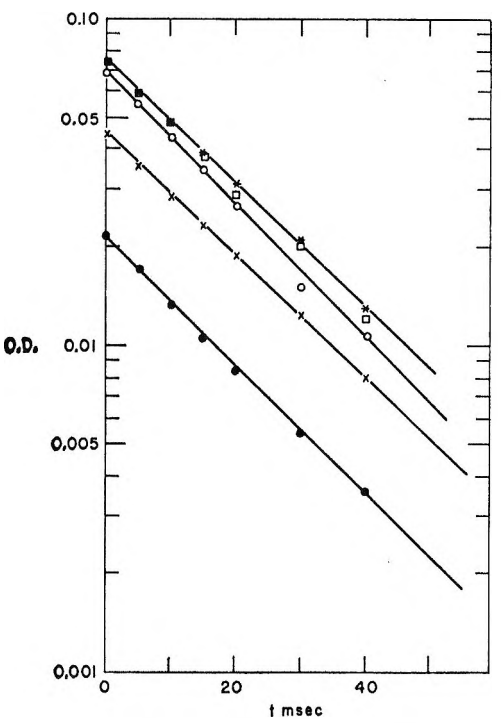

Figure 3. Decay of the ozonide ion at 4300 A produced in 0.3 *N* $Ba(OH)_2$ saturated with 1 atm of oxygen.

changed by fivefold, the half-lifetime changes by less than 10%.

The decay rate was found to be pH independent from pH 12.7 up to 14 and did not depend on the O_2–N_2O but on oxygen concentration only. The results are summarized in Figure 4, which shows the half-lifetime to be linear with O_2 concentration in He–O_2 and N_2O–O_2 mixtures over the pH range studied

At 2400 A in the time range of 1–20 msec no decay was found in O_2 or O_2–N_2O alkaline solutions, as was reported before.[6] The decay rate was pH dependent but did not change with oxygen concentrations. The decay of the absorption at 4300 A was found to depend on the number of pulses received by the solution. At very high doses or after repetitive pulses, the half-lifetime decreases and the reciprocal of the half-lifetime is linear with the number of pulses received by the solution, as shown in Figure 5. Hydrogen peroxide accumulates in the solution with repetitive pulses and the addition of H_2O_2 decreases the half-life of the absorption at 4300 A, as shown in Figure 6.

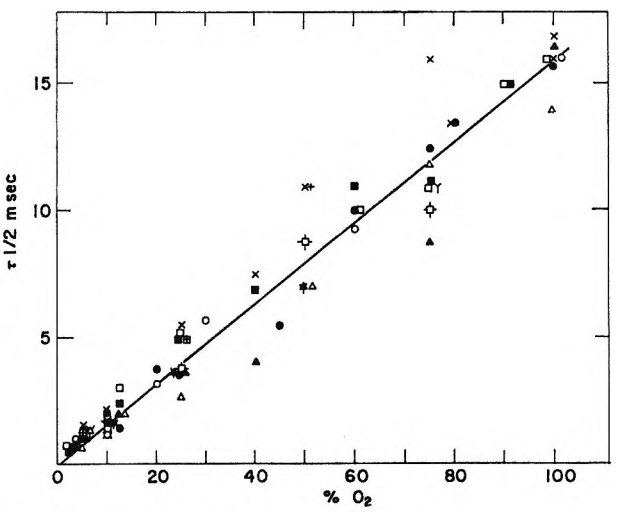

Figure 4. Dependence of ozonide half-life on the oxygen concentration in solution saturated with 1 atm of gas, at different acidities. Symbols as in Figure 1.

Discussion

Absorption and Identity of the Intermediates. The absorbing species at 4300 A was found in pulse radiolysis[6,7] and flash photolysis[10] of O_2-saturated alkaline solutions.

The species was assumed to be either O_3^- [6,7,10,15] or O_3^{2-} [6] being formed in one of the reactions

$$OH + OH^- \longrightarrow O^-, \quad O^- + O_2 \longrightarrow O_3^- \qquad (a)$$

$$OH + OH^- \longrightarrow O^-, \quad e_{aq} + O_2 \longrightarrow O_2^-,$$
$$O^- + O_2^- \longrightarrow O_3^{2-} \qquad (b)$$

(15) A. D. McLachlan, M. C. R. Symons, and M. G. Townsend, *J. Chem. Soc.*, 952 (1959).

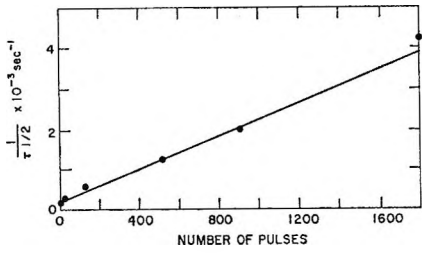

Figure 5. Dependence of the reciprocal of the ozonide half-life on the number of pulses the solution received in 0.3 *N* $Ba(OH)_2$.

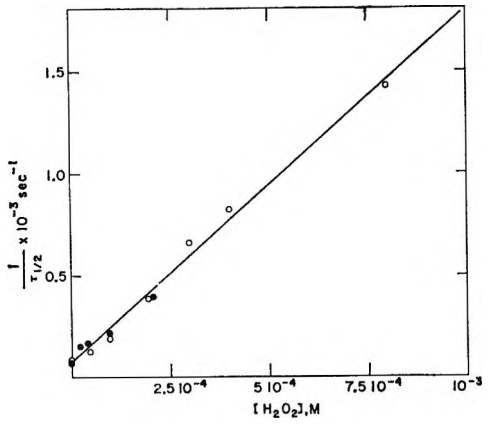

Figure 6. Dependence of the decay rate on peroxide concentration in oxygen-saturated solutions: ○, 0.1 *N* $Ba(OH)_2$; ●, 0.3 *N* $Ba(OH)_2$.

Now there seems to be very good evidence for the identification as O_3^-. The spectra is very similar to the reflectance spectra of solid ozonides[15] and alkali ozonides in liquid ammonia.[14] It was shown[6] that the precursor of the absorption is the OH radical, as OH scavengers such as alcohols suppressed the formation of the species. As it is formed only in alkaline solutions, one concludes the O^- to be a precursor. Oxygen was found to be necessary for its formation as well.

Further evidence for the identification as O_3^- was provided by Adams,[7] *et al.* They found the formation was first order with O_2 concentration and they showed that the addition of N_2O in excess of O_2 doubles the yield of the intermediate (Figure 1). Under these conditions the solvated electron reacts with N_2O rather than with O_2; thus the electrons are converted into O^- according to the reaction

$$e_{aq} + N_2O \longrightarrow N_2O^-$$

Therefore N_2O must prevent O_2^- formation. That N_2O increases the absorption rather than decreasing it proves that reaction b cannot be responsible for the absorption.

Although there seems to be full agreement as to the formation of O_3^-, which has an absorption peak at 4300 A, there is some controversy as to the existence of a second absorption peak of the O_3^- in the ultraviolet region[6,7] (2400 A). The HO_2 and O_2^- show an absorbance in the ultraviolet region at 2400 A. Above pH 6 practically no HO_2 is found and all the hydroperoxy radical should exist as O_2^-. As has been shown,[6] the spectrum in the ultraviolet region does not change its shape in the pH range 6–14, except for a change in the intensity of the absorption which increases with the pH and in the lifetime of the intermediates. The absorption at 2400 A in alkaline solutions is approximately doubled if CH_3OH is added to the solutions.[6] This indicates that at least part of the absorption in this region is due to O_2^- or a product of it, rather than to the O_3^-. Adams, *et al.*,[7] found the absorption at 2400 and 4300 A decayed with equal rates except that at 2400 A a second slower decay is followed. The present results and previous results[6] did not confirm their findings. We were unable to observe any decay at 2400 A with the same rate as found at 4300 A under the same conditions. At pH 12.7, the decay at 2400 A is slower by more than an order of magnitude. After this slow decay, a residual absorption at 2400 A remains owing to HO_2^- formed as a final product. In experiments with 0.1 *N* NaOH containing some carbonate, a decay at 2400 A occurred with a similar lifetime to the decay at 4300 A, which suggests that a carbonate radical may be responsible for some absorption formed in the ultraviolet region.

The transient species absorbing at 2400 A in alkaline solution is formed from O_2 and e_{aq}; thus we expect it to be O_2^-. Nevertheless, its behavior is different from the O_2^-, having a stronger absorbance although the peak is of similar shape. Its decay is orders of magnitude slower than that of the O_2^-. These species must be either an alkaline-stabilized form of O_2^- or its dimer or an alkali-stabilized form of the disproportionation product of the O_2^-.

Decay of the O_3^-. The decay kinetics observed here may be summarized by the equation

$$-\frac{d[O_3^-]}{dt} = \left[\frac{k_a}{[O_2]} + k_b[H_2O_2]\right][O_3^-] \qquad (I)$$

From Figures 4 and 6 we derive the values

$$k_a = 0.06\ M\ \text{sec}^{-1}$$

$$k_b = 1.6 \times 10^6\ M^{-1}\ \text{sec}^{-1}$$

Ozonized Solutions. The absence of any initial absorption at 4300 A in neutral solutions containing

O_3 and O_2 can be explained according to the possible reactions occurring.

$$O_3 + e_{aq} \longrightarrow O_3^- \quad (p)$$

$$O_2 + e_{aq} \longrightarrow O_2^- \quad (q)$$

$$O_3 + e_{aq} \longrightarrow O_2 + O^- \quad (r)$$

If reaction p is slower than (q) and/or (r), no ozonide is expected to be formed.

As O_3 and O_2 concentrations were comparable, we are forced to assume that either e_{aq} reacts slowly with ozone or the main pathway of the reaction is (r) rather than (p).

Decay Mechanism. Stabilization by oxygen of the 4300-A absorption indicates an equilibrium of the type $x + O_2 \rightleftharpoons y$, where the reaction proceeds through the first-order decay of x. (The equilibrium must lie to the right.) If the equilibrium were $O^- + O_2 \rightleftharpoons O_3^-$, the O^- would have to decay in a first-order process, although the contrary is found experimentally.[12] Such a mechanism could hold only if O^- reacts with an impurity. There is no such impurity either in the $Ba(OH)_2$ or in the gases, as the half-life does not decrease with increasing concentrations of these reagents (Figure 4), nor in the triply distilled water, since water from different stills gave the same results.

A mechanism which agrees with the ozonide decay would be

$$O^- + O_2 \longrightarrow O_3^- \quad (1)$$

$$2O_3^- \rightleftharpoons O_6^{2-} \quad (2)$$

$$O_6^{2-} \rightleftharpoons O_4^{2-} + O_2 \quad (3)$$

$$O_4^{2-} \longrightarrow O_2 + O_2^{2-} \quad (4a)$$

or

$$O_4^{2-} \longrightarrow 2O_2^- \quad (4b)$$

$$O_4^{2-} + H_2O_2 \longrightarrow 2O_2 + 2OH^- \quad (5a)$$

or

$$O_6^{2-} + H_2O_2 \longrightarrow 3O_2 + 2OH^- \quad (5b)$$

Reaction 1 is fast, as Adams,[7] *et al.*, measured $k_{O^- + O_2} = 2.5 \times 10^9\ M^{-1}\ \text{sec}^{-1}$.

In order to predict a first-order decay of the intermediate and a reverse oxygen concentration dependence as observed, the following restrictions have to be added to the above mechanism.

(a) Equilibrium 2 has to be to the right, which means that the ozonide ion exists in solution mainly as its dimer O_6^{2-}. The proposed dimerization of O_3^- in a strongly alkaline solution is analogous to the dimerization of the periodate ion[16] known to occur at pH >10.

(b) As O_3^- is formed in alkaline oxygenated solutions more rapidly than would be possible for O_3^- to associate into O_6^{2-} at the low concentrations in which O_3^- is formed, we expect to be able to observe the formation of O_6^{2-}. As no change in the absorption at 4300 A was observed during the time of the formation of O_6^{2-}, we must conclude that O_3^- and its dimer, O_6^{2-}, have very similar extinction coefficients per O atom.

(c) The observed decay expression fits the proposed mechanism if an additional assumption is made. We have to assume that equilibrium 3 lies to the left, otherwise the first-order rate constant would not be proportional to $1/[O_2]$ as it was observed.

The proposed mechanism is rather speculative, as it predicts two new intermediates, O_6^{2-} and O_4^{2-}, where no direct evidence for their existence is known; however, the existence of H_2O_4, the acid form of O_4^{2-}, has been shown.[17,18] (If O_4^{2-} and O_6^{2-} do exist, some ring structure might stabilize these hypothetical intermediates.)

We propose this mechanism in spite of the speculative assumption needed, as we cannot see any alternative explanation for the observed results. Reaction scheme 1–5a or 1–5b will give the values $k_a = k_4k_3/k_{-3}$ and $k_b = k_{5a}k_3/k_{-3}$ or $k_{5b} = k_b$.

The absorption of O_2^- at 2400 A also raises some difficulties. Above pH 10 the decay is not second order, but first order, with half-lifetime that increases with the pH.

This behavior was attributed[6] to the scheme

$$2O_2^- \longrightarrow O_2^{2-} + O_2$$

$$O_2^{2-} + H^+ \longrightarrow HO_2^-$$

$$O_2^{2-} + H_2O \longrightarrow HO_2^- + OH^-$$

Below pH 7 the first step is rate determining; thus second-order decay is observed. At higher pH the second and third steps are the slow ones; this will predict first-order decay and a pH dependence similar to the one observed. The only difficulty to this assumption is the lack of any change in absorption in the time range where the reaction $2O_2^- \rightarrow O_2 + O_2^{2-}$ occurs. This would force us to assume that there is no difference in the absorption of two O_2^- radicals and one O_2^{2-} ion.

As O_2^-, O_4^{2-}, and O_2^{2-} are possible intermediates in the decay of both O_3^- and O_2^- in alkaline solutions, it would seem that more work should be done in order

(16) I. I. Skorokhodov, L. I. Nekrasov, and N. I. Kobozev, *Russ. J. Phys. Chem.*, 38, 1188 (1964).

(17) Z. P. Zagorski and K. Sehested, "Pulse Radiolysis 43," Academic Press Inc., New York, N. Y., 1965.

(18) G. J. Buist and J. D. Lewis, *Chem. Commun.*, 66 (1965).

to understand this complicated system, studying simultaneously the decay at both wavelengths 2400 and 4300 A.

Acknowledgment. The author wishes to thank Drs. A. O. Allen, H. A. Schwarz, and A. Treinin for valuable suggestions and discussions.

Refractometry in Fused Alkali Nitrates and Thiocyanates

by Hans R. Jindal and George W. Harrington

Department of Chemistry, Temple University of the Commonwealth System of Higher Education, Philadelphia, Pennsylvania *(Received September 8, 1966)*

Refractive index and density measurements were performed on various alkali nitrates, alkali nitrate mixtures, and solutions of alkali halides in the nitrate systems. In addition, molten alkali thiocyanates and saturated aqueous solutions of alkali thiocyanates were studied. Molar refractions, polarizabilities, and fundamental absorption frequencies were calculated.

Introduction

Work on refractive index measurements in molten salts dates back to comparatively recent years. It has, however, received impetus during the past 10 years or so with a view to utilizing this property for determination of complex ions formed, if any,[1,2] and for attempting to elucidate the structure of melts.[3,4] Meyer[5] and Meyer and Heck[6] in 1922 determined for the first time the refractive indices of fused $NaNO_3$, KNO_3, NaOH, and KOH and calculated their molar refractions. Wagner[7] in 1928 extended this work to a larger number of salts and to higher temperatures using light of six different wavelengths. After a long gap of some 30 years Bloom and Rhodes[1] determined the molar refractions of $NaNO_2$, $NaNO_3$, KNO_2, KNO_3, $AgNO_3$, and $NaNO_3$–KNO_3, $NaNO_3$–$AgNO_3$, and KNO_3–$AgNO_3$ mixtures of varying compositions. They obtained almost straight-line plots for molar refraction *vs.* mole fraction of a component for these mixtures concluding that there is little or no additional ionic interactions in these systems. Murgulescu and Volanschi[2] in 1961 carried out refractive index measurements of $LiNO_3$–$NaNO_3$ and $LiNO_3$–KNO_3 systems and calculated their molar refractions. They found that the rule of mixtures holds indicating that the deformation action of the small-sized and highly charged Li^+ ion has little effect on the refractometric behavior of these mixtures. During the last few years Zarzycki and Nandin[3,4] have made measurements of refractive index and magnetic rotation of a good many solid and fused salts and have calculated their molar refractions and molar magnetic rotations. Since these molar constants are related to the frequencies of absorption bands for the same compounds[3,4,8] they also determined the absorption frequencies as a function of temperature. Comparing this variation of absorption frequency with the variation experimentally obtained for the same

(1) H. Bloom and D. C. Rhodes, *J. Phys. Chem.*, **60**, 791 (1956).

(2) I. G. Murgulescu and C. Volanschi, *Rev. Chim. Acad. Rep. Populaire Roumaine*, **6**, 45 (1961).

(3) J. Zarzycki and F. Nandin, *Compt. Rend.*, **256**, 634, 1252, 3078, 5344 (1963); **257**, 3163 (1963); **258**, 1488 (1964).

(4) J. Zarzycki and F. Nandin, *Rev. Hautes Temp. Refractaires*, **1**, 121 (1964).

(5) G. Meyer, *Z. Electrochem.*, **28**, 21 (1922).

(6) G. Meyer and H. Heck, *Z. Physik Chem.* (Leipzig), **100**, 316 (1922).

(7) O. H. Wagner, *ibid.*, **131**, 409 (1928).

(8) M. R. Mallemann, *J. Phys. Radium*, **7**, 295 (1926).

compounds, they have tried to lend support to the "free space" model for fused salts.

We have extended the refraction studies of alkali metal nitrates, their binary mixtures, and mixtures with alkali metal halides and also those of alkali metal thiocyanates and their binary mixtures.

Experimental Section

Materials Used. All salts used were of reagent grade quality. They were powdered, dried in a vacuum oven at about 110° for 3–4 hr, and finally vacuum desiccated over P_2O_5. Further handling was performed using carefully observed anhydrous techniques including use of a glove box. This procedure was found particularly essential for thiocyanates and lithium salts which are extremely hygroscopic.

Method. The method employed for refractive index determination involved the measurement of the angle of minimum deviation of the emergent ray from a hollow Pyrex or quartz 60° prism and the application of Snell's law.[9] The prism was 1.5 in. per side and held 12–15 g of melt.

The furnace used was constructed of a brass rod 6 in. long and 3 in. in diameter. The center of the block had a triangular hole through its entire length of such dimensions that the prismatic cell could go in as a snug fit. The bottom section of the furnace consisted of a brass plate 0.75-in. thick having a triangular groove in the center corresponding to the hole in the main block. The main block and the bottom plate were held together by connecting pins and spacers to allow a $^1/_6$-in. opening for the light path. The depth of the prism well and the height of the prism were such that approximately 4 in. of brass block were above the top of the prism. Thus, temperature gradients even at the surface were negligible. Three 250-w rod heaters were inserted in the block in a symmetrical arrangement around the prism well. The heaters extended from the top of the main block into the bottom plate. These heaters were controlled by a Proportio-Null 1300 series temperature controller. The sensing element for the controller was placed in a well in the block. The bottom plate was also heated by resistance wire wound around its circumference. This was regulated by a variable-dc source.

The main block and bottom plate were well insulated with approximately 2 in. of porcelain cement, alundum, and asbestos. A temperature as high as 500° could be attained with control to within ±0.1° and it was measured by a sheathed chromel–alumel thermocouple placed in the melt, using a Leeds and Northrup AZAR recorder.

The entire assembly was mounted on the table of an AO Spencer No. 3670 spectrometer in such a fashion that it could be raised out of the light path by a chain and pulley arrangement. The movement was necessary for setting the instrument for the undeviated ray.

Density measurements were made using the well-known sinker method. The basic apparatus has been described elsewhere.[10] The method was modified slightly for this study to work with smaller samples and to permit more efficient blanketing with dry HP nitrogen. The refractive index measurements were also performed with the melt blanketed with dry HP nitrogen. This was achieved by appropriately placed bubblers and gas-supply tubes in the furnace well and prism.

The wavelengths of light used were (i) blue-violet line of mercury (435.8 mμ), (ii) green line of mercury (546.1 mμ), and (iii) yellow line of sodium (589.0 mμ). The appropriate elemental lamps were used as sources.

The aqueous solutions were prepared in a flask fitted with a mechanical stirrer and immersed in a constant-temperature water bath. The solubility of the thiocyanates was determined by titration with a standard $AgNO_3$ solution using 0.2–0.5 *M* HNO_3 containing a few drops of ferric ammonium sulfate as indicator.[11]

The refractive indices are accurate to ±0.0002 and the densities to ±0.001 g/cc. These errors lead to a maximum error of ±0.02 cc mole^{-1} in the calculated molar refractions reported below.

Results

The refractive indices (η) and densities (ρ) of the systems studied are a linear function of temperature over the ranges examined and are, therefore, presented in the form of equations determined by least-squares calculations

$$\eta = \eta_0 - at$$

$$\rho = \rho_0 - bt$$

where η_0, ρ_0, a, and b are empirically defined constants and t is the temperature in degrees centigrade. Tables I–V summarize data pertaining to alkali metal nitrates, their eutectics, alkali halide additions to $NaNO_3$, KNO_3, (Li, K)NO_3 eutectic, (Na, K)NO_3 eutectic, and KNCS, NaNCS, and their mixtures.

The maximum concentrations of added halide are

(9) F. W. Sears and M. W. Zemansky, "University Physics," 2nd ed, Addison Wesley Publishing Co., Inc., Reading, Mass., 1955, p 736.

(10) P. Papaioannou and G. W. Harrington, *J. Phys. Chem.*, **68**, 2424 (1964).

(11) I. M. Kolthoff and E. B. Sandell, "Text Book of Quantitative Inorganic Analysis," 3rd ed, The Macmillan Co., New York, N. Y., 1952, pp 455, 456.

Table I: Refractive Index and Molar Refraction of Nitrates and Thiocyanates

Melt	Refractive index: Blue-violet line η_0	Blue-violet line $a \times 10^4$, deg^{-1}	Green line η_0	Green line $a \times 10^4$, deg^{-1}	Yellow line η_0	Yellow line $a \times 10^4$, deg^{-1}	Molar refraction, Yellow line, cc mole^{-1}
$LiNO_3$ (270–380°)	1.5215	1.25	1.5070	1.26	1.5039	1.26	10.95 (375°)
$NaNO_3$ (320–384°)	1.4885	1.47	1.4742	1.44	1.4709	1.43	11.52 (375°)
KNO_3 (345–410°)	1.4826	1.62	1.4693	1.58	1.4677	1.61	13.51 (375°)
KNCS (180–200°)	1.6092	1.68	1.5940	1.91	1.5893	1.87	19.61 (190°)
NaNCS (315–345°)	...	...	...	...	1.6287	1.87	...
(Na, K)NCS (145–345°)	1.6324	2.40	1.6082	2.16	1.6060	2.30	18.71 (190°)

Table II: Refractive Index, Density, and Molar Refraction of Alkali Halide Additions to Nitrates

	Mole % of alkali halide	Refractive index: Blue-violet line η_0	Blue-violet line $a \times 10^4$, deg^{-1}	Green line η_0	Green line $a \times 10^4$, deg^{-1}	Yellow line η_0	Yellow line $a \times 10^4$, deg^{-1}	Density ρ_0, g cc^{-1}	Density $b \times 10^4$, g cc^{-1} deg^{-1}	Molar refraction 375°, Yellow line, cc mole^{-1}
$NaNO_3$ (320–410°)	3.0 LiCl	...	...	...	...	1.4760	1.45	2.147	7.97	11.51
	5.0	1.4930	1.42	1.4790	1.40	1.4709	1.55	2.122	7.37	11.44
	8.0	1.4959	1.42	1.4796	1.35	1.4771	1.38	2.108	7.12	11.34
	5.0 NaCl	1.4901	1.45	1.4769	1.45	1.4752	1.49	2.135	7.27	11.36
	8.0	1.4899	1.33	1.4750	1.29	1.4761	1.41	2.152	7.88	11.37
	10.0	1.4916	1.34	1.4727	1.21	1.4726	1.28	2.118	7.03	11.35
	3.0 KCl	1.4946	1.52	1.4771	1.42	1.4730	1.39	2.141	7.58	11.56
	5.0	1.4918	1.42	1.4793	1.44	1.4775	1.47	2.122	7.13	11.59
	8.0	1.4923	1.43	1.4778	1.40	1.4751	1.40	...	...	...
KNO_3 (340–420°)	3.0 LiCl	...	...	...	...	1.4702	1.57	2.070	6.61	13.54
	5.0	1.4846	1.51	1.4697	1.44	1.4709	1.55	2.085	7.07	13.44
	8.0	1.4868	1.52	1.4762	1.56	1.4754	1.63	2.096	7.48	13.28
	3.0 NaCl	1.4895	1.70	1.4731	1.59	1.4713	1.61	2.113	7.50	13.52
	5.0	1.4885	1.62	1.4732	1.53	1.4732	1.60	2.119	7.70	13.49
	8.0	1.4922	1.72	1.4769	1.63	1.4750	1.64	...	...	...
	5.0 KCl	1.4813	1.53	1.4692	1.53	1.4661	1.52	2.106	7.37	13.49
	8.0	1.4866	1.58	1.4721	1.52	1.4705	1.55	2.113	7.60	13.49
	10.0	1.4869	1.57	1.4729	1.52	1.4705	1.53	2.110	7.56	13.44

believed to be representative of the limits of solubility, for the temperature ranges studied, as evidenced by no significant change in refractive index on subsequent additions. Literature values of density were used for the pure salts and the (Li, K)NO_3 eutectic.[12,13]

Discussion

A. Molar Refractions. The molar refractions (R) of the melts were calculated by the usual Lorentz–Lorenz relation.[14] In the case of mixtures, the molecular weight, M, is given by $M = \sum x_i M_i$, where x_i and M_i are the mole fraction and molecular weight of the ith component. The calculated molar refractions for the yellow line are included in Tables I–V. In the last column of Tables III and IV are also listed the molar refractions (R') for the mixtures assuming the rule of mixtures holds, *i.e.*, the molar refractions calculated as

$$R' = \sum x_i R_i$$

where x_i and R_i refer to the mole fraction and molar refraction for the ith component.

The molar refractions are reported for specific tem-

(12) G. J. Janz, A. T. Ward, and R. D. Reeves, "Molten Salt Data," Rensselaer Polytechnic Institute, Troy, N. Y., 1964.

(13) M. Goffman, Ph.D. Thesis, Temple University, 1965.

(14) "Physical Methods of Organic Chemistry," Vol. I, Part II, A. Weissberger, Ed., Interscience Publishers, Inc., New York, N. Y., 1960, Chapter 18.

Table III: Refractive Index, Density, and Molar Refraction of Nitrate Eutectics (Yellow Line)

Melt	Refractive index: η_0	Refractive index: $a \times 10^4$, deg^{-1}	Density: ρ_0, g cc^{-1}	Density: $b \times 10^4$, g cc^{-1} deg^{-1}	Molar refraction: R, cc mole^{-1}	Molar refraction: R', cc mole^{-1}
(Li, Na)NO_3 (245–345°)	1.4879	1.32	2.015	6.26	11.20 (320°)	11.18
(Li, K)NO_3 (155–255°)	1.4844	1.60	1.949	7.0 (t − 160)[a]	12.27 (200°)	
(Na, K)NO_3 (255–345°)	1.4726	1.61	2.129	7.57	12.60 (345°)	12.56

[a] See ref 13.

Table IV: Refractive Index, Density, and Molar Refraction of Alkali Halide Addition to Nitrate Eutectics (Yellow Line)

Eutectic	Mole % alkali halide	Refractive index: η_0	Refractive index: $a \times 10^4$, deg^{-1}	Density: ρ_0, g cc^{-1}	Density: $b \times 10^4$, g cc^{-1} deg^{-1}	Molar refraction: R, cc mole^{-1}	Molar refraction: R', cc mole^{-1}
(Li, K)NO_3	8.0 LiCl	1.4890	1.64	2.074	8.25	11.93 (200°)	...
(155–255°)	8.0 NaCl	1.4855	1.59	2.094	8.38	11.94	...
	8.0 KCl	1.4851	1.60	2.088	8.11	12.11	...
	8.0 RbCl	1.4855	1.59	2.157	8.50	12.26	...
	8.0 CsCl	1.4901	1.67	2.244	9.69	12.43	...
(Na, K)NO_3	5.0 LiCl	1.4811	1.75	2.116	7.63	12.45 (340°)	12.49
(250–340°)	8.0 LiCl	1.4799	1.66	2.097	7.23	12.32	12.35
	5.0 NaCl	1.4746	1.58	2.121	7.54	12.49	12.46
	8.0 NaCl	1.4735	1.51	2.119	7.50	...	...
	5.0 KCl	1.4667	1.67	2.125	7.56	12.56	12.58
	8.0 KCl	1.4772	1.65	2.125	7.61	...	...

Table V: Refractive Index, Density, and Molar Refraction of NaNCS Additions to KNCS (145–200°) (Yellow Line)

Mole % NaNCS	Refractive index: η_0	Refractive index: $a \times 10^4$, deg^{-1}	Density: ρ_0, g cc^{-1}	Density: $b \times 10^4$, g cc^{-1} deg^{-1}	Molar refraction R, cc mole^{-1}
10.0	1.5956	2.04	1.7284	6.86	19.25 (190°)
20.0	1.6013	2.12	1.7115	5.95	19.04
30.0	1.6060	2.30	1.7195	6.23	18.71
50.0	1.6102	1.94	...	...	...
80.0	1.6271	2.09	...	...	...
100.0	1.6287	1.87	...	...	...

peratures. Although expected to be independent of temperature, the molar refraction does increase slightly (approximately 0.02–0.05 cc mole^{-1}/50°) with rise in temperature. This has been observed by others.[1-3] R' is thus calculated only for systems in which the components were studied at temperatures comparable to those of the mixtures.

Taking the case of alkali halide additions to $NaNO_3$, Table II, it is seen that for LiCl additions there is a distinct decrease in molar refraction with increasing concentration of LiCl; for NaCl additions the value is lower than that for pure $NaNO_3$ but to a lesser extent, while for KCl additions there is a slight increase in molar refraction. The added alkali halide has a different molar refraction than $NaNO_3$ and makes a different contribution toward the total molar refraction and it is the sum of the contributions of the two components which equals the calculated value. This is confirmed by the values of molar refraction for fused LiCl, NaCl, and KCl as determined by Zarzycki and Nandin.[3] The reported values for the green line of mercury are 8.32–8.41, 9.65–9.71, and 11.75–11.85 cc mole^{-1} for LiCl, NaCl, and KCl, respectively. (Assuming continuance of the liquid state, these values would probably be 0.1–0.2 cc mole^{-1} lower at the temperatures of the nitrate solutions.)

If the behavior of these alkali halides as solutes in the fused nitrates was similar to their behavior in the pure molten state, then the contribution of a certain mole per cent of LiCl toward molar refraction is the least among the three alkali halides and is less than that of $NaNO_3$. This explains the lowest values obtained for LiCl additions. In the same way, since the molar refraction of molten KCl is highest among the three alkali halides and higher than that of $NaNO_3$, slightly higher values for KCl additions are justified. Similar arguments explain the molar refraction values for alkali halide additions to KNO_3.

The molar refraction values of alkali nitrate eutectics are given in Table III and a comparison of the experimental values with those calculated from the rule of mixtures as given in the last column of the table supports the same assumption in the case of nitrate mixtures.

The results of molar refractions of 8 mole %, additions of LiCl, NaCl, KCl, RbCl, and CsCl to (Li, K)NO_3 eutectic as presented in Table IV also point in the same direction. The molar refraction of the eutectic is 11.27 cc mole^{-1}; for the LiCl addition it is 11.93 and then increases through the CsCl addition, being almost equal to that of the eutectic at the RbCl addition. That the RbCl mixture has the same molar refraction as the eutectic itself can be explained on the basis of the rule of the mixtures if the molar refraction of RbCl as solute is equal to that of the eutectic. Although we do not at present know the exact value of the molar refraction of RbCl, a glance at the values of LiCl, NaCl, and KCl as reported by Zarzycki and Nandin[3] mentioned earlier in this paper would indicate that the molar refraction of RbCl could fall around 12.5 cc mole^{-1}, which is not much different from 12.27.

The results of LiCl, NaCl, and KCl additions to (Na, K)NO_3 eutectic as given in Table IV justify the additive character of molar refraction in the case of these three-component systems as well.

To see if the same rule holds in case of thiocyanates, the values of molar refraction of KNCS and its mixtures containing 10, 20, and 30 mole % NaNCS were plotted *vs.* mole % NaNCS. An almost linear graph (Figure 1) was obtained. Mixtures with higher than 30 mole % NaNCS and pure NaNCS were found to undergo slow decomposition above their melting points. This did not interfere with refractive index measurements since small quantities of melt were required and temperature equilibration was rapidly attained, but the density measurements could not be performed satisfactorily by the method used and the presence of the platinum bob appeared to enhance the decomposition rate. An extrapolation by a least-square calculation of the above straight-line graph to 100 mole % NaNCS gave a value of 16.5 cc mole^{-1} for the molar refraction of NaNCS.

The rule of mixtures for melts appears quite reasonable if the components do not cause any additional interactions like the formation of complex ions or new kinetic species. In a mixture of, say, two salts, M_1X_1 and M_2X_2, the environment of X_2 is altered by the presence of M_1 causing a certain change in molar refraction of M_2X_2 in a direction depending upon the charge density of M_1 compared to that of M_2, but simultaneously the environment of X_1 is changed by the

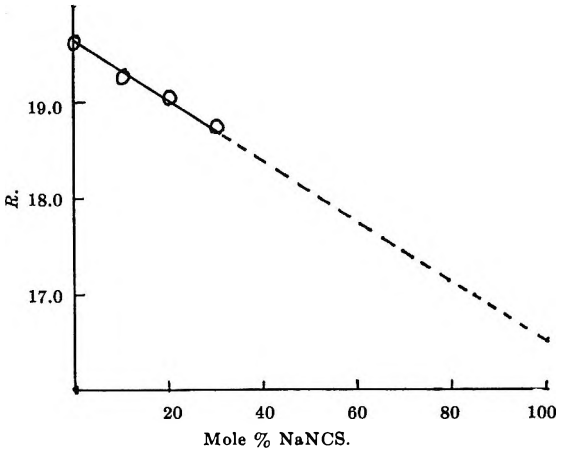

Figure 1. Molar refraction *vs.* mole % NaNCS in (Na, K)NCS mixtures.

closeness of M_2 and the molar refraction of M_1X_1 changes in a direction opposite to that of M_2X_2 resulting in no net change in total molar refraction of the mixture. That is, the mixture behaves from the molar refraction point of view as if the ions of the two components did not influence each other.

B. Polarizabilities and Ionic Radii. Since molar refraction for light of infinite wavelength (R_∞) is related to the polarizability (α) of the compound as $R_\infty = {}^4/_3\pi N\alpha$ we can calculate α if we know R_∞. To obtain the value of R_∞ for a particular compound we have used the following expression[14] (for the dispersion) originating from classical electromagnetic theory and applicable to normal dispersion not too close to absorption bands

$$\phi = \frac{\eta_\lambda^2 - 1}{\eta_\lambda^2 + 2} = \sum \frac{C_i}{(\gamma_0)_i^2 - \gamma^2}$$

where η_λ is the refractive index for a particular wavelength λ, C_i is a constant related to transition probabilities, $(\gamma_0)_i$ is a characteristic frequency related to the frequency of light absorption, and γ is the frequency of the light used. If it is assumed, as it is found to hold in practice, that for colorless compounds only one term out of $C_i/[(\gamma_0)_i^2 - \gamma^2]$ contributes to dispersion, the above relationship reduces to

$$\phi = \frac{\eta_\lambda^2 - 1}{\eta^2 + 2} = \frac{C}{\gamma_0^2 - \gamma^2}$$

or

$$\frac{1}{\phi} = \frac{\gamma_0^2}{C} - \frac{1}{C}\gamma^2$$

That is, a plot of $1/\phi$ *vs.* γ^2 should give a straight line,

as it does, especially for colorless compounds in the visible region of the spectrum.

This procedure has been adopted in the present case and the value of $1/\phi$ extrapolated to infinite wavelength is obtained. From the value of $1/\phi_\infty$, the corresponding $R_\infty = \phi_\infty(M/\rho)$ is calculated.

The polarizability of a compound is a measure of its molecular volume and in the case of ionic compounds, as fused salts are, it is equal to the sum of the volumes of the cation and the anion constituting the compound. In the phenomenon of refraction of light it is the loosely bound (called active) electrons of the ions which play a prominent role. Since the electrons of the cation are very firmly held owing to the positive charge and the opposite holds in the case of the anion, it is the latter ion which makes the principal contribution to the molar refraction. There is no way as yet known to ascertain what fraction of the total refraction of an ionic compound is due to the cation. Pauling[15] has calculated on theoretical grounds the molar refraction of Li^+ ion as 0.1 cc mole^{-1}. Subtracting this from the molar refraction of $LiNO_3$ for infinite wavelength, R_∞ for NO_3^- ion comes out to be 10.41 cc mole^{-1} and α is calculated to be 4.13×10^{-24} cm^3.

Knowing α, the radius of the nitrate ion is calculated as $\alpha = \gamma^3$ or $\gamma_{NO_3^-} = \sqrt[3]{\alpha_{NO_3^-}} = \sqrt[3]{4.13 \times 10^{-24}} = 1.60$ A.

Considering the molar refractive values at infinite wavelength of NO_3^-, KNO_3, and KNCS and by appropriate addition and subtraction, R_∞ for NCS^- ion is 16.21 cc mole^{-1}. This gives the values for the polarizability and radius of NCS^- ion as 6.43×10^{-24} cm^3 and 1.86 A, respectively.

The above values for radii of NO_3^- and NCS^- ions are in reasonable agreement with the over-all radii calculated from consideration of the reported covalent bond lengths and ionic sizes.[16,17] The nitrate radius is, however, smaller than the thermochemical radius.[18]

C. Characteristic Absorption Frequencies. Molar refraction is related to the frequencies of the high-energy absorption bands and the number of electrons in the molecule of the compound through the relation[3,4,8]

$$R = \frac{Ne^2}{3\pi\mu}\left(\frac{p_1}{\gamma_1^2 - \gamma_L^2} + \frac{p_2}{\gamma_2^2 - \gamma_L^2}\right)$$

where N is Avogadro's number, e and μ are the charge and mass of the electron, p_1 and p_2 are the numbers of the active and the remaining electrons, τ_L is the frequency of light used for refractive index measurements, and γ_1 and γ_2 are the fundamental frequencies of the absorption bands. In the case of ionic compounds, p_1 and p_2 refer to the electrons of the anion alone.

If one considers the NO_3^- ion as a planar and symmetrical structure[19] with sp^2 hybridization of the nitrogen atom and delocalization of the electrons involved in N–O bonds, then there are three active electrons. With $p_1 = 3$ and $p_2 = 29$ and the use of the values of R for the blue-violet and yellow lines for $LiNO_3$, $NaNO_3$, and KNO_3, we have calculated γ_1 and γ_2 for the nitrate ion. These values appear in Table VI.

Table VI: Absorption Frequencies for Nitrates and Thiocyanates

	γ_1, mμ	γ_2, mμ
$LiNO_3$	126.1	19.6
$NaNO_3$	123.9	23.6
KNO_3	129.9	27.4
KNCS	135.4	34.8
NaNCS	134.0	25.0

Similarly, the linearity of the NCS^- ion[20] and supposition of sp hybridization for the carbon atom give $p_1 = 4$ and $p_2 = 26$ for this ion. Utilizing these values and also the molar refraction values of KNCS for the blue-violet and yellow lines, γ_1 and γ_2 were calculated and are given in Table VI.

If the extrapolated value for molar refraction of NaNCS for the yellow line is accepted as correct and it is assumed that its molar refraction for the blue-violet line differs to the same extent as does that of KNCS, R for NaNCS for the blue-violet line is 17.2 cc mole^{-1}. The values of γ_1 and γ_2 thus calculated for NaNCS are also reported in Table VI.

Our values of γ_1 and γ_2 for nitrates have the same order of magnitude as those reported by Zarzycki and Nandin.[3,4] For thiocyanates γ_1 is nearly 135 mμ and γ_2 is about 30 mμ. It appears that the magnitude of γ_1 is not much influenced, but that of γ_2 is, by the nature of the cation.

(15) K. Fajans, *Z. Physik. Chem.* (Frankfurt), 24, 103 (1934).

(16) F. A. Cotton and G. Wilkinson, "Advanced Inorganic Chemistry," Interscience Publishers, Inc., New York, N. Y., 1962, p 93.

(17) E. A. Moelwyn-Hughes, "Physical Chemistry," Pergamon Press Ltd., Oxford, England, 1961, Chapters XI, XII, and XX.

(18) C. G. S. Phillips and R. J. P. Williams, "Inorganic Chemistry," Vol. I, Oxford University Press, New York, N. Y., 1965, p 158.

(19) N. Elliot, *J. Am. Chem. Soc.*, 59, 1380 (1937).

(20) Z. V. Zvonhova, *Zh. Fiz. Khim.*, 26, 1798 (1953).

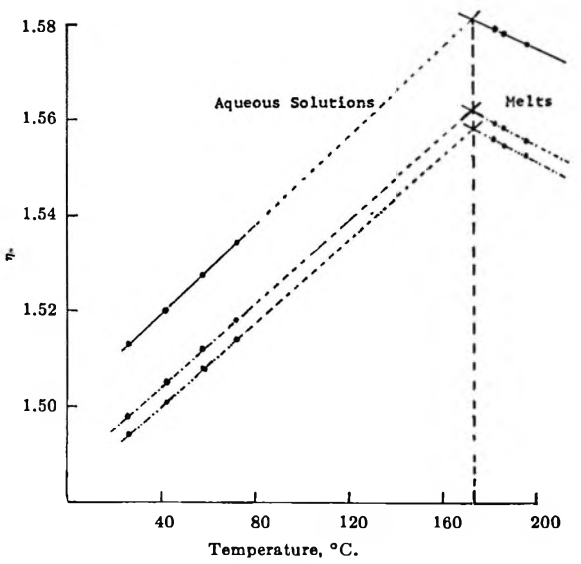

Figure 2. Refractive index *vs.* temperature for molten KNCS and its saturated aqueous solutions: ———, blue-violet line; — · —, green line; —· ·—, yellow line.

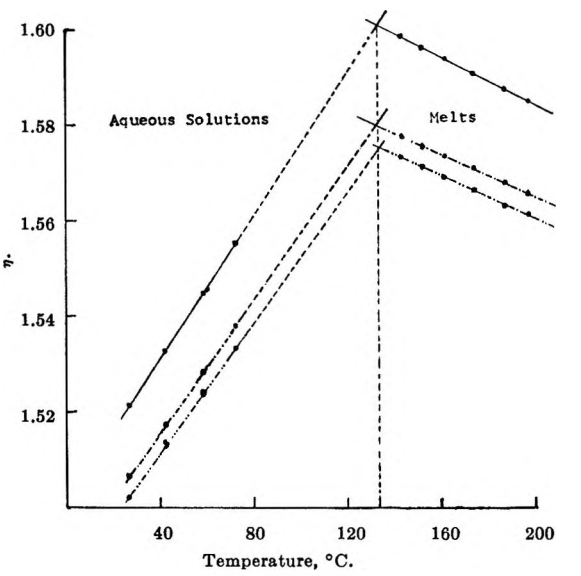

Figure 3. Refractive index *vs.* temperature for molten (Na, K)NCS eutectic and its saturated aqueous solutions: ———, blue-violet line; — · —, green line; —· ·—, yellow line.

D. Aqueous Solutions. Because of the relatively high aqueous solubility of KSCN, the refractive properties of saturated aqueous solutions of pure KSCN and KSCN–NaSCN eutectic were examined for any similarities between such solutions and the melts. The rather interesting results are shown in Figures 2 and 3. The solubilities and approximate densities are given in Table VII. The latter were determined by weighing a known volume taken from the saturating vessel at the temperature indicated. It will be noticed that in each case the extrapolated intercept of the aqueous solution and melt plots occurs at the melting point of the salt and eutectic. Other saturated aqueous solutions were studied involving salts used in this study and by others.[1] A similar linear type of relationship could not be found.

In theory, one would expect such plots to intercept at the melting point, but our study suggests that aqueous solutions of alkali nitrates and nitrites would show considerable curvature at higher temperatures.

Table VII

	KSCN		KSCN–NaSCN	
Temp, °C	Solubility, g/g of H_2O	Density, g/cc	Solubility, g/g of H_2O	Density, g/cc
26.5	2.41 ± 0.01	1.45 ± 0.02		
27.0			2.48 ± 0.01	1.45 ± 0.02
42.0	2.84	1.47	3.02	1.48
57.0	3.47	1.49		
57.5			4.02	1.51
72.0	4.28	1.51	5.28	1.55

The linearity in the case of the thiocyanates may merely be the result of a fortuitous combination of effects.

Acknowledgment. This work was partially supported by funds granted by the Wagner Free Institute, Philadelphia, Pa.

The γ Radiolysis of Liquid 2-Propanol. III.[1] Chain Reactions in Alkaline Solutions Containing Nitrous Oxide

by Warren V. Sherman[2]

Soreq Nuclear Research Centre, Yavne, Israel *(Received September 8, 1966)*

A study has been made of the γ radiolysis of solutions of potassium hydroxide and nitrous oxide in 2-propanol. The major products identified were nitrogen, methane, acetone, and potassium acetate. The exceptionally high product yields ($G(N_2) > 10^3$ was observed) indicate a chain mechanism. Yields were determined as a function of dose, dose rate, and concentrations of potassium hydroxide and nitrous oxide. The observed dependence of yields on the reciprocal of the square root of the dose rate is consistent with bimolecular termination being of major importance. The yields were independent of the potassium hydroxide concentration when $[KOH] > 2 \times 10^{-2}$ M, but were proportional to the concentration of nitrous oxide. Large yields of hydrogen ($G(H_2) \simeq 20$) were noted at certain nitrous oxide concentrations. Evidence is presented to support the suggestion that the 2-propoxide radical anion (I) is the chain carrier and that the propagation steps for the formation of nitrogen and acetone involve the reactions

$$Me_2\dot{C}O^- \text{ (I)} + N_2O \longrightarrow Me_2CO + N_2 + O^-$$

$$O^- + Me_2CHOH \longrightarrow OH^- + Me_2\dot{C}OH$$

$$Me_2\dot{C}OH + Me_2CHO^- \longrightarrow I + Me_2CHOH$$

Inhibition and retardation of the chain reaction was observed in the presence of a number of organic solutes.

Introduction

A preliminary study of the radiolysis of 2-propanol solutions containing potassium hydroxide and nitrous oxide has been published recently.[3] This present report is concerned with a more complete study of the observed chain reactions.

Experimental Section

2-Propanol (Eastman Spectrograde) and nitrous oxide (Matheson) were purified as described previously.[4] Potassium hydroxide (Baker reagent) was used without further purification. (It was stated by the manufacturers to contain 1.7% K_2CO_3.) All other solutes were of reagent grade and used as received.

Standard solutions of the solutes were prepared, and aliquots (2 ml) were placed in Pyrex reaction vessels consisting of a 20-mm diameter tube fitted with a break-seal and standard-taper joint. The solutions were then thoroughly degassed and nitrous oxide was added; the vessels were sealed and irradiated as described previously.[4] Unless otherwise stated, a period of at least 10 hr was allowed to elapse between removal from the cobalt source and product analysis. Gaseous products volatile at liquid-air temperature (H_2, N_2, CH_4, and CO) were analyzed by gas chromatography on a 2-m column of Molecular Sieve 5A (Linde) at room temperature. Helium was the carrier. The detector consisted of 8-K thermistors (Gow-Mac) and was maintained at 0° by submerging in an ice–water bath. (The author is grateful to Dr. Miguel Wernick for invaluable advice in constructing the gas chroma-

(1) Part II: W. V. Sherman, *J. Phys. Chem.*, **70**, 2872 (1966).

(2) The Radiation Laboratory, University of Notre Dame, Notre Dame, Ind. 46556.

(3) W. V. Sherman, *Chem. Commun.*, 250 (1966).

(4) W. V. Sherman, *J. Phys. Chem.*, **70**, 667 (1966).

tograph.) The relative response of the detector to H_2, N_2, CH_4, and CO was 1:25:24:24. It was not possible to detect H_2 in an excess of N_2 when the former was present at a concentration of less than 1 part/hundred. Thus, when $G(N_2) = 10^3$, the lower limit of detection was $G(H_2) = 10$. Acetone was identified and analyzed on an F & M Model 810 gas chromatograph. The column used was 10% Carbowax 20M on Chromosorb S. Potassium acetate was analyzed as acetic acid on a Perkin-Elmer Fraktometer. The column ("BA") contained a mixture of di-2-ethylhexyl sebacinate and sebacic acid. The irradiated solution from a typical experiment in which considerable yields of gaseous products occurred was injected onto the column. Either no peak or a small peak corresponding to acetic acid was observed. The solution was then acidified with hydrochloric acid and injected again. In all cases a considerable increase in peak size was found. These observations are consistent with the formation of acetic acid from potassium acetate on acidification with hydrochloric acid.

The Co^{60} source used in most of the experiments was a Gammacell 200 (Atomic Energy of Canada, Ltd.). The dose rate received by 2-propanol solutions was 3.6×10^{17} ev ml^{-1} min^{-1}. By placing the reaction vessels in a cylindrical lead shield the dose rate was reduced to 7.2×10^{16} ev ml^{-1} min^{-1}. The other two dose rates were obtained with the Co^{60} source in the pool of the Israel Research Reactor I.

Results

The products identified in the radiolysis of solutions of potassium hydroxide and nitrous oxide with doses in the range 2×10^{16} to 1×10^{18} ev ml^{-1} were nitrogen, methane, acetone, and potassium acetate. No attempt was made to analyze the last named quantitatively. Hydrogen, identified as a reaction product previously at higher doses,[3] was observed only at certain nitrous oxide concentrations (see below). No change in the nature and yields of the chain products was noted when potassium 2-propoxide or sodium hydroxide was substituted for potassium hydroxide. However, when the latter was replaced by 5×10^{-2} *M* ammonia or a saturated solution of potassium chloride, no chain reaction was observed.

1. Effect of Dose and Dose Rate. The yields of nitrogen, methane, and acetone are set out in Table I. At a dose rate of 7.2×10^{16} ev ml^{-1} min^{-1} the yield of all three products remained essentially constant over the range $(1.2\text{–}2.4) \times 10^{17}$ ev ml^{-1}. At lower doses an increase of yield with dose may be observed, while rapidly decreasing yields with dose occurred at higher doses. For a given total dose [$(2.1\text{–}2.2) \times 10^{17}$ ev ml^{-1}] the yields decreased with increasing dose rate. No hydrogen was detectable in these runs.

Table I: Radiolysis of Solutions of Potassium Hydroxide and Nitrous Oxide in 2-Propanol. Yields as a Function of Dose and Dose Rate[a]

Dose rate $\times 10^{-16}$, ev ml^{-1} min^{-1}	Dose $\times 10^{-16}$, ev ml^{-1}	$10^{-1}G(N_2)$	$10^{-1}G(CH_4)$	$10^{-1}G((CH_3)_2CO)$
7.2	2.4	2.24	0.76	...
7.2	3.7	2.70	1.95	3.0
7.2	7.3	2.88	1.77	2.3
7.2	12	3.33	2.30	2.3
7.2	18	3.40	2.30	2.5
7.2	22	3.35	2.25	2.9
7.2	24	3.33	2.35	2.6
7.2	29	2.85	1.87	2.2
7.2	44	1.70	0.74	2.6
7.2	122	1.66	1.27	1.2
0.15	21	10.6	7.25	7.5
0.30	21	7.70	4.85	5.6
36	22	2.00	1.26	1.6

[a] [KOH] = 5×10^{-2} *M*; [N_2O] = 5×10^{-2} *M*.

2. Effect of the Variation of the Initial Concentrations of Potassium Hydroxide and Nitrous Oxide. A series of radiolyses was carried out in which the initial concentration of nitrous oxide was kept constant (5×10^{-2} *M*) and potassium hydroxide varied (Table II, Figure 1). With 5×10^{-4} *M* potassium hydroxide the yields were similar to that observed in the absence of potassium hydroxide.[4] As the concentration was increased, the yields increased rapidly, reached limiting values at about 2×10^{-2} *M*, and then remained relatively insensitive to further increases in the concentration of potassium hydroxide. The profile (Figure 1) has a shape similar to that observed previously at a higher dose and dose rate.[3] However, the limiting values for $G(N_2)$ and $G(CH_4)$ (3.5×10^3 and 2.3×10^2, respectively) are significantly higher than observed previously (1.6×10^3 and 1.0×10^2, respectively).

With the initial concentration of potassium hydroxide kept constant (5×10^{-2} *M*), yields were observed to increase proportionally with increasing concentration of nitrous oxide (Figure 2). The slope of the yield *vs.* [N_2O] plot was unaffected by a fivefold increase in dose rate though the actual yields were decreased considerably.

In the majority of runs it was not possible to detect hydrogen as a reaction product. However, in three cases (see Table II) exceptionally large yields of hydrogen were noted.

Table II: Radiolysis of Solutions of Potassium Hydroxide and Nitrous Oxide in 2-Propanol. Yields as a Function of the Concentration of the Two Solutes[a]

10^{-17} × dose rate, ev ml^{-1} min^{-1}	[KOH], mM	[N_2O], mM	$G(N_2)$	$G(CH_4)$	$G((CH_3)_2CO)$
0.72	0.50	50	2.92[b]	1.40	...
0.72	0.80	50	3.02×10^2	2.28×10	...
0.72	1.0	50	3.73×10^2	2.30×10	2.5×10^2
0.72	2.0	50	1.25×10^3	5.90×10	1.1×10^3
0.72	5.0	50	2.60×10^3	1.76×10^2	1.9×10^3
0.72	10	50	2.96×10^3	1.96×10^2	2.2×10^3
0.72	25	50	3.62×10^3	2.36×10^2	2.5×10^3
0.72	50	50	3.35×10^3	2.25×10^2	2.9×10^3
0.72	180	50	3.67×10^3	2.21×10^2	3.1×10^3
0.72	50	0.50	5.80×10	~ 5	...
0.72	50	1.0	1.25×10^2	8.40	1.0×10^2
0.72	50	2.5	2.74×10^2	2.00×10	2.5×10^2
0.72	50	5.0	5.17×10^2[c]	3.30×10	4.4×10^2
0.72	50	10	1.04×10^3[d]	4.80×10	7.9×10^2
0.72	50	100	6.30×10^3	4.51×10^2	4.7×10^3
0.72	50	200	7.13×10^3	5.13×10^2	5.3×10^3
3.6	50	1.0	7.01×10	...	...
3.6	50	2.5	1.27×10^2[e]	9.30	1.3×10^2
3.6	50	5.0	4.27×10^2[f]	3.30×10	4.0×10^2
3.6	50	10	5.00×10^2[g]	3.35×10	4.1×10^2
3.6	50	50	2.01×10^3	1.26×10^2	1.6×10^3
3.6	50	200	4.80×10^3	2.43×10^2	3.1×10^3

[a] Dose = 2.2×10^{17} ev ml^{-1}. [b] Dose = 6.6×10^{17} ev ml^{-1}; $G(H_2) = 2.8$. [c–g] Hydrogen detected with G values of 5.5 ± 1.0, 23 ± 4, 11 ± 1, 21 ± 4, and 4.0 ± 1.0, respectively.

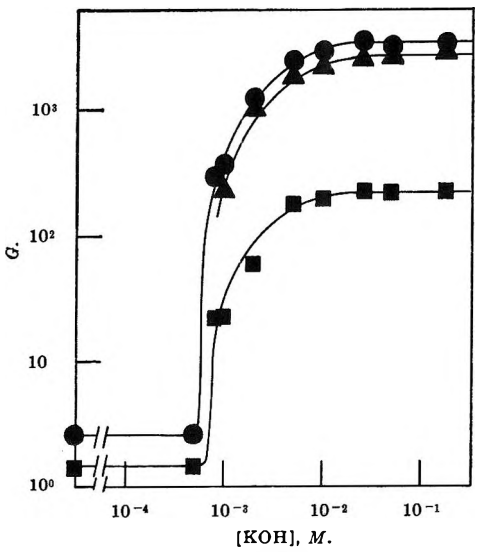

Figure 1. Product yields as a function of potassium hydroxide concentration. [N_2O] = 5×10^{-2} M; dose rate = 7.2×10^{16} ev ml^{-1} min^{-1}; dose = 2.2×10^{17} ev ml^{-1}: nitrogen, ●; acetone, ▲; methane, ■.

3. Postirradiation Yields. It was found that if an irradiated solution was plunged into liquid air immediately on removal from the cobalt source and kept at this temperature until product analysis, the yields of gaseous products were considerably less than that obtained from a solution which had been allowed to stand at room temperature for a period of time prior to freezing for the analysis of gaseous products. Additional but diminishing amounts of the latter could be recovered on subsequent thaw–freeze cycles while the reaction vessel was still attached to the vacuum line. A typical run is shown in Table III. The total yields of nitrogen and methane recovered in these runs were

Table III: Radiolysis of Solutions of Potassium Hydroxide and Nitrous Oxide in 2-Propanol. Postirradiation Yields[a]

Thawing interval no.	Time thawed, min	"$G(N_2)$"	"$G(CH_4)$"
...	...	2.16×10^3	1.41×10^2
1	3.0	9.20×10^2	7.10×10
2	3.0	1.91×10^2	1.34×10
3	3.0	4.50×10	6.9
4	30	$<9.0 \times 10$	...

[a] [KOH] = 5×10^{-2} M; [N_2O] = 5×10^{-2} M; dose rate = 7.2×10^{16} ev ml^{-1} min^{-1}; dose = 2.2×10^{17} ev ml^{-1}.

Table IV: Solute Effects in the Radiolysis of Solutions of Potassium Hydroxide and Nitrous Oxide in 2-Propanol[a]

[Solute], M		10^{-17} × dose rate, ev ml^{-1} hr^{-1}	10^{-17} × dose, ev ml^{-1}	G(gas)	$G(H_2)$	$G(N_2)$	$G(CH_4)$
Benzene	5.0×10^{-2}	3.6	11[b]	1.6×10^3	...	1.49×10^3	1.03×10^2
Benzene	2.5×10^{-1}	3.6	11[b]	9.1×10^2	4.5	8.50×10^2	5.40 × 10
Nitrobenzene	5.0×10^{-5}	0.72	2.2	4.5	...	...	...
Nitrobenzene	5.0×10^{-3}	0.72	2.2	9.4	...	...	...
Nitrobenzene	5.0×10^{-2}	3.6	11[b]	6.2[c]	2.4	0.67	0.67
Nitrobenzene	2.5×10^{-1}	3.6	11[b]	4.7[d]	1.7	0.26	0.60
Benzophenone	5.0×10^{-2}	3.6	11[b]	9.5[e]	3.0	3.50	1.32
Acetone	1.0×10^{-3}	0.72	2.2	1.4 × 10	...	...	...
Acetone	5.0×10^{-3}	0.72	2.2	6.7	...	...	...
Carbon tetrachloride	5.0×10^{-3}	0.72	2.2	1.1×10^2	...	1.03×10^2	6.45
Carbon dioxide	5.0×10^{-2}	3.6	11[b]	6.6	2.9	2.60	1.06

[a] [KOH] = [N_2O] = 5.0×10^{-2} M. [b] Yields at this dose rate and total dose in the absence of solutes are $G(N_2) = 1.55 \times 10^3$ and $G(CH_4) = 1.03 \times 10^2$. [c–e] Carbon monoxide identified with G values of 2.50, 2.18, and 1.66, respectively.

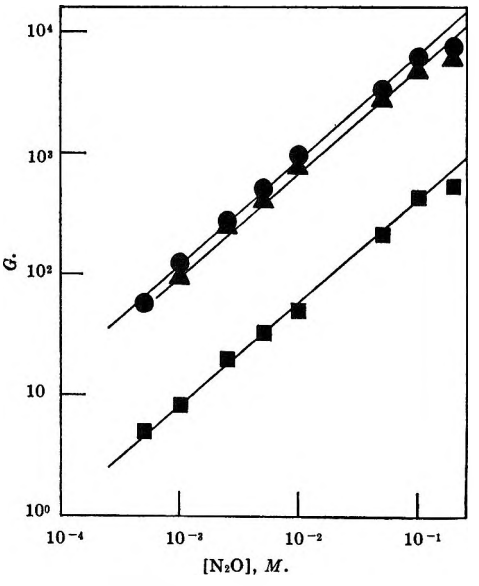

Figure 2. Product yields as a function of nitrous oxide concentration. [KOH] = 5×10^{-2} M; dose rate = 7.2×10^{16} ev ml^{-1} min^{-1}; dose = 2.2×10^{17} ev ml^{-1}: nitrogen, ●; acetone, ▲; methane, ■.

approximately equal to those obtained from solutions which had been allowed to stand at room temperature for several hours before analysis.

4. Effect of Organic Solutes. The presence of small concentrations of a number of organic solutes was found to retard and inhibit the formation of the chain products (Table IV). Of the solutes studied, only with benzene was a high concentration (>0.1 M) necessary to produce a significant diminution of the product yields. Carbon monoxide was identified in the presence of nitrobenzene (5×10^{-2} and 2.5×10^{-1} M) and benzophenone (5×10^{-2} M). Precipitation of potassium chloride was observed on prolonged irradiation of the solution containing carbon tetrachloride.

Discussion

In all of the experiments where the chain reaction was observed, the ratio of yields of nitrogen to methane remained essentially constant (14 ± 2). This ratio was also observed in the presence of benzene and carbon tetrachloride where the chain was retarded. The yields of nitrogen and acetone were always of the same order of magnitude, the latter being consistently 10–30% lower than the former. These constant product yield ratios are in accord with nitrogen and acetone having their origin in a common intermediate(s), and with the minor product methane (and presumably potassium acetate) originating in a side reaction. Two stoichiometric reactions (1 and 2) may then be written to describe the observed products.

$$N_2O + Me_2CHOH \longrightarrow Me_2CO + N_2 + H_2O \quad (1)$$

$$N_2O + Me_2CHOH \longrightarrow MeCO_2H + N_2 + CH_4 \quad (2)$$

The formation of an additional oxidation product derived from 2-propanol, *e.g.*, pinacol, could account for the inequality of nitrogen and acetone yields, but attempts to identify this product were unsuccessful.

The observation that the yields of nitrogen, methane, and acetone are proportional to the initial concentration of nitrous oxide (Figure 2) is consistent with the latter taking part in a rate-determining first-order propagation step. The lack of dependence of product yields on potassium hydroxide concentration (when [KOH] > 2×10^{-2} M) indicates that this solute

is not rate determining provided a minimal concentration is present. Since the chain reaction is observed only in strongly alkaline solution and not under acid or neutral conditions, it is evident that the chain carrier is not a protonated species or a neutral radical, but an anionic species.

A chain reaction involving 100-ev yields of nitrogen and acetone of up to 60 ev was noted in the radiolysis of alkaline aqueous solutions of nitrous oxide and 2-propanol.[5] It was proposed that the 2-propoxide radical anion (I) is the chain carrier in this reaction. By analogy, it is suggested that the chain carrier in 2-propanol solution is also I and that reactions 3–5 constitute the propagation steps for the major products nitrogen and acetone.

$$Me_2\dot{C}O^- \text{ (I)} + N_2O \longrightarrow Me_2CO + N_2O^- \longrightarrow N_2 + O^- \quad (3)$$

$$O^- \text{ (or } N_2O^-) + Me_2CHOH \longrightarrow OH^- \text{ (or } N_2 + OH^-) + Me_2\dot{C}OH \text{ (II)} \quad (4)$$

$$II + Me_2CHO^- \longrightarrow I + Me_2CHOH \quad (5)$$

The 2-propoxyl radical (II) may be formed in the radiolysis of 2-propanol solutions of nitrous oxide in three ways: (i) as a primary product (reaction 6), (ii) by the abstraction of the carbinol hydrogen atom of the solvent by other primary radicals, R (reaction 7), and (iii) by reaction 4 involving O^- produced by the reaction of solvated electrons with nitrous oxide (reaction 8). Since the pK_a of a radical is greater than that

$$Me_2CHOH \text{ —}\sim\!\!\rightarrow e_{sol}^- + R\cdot + \text{other products} \quad (6)$$

$$R\cdot + Me_2CHOH \longrightarrow RH + II \quad (7)$$

$$e_{sol}^- + N_2O \longrightarrow N_2O^- \longrightarrow N_2 + O^- \quad (8)$$

of the compound from which it has been derived by the loss of a hydrogen atom, the ionization of II in a solution containing 2-propoxide anions (reaction 5) should be particularly favorable. Reactions 5–8 may therefore be considered to constitute the initiation steps of the chain reaction.

In order to verify that the production of radicals in an alkaline solution of nitrous oxide in 2-propanol would lead to a chain reaction, *t*-butoxy radicals were generated photochemically by exposing solutions containing di-*t*-butyl peroxide to ultraviolet light from a high-pressure mercury lamp.[6] Large yields of nitrogen, methane, acetone, and potassium acetate were observed. The light-induced reaction closely paralleled the γ-ray reaction in four salient features: (i) the similarity between the yields of nitrogen and acetone; (ii) the constant ratio of the yields of nitrogen to methane (14 ± 2); (iii) the yield–[KOH] profile (at $[KOH] > 2 \times 10^{-2}$ *M* the product yields were independent of [KOH]); (iv) the product yields proportional to $[N_2O]$.

The observed retardation and inhibition of the chain reaction (Table IV) by solutes which are good electron acceptors is supporting evidence for a negatively charged species being an intermediate in the chain reaction. It has been shown[4] that nitrobenzene, benzophenone, acetone, and carbon tetrachloride compete effectively with nitrous oxide for solvated electrons. In addition, the reactivity of these compounds toward solvated electrons was determined to be of the same order of magnitude. The fact that the presence of only 5×10^{-5} *M* nitrobenzene completely inhibits the chain reaction indicates that inhibition is not solely at the initiation stage (competition with nitrous oxide for the solvated electron) but also involves an intermediate in one of the propagation steps. Competition between nitrous oxide and an electron acceptor S (reaction 9) for the electron of radical anion I is

$$I + S \longrightarrow Me_2CO + S^- \quad (9)$$

consistent with the experimental observations. Further support for the proposed mechanism is that benzene, a poor electron acceptor, has little effect on the product yields even when present at concentrations in excess of that of nitrous oxide.

It is noteworthy that the efficiency of carbon tetrachloride as an inhibitor is lower than that of nitrobenzene and acetone. Since the reactivity of carbon tetrachloride toward solvated electrons in 2-propanol is greater than that of acetone,[4] and not significantly less than that of nitrobenzene,[4] it is evident that while electron transfer from I to carbon tetrachloride is thermodynamically favorable, not every transfer occurrence (reaction 9) results in termination of the chain. A possible explanation is that the carbon tetrachloride anion is unstable and can dissociate to give a trichloromethyl radical (reaction 10). The latter can then initiate a new chain by abstracting the carbinol hydrogen of the solvent (reaction 11). Based on gas-phase data,

$$I + CCl_4 \longrightarrow Me_2CO + CCl_3\cdot + Cl^- \quad (10)$$

$$CCl_3\cdot + Me_2CHOH \longrightarrow CHCl_3 + II \quad (11)$$

reaction 10 might be expected to be endothermic, but in a solvent of relatively high dielectric constant such as 2-propanol the energy of solvation of the small chloride ion could be great enough to provide the driving

(5) G. Scholes, M. Simic, and J. J. Weiss, *Discussions Faraday Soc.*, **36**, 214 (1963).

(6) W. V. Sherman, *J. Am. Chem. Soc.*, **89**, 1302 (1967).

force for reaction 10. The observation of potassium chloride as a product is in agreement with dissociative electron capture by carbon tetrachloride.

If the foregoing mechanism is correct, then, in view of the fact that carbon tetrachloride can decrease the rate of reaction, it must be concluded that either the process leading to trichloromethyl radicals is less than 100% efficient, or combination reactions of the latter (*e.g.*, dimerization) compete favorably with the abstraction reaction 11.

The observation that the presence of small concentrations of acetone retard and inhibit the chain requires comment. Electron capture by acetone gives the same radical anion, I, which is the proposed chain carrier. Taken at face value, the effect of acetone would appear to be in conflict with the proposed mechanism for the chain reaction. However, acetone was found to have no measurable effect on the light-induced reaction initiated by di-*t*-butyl peroxide even when present in high concentration.[6] Since the γ-ray and light-induced reactions appear to differ only in their mode of initiation, it may be assumed that the apparently anomalous inhibition by acetone is due to its interaction with the initial steps of the chain. In the light-induced reactions initiation is *via* homogeneously produced reactive centers. In the early stages of the γ-ray reaction the reactive centers are not distributed homogeneously, but rather in areas of high concentration (spurs[7]). Acetone can act as a trap for the radiolytic radicals and negatively charged species. The resulting acetone radicals or radical anions may then undergo combination and charge neutralization reactions with the primary radicals and positive holes before they are able to diffuse away from the parent spurs. To sustain the chain, nitrous oxide must compete with these reactions. The fact that retardation and inhibition of the chain is observed in the presence of acetone indicates that the reaction of nitrous oxide with the acetone radical anion is slow compared with radical combination or charge-neutralization processes. Benzene, a good radical scavenger but poor electron scavenger, does not significantly retard the chain unless present at very high concentration. It may therefore be concluded that only charge transfer is important in inhibition by acetone.

The observed decrease in product yields with increasing dose on prolonged irradiation (Table I) is consistent with acetone formed as a reaction product acting as an inhibitor. The low yields at very low doses probably indicate the presence of an impurity which can terminate the chain but is rapidly consumed. The potassium hydroxide used in the experiments was contaminated with small amounts of potassium carbonate (see Experimental Section). The observed inhibition of the chain in the presence of added carbon dioxide indicates that this could be the cause of the low yields at low doses.

Mathematical analysis of the chain reaction using homogeneous steady-state kinetics is valid provided that the radiation spurs have a homogeneous distribution and that the lifetime of any particular spur is short compared with the average life of the chain centers between propagation steps. Assuming initiation by reactions 5–8 and propagation by reactions 3–5, then in the case of bimolecular termination[8–10]

$$\mathrm{I} + \mathrm{I} \xrightarrow{\mathrm{Me_2CHOH}} \mathrm{Me_2CO} + 2\mathrm{Me_2CHO^-} \qquad (12)$$

the yields of nitrogen and acetone are given by expressions A and B, where D is the dose rate, G_e the yield of electrons scavengeable by nitrous oxide, and G_R the yield of radicals R.

$$G(\mathrm{N_2}) = G_e + k_3[\mathrm{N_2O}]\left[\frac{G_e + G_R}{k_{12}D}\right]^{1/2} \qquad (A)$$

$$G(\mathrm{Me_2CO}) = G_e + G_R + k_3[\mathrm{N_2O}]\left[\frac{G_e + G_R}{k_{12}D}\right]^{1/2} \qquad (B)$$

For first-order termination by an impurity M, reac-

$$\mathrm{I} + \mathrm{M} \longrightarrow \mathrm{Me_2CO} + \mathrm{M^-} \qquad (13)$$

tion 13, the yields of nitrogen and acetone are given by expressions C and D.

$$G(\mathrm{N_2}) = G_e + \frac{k_3[\mathrm{N_2O}](G_e + G_R)}{k_{13}[\mathrm{M}]} \qquad (C)$$

$$G(\mathrm{Me_2CO}) = (G_e + G_R)\left[1 + \frac{k_3[\mathrm{N_2O}]}{k_{13}[\mathrm{M}]}\right] \qquad (D)$$

A straight line is obtained in a plot of $G(\mathrm{N_2})$ and $G(\mathrm{Me_2CO})$ *vs.* $(1/D)^{1/2}$ (Figure 3). This is consistent with bimolecular termination (reaction 12) being of major importance in the chain reaction. However, the positive intercept at $(1/D)^{1/2} = 0$ (*i.e.*, $D \rightarrow \infty$) indicates an additional first-order termination process. With a knowledge of k_{12} and $(G_e + G_R)$ it would be possible to obtain a value for k_3 from the slope of the $G(\mathrm{N_2})$ *vs.* $(1/D)^{1/2}$ plot. While an accurate figure for

(7) A. H. Samuel and J. L. Magee, *J. Phys. Chem.*, 21, 1080 (1953).

(8) The reaction between two identical ketyl radical ions has been written as giving the corresponding pinacol anion.[9] However, it has been pointed out[10] that, since a pinacol is not an observed product in this type of reaction, it is perhaps better to write it as a disproportionation reaction involving a simultaneous proton transfer from the solvent.

(9) A. Beckett and G. Porter, *Trans. Faraday Soc.*, 59, 2038 (1963).

(10) S. G. Cohen and W. V. Sherman, *J. Am. Chem. Soc.*, 85, 1642 (1963).

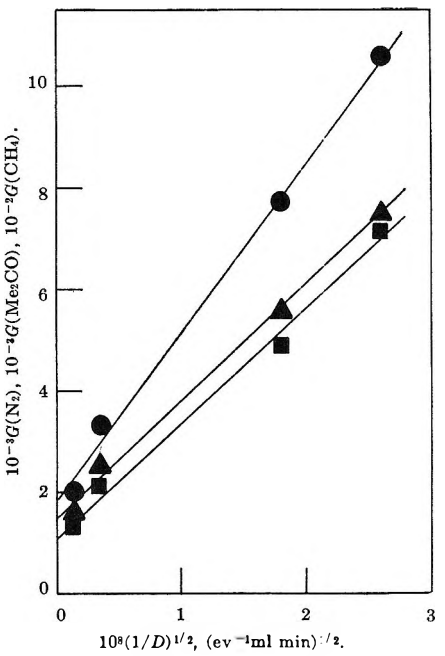

Figure 3. Product yields as a function of dose rate. [KOH], $[N_2O] = 5 \times 10^{-2}$ *M*; dose = (2.1–2.2) × 10^{17} ev ml^{-1}: nitrogen, ●; acetone, ▲; methane, ■.

both of these is not available, it is possible to make an estimate of an upper limit for k_3. The upper limit for k_{12} would be that of a diffusion-controlled reaction. Using the Debye equation[11] this is $k_{12} = 3 \times 10^9\ M^{-1}$ sec^{-1}. In the absence of an accurate value for G_R, a lower limit for ($G_e + G_R$) could be the yield of solvated electrons scavengeable by 5×10^{-2} *M* nitrous oxide. This may be equated with the yield of nitrogen ($G(N_2) = 2.7$) found in the radiolysis of a neutral solution of nitrous oxide in 2-propanol.[4] Using these numbers it is calculated that the upper limit for $k_3 = 10^5\ M^{-1}$ sec^{-1}. This low value for the upper limit of k_3 is consistent with the explanation of inhibition by acetone given above, namely, that charge transfer from the acetone radical anion I to nitrous oxide competes unfavorably with charge neutralization at positive holes.

The additional quantities of gaseous products recovered on each additional thaw–freeze cycle from solutions which had been frozen in liquid air immediately after irradiation are much too large to be attributable to gases produced during the irradiation period and subsequently trapped when the solutions were frozen. The additional yield must be produced after the removal of the solution from the radiation source. The magnitude of the postirradiation yields (Table III) indicates that the average lifetime of the chains between creation and destruction, *T*, is of the order of 1 min. *T* is defined by $T = \bar{l} \times$ kcl, where $\bar{l}$ is the average life in seconds of the chain centers between propagation steps and kcl is the kinetic chain length (product yield/yield of initiators). Since $\bar{l} = 1/k_3[N_2O]$,[12] an estimate for k_3 based on the postirradiation yields is $k_3 = 10^{2+1}\ M^{-1}$ sec^{-1}.

The occurrence of postirradiation yields was not recognized at the time when the preliminary results were communicated.[3] The observation of an apparent dose effect at doses in the range (1.8–3.6) × 10^{17} ev ml^{-1} which was attributed to a buildup of chain-carrying intermediates was in fact a result of carrying out the product analyses too quickly after the radiolyses. On repeating these experiments and allowing sufficient time to elapse before analysis, no dose effect was noted at these doses.

As was pointed out at the beginning of this section the constancy of the $G(N_2):G(CH_4)$ ratio is consistent with the two products having a common precursor. The oxygen radical anion produced in reaction 3 is initially in close proximity to an acetone molecule. The addition of O^- to acetone (reaction 14) is a possible reaction and the resulting radical ion III may be expected to lose a methyl radical to give the acetate ion (reaction 15) and subsequently methane (reaction 16).

$$Me_2CO + O^- \longrightarrow Me_2C(O\cdot)(O^-) \quad \text{(III)} \qquad (14)$$

$$\text{III} \longrightarrow Me\cdot + MeCO_2^- \qquad (15)$$

$$Me\cdot + Me_2CHOH \longrightarrow CH_3 + \text{II} \qquad (16)$$

The yield of hydrogen in the radiolysis of neutral solutions of 5×10^{-2} *M* nitrous oxide in 2-propanol is $G = 3.1$.[4] In the preliminary experiments[3] a small increase in hydrogen yield (to $G = 4$) was consistently noted in the presence of potassium hydroxide. In these experiments gas analysis was made using a gas chromatograph with a smaller response to nitrogen. The gas chromatograph used in the present work was more easily overloaded by nitrogen and this limited the level of detection to 1 part/hundred of hydrogen in nitrogen. Hence, $G(H_2) = 4$ would not be detectable in most of the runs in which the chain reaction was observed. No hydrogen was in fact detected in the majority of the runs. However, in certain experiments

(11) P. J. W. Debye, *Trans. Electrochem. Soc.*, 82, 205 (1942).

(12) F. S. Dainton, "Chain Reactions," Methuen and Co., Ltd., London, 1956, Chapter IV.

(see Table II) where the initial concentration of nitrous oxide was relatively small, exceptionally high values were found for $G(H_2)$. These yields are too large to be solely due to increased primary yields of atomic or molecular hydrogen, and it must therefore be concluded that in these runs hydrogen is formed as an additional chain product. It is noteworthy that this is the first recorded instance where hydrogen is produced with G values exceeding 10 from an organic solvent subjected to Co^{60} γ rays. A mechanism for this enhanced hydrogen yield is not readily formulated. More experiments are required in order to determine the exact dependence of $G(H_2)$ on such reaction parameters as dose rate and nitrous oxide concentration.

Another unexpected result for which a mechanism is unclear is the formation of significant yields of carbon monoxide (see Table IV) when the chain reaction is inhibited by nitrobenzene or benzophenone.

Acknowledgments. This work was carried out during the tenure of an Israel Atomic Energy Commission fellowship. The author wishes to thank Dr. Arie Rajbenbach for many helpful discussions.

The Reaction of $O(^3P)$ with Acetaldehyde in a Fast-Flow System[1]

by R. D. Cadle and J. W. Powers[2]

National Center for Atmospheric Research, Boulder, Colorado *(Received September 29, 1966)*

The kinetics and products of the reaction of $O(^3P)$ with acetaldehyde in a fast-flow system have been investigated. The only products detected under these conditions were methane, water, carbon dioxide, carbon monoxide, and a trace of formaldehyde. Rate constants were calculated from the initial rate of reaction of $O(^3P)$, k_0, and from the over-all rate of disappearance of H_3CCHO, k_a. Values of k_a were about twice those for k_0, for which the rate equation was found to be $k_0 = 1.1\ (\pm 0.3) \times 10^{13} \exp(-2300/RT)$ cm^3 mole^{-1} sec^{-1}. Values for k_0 were essentially the same whether the atomic oxygen was produced by titrating atomic nitrogen with nitric oxide or by subjecting molecular oxygen to a microwave discharge.

Introduction

The reaction of atomic oxygen in the ground (^3P) electronic state with acetaldehyde has been investigated by Cvetanović,[3] Avery and Cvetanović,[4] and by Avramenko and his co-workers.[5-8] The first two investigators[3,4] produced oxygen atoms by the mercury-photosensitized decomposition of nitrous oxide and by the photolysis of nitrogen dioxide at 3660 A. The major products of the reaction were found to be water and diacetyl, suggesting that the primary attack involves the abstraction of the aldehydic hydrogen atoms. Cvetanović reported that the rate constant at room temperature was 0.7 ± 0.1 times that for the atomic oxygen–ethylene reaction and suggested that the activation energy is about 3 kcal/mole. Combining this

(1) This work was supported by Grant No. AP-00343-02, Division of Air Pollution, Bureau of State Services, U. S. Public Health Service.

(2) On leave of absence from Ripon College, Ripon, Wis.

(3) R. J. Cvetanović, *Can. J. Chem.*, **34**, 775 (1956).

(4) H. E. Avery and R. J. Cvetanović, *J. Chem. Phys.*, **43**, 3727 (1965).

(5) L. I. Avramenko and R. V. Lorentso, *Zh. Fiz. Khim.*, **26**, 1084 (1952).

(6) L. I. Avramenko and R. V. Kolesnikova, *Izv. Akad. Nauk SSSR, Otd. Khim. Nauk*, 1231 (1961).

(7) L. I. Avramenko, R. V. Kolesnikova, and M. F. Sorokima, *ibid.*, 1005 (1961).

result with the value of Elias and Schiff[9] for the atomic oxygen–ethylene rate constant at room temperature, the atomic oxygen–acetaldehyde rate constant is 4.6×10^{11} cm^3 mole^{-1} sec^{-1}. If Cvetanović's data for rate constant ratios[3,10] are combined with those for the reaction of O with NO_2,[11] the value 1.9×10^{11} cm^3 mole^{-1} sec^{-1} is obtained. If Cvetanović's data are combined with those of Ford and Endow,[12] the value is 3.2×10^{11} cm^3 mole^{-1} sec^{-1}. Avramenko, *et al.*, produced oxygen atoms by the mercury-photosensitized decomposition of nitrous oxide[6] and by passing molecular oxygen through an electrical discharge.[5,7,8] The reaction products included acetic acid, glycolic aldehyde, ketene, and formaldehyde, but no diacetyl was found. They suggested three possible types of reactions: scission of the C–C bond, the formation of water and ketene, and incorporation of an oxygen atom at the C–H bond to form acetic acid or glycolic aldehyde. From the amounts of acetic acid produced they obtained the rate equation

$$k = 3.6 \times 10^{11} \exp(-2750/RT) \text{ cm}^3 \text{ mole}^{-1} \text{ sec}^{-1}$$

This corresponds to a rate constant at 300°K of about 2×10^9 cm^3 mole^{-1} sec^{-1}, smaller than the value of Cvetanović by more than two orders of magnitude.

In view of these discrepancies, an investigation was undertaken in these laboratories of the O(^{3}P)–H_3CCHO reaction using a fast-flow system and following the course of the reaction by measuring atomic oxygen concentrations with the air afterglow[13] or by measuring acetaldehyde concentrations with gas chromatography. Thus rate constants were measured directly without the need to assume that some product is a "primary" product. The use of this technique also provided an opportunity to investigate the nature of the products when there is a relatively large ratio of the concentration of atomic oxygen to that of acetaldehyde.

Experimental Section

The flow system and experimental technique have been described previously.[14] Atomic oxygen was usually produced by subjecting molecular nitrogen to a microwave discharge and converting the atomic nitrogen thus produced to atomic oxygen by titration with nitric oxide.[13] In a few experiments the atomic oxygen was produced by subjecting molecular oxygen to the discharge.

The acetaldehyde (Eastman) was purified by trap-to-trap distillation *in vacuo* before admitting it to the storage flask. Cylinder nitric oxide (Matheson) was passed over Ascarite to remove N_2O_3 before admitting it to the storage flask. The nitrogen and oxygen were National Cylinder Gas. The former was specified to be typically 99.98% nitrogen; the oxygen was water pumped and the main impurity, about 0.2%, was argon.

Samples of the effluent were analyzed by infrared spectroscopy, mass spectroscopy, gas chromatography, and a colorimetric method for formaldehyde.[15] Samples for analysis by infrared and mass spectroscopy and for formaldehyde were collected by passing all of the gases from the reaction tube through a trap cooled with liquid nitrogen. Silica gel was placed in the trap when methane and carbon monoxide were to be collected.

Rate constants were calculated in two ways. One involved calculations from the rates of atomic oxygen decrease at zero time, corrected for the slight decrease in the absence of acetaldehyde. The other involved calculations from the decrease in acetaldehyde concentration during a time determined by the position of the reaction-quenching silver oxide-coated screen using the equation[9]

$$\ln \frac{[H_3CCHO]_1}{[H_3CCHO]_2} = k \int_{t_1}^{t_2} [O] dt$$

The values of the integral were determined graphically from the scans of the airglow.

The total pressure in the reaction tube was varied from 1.2 to 4.4 mm. Concentrations of atomic oxygen were varied from about 4×10^{-11} to 6×10^{-9} mole cm^{-3}. Concentrations of acetaldehyde were varied from about 5×10^{-11} to 2.0×10^{-9} mole cm^{-3}. The effect of temperature was studied over the range 299–476°K. A thermocouple in an appropriate well was used to demonstrate that the reaction did not appreciably change the temperatures.

Results

Only two peaks were observed on the chromatogram of the partially reacted gases when a dinonylphthalate column was used, even when only a few per cent of the acetaldehyde had reacted. One was produced by acetaldehyde and the other, as confirmed by further studies, by methane. No diacetyl or acetic acid was detected, although chromatograms prepared from actual samples of these substances demonstrated that they would have been detected if formed in appreciable

(8) L. I. Avramenko and R. V. Kolesnikova, *Advan. Photochem.*, **2**, 25 (1964).

(9) L. Elias and H. I. Schiff, *Can. J. Chem.*, **38**, 1657 (1960).

(10) R. J. Cvetanovic, *Advan. Photochem.*, **1**, 115 (1963).

(11) F. S. Klein and J. T. Herron, *J. Chem. Phys.*, **41**, 1285 (1964).

(12) H. W. Ford and N. Endow, *ibid.*, **27**, 1277 (1957).

(13) F. Kaufman, *Progr. Reaction Kinetics*, **1**, 3 (1961).

(14) R. D. Cadle and E. R. Allen, *J. Phys. Chem.*, **69**, 1611 (1965).

(15) A. P. Altshuller, L. J. Lang, and A. F. Wartburg, *Intern. J. Air Water Pollution*, **6**, 381 (1962).

yields. The yield of methane accounted for an average of about 9% of the acetaldehyde carbon reacted.

When all of the acetaldehyde was allowed to react, the only bands in the infrared spectra of products collected at the temperature of liquid nitrogen in the absence of silica gel were from carbon dioxide and water. The yield of carbon dioxide varied from 32 to 62% of the acetaldehyde carbon. The only condensable gaseous products observed with the mass spectrometer were carbon dioxide and water.

The presence among the products of carbon monoxide was established and that of methane confirmed by the infrared spectra of the products collected on and desorbed from silica gel. When the nitric oxide was purified to eliminate nitrous oxide (the main impurity in Matheson nitric oxide) by trap-to-trap distillation, all of the bands could be accounted for as resulting from carbon monoxide, methane, carbon dioxide, water, and formaldehyde. Those possibly due to formaldehyde were very small. Yields calculated from the spectra showed that the acetaldehyde was oxidized almost entirely to carbon dioxide, carbon monoxide, methane, and water (Table I).

Table I: Yields of Carbon Dioxide, Carbon Monoxide, and Methane Calculated from the Infrared Spectra of the Products Collected on and Then Desorbed from Silica Gel[a]

Run no.	Yield, moles per mole of H_3CCHO reacted		
	CO_2	CO	CH_4
1	0.72	1.12	0.19
2	0.81	1.23	0.15

[a] All of the acetaldehyde had been allowed to react. The two runs were essentially duplicates, at about 299°K.

The chemical analyses for formaldehyde showed that small amounts were formed, about 0.1–1.5 mole % of the acetaldehyde reacted.

The mole ratio of atomic oxygen reacted to acetaldehyde reacted varied with the ratios of the initial concentrations of the reactants, increasing with increasing $[O]_0/[H_3CCHO]_0$ as shown in Table II. Varying these ratios had little effect on the methane yield.

All of the above results were obtained when producing the atomic oxygen by titration of atomic nitrogen with nitric oxide.

Reaction orders were determined in the conventional manner by maintaining the initial concentration of one reactant and the total pressure constant while varying the concentration of the other reactant and measuring initial rates of atomic oxygen decrease. Regression lines fitted to the plots of initial rates *vs.* logarithms of the concentrations had slopes of about unity, demonstrating that the rates were essentially first order in acetaldehyde and in atomic oxygen. The rates were independent of the total pressure over the range investigated.

Second-order rate constants calculated from the atomic oxygen concentrations (k_0) and from the acetaldehyde concentrations (k_a) as described above are shown in Tables II and III. Standard deviations (σ) for the results at room temperature are included in Table III. There was much more scatter in the values for k_a than in those for k_0. The activation energy, 2.3 kcal mole^{-1}, was calculated from the slope of the regression line fitted to the usual Arrhenius plot. This leads to the rate equation

$$k_0 = 1.1\ (\pm 0.3) \times 10^{13} \exp(-2300/RT)\ \text{cm}^3\ \text{mole}^{-1}\ \text{sec}^{-1}$$

The ratio k_a/k_0 was greater than unity for every run, varying from 1.4 to 6.3 with an average of about 2, as shown in Table II. There was no significant difference between the rate constants for the reaction in nitrogen and for that in oxygen and the above ratio was greater than unity in both cases.

Discussion

As indicated above, the only products detected were water, methane, carbon dioxide, carbon monoxide, and a trace of formaldehyde, and they accounted for essentially all of the acetaldehyde reacted. The difference between the nature of the products obtained in the present study and those obtained in the investigations of Cvetanović and of Avery and Cvetanović almost certainly results from the difference in the relative acetaldehyde and oxygen atom concentrations. The ratios of atomic oxygen to acetaldehyde were much higher in the present study, with a result that many intermediate products reacted with atomic oxygen. Possibly the same explanation holds for some of the differences between the nature of the products obtained in the present study and those obtained in the investigations of Avramenko, *et al.* Cvetanović found methane among the reaction products but explained it as resulting from methyl radicals produced as a primary product of the mercury-sensitized decomposition of acetaldehyde.

The rate constants obtained in the present study agreed very well with those obtained by combining the relative rate constants of Cvetanović with the absolute rate constants of others. The activation energy agreed fairly well with that predicted by Cvetanović and that measured by Avramenko, *et al.*

Table II: The Effect of the Initial Ratio of the Concentrations of Atomic Oxygen to Those of Acetaldehyde on Various Parameters of the Reaction at 298°K

$[O]_0 \times 10^{10}$, moles cm^{-3}	$[H_3CCHO]_0 \times 10^{16}$, moles cm^{-3}	CH_4 yield $\times 10^2$, moles of CH_4 per mole of H_3CCHO reacted	$\Delta[O]/\Delta[H_3CCHO]$	$k_0 \times 10^{-11}$, cm^3 mole^{-1} sec^{-1}	$k_a \times 10^{-11}$, cm^3 mole^{-1} sec^{-1}
2.0	17	13	0.31	2.8	...
6.1	20	9.4	0.76	3.0	5.1
5.8	9.4	13	1.0	3.5	8.1
6.2	10	15	1.0	3.2	5.6
8.1	6.7	12	1.4	3.8	9.5
5.8	3.1	...	2.5	2.4	9.2
12	5.1	19	2.6	3.5	7.4
13	2.3	...	6.5	2.0	4.3

Table III: Rate Constants and Activation Energies for the O(^{3}P)–H_3CCHO Reaction Obtained in This and Other Investigations

Ref	T, °K	k	k_0	k_a	Activation energy, kcal mole^{-1}
		cm^3 mole^{-1} sec^{-1}			
Cvetanović[a]	298	4.6×10^{11}			3
Cvetanović[b]	298	1.9×10^{11}			
Cvetanović[c]	298	3.2×10^{11}			
Avramenko[7]	343	6.6×10^{9}			2.75 ± 0.5
	353	7.4×10^{9}			
	373	1.1×10^{10}			
	393	1.14×10^{10}			
	428	1.41×10^{10}			
Cadle and Powers					
(N_2)[d]	299		2.7×10^{11} ($\sigma = 0.9$)	6.4×10^{11} ($\sigma = 2.4$)	2.3
	369		5.4×10^{11}		
	412		7.4×10^{11}		
	476		12×10^{11}		
(O_2)[e]	299		2.6×10^{11} ($\sigma = 1.0$)	13×10^{11} [f]	

[a] Combined data of Cvetanović[8] and Elias and Schiff.[9] [b] Combined data of Cvetanović[3,10] and Klein and Herron.[11] [c] Combined data of Cvetanović[3,10] and Ford and Endow.[12] [d] O(^{3}P) obtained by NO titration of N. [e] O(^{3}P) obtained by passing O_2 through a microwave discharge. [f] Insufficient values were obtained to calculate σ.

The reason for the marked disagreement between the rate constants obtained in this study and those obtained by Avramenko, *et al.*, is not known, but possibly resulted from an erroneous assumption by Avramenko, *et al.*, that acetic acid is a primary product of the reaction.

The following sequence of reactions could explain the formation of methane and, if reaction 2 is fast, the fact that k_a/k_0 is greater than one.

$$CH_3CHO + O \longrightarrow CH_3CO + OH \quad (1)$$

$$CH_3CHO + OH \longrightarrow CH_3CO + H_2O \quad (2)$$

$$CH_3CO + O \longrightarrow CH_3CO_2 \quad (3)$$

$$CH_3CO_2 \longrightarrow CH_3 + CO_2 \quad (4)$$

$$CH_3 + CH_3CHO \longrightarrow CH_4 + CH_3CO \quad (5)$$

This reaction sequence is essentially that proposed by Cvetanović. In addition, the following reactions must be occurring.

$$CH_3CO \longrightarrow CH_3 + CO \quad (6)$$

$$OH + CO \longrightarrow CO_2 + H \quad (7)$$

$$CH_3 + O \longrightarrow \text{products} \quad (8)$$

The methyl radical must undergo reactions such as (8) in addition to hydrogen abstraction, since the yield of

carbon dioxide plus carbon monoxide is much greater than that of methane. The above equations do not constitute a complete mechanism and the reason for the relative lack of dependence of methane yield on the $[CH_3CHO]_0/[O]_0$ ratio (Table II) is not obvious.

The increasing ratio of atomic oxygen reacted to acetaldehyde reacted with increasing $[O]_0/[H_3CCHO]_0$ (Table II), together with the fact that the former ratios varied from fractional values to severalfold, agrees with the concept that both atomic oxygen and acetaldehyde are involved in secondary reactions. Such secondary reactions may have a much greater effect on k_a than on k_0, since the latter is calculated from initial rates when the concentrations of intermediate products are small. This, of course, will only be true if the rate constants for the reaction of atomic oxygen with the intermediate products are not markedly greater than that for the primary reaction of atomic oxygen with acetaldehyde.

Another possible explanation for k_a/k_0 exceeding one is that the measured values for atomic oxygen concentrations were too low. These were used for calculating k_a but only relative values were needed for calculating k_0. The measured values would have had to be low both when atomic oxygen was prepared from nitrogen and when it was prepared from oxygen. This could also explain the fractional values for the ratio of atomic oxygen reacted to acetaldehyde reacted. If either of these explanations is correct, k_0 represents the primary reaction step much better than k_a.

Kinetics of Deuterium Exchange of Trimethylammonium Ion in D_2SO_4[1]

by Gideon Fraenkel and Yutaka Asahi[2]

Evans Chemistry Laboratory, The Ohio State University, Columbus, Ohio 43210 *(Received October 3, 1966)*

The kinetics of exchange protolysis of trimethylammonium nitrate in D_2SO_4 have been examined over the temperature range 41–103° employing nmr integration to determine the rate constants. The exchange reaction is first order in the protonated base and the rate constants correlate well with Arnett's acidity function H'''. The mechanism proposed to account for these results involves the rate-determining dissociation $BH^+ + D_2O \xrightarrow{k_{15}} B + HD_2O^+$. The rate constants are given by $\log (k_{15}/T) = -(3313/T) + 8.08 \log T - 12.18$. At 50° $\Delta H^{\ddagger}$ is 22 kcal.

Introduction

The kinetics of exchange protolysis of the methylammonium ions have been studied by Meiboom, Grunwald, and co-workers[3-8] employing nmr line shape measurements and by Swain[9,10] who found that at 0° in methanol the exchange rates were sufficiently slow to follow with deuterium labeling techniques. Meiboom, *et al.*,[3-5] showed that in water the fast steps in the exchange protolysis of amines are

$$BH^+ + H_2O + B \longrightarrow B + H_2O + BH^+ \quad (1)$$

$$BH^+ + B \longrightarrow B + BH^+ \quad (2)$$

and at high acidities they detected the step

$$BH^+ + H_2O \longrightarrow B + H_3O^+ \quad (3)$$

(1) Presented at the Nmr Symposium, Tokyo, Japan, Sept 1965.

(2) Takeda Chemical Industries, Osaka, Japan.

(3) E. A. Grunwald, A. Loewenstein, and S. Meiboom, *J. Chem. Phys.*, **27**, 630, 641 (1957).

(4) A. Loewenstein and S. Meiboom, *ibid.*, **27**, 1067 (1957).

(5) Z. Luz and S. Meiboom, *ibid.*, **39**, 366 (1963).

(6) E. Grunwald and E. Price, *J. Am. Chem. Soc.*, **86**, 2965, 2970 (1964).

(7) Z. Luz and S. Meiboom, *ibid.*, **86**, 4764 (1964).

(8) M. Cocivera and E. Grunwald, *ibid.*, **87**, 2070 (1965).

Grunwald and co-workers reported the kinetics of exchange of N-deuterated methylammonium salts in H_2SO_4 by integrating the nmr peaks for the different species.[11] Their results were in accord with a two-step exchange at high acidities

$$BH^+\cdots H_2O \rightleftharpoons B\cdots HOH + H^+ \quad (4)$$

$$B\cdots HOH \rightleftharpoons B + H_2O \quad (5)$$

the apparent rate constants being proportional to $(\kappa/\kappa_0)(1/h_0)$. Here κ and h_0 refer to the viscosity and Hammett acidity function, respectively. However, in the case of $(CH_3)_3ND^+$ this correlation does not hold. In aqueous HCl the rate of proton exchange of trimethylammonium ion was found to be proportional to $(BH^+)/(H^+)$.[12] After correction for salt effects these data fitted a mechanism similar to steps 4 and 5 but involving more water molecules.

$$BH^+ + nH_2O \rightleftharpoons B\cdots(HOH)_m + H(OH_2)^+_{n-m} \quad (6)$$

$$B\cdots(HOH)_m \xrightarrow[k_H]{} B + mH_2O \quad (7)$$

In attempts to use trimethylammonium ion as an internal standard in D_2SO_4 we have now found that the rate of NH exchange with deuterium is so slow, even at elevated temperatures, that it is easily followed by integrating the nmr curves for the different species present.[11]

It was the purpose of this work to investigate the kinetics of deuterium exchange of $(CH_3)_3NH^+$ in D_2SO_4.

Experimental Section

Chemicals. The following materials were obtained commercially: trimethylamine, Eastman Kodak; deuterium oxide, Columbia Chemical Co; and sulfur trioxide, Allied Chemicals. Deuteriosulfuric was prepared by adding the appropriate quantity of D_2O to SO_3 to 0°. Trimethylammonium nitrate was made by dissolving trimethylamine in 5 *M* nitric acid and recrystallizing the salt from absolute ethanol.

Samples. Solutions were made up by adding the acid to a weighed quantity of ammonium salt in a 1- or 5-ml volumetric flask. Most solutions had to be used immediately; however, samples in very strong acid could be stored at −78°.

Kinetic Run Procedure. The solution to be studied was transferred to a 5-mm nmr tube. For fast exchange rates the sample was kept in the thermostated nmr insert for the duration of the run. In the case of slow runs several identical samples were placed in a thermostat and removed for nmr analysis at convenient intervals.

Nmr Analysis. The Varian A60 nmr spectrometer with variable temperature probe was used. Analysis was accomplished by integrating the methyl resonances for the N-deuterio and N-protio ions at a sweep width of 1 cps/cm, the error being ±1%.

Results and Discussion

Figure 1 illustrates the N-methyl proton nmr absorption for a mixture of $(CH_3)_3NH^+$ (doublet) and $(CH_3)_3ND^+$ (triplet) in D_2SO_4 at different times after mixing the protio salt with the acid. It is seen that the coupling constants $J_{H,H}$ and $J_{H,D}$ are 5.3 and 0.6 cps, respectively. The former value is a function of acid concentration as is shown in Table I.

The rate of deuterium exchange was determined by integrating the methyl absorptions for the two species as a function of time. A typical run is illustrated in Figure 2. The rate of deuterium exchange is first

Table I: Nmr Parameters for Trimethylammonium Nitrate in D_2SO_4

D_2SO_4 concn, wt %	τ_{CH_3}	$J_{H,H}$, cps
0	7.08	4.8
2	7.04	5.0
9	7.04	5.1
27.8	7.03	5.2
46.3	7.03	5.3
64.8	7.02	5.4
83.3	7.03	5.4
89.4	7.06	5.4

Table II: First-Order Rate Constant, k_1, for Deuterium Exchange of Trimethylammonium, BH^+, Nitrate in 47% D_2SO_4 at 97°

(BH^+), *M*	k_1, sec^{-1}
2.2	0.42
0.73	0.44
0.38	0.44
0.15	0.42
0.077	0.42
0.039	0.41

(9) C. G. Swain and M. M. Labes, *J. Am. Chem. Soc.*, **79**, 1084 (1957).

(10) C. G. Swain, J. T. McKnight, and V. R. Kreiter, *ibid.*, **79**, 1088 (1957).

(11) M. T. Emerson, E. Grunwald, M. L. Kaplan, and R. A. Kromhout, *ibid.*, **82**, 6307 (1960).

(12) E. Grunwald, *J. Phys. Chem.*, **67**, 2208, 2211 (1963).

Table III: First-Order Rate Constants, k_1, sec^{-1}, for Deuterium Exchange of Trimethylammonium Ion, 0.1 *M*, in D_2SO_4

41°		97°		103°	
% D_2SO_4	k_1	% D_2SO_4	k_1	% D_2SO_4	k_1
61.73	3.83×10^{-7}	66.13	2.77×10^{-5}	80.80	2.16×10^{-7}
47.40	4.33×10^{-5}	61.58	1.95×10^{-4}	75.83	1.63×10^{-6}
41.30	2.01×10^{-4}	49.00	7.45×10^{-3}	70.28	1.45×10^{-5}
38.18	6.33×10^{-4}	45.90	1.63×10^{-2}	62.31	3.00×10^{-3}
34.50	1.45×10^{-3}	41.26	3.82×10^{-2}	49.12	1.35×10^{-2}
31.77	2.35×10^{-3}	40.58	4.38×10^{-2}	43.08	6.70×10^{-2}

Figure 1. Nmr absorption for methyl hydrogens in sample initially 0.1 *M* $(CH_3)_3NH^+NO_3^-$ in 37.6% D_2SO_4, 41° at different times after mixing: a, 0.6 min; b, 12 min; c, 43 min.

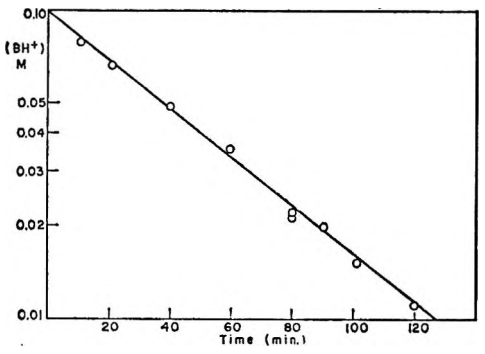

Figure 2. Deuterium exchange of 0.1 *M* $(CH_3)_3NH^+NO_3^-$ in 50.4% D_2SO_4, 60°.

order in, and the rate constants are independent of, the concentration of protonated base, Table II. First-order rate constants for deuterium exchange as a function of acid concentration and temperature are listed in Table III.

The H_0[13] acidity function for H_2SO_4 was determined by Gel'bshtein between 20 and 80°.[14] The corresponding acidity function for D_2SO_4 at 22° was found to be very close to that for H_2SO_4[15] within the range 0.1–12 *M*. Employing Gel'bshtein's values for H_0[14] and when necessary extrapolating his data to other temperatures it is found that at 41°

$$\log k_1 = 1.5H_0 \quad (8)$$

and at 103°

$$\log k_1 = 1.2 + 1.5H_0 \quad (9)$$

An estimate of J_0[16] for D_2SO_4 at different temperatures was made by assuming that

$$J_0 = H_0 + \log a_{H_2O} \quad (10)$$

The activity of water was calculated from $P_{H_2SO_4}/P_{H_2O}$ for sulfuric acid–water mixtures at different temperatures.[17] The values of H_0 were obtained as described above and it was assumed that J_0 for H_2SO_4 and D_2SO_4 would be very similar. The results are at 41°

$$\log k_1 = -0.4 + J_0 \quad (11)$$

and at 103°

$$\log k_1 = 1.4 \times 1.2J_0 \quad (12)$$

Deno's acidity function, C_0,[18] does not correlate the rate constants for exchange obtained in this work.

By far the best correlation is obtained with the acidity function H''' of Arnett,[19] at 41°

$$\log k_1 = 0.1 + 1.1H''' \quad (13)$$

and at 103°

$$\log k_1 = 2.4 + 0.95H''' \quad (14)$$

Furthermore, the structural similarity of trimethylamine to the N,N-dimethylaniline indicators used to determine H'''[19] strengthens the view that this last correlation should be taken seriously. It is interesting that these first-order rate constants are not linear with $\kappa/\kappa_0 h_0$ *or even* $\kappa/\kappa_0 h'''$.

(13) L. P. Hammett and A. J. Deyrup, *J. Am. Chem. Soc.*, **54**, 2721 (1932).

(14) A. I. Gel'bshtein, *Russ. J. Inorg. Chem.*, **1**, 282, 506 (1956).

(15) E. Högfeldt and J. Bigeleisen, *J. Am. Chem. Soc.*, **82**, 15 (1960).

(16) V. Gold and E. W. V. Hawes, *J. Chem. Soc.*, 2102 (1951).

(17) "International Critical Tables," Vol. 3, p 302.

(18) N. C. Deno, J. J. Jaruzelski, and A. Schriesheim, *J. Am. Chem. Soc.*, **77**, 3044 (1955).

(19) E. M. Arnett and G. W. Mach, *ibid.*, **86**, 2671 (1964).

The correlation with H''' implies that the over-all rate-determining step in the deuterium exchange of trimethylammonium ion in D_2SO_4 is

$$BH^+ + D_2O \longrightarrow B + HD_2O^+ \quad (15)$$

or more generally[12]

$$BH^+ + nD_2O \rightleftharpoons B\cdots HOD(D_2O)_{m-1} + D(D_2O)^+_{m-n} \quad (16)$$

$$B\cdots HOD(D_2O)_{m-1} \longrightarrow B + HOD + (m-1)D_2O \quad (17)$$

The results reported here essentially agree with those of Meiboom[4,5] and Grunwald.[11,12] For instance, Grunwald's value for k_H, reaction 7, at 41° is 1.39×10^{10} sec^{-1},[20] whereas the corresponding rate constant in this work, k_{17}, is 3.6×10^9 sec^{-1}, by integration. However, these results are not strictly comparable since the exchanges were studied under different conditions with different methods and Grunwald's values were corrected for salt effects.

The main conclusion from the present work is that the correlation obtained with H''' over such a wide range of temperature and acid concentration strongly supports steps 16 and 17 or 4 and 5 as the rate-determining steps for proton exchange of trimethylammonium ion in strong acids.

Arnett[19] has warned of the dangers of applying acidity function criteria indiscriminately to data for acid-catalyzed reactions. The use of H''' in the present treatment is justified because tertiary amines are more similar in their behavior to one another than to other types of amines.

It is still possible that exchange steps of the type $BH + S \rightarrow B + SH^+$ might take place where S is H_2SO_4, HSO_4^-, or SO_4^{2-}. Evidently these steps are too slow to be detected.

The thermodynamic activation parameters for reaction 15 were estimated by extrapolating the rate constants for exchange to $H''' = 0$ between 41 and 103°. The Eyring plot so obtained, illustrated in Figure 3, is definitely curved, the slope increasing with temperature. From the slope in the center of the above temperature range $\Delta H^{\ddagger}$ is 22 kcal. Substituting the known dependence of $\Delta H^{\ddagger}$ and $\Delta S^{\ddagger}$ on temperature into the Eyring equation, it is found that

$$\log \frac{k_{15}}{T} = \frac{-3313}{T} + 8.08 \log T - 12.18 \quad (18)$$

accurately fits the data. Hence the corrected activation parameters are $\Delta H_{15}^{\ddagger} = 15.1$kcal, $\Delta S_{15}^{\ddagger} = 7.5$ eu, and $\Delta C_p = 16$ cal/mole °K. Grunwald's values[12] for reaction 3, obtained with aqueous HCl solutions (line shape method), are $\Delta H_3^{\ddagger} = 11.29$ kcal, $\Delta S_3^{\ddagger} = -17.9$ eu, and $\Delta C_p = 80$ cal/mole °K.

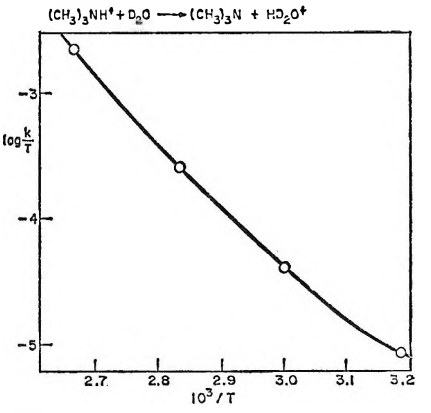

Figure 3. Eyring plot for deuterium exchange of trimethylammonium nitrate, 0.1 M in 49% D_2SO_4.

Acknowledgment. This research was supported by the National Institutes of Health Grant No. GM-08686-03

(20) Interpolated from the data in ref 12, p 2214.

Indirect Inactivation of Deoxyribonucleic Acid

by Kenneth H. Kingdon

1174 Phoenix Avenue, Schenectady, New York 12308 *(Received October 3, 1966)*

This paper explores the concept that radiation inactivation of a DNA molecule is caused by the generation of a single pair of H radicals in a sugar, which migrate through the adjacent bases by a two-dimensional random walk, caused by excitation of the electron atmosphere of the molecule by the radiation which generated the H radicals. The chance is estimated that this single pair of H radicals shall react with both members of an adjacent base pair, thus leading to the formation of a covalent cross-link between the bases and inactivation of the entire molecule. This chance is estimated to be 0.12, and from this and the experimental G value of 2.0 for producing the H radicals, the D_{37} for virus DNA is found to be 7.5×10^{12}/(molecular weight) rads, in fair agreement with experiment. A molecule of diploid cell DNA has much lower sensitivity to radiation than a molecule of equal mass of virus DNA. Part of this is due to the duplication of genes, but it is suggested that another factor is the existence of a three-dimensional secondary structure in the diploid DNA formed by H bonds with adsorbed water, in which the pair of H radicals is much more widely dispersed by a three-dimensional random walk and therefore is less effective for cross-linking the bases. An initial effect of radiation on a diploid cell is to break some of these water H bonds, giving isolated pieces of virus-like twin DNA helix, which are more sensitive to radiation. The production of isolated twin helix DNA by the radiation is estimated, and it is shown that a log–log plot of the fraction of diploid cells surviving at dose D, against cosh (D/D_{37}), should be linear, with a slope of -2.3. This is in agreement with experiment.

I. Introduction

One process by which radiation is known to inactivate DNA is by the formation of a covalent cross-link between the two bases in a pair of nucleotides.[1] Such cross-links may inactivate the DNA biologically by preventing complete separation of the strands of a twin helix. In other experiments a cross-link may serve as an anchor to locate the partially separated strands of a twin helix, giving the "reversible DNA" studied by Geiduschek.[2] These cross-links presumably result from chemical interactions of radicals formed in the two bases. However, all bases are resonating ring structures and are therefore quite insensitive to radiation, so the possibility should be considered that other radicals are produced by the radiation elsewhere and that these radicals migrate to the bases and put them in a chemically reactive condition.

Although indirect inactivation is usually thought to be due to radicals formed from water, which diffuse into the molecule to be inactivated, it is true that for ionizing radiations some organic substances such as n-octane, cyclohexane, alanine, and glutamic acid have radical yields greater than that for water.[3,4] It seems clear, therefore, that nonaqueous sources of radicals, such as other components of DNA, may be important. Biemann and McCloskey[5,6] have demonstrated from the mass spectra of nucleosides that H

(1) J. Marmur and L. Grossman, *Proc. Natl. Acad. Sci. U. S.*, **47**, 778 (1961).

(2) E. P. Geiduschek, *ibid.*, **47**, 950 (1961).

(3) L. Bouby, A. Chapiro, M. Magat, E. Migirdicyan, A. Prevot-Bernas, L. Reinisch, and J. Sebban, *Proc. Intern. Conf. Peaceful Uses At. Energy, Geneva, 1955*, **7**, 526 (1956).

(4) T. Henriksen, T. Sanner, and A. Pihl, *Radiation Res.*, **18**, 147 (1963).

(5) K. Biemann, "Mass Spectrometry," McGraw-Hill Book Co., Inc., New York, N. Y., 1962, p 351.

(6) K. Biemann and J. A. McCloskey, *J. Am. Chem. Soc.*, **84**, 2005 (1962).

atoms are produced in the sugar and migrate to the base. The very great intensity of the (base + H) and (base + 2H) peaks shows that this is a very probable process and illustrates the stability of the bases against ionizing radiations, as compared with the sugars.

A very large DNA molecule is formed from only six kinds of small molecules—the four bases, the sugar, and the phosphate. The bonds between phosphorus and oxygen are known to be very strong and therefore radiation resistant; and the work of Biemann and McCloskey[6] demonstrates that the bases are much more radiation resistant than the sugar. Accordingly, we shall assume that the G of 2.0 for DNA, as found by Lett, Parkins, Alexander, and Ormerod,[7] is due entirely to H atoms liberated from the sugar and shall attempt to show that the migration of these H atoms to the bases can account quantitatively for the inactivation of virus twin helix DNA by ionizing radiation.

II. Abundance of Radicals Formed in DNA

It will clarify our thinking to state quantitatively the abundance of radicals formed in DNA by radiation. In what follows we shall refer to the entire DNA content of a virus (for example) as a single molecule and consider that a structure of molecular weight 10^8 can be inactivated by formation of a single covalent cross-link between a pair of bases.[1]

A typical twin helix DNA molecule of molecular weight 6×10^7 has a D_{37} of about 10^5 rads. This amount of radiation will, on the average, deliver 630 ev/molecule, which with a G of 2.0 will produce about 12 H radicals/molecule, or 6 pairs of H radicals/10^5 pairs of nucleotides. It is evident from these figures that it is extremely improbable that a second pair of radicals will be formed in a given pair of nuclectides during the irradiation and that therefore the radical attack and cross-linking of a pair of bases must be carried out by a single pair of H radicals produced in an adjacent sugar.

III. Migration of Radicals

The H radicals have to migrate from the sugar to the bases in order to produce inactivation and, from what has been said about the abundance of radicals formed in DNA, it is clear that there is no concentration gradient for conventional diffusion. Biemann and McCloskey[6] have demonstrated the rapid migration of H radicals from the sugar to the base in the mass spectra of nucleosides. It has also been shown by Tikhomirova, Malinskii, and Karpov[8] that gases migrate through polyethylene 10–15 times faster than normally while the polyethylene is exposed to a γ-ray flux of 730 r/min, the migration rate returning to its normal value as soon as the radiation is stopped. It is suggested here that these effects are caused by each incident electron of the ionizing radiation momentarily heating the electron atmosphere of a molecule locally to a high temperature, thus creating local fluctuations of the energy levels of the molecule and causing the H radicals or other small molecules to perform random walks between these momentarily fluctuating energy levels. The usual concept of diffusion of atoms is based on the idea that an atom statistically acquires an unusually high energy which enables it to surmount a potential barrier and move to a different site in a static system of energy levels. The migration concept suggested here is that an atom of average energy is enabled to move to a different site by a statistical disturbance of the system of energy levels by incident radiation.

Biemann and McCloskey's experiments[6] show that a single excitation of the electron system has a very high probability of transporting an H radical from the sugar to the base, a distance of about 5 atomic spacings, or a random walk of about 25 steps. It therefore seems correct to assume that a single excitation of the electron atmosphere of the molecule lasts long enough to permit the H radicals to migrate from the sugar to the nearest pair of bases, and perhaps farther.

IV. Inactivation of Virus Two-Strand DNA

Figure 1 shows a projection of a short section of a two strand Watson–Crick helix, based on a figure of Wilkins,[9] but with the bases rotated about 45°, so as to make evident their structure and hydrogen bonding. The bases adenine, thymine, cytosine, and guanine are labeled A, T, C, and G, and the sugar and phosphate, S and P, respectively.

Suppose a pair of H radicals is generated in the sugar ring at left center of Figure 1. A minimum random walk of 9 atomic spaces (including one hydrogen bond), about 81 random steps, would carry one of these H radicals through the adenine to the C_6 of the thymine, where it might add to C_6, breaking the double bond and producing a radical on C_5. The other H radical of the pair might interact with the adenine. We shall attempt to estimate quantitatively the chance that a

(7) J. T. Lett, G. Parkins, P. L. Alexander, and M. G. Ormerod, *Nature*, 203, 593 (1964).

(8) N. S. Tikhomirova, Yu. M. Malinskii, and V. L. Karpov, *Vysokomolekul. Soedin.*, 2, 1335 (1960); see *Chem. Abstr.*, 55, 19312*d* (1961).

(9) M. H. F. Wilkins in "Comprehensive Biochemistry," Vol. 8, Florkin and Stotz, Ed., Elsevier Publishing Co., New York, N. Y., 1963, p 272.

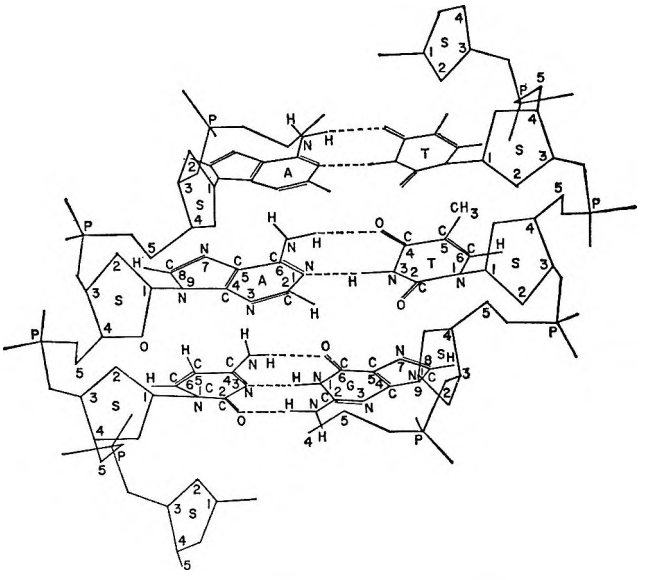

Figure 1. Migration paths for H radicals in DNA helix.

single pair of H radicals will intereact with both members of this pair of bases so as to produce a cross-link between them. It should be stated explicitly that this calculation is intended only to demonstrate that, with a particular set of assumptions, which are based as far as possible on observed experimental data, the calculated probability of cross-linking a pair of bases is in approximate agreement with the observed value of D_{37} for DNA. The inference should not be drawn that this is intended as a definitive treatment of this difficult problem.

The assumptions needed for this calculation are as follows. The first assumption specifies the reactive sites for the radicals in the purine and pyrimidine bases, and in the sugar–phosphate strands. The radiation chemistry of aqueous solutions of nucleic acids, as reviewed by Scholes,[10] indicates that the 5,6 carbon double bond in a pyrimidine and the 4,5 carbon double bond in a purine are the most probable sites for attack by the H and OH radicals formed in water. The double bond becomes saturated, leaving a new radical on one of the carbons. Other chemical reactions usually follow this initial step. In the present case, we are postulating that the subsequent chemical reaction is the reaction of the two new radicals, one on each base, to form a covalent cross-link between the purine and the pyrimidine. In addition to reacting with the adjacent bases, H radicals will also migrate along the sugar–phosphate strands of the twin helix and presumably will react with the singly bonded oxygen atoms in the phosphate groups. For a pair of H radicals originating in the ring of the sugar to the left center of Figure 1, there will thus be 6 reactive sites, with the following atomic bond spacings from the nearest point of the sugar ring: O in one phosphate (3), O in the other phosphate (4), C_4 in adenine (2), and C_5 (4), C_5 in thymine (8), and C_6 (9). Since the number of random walk steps required to traverse a given distance is proportional to the square of the distance and if each atomic spacing is traversed in one step (as discussed in section III), the number of random steps required to reach each of the above reactive sites will be 9, 16, 4, 16, 64, and 81, respectively. Our second assumption is that the probability of reaching a particular site is inversely proportional to the number of random steps required, so that the probabilities for reaching the various sites are $k/9$, $k/16$, $k/4$, $k/16$, $k/64$, and $k/81$, respectively. The constant k may be evaluated by setting the sum of the probabilities equal to unity. This scheme of calculation neglects H radicals which pass through the phosphate groups without reacting and those which pass through the adenine and thymine without reacting. For such a pair of H radicals to reach the nearest reactive sites in the A–T base pair at the top of Figure 1 would require random walks of 81 and 400 steps, respectively, so that the neglect of this group is justified for the elementary calculation.

H radicals migrating from the sugar ring at left center of Figure 1 may form cross-links between the adjacent adenine and thymine by two mutually exclusive processes.[11] In part a of process 1, the first H radical reacts in the adenine, whereas, in part b, the second H radical passes through the adenine and reacts in the thymine. In part a of process 2, the first H radical passes through the adenine and reacts in the thymine, whereas, in part b, the second H radical reacts in the adenine. The total probability will be the sum of the probabilities for these two mutually exclusive processes. Table I lists the reactive sites, and the probabilities for reaching each site by a random walk, as outlined above. This is followed by the detailed calculations for the two processes. In part a of the first process, the sum of the probabilities has been set equal to unity, and k was found to be 1.94, so that the individual probabilities are as listed. The probability for reaction in A is 0.608, made up of 0.486 on C_4 and 0.122 on C_5, so that 0.608 is the probability for part a of process 1. Part b of process 1 must be divided into two cases:

(10) G. Scholes, *Progr. Biophys. Mol. Biol.*, 13, 59 (1963). In Scholes' article the reactive bond for radicals in a pyrimidine is referred to as the 4,5 double bond. In the present article this bond is referred to as the 5,6 double bond, in accordance with most recent references. The pyrimidine ring is symmetrical about a 2–5 line, so that a dual numbering system is possible.

(11) The author is indebted to a referee for pointing out this approach to the calculation.

Table I: Chance of H Radical Reaction with A and T

Reactive Sites and Probabilities for A → T

	Oxygens		Adenine		Thymine		k	Case fraction
Reaction sites	1	2	C_4	C_5	C_5	C_6		
Probabilities	$k/9$	$k/16$	$k/4$	$k/16$	$k/64$	$k/81$		
Process 1, Part a	0.216	0.122	0.486	0.122	0.030	0.024	1.94	
			0.608					
Case b_1	0.421	0.237	0	0.236	0.059	0.047	3.79	0.80
					0.106			
Case b_2	0.246	0.138	0.554	0	0.035	0.027	2.22	0.20
					0.062			
Process 2, Part a	0.216	0.122	0.486	0.122	0.030	0.024	1.94	
					0.054			
Case b_1	0.222	0.125	0.500	0.125	0	0.025	2.00	0.56
			0.625					
Case b_2	0.221	0.124	0.498	0.124	0.031	0	1.99	0.44
			0.622					

$b_1 + b_2 = (0.80 \times 0.106) + (0.20 \times 0.062) = 0.097$

Probability of process 1: $0.608 \times 0.097 = 0.059$

Probability of process 2: $0.623 \times 0.054 = 0.034$

Total cross-links for both processes: $0.059 + 0.034 = 0.093$

Reactive Sites and Probabilities for T → A

	Oxygens		Thymine		Adenine	
Reaction sites	1	2	C_5	C_6	C_4	C_6
Probabilities	$k/9$	$k/16$	$k/25$	$k/4$	$k/49$	$k/36$
Probability of process 1				0.098		
Probability of process 2				0.056		
				0.154		

Average for sources in both strands: $0.5(0.093 + 0.154) = 0.123$

case b_1 where the first H radical has reacted with the C_4 of A so that a new radical exists on C_5, and case b_2 where the first H radical has reacted with C_5 of A and the new radical exists on C_4. Case b_1 will appear in 0.486/0.608 or 0.80 of the process 1 reactions, and case b_2, in 0.20. In case b_1 the probability of reaction on C_4 of A is zero, so that setting the sum of the other probabilities equal to unity gives a k of 3.79 and the values listed in the b_1 line of the table. The situation is similar for b_2. From the probabilities listed for case b_1 it will be seen that the chance for its occurrence is 0.80 (0.059 + 0.047), or 0.80(0.106), whereas the corresponding value for case b_2 is 0.20(0.062). The probability for b is the sum of these, or 0.097, and the probability for process 1 is the product of the probabilities for parts a and b, 0.608 × 0.097, or 0.059. The calculation for process 2 is similar, leading to a probability of 0.034. Hence, the chance of forming a cross-link by both mutually exclusive processes is 0.059 + 0.034, or 0.093.

H radicals will also be produced in the sugar ring at right center of Figure 1 and will migrate through T and A, in that order. The distances to the reactive sites in T and A are now different from before, and the new reaction probabilities are listed in the lower part of Table I. Carrying out the calculation in the same way shows that the probability for process 1 is 0.098, and for process 2, 0.056, giving a total of 0.154.

Since there is an equal chance that H radicals will originate in the sugar ring in either strand, the total probability for cross-linking the AT pair of bases by a single pair of H radicals is 0.5(0.093 + 0.154), or 0.123. Within the assumptions of our calculation, this is also the probability that a single pair of H radicals will form a cross-link between a cytosine–guanine pair of bases, so that no allowance need be made for the difference in abundance of the different base pairs. The end result of the calculation therefore is that a radiation dose sufficient to produce on the average a single pair of H radicals in each DNA molecule will inactivate 0.12 of the molecules.

The estimation of this probability, together with the

experimental value of G for DNA, makes possible a direct calculation of D_{37} for DNA. A dose of 100 ev/molecule produces experimentally on the average 1 pair of H radicals/molecule.[7] This dose is equivalent to $9.60 \times 10^{11}/M$ rads, where M is the molecular weight. With this dose we have estimated above that 0.88 of the molecules survive, so that the exponential survival law gives

$$D_{37} = -(9.60 \times 10^{11}/M)/\ln 0.88 = 7.5 \times 10^{12}/M \text{ rads}$$

The values of $D_{37} \times M$ listed by Kaplan and Moses[12] for two-strand DNA viruses range from 4.6×10^{12} to 6.9×10^{12}, with an average of 5.8×10^{12}. Our calculation agrees satisfactorily.

V. Inactivation of Diploid Cell DNA

In 1961, Terzi[13] pointed out that, per *in vivo* molecule of DNA inactivated, the amount of radiation for a diploid cell was over 100 times that required for a twin helix DNA virus of equal molecular weight. This is due in part to the duplication of genes in the diploid cell, but some additional factor seems necessary to account for the great difference. Besides this quantitative difference, there is the qualitative difference that the plot of log (surviving fraction) against dose is sigmoidal for the diploid cell, but linear for the DNA virus. We shall try to explain both of these differences in terms of indirect inactivation by radicals.

Langridge, Marvin, Seeds, Wilson, Hooper, Wilkins, and Hamilton[14] have pointed out that water molecules may be hydrogen bonded in a single nucleotide of DNA, or between neighboring nucleotides, to establish the secondary structure of a DNA crystal, as studied by X-ray diffraction. We assume that the arrangement of the folded DNA in a diploid cell is similar to that of DNA in the crystal and that water molecules will form hydrogen bonds between neighboring nucleotides. A second assumption is that the diploid cell DNA contains much more water than virus DNA. A third assumption is that in the diploid cell the radiation produces H radicals principally from the sugars, the adsorbed water being so tenuously distributed that the processes which give rise to H and OH radicals in bulk water are much less efficient here. It is planned to discuss the evidence for this in a subsequent publication. Under these assumptions it is clear that the additional water–hydrogen bonds of a diploid cell give the H radicals generated in the sugars many more migration paths than are available in dry DNA. Therefore the chance that a single pair of H radicals shall cross-link an adjacent pair of bases is greatly reduced in the diploid cell, thus accounting in part for its much lower sensitivity per molecule to radiation. Migration of H radicals in the bases of virus DNA is two dimensional, whereas in diploid cell DNA the migration is three dimensional, leading to much wider dispersion of a pair of H radicals.

It has been suggested often that a likely effect of radiation on DNA is to break hydrogen bonds. Accordingly, it is likely that an initial effect of radiation on diploid cell DNA is to break some of the water H bonds which determine the secondary structure of the DNA. This will lead to local separations of one twin Watson–Crick helix from another, thus converting a small region of three-dimensional migration into two small regions of two-dimensional migration in isolated twin helix DNA, which will be more sensitive to radiation than the three-dimensional region. We assume that inactivation of diploid cells is due entirely to cross-linking of bases by radiation in the isolated twin helix DNA produced by the radiation. The individual strands of a twin helix are not separated, and the isolated twin helices will recombine to the three-dimensional structure whenever conditions become favorable. The isolated lengths of twin helix may be thought of as the products of a photochemical dissociation, and the chance of their recombining will be proportional to the square of their concentration. It is not necessary that an isolated length of twin helix should recombine with its original partner. The formation of water H bonds with any other piece of isolated twin helix will give the secondary structure which protects from radiation and will leave the biological function of the twin helix unimpaired.

Let M_{30} be the initial amount of three-dimensional DNA, M_3, and let M_2 be the fraction of this converted to two-dimensional DNA after the incidence of D units of radiation, at intensity $I = \mathrm{d}D/\mathrm{d}t$. We assume that M_2 is always small, so that the radiation is always acting on an essentially constant amount of M_3. Then, for an additional amount of radiation, $\mathrm{d}D$

$$\mathrm{d}M_2 = c_1 M_{30}\mathrm{d}D - c_2 M_2^2 \mathrm{d}t$$

$$\mathrm{d}M_2 = c_1 M_{30}\mathrm{d}D - c_2 M_2^2 \mathrm{d}D/I \qquad (1)$$

$$\mathrm{d}D = \frac{\mathrm{d}M_2}{c_1 M_{30} - c_2 M_2^2/I}$$

Integrating

$$D = \frac{1}{\sqrt{c_1 M_{30} c_2/I}} \tanh^{-1}\left(M_2\sqrt{\frac{c_2}{I c_1 M_{30}}}\right)$$

(12) H. S. Kaplan and L. E. Moses, *Science*, **145**, 21 (1964).

(13) M. Terzi, *Nature*, **191**, 461 (1961).

(14) R. Langridge, D. A. Marvin, W. E. Seeds, H. R. Wilson, C. W. Hooper, M. H. F. Wilkins, and L. D. Hamilton, *J. Mol. Biol.*, **2**, 38 (1964); see p 64.

Since M_2 is assumed zero when D is zero, the integration constant is zero. Solving for M_2 and writing K for $\sqrt{c_1 M_{30} c_2 / I}$

$$M_2 = \frac{\tanh (KD)}{\sqrt{c_2/(Ic_1M_{30})}} \qquad (2)$$

This gives the production of M_2 in a population of diploid cells as a function of total dose D. Even though most of the population becomes inactivated biologically, the production of M_2 continues at approximately this rate, since the inactivated molecules will continue to produce approximately the normal amount of M_2.

If a population M_3 of diploid cells has been subjected to a dose D, the number inactivated by a further dose dD is

$$dM_3 = -c_3 M_3 M_2 dD$$

Substituting for M_2 from eq (2) and integrating

$$\ln M_3 = -\frac{c_3 I}{c_2} \ln \cosh (KD) + \text{constant}$$

Since $M_3 = M_{30}$ when D is zero, the constant is $\ln M_{30}$, so that

$$\ln \frac{M_3}{M_{30}} = -\frac{c_3 I}{c_2} \ln \cosh (KD)$$

Since $\ln (M_3/M_{30})$ is -1 when D is D_{37}, $c_3 I/c_2$ is $1/\ln \cosh (KD_{37})$ and

$$\ln \frac{M_3}{M_{30}} = -\frac{\ln \cosh (KD)}{\ln \cosh (KD_{37})}$$

Expressing D in units of (KD_{37}) and inserting the value of ln cosh (1) give finally

$$\ln \frac{M_3}{M_{30}} = -2.30 \ln \cosh (D/D_{37}) \qquad (3)$$

Thus a plot on log-log paper of surviving fraction as a function of cosh (D/D_{37}) should be linear, with a slope of -2.3.

Three examples of inactivation plots, selected at random from the literature, are shown in Figure 2: for hamster cells in tissue culture, from Elkind and Sutton;[15] for hela cells in tissue culture, from Puck and Marcus;[16] and for normal mouse bone marrow cells, from Till and McCullough.[17] These plots were constructed by measuring the points on published figures. The plots are approximately linear and have the slopes: mouse, -2.0; hamster, -2.1; and hela, -3.5. Two of these slopes are near the calculated -2.3. In the hela cell measurements it appears that there was a strong photoelectric component of backscatter from the glass slides on which the cells were

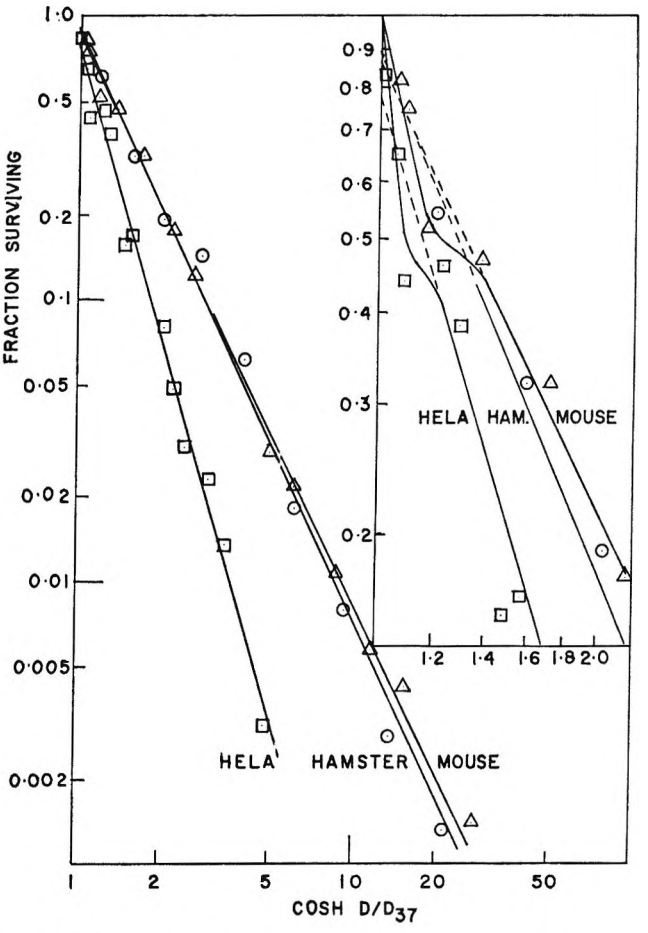

Figure 2. Irradiation plots to test eq 3.

mounted, so that there might have been a mixture of radiations with different LET. This is possibly the reason for the slope being too large. In order to get more information on the slope, two more readily available plots of data were analyzed: diploid *Saccharomyces cerevisiae* (X 320 yeast), from Mortimer;[18] and chicken embryo wing bud cells irradiated *in ovo*, from Philpott, Shaeffer, and Tolmach.[19] Log–log plots of surviving fraction as a function of cosh (D/D_{37}) had slopes of -2.1 and -2.6, respectively. It is concluded from these examples that the normal slope for such plots is about -2.3, in agreement with our eq 3.

The two plots last mentioned intersect the axis of ordinates very close to unity, but in Figure 2 there is

(15) M. M. Elkind and H. Sutton, *Nature*, **184**, 1293 (1959).

(16) T. T. Puck and P. I. Marcus, *J. Exptl. Med.*, **103**, 653 (1956).

(17) J. E. Till and E. A. McCullough, *Radiation Res.*, **14**, 213 (1961).

(18) R. K. Mortimer, *ibid.*, **9**, 312 (1958).

(19) B. W. Philpott, C. W. Shaeffer, and L. J. Tolmach, *ibid.*, **17**, 508 (1962).

no doubt that the main part of each line intersects the axis of ordinates below 1.0. The intercepts are: hela, 0.78; mouse, 0.88; and hamster, 0.90. The initial portions of the plots are shown on a larger scale at the upper right of Figure 2, and in the enlarged figure nonlinear curves have been fitted to the upper parts of the hela and hamster plots to match the data points as closely as possible. The reason for an initial high sensitivity is thought to be as follows. It has been recognized for many years that "the sensitivity of cells to irradiation is in direct proportion to their reproductive activity." Since reproductive activity involves the production of new DNA, which presumably is initially not protected with the three-dimensional secondary structure due to water H bonds, the high sensitivity of reproducing cells is entirely in line with the ideas discussed above. Moreover, it is likely that the majority of cells will have some isolated DNA helix which has not yet entered the protective secondary structure or which has been withdrawn from that structure for replication purposes. Accordingly, it seems reasonable that the more rapid inactivation shown in the plots of Figure 2 is due to the rapid destruction of isolated DNA helix already in the cell at the start of the irradiation.

Elkind and Sutton[15] studied the recovery of irradiated hamster cells as a function of the resting time between two irradiations. Following the ideas advanced above, the rate of recovery, as shown in their Figure 1, would measure the rate at which M_2 recombined to M_3, according to our eq 1. The measured recovery proceeds initially exponentially as a function of time, with a time constant of about 80 min for the amount of M_2 to fall to $1/e$. This recombination would therefore have little effect on the fraction surviving, since the largest dose of about 1200 rads was given in less than 2 min. This is in accordance with the usual experience that the fraction surviving does not depend critically on the rate at which the dose is given.

One artifact may be noted in connection with survival plots. For diploid cells, plots of log (surviving fraction) as a function of $D^{3/2}$ are quite linear. It is thought that this is due to the fact that log cosh (D/D_{37}) increases proportionally to $(D/D_{37})^{3/2}$ over a range of D/D_{37} from 0.8 to 4.0, which covers the range of dose used in many investigations.

VI. Discussion

In conclusion, since this paper presents some novel ideas about the radiation inactivation of DNA, it may be well to summarize the experimental facts on which the ideas are based and the scope of the understanding to which these ideas lead. The main experimental facts used are as follows. That DNA molecules can be inactivated by some form of cross-linking is very old. Inactivation by cross-linking of bases is discussed by Marmur and Grossman,[1] and the "reversible DNA" of Geiduschek[2] makes use of the same fact. The great radiation stability of bases in nucleosides and the plentiful generation of H radicals from sugars in nucleosides are based on the mass spectra of Biemann and McCloskey.[6] The migration of atoms and molecular fragments in molecules is demonstrated by all mass spectrometry[6] and by Tikhomirova, *et al.*,[8] in bulk polyethylene. The G value for DNA was given by Lett, *et al.*[7] The principal reaction sites for H radicals in the bases are discussed by Scholes[10] from the aqueous solution chemistry point of view. X-Ray crystallographic data on the presence of water in DNA are discussed by Langridge, *et al.*[14]

The major results derived from this experimental basis are as follows: (a) a single mechanism correlating radiation inactivation of virus DNA, inactivation of diploid cell DNA, and restoration effects after irradiation of diploid cells; (b) a direct calculation of D_{37} for virus DNA, in fair agreement with experiment; (c) a direct calculation of the shape and slope of the inactivation curve for diploid cells, in agreement with experiment.

Acknowledgments. The author is grateful to Dr. Hillel Poritsky for help with the integrations of section V. His thanks are also due to a referee for detailed criticism of the calculations of section IV, which led to the improved treatment given here.

High-Temperature Infrared Spectroscopy of Olefins Adsorbed on Faujasites

by P. E. Eberly, Jr.

Esso Research Laboratories, Humble Oil and Refining Company, Baton Rouge Refinery, Baton Rouge, Louisiana *(Received October 11, 1966)*

A high-temperature infrared cell for recording spectra of solids and adsorbed species at temperatures up to 650° and pressures from 10^{-5} to 760 mm is described. Thus, spectra recorded at 427° show that hydrogen faujasite (HY) produced by calcining NH_4Y under vacuum to 427° contains three different hydroxyl groups having absorption frequencies of 3740, 3635, and 3540 cm^{-1}. These groups readily exchange with deuterium gas to form their OD analogs. When hexene-1 is adsorbed on HY at 93°, the double-bond character disappears. At 150°, polymerization and dehydrogenation processes begin to occur to form a conjugated polyene type of structure as evidenced by a band at 1600 cm^{-1}. Upon heating to 260°, cyclization occurs to form a hydrogen-deficient aromatic ring structure characterized by a band at 1580 cm^{-1}. With the exception of ethylene, which formed no adsorbed species capable of detection, similar results were observed with other low molecular weight olefins, although differences in extent of reaction were found. The condensed-ring structure was not produced on other ion-exchanged forms of zeolite Y with the possible exception of AgY in which partial reduction could have occurred to form some HY. The main reaction on other ion-exchanged forms involved the loss of double-bond character.

I. Introduction

In the characterization of solid surfaces and adsorbed species by infrared spectroscopy, almost no spectra have been obtained at elevated temperatures. Since most catalytic reactions of practical importance occur at high temperatures, the need for spectral studies *in situ* at these conditions is obvious. First of all, with high-temperature spectroscopy, changes in catalyst structure, particularly with regard to the hydroxyl groups, can be directly observed. With *in situ* measurements, it is possible to avoid partial rehydration which sometimes occurs when the solid is lowered to room temperature for spectral studies. This effect can be particularly serious in systems which are not completely baked out. A second advantage of high-temperature infrared spectroscopy lies in the possibility of studying adsorbed species at actual reaction conditions, provided that their surface concentration is sufficiently large to permit their detection.

This paper describes a new high-temperature infrared cell and associated equipment for recording spectra of solids. Results are presented on the interaction of the various ion-exchanged faujasites with hexene-1 and other olefins at 90–427°.

Faujasite, a crystalline sodium alumino-silicate belonging to the zeolite family, can be readily synthesized and is frequently referred to as zeolite Y. This material has a silica:alumina molar ratio of near 5:1 and consequently is more stable to heat and steam than its counterpart, zeolite X, which has a silica:alumina ratio of only 2.5:1. Outside of the difference in composition, however, the anionic frameworks are structurally identical.[1,2] Heats of adsorption[3] as well as catalytic activity[4] depend strongly on the nature of the exchangeable ions. A number of investigators have recorded the spectra of various ion-exchanged faujasites at room temperature after activation at elevated temperatures.[5–8] With the exception of the

(1) L. Broussard and D. P. Shoemaker, *J. Am. Chem. Soc.*, 82, 1041 (1960).

(2) D. W. Breck, *J. Chem. Educ.*, 41, 678 (1964).

(3) P. E. Eberly, Jr., *J. Phys. Chem.*, 66, 812 (1962).

(4) J. A. Rabo, P. E. Pickert, D. N. Stamires, and J. E. Boyle, *Actes Congr. Intern. Catalyse, 2e, Paris, 1960*, 2055 (1961).

(5) L. Bertsch and H. W. Habgood, *J. Phys. Chem.*, 67, 1621 (1963).

(6) J. L. Carter, P. J. Lucchesi, and D. J. C. Yates, *ibid.*, 68, 1385 (1964).

(7) J. B. Uytterhoeven, L. G. Christner, and W. K. Hall, *ibid.*, 69, 2117 (1965).

hydrogen or "decationized" form, faujasites do not contain large concentrations of hydroxyl groups. Carter, Lucchesi, and Yates,[6] as well as Angell and Schaffer,[8] detected their existence on zeolites X and Y. Their concentration, however, appears to be small. By a deuterium-exchange technique, Uytterhoeven, Christner, and Hall[7] determined that the amount of such groups on NaY is 0.15×10^{20} OH/g for 1-μ crystals. This quantity is commensurate with the number of groups needed to terminate the external crystal faces. On the other hand, hydrogen faujasite contains nearly 50 times as many hydroxyl groups, which is sufficient to account for the number of "decationized" sites.

Although studies of olefin adsorption on other types of solids have been made,[9,10] work on zeolites has only recently begun to appear. Ethylene adsorption at room temperature on faujasite-type catalysts has been studied by Carter, *et al.*,[11] and Liengme and Hall.[12]

II. Experimental Section

Materials. The composition of sodium faujasite (NaY) is given in Table I. Other forms were obtained from this material by standard methods of ion exchange. HY was prepared by first exchanging the sodium with ammonium ions. For this purpose, 180 g of NaY was treated with a solution of 333 g of NH_4NO_3 dissolved in 3 l. of water. The exchange was conducted for 2 hr at 70°. After allowing settling and decanting the supernatant liquid, a fresh solution of NH_4NO_3 was added and the treatment repeated. After a total of five such treatments, the solid was filtered, thoroughly washed, and oven dried at 150° overnight. Analysis of this sample is given in Table I.

Table I: Properties of Na and NH_4 Faujasites

	NaY	NH_4Y
Composition as expressed by empirical formula, moles		
Na_2O	1.13	0.08
$(NH_4)_2O$	0	0.87
Al_2O_3	1.00	1.00
SiO_2	4.72	4.67
Relative crystallinity	1.00	0.93
Toluene adsorption capacity at 93° and 1 mm, mmoles/g[a]	2.4	2.1

[a] Prior to adsorption, samples were degassed at 427°.

Since, for electrical neutrality, the sum of the moles of exchangeable cation oxides should equal the moles of alumina, there appears to be a 13% excess of extraneous soda in NaY. On the other hand, the ammonium form has a 5% deficiency in cations. This small amount may be due to errors inherent in the analyses or to the presence of some alumina not incorporated in the zeolite structure. By comparing the intensity of the X-ray diffraction lines, the crystallinity of the NH_4Y was estimated to be over 90% of that of NaY. Adsorption capacity at low pressure, which constitutes an alternate method for estimating structure retention, gave essentially the same results.

To prepare HY, NH_4Y was heated *in situ* in the infrared cell up to 427° under vacuum. This process removed the physically adsorbed water and liberated NH_3 gas to produce HY in which the hydrogen atoms exist in the form of hydroxyl groups.

Other forms of faujasite were prepared by ion exchanging with the chloride salts of the desired ion. For AgY, the nitrate salt was used. In general a threefold excess of the ion was employed and the treatment was repeated three times.

Sample Preparation. For infrared examination, the solids were ground with a mortar and pestle. Then they were compressed under 30,000 psi into 1.25-in. diameter disks. These disks were about 8–16 mils thick and contained 12–22 mg of solid/cm^2. One of the difficulties in this procedure was the removal of the disk from the die for insertion into the sample disk holder. This was overcome by putting a slight bevel on the circumference of the plunger used for compression. Thus during fabrication, the pressure at the edge of the disk was much less than that at the middle and the powder did not bind strongly to the die.

Apparatus. Spectra were recorded with a Cary-White Model 90 infrared spectrophotometer. An important advantage of this instrument is its ability to measure spectra at elevated temperatures without undue interference from the furnace radiation. In this double-beam instrument, the infrared radiation is chopped prior to passing through the sample. Since the detection system is designed to respond only to the chopped radiation, the continuous radiation from the hot sample and furnace is not observed. In general, spectra were obtained in the region of 4000–1200 cm^{-1} at a spectral slit width of 4 cm^{-1} and a scan speed of 3 cm^{-1}/sec.

The high-temperature infrared cell used in this

(8) C. L. Angell and P. C. Schaffer, *J. Phys. Chem.*, 69, 3463 (1965).

(9) R. P. Eischens and W. A. Pliskin, *Advan. Catalysis*, 10, 2 (1958).

(10) D. J. C. Yates and P. J. Lucchesi, *J. Phys. Chem.*, 67, 1197 (1963).

(11) J. L. Carter, D. J. C. Yates, P. J. Lucchesi, J. J. Elliott, and V. Kevorkian, *ibid.*, 70, 1126 (1966).

(12) B. V. Liengme and W. K. Hall, *Trans. Faraday Soc.*, 62, 3229 (1966).

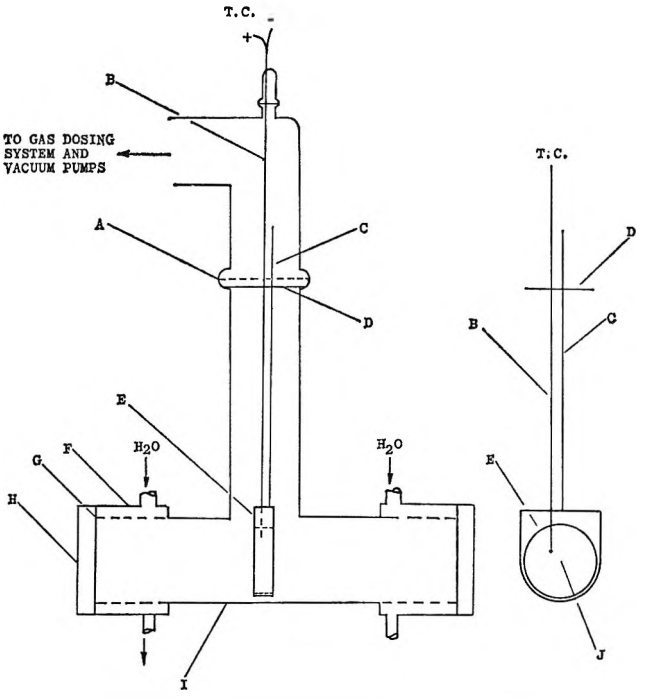

Figure 1. Diagram of high-temperature infrared cell and sample holder: A, O-ring seal; B, chromel–alumel thermocouple; C, handle for sample disk holder; D, supporting ring; E, stainless steel sample disk holder; F, water-cooling jacket; G, Glyptal seal; H, $2^5/_8 \times {}^1/_4$ in. KBr disk; I, 2-in. "Vycor" glass tube; J, $1^1/_4$-in. diameter sample disk.

study is shown in Figure 1. It was constructed from 2-in. diameter "Vycor" glass tubing and was connected to the associated vacuum and gas-dosing system by an O-ring seal (A). Two KBr disks (H) were attached to the ends of the tubing with "Glyptal." To keep these seals (G) cool during high-temperature operation, water-cooling jackets (F) were installed at each end. The central portion of the cell was wound with heating wire and carefully insulated so that the sample disks could be heated up to 650°.

A front view of the sample holder is shown in the right-hand portion of Figure 1. The sample disk (J) is inserted into a slot in the holder. With handle (C), the holder can be inserted into the cell and supported on a glass lip by ring D. A sheath containing two chromel–alumel thermocouples (B) is then inserted into the holder so that the junctions are near the center of the disk. The output of one thermocouple is sent to a recorder and that of the second to a stepless, proportional controller for accurate temperature control. With this system, spectra of solids can be measured *in situ* up to 650° and 10^{-5}–760 mm. Upon introducing gases to the high-vacuum system, the temperature of the disk was sometimes observed to increase momentarily 10–15° above the set point owing to increased heat conduction. In experiments where temperature control was critical, about 1 mm of helium was introduced to the system prior to hydrocarbon injection to eliminate this effect. To cancel out the absorption of infrared radiation by the gas phase, a dummy cell is placed in the reference beam and connected to the same vacuum and gas-dosing system.

III. Results

Hexene-1 Adsorption on Deuterium Faujasite (DY). Upon heating to 427° under vacuum, NH_4Y loses both adsorbed water and NH_3 gas to form HY. The hydrogen exists in the form of characteristic OH groups as shown by the solid-line spectrum in Figure 2 taken at 427°. Three distinct hydroxyl groups are observed at 3740, 3635, and 3540 cm^{-1}. This spectrum is similar to those recorded previously for HY at room temperature.[7,8] No evidence is observed for decreases in intensity of the OH bands with temperature.

Upon exposure of HY to 50 mm of deuterium gas at 427°, the three OH groups can be almost quantitatively converted to their OD analogs as observed by a shift in the infrared bands to 2750, 2680, and 2610 cm^{-1}, respectively. The spectrum of DY, recorded at 427°, is given by the dashed line in Figure 2.

DY exhibits strong interactions with adsorbed olefins. After recording the dashed-line spectrum in Figure 2, the excess deuterium gas was evacuated from the system and the sample cooled to 93° under vacuum. The sample was then exposed to 2-mm pressure of hexene-1 for 15 min and the spectrum in the bottom portion of Figure 3 was obtained.

First of all, hexene-1 upon adsorption loses its double-bond character as shown by the absence of an

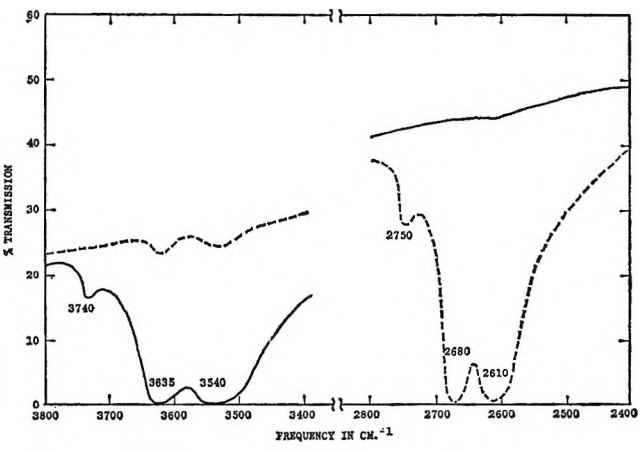

Figure 2. Infrared spectra of H(D)Y at 427°. The solid line represents the spectrum of HY. The dashed line represents the spectrum obtained after exposure to 50 mm of D_2 at 427°. The original disk contained 19 mg/cm² of NH_4Y.

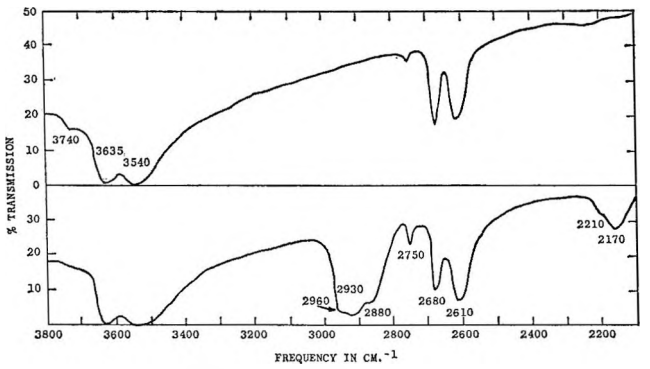

Figure 3. Infrared spectra of DY after exposure to hexene-1 at 2-mm pressure. The bottom spectrum is that obtained upon exposure of DY to 2-mm pressure of hexene-1 at 93°. After heating the sample to 427° the upper spectrum was obtained. The original disk contained 19 mg/cm² of NH_4Y.

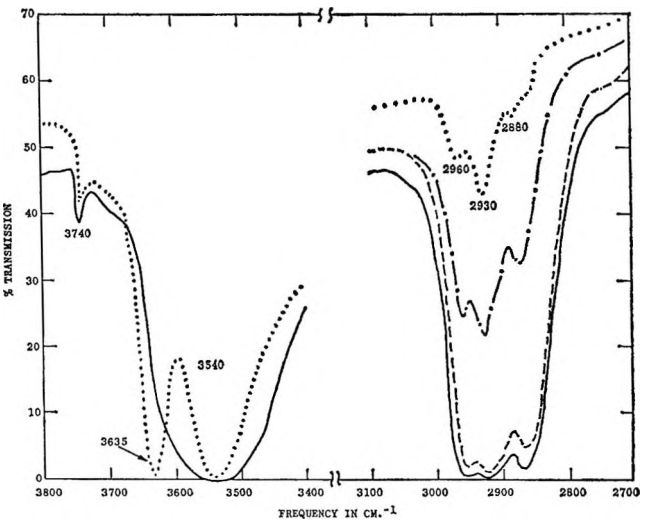

Figure 4. Infrared spectra in the OH and CH stretch regions of adsorbed species created by exposure of HY to hexene-1. The solid line represents the spectrum of HY exposed to 2 mm of hexene-1 at 93°. The remaining spectra were taken as the temperature was raised to successively higher values: – – –, 149°; — · —, 204°; and · · · ·, 260°. The original disk contained 16 mg/cm² of NH_4Y.

olefinic CH stretch band which normally occurs at 3090 cm^{-1} in pure gas-phase hexene-1. At the same time, a rapid exchange occurs between the hydrogen atoms in the adsorbed species and deuterium in the OD groups. This is shown by the appearance of CD linkages absorbing at 2210 and 2170 cm^{-1} and by the regeneration of the characteristic OH frequencies which blank out even at short exposure times. Relative to the 2610-cm^{-1} band, the band at 2680 cm^{-1} has become weaker, suggesting that the hydrocarbon has preferentially adsorbed near these groups causing a lowering in absorption frequency and/or broadening of the band. Upon removal of the adsorbed material by evacuation and heating to 427°, the 2680-cm^{-1} band again becomes the more intense, as shown by the spectrum in the upper portion of Figure 3.

Adsorption of Various Olefins on Hydrogen Faujasite (HY). The interaction of hexene-1 with HY was studied in more detail under conditions in which temperature surges were eliminated by prior injection of a small amount of helium. After injection of 1 mm of helium at 93°, hexene-1 was introduced to the system until the pressure reached 2 mm. The spectrum was recorded after a 1-hr exposure. Additional spectra were recorded after a 1-hr exposure at successively higher temperatures of 149, 204, and 260°. Spectra in the OH and CH stretch region are given in Figure 4. As the temperature is raised, progressively less material is adsorbed on the surface, as evidenced by the decreasing absorbance of the CH stretching bands at 2960, 2930, and 2880 cm^{-1}. Olefinic CH stretch vibrations, which occur above 3000 cm^{-1}, were not observed at any temperature investigated. The adsorbed material is seen to interact preferentially with the hydroxyl groups at 3635 cm^{-1}. Such an interaction normally results in the displacement of the band to lower frequencies. However, no discrete, additional bands were found to occur, the spectrum merely exhibiting a small depression in transmission throughout the whole OH stretch region.

In addition to these effects, reactions leading to cyclization and formation of aromatic ring structures were also observed. Spectra illustrating these phenomena are shown in Figure 5 and were taken at the same conditions as those in Figure 4. In this region of the spectrum, bands due to C=C stretching modes, aromatic ring vibrations, and CH bending modes occur.

At 93°, where the concentration of adsorbed material is highest, as indicated by the intense CH band absorption at 1460 and 1380 cm^{-1}, no olefinic vibration at 1630 cm^{-1} owing to the C=C stretching mode is observed. The broad, low-intensity band in this region is due to some vibration of the solid, since it is present even before exposure to the olefin. At 149°, however, a new band appears at 1600 cm^{-1} which is indicative of the formation of olefinic groups in a conjugated polyene type of structure.[13,14] This structure must be highly unsaturated, since no olefinic CH stretch vibrations are observed. At the same time, the intensity

(13) R. N. Jones and C. Sandorfy, "Chemical Applications of Spectroscopy," Interscience Publishers, Inc., New York, N. Y., 1956, Chapter 4.

(14) E. R. Blout, M. Fields, and R. Karplus, *J. Am. Chem. Soc.*, **70**, 194 (1948).

Table II: Absorbance[a] of Bands in 1600–1580-cm^{-1} Region on HY at 2-mm Pressure

Temp, °C	Hexene-1	Pentene-1	Butene-1	Isobutylene	Propylene
93	0	0	0	0	0
149	0.93 (1600)[b]	0.71 (1600)	0.92 (1600)	3.91 (1590)	2.00 (1600)
204	3.48 (1590)	0.67 (1595)	1.04 (1590)	3.48 (1590)	5.38 (1590)
260	4.13 (1580)	4.18 (1580)	2.45 (1585)	4.27 (1585)	9.40 (1580)

[a] Per gram of solid. [b] Numbers in parentheses represent wavenumbers (cm^{-1}).

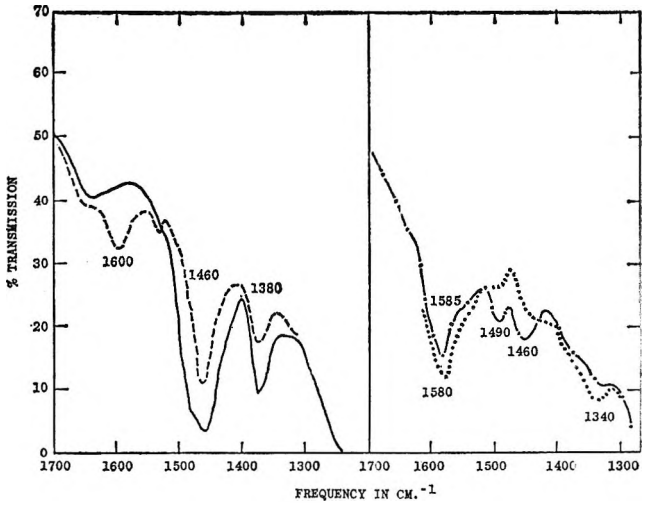

Figure 5. Infrared spectra in the 1700–1200-cm^{-1} region of adsorbed species created by exposure of HY to hexene-1. The lines have the same significance as those in Figure 4.

of the saturated CH bending frequencies decreases. Upon successive increases of temperature to 204 and 260°, the new band becomes more intense and shifts progressively to a lower frequency near 1580 cm^{-1}. This latter band is characteristic of an aromatic ring vibration associated with the carbon skeleton and is not due to CH linkages.[13,15] Its intensity, in fact, varies inversely with those associated with carbon–hydrogen vibrations. This aromatic species is tightly adsorbed, since the 1580-cm^{-1} band cannot be lowered in intensity by further evacuation and heating up to 427°. The discharged disk was brownish in color.

Similar results are observed with other low-molecular weight olefins, although differences in extent of reaction exist. Data are listed in Table II and were obtained in the same manner as described for hexene-1. With ethylene under the same conditions, no bands due to adsorbed species were observed. At 150°, all the other olefins produce the new band at 1600 cm^{-1} due to a conjugated polyene structure. At higher temperatures, the band in all cases shifts to 1585–1580 cm^{-1} characteristic of the aromatic ring structure.

Hexene-1 Adsorption on Other Ion-Exchanged Faujasites. The degree of interaction of hexene-1 with various faujasites depends on the nature of the cation. The reactions to produce aromatic ring structures appear to be peculiar to HY and AgY. With the latter material, however, some reduction of the silver occurred during exposure to the hydrocarbon. This could have resulted in the formation of HY, accounting for their similarity in behavior.

With the other ion-exchanged faujasites, the main effect was the loss of double-bond character in the adsorbed material. An estimate of this loss is obtained by dividing the absorbance at 1630 cm^{-1} due to C=C stretching by that at 1460 cm^{-1} due to CH band vibrations. Values are listed in Table III. In all cases, the C=C vibration occurs near 1630 cm^{-1} which represents a shift of 12 cm^{-1} from that in liquid hexene-1. For the alkali metal forms, the intensity ratio is about the same as observed for liquid-phase hexene-1. The ratio is markedly lower for the divalent forms, and with AgY and HY, no double frequency is observed.

Table III: Hexene-1 Adsorption at 93° and 2 mm. Amount of Double-Bond Character in Adsorbed Phase

Solid	% exchange	A_{1630}/A_{1460}
NaY	100	1.53
LiY	64	1.45
KY	95	1.34
CaY	75	0.84
MgY	67	0.35
CdY	73	0.20
AgY	100	0
HY	92	0

IV. Discussion

High-temperature infrared spectroscopy shows that the OH groups on hydrogen faujasite exhibit nearly

(15) C. N. R. Rao, "Chemical Applications of Infrared Spectroscopy," Academic Press Inc., New York, N. Y., 1963, Chapter 2.

the same infrared spectrum at 427° as that at 93°. In this range, we see no evidence for proton delocalization. This effect has been observed on micas[16] and also on decationized faujasite.[17] Since the predominant OH bands blank out at both conditions, it is possible that some loss of intensity may have occurred which would have been beyond our detection. This loss, however, could not have been large.

The OH groups absorb at 3740, 3635, and 3540 cm^{-1}. The groups at 3740 cm^{-1} are almost universally observed on silica-containing materials and are not believed to be necessarily characteristic of HY. Since zeolites are rarely completely free of amorphous material, it is possible that they could be associated with such an impurity rather than the crystalline faujasite. The OH groups at 3635 and 3540 cm^{-1} appear to be peculiar to HY. Some authors have attributed the lower frequency band to interaction between two adjacent hydroxyl groups.[8] Liengme and Hall,[12] however, suggested that the two bands may result from OH groups in different, crystallographic locations. The data in the present report favor the latter explanation. The groups at 3635 cm^{-1} are believed to be located inside the adsorption cages near six-membered oxygen rings. The other groups at 3540 cm^{-1} are in inaccessible bridge positions located between two sodalite units. The assignment of the lower frequency to the bridge position is consistent with the possibility of the proton being able to interact with twice as many oxygen anions as its counterpart in the cage position. Also, it explains the preferential interaction of olefins with the 3635-cm^{-1} band. The fact that both groups in their deuterated form can be transformed into their hydrogen analogs upon exposure to hexene-1 is probably due to the formation of hydrogen during the adsorption process.

HY reacts strongly with adsorbed olefins causing them to polymerize, dehydrogenate, and cyclize to form aromatic ring structures. These reactions occur on the surface at 150–260°, which is an unusually low temperature since normal aromatization processes operate at 500–600°. The polymerization reaction is the first to occur near 150°, as evidenced by the appearance of a band at 1600 cm^{-1}, indicative of a polyene structure. Propylene and isobutylene, being the most easily polymerized, show the greatest intensity of this band. At higher temperatures, the band shifts to 1585–1580 cm^{-1}, characteristic of the aromatic ring structure. This sequence of reactions is one of the mechanisms of carbon formation. A band in this region has been reported for cokes isolated from silica–alumina catalysts.[18]

The interaction of olefins with other ion-exchanged faujasites is less intense. The spectra of hexene-1 on alkali metal forms are not too dissimilar from that of pure liquid hexene-1. With divalent zeolites, there is a loss in double-bond character, as indicated by a decrease in intensity of the 1630-cm^{-1} band. This may result from an interaction of the π electrons with the surface to form carbon to surface bonds or to the occurrence of some polymerization.

(16) J. J. Fripiat, P. Rouxhet, and J. Jacobs, *Am. Mineralogist*, **50**, 1937 (1965).

(17) Private communication.

(18) P. E. Eberly, Jr., C. N. Kimberlin, Jr., W. H. Miller, and H. V. Drushel, *Ind. Eng. Chem. Process Design Develop.*, **5**, 193 (1966).

Regularities and Specific Effects in Enthalpies of Transfer of Ions from Water to Aprotic Solvents[1]

by Harold L. Friedman

Department of Chemistry, State University of New York, Stony Brook, New York *(Received October 11, 1966)*

Some regularities in published data for enthalpies of transfer of ions from water to propylene carbonate, dimethyl sulfoxide, formamide, and N-methylformamide are pointed out. The qualitative trend of the halide ions is the same in each case, while the varying trend of the alkali metal ions seems to reflect differences in solvent basicity. There is evidence for a large specific interaction of $AsPh_4^+$ and BPh_4^- with at least one of the first two solvents.

It is often said that aqueous electrolyte solutions are so complicated that we shall have an easier time understanding electrolyte solutions in general when we have a much wider selection of data for solutions in less complicated solvents. It is our purpose to show here, on the basis of some recent results for enthalpies of solution, that even in aprotic solvents one may find large effects that are not expected on the basis of the simplest models. Our method is first to extract some regularities and then to examine deviations from the regular behavior.

The measurement of heats of solution of a salt in an organic solvent and in water, together with appropriate extrapolation to infinite dilution, may be combined to get ΔH° of process 1

$$A^+(aq) + B^-(aq) \longrightarrow A^+(org) + B^-(org) \quad (1)$$

We will call this ΔH_{tr}. If an assumption is made regarding the separation of ΔH_{tr} into the ionic contributions, one may represent the data for a series of salts and a particular organic solvent as shown in Figure 1 for solutions in propylene carbonate[2]

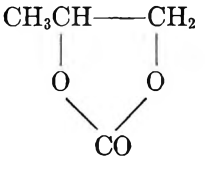

If the separation assumption is made in a different way, the effect is only to shift the anion and cation curves up or down with respect to each other. We shall focus our attention on the *shape* of each curve and its dependence upon organic solvent. These features are independent of the separation assumption.

In a similar way the choice of ionic radii used as abscissa in Figure 1 is somewhat arbitrary, but it is not crucial in determining the qualitative shapes of the curves. For simple ions the Pauling crystal radii have been used. For complex ions the radii are estimated from sums of bond lengths plus an allowance of 1 A for the van der Waals radius of the outermost atom or they are estimated form ionic volumes. These estimates are described in detail by Robinson and Stokes[3] and we have used their results when available.

While ΔH_{tr} is more complicated to interpret than enthalpies of transfer from solution to gas phase, *i.e.*, solvation enthalpies, the latter are not at present experimentally accessible for complex ions. It is valuable to include these because of their intrinsic chemical interest as well as because they extend the field of ions available for study.

The ionic enthalpy of transfer may be estimated from the Born charging equation[2] if it is assumed that the ionic-size parameter is independent of temperature. From the calculated function shown in Figure 1 it is clear that the macroscopic dielectric effects which are

(1) Research supported by the Office of Saline Water.

(2) Y. C. Wu and H. L. Friedman, *J. Phys. Chem.*, **70**, 2020 (1966).

(3) R. A. Robinson and R. H. Stokes, "Electrolyte Solutions," Butterworth and Co. Ltd., London, 1955, Table 6.2.

accounted for by the Born equation are negligible here except in the case of Li^+.

Wu and Friedman[2] have indicated that the curves in Figure 1 are qualitatively what one would expect on the basis of two assumptions.

(1) Propylene carbonate is nearly an ideal solvent for ions—one in which the thermodynamics of solvation can be calculated from macroscopic electrostatics, *i.e.*, from the Born equation, with allowance for a region about each ion that is not penetrated by the dielectric.[4,5] This region is the crude macroscopic equivalent of the region that is inaccessible to the centers of charge of the solvent molecules.

(2) An ion in water may produce three types of structural modification as depicted in the models of Frank and Evans.[6,7] These are an inner cosphere of water oriented by the ionic fields, an outer cosphere of water in a state of more orientational randomness than bulk water at the same temperature, and possibly a cosphere region in which water has more orientational order than bulk water at the same temperature. The different dependence of the first and second effects on ionic size determines the left branches of the curves in Figure 1, while the right branch is due to the third effect becoming dominant for large ions with hydrophobic surfaces.[7]

In Figure 2 we present the corresponding data for solutions in dimethyl sulfoxide (DMSO) obtained by Arnett and McKelvey.[8] It is striking that the anion behavior is so closely similar to that in propylene carbonate (PC) while the cation behavior is very different. This may be attributed to the greater basicity of DMSO which makes it basic enough to enter into specific interaction with the smaller cations although it is nearly an ideal solvent for anions.[8] Independent evidence for this basicity difference is furnished by the comparison of ΔH° of solution of water in the two solvents: 2.00 kcal/mole in PC and −1.28 kcal/mole in DMSO.[2,8]

Some confirmation of this effect is furnished by data in formamide[9] and N-methylformamide[10] shown in Figure 3, although these are not so nearly aprotic solvents as PC and DMSO. In each case the anion dependence is qualitatively similar to that in PC. The differences are presumably due to hydrogen bonding to the anions for the systems in Figure 3, but they are not easy to interpret because each is the net effect of forming solvent–anion hydrogen bonds while breaking solvent–solvent hydrogen bonds. However, it seems reasonable that formamide, which can form three-dimensional hydrogen-bonded networks like water, produces smaller effects (*i.e.*, ΔH_{tr} is less sensitive to the size of the anion) and so is more similar to water by this measure than N-methylformamide, which can only form H-bonded chains. On the other hand, the cation dependence is that expected if both solvents are more basic than PC. By this criterion the basicity of

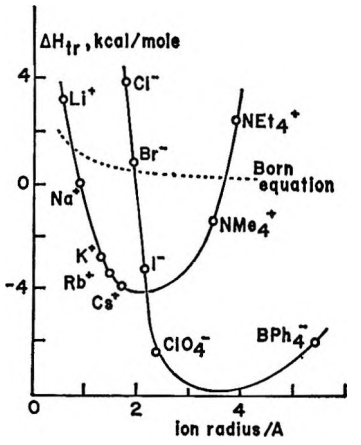

Figure 1. Enthalpies of transfer from water to propylene carbonate. The data are from ref 2 where the separation assumption is made on the basis that ΔH_{tr} is the same for Cs^+ and I^- except for certain small effects in the water.

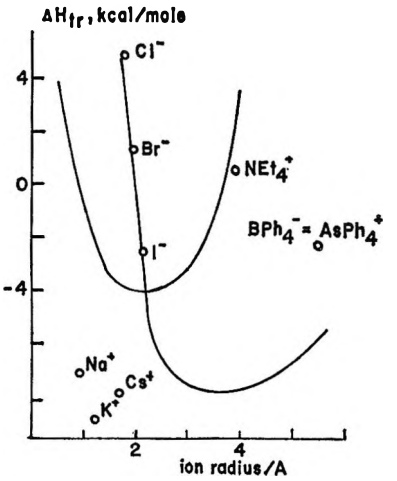

Figure 2. Enthalpies of transfer from water to DMSO. The data are from ref 8 where the assumption is made that ΔH_{tr} is the same for $AsPh_4^+$ and BPh_4^-. The curves are copied from Figure 1.

(4) A. Voet, *Trans. Faraday Soc.*, 32, 1301 (1936).

(5) W. M. Latimer, K. Pitzer, and C. M. Slansky, *J. Chem. Phys.*, 7, 108 (1939).

(6) H. S. Frank and M. W. Evans, *ibid.*, 13, 507 (1945).

(7) H. S. Frank and W. Y. Wen, *Discussions Faraday Soc.*, 24, 133 (1957).

(8) E. M. Arnett and D. R. McKelvey, *J. Am. Chem. Soc.*, 88, 2598 (1966).

(9) G. Somsen and J. Coops, *Rec. Trav. Chim.*, 84, 985 (1965).

(10) R. P. Held and C. M. Criss, *J. Phys. Chem.*, 69, 2611 (1965).

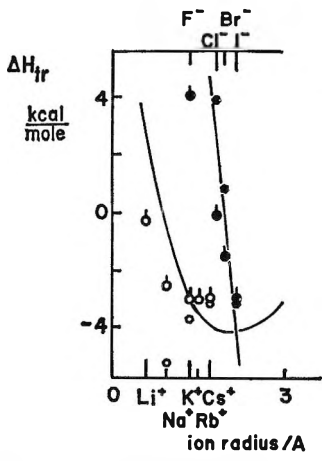

Figure 3. Enthalpies of transfer from water to formamide (ó) and N-methylformamide (○). The data are from ref 9 and 10, respectively, together with the assumption that ΔH_{tr} is the same for Cs^+ and I^-. The curves are copied from Figure 1.

all these solvents may be ordered PC < formamide < DMSO < N-methylformamide. Arnett[11] has reviewed other measures of the strengths of very weak bases and one such measure, the ionization constant, K_a, of the conjugate acid related to aqueous media at 25°, is given for two of these compounds as follows: formamide, $pK_a = -2.7$; DMSO, $pK_a = 0$. This is consistent with the above order.

The effect of the solvent basicity difference should diminish as cations get larger and thus ΔH_{tr} should be the same for PC and DMSO for large enough cations. However we find ΔH_{tr} of Cs^+ is 6.6 kcal/mole less than that of NEt_4^+ in PC while the corresponding difference in DMSO is 8.3 kcal/mole. The difference suggests residual specific effects in at least one of the solvents, even for ions as large as Cs^+.

It is also remarkable that in DMSO the ΔH_{tr} of $AsPh_4^+$ is 2.9 kcal/mole less than for NEt_4^+, inasmuch as both are expected to be iceberg makers in the aqueous phase and to be quite inert in the organic phase. That the effect is due to a peculiarity of the aryl complex in the organic phase is suggested by the comparison of ΔH_{tr} of I^- with BPh_4^-. The order is reversed on going from PC to DMSO. This reversal amounts to a shift of 3 kcal/mole in the enthalpy of BPh_4^- relative to that of I^- between the two solvents.

It is of interest to note that the enthalpy of hydration of gaseous C_2H_6 is −4.4 kcal/mole while that of C_6H_6 is −7.7 kcal/mole. This difference makes a large contribution to the enthalpy of transfer that is opposite in sign to that needed to account for the difference between NEt_4^+ and $AsPh_4^+$ in DMSO, provided we assume that the ionic enthalpies of transfer have additive contributions from the substituent alkyl or aryl groups. Other experimental evidence against the relevance of such an additivity concept is found in the values of ΔH_{tr} from water to DMSO of various R–Ph and R–OH compounds reported by Arnett and McKelvey.[8] (The necessary heats of solution of the hydrocarbons in water were derived[8] from data on the temperature dependence of solubilities and are quite uncertain because of the strong curvature of the log K *vs.* $1/T$ plots.) Such additivity relations would be useful here if they were valid, but we cannot be sure whether their failure is due to effects in the aqueous phase or DMSO phase or both.

A physical effect which may be responsible for the difference in ΔH_{tr} or NEt_4^+ and $AsPh_4^+$, and which is consistent with the other observations as well, is the inductive interaction $\mu^2\alpha/r^6$ where α is the polarizability of the solute, μ is the electric dipole moment of the solvent, and r is the equilibrium separation of solvent and solute molecules. While the expression given is for the interaction of point molecules and what is required here is an ensemble average of orientations and separations of solvent molecules in contact with the solute,[12] some idea of the magnitude of the effect may be obtained by considering the inductive term in the interaction of a single DMSO molecule and a C_2H_6 or C_6H_6 molecule in contact in the gas phase. With the parameters $\alpha = 4.33$ A^3 for C_2H_6 and 9.89 A^3 for C_6H_6[12] and $\mu = 4.94$ D. for PC[13] and 3.96 D. for DMSO[14] and $r = 4$ A, we find 0.54 kcal/mole for the DMSO–C_6H_6 interaction and 0.27 kcal/mole for the DMSO–C_2H_6 interaction and somewhat larger values for the interactions with PC. With n hydrocarbon–DMSO contacts in solution this interaction would be increased n-fold, although it tends to be reduced when allowance is made for interrupting DMSO–DMSO interactions when the hydrocarbon is introduced. It would require much more detailed calculations to get quantitative estimates, because the energies are not small compared to $RT = 600$ cal/mole so the usual[12] high-temperature approximation orientational average does not apply. The orientational dependence of the potentials would also make the effects nonadditive for neighboring groups, so both in this respect and in magnitude the inductive effect seems to be in qualitative agreement with the observations.

In order to obtain single-ion free energies of transfer it is sometimes assumed that for large ions (ferro-

(11) E. M. Arnett, *Progr. Phys. Org. Chem.*, 1, 223 (1963).

(12) J. O. Hirschfelder, C. F. Curtiss, and R. B. Bird, "Molecular Theory of Gases and Liquids," John Wiley and Sons, Inc., New York, N. Y., 1954.

(13) R. Kempa and W. H. Lee, *J. Chem. Soc.*, 1936 (1958)

(14) H. Dreizler and G. Dendl, *Z. Naturforsch.*, 19a, 512 (1964).

cinium, cobalticinium,[15] tetraphenylphosphonium, and tetraphenylborate[16]) the free energy of solvation is that of the corresponding uncharged species plus a Born charging term. Indeed in each case the assumptions seem quite consistent with the observations. This suggests that specific effects of the kind discussed here are not important for other (less polar?) solvents or else they are much more easily seen in the enthalpy or entropy than in the free energy, just as for structural effects in aqueous solutions.

Finally, it must be remarked that the assumption that propylene carbonate is a nearly ideal solvent for ions may be of limited significance, although it has been useful in this discussion. For one thing, the solvation energies of the monatomic ions in this solvent do not agree with the Born equation within the experimental error, although the agreement is better than for solvation enthalpies in water.[2] Also, although solvent basicity seems to contribute less to the nonideality of propylene carbonate than for the other solvents discussed here, there is no indication that the less well-defined specific effects mentioned above are smaller for propylene carbonate than for the other solvents.

Acknowledgment. The author is grateful to Professor E. M. Arnett for many suggestions concerning this problem.

(15) H. M. Koepp, H. Wendt, and H. Strehlow, *Z. Elektrochem.*, **64**, 483 (1960).

(16) E. Grunwald, G. Baughman, and G. Kohnstamm, *J. Am. Chem. Soc.*, **82**, 580 (1960).

Reactions of Ammonia with Porous Glass Surfaces

by M. J. D. Low, N. Ramasubramanian, and V. V. Subba Rao

School of Chemistry, Rutgers, The State University, New Brunswick, New Jersey *(Received October 13, 1966)*

Infrared spectra of NH_3 sorbed on highly dehydroxylated, deuterated, and fluoridated porous glass were recorded. Two pairs of bands at 3409 and 3320 cm^{-1} and at 3350 and 3308 cm^{-1} were attributed to physically adsorbed NH_3, hydrogen bonded to the SiOH and BOH groups of the glass surface, respectively. Bands at 3368 and 3282 cm^{-1} were ascribed to a $\equiv B-NH_3$ complex. Two pairs of bands at 3569 and 3479 cm^{-1} and at 3543 and 3459 cm^{-1} were ascribed to $=BNH_2$ and $\equiv SiNH_2$ groups, respectively. A single band at 3455 cm^{-1} was tentatively assigned to the N–H stretching vibration of a secondary amine, the nitrogen atom being bonded to two surface boron atoms.

There have been numerous reports dealing with the sorption of NH_3 on porous glass.[1–15] A variety of experimental techniques has been used and there seems to be a general agreement about the role of surface silanol groups as sites for a weakly bonded NH_3 adsorption. A strong adsorption requiring sites other than silanols has also been reported. Folman and Yates suggested that the strong sites were silicon or oxygen atoms.[1] However, Cant and Little pointed out that porous glass contained 3% B_2O_3 and stated that it was not impossible that strongly bound NH_3 was adsorbed on electron-deficient surface boron atoms themselves.[12] Chapman and Hair similarly concluded that strong NH_3 adsorption occurred on

(1) D. J. C. Yates, N. Sheppard, and C. L. Angell, *J. Chem. Phys.*, **23**, 1980 (1955).

(2) M. Folman and D. J. C. Yates, *Proc. Roy. Soc.* (London), **A246**, 32 (1958).

(3) M. Folman and D. J. C. Yates, *Trans. Faraday Soc.*, **54**, 429 (1958).

(4) U. Feldman, C. Schonfeld, and M. Folman, *ibid.*, **59**, 2394 (1963).

(5) I. Lubezky, U. Feldman, and M. Folman, *ibid.*, **61**, 940 (1965).

boron atoms which acted as Lewis acid sites on the surface.[14] Further support for this conclusion was presented by Hair and Chapman.[15]

Much of the evidence for the existence of the strong adsorption and deductions about the nature of the strong adsorption site come from infrared spectroscopic examination of specimens after various treatments with NH_3, desorption, and the like. However, the specimens were not subjected to prolonged initial degassing at high temperatures, which would lead to severe dehydration of the surface. Also, the existence of hydroxyl groups bonded to surface atoms other than silicon and the possible effects of such species on the sorption reaction were not considered in those studies. In contrast, recent studies of porous glass have provided evidence for the existence of surface BOH groupings, for the action of surface boron as adsorption center for the sorption and reaction of water, and for the migration of boron from within the bulk to the porous glass surface.[16–19] As multiple hydroxyl species may influence the interaction of NH_3 and the glass surface, we have again studied the sorption of NH_3 by porous glass, employing infrared spectroscopic methods. Well-dehydroxylated specimens were used as well as fluoridated or deuterated glasses. Some new infrared bands were observed. The results of the present study agree with previous work in that the same gross, over-all sorption effects were observed, but they differ significantly in the detail of all aspects.

Experimental Section

The general procedures employed were described elsewhere.[17] Porous glass,[20] Corning Code 7930, was purchased from Corning Glass Co. in the form of 1-mm thick sheets. Specimens 1 × 2.5 cm were cut from the sheets, heated in oxygen (~60 torr) at 700° for 3–4 hr in order to remove carbonaceous impurities, and were then degassed at 800° for 30 hr.

Specimens were deuterated by exposing samples to D_2O vapor at 200° for 12 hr and then degassing for 4 hr at 400°. Three or four repetitions of this treatment led to a conversion of approximately 80% of the hydroxyl groups. Fluoridation was done[14] by treating a fresh specimen with 30% NH_4F solution for 20 min, washing thoroughly, and air drying at 100° for 15 hr. The specimen was then degassed at 700° for 3 hr.

Spectra over the region 4000–2000 cm^{-1} were recorded with Perkin-Elmer Models 521 or 621 spectrophotometers. The ordinates of some of the spectra shown in the figures were displaced in order to avoid overlapping of traces. The number next to each spectrum near the left ordinate shows the per cent transmittance.

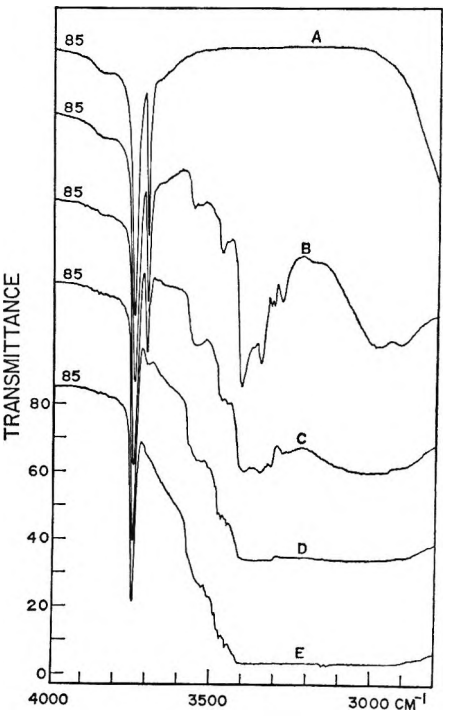

Figure 1. Effect of pressure on NH_3 sorption. A, background spectra of porous glass degassed for 30 hr at 800°. The specimen was exposed to NH_3 at room temperature. The pressure in torr was B, 8.5; C, 25; D, 80; E, 220.

Results

Typical results on the effects of pressure on NH_3 sorption are given by the sequence of spectra A–M of Figures 1 and 2. Spectra B–E were recorded with dif-

(6) D. Fiat, M. Folman, and U. Garbatski, *Proc. Roy. Soc.* (London), **A260**, 409 (1961).
(7) L. H. Little, N. Sheppard, and D J. C. Yates, *ibid.*, **A259**, 242 (1960).
(8) U. Feldman and M. Folman, *Trans. Faraday Soc.*, **60**, 440 (1964).
(9) M. Folman and D. J. C. Yates, *J. Phys. Chem.*, **63**, 183 (1959).
(10) A. N. Sidorov, *Dokl. Akad. Nauk SSSR*, **95**, 1235 (1954).
(11) A. N. Sidorov, *Zh. Fiz. Khim.*, **30**, 995 (1956).
(12) N. W. Cant and L. H. Little, *Can. J. Chem.*, **42**, 802 (1964).
(13) M. Folman, *Trans. Faraday Soc.*, **57**, 2000 (1961).
(14) I. D. Chapman and M. L. Hair, *ibid.*, **61**, 1507 (1965).
(15) M. L. Hair and I. D. Chapman, *J. Am. Ceram. Soc.*, in press.
(16) M. J. D. Low and N. Ramasubramanian, *Chem. Commun.*, No. 20, 1965.
(17) M. J. D. Low and N. Ramasubramanian, *J. Phys. Chem.*, **70**, 2740 (1966).
(18) M. J. D. Low and N. Ramasubramanian, unpublished data.
(19) M. J. D. Low and N. Ramasubramanian, unpublished data.
(20) M. E. Nordberg, *J. Am. Ceram. Soc.*, **27**, 299 (1944).

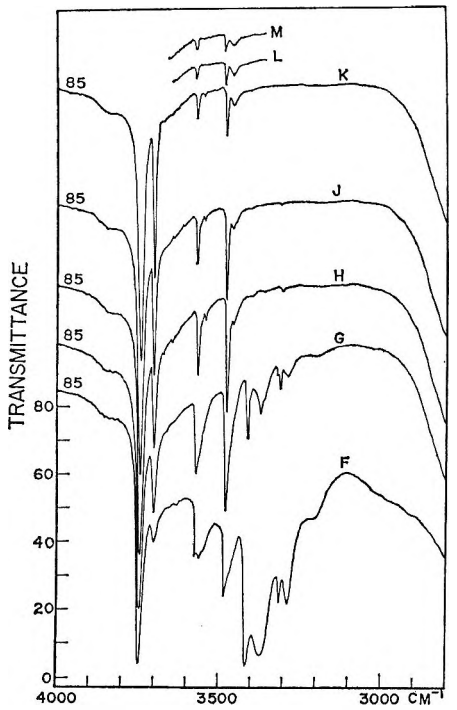

Figure 2. NH_3 desorption. Subsequent to spectrum E of Figure 1, the specimen was degassed. The temperature and degassing periods (hr) were: F, room temperature, 12; G, 100°, 5; H, 200°, 15; J, 300°, 3; K, 400°, 3; L, 500°, 2; M, 600°, 2.

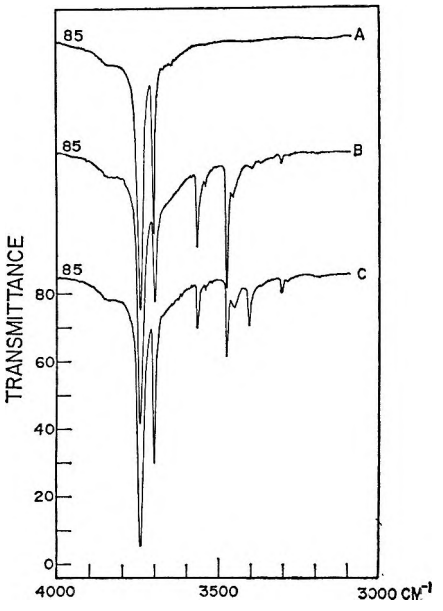

Figure 3. Heat treatment in closed cell: A, base spectrum of porous glass, after 30 hr degassing at 800°; B, after exposure to 130 torr of NH_3 at room temperature for 2 hr and degassing at 150° for 15 hr; C, after heating specimen in the closed cell at 400° for 3 hr and cooling to room temperature.

ferent pressures of NH_3 in the cell. The prominent features of spectrum A of the degassed specimen are a sharp band at 3748 cm^{-1} assigned to isolated surface silanol groups and a sharp band at 3703 cm^{-1} assigned to BOH groups.[16,17] With increasing NH_3 pressure and increasing NH_3 sorption, the BOH band broadened, declined in intensity, shifted to lower wavenumbers, and eventually disappeared, as in the sequence of spectra A–E of Figure 1. The band reappeared near 3699 cm^{-1} when the pressure was reduced. On successively degassing the specimen, as in the sequence of spectra F–K of Figure 2, the BOH band narrowed, shifted to 3703 cm^{-1}, and increased in intensity. The intensity of the 3703-cm^{-1} band after a sorption–desorption cycle, such as that illustrated by Figures 1 and 2, was slightly greater than that found prior to exposure to NH_3. The 3748-cm^{-1} silanol band exhibited similar although not as pronounced changes.

NH_3 sorption at room temperature brought about a series of bands near 3562, 3474, 3410, 3350, 3320, 3310, 3285, and 3200 cm^{-1}, as well as a very broad band near 3000 cm^{-1}. The intensities of all bands decreased on degassing at increasingly higher temperatures and there were small but significant changes in band positions. After degassing at 100°, bands were located near 3565, 3478, 3409, 3368, 3350, 3308, and 3282 cm^{-1}. Degassing at 200° and above caused the disappearance of most of these bands. However, heating caused changes in the bands near 3565 and 3478 cm^{-1}.

Some changes typical of those observed on heating an NH_3-treated sample in a closed cell are shown in Figure 3. A well-degassed sample (spectrum A) was exposed to 130 torr of NH_3 at room temperature for 2 hr and was then degassed for 15 hr at 150° (spectrum B). The cell was then closed off and the specimen was heated at 400° for 3 hr, cooled to room temperature, and spectrum C was recorded. Heating in the closed cell caused these changes: (a) the BOH band increased, (b) most bands in the 3600–3400-cm^{-1} region decreased, (c) bands near 3409 and 3307 cm^{-1} increased, and (d) a small band on the low-wavenumber side of the asymmetric 3478-cm^{-1} band in spectrum B became more distinct as in spectrum C. Changes of a similar nature were also produced when NH_3-treated specimens were heated during degassing, as shown in detail by the sequence of spectra A–H of Figure 4.

Specimen A of Figure 4 is the "background" spectrum of a well-dehydroxylated specimen. The specimen was exposed to 25 torr of NH_3 for 0.5 hr at room temperature and spectrum B was recorded in the presence of the gas. The bands of sorbed NH_3 became

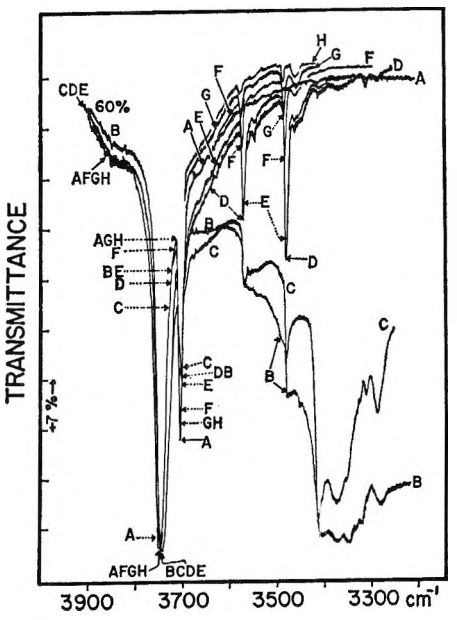

Figure 4. High-temperature degassing. The specimen was subjected to the following successive treatments: A, degassing for 1 day at 800°; B, exposed to 25 torr of NH_3 at room temperature for 0.5 hr; C, degassing at room temperature for 15 min. The specimen was then degassed for 0.5 hr at D, 250°; E, 300°; F, 400°; G, 500°; H, 650°.

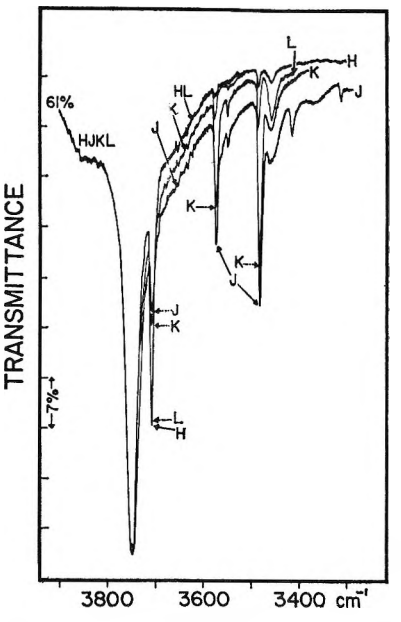

Figure 5. NH_3 treatment. Spectrum H is the same as spectrum H of Figure 4. The specimen was exposed to 25 torr of NH_3 at 200° for 1 hr, was then degassed for 5 min at 200°, cooled to room temperature, and spectrum J was recorded. The specimen was then degassed for 0.5 hr at 400° (spectrum C) and for 0.5 hr at 700° (spectrum D).

well defined after a short evacuation (spectrum C) and became less intense on heating and pumping (spectrum D). The asymmetry of the low-wavenumber sides of bands at 3565 and 3478 cm^{-1} decreased and the bands shifted to 3568 and 3479 cm^{-1}, there also being small but distinct bands at 3546 and 3459 cm^{-1}. These bands decreased on heating and pumping, but the band near 3459 cm^{-1} decreased more slowly than other bands and apparently shifted to 3755 cm^{-1}.

The changes in the 3600–3400-cm^{-1} region were accompanied by changes in the OH bands. The 3748-cm^{-1} silanol band shifted to lower wavenumbers, its intensity increased slightly, and the band broadened slightly after the first exposure to NH_3. Both the band position and intensity remained unaffected (spectra B–E) until much of the sorbed NH_3 had been removed. The band then narrowed and shifted to 3748 cm^{-1} (spectra F, G, and H). The 3703-cm^{-1} BOH band showed larger changes, however. Its intensity decreased on NH_3 sorption and did not increase to a large extent until degassing was carried out at temperatures above 300° (spectra F, G, and H).

The intensities of the bands in the 3600–3400-cm^{-1} region could be increased by heating in NH_3. Some results are shown in Figure 5. The specimen which had been subjected to the sorption–desorption cycle of Figure 4 was heated in 25 torr of NH_3 at 300° for 1 hr and was then degassed for 5 min at 300°. Spectrum J of Figure 5 was recorded after the specimen had cooled to room temperature. The NH_3 treatment had caused a marked decrease in the BOH band, a minor change in the silanol band, and marked increases in bands at 3569, 3546, 3479, and 3459 cm^{-1}. These bands decreased on degassing, changes similar to those shown by Figure 4 being observed. The remnants of the bands in the 3600–3400-cm^{-1} region could be observed even after a 700° degassing.

The band peaking at 3459 cm^{-1} decreased more slowly than the other bands, becoming relatively better formed and more pronounced with increased degassing, as in spectrum L. Also, there was an apparent shift to 3755 cm^{-1}. However, the two prominent bands at 3769 and 3479 cm^{-1} and also the minor band at 3546 cm^{-1} were sharp, as shown by spectra J and K of Figure 5, whereas the 3455-cm^{-1} band was relatively broad. The difference and changes in band shape consequently suggest that a small but relatively sharp band near 3459 cm^{-1} was superimposed on a broader band centering near 3455 cm^{-1}.

The effects of NH_3 sorption on a deuterated porous glass surface are shown by the spectra of Figure 6. The spectrum of a well-degassed, deuterated surface showed small bands at 3475 and 3699 cm^{-1} due to resid-

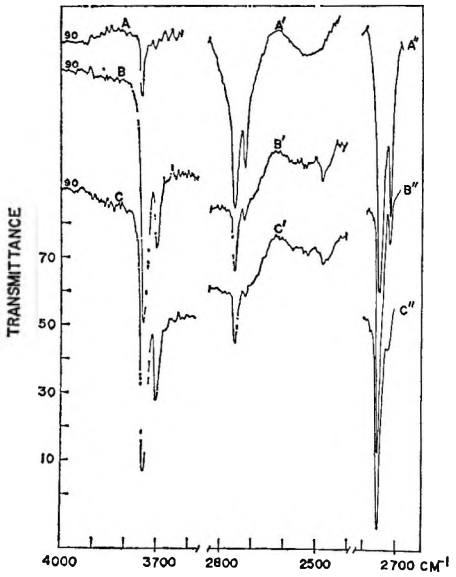

Figure 6. NH_3 sorption on deuterated glass. A, A′, A″, deuterated, degassed porous glass. The specimen was exposed to 6 torr of NH_3 at room temperature for 2.5 hr (spectra B, B′, B″) and 20 hr (spectra C, C′, C″). Spectra A″, B″, C″ are expansions of the respective spectra A′, B′, C′.

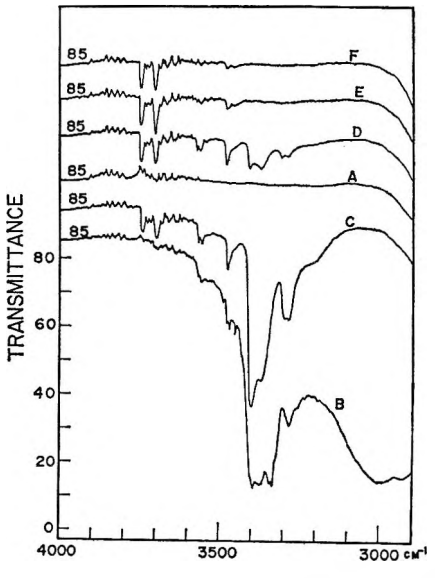

Figure 7. NH_3 sorption on fluoridated glass: A, spectrum of fluoridated glass sample; B, after exposure of 35 torr of NH_3 at room temperature. The specimen was then degassed. The pumping times and temperatures were: C, 15 hr, room temperature; D, 6 hr, 100°; E, 15 hr, 200°; F, 3 hr, 300°.

ual OH groups (spectrum A) and bands at 2756 and 2723 cm^{-1} due to OD groups (spectrum A′). The OD bands were superimposed on a BO band of the support. The spectra in the OD region were consequently expanded by attenuating the reference beam of the spectrophotometer with a screen. The letters identifying such expanded spectra are marked with double primes. There was a large increase of bands in the OH region when the specimen was exposed to NH_3 at room temperature, as shown by spectra B and C; also, there was a decrease of bands in the OD region, shown by spectra B′, B″, C′, and C″. The bands due to sorbed NH_3 were essentially the same as those found with hydroxylated surfaces, *e.g.*, as shown in Figures 1 and 2. Small bands near 2482 and 2420 cm^{-1} were noticed, but these could be easily removed by pumping at 200° and are attributed to N–D vibrations of physically adsorbed ND_3.

Typical results of NH_3 sorption on fluoridated glass are shown in Figure 7. The surface hydroxyl groups had been completely removed by the fluoridation procedure, as shown by spectrum A. The spectra of NH_3 sorbed on such surfaces, as well as after degassing, showed essentially the same band structure as those of Figures 1–5. The NH_3 bands declined with increasing degassing temperature and were removed at 400°. Small bands near 3743 and 3699 cm^{-1} were formed on NH_3 sorption. These grew somewhat when the specimen was degassed, indicating that some formation of hydroxyl groups occurred.

Discussion

The positions, symmetry, and occurrence of the various infrared bands described above were affected by surface coverage and degassing conditions. For the purpose of discussion and comparison with previous results, however, the bands may be grouped as follows: group I: 3409, 3350, 3320, and 3308 cm^{-1}; group II: 3368 and 3282 cm^{-1}; group III: 3565 and 3474 cm^{-1}; group IV: 3569, 3479, 3543, and 3459 cm^{-1}; group V: 3455 cm^{-1}. Comparison with previous results is possible although difficult. As shown by the lack of detail of published spectra, many of these were recorded under conditions of low resolution. This would have the effect of averaging closely spaced bands and distorting band shapes and positions. Some differences in band positions may also arise because of changes in the nature of the surfaces caused by differences in the degree of degassing. For example, Abramov, Kiselev, and Lygin[21] listed the values of 3410, 3402, 3350, and 3370 cm^{-1} for the ν_3 band of NH_3 adsorbed on silica gel, Aerosil silica, aluminosilicate catalyst, and a sodium faujasite, respectively.

Group I. Cant and Little[12] reported that NH_3

(21) V. N. Abramov, A. V. Kiselev, and V. I. Lygin, *Russ. J. Phys. Chem.* **38**, 1020 (1964).

weakly held by the glass surface caused absorptions at 3400 and 3320 cm^{-1}. This observation was confirmed by Chapman and Hair.[14] Folman[13] reported bands at 3380 and 3290 cm^{-1}. All such bands were ascribed to physically adsorbed NH_3. The group I bands, which were greatly reduced in intensity on pumping at room temperature or were completely removed near 100°, are similarly ascribed to NH_3 adsorbed on hydroxyl groups by hydrogen bonding.

As pointed out in a preliminary communication by Yates, Sheppard, and Angell[1] and later by Folman and Yates,[2] the hydrogen bonding of NH_3 to surface OH is more likely to be of the OH···N rather than the NH···O type. Adsorption with the formation of NH···O bonding would not be expected to influence the intensity of the original OH band significantly. Conversely, it was reported that NH_3 adsorption caused large diminutions of silanol bands, so that the OH···N bonding is preferred. Such a diminution of the silanol band on NH_3 sorption and its growth on desorption are illustrated by Figures 1 and 2. In concurrence with others, those changes are considered to be caused by $\equiv$SiOH···NH_3 bonding and the 3409- and 3320-cm^{-1} bands are ascribed to the N–H vibrations of such structures. Figures 1 and 2 also show that the behavior of the 3703-cm^{-1} BOH band on NH_3 sorption and desorption was like that of the 3748-cm^{-1} silanol band. By analogy, that behavior is ascribed to the formation of BOH···NH_3 groupings and the bands at 3350 and 3308 cm^{-1} are ascribed to the N–H vibrations of such structures.

As noted by Cant and Little,[14] adsorbed NH_3 exchanges rapidly with surface OD groups. The spectra of Figure 6 similarly show that both SiOD and BOD groups are converted to the corresponding hydroxyl structures. However, spectra B′, B″ and C′, C″ show that appreciable amounts of SiOD groups remained on the surface after long reaction times, whereas the BOD band was greatly diminished, suggesting that BOD groups were more reactive for the exchange reaction than SiOD groups.

Group II. The 3368- and 3282-cm^{-1} bands of group II were observed on exposing porous glass to NH_3 at room temperature, were stable at 100°, but could be removed by degassing at 200°. Similar bands showing such behavior have been described by others.[12,14,15] Cant and Little reported bands at 3365 and 3280 cm^{-1} and, on the basis of comparison with the spectrum of the Lewis acid–base complex F_3B–NH_3, suggested the possibility of NH_3 adsorption on electron-deficient boron atoms on the glass surface. This suggestion was supported by the observations of Cant and Little[22] and of Chapman and Hair,[14] which we have confirmed in this laboratory, that the group II bands were not produced when NH_3 was adsorbed on pure silica. In concurrence with others, the group II bands are ascribed to $\equiv$B–NH_3 structures which could form on the boria-containing porous glass surface but could not occur on pure silica. Experiments with boria-doped silica described elsewhere[23] provide further support for this assignment. Only the bands ascribed to physically adsorbed NH_3 were found with pure Cab-O-Sil silica, but the bands of groups II, III, and IV were found with Cab-O-Sil impregnated with boria.

The formation of the $\equiv$B···NH_3 complex is taken as a chemisorption. The adsorption may be completely reversible, because the group II bands can be removed by pumping. However, the possibility that the complex is the precursor of dissociated, more tightly bonded species cannot be ruled out.

Group III. A pair of bands near 3562 and 3474 cm^{-1} was observed at room temperature as, for example, in spectrum G of Figure 2. The band positions shifted to higher wavenumbers near 3565 and 3478 cm^{-1} when the surface coverage was decreased by degassing. Each band was asymmetric on the low-wavenumber side and, on heating or degassing above 200°, became smaller and less asymmetric to form what have been termed group IV bands. However, the bands of group IV are frequently poorly or not at all resolved under conditions of high surface coverage, the two minor bands not being distinguishable, and hence appear as a pair of asymmetric bands, *i.e.*, as group III bands. Group III and group IV bands are consequently considered to be brought about by the same surface species.

The group III and group IV bands apparently have not been previously described in detail. However, Folman studied the sorption of NH_3 on chlorinated porous glass and reported that two bands at 3520 and 3445 cm^{-1} remained after degassing at 450°, their intensities becoming stronger with each sorption–desorption cycle up to a certain point where saturation of the surface was obtained and no further changes were observed.[13] Folman ascribed the two bands to NH_2 groups attached to surface Si atoms. As the over-all behavior of those bands was similar to that of group III or group IV bands as described above, it seems plausible that Folman's bands were group IV bands but were not well developed or resolved under the conditions of his experiments.

Also, Chapman and Hair studied the sorption of NH_3

(22) N. W. Cant and L. H. Little, *Can. J. Chem.*, **43**, 1252 (1965).

(23) M. J. D. Low, N. Ramasubramanian, and P. Ramamurthy, unpublished data.

on fluoridated porous glass.[14] They reported (a) the formation of a distinct shoulder at 3460 cm^{-1} when NH_3 was sorbed on partially fluoridated glass; (b) on degassing at 200°, the shoulder became a well-defined band at 3450 cm^{-1} which was retained after degassing at 250°; and (c) the 3450-cm^{-1} band was not formed on a completely fluoridated surface. The 3450-cm^{-1} band was ascribed to the fundamental N–H stretching of the NH_4^+ ion. However, the 3450-cm^{-1} band is much like Folman's 3445-cm^{-1} band. Also, some of Chapman and Hair's spectra suggest the presence of shoulders between 3500 and 3600 cm^{-1}, although it is difficult to make an exact comparison because the published spectra are small and not well defined. As the spectra of Figure 7 showed that group III, group IV, and group V bands were formed with completely fluoridated glass, it seems likely that group III bands were produced in Chapman and Hair's experiments.

Group IV. Two relatively sharp, intense bands near 3565 and 3478 cm^{-1} were observed. Each band was asymmetric on the low-wavenumber side and, on heating and pumping, the asymmetry decreased along with the band intensity. A small but distinct band occurred on the asymmetric side of each band. All four bands could be enhanced by means of a sorption-desorption cycle, as shown in Figure 5, but were retained even after a 700° degassing. Such behavior, as noted by Folman,[13] indicates a strong bonding of the sorbed material. Group IV bands were consequently caused by surface species more tightly bound and distinct from those responsible for the group I and group II bands.

Folman suggested that the surface become aminated and ascribed his 3520- and 3445-cm^{-1} bands to the symmetric and antisymmetric N–H stretching of surface $-NH_2$ groups. A similar assignment is made for the group IV bands based on Folman's suggestion and reasons for the assignment, each of the pairs of bands at 3569 and 3479 cm^{-1} and at 3546 and 3459 cm^{-1} being attributed to surface $-NH_2$ groups.

Bellamy and Williams[24] pointed out that both the asymmetric and symmetric stretching frequencies depend basically on the same force constant and must consequently be directly related to each other. They found the relation, $\nu_{sym} = 345.53 + 0.876\nu_{as}$, was obeyed with a standard deviation of 4.8 cm^{-1} for 64 primary amines. Using the observed values of 3569 and 3546 cm^{-1}, Bellamy and Williams' equation leads to the values of 3472 and 3452 cm^{-1}, each differing by 7 cm^{-1} from the observed values of 3479 and 3459 cm^{-1}, respectively. The constant frequency relations of the two group IV pairs suggest that one type of surface structure was responsible for both pairs of absorptions, *i.e.*, a primary amine bonded to two different surface sites, and supports the previous suggestion that the small 3459-cm^{-1} band was superimposed on the broader 3455-cm^{-1} band.

Results such as those of Figures 4 and 5 indicate that, although all the group IV bands decreased on degassing, the greatest intensity changes were shown by the pair of bands at 3569 and 3479 cm^{-1} as well as by the 3703-cm^{-1} BOH band. Relatively high degassing temperatures were required to cause increases in intensity of the 3703-cm^{-1} band, so that a hydrogen bonding of molecular NH_3 to surface BOH groups can be reasonably ruled out. In view of such behavior, the 3569- and 3479-cm^{-1} bands are ascribed to surface $=BNH_2$ structures.

Similar although less pronounced behavior was exhibited by the 3546- and 3459-cm^{-1} pair and the silanol band. By analogy, the 3546- and 3459-cm^{-1} pair are ascribed to a surface $\equiv SiNH_2$ structure of the type postulated by Folman.

The formation of a primary amine requires a dissociative reaction such as

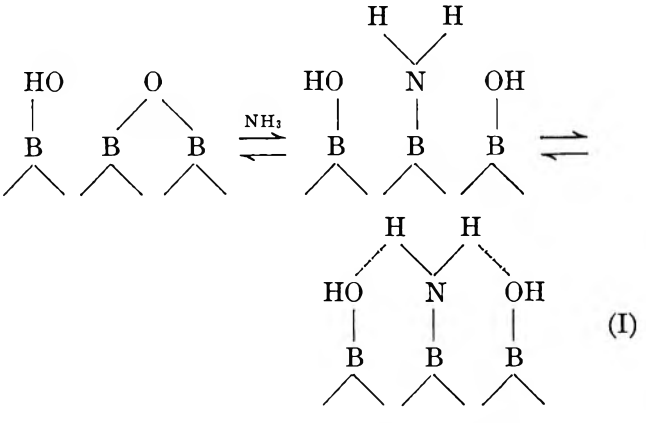

(I)

an analogous reaction scheme being required for the breaking of siloxane bridges. The reaction scheme is given in two reversible steps and requires the formation of hydroxyl groups.

Spectrum B of Figure 3 shows that (a) physically adsorbed NH_3 had been almost completely removed, because the group I bands were quite small, and (b) the BOH band was smaller than that of spectrum A of Figure 3. Spectrum C was recorded after the sample had been heated and cooled within the closed cell and shows that the group IV bands have declined and the BOH band and the group I bands have increased in intensity. Such behavior suggests that (a) NH_3 was formed when the sample was heated, so that the

(24) L. J. Bellamy and R. L. Williams, *Spectrochim. Acta*, 9, 341 (1957).

group IV bands decreased, and (b) when the sample was cooled in the closed cell, the NH_3 became physically adsorbed, so that the group I bands increased. Similar intensity relations between the BOH and group IV bands are shown by Figures 4 and 5; the growth of the BOH band was accompanied by a decrease in intensity and a decrease in asymmetry of the prominent 3569- and 3479-cm^{-1} bands. Such behavior suggests that the reactions were reversible, at least to some extent, and that the asymmetry on the low-wavenumber sides of the 3569- and 3479-cm^{-1} bands was produced by hydrogen bonding of the amine to BOH groups produced by the reaction as well as to BOH groups already present on the surface.

Group V. As shown by the sequence of spectra D–L of Figures 4 and 5, the relatively broad 3455-cm^{-1} band became more distinct when the superimposed 3459-cm^{-1} band was removed by degassing. The single group V band could be enhanced by NH_3 treatment and was not completely removed by pumping at 700°, as shown by the spectra of Figure 5, and was consequently produced by a tightly bonded surface species.

Chapman and Hair[14] reported the formation of a band at 3450 cm^{-1} when NH_3 was sorbed by fluoridated porous glass and assigned that absorption to the N–H stretching vibration of an NH_4^+ ion formed by chemisorption of NH_3 upon strong protonic sites on the surface. They recognized that the 3450-cm^{-1} value was higher than any previously reported for ammonium salts, but pointed out that a close examination of the published values for the fundamental N–H stretching frequencies for a series of ammonium salts revealed a definite trend in which this N–H stretching frequency increased as the strength of the complementary acid increased. As they had previously suggested[25] that the introduction of fluorine atoms for hydroxyl groups on the surface of porous glass might give rise to an inductive effect through the surface with the production of strong protonic sites, their assignment of the 3450-cm^{-1} band to NH_4^+ groups seemed reasonable. A similar reaction

$$\equiv SiOH + NH_3 \longrightarrow \equiv SiO^-NH_4^+$$

was postulated by Felden[26] and by Boyle, Gaw, and Ross.[27]

The 3455-cm^{-1} band was formed on untreated as well as on fluoridated surfaces, as shown above. Consequently, if the reasonable assumption is made that the 3455-cm^{-1} band and Chapman and Hair's 3450-cm^{-1} band were produced by the same species, the formation of surface NH_4^+ groups because of an inductive effect becomes uncertain. A reasonable alternative is the formation of a secondary amine.

The value of 3455 cm^{-1} falls in the frequency range found for the single N–H vibration of secondary amines.[28] If surface $\equiv BNH_2$ groups are formed, it seems not unreasonable to postulate that the reaction proceed one step further to produce secondary amines. The 3455-cm^{-1} band is tentatively assigned to the N–H vibration of a surface group formed by the bonding of the nitrogen atom of an NH group to two neighboring boron atoms.

The formation of secondary and primary amines requires the abstraction of hydrogen from NH_3 and, unless molecular hydrogen is formed and desorbed or a protonic type[29] of binding exists, the formation of surface hydroxyl groups. That such reactions occur is shown by (a) small increases in the intensities of both the SiOH and BOH bands after a sorption–desorption cycle during which the glass was exposed to a relatively high pressure of NH_3, as illustrated by the spectra of Figures 1 and 2; (b) small increases in the SiOH band immediately after exposure to NH_3 at low pressures, such as that shown by Figure 4 (increases in the BOH band would be masked by hydrogen bonding to the BOH groups); (c) the exchange data of Figure 6, which suggest, although quantitative interpretation is not possible, that some hydroxyl formation had occurred because the two OH bands grew appreciably while the OD bands remained fairly large; and (d) the formation of SiOH and BOH bands on completely fluoridated surfaces, as shown by the spectra of Figure 7.

Chapman and Hair[14] similarly reported an increase in the SiOH band when NH_3 reacted with fluoridated porous glass and concluded that it was probable that this effect was caused by the opening of surface siloxane groups. They also reported the formation of a small band at 3700 cm^{-1}, which they attributed to the N–H vibration of a secondary amine but which, in view of the present and other[16–18] results, is attributed to BOH groups formed by the reaction of NH_3 with BOB groups.

Although the various data show that surface hydroxyls were produced, there is some uncertainty about the mechanism(s) involved in their production. Various

(25) I. D. Chapman and M. L. Hair, *J. Catalysis*, 2, 145 (1963).

(26) M. Felden, *Compt. Rend.*, 249, 682 (1959).

(27) T. W. Boyle, W. J. Gaw, and R. A. Ross, *J. Chem. Soc.*, 240 (1965).

(28) L. J. Bellamy, "The Infrared Spectra of Complex Molecules," 2nd ed, John Wiley and Sons, Inc., New York, N. Y., 1954, pp 251 ff.

(29) R. P. Eischens, W. A. Pliskin, and M. J. D. Low, *J. Catalysis*, 1, 180 (1962).

infrared spectroscopic data indicated that boron on the porous glass surface played an important role as adsorption center in the hydration of the glass surface.[18] Also, NH_3 sorption on Cab-O-Sil did not enhance the silanol band intensity. Cant and Little[22] and also Chapman and Hair,[14] who studied NH_3 sorption on silica, did not mention an increase of the silanol band due to reaction of the silica with NH_3. Also, NH_3 sorption by silica produced only group I bands. More recently, Peri reported that NH_3 was slowly chemisorbed by a limited number of sites on pure aerogel silica with the formation of NH_2 and OH groups.[30] However, the maximum NH_3 chemisorption after 8 days at 100 torr at room temperature was only 1.3–1.4 molecules/100 A^2.

Such results raise some doubt about the extent of direct reactions of NH_3 with siloxane bridges on the porous glass surface. A direct reaction to produce primary amine and SiOH groups *via* a reaction scheme analogous to reaction I may occur, as implied by Peri's results.[30]

However, an additional reaction, such as reaction II might be operative for the production of SiOH groups, because the silica network of the glass appears to be relatively inert. In such a case the surface boron would

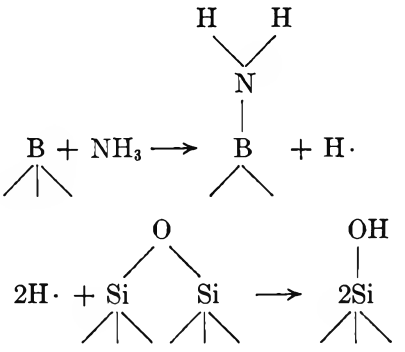

(II)

act as adsorption center or active site, one fragment resulting from the dissociation of NH_3 reacting with a neighboring siloxane bridge. It might also be possible that surface boron acts as dissociation center, both NH_2· and H· fragments migrating to and reacting with a neighboring siloxane.

Acknowledgment. Support for this work by Grant ES-00088-01 from the Division of Environmental Health, Bureau of State Services, Public Health Service, Contract Nonr 404(19) from the Office of Naval Research, and NSF Grant GP 1434, is gratefully acknowledged.

(30) J. B. Peri, *J. Phys. Chem.*, **70**, 2937 (1966).

Mechanisms for Some High-Temperature Gas-Phase Reactions of Ethylene, Acetylene, and Butadiene[1]

by S. W. Benson and G. R. Haugen

Department of Thermochemistry and Chemical Kinetics, Stanford Research Institute, Menlo Park, California 94025
(Received October 17, 1966)

Sufficient information concerning the rate parameters of the individual propagation and termination steps of radical reactions now exists so that it is possible to predict the kinetic behavior of a chain mechanism with better than order-of-magnitude reliability. This precision comes from the similarities that exist between the A factors and activation energies of homologous reactions. In particular, the creditability of a proposed chain mechanism for the high-temperature gas-phase reaction of unsaturated hydrocarbons can be tested by comparing the observed kinetic behavior with that predicted by the mechanism. A pyrolytic chain was proposed that adequately describes the experimentally observed high-temperature hydrogenation of acetylene and also the high-temperature pyrolysis of ethylene. The propagation steps representing the formation of the major products of these system are $C_2H_3\cdot + M \underset{-1}{\overset{1}{\rightleftharpoons}} C_2H_2 + H\cdot + M$ ($k_1 = 10^{11.9-31.5/\theta}$ l. mole^{-1} sec^{-1}; $k_{-1} = 10^{7.9+15.0/\theta}$ l.^{2} mole^{-2} sec^{-1}) where $\theta = 2.303RT$ in kcal/mole, and $H\cdot + C_2H_4 \underset{-2}{\overset{2}{\rightleftharpoons}} H_2 + C_2H_3\cdot$ ($k_2 = 10^{10.8-6/\theta}$ l. mole^{-1} sec^{-1}; $k_2 = 10^{9.9-7.4/\theta}$ l. mole^{-1} sec^{-1}), respectively. The minor product in both systems is 1,3-butadiene. In the pyrolysis of ethylene, the side reaction, $C_2H_3\cdot + C_2H_4 \underset{-3}{\overset{3}{\rightleftharpoons}} C_4H_6 + H\cdot$ ($k_3 = 10^{8.7-7.3/\theta}$ l. mole^{-1} sec^{-1}; $k_{-3} = 10^{9.8-1.0/\theta}$ l. mole^{-1} sec^{-1}), accounts for the production of butadiene. In the case of the hydrogenation of acetylene, a concurrent chain is responsible for the side products, $C_2H_3\cdot + C_2H_2 \overset{4}{\longrightarrow} C_4H_5\cdot$ ($k_4 = 10^{8.3}$ l. mole^{-1} sec^{-1}) and $C_4H_5\cdot + H_2 \overset{5}{\longrightarrow} C_4H_6 + H\cdot$ ($k_5 = 10^{9.4-5.9/\theta}$ l. mole^{-1} sec^{-1}).

Introduction

The successful interpretation of both the hydrogenation and the isotope exchange kinetics of the acetylene–deuterium system by a radical mechanism with a long chain length[2] stimulated consideration of this mechanism for the single-pulse shock-tube pyrolysis of ethylene.[3] The dwell time in these pyrolysis experiments being a factor of 10 to 100 longer than the dwell time in the isotope exchange experiments, the complications of nonsteady-state kinetics is avoided. In particular, possible catalysis of the induction period by impurities does not influence the kinetic behavior of the system. Consequently, this investigation afforded an excellent opportunity to test the steady-state kinetics predictions of the radical mechanism.

Skinner and Sokoloski[3] studied both the kinetics of formation of acetylene from the pyrolysis of ethylene and the reverse process, the hydrogenation of acetylene. The pyrolysis was relatively clean. The only other product of importance was butadiene. Accordingly, the kinetics of both the formation and decomposition

(1) The authors are indebted to the Department of Health, Education, and Welfare, U. S. Public Health Service, for support of this study through Research Grant No. AP-00353-02 from the Division of Air Pollution.

(2) S. W. Benson and G. R. Haugen, submitted for publication.

(3) G. B. Skinner and E. M. Sokoloski, *J. Phys. Chem.*, **64**, 1028 (1960).

Table I: Rates of Formation of Acetylene and 1,3-Butadiene from Ethylene (Dwell Time 2 msec)

T, °K	$(C_2H_4)_0$[a]	$(Ar)_0$[a]	$R_{C_2H_2}$,[b,c]	$R_{C_4H_6}$,[b,d]	% conversion of C_2H_4
			Mixture 1		
1276	2.23×10^{-4}	4.76×10^{-2}	1.9×10^{-3}	1.6×10^{-4}	1.7
1329	2.14×10^{-4}	4.58×10^{-2}	4.1×10^{-3}	...	3.8
1329	2.14×10^{-4}	4.58×10^{-2}	4.2×10^{-3}	1.5×10^{-4}	3.9
1372	2.07×10^{-4}	4.43×10^{-2}	5.8×10^{-3}	1.4×10^{-4}	5.8
1444	1.97×10^{-4}	4.21×10^{-2}	1.3×10^{-2}	8.1×10^{-5}	13
1475	1.93×10^{-4}	4.13×10^{-2}	1.5×10^{-2}	7.6×10^{-5}	17
1502	1.90×10^{-4}	4.05×10^{-2}	1.9×10^{-2}	...	20
1535	1.85×10^{-4}	3.97×10^{-2}	2.3×10^{-2}	...	25
1587	1.79×10^{-4}	3.83×10^{-2}	4.0×10^{-2}	...	46
1625	1.75×10^{-4}	3.74×10^{-2}	4.5×10^{-2}	...	54
1666	1.71×10^{-4}	3.65×10^{-2}	6.2×10^{-2}	...	82
1740	1.64×10^{-4}	3.49×10^{-2}	7.2×10^{-2}	...	~100
1784	1.59×10^{-4}	3.41×10^{-2}	7.6×10^{-2}	...	~100
			Mixture 2		
1169	3.13×10^{-3}	4.90×10^{-2}	1.4×10^{-3}	4.7×10^{-3}	0.09
1170	3.13×10^{-3}	4.91×10^{-2}	2.0×10^{-3}	4.2×10^{-3}	0.13
1205	3.04×10^{-3}	4.76×10^{-2}	4.6×10^{-3}	...	0.31
1215	3.02×10^{-3}	4.73×10^{-2}	4.8×10^{-3}	5.4×10^{-3}	0.32
1241	2.95×10^{-3}	4.62×10^{-2}	9.4×10^{-3}	1.0×10^{-2}	0.63
1242	2.95×10^{-3}	4.61×10^{-2}	1.1×10^{-2}	8.8×10^{-3}	0.73
1264	2.90×10^{-3}	4.54×10^{-2}	2.2×10^{-2}	1.5×10^{-2}	1.5
1325	2.76×10^{-3}	4.33×10^{-2}	5.1×10^{-2}	1.9×10^{-2}	3.6
1332	2.75×10^{-3}	4.31×10^{-2}	5.3×10^{-2}	...	3.8
1345	2.72×10^{-3}	4.26×10^{-2}	5.9×10^{-2}	1.9×10^{-2}	4.3
1423	2.57×10^{-3}	4.03×10^{-2}	2.0×10^{-1}	2.0×10^{-2}	15
1426	2.57×10^{-3}	4.02×10^{-2}	2.1×10^{-1}	...	16

[a] Concentration units, moles liter^{-1}. [b] Units of rate, moles liter^{-1} sec^{-1}. [c] $R_{C_2H_2}$ represents the average rate of production of acetylene over the dwell time interval, t_d.

$$R_{C_2H_2} = \frac{12.2}{T}\frac{1}{t_d}\int_{t=0}^{t=t_d} k_a(0.0233)e^{-k_a t}dt$$

where k_a is the apparent rate constants for acetylene production reported in ref 3. The quantity $12.2/T$ represents the conversion factor for the change of concentration units. [d] Similarly, $R_{C_4H_6}$ represents the average rate of production of 1,3-butadiene over the dwell time interval, t_d.

$$R_{C_4H_6} = \frac{12.2}{T}\frac{1}{t_d}\frac{1}{2}\int_{t=0}^{t=t_d} k_b(0.0233)^2e^{-2k_a t}dt$$

where k_b is the apparent rate constant for butadiene production reported in ref 3.

of 1,3-butadiene were investigated. The data for these systems are reproduced in Tables I, II, and III. The measurements of the pyrolysis of a mixture of ethylene and acetylene has been excluded from this discussion on account of the complications issuing from simultaneous occurrence of several competing initiation and termination steps.

Discussion of the Pyrolysis of Ethylene

The over-all stoichiometry can be represented by partial contribution from each of the two reactions

$$C_2H_4 \longrightarrow C_2H_2 + H_2$$

$$2C_2H_4 \longrightarrow C_4H_6 + H_2$$

The paths for production of the minor quantities of methane and propylene observed will not be considered. The proposed mechanism for the initial formation of the major products (C_2H_2, C_4H_6, and H_2) is shown below.[4]

$$2C_2H_4 \xrightarrow{i} \cdot C_2H_5 + \cdot C_2H_3 \quad \text{(initiation)}$$

Table II: Kinetics of the Hydrogenation of Acetylene (Mixture 5) (Concentrations, moles liter^{-1})

T, °K	$(C_2H_2)_0 \times 10^4$	$(H_2)_0 \times 10^3$	$(Ar)_0 \times 10^2$	$(C_2H_2) \times 10^4$	$(C_2H_4) \times 10^5$	$(C_4H_6) \times 10^6$	$(CH_4) \times 10^6$
			(Dwell Time 2 msec)				
1187	7.24	4.35	4.63	6.87	0.65	2.89	...
1279	6.74	4.15	4.30	6.28	1.01	4.05	...
1384	6.22	3.74	3.97	5.86	1.68	4.36	...
1484	5.81	3.49	3.71	5.31	2.04	4.66	...
1502	5.74	3.44	3.67	5.25	2.12	4.60	...
1635	5.28	3.17	3.37	4.80	1.85	7.92	...
1774	4.85	2.91	3.10	4.31	1.21	10.2	...
			(Dwell Time 10 msec)				
1180	7.30	4.39	4.66	6.66	3.21	10.2	...
1260	6.84	4.11	4.38	6.12	5.20	...	5.48
1363	6.32	3.79	4.07	5.52	5.70	8.22	...
1436	5.98	3.60	3.83	5.14	5.32	...	7.78
1530	5.64	3.38	3.60	4.98	4.06	7.34	...
1677	5.13	3.08	3.28	4.61	2.00	...	9.25

Table III: Kinetic Behavior of the Decomposition of 1,3-Butadiene (Mixture 4, Dwell Time 10 msec)

T, °K	$(C_4H_6)_0 \times 10^4$ [a]	$(Ar)_0 \times 10^2$ [a]	$(C_4H_6) \times 10^4$ [b]	$(C_2H_2) \times 10^5$ [b]	$(C_2H_4) \times 10^5$ [b]	$(H_2) \times 10^5$ [b]	% conversion of C_4H_6	$R_{C_4H_6}$ [c]
1209	1.34	5.03	1.23	0.86	0.90	0.32	8.1	1.1×10^{-3}
1242	1.30	4.88	1.14	0.91	1.02	0.29	12.6	1.6×10^{-3}
1289	1.25	4.70	0.84	2.95	2.72	0.99	33.0	4.1×10^{-3}
1334	1.22	4.56	0.63	4.42	3.57	1.55	48.8	6.0×10^{-3}
1381	1.17	4.40	0.33	6.74	4.25	2.30	71.9	8.5×10^{-3}
1412	1.15	4.30	0.22	8.80	4.26	3.92	80.8	9.4×10^{-3}

[a] Initial concentration of reactant, moles liter^{-1}. [b] Final concentration of reactant and products, moles liter^{-1}. [c] $R_{C_4H_6}$ represents the average rate of disappearance of 1,3-butadiene over the dwell time, t_d

$$R_{C_4H_6} = \frac{12.2}{T}\frac{1}{t_d}\int_{t=0}^{t=t_d} k_c(0.0133)e^{-k_c t}dt$$

where k_c is the apparent rate constant for the disappearance of C_4H_6 reported in ref 3.

$$\left.\begin{aligned} C_2H_3\cdot + M &\xrightarrow{1} C_2H_2 + H\cdot + M \\ H\cdot + C_2H_4 &\xrightarrow{2} H_2 + C_2H_3\cdot \end{aligned}\right\}\text{(chain)}$$

$$C_2H_3\cdot + C_2H_4 \xrightarrow{3} CH_2{=}CHCH{=}CH_2 + H\cdot$$

(path for butadiene formation)

$$\cdot C_2H_5 + M \underset{-8}{\overset{8}{\rightleftarrows}} C_2H_4 + \cdot H + M$$

$$2H\cdot + M \xrightarrow{tH}$$

$$C_2H_3\cdot + H\cdot \xrightarrow{tHV} \text{(termination)}$$

$$2C_2H_3\cdot \xrightarrow{tV}$$

The radical $C_2H_5\cdot$ will disappear more rapidly than $C_2H_3\cdot$ since it has a weaker bond strength and is closer to its high pressure limit. It is also not a propagating species since it is not reproduced by any favorable or fast chain. Under the steady-state conditions, the equilibrium

$$M + C_2H_5\cdot \underset{-8}{\overset{8}{\rightleftarrows}} C_2H_4 + H\cdot + M$$

will be established [$(k_8/k_{-8})_{1400°K} = 10^{3.89}10^{-41.2/\theta}$ mole l.$^{-1}$]. At 1400°K and C_2H_4 $\sim 10^{-3.5}$ M, the equilibrium dissociation of the radical will be $\geq 90\%$.

(4) The formation of a biradical from the molecular condensation of two ethylenes was also considered as a possible initiation process. The rate of formation of the biradical and the consequential unimolecular and bimolecular reactions of this radical are much too slow to be significant. However, the exchange of hydrogen atoms of ethylene may proceed rapidly through the intermediate cyclobutane (see Appendix).

The absence of ethane demonstrates the minor contribution of the abstraction of a hydrogen atom from ethylene by this radical.

The ratio of the steady-state concentration of the radicals $C_2H_3\cdot$ and $H\cdot$ is controlled by the propagation chain. Assuming no contribution of the back reactions, we find the simple expressions

$$\omega = \frac{(C_2H_3\cdot)_{ss}}{(H\cdot)_{ss}} = \frac{k_2(C_2H_4)}{k_1(M)} \qquad (1)^5$$

Noting that the steady-state rates of formation of acetylene and hydrogen are determined by the propagation chain, a consequence of its long chain length, we find that the rates of production of hydrogen and acetylene are equal, as long as the rate of production of butadiene is negligible. The rate of formation of acetylene is given by

$$R_{C_2H_2} = k_1(M)(C_2H_3\cdot) \qquad (2)$$

Since hydrogen atom abstraction (reaction 2) is a few powers of ten faster than the low-pressure limit of the elimination of a hydrogen atom from vinyl radical (reaction 1), see Appendix, the vinyl radical, $C_2H_3\cdot$, predominates in this system. Thus, termination occurs mainly between two of these radicals, and the absolute rate is given by

$$R_{C_2H_2} = k_1\left(\frac{k_i}{k_{tv}}\right)^{1/2}(C_2H_4)(M) \qquad (3)$$

Substituting appropriate numbers for the rate constants (see Appendix) the apparent rate constant, $k_1(k_i/k_{tv})^{1/2}(M)$ becomes $10^{11.4-63.9/\theta}$ sec^{-1}. This predicts an absolute rate of $10^{-1.6}$ mole $l.^{-1}$ sec^{-1} at the typical conditions used by Skinner and Sokoloski[3] [temp 1500 °K and $(C_2H_4) \sim 10^{-3.7}$ mole $l.^{-1}$] which agrees with their experimental rate of $10^{-1.7}$ mole $l.^{-1}$ sec^{-1}. At high temperatures and low ethylene concentrations, the steady-state concentrations of the radicals $\dot{C}_2H_3$ and $\dot{H}$ equalize. Under these conditions, we must include termination between $H\cdot$ and $\dot{C}_2H_3$. The steady-state rate expression becomes

$$R_{C_2H_2} = \left(\frac{k_i}{k_{tv}}\right)^{1/2}\frac{k_2(C_2H_4)^2}{\{\alpha\omega + \omega^2\}^{1/2}} \qquad (4)$$

where, $\alpha = k_{tHv}/k_{tv}$. Substituting values for the rate constants in eq 4 permits the prediction of the average rate of formation of acetylene. Comparison of calculated and observed rates is shown in Table IV. This comparison is meaningful only as long as the back reactions, omitted in the mechanism, are negligible. The agreement between the observed concentration and temperature behavior and that predicted by the mechanism is good. Agreement is maintained over a 620° range in temperature and a tenfold change in concentration. Part of the pyrolysis could be proceeding by a concurrent molecular mechanism. The rate parameters for the direct molecular elimination of H_2 from ethylene have been estimated,[6] $R_{C_2H_2}^{(mole)} = 10^{13.5-85/\theta}$ (C_2H_4). The fraction of the pyrolysis proceeding by a molecular mechanism is shown in Table V. This mechanism is only important at very high temperatures, where the per cent conversion is large. Consequently, the effect of neglecting the back reactions becomes increasingly important and the refinement of the concurrent molecular elimination is not warranted.

The path for formation of butadiene is assumed to be a reaction between the vinyl radical and ethylene, reaction 3, with a rate of production of 1,3-butadiene, expressed by

$$R_{C_4H_6} = k_3(C_2H_4)(C_2H_3\cdot) \qquad (5)$$

Accordingly, the steady-state rate is

$$R_{C_4H_6} = \frac{k_3(C_2H_4)}{k_1(M)}R_{C_2H_2} \qquad (6)$$

which agrees reasonably with the observed kinetics of formation (see Table IV).

Lin[7] has proposed a chain mechanism for the low-temperature hydrogenation of ethylene that is initiated by vinyl and ethyl radicals

$$2C_2H_4 \xrightarrow{i} C_2H_3\cdot + C_2H_5\cdot \quad \text{(initiation)}$$

$$\left.\begin{aligned} C_2H_5\cdot + H_2 &\xrightarrow{9} C_2H_6 + H\cdot \\ H\cdot + C_2H_4 &\xrightarrow{10} C_2H_5\cdot \end{aligned}\right\} \text{(chain)}$$

$$C_2H_3\cdot + H_2 \underset{2}{\overset{-2}{\rightleftharpoons}} C_2H_4 + H\cdot$$

$$2C_2H_5\cdot \xrightarrow{tEt} \text{(termination)}$$

The vinyl and hydrogen atoms equilibrate rapidly in this system ($k_2/k_{-2} = 10^{-1.32-0.6/\theta}$); consequently, the steady-state rate of formation of ethane is equal to $k_9(k_i/k_t)^{1/2}(C_2H_2)(H_2)$. The value of the ratio

(5) At high ethylene concentrations and low temperatures, reaction 3 starts to compete with reaction 1. Under these conditions, ω is determined by the expression

$$\omega = [k_2(C_2H_4)]/[k_1(M) + k_3(C_2H_4)]$$

Mixture 2 satisfied these prerequisites; consequently, the calculations of the steady-state rate required the use of the above relations.

(6) S. W. Benson and G. R. Haugen, *J. Phys. Chem.*, 70, 3336 (1966): $C_2H_4 \rightarrow C_2H_2 + H_2$; $\Delta H°$ (1400°K) $\simeq$ 45.1 kcal/mole; E_{act} (1400°K) $\simeq$ 85 kcal/mole.

(7) M. C. Lin, *Can. J. Chem.*, 44, 1237 (1966).

Table IV: Comparison of the Observed Rate of Formation of C_2H_2 and C_4H_6 from Ethylene with That Predicted by Eq 4 and 6[a]

T, °K	Log $R^0_{C_2H_2}$ calcd [b]	$R_{C_2H_2}$ calcd / $R_{C_2H_2}$ obsd [c]	Log $R^0_{C_4H_6}$ calcd [b]	$R_{C_4H_6}$ calcd / $R_{C_4H_6}$ obsd [c]
Mixture 1, Dwell Time 2 msec				
1276	−3.13	0.4	−3.76	0.2
1329	−2.78	0.4	−3.58	...
1329	−2.78	0.4	−3.58	0.3
1372	−2.44	0.6	−3.36	0.5
1444	−2.01	0.7	−3.12	1.4
1475	−1.79	0.9	−2.98	1.4
1502	−1.67	0.9	−2.92	...
1535	−1.50	1.1	−2.82	...
1587	−1.25	0.8	−2.68	...
1625	−1.06	1.0	−2.56	...
1666	−0.88	0.7	−2.46	...
1740	−0.58	0.9	−2.29	...
1784	−0.43	1.2	−2.21	...
	Av	0.8 ± 0.2		
Mixture 2, Dwell Time 2 msec				
1169	−3.05	1.4	−2.25	0.5
1170	−3.05	0.9	−2.25	0.6
1205	−2.85	0.6	−2.14	...
1215	−2.77	0.8	−2.07	0.6
1241	−2.52	0.5	−1.92	0.4
1242	−2.52	0.5	−1.92	0.4
1264	−2.36	0.3	−1.83	0.3
1325	−1.88	0.4	−1.54	0.4
1332	−1.81	0.4	−1.49	...
1345	−1.73	0.4	−1.46	0.4
1423	−1.20	0.4	−1.14	0.6
1426	−1.20	0.4	−1.14	...
	Av	0.5 ± 0.2	Av	0.5 ± 0.1

[a] Values of rate constants of individual steps of mechanism used in estimating over-all rates: $k_i = 10^{11.7-64.7}$ l. mole^{-1} sec^{-1}; $k_1 = 10^{11.9-31.5/\theta}$ l. mole^{-1} sec^{-1}; $k_2 = 10^{10.8-6/\theta}$ l. mole^{-1} sec^{-1}; $k_3 = 10^{8.7-7.3/\theta}$ l. mole^{-1} sec^{-1}; $k_{tv} = 10^{10.0}$ l. mole^{-1} sec^{-1}; $k_{tHv} = 10^{9.6}$ l. mole^{-1} sec^{-1}; $k_{tEt} = 10^{10.0}$ l. mole^{-1} sec^{-1}. [b] $R^0_{C_2H_2}$ calcd and $R^0_{C_4H_6}$ calcd represent the calculated initial rates in units of mole liter^{-1} second^{-1}. [c] $R_{C_2H_2}$ calcd and $R_{C_4H_6}$ calcd represent the average rates over the dwell time interval

$$R_{C_2H_2} = R^0_{C_2H_2}\left(1 - \frac{\%\text{ conversion}}{200}\right)^2;$$

$$R_{C_4H_6} = R^0_{C_4H_6}\left(1 - \frac{\%\text{ conversion}}{200}\right)^3$$

Table V: Fraction of the Ethylene Pyrolysis Occurring by a Molecular Mechanism

T, °K	$R_{C_2H_2}^{(mole)} / R_{C_2H_2}^{(rad)}$ [a]	$\frac{R_{C_2H_2}^{(rad)} + R_{C_2H_2}^{(mole)}}{R\text{ (obsd)}}$	% conversion of C_2H_4
Mixture 1, Dwell Time 2 msec			
1276	0.061	0.4	1.7
1329	0.084	0.4	3.8
1329	0.084	0.4	3.9
1372	0.12	0.7	5.8
1444	0.23	0.9	13
1475	0.28	1.2	17
1502	0.32	1.2	20
1535	0.43	1.6	25
1587	0.65	1.3	46
1625	0.93	1.9	54
1666	1.35	1.6	82
1740	2.45	3.1	~100
1784	4.26	6.3	~100
Mixture, 2, Dwell Time 2 msec			
1169	0.01	1.4	0.09
1170	0.01	0.9	0.13
1205	0.02	0.6	0.31
1215	0.02	0.8	0.32
1241	0.03	0.5	0.63
1242	0.03	0.5	0.73
1264	0.04	0.3	1.5
1325	0.06	0.4	3.6
1332	0.07	0.4	3.8
1345	0.06	0.4	4.3
1423	0.15	0.5	15
1426	0.15	0.5	16

[a] $R_{C_2H_2}^{(mole)}$ represents the rate for the molecular mechanism average over the dwell-time interval. $R_{C_2H_2}^{(rad)}$ represents the rate for the radical mechanism average over the dwell-time interval.

$$\frac{R_{C_2H_2}^{(mole)}}{R_{C_2H_2}^{(rad)}} = \frac{R^0_{C_2H_2}{}^{(mole)}}{R^0_{C_2H_2}{}^{(rad)}} \frac{1}{1 - \left(\frac{\%\text{ conversion}}{200}\right)}$$

where $R^0_{C_2H_2}{}^{(mole)}$ and $R^0_{C_2H_2}{}^{(rad)}$ represent the initial rates for the molecular and radical mechanism, respectively. [b] Experimental rates below the dashed line cannot be compared with the calculated ones because of the high conversion of ethylene occurring during the reaction interval.

(k_i/k_t), estimated for the high-temperature pyrolysis of ethylene, can be corrected for ΔC_p to the lower temperature, 750°K; $k_i/k_t = 10^{1.06-64.9/\theta}$. A reasonable value for k_9 is $10^{9.5-13/\theta}$ l. mole^{-1} sec^{-1}; this gives an acceptable rate constant for the inverse reaction, k_{-9}, $10^{10.8-7.0/\theta}$ l. mole^{-1} sec^{-1} (a consequence of the equilibrium constant k_9/k_{-9}, at 750°K, $10^{-1.29-5.7/\theta}$).[8]

Thus, the rate of ethane formation is $10^{10.0-45.5/\theta}$ mole l.$^{-1}$ sec^{-1}. At 750°K, the absolute rate is $10^{-3.3}$ mole l.$^{-1}$ sec^{-1}, about a factor of 3 slower than the observed rate ($10^{-2.8}$ mole l.$^{-1}$ sec^{-1}).[9] This suggests that the ratio k_i/k_t might be larger than estimated. In fact, an increase of six-tenths of a power of ten ($10^{0.6}$)

(8) B. de B. Darwent and R. Roberts, *Discussions Faraday Soc.*, **14**, 55 (1953).

(9) R. N. Pease, *J. Am. Chem. Soc.*, **54**, 1877 (1932).

Table VI: Comparison of the Predicted and Observed Rates of Hydrogenation of Acetylene[a]

T, °K	Log $R^0_{C_2H_4}{}^{calcd}$ [b]	$R_{C_2H_4}{}^{calcd}/R_{C_2H_4}{}^{obsd}$ [c]	Log $R^0_{C_4H_6}{}^{calcd}$ [b]	$R_{C_4H_6}{}^{calcd}/R_{C_4H_6}{}^{obsd}$ [c]	Log $[(C_2H_4)/(C_2H)_{4e}]$ [d]	Log $[(C_4H_6)/(C_4H_6)_e]$ [e]
			Mixture 5, Dwell Time 2 msec			
1187	−2.09	2.5	−3.10	0.6	−2.92	−2.24
1279	−1.87	2.6	−2.99	0.5	−2.08	−0.89
1384	−1.59	3.0	−2.80	0.6	−1.20	0.35
1484	−1.40	3.8	−2.69	0.8	−0.57	1.38
1502	−1.37	3.9	−2.67	0.8	−0.48	1.50
1635	−1.23	6.0	−2.62	0.5	0.06	2.86
1774	−1.15	11.0	−2.61	0.4	0.43	3.98
			Mixture 5, Dwell Time 10 msec			
1180	−2.21	1.8	−3.21	0.5	−2.26	−1.75
1260	−1.89	2.3	−2.97	...	−1.47	...
1363	−1.62	4.0	−2.81	1.6	−0.75	−0.64
1436	−1.48	5.7	−2.73	...	−0.39	...
1530	−1.35	10.3	−2.67	2.4	−0.04	2.01
1677	−1.22	29.0	−2.63	...	0.26	...

[a] Values of rate constants of individual steps of mechanism used in estimating over-all rate: $k_i = 10^{9.7-60.7/\theta}$ l. mole^{-1} sec^{-1}; $k_1 = 10^{11.9-31.5/\theta}$ l. mole^{-1} sec^{-1}; $k_{-1} = 10^{7.9+15.0/\theta}$ l.^{2} mole^{-2} sec^{-1}; $k_{-2} = 10^{9.9-7.4/\theta}$ l. mole^{-1} sec^{-1}; $k_4 = 10^{8.3}$ l. mole^{-1} sec^{-1}; $k_5 = 10^{9.4-5.9/\theta}$ l. mole^{-1} sec^{-1}; $k_{tHv} = 10^{9.6}$ l. mole^{-1} sec^{-1}; $k_{tH} = 10^{9.0}$ l. mole^{-1} sec^{-1}. [b] $R^0_{C_2H_4}{}^{calcd}$ and $R^0_{C_4H_6}{}^{calcd}$ represent initial rates calculated in mole liter^{-1} second^{-1}. [c] $R_{C_2H_4}{}^{calcd}$ and $R_{C_4H_6}{}^{calcd}$ represent the average rate over the dwell time interval.

$$R_{C_2H_4}{}^{calcd} = R^0_{C_2H_4}{}^{calcd}\left(1 - \frac{\%\ \text{conversion}}{200}\right); \quad R_{C_4H_6}{}^{calcd} = R^0_{C_4H_6}{}^{calcd}\left(1 - \frac{\%\ \text{conversion}}{200}\right)^2$$

[d] $(C_2H_4)/(C_2H_4)_e = (C_2H_4)_{obsd}/(C_2H_2)_{obsd}(H_2)_{obsd} \times 10^{4.87-44.03/\theta}$. The quantity $10^{4.87-44.03/\theta}$ mole^{-1} l. is the equilibrium constant for the process $C_2H_2 + H_2 \rightleftarrows C_2H_4$ at 1400°K. [e] $(C_4H_6)/(C_4H_6)_e = (C_4H_6)_{obsd}/(C_2H_2)^2_{obsd}(H_2)_{obsd} \times 10^{9.92-82.9/\theta}$. The equilibrium constant for the process, $2C_2H_2 + H_2 \rightleftarrows C_4H_6$ at 1400°K, is $10^{9.92-82.9/\theta}$ l.^{2} mole^{-2}. The over-shoot of equilibrium suggests that the formation of 1,3-butadiene is occurring during the quenching interval, *i.e.*, lower temperature. [f] Experimental rates below the dashed lines cannot be compared with the calculated ones because of the important contribution of the neglected back reactions.

will bring the calculated and observed absolute rates for both the low-temperature hydrogenation of ethylene and its high-temperature pyrolysis into better agreement. This can be considered an indication of a slower rate of termination ($10^{9.4}$ l. mole^{-1} sec^{-1}) between either two ethyl radicals or two vinyl radicals. This is reasonable for a disproportionation rate. As will be seen later, a value of $10^{9.4}$ l. mole^{-1} sec^{-1} for the vinyl–vinyl termination gives a better correlation for the 1,3-butadiene pyrolysis.

Hydrogenation of Acetylene

The high-temperature hydrogenation of acetylene yields mainly ethylene and 1,3-butadiene. It is easily ascertained that the hydrogen–acetylene–ethylene equilibrium is established at high temperatures (See Table VI). Consequently, the simple mechanism displayed below correlates with the pyrolysis, only if the temperature is low and the dwell time is short.

$$C_2H_2 + H_2 \xrightarrow{i} C_2H_3\cdot + H\cdot \quad \text{(initiation)}$$

$$C_2H_3\cdot + H_2 \xrightarrow{-2} C_2H_4 + H\cdot$$

$$C_2H_3\cdot + M \underset{-1}{\overset{1}{\rightleftarrows}} C_2H_2 + H\cdot + M \quad \text{(chain-forming ethylene)}$$

$$C_2H_3\cdot + C_2H_2 \xrightarrow{4} C_4H_5\cdot{}^{11}$$

$$C_4H_5\cdot + H_2 \xrightarrow{5} C_4H_6 + H\cdot \quad \text{(chain forming 1,3-butadiene)}^{10}$$

$$2H\cdot + M \xrightarrow{tH}$$

$$H + C_2H_3\cdot \xrightarrow{tHv} \quad \text{(termination)}$$

Supposing steady-state conditions and long propagation chains exist, the expression for the initial rate of production of ethylene can be formulated as

(10) Assume this chain length is smaller than that of the preceding one. In other words, the ratio $[C_2H_3\cdot]/[H\cdot]$ is determined by the first chain, and the ratio $[C_4H_5\cdot]/[C_2H_3\cdot]$ is determined by the second chain. This assumption is justified in the Appendix.

(11) Assume this radical has a minor role in termination.

$$R_{C_2H_4} = k_{-2}\left(\frac{k_i}{k_{tH}}\right)^{1/2} \frac{\omega(H_2)^{3/2}(C_2H_2)^{1/2}}{[(M) + \alpha\omega]^{1/2}} \quad (7)$$

where

$$\alpha = \frac{k_{tHv}}{k_{tH}}$$

$$\omega = \frac{(C_2H_3\cdot)_{ss}}{(H\cdot)_{ss}} = \frac{k_{-1}(C_2H_2)(M)}{k_{-2}(H_2) + k_1(M)}$$

At low temperatures, where $(C_2H_3\cdot) \approx (H\cdot)$, termination occurs between a vinyl radical and a hydrogen atom. As the temperature is increased, concentration of hydrogen atoms exceeds that of the other radicals, $(H\cdot) > (C_2H_3\cdot)$, and the termination of two hydrogen atoms by a collision with a third body competes with the mixed termination at the highest temperatures. The agreement between the predicted and observed absolute rates is gratifying (Table VI). The neglected back reactions become important at high temperatures, and near the end of the dwell-time interval, this is evident by the establishment of the equilibrium concentration of ethylene (next to the last column, Table VI). This accounts for the increase in the ratio, $R_{C_2H_4}^{calcd}/R_{C_2H_4}^{obsd}$, at high temperatures and long dwell times. It would be advantageous to exhaust the possibility of a contribution from a molecular mechanism. To this end, the kinetic parameters for the process, $C_2H_2 + H_2 \rightarrow C_2H_4$, were estimated, $k = 10^{8.56-41/\theta}$ l. mole^{-1} sec^{-1} (see ref 6), with the outcome that the molecular mechanism, concurrent with the radical mechanism, does not contribute a sufficient fraction to the over-all rate (see Table VII).

The chain composed of reactions 4, 5, and −1 is assumed responsible for the formation of 1,3-butadiene. The steady-state rate of formation for 1,3-butadiene is related to the steady-state rate of formation of ethylene (eq 7) by

$$R_{C_4H_6} = \frac{k_5}{k_{-2}}\phi R_{C_2H_4} \quad (8)$$

where, $\phi = (C_4H_5\cdot)_{ss}/(C_2H_3\cdot)_{ss} = k_4(C_2H_2)/k_5(H_2)$. The rates calculated with this equation are compared to the observed values in Table VI. The absolute rate calculated for the formation of 1,3-butadiene agrees with the observed rates as long as the dwell time is short. This is perhaps caused by the neglect of the back reactions. However, the behavior is irregular in that the final concentration of 1,3-butadiene in some cases is greater than that expected from the equilibrium $2C_2H_2 + H_2 \rightleftarrows C_4H_6$, a consequence not easily explained, except as a continuation of the chain during the quenching period.

Table VII: Comparison of Molecular and Radical Mechanism for the Hydrogenation of Acetylene

T, °K	Log $R_{C_2H_4}^{mole}/R_{C_2H_4}^{rad}$ [a]
Mixture 5, Dwell Time 2 msec	
1187	−2.41
1279	−2.08
1384	−1.95
1484	−1.70
1502	−1.73
1635	−1.25
1774	−1.18
Mixture 5, Dwell Time 10 msec	
1180	−2.29
1260	−2.16
1363	−2.00
1436	−1.88
1530	−1.67
1677	−1.38

[a] $R_{C_2H_4}^{mole} = 10^{8.6} \times 10^{-41/\theta}(H_2)(C_2H_2)$.

Discussion of 1,3-Butadiene Pyrolysis

A brief kinetic study of the pyrolysis of 1,3-butadiene was reported.[3] Rudimentary data on the rate of disappearance of butadiene and the distribution of products (acetylene, ethylene, and hydrogen) were recorded for butadiene conversions ranging from 8% to slightly over 80%. The material balance was very good for the low conversion runs (1–2% error in material balance at 8% conversion), but becomes larger as the per cent conversion is increased (20–25% error in material balance at 80% conversion). A simple mechanism, which reproduces the observed rate and product distribution, is given below

$$C_4H_6 \xrightarrow{i} 2C_2H_3\cdot \quad \text{(initiation step)}$$

$$\left.\begin{aligned} &C_2H_3\cdot + M \xrightarrow{1} C_2H_2 + H\cdot + M \\ &H\cdot + C_4H_6 \xrightarrow{-3} C_2H_3\cdot + C_2H_4 \\ &H\cdot + C_4H_6 \xrightarrow{-5'} C_4H_5\cdot + H_2 \\ &C_4H_5\cdot \xrightarrow{-6'} C_4H_4 + H\cdot \end{aligned}\right\} \text{(chain)}$$

$$\left.\begin{aligned} &2C_2H_3\cdot \xrightarrow{tv} C_4H_4 + H_2(C_4H_6) \\ &2C_4H_5\cdot \xrightarrow{tR} \\ &C_4H_5\cdot + C_2H_3\cdot \xrightarrow{tvR} \end{aligned}\right\} \text{(termination)}$$

Starting with the steady-state hypothesis and the assumption of long chain length, a simple expression for the ratio of the steady-state concentration of the radicals $(C_2H_3\cdot)/(H\cdot)$ and $(C_4H_5\cdot)/(H\cdot)$ is obtained.

$$\Omega = \frac{(C_2H_3\cdot)}{(H\cdot)} = \frac{k_{-3}(C_4H_6)}{k_1(M)} = 10^{-2.1+30.5/\theta}\frac{(C_4H_6)}{(M)} \quad (9)$$

$$\psi = \frac{(C_4H_5\cdot)}{(H\cdot)} = \frac{k_{-5'}(C_4H_6)}{k_{6'}} = 10^{-4.8+5.4/\theta}(C_4H_6) \quad (10)$$

Using physically defensible values for the rate constants (see Appendix) and the typical experimental condition,[3] we find that the vinyl radicals and the $C_4H_5\cdot$ radical (resonance stabilized) predominate over the hydrogen atoms, and most certainly, termination occurs between two of these radicals.

The rates of formation of the products and rate of disappearance of butadiene are solely determined by the propagation chain, a consequence of the long chain length. These rates can be related to the elementary steps of the chain by a simple application of steady-state kinetics

$$-R_{C_4H_6} = k_1(M)\left(1 + \frac{k_{-5'}}{k_{-3}}\right)(C_2H_3\cdot) \quad (11)$$

$$R_{C_2H_2} = k_1(M)(C_2H_3\cdot) \quad (12)$$

$$R_{C_2H_4} = k_1(M)(C_2H_3\cdot) \quad (13)$$

$$R_{H_2} = k_1(M)\frac{k_{-5'}}{k_{-3}}(C_2H_3\cdot) \quad (14)$$

and

$$R_{C_4H_4} = k_1(M)\frac{k_{-5'}}{k_{-3}}(C_2H_3\cdot) \quad (15)$$

The steady-state concentration of the vinyl radical is approximately

$$(C_2H_3\cdot)_{ss} = \left(\frac{k_i}{k_t}\right)^{1/2}(C_4H_6)^{1/2} \quad (16)$$

where k_t is an average termination rate $10^{10.0}$ l. mole^{-1} sec^{-1}.[12] Substituting the most probable values for the rate constants (see Appendix) into these equations, the initial rate of disappearance of butadiene becomes $10^{14.7-81.3/\theta}(M)(C_4H_6)^{1/2}$ mole l.$^{-1}$ sec^{-1} and the initial rate of formation of acetylene $10^{14.6-81.3/\theta}$ (M)-$(C_4H_6)^{1/2}$ mole l.$^{-1}$ sec^{-1}.[13] At the mean condition used by Sokoloski and Skinner,[3] the above rates give absolute values of $10^{-2.4}$ mole l.$^{-1}$ sec^{-1} and $10^{-2.5}$ mole l.$^{-1}$ sec^{-1}, respectively. This is in unexpectedly good agreement with the observed values of $10^{-2.4}$ mole l.$^{-1}$ sec^{-1} and $10^{-2.5}$ mole l.$^{-1}$ sec^{-1}. respectively. A more critical comparison between the calculated and observed rates is shown in Table VIII; good agreement is exhibited as long as conversion of the butadiene is 50% or less. Consideration of the equilibrium constants for the equilibria $C_4H_6 \rightleftarrows C_2H_2 + C_2H_4$; K-(1400°K) = $10^{+5.06-38.9/\theta}$ mole l.$^{-1}$, $C_4H_6 \rightleftarrows 2C_2H_2 + H_2$; $K = 10^{+9.93-82.9/\theta}$ mole^2 l.$^{-2}$, and $C_4H_6 \rightleftarrows C_4H_4 + H_2$; $K = 10^{4.82-44.5/\theta}$ mole l.$^{-1}$, confirm the unimportance of the back reactions. However, it is possible that some of the reverse reactions of the individual steps of the mechanism are proceeding at high conversions. In fact, the ethylene concentration in this system is more than a factor of 100 greater than the equilibrium value prescribed by the equilibrium $C_2H_4 \rightleftarrows C_2H_2 + H_2$. A catalyst for the attainment of equilibrium should remove ethylene while the acetylene–hydrogen ratio remains constant. This seems to agree with the observations. At high conversion, the system loses ethylene, yet the ratio of acetylene to hydrogen remains constant (see Table VIII). A possible catalyst for establishing the equilibrium is hydrogen atoms. This is accomplished by the mechanism

$$C_2H_4 + H\cdot \xrightarrow{2} C_2H_3\cdot + H_2$$

$$C_2H_3\cdot + M \xrightarrow{1} C_2H_2 + H\cdot + M$$

The rate of disappearance of ethylene compared to the rate of disappearance of butadiene under steady-state conditions is given by

$$\frac{R_{C_2H_4}}{R_{C_4H_6}} = \left(\frac{k_2}{k_{-3} + k_{-5'}}\right)\frac{(C_2H_4)}{(C_4H_6)} = 10^{0.9-5/\theta}\frac{(C_2H_4)}{(C_4H_6)} \quad (17)$$

Under the best conditions for the decomposition of ethylene, high temperature, and 80% conversion, the rates of disappearance of ethylene and butadiene compete. Let us compare the reverse of reaction −3 with the rate of disappearance of butadiene, $R_{C_4H_6}$

$$\frac{R_{C_2H_4}}{R_{C_4H_6}} = \frac{k_3(C_2H_4)}{k_1(M)\left[1 + \left(\frac{k_{-5'}}{k_{-3}}\right)\right]} \cong 10^{-3.3+24.2/\theta}\frac{(C_2H_4)}{(M)} \quad (18)$$

(12) A rigorous derivation of the steady-state concentration of vinyl radical is expressed by the relation

$$(C_2H_3\cdot)_{ss} = \left(\frac{k_i}{k_{tv} + k_{tR}(\psi/\Omega)^2 + k_{tvR}(\psi/\Omega)}\right)^{1/2}(C_4H_6)^{1/2}$$

The denominator in this equation is independent of butadiene concentration. Substituting the most probable values for the rate constants, the denominator becomes

$$10^{9.4}\{1 + [10^{-2.7+23.5/\theta}(M)][1 + 10^{-2.7+23.5/\theta}(M)]\}$$

l. mole^{-1} sec^{-1}

Over the entire temperature range studied, the square root of the denominator varies only by a factor of 2. Consequently, for the sake of simplicity, we have replaced the denominator with an average termination rate. The accuracy of the data does not warrant the rigorous analysis.

(13)

$$\frac{R_{C_2H_2}}{-R_{C_4H_6}} = \left(\frac{k_{-3}}{k_{-3} + k_{-5'}}\right) = 0.72$$

Table VIII: Comparison of the Predicted and Observed Kinetic Behavior of the Pyrolysis of 1,3-Butadiene[a] (Mixture 4, Dwell Time 10 msec)

T, °K	Log $R^0_{C_4H_6}{}^{calcd}$ [b]	$R_{C_4H_6}{}^{calcd}/R_{C_4H_6}{}^{obsd}$ [c]	$R_{C_2H_2}{}^{calcd}/R_{C_2H_2}{}^{obsd}$ [d]	$(R_{C_2H_4}/R_{C_2H_4})_{obsd}$	$(R_{C_2H_2}/R_{H_2})_{obsd}$	$(R_{C_4H_6}/R_{H_2})_{obsd}$ [f]
1209	−3.27	0.5	0.5	1.0	2.7	0.7
1242	−2.85	0.8	1.1	0.9	3.1	2.2
1289	−2.36	1.0	1.1	1.1	2.9	1.3
1334	−1.95	1.7	1.7	1.2	2.9	1.2
1381	−1.50	3.0	2.8	1.6	2.9	1.3
1412	−1.23	4.9	3.8	2.0	2.2	0.7
		2 ± 1	2 ± 1			

[a] Values of rate constants of individual steps of mechanism used in estimating the over-all rate: $k_i = 10^{15.4-99.5/\theta}$ sec^{-1}; $k_1 = 10^{11.9-31.5/\theta}$ l. mole^{-1} sec^{-1}; $k_{-3} = 10^{9.8-1.0/\theta}$ l. mole^{-1} sec^{-1}; $k_{-5'} = 10^{10.0-4.7/\theta}$ l. mole^{-1} sec^{-1}; $k_{-6'} = 10^{14.8-58/\theta}$ sec^{-1}; $k_{tv} = 10^{9.4}$ l. mole^{-1} sec^{-1}; $k_{tR} = k_{tvR} = 10^{9.4}$ l. mole^{-1} sec^{-1}; $k_{t\,av} = 10^{10.0}$ l. mole^{-1} sec^{-1}. [b] Initial rate predicted by mechanism $R^0_{C_4H_6}{}^{calcd} = 10^{14.7-81.3/\theta}$ (M)$(C_4H_6)^{1/2}$ mole l.$^{-1}$ sec^{-1}. [c] $R_{C_4H_6}{}^{calcd} = R^0_{C_4H_6}{}^{calcd}[1 - (\%\text{ conversion}/200)]^{1/2}$. [d] $R_{C_2H_2}{}^{calcd} = k_{-3}/(k_{-3} + k_{-5}) \times (-R_{C_4H_6}{}^{calcd})$. [e] Below the dashed line the conversion is greater than 50%. [f] Ratio of hydrogen produced to the unaccountable decomposed butadiene.

Taking the conditions for the largest conversion, greatest concentration of ethylene near the end of the reaction interval, we find that the rate of butadiene disappearance is about two orders of magnitude faster than the loss of ethylene. Apparently, this reverse reaction does not contribute to the kinetic behavior of this system. The poor material balance is likely to obscure a correlation between the observed and calculated product distribution. This problem is minimized if the ratios of products are correlated. To this end, the observed and calculated ratios, $R_{C_2H_2}/R_{C_2H_4}$, and $R_{C_2H_2}/R_{H_2}$, will be compared. Equations 12 through 15 give

$$\frac{R_{C_2H_4}}{R_{C_2H_4}} = 1 \tag{19}$$

$$\frac{R_{C_2H_2}}{R_{H_2}} = \frac{k_{-3}}{k_{-5'}} = 10^{-0.2+3.7/\theta} \tag{20}$$

and, for the sake of completeness

$$\frac{R_{C_2H_2}}{R_{C_4H_4}} = \frac{k_{-3}}{k_{-5'}} = 10^{-0.2+3.7/\theta} \tag{21}$$

According to the proposed mechanism, the acetylene and ethylene should always be produced in a 1:1 ratio, while approximately three times more acetylene should be formed than hydrogen. Vinylacetylene should be produced at the same rate as hydrogen. These product ratios are in reasonable agreement with the observed values (Table VIII). It appears that the ethylene to hydrogen ratio changes from a value of 2.8, for conversion of 50% or less, to a value of 1.1 at very high conversions; thus, hydrogen is gained at the expense of ethylene. The decomposed butadiene that was not recovered in the analysis appears to be an unidentified product which is formed 1.2 times faster than hydrogen (see Table VIII). Our mechanism suggests that a mole of vinylacetylene is produced for every mole of hydrogen formed, which is sufficient to establish a material balance good to about 10%. The radical $C_4H_5\cdot$ has two isomers, $H\dot{C}{=}CHCH{=}CH_2$ and $H_2C{=}\dot{C}CH{=}CH_2$. The resonance stabilized radical, $CH_2{=}\dot{C}CH{=}CH_2$ has an entropy only 0.7 cal/deg mole larger than the isomeric radical, $\dot{C}H{=}CHCH{=}CH_2$; however, in terms of enthalpy, it is 13 kcal/mole more stable (see Appendix, ref 2). The competition between these two radicals

$$C_4H_6 + CH_2{=}\dot{C}CH{=}CH_2 \underset{b}{\overset{f}{\rightleftarrows}} \dot{C}H{=}CHCH{=}CH_2 + C_4H_6$$

will favor the radical $CH_2{=}\dot{C}CH{=}CH_2$ [K (1400°K) = $k_f/k_b = 10^{-0.15-13.3/\theta}$]. The kinetic competition between the two hydrogen atom abstractions

$$H\cdot + C_4H_6 \xrightarrow{-5} \dot{C}H{=}CHCH{=}CH_2 + H_2$$

$$H\cdot + C_4H_6 \xrightarrow{-5'} CH_2{=}\dot{C}CH{=}CH_2 + H_2$$

should favor reaction $-5'$; the attack of the relatively weaker bonded hydrogen will be more profitable kinetically speaking. The fate of the resonance-stabilized radical is restricted to the loss of a hydrogen atom forming vinylacetylene, $CH{\equiv}CCH{=}CH_2$. Similarly, hydrogen atoms can add either at the primary or secondary hydrogen sites yielding, respectively, the radicals, $CH_3\dot{C}HCH{=}CH_2$ and $\dot{C}H_2CH_2CH{=}CH_2$.

The resonance-stabilized radical's ($CH_3\dot{C}HCH{=}CH_2$) most probable path is the reverse of its formation—consequently no net reaction. On the other hand, the fate of radical $\dot{C}H_2CH_2CH{=}CH_2$ is determined by the competition between the reverse of its formation and the carbon bond split, $\dot{C}H_2CH_2CH{=}CH_2 \rightarrow C_2H_4 + C_2H_3\cdot$. Thus, reaction -3 must correspond to the hydrogen atom addition at the secondary hydrogen site.

Appendix

The formulation of reliable conclusions from these mechanisms necessitates a meaningful discrimination of the values employed for the rate constants based on the known kinetic parameters of similar systems. This section presents the arguments defending the selection of kinetic parameters utilized in this study.

The pertinent equilibrium constants relating the rate constants associated with the mechanisms can be evaluated from the thermochemical parameters tabulated in Appendix A of ref 2. These are

$$C_2H_3\cdot + M \underset{-1}{\overset{1}{\rightleftarrows}} C_2H_2 + H\cdot + M;$$
$$K(1400°K) = 10^{4.01-46.5/\theta} \text{ mole liter}^{-1}$$

$$H\cdot + C_2H_4 \underset{-2}{\overset{2}{\rightleftarrows}} H_2 + C_2H_3\cdot;$$
$$K(1400°K) = 10^{0.88+1.4/\theta}$$

$$C_2H_3\cdot + C_2H_4 \underset{-3}{\overset{3}{\rightleftarrows}} CH_2{=}CHCH{=}CH_2 + H\cdot;$$
$$K(1400°K) = 10^{-1.05-6.3/\theta}$$

$$C_2H_3\cdot + C_2H_4 \underset{-4}{\overset{4}{\rightleftarrows}} \dot{C}H{=}CHCH{=}CH_2;$$
$$K(1400°K) = 10^{-5.37+40.0/\theta} \text{ l. mole}^{-1}$$

$$\dot{C}H{=}CHCH{=}CH_2 + H_2 \underset{-5}{\overset{5}{\rightleftarrows}} C_4H_6 + H\cdot;$$
$$K(1400°K) = 10^{-0.57-1.2/\theta}$$

$$H_2 + CH_2{=}\dot{C}CH{=}CH_2 \underset{-5'}{\overset{5'}{\rightleftarrows}} C_4H_6 + H\cdot;$$
$$K(1400°K) = 10^{-0.72-14.5/\theta}$$

$$\dot{C}H{=}CHCH{=}CH_2 \underset{-6}{\overset{6}{\rightleftarrows}} C_4H_4 + H\cdot;$$
$$K(1400°K) = 10^{4.25-45.7/\theta} \text{ mole l.}^{-1}$$

$$CH_2{=}\dot{C}CH{=}CH_2 \underset{-6'}{\overset{6'}{\rightleftarrows}} C_4H_4 + H\cdot;$$
$$K(1400°K) = 10^{4.10-58.7/\theta} \text{ mole l.}^{-1}$$

$$C_2H_3\cdot + C_4H_6 \underset{-7}{\overset{7}{\rightleftarrows}} C_2H_4 + \dot{C}H{=}CHCH{=}CH_2;$$
$$K(1400°K) = 10^{-0.31-0.2/\theta}$$

$$C_2H_3\cdot + C_4H_6 \underset{-7'}{\overset{7'}{\rightleftarrows}} C_2H_4 + CH_2{=}\dot{C}CH{=}CH_2;$$
$$K(1400°K) = 10^{-0.15+12.9/\theta}$$

$$2C_2H_4 \underset{t}{\overset{i}{\rightleftarrows}} C_2H_5\cdot + C_2H_3\cdot; \quad K(1400°K) = 10^{1.08-64.7/\theta}$$
$$K(750°K) = 10^{1.06-64.9/\theta}$$

$$C_2H_2 + H_2 \underset{t}{\overset{i}{\rightleftarrows}} C_2H_3\cdot + H\cdot;$$
$$K(1400°K) = 10^{0.07-60.7/\theta}$$

$$C_4H_6 \underset{t}{\overset{i}{\rightleftarrows}} 2C_2H_3\cdot;$$
$$K(1400°K) = 10^{6.00-99.5/\theta} \text{ mole l.}^{-1}$$ [14]

$$C_2H_5\cdot + H_2 \underset{-9}{\overset{9}{\rightleftarrows}} C_2H_6 + H\cdot;$$
$$K(750°K) = 10^{-1.29-5.7/\theta}$$

$$H\cdot + C_2H_4 \underset{-10}{\overset{10}{\rightleftarrows}} C_2H_5\cdot;$$
$$K(750°K) = 10^{-5.13+42.0/\theta} \text{ l. mole}^{-1}$$

$2C_2H_4 \underset{-11}{\overset{11}{\rightleftarrows}} \square$; $K(1400°K) =$
$10^{-6.72+18.0/\theta}$ l. mole^{-1} [15]

$\square \underset{-12}{\overset{12}{\rightleftarrows}} \overset{\cdot}{\square}\overset{\cdot}{}$; $K(1400°K) = 10^{+3.22-56.4/\theta}$ [15]

$\overset{\cdot}{\square}\overset{\cdot}{} \underset{-13}{\overset{13}{\rightleftarrows}} \overset{\cdot}{\square} + H\cdot$; $K(1400°K) =$
$10^{+3.55-38.3/\theta}$ mole l.$^{-1}$ [15]

$\overset{\cdot}{\square}\overset{\cdot}{} + C_2H_4 \underset{-14}{\overset{14}{\rightleftarrows}} \overset{\cdot}{\square} + C_2H_3\cdot;$
$K(1400°K) = 10^{-0.15-5.0/\theta}$ [15]

(14) The kinetics of the butadiene pyrolysis are consistent with the adoption of a symmetry number of 2 for the vinyl radical; this suggests that the radical site has acetylene symmetry. In ref 2, a symmetry number of 1 was used for the vinyl radical. This assumed that the radical site has ethylene symmetry. In most cases, this change in symmetry number produces a variation in the estimated A factor of the elementary process involving the vinyl radical of only a factor of 2. This difference will not influence the conclusions reached, since the reliability in estimating the absolute rate of a chain mechanism is only better than order of magnitude.

(15) Thermodynamic parameters of cyclobutane are $\Delta H_f° = 6.3$ kcal/mole [S. W. Benson, *J. Chem. Educ.*, **42**, 502 (1965)], $S°_{1400°K} = 120.3$ eu [calculated by group additivity rules: S. W. Benson and J. H. Buss, *J. Chem. Phys.*, **29**, (1958), ring correction + 28.6 eu], and $C_p°$ (1400°K) = 56.3 eu, $C_p°$ (300°K) = 17.4 eu (calculated by group additivity, ring corrections -4.61 and -0.67, respectively). The heat of formation of the biradical i, $\Delta H_f° = 61.6$ kcal/mole, was estimated, assuming the C–H bond energy in C_4H_{10} and $\dot{C}_4H_9$ is the same as it is in C_2H_6 (98 kcal/mole). The entropy

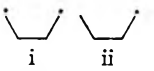

i ii

and heat capacity of ii and i were estimated from the relationships

Rate constants for termination processes vary between $10^{10.6}$ and $10^{9.0}$ l. mole^{-1} sec^{-1}.[16] The appropriate value and the equilibrium constants for the initiation processes assign values of $10^{11.7-64.7/\theta}$ l. mole^{-1} sec^{-1}, $10^{9.7-60.7/\theta}$ l. mole^{-1} sec^{-1}, and $10^{15.4-99.5/\theta}$ sec^{-1} to the rate constants for the respective initiation steps, $2C_2H_4 \rightarrow C_2H_5\cdot + C_2H_3\cdot$, $C_2H_2 + H_2 \rightarrow C_2H_3\cdot + H\cdot$, and $C_4H_6 \rightarrow 2C_2H_3\cdot$.

The low-pressure limit of the classical rate of unimolecular decomposition of the vinyl radical ($C_2H_3\cdot$) had been calculated from the RRK theory in Appendix B of ref 2. A value of $10^{11.9-31.5/\theta}$ l. mole^{-1} sec^{-1} was found for the rate constant k_1. Combining this value with the equilibrium constant, k_1/k_{-1} ($10^{4.01-46.5/\theta}$ mole l.$^{-1}$) gave a value of $10^{7.9+15.0/\theta}$ l.^{2} mole^{-2} sec^{-1} for the rate constant of the back reaction, k_{-1}.

The abstraction of a hydrogen atom from ethylene by a hydrogen atom has a rate constant (k_2) of about $10^{10.8-6.0/\theta}$ l. mole^{-1} sec^{-1}. This value was obtained by analogy with similar abstraction reactions.[16,17] Noting the magnitude of the equilibrium constant, k_2/k_{-2} ($10^{0.88+1.4/\theta}$), k_{-2} can be appraised as $10^{9.9-7.4/\theta}$ l. mole^{-1} sec^{-1}.

We have arbitrarily selected a value for k_{-3} of $10^{9.8-1.0/\theta}$ l. mole^{-1} sec^{-1}. A 1 kcal/mole activation energy seems reasonable in the light of the small activation energies reported for the addition of hydrogen atoms to olefins.[18] An A factor of this magnitude is quite plausible when it is recognized that 10^{10} l. mole^{-1} sec^{-1} is a typical A factor for reactions classed as bimolecular exchange reactions.[16,19] The rate constant for the reverse reaction, k_3, is determined by uniting the ratio k_3/k_{-3} (equilibrium constant $10^{-1.05-6.3/\theta}$) with the rate constant k_{-3} ($10^{9.8-1.0/\theta}$ l. mole^{-1} sec^{-1}); the rate constant k_3 is quite simply $10^{8.7-7.3/\theta}$ l. mole^{-1} sec^{-1}.

The rate constant, k_4, for the addition of vinyl radical to acetylene was assigned a value of $10^{8.3}$ l. mole^{-1} sec^{-1}, a consequence of the values reported for the addition of alkyl radicals to conjugated dienes, or acetylene.[16] (A factors range between $10^{8.5}$ and $10^{7.7}$ l. mole^{-1} sec^{-1}.) Although these systems have an activation energy of about 6 kcal/mole, a considerably smaller value is expected for the addition of vinyl radical to an unsaturated system. The estimated equilibrium constant k_4/k_{-4} ($10^{-5.37+40.0/\theta}$ l. mole^{-1}) allows an evaluation of the rate parameters of the unimolecular rate of decomposition of the radical $C_4H_5\cdot$, k_{-4} ($10^{13.7-40.0/\theta}$ sec^{-1}).

A characteristic value of the rate constant for the abstraction of a hydrogen atom from alkane by a hydrogen atom is $10^{10.5-7.0/\theta}$ l. mole^{-1} sec^{-1}.[16,17] The abstraction of a hydrogen atom from an unsaturated compound by a hydrogen atom has nearly as large an A factor and a slightly smaller activation energy.[20] This suggests a value for k_{-5} of $10^{10.0-4.7/\theta}$ l. mole^{-1} sec^{-1}. Then the ratio k_5/k_{-5} (equilibrium constant $10^{-0.57-1.2/\theta}$) ascribes a magnitude of $10^{9.4-5.9/\theta}$ l. mole^{-1} sec^{-1} to k_5. Similarily, k_{-5}' is $10^{10.0-4.7/\theta}$ l. mole^{-1} sec^{-1}, which ascribes a value of $10^{9.3-19.2/\theta}$ l. mole^{-1} sec^{-1} to k_5'.

The kinetic parameters of the hydrogen atom transfer reaction of radicals can be grouped into definite limits. The A factors fall between 10^7 and 10^9 l. mole^{-1} sec^{-1} and the activation energy between 1 and 10 kcal/mole.[16] Apparently, a value for k, of $10^{8.5-8.0/\theta}$ l. mole^{-1} sec^{-1} would be reasonable. This establishes k_{-7} as $10^{8.8-7.8/\theta}$ l. mole^{-1} sec^{-1}, a value characteristic of hydrogen atom transfer reaction.

The rate constant k_6 can be obtained from the value of the ratio k_6/k_{-6} ($10^{4.25-45.7/\theta}$ mole l.$^{-1}$) and an estimation of k_{-6}. The rate constant k_{-6} is analogous to the rate constants for the addition of hydrogen atoms to 1,3-butadiene, and ethylene, which have A-factor values between $10^{10.0}$ and $10^{10.7}$ l. mole^{-1} sec^{-1} and extremely small activation energies.[17] Accordingly, k_6 must be approximately $10^{14.7-45.7/\theta}$ sec^{-1}. A similar analysis gives $10^{10.7}$ l. mole^{-1} sec^{-1} and $10^{14.8-58.7/\theta}$ sec^{-1} for k_{-6}' and k_6', respectively.

In the ethylene pyrolysis, the radical $C_2H_5\cdot$ was assumed to be inactive in the propagation steps. The equilibrium constants for the process $M + C_2H_5\cdot \underset{-8}{\overset{8}{\rightleftarrows}} C_2H_4 + H\cdot + M$ at 1400°K is $10^{3.88-41.2/\theta}$ mole l.$^{-1}$. Under the experimental condition of the pyrolysis, the radical $C_2H_5\cdot$ has a very small concentration, if the equilibrium is maintained. The estimation of the low-pressure limits of the forward and reverse reaction by the RRK theory indicated that the equilibrium is attained if the steady concentrations of the radicals are reasonably large.

The preferred value for k_{-9} is $10^{10.8-7.3/\theta}$ l. mole^{-1}

(see Appendix A, ref 2): $S°$ (C_4H_{10}) $-$ S (C–H) $+ R \ln q - R \ln \sigma$; $C_p°$ (C_4H_{10}) $-$ C_v (C–H); and $S°$ ($C_4H_9\cdot$) $-$ S (C–H) $+ R \ln q - R \ln \sigma$; $C_p°$ ($C_4H_9\cdot$) $-$ C_v (C–H), respectively. The monoradical $S°$ (1400°K) = 137.4 eu and $C_p°$ (1400°K) = 57.8 eu, $C_p°$ (300°K) = 22.9 eu. The biradical $S°$ (1400°K) = 135.0 eu and $C_p°$ (1400°K) = 53.4 eu, $C_p°$ (300°K) = 22.4 eu.

(16) S. W. Benson and W. B. DeMore, *Ann. Rev. Phys. Chem.*, **16**, 397 (1965); S. W. Benson, *Ind. Eng. Chem.*, **56**, 18 (1964).

(17) B. A. Thrush, *Progr. Reaction Kinetics*, **3**, 65 (1965).

(18) K. R. Jennings and R. J. Cvetanovic, *J. Chem. Phys.*, **35**, 1233 (1961); K. Yang, *J. Am. Chem. Soc.*, **84**, 719, 3795 (1962).

(19) S. W. Benson, "The Foundation of Chemical Kinetics," McGraw-Hill Book Co. Inc., New York, N. Y., 1960.

(20) V. V. Voevodsky and V. N. Kondratiev, *Progr. Reaction Kinetics*, **1**, 43 (1961).

sec^{-1},[16] when multiplied by the equilibrium constant k_9/k_{-9}, yields k_9, $10^{9.5-13.0/\theta}$ l. $mole^{-1}$ sec^{-1}.

The rate constants k_{-6} and k_{10} most likely have the same value, $10^{10.4}$ l. $mole^{-1}$ sec^{-1}. From the equilibrium constant k_{10}/k_{-10} we find k_{-10} is $10^{15.5-42.0/\theta}$ sec^{-1}.

Taking k_{11} equal to $10^{7.4-24/\theta}$ l. $mole^{-1}$ sec^{-1}, the rate constant found for the condensation of $CF_2{=}CF_2$,[16] the equilibrium constant k_{11}/k_{-11} lets us determine the magnitude of the unimolecular rate constant k_{-11}, $10^{14.1-42.0/\theta}$ sec^{-1}.

Internal ring formation apparently has no activation energy and an A factor of $10^{11.5}$ sec^{-1}.[16] This means that the ring fission rate constant should be $10^{14.7-56.4/\theta}$ sec^{-1}.

The rate constant for the addition of a hydrogen atom to ethylene is about $10^{10.4}$ l. $mole^{-1}$ sec^{-1}. See arguments on the magnitude of k_{-6}. Thus, k_{13} is equal to $10^{14.0-38.3/\theta}$ sec^{-1}.

Equating the rate constants k_{-7} and k_{14}, $10^{8.8-7.8/\theta}$ l. $mole^{-1}$ sec^{-1} requires that k_{-14} be $10^{9.0-2.8/\theta}$ l. $mole^{-1}$ sec^{-1}.

The chain lengths (φ) for the formation of ethylene and butadiene in the hydrogenation of acetylene are, respectively

$$\varphi_{C_2H_4} = \frac{k_{-2}(H_2)}{k_{tHv}(H\cdot)_{ss}}$$

and

$$\varphi_{C_4H_6} = \frac{k_5(H_2)(C_4H_5\cdot)_{ss}}{k_{tHv}(C_2H_3\cdot)_{ss}(H\cdot)}$$

Now, comparing the chain length (φ) for the two chains, we find

$$\frac{\varphi_{C_2H_4}}{\varphi_{C_4H_6}} = \frac{k_{-2}}{k_5}\frac{(C_2H_3\cdot)_{ss}}{(C_4H_5\cdot)_{ss}} = \frac{k_{-2}}{k_4}\frac{(H_2)}{(C_2H_2)}$$

This ratio is equal to $10^{2.4-7.4/\theta}$, since in mixture 5, the hydrogen concentration is six times the acetylene concentration. Thus, $\varphi_{C_2H_4}/\varphi_{C_4H_6} \geq 10$, which justifies the assumption of independent chains.

An Empirical Corresponding-States Relationship for Liquid Viscosity

by R. J. Greet and J. H. Magill

Mellon Institute, Pittsburgh, Pennsylvania 15213 *(Received October 18, 1966)*

An empirical corresponding-states relation for liquid viscosity for a wide variety of substances is given. This relationship, which correlates the experimental viscosity with the reduced temperature parameter T_m/T, allows liquids to be categorized according to their chemical and molecular nature. The status of other empirical viscosity–temperature correlations is also discussed.

I. Introduction

There exist, at present, numerous models and theories for the temperature dependence of fluid viscosity at constant pressures.[1-7] We shall discuss some of these descriptions of viscous behavior in this paper (primarily ref 1–7). Because no one theory of liquid transport has yet proven to be universally applicable, empirically discovered relationships still serve as practical aids. Correlating new data on reduced variable plots provides both a first check for consistency with

(1) R. M. Barrer, *Trans. Faraday Soc.*, **39**, 48 (1943).

(2) S. Glasstone, K. J. Laidler, and H. Eyring, "The Theory of Rate Processes," McGraw-Hill Book Co., Inc., New York, N. Y., 1941, Chapter 10, p 477.

other data on similar systems and a means of extrapolating values from limited available data.

While viscosity is often measured over an extended temperature range, it is only when the viscosity changes by many orders of magnitude in the measured interval that a corresponding-states relationship can be tested. Recently, fairly extensive viscosity data have been determined for two nonpolar van der Waals bonded glass-forming liquids. These systems, 1,3,5-tri-α-naphthylbenzene (TαNB)[8-10] and 1,2-diphenylbenzene (O-TER),[5,11,12] exhibit the viscosity behavior shown in Figure 1. In Figure 2, these viscosity data are plotted against two different reduced variables. ΔH_v is the latent heat of vaporization, k is the Boltzmann constant, and T_m is the normal melting temperature at 1 atm of pressure. For these systems

TαNB: $\Delta H_v = 27.9$ kcal/mole; $T_m = 472$°K

O-TER: $\Delta H_v = 14.8$ kcal/mole; $T_m = 329$°K

The use of the latent heat of vaporization to define a reduced temperature parameter has previously been used for somewhat limited viscosity data of a few molecular liquids.[6,13] The correlation with ΔH_v has been preferred in the past because of the fundamental significance which one can attach to it. The linearity of plots[11] of Arrhenius activation energy *vs.* ΔH_v for a variety of materials is partly responsible for this view though, again, activation energy values were mostly obtained from data which covered a limited range, where the transport processes followed an Arrhenius relationship. It was the failure of this variable to bring about a reduction of the 1,3,5-tri-α-naphthylbenzene and *o*-terphenyl data, coupled with the success of using the melting temperature in a reduced variable definition, which initiated the investigation of the correlations presented in the next section. There is an overlap of nine logarithmic decades in the data reduced in the T_m/T plots of Figure 2.

II. Reduced Variable Plots

Plotting viscosity data of different materials against the reduced parameter T_m/T causes these data to fall into several groups. These groups are comprised of materials which generally exhibit the same type of intermolecular bonding. There are still some differences in the magnitude of the viscosities of substances within a given category. In the next section, we discuss some of the parameters for reduced viscosity which have been used. These reduced viscosity parameters do not, however, bring all the various classes of systems together, so we have plotted the experimental viscosity values against T_m/T in the figures to follow.

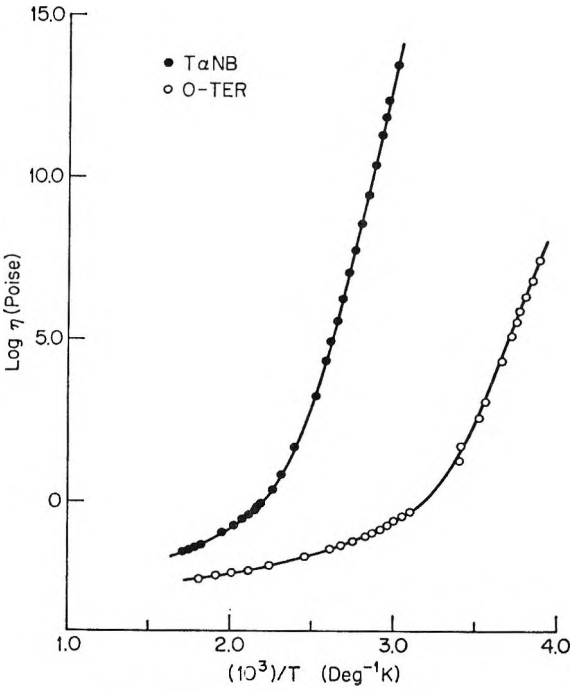

Figure 1. Log (viscosity) *vs.* reciprocal temperature (°K) for 1,3,5-tri-α-naphthylbenzene and *o*-terphenyl.

General Organic Compounds. The viscosity data[5,8-12,14-17] of Figure 3, plotted against the reduced parameter T_m/T, illustrate the validity of this empirical relationship for a variety of organic molecules. Those liquids with similar shapes and force fields behave similarly. Substances which differ widely on an Arrhenius plot (see Figure 1 of this work and Figure 2 of

(3) A. Jobling and A. S. C. Lawrence, *Proc. Roy. Soc.* (London), **A206**, 257 (1951).

(4) A. J. Matheson, *J. Chem. Phys.*, **44**, 695 (1966).

(5) E. McLaughlin and A. R. Ubbelohde, *Trans. Faraday Soc.*, **56**, 988 (1960).

(6) D. Turnbull, "Modern Aspects of the Vitreous State," Vol. I, J. D. Mackenzie, Ed., Butterworth and Co. Ltd., London, 1960, Chapter 3, p 38.

(7) A. G. Ward, *Trans. Faraday Soc.*, **33**, 88 (1937).

(8) J. H. Magill and D. J. Plazek, *J. Chem. Phys.*, in press.

(9) J. H. Magill and A. R. Ubbelohde, *Trans. Faraday Soc.*, **54**, 1811 (1958).

(10) D. J. Plazek and J. H. Magill, *J. Chem. Phys.*, **45**, 3038 (1966).

(11) J. N. Andrews and A. R. Ubbelohde, *Proc. Roy. Soc.* (London), **A228**, 435 (1955).

(12) R. J. Greet and D. Turnbull, *J. Chem. Phys.*, **46**, 1243 (1967).

(13) D. Turnbull and M. H. Cohen, *ibid.*, **34**, 120 (1961).

(14) A. J. Barlow, J. Lamb, and A. J. Matheson, *Proc. Roy. Soc.* (London), **A292**, 322 (1966).

(15) R. K. Hind, E. McLaughlin, and A. R. Ubbelohde, *Trans. Faraday Soc.*, **56**, 331 (1960).

(16) M. F. Mole, W. S. Holmes, and J. C. McCoubrey, *J. Chem. Soc.*, 5144 (1964).

(17) O. Jäntsch, *Z. Krist.*, **108**, 185 (1956).

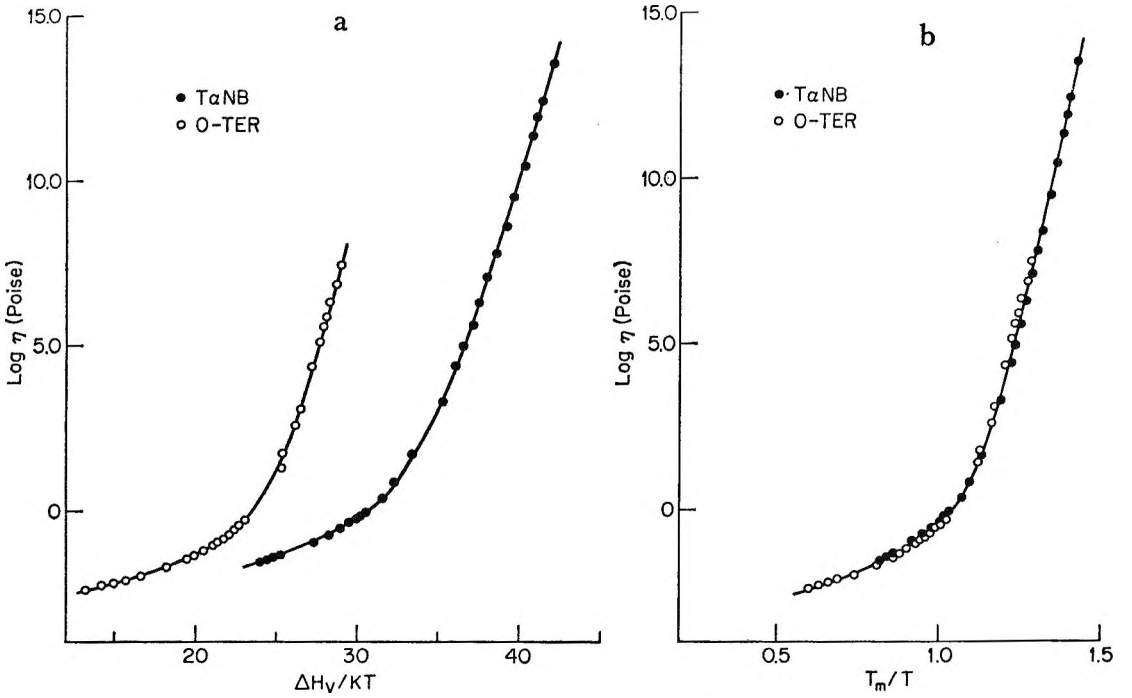

Figure 2. (a) Log (viscosity) *vs.* reduced temperature parameter, $\Delta H_v/kT$, for 1,3,5-tri-α-naphthylbenzene and *o*-terphenyl. ΔH_v is the heat of vaporization. (b) Same viscosity data as part a plotted against the normalizing parameter, T_m/T. T_m is the melting point of the material.

ref 18)[18] can be merged and often superimposed by this procedure (see Figure 2b). It is obvious that under corresponding conditions, as for example in the alkylbenzenes[14] where T_m/T is unity, there is a trend or shift toward higher viscosity values as the anisotropy of the molecules increases, *i.e.*, as the substituent gets larger. On the other hand, pairs of liquids like pyrrole and pyrrolidine[15] and triphenylphosphate and triphenylphosphite[16] are practically reduced to a single curve when plotted against T_m/T. The magnitude of the viscosity of the planar 1,3,5-triphenylbenzene[9] is lower than that of its more complex higher homolog,[9] which in turn is not so great as that of the nonplanar 1,3,5-tri-α-naphthylbenzene[8-10] and 1,2-diphenylbenzene[5,11,12] which coincide under corresponding conditions. Admittedly, the results of Figure 3 comprise only a small portion of the literature data on such substances. We have been selective with the results presented, since existing experimental data are sometimes unsatisfactory for testing transport relationships because they are not extensive enough or the purity and melting points of the materials may sometimes be suspect. Data[19] on isobutyl bromide and isoamyl bromide depart significantly from the general format of Figure 3, both in the shape of their curves and magnitude of the viscosities at corresponding temperatures. In this respect, too, di-*n*-butyl phthalate[14] also deviates from the general pattern. The alkyl bromides show negative deviations and the phthalate compound shows positive deviations in the magnitude of the viscosity at any given T_m/T value with respect to the over-all pattern presented in Figure 3.

Alcohols and Water. In Figure 4, viscosity data[20] on several alcohols with widely different melting points (*e.g.*, glycerol,[20] $T_m = 17.5°$, and ethyl alcohol,[20] $T_m = -117.3°$) readily reduce to a single curve. The Arrhenius plots of these substances are widely separated. The alcohols further demonstrate that materials with related liquid structures should behave similarly when reduced to corresponding temperature. The utility of this plot may lie in the fact that the graph may be used to obtain an estimate of the viscosity of the different alcohols outside their existing experimental ranges.

The data on water[21,22] have been included in Figure

(18) T. A. Litovitz and P. Macedo, "Physics of non-Crystalline Solids," J. A. Prins, Ed., North-Holland Publishing Co., Amsterdam, 1965, p 220.

(19) D. J. Denny, *J. Chem. Phys.*, **30**, 159 (1959).

(20) "American Institute of Physics Handbook," Section 2-181, 2nd ed, American Institute of Physics, New York, N. Y., 1963.

(21) J. Hallett, *Proc. Phys. Soc.* (London), **82**, 1046 (1963).

(22) R. Mills and R. H. Stokes, "Viscosity of Electrolytes and Related Compounds," Pergamon Press, London, Ltd., 1965, Appendix 1.1.

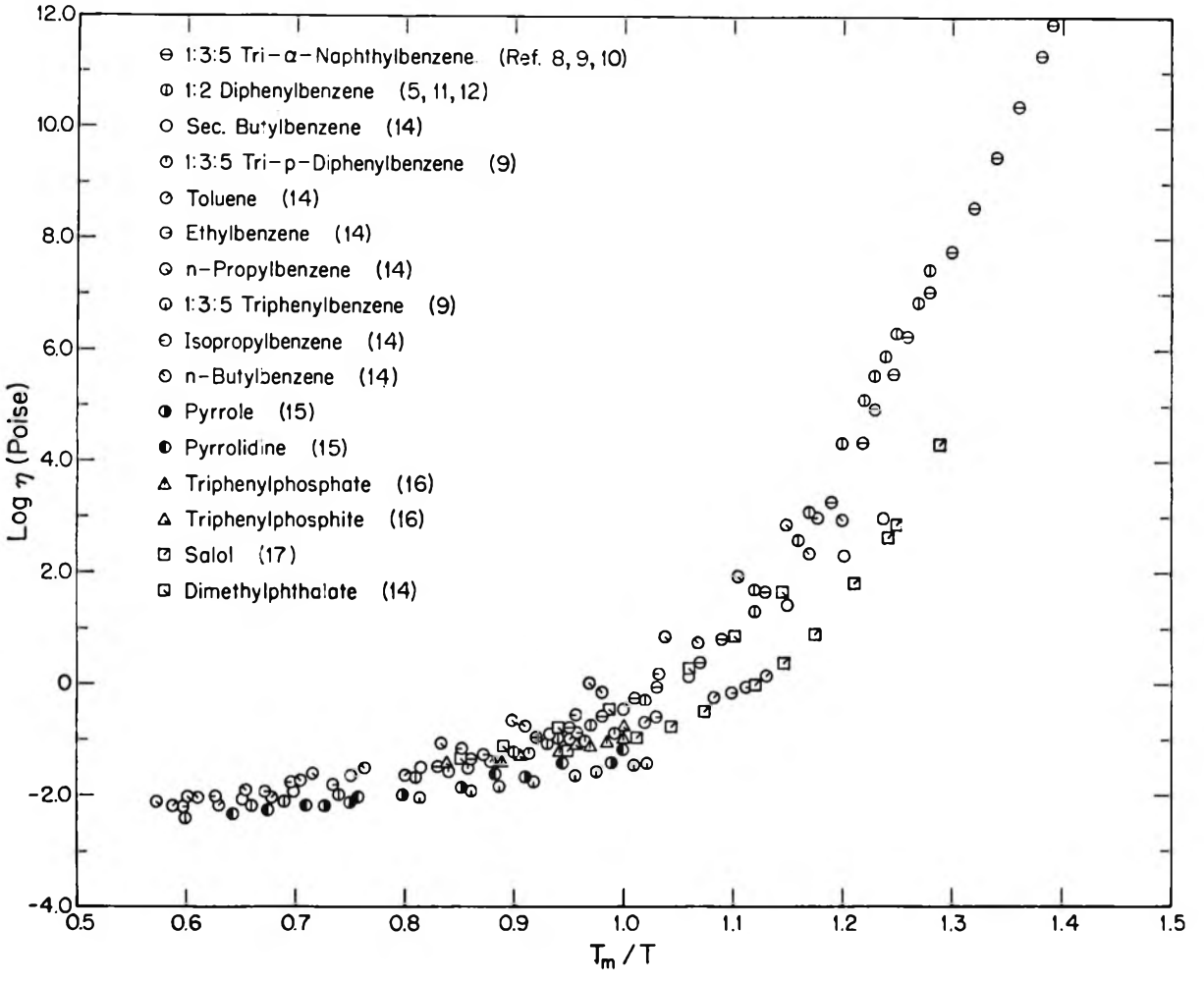

Figure 3. Log (viscosity) *vs.* reduced parameter T_m/T for a wide variety of organic compounds.

4 since, in some respects, this liquid may be considered to be related chemically to the alcohols. However, water really exhibits unique behavior in most respects. It is considered to consist of two species, namely "structured" and "nonstructured" water.[23] The former species is predominant at the lower temperatures while the latter one (which is attributed to freely rotating molecules) is more abundant at the higher temperature. In the case of water, it is noteworthy that it does not show anomalous viscosity behavior in the 4° region, even though its density passes through a maximum value at this temperature.

Inorganic Oxides. The inorganic oxides[10,24-37] are more diverse in their behavior than the other groups of substances (Figure 5). However, it should be noted that Arrhenius plots of the data give a broad spread on the temperature scale (see Figures 1 and 2, ref 18 and 24, respectively). Several explanations can be forwarded to account for this cacophony of data.

These oxide melts, although somewhat chemically similar in character, are believed to exhibit varying

(23) H. S. Frank, *Federation Proc. Suppl.*, **24**, No. 15, Part 3, 1 (1965).

(24) J. D. Mackenzie, "Modern Aspects of the Vitreous State," Vol. I, Butterworth and Co. Ltd., London, 1960, Chapter 8, p 188.

(25) C. R. Kurkjian and R. W. Douglas, *Phys. Chem. Glasses*, **1**, 19 (1960).

(26) J. D. Mackenzie, *J. Chem. Phys.*, **29**, 605 (1958).

(27) J. R. Bacon, A. A. Hasapis, and J. W. Wholley, *Phys. Chem. Glasses*, **1**, 90 (1960).

(28) J. Yovanovitch, *Compt. Rend.*, **253**, 853 (1961).

(29) M. P. Volarovich and A. A. Leontieva, *J. Soc. Glass Technol.*, **20**, 139 (1939).

(30) G. S. Parks and M. E. Spaght, *Physics*, **6**, 69 (1935).

(31) A. Napolitano, P. B. Macedo, and E. G. Hawkins, *J. Am. Ceram. Soc.*, **48**, 613 (1965).

(32) I. Karutz and I. N. Stranski, *Z. Anorg. Chem.*, **292**, 330 (1957).

(33) J. P. Poole, *J. Am. Ceram. Soc.*, **32**, 30 (1949).

(34) I. Shartis, S. Spinner, and W. J. Capps, *ibid.*, **35**, 155 (1952).

(35) H. R. Lillie, *ibid.*, **22**, 367 (1939).

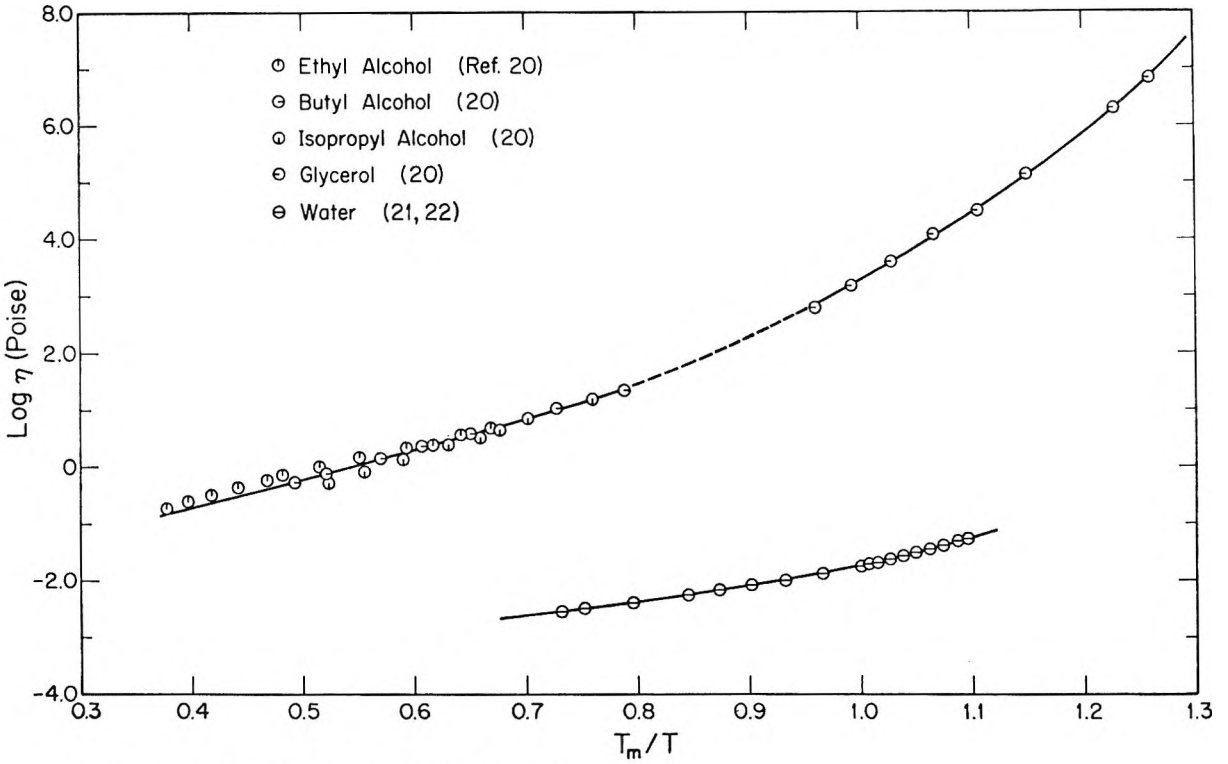

Figure 4. Log (viscosity) *vs.* T_m/T for a series of alcohols and water.

degrees of "structuredness," not only among materials but also with temperature. The quality of the materials measured has not always been well characterized. The high temperatures required in the study of these molten refractories also impose a limitation on the experimental techniques available to the investigators. All of these factors contribute adversely. Nevertheless, the viscosity data[30,31] on B_2O_3 correspond fairly well except for the low-temperature region. In this region, the most recent results[31] are to be preferred. The sodium[33-36] and potassium[10,33,34] disilicate viscosity data also diverge at the lower temperatures, but this may be attributed in part to the difference in ion size in the region where volume effects are becoming important. The As_2O_3 data[32] have approximately the same slope as the B_2O_3 results, but lie surprisingly higher in magnitude. At any rate, there is some uniformity in the observed behavior of these materials when displayed on a log η *vs.* T_m/T plot. The measurements on GeO_2[25,26] and SiO_2[27-29,37] clearly call for more extensive and better data, although the experimental difficulties in this instance are appreciated. (Very recent data[38,39] on these compounds are represented in Figure 5 by solid and dashed lines for SiO_2 and GeO_2, respectively.) Still, the steep curvature in some of the GeO_2 and SiO_2 data[26,37] and the discrepancies between these and other sets of results lie outside experimental uncertainty.[18,25] The same upward trend in the GeO_2 and SiO_2 data[26,37] over a small temperature interval has been attributed to calibration errors.[27,38]

In addition to the oxide network liquids,[24] we also examined the viscosity data[40] of BeF_2. Although this material is not an oxide, it may be categorized with these supposedly two- and three-dimensional "structured" liquids. The reduced-temperature–viscosity plot for this liquid also exhibits some unexpected curvature with an activation energy comparable with oxide materials.

The viscosity results[41-43] of Se and $ZnCl_2$ fall on the same curve but lie at a much lower viscosity level (about two decades) than the disilicate data. However, in the region of $T_m/T > 1$, their activation energy is comparable with the disilicates. At much lower tempera-

(36) B. A. Pospelov and K. S. Evstrop'ev, *Zh. Fiz. Khim.*, **15**, 125 (1941).

(37) J. O'M. Bockris, J. D. Mackenzie, and J. A. Kitchner, *Trans. Faraday Soc.*, **51**, 1734 (1955).

(38) E. H. Fontana and W. A. Plummer, *Phys. Chem. Glasses*, **7**, 139 (1966).

(39) R. Bruckner, *Glastech. Ber.*, **37**, 413 (1964).

(40) J. D. Mackenzie, *J. Chem. Phys.*, **32**, 1150 (1960).

(41) A. Eisenberg and A. V. Tobolsky, *J. Polymer Sci.*, **61**, 483 (1959).

(42) D. E. Harrison, *J. Chem. Phys.*, **41**, 844 (1964).

(43) J. D. Mackenzie and W. K. Murphy, *ibid.*, **33**, 366 (1960).

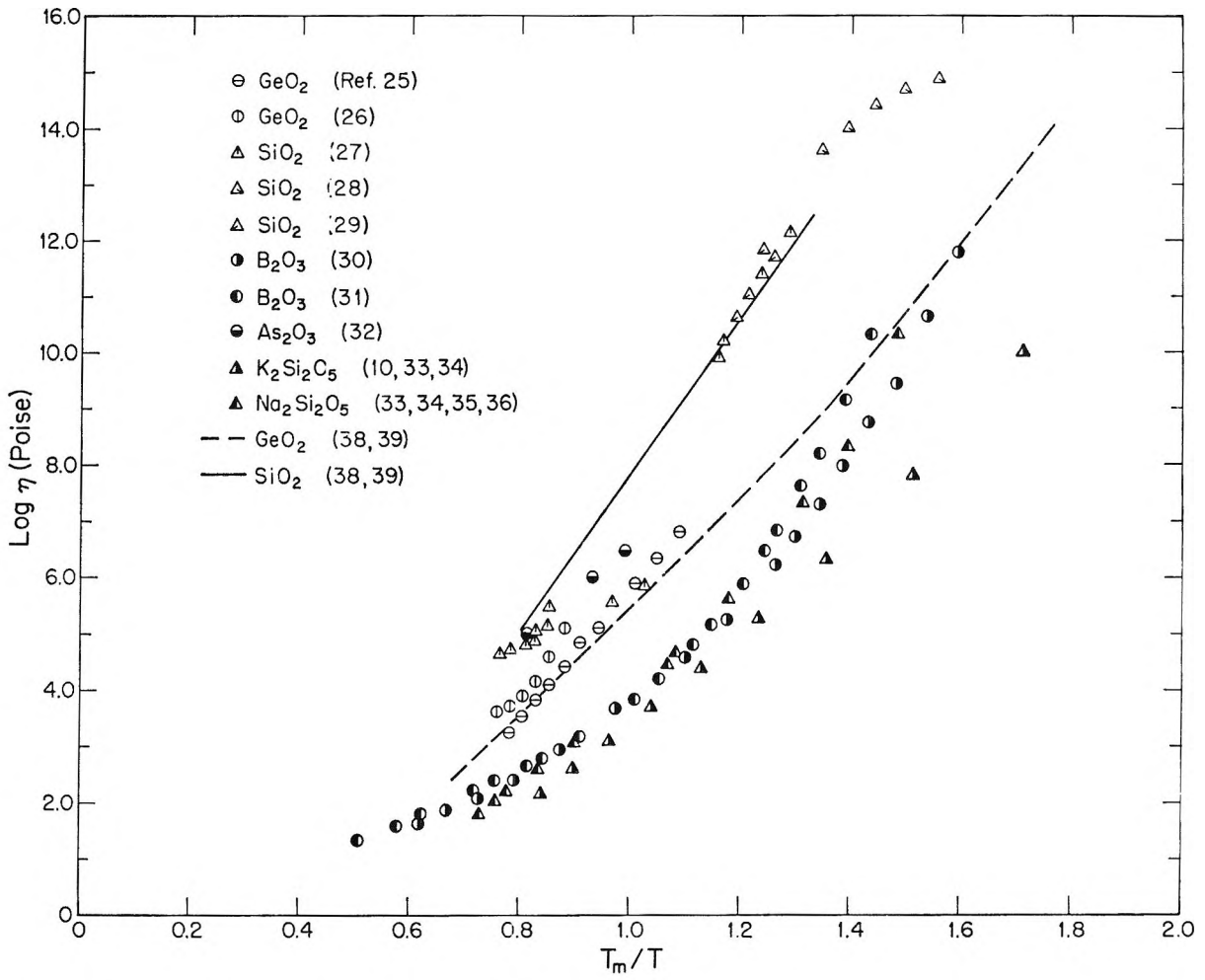

Figure 5. Log (viscosity) *vs.* reduced parameter T_m/T for a variety of inorganic oxides.

tures, $1.5 < T_m/T < 1.6$, the apparent energy for viscous flow of the Se exceeds that for the disilicates. Although it is known that Se displays polymeric character, we cannot explain this behavior in the absence of more detailed knowledge of the liquid state.

Metals. Figure 6a shows the experimental data[44-48] of various metallic systems plotted against reciprocal temperature. The data available for any particular system exhibit Arrhenius behavior with the apparent activation energy for viscous flow increasing as the melting temperature increases. This leads to the reduction shown in Figure 6b, when log η is plotted as a function of T_m/T. The reduced data can be described approximately by the equation

$$\log \eta = -2.4 + 0.80(T_m/T) \quad \text{poise}$$

This is equivalent to a relationship of the form

$$\eta = A\epsilon^{-\Delta S \Delta T/RT}$$

with $A = 2.5 \times 10^{-2}$ poise, $\Delta S = 3.7$ cal/mole deg, and ΔT is the amount of superheating ($\Delta T = T - T_m$).

While the viscosity behavior of all of these metals can be approximately described with a single value for ΔS, this constant is not simply related to the entropy of fusion for these materials. Those metals which crystallize into a BCC structure have an entropy of fusion[49] of approximately 2.0 cal/mole deg; the close-packed structures have an entropy of fusion of approximately 2.3 cal/mole deg. However, other ma-

(44) G. Cavalier, *Compt. Rend.*, 256, 1308 (1963).

(45) H. Schenck, M. G. Frohberg, and K. Hoffman, *Archiv. Eisenhuttenw.*, 34, 93 (1963).

(46) D. Ofte and L. J. Wittenberg, *Trans. AIME*, 227, 706 (1963).

(47) "Handbook of Chemistry and Physics," 31st ed, Chemical Rubber Publishing Co., Cleveland, Ohio, 1949, p 1756.

(48) "Metals Reference Book," Butterworth Inc., Washington, D. C., 1962, p 698.

(49) B. Chalmers, "Principles of Solidification," John Wiley and Sons, Inc., New York, N. Y., 1964, p 41.

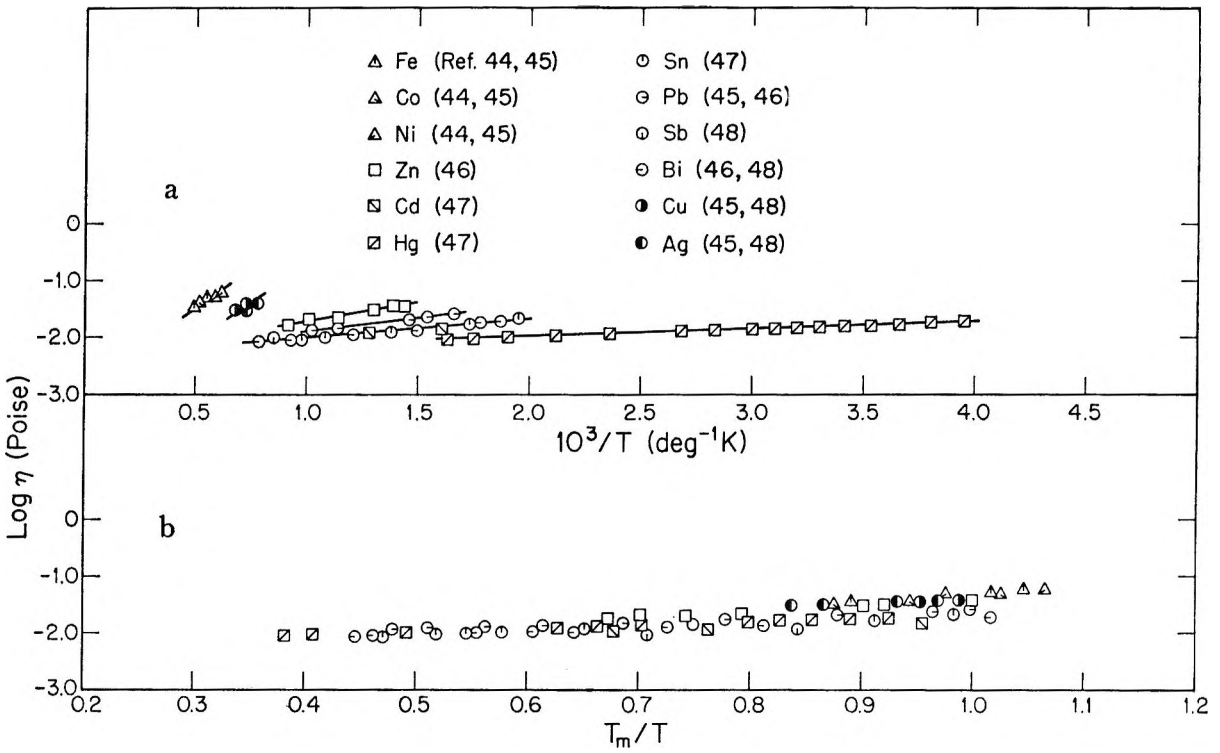

Figure 6. (a) Arrhenius plots—log (viscosity) *vs.* reciprocal absolute temperature for a variety of molten metals. (b) The same viscosity results of part a plotted with the reduced parameter T_m/T as the abscissa.

terials which are less metallic in character have much higher entropies of fusion: 3.4 eu for Sn, 4.8 eu for Bi, and 5.1 eu for Sb.

In addition to the uniformity of the reduced results for molten metals, it is found that liquefied inert gases[50-52] (Ne, Ar, and Kr), molecular gases[50,51] (N_2 and O_2), and simple hydrocarbons[50,53] (CH_4, CCl_4, and neopentane) also exhibit Arrhenius behavior. Their activation energy for flow is practically constant with a value of 3.4 kcal/mole approximately. The principle of corresponding states holds for these materials since the reduced viscosity temperature plots give a single curve. It is significant that Arrhenius behavior is displayed over the entire liquid life of all these essentially spherical molecules which are presumed to rotate freely in the liquid state. With the exception of molten metals, the liquid range of these other substances is short, which seems to be a characteristic feature of such isotropic materials where their symmetric geometry does not impose flow restrictions which affect mass transport.

III. Discussion

Models for Viscous Flow. We make brief mention here of some of the formulas used to describe viscosity behavior, in order to provide a context for the present correlations. Since composition is constant in the systems considered, the thermodynamic state of these liquids is uniquely determined by specifying either the temperature and pressure or the temperature and specific volume of the system. This permits two definitions for an "apparent activation energy" for viscous flow to be used in describing the experimental data.

$$\Delta E_p = k\left(\frac{\partial \ln \eta}{\partial(1/T)}\right)_p \quad (1)$$

$$\Delta E_v = k\left(\frac{\partial \ln \eta}{\partial(1/T)}\right)_v \quad (2)$$

Since pressure and volume are alternative variables, these definitions are related to one another through other derivative properties.

$$\Delta E_p - \Delta E_v = \frac{k\alpha T^2}{\beta}\left(\frac{\partial \ln \eta}{\partial P}\right)_T \quad (3)$$

(50) J. P. Boon and G. Thomas, *Physica*, **29**, 208 (1963).

(51) H. Eyring and R. P. Marchi, *J. Chem. Educ.*, **40**, 562 (1963).

(52) F. Hirth, *Cryogenics*, **2**, 368 (1962).

(53) J. Timmermanns, "Physico-chemical Constants of Pure Organic Compounds," Elsevier Publishing Co., New York, N. Y., Vol. I, 1950, p 227, and Vol. II, 1965, pp 8, 14, 433.

$$\Delta E_p - \Delta E_v = -kv\alpha T^2\left(\frac{\partial \ln \eta}{\partial v}\right)_T \quad (4)$$

where α and β are the usual coefficients of volume thermal expansion and compressibility, namely

$$\alpha = \frac{1}{v}\left(\frac{\partial v}{\partial T}\right)_P \quad (5)$$

$$\beta = \frac{-1}{v}\left(\frac{\partial v}{\partial P}\right)_T \quad (6)$$

One of the first expressions derived for the viscosity was that which results from postulating that viscous flow is an activated process with the energy distribution of the flow units obeying Boltzmann statistics.[54] This resulted in the relationship

$$\eta = A\epsilon^{B/kT} \quad (7)$$

where A and B are taken to be functions of the pressure only. If this expression were universally obeyed, then ΔE_p would be a constant for all of the temperatures investigated and equal in the parameter B of eq 7. In fact, the experimental evidence is that this is virtually never true when the data cover a change of many orders of magnitude in viscosity. While Arrhenius behavior is exhibited by liquids at temperatures well above their melting point, a temperature-dependent activation energy under constant pressure conditions must be used to describe the high viscosity behavior of undercooled anisotropic liquids.

It has been suggested[14] that there exists a transition temperature near the melting temperature of a liquid and that viscous flow is determined by different mechanisms above and below this temperature. If this is true, then a single model for viscous flow would not be expected to describe the entire experimental data. Rather, a viscosity relationship for a particular model may be fitted to the experimental data above and below the transition temperature. This, of course, assures a closer agreement between any model and the data, but there appears at present to be no direct experimental evidence that such a transition temperature actually exists.

One might formally alter eq 7 by permitting A and B to be functions of the temperature as well as the pressure. With an activated flow interpretation, one might consider this temperature dependence to be reflecting the anisotropy of the flow unit. Those systems which can be readily undercooled to high viscosities contain anisotropic molecular constituents which exhibit greatly increased steric hindrance to reorientation as the temperature is decreased. In these circumstances, the nature of the flow unit is changing with temperature, with greater cooperation among molecular units necessary at the lower temperatures. However, this alteration of eq 7 results in an expression which is too general in that $A(T,P)$ and $B(T,P)$ cannot uniquely be associated with the experimental numbers.[7]

A more specific modification of eq 7 is to postulate that the temperature and pressure dependence of the parameters A and B enters only through the specific volume.[55] In other words

$$A = A(v)$$

$$B = B(v)$$

and ΔE_v is now predicted to be constant and equal to B over all of the temperatures measured. The somewhat limited measurements of the pressure dependence of the viscosity suggest that this relationship might be valid.[3] However, the experimental range over which the investigations have been made needs to be considerably expanded before the constancy of ΔE_v can confidently be taken to be generally true.

Alternative expressions for viscous behavior have evolved from what has been termed the free-volume model. One form of this relationship was first proposed empirically by Vogel[56] and was later modified by Doolittle.[57] The Doolittle formula implies that the cell volumes of the molecules, rather than the energies of the flow units, are given by Boltzmann statistics. Later, other approximations were assumed in an attempt to make the derivation more rigorous.[58] The free-volume relationship as expressed by Doolittle is

$$\eta = A'\epsilon^{B'/(v-v_0)} \quad (8)$$

where A', B', and v_0 are taken to be functions of the pressure only. With this formulation, neither ΔE_p nor ΔE_v is expected to be constant, and may be written as

$$\Delta E_p = \frac{kB'v\alpha T^2}{(v - v_0)^2} \quad (9)$$

$$\Delta E_v = -\frac{k\alpha T^2}{\beta}\left[\frac{\partial \ln A}{\partial P} + (v - v_0)^{-1}\frac{\partial B'}{\partial P} + B'(v - v_0)^{-2}\left(\frac{\partial v_0}{\partial P}\right)\right] \quad (10)$$

The value of ΔE_p given by eq 9 can be made to fit approximately much of the experimental data. How-

(54) E. N. da C. Andrade, *Nature*, **125**, 309 (1930).
(55) E. N. da C. Andrade, *Phil. Mag.*, **17**, 698 (1934).
(56) H. Vogel, *Physik. Z.*, **22**, 645 (1921).
(57) A. K. Doolittle, *J. Appl. Phys.*, **22**, 1471 (1951).
(58) M. H. Cohen and D. Turnbull, *J. Chem. Phys.*, **31**, 1164 (1959).

ever, this expression appears to be insufficient to fit the entire data for those systems in which the viscosity has been measured over many orders of magnitude.[10]

In this instance, eq 8 has also been rewritten to be explicitly a function of temperature by substituting[56,59]

$$(v - v_0) = \alpha'(T - T_0) \qquad (11)$$

The free-volume concepts and the extension of eq 11 have particularly been applied to the viscous and viscoelastic behavior of polymer systems.[60] We shall not discuss these systems here as molecular weight distributions and dependence of melting temperature on sample history make these systems especially difficult to evaluate for a corresponding-states relationship. Yet another modification of eq 8 has been to consider that v_0 is also temperature dependent.[4] This is a different fundamental postulate from that first proposed by Doolittle.[57]

Reduced-Viscosity Parameters. Turnbull and Cohen[13] have defined a reduced-viscosity parameter (η/γ) to be

$$(\eta/\gamma) = \eta v^{2/3}(mT)^{-1/2} \qquad (12)$$

where η is the viscosity, v is the average molecular volume, m is the mass of a molecule, and T is the absolute temperature. This expression has the dimensions of $(\text{mass})^{1/2}(\text{length})(\text{time})^{-1}(\text{temperature})^{-1/2}$, and the logarithmic scale of such a variable will thus be shifted, depending upon the system of units used. A dimensionless reduced parameter can be defined which has the same temperature dependence as the Turnbull–Cohen parameter by introducing the Boltzmann constant in the following way

$$(\eta/\gamma') = \eta v^{2/3}(mkT)^{-1/2} \qquad (13)$$

However, for most systems, the temperature variation of $v^{2/3}T^{-1/2}$ is small compared with the temperature variation of η. The total temperature variation of the above reduced parameters is therefore not substantially different from that of η alone.

In view of the reduction achieved by using T_m/T as a reduced-temperature variable, one might also use $\log(\eta/\eta_m)$ as a reduced-viscosity variable, where η_m is the viscosity at the melting point. This variable does not, however, bring the various classes of systems into coincidence, and since it forces all of the curves to pass through the coordinates (1, 0), evaluation of the amount of reduction achieved is difficult.

A complete corresponding-states relationship should incorporate the viscosity into a nondimensionalized parameter. Because the existing suggestions for defining a reduced viscosity appear to be only partially successful, we feel that plotting the experimental viscosity data directly gives a more accurate test of the correspondence achieved with a reduced-temperature variable.

Reduced-Temperature Parameters. The use of the latent heat of vaporization in the definition of a reduced temperature implies that viscous flow is an activated process involving individual molecules. The heat of vaporization should reflect the degree of intermolecular bonding of a system, and for an activated process involving individual molecules, the important parameter should be the ratio of the thermal energy to the bonding energy. This simple picture of viscous flow breaks down, however, at low temperatures where the apparent activation energy for viscous flow, taken from the slopes of Arrhenius plots, becomes as much as five times greater than the energy needed to vaporize a molecule.[8,12] This unrealistic activation energy in terms of individual molecular movements is qualitatively explained by saying that viscous flow, particularly viscous flow at low temperatures, is a cooperative process involving the associated reorientation of many molecules simultaneously.

As mentioned in the Introduction, the apparent linear relationship between ΔE_p and ΔH_v has been responsible in part for the postulate that ΔH_v should play a central role in the definition of reduced temperature.[2] As pointed out earlier in this section, increased experimental data indicate that ΔE_p is most always temperature dependent whenever a large change in viscosity is measured.

Theories involving the melting process and particularly predictions of the melting temperature T_m are far from rigorous and universally applicable at present. Since T_m represents the transition point between two condensed phases, it does reflect the cooperative modes of a system in the rigid and fluid states, contrasted with ΔH_v, which more closely represents a property attributable to individual molecules. In this sense, T_m is not an unreasonable variable to introduce into a viscosity description, although we have only empirical evidence at present for using it as we have illustrated in the figures.

Cohen and Turnbull[6] have sometimes presented schematic curves of viscosity behavior using T_m/T as a variable, but they apparently have not tested the relationships with experimental data points. Eyring and Marchi[51] have also suggested that the melting temperature T_m is reflected in the fluid viscosity behavior. They comment that, since most liquids have nearly the

(59) M. L. Williams, R. F. Landel, and J. D. Ferry, *J. Am. Chem. Soc.*, 77, 3701 (1955).

(60) G. C. Berry and T. G Fox, unpublished results.

same concentration of vacancies and rate of molecular jumping at their melting points, one would expect that liquids would have similar viscosities at their very different melting temperatures. The concept of liquid vacancies is a consequence of a particular model developed by Eyring, *et al.*[2,51]

Ubbelohde and co-workers[5,9,11,61,62] have also ascribed particular significance to liquid transport properties in the vicinity of T_m through the concept of specific molecular associations. Viscosity "anomalies" have been explained by this approach which differs from the quasi-lattice picture mentioned by Eyring.

One further observation is relevant, pertaining to the 1,3,5-tri-α-naphthylbenzene and o-terphenyl data of Figures 1 and 2. These systems have an identical ratio of melting temperature T_m to glass transition temperature T_g, determined by specific volume measurements ($T_m/T_g = 1.36$). Thus, Figure 2b is equivalent, through a change in scale, to a correlation of viscosity as a function of T_g/T. The parameter T_0 of eq 11 represents the temperature at which viscous flow becomes impossible for a particular system since inadequate free volume is present for this process. The glass transition occurs at a some higher temperature than T_0 and is governed by the nature of the system and experimental conditions. One might therefore expect that T_0 would be a more appropriate temperature than T_g for defining a reduced parameter. However, values of T_0 are not available for many of the systems correlated here which makes T_m a more useful normalizing parameter at the present time.

High-Temperature Behavior. A striking feature of the log η *vs.* T_m/T graphs is that all the liquids of a given class appear to converge to a common slope at temperatures well above their respective melting points, where the space available for molecular motion in the liquid is believed to be unrestricted and the shape of the molecule is comparatively unimportant under these conditions, *i.e.*, where the Arrhenius relationship is observed. The nature of our empirical plots demonstrates this trend for all the classes of materials which we have examined. A straight line on the plot of log η *vs.* T_m/T represents a region in which the viscosity is described by the equation

$$\eta = A\epsilon^{-\Delta S \Delta T/RT}$$

where A and ΔS are constants and ΔT is the departure from the melting temperature. From the slopes of the high-temperature tangents, the values in Table I represent the values of ΔS found for the various classes.

The concentration of available free space in the liquid state decreases with decreasing temperature and there is also a corresponding change in the coordination number of any system under such conditions.[63] The volume available for translational processes is therefore gradually diminished. A smaller and smaller number of molecules have, or acquire, the necessary energy for transport, but even if this condition is realized, the influence of molecular anisotropy can impede the progress of molecules in a specific direction. The over-all form of the nonlinear plots raises the question of the validity of a single activation to describe momentum transfer except in the simple systems (metals, liquefied gases, and simple spherical or pseudospherical organic molecules) or under conditions where unrestricted motion is attainable at high temperatures in the more complex molecules. For anisotropic molecules, there is no unique activation energy which will describe a particular material over its entire liquid life. Only in the region well above the sodidification point of the liquid can a single value describe the flow behavior of such substances. At all other temperatures and especially in the supercooled stage, a temperature-dependent activation energy must be applied to describe momentum transfer processes. At large degrees of supercooling where this energy is very high (many times the latent heat of vaporization of the material), we are forced to modify our approach to the liquid state, since non-Arrhenius behavior results. An additional parameter invoking molecular geometry should be introduced into the transport equations to describe these results.

Table I

	ΔS, cal/mole deg
Metals (Figure 6)	~4
General organics (Figure 3)	~12
Alcohols (Figure 4)	~24

IV. Summary

The reduced temperature–viscosity relationship provides us with an empirical correlation which has been demonstrated to be of practical value. Particularly, it may be used to test the consistency of new data with existing viscosity results, as well as their conformity to

(61) A. R. Ubbelohde, "Symposium on Liquids: Structure, Properties and Solid Interactions," T. H. Hugel, Ed., Elsevier Publishing Co., Amsterdam, 1965, p 226.

(62) E. McLaughlin and A. R. Ubbelohde, *Trans. Faraday Soc.*, **54**, 1804 (1958).

(63) J. Zarzycki, "Physics of non-Crystalline Solids," J. A. Prins, Ed., North-Holland Publishing Co., Amsterdam, 1965, p 525.

a given class of liquids. Reduced plots should provide a reasonable estimate of liquid viscosity outside existing experimental ranges for many materials.

In contrast with spherical or pseudo-spherical molecules, anisotropic molecules exhibit no unique activation energy which will describe mass transport over the entire liquid range.

Acknowledgments. This work was supported in part by the Office of Naval Research under Contract No. Nonr 2693(00).

Conductances and Dissociation of Some 5-Substituted Tetrazoles in 1,1,3,3-Tetramethylguanidine at 25°

by Joseph A. Caruso, Paul G. Sears,[1] and Alexander I. Popov

Department of Chemistry, Michigan State University, East Lansing, Michigan 48823 *(Received October 28, 1966)*

Electrical conductances of tetrazole, nine 5-substituted tetrazoles, picric acid, tetrabutylammonium iodide, and tri(isoamyl)butylammonium tetraphenylborate were measured in 1,1,3,3-tetramethylguanidine (TMG) at 25°. Dissociation constants of these compounds were determined from the conductance data. The inductive effect of the substituent groups on the acid strength of the 5-substituted tetrazoles is illustrated by a reasonable linearity of the Taft plot. The dielectric constant of TMG was found to be 11.00 ± 0.02 at 25°.

Introduction

While it has been known for some time that tetrazole and the 5-substituted tetrazoles have definite acidic properties, the relative acidities and the influence of structure factors upon the proton-donor ability of these compounds have not been thoroughly investigated. Dissociation constants of some water-soluble tetrazoles have been determined conductometrically by Oliveri-Mandala,[2] who found that unsubstituted tetrazole had approximately the same acid strength (K_a = 1.54×10^{-5}) as acetic acid. More recently, the acidic dissociation constants of a number of alkyl- and aryl-substituted tetrazoles have been determined potentiometrically by Herbst and co-workers.[3,4] In the case of tetrazole, the K_a value of 1.62×10^{-5} agrees well with that of Oliveri-Mandala. In a number of cases, however, the tetrazole derivatives were insoluble in water, and water–alcohol mixtures of varying composition were used as solution media. Since the change in the composition of the solvent should also change the liquid junction potential (aqueous sce used as reference), it is possible that the relative acid strengths of the tetrazoles may have been altered by this procedure.

In connection with a comprehensive study of the chemistry of tetrazoles carried out in this laboratory, it was of interest to us to determine the influence of substituent groups on the acidity of 5-substituted tetrazoles. Since most of these compounds are insoluble in water, a suitable nonaqueous solvent had to be used.

A relatively new nonaqueous solvent, 1,1,3,3-tetramethylguanidine (hereafter abbreviated as TMG) was

(1) On sabbatical leave from University of Kentucky, Lexington, Ky.

(2) E. Oliveri-Mandala, *Gazz. Chim. Ital.*, 44, II, 175 (1914).

(3) T. S. Mihina and R. M. Herbst, *J. Org. Chem.*, 15, 1082 (1950).

(4) R. M. Herbst and K. R. Wilson, *ibid.*, 22, 1142 (1957).

recently studied in this laboratory.[5] This substance was found to be strongly basic ($pK_a \approx 13$ in aqueous solution[6]) and a good solvent for the tetrazoles. It does have a rather low dielectric constant ($D = 11.00$) so that a considerable amount of ion pairing is to be expected. However, since the solvent properties of TMG have not been explored to any significant extent, it was decided to combine the study of the tetrazoles with the study of the solvent properties of TMG.

Experimental Section

Reagents. 1,1,3,3-Tetramethylguanidine was obtained from American Cyanamid and was purified by vacuum distillation over granulated barium oxide at 36–38° under about 0.1 mm pressure. The system containing about 2 l. of TMG was first refluxed for several hours, a first fraction of 100 ml was collected and discarded, and then a final fraction of about 700 ml was collected and used immediately. Solvent prepared in such a manner exhibited specific conductances within the range of $5–10 \times 10^{-8}$ ohm^{-1} cm^{-1}. Gas chromatograms taken on an F & M Model 700 gas chromatograph equipped with a hydrogen flame detector showed only one peak, whereas solvent purified at atmospheric pressure exhibited three peaks with the area ratios of about 2:2:96.

Tetramethylguanidine is a solvent with bp 159–160°.[5] Its freezing point could not be determined since it congeals to a glassy state. The viscosity is 0.0140 poise and the density is 0.9136 g/ml at 25°.[5] The dielectric constant of the solvent was measured by a previously described technique[7] and was found to be 11.00 ± 0.02 at 25°.

Conductance water for potassium chloride solutions was prepared by passing distilled water through a mixed-bed resin obtained from Crystalab Research Laboratories. The specific conductance of such water ranged from 5 to 7×10^{-7} ohm^{-1} cm^{-1}.

Potassium chloride, Matheson Coleman and Bell Reagent, ACS, Crystals, was fused in a platinum crucible, ground in an agate mortar, oven dried, and stored.

The preparation and purification of tri(isoamyl)-butylammonium tetraphenylborate has been described previously.[8] The melting point of our product was 264–265°.

Picric acid, Matheson Coleman and Bell Reagent Crystals, was recrystallized twice from ethanol and dried to constant weight.

Some of the 5-substituted tetrazoles were available as a result of previous work in this laboratory;[3] others were prepared according to the procedure of Finnegan, *et al.*[9] The compounds were purified as follows.

The 5-ethyl (mp 86.5–89.5°) and 5-*n*-propyl (mp 60–62°) tetrazoles were purified by triple sublimation. Since they were in such short supply, further purification was not attempted, and consequently the purities may not be as high as would be desirable.

The 5-*p*-nitrophenyl (mp 226–227° dec), 5-*p*-chlorophenyl (mp 260–261° dec), 5-*p*-methoxyphenyl (mp 239–240°), 5-phenyl (mp 221–222°), 5-methyl (mp 148°), 5-benzyl (mp 124–125°), and 5-*p*-chlorobenzyl (mp 162–163°) tetrazoles were all recrystallized twice. The respective tetrazole was added to 1,2-dichloroethane and the mixture was brought to boiling. Just enough methanol was then added to dissolve the tetrazole. The solution was allowed to cool and the needle-like crystals filtered off. The crystals were then dried in a vacuum desiccator for 24 hr. The melting points, as given above, compare favorably with the literature values.[3,9]

Tetrazole was obtained from City Chemical Co. and was purified by recrystallizing from a 1:5 methanol–benzene mixture. The needle-like crystals were dried to constant weight *in vacuo*. The melting point of 155° coincided with the literature value.[10]

Apparatus. All melting points were taken on a Fisher–Johns melting point block for which the usual stem corrections were made. The conductance bridge has been described previously,[11] and was operated at a frequency of 2000 cps.

The cells were similar to those described by Daggett, Bair, and Kraus.[12] The electrodes were platinized according to the technique of Jones and Bollinger.[13] Potassium chloride solutions were made up by weight, the molar concentrations were calculated, and the equivalent conductances were calculated from the Lind, Zwolenik, and Fuoss equation.[14] The constants of the four cells used in this investigation were calculated in the usual manner and they are as follows: 0.2409 ± 0.0001, 0.2320 ± 0.0001, 0.1216 ± 0.0002, and 0.4421 ± 0.0004 cm^{-1}.

The temperature of 25.00 ± 0.03° was provided by a

(5) M. L. Anderson, Ph.D. Thesis, Michigan State University, 1965.

(6) S. J. Angyal and W. K. Warburton, *J. Chem. Soc.*, 2492 (1951).

(7) J. W. Vaughn and P. G. Sears, *J. Phys. Chem.*, **62**, 183 (1958).

(8) M. A. Coplan and R. M. Fuoss, *ibid.*, **68**, 1177 (1964).

(9) W. G. Finnegan, R. A. Henry, and R. Lofquist, *J. Am. Chem. Soc.*, **80**, 3908 (1958).

(10) F. R. Benson, *Chem. Rev.*, **41**, 5 (1947).

(11) H. B. Thompson and M. T. Rogers, *Rev. Sci. Instr.*, **27**, 1079 (1956).

(12) H. M. Daggett, E. J. Bair, and C. A. Kraus, *J. Am. Chem. Soc.*, **73**, 799 (1951).

(13) G. Jones and D. M. Bollinger, *ibid.*, **57**, 280 (1935).

(14) J. E. Lind, J. J. Zwolenik, and R. M. Fuoss, *ibid.*, **81**, 1557 (1959).

Sargent S-84805 thermostatic bath assembly filled with light mineral oil.

Procedure. Freshly distilled solvent was weighed into two of the cells which had been previously steamed, rinsed with acetone, and dried by a stream of dry nitrogen. The cells were then immersed in the thermostatic bath and allowed sufficient time to equilibrate. The parallel resistance readings (30,000 ohms in shunt across the cell) were then taken and converted to series cell resistances. Stock solutions were prepared by weighing solvent into a flask containing previously weighed solute. The stock solutions were then added by means of weight burets and the contents of the cells were thoroughly mixed. After equilibration, the contents of the cells were remixed in the bath and the resistance readings were taken. All weights were corrected to their equivalent weights *in vacuo*.

Results and Discussion

Conductance data were obtained for tetrazole, nine 5-substituted tetrazoles, tetrabutylammonium iodide, tri(isoamyl)butylammonium tetraphenylborate, and picric acid solutions in TMG. The results are shown in Table I. It should be noted that the concentration range of our solutions is perhaps somewhat narrower than that usually found in similar studies. In general, the upper limit of concentration was determined by the Fuoss equation, $C_{max} = 3.2 \times 10^{-7} D^3$, where D is the dielectric constant,[15] since at higher concentrations the simple laws of dilute solutions of electrolytes are no longer obeyed. The lower limit was taken such that the specific conductance of the solvent would be less than 5% of the specific conductance of the most dilute solution. Under these conditions, the solvent correction was made by subtracting the specific conductance of the solvent from that of the respective solution.

The experimental data were evaluated according to the method of Fuoss and Shedlovsky[16] using a FORTRAN computer program run on the CDC 3600 computer. The results including the respective standard deviations are given in Table II, and typical plots for four of the 5-substituted tetrazoles are illustrated in Figure 1. It is seen that satisfactory linear plots were obtained.

Recently, Bellobono and Favini, who studied conductances of electrolytes in ethylenediamine, reported that they obtained satisfactory values of Λ_0 and K by simple extrapolation of the $1/\Lambda$ *vs.* $C\Lambda$ plots,[17] *e.g.*, by using the Ostwald dilution equation. This method was applied to the data obtained in this investigation, but the plots were curved and the extrapolation was much more uncertain than that associated with the Fuoss–Shedlovsky treatment.

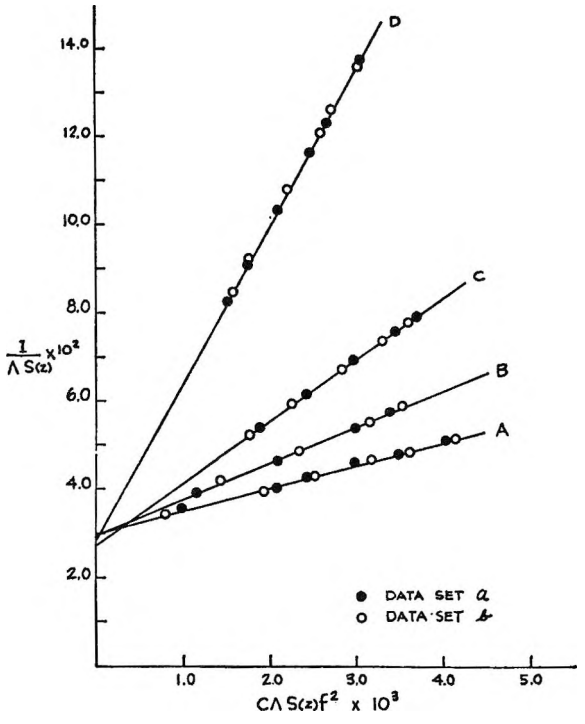

Figure 1. Shedlovsky plots for A, 5-*p*-NO_2PhTz; B, 5-*p*-ClPhTz; C, 5-PhTz; and D, 5-EtTz.

As expected for a solvent with a dielectric constant of 11.00, all of the compounds studied are rather weak electrolytes. The leveling effect of the basic solvent on acids is also evident from the relatively narrow range of the acid dissociation constants. For example, while the dissociation constants of picric acid and of tetrazole differ by a factor of 138,000 in aqueous solutions[2,3,18] (2.12 and 1.54×10^{-5}), the difference is only 19.5 in TMG. We have to deal not only with the ionization process, but also with the incomplete dissociation of the resulting ion pairs. In fact, the dissociation constants reported in Table II are the "over-all" dissociation constants

$$K_{HA} = \frac{(H^+)(A^-)}{(HA) + (H^+A^-)} = \frac{K_i K_d}{1 + K_i}$$

where K_i is the ionization constant and K_d is the ion-pair dissociation constant.[19] In the case of tetrazole, the over-all constant in TMG is greater than in water because of the basic nature of the solvent $K_i^{TMG} >>$

(15) R. M. Fuoss, *J. Am. Chem. Soc.*, **57**, 2604 (1935).

(16) T. Shedlovsky, *J. Franklin Inst.*, **225**, 739 (1938); R. M. Fuoss and T. Shedlovsky, *J. Am. Chem. Soc.*, **71**, 1496 (1949).

(17) I. R. Bellobono and G. Favini, *Ann. Chim.* (Rome), **56**, 32 (1966).

(18) D. J. G. Ives and P. G. N. Musley, *J. Chem. Soc.*, 757 (1966).

(19) I. M. Kolthoff and S. Bruckenstein, *J. Am. Chem. Soc.*, **78**, 1 (1956).

Table I: Equivalent Conductances in TMG at 25° (Superscripts a and b Designate Series of Determinations)

10^4C	Λ	10^4C	Λ	10^4C	Λ
5-*p*-NO_2PhTz[a]		5-*p*-MeOPhTz		5-*p*-ClPhTz	
0.4551	26.93[a]	0.6704	19.01[a]	0.6051	24.40[a]
1.297	23.32	1.618	14.66	1.517	20.11
1.731	21.66	2.427	12.78	2.809	17.03
2.401	20.04	3.399	11.33	3.547	15.90
3.166	18.87	4.152	10.54	0.8480	22.97[b]
4.112	17.68	4.666	10.09	1.773	19.36
0.3510	27.75[b]	1.210	16.08[b]	3.051	16.64
1.165	23.89	2.369	12.89	3.841	15.51
1.737	22.07	3.357	11.39		
2.585	20.17	4.367	10.35		
3.223	19.10	5.202	9.705		
4.303	17.72	5.876	9.279		
5-PhTz		Tetrazole		5-MeTz	
1.525	17.39[a]	1.703	16.75[a]	2.878	10.41[a]
2.435	15.02	3.359	13.15	5.014	8.364
3.560	13.29	5.038	11.26	8.835	6.708
4.858	11.97	6.575	10.20	1.546	12.84[b]
5.542	11.45	7.922	9.530	3.864	9.314
1.381	17.84[b]	9.451	8.913	4.961	8.419
2.126	15.67	2.089	15.71[b]	6.253	7.705
3.322	13.57	3.733	12.74	7.667	7.122
4.487	12.28	5.885	10.72	9.140	6.637
5.372	11.53	7.633	9.707		
		9.382	8.986		
		11.21	8.388		
Bu_4NI					
0.4366	22.97[a]				
1.226	16.50				
1.779	14.41				
2.641	12.49				
3.220	11.58				
3.673	11.04				
0.4259	23.38[b]				
1.042	17.61				
1.739	14.68				
2.373	13.11				
2.910	12.14				
3.617	11.19				
5-EtTz		5-PrTz		5-BzTz	
1.799	11.43[a]	1.889	10.80[a]	1.251	13.71[a]
2.330	10.38	3.437	8.647	2.823	10.23
3.349	9.053	4.954	7.485	4.319	8.695
4.678	7.990	6.923	6.572	5.467	7.925
5.417	7.515	8.687	5.996	6.569	7.370
7.220	6.710	10.03	5.617	7.609	6.948
1.883	11.17[b]	1.944	10.73[b]	1.070	14.40[b]
2.414	10.19	3.505	8.597	2.320	10.97
3.739	8.633	5.715	7.098	3.380	9.524
5.108	7.648	7.400	6.417	4.274	8.705
5.704	7.328	9.075	5.912	5.337	7.986
7.253	6.669	10.60	5.563	6.186	7.538
5-*p*-ClBzTz		Picric Acid		(i-Am)$_3$BuNBPh$_4$	
1.525	14.55[a]	0.7588	33.30[a]	0.3702	24.60[a]
3.008	11.69	1.720	30.64	0.6467	24.15
5.031	9.748	3.334	27.84	1.246	23.38
6.331	8.985	4.342	26.66	2.916	21.67
7.540	8.419	5.475	25.57	4.044	20.86
8.578	8.023	6.487	24.98	1.979	22.52
1.172	15.79[b]	0.4806	34.04[b]	0.3295	24.78[b]
2.178	13.05	1.188	31.96	0.5731	24.35
3.169	11.48	2.504	29.10	1.078	23.58
3.978	10.61	3.508	27.63	1.695	22.75
4.842	9.892	5.190	25.85	2.484	21.98
5.671	9.343	5.912	25.25	3.542	21.14

[a] Tz = tetrazole; Bz = benzyl; Ph = phenyl; Bu = *n*-butyl; *i*-Am = isoamyl; Me = methyl; Et = ethyl; Pr = *n*-propyl; MeO = methoxy.

Table II: Conductance Results in TMG at 25°

Substance	Λ_0	$\sigma\Lambda_0$	$K_a \times 10^5$	$\sigma K_a \times 10^5$
Tetrazole	45.5	1.2	2.94	0.16
5-MeTz	36.3	1.5	2.52	0.21
5-EtTz	34.9	1.0	2.31	0.14
5-PrTz[a]	34.6	...	2.18	...
5-BzTz	36.0	0.5	2.45	0.07
5-*p*-ClBzTz[a]	32.6	...	4.56	...
5-PhTz	35.5	0.3	5.77	0.10
5-*p*-MeOPhTz	35.1	0.4	3.89	0.10
5-*p*-ClPhTz	34.1	0.3	10.5	0.25
5-*p*-NO_2PhTz	33.0	0.5	18.9	0.72
Picric acid	38.2	0.2	55.8	1.2
(i-Am)$_3$BuNBPh$_4$	26.4	0.1	179	8.9
Bu_4NI	42.7	0.9	2.48	0.11

[a] Evaluated by taking the mean of both data sets; all others were evaluated by combining both data sets.

$K_i^{H_2O}$, which more than compensates for the ion-pair formation in TMG. On the other hand, picric acid is a strong acid in water and, $K_i^{H_2O} \approx K_i^{TMG}$, but the over-all constant is smaller in TMG than in water because of the low dielectric constant of the former solvent.

The over-all constant, however, still reflects the inductive effect of the substituent group on the acidity of the tetrazoles. Thus, for example, the acid strength varies in the order: HTz > 5-MeTz > 5-EtTz > 5-PrTz. With the phenyl derivatives we have 5-*p*-NO_2-PhTz > 5-*p*-ClPhTz > 5-PhTz > 5-*p*-MeOPhTz, and with benzyl derivatives 5-*p*-ClBzTz > 5-BzTz.

The discrepancy between the ion-pair dissociation constants of tri(isoamyl)butylammonium tetraphenylborate and the tetrabutylammonium iodide is puzzling, especially in view of the fact that both electrolytes

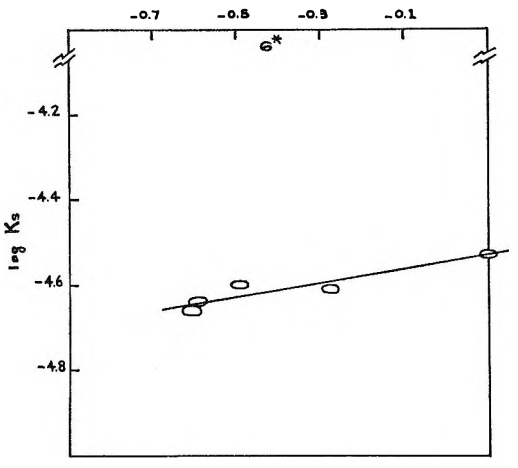

Figure 2. Relationship between log K_s and σ^* for some 5-aliphatic-substituted tetrazoles.

exhibit normal behavior in adiponitrile solutions.[20] It should be pointed out, however, that tetraalkylammonium halides show appreciable association even in solvents of high dielectric constant such as acetonitrile,[21] where the ion-pair dissociation constant for tetramethylammonium iodide, for example, is 3.62×10^{-2}.

The limiting conductance follows the usual trend of varying inversely with the size of the ions. In this respect, it is interesting to compare our results with those of Bellobono and Favini,[17] since ethylenediamine has approximately the same dielectric constant as TMG (12.9 *vs.* 11.00) and both solvents are strongly basic in nature. The limiting conductances of alkali halides in ethylenediamine, for example, in general, increase with the size of the ions. Thus $\Lambda_0^{LiI} < \Lambda_0^{NaI} \approx \Lambda_0^{CsI}$, and $\Lambda_0^{LiBr} < \Lambda_0^{NaBr} < \Lambda_0^{KBr} > \Lambda_0^{CsBr}$. Also, the limiting conductances of the bromides are, in general, higher than those of the iodides. The limiting conductances of the organic acids and their alkali salts showed little correlation with the ionic size since in some cases the Λ_0 for an acid was greater than that of the salt, while in other cases the opposite results were obtained.

An attempt was made to correlate the inductive effect of the substituent groups with the Taft σ^* constant for the series of 5-aliphatic substituted tetrazoles. With tetrazole as a reference, σ^* values[22] were plotted *vs.* log K_s. As seen from Figure 2, the result is a fairly reasonable linear plot which may be described by the equation

$$\log K_s = \rho^*\sigma^* + \log K_0 = 0.173\sigma^* - 4.53$$

These data, also shown in Table III, support the conclusion that the Taft σ^* values provide a useful correlation for the estimation of acid strengths of weak acids, although as given by Taft, the σ^* values are for hydrolysis of esters in acidic or basic solutions. It has also been previously shown that log K_f is a linear function of the Taft σ^* constant, where K_f is the formation constant of various halogen complexes.[23]

Table III: Constants for Various Tetrazoles[a,b]

Substance	Log K_s	σ^*
5-MeTz	−4.60	−0.490
5-EtTz	−4.64	−0.590
5-PrTz	−4.66	−0.605
5-BzTz	−4.61	−0.275
Tetrazole	−4.53	0.000

[a] The above σ^* values are relative to tetrazole (containing the hydrogen substituent) with the reference value of 0.000. Taft gives the methyl substituent as the reference. To convert these values to those given by Taft,[22] 0.490 is added to each value. [b] Taft gives median deviations for the σ^* values of ±0.02 to ±0.04.

Acknowledgment. The authors gratefully acknowledge the support of this work by Research Grant MH 07825 from the Institute of Mental Health, U. S. Public Health Service. They are also indebted to Professor R. M. Herbst and to Mr. Thomas Wehman of this Laboratory for some of the 5-substituted tetrazoles.

(20) P. G. Sears, J. A. Caruso, and A. I. Popov, *J. Phys. Chem.*, **71**, 905 (1967).

(21) A. I. Popov and N. E. Skelly, *J. Am. Chem. Soc.*, **76**, 5309 (1954).

(22) R. W. Taft, in M. S. Newman, Ed., "Steric Effects in Organic Chemistry," John Wiley and Sons, Inc., New York, N. Y., 1956, Chapter 13.

(23) W. B. Person, W. C. Golton, and A. I. Popov, *J. Am. Chem. Soc.*, **85**, 891 (1963).

A Calculation of the Geminal Coupling Constant Based upon the Dirac–Van Vleck Vector Model[1]

by Harry G. Hecht

University of California, Los Alamos Scientific Laboratory, Los Alamos, New Mexico 87544
(Received October 28, 1966)

The geminal proton–proton coupling constant is calculated using the Voge formulation of the methane problem. This is more general than the previous calculations in that valence-state promotion is considered explicitly by configuration interaction with the s^2p^2 and p^4 atomic states of carbon. The energy matrix is solved for four different sets of empirical integrals. It is found that although the calculated coupling constant is still positive, it does not depend so critically on the precise values of the integrals used as was the case in former calculations.

I. Introduction

The early calculations of nuclear spin–spin coupling constants by the valence bond method appeared remarkably successful,[2a-e] but at present these results are regarded by most workers as somewhat fortuitous. Although the valence bond approach continues to be used for the correlation of some effects,[2f] it is generally viewed with much skepticism, since it has been shown to predict positive constants for both geminal and vicinal couplings,[2b,c] whereas the recent experiments show that they are of opposite relative sign,[3] with the geminal coupling presumably the negative one.

It is supposed that there is no fundamental difficulty with the method,[4] but that the approximate nature of the molecular wave functions is responsible for the discrepancy. More specifically, Karplus[5] has pointed out that a near cancellation of the exchange integrals, β and γ (see notation of Section III), leads to a geminal coupling constant nearly proportional to δ.

$$J_{HH'} \simeq \lambda(2\delta - \beta - \gamma) \qquad (1)$$

δ is not known with certainty[2f] and it has been shown that the calculated geminal coupling constant can be changed by more than ± 30 cps by varying the exchange integrals within reasonable limits.[6] Thus it would appear that the valence bond method is severely limited by the inaccuracies inherent in the evaluation of the necessary exchange integrals.

The molecular orbital calculation of coupling constants had a much different genesis. The initial calculations did not look very promising.[7] Here again only positive contact couplings were calculated and it seemed that the difficulty in determining the extent of configuration interaction would seriously limit the method. The delocalized molecular orbital method of Pople and Santry[8] does allow for both signs, but again cancellations occur which preclude any quantitative calculations.

(1) Work performed under the auspices of the U. S. Atomic Energy Commission.

(2) (a) E. Aihara, *J. Chem. Phys.*, **26**, 1347 (1957); (b) M. Karplus and D. H. Anderson, *ibid.*, **30**, 6 (1959); (c) M. Karplus, *ibid.*, **30**, 11 (1959); (d) H. S. Gutowsky, M. Karplus, and D. M. Grant, *ibid.*, **31**, 1278 (1959); (e) S. Alexander, *ibid.*, **34**, 106 (1961); (f) M. Barfield and D. M. Grant, *J. Am. Chem. Soc.*, **83**, 4726 (1961); **85**, 1899 (1963); *J. Chem. Phys.*, **36**, 2054 (1962).

(3) R. R. Fraser, R. U. Lemieux, and J. D. Stevens, *J. Am. Chem. Soc.*, **83**, 3901 (1961); R. R. Fraser, *Can. J. Chem.*, **40**, 1483 (1962); F. Kaplan and J. D. Roberts, *J. Am. Chem. Soc.*, **83**, 4666 (1961); C. A. Reilly and J. D. Swalen, *J. Chem. Phys.*, **35**, 1522 (1961); R. Freeman and K. Pachler, *Mol. Phys.*, **5**, 85 (1962); H. S. Gutowsky and C. Juan, *J. Chem. Phys.*, **37**, 120 (1962); F. A. L. Anet, *J. Am. Chem. Soc.*, **84**, 1053, 3767 (1962); P. C. Lauterbur and R. J. Kurland, *ibid.*, **84**, 3405 (1962).

(4) M. Barfield and D. M. Grant in "Advances in Magnetic Resonance Spectroscopy," Vol. I, J. S. Waugh, Ed., Academic Press Inc., New York, N. Y., 1965.

(5) M. Karplus, *J. Am. Chem. Soc.*, **84**, 2458 (1962).

(6) M. Barfield and D. M. Grant, Abstracts, 144th National Meeting of the American Chemical Society, Los Angeles, Calif., April 1963.

(7) H. M. McConnell, *J. Chem. Phys.*, **24**, 460 (1956).

(8) J. A. Pople and D. P. Santry, *Mol. Phys.*, **7**, 269 (1964); **9**, 301, 311 (1965).

It is probably fair to say that on the whole the valence bond method has been favored for the interpretation of coupling constants, because of the intimate way in which the pairwise coupling of spins is incorporated. The same can of course be said for the Dirac–Van Vleck vector model.[9] Because of the conceptual simplicity of this approach, it seems that calculations based upon a more complex model, in an attempt to better understand the nature of its limitations, can be justified.

II. The Model

It might be supposed that it is better to evaluate the required molecular integrals theoretically, because of the inherent difficulties in estimating them empirically with sufficient accuracy to make meaningful calculations. A problem is encountered here, however. Although wave functions have been tabulated for most of the atomic states of carbon,[10] any quantitative calculation would require the wave function for the so-called valence state.[9,11] Thus, even Slater orbitals may be more accurate for the calculation of the molecular integrals than more exact solutions, because of the way in which an empirical account is taken of overlap and valence-state promotion. Because of such considerations, empirical integrals probably offer the best approach and other factors must be sought in order to achieve the necessary improvement in the molecular wave function.

It seems that although some account is taken of valence-state promotion by use of empirical integrals, a model which treats it explicitly is to be preferred. In the usual valence bond treatment, only the quadrivalent sp^3 configuration is considered. A more exact calculation involves interaction with other configurations, particularly the divalent s^2p^2 ground state of the carbon atom. This problem has been considered by Voge,[12] who shows that the A_1 states of Eyring, Frost, and Turkevich[13] can be regarded as providing the three spin-paired basis functions out of a set of seven functions for a complete calculation. The calculation of the geminal proton coupling in methane by Karplus and Anderson[2b] used just these three symmetry-adapted functions. As Voge points out,[12] the energy is not greatly changed by resonance with the other atomic states, but the promotional energy of the valence state and the wave function are altered considerably. Of course, just such changes are of utmost significance in the nuclear spin–spin coupling problem and one might hope that the critical dependence upon δ might be minimized, although there is probably no *a priori* reason for optimism on this point.

The formulation in terms of the Dirac–Van Vleck vector model need not be repeated here; Voge[12] has solved the problem using the elegant method of treating permutation degeneracy developed by Serber.[14] It is found that the 7×7 problem involves three states of spin-paired configuration (A), $t_a t_b t_c t_d$, as previously mentioned, together with three states with one orbital occupied by two electrons (B), $t_a^2 t_b t_c$, and one state with two filled orbitals (C), $t_a^2 t_b^2$. Voge shows that this is tantamount to consideration of the carbon atom configurations, sp^3, s^2p^2, and p^4.

III. Calculations and Results

Following Voge,[12] we use the following notation for the molecular integrals in terms of which the energy matrix is expressed

$$
\begin{aligned}
H_I^{AA} &= (A|\mathbf{H}|A) & H_I^{CC} &= (C|\mathbf{H}|C)\\
H_I^{BB} &= (B|\mathbf{H}|B) & H_I^{BA} &= (B|\mathbf{H}|A)\\
\alpha &= (t_a h_a;\ h_a t_a) & \theta &= (t_a t_b;\ t_c t_a)\\
\beta &= (h_a h_b;\ h_b h_a) & \kappa &= (t_a h_c;\ h_c t_b)\\
\gamma &= (t_a t_b;\ t_b t_a) & \lambda &= (t_a t_b;\ t_a t_c)\\
\delta &= (t_a t_b;\ h_b t_a) & \mu &= (t_a t_b;\ t_c t_d)\\
\eta &= (t_a h_a;\ h_a t_b)
\end{aligned}
\qquad (2)
$$

where

$$(t_a h_a;\ h_a t_a) \equiv \iint t_a(1) h_a(2) \mathbf{H} h_a(1) t_a(2) d\tau_1 d\tau_2 \qquad (3)$$

etc.

Some of these integrals are purely atomic quantities (γ, θ, λ, μ) and can be expressed in terms of the Slater parameters.[15] The remaining integrals require a knowledge of the molecular properties. Our calculations were performed for the following four sets of integrals.

Set I uses Beardsley's formulas[16] for $F_0(2s, 2s)$, $F_0(2s, 2p)$, and $F_0(2p, 2p)$, together with the values of G_1, F_2, and $I(2p) - I(2s)$ derived by Van Vleck[17] by fitting to the sp^3 atomic energy levels. The molecular integrals assume $N_{s\sigma} = 1.91$ ev, $N_{ss} = 2.0$ ev, $N_{\sigma\sigma} = 2.2$ ev, $N_{\pi\pi} = -0.6$ ev (see Van Vleck[11] for the definition of these integrals in terms of which α, δ, η, and κ

(9) J. H. Van Vleck and A. Sherman, *Rev. Mod. Phys.*, 7, 167 (1935).
(10) A. Tubis, *Phys. Rev.*, 102, 1049 (1956).
(11) J. H. Van Vleck, *J. Chem. Phys.*, 2, 20 (1934).
(12) H. H. Voge, *ibid.*, 4, 581 (1936).
(13) H. Eyring, A. A. Frost, and J. Turkevich, *ibid.*, 1, 777 (1933).
(14) R. Serber, *ibid.*, 2, 697 (1934); 3, 81 (1935).
(15) J. C. Slater, *Phys. Rev.*, 34, 1293 (1929).
(16) N. F. Beardsley, *ibid.*, 39, 913 (1932).
(17) J. H. Van Vleck, *J. Chem. Phys.*, 2, 297 (1934).

Table I: Results of Calculations of Geminal Contact Spin–Spin Coupling Interaction of Protons in Methane, Using the Four Sets of Integrals Discussed in the Text (All Integrals are in Electron Volts and $J_{HH'}$ is in Cycles per Second)

Set	H_I^{AA}	H_I^{BB}	H_I^{CC}	H_I^{BA}	α	β	γ	δ	μ	η	θ	κ	$J_{HH'}$
I	9.745 + x	12.489 + x	15.233 + x	−2.467	−3.804	−1.060	0.901	0.268	−0.471	−0.501	−0.067	−0.332	10.8
II	9.774 + x	12.644 + x	15.514 + x	−2.472	−3.804	−1.060	0.336	0.268	−0.499	−0.501	−0.097	−0.332	15.7
III	9.774 + x	12.644 + x	15.514 + x	−2.472	−3.091	−1.060	0.336	−0.003	−0.499	−0.214	−0.097	−0.603	16.8
IV	9.774 + x	12.644 + x	15.514 + x	−2.472	−3.969	−1.060	0.336	0.323	−0.499	−0.556	−0.097	−0.277	15.6

are expressed), which are the values found by Voge[18] by fitting to the heat of sublimation of graphite, 170 kcal.[19] These values closely parallel those used by Karplus and Anderson,[2b] but they do not contain the correction for zero-point vibrations.

Set II uses Ufford's atomic states[20] for $F_0(2s, 2s)$, $F_0(2s, 2p)$, and $F_0(2p, 2p)$. They are perhaps better than those derived by Beardsley,[16] since they are based on SCF functions for carbon given by Torrance.[21] G_1, F_2, and $I(2p) - I(2s)$ were taken from Voge's reexamination[18] of the methane problem and the same N values were used as in set I.

Set III is the same as set II for the atomic integrals, but the set $N_{ss} = 2.0$ ev, $N_{\sigma\sigma} = 2.3$ ev, $N_{s\sigma} = 1.0$ ev, $N_{\pi\pi} = -0.6$ ev, derived by Van Vleck,[11] is used for the molecular integrals.

Set IV is the same as set II for the atomic integrals, but the set $N_{ss} = 2.0$ ev, $N_{\sigma\sigma} = 2.2$ ev, $N_{s\sigma} = 2.1$ ev, $N_{\pi\pi} = -0.6$ ev, derived by Penney[22] by fitting to the bending vibration of methane, is used for the molecular integrals.

In each case, $\beta = -1.06$ ev is used, which is 0.9 of the Morse function for H_2 for the proton separation appropriate to methane. The term

$$Z = M_{ss} - {}^1/_3 M_{\sigma\sigma} - {}^2/_3 M_{\pi\pi} \qquad (4)$$

also enters the energy matrix, where the M values are defined by

$$M_{kk} = \iint \psi_k(1)h(2)\left[\frac{e^2}{r_{12}} - \frac{e^2}{r_{H1}}\right]\psi_k(1)h(2)d\tau_1 d\tau_2 \qquad (5)$$

These integrals were evaluated using the screening constants for the carbon 2s and 2p orbitals given by Hartree[23] and the tables of Kotani and Amemiya.[24] It was found that $Z = 0.064$ ev.

Since the average energy approximation has been well justified for this case,[25] we used the following equation for the contact coupling constant.[2b]

$$J_{HH'} = \frac{1}{4\Delta E}\left(\frac{2}{3h}\right)\left(\frac{16\pi\beta\hbar}{3}\right)^2 \times \gamma_H^2\left(\Psi_0\left|\sum_{K,K'}\delta(\mathbf{r}_{KH})\delta(\mathbf{r}_{KH'})(2P_{KK'} + 1)\right|\Psi_0\right) \qquad (6)$$

Here $P_{KK'}$ is an electron transposition operator and Ψ_0 is the ground-state electronic wave function. The assumptions involved in the actual calculations are similar to those used by Karplus and Anderson.[2b] The necessary spin functions for the 14 coupling schemes are not given by Voge,[12] but they can easily be written using Clebsch–Gordon coefficients. The results of the calculations are summarized in Table I.

IV. Conclusions

The techniques used to evaluate the integrals mentioned in Section III are those that have been frequently employed by various workers and it is felt that the ranges of values for these integrals listed in Table I are fairly representative of the uncertainties inherent in an empirical evaluation of them. It will be observed that the lack of precision in many cases is quite considerable.

The calculated proton spin–spin coupling constants compare favorably in magnitude with the experimental value of 12.4 cps[26] and are quite constant considering the magnitude of the changes in several of the integrals. By comparison, eq 1 (with $\lambda = 30$ cps) leads to values 20.9, 41.9, 21.5, and 41.1 cps for sets I, II, III, and IV, respectively. Thus, the critical dependence on δ, β, and γ implied by eq 1 is at least in part an artifact of the simplified perturbation approach[2d] and it does appear that more complete calculations based on empirical estimates of the integrals can lead to more stable results.

It will be noted that the geminal coupling constants calculated here are still of what appears to be the

(18) H. H. Voge, *J. Chem. Phys.*, 16, 984 (1948).

(19) W. A. Chupka and M. G. Ingram, *J. Phys. Chem.*, 59, 100 (1955); F. H. Field and J. L. Franklin, "Electron Impact Phenomena," Academic Press Inc., New York, N. Y., 1957.

(20) C. W. Ufford, *Phys. Rev.*, 53, 569 (1938).

(21) C. C. Torrance, *ibid.*, 46, 388 (1934).

(22) W. G Penney, *Trans. Faraday Soc.*, 31, 734 (1935).

(23) D. R. Hartree, "The Calculation of Atomic Structures," John Wiley and Sons, Inc., New York, N. Y., 1957.

(24) M. Kotani and A. Amemiya, *Proc. Phys-Math. Soc. Japan*, 22, 1 (1940).

(25) M. Karplus, *J. Chem. Phys.*, 33, 941 (1960).

(26) M. Karplus, D. H. Anderson, T. C. Farrar, and H. S. Gutowsky, *ibid.*, 27, 597 (1957).

wrong sign. Although we still cannot rule out the possibility that integral variations are responsible for this discrepancy, the improved stability of the above calculations with respect to such variations suggests that this factor is not as significant as previously thought. Thus, the neglect of other factors, such as ionic terms and multiple exchange integrals, may be quite important. Ionic terms are not easily included in the usual formulation of the theory, but could be incorporated in a manner similar to that reported by Craig.[27] It is very unlikely that this would be fruitful, however, in view of the relatively small changes in couplings calculated by Hiroike[28] and Ranft,[29] where ionic character was introduced in a more empirical way. Multiple-exchange interactions are almost always excluded, apparently in many cases for no better reason than that they are difficult to calculate. They probably are worthy of consideration, even if they could only be dealt with in a very approximate way.

(27) D. P. Craig, *Proc. Roy. Soc.* (London), **A200**, 272, 390, 401 (1950).

(28) E. Hiroike, *J. Phys. Soc. Japan*, **15**, 270 (1960); *Progr. Theoret. Phys.* (Kyoto), **26**, 283 (1961).

(29) J. Ranft, *Ann. Physik.*, **8**, 322 (1961); **9**, 124 (1962).

Transference Numbers and Ionic Mobilities from Electromotive Force Measurements on Molten Salt Mixtures[1]

by Wishvender K. Behl and James J. Egan

Brookhaven National Laboratory, Upton, New York *(Received November 4, 1966)*

Transference numbers and ionic mobilities of the cations relative to the chloride ion in the mixtures of molten chlorides LiCl–$PbCl_2$, KCl–$PbCl_2$, KCl–$CaCl_2$, KCl–$MgCl_2$, and KCl–NaCl were determined over the entire composition range from electromotive force measurements. The experimental arrangement of the cell employs a special junction using alumina powder to join the two salt compartments. The relative ionic mobilities of the cations were equal in the system KCl–NaCl over the whole concentration range, while in other systems the alkali ion had a greater mobility than the divalent cation. The transference numbers and ionic mobilities obtained in the present measurements for the systems KCl–$PbCl_2$ and LiCl–$PbCl_2$ agree very well with literature values obtained by moving-boundary and Hittorf-type measurements. The systems KCl–$CaCl_2$, KCl–$MgCl_2$, and NaCl–KCl have not been previously studied.

Introduction

Transference numbers in molten salt mixtures are in general determined by one of three methods—Hittorf-type measurements, moving-boundary measurements, or studies of emf of cells with transference. Examples of Hittorf-type measurements may be found in the works of Aziz and Wetmore, Duke, Laity, and co-workers.[2-5] The moving-boundary method has been used by Klemm and co-workers.[6,7] Also, Berlin, *et al.*,[8] have studied trace amounts of cations in nitrate melts by countercurrent electromigration experiments. Emf

(1) This work was performed under the auspices of the U. S. Atomic Energy Commission.

(2) P. M. Aziz and F. E. W. Wetmore, *Can. J. Chem.*, **30**, 779 (1952).

(3) F. R. Duke and G. Victor, *J. Am. Chem. Soc.*, **83**, 3337 (1961).

cells with transference have been used by Schwarz,[9] Murgelescu and co-workers,[10-12] Stern,[13,14] Laity,[15] and Bloom and Easteal.[16]

In the present study, emf's of cells of the types

$$Cl_2(g)\text{-}C|KCl(l)\left\|\begin{matrix}KCl\\MCl_n\end{matrix}\right.(l)|C\text{-}Cl_2(g) \qquad (I)$$

and

$$Cl_2(g)\text{-}C\left|\begin{matrix}KCl\\MCl_n\end{matrix}\right.(l)\left\|MCl_n(l)\right|C\text{-}Cl_2(g) \qquad (II)$$

were measured as a function of the concentration of the molten salt mixtures, where M was Na^+, Pb^{2+}, Ca^{2+}, or Mg^{2+}. For the study of the system LiCl–$PbCl_2$, KCl in cell I was replaced by LiCl and MCl_n by $PbCl_2$. From the results of these measurements and the thermodynamic properties of the mixtures, transference numbers of the cations relative to the chloride ion were determined. The relative ionic mobilities (internal mobilities) were calculated from the above transference numbers using known data on density and conductance of the molten salt mixtures.

It was found that the usual quartz frit, used to connect the two salt compartments in the above cells, gave results in disagreement with previous reliable measurements so that a special junction was designed and is described in the experimental section. It was also found that the elimination of metal electrodes was very helpful.

Experimental Section

Purification of Materials. Reagent grade chemicals were used. Sodium and potassium chloride were melted under vacuum and stored in an argon atmosphere in storage tubes. Lithium chloride, lead chloride, and magnesium chloride (anhydrous) were heated at 100° under a flowing atmosphere of hydrogen chloride gas for 24 hr. The temperature was then slowly raised to the melting point and HCl gas bubbled through the molten chlorides for a period of 3–4 hr. The temperature was then lowered and the anhydrous salts so obtained were remelted and filtered in an inert atmosphere of argon gas, cooled, and stored. Calcium chloride dihydrate ($CaCl_2 \cdot 2H_2O$) was similarly heated under a flowing atmosphere of HCl gas at 100° for 24 hr and the temperature then raised to 280° when $CaCl_2 \cdot H_2O$ melted and HCl gas was allowed to bubble for another 8–10 hr. After all the water of hydration was removed, the temperature was gradually raised to the melting point of calcium chloride and HCl gas was bubbled for another 3–4 hr. Finally the anhydrous salt was allowed to solidify. It was then transferred to the filter tube, remelted, filtered in an inert atmosphere of argon, cooled, and stored.

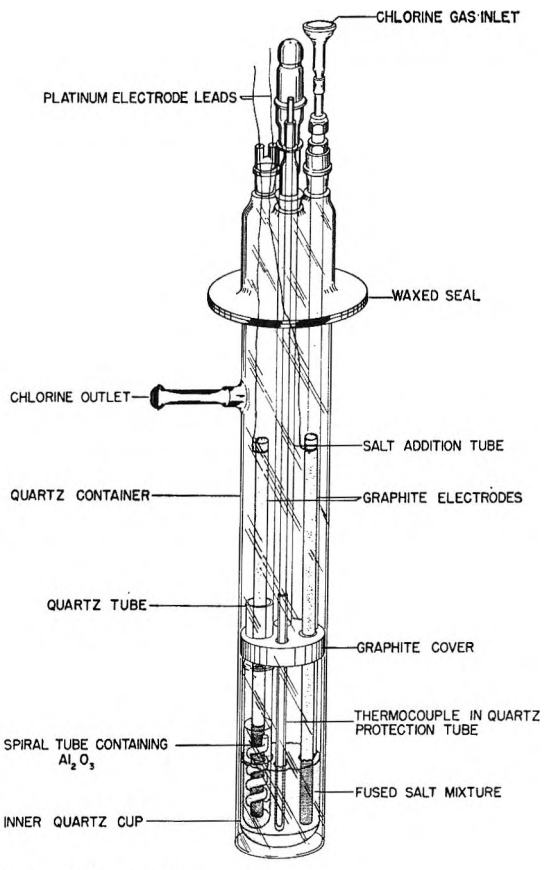

Figure 1. Cell assembly.

Apparatus. The cell assembly used is shown in Figure 1. A 5-in. long quartz tube (25-mm diameter) closed at the bottom was used as one compartment of the cell. This was placed in an outer Vycor container (57-mm diameter), which was used as the second

(4) (a) F. R. Duke, R. W. Laity, and B. Owens, *J. Electrochem. Soc.*, **104**, 299 (1957); (b) F. R. Duke and R. A. Fleming, *ibid.*, **106**, 130 (1959).

(5) C. T. Moynihan and R. W. Laity, *J. Phys. Chem.*, **68**, 3312 (1964).

(6) A. Klemm in "Molten Salt Chemistry," Milton Blander, Ed., Interscience Publishers, Inc., New York, N. Y., 1964.

(7) A. Klemm and E. U. Monse, *Z. Naturforsch.*, 12a, 319 (1957).

(8) A. Berlin, F. Ménès, S. Forcheri, and C. Monfrini, *J. Phys. Chem.*, **67**, 2505 (1963).

(9) K. E. Schwarz, *Z. Elektrochem.*, **47**, 144 (1941).

(10) I. G. Murgelescu and D. I. Marchidan, *Russ. J. Phys. Chem.*, **34**, 1196 (1960).

(11) I. G. Murgelescu and S. Sternberg, *Discussions Faraday Soc.*, **32**, 107 (1961).

(12) I. G. Murgelescu and D. I. Marchidan, *Acad. Rep. Populare Romine, Studii Cercetari Chim.*, **8**, 383 (1960).

(13) K. H. Stern, *J. Phys. Chem.*, **63**, 741 (1959).

(14) K. H. Stern, *J. Electrochem. Soc.*, **112**, 1049 (1965).

(15) R. W. Laity, *J. Am. Chem. Soc.*, **79**, 1849 (1957).

(16) H. Bloom and A. J. Easteal, *Australian J. Chem.*, **18**, 2039 (1965).

compartment. The small compartment contained the pure chloride while the other compartment contained the mixture. The mole fraction of the mixture was varied from 0.1 to 0.9. The liquid junction between the two solutions was established through a 5-in. length of 6-mm diameter tubing, formed in a spiral and opening to the second compartment as shown. The spiral was filled with powdered alumina T-61 (120 mesh, Aluminum Co. of America). The powdered alumina was found ideal for these experiments as it prevented any gravitational flow from one side to the other due to any difference in levels. It generally took 24 hr for the molten salt to flow through the alumina column and establish contact with the solution in the outside container. However, this process was hastened by evacuating the cell for 1–2 min after the salts were molten in the two compartments and when the pressure was brought back to atmospheric pressure with argon, the alumina column was filled with the molten salt. The contact was then confirmed by measuring the resistance across the two carbon electrodes; it was usually about 100–200 ohms, if proper contact was established.

In earlier experiments the liquid junction was established by using a fine-porosity quartz disk between the two compartments. However, while working on the system LiCl–$PbCl_2$, it was observed that the emf increased steadily with time. This was interpreted as an indication that Li^+ from the melt was exchanging with the quartz disk. The alumina was found to be inert.

Spectroscopic carbon rods were used as the electrodes and platinum wires were used as leads. The whole cell assembly was heated at 825° under vacuum for 3–4 hr and under chlorine atmosphere for a period of 24 hr before loading the cell with salts.

The chlorine gas was used from the cylinder. A wire-wound cylindrical furnace was used to heat the cell assembly and the temperature of the cell was controlled within ±2° with a Honeywell Brown Pyr-o-vane temperature controller.

Results and Discussion

The transport number, t_i, of the ion i is given by

$$t_i = \frac{z_i c_i \mathfrak{F} b_i}{\kappa} \tag{1}$$

where z_i is charge, c_i the concentration in moles per cubic centimeter of the ions i, $\mathfrak{F}$ is the Faraday constant, b_i the mobility of ion i, and κ the specific conductance. Following Klemm[6] we can define two sets of transport numbers by choosing two different references to measure the mobilities of the ions. Thus, if we choose walls of the cell as the references, we have

$$t_{iw} = \frac{z_i c_i \mathfrak{F} b_{iw}}{\kappa} \tag{2}$$

The transference number so defined is called the "external transport number" and is identical with the transport numbers obtained by several workers by Hittorf-type measurements. However, if we choose one of the ions as a reference, then we have

$$t_{ij} = \frac{z_i c_i \mathfrak{F} b_{ij}}{\kappa} \tag{3}$$

The transport number so defined is called the "internal transport number" and is identical with the quantity ϕ used by Aziz and Wetmore.[2] The relation between the internal and external transport numbers in the case of a binary mixture of molten salts with the common ion as the reference can be easily shown to be

$$t_{13} = t_{1w} + E_{13} t_{3w} \tag{4}$$

$$t_{23} = t_{2w} + E_{23} t_{3w} \tag{5}$$

where t_{13} and t_{23} are the internal transport numbers of the cations, t_{1w} and t_{2w} are the corresponding external transport numbers, and E_{13} and E_{23} are the equivalent fractions of the salts 13 and 23. t_{3w} is the external transport number of the anion. Thus, according to the definition

$$\begin{aligned} t_{13} + t_{23} &= t_{1w} + t_{2w} + (E_{13} + E_{23}) t_{3w} \\ &= t_{1w} + t_{2w} + t_{3w} = 1 \end{aligned} \tag{6}$$

Now consider the cell

$$\underset{\text{A}}{\text{Cl}_2(\text{g})\text{–C}|\text{KCl(l)}||} \underset{\text{PbCl}_2}{\overset{\text{KCl}}{}} \underset{\text{B}}{\text{(l)}|\text{C–Cl}_2(\text{g})}$$

The emf of the above cell may be expressed by the equation

$$E_{\text{cell}} = -\frac{1}{\mathfrak{F}} \int_A^B t_{13}\, d\mu_{KCl} - \frac{1}{2\mathfrak{F}} \int_A^B t_{23}\, d\mu_{PbCl_2} \tag{7}$$

where t_{13} and t_{23} are the internal transport numbers of the ions K^+ and Pb^{2+}, respectively, and μ_{KCl} and μ_{PbCl_2} are the chemical potentials of the respective chlorides. The derivation of this equation is discussed in detail by Wagner.[17] Now, using the Gibbs–Duhem equation, we have

$$d\mu_{PbCl_2} = -\frac{x_{KCl}}{1 - x_{KCl}}\, d\mu_{KCl} \tag{8}$$

(17) C. Wagner, *Advan. Electrochem. Electrochem. Eng.*, **4**, 1 (1966).

and from the definition of internal transport numbers

$$t_{23} = 1 - t_{13} \tag{9}$$

Substituting eq 8 and 9 into eq 7

$$E_{cell} = -\frac{1}{\mathfrak{F}}\int_A^B t_{13}\, d\mu_{KCl} + \frac{1}{2\mathfrak{F}}\int_A^B (1 - t_{13})\frac{x_{KCl}}{1 - x_{KCl}}\, d\mu_{KCl}$$

$$= -\frac{1}{2\mathfrak{F}}\int_A^B \left(\frac{2t_{13} - t_{13}x_{KCl} - x_{KCl}}{1 - x_{KCl}}\right) d\mu_{KCl} \tag{10}$$

Since

$$d\mu_{KCl} = 2.303RT\ d \log a_{KCl} \tag{11}$$

therefore

$$E_{cell} = \frac{-2.303RT}{2\mathfrak{F}}\int_A^B \frac{2t_{13} - t_{13}x_{KCl} - x_{KCl}}{1 - x_{KCl}}\, d \log a_{KCl} \tag{12}$$

Differentiating eq 12

$$\left(\frac{\partial E_{cell}}{\partial \log a_{KCl}}\right)_B = \frac{-2.303RT}{2\mathfrak{F}}\left(\frac{2t_{13} - t_{13}x_{KCl} - x_{KCl}}{1 - x_{KCl}}\right)_B \tag{13}$$

Thus, if the measurements of the cell potential are made over the whole composition range, the transport number t_{13} can be calculated by use of eq 13 using graphical differentiation. The transport number t_{23} will then be given by eq 9. Similar equations can be derived for cells of type II.

The internal mobilities of the cations relative to the chloride ion can then be calculated by use of eq 3. Thus

$$b_{13} = \frac{t_{13}\kappa}{z_1 c_1 \mathfrak{F}}$$

and

$$b_{23} = \frac{t_{23}\kappa}{z_2 c_2 \mathfrak{F}} \tag{14}$$

where κ is the specific conductance of the mixture, z_1 and z_2 are the charges on cations 1 and 2, and c_1 and c_2 are their concentrations in moles per cubic centimeter.

Since the equivalent conductance λ is related to the specific conductance κ and equivalent volume v by the equation

$$\lambda = \kappa v = \frac{\kappa}{z_1 c_1 + z_2 c_2} \tag{15}$$

Table I

$z_{alkali\ chloride}$	System[a] KCl–PbCl₂ Cell B at 526° E_{cell}, mv	KCl–PbCl₂ Cell A at 825° a_{KCl}	KCl–PbCl₂ Cell A at 825° E_{cell}, mv	LiCl–PbCl₂ Cell C at 650° a_{LiCl}	LiCl–PbCl₂ Cell C at 650° E_{cell}, mv	KCl–CaCl₂ Cell A at 825° a_{KCl}	KCl–CaCl₂ Cell A at 825° E_{cell}, mv	KCl–CaCl₂ Cell B at 825° a_{KCl}	KCl–CaCl₂ Cell B at 825° E_{cell}, mv	KCl–MgCl₂ Cell A at 825° a_{KCl}	KCl–MgCl₂ Cell A at 825° E_{cell}, mv	KCl–NaCl Cell A at 825° a_{KCl}	KCl–NaCl Cell A at 825° E_{cell}, mv
0.1	0.010	0.017		0.120	20.7	0.013	80.9	0.013	8.6	0.0018	25.0	0.1	2.5
0.2	0.020	0.039	5.1	0.244	18.8	0.038	79.2	0.038	10.3	0.0060	25.2	0.2	0.2
0.3	0.045	0.077	6.5	0.363	16.8	0.076	75.1	0.076	14.3	0.0157	23.6	0.3	−0.7
0.4	0.100	0.144	9.2	0.472	14.2	0.139	67.9	0.139	21.3	0.0359	21.1	0.4	−1.0
0.5	0.190	0.245	13.5	0.563	11.4	0.224	57.8	0.224	31.3	0.0800	17.3	0.5	0.0
0.6	0.340	0.398	20.5	0.656	8.8	0.360	45.7	0.360	43.6	0.169	11.8	0.6	−0.2
0.7	0.530	0.571		0.740	6.6	0.529	31.7	0.529	57.7	0.369	6.6	0.7	−2.0
0.8	0.740	0.800			4.8	0.707	19.9	0.707	70.8	0.644	2.8	0.8	−0.5
0.9	0.900	0.900				0.885	8.4	0.885		0.864		0.9	

[a] Cell A, $Cl_2(g)$–C|KCl(l)‖$\frac{KCl}{MCl_n}$(l)|C–$Cl_2(g)$; cell B, $Cl_2(g)$–C‖$\frac{KCl}{MCl_n}$(l)‖MCl_n(l)|C–$Cl_2(g)$; cell C, $Cl_2(g)$–C|LiCl‖$\frac{LiCl}{PbCl_2}$(l)|C–$Cl_2(g)$; where M = Pb^{2+}, Ca^{2+}, Mg^{2+}, and Na^+.

Table II

$x_{\text{alkali chloride}}$	KCl–$PbCl_2$ at 525°: t_{13}, present measurements	KCl–$PbCl_2$ at 525°: t_{13}, from the data of Duke, *et al.*[4b]	KCl–$PbCl_2$ at 825°: t_{13}, present measurements	KCl–$PbCl_2$ at 825°: t_{13} at 850°, from the data of Duke, *et al.*[4b]	KCl–$CaCl_2$ at 825°: t_{13}	KCl–$MgCl_2$ at 825°: t_{13}	KCl–NaCl at 825°: t_{13}	LiCl–$PbCl_2$ at 650°: t_{13}
0.1	0.076	0.075			0.060	0.05	0.10	0.064
0.2	0.142	0.150			0.150	0.16	0.20	0.163
0.3	0.211	0.235			0.260	0.36	0.30	0.257
0.4	0.302	0.325	0.338		0.375	0.58	0.40	0.366
0.5	0.414	0.430	0.452		0.490	0.76	0.50	0.458
0.6	0.559	0.560	0.564		0.615	0.83	0.60	0.559
0.7			0.677	0.670	0.740	0.87	0.70	0.655
0.8			0.780	0.780	0.845	0.91	0.80	0.751
0.9			0.882	0.885	0.930	0.95	0.90	0.897

we now have the equations

$$b_{13} = \frac{(z_1c_1 + zc_{22})t_{13}\lambda}{z_1c_1\mathcal{F}}$$

and

$$b_{23} = \frac{(z_1c_1 + z_2c_2)t_{23}\lambda}{z_2c_2\mathcal{F}} \qquad (16)$$

or

$$b_{13} = \frac{t_{13}\lambda}{E_{13}\mathcal{F}}$$

and

$$b_{23} = \frac{t_{23}\lambda}{E_{23}\mathcal{F}} \qquad (17)$$

where E_{13} and E_{23} are the equivalent fractions of the salts 13 and 23, respectively.

The emf measurements on the various molten salt mixtures are summarized in Table I. The activities of KCl in the systems KCl–$PbCl_2$, KCl–$MgCl_2$, KCl–$CaCl_2$, and KCl–NaCl and of LiCl in the system LiCl–$PbCl_2$ were taken from the unpublished results of Egan.[18] The emf's of the cells in all the cases except for the system KCl–NaCl were nonzero and varied with concentration. In the case of the system KCl–NaCl, the emf was 0 within ±2 mv over the whole concentration range.

The transference number of the potassium ion (t_{13}) relative to the chloride ion in the system KCl–$PbCl_2$ was calculated by use of eq 13 at various concentrations of the mixture. These values are shown in Table II as a function of the potassium chloride mole fraction. The system KCl–$PbCl_2$ was also investigated by Duke and Fleming[4b] by Hittorf-type measurements. The values of ϕ for the potassium ion, which

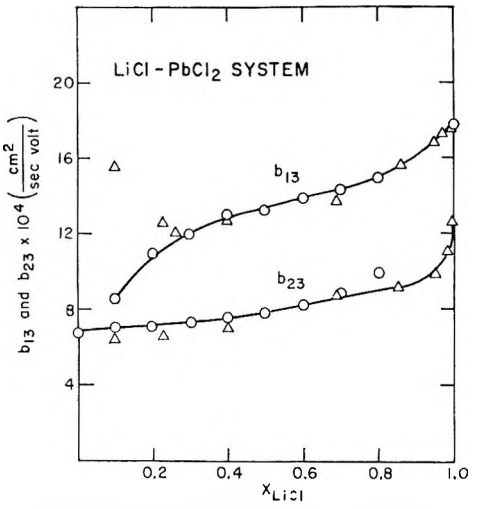

Figure 2. Internal mobilities of Li^+ and Pb^{2+} ions relative to the chloride ions as a function of composition: O, mobilities obtained from the present measurements; Δ, mobilities taken from the data of Klemm, *et al.*[7]

are the same as the internal transport numbers (t_{13}) obtained in the present measurements, are also shown in Table II and there is an excellent agreement between the two sets of data.

The internal transport numbers of the potassium ion relative to the chloride ion in the systems KCl–$CaCl_2$ and KCl–$MgCl_2$ and that of the lithium ion in the system LiCl–$PbCl_2$ were similarly calculated by use of eq 13 and are given as a function of the alkali chloride mole fraction in Table II.

Since the emf for the cell

$$Cl_2(g)\text{–}C|KCl(l)\left\|\begin{matrix}KCl\\NaCl\end{matrix}(l)\right|C\text{–}Cl_2(g)$$

(18) J. J. Egan, unpublished results; see Abstracts of the Electrochemical Society Meeting, San Francisco, Calif., May 1965, and also BNL 954 (S-68).

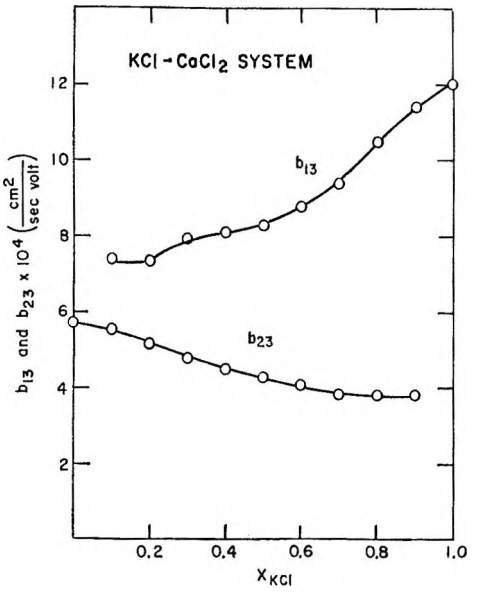

Figure 3. Internal mobilities of K^+ and Ca^{2+} ions relative to the chloride ion as a function of composition.

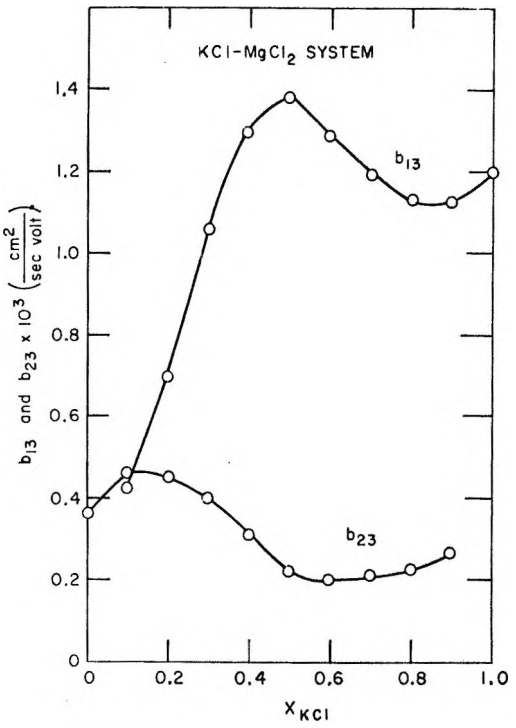

Figure 4. Internal mobilities of the K^+ and Mg^{2+} ions relative to the chloride ion as a function of composition.

was zero over the whole concentration range, it can be easily shown that the internal transport number for the potassium ion at any concentration is equal to the mole fraction of potassium chloride in the mixture.

Internal Mobilities. The internal mobilities of the cations Li^+ and Pb^{2+} in the system LiCl–$PbCl_2$ were calculated by use of eq 17. The internal transport numbers determined in the present measurements were used. The specific conductance values were taken from the data of Klemm and Monse[7] and the equivalent conductance was calculated by use of eq 15. Since the density data for this system were not available, it was assumed that the relationship between the equivalent volume and mole fraction was linear.

The values of the internal mobilities so obtained are plotted in Figure 2. Also plotted are the internal mobilities obtained by Klemm and Monse[7] from the moving-boundary experiments. There is a good agreement between the two sets of data except at concentrations below 0.4 mole fraction of lithium chloride. Klemm and Monse observed an increase in the internal mobility of lithium ion as the concentration of LiCl decreased below $0.4x_{LiCl}$. This increase was not observed in the present measurements.

The internal mobilities of the cations relative to the chloride ions in the systems KCl–$CaCl_2$ and KCl–$MgCl_2$ were similarly calculated by use of eq 17 and are plotted in Figures 3 and 4. The specific conductance and density data for these systems were taken from the literature.[19,20]

In each of the systems studied, the alkali ion was observed to have a relatively larger mobility than that of the alkaline earth ion.

In the system NaCl–KCl, the cell potential was observed to be zero over the whole concentration range and hence it was concluded that the internal mobilities of the sodium and potassium ions are the same over the whole concentration range.

Acknowledgments. The authors wish to acknowledge the help of Mr. John Bracker and Mr. R. J. Heus with the experiments and the helpful suggestions of Dr. R. H. Wiswall.

(19) R. W. Huber, E. V. Potter, and H. W. St. Clair, Bureau of Mines Report of Investigation 4858, U. S. Department of the Interior, Washington, D. C., March 1952.

(20) C. Sanconnini, *Gazz. Chim. Ital.*, **51**, 289 (1920).

Pole-Figure Inversion for the Triclinic Crystal Class. Polyethylene Terephthalate[1]

by W. R. Krigbaum and Y. I. Balta

Department of Chemistry, Duke University, Durham, North Carolina *(Received November 11, 1966)*

The Roe–Krigbaum procedure for determining the crystallite orientation distribution function is applied to four drawn samples of polyethylene terephthalate having fiber texture. This is the first example of pole-figure inversion for a material belonging to the triclinic crystal class. Application of the procedure to this polymer is particularly difficult because the plane-normal distributions are rapidly varying functions containing sharp peaks, and the triclinic system offers no simplification due to symmetry. Seventeen plane normals (all composite) were investigated for each sample. The crystallite orientation distributions obtained are broadened due to unavoidable series termination errors, but useful information can be gained concerning the qualitative aspects of the distributions. Polyethylene terephthalate has a unique preferred crystallite orientation with the fiber axis 6° from the c axis and making an azimuthal angle of approximately 50° with the plane containing the a^* and c axes. This orientation is already achieved with considerable perfection at a drawing ratio of 3.

I. Introduction

When a polycrystalline sample, such as a metal or polymer, is deformed mechanically by drawing or rolling, the crystalline regions generally exhibit some preferred orientation or texture. Again, when such materials are crystallized from a melt which has been rendered anisotropic by flow or deformation, a nonrandom orientation of the crystalline domains is observed.

Let us suppose that one wishes to characterize, as completely as possible, the distribution of crystallite orientations in such a material. This can be accomplished, in principle, by selecting one coordinate axis in the macroscopic sample and a second in the crystallographic unit cell, and expressing the orientation distribution of one of these with respect to the other. Such a distribution is termed either the crystallite orientation distribution or inverse pole figure, depending upon which of the two coordinate systems is regarded as the fixed frame of reference. If the sample exhibits cylindrical symmetry (fiber texture), these two distributions are interrelated in a very simple manner. From the experimental point of view, there are a number of texture-sensitive properties which could be studied to obtain relevant information. Of these, wide angle X-ray diffraction is most directly related to the orientation of the polycrystalline domains and furnishes the most quantitative information. However, what one obtains directly from these measurements is not the desired crystallite orientation, or inverse pole figure, but the orientation distributions of the normals to a number of different crystallographic planes. This information can be displayed as the pole-figure diagram. One is then faced with the problem of pole-figure inversion which, in many respects, is analogous to the Fourier transformation involved in deducing, from the diffracted intensities or structure factors represented in reciprocal space, the distribution of electron density in real space representing the crystal structure.

A suggested procedure for performing this transformation was contained in a paper by Sack;[2] however, his objective was the more limited one of calculating $\langle\cos^2\chi\rangle$ for an unobservable plane normal from values of $\langle\cos^2\chi\rangle$ for other planes which could be measured.

(1) Supported by the U. S. Army Research Office (Durham) under Grant 31-134-G202.

(2) R. A. Sack, *J. Polymer Sci.*, **54**, 543 (1961).

Bunge[3–5] was the first to describe a complete analytical procedure for the derivation of inverse pole figures for materials having fiber texture. His method was somewhat cumbersome, and his illustration of its application was restricted to materials belonging to the cubic crystal class. Somewhat later, Roe and Krigbaum[6] showed that the procedure of Sack could be generalized for the treatment of materials having fiber texture, and belonging to any crystal class. The restriction to fiber textures was removed by Roe,[7] who further generalized the foregoing treatment for application to materials of general texture.

Our interest here concerns the effect of symmetry elements in the pole-figure inversion problem for materials having fiber texture. In order to facilitate further discussion, we will outline the Roe–Krigbaum procedure.

Two coordinate systems are designated. One of these, *o–xyz*, is fixed with respect to the macroscopic sample, while the other, O–*XYZ*, is fixed in the crystallographic unit cell. For example, we may let the *Z* axis coincide with the direct lattice vector *c*. The orientation of O–*XYZ* with respect to *o–xyz* is then specified by the three Eulerian angles θ, ψ, and φ, or their equivalent, ξ, ψ, φ, where

$$\xi = \cos\theta \tag{1}$$

as illustrated in Figure 1. One observes, for each reflection, the intensity distribution $I(\chi_i)$, where χ_i is the angle between the ith reciprocal lattice vector $\mathbf{r}_i$ and the fiber (z) axis. After correction for background, the observed $I(\chi_i)$'s are converted into the plane-normal orientation distributions, $q_i(\zeta_i)$, through normalization

$$q_i(\zeta_i) = \frac{I(\chi_i)}{\int_0^{\pi} I(\chi_i)\sin\chi_i\,d\chi_i} \tag{2}$$

where

$$\zeta_i = \cos\chi_i \tag{3}$$

The plane-normal orientation distribution for each reflection may be expanded in a series of normalized Legendre polynomials

$$q_i(\zeta_i) = \sum_{l=0}^{\infty} Q_{2l}{}^{i} P_{2l}(\zeta_i) \tag{4}$$

in which, because of the orthogonal properties of these polynomials, the coefficient $Q_{2l}{}^{i}$ is given by

$$Q_{2l}{}^{i} = \int_{-1}^{1} q_i(\zeta_i) P_{2l}(\zeta_i)\,d\zeta_i \tag{5}$$

Due to Friedel's law, $q_i(\zeta_i)$ is an even function of ζ_i, and hence all odd coefficients vanish. Also, for samples having fiber texture, the crystallite orientation distribution will be symmetrical about the fiber axis, and hence independent of ψ. This desired function, $w(\xi,\varphi)$, therefore may be represented by a series of spherical harmonics

$$w(\xi,\varphi) = \sum_{l=0}^{\infty} \sum_{m=-l}^{l} W_{lm} P_l{}^{m}(\xi) e^{-im\varphi} \tag{6}$$

in which the coefficients, W_{lm}, are given by

$$W_{lm} = \frac{1}{2\pi} \int_0^{2\pi} \int_{-1}^{1} w(\xi,\varphi) P_l{}^{m}(\xi) e^{im\varphi}\,d\xi\,d\varphi \tag{7}$$

Application of the Legendre addition theorem to the relation

$$\cos\chi_i = \cos\theta\cos\Theta_i + \sin\theta\sin\Theta_i\{\cos[\varphi - (\pi - \Phi_i)]\} \tag{8}$$

where Θ_i and Φ_i are the polar and azimuthal angles of the reciprocal lattice vector $\mathbf{r}_i$ in the *O–XYZ* coordinate system, yields a relationship between the $P_i(\zeta_i)$ and $P_l{}^{m}(\xi)$

$$P_i(\cos\chi_i) = [2/(2l+1)]^{1/2} \sum_{m=-l}^{l} P_l{}^{m}(\cos\theta) \times P_l{}^{m}(\cos\Theta_i) e^{im(\varphi+\Phi_i-\pi)} \tag{9}$$

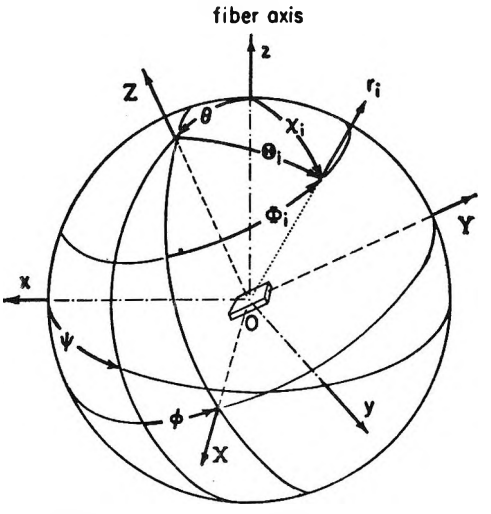

Figure 1. An illustration of the Eulerian angles θ, ψ, and φ, and the orientation of a reciprocal lattice vector $\mathbf{r}_i$, with respect to the sample coordinate system *xyz* and the unit cell coordinate system *XYZ*.

(3) H. J. Bunge, *Monatsber. Deut. Akad. Wiss. Berlin*, 1, 400 (1959); 2, 479 (1960); 3, 97, 285 (1961); 5, 293 (1963).

(4) H. J. Bunge, *Acta Cryst.*, 15, 612 (1962).

(5) H. J. Bunge and H. Sanderman, *Monatsber. Deut. Akad. Wiss. Berlin*, 5, 343 (1963).

(6) R.-J. Roe and W. R. Krigbaum, *J. Chem. Phys.*, 40, 2608 (1964).

(7) R.-J. Roe, *J. Appl. Phys.*, 36, 2024 (1965).

Recalling that $q_i(\xi_i)$ is a normalized distribution function, one sees from eq 5 that the coefficient Q_{2l}^{i} is just the average value of $P_{2l}(\cos \chi_i)$ for all crystallites in the sample. This same average can also be obtained from eq 9. If this equation is multiplied by $w(\xi,\varphi)\ d\xi d\varphi$, and the result is integrated over all the ranges of ξ and φ, then in view of eq 7 one obtains

$$Q_{2l}^{i} = 2\pi[2/(2l + 1)]^{1/2} \times \sum_{m=-l}^{l} (-1)^m W_{2lm} P_{2l}^{m}(\cos \Theta_i) e^{im\Phi_i} \quad (10)$$

Since Θ_i and Φ_i are known from the unit cell parameters, eq 10 represents a set of simultaneous linear equations involving the known Q_{2l}^{i} and the unknown coefficients W_{2lm}. For a selected value of l there will be, in the absence of symmetry elements, $(2l + 1)$ unknown W_{2lm}. If $(2l + 1)$ reflections can be investigated and the corresponding Q_{2l}^{i} coefficients are determined, then the set of $(2l + 1)$ simultaneous equations can be solved to determine all the required W_{2lm}. In general, the W_{2lm} will be complex quantities. If these are written

$$W_{2lm} = A_{2lm} + iB_{2lm}$$
$$W_{2l\bar{m}} = A_{2lm} - iB_{2lm} \quad (11)$$

where $\bar{m} = -m$, then eq 10 becomes

$$Q_{2l}^{i} = 2\pi[2/(2l + 1)]^{1/2}\{A_{2l0}P_{2l}^{0}(\cos \Theta_i) + 2\sum_{m=i}^{l} (-1)^m [A_{2lm} \cos m\Phi_i - B_{2lm} \sin m\Phi_i]P_{2l}^{m}(\cos \Theta_i)\} \quad (12)$$

However, the previous comment concerning the number of reflections which must be measured to determine all of the unknown coefficients for a particular value of l remains unchanged.

With this background we are prepared to consider briefly the effect of symmetry upon $w(\xi,\varphi)$. We have already observed that all Q_l^{i} with l odd vanish due to Friedel's law. From eq 10 one finds that all W_{lm} having odd values of l must likewise vanish. The sample may contain symmetry elements of two types. The first arises from the crystalline texture. For example, we have noted that, for samples exhibiting fiber texture, the crystallite orientation distribution function is independent of ψ. The second type of symmetry element arises from the crystal class. Thus Roe and Krigbaum[6] have pointed out that for a unit cell belonging to the orthorhombic class, A_{2lm} for m odd, and all B_{2lm}, will vanish. The effect of either type of symmetry is to reduce the number of unknown coefficients, and hence the number of reflections, required to represent the crystallite orientation distribution by a truncation of the series appearing in eq 6 containing, as its highest term, a coefficient having a specified value of l.

Krigbaum and Roe[8] tested their procedure using samples of cross-linked polyethylene which had been deformed uniaxially in the melt and crystallized at fixed strain. They investigated 16 reflections, some of which were composite, and from these data they were able to obtain a description of the crystallite orientation distributions for these samples in considerable detail. Indeed, the major aspects of the crystallite orientation distribution were resolved when the procedure was applied to data from as few as four reflections (terminating the series at $l = 3$). Polyethylene has a unit cell belonging to the orthorhombic class, and the application of their procedure was therefore considerably simplified by the symmetry elements present. This leaves unanswered the feasibility of their procedure for fiber texture samples belonging to crystal classes of lower symmetry, and the investigation reported here was undertaken to resolve this specific question. The most severe test would be provided by a triclinic crystal, and we have chosen one of these, polyethylene terephthalate, for this study.

II. Experimental Section

We wish to thank Dr. Carl Heffelfinger of the Film Department, E. I. du Pont de Nemours and Co., Circleville, Ohio, who furnished the samples studied. Quenched films of polyethylene terephthalate were stretched to various elongations near the glass transition temperature, 70°. These films, as received, exhibited no discrete X-ray diffraction peaks, and after crystallization they had fiber texture. From the results of Sadamatsu,[9] 160° was taken as a suitable temperature for crystallization. The samples were clamped at fixed length during the crystallization, and all samples except S3 were maintained at 160° for sufficient time to obtain a high degree of crystallinity. Densities of the crystallized samples were determined in a calibrated density gradient column composed of chlorobenzene and carbon tetrachloride. Degrees of crystallinity were calculated by assigning to the amorphous and crystalline portions the densities of 1.335 and 1.455 g/cm^3, respectively.[10] A summary of the relative elongation α, crystallization temperature T_x, and time t, and per cent crystallinity for the various samples studied appears in Table I.

(8) W. R. Krigbaum and R.-J. Roe, *J. Chem. Phys.*, **41**, 737 (1964).
(9) S. Sadamatsu, *Rept. Progr. Polymer Phys. Japan*, **8**, 97 (1965).
(10) R. de P. Daubeny, C. W. Bunn, and J. C. Brown, *Proc. Roy. Soc.* (London), **A226**, 531 (1954).

Table I: Characterization of the Polyethylene Terephthalates Samples

Sample	α	T_x, °C	t, min	% crystallinity
S1	2.0	162 ± 1	30	25.0
S2	3.0	159 ± 1	45	27.5
S3	3.5	159 ± 1	8	16.7
S4	3.5	160 ± 1	35	28.0

Intensity measurements were performed by counting, using a diffractometer equipped with a single-crystal orienter. Sample S4 was studied using a General Electric XRD-5 unit, while the remaining samples were investigated using a Picker Automated four-angle system. The latter, of course, considerably reduced the time required to collect data. The geometry utilized in either case permits the fiber axis to remain always normal to the bisector of the external angle formed by the incident and diffracted beams, so that χ coincides with the angle between the fiber axis and the reciprocal lattice vector. Data were collected using single-crystal collimators and fixed-point counting, the times ranging between 80 and 400 sec, depending upon the intensity of the particular reflection. Measurements were performed at χ intervals of 2 to 4°, depending upon the rate of variation with χ.

The unit cell parameters of polyethylene terephthalate are[10] a = 4.54 A, b = 5.94 A, c = 10.75 A; α = 98.5°, β = 118.0°, and γ = 112.0°. The 17 reflections investigated are designated by the numbers appearing in the left-hand column of Table II. There was some overlapping in every case, and the other planes which contributed to the observed intensities are also listed in the table. Column 2 gives values for twice the Bragg diffraction angle (which is not to be confused with the Euler angle θ appearing in eq 1), and the angles Θ_i and Φ_i are given for a^* along OX, c along OZ, and b^* in the plane defined by OX and OY. The composite intensity distribution was resolved graphically to obtain the component making the largest contribution at that Bragg angle by assuming that the χ distribution of that component is symmetrical with respect to its maximum. This resolution is illustrated in Figure 2 for three reflections of sample S2. The dashed curve represents the observed intensity distribution, and the full curve represents that of the component making the major contribution. The right-hand column of Table II gives the magnitudes of the structure factors as measured by Bunn, *et al.*[10] The observed intensities must be corrected for background before the plane-normal orientation distributions can be calculated. The

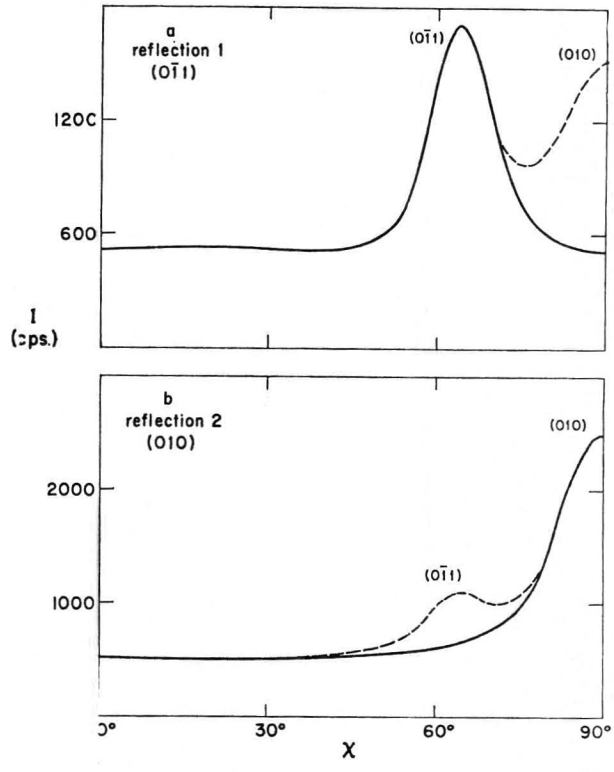

Figure 2. Resolved intensity distributions (full curves) of three reflections for sample S2, and the observed composite intensities (dashed).

contribution to this background due to instrumental noise can be readily determined, but the amount, and particularly the angular distribution, of the remainder of the background is more difficult to evaluate. For this purpose the stretched, amorphous samples were step-scanned in 2θ at four different χ values: 0, 30, 60, and 90°. These data were plotted as four continuous curves, one for each χ. Similar data were collected for the isotropic (α = 1), amorphous sample and for the drawn, crystallized samples. For each of the latter, the background curve was constructed such that the level at any 2θ never exceeded the smallest of the four values measured for the crystalline sample at different χ values, and that the shape of the curve should resemble that observed for the isotropic, amorphous sample. Finally, it was assumed that this background is independent of χ.

III. Results

For the triclinic crystal class only those reflections related by Friedel's law (*e.g.*, (hkl) and ($\bar{h}\bar{k}\bar{l}$)) are equivalent. When the Θ_i and Φ_i corresponding to these reflections are inserted into eq 12, the same set of $Q_{2l}{}^i$ must be recovered. Upon performing this operation, one finds that there is no simplification for a material

Table II: Crystallographic Data for All Plane Normals Contributing to the Measured Intensity

i	hkl	2θ	Θ_i	Φ_i	F_i
1	$(0\bar{1}1)$	16.42	59.85	257.43	12.0
2	(010)	17.53	90.00	59.44	18.0
3	$(\bar{1}11)$	21.31	67.24	123.86	10.0
4	$(\bar{1}10)$	22.54	90.00	138.02	20.0
	(011)	23.57	69.44	47.95	8.0
5	$(\bar{1}12)$	24.71	47.16	106.30	11.0
6	(100)	25.69	90.00	0.00	37.0
7	$(\bar{1}03)$	26.44	20.02	155.79	7.0
8	$(1\bar{1}1)$	27.84	72.72	328.48	14.0
	$(0\bar{1}3)$	28.75	150.07	126.94	3.8
9	(003)	30.77	35.81	11.96	7.0
	$(11\bar{2})$	31.15	112.19	28.80	2.0
	$(1\bar{2}0)$	31.44	90.00	285.60	3.0
	(012)	31.96	58.61	40.52	3.0
10	$(\bar{1}\bar{1}3)$	32.44	39.75	213.62	7.2
11	$(0\bar{2}1)$	32.73	75.26	247.48	9.5
	$(\bar{1}21)$	32.87	75.32	93.64	7.0
	$(0\bar{2}2)$	33.18	59.85	257.43	4.2
	$(1\bar{2}1)$	33.37	75.56	295.31	4.0
12	$(\bar{1}05)$	42.66	9.70	61.00	...
13	$(0\bar{2}4)$	42.73	38.07	282.20	1.3
	(111)	45.27	79.29	22.00	3.1
14	$(\bar{2}10)$	45.91	90.00	160.43	11.0
15	$(\bar{1}\bar{2}4)$	47.38	44.44	231.21	11.0
	$(1\bar{3}2)$	48.31	69.49	283.93	7.0
16	$(\bar{2}05)$	48.54	29.26	164.53	7.0
17	$(\bar{1}31)$	49.04	80.05	81.60	7.0
	$(12\bar{1})$	49.59	99.85	37.53	5.2
	$(03\bar{2})$	49.66	109.97	70.56	4.5

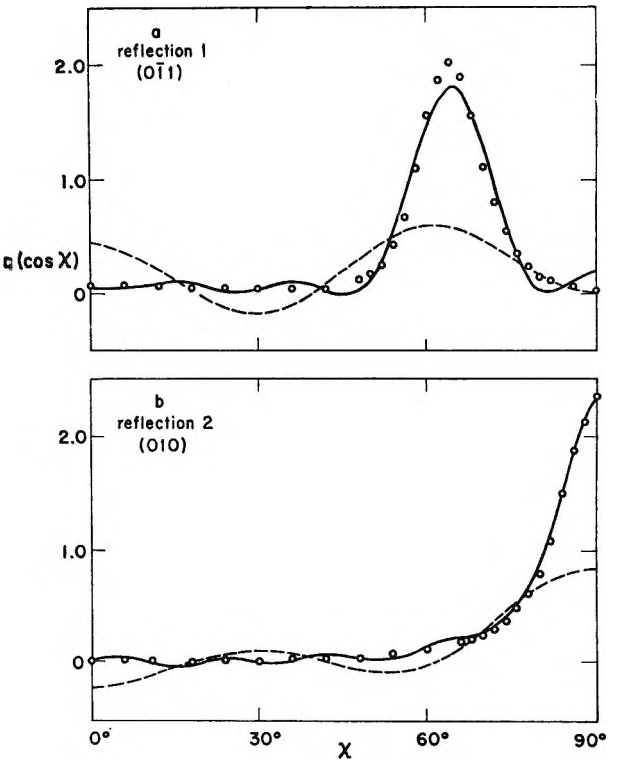

Figure 3. Comparison of the observed plane-normal orientation distributions $q_i(\zeta_i)$ (circles) for two reflections of sample S2 with those calculated for $l \leqslant 8$ (full curve) and $l \leqslant 3$ (dashed curve).

belonging to the triclinic class. Hence, if the $q_i(\zeta_i)$'s are determined for N reflections, one finds from eq 12 that W_{2lm} can be determined through $l = (N - 1)/4$. In the present investigation, 17 planes were studied, so that we may hope to determine W_{2lm} through $l = 4$. On substituting eq 11 into 6, there is obtained

$$w(\xi,\varphi) = \sum_{l=0}^{\infty} A_{2l0} P_l^0(\xi) + 2\sum_{l=1}^{\infty}\sum_{m=1}^{l} [A_{2lm}\cos m\varphi + B_{2lm}\sin m\varphi] P_{2l}^m(\xi) \quad (13)$$

If N nonequivalent $q_i(\zeta_i)$ are determined, the maximum number of coefficients, A_{2lm} and B_{2lm}, which can be evaluated is

$$C = (N + 1)(N + 3)/8 \quad (14)$$

which, for $N = 17$, is 45.

The limitation to $l = 4$ means that the infinite series representation of the plane-normal distributions (eq 4), must be replaced by a five-term series ($l = 0$ to 4) for the purpose of deducing the crystallite orientation distribution. This will not give rise to a serious loss of information if the plane-normal distributions are broad, slowly varying functions. Two typical examples of the distributions actually observed, those for the $(0\bar{1}1)$ and (010) reflections of sample S2, are designated by the open circles in Figure 3. One sees that, contrary to our hopes, these are very sharply peaked distributions. In fact, they are more sharply peaked than those encountered in the earlier study of polyethylene. A test of the series approximation is illustrated by the dashed curve in this figure, representing a four-term series ($l \leqslant 3$), and by the full curve representing a nine-term series ($l \leqslant 8$). One sees immediately that at least nine terms are required to render a faithful representation of the details of these distributions. The four-term series gives a maximum in approximately the correct location, but the maximum is too low in magnitude, and it is distributed over too broad a range of χ. Furthermore, the four-term representation exhibits negative values which, of course, have no physical significance. The standard deviations for these two reflections are 0.55 and 0.40, respectively, using $l \leqslant 3$, and 0.15 and 0.05 using $l \leqslant 8$.

The set of simultaneous equations (12) was next solved for the coefficients A_{lm} and B_{lm} through $l = 4$, and the crystallite orientation distribution function $w(\xi,\varphi)$ was calculated according to eq 13. The resulting distribution exhibited maxima and minima of large magnitude, and some of the maxima were judged to be spurious because they appeared in locations which would be difficult to rationalize on physical grounds. When the data for all 17 plane-normal distribution functions were utilized to determine only A_{2lm} and B_{2lm} through $l = 3$, the computed crystallite orientation distribution $w(\xi,\varphi)$ appeared perfectly reasonable. In explanation of this observation, we note that for the coefficients having low l values, the number of simultaneous equations exceeds the number of unknown A_{2lm} and B_{2lm} to be determined. Therefore, the effect of any abnormalities in the experimental data is diminished by the least-square procedure employed in solving for the A_{2lm} and B_{2lm}. On the other hand, all of the experimental information is required when the A_{8m} and B_{8m} are sought, and defects in one or more of the plane-normal distributions can greatly affect these values.

In an effort to investigate this behavior further, the A_{6m} and B_{6m} were computed anew from the values of Q_{2l}^{t} for only the first 13 numbered reflections in Table II. These values showed good agreement with those obtained using all 17 reflections. However, if the information from the first 12 reflections, and any other from the group 14–17, was used in the solution for A_{6m} and B_{6m}, these latter values differed considerably from those obtained from the data for all 17 planes, and the resulting $w(\xi,\varphi)$ exhibited maxima and minima of large magnitude, as well as additional false maxima. The Roe–Krigbaum procedure allows the assignment of a weighting factor ρ_t to each plane-normal distribution. Some attempts were made to reduce the ill-conditioned behavior of the set of simultaneous equations in this manner, but these were not successful.

We have therefore calculated $w(\xi,\varphi)$ in each case using A_{lm} and B_{lm} through $l = 3$, as evaluated using the data for 17 reflections. The number of crystallites, dn, having orientation (θ,φ) to within $d\theta$ and $d\varphi$, is $w(\xi,\varphi) \sin\theta\, d\theta d\varphi$. The corresponding number, dn_0, for an isotropic sample is $(1/4\pi) \sin\theta\, d\theta d\varphi$. The orientation function $G(\xi,\varphi)$ defined by the ratio of these numbers

$$G(\xi,\varphi) = (dn/dn_0) = 4\pi w(\xi,\varphi) \qquad (15)$$

possesses some advantages for graphical representation, since where $G(\xi,\varphi)$ is unity, just as many crystallites have that particular orientation as would be found in a perfectly random, isotropic sample. Contour maps[11] of $G(\xi,\varphi)$ for two of the four samples studied appear in Figure 4. The particular ranges of θ and φ chosen for this plot were unfortunate, since there appear to be two high-density regions: one near $\theta = 0°$ and one near

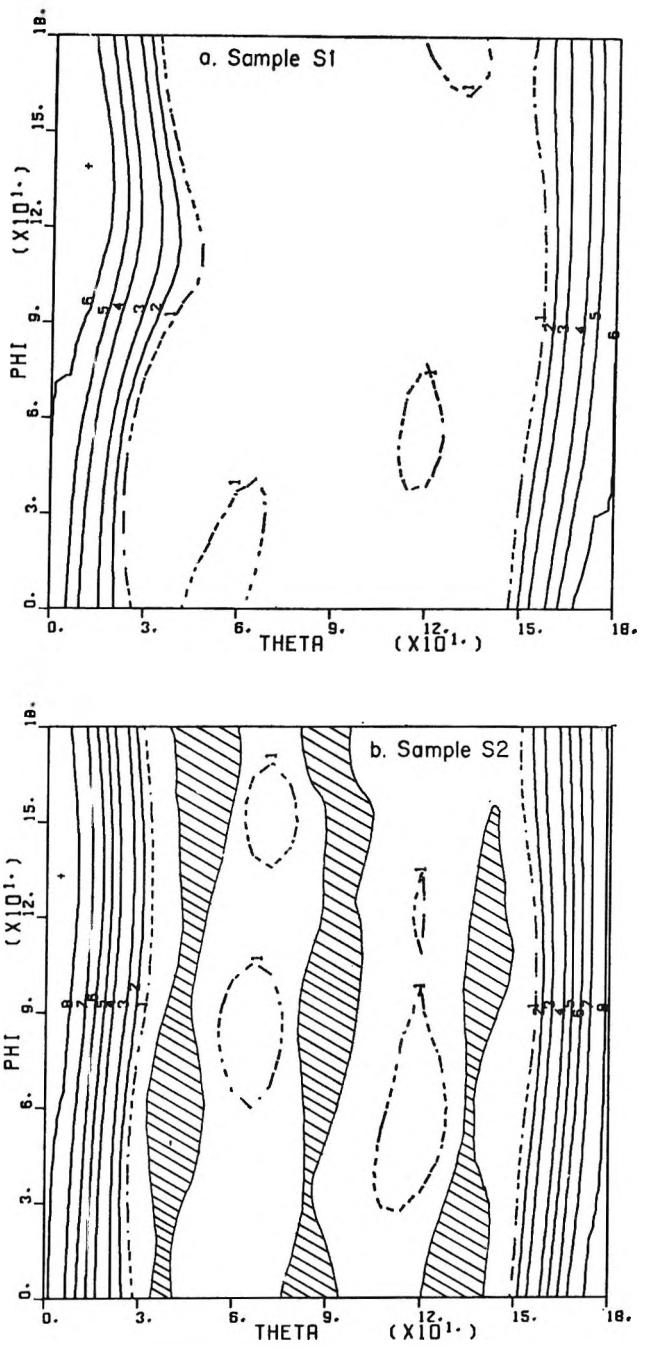

Figure 4. Contour maps representing G (ξ, φ) for two of the four samples studied. Contour lines 1–8 are drawn at densities 1.5, 3, 5, 8, 10, 12, 14, and 16. The shaded areas, (shown only in b) represent negative density regions arising from series termination errors.

(11) M. O. Dayhoff, *Comm. Assoc. Comp. Mach.*, 6, 620 (1963).

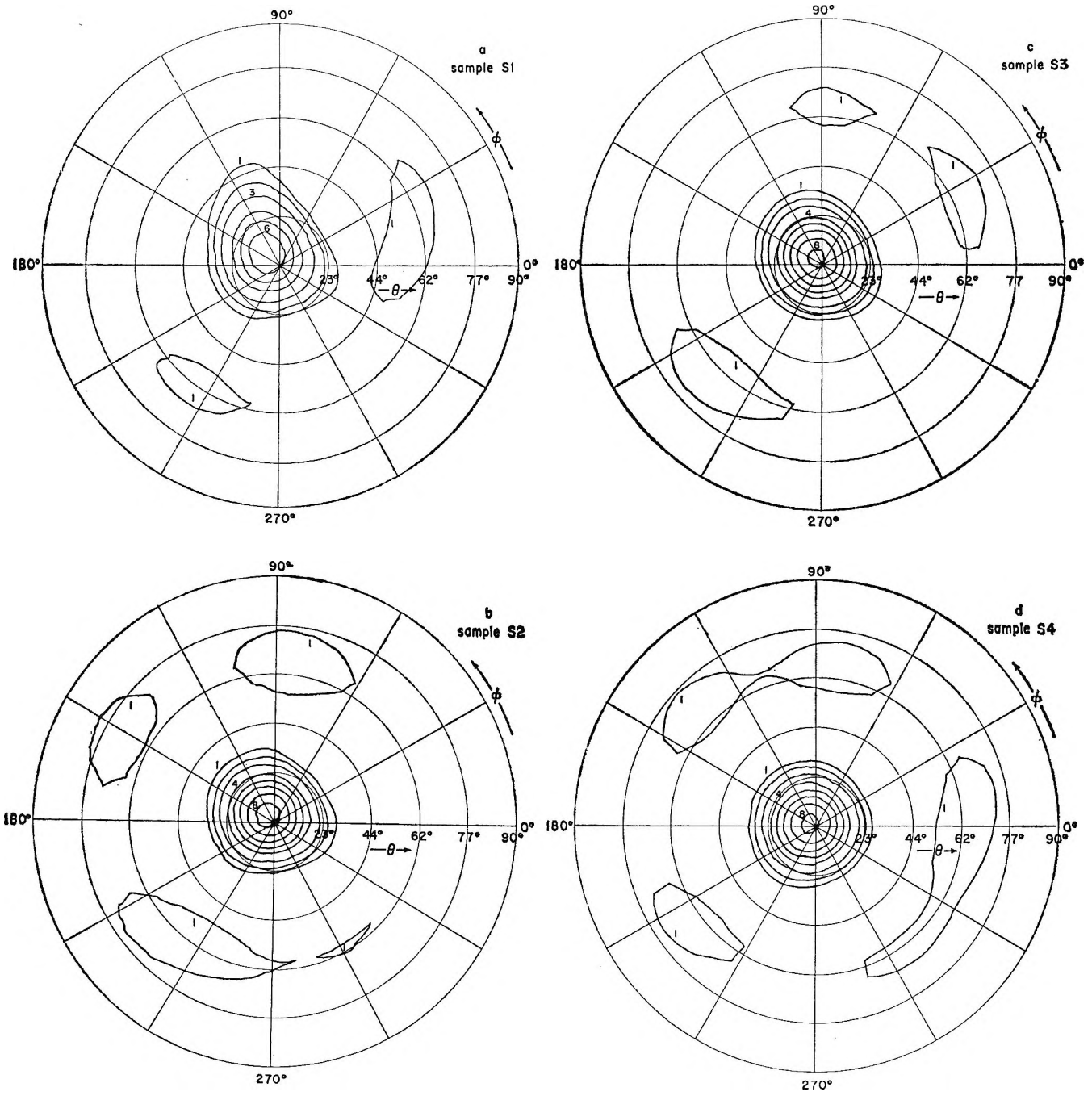

Figure 5. Contour maps of $G(\xi,\varphi)$ shown in stereographic polar projection. Contours correspond to the probability density values indicated in Figure 4.

$\theta = 180°$. However, if we recall that (θ,φ) and $(\pi - \theta,\pi + \varphi)$ are corresponding points, it is evident that the lower right-hand portion of these diagrams could appear just above the upper left-hand region. In this case, θ would range from 0 to 90° and φ from 0 to 360°, and only one region of high probability would appear.

As pointed out previously,[8] the variation in probability density along a vertical line in Figure 4 is, aside from a normalization constant, the conditional probability $w_\xi(\varphi)$ of finding a crystallite with an orientation φ when the c axis has a fixed inclination to the fiber axis. In a like manner, the variation along any horizontal line represents, again apart from a constant, the conditional probability $w_\varphi(\xi)$ of finding the

c axis at θ when the plane containing a^* and b^* has a fixed rotation with respect to the plane containing the fiber and c axes.

The contour diagrams shown in Figure 4 are replotted in polar stereographic projection[12] in Figure 5. From Figure 1 this map can be interpreted as the projection of the hemispherical surface $z \geq 0$ on a plane perpendicular to OZ. The function $G(\xi,\varphi)$ may be transformed into the inverse pole figure by replacement of φ by $(\pi - \varphi)$. Thus, if we imagine all of the crystallites in the anisotropic sample to be rotated so that the corresponding crystallographic axes coincide, the resulting spacial distribution of the fiber axis will be illustrated by Figure 5 after changing φ to $(\pi - \varphi)$. An alternative interpretation of $G(\xi,\varphi)$ depends upon the use of Figure 6, showing the poles of the 17 plane normals investigated plotted in stereographic projection. If this is superimposed on one of the contour diagrams of Figure 5, then the magnitude of $G(\xi,\varphi)$ at any pole is proportional to the probability that the plane normal in question will lie along the fiber axis. It can be seen that no $(hk0)$ plane normals point toward the stretching direction, whereas normals belonging to planes of the type $(h0l)$ align preferentially toward the fiber axis. Among the latter group, the tendency for collinearity of the plane normal and the fiber axis increases with the l/h ratio. Heffelfinger and Schmidt[13] reported that the $(\bar{1}05)$ plane is perpendicular to the fiber direction, in qualitative agreement with this observation.

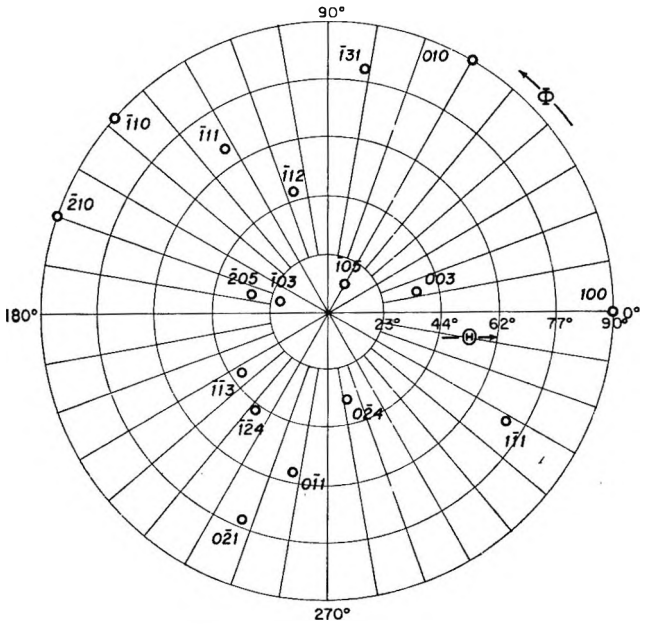

Figure 6. Poles of selected reciprocal lattice points inside the reflection sphere $2\theta < 60°$.

IV. Conclusions

Before examining the details of the crystallite orientation distribution functions, we will investigate its standard deviation, σ_w. Although σ_q can be calculated, no direct method is available to obtain σ_w. Roe and Krigbaum[7] derived the approximate relation

$$\sigma_w = \frac{1}{\pi} \sum_{l=\lambda+1}^{\infty} (l + 1/2)\langle Q_{2l}^2 \rangle \qquad (16)$$

based upon the assumption that all reciprocal lattice points are continuously and uniformly distributed with respect to Θ and Φ. Here λ is the maximum value of l appearing in the terms retained. These authors also showed that, with the same assumption, the following should apply

$$\langle Q_{2l}^2 \rangle \cong 2\pi^2[2/(2l + 1)][A_{2l0}^2 + 2\sum_{m=1}^{l} (A_{2lm}^2 + B_{2lm}^2)] \qquad (17)$$

Figure 7 presents a test of eq 17 using the data for sample S2. The open circles indicate average squares of Q_{2l} for all 17 reflections. It is interesting to observe that $\langle Q_{2l}^2 \rangle$ appears to be an exponentially decaying function of l^2 for polyethylene terephthalate, whereas it decreased exponentially with l for polyethylene. The filled circles in Figure 7 represent values of the right-hand member of eq 17. These appear to parallel the $\langle Q_{2l}^2 \rangle$, but to differ by a constant factor of about 1.3. If the linear behavior of $\langle Q_{2l}^2 \rangle$ is assumed to extend beyond the region investigated ($l = 8$), then eq 16 may be replaced by

$$\sigma_w^2 = \frac{1}{\pi} \int_{l=8}^{\infty} (l + 1/2) a e^{-bl^2} \, dl \qquad (18)$$

and with the values 0.737 and 0.012 for a and b, obtained from the intercept and slope of the line appearing in Figure 7, σ_w is found to be 2.12 for sample S2.

When the crystallite orientation distribution function is represented in series form by a small number of terms, as is the case here, it cannot furnish information on the detailed aspects of the orientation distribution. It may, however, indicate the essential characteristics of the crystallite orientation in the sample, as pointed out by Krigbaum and Roe.[8] We therefore begin our discussion of the crystallite orientation in polyethylene terephthalate with a consideration of the qualitative aspects of $G(\xi,\varphi)$. One sees from

(12) We wish to express our appreciation to Mr. Richard Pritchard of the Duke University Computing Laboratory for programming assistance throughout, and in particular for the modification of the Dayhoff CALCOMP program to yield stereographic projections.

(13) C. J. Heffelfinger and P. G. Schmidt, *J. Appl. Polymer Sci.*, 9, 2661 (1965).

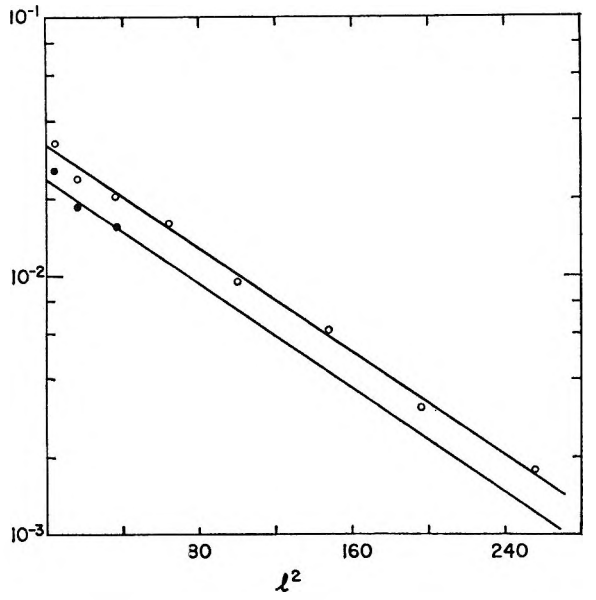

Figure 7. A test of eq 17 (see text).

Figure 5 that the crystallite orientation distributions of all samples are similar in nature, and that the largest change occurs on going from $\alpha = 2$ to $\alpha = 3$. We conclude that there is a unique preferred crystallite orientation in polyethylene terephthalate, and that this orientation is achieved with considerable perfection at relatively low drawing ratios. This behavior stands in contrast to that observed[8] for polyethylene, in which the character of the crystallite orientation changes more or less continuously with the drawing ratio prior to crystallization.

The highest contours of $G(\xi,\varphi)$ in Figure 5 occur for small values of θ. This indicates that the c axis tends to align along the stretching direction. The same conclusion also follows, of course, from the observation that the normals of the $(\bar{h}0l)$ planes having large (l/h) ratios orient most strongly in the direction of the fiber axis. If the distribution of the crystallographic c axis is limited within a small range in θ, and the distributions of a^* and b^* are random with respect to the fiber axis, $G(\xi,\varphi)$ will be independent of φ. The resulting function would appear in stereographic projection as a circle in the center of the diagram. The contours in Figure 6 deviate somewhat from circular shape and, more important, their center is displaced from the center of the coordinate system. This means not only that the c axis is restricted within a narrow range of θ, but also that all rotational positions about the c axis are not equally probable. From the point of view of crystallization kinetics, the preferential orientations of all three axes may mean that there are at least two forces which govern the final crystallite orientation.

The location of the largest value of $G(\xi,\varphi)$ for each sample is indicated by a cross in Figure 4. Thus, for example, the highest probability for sample S2 occurs at $\theta = 6°$ and $\varphi = 132°$. In terms of the inverse pole figure based on the coordinate system defined by c, a^*, and b^*, this means that the most probable location of the fiber axis is 6° away from the c axis and 48° from the a^*c plane. Once the most probable orientation of the unit cell has been determined, the orientation of the a and b axes can be calculated from the relations

$$\varphi_a = \varphi + \gamma^* - \pi/2$$

$$\phi_b = \varphi + \pi/2$$

$$\cos\theta_a = \cos\beta\cos\theta_c + \sin\beta\sin\theta_c\cos(\pi - \phi_a)$$

$$\cos\theta_b = \cos\alpha\cos\theta_c + \sin\alpha\sin\theta_c\cos(\pi - \phi_b)$$

Table III summarizes the most probable orientations of all of the crystallographic axes for the four samples studied. The major change with draw ratio is the shift from $\theta_c = 12°$ for sample S1 to 6° for the remaining samples. Daubeny, Bunn, and Brown[10] reported that for their polyethylene terephthalate sample, which had been crystallized and allowed to relax, the c axis was inclined from the fiber axis by approximately 5°. The remainder of the table reinforces our previous conclusion that there is one highly preferred crystallite orientation in polyethylene terephthalate.

Table III: Most Probable Orientation of Unit Cell Axes

			c axis	a axis		b axis	
Sample	α	φ	θ_c	θ_a	ϕ_a	θ_b	ϕ_b
S1	2.0	135	12	114	104	91	225
S2	3.0	132	6	116	104	94	222
S3	3.5	129	6	117	98	94	219
S4	3.5	159	6	114	128	96	249

In summary, we have found that polyethylene terephthalate represents a difficult case for the application of the Roe–Krigbaum treatment in two respects: the plane-normal distributions are sharp, rapidly varying functions, and the triclinic unit cell offers no simplification due to symmetry. Even under these circumstances, useful information concerning the crystallite orientation can be gained from the qualitative aspects of the orientation distribution function. However, it must be recognized that a significant fraction of the information contained in the measured plane-normal distributions could not be utilized.

One obvious remedy for this shortcoming involves the study of a larger number of reflections. Procedures are available for the resolution of a steady signal from a high background of random noise. Also, the use of a higher crystallization temperature might have increased the number of reflections accessible to our measurements. A second, and perhaps more fundamental, problem arises from our observation of the necessity to have more equations than unknown coefficients A_{lm} and B_{lm}. This indicates that the data for the various plane normals do not form an entirely self-consistent set. The most likely cause of this inconsistency is uncertainty in the level, and orientation dependence, of the background correction. This indicates the need for a procedure which permits the background for each reflection to be adjusted until internal consistency, for example, among the values of Q_2^i and Q_4^i, is achieved.

Electrolyte Concentration Effects in the Formation of Pentaaquochlorochromium(III) Ion in Aqueous Perchloric Acid Solution[1]

by Clarence F. Hale and Edward L. King

Department of Chemistry, University of Colorado, Boulder, Colorado *(Received November 14, 1966)*

Equilibrium in the reaction forming inert inner-sphere pentaaquochlorochromium(III) ion, $Cr(OH_2)_6^{3+} + Cl^- = Cr(OH_2)_5Cl^{2+} + H_2O$, has been studied at 40.0, 60.2, and 80.5° in solutions of ionic strength 0.98, 4.00, 6.70, and 10.0 M, with perchloric acid as the principal electrolyte. The formation of $Cr(OH_2)_5Cl^{2+}$ increases with an increase in electrolyte concentration, in part owing to the lower activity of water in concentrated electrolyte solutions. With increasing concentration of electrolyte, the reaction becomes less endothermic, ΔH° = 6.0 ± 0.7, 5.6 ± 0.4, 3.6 ± 0.3, and 3.1 ± 1 kcal mole^{-1}, respectively, at the indicated four values of ionic strength.

Although association of ions of opposite charge decreases with increasing electrolyte concentration in dilute solution, an opposite trend, increasing association with increasing electrolyte concentration, is observed in concentrated electrolyte solution. Coll, Nauman, and West[2] observed a dramatic increase in the stability of chloroiron(III) ion relative to the dissociated ions with increasing electrolyte concentration in concentrated perchloric acid. The present study deals with the reaction forming inert inner-sphere pentaaquochlorochromium(III) ion[3]

$$Cr(OH_2)_6^{3+} + Cl^- = Cr(OH_2)_5Cl^{2+} + H_2O$$

in relatively concentrated perchloric acid solution. Because of the slowness with which this equilibrium is established, study of it offers advantages over similar studies on relatively labile systems, *e.g.*, iron(III)–chloride, in which it is not possible to distinguish outer-sphere (ion-pair) and inner-sphere species.[4] The inability to distinguish outer-sphere and inner-sphere species in a labile system complicates interpretation of

(1) Supported by the National Science Foundation, Grant GP-680.

(2) H. Coll, R. V. Nauman, and P. W. West, *J. Am. Chem. Soc.*, 81, 1284 (1959).

(3) Hereafter, $Cr(OH_2)_5Cl^{2+}$ will be called simply chlorochromium(III) ion.

(4) M. J. M. Woods, P. K. Gallagher, and E. L. King, *Inorg. Chem.*, 1, 55 (1962).

electrolyte concentration effects since the number of water molecules involved specifically in the association reaction differs in two cases. In addition, most types of experimental data on systems at equilibrium yield the sum of the concentrations of outer-sphere and inner-sphere species. In the reaction of chromium(III) under consideration, the coordination number of the metal ion is the same in the reactant and product species and it is certain that one water molecule is replaced by one chloride ion. Of course, taking into account the one water molecule which appears in the balanced equation for the formation of chlorochromium(III) ion does not settle the role of solvent in the reaction. It is, however, a needed step toward understanding the effect of electrolyte concentration upon ionic equilibria in concentrated solutions.

In the present work, studies were made at 40.0, 60.2, and 80.5°. At each temperature, the ionic strength was maintained at 0.98, 4.00, 6.70, and 10.0 *M*. To minimize formation of dichlorochromium(III) species, the concentration of chloride ion was kept low; the stoichiometric concentration of chromium(III) was much larger than that of chloride ion. Chromium(III) perchlorate made an appreciable contribution to the ionic strength, but the hydrochloric acid did not and the change in ionic strength with occurrence of reaction was not significant. The decision to study solutions with particular values of molar ionic strength was somewhat arbitrary; it was not based on any belief that the ionic strength principle was valid at the high electrolyte concentrations studied. (Appropriate interpolation allows equilibrium quotients based on the experimental observations to be converted to values appropriate for other comparisons, *e.g.*, on solutions of constant molal ionic strength, perchlorate molarity, etc.)

Experimental Methods

Reagents. Solutions of perchloric acid and hydrochloric acid, prepared by dilution of reagent grade concentrated solutions, were standardized using sodium carbonate. Solutions of chromium(III) perchlorate in perchloric acid were prepared by reaction of hydrogen peroxide and chromium(VI) oxide in perchloric acid solution. The slight excess of peroxide which was used was decomposed by heating the solution at 75°. (The absence of peroxide in the final stock solution was demonstrated by making a portion alkaline; if peroxide were present, chromium(VI) would be produced. Its absence was checked with diphenylcarbazide.) As indicated in an earlier paper,[5] the ratio of absorbance at 230 and 260 mμ (A_{230}/A_{260}) is a useful measure of solution contamination by polymeric chromium(III) species. The value ~0.26 found in the stock solutions prepared for this study is slightly higher than the value (0.22) found in the earlier study,[5] but it corresponds to a negligible amount of polymeric chromium(III) species in the stock solutions.

Analysis of Equilibrated Solutions. The absorbancy indices of some chromium(III) species in solution may be sensitive to temperature and electrolyte concentration.[6,7] The procedure was adopted, therefore, of making all spectral measurements at room temperature (approximately 25°) on solutions which had been diluted to a stoichiometric ionic strength of 1 *M;* under these conditions the rate of reequilibration from the state achieved in the period at higher electrolyte concentration and temperature to the equilibrium state corresponding to 25° and 1 *M* ionic strength is very low.[8] The molar absorbancy indices of hexaaquochromium(III) ion and chlorochromium(III) ion were determined independently. Measurements on three independent solutions of approximately 10^{-2} *M* chromium(III) perchlorate in approximately 1 *M* perchloric acid yielded values (based on decadic logarithms): 230 mμ, 1.24 l. mole^{-1} cm^{-1}; 225 mμ, 1.46 l. mole^{-1} cm^{-1}; and 220 mμ, 2.98 l. mole^{-1} cm^{-1}. Judged by the consistency of values determined from the three solutions, these quantities are known to ~1%. Since equilibrated solutions contain chloride ion, its effect upon the light absorption by hexaaquochromium(III) ion was checked. Although an effect, interpretable in terms of "ion pairing"[9] is observed in solutions of higher concentration of chloride, the effect was negligible at most of the chloride ion concentrations of the present study. At 220 mμ, the extinction coefficient of hexaaquochromium(III) ion is raised by ~0.02 l. mole^{-1} cm^{-1} for an increase of concentration of chloride ion by 10^{-3} *M*. The concentrations of free chloride in the equilibrated solutions after dilution for spectral measurements were in the range 10^{-2} to 10^{-3} *M;* in most solutions the concentration was nearer the lower limit. Only in the solutions equilibrated at ionic strength 0.98 *M* was it necessary to correct the absorbancy index of hexaaquochromium(III) ion for the effect of chloride ion. Solutions containing chlorochromium(III) ion as the only chromium-containing species were prepared by an ion-exchange procedure

(5) C. Altman and E. L. King, *J. Am. Chem. Soc.*, **83**, 2825 (1961).

(6) E. L. King, M. J. M. Woods, and H. S. Gates, *ibid.*, **80**, 5015 (1958).

(7) J. E. Finholt, K. G. Caulton, and W. J. Libbey, *Inorg. Chem.*, **3**, 1801 (1964).

(8) T. W. Swaddle and E. L. King, *ibid.*, **4**, 532 (1965); the half-time for aquation of $Cr(OH_2)_5Cl^{2+}$ in 1 *M* $HClO_4$ at 25° is approximately 600 hr. Under our concentration conditions, this is also approximately the half-time for establishment of equilibrium.

(9) H. S. Gates and E. L. King, *J. Am. Chem. Soc.*, **80**, 5011 (1958).

similar to that used previously.[9] Measurements on two to four independently prepared solutions yielded values for the absorbancy indices of chlorochromium(III) ion: 230 mμ, 785 l. mole^{-1} cm^{-1}; 225 mμ, 1.36 × 10^3 l. mole^{-1} cm^{-1}; and 220 mμ, 2.37 × 10^3 l. mole^{-1} cm^{-1}.

Solutions for equilibration were prepared to have the ionic strength values of 0.98, 4.00, 6.70, and 10.0 *M* at each of the temperatures studied. Some solutions were preequilibrated at 75–80° before being placed in a thermostat for equilibration. In these solutions the equilibrium concentration of chlorochromium(III) ion was approached from a value greater than the equilibrium value. The time periods during which solutions were kept in the thermostat ranged from 14 to 48 days at 40°, 2 to 6.5 days at 60°, and 5 to 10 hr at 80°. Based on existing kinetic studies[8] and the present measurements, these time intervals were generally long enough for equilibration. (In a few samples open to question, appropriate allowance was made in the plots of log Q' *vs.* C_{Cr} (to be discussed) for whether or not equilibrium was approached from too high or too low a concentration of chlorochromium(III) ion.)

Light absorption of the quenched and diluted equilibrated solutions at 220, 225, and 230 mμ (measured with a Cary Model 15 spectrophotometer) was used to obtain the concentration of chlorochromium(III) ion, it being assumed that chlorochromium(III) ion and hexaaquochromium(III) ion were the only absorbing species in the solution. The calculation involved the equation $[CrCl^{2+}] = (A' - a_0C_{Cr})/(a_1 - a_0)$, in which A' is the measured light absorption per centimeter of path (corrected for dilution), a_1 and a_0 are the molar absorbancy indices of $Cr(OH_2)_5Cl^{2+}$ and $Cr(OH_2)_6^{3+}$, respectively, and C_{Cr} is the stoichiometric molarity of chromium(III).

Agreement between values of the concentration of chlorochromium(III) ion calculated from the data obtained at different wavelengths is evidence that other light-absorbing species are not interfering. The ratio of absorbancy indices (a^{220}/a^{230}) for each isomeric dichlorochromium(III) ion is approximately 1.8, compared to 3.0 for chlorochromium ion.[5] It would be fortuitous for any other possible contaminant to have a ratio of absorbancy indices (a^{220}/a^{230}) equal to that of chlorochromium (III) ion. Generally good agreement (to 1–3%) of calculated concentrations of chlorochromium(III) ion was obtained using data from the different wavelengths. The absorbancy indices at 220 mμ are more appropriate for the analysis and it is upon the measurements at this wavelength that our calculations are based.[10]

Evaluation of the Empirical Equilibrium Quotient $Q' = [CrCl^{2+}]/([Cr^{3+}][Cl^-])$.[10] At each temperature and electrolyte concentration, solutions with a range of concentrations of chromium(III) and chloride ion were studied. The derived values of Q' from solutions with constant chromium(III) and varying chloride ion concentrations were in good agreement. Over a four- to fivefold change in stoichiometric concentration of chloride (and a similar range of calculated concentrations of free chloride ion), the average difference between individual values of Q' and the average value for the particular series (*i.e.*, particular temperature and electrolyte concentration) was approximately 2%. (This omits one solution with the highest chloride ion concentration (2.3 × 10^{-4} *M* chloride ion) in the series at 60° and 10 *M* perchloric acid.) This demonstrates that inappreciable dichlorochromium(III) ion was present in the solutions being considered; the highest concentration of chloride ion studied under each set of conditions was approximately 10^{-2} *M* at all temperatures in solutions with ionic strength 0.98 and 4.0 *M*, 4–7 × 10^{-3} *M* at all temperatures in solutions with ionic strength 6.7 *M*, and 2–4 × 10^{-4} *M* at all temperatures in solutions with ionic strength 10.0 *M*.

At each temperature and ionic strength, the concentration of chromium(III) was varied between 0.006 and 0.031 *M*. The calculated equilibrium quotient showed in most of the series a mild dependence upon the concentration of chromium(III) ion. In the series of experiments at 60°, I = 4.0 *M*, the derived values of Q' as a function of chromium(III) concentration are (given as C_{Cr}, Q') 6.2 × 10^{-3}, 1.07; 1.24 × 10^{-2}, 1.06; 2.49 × 10^{-2}, 0.99; and 3.11 × 10^{-2}, 0.95. Corresponding data for 80°, I = 4.0 *M* are 5.85 × 10^{-3}, 1.89; 1.17 × 10^{-2}, 1.69; 2.34 × 10^{-2}, 1.64; and 2.92 × 10^{-2}, 1.55. A dependence of this sign, a decrease in Q' with an increase in concentration of chromium(III), could be caused by ion pairing of aquochromium(III) ion and chloride ion if appreciable chloride ion was tied up as the ion-pair species. Under such circumstances, the concentration of chloride should be calculated using $[Cl^-] = C_{Cl} - [CrCl^{2+}] - [Cr^{3+}Cl^-]$, not $[Cl^-] = C_{Cl} - [CrCl^{2+}]$. Since the trend is observed in series of experiments in which only 1–3% of the chloride ion was tied up as inner-sphere complex (*e.g.*, the series at 60° cited above) and the amount tied up as ion pair

(10) Tables giving stoichiometric concentration conditions and calculated values of Q have been deposited as Document Number 9270 with the ADI Auxiliary Publications Project, Photoduplication Service, Library of Congress, Washington 25, D. C. A copy may be secured by citing the document number and by remitting $1.25 for photoprints or $1.25 for 35 mm microfilm. Advance payment is required. Make checks or money orders payable to Chief, Photoduplication Service, Library of Congress.

is unlikely to be greater than this,[9] this particular explanation for the trend is not acceptable. Rather the trend is assumed to be an ill-defined medium effect due to variation of perchlorate ion concentration, which varied as the concentration of chromium(III) varied ($[ClO_4^-] = I - 3C_{Cr}$); the change of concentration of chromium(III) is appreciable.[11] The data at each temperature and ionic strength were plotted as log Q' *vs.* the stoichiometric concentration of chromium(III). Straight lines were drawn to extrapolate the value of log Q' to zero chromium(III) concentration. These values of Q' correspond, therefore, to media in which the ionic strength is due only to perchloric acid (ignoring the very small concentration of hydrochloric acid). Values of Q' obtained in this way are presented in Table I. (Erratic results were obtained in the series of experiments in media of $I = 10.0\ M$, 40° and these data are omitted.) The uncertainties given are based upon the uncertainty in the experimentally measured absorbancies and scatter of the experimental points in plots of log Q' *vs.* C_{Cr}.

Table I: Experimental Values[a] of the Equation

$$Q' = \frac{[CrCl^{2+}]}{[Cr^{3+}][Cl^-]}$$

I,M	40.0°	60.2°	80.5°
0.98	0.17 ± 0.02	0.33 ± 0.02	0.53 ± 0.03
4.00	0.63 ± 0.01	1.10 ± 0.04	1.8 ± 0.1
6.70	6.0 ± 0.1	8.3 ± 0.6	12.0 ± 0.3
10.0		130 ± 10	140 ± 7

[a] Values are based upon the molar concentration scale at each particular temperature. The values have been extrapolated to zero concentration of chromium(III).

Results

The equilibrium quotient associated with the reaction

$$Cr(OH_2)_6^{3+} + Cl^- = Cr(OH_2)_5Cl^{2+} + H_2O$$

is obtained from the empirical equilibrium quotient, Q', by multiplication by the activity of water, a_w

$$Q = \frac{[Cr(OH_2)_5Cl^{2+}]a_w}{[Cr(OH_2)_6^{3+}][Cl^-]} = Q'a_w$$

Values of the activity of water have not been measured for the solutions studied and the needed values were obtained by interpolation, or in a few cases by extrapolation, of existing data.[12] (Density data for perchloric acid solutions as a function of temperature[13] were used to calculate the molality of perchloric acid corresponding to each temperature–molarity combination. The values so obtained (given as molarity, molality at 40, 60, and 80°) are 0.98 M, 1.060, 1.047, 1.035; 4.00 M, 5.076, 5.00, 4.91; 6.70 M, 9.91, 9.70, 9.49; and 10 M, 18.81, 18.30, 17.83. The density data as a function of temperature are needed also in calculation of the enthalpy change.) Extrapolation of values of the activity of water at 25° beyond the highest molality of perchloric acid for which data are available (16 m) to the highest molality needed for the correlation of our data (18.8 m) was made with the equation which correlates data from 10 to 16 m[14]

$$\frac{232ma_w}{55.51(1 - a_w)} = 1 + 58.0a_w$$

To evaluate the activity of water at the temperatures in question, use was made of existing apparent molal heat data.[15] Values of $\bar{L}$ for perchloric acid were assumed to be independent of temperature and the values obtained for 25° were used. An extrapolation was needed to obtain the value for 25° for 10 M perchloric acid, but values for the other concentrations were obtained by interpolation. Based on the cited studies and these stated assumptions, the values of activity of water used in the present study were obtained. They are (given as C_{HClO_4} (molarity), a_w) for 40°, 0.98, 0.963; 4.0, 0.726; and 6.7, 0.367; for 60°, 0.98, 0.961; 4.0, 0.723; 6.7, 0.365; and 10.0, 0.0738; for 80°, 0.98, 0.961; 4.0, 0.718; 6.7, 0.360; and 10.0, 0.0918. Values of Q ($=Q'a_w$) obtained using these values of activities are presented in Table II. Values of ΔH for the reaction have been obtained for each medium from plots of log Qd *vs.* T^{-1}, where d is the density of the solution. (Incorporation of factor d corrects for temperature dependence of the molarity.) Although one can expect a reaction of this charge type to have associated with it an appreciable value[16] of ΔC_p, the quality of the data does not allow evaluation of ΔC_p and $\Delta H°$ was assumed to be independent of

(11) The extent of formation of hydrolytic dimer of chromium(III) in these solutions is negligible, based on equilibrium data of G. Thompson, Thesis, University of California, Berkeley, Calif., June 1964 (U. C. R. L. 11410). If appreciable light absorption were due to hydrolytic dimer, the trend in Q' with the concentration of chromium(III) would be opposite that observed.

(12) J. N. Pearce and A. F. Nelson, *J. Am. Chem. Soc.*, 55, 3075 (1933); R. A. Robinson and O. J. Baker, *Trans. Proc. Roy. Soc. New Zealand*, 76, 250 (1946).

(13) L. H. Brickwedde, *J. Res. Natl. Bur. Std.*, 42, 309 (1949).

(14) R. H. Stokes and R. A. Robinson, *J. Am. Chem. Soc.*, 70, 1870 (1948).

(15) C. E. Vanderzee and J. A. Swanson, *J. Phys. Chem.*, 67, 285 (1963).

(16) For the reaction of chromium(III) ion and thiocyanate ion, the value of $\Delta C_p°$ is approximately 70 cal mole^{-1} deg^{-1} (C. Postmus and E. L. King, *J. Phys. Chem.*, 59, 1208 (1955)).

temperature. Values of $\Delta H°$ so obtained are 0.98 M, 6.0 ± 0.7 kcal mole^{-1}; 4.0 M, 5.6 ± 0.4 kcal mole^{-1}; 6.7 M, 3.6 ± 0.3 kcal mole^{-1}; and 10.0 M, 3.1 ± 1 kcal mole^{-1}.[17]

Table II: Values[a] of $Q = \dfrac{[CrCl^{2+}]a_w}{[Cr^{3+}][Cl^-]}$

I, M	40.0°	60.2°	80.5°
0.98	0.16	0.32	0.51
4.00	0.46	0.80	1.3
6.70	2.2	3.0	4.3
10.0		9.6	12.8

[a] The percentage uncertainties corresponding to the values given in Table I are appropriate here, except for the value for 10 M perchloric acid. Uncertainty in the activity of water in such solutions may exceed the uncertainty in the empirical equilibrium quotient, Q'.

Discussion

The equilibrium being studied is amenable to careful characterization and the present study contributes relevant information. It is open to question, however, whether all interactions other than those specifically given in the balanced chemical equations should be lumped together in the activity coefficient factor $f_{Cr(OH_2)_5Cl^{2+}}/f_{Cl}f_{Cr(OH_2)_6^{3+}}$. The additional possible interactions which one might wish to describe in chemical terms are (a) inner-sphere interactions of cationic chromium(III) species with perchlorate ion, (b) outer-sphere (ion-pair) interactions of cationic chromium(III) species with chloride ion or perchlorate ion, and (c) interactions involving solvent.

Inner-sphere coordination of perchlorate ion may occur to an appreciable extent in the most concentrated perchloric acid solutions studied. Jones and Bjerrum[18] have observed slow spectral changes occurring when the concentration of perchloric acid in a solution of hexaaquochromium(III) ion is raised to 10.6 M and they have interpreted these changes in terms of the formation of pentaaquoperchloratochromium(III) ion. The equilibrium quotient for formation of this species is relatively uncertain,[19] however, and no account of its presence has been taken in treatment of our data. The trend in $\Delta H°$ values observed in the present study may be due to an appreciable fraction of the reactant cation being present as the "endothermic" species $Cr(OH_2)_5OClO_3^{2+}$ in the more concentrated perchloric acid solutions.

In the most concentrated electrolyte solutions studied, it is reasonable that the second coordination shell around chromium contains perchlorate ion. At 6.7 M perchloric acid (9.9 m at 80.5°), there are only 2.3 water molecules per ion of supporting electrolyte (hydronium ion H_3O^+ and perchlorate ion); at 10.0 M perchloric acid (18.8 m at 80.5°), the figure is 1.0. It seems hopeless, however, to incorporate into the treatment of our data a quantitative account of the competition between water and perchlorate ion for sites in the second coordination shell around hexaaquochromium(III) ion and pentaaquoclorochromium-(III) ion. It must be recognized, nevertheless, that a relevant factor in determining the position of an equilibrium involving cationic species is the interaction of these species and perchlorate ion.

Considering the data at 60.2°, the empirical equilibrium quotient, Q', increases by a factor of 400 with an increase of the concentration of perchloric acid from 0.98 to 10.0 M. This factor is lowered to 30 if the specific participation of one water molecule is taken into account, that is, if values of $Q(=Q'a_w)$ are considered. Solvation of chloride ion has been ignored as well as differences of the secondary solvation of the cationic reactant and product. If one more water molecule were introduced on the product side of the balanced chemical equation, the trend in the corresponding equilibrium quotients would be reduced still more. For 60.2°, values of $Q'a_w^2$ are 0.98 M, 0.31; 4.00 M, 0.58; 6.70 M, 1.1; and 10.0 M, 0.94. A factor of 4 now encompasses all of the values and there might seem to be a reason for taking this calculation seriously, that is, the product species are hydrated by two fewer water molecules than the reactants. It does not seem reasonable, however, that this approach to determination of relative hydration of species, with its tacit assumption that the activity coefficient quotient $f_{CrCl^{2+}}/(f_{Cr^{3+}}f_{Cl^-})$ is medium independent in this electrolyte concentration range, is correct.

The dependence of the standard entropy change upon electrolyte concentration is of interest. Combination of values of $\Delta H°$ already presented with values of $\Delta G°$ calculated from the values of Q for 60.2° given in Table II give the values of $\Delta S°$ summarized in Table III.

(17) Earlier studies of this reaction (ref 9 and R. J. Baltisberger and E. L. King, *J. Am. Chem. Soc.*, 86, 795 (1964)) gave a value of 6.1 kcal mole^{-1} for ΔH for a solution with a total anion molality of 4.44 and a value of 7.0 kcal mole^{-1} for an aqueous solution of ionic strength at 0.42 M.

(18) K. M. Jones and J. Bjerrum, *Acta Chem. Scand.*, 19, 974 (1965).

(19) Evaluation of the equilibrium quotient depends upon the assumption that hexaaquochromium(III) ion is present predominantly as an ion pair (with perchlorate ion) and also upon uncertain extrapolation to obtain the activity of water in 10.6 M perchloric acid.

Table III: Thermodynamic Quantities[a] Associated with the Reaction $Cr(OH_2)_6^{3+} + Cl^- = Cr(OH_2)_5Cl^{2+} + H_2O$

I,M	$\Delta G_{333.4}°$, kcal mole^{-1}	$\Delta H°$, kcal mole^{-1}	$\Delta S°$, cal mole^{-1} deg^{-1}
0.98	0.75	6.0 ± 0.7	15.7 ± 2
4.00	0.15	5.6 ± 0.4	15.7 ± 1
6.70	−0.73	3.6 ± 0.3	13.0 ± 1
10.0	−1.50	3.1 ± 1	13.8 ± 3

[a] Based on the hypothetical ideal 1 M solution of solute species in the indicated concentration of perchloric acid as the standard state.

The reaction under consideration is one for which values of the equilibrium quotient and $\Delta S°$ depend upon the choice of standard state for the solute species. The values of Q given in Table II and the thermodynamic quantities given in Table III correspond to a hypothetical ideal 1 M solution of the solute species in a solution of the indicated molarity of perchloric acid as the standard state at each temperature. This is a convenient standard state, but it does not seem possible to claim that it is more rational than other possibilities based on other solute concentration scales; for instance, moles per 1000 g of water, moles per 1000 g of "free" water, or mole fraction. For 60°, conversion of the values of Q to values based on the conventional molal scale give Q_m = 0.30, 0.64, 2.07, and 5.3 for solutions 0.98, 4.00, 6.70, and 10.0 M perchloric acid, respectively. To convert these to values corresponding to a modified molality concentration scale, moles per 1000 g of "free" water, they can be multiplied by the activity of water. (This is based on the simple view that $(1000/a_w)$ g of water in the perchloric acid solutions contain 1000 g of "free" water.) The resulting values are $Q_m a_w$ = 0.29, 0.46, 0.76, and 0.39 for solutions 0.98, 4.00, 6.70, and 10.0 M perchloric acid, respectively. Clearly, the medium effect has just about disappeared when equilibrium quotients are based on this scale. (Except for use of the molal scale, this last calculation is, of course, very similar to that in which Q was multiplied by the activity of water or Q' by the square of the activity of water.)

The final conclusions which can be drawn may be summarized. (1) Inclusion of the activity of water in the equilibrium constant expression for the reaction in question removes a large fraction of its medium dependence in concentrated electrolyte solution. (2) Further refinement of the medium effect depends, in part, on the choice of concentration scale for considering such equilibrium constants.

Electrochemical Studies in a Solid Electrolyte System

by Douglas O. Raleigh

North American Aviation Science Center, Thousand Oaks, California *(Received November 21, 1966)*

Previous studies of the double-layer capacitance of solid AgBr against metallic electrodes at elevated temperatures were extended to include new electrode materials, electrode interface preparations, and electrochemical techniques. In addition, monolayer-level electrodeposition characteristics were investigated. Results with polycrystalline and single-crystal Pt electrodes show that the high double-layer capacitance previously reported is more likely an intrinsic property of the AgBr|Pt interface than due to surface inhomogeneities. With a crystalline graphite electrode, capacitances an order of magnitude smaller were obtained that are in reasonable agreement with diffuse double-layer theory. Galvanostatic experiments showed that Ag electrodeposition onto Pt involves the buildup of a preplated Ag monolayer, while nucleated deposition occurs on graphite, resulting in dendritic growth. Activity-coverage data were obtained for the Ag monolayer buildup process on Pt. For deposition on graphite, the amount of Ag involved at the critical nucleation stage was obtained. The contrasting over-all results with Pt and graphite are analyzed in terms of the relative Ag–Ag, Ag–Pt, and Ag–C bond strengths, resulting in the tendency of Pt to adsorb both Ag atoms and ions and the absence of this tendency with graphite. In all the double-layer charging studies, low-level residual charging currents were observed which are attributed to slow relaxation processes in the diffuse double layer.

Introduction

There has been a developing interest in electrochemical systems employing solid electrolytes.[1-3] Solid electrolyte cells have been used in thermodynamic and phase diagram studies, studies of transport and polarization phenomena in ionic solids, solid-state reaction studies, and device applications. Most of the work, however, has involved the *application* of a solid electrolyte cell to a particular problem, rather than the intrinsic interest of such cells as electrochemical systems. Such systems are, in fact, electrochemically unique in a number of aspects: a highly structured electrolyte, charge transport by lattice defect migrations, the solid–solid nature of the electrode interfaces, and the absence of hydration and solvent effects. It was the purpose of this work to study two phenomena of electrochemical interest, double-layer capacitance and electrodeposition, in a simple solid electrolyte system.

Silver bromide has been studied intensively in our laboratory as a representative solid electrolyte because of its high intrinsic ionic conductivity at convenient working temperatures,[4] its reasonably well-understood ionic conduction mechanism,[5] its availability as high-purity single crystals, and the interest of solid-state processes in AgBr in photographic studies. In a previous publication,[6] results were reported on the double-layer capacitance of AgBr against Pt and Au electrodes. The present work was motivated in part by a desire to extend these studies and attempt to answer some unresolved questions.

To review the previous work briefly, voltage steps were applied to the so-called polarization cells (type I)

(1) C. Wagner, *Proc. Intern. Comm. Electrochem. Thermodyn. Kinet.*, 7, 361 (1957); *Z. Elektrochem.*, 60, 4 (1956).

(2) F. A. Kroger, "The Chemistry of Imperfect Crystals," Interscience Publishers, Inc., New York, N. Y., 1964, Chapter 22.

(3) D. O. Raleigh, *Progr. Solid State Chem.*, 3, 83 (1967).

(4) J. Teltow, *Ann. Physik*, 5, 63 (1949).

(5) See, for instance, A. W. Lawson, *J. Appl. Phys. Suppl.*, 33, 466 (1962).

(6) D. O. Raleigh, *J. Phys. Chem.*, 70, 689 (1966).

$$C,Br_2(g)|AgBr|(Pt \text{ or } Au) \qquad (I)$$

in which the voltage was always maintained in a suitable range to prevent any steady-state ionic discharge at the Pt or Au "blocking" electrode. This was done by biasing the bromine electrode positively at least several tenths of a volt, but less than the potential required to decompose AgBr into Ag(s) and $Br_2(g)$ at the ambient electrode pressure. Under these conditions, there is only an extremely small electronic cell current, the blocking electrode interface behaving as a purely capacitative circuit element for ionic current. Since AgBr at the temperatures of interest is a predominant ionic conductor, voltage steps act merely to recharge the blocking interface at the new potential. Moreover, if the bromine electrode behaves as a "reversible" or ideally unpolarized electrode in response to voltage steps, as the experimental evidence indicated, the cell then formally resembles an RC series load, R being the electrolyte resistance. Under these conditions, the transient cell current in response to voltage steps gives information on the capacitative properties of the blocking interface. Finally, since the cell under a fixed polarizing voltage is at electrochemical equilibrium, the thermodynamic activities of Ag and Br_2 are jointly fixed at the blocking interface by the applied voltage, allowing study of its capacitative properties as a function of one of these complementary variables.

In the above work, oscillographic current–time data in response to voltage steps were obtained which represented the bulk ($\sim$97%) of the total voltage change across the blocking interface. It was found that the recharging current, which decayed monotonically to zero as expected, did not decay with a single time constant, indicating a dispersion behavior in the capacitance. Under the best defined cell conditions, it was possible by graphical analysis to resolve the current–time data into a mixture of two time constants, but a slowly decaying low-level current was also observed. Moreover, possible effects due to current-flow geometry and the reversible electrode could not be definitely ruled out.

The graphical analysis nonetheless served to determine the electrode double-layer capacitance on the time scale of the bulk of the recharging process. Large (200–300 $\mu f/cm^2$) C_{dl} values were obtained that were roughly independent of temperature and cell potential at values of the latter corresponding to low Ag activities at the interface. At higher a_{Ag}, large increases in the total charge transfer were obtained which were attributed to gradual electrodeposition of an Ag monolayer as the decomposition potential ($a_{Ag} = 1$) was approached. The large C_{dl} values in the low a_{Ag} range were tentatively attributed to ion adsorption on the electrode surface, but the possible role of surface inhomogeneities could not be ruled out.

In the present work, it was desired to (1) use a cell arrangement that simultaneously provided a good uniaxial current-flow geometry and removed any effects associated with the "reversible" electrode to see if C_{dl} still showed dispersion behavior; (2) carry out tests with both single-crystal Pt and polycrystalline Pt foil, using a number of electrode-interface preparation techniques, to observe the effect on both the size and degree of dispersion of C_{dl}; (3) measure any long term, low-level portion of the total charge transfer, determining both its size and duration, and try to ascertain its origin; and (4) repeat all the above with a reasonably well-defined electrode surface of a material appreciably different from Pt.

For these purposes, the cell arrangement

$$Ag|AgBr|\text{inert electrode} \qquad (II)$$

was employed, a polarization cell of the type used by Ilschner[7] to measure electronic conductivity in AgBr. The cell consisted of a cylindrical AgBr pellet spring-loaded between an Ag foil and a planar surface of the inert electrode material. In contrast to previous cells of this type, however, a three-electrode arrangement was employed, in which an Ag wire embedded in the AgBr pellet about halfway between the two above electrodes served as the reference electrode, the Ag foil serving as counterelectrode. In analogy to the cell with a Br_2 electrode, steady-state ionic current blocking was achieved by biasing the Ag foil electrode 0–0.3 v negative with respect to the inert or blocking electrode. Under these conditions, the steady-state silver activity at the blocking electrode (referred to unit activity for pure Ag) is given by $a_{Ag} = \exp[-\mathcal{E}\mathfrak{F}/RT]$, where $\mathcal{E}$ is the potential between the blocking electrode and either the reference or counterelectrode (the latter two being essentially equipotential in the steady-state condition of zero ionic cell current).

Both the steady-state cell bias and voltage steps were applied *via* a standard potentiostat arrangement. In this, the potentiostat applies across the cell whatever voltage is required to maintain the voltage between reference and blocking electrodes equal to the potentiostat input voltage. When a step is applied to the potentiostat input, the cell voltage is rapidly altered to raise the reference-to-blocking electrode voltage to the new input level. Since the blocking electrode must be repolarized at the new potential and

(7) B. Ilschner, *J. Chem. Phys.*, 28, 1109 (1958).

this requires a finite amount of charge transfer, the step voltage will initially appear as iR drop in the electrolyte between the reference and blocking electrodes. Eventually, when recharging is complete, the step voltage will be taken up entirely as altered voltage across the blocking electrode. The net result of this arrangement is the same as if the voltage step were applied directly across the cell with a two-electrode setup employing an ideal unpolarizable counterelectrode. Thus, counterelectrode effects in the blocking electrode recharging kinetics are avoided.

In further efforts to meet the above-listed objectives, both single-crystal and polycrystalline Pt foil were employed as blocking electrodes, as well as stress-annealed pyrolytic graphite, which provides a smooth, nonporous cleavage surface with a high degree of c-axis orientation. A number of electrode-interface preparations were used. A current-integrating function was added to the circuitry to measure long-term, low-level charging effects.

In addition to the potentiostatic studies, it was of interest to examine some aspects of the AgBr|blocking electrode interface under constant-current conditions. Galvanostatic experiments would be expected to yield both independent information on double-layer capacitance and a picture of the voltage requirements for plating out the first few monolayers of metallic Ag on an initially bare blocking electrode. The latter information should provide a check on our previous suggestions regarding Ag monolayer buildup as the decomposition potential is approached and be of intrinsic interest as well.

Consider a galvanostatic experiment on cell II above, where a constant current is to be passed through the cell and the voltage, V, between reference and blocking electrodes monitored. If the cell is initially potentiostated at a polarizing voltage V_0 where a_{Ag} is low (typically -0.3 v, where $a_{Ag} \sim 0.0015$ at our temperatures) and then switched to a constant-current source which conducts Ag^+ ions to the blocking interface, there should be a considerable voltage span, before the decomposition potential is reached, in which the predominant electrode process is double-layer charging. In this range, the effective double-layer capacitance, C, in response to the charging current is given by $\partial V/\partial t = i/C$. If C is relatively constant in this range, the integrated voltage–time expression will be

$$V = V_0 + iR + (it/C) \qquad (1)$$

where R is the effective electrolyte resistance between the reference and blocking electrodes. The situation is shown schematically in Figure 1. As decomposition potential $\mathcal{E}_d$ (0 v in cell II) is approached, faradaic or

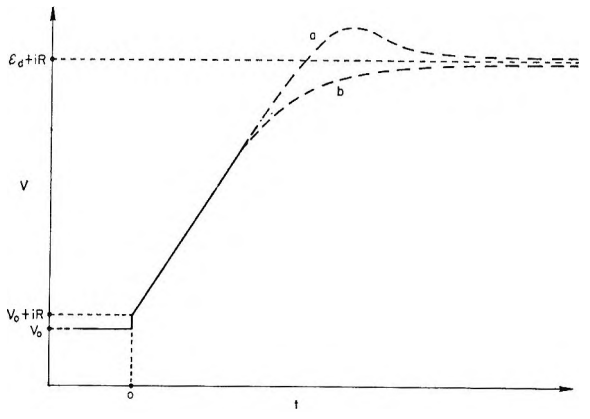

Figure 1. Schematic of expected galvanostatic voltage–time behavior in cell II for the cases of (a) discharge with an activation barrier and (b) discharge commencing with monolayer buildup.

Ag electrodeposition effects should set in. Two possible results are depicted. In one case, if an activation barrier were involved in the discharge of the first few Ag° atoms, a transient overvoltage peak would result, with a relatively linear double-layer charging slope up to this point. In the second case, if Ag discharge at subunit activity and consequent monolayer buildoccurred as $\mathcal{E}_d$ was approached, one would expect a voltage roundoff and nc activation overvoltage peak, since steady-state discharge would be occurring onto a preplated Ag surface.

Further information may also be obtained from such charging curves. If the double-layer capacitance were found to be relatively constant in the low a_{Ag} voltage region, it should be possible to subtract its contribution from the total charge transfer it at time t to obtain the faradaic contribution. This should allow estimates of the number of Ag atoms involved in nucleation if an activated discharge were involved or of the fractional monolayer coverage as a function of a_{Ag} in the case of monolayer buildup. Galvanostatic experiments of this type were carried out with both Pt and graphite electrodes.

Experimental Section

Materials. A 0.25-in. diameter single-crystal rod of 99.999% AgBr received from Semi-Elements, Inc. was machined into $^1/_4$- or $^3/_{16}$-in. diameter pellets $\sim$0.1 in. thick, using a diamond or tungsten carbide cutting tool. The pellets were cleaned as previously described.[8] High-purity 1-mil silver foil, employed for the counterelectrode, was washed in 2 M KCN, thoroughly rinsed, and tissue dried before cell assembly.

(8) D. O Raleigh, *J. Phys. Chem. Solids*, 26, 329 (1965).

In one cell, the blocking electrode was mirror-smooth, high-purity polycrystalline Pt foil of the type employed previously.

For Pt single-crystal runs, it was desired to obtain a smooth single-crystal surface with a relatively low dislocation density but no particular crystallographic orientation. For this purpose, a $^1/_{16}$-in. thick slice from a $^1/_4$-in. diameter high-purity single-crystal Pt rod was obtained from the Materials Research Corp. An X-ray Laue pattern showed a good deal of surface damage from cutting, so 10 mils of one face was removed by spark cutting. The crystal pellet was then electropolished to a semismooth finish, annealed overnight in air at 1500°, and further electropolished to a specular finish. A final X-ray Laue pattern showed only a small amount of remnant nonideality, whose quality suggested the presence of some subboundaries rather than surface dislocations.

Obtaining a specular surface by electropolishing involved a good deal of trial and error. After a number of aqueous polishing baths were tried without success, a 48 mole % KCl–52 mole % NaCl fused-salt bath, as recommended by Brouillet and Epelboin,[9] was employed. The salt melt, contained in a Pt crucible that served as cathode, was centered in a vertical tube furnace through which the crystal pellet, suspended by a Pt wire, was lowered and raised gradually to minimize thermal shock. A temperature range 720–750° was employed. Best results were obtained with a 0.25-amp/cm^2 current density and gentle pendulation of the pellet during polishing. Following electropolishing and cooling, the pellet was rinsed and gently tissue dried. In one run, no further surface treatment was carried out, while in another, the pellet was boiled in concentrated HBr and then rinsed and dried to observe the relative effects.

For graphite blocking electrodes, several pieces of stress-annealed pyrolytic graphite were obtained from Dr. Paul Schlichta of the Jet Propulsion Laboratory. These cleaved readily to provide a fairly smooth and planar light-reflecting surface. In view of their high degree of *c*-axis orientation (perpendicular to the cleavage plane), such surfaces were felt to represent the best approach to a single-crystal graphite surface.

Apparatus and Procedures. Cells were assembled by springloading the AgBr electrolyte pellet between the counter- and blocking electrodes in an apparatus similar to that used previously[8] in bromine electrode runs, except that the concentric tube arrangement used for the bromine electrode was replaced by a simple Pyrex plunger tube with a fitted nickel block on the end. All cell leads were platinum, the reference electrode consisting of a short length of 20-mil Ag wire spot-welded to a Pt lead wire. The reference electrode was attached by resting its tip on the periphery of the AgBr pellet in the assembled cell, directing a stream of argon to the area, and briefly heating the wire with a microtorch to melt the AgBr locally at the point of contact. This resulted in a secure attachment.

The cell arrangement was placed in the furnace tube setup described previously[8] and outgassed overnight at room temperature and for one to several hours at 200° with a polarizing cell bias. Subsequent procedures were deliberately varied from run to run. In one run with polycrystalline Pt foil, the cell was heated to 410° in flowing argon and manually compressed as a means of forming the electrode contacts. (AgBr at these temperatures is quite plastic and readily adapts to the electrode surface.) In the next run with the same cell, the cell was briefly heated in argon to the melting point of AgBr (425°) to cause local melting at both electrodes. In two runs with single-crystal Pt, the cell was heated under compression to within 1–2° of the melting point, using an argon atmosphere in the first and vacuum in the second. In the two graphite runs, local electrolyte melting was carried out in both, using argon in the first run and vacuum in the second. Following the above, the cell was cooled under flowing argon to one of the two measuring temperatures (244 and 292°) used in our studies. In all runs, the cell was always maintained under a polarizing potential (except during the brief galvanostatic sweeps) to preserve the character of the blocking interface.

Circuitry. The cell circuitry, consisting of a potentiostat, galvanostat, a means of fast switching between the two types of operation, and a current integrator, is shown in Figure 2. The potentiostatic portion is the same as used previously,[6] except that the amplifier feedback is connected to the reference electrode through a follower amplifier as in conventional potentiostatic operation.[10] As before, the input base and step voltages for voltage step studies are provided by a pair of battery-operated voltage dividers connected by a mercury relay (S1). Current–time transients in response to steps were monitored with a differential-amplifier oscilloscope across a 50–200-ohm measuring resistance, adjusted to provide approximate full-scale deflection. In the present arrangement, it was found necessary to include a 50-pf stabilizing capacitor across the amplifier during steady-state operation and 400 pf additional capacitance during warmup to achieve stable

(9) P. Brouillet and I. Epelboin, *Compt. Rend.*, 237, 895 (1953).

(10) See, for instance, G. Lauer and R. A. Osteryoung, *Anal. Chem.*, 38, 1106 (1966).

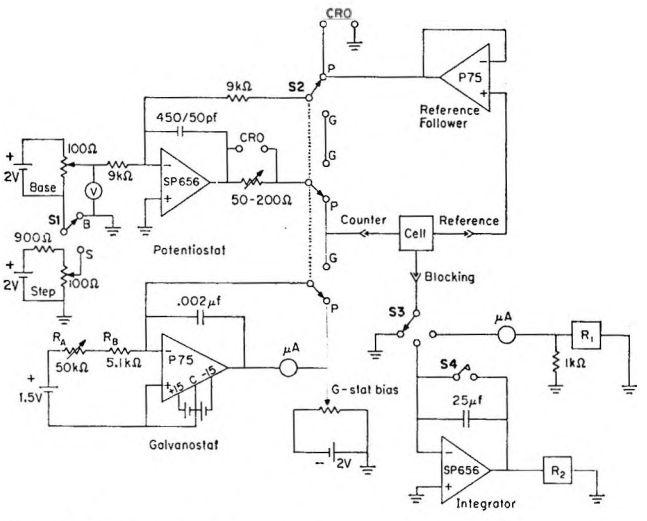

Figure 2. Circuitry diagram.

operation. In steady-state operation, voltage steps with a 10-μsec rise time were obtained.

Noise-free constant-current operation in the 25–250-μa range was obtained as shown with an ungrounded and battery-operated Philbrick P75 operational amplifier, resistors R_A and R_B providing current-adjusting and current-limiting functions. Fast switching from potentiostatic to galvanostatic operation was achieved with three Clare mercury relays in tandem (S2), P and G showing the switch positions for the two operations. Current surges in P → G switching were avoided by biasing the galvanostat output in the P position at a voltage equal to the potentiostat output. In galvanostatic operation, the cell voltage was oscilloscope monitored from the reference follower output. With this arrangement, voltage–time data reflecting submonolayer level electrodeposition could be conveniently obtained.

Switch S3, which is normally to ground, may be switched to the middle position to provide a current-integrating function or to the right position to monitor any steady-state cell current *via* a microammeter and strip-chart recorder R_1. Opening shunt switch S4 initiates current integration, in which the accumulated charge across a 25-μf precision polystyrene capacitor is measured by R_2, a Moseley Model 2D2A X–Y recorder. Charge accumulations could be conveniently measured to the nearest 0.01 μcoulomb with this arrangement. For stablest operation, it was found necessary to separate the recorder and integrator by a voltage follower.

Results

Potentiostatic. Cells assembled and pretreated as above were found to exhibit the same ideal ionic current-blocking behavior as the previous bromine electrode cells. In the range of polarizing potential employed (0.02–0.3 v), the steady-state cell current, presumably electronic, ranged from 0.1 to 0.2 μa at 292° and was considerably smaller at 244°. As expected, voltage step application gave reproducible current transients that decayed asymptotically toward zero on the millisecond time scale. Peak current values showed an average electrolyte resistance between reference and blocking electrodes of about 20 ohms at 292° and 100 ohms at 244°. As determined by the steady-state voltage between reference and counterelectrodes, the reference electrode voltage was stable and drift free to within 1 mv.

In Pt runs, much the same qualitative results were obtained as in the previous work with bromine electrode cells. At both temperatures, 50- or 100-mv voltage steps at cell voltages corresponding to a low a_{Ag} (0.1–0.3 v) gave similar oscillographic current–time traces that were symmetric with respect to step direction. At higher a_{Ag} values (0.02–0.1 v), the current duration and hence the total charge transfer increased considerably. In addition, asymmetry with respect to the step direction set in, repolarization appearing to take longer for steps that increased a_{Ag} than for steps that decreased it. All this is consistent with the previously suggested picture of the gradual electrodeposition of an Ag° monolayer as $a_{Ag} = 1$ is approached.

In graphite runs, current transients decayed much more rapidly, indicating at least an order of magnitude smaller total charge transfer. Moreover, current–time traces were extremely symmetric with respect to step direction throughout the entire voltage range and showed no particular increase in charge transfer at high a_{Ag} voltages. Charge transfers at the two temperatures were comparable. These results were taken to indicate an absence of any tendency for either Ag^+ ions or Ag° atoms to adsorb on the graphite surface, the low charge transfer seeming to indicate pure diffuse double-layer charging.

A common result of all runs, regardless of electrode or cell preparation, was the failure of the current transients to decay with a single time constant. Thus, in no instance did the electrode interface behave as an ideal capacitor, even with uniaxial current flow geometry and counterelectrode effects compensated for. This is perhaps to be considered in the light of similar results for solid electrodes in aqueous media,[11] where the analogous effect is a frequency dependence of the ac capacitance. As before, log *i vs. t* plots could be

(11) See, for instance, P. Delahay, "Double Layer and Electrode Kinetics," Interscience Publishers, Inc., New York, N. Y., 1965, p 129.

graphically resolved into a mixture of two time constants with a good fit, but the occasional indication of a small, short-lived third component and the inevitable presence of a long-time low-level "tail" component indicates the two-time-constant model may be little more than an empirical first-order description of the recharging kinetics accompanying the bulk of the voltage change across the blocking interface.

Use of the current integrator permitted direct observation of the above-mentioned long-term low-level currents and their contribution to the total charge transfer. When a voltage step $V_0 \rightarrow V_1$ was applied, an immediate recorder pen displacement occurred, measuring the accumulated fast charge transfer up to ~0.25 sec. This was followed by a slow further charge accumulation lasting some tens of seconds in platinum cells and several minutes in graphite cells. In all cases, there appeared an eventual cessation in the charge transfer as the cell current fell to its small steady-state value. When a reverse voltage step $V_1 \rightarrow V_0$ was subsequently applied, the same general behavior with reversed current was observed. Figure 3 shows a schematic of typical charge-transfer data obtained in this manner.

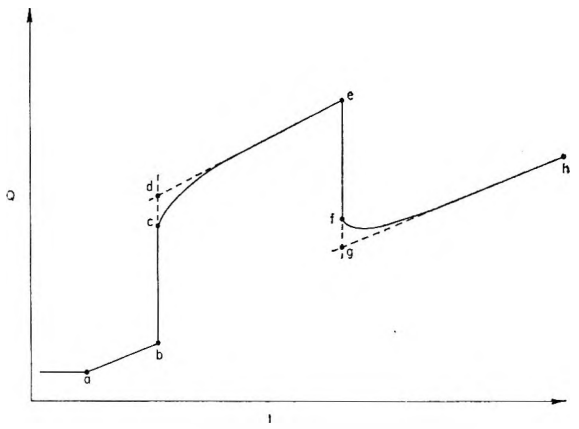

Figure 3. Schematic current integrator data trace: a, prestep integration started; ab, steady-state cell current slope at V_0; bc, fast response to voltage step $V_0 \rightarrow V_1$; bd, total charge transfer for $V_0 \rightarrow V_1$; de, steady-state current slope at V_1; ef and eg, fast and total charge transfers for return step $V_1 \rightarrow V_0$; gh, steady-state current slope at V_0.

For comparison with current integrator data, "fast" charge-transfer values were calculated as in the previous work by straightforward integration of the oscillographic current–time data on the basis of the two-time-constant model. The comparison showed, as Figure 3 indicates, a considerable contribution from slow charge transfer, ranging from as little as 5% of the total in Pt cells to as much as 78% in graphite cells. Actual ranges were 5–33% with Pt and 64–78% with graphite. The immediate recorder pen displacement on the current integrator, to which no special significance is attached, but which serves as an intermediate time scale between the "fast" and total charge transfers, gave values of the order of or somewhat larger than the "fast" transfers in Pt cells and distinctly intermediate values with graphite cells. From these results and the above-noted longer duration of charging currents with graphite, it is apparent that the total charging or interface repolarization process goes much more slowly with graphite.

It was at first thought that these residual currents might be faradaic diffusion currents rather than true double-layer charging currents, representing Ag discharge and diffusion into the bulk of the electrode. Since applying a steady-state voltage, V, fixes a silver activity $\exp[-V\mathfrak{F}/RT]$ at the electrode interface, voltage steps that increase a_{Ag} result in whatever charge transfer is required to achieve the new activity at the interface. This will include both double-layer recharging and whatever Ag^+ discharge is required to saturate the interface with Ag° atoms at the new activity. If significant diffusion of Ag° atoms into the electrode can occur at this activity, charge transfer will continue in order to replace those Ag° atoms lost into the electrode. A cell current would then persist until the kinetics of the diffusion process became negligible. Likewise, voltage steps that reduced a_{Ag} could result in a residual cell current representing extraction of Ag° atoms from electrode regions near the interface.

All the experimental findings, however, indicate that a diffusion current was not involved. First, any contribution to the total charge transfer from diffusion should be greater at cell voltages corresponding to a high a_{Ag}. Instead, the residual charge transfer at low a_{Ag} biases was at least as great and was generally a greater fraction of the total charge transfer than at high a_{Ag} values. Second, current effects from diffusion should be larger and longer lived at the higher temperature. Instead, the residual charge-transfer contribution was about the same fraction of the total at the two temperatures and was actually somewhat longer lived at the lower temperature. Moreover, diffusion should involve a nonconservation of charge transfer, in that a portion of the Ag° transferred into the electrode in an a_{Ag} increasing step should be irrecoverable on subsequently applying the reverse step. Total charge transfers were, in fact, found to be independent of step direction within the limit of error of the measurement (1–3%). Accordingly, it is concluded that the residual cell currents reflect some slow relaxation process in the double-layer charging rather than an electrode diffusion effect.

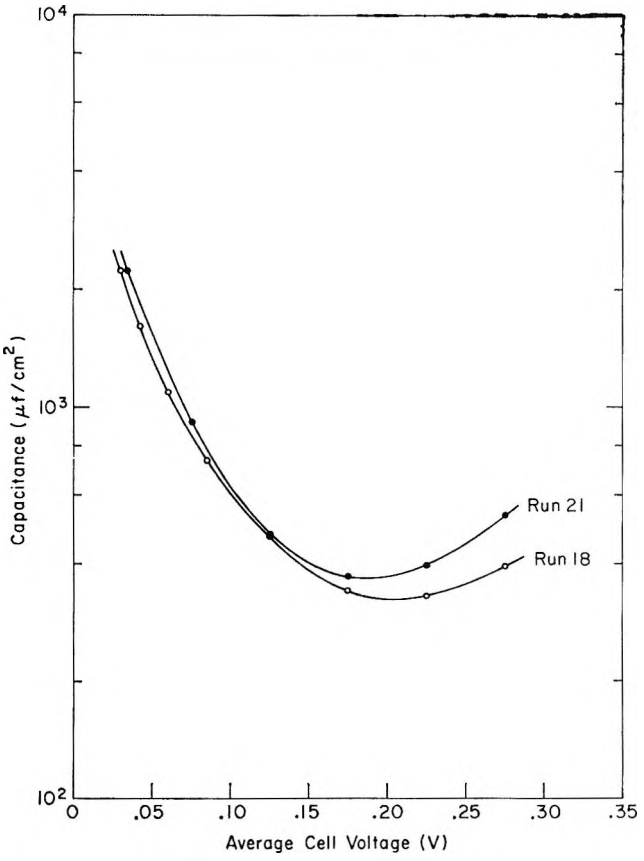

Figure 4. Effective total capacitance of the AgBr|Pt interface as a function of average cell voltage in runs 18 and 21. Capacitance values were calculated from charge transfers in response to 50-mv voltage steps.

The general result of charge-transfer comparisons for Pt cells with various electrode types and interface preparations was that, while such factors result in second-order differences in the capacitance–voltage curves, their general character and high double-layer capacitance are an intrinsic property of the AgBr|Pt interface, not substantially affected, for instance, by whether the Pt electrode is polycrystalline or single crystal. Figure 4, for example, shows the total (current integrator) capacitance as a function of cell voltage from two runs in which charge-transfer data were taken in sufficient detail (at 50-mv intervals) to provide curves which approximate fairly well the effective differential capacitance. In run 18, a polycrystalline Pt foil was employed and the electrolyte interface was melted at the start of the run. In run 21, the Pt single crystal, prerinsed in boiling HBr, was employed and the interface was heated to within 1–2° of the electrolyte melting point under compression and under vacuum at the start of the run. The data shown were obtained at 292°; similar though somewhat smaller (~10%) capacitance data were obtained at 244°. The Figure 4 curves show a real difference at the high-voltage (low a_{Ag}) end, but generally similar values and variation with cell voltage.

Table I: Comparative Total Charge-Transfer Data with Polycrystalline and Single-Crystal Platinum

Temp, °C	Voltage step, v	Charge transfer, μcoulombs/cm² Run 18	Run 20
292	0.1 → 0.2	40.5	40.4
292	0.2 → 0.3	36.4	33.8
244	0.1 → 0.2	36.1	34.9
244	0.2 → 0.3	36.0	32.2

In another comparison, Table I shows the total charge-transfer values measured with low a_{Ag} voltage steps in runs 18 and 20 at the two temperatures. In run 20, the single crystal was used without HBr pretreatment and the interface heated to within 1–2° of the electrolyte melting point under argon. Charge-transfer values agree to an average of ~5%. Since it would seem highly unlikely that the same degree of surface inhomogeneity would exist in run 18 with a polycrystalline foil and run 20 with an annealed, electropolished single crystal, it must be concluded that such inhomogeneities are not primarily reponsible for the high double-layer capacitances observed.

A good deal more scatter was observed in the "fast" capacitance values determined from graphical analysis of oscillographic sweeps. Figure 5 shows rough capacitance–voltage curves at 292° from three runs, together with the total capacitance curve from run 18 for comparison. Again, values at 244° were similar, though ~10% smaller. The dashed curves are rather rough approximations to the differential capacitance in that 100-mv voltage steps were employed. Run 17 was made with the same cell as run 18, except that the cell was heated to 410° in argon and manually compressed to form the interface contacts. The Figure 5 data show the same general voltage dependence as the total charge-transfer data, consisting of a relatively flat portion at low a_{Ag} voltages (somewhat obscured in the semilog plots) and an abrupt rise as the Ag discharge potential is approached. Values at the capacitance minimum appear to straddle the previously reported value of 200 $\mu f/cm^2$ from Br_2 cells. Because of the greater degree of scatter than in the total charge-transfer data, it is felt that the latter represent the more physically significant measurement.

As indicated, both the "fast" and total charge-

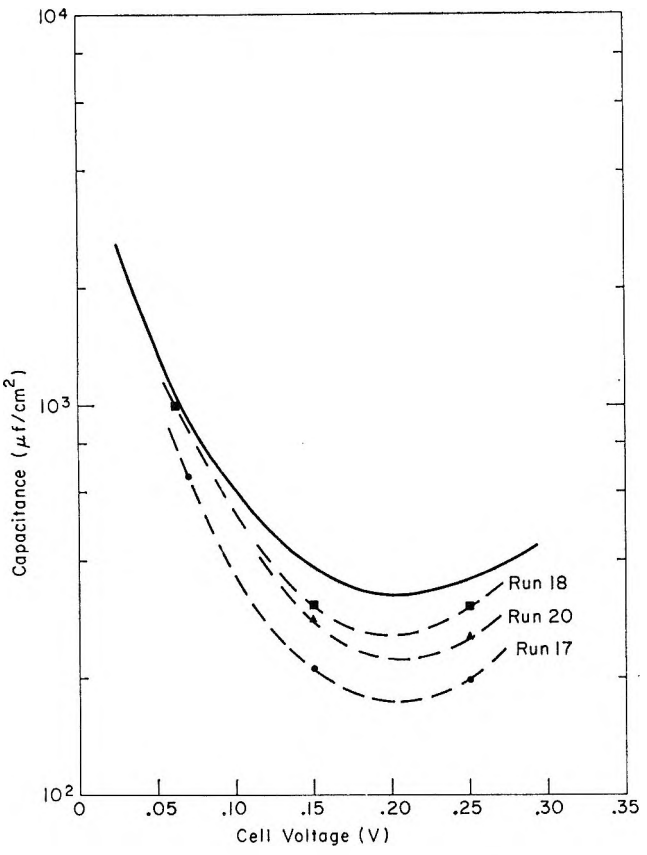

Figure 5. Effective "fast" capacitance of the AgBr|Pt interface as a function of average cell voltage in runs 17, 18, and 20 (dashed lines), compared with effective total capacitance in run 18 (solid line). Capacitance values were calculated from charge transfers in response to 100-mv voltage steps.

transfer values were an order of magnitude lower for graphite cells and showed none of the capacitance–voltage behavior in Pt indicative of preplating or monolayer buildup as the Ag discharge potential was approached. Since the relatively large double-layer capacitance against Pt is attributed to ion-adsorption effects on the electrode, it is of interest to compare the graphite C_{dl} results with theoretical predictions on the basis of a pure diffuse double-layer model. As noted previously,[6] Grimley and Mott[12] developed such a model for discussing equilibria at the Ag|AgBr interface, which may be generalized to AgBr|inert electrode interfaces in a straightforward manner. The result is the capacitance equation

$$C_{dl} = \left(\frac{KN}{8\pi kT}\right)^{1/2}\left\{\frac{eV}{kT} + \ln\frac{n_0}{N}\right\}^{-1/2} \qquad (2)$$

where K is the static dielectric constant of AgBr, n_0 is the equilibrium concentration of ionized Frenkel defect pairs in the bulk of the AgBr crystal, N is the number density of anionic or cationic lattice sites, and V is the potential across the interface. In this model, a diffuse double-layer charge is developed in AgBr, which is known to conduct ionic current *via* a Frenkel defect structure,[5] as an excess of Ag^+ cation vacancies over Ag^+ interstitials in the neighborhood of the interface. Capacitance or charge storage results from alteration of the defect concentration profiles as voltage V is changed.

Predicted values of C_{dl} were calculated from eq 2, using available values[13,14] of K and n_0/N together with the Grimley–Mott estimate of the Ag|AgBr absolute electrode potential to obtain values of V corresponding to our cell potentials. As noted previously, the expression predicts a very small temperature dependence for C_{dl} under our conditions. In Table II, observed total charge transfers from current integrator data on a graphite cell prepared by interface melting under vacuum are converted to average capacitances by dividing by the size of the voltage step and compared with the prediction of eq 2. Surprisingly good agreement is seen for the results at 292° and factor-of-two agreement at 244°. It would seem, then, that the assumption of pure diffuse double-layer charging in graphite is a reasonable one. It would also seem indicated, from the more long-lived nature of the charging process in graphite than with Pt, that the slow relaxation process previously referred to is more likely to be associated with the diffuse double layer, since the preponderant charging process in Pt is assumed to be ion adsorption. Frenkel pair formation and recombination in the diffuse double layer, as discussed briefly by Friauf,[15] is a possible source of the slow relaxation

Table II: Observed and Predicted Capacitances for Graphite Cell

Temp, °C	Voltage step, v	Capacitance, μf/cm² Observed	Predicted
292	0.02 → 0.1	41.3	49.5
292	0.1 → 0.2	40.5	47.6
292	0.2 → 0.3	45.5	45.7
244	0.02 → 0.1	29.3	48.3
244	0.1 → 0.2	25.9	46.5
244	0.2 → 0.3	33.5	44.4

(12) T. B. Grimley and N. F. Mott, *Discussions Faraday Soc.*, **1**, 3 (1947).

(13) G. Everett, A. W. Lawson, and G. E. Smith, *Phys. Rev.*, **123**, 1589 (1961).

(14) J. Teltow, *Ann. Physik*, **5**, 71 (1949).

(15) R. J. Friauf, *J. Chem. Phys.*, **22**, 1329 (1954).

process. The scatter, however, in the "fast" charge transfer results for Pt indicate the precise nature of the interface may also play a role.

Galvanostatic: Platinum. Galvanostatic experiments were carried out in two of the Pt runs (18 and 20) and in two graphite runs. In these, the cell was initially potentiostatted at −0.3 v to provide a low steady-state silver activity and then switched to a 25–250-μa constant current, the blocking electrode voltage being monitored oscillographically as described. Results will first be reported for the case of Pt electrodes.

Figure 6 shows a typical voltage–time sweep for a Pt cell, using two oscilloscope sweep rates to display both the initial rise and plateau portions of the curve. The degree of electrodeposition involved is in the fractional- to several-monolayer region. In each sweep picture, the bottom horizontal line shows the initial "presweep" polarizing voltage and the top line the theoretical cell discharge potential, $\mathcal{E}_d$, (0 v). The same general voltage–time behavior was observed with polycrystalline and single-crystal Pt electrodes and at both temperatures. In all cases with Pt electrodes, the voltage first rose monotonically through an approximately linear region and then rounded out to a very flat plateau quite close to the theoretical $\mathcal{E}_d$, with no observable overvoltage peak. The small plateau voltage in excess of $\mathcal{E}_d$ was in all cases largely, though not entirely, accountable as iR drop between the reference and blocking electrodes. It appears, then, that the platinum electrode behavior at $\mathcal{E}_d$ closely resembles that of an ideal silver electrode, even when no more than one to several monolayers of silver have been discharged.

Repeat galvanostatic sweeps under the same conditions were found to be precisely reproducible, provided the cell was returned to a polarizing potential to strip off the plated Ag after no more than several monolayers of plating current were passed (~1500 μcoulombs/cm^2). For substantially greater total charge transfers, the fine details of the voltage behavior in the late plateau region became somewhat irreproducible from sweep to sweep and some interface deterioration was observed on return to the polarizing potential. This deterioration showed up as a lowered double-layer capacitance for the bare Pt interface. Since the primary interest in this work was in the *initial* electrodeposition behavior, total charge transfers on galvanostatic sweeps were limited to several monolayers to avoid these effects.

Voltage–time traces obtained at various current levels were compared directly by displaying them superposed on the storage mode of the oscilloscope screen, using appropriate sweep rates so that the same

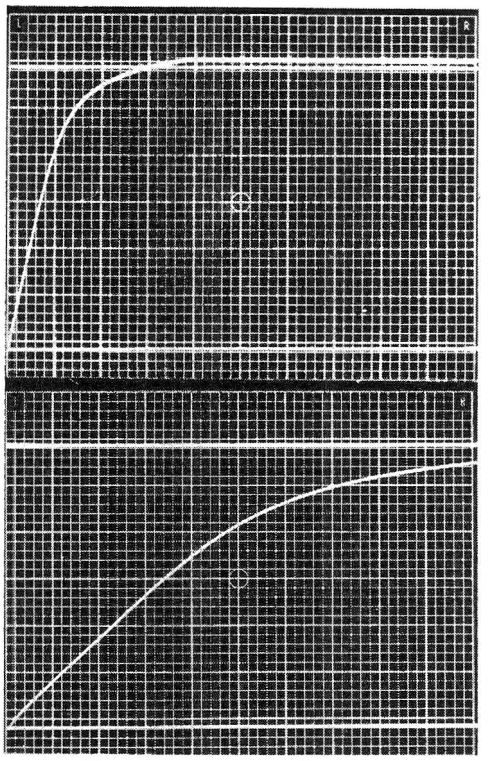

Figure 6. Galvanostatic voltage–time sweeps in run 18 (polycrystalline Pt electrode) at 244°: current, 50 μa (≈140 μa/cm^2); vertical scale, 50 mv/cm; horizontal scale, 0.5 sec/cm (upper), 0.1 sec/cm (lower); two successive sweeps superposed in each case.

displacement along the abscissa corresponded to the same total charge transfer at each current level. A result for run 18 at 292° is shown in Figure 7. The small spread in the traces is narrowed even further if different iR corrections in the separate sweeps are accounted for. The essential congruence of the sweeps shows that the charging and electrodeposition processes at these current levels occur essentially as equilibrium processes.

As noted, the initial portions of the galvanostatic curves show an approximately linear voltage rise, attributed to pure capacitative charging. Capacitances calculated from the slopes of these voltage rises were in reasonable agreement with, though generally somewhat higher (5–10%) than the "fast" capacitances graphically derived from the oscillographic potentiostat data on the basis of the two-time-constant model. This might be expected, since a longer time scale is involved in the galvanostatic charging process, allowing some contribution from the slow charging effects previously discussed.

Two additional details of the initial galvanostatic voltage rises are of interest. At the higher temperature some concave upward curvature (*e.g.*, Figure 7) was

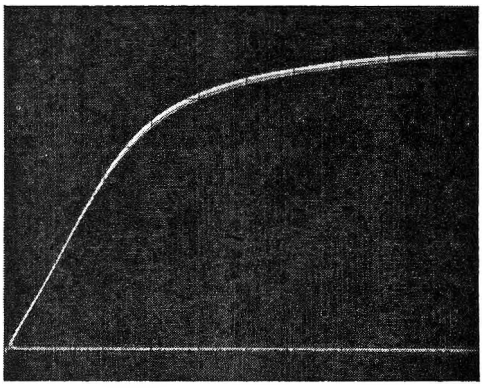

Figure 7. Superposed galvanostatic voltage–time sweeps in run 18 at 50, 100, and 200 μa (292°): vertical scale, 50 mv/cm; horizontal scale, 10 μcoulombs/cm (0.2 sec/cm for 50 μa, 0.1 sec/cm for 100 μa, 0.05 sec/cm for 200 μa). Horizontal zero-voltage line omitted for clarity.

always noted at the start of the voltage rise. This is in agreement with the finding that both "fast" and total capacitances were always somewhat greater at the high-voltage end (0.3 v) than in the middle of the cell voltage span, so is not surprising. At the lower temperature, however, the curvature in this region was always *convex* upward. This is especially interesting since it is the behavior one would expect at this temperature from the two-time-constant model. The equivalent electrical circuit for this model consists of two RC series loads in parallel. If a constant current is applied to such a circuit, it can be shown that its final ($t = \infty$) effective capacitance in the charging process will be given by $(C_1 + C_2)$, but that a smaller effective capacitance will initially obtain for a time comparable with the average of the RC charging times involved. At 292°, the RC charging times involved were too fast to be seen on the time scale of the galvanostatic sweep but, at 244°, they represent the order-of-magnitude time span in which the concave upward curvature is observed. Thus, the two-time-constant model appears to continue to be a useful one in describing relatively rapid charging processes at the interfaces in question.

Despite the above-noted deviations from linearity, the initial voltage rise curves nonetheless displayed sufficiently linear behavior over a wide enough portion of the total voltage span to derive a single effective capacitance value to describe the over-all capacitative charging behavior fairly well. This characteristic is especially useful, since it permits us to divide the total charge transfer, Q, at any point (V, t) on a curve into capacitative (or double-layer) charging and faradaic (or Ag electrodeposition) components with reasonable accuracy. The result permits a test of the monolayer deposition model for the buildup of plated Ag as $\mathcal{E}_d$ is approached. If the galvanostatic sweep was started at voltage V_0, then the faradaic contribution at point (V, t) should be

$$Q_f = it - C[(V - iR) - V_0] \qquad (3)$$

where R can be determined from the potentiostatic data. Moreover, since 240 μcoulombs/cm^2 is the charge required to plate a monolayer of metallic silver, Q_f can be reduced to the fraction of full monolayer coverage at the point (V, t), assuming the geometric electrode interface area to be the actual area. Furthermore, since $(V - iR)$ is the galvanic potential of the cell Ag|AgBr|Pt(Ag), this voltage may be directly converted to the activity of silver at the blocking interface, as discussed previously. Thus, the net result is data on the activity of silver at the interface as a function of the fraction of ideal monolayer coverage by plated Ag.

Figure 8 shows a log–log plot of galvanostatic data from run 18 (polycrystalline Pt) reduced in this manner, using data from two current levels at the lower temperature. Substantially identical data were obtained with the single-crystal Pt electrode. In all cases, the silver activity data showed a roundoff to a plateau in the neighborhood of 1.0 ideal monolayer coverage, indicating the general validity of the monolayer buildup model. A further general result was the apparent well-defined power relationship between silver activity and fractional coverage over a wide range of these values. From the slopes of the curves in Figure 8 and those obtained in the single-crystal run at the two temperatures, a_{Ag} = (fractional coverage)^n with $n = 0.57 \pm 5\%$. From mass-action considerations, such a power dependence would suggest some random degree of association of plated Ag atoms on the Pt surface, though other factors may also be involved.

It was mentioned previously that a small, constant plateau voltage above the theoretical $\mathcal{E}_d$ was generally obtained, in excess of that attributable to iR drop.

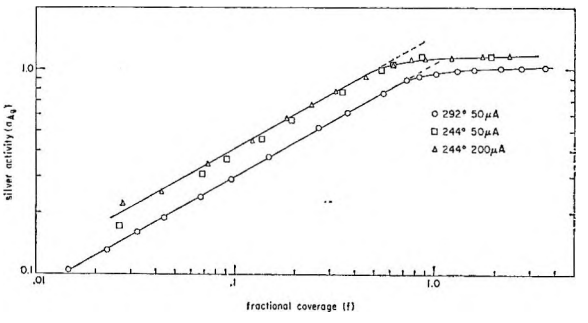

Figure 8. Log–log plot of silver activity at Pt interface *vs.* fraction of ideal monolayer coverage derived from run 18 galvanostatic data.

This excess voltage, which appears in the 244° curve of Figure 8 as a silver activity in excess of unity, amounted to about 6 mv at 244° in the two runs and some smaller, less certain value in 292° sweeps. Because of its apparent independence of the current level, it was felt at first to represent some variety of thin-film activity augmentation above that characteristic of bulk Ag. In a test in a single-crystal run, however, the cell was momentarily disconnected during a galvanostatic sweep without placing it back on the potentiostat, *i.e.*, isolated, and the effect on this excess voltage observed. The result is shown in Figure 9 in an oscillograph that greatly magnifies the plateau-level voltage. In this sweep, the cell had just reached plateau voltage and was disconnected midsweep. Cessation of the galvanostatic current was seen to result in an immediate voltage drop that matched the expected iR contribution and a finite-lived further drop to the theoretical $\mathcal{E}_d$. This result suggests the excess voltage represents some manner of polarization, but the occurrence of some type of stress relaxation in the thin Ag electrodeposit cannot be ruled out. In short, the slight excess voltages observed suggest some type of second-order nonequilibrium effect, but the data are insufficient to ascertain its nature.

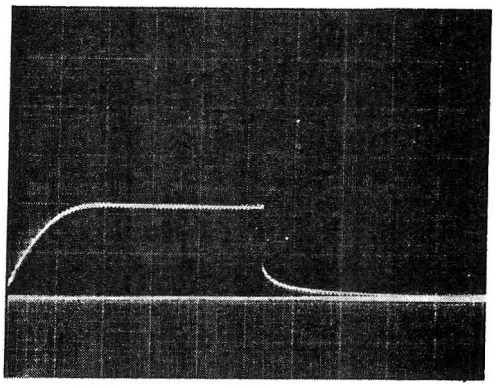

Figure 9. Effect of cell isolation on excess plateau voltage during galvanostatic sweep. Run 20, 244°, 100-μa current level: vertical scale, 10 mv/cm; horizontal scale, 0.2 sec/cm. Bottom horizontal line is theoretical $\mathcal{E}_d$ (0 v).

Galvanostatic: Graphite. Considerably different galvanostatic behavior was observed with graphite electrodes. All the features of this behavior, in fact, indicate an activated electrodeposition involving a relatively small number of sites on the graphite surface and leading to dendritic growth rather than smooth deposition of monolayers. Figure 10 shows two successive galvanostatic sweeps on a graphite cell, using different sweep speeds. In all such curves, an overvoltage peak was obtained, with a subsequent dropoff to a relatively slow-falling voltage still considerably in excess of the theoretical $\mathcal{E}_d$. Such peaks always occurred at total charge transfers quite small compared to that required to discharge an ideal Ag monolayer. In Figure 10, for instance, the *total* charge transfer at the overvoltage peak, containing an obviously large capacitative charging contribution, amounts to about 2% of an Ag monolayer. The occurrence of dendritic growth was ascertained by microscopic examination of the electrode interface after a run in which a relatively large amount of discharge current was applied as a final step. The microdendrite pattern appeared randomly distributed, bearing no particular relation to topographical features of the pyrolytic graphite cleavage surface.

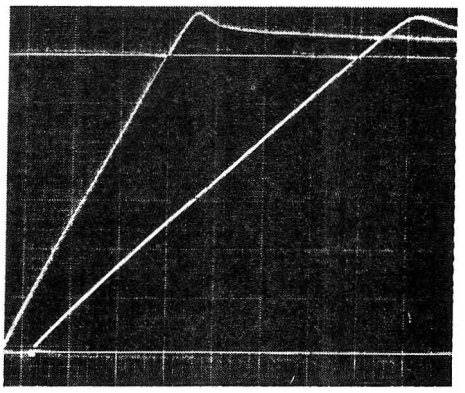

Figure 10. Galvanostatic voltage–time sweeps in run 22 (graphite, interface preparation by vacuum melting) at 292°: current, 50 μa ($\approx$125 μa/cm^2); vertical scale, 50 mv/cm; horizontal scale, 5 msec/cm (right curve), 10 msec/cm (left curve).

Individual galvanostatic sweeps were precisely reproducible up to the neighborhood of the overvoltage peak and fairly, though not exactly, reproducible thereafter. Peak heights at the 50-μa current level ranged from 40 to 45 mv at 292°, about twice this large at 244°, and increased considerably with increasing current level. Figure 11 shows the effect of current, again using sweep rates for the different current levels such that the total charge transfer at a given horizontal displacement from the start of the sweep is the same in each case. As in the platinum runs, electrode interface deterioration was observed to occur if excessive total charge transfers were applied, though the maximum acceptable charge transfer (one to several microcoulombs) was very much lower than for Pt.

As noted before, the electrode interface preparation in the two graphite runs involved flash melting of the pellet to the electrode in both, but with an argon atmosphere in one run and under vacuum in the other. The qualitative results in the two runs were the same in all respects but one. In the run using

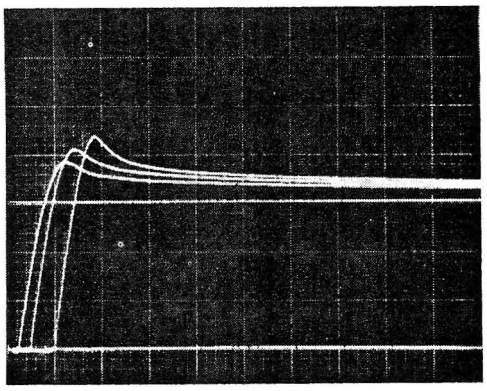

Figure 11. Galvanostatic voltage–time sweeps at 292° in run 19 (graphite, interface preparation by melting in argon) at 50, 100, and 200 μa (125, 250, and 500 μa/cm^2). Peak height increases with current level: vertical scale, 100 mv/cm; horizontal scale, 20 msec/cm (50 μa), 10 msec/cm (100 μa), 5 msec/cm (200 μa).

vacuum melting, the voltage-rise portions of the galvanostatic curves were extremely linear, as seen in Figure 10. The capacitances derived from the curve slope in this region were about 50% larger than those from the graphical analyses of the oscillographic potentiostatic data, but gave an excellent match to values derived from the "immediate" portion of the current integrator data (Figure 3, line *bc*). Since the latter values represent a somewhat comparable time scale to the galvanostatic charging, this result is reasonable and is consistent with the relatively protracted nature of the over-all charging process with a graphite electrode. In the run using argon melting, however, the voltage-rise portions of the galvanostatic curves showed a general curvature and, more importantly, gave capacitance values even smaller than those derived from the oscillographic potentiostatic data. This result seems to defy explanation. It was felt to reflect some unusual interface condition, possibly resulting from the presence of adsorbed furnace gas molecules at the interface. At any rate, in view of the more reasonable results obtained in the run with vacuum melting, it was felt that the latter run offered results of greater physical significance.

The good linearity in the voltage-rise portions of curves from the latter run offers a means of estimating the total faradaic charge transfer involved in reaching the overvoltage peak. In view of the apparent nucleated nature of the electrodeposition process, this estimate should relate to the amount of electrodeposited Ag involved in reaching the critical nucleation stage, a process which will be discussed presently. If the linear region of a curve is extrapolated to a voltage V' corresponding to the time t at which the peak overvoltage, V_p is reached, then V' is the voltage the cell would reach at time t, were there no faradaic contribution. Since the voltage only reaches V_p, the faradaic contribution must be $C(V' - V_p)$, where C is the capacitance derived from the slope of the linear portion. Values obtained in this manner at 292° were 0.23, 0.19, and 0.165 μcoulomb/cm^2 at current levels 25, 50, and 100 μa, respectively, corresponding to 0.096, 0.079, and 0.069% of an ideal Ag monolayer or to atomic concentrations of 1.45_5, 1.2_0, and 1.05×10^{12} cm^{-2}. The general picture, then, is of an extremely localized Ag discharge pattern, in which activation energy is required to build up a number of minute nucleation sites that serve as centers for subsequent steady-state discharge.

Discussion

Perhaps the most interesting characteristic of solid electrolyte cells such as the above is their extreme electrochemical simplicity. The one-component nature of the electrolyte allows the study of ideal polarized solid electrodes under thermodynamically well-defined conditions and in the absence of side effects due to solvents. Thus, hydrolytic oxide layers, hydration sheaths, and the like are absent. In the above work under these conditions, two distinct types of electrode behavior were nonetheless observed. In what follows, we shall consider what factors may be responsible.

Whether a metal electrodeposits on a bare foreign substrate uniformly or dendritically at the monolayer level presumably depends on the relative bond strengths of the metal atoms with themselves and with atoms of the electrode material. Alternately stated, the relative sublimation energy of the metal and adsorption energy of the metal atoms on the substrate electrode are involved. Rogers,[16] *et al.*, have considered a number of classes of electrodeposition behavior in this respect. If the two energies or bond strengths are comparable, entropy considerations will favor uniform monolayer buildup as the theoretical electrodeposition potential is approached. If the adsorption energy or bond strength is relatively small, an overvoltage will be required to discharge even a relatively small amount of the metal and subsequent discharge will be on the metal nuclei thus formed.

A useful concept in this respect is that of surface solubility. In this, the difference between the sublimation and adsorption energies of the electrodeposit metal becomes the "heat of solution." In the present study, silver and platinum possess identical crystal structure (face-centered cubic) and their lattice parameters differ

(16) J. T. Byrne and L. B. Rogers, *J. Electrochem. Soc.*, 98, 457 (1951).

by only 4%. Because of this and their similar metallic nature, one might expect both comparable energies for the Ag–Ag and Ag–Pt bonds and a capability for epitaxial deposition. If this were so, the result would be a good surface solubility on Pt for Ag atoms at any significant activity, possibly leading to full monolayer coverage at unit activity. Rogers, *et al.*,[17] found comparable results for Ag on Pt in aqueous solutions, though the detailed results were more complicated and difficulties were encountered with reproducibility and possible contaminant effects. Schottky,[18] on the other hand, found a nucleated deposition behavior for Ag on Pt in aqueous solutions. In our own work, it is felt that the elevated temperatures employed and the absence of solvent effects may remove a number of extraneous factors significant for aqueous solutions and thus yield a more clear-cut picture of the intrinsic deposition behavior.

In the case of graphite, no silver graphitic compounds have been reported and compounds such as Ag_2C_2 are unstable at elevated temperatures. Accordingly, we may assume that the Ag–C bond is relatively weak. Thus, we would expect a very small surface solubility, even at $a_{Ag} = 1$. Figure 10, in fact, indicates this by the linearity of the galvanostatic sweep even where it crosses $\mathcal{E}_d$.

It is of interest to pursue the surface solubility picture for describing the process of Ag discharge on the graphite surface. As a galvanostatic sweep is carried out, Ag^+ ions arrive at the interface at a constant rate. A few discharge to correspond to the Ag° surface solubility at each momentary activity during the sweep, but most go to increase the double-layer charge. When a_{Ag} exceeds unity, agglomeration or "precipitation" of isolated Ag° atoms becomes a spontaneous process. The process is self-catalyzed, since agglomeration creates local activity gradients on the graphite surface which increase with increasing agglomerate size. The latter occurs because increasing size reduces a_{Ag} in agglomerates as bulk free energy becomes significant compared with surface free energy (*i.e.*, as the ratio of Ag–Ag bonds to Ag–C bonds increases). At the overvoltage peak, the agglomeration rate becomes equal to the rate of arrival of new Ag^+ ions. As agglomerate growth continues, a_{Ag} is further reduced toward that of bulk Ag, resulting in the observed overvoltage drop, but a steady-state activation overvoltage is still required to drive the process of diffusion to agglomerate sites. Increasing the current level results in a greater overvoltage requirement, since less time is available for the agglomeration process during a given amount of charge transfer. The result is smaller, more closely spaced agglomerates of higher a_{Ag} at the critical nucleation stage. Decreasing temperature increases the peak overvoltage requirement by slowing down the agglomeration and steady-state diffusion rates. A similar nucleation process in three dimensions, that of Ag in Ag_2S, has been studied by Schmalzried and Wagner,[19] using a solid electrolyte cell.

Finally, it is of interest to note in this work that a high double-layer capacitance, presumably involving an adsorbed cation layer, and the tendency to build up a monolayer of adsorbed metal atoms as $\mathcal{E}_d$ is approached are apparently correlated. A number of preliminary results with electrode materials other than Pt and graphite support this correlation. This seems reasonable, since similar factors must be involved in the ability of an electrode material to adsorb ions of a metal and atoms of the same metal. In both cases, the adsorption should involve some manner of quasi-chemical bonding in which there is a degree of electron sharing between metal ions or atoms and the metallic substrate. The question, in fact, arises as to whether adsorbed ions and atoms in this instance are quantum-mechanically distinguishable. It is felt that they are, since the electrolyte lattice in the neighborhood of an adsorbed ion should be electrostatically polarized, thus providing different nearest-neighbor configurations for adsorbed ions and atoms. While electron exchange *via* the electrode surface could occur between such atoms and ions in consequence of thermal lattice vibrations, this process would be far too slow to have the nature of a quantum-mechanical resonance. Nonetheless, similar factors should apply to the ability of a surface to adsorb ions and atoms of the same metal, suggesting a general correlation between large double-layer capacitance and electrodeposition *via* monolayer buildup.

Acknowledgments. The author is greatly indebted to Mrs. Barbara Vaudreuil and to Mr. Harry Crowe for considerable assistance in all phases of the experimental work. Thanks are due to Dr. Paul Schlichta for providing samples of stress-annealed pyrolytic graphite.

(17) J. T. Byrne, L. B. Rogers, and J. C. Griess, *J. Electrochem. Soc.*, 98, 452, (1951).

(18) W. F. Schottky, *Z. Physik. Chem.* (Frankfurt), 31, 40 (1962).

(19) H. Schmalzried and C. Wagner, *Trans. AIME*, 227, 539 (1963).

Photochemical Formation of Free Radicals from Hydrogen Sulfide, Mercaptans, and Cysteine[1]

by D. H. Volman, J. Wolstenholme, and S. G. Hadley

Department of Chemistry, University of California, Davis, California
(Received November 21, 1966)

Electron spin resonance studies of H_2S, CH_3SH, C_2H_5SH, L-cysteine, aqueous solutions of H_2S, D_2S, CH_3SH, CH_3SD, and L-cysteine, and L-cysteine in aqueous hydrogen peroxide ultraviolet irradiated at 77°K have been made. The primary photochemical process established for each of these compounds is cleavage of the sulfur–hydrogen bond to yield a hydrogen atom and the corresponding thiyl free radical. For methanethiol in water, the free radicals $\cdot CH_3$ and $\cdot CH_2SH$ were identified and evidence that $\cdot CH_2SH$ did not come from a primary photochemical process was obtained. Hydroxyl radicals from the photolysis of hydrogen peroxide yielded thiyl free radical by abstraction of hydrogen atom from the sulfhydryl group of L-cysteine.

Introduction

There have been a number of esr studies of free radicals produced in molecules containing the sulfhydryl group by γ, X-, and ultraviolet irradiation. Much of this work has been stimulated by the importance of sulfur-containing radicals of biological interest, particularly because they may be formed as a result of radiation damage in proteins. The spectra obtained have generally been interpreted on the basis of the formation of a thiyl free radical in the primary process. Mercaptans are the simplest compounds capable of yielding thiyl free radical on irradiation; however, of the simple thiols, only benzyl mercaptan seems to have been studied in ultraviolet irradiation experiments.[2] Because of the biological interest and because the system seemed inherently of photochemical interest, we report here on investigations of ultraviolet-irradiated simple thiols, methane and ethane, and hydrogen sulfide which is, although not a thiol, analogous and the simplest molecule containing the sulfhydryl group. Experiments on cysteine are also reported.

Experimental Section

The experimental procedures and apparatus were similar to those reported in earlier work from this laboratory[3] and fuller details may be found therein. The volatile compounds were vacuum distilled into 4-mm quartz sample tubes, degassed by several freeze–pump–thaw cycles, and sealed while frozen with liquid nitrogen. Irradiations were carried out and spectra were recorded at 77°K by keeping the sample tube in a Varian liquid nitrogen quartz dewar insert. Annealing at higher temperatures was accomplished by using nitrogen gas cooled by passage through a heat exchanger in liquid nitrogen or at 195°K by use of solid carbon dioxide. Two light sources were used: a low-pressure mercury resonance arc housed in Vycor from which the transmitted light was chiefly 2537 A as Vycor is opaque to 1849-A light; a high-pressure arc which, in conjunction with a Pyrex filter, transmitted above 2800 A. The spectrometer was a Varian 4501 X-band instrument with 100-kc field modulation. Spectra were taken as first derivatives. Calibration of the scanning rate, gauss per minute, was made with peroxylamine disulfonate.

Results and Interpretation

Hydrogen Sulfide. Spectra obtained from the ul-

(1) This investigation was supported by Public Health Service Research Grant No. CA-05528 from the National Cancer Institute and in part by the National Science Foundation through Grant No. GP-3652.

(2) J. J. Windle, A. K. Wiersma, and A. L. Tappel, *J. Chem. Phys.*, 41, 1996 (1964).

(3) D. H. Volman, K. A. Maas, and J. Wolstenholme, *J. Am. Chem. Soc.*, 87, 3041 (1965).

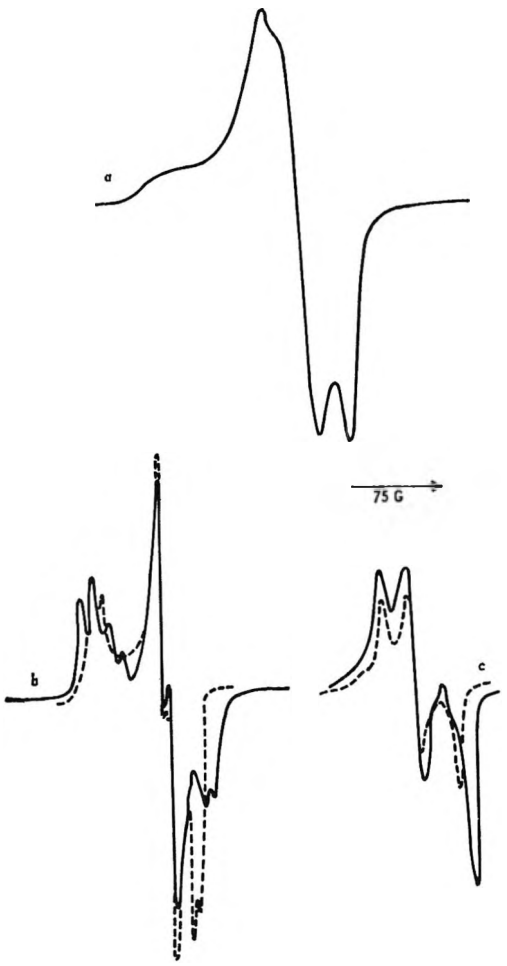

Figure 1. Esr spectra of hydrogen sulfide irradiated at 2537 A and 77°K (spectra recorded at 77°K): a, not annealed; b, annealed 2 min at 115°K; c, annealed 11 min at 115°K; broken line, comparison spectra (see text).

traviolet (2537 A) irradiation of hydrogen sulfide for 30 sec at 77°K are shown in Figure 1. After irradiation the samples were held at 115°K for the periods indicated, after which they were cooled to 77°K and the spectra recorded. For comparison, we have indicated the spectrum of ultraviolet-irradiated elementary sulfur in Figure 1c and the spectrum given by Sergeev, *et al.*,[4] for ultraviolet-irradiated hydrogen sulfide in Figure 1b.

The sulfur spectrum was obtained by irradiating elementary sulfur (Allied Chemical Corp. precipitated sulfur) at 77°K and 2537 A. The sample was warmed to 165°K, where the signal was slowly decaying, and the spectrum was recorded. The spectrum is very similar to that obtained by Radford and Rice[5] for sulfur condensed from the heated vapor on cold surfaces.

The comparison hydrogen sulfide spectrum is from the only reported esr results on hydrogen sulfide of which we are aware. The study[4] was incidental to work directed at the effect of temperature on radical stabilization and, hence, quite fragmentary. Moreover, the results are contained in a preprint of an oral presentation and are difficult to evaluate because of insufficient information. The sample was apparently irradiated at 77°K, but we do not know how it was treated subsequently.

The spectra of a sample prepared by saturating water with hydrogen sulfide are shown in Figure 2. The sample was irradiated for 30 min at 77°K and 2537 A. Both spectra were recorded at 77°K, but Figure 2b represents the center portion after the irradiated sample was held at 195°K for 13 days.

Identical procedures were carried out with D_2S, prepared by the reaction of D_2O with aluminum sulfide, dissolved in D_2O. These results are shown in Figure 3.

From the results presented it may be concluded that the primary photochemical processes for hydrogen sulfide is

$$H_2S + h\nu \longrightarrow \cdot H + HS\cdot \qquad (1)$$

as all the available photochemical evidence indicates.[6] That hydrogen atoms are formed is clearly evident in Figures 2 and 3. In Figure 3a both H (the outer doublet) and D (inner triplet) are obvious. The proton splitting in this spectrum is 506 gauss and the deuteron splittings are each 76.8 gauss, virtually the same as the free atom values, 507 and 77.6 gauss, respectively. These results are analogous to those reported by Livingston, Zeldes, and Taylor[7] in the γ radiation of some aqueous solutions of inorganic oxygen acids (sulfuric, perchloric, and phosphoric) at 77°K. Hydrogen atom spectra were not observed in the spectra obtained from pure hydrogen sulfide; this is consistent with the well-known observations that stabilization of free radicals is strongly dependent on the solvent matrix and that hydrogen atom spectra cannot be obtained in irradiated pure water at 77°K.[8]

Figure 1c indicates that elementary sulfur is formed, as is also observed in the photolysis of gaseous hydrogen sulfide. The mechanism for the formation of sul-

(4) G. B. Sergeev, V. S. Gourman, V. I. Papissova, and E. I. Yakovenko in "Preprints of Papers Read at the Fifth International Symposium on Free Radicals, July 6–7, 1961," Almqvist and Wilksell, Uppsala, Sweden, 1961.

(5) H. E. Radford F. O. Rice, *J. Chem. Phys.*, **33**, 774 (1960).

(6) B. de B. Darwent and R. Roberts, *Proc. Roy. Soc.* (London), **A216**, 344 (1953).

(7) R. Livingston, H. Zeldes, and E. H. Taylor, *Discussions Faraday Soc.*, **19**, 166 (1955).

(8) L. H. Piette, R. C. Remkel, and H. E. Weaver, *J. Chem. Phys.*, **30**, 1623 (1959).

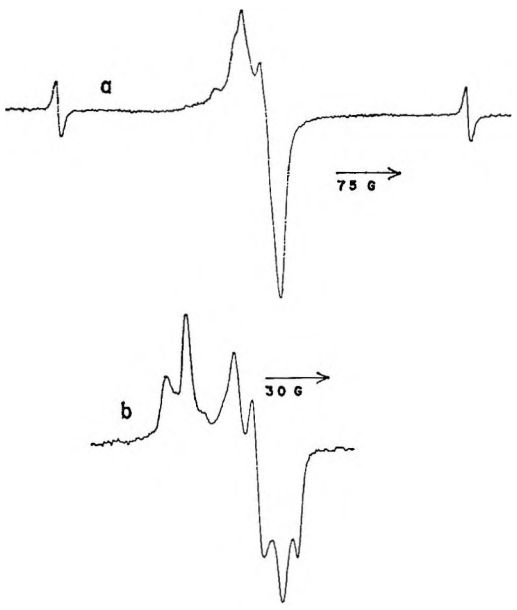

Figure 2. Esr spectra of aqueous hydrogen sulfide irradiated at 2537 A and 77°K (spectra recorded at 77°K): a, not annealed; b, annealed 13 days at 195°K.

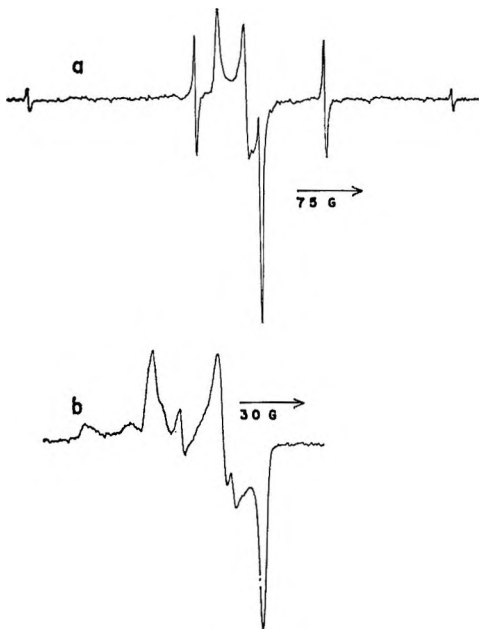

Figure 3. Esr spectra of aqueous (D_2O) hydrogen sulfide (D_2S) irradiated at 2537 A and 77°K (spectra recorded at 77°K): a, not annealed; b, annealed 13 days at 195°K.

fur has been considered in detail by Darwent and Roberts,[6] who gave a number of energetically possible routes, all of which involve HS· free radical.

Figure 1b shows structures which may be attributed to proton splittings of a sulfur free radical, inferentially the HS· radical. This is borne out by the experiments in water solution. Figure 2b shows the kind of structure which would be expected if the elementary sulfur radical spectrum were modified by coupling with a single proton; the three sulfur lines, having anisotropic g values,[5] are split into doublets with almost identical splittings of 9.5 gauss. A comparison with the results obtained with D_2S in D_2O, with some proton contamination (Figure 3b) is further indication that the splittings observed are due to proton interactions. Recent studies of McDonald[9] on gaseous ·SH at room temperature yield 5.4 gauss for the proton coupling constant while Henriksen[10] and Kurita and Gordy[11] report about 9-gauss splitting attributed to a proton in the $COOHCH(NH_2)CH_2S$· radical.

Methane- and Ethanethiol. The pure compounds in the frozen state at 77°K were irradiated at 2537 A and the spectra, Figure 4, were recorded at 77°K immediately after irradiation. The results obtained are similar to those reported for optically bleached γ-irradiated methyl disulfide,[12] where CH_3S· is presumed formed, and to those reported for X-irradiated cysteine and cysteamine hydrochloride at 77°K.[10] For the latter thiols, the esr spectra have been interpreted as arising from RCH_2S· radicals with an anisotropic g factor and hyperfine coupling with only one of the protons on the carbon atom adjacent to sulfur. The doublets due to this hyperfine coupling may be clearly seen in the two lowest field lines, where they appear in the spectra of Henriksen, and the coupling constant is about 9 gauss, in good agreement with the value reported by Henriksen and by Kurita and Gordy.[11] This is also about equal to the coupling constant we have assigned to the proton in the ·SH free radical.

From these results it may be inferred that the primary photochemical process in both pure solid methanethiol and ethanethiol is

$$RSH + h\nu \longrightarrow RS\cdot + \cdot H \qquad (2)$$

This is an agreement with the conclusion of Inaba and Darwent[13] that eq 2 is probably the only primary process occurring in gaseous methanethiol.

A saturated solution of methanethiol in water frozen at 77°K was also irradiated at 2537 A and the spectrum, Figure 5, was recorded at 77°K. The spectrum

(9) C. C. McDonald, *J. Chem. Phys.*, 39, 2587 (1965).

(10) T. Henriksen, *ibid.*, 37, 2189 (1962).

(11) Y. Kurita and W. Gordy, *ibid.*, 34, 282 (1961).

(12) F. K. Truby, D. C. Wallace, and J. E. Hesse, *ibid.*, 42, 3845 (1965).

(13) T. Inaba and B. de B. Darwent, *J. Phys. Chem.*, 64, 1431 (1960).

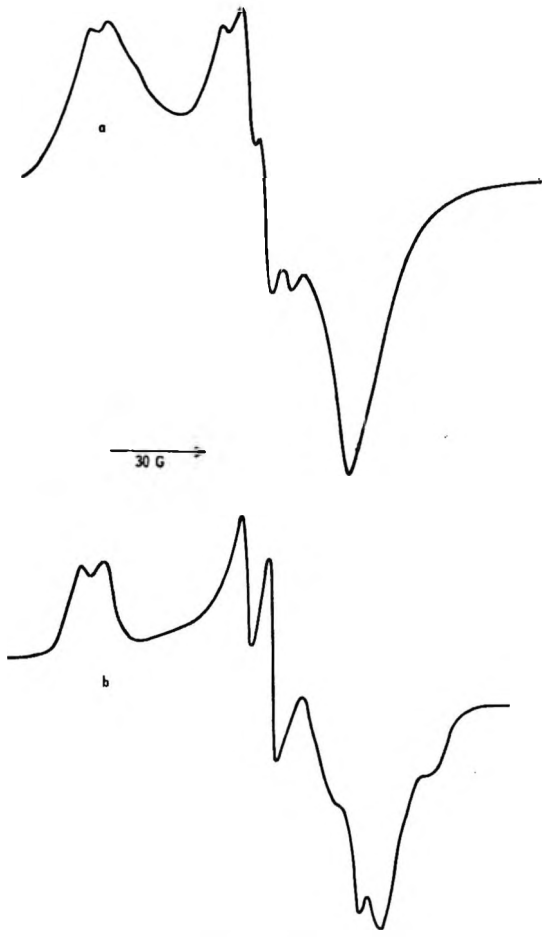

Figure 4. Esr spectra of (a) methanethiol and (b) ethanethiol irradiated at 2537 A and 77°K.

of free H atom, a doublet split by some 500 gauss, was also obtained but is outside of the field shown.

The low-field portion is very much like the spectrum obtained from the irradiation of pure methanethiol, Figure 4, which we have identified as the $CH_3S\cdot$ radical. The remainder of the spectrum is analogous to that observed by Sullivan and Koski[14] in the ultraviolet irradiation of methanol at 77°K, a 1:3:3:1 quartet with 23.5-gauss splittings attributed to methyl radicals and a 1:2:1 triplet with 18-gauss splitting. Our spectrum may be interpreted in similar fashion: a quartet (about 1:3:3:1) with an average coupling of 23 gauss and a triplet (probably 1:2:1) with an average coupling of 19 gauss. These spectra are attributed to $\cdot CH_3$ and $\cdot CH_2SH$, respectively.

Except for radical–radical combination, the only secondary reaction of importance reported in the study by Inaba and Darwent[13] is

$$H\cdot + CH_3SH \longrightarrow H_2 + CH_3S\cdot \qquad (3)$$

This reaction cannot account for the radicals observed

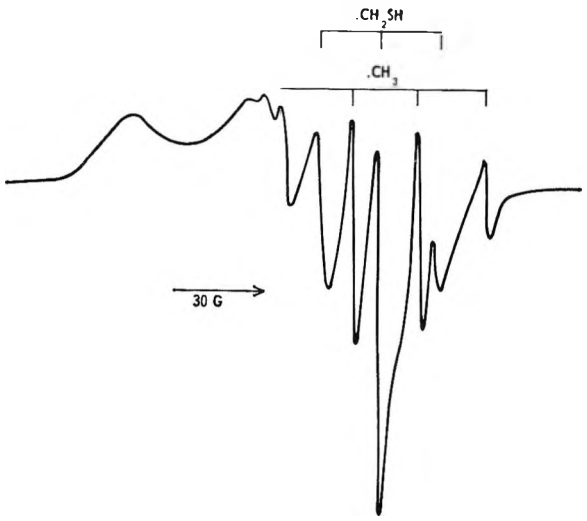

Figure 5. Esr spectrum of aqueous methanethiol irradiated at 2537 A and 77°K.

in water solution. Although it is possible that $\cdot CH_2SH$ may arise from a primary process involving cleavage of a carbon–hydrogen bond, contrary evidence was obtained. Irradiation of a 40:1 mole ratio D_2O to methanethiol solution, in which the thiol should be present almost entirely as CH_3SD, yielded the esr spectrum of D atoms with only traces of H atoms. This is unequivocal evidence that hydrogen atoms are formed only by cleavage of the sulfur–hydrogen bond. Therefore, it may be concluded that the radical is produced by hydrogen atom abstraction

$$R\cdot + CH_3SH \longrightarrow RH + \cdot CH_2SH \qquad (4)$$

This reaction may be favored in the water system because it might be expected that the hydrogen atom bonded to sulfur would be shielded by strong interaction with water. It may be noted that ethanethiol is reported to form the hydrate, $C_2H_5SH\cdot 18H_2O$.[15] The change of free methyl being produced by secondary reactions appears remote, and the most logical mechanism for its formation is by cleavage of the carbon–sulfur bond in the primary photochemical process as an alternative to reaction 2 in frozen water solution. If free methyl radical is formed by cleavage of the carbon–sulfur bond, equivalent amounts of $HS\cdot$ should be formed. The spectrum of $HS\cdot$ is very similar to that of $CH_3S\cdot$ and it is therefore possible that the low-field portion of Figure 5, which we have attributed to $CH_3S\cdot$, contains a contribution from $HS\cdot$. It is

(14) P. J. Sullivan and W. S. Koski, *J. Am. Chem. Soc.*, 84, 1 (1962).
(15) E. E. Reid, "Organic Chemistry of Bivalent Sulfur," Vol. I, Chemical Publishing Co., Inc., New York, N. Y., 1958, p 109.

also possible that this cleavage occurs in pure methanethiol but that methyl radicals are not observed because subsequent hydrogen atom abstraction analogous to reaction 3 is extremely rapid.

A detailed argument for observing coupling of only one proton of the two on the carbon atom adjacent to sulfur has been presented by Kurita and Gordy[11] for the $COOHCH(NH_2)CH_2S\cdot$ radical. They assume that the bonding orbital of sulfur is an sp^2 hybrid and that the occupied atomic orbitals of the valence shell are three sp^2 hybrids directed in a common plane. The orientation of the orbitals is assumed fixed, probably by hydrogen bonding to amine groups on neighboring molecules. The unpaired electron is taken to be in a p orbital perpendicular to the plane of the sp^2 orbitals. If free rotation does not occur about the C–S bond, this configuration can lead to major coupling with only one of the two protons. A similar argument may be used for $CH_3CH_2S\cdot$ and $CH_3S\cdot$ radicals. In this case it is likely that hydrogen bonding would occur either with hydrogen atoms attached to sulfur in neighboring molecules or with hydrogen atoms attached to oxygen in a water matrix. On this basis, coupling with one of the protons could be three or four times greater than with the other proton or protons. The weaker couplings would, therefore, go undetected as they would amount to only some 2–3 gauss.

Cysteine. Pure L-cysteine was irradiated at 2537 A and 77°K. The spectra obtained are shown in Figure 6. These results are similar to those obtained by Henriksen[10] in the X-irradiation of L-cysteine. Proton coupling is observed at 160°K, whereas Henriksen obtained proton coupling at 77°K but not at 295°K.

A 0.3 *M* solution of L-cysteine in water frozen at 77°K was also irradiated at 2537 A and spectra similar to that obtained with the pure solid were obtained. In contrast to the results obtained with methanethiol, the spectrum of hydrogen atom was not observed. As the trapping of hydrogen atoms at 77°K seems to be quite sensitive to the specific matrix and since solutions of sulfuric acid are known to be particularly effective,[7] experiments were carried out in solutions to which sulfuric acid were added. Irradiation of a 0.3 *M* sulfuric acid solution at 2537 A and 77°K did not yield a hydrogen atom spectrum; irradiation of a solution 0.3 *M* sulfuric acid and 0.3 *M* L-cysteine at 2537 A and 77°K did yield a hydrogen atom spectrum. Thus, there is good evidence for the production of both thiyl and hydrogen atom in the primary photochemical process in L-cysteine, analogous to the results obtained for hydrogen sulfide and methane- and ethanethiol.

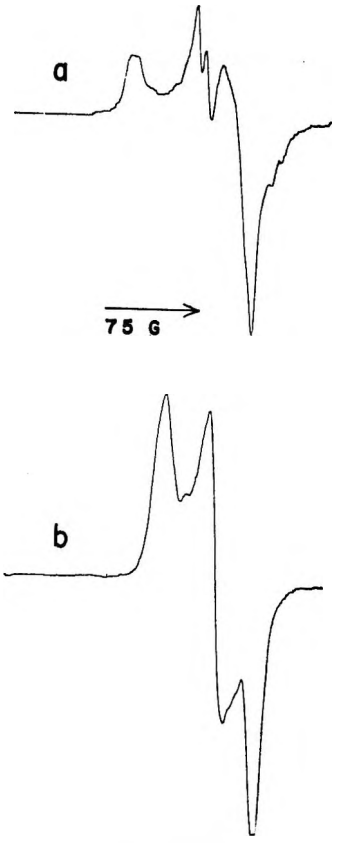

Figure 6. Esr spectra of L-cysteine irradiated at 2537 A and 77°K: a, recorded at 160°K; b, recorded at 293°K.

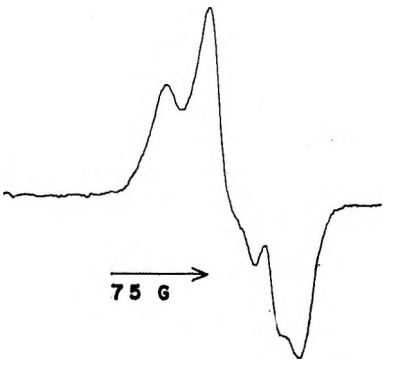

Figure 7. Esr spectrum of aqueous L-cysteine–hydrogen peroxide irradiated at $\lambda > 2800$ A and 77°K. Recorded at 165°K.

As hydroxyl free radicals derived from water are expected to be involved in radiation damage in biological systems, we have carried out experiments directed at observing the products of the reaction of hydroxyl radicals with L-cysteine. A solution of 0.3 *M* hydrogen peroxide and 0.3 *M* L-cysteine frozen at 77°K was irradiated with light from a high-pressure mercury arc through a Pyrex filter. Under these

conditions the transmitted radiation, $\lambda > 2800$ A, is not absorbed by L-cysteine and is absorbed by hydrogen peroxide with the formation of hydroxyl radicals. In the absence of cysteine, the spectrum obtained is that typical of irradiated hydrogen peroxide, decaying with increasing temperature and disappearing completely in a few minutes at 150°K. In the presence of L-cysteine, a broad line with little evidence of structure was obtained at 77°K. On raising the temperature to 165°K the spectrum shown in Figure 7 was obtained. Although not identical with that obtained from pure solid cysteine, the similarity, particularly when compared to Figure 6b, is good evidence that thiyl radical is formed. Thus, the secondary reaction is the abstraction of the sulfhydryl hydrogen atom by hydroxyl radical. These results confirm conclusions reached by Henriksen[16] from studies of X-irradiated aqueous solutions of L-cysteine. It may be emphasized that a major difference in these studies is that the X-irradiation of thiols in water yields both hydroxyl and thiyl radicals as primary irradiation products, whereas ultraviolet irradiation at $\lambda > 2800$ A in solutions with hydrogen peroxide yields hydroxyl but not thiyl radicals as primary irradiation products.

(16) T. Henriksen, *J. Chem. Phys.*, 38, 1926 (1963).

Kinetics of Decomposition of Chloroformic Acid by Rapid-Scan Infrared Spectroscopy

by Reed J. Jensen and George C. Pimentel

Chemistry Department, University of California, Berkeley, California *(Received December 2, 1966)*

The 768-cm^{-1} absorption produced by flash photolysis of chlorine–formic acid mixtures has been reexamined under higher resolution and its kinetic behavior has been studied as a function of temperature. The assignment of this band as the C–Cl stretching motion of chloroformic acid is corroborated by the band width, 17.5 cm^{-1}, and the absence of frequency shift on deuteration. The decomposition is unimolecular over the temperature range 288–343°K and the rate constant equals $5 \times 10^{13} \exp(-14{,}000/RT)$. The implied activation enthalpy and entropy indicate that the rate-limiting step is probably the *cis–trans* isomerization of chloroformic acid. Bond length and energy considerations indicate that bromoformic acid will be similarly labile.

Introduction

West and Rollefson[1] studied the gas-phase photolysis of chlorine and formic acid and postulated the following mechanism to explain their observed quantum yield of several thousand.

$$Cl_2 \xrightarrow{h\nu} 2Cl \quad (1)$$

$$Cl + HCOOH \longrightarrow HCl + COOH \quad (2)$$

$$COOH + Cl_2 \longrightarrow ClCOOH + Cl \quad (3)$$

$$ClCOOH \longrightarrow HCl + CO_2 \quad (4)$$

$$COOH \longrightarrow CO_2 + H \quad (5)$$

$$H + Cl_2 \longrightarrow HCl + Cl \quad (6)$$

$$2Cl + M \longrightarrow Cl_2 \quad (7)$$

(1) W. West and G. K. Rollefson, *J. Am. Chem. Soc.*, 58, 2140 (1936).

Herr and Pimentel[2,3] studied the reaction intermediates of the above reaction by rapid-scan infrared spectroscopy. They detected, at 768 cm^{-1}, the absorption of the C–Cl stretch of the ClCOOH molecule. The half-life of the unstable molecule at temperatures typical of their reaction conditions was estimated to be 50–70 μsec.

The present work further explores, by rapid-scan infrared spectrophotometry, the kinetics of the decomposition of this intermediate species in the chlorine–formic acid photochemical reaction.

Experimental Section

The formic acid in this study was Baker and Adamson 98 to 100%, the chlorine was Matheson 99.5%, the deuterium oxide was Bio-Rad 99.94%, and the calcium sulfate was Hammond indicating $CaSO_4$ (Drierite).

The spectral region near 800 cm^{-1} was studied at two spectral slit widths, 8 or 9 cm^{-1} and 40 cm^{-1}, using the rapid-scan infrared spectrometer built by Herr and Pimentel[2,3] and modified by Carlson.[4] The instrument was used with an NaCl prism, Nernst glower source, and a zinc-doped Ge detector at 20°K. With the 40-cm^{-1} spectral slit width, the scan rate was 900 cm^{-1}/100 μsec. For the smaller spectral slit width, the rotating Littrow mirror was replaced by a 40-line/mm grating. With this grating and a scan rate of 200 cm^{-1}/100 μsec, the 9.4-cm^{-1} interference fringes of an AgCl film were resolved.

For study of the spectral region near 1800 cm^{-1}, a 100-line/mm rotating grating and a mercury-doped Ge detector at 20°K were substituted. Resolution of water lines indicated that the spectral slit width was about 5 cm^{-1} at scan rates of 1000 cm^{-1}/100 μsec.

For photolysis, a bank of condensers (0.5, 9, 17.5, or 32.5 μf) charged to voltages in the range 7 to 18 kv was discharged through a 58-cm quartz flash tube filled with 20 mm of xenon. The flash duration (at half-height) was about 30 μsec for low capacitance and 60 μsec for the higher capacitances. Throughout this work, a Pyrex reaction cell was used, so that very little light of wavelength less than 3100 A was admitted. The number of photons in the effective region, 3100 to 3900 A, was about 40 μmoles per 1000-joule flash.[5] The cell and flash tube were optically coupled by wrapping them together in aluminum foil.

Temperature measurement and control were important in this experiment. Fortunately, the formic acid monomer–dimer equilibrium furnishes temperature information through the spectral intensities. About 40 μsec after each measurement of the 768-cm^{-1} band of ClCOOH, the spectral scan encompasses the 917-cm^{-1} band of formic acid dimer and 30 μsec later, the 1105-cm^{-1} band of formic acid monomer. With the assumption of Beer's law, the following expression can be derived

$$T_2 = \frac{T_1 \Delta H}{\Delta H - RT_1 \ln \frac{r_2}{r_1}}$$

where $r_i = (D_i/M_i^2)$, D_i is the optical density of the dimer band at 917 cm^{-1} at temperature T_i, M_i is the optical density of the monomer band at 1105 cm^{-1} at temperature T_i, and ΔH is minus the heat of dissociation per mole of dimer (= −14.5 kcal/mole[6]).

This temperature calculation also tacitly assumes that equilibrium is rapidly established within the 20- or 30-μsec period following the flash and preceding the spectral scan. This is undoubtedly so, since the half-time for dissociation of the dimer at 300°K is of the order of 10^{-12} sec if $\Delta F^{\ddagger}$ for bond rupture is close to ΔF of dissociation of the dimer (1.64 kcal/mole).[6] We see, then, that T_2 can be estimated from a reference spectrum at room temperature, T_1, before the flash and a measurement of the optical densities at 917 and 1105 cm^{-1} at the unknown temperature.

The applicability of this temperature T_2 in the present work depends upon one more factor. The temperature rise after cessation of the flash must be small enough so that the temperature is essentially constant (and equal to T_2) for the period between flash termination and the recording of the band at 768 cm^{-1}. For kinetic studies below 40°, the heating that accompanies the flash sufficed to warm the gas to the desired temperature. Variation of flash energy and Cl_2 pressure provided control. For reaction temperatures above 45°, the cell was heated externally to a temperature 10 or 15° below the desired temperature. Thus the temperature rise due to flash heating and subsequent reactions never exceeded 15°. Since a large fraction of this rise must have occurred during the flash, the error involved in the use of T_2 is at most a few degrees.

In a typical kinetic experiment, a mixture of 20 mm of HCOOH, 20 mm of Cl_2, and 720 mm of N_2 was photolyzed with a 1300-joule flash to give a 10 or 15° temperature rise. Doubling the chlorine pressure increased the temperature rise to 40–50°. If the chlo-

(2) G. C. Pimentel and K. C. Herr, *J. Chim. Phys.*, **61**, 1509 (1964).

(3) K. C. Herr and G. C. Pimentel, *Appl. Opt.*, **4**, 25 (1965).

(4) G. A. Carlson, Ph.D. Dissertation, University of California, Berkeley, Calif., 1966.

(5) Based on actinometry performed by G. A. Carlson.

(6) G. C. Pimentel and A. L. McClellan, "The Hydrogen Bond," W. H. Freeman and Co., San Francisco, Calif., 1960.

rine pressure were raised to 250 mm and N_2 pressure dropped to 500 mm, the cell would explode.

Time measurement was entirely based upon the time scale of the Tektronix 535A oscilloscope horizontal sweep. The 50-μsec/cm and 20-μsec/cm sweep scales were used and each was calibrated to ±1% with a Tektronix RM187 time mark generator. Time was measured from the beginning of the flash since this time is well defined, and for first-order kinetics, the error involved affects the intercept but not the slope. The slope, of course, fixes the rate constant.

Results

Identification of ClCOOH. The 768-cm^{-1} C–Cl stretching mode of ClCOOH was studied under higher resolution than was available in the earlier work[2,3] (about 20 cm^{-1}) to seek band contour verification of the identification. Figure 1 shows this band under the optimum conditions that could be obtained in this work with a spectral slit width of about 8 cm^{-1} (trace a). Trace b in Figure 1 contrasts the spectrum of formic acid before the flash with a superimposed interference spectrum generated by a piece of AgCl sheet placed in the optical path. The 9.4-cm^{-1} spacings of the fringes furnish calibration marks and a qualitative measure of the resolution. An optical density plot of trace a shows that the band width at half-height, under this resolution, is about 17.5 ± 1 cm^{-1}. The uncertainty is connected with the difficulty in fixing the I_0 line and the zero transmission base line.

Because of the chlorine atom mass, chloroformic acid is approximately a prolate symmetrical top and the axis of least moment of inertia is close to the carbon–chlorine bond. Thus the C–Cl stretch is expected to exhibit the PQR structure of a parallel band. With reasonable bond lengths and angles, the value of $\frac{1}{2}(B + C)$ is about 0.12 cm^{-1}. At 300°K, the PR peak spacing is expected to be near 14 cm^{-1}. With an 8-cm^{-1} spectral slit width, it is unlikely that such a fine structure would be resolved. Furthermore, the measured band width of 17.5 cm^{-1} is reasonably close to the expected value, certainly consistent with the interpretation.

The 1600–2000-cm^{-1} region was carefully examined for evidence of the carbonyl stretching motion of chloroformic acid. The HCOOH pressure was varied from 1.5 to 20 mm with a Cl_2 pressure of 25 mm and an N_2 pressure of 700 to 730 mm. The spectral slit width in this region was 5 cm^{-1}. No trace could be found of a carbonyl absorption outside of the region of the formic acid bands, 1690–1800 cm^{-1}. There was, however, evidence that chloroformic acid may absorb within this region, perhaps near 1800 and 1760 cm^{-1}, though

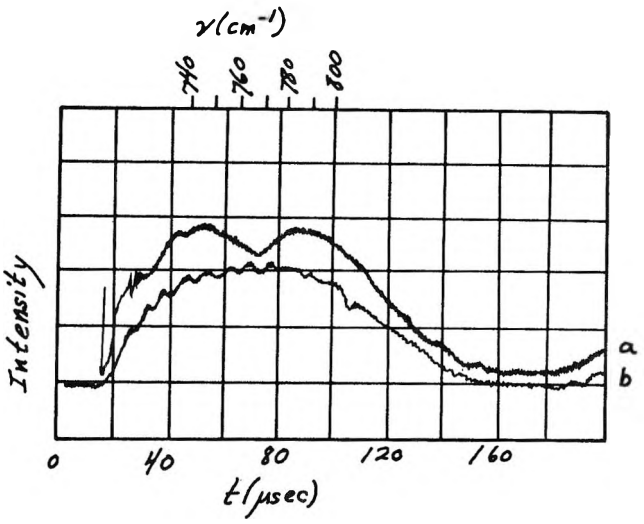

Figure 1. Band contour of 768-cm^{-1} band; spectral slit width, 8 cm^{-1}: a, 768-cm^{-1} band immediately after flash; time measured from flash trigger; b, before flash, formic acid and interference fringes from AgCl sheet; time measured from sweep trigger.

the interpretation is difficult if any temperature changes occur because of attendant displacement of the formic acid monomer–dimer equilibrium.

As one further verification of identification, 18 mm of 97% HCOOD, 25 mm of Cl_2, and 715 mm of N_2 was photolyzed in the usual way. The transient spectrum was indistinguishable from that recorded in similar experiments with HCOOH. The absence of a noticeable frequency shift is consistent with the assignment of the 768-cm^{-1} transient to a C–Cl stretching motion of chloroformic acid and it eliminates the possibility that the motion is connected with a hydrogen bending motion in such a species as carboxyl radical.

Choice of Conditions for Kinetic Studies. Reproducibility was, at first, quite a problem. It was discovered early that unless air was excluded and the sample was carefully dried with anhydrous $CaSO_4$ as the cell was filled, the transient absorption intensity was variable. Furthermore, after a replacement of a section of vacuum line or cleaning of the photolysis cell, the transient was diminished or lost until several experiments had been performed, after which the transient was again reproducible.

The effect of flash energy on intensity of the 768-cm^{-1} transient was investigated for two types of mixtures, chlorine in small excess (14 mm of HCOOH, 23.8 mm of Cl_2, and 722 mm of N_2) and chlorine in large excess (13 mm of HCOOH, 195 mm of Cl_2, and 550 mm of N_2). In the latter case, the intensity of the 768-cm^{-1} band was found to increase to a maximum at about 500 joules and then decrease at higher

flash energies, diminishing by about 30% at a flash energy of 1150 joules. At still higher flash energies, cell destruction is likely to occur. The transient can be detected only for one or two flashes of a given mixture, indicating that the chains furnished by reactions 2 and 3 are long enough to consume the formic acid. Thus the high chlorine mixtures are quite unsuited to kinetic studies: the amount of transient depends sensitively upon flash intensity, there is a large temperature rise, and the mixture must be replaced after each flash.

For chlorine in small excess (Cl_2/HCOOH = 1.7) the transient intensity was constant and reproducible within 5% over the flash energy range 400 to 1200 joules. Furthermore, the amount of heating was small and reasonably constant over this flash range, about 10°. Most important, it was possible to flash a given sample five or six times and obtain the same optical density of the 768-cm^{-1} transient repetitiously if delay time was held constant. The small temperature rise and the repeated appearance of the transient at constant intensity show that the chains cannot be long enough to consume a large fraction of the formic acid. Furthermore, the amount of transient produced by the flash must be relatively independent of the more important experimental variables: the flash energy, the formic acid pressure, and the chlorine pressure. In view of these favorable features, all kinetic studies were conducted with chlorine in small excess and with flash energies near 1000 joules.

Kinetic Study. Figure 2 shows the optical density–delay time data recorded in a typical kinetic study

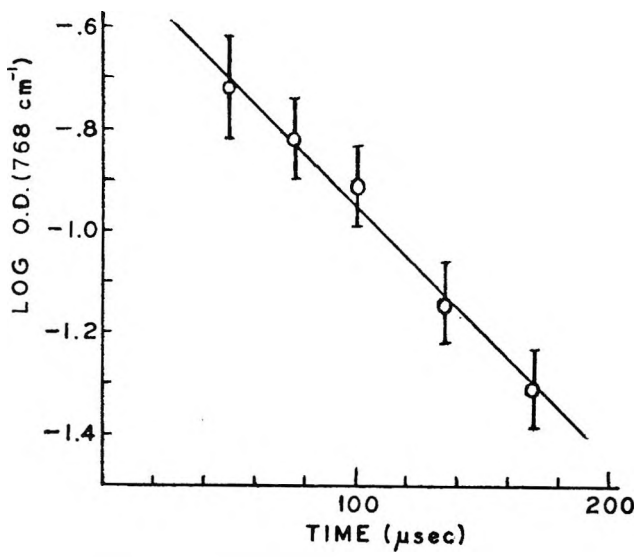

Figure 2. Plot of log OD (768 cm^{-1}) *vs.* time (T, 308°K); time measured from flash trigger to time of scan through 768 cm^{-1}.

of a low-excess Cl_2 mixture. The five data points were obtained from a single filling of the sample cell and with delay times varied nonsystematically: 49, 170, 75, 100, and 135 μsec. The linearity of the plot indicates that the 768-cm^{-1} band is lost in a first-order process, presumably reaction 4. The slope gives the rate constant 1.1 ± 0.5 × 10^4 sec^{-1}, and the formic acid bands indicate that the reaction temperature was 308 ± 2°K.

Similar kinetic studies were conducted at nine temperatures in the range 288 to 343°K. The data, collected in Table I, provide a basis for a plot of log k − log T *vs.* T^{-1}, as shown in Figure 3. The least-squares straight line shown has a slope of −3.0 ± 0.4 × 10^3. This line gives an activation enthalpy, $\Delta H^{\pm}$ = 13.8 ± 1.6 kcal/mole (2σ) and activation entropy

Table I: Kinetic Data: Decomposition of Chloroformic Acid

Temp, °K	Delay time, μsec	Log OD transient	Log k
343 ± 2°	48 ± 2	−0.39 ± 0.1	5.04 ± 0.2
	71 ± 2	−0.94 ± 0.08	
	83 ± 2	−1.40 ± 0.08	
	110 ± 2	−3.00 + 0.8, −3.0	
338 ± 2°	68 ± 2	−0.78 ± 0.1	4.86 ± 0.2
	95 ± 2	−1.01 ± 0.08	
	130 ± 2	−2.73 ± 0.4	
323 ± 2°	60 ± 2	−1.06 ± 0.1	4.61 ± 0.15
	109 ± 2	−1.17 ± 0.08	
	140 ± 2	−2.11 ± 0.2	
318 ± 2°	70 ± 2	−0.79 ± 0.1	4.32 ± 0.15
	103 ± 2	−1.00 ± 0.08	
	131 ± 2	−1.24 ± 0.1	
311 ± 2°	70 ± 2	−0.78 ± 0.1	4.15 ± 0.15
	109 ± 2	−0.80 ± 0.08	
	135 ± 2	−0.95 ± 0.08	
308 ± 2°	49 ± 2	−0.72 ± 0.1	4.04 ± 0.15
	75 ± 2	−0.82 ± 0.08	
	100 ± 2	−0.91 ± 0.08	
	135 ± 2	−1.14 ± 0.08	
	170 ± 2	−1.31 ± 0.08	
295 ± 2°	85 ± 2	−0.75 ± 0.1	3.72 ± 0.15
	149 ± 2	−0.84 ± 0.08	
	200 ± 2	−0.95 ± 0.08	
293 ± 2°	80 ± 2	−0.69 ± 0.1	3.38 ± 0.15
	164 ± 2	−0.88 ± 0.08	
	240 ± 2	−0.95 ± 0.08	
288 ± 2°	105 ± 2	−0.63 ± 0.1	3.25 ± 0.15
	170 ± 2	−0.67 ± 0.1	
	248 ± 2	−0.72 ± 0.08	
	372 ± 2	−0.84 ± 0.08	

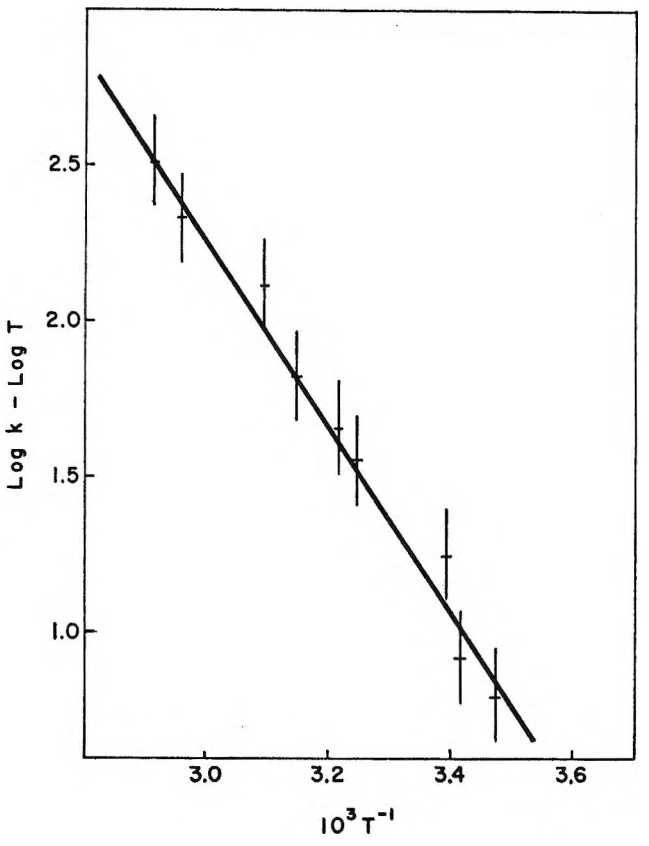

Figure 3. Temperature dependence of ClCOOH decay constant.

$\Delta S^{\pm} = 5 \pm 5$ cal/mole deg (2σ). These results correspond to a frequency factor, $A = 5 \times 10^{13}$.

The uncertainty in the activation energy is rather large, as is appropriate to the scatter of the data in some of the determinations of k. However, a more sinister experimental error lies, perhaps, in the temperature measurement. The decomposition of ClCOOH is undoubtedly exothermic, probably by 10 or 12 kcal/mole. It is implied that there might be a 2 or 3° temperature rise during the time of study and, indeed, there was evidence from the formic acid dimerization that this was probably so. Such an effect would, of course, cause a deviation from linearity in the plots such as Figure 2, and it would tend to give a k that is too large. On the other hand, there is a tendency for the implied error to be about the same at various temperatures since the optical density range is about the same. Hence, the temperature dependence (leading to $\Delta H^{\pm}$) is more reliable than the absolute values of k (which lead to $\Delta S^{\pm}$ or to A). In any event, the implied curvature is not in evidence in Figure 2, so it must be smaller than the uncertainty introduced in the photometry.

Discussion

The low value of $\Delta H^{\pm}$ rules out bond rupture mechanisms. A bimolecular process is ruled out, of course, by the linear plot shown in Figure 2. An intramolecular mechanism is suggested. An obvious process is the two-step mechanism, (4a) and (4b). The barrier to rotation has been measured for formic acid by

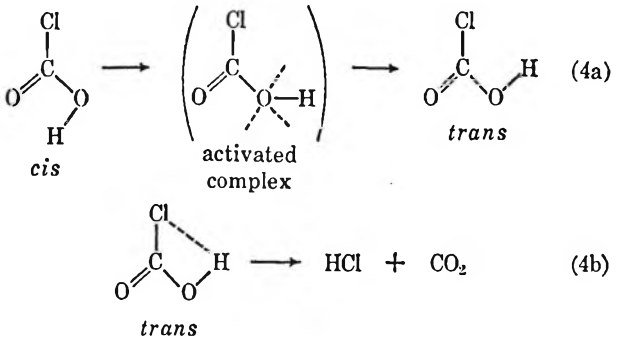

Lerner and Dailey,[7] who found 17 kcal/mole. Our value for $\Delta H^{\pm}$ is sufficiently close to this value to suggest that *reaction 4a is the rate-determining step* and that reaction 4b is rapid in comparison. Furthermore, the positive value of $\Delta S^{\pm}$ can be associated with the bending mode of the OH group which, in the activated complex, is no longer restrained. The reasonableness of this deduction can be tested by examining the probable interatomic distances in the *trans*-ClCOOH as well as in the stable counterparts HCOOH and FCOOH and the as yet unknown counterpart, BrCOOH. These distances can be compared to those in the product molecule, HX, which must be formed. Table II shows these calculated distances using conventional C–X bond lengths, the formic acid C–O distance, and hypothetical bond angles ($\angle$X–C–O = 120°, $\angle$C–O–H = 90°). The last column shows that the bond length discrepancy is a minimum for X = Cl.

Table II: Calculated X···H Distances in *trans*-XCOOH

X	$r_{X\cdots H}^{calcd}$, A	r_{HX}, A	Discrepancy, A
H	1.86	0.74	1.12
F	2.00	0.92	1.08
Cl	2.24	1.28	0.96
Br	2.47	1.41	1.06

Another quantity of importance is the trend in the energy needed to rupture a C–X bond minus the energy released in formation of an H–X bond. Of

(7) R. S. Lerner and B. P. Dailey, *J. Chem. Phys.*, **26**, 680 (1957).

course there are other energy contributions to the over-all process, but they may be relatively constant as X varies. Table III shows these bond energies and, again, the difference. For consistency, the C–X bond energy in CF_3X molecules is listed in the second column.[8]

Table III: Bond Energy Differences between C–X and H–X Bonds (kcal/mole)

X	D_0(C–X) in F_3CX	D_0(H–X)	D_0(C–X) − D_0(H–X)
H	103	103	0
F	121	134	−13
Cl	83	102	−19
Br	65	87	−22

Both Tables II and III provide a basis for understanding the ease of decomposition of ClCOOH relative to FCOOH and HCOOH. For chlorine, the X···H distance discrepancy is smallest, facilitating the hydrogen atom transfer. At the same time, the bond energy discrepancy contributes most to exothermicity. Using these quantities as guides, we see that the bromine counterpart is sufficiently like ClCOOH that its decomposition should be similar. In particular, if the *cis–trans* isomerization is the rate-determining step for ClCOOH, it will probably also be so for BrCOOH. It is implied that BrCOOH should also have only transient existence under normal conditions.

Conclusions

This study confirms the earlier identification of chloroformic acid[2,3] as a transient intermediate in the photolytic reaction between chlorine and formic acid. Hence, it verifies further the reaction mechanism of West and Rollefson.[1] The energy of activation provides a basis for concluding that the unimolecular decomposition is probably rate-limited by the *cis–trans* isomerization around the C–O bond.

In addition to the specific result, we note that this study provides an encouraging prototype in the use of rapid-scan infrared spectroscopy. The versatility of the infrared technique now is available for the direct detection and kinetic study of reaction intermediates.

Acknowledgments. We gratefully acknowledge postdoctoral fellowship support (for R. J. J.) provided by the National Institute of Health and research support by the Air Force Office of Scientific Research.

(8) T. L. Cottrell, "The Strengths of Chemical Bonds," 2nd ed Butterworth and Co. Ltd., London, 1958.

Relative Signs of H–H Coupling Constants for ABX Systems in Four- and Five-Membered Saturated Ring Compounds

by Richard H. Cox and Stanford L. Smith

Department of Chemistry, University of Kentucky, Lexington, Kentucky 40506 *(Received December 5, 1966)*

Double irradiation (spin-tickling) experiments on the ABX portions of the nmr spectra from 1,4-diphenyl-2-azetidinone, styrene carbonate, and the vinyl chloride Diels–Alder adduct of hexachlorocyclopentadiene are described. The geminal and vicinal H–H coupling constants are shown to have opposite signs in all three molecules. These results are in accord with recent theoretical predictions.

Exact computer analyses[1–7] of carefully calibrated nmr spectra for systems of three or more spins have shown that geminal and vicinal H–H couplings may have either the same or opposite signs. In recent years these conclusions have been verified by double-resonance experiments.[8–13] Thus, $^2J_{HH}$ couplings across sp^3 hybridized carbons in saturated systems are usually found to be negative,[1–4,7–10,12,13] whereas for sp^2 hybridized systems $^2J_{HH}$ may be either positive or negative depending on the nature of substituents attached to the system.[14] Similarily, the sign of $^2J_{HH}$ in three-membered heterocyclic systems[5,6,11,13] depends on the heteroatom (*e.g.*, $^2J_{HH}$ in styrene oxide is +5.66 Hz while $^2J_{HH}$ in styrene sulfide is −1.38 Hz).[15] This problem is of continuing significance, both from the practical aspect of spectral analysis and from the theoretical viewpoint of elucidating the quantum mechanical origin and mechanism(s) of spin–spin coupling.

Recently, while investigating the solvent dependence of H–H couplings in small ring compounds, the relative sign of the geminal H–H coupling constant in these systems became of critical importance.[15] In order to obtain further information concerning the sign of $^2J_{HH}$ in saturated ring systems, spin-tickling experiments were carried out on the ABX system in four- and five-membered saturated ring compounds. We report here the relative signs of the H–H coupling constants in 1,4-diphenyl-2-azetidinone (I), styrene carbonate (II), and the vinyl chloride Diels–Alder adduct of hexachlorocyclopentadiene (III).

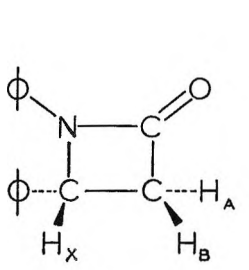

I

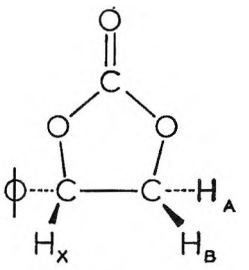

II

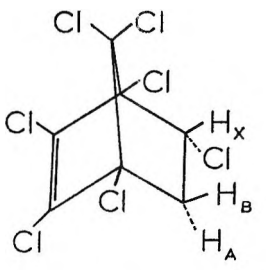

III

(1) R. R. Fraser, R. V. Lemieux, and J. D. Stevens, *J. Am. Chem. Soc.*, **83**, 3901 (1961).

(2) F. Kaplan and J. D. Roberts, *ibid.*, **83**, 4474 (1961).

(3) K. L. Servis and J. D. Roberts, *J. Phys. Chem.*, **67**, 2885 (1963).

(4) R. R. Fraser, *Can. J. Chem.*, **40**, 1483 (1962).

(5) C. A. Reilly and J. D. Swalen, *J. Chem. Phys.*, **32**, 1378 (1960).

(6) C. A. Reilly and J. D. Swalen, *ibid.*, **35**, 1522 (1961).

(7) H. Finegold, *Proc. Chem. Soc.*, 213 (1962).

(8) R. Freeman, K. A. McLaughlan, J. I. Musher, and K. G. R. Pachler, *Mol. Phys.*, **5**, 321 (1962).

Experimental Section

Procedures described in the literature were used to prepare 1,4-diphenyl-2-azetidinone (I)[16] and styrene carbonate (II).[17] The vinyl chloride Diels–Alder adduct of hexachlorocyclopentadiene (III) was a gift from Dr. P. E. Hoch. Samples were prepared as 10 mole % solutions in *d*-chloroform containing about 4% TMS as an internal standard and lock signal.

Spectra were obtained with a Varian HA-60-IL spectrometer operating in the frequency-sweep mode. A Hewlett-Packard 201CR frequency oscillator monitored by a Hewlett-Packard 521CR frequency counter was employed to provide the weak perturbing radiofrequency field applied to a particular transition.

Results and Discussion

Freeman and Anderson[9] have described the effect of a weak perturbing radiofrequency field when applied to individual lines in an nmr spectrum. When the perturbing radiofrequency field is set at the frequency of a particular resonance line and the magnitude of this field is about equal to the line width in Hz, transitions which share a common energy level with the irradiated line (and only those transitions) will be split into doublets. From results obtained by irradiating, in turn, several lines in the spectrum, it is then possible to trace out the energy level diagram of a nuclear spin system and, if the spectrum is close to first order, to determine the relative signs of the coupling constants.

Figure 1A shows the ABX portion of the nmr spectrum of 1,4-diphenyl-2-azetidinone (I). The results of an experiment in which line 12 was irradiated are shown in Figure 1B. Changes in the spectrum show that line 1 and 2 of the A region have the same X spin state as do lines 5 and 6 of the B region. The results show J_{AB} (*gem*) to be different in sign from J_{AX} (*trans*) and J_{BX} (*cis*).[18] A similar experiment in which line 9 of the X region was irradiated (Figure 1C) is consistent with the geminal coupling constant being opposite in sign to the two vicinal coupling constants. The nmr spectra of II and III are similar to the one shown in Figure 1A for I. Experiments, similar to the above, carried out on II and III give identical results.

The chemical shifts and coupling constants obtained from exact computer analysis[19] of the nmr spectra of I, II, and III are given in Table I. Making the usual assumption that vicinal H–H couplings are positive,[20,21] the absolute sign of the geminal H–H coupling constants is given as negative.

The sign of the geminal H–H coupling constant in III has been suggested earlier to be negative[22] and is verified here. Since it is highly unlikely that changing β substituents in the hexachlorobicycloheptene system would cause $^2J_{HH}$ to change by a factor of 2, it follows that the sign of $^2J_{HH}$ in the remainder of these adducts studied previously[23] is also negative. For I and II, computer analyses with both a positive and a negative

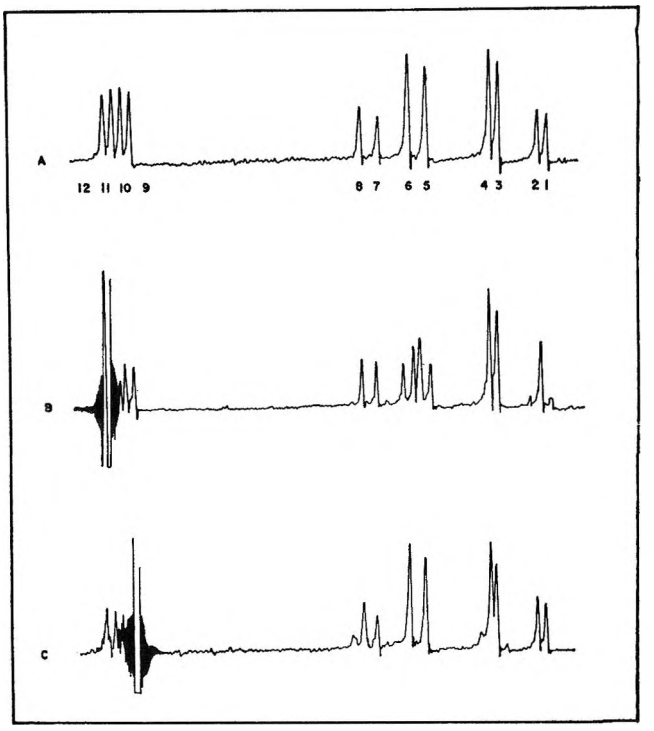

Figure 1. The ABX portion of the 60-MHz spectra of 1,4-diphenyl-2-azetidinone (I): A, normal spectrum; B, line 12 irradiated; C, line 9 irradiated.

(9) R. Freeman and W. A. Anderson, *J. Chem. Phys.*, **37**, 2053 (1963).

(10) R. Freeman and N. S. Bhacca, *ibid.*, **38**, 1088 (1963).

(11) D. D. Elleman and S. L. Manatt, *J. Mol. Spectry.*, **9**, 477 (1962).

(12) K. A. McLaughlan and D. H. Whiffen, *Proc. Chem. Soc.* (London), 144 (1962).

(13) S. L. Manatt, D. D. Elleman, and S. J. Brois, *J. Am. Chem. Soc.*, **87**, 2220 (1965).

(14) C. N. Banwell and N. Sheppard, *Discussions Faraday Soc.*, **34**, 115 (1962), and references contained therein.

(15) Both couplings are solvent dependent. S. L. Smith and R. H. Cox, *J. Chem. Phys.*, **45**, 2848 (1966).

(16) H. Gilman and M. Speeter, *J. Am. Chem. Soc.*, **65**, 2255 (1943).

(17) L. R. Morris and D. J. Hubbard, *J. Org. Chem.*, **27**, 1451 (1962).

(18) A mnemonic method for establishing the relative signs of coupling constants from double-resonance data has recently been given. E. F. Friedman and H. S. Gutowsky, *J. Chem. Phys.*, **45**, 3158 (1966).

(19) J. D. Swalen and C. A. Reilly, *ibid.*, **37**, 21 (1962).

(20) M. Karplus, *J. Am. Chem. Soc.*, **84**, 2458 (1962).

(21) P. C. Lauterbur and R. J. Kurland, *ibid.*, **84**, 3405 (1962).

(22) A. A. Bothner-By, private communication reported in ref 23.

(23) K. L. Williamson, *J. Am. Chem. Soc.*, **85**, 516 (1963).

Table I: Calculated Chemical Shifts and Coupling Constants at 60 MHz[a]

Compound	J_{AB} (*gem*)	J_{AX} (*trans*)	J_{BX} (*cis*)	ν_A[b]	ν_B[b]	ν_X[b]
I	−15.16	2.73	5.66	174.17	210.70	298.41
II	−8.64	7.78	8.07	258.22	286.35	339.26
III[c]	−13.32	3.16	8.20	130.23	179.78	278.89

[a] Calculated probable errors are < ±0.06 Hz in all cases. [b] In Hz downfield from internal TMS. [c] Results from 5 mole % solution in cyclohexane.

sign for $^2J_{HH}$ did not allow a distinction between the two signs to be made. The results obtained for I are in agreement with those obtained for the similar compound 2,2-dibromocyclobutanone.[3] Compounds similar to II have also been examined[1] where the sign of $^2J_{HH}$ was found to be negative.

It appears, from these results and others from the literature, that the sign of geminal H–H coupling constants in four- and five-membered saturated ring systems is negative. One exception appears to be $^2J_{HH}$ for the C_2 methylene group of 1,3-dioxolanes where it has been suggested from the solvent dependence of $^2J_{HH}$ that this coupling is probably positive.[15] This type of deviation has been discussed previously in relation to the contributions of the two neighboring oxygens to the coupling constant.[24,25] Both the magnitude and the sign of the geminal couplings found in this investigation are in complete accord with the MO theory for trends in geminal H–H coupling constants[24] caused by substituents and changing hybridization.

Acknowledgment. The authors wish to thank Dr. P. E. Hoch of the Hooker Chemical Co. for the donation of the Diels–Alder adduct of hexachlorocyclopentadiene.

(24) J. A. Pople and A. A. Bothner-By, *J. Chem. Phys.*, 42, 1339 (1965).

(25) A. A. Bothner-By in "Advances in Magnetic Resonance," Vol. I, J. S. Waugh, Ed., Academic Press, Inc., New York, N. Y., 1965, p 195.

The Crystal Structures of Hydrated and Dehydrated Synthetic Zeolites with Faujasite Aluminosilicate Frameworks. I. The Dehydrated Sodium, Potassium, and Silver Forms

by G. R. Eulenberger, D. P. Shoemaker,[1] and J. G. Keil

Department of Chemistry and Center for Materials Science and Engineering, Massachusetts Institute of Technology, Cambridge, Massachusetts 02139 *(Received December 7, 1966)*

The cation positions in dehydrated synthetic faujasite (zeolite 13Y, with a unit cell content approximately represented by $Na_{57}Si_{135}Al_{57}O_{384}$, Fd3m, $a_0 = 24.71 \pm 0.02$ A) and the analogous K- and Ag-exchange compounds ($K_{57}Si_{135}Al_{57}O_{384}$, $a_0 = 24.80 \pm 0.02$ A; $Ag_{57}Si_{135}Al_{57}O_{384}$, $a_0 = 24.85 \pm 0.03$ A) were determined with X-ray powder diffraction data by means of three-dimensional Fourier syntheses and the structures were refined by least squares. The cations Na^+, K^+, and Ag^+ were found to occupy three different kinds of sites (I, II, III) on the threefold symmetry axes of the faujasite framework structure. These sites are associated with two sets of tetrahedrally arranged $(Si, Al)_6O_6$ rings which with additional oxygen atoms define the "sodalite unit." Site I approaches, from outside of the sodalite unit, the center of the six-membered ring that faces the large absorption cavity of the structure; site II, from inside of the sodalite unit, approaches the second six-membered ring which faces the center of symmetry. Site III is at the center of symmetry. A cation in site I or II has three nearest oxygen neighbors forming a regular triangle; in site III it is surrounded by six equidistant oxygens forming a moderately distorted octahedron. In all cases, site II has the smallest occupancy factor. The occupancy factor is close to unity for site I with Na^+ and K^+ and for site III with Ag^+. For site I, the distances Na–O 2.33 A, K–O 2.72 A, and Ag–O 2.32 A were observed.

Introduction

The dehydrated forms of synthetic zeolites, well known as "molecular sieves," have attracted much attention in recent years because of their unique physicochemical properties, such as their capacity for selective absorption and catalysis due to the presence of interconnecting channels and cavities of definite shape and uniform size.

The crystal structure of zeolite X (near-faujasite) in its hydrated form was determined by Broussard and Shoemaker[2a] from powder data and was found to be almost identical with that of the naturally occurring mineral faujasite.[2b,3] Zeolite Y, or "synthetic faujasite"[4] is a sodium aluminosilicate which has essentially the same framework structure as zeolite X but differs in its Si:Al ratio which varies from 2.2 to 3.0 as in natural faujasite while the same ratio is near 1.5 in zeolite X. As repeatedly mentioned elsewhere, the faujasite framework structure may be described as a diamond array of cuboctahedral aluminosilicate units composed of 24 (Si, Al) atoms and 36 oxygen atoms. This structural unit is usually referred to as the "sodalite unit" because of its occurrence in the mineral sodalite. It may be envisioned as an arrangement of two sets of tetrahedrally positioned rings each containing six linked $(Si, Al)O_4$ tetrahedra. Each sodalite

(1) Author to whom correspondence and reprint requests should be sent.

(2) (a) L. Broussard and D. P. Shoemaker, *J. Am. Chem. Soc.*, 82, 1041 (1960); (b) G. Bergerhoff, W. H. Baur, and W. Nowacki, *Neues Jahrb. Mineral. Monatsh.*, 193 (1958).

(3) W. H. Baur, *Am. Mineralogist*, 49, 697 (1964).

(4) D. W. Breck, Belgian Patent No. 577642, 1959.

unit is connected at the (Si, Al)O rings of one such set to each of four other sodalite units by six "bridge" oxygen atoms O(1), so that the 12 oxygen atoms in the two rings define a distorted hexagonal prism. The deformation is such that the six oxygens closest to the center of the prism (at a center of symmetry) form an octahedron, which may be nearly regular or moderately distorted. There are, per unit cell, eight large absorption cages with about 13.7 A free diameter (which have been repeatedly referred to in the literature as "supercages"), eight sodalite units, and 16 hexagonal prisms. The "supercages" meet at windows with approximately 7.5 A free diameter formed by (Si, Al)$_{12}$O$_{12}$ rings shared between them.

The sodium ions in zeolites X and Y have been successfully exchanged by various uni-, di-, and trivalent cations and exchange equilibria have been extensively studied.[5-10] The absorptive and catalytic properties of dehydrated near-faujasites and faujasites are known to be strongly influenced by the type of cations which are present in the structure. Frilette, Weisz, and Golden[11] report that the catalytic cracking of hydrocarbons on a near-faujasite catalyst follows different mechanisms with the sodium and calcium forms. Carter, Yates, Lucchesi, Elliott, and Kevarkian[12] studied the adsorption of ethylene on a series of cation-exchanged faujasites by infrared spectroscopy and calorimetry and observed that the spectral features attributable to the adsorbed hydrocarbon as well as the thermodynamic quantities describing the adsorption equilibria are greatly influenced by the choice of cation.

The problem of cation bonding in the hydrated faujasites will not be discussed in this paper and the results of this study should not be regarded as applicable to these cases.

Experimental Section

A sample of zeolite Y powder was kindly furnished by Drs. P. Eberly and H. E. Robson of Esso Research Laboratories. Two independent chemical analyses of the sample confirmed the composition as $Na_{57}Si_{135}Al_{57}O_{384}\cdot nH_2O$ (written in terms of one unit cell), with error limits of approximately ± 0.5 in the number of Na or Al (= 192 − Si). The number n in the fully hydrated form is approximately 260. A Debye–Scherrer diagram showed rather sharp lines in the back reflection region; no additional lines corresponding to crystalline impurities could be detected.

The potassium form of the zeolite was prepared by cation exchange employing 1 N KOH solution in a batch procedure which was repeated until no further change in the powder line intensities could be observed. Complete replacement of sodium by potassium has been reported by several workers.[5,6,9,10] The Debye–Scherrer photograph did not reveal any decomposition of the lattice or the formation of another crystalline phase.

The preparation of the silver zeolite was accomplished with silver acetate solutions (pH near 6) after previous attempts with the more acidic silver nitrate solutions had been found to produce considerable decomposition. Light was excluded as much as possible. A chemical analysis confirmed complete replacement of Na^+ by Ag^+.

Specimens for Debye–Scherrer powder photography were prepared with the apparatus and the procedure described by Seff and Shoemaker.[13] The dehydration of the samples was carried out at 350° to a pressure of approximately 10^{-5} torr. The diffraction photographs revealed significant changes in the line intensities upon dehydration, particularly in the case of the silver zeolite. No structural damage due to dehydration was observed.

The camera used was a standard 114.6-mm Debye–Scherrer powder X-ray diffraction camera (Straumanis arrangement). A least-squares program incorporating the Nelson–Riley extrapolation procedure was used for refining the lattice parameters. The values obtained are (at room temperature): Na zeolite, a_0 = 24.71 ± 0.02 A; K zeolite, a_0 = 24.80 ± 0.02 A; Ag zeolite, a_0 = 24.85 ± 0.03 A (λ for Cu Kα = 1.5418 A).

Structure Determination, Refinement, and Discussion

The techniques employed were those developed and applied by Broussard and Shoemaker[2a] and particularly by Seff and Shoemaker[13] for three-dimensional structure analysis based on powder X-ray diffraction data. The program MIFR2A, a modification of ERFR2,[14] was employed to prepare the Fourier maps.

(5) R. M. Barrer, W. Gruser, W. F. Grutter, *Helv. Chim. Acta*, **39**, 518 (1956).

(6) L. L. Ames, Jr., *Am. Mineralogist*, **49**, 127 (1964).

(7) L. L. Ames, Jr., *ibid.*, **49**, 1099 (1964).

(8) L. L. Ames, Jr., *J. Inorg. Nucl. Chem.*, **27**, 885 (1965).

(9) R. M. Barrer, L. V. C. Rees, and M. Shamsuzzoha, *ibid.*, **28**, 628 (1966).

(10) H. S. Sherry, *J. Phys. Chem.*, **70**, 1158 (1966).

(11) V. J. Frilette, P. B. Weisz, and R. L. Golden, *J. Catalysis*, **1**, 301 (1962).

(12) J. L. Carter, D. J. C. Yates, P. J. Lucchesi, J. J. Elliott, and V. Kevarkian, *J. Phys. Chem.*, **70**, 1126 (1966).

(13) K. Seff and D. P. Shoemaker, *Acta Cryst.*, **22**, 162 (1967).

(14) W. G. Sly, D. P. Shoemaker, and J. H. van der Hende, ERFR2 Fourier Summation Program, CBRL-22M-62, Esso Research and Engineering Co., 1962.

Table I: Atomic Parameters (Origin at $\bar{3}$m)

Atom	Position	Structure	x	y	z	B, A²	Occupancy factor
(Si, Al)	192(i)	I	0.1285	0.9453	0.0368	4.29	1.0
		II	0.1262	0.9434	0.0359	2.68	1.0
		III	0.1238	0.9470	0.0365	1.48	1.0
O(1)	96(h)	I	0.1035	0.8965	0.0000	10.09	1.0
		II	0.1063	0.8937	0.0000	6.46	1.0
		III	0.1025	0.8975	0.0000	3.69	1.0
O(2)	96(g)	I	0.2569	0.2569	0.1418	4.89	1.0
		II	0.2510	0.2510	0.1379	5.48	1.0
		III	0.2532	0.2532	0.1420	3.82	1.0
O(3)	96(g)	I	0.1798	0.1798	0.9637	4.22	1.0
		II	0.1749	0.1749	0.9685	5.07	1.0
		III	0.1801	0.1801	0.9603	4.47	1.0
O(4)	96(g)	I	0.1802	0.1802	0.3232	3.98	1.0
		II	0.1835	0.1835	0.3227	1.32	1.0
		III	0.1719	0.1719	0.3151	7.34	1.0
M(1)	32(e)	I	0.2235	0.2235	0.2235	4.43	0.947
		II	0.2501	0.2501	0.2501	5.13	0.938
		III	0.2285	0.2285	0.2285	6.94	0.885
M(2)	32(e)	I	0.0609	0.0609	0.0609	18.70	0.612
		II	0.0748	0.0748	0.0748	6.00	0.444
		III	0.0752	0.0752	0.0752	6.42	0.333
M(3)	16(c)	I	0.0	0.0	0.0	2.76	0.484
		II	0.0	0.0	0.0	3.15	0.751
		III	0.0	0.0	0.0	6.61	1.000

For the first Fourier maps only diffraction lines with $N \leq 140$, where

$$N = h^2 + k^2 + l^2 \quad (1)$$

were included and the Fourier coefficients were computed with signs and intensity ratios for the empty framework as approximately defined by the coordinates given by Broussard and Shoemaker.[2a] The positions indicated by additional electron density maxima were subjected to a least-squares analysis in the course of which they either showed convergent behavior or else tended to disappear from the structure. These least-squares analyses were carried out by means of the FORTRAN II program LSPOW 1, a program for structure refinement with powder data for any cubic space group for which corresponding subroutines have been written. It constitutes a generalization of LSPOW.[13] Since for large N, pairs of lines differing only by 1 in N were frequently unresolved, in each cycle the total observed intensity for each such pair was apportioned between the two lines in the ratio of the calculated intensities from the previous cycle. A new Fourier map was generated to check the convergence of the procedure and to detect new cation positions. The structure arrived at in this way was then refined with the intensity data for all lines actually observed. Different combinations of variables were simultaneously varied in subsequent runs each composed of four to eight cycles of full matrix refinement. As a rule, positional parameters together with occupancy factors and temperature factors were varied alternatively. Although the correlation between occupancy and temperature factors is very close and these variables cannot be refined together in the same cycle, slow convergence was achieved in this way. The very intense (111) reflection was found to be much weaker than calculated in all three cases, possibly owing to secondary extinction, and therefore was always omitted from the refinement. An absorption correction corresponding to $\mu R = 0.4$ was applied in all cases and no further attempts were made to optimize this parameter. The atomic form factors were taken from International Tables, Vol. III, 1962; for the framework atoms the ionic charges were taken to be one-half of the nominal values and appropriate averages were taken. For the exchangeable cations, however, the form factors were based on their theoretical charge, +1. No dispersion corrections were included; the

Table II: Interatomic Distances and Bond Angles

	Structure I	Structure II	Structure III
(a) (Si, Al)-O_4 tetrahedron			
(Si, Al)-O(1)	1.63 A	1.60 A	1.62 A
(Si, Al)-O(2)	1.63 A	1.68 A	1.65 A
(Si, Al)-O(3)	1.70 A	1.71 A	1.61 A
(Si, Al)-O(4)	1.58 A	1.66 A	1.61 A
Mean value	1.635 A	1.662 A	1.623 A
(Si, Al)-O(1)-(Si, Al)	150°	142°	144°
(Si, Al)-O(2)-(Si, Al)	156°	150°	145°
(Si, Al)-O(3)-(Si, Al)	141°	135°	145°
(Si, Al)-O(4)-(Si, Al)	138°	136°	157°
Mean value	146.2°	140.8°	147.8°
O(1)-O(2)	2.57 A	2.73 A	2.66 A
O(1)-O(3)	2.57 A	2.74 A	2.47 A
O(1)-O(4)	2.67 A	2.66 A	2.76 A
O(2)-O(3)	2.71 A	2.56 A	2.71 A
O(2)-O(4)	2.68 A	2.69 A	2.65 A
O(3)-O(4)	2.80 A	2.88 A	2.62 A
Mean value	2.667 A	2.710 A	2.645 A
O(1)-(Si, Al)-O(2)	104°	113°	109°
O(1)-(Si, Al)-O(3)	101°	112°	100°
O(1)-(Si, Al)-O(4)	112°	109°	117°
O(2)-(Si, Al)-O(3)	109°	98°	113°
O(2)-(Si, Al)-O(4)	113°	107°	109°
O(3)-(Si, Al)-O(4)	117°	117°	109°
Mean value	109.3°	109.3°	109.5°
(b) Cation coordination			
M(1)-O(2)	2.33 A	2.78 A	2.32 A
M(1)-O(4)	2.89 A	2.95 A	2.93 A
M(2)-O(3)	2.44 A	2.64 A	2.86 A
M(2)-O(2)	3.10 A	3.08 A	3.22 A
M(3)-O(3)	2.71 A	2.75 A	2.65 A
M(3)-O(2)	3.51 A	3.42 A	3.53 A
M(3)-O(1)	3.62 A	3.73 A	3.60 A
M(2)-M(2)	4.48 A	3.52 A	3.50 A
M(2)-M(3)	2.61 A	3.21 A	3.24 A

function minimized in the refinement, the weighting scheme (except that unobserved reflections were omitted), and the R index for intensities were the same employed by Seff and Shoemaker.[13] The R indices in this paper are based on all intensities $N \leq N_{max}$ with unobserved reflections set equal to $I_{min}/2$ and the (111) reflection excluded. Standard deviations were computed in the conventional way from the residuals; however, examination of the calculated interatomic distances suggests that these standard deviations are unrealistically small and accordingly their values are not given. Bond distances and angles were computed employing a special FORTRAN II program written by G. R. E.

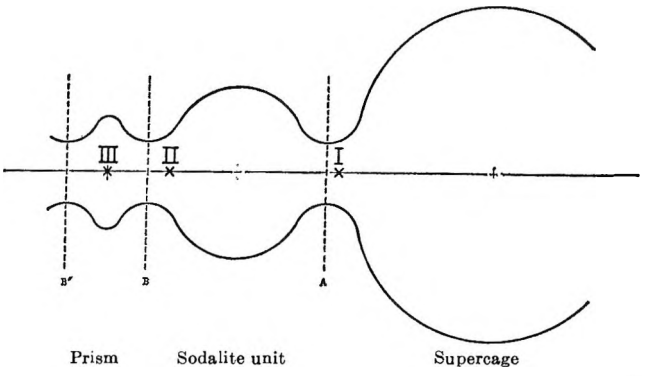

Figure 1. Schematic diagram of cages in synthetic faujasites showing cation positions. Center line is a threefold rotation axis (3m) of the structure. Heavy solid line represents boundary of cavities, as defined by oxygen ionic radii. Roman numerals identify cation positions (see text).

Dehydrated Sodium Faujasite (Structure I). The parameters, interatomic distances and angles, and observed and calculated intensities are presented in Tables I, II, and III, respectively. A final intensity R index of 0.19 was attained. This value was computed using all intensities with $3 < N \leq 384$.

The Na^+ ions were found to occupy three different sites on the threefold axis of the faujasite structure. These sites are associated with the $(Si, Al)_6O_6$ rings ("six rings") of the sodalite unit. The atoms of such a ring lie in three closely spaced parallel planes, one for six (Si, Al) atoms and two for groups of three oxygen atoms. A median plane halfway between the two oxygen planes will be used as a reference plane in the discussion of the cation positions.

Site I approaches, from outside of the sodalite unit, the center of the six-membered ring which faces the supercage of the faujasite structure (referred to as "ring A"); the cation lies almost exactly in the reference plane (see Figure 1). There are 30.0 ± 0.5 cations per unit cell at this site (for occupancy factors, see corresponding column in Table I). Each cation has three nearest oxygen neighbors [O(2)] at 2.33 A and three further ones [O(4)] at 2.89 A. Site II approaches, from inside of the sodalite unit, the six ring that forms the base of the pseudohexagonal prism around the center of symmetry ("ring B"). The reference plane to cation distance in this case is 0.91 A; there are 19.5 ± 0.5 cations in this position. Each is coordinated by three O(3) atoms at a distance of 2.44 A and three O(2) atoms at a distance of 3.10 A. Site III is at the center of symmetry, flanked by two ring B planes at 1.70 A distance. There are 7.5 ± 0.5 cations at this site which are surrounded by six O(3) atoms forming a slightly distorted octahedron, the Na-

Table III: Calculated and Observed Intensities ($\times 10^{-4}$)[c]

	Structure I		Structure II		Structure III			Structure I		Structure II		Structure III	
N	I_C	I_O	I_C	I_O	I_C	I_O	N	I_C	I_O	I_C	I_O	I_C	I_O
3	1988	621[b]	2129	809[b]	4510	1898[b]	187	469	497	534	373	1542	1674
8	624	637	492	564	182	151	192	42	75	357	291	439	385
11	743	647	743	779	1265	1000	195	610	576	746	729	1314	1448
12	29	31	91	128	63	45	196	7	32[a]	71	64[a]	83	162[a]
16	15	62	121	136	1216	1165	200	1087	1299	1661	1886	4210	4495
19	1528	1750	881	630	1070	1063	203	19	33[a]	181	67[a]	291	170[a]
24	28	3[a]	69	57	7	16[a]	204	192	156	156	67[a]	1080	850
27	262	369	349	516	332	491	208	78	34[a]	570	506	494	484
32	528	492	104	150	441	585	211	1242	1549	1570	1613	886	830
35	178	147	172	181	1396	1676	212	25	35[a]	364	447	247	179[a]
36	48	79	182	186	15	25[a]	216	76	167	142	72[a]	892	658
40	100	83	128	208	14	27[a]	219	173	170	393	473	934	667
43	2076	2047	2077	2527	1145	1542	224	300	335	15	75[a]	2	191[a]
44	2	6[a]	194	205	194	137	227	221	153	484	254	1837	1632
48	23	30	122	133	608	813	228	246	179	55	77[a]	145	195[a]
51	117	88	253	152	1138	1163	232	83	39[a]	9	78[a]	617	455
56	1458	1663	1435	1744	2592	2942	235	269	183	340	480	303	203[a]
59	44	65	257	189	1020	708	236	873	598	277	194	2022	1603
64	43	74	77	41	267	405	243	1793	1805	2322	2504	4097	5270
67	206	304	675	629	8	48[a]	244	48	42[a]	31	83[a]	897	1213
68	0	9[a]	1	19[a]	492	562	248	80	103	269	349	5	216[a]
72	546	706	1147	1315	951	879	251	561	566	981	679	2515	2395
75	2634	2602	2436	2474	5044	5011	256	269	130	1163	793	368	513
76	0	11[a]	96	46	368	357	259	573	400	636	580	347	228[a]
80	785	922	2855	2835	5786	5380	260	75	45[a]	47	90[a]	42	229[a]
83	219	122	641	431	2216	2012	264	184	110	319	309	391	691
84	393	235	270	185	1597	1210	267	649	845	1126	824	845	788
88	1862	1419	1078	1367	3512	3787	268	0	47[a]	57	94[a]	1356	1333
91	627	768	1246	1660	5297	5273	272	666	628	2877	3126	2410	2474
96	233	436	1457	1762	2661	3664	275	560	558	394	459	1295	2507
99	190	222	165	91	756	909	276	38	48[a]	253	300	11	247[a]
104	99	234	111	109	68	261	280	821	785	1131	776	1759	1171
107	35	32	72	75	1971	1739	283	144	121	293	277	554	254[a]
108	899	861	509	512	812	977	288	858	926	1514	1473	2884	2651
115	33	17[a]	81	34[a]	480	351	291	217	152	627	1126	2230	2865
116	51	42	310	271	129	210	292	1	52[a]	3	104[a]	243	264[a]
120	12	18[a]	0	36	153	91[a]	296	1143	1560	1060	1029	2505	2195
123	619	765	182	330	716	957	299	152	129	238	260	1472	1416
128	844	912	2325	3346	2580	3199	300	46	53[a]	76	107[a]	228	273[a]
131	706	634	427	350	5110	4613	304	4	54[a]	106	109[a]	15	277[a]
132	116	107	163	40[a]	1140	1222	307	88	55[a]	38	110[a]	243	280[a]
136	15	21[a]	123	94	162	105[a]	308	25	55[a]	14	111[a]	340	281[a]
139	792	1278	482	585	1009	1394	312	6	56[a]	82	112[a]	288	286[a]
140	25	21[a]	902	817	288	335	315	65	56[a]	105	114[a]	565	289[a]
144	520	574	2	44[a]	3	113[a]	320	98	58[a]	13	116[a]	15	294[a]
147	20	23[a]	148	110	79	115[a]	323	236	226	390	449	766	603
152	6	23[a]	143	206	709	1479	324	309	296	261	359	1793	2035
155	135	112	198	48[a]	14	123[a]	328	1854	2441	2571	3152	3959	3525
160	16	25[a]	253	158	78	127[a]	331	263	202	377	327	1970	2588
163	132	184	343	287	1613	1429	332	4	60[a]	410	362	791	983
164	917	768	692	453	2948	2589	336	126	148	58	122[a]	118	311[a]
168	862	833	980	818	95	135[a]	339	1048	1051	1742	1673	2969	2476
171	194	126	275	351	1153	1236	344	926	851	1010	1204	1064	674
172	4	27[a]	38	55[a]	78	139[a]	347	87	154	324	309	907	828
176	1	28[a]	314	441	411	395	352	26	64[a]	0	129[a]	0	328[a]
179	660	657	715	711	1883	1809	355	417	344	518	609	981	919
180	221	241	125	58[a]	2	147[a]	356	49	65[a]	116	131[a]	192	333[a]
184	33	29[a]	295	144	173	151[a]	360	446	307	891	660	1952	1573

Table III (*continued*)

	Structure I		Structure II		Structure III	
N	I_C	I_O	I_C	I_O	I_C	I_O
363	1284	1912	1543	2126	2875	3731
364	19	67[a]	7	134[a]	491	1084
371	313	440	735	829	344	348[a]
372	39	68[a]	37	137[a]	3	349[a]
376	61	69[a]	210	139[a]	118	353[a]
379	842	864	738	795	1270	1664
384	418	351	2011	2259		
388			26	144[a]		
392			856	824		

[a] Unobserved intensities, taken as $I_{min}/2$. [b] Not included in the computation of the R factor. [c] The Lorentz polarization factor was omitted from the calculated intensities and divided out of the observed ones.

(3)–O(3) distance being 2.77 A. The total number of cations computed from the occupancy factors agrees with the figure given by chemical analysis within limits of error. Figure 2 shows a sodalite unit with associated Na^+ cations. The apparent temperature factors encountered in this work are higher than in other tectosilicates and closer to values familiar from organic compounds. Reasons for this behavior have been discussed previously.[13] The apparent temperature factor associated with Na(2) is unusually high, with a value of 18.7 A.[2] Moreover, the sodium peak in the electron density map is more elongated in the direction of the 3 axis than would be expected from ordinary anisotropic thermal motion. This effect is quite possibly due to a positional disorder along this axis, since a small proportion of the cation occupying this kind of site may have as near neighbors other cations on the opposite side of ring B, thus experiencing a considerable electrostatic repulsion (Na(2)–Na(3) = 2.61 A) which stabilizes the cation in a position closer to the center of the sodalite unit. Therefore, the coordinate 0.0609 should be considered an averaged value connected with two or more actual positions.

The Na(1)–O(2) and Na(2)–O(3) distances agree with values found in other tectosilicates. The relatively long Na(3)–O(3) distances are fixed by the aluminosilicate framework.

Dehydrated Potassium Faujasite (*Structure II*). The final R index as defined previously and computed including intensities with $3 < N \leqq 392$ is 0.22. Results are given in Tables I, II, and III. The same cation arrangement as in the sodium zeolite was found but with larger bond distances and somewhat different occupancy factors. The number of cations located corresponds well to the figure arrived at by chemical

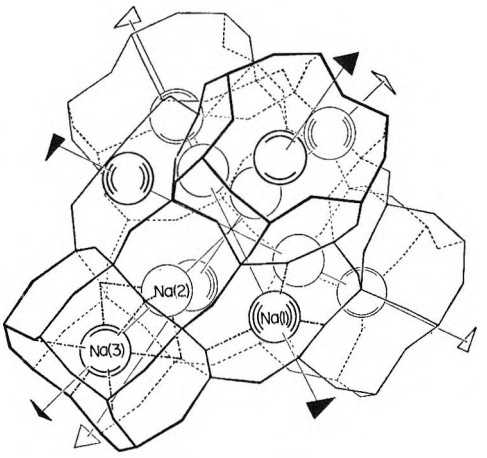

Figure 2. The structure of one sodalite unit with adjacent distorted prisms, showing the aluminosilicate framework (solid and dashed lines), cations (circles, variously shaded according to type of position), nearest cation–oxygen distances (dash–dot lines), and threefold symmetry axes.

analysis. Site I is occupied by 30.0 ± 0.3 K^+ ions surrounded by three O(2) and three O(4) atoms at respective distances of 2.78 and 2.95 A. The distance of the cation from the ring A reference plane is 1.22 A. In site II, 14.2 ± 0.3 cations are found with three O(3) at 2.64 A and three additional O(2) atoms at 3.08 A. The cation is recessed from the ring plane B toward the center of the sodalite unit 1.39 A along the threefold axis. Site III at the center of a moderately distorted octahedron composed of six O(3) atoms at a distance of 2.75 A from the center of symmetry contains 12.0 ± 0.3 cations. In this case the ring B plane to cation distance is 1.82 A. The values predicted from ionic radii in Goldschmidt's and Pauling's systems for K^+–O^{2-} distances are, respectively, 2.65 and 2.73 A. The observed values are in reasonable agreement with those theoretical distances, particularly the former one.

Dehydrated Silver Faujasite (*Structure III*). Including intensities $3 < N \leqq 379$, the R index 0.19 was attained. The Ag^+ ions were found to occupy positions[15] on the threefold axes analogous to the previous cases. The occupancy factors indicate a total number of 55 silver cations in the structure; within reasonable limits all cations were located. The numerical data are presented in Tables I, II, and III.

There are 16 ± 0.6 cations at site III, 10.7 ± 0.6 at site II, and 28.3 ± 0.6 at site I. Regarding the sites II and III the trends characterizing the transition from Na to K are again observed; the occupancy factor

(15) The Ag^+ positions found were roughly the same as those found previously on a Fourier line (*xxx*) in unpublished work on a similar material by L. Broussard and D. P. Shoemaker, Esso Research Laboratories, Baton Rouge, La.

of site III increases to unity while that for site II decreases further. There are also somewhat fewer cations at site I. Site II has three O(3) neighbors at 2.86 A and three more oxygens [O(2)] at 3.22 A; the cation is positioned inside of the sodalite unit at 1.55 A from the ring B reference plane. Site I has three ligands O(2) at 2.32 A and three additional ligands O(4) at 2.93 A; its displacement from ring A toward the center of the supercage is only 0.46 A. The O(3) ligands of the distorted octahedron are connected with site III at a distance of 2.65 A from the center of symmetry. The distance from ring B plane to site III is 1.69 A.

The sum of the Ag^+ and O^{2-} radii is 2.45 A if Goldschmidt ionic radii are employed or 2.66 A if Pauling ionic radii are used. The crystal structures of several oxygen-containing silver salts have been determined; the smallest approach distances of Ag to O reported vary between 2.23 A in silver tetraborate $Ag_2O \cdot 4B_2O_3$[16a] or 2.37 A in silver polyphosphate $(AgPO_3)_z$[16b] and approximately 2.5 A, *e.g.*, 2.48 A in $AgNO_3$.[17] In Ag_2O, there is a linear O–Ag–O arrangement with only 2.05 A for the Ag–O distance. These data suggest varying degrees of covalency in the Ag–O bond. It appears justified to assume some degree of covalent bonding for site I with its comparatively short Ag–O distances (2.32 A). The remarkably long recession of Ag(2) toward the interior of the sodalite unit which gives rise to an Ag–O distance of 2.86 A is probably due to the electrostatic repulsion from the Ag^+ ion at the center of symmetry at a distance of 3.24 A.

Aluminosilicate Framework. Smith and Bailey[18] summarize the results of the structural investigations of the framework silicates, predominantly feldspars, and find a linear relationship between the percentage of Al in a particular tetrahedral (Si, Al)O_4 site and the mean (Si, Al)–O distance averaged for the same (Si, Al)O_4 tetrahedron. Furthermore, considerable differences up to approximately 0.1 A occur between different (Si, Al)–O bonding lengths of a particular tetrahedron. The O–(Si, Al)–O and particularly the (Si, Al)–O–(Si, Al) angles are more flexible; for the latter, values between 120 and 180° have been observed. The distance rules may be considered valid for the Na and K zeolites; there is some doubt about their applicability to the Ag zeolite as some degree of covalent cation bonding appears to be involved.

The mean (Si, Al)–O distance for the structures I and II, 1.648 A, compares favorably with 1.652 A for feldspars with the same Si:Al ratio. It also agrees with the value (1.647 A) found by Baur[3] for the hydrated Na zeolite. The difference between 1.635 A for the tetrahedral average for structure I and 1.662 for structure II has no ready explanation in physical terms and perhaps gives a better measure of the uncertainties in the bond distances than do the least-squares estimates. The differences between the extreme (Si, Al)–O distances, which are 0.12 in structure I and 0.11 in structure II, do not violate the rules set forth above. The mean angle (Si, Al)–O–(Si, Al) is 143.5°, which is close to the general average of 141°.[19] The maximum deviations from the mean for this angle and the O–(Si, Al)–O angle are also within usual boundaries. In the case of structure III, a larger uncertainty is probable in Si–O distances since the photographs are somewhat inferior to those of the other materials and since the cation makes a much larger contribution to the structure factors.

Other Results on Cation Positions in Related Zeolites. Structure determinations of dehydrated synthetic zeolite type "A" and dehydrated natural chabazite reveal a similar pattern of cation complexing.

The structure of dehydrated zeolite 5A ($Ca_4Na_4Al_{12}Si_{12}O_4$l) was investigated by Seff and Shoemaker.[13] The Ca^{2+} ion apparently prefers a position near the middle of the oxygen plane associated with the six-membered ring, with three oxygen neighbors at a distance of 2.32 A and three further ones at 2.84 A, while the Na^+ cation is apparently recessed into the sodalite unit 0.37 A along the threefold axis having oxygen neighbors at 2.33 and 2.86 A. This interpretation is not, however, entirely clear-cut, as the apparent resolution of the two cations may be in part a result of anisotropic thermal motion.

The framework of calcium chabazite may be characterized as a rhombohedral arrangement of double six-membered rings (pseudohexagonal prisms) which are similar to those found in the faujasite structure and interconnected by four-membered rings. According to Smith,[20] 0.6 Ca^+ ions out of 1.95 in the unit cell occupy the centers of the distorted pseudohexagonal prisms (corresponding to site III in this paper), surrounded by a slightly distorted oxygen octahedron at a distance of 2.38 A; 0.7 Ca^{2+} are apparently located on the 3 axis close to the center of the six-membered rings with a 3 + 3 oxygen coordination at distances of 2.37 and 2.84 A, respectively (this position corresponds to site II). The rest of the cations are believed to occupy

(16) (a) J. Krogh-Moe, *Acta Cryst.*, 18, 77 (1965); (b) K. H. Jost, *ibid.*, 14, 779 (1961).

(17) P. F. Lindley and P. Woodward, *J. Chem. Soc.*, 123 (1966).

(18) J. V. Smith and S. W. Bailey, *Acta Cryst.*, 16, 801 (1963).

(19) F. Liebau, *ibid.*, 14, 1103 (1961).

(20) J. V. Smith, *ibid.*, 15, 835 (1962).

a position of lower symmetry; however this has not been firmly established.

Acknowledgments. We wish to thank Drs. P. Eberly and H. E. Robson of Esso Research Laboratories (Baton Rouge, La.) for the specimen of synthetic faujasite used in this work, and Dr. Leo Broussard of those laboratories for valuable discussions. We thank the Humble Oil and Refining Co. (Esso Research Laboratories) for financial support. Computations were done principally at the Massachusetts Institute of Technology Computation Center.

Association in Vapors of Ionic Salts. The Vapor Mixtures Potassium Chloride–Lead Chloride and Rubidium Chloride–Lead Chloride

by K. Hagemark, D. Hengstenberg, and M. Blander

North American Aviation Science Center, Thousand Oaks, California 91360 *(Received December 8, 1966)*

Pressure–temperature relations at constant density have been measured at 1260–1430°K for binary mixtures of KCl–$PbCl_2$ and RbCl–$PbCl_2$ using a liquid gold isotensoscope. The large deviations from ideal gas behavior are consistent with the presence of the associated vapor species K_2Cl_2, Rb_2Cl_2, $KPbCl_3$, and $RbPbCl_3$. The association constants, K (liters per mole), for $KPbCl_3$ and $RbPbCl_3$ are calculated from the data. The magnitude of the association constants is the same as that of the dimerization constants for the alkali halides; however, unlike the case of the dimerization constant, the values for the association constant increase with increasing alkali cation radius. For example, at 1300°K, the values for log K are 3.45 and 3.66 for $KPbCl_3$ and $RbPbCl_3$, respectively.

Introduction

Single component alkali halide vapors have been comprehensively and quantitatively investigated,[1-3] and the data on alkali halide dimers have been useful in developing theories of these systems.[1,4]

There have been many investigations of vapor compounds in binary mixtures containing an alkali halide: molecular beam experiments,[5] mass spectrometry,[6-10] electronic absorption spectra,[11] and combined vapor "pressure" techniques;[7,12] however, no unified quantitative work has been done. Such work, in which one investigates systematically the influence of various ionic parameters on association constants, is necessary for the ultimate development of a theoretical understanding of these vapors. Quantitative data for the equation of state of binary salt vapors are also required for evaluation of thermodynamic functions of liquid or solid mixtures from vapor pressure measurements.

(1) S. H. Bauer and R. F. Porter, "Molten Salt Chemistry," M. Blander, Ed., Interscience Publishers, Inc., New York, N. Y., 1964, p 607.

(2) S. Datz, W. T. Smith, Jr., and E. H. Taylor, *J. Chem. Phys.*, **34**, 558 (1961).

(3) K. Hagemark, M. Blander, and E. B. Luchsinger, *J. Phys. Chem.*, **70**, 276 (1966).

(4) M. Blander, *J. Chem. Phys.*, **41**, 170 (1964).

(5) V. S. Rao and P. Kusch, *ibid.*, **34**, 832 (1961).

(6) J. Berkowitz and W. A. Chupka, *Ann. N. Y. Acad. Sci.*, **69**, 1073 (1960).

(7) C. Beusmann, "Activities in the KCl–$FeCl_2$ and LiCl–$FeCl_2$ Systems," ORNL-2323, Office of Technical Services, U. S. Department of Commerce, Washington 25, D. C., 1957.

(8) R. F. Porter and E. E. Zeller, *J. Chem. Phys.*, **33**, 858 (1960).

(9) A. Büchler and J. L. Stauffer, "Thermodynamics of Nuclear Materials," Vol. I, IAEA, Vienna, 1965, p 271.

In the present work, measurements of the pressure–temperature relations at constant density were made for the binary gas mixtures KCl–$PbCl_2$ and RbCl–$PbCl_2$. The large deviations from ideal gas behavior are accounted for by assuming the presence of the associated vapor species K_2Cl_2, Rb_2Cl_2, $KPbCl_3$, and $RbPbCl_3$. Association constants for the latter two species are deduced from our data. Previously the dimerization constants for KCl and RbCl have been obtained.[2] $PbCl_2$ has been shown by mass spectrometry to be monomeric in the vapor.[13] Qualitative observations of 1:1 compounds between alkali chlorides and $PbCl_2$ have been reported.[10]

Experimental Method

Our experimental method is a modification[3] of the technique used by Datz, *et al.*,[2] in which the pressures of weighed amounts of completely vaporized salts are measured at several temperatures in a vessel of known volume. The method has the advantage that the partial pressures of both components may be independently varied. This allows one to make an independent check of the stoichiometry of the associated vapor species and to obtain absolute values of the association constants.

A detailed description of the apparatus is given in a previous paper;[3] thus, only the principal features will be described. A fused silica vessel of known volume is connected to one side of a U-tube filled with liquid gold. Argon pressure on the other side of the U-tube is controlled so that it equalizes the pressure exerted by the ionic salt vapor in the silica vessel. This equalization is indicated by the gold levels being equal on both sides of the U-tube. The compensating Ar pressure is determined by a Hg manometer. A cathetometer is used to observe the levels in the U-tube containing the gold and in the mercury manometer. The upper temperature limit of the measurements is about 1150°, the softening point of the silica. Because we are interested only in unsaturated vapors, the lower temperature limit is dependent on the amount of salt introduced into the vessel. The more salt that is added, the higher is the temperature necessary to evaporate the salt completely and the narrower is the temperature range of the measurements. The materials $PbCl_2$ and KCl were Baker Analyzed reagents and the RbCl, from Alfa Inorganics, Inc., was 99.9% pure. The salts were used without further purification.

Thermodynamic Calculations

The total pressure, p, of a gas mixture is given by the sum of the partial pressures, p_i, of all the gas species, i. As will be shown later, our data are consistent with the presence of the species MCl, M_2Cl_2, $PbCl_2$, and $MPbCl_3$, where M = K or Rb, so that

$$p = \Sigma p_i = p_{MCl} + p_{M_2Cl_2} + p_{PbCl_2} + p_{MPbCl_3} \quad (1)$$

The partial pressure of species i can be calculated from

$$p_i = \frac{n_i R^* T}{V} \quad (2)$$

where n_i is the number of moles of species i present in the vapor, $R^* = 62.360$ l. mm $mole^{-1}$ deg^{-1}, and V is the volume of the vessel. Further, the n_i values are related to the respective weights of material by

$$n_{PbCl_2} + n_{MPbCl_3} = \frac{W_{PbCl_2}}{M_{PbCl_2}} \quad (3)$$

$$n_{MCl} + 2n_{M_2Cl_2} + n_{MPbCl_3} = \frac{W_{MCl}}{M_{MCl}} \quad (4)$$

W_{MCl} and M_{MCl} (or W_{PbCl_2} and M_{PbCl_2}) are the actual weights and the molecular weights, respectively, of alkali chloride (or lead chloride). The dimerization constants (liters per mole) for alkali halides are given by

$$K_2 = R^* T \frac{p_{M_2Cl_2}}{p^2_{MCl}} \quad (5)$$

and have been measured previously.[2] The association constants, K, for the vapor phase reaction

$$MCl + PbCl_2 \rightleftarrows MPbCl_3 \quad (A)$$

are given by

$$K = R^* T \frac{p_{MPbCl_3}}{p_{MCl} p_{PbCl_2}} \quad (6)$$

K may be calculated from eq 1–6 with the aid of the measured parameters p, V, W_{MCl}, W_{PbCl_2}, and the known values of the dimerization constant, K_2. If we subtract eq 3 from eq 1 we obtain

$$p - \frac{W_{PbCl_2} R^* T}{M_{PbCl_2} V} = p_{MCl} + p_{M_2Cl_2} = p_{MCl} + \frac{K_2}{R^* T} p_{MCl}^2 \quad (7)$$

This quadratic equation can be solved for p_{MCl} and $p_{M_2Cl_2}$ when K_2 is known. Knowing p_{MCl} and $p_{M_2Cl_2}$,

(10) H. Bloom and J. W. Hastie, *Australian J. Chem.*, 19, 1003 (1966).

(11) D. M. Gruen and C. W. Decock, *J. Chem. Phys.*, 43, 3395 (1965).

(12) E. E. Schrier and H. M. Clark, *J. Phys. Chem.*, 67, 1259 (1963).

(13) A. Büchler, J. L. Stauffer, and W. Klemperer, *J. Am. Chem. Soc.*, 86, 4544 (1964).

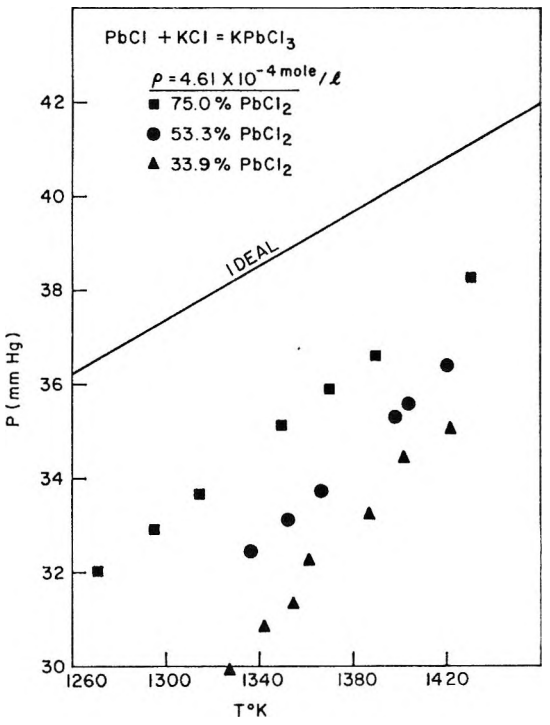

Figure 1. Experimental data for vapor mixtures of KCl–$PbCl_2$ shown as p (mm) *vs.* T (°K). The line corresponds to p^{ideal}.

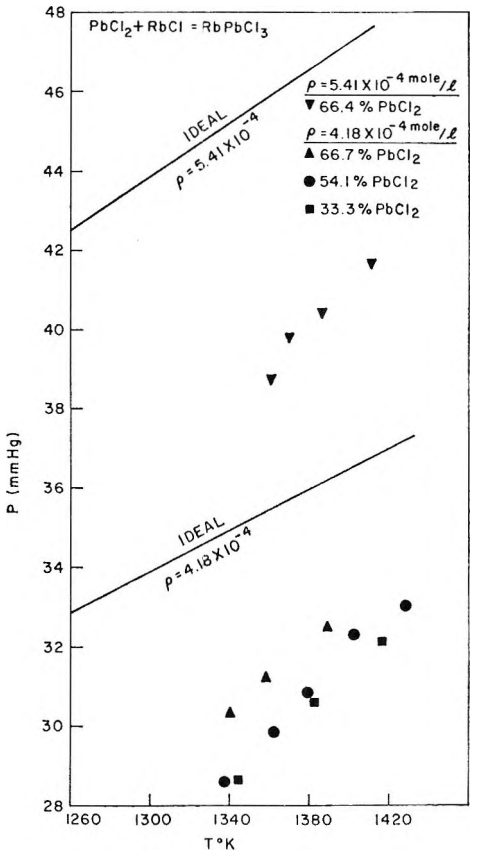

Figure 2. Experimental data for vapor mixtures of $RbCl$–$PbCl_2$ shown as p (mm) *vs.* T (°K). The two lines correspond to p^{ideal} for the vapor mixtures of densities $\rho = 5.41 \times 10^{-4}$ mole $l.^{-1}$ and $\rho = 4.18 \times 10^{-4}$ mole $l.^{-1}$, respectively.

we may calculate p_{MPbCl_3} from eq 2 and 4. From this value of p_{MPbCl_3} and eq 2 and 3 we may calculate p_{PbCl_2} and consequently the association constant, K, for reaction A.

The assumption that the only significant species formed between $PbCl_2$ and the alkali halide is the 1:1 compound can be tested by varying the partial pressures (and the ratios) of the two salts in the binary mixtures. The constancy of the apparent association constants is evidence that the assumption is correct. The assumption is also consistent with mass spectrometric observations.[10]

Results

The experimental data are shown in Figures 1 and 2, where the observed pressure is plotted as a function of temperature for seven series of measurements. In each series, several measurements were made in an ascending and several in a descending set of temperatures with approximately 3 hr being allowed at each temperature for the attainment of equilibrium. For the binary system KCl–$PbCl_2$, three series of measurements were made at a total density, ρ, of 4.61×10^{-4} mole/l. with the individual series containing 75.0, 53.3, and 33.9 mole % $PbCl_2$. Four series of measurements were carried out in the $RbCl$–$PbCl_2$ system, one with a density of 5.41×10^{-4} mole/l. and 66.4 mole % $PbCl_2$ and three with a density of 4.18×10^{-4} mole/l. with 66.7, 54.1, and 33.3 mole % $PbCl_2$. The ideal total pressure, given by

$$p^{ideal} = \rho RT \qquad (8)$$

is shown as a solid line in the figures, where ρ is the ideal density. The negative deviations from ideal gas behavior are of the order of 4–6 mm. Because of the contribution of the alkali chloride dimer, the negative deviations are greater for mixtures which are lower in the percentage of $PbCl_2$ (and higher in the partial pressure of the alkali chloride). All the deviations from ideal gas behavior cannot be accounted for by the dimer and one must postulate a compound between the alkali chloride and $PbCl_2$. If we assume the simplest compound, $MPbCl_3$, we may calculate values of the partial pressures of all the species and the association constants (K) for reaction A. These data are given in Table I and a plot of the log of the association constants (K) *vs.* T^{-1} is given in Figures 3 and 4. The

Table I: Experimental Data, Calculated Partial Pressures of Vapor Species, and Equilibrium Constants for the Compound $KPbCl_3$

Run, $\rho = 4.61 \times 10^{-4}$ mole/l.	T, °K	p_{obsd}	p^{ideal}	p_{KCl}	$p_{K_2Cl_2}$	p_{PbCl_2}	p_{KPbCl_3}	Log K
53.3% $PbCl_2$	1336	32.47	38.44	9.67	2.31	16.83	3.66	3.27
	1403	35.70	40.37	12.46	1.74	18.58	2.93	3.04
	1398	35.32	40.23	12.13	1.74	18.27	3.17	3.09
	1366	33.75	39.30	10.80	2.00	17.40	3.55	3.21
	1420	36.42	40.86	13.06	1.58	18.92	2.86	3.01
	1352	33.15	38.90	10.28	2.14	17.12	3.61	3.24
75.0% $PbCl_2$	1314	33.68	37.83	4.62	0.69	24.91	3.46	3.39
	1389	36.60	39.98	6.12	0.49	27.10	2.89	3.18
	1430	38.28	41.16	7.00	0.41	28.40	2.47	3.05
	1349	35.13	38.83	5.39	0.61	26.03	3.09	3.26
	1369	35.89	39.41	5.78	0.55	26.59	2.97	3.22
	1295	32.91	37.28	4.21	0.74	24.33	3.63	3.46
	1271	32.01	36.59	3.76	0.81	23.67	3.77	3.53
33.9% $PbCl_2$	1361	32.22	39.14	14.92	4.05	10.38	2.87	3.20
	1401	34.47	40.29	17.38	3.46	11.28	2.36	3.02
	1327	29.89	38.16	12.59	4.38	9.03	3.89	3.45
	1342	30.84	38.59	13.56	4.22	9.53	3.53	3.36
	1354	31.34	38.93	14.18	3.98	9.57	3.61	3.35
	1387	33.26	39.88	16.23	3.54	10.42	3.08	3.20
	1421	35.07	40.86	18.20	3.03	11.07	2.76	3.08

Table II: Experimental Data, Calculated Partial Pressures of Vapor Species, and Equilibrium Constants for the Compound $RbPbCl_3$

Run	T, °K	p_{obsd}	p^{ideal}	p_{RbCl}	$p_{Rb_2Cl_2}$	p_{PbCl_2}	p_{RbPbCl_3}	Log K
$\rho = 4.18 \times 10^{-4}$ mole $l.^{-1}$ 54.1% $PbCl_2$	1337	28.63	34.85	8.92	0.85	13.49	5.37	3.57
	1379	30.87	35.95	10.67	0.75	15.12	4.33	3.36
	1428	33.03	37.22	12.31	0.58	16.54	3.60	3.20
	1402	32.32	36.55	11.82	0.71	16.25	3.53	3.21
	1362	29.88	35.50	9.89	0.78	14.36	4.85	3.46
$\rho = 4.18 \times 10^{-4}$ mole $l.^{-1}$ 33.3% $PbCl_2$	1416	32.12	36.91	18.37	1.48	8.96	3.31	3.25
	1382	30.60	36.02	16.82	1.80	8.36	3.62	3.35
	1344	28.65	35.03	14.84	2.16	7.43	4.22	3.51
$\rho = 4.18 \times 10^{-4}$ mole $l.^{-1}$ 66.7% $PbCl_2$	1358	31.21	35.42	7.14	0.42	19.86	3.79	3.36
	1389	32.50	36.22	7.94	0.37	20.84	3.35	3.24
	1340	30.32	34.95	6.54	0.44	19.15	4.19	3.45
$\rho = 5.41 \times 10^{-4}$ mole $l.^{-1}$ 66.4% $PbCl_2$	1370	39.82	46.18	8.62	0.54	24.84	5.82	3.37
	1411	41.73	47.56	9.71	0.44	26.19	5.39	3.27
	1361	38.73	45.87	7.78	0.49	23.81	6.65	3.48
	1386	40.42	46.72	8.92	0.48	25.20	5.82	3.35

precision of the association constants is lowered by the uncertainties in calculating and correcting for the amount of alkali halide dimer. Within the uncertainties in the data, the association constants are independent of the partial pressure of each of the components. Thus, if compounds other than $MPbCl_3$ are present, the amounts are relatively insignificant. For example, the presence of a significant amount of M_2PbCl_4 would lead to apparent values of K which would increase with the partial pressure of the alkali halide monomer.

A least-squares treatment of the data leads to the two equations $\log K = -1.399 + 6310/T$ for the KCl–$PbCl_2$ system and $\log K = -1.559 + 6782/T$ for the

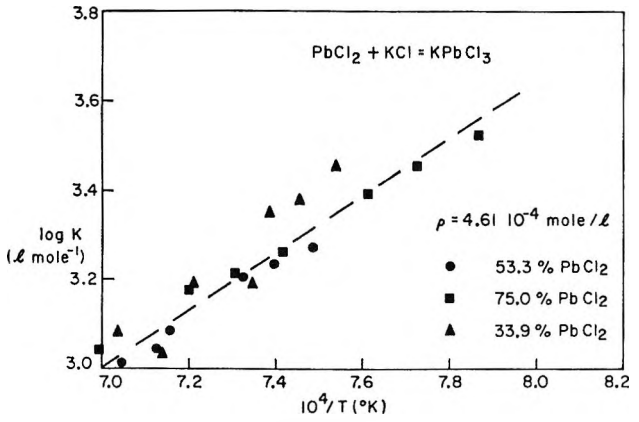

Figure 3. The calculated association constants for the equilibrium KCl + $PbCl_2$ = $KPbCl_3$.

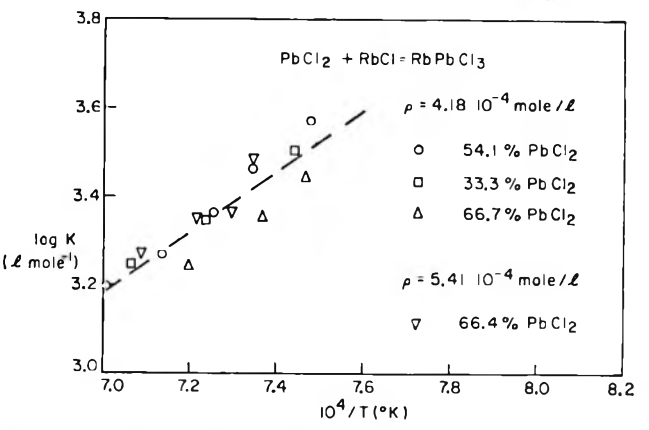

Figure 4. The calculated association constants for the equilibrium RbCl + $PbCl_2$ = $RbPbCl_3$.

RbCl–$PbCl_2$ system, which represent the data with a standard deviation of 5×10^{-2}. From these equations we can calculate the energies (ΔE) and the entropies of association (ΔS_p) of −29 kcal/mole and −17.7 eu for $KPbCl_3$ and −31 kcal/mole and −18.4 eu for $RbPbCl_3$. The standard states for the entropies are 1 atm. However, the scatter displayed by the data leads to large uncertainties in the values for the energy and entropy of association. At 1300°K, the value of log K for the formation of $KPbCl_3$ is 3.45 and for $RbPbCl_3$, 3.66. Thus, these association constants are of the same magnitude as the dimerization constant for alkali halides, but the association constants are larger the larger the alkali cation radius. (The dimerization constants for the alkali halides decreased with increasing alkali cation radius.) (See Table II.)

The apparent entropies of association are considerably less negative than the entropies of dimerization of alkali halides. Consistent with the present entropy values are the reported values of the entropies of dimerization of TlF and TlCl.[11] These latter entropies appear to be consistent with linear molecules of Tl_2X_2 and one might postulate that a linear arrangement M–Cl–Pb exists. However, such speculation is unwarranted without more precise thermodynamic data and some structural studies as with electron diffraction or absorption spectra. We plan further studies of similar mixtures as well as of mixtures of two alkali halides.

Acknowledgments. The authors wish to thank Mr. Ernest Eisel, who constructed the fused silica apparatus.

(14) F. J. Keneshea and D. Cubiocciotti, *J. Phys. Chem.*, 69, 3910 (1965).

Potentiometric Titration of Amphoteric Surfactants in Micellar Solutions

by Fumikatsu Tokiwa and Kenji Ohki

Research Laboratories, Kao Soap Company, Wakayama-shi, Japan *(Received December 9, 1966)*

Potentiometric titration curves have been obtained for micellar solutions of amphoteric surfactants, N-dodecyl-β-aminopropionic acid (DAPA) and N-dodecyl-β-iminodipropionic acid (DIPA), in the presence of 0.10 *M* sodium chloride. The potentiometric equation for surfactant micelles, proposed in the previous paper, has been developed to describe the electrochemical behavior of these amphoteric surfactants. The surface potential, evaluated from the titration curves, of the DAPA micelle is higher than that of the DIPA micelle, and their potentiometric behavior was discussed on the basis of a Gouy–Chapman model for a uniformly charged plane. The different potentiometric behavior between DAPA and DIPA micelles may be accounted for by different structural features of the micelles, probably the DIPA micelle having a looser structure.

Introduction

In the previous paper[1] the general potentiometric titration equation for polyelectrolytes[2,3] has been successfully applied to the interpretation of potentiometric titration data of a nonionic–cationic surfactant, dimethyldodecylamine oxide ($C_{12}H_{25}N(CH_3)_2OH^+ \rightleftarrows C_{12}H_{25}N(CH_3)_2O + H^+$), by taking into account the micelles formed in the solution above its critical micelle concentration (cmc). An expression for the potentiometric behavior of the micelle of this surfactant can be written[1]

$$\mathrm{pH} + \log \frac{\beta_M}{1 - \beta_M} = \mathrm{p}K_{0,M} - \frac{0.434}{kT}\left(\frac{\partial G_{el}}{\partial \zeta}\right) \quad (1)$$

where $\mathrm{p}K_{0,M}$ is the negative logarithm of the intrinsic dissociation constant of the micelle and G_{el} is the electrostatic free energy of the micelle carrying ζ positive charges. Here, the β_M in eq 1 can be expressed as[1]

$$\beta_M = (\beta - x\beta_m)/(1 - x); \quad x = c_0/c \quad (2)$$

where β is the observed degree of ionization of the surfactant, β_m and β_M are the degrees of ionization of the monomer and of the micelle, respectively, c is the total concentration of the surfactant, and c_0 is the monomer concentration which can be assumed to be nearly equal to the cmc.[4,5] For sufficiently concentrated solutions where c is very large compared to c_0, x approaches zero and then β_M also approaches β, as described in eq 2. Thus, when we choose a solution of such high concentrations as a test solution, the experimentally measurable β can be used as β_M.

The purpose of the present paper is to extend the above potentiometric equation for micelles to the interpretation of the electrochemical behavior of amphoteric surfactants. The micelles of amphoteric surfactants composed of acidic and basic groups are of interest as a model of amphoteric colloids. The electrochemical behavior of these micelles resembles that of proteins, while their chemical structure relates them to the common surfactants.

The amphoteric surfactants studied are N-dodecyl-β-aminopropionic acid (abbreviated as DAPA) and N-dodecyl-β-iminodipropionic acid (abbreviated as DIPA) which can exist in both anionic and cationic forms depending upon the pH of the solutions. With DAPA, these two forms are related by the equilibrium (where R = $C_{12}H_{25}$)

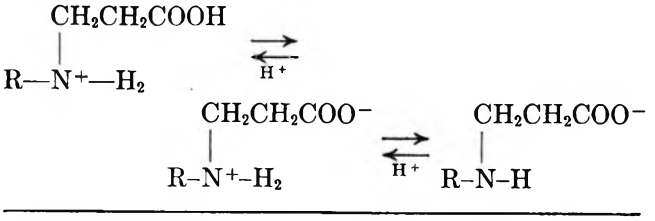

(1) F. Tokiwa and K. Ohki, *J. Phys. Chem.*, **70**, 3437 (1966).

(2) A. Katchalsky and J. Gillis, *Rec. Trav. Chim.*, **68**, 879 (1949).

(3) R. Arnold and J. Th. G. Overbeek, *ibid.*, **69**, 192 (1950).

(4) E. Hutchinson, *Z. Physik. Chem.* (Frankfurt), **21**, 38 (1959); E. Hutchinson, V. E. Sheaffer, and F. Tokiwa, *J. Phys. Chem.*, **68**, 2818 (1964).

With DIPA, the equilibrium is

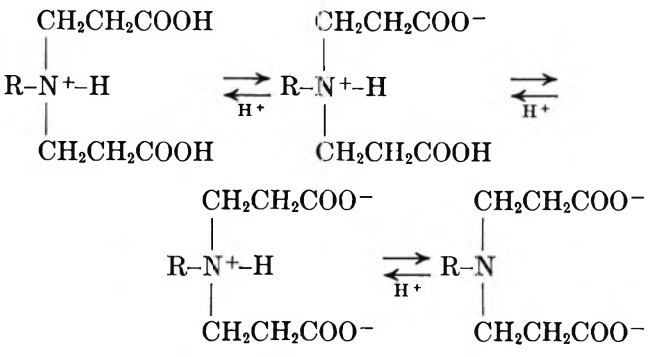

Expressing the degree of ionization of the carboxyl group as α and that of the amino (or imino) group as β, we may write the forms of the potentiometric equations for the micelles of these surfactants as

$$\mathrm{pH} - \log \frac{\alpha_M}{1 - \alpha_M} = \mathrm{p}K^{(a)}{}_{0,M} + \frac{0.434}{kT}\left(\frac{\partial G_{el}(\zeta, \nu)}{\partial \nu}\right) \quad (3)$$

$$\mathrm{pH} + \log \frac{\beta_M}{1 - \beta_M} = \mathrm{p}K^{(b)}{}_{0,M} - \frac{0.434}{kT}\left(\frac{\partial G_{el}(\zeta, \nu)}{\partial \zeta}\right) \quad (4)$$

where $\mathrm{p}K^{(a)}{}_{0,M}$ and $\mathrm{p}K^{(b)}{}_{0,M}$ are the intrinsic dissociation constants of the acidic and of the basic group, respectively, and the subscript, M, refers to the micelles. The state of ionization of the amphoteric micelles is given by the number of positive (ζ) and negative (ν) ionized groups carried by each micelle, and the net charge ($\zeta - \nu$) substantially contributes to the electrostatic free energy of the micelle.

Experimental Section

Materials. N-Dodecyl-β-aminopropionic acid (DAPA) was prepared by the reaction of dodecyl amine with β-propiolactone in acetonitrile at 25–30° for 4 hr, according to Gresham, *et al.*[6] (The dodecylamine used was shown to be more than 99.5% pure by gas chromatography.) The crude product was purified by repeated recrystallization from a mixture of acetone and water and then dried under vacuum. Thin layer chromatography showed that the purified sample was free of the unreacted amine but contained a very small amount of N-dodecyl-β-iminodipropionic acid (less than 1.0% by mass spectroscopy).

N-Dodecyl-β-iminodipropionic acid (DIPA) was prepared by the reaction of the dodecylamine with methyl acrylate in methanol at 70–75° for 15 hr, followed by saponification of the methyl ester of DIPA with sodium hydroxide.[7] The product obtained was in the form of the sodium salt of DIPA. It was repeatedly recrystallized from a mixture of acetone and water and then dried under vacuum. The presence of DAPA could not be detected by thin layer chromatography and mass spectroscopy.

Preparation of Solutions. Stock solutions were prepared on a weight per volume basis and diluted volumetrically to the desired concentrations. Glass-redistilled water was used to make up all solutions.

pH Measurements. A Potentiograph E-336 pH meter (Metrohm Herisau Cc.), accurate to 0.01 pH unit, was used with Beckman standard buffers. The titrations were carried out in an atmosphere of purified nitrogen at 25°, using standardized hydrochloric acid and sodium hydroxide solutions containing sodium chloride of a concentration equal to that in the sample solutions, the procedure described in the previous paper being employed.[1] The concentration of free acid is deduced from the measured pH assuming that the activity coefficient of hydrogen ion in the surfactant solution is the same as that in a corresponding hydrochloric acid or sodium hydroxide solution containing no surfactant.

The forward titration curve, *i.e.*, from the acid to the alkaline side, was compared with the backward curve to check the titration process. They were almost coincident with each other. In the present experiment, the titration on the acid side of the pH which the sample solution exhibited was carried out by using the acid titer, and the titration on the alkaline side was done by the alkaline titer to minimize a change in surfactant concentration during the course of the titration. With DAPA, the solution was viscous and turbid in the region of pH 3.0–4.5. With DIPA, the solution was also in the similar state in the region of pH 2.3–4.2.

Determination of Critical Micelle Concentrations. The cmc values of DAPA and DIPA at different pH were determined by the solubilization method described elsewhere.[8]

Results

Figure 1 shows the modified potentiometric titration curves for the carboxyl group of DAPA, pH − log $[\alpha/(1 - \alpha)]$ *vs.* α, at different concentrations in 0.10 *M* NaCl solution. While the quantities of pH −

(5) K. Shinoda, "Colloidal Surfactants," Academic Press Inc., New York, N. Y., 1963, p 25.

(6) T. L. Gresham, J. E. Jansen F. W. Shaver, R. A. Bankert, and F. T. Fiedorek, *J. Am. Chem. Soc.*, **73**, 3168 (1951).

(7) E. H. Riddle, "Monomeric Acrylic Esters," Reinhold Publishing Corp., New York, N. Y., 1954, p 153.

(8) F. Tokiwa, *Bull. Chem. Soc. Japan*, **36**, 222 (1963).

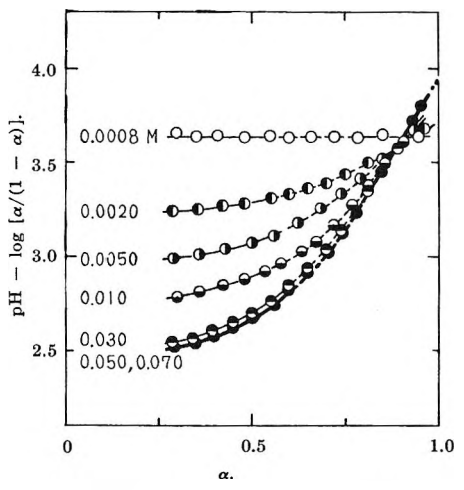

Figure 1. The modified potentiometric titration curves for the carboxyl group of DAPA at different concentrations in 0.10 *M* NaCl solution. The part indicated by a broken line denotes the region where the solution was turbid and viscous.

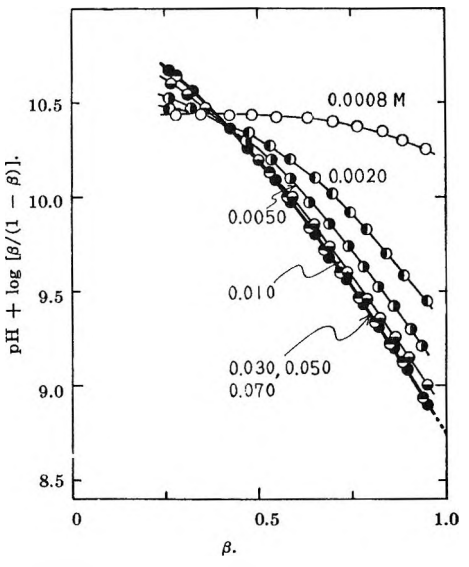

Figure 2. The titration curves for the amino group of DAPA at different concentrations in 0.10 *M* NaCl solution.

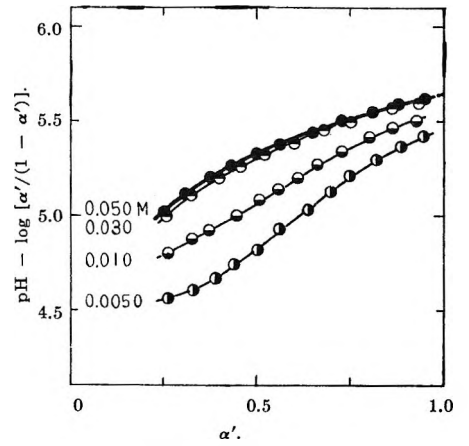

Figure 3. The titration curves for the second carboxyl group of DIPA at different concentrations in 0.10 *M* NaCl solutions.

log $[\alpha/(1 - \alpha)]$ are practically independent of α below the cmc, they are markedly dependent on α at concentrations higher than the cmc. The cmc of DAPA in 0.10 *M* NaCl solution lies at (0.3–3.5) $\times 10^{-3}$ *M* in the range of pH 2.3–11.0, although it changes with pH.

At high concentrations where c is very large compared to c_0, *i.e.*, x $(=c_0/c)$ is near zero, α_M approaches α since $\alpha_M = (\alpha - x\alpha_m)/(1 - x)$. In fact, the pH − log $[\alpha/(1 - \alpha)]$ *vs.* α curves at concentrations higher than 0.03–0.05 *M* converges to a single curve. The curve at such high concentrations thus represents the pH − log $[\alpha_M/(1 - \alpha_M)]$ *vs.* α_M relation for the micelle, which is shown by a thick line in Figure 1.

Figure 2 shows the titration curves for the amino group of DAPA at different concentrations. The thick line also represents the pH + log $[\beta_M/(1 - \beta_M)]$ *vs.* β_M curve for the micelle.

Figure 3 shows the titration curves for the second carboxyl group of DIPA, where α' is the degree of ionization of the second carboxyl group. Unfortunately, the curves for the first carboxyl group could not be obtained because of formation of insoluble material and high viscosity in the region of interest. The cmc values of DIPA in 0.10 *M* NaCl solution were found to be (0.7–1.8) $\times 10^{-3}$ *M* in the range of pH 4.8–11.0.

Figure 4 shows the titration curves for the imino group of DIPA. Variation of pH + log $[\beta/(1 - \beta)]$ with β is rather small even at high concentrations.

Discussion

The electrostatic potential at the surface of the amphoteric micelle carrying $(\zeta - \nu)$ charges is related to the electrostatic free energy of the micelle which is essentially governed by the degrees of ionization of the acidic and basic groups.[9,10] In the first instance, let us consider the surface potential of the DAPA micelle on the acid side of the isoelectric point. Since the last term of eq 3, $\partial G_{el}(\zeta, \nu)/\partial\nu$, represents the electrical work necessary to remove a hydrogen ion from the micelle with $(\zeta - \nu)$ charges, eq 3 can be rewritten

$$\text{pH} - \log \frac{\alpha_M}{1 - \alpha_M} = \text{p}K^{(a)}_{0,M} - \frac{0.434}{kT}\epsilon\psi_0(\alpha_M, \beta_M) \qquad (5)$$

(9) A. Katchalsky and I. R. Miller, *J. Polymer Sci.*, **13**, 57 (1954).
(10) A. Katchalsky, N. Shavit, and H. Eisenberg, *ibid.*, **13**, 69 (1954).

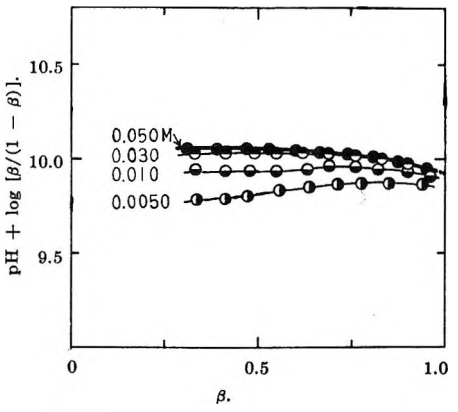

Figure 4. The titration curves for the imino group of DIPA at different concentrations in 0.10 M NaCl solution.

where ψ_0 is the electrostatic potential at the surface of the micelle and ϵ is the elementary charge. In the present case, $pK^{(a)}{}_{0,M}$ and $pK^{(b)}{}_{0,M}$ are separate enough to consider the ionization of the carboxyl group and of the amino group to be independent of each other. Namely, under the condition where the ionization of the carboxyl group takes place, it remains that $\beta_M = 1$ and then the potential in eq 5 is reduced to

$$\psi_0(\alpha_M, \beta_M) = \psi_{0,\beta_M=1}(\alpha_M) \quad (6)$$

As is easily understood from eq 5 and 6, a difference between the quantities of pH − log $[\alpha_M/(1 - \alpha_M)]$ at $\alpha_M = 1$ and at a certain α_M corresponds to $0.434(\epsilon\psi_0/kT)$. Using Figure 1, the surface potential at each α_M can be obtained from this difference.[1]

From a similar consideration, we obtain the following expression for evaluating the surface potential of the DAPA micelle on the alkaline side—the electrical work in this case, however, is the one required in combining a hydrogen ion with the micelle carrying $(\zeta - \nu)$ charges.

$$\text{pH} + \log \frac{\beta_M}{1 - \beta_M} = pK^{(b)}{}_{0,M} - \frac{0.434}{kT}\epsilon\psi_{0,\alpha_M=1}(\beta_M) \quad (7)$$

The surface potential at each β_M can be evaluated from the pH + log $[\beta_M/(1 - \beta_M)]$ *vs.* β_M curve shown in Figure 2. Combining the surface potential thus obtained on the acidic side with that on the basic side, we can construct Figure 5 in which ψ_0 is plotted against ρ, where $\rho = \alpha_M - \beta_M$. For reference, the ψ_0 *vs.* pH curve for the DAPA micelle is illustrated in Figure 6, together with the curve for the DIPA micelle, to show how the surface potential depends on pH.

On the other hand, the construction of the surface potential curve for the DIPA micelle is somewhat complicated. For the sake of understanding, the titration behavior of the DIPA micelle is schematically shown in Figure 7. In the region indicated by a broken line in Figure 7, the observed pH values were unreliable because of the reason already described, and therefore the potential on the acid side of the isoelectric point could not be estimated.

Now let us turn our attention to the surface potential of the DIPA micelle on the alkaline side. In order to

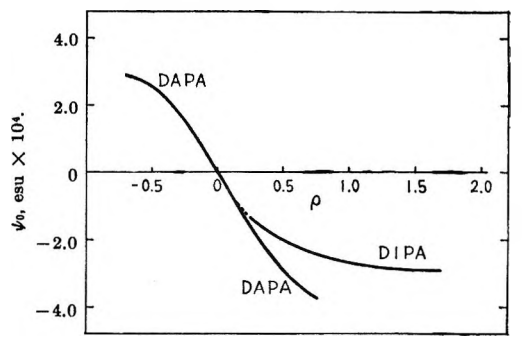

Figure 5. The ψ_0 *vs.* ρ curves for the micelles of DAPA and DIPA, where ρ is $(\alpha_M - \beta_M)$ for DAPA and $(\alpha_M + \alpha'_M - \beta_M)$ for DIPA.

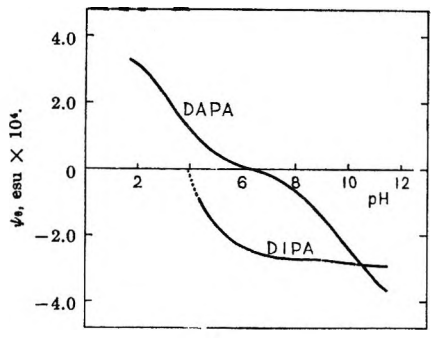

Figure 6. The dependence of ψ_0 on pH for the micelles of DAPA and DIPA.

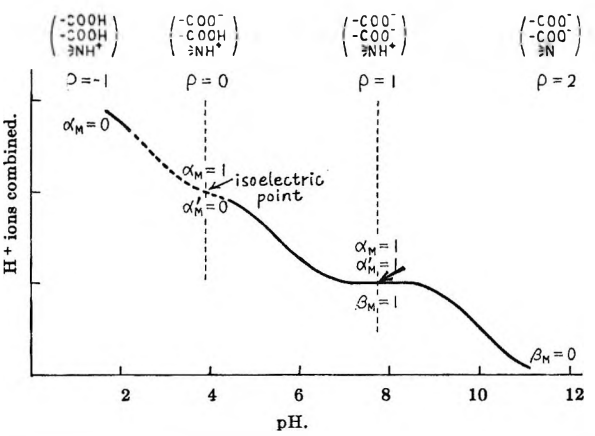

Figure 7. The schematic titration behavior of the DIPA micelle.

evaluate the potential, the point where $\alpha_M = 1$, $\alpha'_M = 1$, and $\beta_M = 1$ was taken as an arbitrary base point of the potential (indicated by an arrow in Figure 7), because it is inadequate in the present case to take the isoelectric point ($\psi_0 = 0$) as a base point. Since the ionizations of the second carboxyl group and of the imino group take place independently of each other, as in the case of DAPA, the potentiometric equation for the second carboxyl group of the DIPA micelle may be written in the form

$$\mathrm{pH} - \log \frac{\alpha'_M}{1 - \alpha'_M} =$$

$$pK^{(a')}_{0,M} - \frac{0.434}{kT}\epsilon\psi_0(\alpha_M, \alpha'_M, \beta_M) =$$

$$pK^{(a')}_{0,M} - \frac{0.434}{kT}\epsilon\psi_{0,\alpha_M=1,\beta_M=1}(\alpha'_M) =$$

$$pK^{(a')}_{0,M} - \frac{0.434}{kT}\epsilon(\psi_0(\alpha_M, \alpha'_M, \beta_M)_{\alpha_M=1,\alpha'_M=1,\beta_M=1} +$$

$$\psi_{0,rel}(\alpha'_M)) = pK^{(a')}_{bp,M} - \frac{0.434}{kT}\epsilon\psi_{0,rel}(\alpha'_M) \quad (8)$$

where $\psi_{0,rel}$ is the potential relative to that at the base point, $pK^{(a')}_{bp,M}$ is the ionization constant of the micelle at the base point, and the superscript a′ refers to the second carboxyl group. Similarly, the equation for the imino group of the micelle is given by

$$\mathrm{pH} + \log \frac{\beta_M}{1 - \beta_M} = pK^{(b)}_{bp,M} - \frac{0.434}{kT}\epsilon\psi_{0,rel}(\beta_M) \quad (9)$$

$$pK^{(b)}_{bp,M} = pK^{(b)}_{0,M} -$$

$$\frac{0.434}{kT}\epsilon\psi_0(\alpha_M, \alpha'_M, \beta_M)_{\alpha_M=1,\alpha'_M=1,\beta_M=1}$$

According to eq 8 and 9, the surface potential at each α'_M and β_M can be obtained from Figures 3 and 4, respectively. Here, it should be remembered that the potential thus obtained is the one between at the base point and at a certain α'_M (or β_M); that is, it is not "absolute" but "relative" potential. An extrapolation to the point where $\psi_0 = 0$, *i.e.*, to the point where $\alpha_M = 1$, $\alpha'_M = 0$, and $\beta_M = 1$, is required to obtain the absolute potential. In Figure 5 the ψ_0 of the DIPA micelle is plotted against ρ, where ρ represents the value of $(\alpha_M + \alpha'_M - \beta_M)$.

A characteristic feature of the surface potential curves shown in Figure 5, especially, of the curve for DIPA, is a decrease in the slope with increasing magnitude of ρ at high charges. If we assume a uniformly charged plane for the micelle, the potential ψ_0 at the surface and the charge density σ are related by the expression[11,12]

$$\psi_0 = \frac{2kT}{\epsilon}\sinh^{-1}\frac{\sigma}{\sqrt{2N_0DkT/\pi}} \quad (10)$$

where D is the dielectric constant and N_0 is the bulk concentration of ionic species which can be assumed to be constant in the present case. The charge density on the micellar surface is given by

$$\sigma = -n\epsilon\rho/A = -\epsilon\rho/(A/n) \quad (11)$$

where n is the number of surfactant molecules per micelle, A is the surface area of the micelle, and therefore A/n represents the surface area occupied by one molecule. Putting $A/n = s$, then eq 11 is

$$\sigma = -\epsilon\rho/s \quad (12)$$

Substituting this expression into eq 10, we obtain

$$\psi_0 = \frac{2kT}{\epsilon}\sinh^{-1} B\frac{\rho}{s} \quad (13)[13]$$

where $B = -\epsilon/\sqrt{2N_0DkT/\pi}$. The potential ψ_0 depends on both ρ and s. The total change in ψ_0 when ρ and s are varied is

$$\Delta\psi_0 = \left(\frac{\partial\psi_0}{\partial\rho}\right)_s\Delta\rho + \left(\frac{\partial\psi_0}{\partial s}\right)_\rho\Delta s \quad (14)$$

where

$$\left(\frac{\partial\psi_0}{\partial\rho}\right)_s = \frac{2kT}{\epsilon}\frac{1}{\sqrt{(s/B)^2 + \rho^2}} \quad (15)$$

$$\left(\frac{\partial\psi_0}{\partial s}\right)_\rho = -\frac{2kT}{\epsilon}\frac{1}{\sqrt{(s^2/B\rho)^2 + s^2}} \quad (16)$$

From eq 15 it can be seen that the slope, $\partial\psi_0/\partial\rho$, decreases as the magnitude of ρ increases at a constant value of s. The value of s tends in general to increase with increasing $|\rho|$ owing to the electrical repulsion between charged groups; this effect results in lowering the potential according to eq 16. Thus, eq 14–16 explain the characteristic feature of the ψ_0 *vs.* ρ curves shown in Figure 5.

As seen in Figure 5, the surface potential of the DIPA micelle is relatively low as compared with that of the DAPA micelle. It is expected from eq 16 that the micelle with a looser structure will have lower poten-

(11) E. J. W. Verwey and J. Th. G. Overbeek, "Theory of the Stability of Lyophobic Colloids," Elsevier Publishing Co., Inc., New York, N. Y., 1948, pp 22–50.

(12) D. J. Shaw, "Introduction to Colloid and Surface Chemistry," Butterworth and Co. Ltd., London, 1966, pp 117–125.

(13) At low charge where $\rho \ll s/B$, eq 13 is reduced to $\psi_0 = (2kT/\epsilon)(B/s)\rho$. The linear portion of the curves shown in Figure 5 may be explained by this expression assuming that s is unchanged.

tial, because the looser the micellar structure, the larger the value of s. The different potentiometric behavior between DAPA and DIPA micelles may be accounted for by different micellar structure, probably the DIPA micelle having a looser structure.

Acknowledgments. The authors express their thanks to Dr. H. Kita, Director of the Research Laboratories, for his encouragement and permission to publish this paper, and to Mr. T. Ohtsuka for his help in preparing the samples.

The Solubility of a Series of Gases in Cyclohexane and Dimethylsulfoxide

by J. H. Dymond

Department of Chemistry, University of California, Berkeley, California 94720 *(Received December 13, 1966)*

An apparatus for determining the solubility of gases in liquids with enhanced speed and precision has yielded figures for the solubility in $(CH_3)_2SO$ at 1 atm and 25° of He, Ne, Ar, Kr, Xe, H_2, D_2, N_2, O_2, CO_2, and CH_4 and for both solubility and entropy of solution in c-C_6H_{12} of Ne, Ar, Kr, Xe, H_2, N_2, CO_2, C_2H_6, and c-C_3H_6. The latter results fall closely on a straight line when the partial molal entropy of solution, $\bar{s}_2 - s_2^g$ (1 atm, 25°) is plotted against $-R \ln x_2$ ($x_2 \equiv$ mole fraction of the gas). The theoretical significance of these results will be discussed in a later paper by J. H. Hildebrand.

Introduction

The work here reported was undertaken, first, to obtain figures of sufficient precision to serve for theoretical study of the solubility and entropy of solution of a series of gases in a single, representative, nonpolar liquid and, second, to secure data for the solubility of gases in dimethylsulfoxide, needed in connection with a study of diffusion in a liquid having high cohesion.

Apparatus and Materials

We designed for our purpose a new apparatus capable of more speed and accuracy than any we have used before. Its design and operation are fully described elsewhere.[1] Its principal features are shown in Figure 1. A bulb of ~250-cc capacity, A, into which degassed solvent is introduced and accurately measured, is connected with bulb B of ~100-cc capacity into which a measured amount of gas is introduced. A manometer connected at D measures the total pressure of gas plus solvent vapor in B. A glass-enclosed pump in the side arm, C, operated magnetically, pumps slugs of solvent into the upper bulb, where it runs down the walls without splashing and exposes fresh surfaces of the solvent. The pressure falls to an equilibrium value from which the amount of gas that has been dissolved and hence that which would be dissolved at 1 atm partial pressure can be calculated. More gas can be added and equilibrated as a check on the attainment of equilibrium and, in the case of a very soluble gas, as a check on the applicability of Henry's law. The temperature is then changed and the system reequilibrated. The relation between log x_2 ($x_2 \equiv$ mole fraction of the solute) and log T is strictly linear and from the straight lines we obtain values for the partial molal entropy of solution, $\bar{s}_2 - s_2^g$ (1 atm) $= R(\Delta \log x_2/\Delta \log T)_P$.

(1) J. Dymond and J. H. Hildebrand, *Ind. Eng. Chem. Fundamentals*, **6**, 130 (1967).

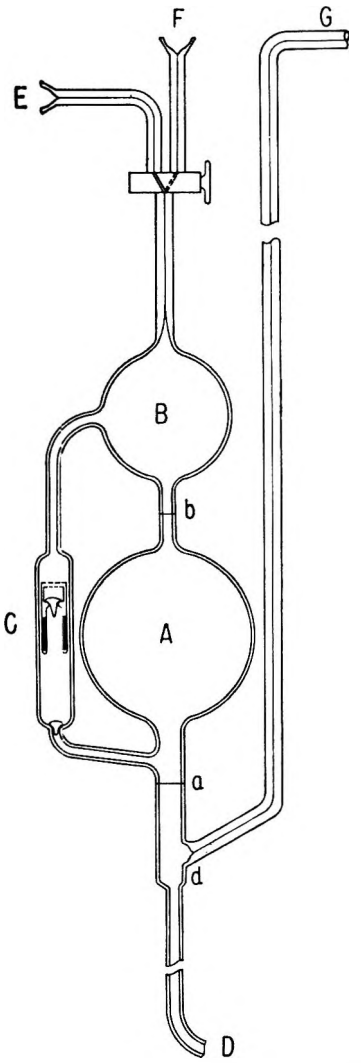

Figure 1. Central part of the solubility apparatus.

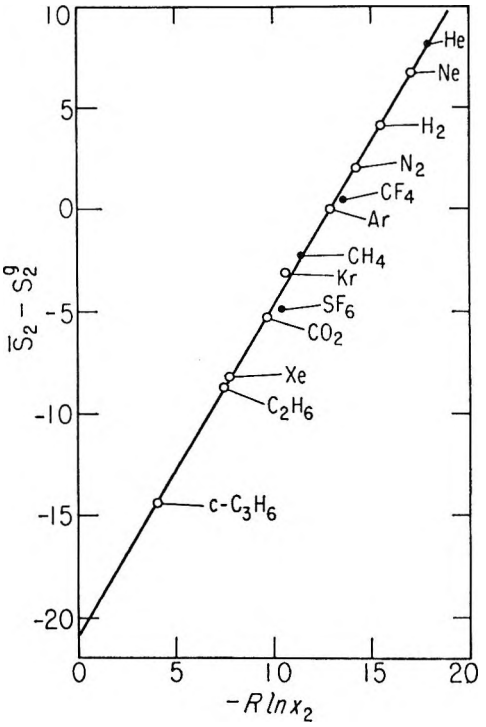

Figure 2. Relation between the solubility of gases in cyclohexane at 25° and 1 atm partial pressure and their entropy of solution obtained from the linear relation $R(\Delta \log x_2/\Delta \log T)$ saturated at constant pressure.

The cyclohexane was Matheson Coleman and Bell Chromatoquality reagent. It was dried over Drierite and a fraction frozen out. It melted at 6.45°. The dimethylsulfoxide was Matheson Coleman and Bell Spectroquality reagent. It was dried by passing through a column of Molecular Sieve, Type 4A, and a fraction frozen out. The melting point was 18.37°. The CO_2 was from Western Gas, Inc.; the N_2 from General Dynamics Corp.; Ar from Linde Argon; Ne, Kr, Xe, and c-C_3H_6 from the Matheson Co.; CH_4 and C_2H_6 (Research grade) from Phillips Petroleum Co.; D_2 from Bio-Rad Labs; and He, H_2, and O_2 from the Stuart Oxygen Co. These gases were dried and passed directly into the apparatus.

Results

The experimental figures for the mole fraction of the gases in cyclohexane saturated at 1 atm partial pressure and at the temperatures stated are given in Table I, together with values interpolated to 25° and entropies of solution calculated from the log x_2 *vs.* log T slopes. Maximum deviations from these lines are less than 0.5% in x_2. Henry's law was found to be obeyed even by c-C_3H_6 in c-C_6H_{12} at a mole fraction of approximately 0.2. Results for the solubility of gases in dimethylsulfoxide are given in Table II.

We redetermined the figures for CF_4 in c-C_6H_{12} in the range 17–34° and confirmed the values found by Archer and Hildebrand:[2] 10^4x_2 (25°) = 10.34 and $\bar{s}_2 - s_2^g = 0.50$; they also found for SF_6 10^4x_2 (25°) = 53.9 and $\bar{s}_2 - s_2^g = -4.9$. Our value for N_2, 10^4x_2 (25°) = 7.68, and for CO_2, 77.1, differ but little from the figures obtained earlier by Gjaldbaek and Hildebrand,[3] 7.55 and 77.2, respectively. Figures for the solubility of the rare gases in c-C_6H_{12} have also been determined by Clever, Battino, Saylor, and Gross[4] as follows for 10^4x_2 (25°): He 1.21, ($\bar{s}_2 - s_2^g = 8.1$), Ne 1.80, Ar 14.9, Kr 46.7, Xe 192. In Figure 2 we

(2) G. Archer and J. H. Hildebrand, *J. Phys. Chem.*, **67**, 1830 (1963).

(3) G. C. Gjaldbaek and J. H. Hildebrand, *J. Am. Chem. Soc.*, **71**, 3147 (1949).

(4) H. L. Clever, R. Battino, J. H. Saylor, and P. M. Gross, *J. Phys. Chem.*, **61**, 1078 (1957); **62**, 89, 375 (1958).

Table I: Solubility and Entropy of Solution of Gases in Cyclohexane at 1 Atm Partial Pressure[a]

					25.00	$\bar{s}_2 - s_2^g$
Ne	19.82	26.40	31.60	37.35		
	1.79	1.93	2.04	2.20	1.90	6.8
Ar	17.80	25.12	31.05	36.30		
	15.25	15.20	15.20	15.30	15.20	0
Kr	20.35	25.00	31.60	36.20		
	48.5	47.3	45.7	44.7	47.3	−3.1
Xe	19.17	24.86	33.00	36.05		
	228.0	210.0	188.5	181.5	210.0	−8.2
H_2	20.80	25.01	31.62	36.38		
	4.02	4.14	4.34	4.47	4.14	4.2
N_2	17.85	25.45	30.70	33.37		
	7.52	7.70	7.87	7.89	7.68	2.0
CO_2	20.24	26.60	31.08	37.40		
	80.2	75.8	73.1	69.4	77.1	−5.2
C_2H_6	19.20	25.45	31.20	34.80		
	258.0	234.0	215.0	205.5	236.0	−8.7
c-C_3H_6	15.50	20.50	25.00	28.72		
	1760	1550	1400	1275	1395	−14.4

[a] The numbers on the first row are °C; the second, 10^4x_2, where x_2 is the mole fraction of gas.

Table II: Solubility of Gases, 10^4x_2 in Dimethylsulfoxide at 25° and 1 Atm Partial Pressure

He	0.284	D_2	0.799	O_2	1.57	Xe	17.0
Ne	0.368	N_2	0.833	CH_4	3.86	C_2H_6	17.8
H_2	0.761	Ar	1.54	Kr	4.46	CO_2	90.8

have plotted entropy of solution in c-C_6H_{12} against the solubility as $-R \ln x_2$. The open circles represent our data, the solid circles those of others referred to above plus a point for CH_4 by Lannung and Gjaldbaek,[5] 10^4x_2 (25°) = 32.7 and $\bar{s}_2 - {}_2s^g = -2.0$.

This method of plotting was first used by Jolley and Hildebrand[6] and since followed in subsequent papers from this laboratory.

We make the following comments on the relations shown in Figure 2.

(1) These results for solutions of gases in C_6H_{12} are more comprehensive and reliable than those for any other solvent. We believe the values of mole fraction to be accurate to well within 1%.

(2) The strictly linear relationship offers a check upon the accuracy of measurements and also a means of predicting temperature coefficients from a single determination of solubility.

(3) H_2, CF_4, and SF_6 conform rather well to this relationship, although they deviate strongly from relations based upon the geometric mean for the attractive potential energy of molecules of different species.

(4) Since the Gibbs free energy $\Delta F = 0$, the entropy of solution can be used to calculate the heat and the energy of solution.

(5) Extrapolation to $x_2 = 1$ gives $\bar{s}_2 - s_2^g$ (1 atm) = −20.9 cal/deg, which can be interpreted as the entropy of condensing C_6H_{12} vapor from a hypothetical pressure of 1 atm. The entropy of condensing it from its vapor pressure at 25°, 96.6 mm, is −26.5 cal/deg. The loss in entropy in changing from 96.6 to 760 mm is 4.1 cal/deg, giving −22.4 cal/deg.

Acknowledgment. We express our appreciation to the National Science Foundation for the support of this work under a contract administered by Dr. J. H. Hildebrand.

(5) A. Lannung and J. C. Gjaldbaek, *Acta Chem. Scand.*, **14**, 1124 (1960).

(6) J. E. Jolly and J. H. Hildebrand, *J. Am. Chem. Soc.*, **80**, 1050 (1958).

The Photolysis of Nitrogen Dioxide in the Presence of Nitric Acid at 3660 A and 25°[1]

by Sigmund Jaffe and Hadley W. Ford

Jet Propulsion Laboratory, California Institute of Technology, Pasadena, California
(Received December 14, 1966)

Nitrogen dioxide was irradiated at 3660 A in the presence of HNO_3. Both NO_2 and HNO_3 were decomposed. The proposed mechanism for HNO_3 decomposition is $O + HNO_3 \rightarrow OH + NO_3$ followed by $OH + HNO_3 \rightarrow H_2O + NO_3$. The specific rate constant for the $O + HNO_3$ reaction is estimated to be $\sim 10^{10}$ l. mole^{-1} sec^{-1}. Quantum yields are reported as a function of NO_2, HNO_3, and NO pressures.

Introduction

This work was performed as part of a continuing study of the photochemistry of NO_2. Its specific purpose was to determine the mechanism of nitric acid decomposition which results from irradiation in the presence of NO_2.

Nitric acid shows continuous absorption below 3300 A indicating dissociation with a primary yield of unity. The process that appears to be energetically possible in solar radiation[2] is

$$HNO_3 + h\nu \longrightarrow OH + NO_2 \ (-53 \text{ kcal})$$

However, in the presence of NO_2, decomposition takes place above 3300 A. Dissociation must, therefore, result from secondary reactions with the products of NO_2 photolysis.

It is well established[3-5] that the primary process in the photolysis of NO_2 at 3660 A is

$$NO_2 + h\nu \longrightarrow NO(^2\pi) + O(^3P)$$

Thus, decomposition of HNO_3 could result from reaction with oxygen atoms

$$O + HNO_3 \longrightarrow OH + NO_3$$

Such reactions of O atoms and OH radicals are of special interest in the photochemistry of air pollution.

Experimental Section

The apparatus and procedures used in this work were the same as those reported earlier.[5a] A 10-cm long quartz cell containing the gas samples was irradiated with monochromatic light derived from a high-pressure mercury arc. The initial and final NO_2 pressures were determined at 4350 A with a Cary Model 11 spectrophotometer. Spectra of pure HNO_3, pure NO_2, and the products of photolysis showed that NO_2 was the only species absorbing appreciably at 4350 A. The initial pressure of HNO_3 was measured with a stainless steel Wallace and Tiernan Bourdon gauge. The use of the stainless steel gauge and Kel-F stopcock grease was necessary because HNO_3 reacts with most stopcock greases and manometer oils.

The NO_2 pressure was followed as a function of time by a continuous record of the ouput of a solid-state photocell. The photocell had a window measuring 1.5 in. square and, when placed at the end of the quartz cell, absorbed the transmitted light which was focused on it. The intensity of the incident and transmitted light was determined by the photolysis of pure NO_2 for which the quantum yields have been established. The NO_2 pressure was calculated from the measurement of the light absorbed using the extinction coef-

(1) This paper presents results of one phase of research carried out at the Jet Propulsion Laboratory, California Institute of Technology, under Contract No. NAS 7-100, sponsored by the National Aeronautics and Space Administration.

(2) P. A. Leighton, "Photochemistry of Air Pollution," Academic Press Inc., New York, N. Y., 1961, pp 62–64.

(3) H. W. Ford, *Can. J. Chem.*, **38**, 1780 (1960).

(4) F. E. Blacet, T. C. Hall, and P. A. Leighton, *J. Am. Chem. Soc.*, **84**, 4011 (1962).

(5) (a) H. W. Ford and S. Jaffe, *J. Chem. Phys.*, **38**, 2935 (1963); (b) J. N. Pitts, Jr., J. H. Sharp, and S. I. Chan, *ibid.*, **40**, 3655 (1964).

ficient 8.15×10^{-3} mm^{-1} cm^{-1} at 3660 A, reported by Holmes and Daniels.[6] Corrections were made for the absorption of light by N_2O_4 using 3.21×10^{-3} mm^{-1} cm^{-1} for the extinction coefficient.[6]

The final pressure of NO was determined by the addition of excess O_2 to the photolysis cell at the end of a run. NO was converted to NO_2 by the reaction

$$2NO + O_2 \longrightarrow 2NO_2$$

The HNO_3 used in this work was prepared by the reaction of Baker's Analyzed anhydrous KNO_3 with pure H_2SO_4. The acid, distilled under vacuum at room temperature, was 99.8% pure and was colorless. When stored in the dark at $-10°$, the HNO_3 did not decompose. Small samples were stored at $-196°$ for use in the present work.

Results

A series of preliminary experiments were carried out with combinations of HNO_3, $HNO_3 + NO_2$, $HNO_3 + NO_2 + O_2$, $HNO_3 + NO_2 + NO$, and $HNO_3 + NO$. These samples were allowed to stand in the dark (up to 15 hr) except for the periodic determination of the NO_2 concentration by means of the Cary spectrophotometer. No reactions were observed except in the case of mixtures containing NO, where a relatively slow conversion to NO_2 was detected.

Assuming the simple mechanism

$$HNO_3 + NO \longrightarrow NO_2 + HNO_2$$

$$HNO_2 + HNO_2 \longrightarrow H_2O + NO + NO_2$$

a second-order rate constant for the $HNO_3 + NO$ reaction equal to 1×10^2 l. $mole^{-1}$ sec^{-1} was obtained. This value is much too small to influence the results of the photochemically induced reactions.

Mixtures of NO_2, HNO_3, and N_2 were photolyzed at 3660 A and 25° to determine the dependence of the quantum yield on the pressures of NO_2 and HNO_3. The results of a typical experiment are shown in Figure 1. It can be seen that there is an initial period during which the rate of dissociation of NO_2 is greater than the rate of formation of NO_2. However, when the NO pressure builds up sufficiently, the formation of NO_2, presumably by the reaction

$$NO + NO_3 \longrightarrow 2NO_2$$

predominates and the NO_2 pressure increases. The NO_2 pressure continues to increase until it reaches a maximum. It is assumed that the HNO_3 is almost completely dissociated at this point and that further photolysis results in the dissociation of NO_2 in the presence of NO, O_2, N_2, H_2O, and small quantities of HNO_3 and perhaps HNO_2. The ratio of (NO_2) to (HNO_3)

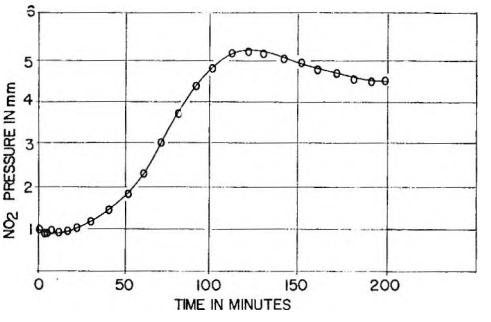

Figure 1. NO_2 pressure as a function of time.

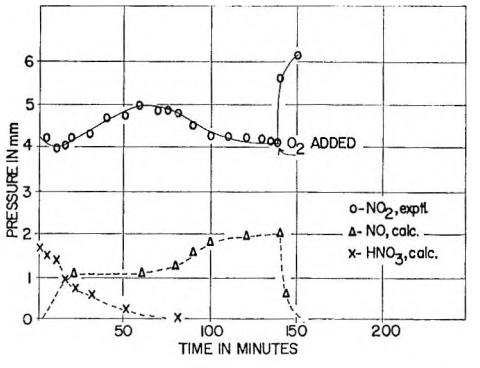

Figure 2. NO_2, NO, and HNO_3 pressures as a function of time (NO calculated from O_2 titration).

was about 20 at the maxima in curves such as that in Figure 1. The dissociation approaches a steady state when the recombination reactions such as

$$2NO + O_2 \longrightarrow 2NO_2$$

$$O + NO + M \longrightarrow NO_2 + M$$

are as fast as the dissociation reactions

$$NO_2 + h\nu \longrightarrow NO + O$$

$$O + NO_2 \longrightarrow NO + O_2$$

Separate samples of $NO_2 + HNO_3$ were titrated with O_2 after a short period of photolysis, at the maximum, and after the system approached the final steady state. Typical results are shown in Figures 2 and 3. The quantity of NO produced at these points suggests that NO builds up slowly at first, reaches a steady state when the NO_2 production becomes linear, and then builds up to the final steady state after the maximum in NO_2 is passed. When NO was added to the system before photolysis, no initial decrease in NO_2 pressure was observed. The NO_2 pressure built up steadily as shown in Figure 4. It appears that the $NO + NO_3$ reaction is rapid under these conditions.

(6) H. H. Holmes and F. Daniels, *J. Am. Chem. Soc.*, **56**, 630 (1934).

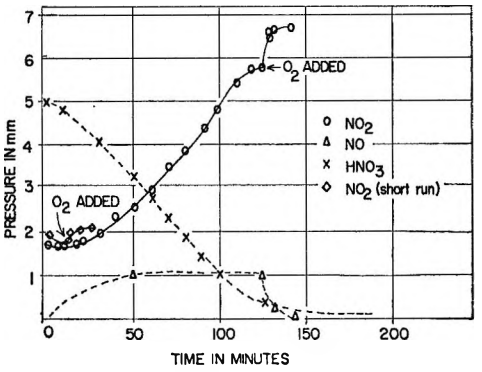

Figure 3. NO_2, NO, and HNO_3 pressures as a function of of time (NO calculated from O_2 titration).

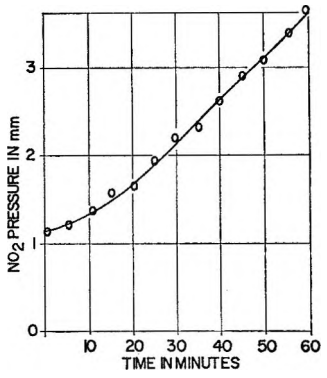

Figure 4. NO_2 pressure as a function of time with added NO (0.55 mm).

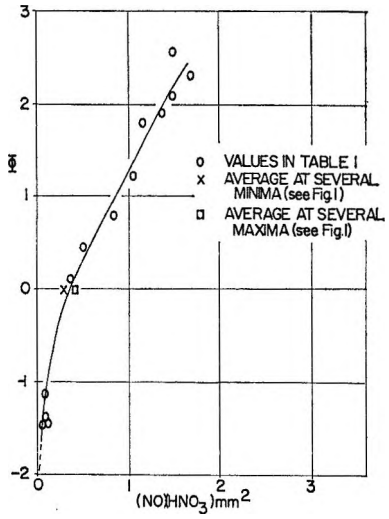

Figure 5.

The presence of OH radicals was qualitatively established by the addition of 1 atm of CO to the system. The reaction

$$OH + CO \longrightarrow CO_2 + H$$

as described by Ung and Back[7] was assumed to have taken place to some extent as evidenced by the appearance of a mass 44 peak in the mass spectrogram of the products of the photolysis. CO does not react readily with O atoms nor does CO affect the rate of normal NO_2 photolysis any more than N_2 or CO_2 does.[8] The OH radical is assumed to result from the reaction

$$O + HNO_3 \longrightarrow OH + NO_3$$

Correlation of the quantum yields with the concentrations of NO_2, HNO_3, and NO revealed that the data could be presented as a function of the product, $(NO)(HNO_3)$. Table I summarizes these data and they are shown in Figure 5.

Table I: Quantum Yields as a Function of $(NO)(HNO_3)$ at 3660 A

Φ	NO, mm	NO_2, mm	HNO_3, mm	$(NO)(HNO_3)$, mm^2	I_a, einsteins $l.^{-1}$ sec^{-1} $\times 10^6$
−2.2	0.02	1.66	4.93	0.10	1.09
−1.5	0.04	6.58	0.86	0.03	3.07
−1.5	0.04	4.32	1.77	0.07	2.53
−1.4	0.47	4.38	1.40	0.07	2.70
0	0.87	4.98	0.24	0.21	2.70
0	0.17	4.01	1.90	0.32	2.42
0.13	0.48	6.28	0.73	0.33	2.94
0.46	0.47	4.32	1.04	0.49	2.68
0.79	0.85	1.70	1.01	0.86	1.91
1.21	0.51	1.03	2.02	1.03	1.24
1.76	0.70	4.26	1.66	1.16	2.27
1.88	0.62	3.84	2.16	1.34	2.12
2.03	0.54	3.42	2.66	1.44	1.97
2.30	0.47	2.86	3.49	1.64	1.73
2.56	0.39	2.48	3.75	1.46	1.56

Experiments were conducted with varying pressures of nitrogen from about 100 to 700 mm. The variation in total pressure did not seem to affect the correlation of quantum yields with the product, $(NO)(HNO_3)$.

The quantum yields approached −2 at the beginning of the process when (NO) was small and they never exceeded +3 in this study. The quantum yields could again approach −2 at the end of the photolysis when (HNO_3) is approaching zero. The limits of −2 at the beginning and end of the process are consistent with the quantum yields for the photolysis of pure NO_2.

(7) A. M. Ung and R. A. Back, *Can. J. Chem.*, **42**, 753 (1964).
(8) H. W. Ford and S. Jaffe, unpublished work.

Discussion

A mechanism that is consistent with the data during the early stages of photolysis is

$$NO_2 + h\nu \longrightarrow NO + O \quad (1)$$

$$O + NO_2 \longrightarrow NO + O_2 \quad (2)$$

$$O + HNO_3 \longrightarrow OH + NO_3 \quad (3)$$

$$OH + HNO_3 \longrightarrow H_2O + NO_3 \quad (4)$$

$$NO + NO_3 \longrightarrow 2NO_2 \quad (5)$$

$$NO_2 + NO_3 \longrightarrow NO + NO_2 + O_2 \quad (6)$$

$$2NO + O_2 \longrightarrow 2NO_2 \quad (7)$$

The quantum yield expression for NO_2 production that results from this mechanism, assuming steady state for O, OH, and NO_3, is

$$\Phi = -1 - \frac{k_2(NO_2)}{k_2(NO_2) + k_3(HNO_3)} + \frac{4k_5(NO)k_3(HNO_3)}{[k_2(NO_2) + k_3(HNO_3)][k_5(NO) + k_6(NO_2)]} + \frac{k_7(NO)^2(O_2)}{I_a} \quad (I)$$

At the beginning of the photolysis, when the NO pressure is very low, the third and fourth terms in eq I will vanish and the slope of (NO_2) *vs.* time will be negative. As the photolysis proceeds, the NO pressure will increase and the third term will become most important. It will eventually be numerically larger than the first two terms and the slope of the curve will become positive. After some time, the (HNO_3) will decrease to the point where the curve will reach a maximum after which the slope will be negative once again. The quantum yield could approach -2 when (HNO_3) is very small, since the second term will approach -1. However, NO_2 regenerating reactions, such as eq 7, will prevent the quantum yield from actually reaching the limit of -2.

By using the data in Table I, the rate constants in Table II, and eq I, one obtains an average value of k_3 equal to $\sim 10^{10}$ l. mole^{-1} sec^{-1}. A rate constant of at least this value would be necessary so that HNO_3 molecules could compete with NO_2 molecules for reaction with O atoms. One could conclude that reaction 3 is at least as fast as

$$O + NO_2 \longrightarrow NO_3^*$$

for which Klein and Herron[9] have reported a rate constant equal to 9.6×10^9 l. mole^{-1} sec^{-1}.

In order for eq I to represent the observed behavior more closely, it would require that $k_6(NO_2)$ be of the same magnitude as $k_5(NO)$. This is true in the early stages of photolysis when (NO) is low. However, if (NO) builds up as shown in Figure 2, k_6 would have to be a few orders of magnitude larger than the value given in Table II. If reaction 6 involved an excited or metastable NO_3, such as OONO, the rate constant, k_6, could be as large as 10^8 l. mole^{-1} sec^{-1}. (The pre-exponential factor[3] for the equivalent thermal reaction is 4×10^9 l. mole^{-1} sec^{-1}.)

Table II: Rate Constants Used in the Calculation of k_3

Constant	Value	Ref
k_2	3.3×10^9 l. mole^{-1} sec^{-1}	*a*
k_5	5.6×10^9 l. mole^{-1} sec^{-1}	*b*
k_6	2.5×10^5 l. mole^{-1} sec^{-1}	*b*
k_7	1.48×10^4 l.^{2} mole^{-2} sec^{-1}	1, p 185
k_8	1.8×10^9 l. mole^{-1} sec^{-1}	1, p 188
k_9	0.24 sec^{-1}	1, p 188

[a] F. S. Klein and J. T. Herron, *J. Chem. Phys.*, **41**, 1285 (1964). [b] C. Schott and N. Davidson, *J. Am. Chem. Soc.*, **80**, 1841 (1948).

There are several reactions that may become significant in the later stages of photolysis. After the maximum in (NO_2) is passed, the system approaches a steady state in all components. Nitric acid may be formed by the process

$$NO_2 + NO_3 \longrightarrow N_2O_5 \quad (8)$$

$$N_2O_5 \longrightarrow NO_2 + NO_3 \quad (9)$$

$$N_2O_5 + H_2O \longrightarrow 2HNO_3 \quad (10)$$

A calculation was made under steady-state conditions, assuming various values for k_{10}. Interpolation of these results where the quantum efficiency for dissociation of NO_2 is equal to that for reformation of NO_2 yielded k_{10} approximately equal to 10^3 l. mole^{-1} sec^{-1}. Another possible reaction for the formation of HNO_3 is

$$NO_2 + OH + M \longrightarrow HNO_3 + M \quad (11)$$

This reaction is similar to that proposed by Johnston, *et al.*,[10,11] for the thermal dissociation of HNO_3. However, no estimate of the value of k_{11} has been made.

It appears at this time that reactions 1–7 describe the system early in the process and up to the maximum

(9) See footnote *a* of Table II.

(10) H. S. Johnston, L. Toering, and R. J. Thompson, *J. Phys. Chem.*, **57**, 390 (1953).

(11) H. S. Johnston, L. Toering, Yu-Sheng Tao, and G. H. Messerley, *J. Am. Chem Soc.*, **73**, 2319 (1951).

in NO_2 pressure. However, it is necessary to consider reactions 8–10 to explain the behavior at the end of the process when (NO_2) is approaching a final steady state. Further investigation of this system at low partial pressures of NO_2 and HNO_3 should prove of interest in atmospheric photochemistry.

Complex Formation in the Gas-Phase Reaction of Hydrogen Bromide with Di-*t*-butyl Peroxide

by Leslie Batt and Frank R. Cruickshank

Department of Chemistry, University of Aberdeen, Old Aberdeen, Scotland

Accepted and Transmitted by the Faraday Society (August 10, 1966)

A mechanism for the decomposition of di-*t*-butyl peroxide (dtBP) in the presence of HBr, 140° and 100 mm, is dtBP → 2*t*-BuȮ (1), *t*-BuȮ + HBr → *t*-BuOH + Ḃr (2), *t*-BuȮ → Me_2CO + Ṁe (3), Ṁe + HBr → CH_4 + Ḃr (4), Me + Br_2 → MeBr + Ḃr (5), Ṁe + Ṁe → C_2H_6 (6), Ḃr + Ḃr + M → Br_2 + M (7), Ṁe + Br + (M?) → MeBr + (M?) (8). Here reaction 7 is the main termination process with reactions 6 and 8 playing minor roles, in contrast to the normal decomposition of dtBP where reaction 6 is the main termination process. Formation of isobutene oxide (IBO) indicates a catalyzed decomposition of dtBP according to Ḃr + dtBP → dtḂP$_{-H}$ + HBr (9), dtḂP$_{-H}$ → IBO + *t*-BuȮ (10). Alternatively, complex formation occurs between dtBP and Br_2 or HBr, IBO being subsequently produced as a result of this. The variation of pressure with time and the very low experimental value of k_5 provide some evidence for complex formation. The following Arrhenius parameters have been estimated. E_2 = 15.5–17.5 kcal/mole (assuming A_2 = $10^{13.5}$ sec^{-1}, A_3 = 10^9 l./mole sec, E_2 = 0–2 kcal/mole); A_4 = $10^{8.95}$ l./mole sec, E_4 = 2.9 kcal/mole, E_5 = 0.9 kcal/mole; E_9 = 17 kcal/mole, E_{-9} = 5 kcal/mole.

Introduction

Di-*t*-butyl peroxide is a very convenient thermal source of *t*-butoxy radicals (*t*-BuȮ) in the gas phase over the temperature range 120–180° (for a static system). This allows a study to be made of the pressure-dependent decomposition of *t*-BuȮ,[1] provided that an efficient radical trap is used to measure its concentration. Raley, Rust, and Vaughan have shown that HBr does not catalyze the decomposition of dtBP[2] and therefore seems to be a suitable radical trap for studying the decomposition of *t*-BuȮ.

Experimental Section

The dtBP was purified as before.[1] The HBr (Matheson) was dried by passing it through a Dry Ice–acetone trap several times, which also removed traces of bromide, bulb-to-bulb distilled, and stored in a 3-l. bulb at −80° in the dark.

The apparatus and essential experimental technique have been described in detail elsewhere.[3] Auramine

(1) L. Batt and S. W. Benson, *J. Chem. Phys.*, **36**, 895 (1962).

(2) J. H. Raley, F. F. Rust, and W. E. Vaughan, *J. Am. Chem. Soc.*, **70**, 2767 (1948).

Table I: Products Formed in the Decomposition of dtBP in the Presence of HBr at 140°.
All Quantities Expressed in μmoles

Run	Length of run, min	Initial dtBP	Final dtBP	CH_4	C_2H_6	CH_3Br	Me_2CO	*t*-BuOH	*t*-BuOBr	IBO	Br_2	Initial HBr	Final HBr
2	13.3	1204	1157	62.2	0.1 → 1	~3	65	34	~2	20.7	~34	87	12.4
3	25.9	1283	1203	72.5	99.8	16.2	129.2	<1	...	2.1	~10	36.7	0

was used to absorb the HBr[4] prior to condensation of the products and the presence of *t*-BuOBr was inferred from the green coloration produced on passing the products and undecomposed reactants from the reaction vessel through the auramine.[5]

Results and Discussion

Three runs were carried out at 140° and a total pressure of 100 mm. The products and the details of the individual concentrations of dtBP and HBr are shown for two of the runs in Table I. In contrast to Tipper, *et al.*,[6] no *t*-BuBr was found. Its formation is probably due to a condensed phase reaction between HBr and *t*-BuOH.

A mechanism for the formation of the products of the reaction other than isobutylene oxide (IBO) is

$$\text{dtBP} \longrightarrow 2t\text{-BuO}\cdot \quad (1)$$

$$t\text{-BuO}\cdot + \text{HBr} \longrightarrow t\text{-BuOH} + \text{Br}\cdot \quad (2)$$

$$t\text{-BuO}\cdot + \text{M} \longrightarrow \text{Me}_2\text{CO} + \text{Me}\cdot + \text{M} \quad (3)$$

$$\text{Me}\cdot + \text{HBr} \longrightarrow \text{CH}_4 + \text{Br}\cdot \quad (4)$$

$$\text{Me}\cdot + \text{Br}_2 \longrightarrow \text{MeBr} + \text{Br}\cdot \quad (5)$$

$$\text{Me}\cdot + \text{Me}\cdot \longrightarrow \text{C}_2\text{H}_6 \quad (6)$$

$$\text{Br}\cdot + \text{Br}\cdot + \text{M} \longrightarrow \text{Br}_2 + \text{M} \quad (7)$$

$$\text{Me}\cdot + \text{Br}\cdot \longrightarrow \text{MeBr} \quad (8)$$

The high yield of CH_4 compared to C_2H_6 (see Table I, run 2) demonstrates the high efficiency of HBr as a radical trap. The high yield of C_2H_6 in run 3 is due to the disappearance of HBr before the end of the run. Using a value of 0.5 μmole for C_2H_6 and an average value of HBr of 37 μmole, the relationship $R_{CH_4}/R^{1/2}_{C_2H_6} = k_4(HBr)/k_6^{1/2}$ produces a value for k_4 of 2.6×10^7 l./mole sec at 140°, assuming Shepp's value for k_6.[7] The standard entropy change computed from listed standard entropies[8,9] is 8.0 eu for the equilibrium $\text{Br}\cdot + \text{CH}_4 \rightleftarrows \text{Me}\cdot + \text{HBr}$. A_{-4} has been measured to be $10^{10.7}$ l./mole sec[10] and hence A_4 is $10^{8.95}$ l./mole sec. Thus our data produce a value for E_4 of 2.9 kcal/mole which is in reasonable agreement with 4.5 kcal/mole found by O'Neal[11] and with 1.7 kcal/mole computed from the results in ref 10. This latter value assumes a standard heat of reaction for reaction 4 of 16.6 kcal/mole derived from listed standard heats of formation.[8,9,12] $E_5 - E_4$ has been measured to be 2 kcal/mole[13] which allows us to give a value for E_5 of 0.9 kcal/mole. From the expression $R_{MeBr}/R_{CH_4} = k_5(\overline{Br_2})/k_4(\overline{HBr})$, we find an impossibly low value for k_5 of 10^5 l./mole sec compared to a literature value of 1.9×10^8 l./mole sec.[13] This suggests a much lower value for $(\overline{Br_2})$ than is estimated (see below).

In the present system, the main termination process is reaction 7. Hence the bromine atom steady-state concentration is given by $(Br)_{ss} = [(k_1/k_7)(dtBP/M)]^{1/2} = [k_1/k_7]^{1/2}$. Taking a value of k_1 from ref 1 and assuming $A_7 = 10^{10}$ l.²/mole² sec,[14] $E_1 = -2$ kcal/mole,[15] $(Br)_{ss}$ turns out to be 2×10^{-8} mole/l.[15a] If IBO is formed *via* the route shown in eq 9 and 10

(3) L. Batt and F. R. Cruickshank, *J. Phys. Chem.*, 70, 723 (1966).

(4) L. Batt and F. R. Cruickshank, *Talenta*, in press.

(5) H. E. O'Neal and S. W. Benson, *J. Chem. Phys.*, 36, 2196 (1962).

(6) A. Hardacre, G. Skirrow, and C. F. H. Tipper, *Combust. Flame*, 9, 53 (1965).

(7) A. Shepp, *J. Chem. Phys.*, 24, 939 (1956).

(8) S. W. Benson, "The Foundation of Chemical Kinetics," McGraw-Hill Book Co., Inc., New York, N. Y., 1960, p 663.

(9) F. D. Rossini, *et al.*, "Selected Values of Chemical Thermodynamic Properties," National Bureau of Standards Circular 500, U. S. Government Printing Office, Washington, D. C., 1952, p 100.

(10) G. B. Kistiakowsky and E. R. Van Artsdalen, *J. Chem. Phys.*, 12, 469 (1944).

(11) H. E. O'Neal, private communication.

(12) D. M. Golden, R. Walsh, and S. W. Benson, *J. Am. Chem. Soc.*, 87, 4053 (1965).

(13) A. F. Trotman-Dickenson, "Gas Kinetics," Butterworth and Co. Ltd., London, 1955, p 191.

(14) See ref 8, p 310.

(15) G. C. Fettis and J. H. Knox, *Progr. Reaction Kinetics*, 2, 28 (1964).

(15a) NOTE ADDED IN PROOF. C. W. Larson and H. E. O'Neal, *J. Phys. Chem.*, 70, 2475 (1966), estimate k_8 as 10^{11} l./mole sec. In this case, termination by Me and Br is as important as Br and Br, but $(Br)_{ss}$ is essentially the same. However, with the relatively few effective degrees of freedom contributing to the decomposition (~6), reaction 8 may well be pressure dependent under our conditions (100 mm, 140°). A falloff in the value of k_8 cited above by 10–100 will leave reaction 7 as the main terminating step.

$$\dot{Br} + dtBP \longrightarrow HBr + dtB\dot{P}_{-H} \quad (9)$$

$$dtB\dot{P}_{-H} \longrightarrow IBO + t\text{-}Bu\dot{O} \quad (10)$$

assuming $dtB\dot{P}_{-H}$ always decomposes, then $R_{chain}/R_{uni} = (k_9/k_1)(\dot{Br}) =$ yield(IBO)/yield(Me_2CO + t-BuOH − IBO)/2 = 21/39, whence k_9 is 1.6×10^3 l./mole sec. The validity of the mass balance relationship yield(CH_4) + yield(t-BuOH) − yield(IBO) = ΔHBr, see Table I, run 2, is in line with such a mechanism. Assuming A_9 is 10^{11} l./mole sec, E_9 turns out to be ~17 kcal/mole. The endothermicity for reaction 9 is of the order of 12 kcal, thus predicting a value for E_{-9} of ~5 kcal/mole. However, there is a very unusual variation in pressure with time during the reaction. Figure 1 shows that there is a marked drop in the pressure initially. The extent of this pressure drop varies directly with the initial HBr concentration. Separate experiments show that this is not due to absorption of dtBP, HBr, or Br_2 in the tap grease. Complex formation occurs between dimethyl ether and HCl[16] and i-PrOH and I_2.[17] The observed fall in pressure may well be due to similar complex formations between dtBP and HBr and dtBP and Br_2. It is possible that these complexes may decompose at a later stage to form t-BuOH and t-BuOBr or 2t-BuOBr, respectively, the latter compound then decomposing unimolecularly to form IBO and HBr, *e.g.*

$$dtBP + Br_2 \rightleftharpoons (dtBPBr_2) \quad (11)$$

$$(dtBPBr_2) \longrightarrow 2t\text{-}BuOBr \quad (12)$$

$$t\text{-}BuOBr \longrightarrow IBO + HBr \quad (13)$$

The erroneously low value for k_5 suggests that this complex formation is more marked for Br_2 and dtBP than for HBr and dtBP. Since t-BuOH could be produced by these reactions, it is possible that this will obscure the kinetics of the decomposition of t-Bu$\dot{O}$. Spurious production of t-BuOH may also occur in the HCl–dtBP system,[18] causing the observed scatter in the relevant graphical plots therein.

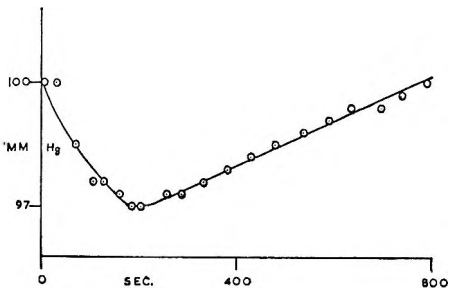

Figure 1. Pressure *vs.* time plot for dtBP + HBr at 140°.

It is concluded that although HBr is a very efficient radical trap, the complicated side reactions make it difficult to come to any worthwhile conclusions about the decomposition of t-Bu$\dot{O}$. The use of HI as a radical trap is also excluded since it reacts heterogeneously with dtBP.[19]

Acknowledgments. F. R. C. gratefully acknowledges the receipt of a Carnegie Scholarship from the Carnegie Trust for the Universities of Scotland. We are grateful to Dr. J. H. Knox for helpful discussions.

(16) K. P. Lawley and L. E. Sutton, *Trans. Faraday Soc.*, **59**, 2630 (1963).

(17) R. Walsh and S. W. Benson, *J. Am. Chem. Soc.*, **88**, 3480 (1966).

(18) M. Flowers, L. Batt, and S. W. Benson, *J. Chem. Phys.*, **37**, 2662 (1962).

(19) L. Batt, S. W. Benson, and H. Hershenson, unpublished results.

Triplet-State Yield of Fluorobenzene by the Sensitization of the Isomerization of *cis*-Butene-2

by David Phillips[1]

Department of Chemistry, The University of Texas, Austin, Texas 78712 *(Received August 19, 1966)*

Triplet-state yields for fluorobenzene excited at 2650, 2537, and 2480 A, respectively, have been determined. The plots all lie on the same smooth curve of quantum yield *vs. cis*-butene-2 pressure, thus indicating that a common level is reached before crossover from excited singlet to triplet state. The asymptotic value for the triplet yield is 0.86 at high pressures of *cis*-butene-2. The sum of triplet state and fluorescent yields is about 1.05 ± 0.09. Comparison with other results is made.

Unger[2] has investigated the fluorescence and triplet-state yields of fluorobenzene using the biacetyl sensitization technique of Ishikawa and Noyes[3] to determine the triplet-state yield quantitatively under a variety of conditions. The Cundall technique[4,5] of the sensitization by a triplet molecule of the *cis–trans* isomerization of butene-2 was also used quantitatively to demonstrate the presence of triplet-state fluorobenzene, and the author indicated that one experiment gave a value for the triplet-state yield in agreement with that found by the biacetyl sensitization technique, although the experimental conditions and method of calculation were not stated.[2]

Standard procedure for the measurement of emission yields in the vapor phase is the use of a T-shaped cell with a phototube at one end of the cell along its axis to measure the light absorbed by material in the cell, and a photomultiplier tube scanning the T-piece for emitted light. Absolute emission yields are determined by calibration of the system with a compound of known emission yield. This arrangement can be the source of extreme error when absorption of incident radiation by the material is high. It can be shown easily that increase in pressure of absorbing material with consequent increase in optical density will cause an increasingly appreciable fraction of the incident light to be absorbed in a region of the cell which is not scanned by the photomultiplier. This leads to artificially low emission yields, and is sometimes given the name "round the corner effect." Interpretation of the effect of pressure upon emission yields must thus be treated with caution, especially if the material under investigation has a discrete absorption spectrum with unresolved rotation lines as is the case in benzene and fluorobenzene.

Since Unger[2] used emission techniques to measure quantitatively both the fluorescence and triplet-state yields of fluorobenzene, it was considered worthwhile to remeasure the triplet-state yield using the technique of Cundall[4,5] in a quantitative manner as this method gives results which are independent of the geometry of the system.

Experimental Section

The vacuum system,[6,7] analytical system,[7] and techniques used[7] have all been described previously.

Fluorobenzene. The fluorobenzene used was Eastman White Label. It was distilled on the vacuum line and the middle third was retained. This fraction was shown to be pure by vpc analysis.

Benzene. Matheson Coleman and Bell chromato-

(1) Department of Chemistry, The University, Southampton, United Kingdom.

(2) I. Unger, *J. Phys. Chem.*, 69, 4284 (1965).

(3) (a) H. Ishikawa and W. A. Noyes, Jr., *J. Am. Chem. Soc.*, 84, 1502 (1962); (b) H. Ishikawa and W. A. Noyes, Jr., *J. Chem. Phys.*, 37, 583 (1962).

(4) R. B. Cundall, F. G. Fletcher, and C. C. Milne, *Trans. Faraday Soc.*, 60, 1146 (1964).

(5) R. B. Cundall and A. S. Davis, *ibid.*, 62, 1151 (1966).

(6) D. Phillips, *J. Phys. Chem.*, 70, 1235 (1966).

(7) D. Phillips, unpublished results.

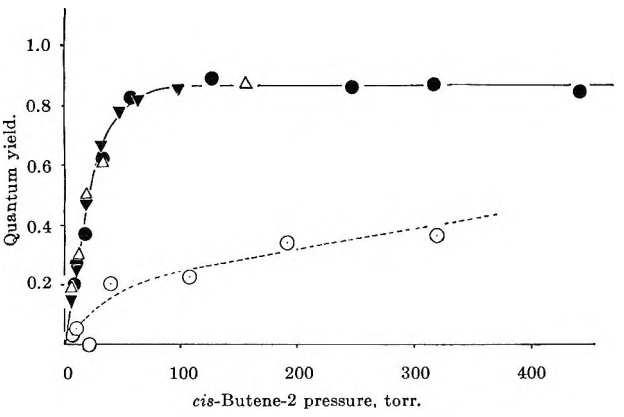

Figure 1. Effect of *cis*-butene-2 pressure on triplet-state yield of fluorobenzene at 25°: ●, 2650 A, C_6H_5F pressure 4 torr; ▼, 2540 A, C_6H_5F pressure 3 torr; △, 2480 A, C_6H_5F pressure 6 torr; ○, 2380 A, C_6H_5F pressure 15 torr.

quality benzene was used without any attempt at purification.

cis-Butene-2. Phillips research grade *cis*-butene-2 was used which contained a single impurity of 0.074% *trans*-butene-2.

Results

The triplet-state yield for fluorobenzene excited at various wavelengths as a function of *cis*-butene-2 pressure is shown in Figure 1. Absolute yields were determined by comparison with the benzene-sensitized isomerization of *cis*-butene-2. The quantum yield for benzene triplet-state formation at 2537 A was taken as 0.63.[5]

The fluorescence yields of fluorobenzene at 25° and various wavelengths were noted for comparison with previously obtained values.[2] At 2537 ± 8 A, 2 torr of fluorobenzene gave an emission yield of 0.180. At 2537 ± 8 A 105 torr of fluorobenzene gave an emission yield of 0.19. Since these wavelengths correspond to regions of high absorption by the fluorobenzene, the variation of fluorescence yield with fluorobenzene pressure was determined at a wavelength where the absorption was smaller. At 2700 ± 8 A, an increase in pressure of fluorobenzene caused an apparent decrease in fluorescent yield, the equation being

$$\frac{1}{Q_{2700}} = 6.1 + 4.8 \times 10^2[\mathrm{M}]$$

where [M] is concentration of fluorobenzene in moles $l.^{-1}$.

At 2380 A, 15 torr of fluorobenzene gave detectable emission, which increased linearly with an increase in *cis*-butene-2 added gas pressure up to 500 torr according to the equation

$$Q_{2380} = 0.039 + 3.15[\mathrm{M}]$$

where [M] is the concentration of *cis*-butene-2 in moles $l.^{-1}$.

In contrast, the emission from 4 torr of fluorobenzene at 2537 A was not altered by the addition of up to 400 torr of *cis*-butene-2.

At 2300 A, the emission from 53 torr of fluorobenzene was very small but detectable; the yield was of the order of 0.01.

All yields quoted above were obtained with reference to the emission from 11 torr of benzene. The absolute fluorescence yield for benzene was taken as 0.18.[8]

Discussion

There are several conclusions to be drawn from Figure 1.

(a) The triplet-state yields at 2650, 2537, and 2480 A all lie on the same curve, indicating that a common level is reached before intersystem crossover occurs. This is probably the equilibrated vibrational level of the excited singlet state of fluorobenzene. This is borne out by the fact that the fluorescence yield of fluorobenzene is independent of the addition of large pressures of *cis*-butene-2.

(b) A high pressure of *cis*-butene-2 is required to capture all of the fluorobenzene triplets. Comparison with the benzene system[5] would indicate that the lifetime of the fluorobenzene triplet is approximately one-tenth of that of benzene, *i.e.*, of the order of 10^{-6} sec.

(c) At 2380 A and above 100 torr of *cis*-butene-2, the triplet-state yield of fluorobenzene, Φ_T, increases with increasing *cis*-butene-2 pressure. The fluorescence yield Q_f at this wavelength also increases with increasing *cis*-butene-2 pressure. Clearly, at 2380 A there is some process occurring which competes effectively with collisional loss of vibrational energy. However, the ratio Q_f/Φ_T remains constant and approximately equal to that measured at longer wavelengths. It is thus unlikely that the competing process is intersystem crossing. It may well be an isomerization step of the type observed recently in substituted benzenes.[9,10]

(d) The asymptotic value of the fluorobenzene triplet at the longer wavelengths is 0.86. A realistic estimate of errors, including that due to the fact that results are dependent upon Cundall's figure[5] of 0.63 ± 0.01 for the benzene triplet yield, would put the value at 0.86 ± 0.04.

(8) W. A. Noyes, Jr., W. A. Mulac, and D. A. Harter, *J. Chem. Phys.*, **44**, 2100 (1966).

(9) L. Kaplan, K. E. Wilzbach, W. G. Brown, and S. S. Young, *J. Am. Chem. Soc.*, **87**, 675 (1965).

(10) K. E. Wilzbach and L. Kaplan, *ibid.*, **87**, 4004 (1965).

Interpretation of the results on fluorescence yields presents some difficulty. At both 2537 and 2700 A, the apparent fluorescence yield of fluorobenzene varied with pressure of fluorobenzene. However, the fluorescence yield of benzene at pressures between 8 and 14 torr also showed a marked variation with pressure, and in this pressure region Noyes, *et al.*, have shown[8] that absolute measurements of the benzene fluorescence yield were independent of pressure. Clearly, in the present system geometrical effects are playing a very important part.

Accordingly, the fluorobenzene fluorescence yield at 2537 A reported earlier was obtained by using a pressure of fluorobenzene which gave the same optical density as 11 torr of benzene and assuming the Noyes figure for the absolute benzene yield of 0.18 ± 0.04. Thus (assuming the fluorescence yield to be the same) under the conditions at which the triplet-state yield of fluorobenzene was measured, the sum of the triplet and fluorescence yields is 1.05 ± 0.09. Because of the "round the corner" effect, we may say nothing about the self-quenching of the fluorebenzene singlet state except that if it is not negligible, then the combined sum above must be adjusted to a higher value.

We may now compare the present results with those obtained by Unger.[2] The maximum sensitized emission yield from biacetyl at 2537 A obtained was 0.136[2] at 3 torr of fluorobenzene and 4.5 torr of biacetyl. Division of this figure by the emission yield of biacetyl of 0.145 ± 0.03[11] gives a triplet-state yield of 0.90 ± 0.18. Under the conditions at which maximum sensitization occurred, the fluorescence yield of fluorobenzene was reported as 0.17 (from Unger's eq 3). Thus, the combined yields of triplet state and fluorescence is 1.06 ± 0.21. However, the fluorescence yield from the same pressure of fluorobenzene in the absence of biacetyl was 0.219 (from Unger's eq 2). Clearly, in Unger's experiments, a significant amount of energy transfer from singlet fluorobenzene molecules to biacetyl had occurred. It can easily be shown that any such process which depletes the concentration of fluorobenzene singlet molecules will lower the value of both fluorescence and triplet-state yields if intersystem crossing occurs from the same state as fluorescence, as is the case here. Thus the yield of 0.90 ± 0.18 found by Unger must also be multiplied by 0.219/0.17 to give the theoretical triplet state yield in the absence of biacetyl. This figure is 1.16 ± 0.25. Thus the combined sum of fluorescence and triplet yield in the absence of any quenching of the triplet state of fluorobenzene by biacetyl is now 1.38 ± 0.29. Even considering the errors of 20% inherent in the measurements, this figure is much too great to be acceptable.

Part of the reason for this high value undoubtedly lies in Unger's acceptance of Ishikawa's value[3b] for the fluorescence yield of benzene, upon which Unger's data depend. Because of possible errors due to geometry, we should only compare results obtained at similar pressures. At 11 torr of benzene, Ishikawa obtained a value of 0.234 for the benzene fluorescence yield. At a similar pressure, Poole obtained a value of 0.17.[12] Both of these values were determined using biacetyl as a standard. The value at this pressure determined by Noyes, *et al.*,[8] in an absolute manner was 0.18. Noyes *et al.*, have already shown[8] that if we assume Ishikawa's value for the fluorescence yield of benzene is too high, and correct the value to 0.18, the resulting triplet-state yield for benzene by the biacetyl sensitization technique becomes 0.63, in exact agreement with the value obtained by Cundall, *et al.*[5]

If we accept that this is not an unreasonable correction, we must also apply it to the data obtained by Unger. Upon multiplication by the factor 0.18/0.234, the fluorescence and triplet-state yields measured by Unger become 0.12 ± 0.02 and 0.69 ± 0.14, respectively, and the values in the absence of biacetyl quenching of the fluorobenzene singlet 0.17 ± 0.03 and 0.95 ± 0.19. The sum of fluorescence and triplet-state yields is now 1.12 ± 0.22, which is unity within the author's stated error, and corresponds quite closely to the values obtained in the present work.

The above demonstrates the difficulty in the determination of emission yields by any method. While it is not suggested that the emission yields for fluorobenzene determined in the present work represent any improvement over previously determined values, it is felt that the triplet yield from the present work is more reliable. However, at the wavelengths where an isomerization may be important, use of Cundall's technique may lead to errors due to the possibility of compound formation with the olefin present.[13] At longer wavelengths, the present system seems to be uncomplicated by such reactions.

Acknowledgments. The author wishes to thank Dr. W. A. Noyes, Jr., for his advice during the course of this work, and one of the referees for pointing out some errors in the original manuscript. Financial support from the U. S. Air Force Office of Scientific Research Grant No. 778-65 is gratefully acknowledged.

(11) G. M. Almy and P. R. Gillette, *J. Chem. Phys.*, **11**, 188 (1943).
(12) G. A. Poole, *J. Phys. Chem.*, **69**, 1343 (1965).
(13) K. E. Wilzbach and L. Kaplan, *J. Am. Chem. Soc.*, **88**, 2066 (1966).

Proton Exchange of Phenol in Aqueous Acid[1]

by Ernest Grunwald and Mohindar S. Puar

Lecks Chemical Laboratories, Brandeis University, Waltham, Massachusetts 02154
(Received November 15, 1966)

This paper reports nmr measurements of the rate of OH–proton transfer between phenol and water at −1, 25, and 50°. Two kinetic processes are recognized, one catalyzed by hydrogen ion and the other by phenoxide ion. For the H^+-catalyzed process, $k = 1.5 \times 10^7$ sec^{-1} M^{-1} at 25°, $\Delta H^{\ddagger} = 5.5_5$ kcal, and $\Delta S^{\ddagger} = -6.8$ gibbs. This rate is too high to be accounted for by the reversible proton-transfer reaction $PhOH + H_3O^+ = PhOH_2^+ + H_2O$ and a concerted termolecular mechanism involving one molecule each of H_3O^+, PhOH, and H_2O is indicated. For the phenoxide-catalyzed process, $k_2 = 5.7 \times 10^3$ sec^{-1} M^{-1} at 25°, $\Delta H^{\ddagger} = 3.2$ kcal, and $\Delta S^{\ddagger} = -7.4$ gibbs. Our data in combination with previous measurements by Luz and Meiboom[2] show that this reaction involves one molecule each of PhOH, HOH, and PhO^-. The lifetime of the PhO^-–HOH hydrogen-bonded complex is estimated to be less than 3×10^{-9} sec in water at 25° on the basis of the kinetic data.

We wish to report a kinetic study of OH–proton exchange between phenol and water in aqueous solution. Rates were measured by nuclear magnetic resonance (nmr) techniques at −1, 25, and 50°, at pH values ranging from 5.8 to 2.2, and at phenol concentrations ranging from 0.25 to 0.5 *M*. Under these conditions the kinetic data are consistent with the rate law, eq 1.

$$\text{rate of exchange} = k[\text{PhOH}][\text{H}^+] + k_2[\text{PhOH}][\text{PhO}^-] \quad (1)$$

Average rate constants, k and k_2, and average activation parameters, $\Delta H^{\ddagger}$ and $\Delta S^{\ddagger}$, are listed in Table I. The results are noteworthy because they help to define the reaction mechanism for both processes as follows.

Acid-Catalyzed Reaction. In principle, the acid-catalyzed reaction can proceed either by a two-step mechanism, such as eq 1a followed by eq 1b, or by a concerted mechanism such as eq 2.[3]

$$\text{PhOH} + \text{H}^1\text{OH}_2^+ \xrightarrow{k_+} \underset{\displaystyle \text{H}^1}{\text{PhOH}^+} + \text{OH}_2 \quad (1a)$$

$$\underset{\displaystyle \text{H}^1}{\text{PhOH}^+} + \text{OH}_2 \xrightarrow{1/2k_-} \underset{\displaystyle \text{H}^1}{\text{PhO}} + \text{HOH}_2^+ \quad (1b)$$

$$\underset{\displaystyle \text{Ph}}{\text{H}_2\text{OH}^+} + \underset{\displaystyle \text{Ph}}{\text{OH}} + \text{OH}_2 \longrightarrow \underset{\displaystyle \text{Ph}}{\text{H}_2\text{O} + \text{HO}} + \text{HOH}_2^+ \quad (2)$$

However, we shall show that the experimental rate constant for the acid-catalyzed reaction is at least a hundred times greater than the *maximum* to be expected for any two-step mechanism (eq 1) in which $PhOH_2^+$ is a reaction intermediate. The ionization of phenol as a base has been measured spectrophotometrially in sulfuric acid–water mixtures[4] and the results have been interpreted with the aid of the Hammett acidity function[5] to give a fairly accurate estimate of the equilibrium constant in dilute aqueous solution, eq 3.

$$K = [\text{PhOH}_2^+]/[\text{PhOH}][\text{H}_3\text{O}^+] = 1.8 \times 10^{-7} \text{ at } 18° \quad (3)$$

(1) Work supported by the Petroleum Research Fund of the American Chemical Society. Grateful acknowledgment is made to the donors of that fund.

(2) Z. Luz and S. Meiboom, *J. Am. Chem. Soc.*, 86, 4766 (1964).

(3) See, for example, E. Grunwald and C. F. Jumper, *ibid.*, 85, 2051 (1963).

(4) E. M. Arnett and C. Y. Wu, *ibid.*, 82, 5660 (1960).

(5) L. P. Hammett, "Physical Organic Chemistry," McGraw-Hill Book Co., Inc., New York, N. Y., 1940, Chapter 9.

Table I: Kinetic Analysis of Nmr Data for OH–Proton Exchange of Phenol in Dilute Aqueous Acid

	Temperature, °C		
	−1.0	25.0	50.5
Acid-Catalyzed Reaction			
$k \times 10^7$, sec^{-1} M^{-1}	0.71	1.46	4.41
$\Delta H^{\pm}$, kcal	...	5.55	...
$\Delta S^{\pm}$, gibbs	...	−6.8	...
Phenoxide-Catalyzed Reaction			
$k_2 \times 10^{-8}$, sec^{-1} M^{-1}	4.0	5.7	12.4
$\Delta H_2^{\pm}$, kcal[a]	...	3.20	...
$\Delta S_2^{\pm}$, gibbs[a]	...	−7.4	...
Auxiliary Data			
δ, at 56.4 MHz, rad/sec	1558	1725	1885[c]
pK_A[b]	10.44	10.02	9.71
S,[d] Debye–Hückel limiting slope	0.486	0.506	0.535

[a] Luz and Meiboom[2] report $\Delta H^{\pm} = 4.2$ kcal, $\Delta S^{\pm} = -5.0$ gibbs; see also Figure 1. [b] D. T. Y. Chen and K. J. Laidler, *Trans. Faraday Soc.*, **58**, 480 (1962). [c] Extrapolated from data at lower temperatures. [d] $-\log y = S\sqrt{\mu}$; y mean ionic activity coefficient of H^+ and PhO^-; μ ionic strength.

In terms of eq 1, $K = k_+/k_-$. Since K is small, reaction 1a is rate-determining and the rate constant, k_1, associated with the cycle 1a followed by 1b is given by eq 4.

$$k_1 = {}^1/_2 k_+ = {}^1/_2 K k_- \qquad (4)$$

To estimate the upper limit to k_1 we estimate the upper limit to k_- by assuming that proton transfer from $PhOH_2^+$ to an *adjacent* water molecule is ultrafast. In that case, k_- is just equal to the rate constant for the dissociation of the conjugate encounter complex, $PhOH{-}HOH_2^+ \rightarrow PhOH + H_3O^+$. A conservative upper limit for the rate constant of the latter process is 10^{12} sec^{-1}.[6] Hence we obtain the limits, $k^- \leq 10^{12}$ sec^{-1} and, because of eq 3 and 4, $k_1 \leq 10^6$ sec^{-1} M^{-1}. By contrast, the experimental rate constant k, interpolated at 18°, is 1.3×10^7 sec^{-1} M^{-1}.

That the acid-catalyzed reaction actually proceeds by a concerted *termolecular* mechanism, as in eq 2, is suggested by the close analogy of the kinetic parameters associated with it and those obtained in symmetrical proton-exchange processes that are known to be termolecular.[3,7]

Phenoxide-Catalyzed Reaction. A kinetic term for OH–proton exchange of the form k_2^*[PhOH][PhO$^-$] was first demonstrated by Luz and Meiboom[2] in their nmr measurements on phenol–phenoxide buffers in the pH range 8.2–9.3. These authors used water enriched in H_2O^{17} and measured the rate of proton exchange *between water molecules*. Under the conditions of their measurements the phenol–phenoxide couple acts as a catalytic carrier of protons from one water molecule to another. On the other hand, the present experiments evaluate the rate of proton exchange, not between different water molecules, but between molecules of water and molecules of phenol. Both experiments require that the reaction be of the type shown in eq 5, but neither experiment taken by

$$PhOH + \left(\begin{matrix} OH \\ | \\ H \end{matrix}\right)_n + OPh^- \longrightarrow PhO^- + \left(\begin{matrix} HO \\ | \\ H \end{matrix}\right)_n + HOPh \qquad (5)$$

itself can evaluate the number, n, of water molecules that participate. However, the two experiments taken in combination do evaluate n, as explained previously.[7,8] The relevant equation is eq 6

$$n = k_2^*/k_2 \qquad (6)$$

where k_2^* is the rate constant obtained in the Luz–Meiboom experiment and k_2 is that obtained in our experiment. The required comparison is made in the upper part of Figure 1. It is clear that in the temperature range in which the measurements overlap, the two rate constants are equal within their experimental error. Thus $n = 1$, that is, reaction 5 involves one water molecule and is termolecular.

Knowledge of the rate constant and of the participation by a water molecule in reaction 5 enables us to set lower limits to the rate of exchange of water molecules between bulk water and hydrogen-bonded sites in the solvation shells of phenol and phenoxide. In order to obtain precise second-order kinetics, it is necessary that the equilibrium between water molecules in the bulk solvent and water molecules in the solvation complexes, $PhOH{-}OH_2$ and $PhO^-{-}HOH$, be established rapidly relative to the time required for proton transfer.[7] Using a kinetic scheme similar to that derived previously for estimating the lifetimes of $R_3N{-}HOH$ hydrogen-bonded complexes[7] and concluding from the data of Luz and Meiboom[2] (which are more precise than ours) that possible deviations from strict second-order kinetics are less than 30% as [PhOH] is increased to 0.3 M and [PhO$^-$] is in-

(6) The Debye–Eigen model of diffusion-controlled rate processes predicts a rate constant of 10^{11} sec^{-1}, M. Eigen, *Z. Physik. Chem.* (Frankfurt), **1**, 176 (1954). For further discussion, see ref 3.

(7) See, for example, E. Grunwald and M. Cocivera, *Discussions Faraday Soc.*, **39**, 105 (1965).

(8) Z. Luz and S. Meiboom, *J. Chem. Phys.*, **39**, 366 (1963).

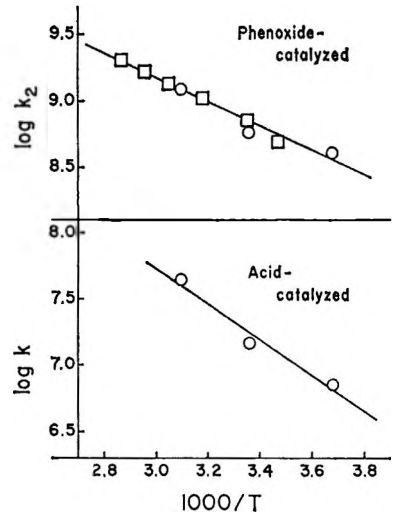

Figure 1. Arrhenius plots of kinetic data: O, present work; □, data of Luz and Meiboom.[2]

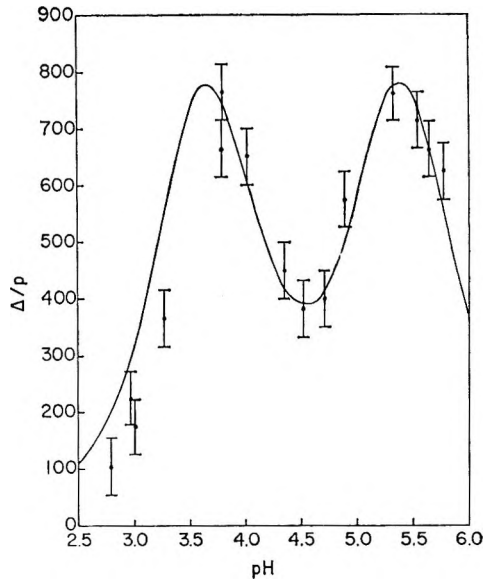

Figure 2. Plot of Δ/p *vs.* pH for dominant nmr line in the phenol–water OH-proton system at −1°. Δ and p are defined in eq 8 and 9. The smooth curve is calculated from eq 1 and 11, using rate constants in Table I and assuming that [PhOH] is constant at 0.42 M. For a previously reported similar relationship with a double maximum, see Figures 3 and 5 in ref 12.

creased to 0.005 M, we obtain the following *upper limit* to the mean lifetime, λ, of a water molecule in the solvation shell of phenoxide ion (eq 7).[9]

$$PhO^-\text{–}HOH + HOH\,(aq) \rightarrow PhO^-\text{–}HOH + HOH\,(aq)$$
$$\lambda < 3 \times 10^{-9}\ \text{sec at } 25° \quad (7)$$

Experimental Section

Materials. Phenol (Mallinckrodt Analytical reagent) was distilled twice at reduced pressure and was solid at room temperature. Water was doubly distilled. Hydrochloric acid was of reagent grade. Reaction mixtures were prepared by standard quantitative techniques; their pH was monitored with a calibrated Beckman pH meter.

Rate Measurements. Rates of OH–proton exchange were derived from measurements of T_1 and T_2' of the dominant nmr line in the water–phenol OH–proton system by spin-echo techniques.[10] The method is similar to one described in a previous paper on neopentyl alcohol in acetic acid.[11] As a measure of exchange broadening we used the quantity Δ, defined in eq 8.

$$\Delta = (1/T_2') - (1/T_1) \quad (8)$$

To relate Δ to the OH–proton exchange rate, R, we introduce two parameters, p and τ, according to eq 9 and 10.

$$p = [PhOH]/([PhOH + 2[H_2O]) \quad (9)$$

$$\tau = 2[H_2O]p/R \quad (10)$$

The desired relationship then becomes eq 11, where δ is the difference in resonance frequency (in radians per second) at the given value of the magnetic field between the phenol and water OH–protons.[12]

$$\frac{\Delta}{p} = \frac{\delta^2\tau}{1 + \delta^2\tau^2} \quad (11)$$

According to eq 11, Δ/p approaches zero as $\delta\tau$ approaches either zero or infinity and it attains a maximum value of $\delta/2$ when $\delta\tau = 1$. According to the rate law (eq 1), R and hence $1/\tau$ goes through a minimum when $[H^+] = k_2[PhO^-]/k$. If $\delta\tau > 1$ at this rate minimum, then the plot of the experimental Δ/p *vs.* pH will look like Figure 2, which shows our data at −1°. The central minimum in Δ/p reflects the minimum in the rate. The two maxima correspond to rates at which $\delta\tau = 1$ and permit evaluation of δ, which is equal

(9) An upper limit to the mean lifetime, λ′, of the $PhOH\text{–}OH_2$ complex is found similarly to be less than 10^{-7} sec. However, this limit is almost certainly far above the true value of λ′ and should not be compared with that obtained for λ in eq 7. To obtain λ one increases [PhOH]; to obtain λ′ one increases $[PhO^-]$. While [PhOH] was moderately high in some experiments, $[PhO^-]$ was very small in all experiments.

(10) S. Meiboom and D. Gill, *Rev. Sci. Instr.*, **29**, 688 (1958). In agreement with previous practice[11] we use the symbol T_2' rather than T_2 to indicate that there is a contribution from proton exchange.

(11) M. Cocivera and E. Grunwald, *J. Am. Chem. Soc.*, **87**, 2551 (1965).

(12) A general treatment of exchange broadening of the dominant nmr line in a system consisting of one intense and a number of weak nmr lines has been given by S. Meiboom, *J. Chem. Phys.*, **34**, 375 (1961).

to $2(\Delta/p)_{max}$. Given δ, we have all the information we need to deduce the rates of OH–proton exchange. The smooth curve in Figure 2 is calculated on the basis of eq 1, 9, 10, and 11, assuming that [PhOH] is constant at 0.42 *M*. Actual values of [PhOH] are not constant, but most of the experimental points in Figure 2 represent aqueous solutions whose phenol concentrations are within 25% of this value.

In calculating [PhO^-] from [PhOH] and the pH, we used K_A values for phenol as reported by Chen and Laidler[13] and estimated activity coefficients from the Debye–Hückel limiting law (see Table I).

At 25° the two maxima in the plot of Δ/p *vs.* pH are barely resolved, that is, $\delta\tau$ at the rate minimum is only slightly greater than one. At 50° the plot shows only one maximum, that is $\delta\tau$ is smaller than one at all values of pH. The required value of δ for rate calculations of 50° was obtained by linear extrapolation of the values at −1 and 25°. The observed dependence of δ on the temperature is analogous to similar observations in methanol[14] and can be said to result from a change in the hydrogen-bonded solvent structure.

(13) See footnote *b* of Table I.

(14) Examples are given by E. Grunwald, C. F. Jumper, and S. Meiboom, *J. Am. Chem. Soc.*, 85, 524 (1963); M. Cocivera, E. Grunwald, and C. F. Jumper, *J. Phys. Chem.*, 68, 3234 (1964).

A Nuclear Magnetic Resonance Study of Acid Dissociation and Proton Exchange of Trimethylammonium Ion in Methanol

by Ernest Grunwald[1]

Bell Telephone Laboratories, Murray Hill, New Jersey 07971 *(Received December 5, 1966)*

Rates of proton exchange have been measured between −0.7 and 50° by nuclear magnetic resonance methods for solutions of trimethylammonium ion (BH^+) in methanol over a wide pH range and are compared with analogous previous measurements in water. Kinetic analysis yields the following rate and equilibrium constants for methanol (numbers in parentheses for water) at 25°: for acid dissociation of BH^+, equilibrium constant K_A = 1.20 (1.57) × 10^{-10}, ΔH_A° = 11.6 (8.8) kcal, ΔS_A° = −6.5 (−15.2) gibbs; forward rate constant k_a = 0.7 (4.7) sec^{-1}, E_{act} = 13 (11.3) kcal; reverse rate constant k_{-a} = 0.6 (3.0) × 10^{10} sec^{-1} M^{-1}, E_{act} = 2 (1.4) kcal. For the symmetrical termolecular proton exchange, $B + HOCH_3 + HB^+ \rightarrow BH^+ + OH \cdot CH_3 + B$, the rate constant k_2 = 3.25 (3.4) × 10^8 sec^{-1} M^{-1}, E_{act} = 2.9 (3.3) kcal. For proton exchange between methanol and methoxide ion, the pseudo-first-order rate constant k_{MeO^-} = 1.84 × 10^{10} sec^{-1}, E_{act} ≈ 2 kcal.

Thermodynamic and kinetic aspects of proton transfer have been studied extensively for solutions of trimethylammonium ion in water.[2-7] The present study provides comparable data for solutions of trimethylammonium ion in methanol. All of the reactions considered here involve at least one molecule of methanol as a reactant.

A comparison of the solvents water and methanol is of interest because the crystal structures of the respective solids[8] suggest that the hydrogen-bonded aggregates that exist in water are three-dimensional "icebergs,"[9] whereas those that exist in methanol are linear polymers. This difference results of course from the presence of two H bond donor sites in the water molecule but only one in the methanol molecule.

In the present study, rate and equilibrium constants for proton transfer of trimethylammonium ion in methanol turn out to be remarkably similar to values obtained for the analogous reactions in water. It appears that the suggested change in hydrogen-bonded solvent structure does not produce any drastic effects.

Results

Our work deals primarily with acid dissociation (eq 1, equilibrium constant K_A) and symmetrical proton exchange (eq 2).[10,11] Values of K_A, k_a, and k_2 were

$$(CH_3)_3NH^+ + CH_3OH \underset{k_{-a}}{\overset{k_a}{\rightleftharpoons}} (CH_3)_3N + CH_3OH_2^+ \quad (1)$$

(1) To whom all correspondence should be addressed at Chemistry Department, Brandeis University, Waltham, Mass. 02154.

(2) D. H. Everett and W. F. K. Wynne-Jones, *Proc. Roy. Soc.* (London), **A177**, 499 (1941).

(3) A. Loewenstein and S. Meiboom, *J. Chem. Phys.*, **27**, 1067 (1957).

(4) A. Loewenstein, *J. Phys. Chem.*, **67**, 1728 (1963).

(5) Z. Luz and S. Meiboom, *J. Chem. Phys.*, **39**, 366 (1963).

(6) E. Grunwald, *J. Phys. Chem.*, **67**, 2208, 2211 (1963).

(7) M. Eigen and G. Schwarz, data cited by M. Eigen and L. De Maeyer in "Technique of Organic Chemistry," Vol. VIII, Part II, 2nd ed, Interscience Publishers, Inc., New York, N. Y., 1963, p 1035.

(8) L. Pauling, "Nature of the Chemical Bond," 3rd ed, Cornell University Press, Ithaca, N. Y., 1960, pp 464, 473.

(9) H. S. Frank, *J. Chem. Phys.*, **13**, 493 (1945); H. S. Frank and M. W. Evans, *ibid.*, **13**, 507 (1945).

(10) On the basis of data in methanol at −80°[11] and in water at 25° (ref 5) it is fairly certain that reaction 2 does not involve more than one molecule of methanol.

(11) E. Grunwald, unpublished research.

$$(CH_3)_3NH^+ + \underset{\underset{CH_3}{|}}{OH} + N(CH_3)_3 \xrightarrow{k_2} (CH_3)_3N + \underset{\underset{CH_3}{|}}{HO} + HN(CH_3)_3^+ \quad (2)$$

derived from measurements of proton-exchange rates by the nuclear magnetic resonance (nmr) method. Measured were (1) R_{NH}, the rate of exchange of the NH protons of trimethylammonium ion, and (2) R_{OH}, the rate of exchange of the OH protons of methanol. These rates were derived from the CH_3 proton resonance spectra of solute and solvent, respectively, according to established methods.[6,12] Rate constants were derived from the rates by usual methods of kinetic analysis; equilibrium constants, K_A, were obtained, as described previously,[12] from the rates R_{OH} in buffered solutions, analysis of which permits a direct determination of the hydrogen ion concentration in equilibrium with the given buffer ratio.

Results Based on R_{OH}. We report a kinetic analysis of data obtained at 25.0 and at −0.7° in buffered solutions containing both trimethylammonium ion (BH^+) and trimethylamine. The work at 25.0° involved 24 independently prepared solutions; that at −0.7 involved 26. The buffer ratio $[BH^+]/[B]$ ranged from 200 to 1, $[BH^+]$ ranged from 0.03 to 0.001 M, and [B] ranged from 0.003 to 1×10^{-4} M. The data at both temperatures conform to eq 3. In eq 3 and throughout this paper, quantities in brackets denote molar concentrations.

$$R_{OH} = k_{MeOH_2^+}[MeOH_2^+] + k_{MeO^-}[MeO^-] + k_2[BH^+][B] \quad (3)$$

The term $k_2[BH^+][B]$ can be assigned to reaction 2. Reaction 1 is too slow to contribute directly and measurably to R_{OH} under these conditions, but its effect can be felt indirectly through contributions to R_{OH} from kinetic terms proportional to the hydrogen ion and methoxide ion concentrations. To express the (unknown) hydrogen ion and methoxide ion concentrations in terms of the (known) buffer ratios, we shall use the Debye–Hückel theory[13] in the form of eq 4 to obtain the required activity coefficients. In eq 4, z is the

$$-\log y_z = \frac{1.826 \times 10^6 D^{-3/2} T^{-3/2} z^2 \sqrt{\mu}}{1 + 252 D^{-1/2} T^{-1/2} \sqrt{\mu}} \quad (4)$$

electric charge (+1, 0, −1) of the given solute, D is the dielectric constant, T the temperature, and μ the ionic strength. The numerical coefficient in the denominator is chosen so as to make the "distance of closest approach" of the ions 5 A. On this basis, thermodynamic expressions for K_A and for K_B of the conjugate base reduce to eq 5.

$$K_A = [B][MeOH_2^+]/[BH^+] \quad (5a)$$

$$K_B = K_{autoprotolysis}/K_A \quad (5b)$$

$$= [BH^+][MeO^-]y_+y_-/[B] \quad (5c)$$

Thus eq 3 can be rewritten in the form of eq 6, where $k = k_{MeOH_2^+}K_A$, $k^1 = k_{MeO^-}K_B$, and $y^2 = y_+y_-$.

$$R_{OH} = k[BH^+]/[B] + k^1y^{-2}[B]/[BH^+] + k_2[BH^+][B] \quad (6)$$

Equation 6 was actually fitted to the data, each experimental point being given a statistical weight in inverse proportion to the measure of its precision. Results are listed in Table I.

Table I: Kinetic and Equilibrium Constants for Proton Transfer in Methanol Solutions of Trimethylamine and Its Conjugate Acid

Constant[a]	Temperature 25.0°	Temperature −0.7°	$\Delta H°$ or E_{act}, kcal	Notes
k	10.5	1.2	...	*b*
k^1	1760	1370	...	*b*
k_2	3.25×10^8	2.06×10^8	2.9	*b*
$k_{MeOH_2^+}$	8.8×10^{10}	6.3×10^{10}	2.1	Ref 12
K_A	1.20×10^{-10}	1.9×10^{-11}	11.6	$k/k_{MeOH_2^+}$
$K_{autoprotolysis}$	1.15×10^{-17}	1.90×10^{-18}	11.3	Ref 14; *c*
K_B	0.96×10^{-7}	1.0×10^{-7}	−0.3	Eq 5b
k_{MeO^-}	1.84×10^{10}	1.4×10^{10}	2	k^1/K_B; *d*

[a] All constants are based on the second as the unit of time and the mole per liter as the unit of solute concentration. [b] Kinetic constants in eq 6. Standard errors are: k^1 and k_2, less than 10%; k, less than 10% at 25°, about 30% at −0.7°. [c] Data of ref 14 were converted to the c scale and are given as a function of temperature by the empirical equation, $\log K_{autoprotolysis} = (-2.03 - 3716/(T - 2.76 \times 10^{-5}T^2))$. [d] Reference 12 reports 1.85×10^{10} for k_{MeO^-} at 25°.

To derive K_A from k, we used the previously reported[12] values of $k_{MeOH_2^+}$; to derive K_B, we used K_A and values of $K_{autoprotolysis}$ based on the work of Koskikallio;[14] to derive k_{MeO^-}, we used K_B and k^1. The value for k_{MeO^-} obtained at 25° is directly com-

(12) E. Grunwald, C. F. Jumper, and S. Meiboom, *J. Am. Chem. Soc.*, **84**, 4664 (1962).

(13) H. S. Harned and B. B. Owen, "The Physical Chemistry of Electrolytic Solutions," Reinhold Publishing Corp., New York, N. Y., 1943.

(14) J. Koskikallio, *Suomen Kemistilehti*, **B30**, 111, 157 (1957).

Table II: Rates of NH Proton Exchange of Trimethylammonium Ion in Methanol

Temp, °C	[BHCl]	[HCl]	$R_{NH}/[BHCl]$	Constants in eq 7		k_2K_A (predicted)[a]	
				k_1	k_2K_A	$\mu = 0$	$\mu = 0.6$
25	0.530	0.0363	0.76	...	...	0.039	...
	0.555	0.216	0.46	0.40	0.025	...	0.026
50	0.514	0.0352	4.50	...	...	0.21	...
	0.538	0.209	2.54	2.1	0.16	...	0.14
0	0.11	0.51	(0.057)	0.056[b]	0.0006[b]	...	...
	0.11	0.51	0.011		(Proton–deuteron exchange)[c]		

[a] k_2K_A at zero ionic strength was calculated from the data in Table I. Variation with ionic strength was assumed to follow the relationship $\delta \log (k_2K_A) = B\delta\mu$. For B we used the value $B = -0.3$ obtained for reaction 2 in water.[6] [b] Obtained by extrapolation from the data at 25 and 50°, using the Arrhenius equation. [c] Results reported in ref 17 for $(CH_3)_3ND^+$ in HCl-containing CH_3OH.

Table III: Acid Dissociation of Trimethylammonium Ion in Methanol

Temp, °C	k_a,[a] $\mu = 0.6$	k_a,[b] $\mu = 0$	K_A,[c] M	k_{-a},[d] sec^{-1} M^{-1}	$P\sigma$,[e] A
50	2.1	4	4.7×10^{-10}	0.8×10^{10}	...
25	0.40	0.7	1.20×10^{-10}	0.6×10^{10}	1.5

[a] k_1, Table II. [b] $\delta \log k_a = -0.4\delta\mu$. [c] Table I. Value at 50° is calculated from data at lower temperatures. [d] $k_a\ (\mu = 0)/K_A$. [e] Equation 8. In methanol at 25°, $D_{MeOH_2^+} = 3.8 \times 10^{-5}$, $D_B \approx 1.5 \times 10^{-5}$ cm²/sec.

parable with the value 1.85×10^{10} sec^{-1} reported previously[12] on the basis of nmr kinetic data for benzoic acid–benzoate buffers in methanol at 25°. The agreement is very good.

Table I also lists values for ΔH° and E_{act} derived from the respective temperature coefficients between 25 and −0.7°. The accuracy of ΔH_A°, ΔH_B°, and of E_{act} for k_{MeO^-} is poor owing to the 30% standard error of k at −0.7°. However, the values obtained are plausible.

Results Based on R_{NH}. NH proton exchange of trimethylammonium ion in methanol was measured at 25 and at 50° in the presence of excess HCl. Results are listed in Table II. The rates are relatively slow under these conditions and, at 25°, are near the lower limit of rate measurability by the nmr method. Nevertheless, the data establish several points of interest.

(1) Reaction 2 is *not* the dominant reaction under these conditions: for a sixfold variation in $[BH^+]/[MeOH_2^+]$, $R_{NH}/[BH^+]$ changes by less than a factor of 2 at both temperatures. If reaction 2 had been dominant, $R_{NH}/[BH^+]$ would have been equal to $k_2K_A[BH^+]/[MeOH_2^+]$.

(2) If the values of $R_{NH}/[BH^+]$ are fitted to a mixed rate law, as in eq 7, the values inferred for k_2K_A are plausible on the basis of data listed in Table I. The

$$R_{NH}/[BH^+] = k_1 + k_2K_A[BH^+]/[MeOH_2^+] \quad (7)$$

results of this analysis are shown in Table II. The agreement between values of k_2K_A as calculated from $R_{NH}/[BH^+]$ and those based on Table I becomes almost exact if it is assumed that salt effects on k_2K_A are the same as in aqueous solution.[6]

(3) Values of k_1 are of the correct magnitude for a mechanism of proton exchange in which acid dissociation (eq 1) is the rate-determining step; that is, $k_1 = k_a$ and $k_1/K_A = k_{-a}$. Since K_A is small we would expect k_{-a} to be in the range of rate constants for diffusion-controlled reactions, as has in fact been found for the analogous reaction of trimethylamine with hydronium ion in water.[6] This interpretation of k_1 is tested in Table III. First, an attempt is made to correct k_1 to zero ionic strength by assuming that the salt effect is equal to the known salt effect on k_a for *p*-toluidinium ion in methanol.[15] The values of $k_1\ (\mu = 0)/K_A$ are then compared with predictions for a diffusion-controlled specific reaction rate based on eq 8,[16] in which D denotes the phenomenological diffusion coef-

(15) M. Cocivera, E. Grunwald, and C. F. Jumper, *J. Phys. Chem.*, 68, 3234 (1964).

(16) Equation 8 is a specialized version of the well-known Debye theory, P. Debye, *Trans. Electrochem. Soc.*, 82, 265 (1942); M. Eigen, *Z. Physik. Chem.* (Frankfurt), 1, 176 (1954).

Table IV: Comparison of Proton Transfer Data for Trimethylammonium Ion in Water and Methanol

(Symbol)[a]	Value at 25°		$\Delta H°$ or E_{act}, kcal	
	Water	Methanol	Water	Methanol
k_2, sec^{-1} M^{-1}	3.4×10^8	3.25×10^8	3.3 at 50°	2.9 at 12°
K_A	1.57×10^{-10}	1.20×10^{-10}	8.82 at 25°[b]	11.6 at 12°[b]
k_a, sec^{-1}	4.7	0.7	11.3 at 50°	13 at 38°
k_{-a}, sec^{-1} M^{-1}	3.0×10^{10}	0.6×10^{10}	1.4 at 50°	2 at 38°
$P\sigma$ for k_{-a}	3.2 A	1.5 A	...	...
k_H, sec^{-1} [c]	1.1×10^{10}	$(1.5 \pm 1.0) \times 10^{10}$	2.3 at 50°	...

[a] Symbols as defined in text. Data taken from Tables I–III and from ref 2 and 6. [b] $\Delta S° = -15.2$ gibbs in water at 25°; $\Delta S° = 6.5$ gibbs in methanol at 12°. [c] k_H is the rate constant for displacement of a solvent molecule from the HOH·B or $CH_3OH \cdot B$ hydrogen-bonded complex in the given solvent.

ficient, σ the encounter diameter, P the probability of reaction per encounter, and N_0 Avogadro's number. To

$$k_{-a} = 4\pi N_0 P\sigma(D_{MeOH_2^+} + D_B)/1000 \qquad (8)$$

obtain exact agreement between k_{-a} and k_1 $(\mu = 0)/K_A$, $P\sigma$ must be taken as 1.5 A, about half as large as the value obtained in a similar analysis in water,[6] and of reasonable magnitude. Furthermore, the formal activation energy of k_1 $(\mu = 0)/K_A$ is about 2 kcal—a reasonable value for a diffusion-controlled reaction in methanol. (The activation energies for viscous flow and for self-diffusion of methanol are also about 2 kcal.)

(4) Extrapolation of the data in Table II to 0° enables us to obtain a rough estimate of the deuterium kinetic isotope effect on $k_1 = k_a$ by comparison of our results for proton–proton exchange with a previously reported[17] result for proton–deuteron exchange. This comparison is made in the last two rows of Table II; the concentrations are those used in the previous work[17] and are such that reaction 2 is relatively negligible. $k_a^{BH^+}/k_a^{BD^+}$ is thus estimated to be about 5.[18]

Discussion

Data for various proton transfer reactions between trimethylammonium ion and water or methanol are compared in Table IV. The two solvents are remarkably similar with respect to most of the quantities tabulated. Of the small differences that do exist, there are two that appear to the author to reflect perhaps a difference in the hydrogen-bonded solvent structure.

(1) The reaction of the solvated hydrogen ion (lyonium ion) with trimethylamine is, according to all available evidence, diffusion controlled. Moreover, in water it has been shown that the reactive encounter complex must be formulated as $B \cdot (H_2O)_n \cdot HOH_2^+$, with $n \geq 1$ and probably $n = 1$.[19] In methanol, data exist for proton transfer involving triethylammonium ion[17,20] which can be analyzed in much the same way to show that the reactive encounter complex must be formulated as $B \cdot (HOCH_3)_n \cdot H_2OCH_3^+$, with $n \geq 1$ and probably $n = 1$.[17]

Let us suppose that $n = 1$ and that the hydrogen-bonded solvent aggregates are linear in methanol and tetrahedral in water. Then eq 9 shows that in water there are two sites (indicated by arrows) at which the addition of a proton will lead to reaction, whereas in methanol there is only one such site. Hence we predict that the parameter $P\sigma$ in eq 8 will be twice as great for reaction in water as for reaction in methanol. The actual values of $P\sigma$ are 3.2 A in water and 1.5 A in methanol, within experimental error of the predicted 2:1 ratio.

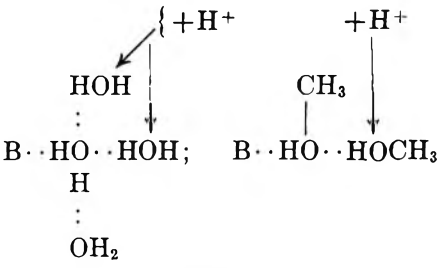

(9)

(2) The significant difference between $\Delta H°$ and $\Delta S°$ for acid dissociation in methanol and water could be attributed largely to the greater alignment of solvent molecules around the hydrogen ion in water than

(17) C. G. Swain, J. T. McKnight, and V. P. Kreiter, *J. Am. Chem. Soc.*, **79**, 1088 (1957).

(18) This estimate may be too high. Previous work for Me_3NH^+ in water[6] and for Et_3NH^+ in methanol[17] has shown that proton exchange due to reversible acid dissociation is not simply a first-order reaction but conforms to the rate law, $R/[BH^+] = k_a/(1 + Q[H^+])$. For Me_3NH^+ in methanol the kinetic constant Q is probably in the range $0.3 < Q < 1.0$. Thus, at 0.51 M HCl, $(1 + Q[H^+])$ can probably not be taken as unity but might be as large as 1.5, so that $k_a^{BH^+}/k_a^{BD^+}$ might be as small as 3.5.

(19) E. Grunwald and M. Cocivera, *Discussions Faraday Soc.*, **39**, 105 (1965).

(20) J. R. Schaefgen, M. S. Newman, and F. H. Verhoek, *J. Am. Chem. Soc.*, **66**, 1847 (1944).

in methanol. The alignment in water could be greater because of a three-dimensional rather than linear hydrogen-bonded aggregation of solvent molecules.

Experimental Section

Materials and Reaction Mixtures. Preparation of pure methanol, of NaOMe in methanol, and of anhydrous HCl in pure methanol followed previous practice.[12] The methanol was neutral by acid–base and nmr analysis. Trimethylammonium chloride was twice recrystallized from pure ethanol[21] and had a chloride equivalent weight of 95.6 (theory 95.6). Sodium chloride, added to some of the reaction mixtures to change the ionic strength, was of ACS reagent grade. Trimethylamine was prepared as a concentrated stock solution in methanol by adding $NaOCH_3$ in methanol to $(CH_3)_3NHCl$ in methanol and distilling in all-glass apparatus protected from the atmosphere by a Dry Ice cold trap.

Reaction mixtures containing the desired solutes and concentrations were prepared from these materials by standard quantitative methods. Samples of the reaction mixtures to be used for the measurement of R_{OH} were introduced into thoroughly clean nmr sample tubes, outgassed in two cycles of freezing (at liquid nitrogen temperature) and thawing, and then frozen and sealed under vacuum. Samples prepared in this way gave unchanging nmr spectra over a monitoring period of several months, thus showing that the solutions are stable. Some of the sample tubes were opened and their contents analyzed for amine. The titers were in every case within 2% of expectation, thus showing that the handling and outgassing does not change the composition of the solutions.[22] Reaction mixtures used in the measurement of R_{NH} were not outgassed.

The Nmr Facts. All measurements were made on Dr. S. Meiboom's nmr spectrometer at Bell Telephone Laboratories. The nmr techniques, temperature control, interpretation of nmr spectra, and calculation of proton exchange rates all followed previous practice[6,12] and need not be described again.

Proton chemical shifts, δ, of trimethylammonium ion and trimethylamine in methanol were found to be as follows: CH_3 protons of methanol, $\delta = 0.00$ ppm (internal standard); $(CH_3)_3N$ protons, 1.09 ppm at $-80°$; $(CH_3)_3NH^+$–methyl protons, 0.45 ppm at $-80°$, 0.38 ppm at 25°; NH protons, -6.8 ppm at 25 and at 50°. The $N^{14}H$ spin–spin interaction of trimethylammonium ion is well resolved at 50°; $J_{NH} = 51$ cps.

(21) E. Grunwald and E. Price, *J. Am. Chem. Soc.*, 86, 2970 (1964).

(22) The author is indebted to Dr. Elton Price for help with preparation of outgassed samples.

The Salting-Out Behavior of Amides and Its Relation to the Denaturation of Proteins by Salts[1]

by Eugene E. Schrier and Evelyn B. Schrier

Department of Chemistry, State University of New York at Binghamton, Binghamton, New York 13901
(Received April 11, 1966)

Salting-out parameters have been obtained by distribution measurements at 25° for the amides N-methyl acetamide and N-methyl propionamide in aqueous solutions of ten different salts. By considering these salting-out parameters to be summations of the corresponding quantities for the methyl, methylene, and amide groups, the contributions from these groups could be calculated for each salt from the experimental data. A test of the additivity of the group salting-out parameters was provided by comparing the amide group parameters with the same quantities calculated from literature data for a compound containing four amide linkages.[2] A model is described for the effect of electrolytes on the transition behavior of proteins. The process is assumed to be the resultant of two opposing effects: (1) the salting-in of amide groups which are exposed to the solvent as the protein unfolds and (2) the salting-out of the nonpolar portions of the molecule. The Flory equation for the effect of equilibrium binding of denaturant on the transition temperature of a protein is modified in the light of this hypothesis. The group salting-out parameters are used together with this equation to calculate the transition temperatures of two proteins, ribonuclease and ichthyocol gelatin, in aqueous salt solutions. The calculated values are generally in agreement with the corresponding experimental quantities.

Introduction

Much attention has been given recently to the effect of electrolytes on the stability of proteins and synthetic polypeptides in solution. Electrolytes modify the character of the thermal transition of proteins in aqueous solution, changing the midpoint temperature, T_m, in a fashion which is dependent on the nature and concentration of added electrolyte. Experimental observations of the salt effects in the isoelectric region have centered upon the globular protein, ribonuclease,[3,4] and various fibrous proteins.[5-7]

The early work of Bello, *et al.*,[5] pointed to the interaction of ions with the peptide groups of gelatin as the mechanism by which salts influence the melting temperature. A different interpretation was proposed by von Hippel and Wong[7] in their investigation of salt effects on various gelatins. According to their view, changes in the degree of ordering of water produced by the addition of salt may affect the extent of nonpolar interaction in a protein, thereby influencing the transition temperature. However, Mandelkern and Stewart[8] (see also Bello[9]) have shown that the experimental results of von Hippel and Wong[7] are consistent with an equation derived by Flory[10] for the change in transition temperature produced by equi-

(1) Presented in part at the 151st National Meeting of the American Chemical Society, Pittsburgh, Pa., March 1966.

(2) D. R. Robinson and W. P. Jencks, *J. Am. Chem. Soc.*, **87**, 2470 (1965).

(3) (a) W. G. Harrington and J. A. Schellman, *Compt. Rend. Trav. Lab. Carlsberg*, **30**, 167 (1957); (b) L. Mandelkern and D. E. Roberts, *J. Am. Chem. Soc.*, **83**, 4292 (1961).

(4) P. H. von Hippel and K-y. Wong, *Science*, **145**, 577 (1964); *J. Biol. Chem.*, **240**, 3909 (1965).

(5) J. Bello, H. Riese, and J. R. Vinograd, *J. Phys. Chem.*, **60**, 1299 (1956); J. Bello, *Biochem. Biophys. Acta*, **109**, 250 (1965).

(6) L. Mandelkern, W. T. Meyer, and A. F. Diorio, *J. Phys. Chem.*, **66**, 375 (1962); L. Mandelkern, J. C. Halpin, A. F. Diorio, and A. S. Posner, *J. Am. Chem. Soc.*, **84**, 1383 (1962).

(7) P. H. von Hippel and K-y. Wong, *Biochemistry*, **1**, 664 (1962).

(8) L. Mandelkern and W. E. Stewart, *ibid.*, **3**, 1135 (1964).

(9) J. Bello, *ibid.*, **2**, 276 (1963).

(10) P. Flory, *J. Cellular Comp. Physiol.*, **49**, 175 (1957).

librium binding of a denaturant to groups which are exposed to the solvent as the protein unfolds.

Evidence for direct binding of ions to peptide groups has been presented recently by Kurtz and Harrington[11] and by Bello, Haas, and Bello.[12] Kurtz and Harrington prepared LiBr complexes of several synthetic polypeptides by acetone precipitation of the complex from very concentrated (10 *M*) aqueous LiBr–polymer solutions. Bello, *et al.*,[12] have presented crystal structures for various amide–salt complexes prepared from solutions of low water content.

While this evidence is rather convincing regarding the equilibrium binding of ions to amide groups in solutions of high ion concentration and low water content, it is not clear whether such binding persists at lower salt concentrations. A further difficulty is the unusual specificity of binding constants, calculated from transition temperature data at 1 *M* salt concentrations, with respect to ion type. An approach to these problems is suggested by the observations of Bello, *et al.*,[5] and of von Hippel and Wong[4,7] that the order of effectiveness of salts in changing the transition temperature of proteins follows the classical Hofmeister behavior.[13] Robinson and Jencks[2] studied the effect of electrolytes on the solubility of a model tetrapeptide, acetyltetraglycine ethyl ester (ATGEE). The behavior of ATGEE in the presence of salts closely parallels the order of salt effects observed for protein transitions. Robinson and Jencks suggested that their results were interpretable as the summation of two effects, an ordinary salting-out effect such as might occur with nonpolar nonelectrolytes and a direct interaction between certain of the anions studied and the amide dipole. Equilibrium constants for the binding of an anion to a single site of the tetrapeptide were calculated for the salts which decreased the activity coefficient of ATGEE.

We report here a study of the salt effects on the distribution behavior of the monoamides, N-methyl propionamide (NMP) and N-methyl acetamide (NMA). The salting-out parameters derived from these data differ significantly from those obtained by Robinson and Jencks[2] for ATGEE. A model is proposed to interpret the data for the amides which is based on the variations of the activity coefficients of (1) the amide group and (2) the alkyl chains with electrolyte concentration. Empirical parameters for these interactions are calculated from the experimentally determined salting-out constants. A modification of the Flory equation[10] is derived which is applicable to changes in protein configuration produced by salt effects on certain constituent groups of the protein. Finally, use of this equation together with the empirical parameters gives results in agreement with experimentally observed changes in T_m produced by added electrolyte.

Experimental Section

Materials. Eastman White Label N-methylacetamide and N-methylpropionamide were used as received. A sample of NMA, fractionally distilled, gave the same results as the unpurified material. Ribonuclease-A was purchased from the Sigma Chemical Co. (Type XIIa). The salts employed were reagent grade or other good quality material and were used without further purification.

Distribution Measurements. Distribution experiments were carried out using ethanol-free chloroform as the reference phase. Aqueous solutions of the amide under study were equilibrated with chloroform for 3 days in a water bath maintained at 25.0 ± 0.05°. Separate experiments were used to determine the time necessary to reach equilibrium.

After the phases were sampled, analysis for amide was carried out by modification of a procedure suggested by Davies and Hallam.[14] An aliquot of the amide solution (usually 5 or 10 ml) was placed in a 500-ml Kjeldahl flask and 25 ml of 25 wt % NaOH were added. Methyl amine was distilled from the mixture over a period of 30 min and was collected in a 25-ml portion of standard 0.1 *M* HCl. Back-titration of the remaining HCl was performed with standard 0.1 *M* NaOH using the mixed methyl red–bromocresol green indicator recommended by Ma and Zuazaga.[15] Because the presence of chloroform led to erratic results in the analysis of the organic phase, we found it necessary to extract the amide in this phase back into water before analysis. Similar procedures were employed for the salt solutions. Salt concentrations were usually between 0.5 and 2 *M*. Duplicate determinations of the distribution ratio were made at each salt concentration. Salt concentrations for the halides and thiocyanates in the equilibrated aqueous phases were obtained by titration with standard $AgNO_3$ using sodium dichlorofluorceinate as the indicator. Final concentrations of salt in the Na_2SO_4–amide solutions were calculated from the molarity of the stock solutions. The solubility of each of the salts employed in this study in

(11) J. Kurtz and W. F. Harrington, *J. Mol. Biol.*, 17, 440 (1966).

(12) J. Bello, D. Haas, and H. R. Bello, *Biochemistry*, 5, 2539 (1966).

(13) F. A. Long and W. G. McDevit, *Chem. Rev.*, 51, 119 (1952).

(14) M. Davies and H. E. Hallam, *Trans. Faraday Soc.*, 47, 1170 (1951).

(15) T. S. Ma and G. Zuazaga, *Ind. Eng. Chem., Anal. Ed.*, 14, 280 (1942).

water-saturated chloroform was found to be undetectable using a gravimetric method which would have been sensitive to between 0.001 and 0.005 M salt concentration.

Since the solubility of NMA is low in chloroform, a fairly high concentration of amide (*ca.* 0.7 M) was employed in the distribution experiments. Lower concentrations of NMP, usually less than 0.4 M, were used. Separate experiments, using various concentrations of amide at fixed salt concentrations, were carried out to determine the dependence of the salting-out parameters on amide concentration.

Ultraviolet Difference Spectral Measurements. The effect of salts on the transition temperature of ribonuclease was investigated using ultraviolet difference spectra. The procedure has been described before.[16] Improved temperature measurement was provided by inserting a thermistor probe directly into the spectrophotometer cell above the light beam. The output was displayed on an Atkins Model 3F01A thermistor bridge, readable to ±0.1°. Salt solutions, made up on molarity basis, were added directly to preweighed samples of ribonuclease and buffer salts. The buffer used was 0.01 M mixed Na_2HPO_4–KH_2PO_4 and 0.12 M KCl. The apparent pH values of the solutions were measured using a Radiometer pHM 4 pH meter.

Difference spectra were usually obtained for salt concentrations near 0.5 and 1.0 M. Only one concentration of NaI, 0.6 M, was used on account of spectral interferences from the iodide ion.

Results

Distribution Experiments. Distribution ratios for the partition of the amides between chloroform and water were obtained in the concentration range 0.07–0.8 M amide in the equilibrated aqueous phase for NMP and from 0.37 to 0.76 M for NMA. The distribution ratio for NMA was found to be independent of concentration in the range investigated. The average value obtained was $K_D = (C_{NMA})_{org}/(C_{NMA})_{aq} = 0.0747 \pm 0.004$ where the error quoted is the standard deviation of the mean of twelve determinations at the various amide concentrations. The average value of the distribution ratio for NMP was 0.300 in the range 0.07–0.25 M NMP. The value rose to 0.367 at 0.78 M aqueous phase amide concentration. Twenty-three determinations of the distribution ratio of NMP were made in all. A plot of aqueous phase NMP concentration *vs.* organic phase NMP concentration was employed for further calculations.

Distribution data for each of the amides in aqueous solutions of ten salts were used to obtain the ratio of the activity coefficients of the amides in the salt solutions to the activity coefficient in pure water. The treatment has been discussed by Long and McDevit.[13] The concentration of amide in water in one experiment and in a salt solution in another may be related to the desired activity coefficients by the equation

$$f_i^\circ c_i^\circ = f_i c_i = \frac{1}{K_D^T} f_i^R c_i^R \qquad (1)$$

Here, f_i°, f_i^R, and f_i are the molar activity coefficient of the amide in water, chloroform, and in the salt solution, respectively, the various c_i are the corresponding molar concentrations of amide, and K_D^T is the thermodynamic distribution constant. The amide concentration is the same in the reference phase in both experiments. Equation 1 reduces to

$$\frac{f_i}{f_i^\circ} = \frac{c_i^\circ}{c_i} \qquad (2)$$

The ratio of eq 2 may be expressed as a function of salt concentration[13] in the form

$$\log \frac{f_i}{f_i^\circ} = \log \frac{c_i^\circ}{c_i} = k_s c_s + k_i(c_i - c_i^\circ) \qquad (3)$$

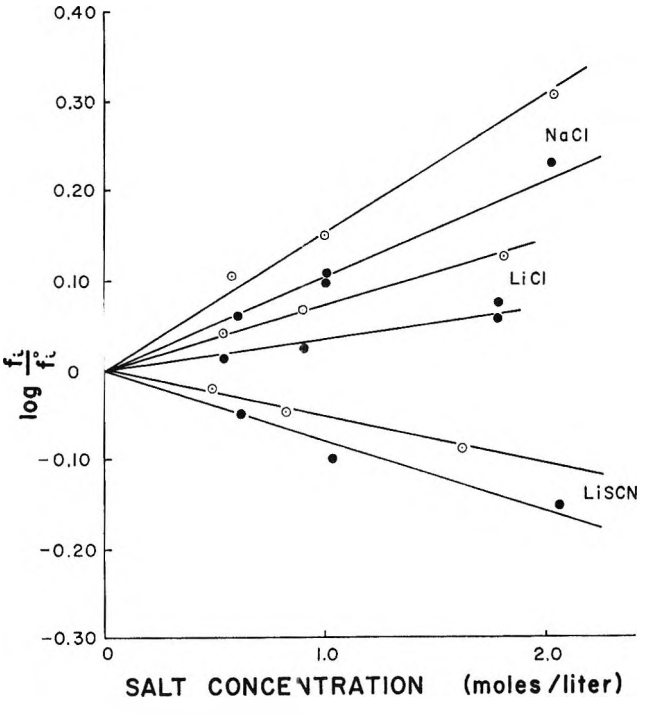

Figure 1. Variation of the activity coefficients of the amides ⊙, NMP and ●, NMA with salt concentration for NaCl, LiCl, and LiSCN.

(16) E. E. Schrier, R. T. Ingwall, and H. A. Scheraga, *J. Phys. Chem.*, 69, 289 (1965).

Table I: Salting-Out Parameters for Aqueous Amides at 25°

Salt	Salting-out parameter, k_s NMP	NMA	ATGEE[a]
Na_2SO_4	0.486 ± 0.003	0.372 ± 0.003	0.48
$CaCl_2$	0.166 ± 0.004	0.076 ± 0.002	−0.09
NaCl	0.164 ± 0.004	0.099 ± 0.003	0.046
NaBr	0.118 ± 0.003	0.065 ± 0.004	0.00
LiCl	0.077 ± 0.003	0.033 ± 0.002	0.021
$CaBr_2$	0.057 ± 0.002	0.000 ± 0.002	−(0.23–0.47)[b]
NaI	0.056 ± 0.002	0.018 ± 0.004	−0.23
LiBr	0.025 ± 0.003	−0.004 ± 0.002	−0.17
NaSCN	0.025 ± 0.002	−0.023 ± 0.002	−0.25
LiSCN	−0.052 ± 0.004	−0.082 ± 0.004	−0.30[b]

[a] Data of Robinson and Jencks. [b] Estimated from the data of Robinson and Jencks.

where c_s is the salt concentration in moles per liter and k_s and k_i are constants called the salting-out parameter and the self-interaction parameter, respectively. The self-interaction term of eq 3 was shown to be negligible by separate experiments with NMP in which the amide concentration was varied at fixed salt concentration for the salts NaI, Na_2SO_4, and LiSCN. Equation 3 can then be simplified to the expression

$$\log \frac{f_i}{f_i^\circ} = k_s c_s \qquad (4)$$

Values of the ratio c_i°/c_i were calculated for each salt–amide combination at each of the experimental points and were plotted as a function of salt concentration. The smoothed data were then used to calculate values of k_s. The constant, k_s, is numerically equal to the logarithm of the ratio of the activity coefficient of the nonelectrolyte in a 1 *M* salt solution to its value in water.

The variation of log (f_i/f_i°) with salt concentration for several of the salts studied is shown for NMP and NMA in Figure 1. Values of the salting-out parameters for the amides are given in Table I. The uncertainties noted are the standard deviations of the mean value of k_s. For comparison purposes, the data of Robinson and Jencks[2] for ATGEE in these salt solutions are also given. The values for ATGEE which are so noted are estimated assuming the additivity of ionic salting-out effects. In the case of $CaBr_2$, a range is given because of uncertainty in the choice of the ions used for estimation.

Salt Effects on the Transition Temperature of Ribonuclease. The results of the ultraviolet difference spectral measurements are given in Table II. The tabulated quantity, ΔT_m, is equal to $T_m - T_m^\circ$, where T_m and T_m° are the transition temperatures in the presence of added salt at 1 *M* concentration and in its absence. The estimated uncertainty in ΔT_m for this work is ±0.6°K/mole. The transition temperature of aqueous ribonuclease solutions (pH 6.80) in the absence of added salts was 61.2°. Apparent pH values for the ribonuclease solutions containing added salts varied between 6.03 and 6.79. Comparison of the data obtained here with that of von Hippel and Wong[4] indicates that the ultraviolet difference spectral method gives results in agreement with those obtained using optical rotation.

Table II: Changes in the Transition Temperature of Ribonuclease in 1 *M* Salt Solutions

Salt	ΔT_m, °K/mole of salt This work	von Hippel and Wong[7]
Na_2SO_4	13.3	
NaCl		1.3
LiCl	−0.1	0
NaBr		−1.9
LiBr	−4.5	−4.3
$CaCl_2$		−6.8
NaI	−8.3	
NaSCN	−14.6	−13.0
LiSCN	−18.5	
$CaBr_2$	−18.7	

Discussion

Salt–Amide Interactions. Reference to Table I reveals distinct differences between the salting-out parameters for monofunctional amides obtained in this study and the same quantities for ATGEE determined by Robinson and Jencks.[2] The salting-out parameters for NMA and NMP are almost always more positive than those for ATGEE.

As mentioned above, Robinson and Jencks con-

sidered the salt effects on ATGEE to be the summation of a salting-out effect on the molecule (perhaps describable by the internal pressure concept of McDevit and Long[17]) and the direct interaction of ions with the amide group. Binding constants calculated from their data did not include a correction for this salting-out effect. In addition, those salts which increased the activity coefficient of ATGEE could not be considered in their interpretation of the data because the salting-out effect and the ion–amide group interaction could not be explicitly separated.

In seeking a rationalization of the discrepancy between the values of the salting-out parameters for the monofunctional amides and ATGEE, consideration must be given to two features of the molecules involved: (1) the larger number of amide groups on the ATGEE molecule as opposed to the monoamides and (2) the larger proportion of nonpolar groups on the monoamides relative to ATGEE. The importance of factor 2 in determining the salting-out parameters for the monoamides is clearly seen in the consistently more positive values of the parameters for NMP as contrasted with the values for NMA.

Some additional data may prove useful. We note that the replacement of a nonpolar group on a molecule by a polar function often reduces the salting-out coefficient of the molecule. This generalization holds best for nonelectrolytes which are neither acidic nor basic in character. For example, the salting-out coefficients for propane[18] in 1 *M* NaCl, LiCl, and KI are, respectively, 0.21, 0.17, and 0.12 in the temperature range 15–25°, while for acetone[13] the salting-out coefficients for the same salts and temperature range are 0.11, 0.06, and 0.02. The decrease in the salting-out parameter in going from propane to acetone may be due to a more favorable interaction of the carbonyl group with the water–salt medium compared to the methylene group which it replaces.

A similar situation may prevail in the contrast between the salt effect data for the monoamides *vs.* those for ATGEE. We mentioned previously that the salting-out parameters for the monoamides are more positive than those for the tetrapeptide, ATGEE. Indeed, several of the salts which increase the solubility of ATGEE salt-out NMP and NMA. The example cited in the previous paragraph illustrates the possibility that the addition of polar groups to a nonpolar molecule can cause a diminution of the salting-out parameter. By extension of this argument, it is possible to conceive that the addition of polar groups to a molecule already containing them might decrease its salting-out constant still further and ultimately allow salting-in to take place.

In order to put these considerations into quantitative terms, we offer the following scheme. We assume that each functional group of the compounds considered makes an independent contribution to the salting-out parameter, k_s. Contributions are assumed to be made by the nonpolar groups as well as by the polar portions of the molecule. This assumption allows us to introduce a correction for salting-out of the molecule which was neglected in the treatment of Robinson and Jencks.[2] The correction is ascribed to the contribution of the alkyl groups to the salting-out parameter. The contribution of the alkyl groups might be expected to be positive by analogy to the behavior of nonpolar molecules in these salt solutions. On the other hand, if amide group contributions are negative, a transition from salting-out in the case of the monofunctional amides to salting-in where four amide groups are present in the molecule is possible. In other words, the variation of the activity coefficients of the amides with electrolyte concentration should be interpretable in terms of the additive effects of the constituent groups of the molecules.

The notion of additivity of functional group effects has been utilized in the past in other connections by many workers.[19,20] A treatment similar to that suggested here has been applied recently by Mukerjee[21] in the interpretation of salt effects on the critical micelle concentration of nonionic detergents. In reference to the theoretical treatment of salting-out of polar molecules, Conway[22] has pointed out that over-all dipole representations are inadequate. The discrete local molecular polarity of the nonelectrolyte as seen by the ion must be taken into account. These considerations apply well to the salt effects on the amides. Electrostatic theories of the Debye–Kirkwood type[13] would predict that the monoamides should be *salted-in* by all the salts considered in this study since the amides have dielectric constants much larger than that of water.

The assumed additivity scheme may be developed in the following way. For the compounds considered in the investigation, the salting-out parameters for each salt studied may be divided as follows: $k_s = 2k_{CH_3} + k_{CH_2} + k_A$ for NMP, while $k_s = 2k_{CH_3} + k_A$ for NMA. Here, k_s is the empirically determined

(17) W. G. McDevit and F. A. Long, *J. Am. Chem. Soc.*, **74**, 1773 (1952).

(18) T. J. Morrison and F. Billet, *J. Chem. Soc.*, 3819 (1952).

(19) E. J. Cohn and J. T. Edsall, "Proteins, Amino Acids, and Peptides," Reinhold Publishing Corp., New York, N. Y., 1943.

(20) C. Tanford, *J. Am. Chem. Soc.*, **84**, 4240 (1962).

(21) P. Mukerjee, *J. Phys. Chem.*, **69**, 4038 (1965).

(22) B. E. Conway, *Ann. Rev. Phys. Chem.*, **17**, 506 (1966).

salting-out parameter for a given salt while k_{CH_3}, k_{CH_2}, and k_A are contributions of the methyl, methylene, and amide groups to k_s. On the basis of these equations, k_{CH_2} is equal to the numerical difference between k_s for NMP and k_s for NMA. An evaluation of k_{CH_3} will then allow k_A to be determined.

The simplest assumption regarding k_{CH_3} is that it is equal to k_{CH_2}. However, there is theoretical justification for the effort to make a more refined hypothesis. McDevit and Long[17] have shown that the salting-out parameter for a nonpolar nonelectrolyte is directly proportional to the partial molar volume of the nonelectrolyte in the salt solution. Masterson[23] has determined the partial molar volumes for the lower alkanes in water. Using these data, it is possible to show that the salting-out parameters for the alkanes[18] are a linear function of their partial molar volumes. Values of $\bar{V}$ at 25° for ethane and propane may be interpolated from Masterson's data. These are 51 cc/mole for ethane and 66.9 cc/mole for propane. We assume that $\bar{V}_{C_2H_6} = 2\bar{V}_{CH_3}$ and $\bar{V}_{C_3H_8} = 2\bar{V}_{CH_3} + \bar{V}_{CH_2}$. Then, from the proportionality between salting-out parameter and partial molar volume mentioned above, we have

$$\frac{k_{CH_3}}{k_{CH_2}} = \frac{\bar{V}_{CH_3}}{\bar{V}_{CH_2}} = \frac{25.5}{15.9} = 1.6 \qquad (5)$$

and, from the values of k_{CH_2} previously determined, k_{CH_3} may be obtained. The amide salting-out parameter, k_A, is then calculated as $k_A = k_{NMA} - 2k_{CH_3}$. Table III gives the values of the salting-out parameters of these groups. The errors listed result from a combination of the standard deviation of the salting-out parameters of NMP and NMA given in Table I.

The trend of the values of k_{CH_2} is noteworthy. The regular change of k_{CH_2} with the nature of the ions is reminiscent of similar trends for nonpolar nonelectrolytes and is encouraging for that reason. In considering k_A, we can see that the values for the alkali halides are almost identical, while those for the calcium halides are nearly twice as large. The k_A values for the thiocyanates are larger than those for the 1:1 halides. This may be a reflection of the larger size of the thiocyanate ion and its anisotropic charge distribution relative to the halides. Finally, the value of k_A for sodium sulfate seems to be out of line with the others.

Table III: Group Salting-Out Parameters for the Methyl, Methylene, and Amide Groups at 25°

Salt	Group salting-out parameters		
	k_{CH_2}	k_{CH_3}	k_A
NaCl	0.065 ± 0.007	0.10 ± 0.01	−0.11 ± 0.03
NaBr	0.053 ± 0.007	0.085 ± 0.011	−0.11 ± 0.03
NaI	0.038 ± 0.006	0.061 ± 0.010	−0.10 ± 0.02
LiCl	0.044 ± 0.005	0.070 ± 0.008	−0.11 ± 0.02
LiBr	0.029 ± 0.005	0.046 ± 0.008	−0.096 ± 0.02
$CaCl_2$	0.090 ± 0.006	0.14 ± 0.01	−0.21 ± 0.02
$CaBr_2$	0.057 ± 0.004	0.091 ± 0.006	−0.18 ± 0.01
NaSCN	0.048 ± 0.004	0.077 ± 0.006	−0.18 ± 0.01
LiSCN	0.030 ± 0.008	0.048 ± 0.013	−0.18 ± 0.03
Na_2SO_4	0.114 ± 0.006	0.182 ± 0.010	0.008 ± 0.02

An approximate theoretical evaluation of the ion–amide group interaction parameter may be made by utilizing an electrostatic model for salt effects. The approach developed by Belton[24] for the salting-out of polar nonelectrolytes is suitable for this purpose. He modified the Debye–McAuley equation[13] for salt effects on nonelectrolytes by explicitly introducing a term expressing the effect of ion–permanent dipole interactions on the activity coefficient of a polar nonelectrolyte. An equation for the activity coefficient of a polar nonelectrolyte is given in his treatment as

$$\log f = n' \frac{4\pi\Sigma z_i^2 e^2}{2\epsilon_0^2 bkT}(\alpha_0 - \alpha_1) + n' \frac{4\pi b\Sigma z_i e}{\epsilon_0 kT}(\mu_0 - \mu_1) \qquad (6)$$

where n' is the number of ions per cubic centimeter; α_0, α_1 the distortion polarizability of solvent and solute, respectively; μ_0, μ_1 the permanent dipole moment of the solvent and solute, respectively; b an adjustable parameter which is related to the sum of the radii of the ions and the nonelectrolyte; ϵ_0 the dielectric constant of the pure solvent; $z_i e$ = the charge of the ion in electrostatic units; k the Boltzmann constant; and T the absolute temperature. We have used this equation to calculate k_A assuming that the dielectric constant of an amide molecule is largely the resultant of the contributions from the amide group. As a crude approximation, the Debye equation was used to calculate the distortion polarizabilities from the known dielectric constants and permanent dipole moments[25,26] of water and the amides. Using a value of b = 2.0 A, $\log f$, which is equal to k_A, was calculated to be −0.13 in a 1 M solution of the 1:1 electrolytes and was −0.20 for the calcium halides for the same salt concentration. The small value of b employed and the neglect of spe-

(23) W. L. Masterson, *J. Chem. Phys.*, **22**, 1830 (1954).

(24) J. W. Belton, *Trans. Faraday Soc.*, **33**, 653 (1937).

(25) C. P. Smyth, "Dielectric Behavior and Structure," McGraw-Hill Book Co., Inc., New York, N. Y., 1955, pp 86, 87.

(26) A. L. McClellan, "Tables of Experimental Dipole Moments," W. H. Freeman and Co., San Francisco, Calif., 1963, p 90.

Table IV: The Values of the Amide Group Salting-Out Parameter

Calculated from Data on ATGEE

Salt	k_{ATGEE}	k_{EtOAc}[a]	$4k_{CH_2}$[b]	k_A ATGEE	k_A This work
NaCl	0.046	0.19	0.26	−0.10	−0.11 ± 0.03
NaBr	0.00	0.12	0.21	−0.083	−0.11 ± 0.03
NaI	−0.23	0.02	0.15	−0.10	−0.10 ± 0.02
LiCl	0.021	0.15	0.18	−0.078	−0.11 ± 0.02
LiBr	−0.17	0.07	0.12	−0.090	−0.096 ± 0.02
$CaCl_2$	−0.09	0.26[c]	0.36	−0.18	−0.21 ± 0.02
$CaBr_2$	−(0.23–0.47)[c]	0.17[c]	0.23	−(0.16–0.21)	−0.18 ± 0.01
NaSCN	−0.25	0.02[c]	0.19	−0.12	−0.18 ± 0.01
LiSCN	−0.30[c]	−0.01[c]	0.12	−0.10	−0.18 ± 0.03
Na_2SO_4	0.48	0.60	0.46	−0.15	0.008 ± 0.02

[a] See ref 27–29. [b] Data from this work. [c] Estimated from various data[2,27–29] on the assumption of additivity of individual ion effects.

cific details of the structure of the solution in the model are significant limitations of the treatment. With these limitations in mind, the agreement of these calculated results with the experimental values for k_A allows us to suggest that the group parameters appear to have a reasonable order of magnitude.

A more exacting test of the validity of the derived empirical parameters may be made by comparing the k_A values of this work with those obtained from the data of Robinson and Jencks.[2] If the assumption of additivity of group salting-out parameters is correct, then values of k_A should be calculable from the data on the salting-out of ATGEE from the following relation: $k_{ATGEE} = 4k_A + 4k_{CH_2} + k_{EtOAc}$ or $k_A = (k_{ATGEE} - 4k_{CH_2} - k_{EtOAc})/4$ where the last term represents the salting-out parameters for ethyl acetate which are available or were estimated from various sources in the literature.[27–29] Table IV indicates the various values used to calculate k_A from data on ATGEE. The values of k_A so obtained are given in the next-to-last column while k_A values obtained from the data of this investigation are included in the last column.

Comparison of the data in the last two columns indicates that the values of k_A for the first seven salts agree within the limits of error of this investigation and the probable limits in the data for ATGEE and ethyl acetate which were employed in the calculation. The limits of error on the salt parameters for these materials are generally unspecified, but they are assumed to be as large for ethyl acetate as the limits of the present results and somewhat larger for ATGEE. The salting-out parameters for ATGEE were regarded as approximate by Robinson and Jencks.[2] Since many of their plots of log activity coefficient of ATGEE *vs.* salt concentration were curved, there was some difficulty in establishing the values of the limiting slope necessary for the estimation of the salting-out parameter. This curvature is evident in the case of NaSCN and may account for a part of the discrepancy noted in the comparison of the k_A values for this salt in Table IV. It is worth noting that the value of the salting-out parameter of ATGEE in the presence of LiSCN is estimated from that reported for NaSCN. Therefore, if the possibility of some error in the NaSCN salting-out parameter for ATGEE is assumed, the similar discrepancy in the comparison of the k_A values for LiSCN cannot be regarded as an independent occurrence. In any event, it does not appear that the differences noted in Table IV between the values of k_A for the thiocyanates invalidate the basic assumptions made in the formulation of the additivity scheme because the magnitude of the k_A values is still approximately consistent with the data for the other salts.

The discrepancy in the k_A values for Na_2SO_4 deserves special attention, however. The value of k_A for sodium sulfate is calculated from the ATGEE data more consistently with k_A values for the other salts than from the monoamide salting-out parameters. The assumption $k_{CH_3} = 1.6\ k_{CH_2}$ may break down in this case. This is suggested by the fact that the ATGEE salt parameter can be treated to obtain k_A without making this assumption. Further work is necessary to clarify this point.

We may conclude from this comparison of the empirical parameters derived from the two sets of

(27) A. P. Altshuller and H. E. Everson, *J. Am. Chem. Soc.*, **75**, 4823 (1953).

(28) S. Glasstone, D. W. Dimond, and E. J. Jones, *J. Chem. Soc.*, 2935 (1926).

(29) J. C. Philip and A. Bramley, *ibid.*, 377 (1915).

data that the assumption of the additivity of group salting-out effects leads to a fairly consistent correlation of salt effects for the amides and electrolytes investigated. A very limited range of compounds has been considered, however. The generality of this approach can only be confirmed or denied by much more extensive investigation. With appropriate caution regarding the preceding development, we turn to its use in interpreting the effects of electrolytes on protein stability.

Electrolyte–Protein Interaction. A quantitative treatment of protein denaturation by electrolytes requires the availability of a theoretical expression relating the change of the transition temperature of proteins with salt concentration to electrolyte–protein interaction. Flory[10,30] has derived an equation relating the lowering of the transition temperature to the equilibrium binding of denaturant molecules or ions to groups on the protein which are exposed to the solvent when the protein molecule unfolds. These groups are considered to be buried and inaccessible to the solvent in the native protein. In addition to this equation which will be modified as described below, a hypothesis regarding the nature of electrolyte–protein interactions is necessary.

As indicated in the Introduction, there are grounds for believing that interaction of ions with the amide groups of the protein which are exposed during the transition is responsible for lowering the transition temperature. It seems reasonable to assume as well that effects on the nonpolar groups of a protein play some part in the over-all transition temperature changes produced by salts. Mention has been made of this possibility by other workers.[2,7]

The clustering of nonpolar side chains in regions away from contact with solvent in a native protein is considered[20] to be an important influence in stabilizing protein configuration. Although there is little experimental evidence pertaining to the number and extent of nonpolar regions in the native as opposed to the denatured state of a protein, the general interpretation of changes in physical properties upon denaturation suggests that they are more numerous in the native state. If salts are added to an aqueous solution of a protein, the already unfavorable positive free energy of transfer of the nonpolar groups from the hydrocarbon-like interior of the protein to water should be increased. This is analogous to the decreased solubility of a hydrocarbon in a salt solution relative to its solubility in water. The positive free energy of transfer of a nonpolar group from water to a salt solution is related to the salting-out parameter for that group. A salting-out effect on the nonpolar groups of a protein should raise its transition temperature to the extent that buried nonpolar groups are more prevalent in the native than in the denatured state.

We therefore regard the transition temperature changes produced by salts to be the resultant of the summation of the interaction of salts with (1) the peptide and (2) the nonpolar groups on the unfolded protein which are inaccessible to the solvent in the native state. Charged groups or the uncharged polar groups of side chains which are exposed to the solvent in both the native and denatured states have been assumed[31] not to contribute significantly to the free energy of unfolding. We will assume in the derivation to follow that essentially all the peptide and nonpolar groups of the protein are inaccessible to the solvent in the native state. This is a fairly good assumption for the nonpolar groups but probably tends to overestimate the number of buried peptide groups. This overestimate will be compensated to some extent by salt effects on the small number of polar side chains which are not exposed to solvent in the native state, *e.g.*, the buried tyrosines of ribonuclease. With these assumptions, it is possible to conceive of the protein as having all groups of interest "inside," *i.e.*, not exposed to the solvent in the native state. The driving force for the change of the transition temperature with added salt then comes from the transfer of these buried groups which are exposed to solvent in the unfolding process from water to the salt solution.

In order to formulate this model in terms suitable for quantitative evaluation, we modify the Flory[10] treatment as follows. An equation[10,30] relating the change in transition temperature of a protein with added salt to changes in the chemical potential of the repeat unit (the amide group and "average" side chain[32]) may be written for a protein solution at fixed concentration as

$$\Delta H_r\left[\frac{T_m - T_m^\circ}{T_m^\circ}\right] = \mu_r - \mu_r^\circ \qquad (7)$$

where ΔH_r is the enthalpy change of unfolding per repeat unit, T_m, T_m° the transition temperatures of the protein in the presence and absence of added salt, respectively, and μ_r, μ_r° the chemical potentials of the repeat unit in the presence and absence of salt. We

(30) L. Mandelkern, "Crystallization of Polymers," McGraw-Hill Book Co., Inc., New York, N. Y., 1964, pp 69–71.

(31) C. Tanford, *J. Am. Chem. Soc.*, **86**, 2050 (1964).

(32) This differs from the usual definition of repeat unit in that it includes the "average" side chain. An "average" side chain is considered to be made up of the total of the –CH, $-CH_2$, and CH_3 groups contained in alkyl and aromatic side chains in a protein divided by its number of amino acid residues. The inclusion of the side chains in the definition is necessary for what follows.

now consider the change in free energy brought about by the transfer of the repeat unit from the aqueous environment to the salt solution. If the concentration of the repeat unit is the same in the salt solution as it is in water, then the free energy change for the transfer of n_r moles of repeat unit from water to the salt solution is given by

$$\Delta F = n_r RT \ln \frac{f_r}{f_r^\circ} \tag{8}$$

The total number of repeat units in the protein may be denoted by $(n_r)_T$. Then, the change of chemical potential per repeat unit is given by

$$\frac{\Delta F}{(n_r)_T} = \mu_r - \mu_r^\circ = \frac{n_r}{(n_r)_T} RT \ln \frac{f_r}{f_r^\circ} = N_r RT \ln \frac{f_r}{f_r^\circ} \tag{9}$$

where N_r is the mole fraction of repeat units which interact with the solvent in the denatured state. The mole fraction, N_r, will have a value equal to 1 if all the repeat units are exposed to the solvent in the unfolded protein, but it will be less than 1 if some remain buried.

The assumption is now made that the behavior of the amide and nonpolar groups on the protein in the presence of salts can be estimated from salting-out data for model amides. We substitute for $\ln (f_r/f_r^\circ)$ by using eq 4 above and obtain

$$\mu_r - \mu_r^\circ = N_r RT k_r c_s \tag{10}$$

where k_r is the salting-out parameter for the repeat unit and c_s is salt concentration. Substituting eq 10 into eq 7 and assuming that T_m is approximately equal to T_m° to obtain the $(T_m^\circ)^2$ term we have

$$T_m - T_m^\circ = \frac{R(T_m^\circ)^2}{\Delta H_r} N_r k_r c_s \tag{11}$$

If the assumption is made that the empirical salting-out parameter of the repeat unit can be divided into group salting-out parameters as above, this equation can be written as

$$T_m - T_m^\circ = \frac{R(T_m^\circ)^2}{\Delta H_r} c_s \Sigma N_i k_i \tag{12}$$

where the summation is over all the interactions of various groups in the repeat unit. This assumption carries with it the implication that the N_i values be considered as independent mole fractions signifying the extent to which the various functional groups of the buried repeat unit interact with the solvent in the unfolded protein. For a given repeat unit of the unfolded protein, it is quite possible that the peptide group will be in contact with the solvent while the side chain will cluster with those of other repeat units, minimizing contact with the solvent.

Equations 11 and 12 are analogous to that developed by Flory[10] to account for lowering of the transition temperature of a protein due to binding of a denaturant to a repeat unit. However, applications of the Flory equation[8] have required further approximations in order to obtain a fit with the experimental results. For example, in the case of salt solutions where T_m depends linearly on salt concentration, it has been assumed[8] that salt activities are equal to concentrations. The dependence of T_m on salt concentration is given without this assumption in the equation derived here.

Equation 12 may be tested against experimentally determined transition temperature changes for ribonuclease and ichthyocol gelatin. As assumed above, we consider only the interaction of peptide and nonpolar groups with salts. Equation 12 takes the form

$$T_m - T_m^\circ = \frac{R(T_m^\circ)^2}{\Delta H_r} c_s (N_A k_A + N_{H\phi} k_{H\phi}) \tag{13}$$

where the subscripts A and Hϕ are used to denote salt–amide group interactions and interaction between salt and nonpolar groups, respectively. The values of k_A may be obtained from Table III. The mole fraction of amide groups in contact with the solvent at the transition temperature is taken as unity for ribonuclease. Schildkraut and Scheraga[33] have demonstrated that all exchangeable hydrogens of ribonuclease are replaced by deuterium at the transition temperature. This suggests the accessibility of all peptide groups to solvent in the unfolded molecule. A value of $N_A = 1$ has been assumed previously for ichthyocol gelatin.[8] To simplify our calculation, we take $k_{H\phi} = k_{CH_2}$. This assumes that the nonpolar groups may be treated as methyl groups instead of complete side chains. If we wished to consider complete (average) side chains, the values of k_{CH_2} for each salt would be multiplied, for a given protein, by the same numerical factor. Since the extent of burial of nonpolar groups in the denatured form of the proteins considered is unknown, $N_{H\phi}$ must be treated as an adjustable parameter. For a given protein, it will have the same value for all salts considered. If we define $N_{H\phi} = N_{CH_2}$, the numerical factor mentioned above will be included in the value of this mole fraction and the value of N_{CH_2} will be larger than if the nonpolar groups were counted as complete side chains. The adjustable parameter,

(33) C. L. Schildkraut and H. A. Scheraga, *J. Am. Chem. Soc.*, **82**, 58 (1960).

N_{CH_3}, is, therefore, the mole fraction of nonpolar side chains counted as methyls which are exposed to the solvent when the protein is in its unfolded state. The values of N_{CH_3} which gave the best fit to the experimental transition temperature data were 1.1 for ribonuclease and 0.8 for ichthyocol gelatin. The enthalpy of unfolding per repeat unit has been previously taken to be 2000 cal/mole for ichthyocol gelatin[9] and 1500 cal/mole for ribonuclease[16] while $T_m°$ is 334.4°K for ribonuclease and 293.4°K for ichthyocol gelatin. The transition temperature changes calculated using eq 13 with the values of K_A and k_{CH_3} given in Table III and the parameters specified above are shown in Table V. They are compared with the experimental values given in Table II for ribonuclease. The experimental ΔT_m values for ichthyocol gelatin are taken from the data of von Hippel and Wong.[7] It should be pointed out that the calculated transition temperature changes are obtained from the difference between numbers having fairly large uncertainties. With this limitation in mind, we can view the generally good agreement between the experimental and calculated transition temperatures in Table V as suggesting the involvement of both ion–amide and ion–nonpolar group interactions in salt effects on protein transitions. This is pointed out in a specific instance by examining the effect of NaCl on the two proteins. While ΔT_m is positive for ribonuclease in 1 M NaCl, it is negative for ichthyocol gelatin with the same salt. A model omitting salt effects on the nonpolar groups, for instance, might not account for the variation of the sign of ΔT_m in this case, but the model proposed here predicts both the sign and approximate magnitude of the values.

The very poor agreement between the calculated and experimental values for the effects of Na_2SO_4 on ribonuclease should be mentioned. This discrepancy is not unexpected in the light of the comparison of the values of k_A mentioned in the previous section. If the value of k_A obtained for the ATGEE data is used for Na_2SO_4, the calculated ΔT_m is 8.3°K/mole of salt which is more in line with the experimental quantity.

One further question arises. The values of k_{CH_3} and k_A which are used here were derived at 25° while they are applied to calculate thermal transition changes at other temperatures. There is good agreement between the experimental and calculated ΔT_m values in cases in which the thermal transition occurs above and below 25° (ribonuclease and ichthyocol gelatin, respectively). Therefore, we may suppose that changes in the k_{CH_3} and k_A values with temperature are either small or, if large, cancel in such a way as to leave the resulting ΔT_m unaffected. There is sufficient data to calculate the effect of temperature on k_{CH_3} and k_A in only one case, for NaI. Robinson and Jencks[2] determined the temperature dependence of the salting-out parameter for ATGEE in sodium iodide solutions. Using these data, together with the temperature coefficients of the salting out parameter for the alkyl groups derived from data given by Long and McDevit,[18] it is possible to calculate k_{CH_3} and k_A at 55°. These values are 0.028 and −0.060, respectively. Even though there is a considerable change in these parameters from their values at 25°, ΔT_m for NaI using the 55° parameters turns out to be −4.4°/mole of NaI *vs.* −5.5°/mole of NaI as calculated using the 25° values. The parameters k_A and k_{CH_3} evaluated at 25° appear to give a useful measure of the transition temperature changes produced by salts at other temperatures.

Table V: Transition Temperature Changes for Ribonuclease and Ichthyocol Gelatin in 1 M Salt Solutions

Ribonuclease

Salt	ΔT_m, °K/mole of salt: Experimental[a]	Calculated[b]
Na_2SO_4	+13.3	+30.8
NaCl	(+1.3)	+0.8
LiCl	+0.1, (0)	−4.5
NaBr	(−1.9)	−1.6
LiBr	−4.5, (−4.3)	−6.7
$CaCl_2$	(−6.8)	−8.0
NaI	−8.3	−5.5
NaSCN	−14.6, (−13.0)	−13.6
LiSCN	−18.5	−18.5
$CaBr_2$	−18.7	−12.1

Ichthyocol Gelatin

Salt	ΔT_m, °K/mole of salt: Experimental[b]	Calculated[c]
NaCl	(−1.6)	−1.8
LiCl	(−4.1)	−4.3
$CaCl_2$	(−8.8)	−8.3
NaSCN	(−10.2)	−9.8

[a] Experimental values in parentheses are the data of von Hippel and Wong.[4,7] [b] Parameters used in eq 13, N_{CH_3} = 1.1, N_A = 1, ΔH_R = 1500 cal/mole, and $T_m°$ = 334.4°K. [c] Parameters used in eq 13, N_{CH_3} = 0.8, N_A = 1, ΔH_R = 2000 cal/mole, and $T_m°$ = 293.4°K.

Acknowledgments. This investigation was supported in part by Public Health Service Research Grant GM-11762 from the Institute of General Medical Sciences. The technical assistance of Mr. Richard Mandel and Mrs. Lois Mackey is gratefully acknowledged. The receipt of preprints in advance of publication from Drs. Jencks and von Hippel and useful discussions and correspondence with them are appreciated.

Theory of Polymeric Dispersants. Statistics of Constrained Polymer Chains

by D. J. Meier

Shell Development Company, Emeryville, California *(Received October 11, 1966)*

A theory is developed for the mutual repulsion of surfaces containing adsorbed polymeric chains. It is assumed that the repulsion is due to (1) the loss of possible chain configurations as the volume available to a chain is reduced between approaching surfaces and (2) the possible change in the free energy of mixing of polymer and solvent as the density of chain segments changes. Both effects are evaluated for a model system in which the polymeric chains are adsorbed by one of their end segments onto planar surfaces. Of the two factors responsible for repulsion, it is concluded that the loss of possible chain configurations due to volume constraints is the more important for sparse surface coverage, while that due to the free energy of mixing is of at least equal importance for extensively covered surfaces in the presence of "good" solvents for the polymer. The theory can be used to predict the effect of molecular weight, solvent type, quantity of adsorbed polymer required, etc.

Introduction

Stable dispersions of particulate matter can often be prepared by adsorption of long-chain molecules. For molecules that are ionizable in polar solvents, it has long been recognized[1] that ionic repulsion provides a key mechanism for dispersion stability. However, in nonpolar media and with nonionic molecules, it is unlikely that ionic effects are important; other mechanisms giving rise to repulsive forces between particles containing adsorbed molecules must be sought. Mackor[2] and Mackor and van der Waals[3] have pointed out that sizeable repulsive forces result from the loss in configurational entropy occurring when chain molecules adsorbed on neighboring particles begin to overlap. By use of a quasi-lattice model, these authors were able to evaluate the configurational entropy of interacting, adsorbed, rodlike molecules and were able to show that the resulting loss in configurational entropy of interacting molecules was sufficiently great to overcome the attractive van der Waals–London forces between particles; *i.e.*, a stable dispersion would result. The basic idea of these authors, *i.e.*, that repulsive forces are generated by configurational changes of adsorbed molecules, will form the basis for this paper. However, the approach and the nature of the system to be treated will be markedly different. The statistical methods used by Mackor and van der Waals[3] limited the type of molecule that could be treated to short, rigid rods. We shall adopt an alternative model in assuming that the adsorbed molecules are sufficiently long and flexible that the chains obey random-flight statistics. In thus restricting the present treatment to long-chain flexible molecules, we shall be able to apply the powerful method of obtaining solutions to the diffusion equation with appropriate boundary conditions[4,5] to evaluate the configurational statistics of adsorbed chains and hence to evaluate configurational free energies.

Model

Since the method to be followed in this paper will be based on obtaining analytical solutions of the diffusion equation

$$\frac{\partial W(\bar{r})}{\partial n} = \frac{l^2}{6}\nabla^2 W(\bar{r})$$

where $W(\bar{r})$ is the probability of end-to-end distance $\bar{r}$ of a chain of n elements of length l, we shall be forced

(1) E. J. W. Verwey and J. Th. G. Overbeek, "Theory of the Stability of Lyophobic Colloids," Elsevier Publishing Co., Amsterdam, 1948.

(2) E. L. Mackor, *J. Colloid Sci.*, 6, 492 (1951).

(3) E. L. Mackor and J. H. van der Waals, *ibid.*, 7, 535 (1952).

(4) E. A. Di Marzio, *J. Chem. Phys.*, 42, 2101 (1965).

(5) S. Chandrasekhar, *Rev. Mod. Phys.*, 15, 1 (1943).

to use a somewhat simplified model of particulate matter with adsorbed chains in order to make the equation tractable. However, it is believed that the simplified model to be used is sufficiently realistic that it demonstrates the salient features of repulsion due to chain-configurational interactions. We shall assume in our model that the particulate matter has planar surfaces, on which chain molecules are adsorbed by one of the chain ends. The planar surfaces present physically impenetrable barriers to other chain segments contacting the surface and have zero interaction energy with segments away from the surface; *i.e.*, the potential at the surface is an infinitely high step function. The assumption that chains are adsorbed at one end of the chain implies, of course, that one end of a chain is unique (perhaps more polar, ionic, etc.). The present restriction to this type of polymer chain excludes the more common nonspecific type of polymer adsorption in which random segments are adsorbed leaving loops of segments[6] projecting into solution. In principle, the methods of the present treatment could be applied to this type of adsorption, but the additional complexities would be formidable.

We shall also assume that the adsorption is irreversible; *i.e.*, the increased free energy of constrained chains does not cause desorption.

Method

The change in the free energy of two planar surfaces having adsorbed chains thereon as the distance of separation is reduced from infinity to d can be divided into contributions from three sources: (1) $\Delta F_V(d)$ associated with the restriction of volume available to the chains, (2) $\Delta F_M(d)$ associated with the changing density of segments and the concomitant change in free energy of mixing of polymer and solvent, and (3) $\Delta F_A(d)$ associated with the attractive free energy of the surfaces, which will be taken as arising from a van der Waals–London type of interaction.

$\Delta F_V(d)$ (per unit area) is obtained from the Boltzmann relation

$$\Delta F_V(d) = -T\Delta S_V(d) = -2\eta kT \ln P_N(d)$$

where $P_N(d)$, in the present case, is the probability that all chain elements of a molecule are within a distance d of the surface on which the chain is adsorbed when the other surface is at infinity, and η is the number of molecules per unit area.

The change in the free energy of mixing $\Delta F_M(d)$ requires an evaluation of the number density $\rho_N(\bar{r})$ of segments between the planar surfaces. This is obtained by summing the probability $W_n(\bar{r})$ of end-to-end distance $\bar{r}$ of a subchain of n elements over the total number of elements N of the chain, *i.e.*

$$\rho_N(\bar{r}) = \sum_{n=1}^{N} W_n(\bar{r})$$

The Flory–Krigbaum[7] method is used with the number density to give the free energy of mixing of polymer and solvent as a function of surface separation.

Since the use of the diffusion equation implies random-flight statistics, we shall follow the lead of Flory[8] in treating the statistics of perturbed chains by use of the familiar isotropic chain expansion parameter α, which will allow for excluded-volume perturbations without changing the form of the equations describing chain statistics.

In the following treatment, f will be used to designate the free energy of a molecule or pair of molecules and F will refer to the free energy per unit area of surface.

Free Energy Change Due to Restricted Volume, $\Delta F_V(d)$. As surfaces containing adsorbed chains are brought closer together, the volume available to the chains necessarily decreases and, as a result, some otherwise possible chain configurations will be lost. The fraction of chain configurations remaining at a separation distance d is just equal to the probability $P_N(d)$ that all chain elements of an adsorbed chain are within a distance d of the surface when the other surface is at infinity. This probability may be determined from the diffusion equation in the following manner. We first obtain the conditional probability $W_N(x,r;x';0;d)\mathrm{d}V$ of finding the second end of a chain of N elements in the volume element $\mathrm{d}V$ at x,r (a cylindrical coordinate system is used) when the first end is at $x = x'$ and $r = 0$, an impenetrable reflective barrier is at $x = 0$, and an absorbing barrier is at $x = d$. The impenetrable barrier will correspond to the surface on which the chain is adsorbed ($x' \rightarrow 0$) while the absorbing barrier removes from the ensemble of configurations those for which any chain element has reached the barrier. The diffusion equation and the boundary conditions for this problem are

$$\frac{\partial W_N}{\partial N} = \frac{l^2}{6}\nabla^2 W_N \qquad (1)$$

$W_N(x = 0) = W_N(x = d) = 0$, where, for simplicity, W_N has been written for $W_N(x,r;\ x';\ 0;\ d)$. It must be noted that the mathematical boundary conditions

(6) C. A. J. Hoeve, E. A. Di Marzio, and P. Peyser, *J. Chem. Phys.*, **42**, 2558 (1965), and references to earlier work cited therein.

(7) P. J. Flory and W. R. Krigbaum, *ibid.*, **18**, 1086 (1950).

(8) P. J. Flory, "Principles of Polymer Chemistry," Cornell University Press, Ithaca, N. Y., 1953.

correspond to absorbing barriers at $x = 0$ and $x = d$, even though the physical surface at $x = 0$ corresponds to an impenetrable reflective surface. This curious feature of the mathematical boundary conditions to be used with the diffusion equation to generate chain statistics of adsorbed chains was apparently first pointed out by Di Marzio.[4]

$W_N(x,r; x'; 0; d)$ is easily obtained from eq 1 by the method of "images"[9] and is

$$W_N(x,r; x'; 0; d)\mathrm{d}V = K \exp(-3r^2/2Nl^2) \sum_{m=-\infty}^{+\infty} \times [\exp\{-3(2md + x' + x)^2/2Nl^2\} - \exp\{-3(2md - x' - x)^2/2Nl^2\}]\mathrm{d}V \quad (2)$$

where K is a normalization constant to be determined. Since we are interested in adsorbed polymers, we let $x' \to 0$ and obtain from eq 2

$$W_N(x,r; \underset{x'\to 0}{x'}; 0; d)\mathrm{d}V = 4K\left(\frac{3}{2Nl^2}\right) x' \exp\left(\frac{-3r^2}{2Nl^2}\right) \sum_{m=-\infty}^{+\infty} \times (x - 2md)[\exp\{-3(2md - x)^2/2Nl^2\}]\mathrm{d}V \quad (3)$$

If eq 3 is now normalized for $d = \infty$, the resulting equation will give the probability that all elements of a chain with ends at $x = 0$, $r = 0$ and $x = x$, $r = r$ are within a distance d of the surface. By integrating eq 3 over volume, we obtain

$$\underset{\substack{x'\to 0 \\ d\to\infty}}{K} = \left[\int_V W_N(x,r; x'; 0; d)\mathrm{d}V\right]^{-1} = \frac{1}{2\pi x'}\left(\frac{3}{2Nl^2}\right) \quad (4)$$

which with eq 3 gives

$$W_N(x,r; 0; 0; d)\mathrm{d}V = \frac{2}{\pi}\left(\frac{3}{2Nl^2}\right)^2 \exp\left(\frac{-3r^2}{2Nl^2}\right) \sum_{m=-\infty}^{+\infty} \times (x - 2md) \exp[-3(x - 2md)^2/2Nl^2]\mathrm{d}V \quad (5)$$

Finally, the required probability $P_N(d)$ that all chain segments are within a distance d of the surface on which the chain is adsorbed and the free end of the chain is anywhere with $x < d$ is obtained by integrating over the volume between the surfaces

$$P_N(d) = 2\pi \int_{r=0}^{\infty} \int_{x=0}^{d} r W_N(x,r; 0; 0; d)\mathrm{d}r\mathrm{d}x$$

which, with eq 5, gives

$$P_N(d) = \sum_{m=-\infty}^{+\infty} [\exp\{-6m^2d^2/Nl^2\} - \exp\{-3(2m - 1)^2d^2/2Nl^2\}] \quad (6)$$

From the Boltzmann relation, the free energy change per chain, $\Delta f_V(d)$, caused by restricting the volume available to a chain as the surfaces are brought together from infinite separation to separation d, becomes

$$\frac{\Delta f_V(d)}{kT} = -\ln \sum_{m=-\infty}^{+\infty} [\exp\{-6m^2d^2/Nl^2\} - \exp\{-3(2m - 1)^2d^2/2Nl^2\}] \quad (7)$$

Figure 1 shows $\Delta f_V(d)/kT$ as a function of the distance (in units of $d/(Nl^2)^{1/2}$) of separation of the surfaces. The repulsion due to volume constraints is seen to be quite large even at moderate distances of separation, *e.g.*, almost $5kT$ when the surface separation is half the root-mean-square end-to-end chain distance (of the free chain).

The repulsive free energy per unit area of surface $\Delta F_V(d)$ will be merely the product of $\Delta f_V(d)$ and the number of chains per unit area η on the two surfaces, *i.e.*

$$\Delta F_V(d) = 2\eta \Delta f_V(d) = -2\eta kT \ln P_N(d) \quad (8)$$

It is assumed, of course, that chains are adsorbed on both surfaces.

Free Energy Change of Mixing. As surfaces containing adsorbed polymer chains are brought together, the density of chain segments in the space between the surfaces increases. The increased density of segments increases the segment–segment interaction, and, depending on this interaction *vis-a-vis* the segment–solvent interaction, the free energy of the system may either increase or decrease. The method used by Flory and Krigbaum[7] to evaluate the change in the free energy of mixing is followed here.

In the model to be treated, it is assumed that molecules adsorbed on opposing surfaces are directly opposite one another but that the surface coverage is sparse enough that overlap between adjacent molecules on the same surface can be neglected. These seemingly incompatible assumptions considerably simplify the present calculations, and, as will be seen, necessary modifications can be made later.

Consider a jth molecule adsorbed on the planar surface $x = 0$ and a kth molecule adsorbed directly opposite on the surface $x = d$. The free energy of mixing $\mathrm{d}f_M$ of polymer segments from the jth and kth molecules with solvent in the volume element $\mathrm{d}V$ is[7]

$$\mathrm{d}f_M = \frac{kT\mathrm{d}V}{V_1}[\ln(1 - \rho_k V_S - \rho_j V_S) + \chi_1 V_S(\rho_k + \rho_j)](1 - \rho_k V_S - \rho_j V_S) \quad (9)$$

(9) H. S. Carslaw and J. C. Jaeger, "Conduction of Heat in Solids," Clarendon Press, Oxford, England 1959.

where V_1 is the solvent molecular volume, V_S is the segment volume, ρ_j and ρ_k are (number) densities of segments from chains on the jth and kth surfaces, respectively, and χ_1 is a solvent–polymer interaction parameter. The free energy of mixing (per pair of molecules on opposing surfaces) is obtained by integrating eq 10 over volume. As the opposing surfaces are brought from infinite separation to a separation d, the change in the free energy of mixing $\Delta f_M(d)$ is

$$\Delta f_M(d) = \int_V (df_M)_d - \int_V (df_M)_\infty \tag{10}$$

where the subscripts refer to separations d and ∞. By expanding the logarithm in eq 9 and retaining terms up to order $\rho^2 V_S^2$, we obtain from eq 10

$$\Delta f_M(d) = \frac{kTV_S^2}{V_1}\left(\frac{1}{2} - \chi_1\right)\left[\int(\rho_j + \rho_k)_d^2 dV - \int(\rho_j + \rho_k)_\infty^2 dV\right] \tag{11}$$

Since $\int(\rho_j)_d^2 dV = \int(\rho_k)_d^2 dV$ and $(\rho_j\rho_k)_\infty = 0$, eq 11 becomes

$$\Delta f_M(d) = \frac{2kTV_S^2}{V_1}\left(\frac{1}{2} - \chi_1\right)\left[\int(\rho_j)_d^2 dV - \int(\rho_j)_\infty^2 dV + \int(\rho_j\rho_k)_d dV\right] \tag{12}$$

The required segment densities are obtained by summing the end-to-end probability functions $W_n(x,r)$ of subchains of n elements over the total number of elements N of the chain. Thus, for the jth chain with its origin on the $x = 0$ surface and the kth chain on the $x = d$ surface, the segment densities $\rho_{Nj}(x,r;\, d)$ and $\rho_{Nk}(x,r;\, d)$ are given by

$$\rho_{Nj}(x,r;\, d) = \sum_{n=1}^{N} W_{nj}(x,r;\, 0;\, 0;\, d) \tag{13}$$

and

$$\rho_{Nk}(x,r;\, d) = \sum_{n=1}^{N} W_{nk}(x,r;\, d;\, 0;\, d) \tag{14}$$

$W_n(x,r;\, x';\, 0;\, d)$ is the probability (per unit volume) of finding the second end of a subchain of n elements at x,r when its origin is at x' and reflective barriers are at $x = 0$ and $x = d$. These probabilities are obtained from the diffusion equation as eq 3 was obtained; *i.e.*, the reflective barriers are replaced in the mathematical boundary conditions by absorbing barriers. The steps leading to eq 6 remain the same, except that now the normalization constant K is obtained by integration over the volume between the surfaces a distance d apart, rather than the infinite separation used previously.

$$\underset{x'\to 0}{K} = \left[2\pi\int_{r=0}^{\infty}\int_{x=0}^{d} rW_n(x,r;\, x';\, 0;\, d)\,dr\,dx\right]^{-1} = \frac{1}{2\pi x'}\left(\frac{3}{2nl^2}\right)\left[\sum_{m=-\infty}^{+\infty}\left[\exp(-6m^2d^2/nl^2) - \exp\{-3(2m-1)^2d^2/2nl^2\}\right]\right]^{-1} \tag{15}$$

The segment density $\rho_{Nj}(x,r;\, d)$ thus becomes, using eq 3 and 15

$$\rho_{Nj}(x,r;\, d) = \frac{2}{\pi}\left(\frac{3}{2l^2}\right)^2 \sum_{n=1}^{N} \frac{\exp(-3r^2/2nl^2)\sum_{m=-\infty}^{+\infty}(x - 2md)\exp[-3(x-2md)^2/2nl^2]}{n^2\sum_{m=-\infty}^{+\infty}\left[\exp(-6m^2d^2/nl^2) - \exp[-3(2m-1)^2d^2/2nl^2]\right]} \tag{16}$$

while $\rho_{Nk}(x,r;\, d)$ is easily obtained from $\rho_{Nj}(x,r;\, d)$ by translation and reflection of the coordinate system

$$\rho_{Nk}(x,r;\, d) = \frac{2}{\pi}\left(\frac{3}{2l^2}\right)^2 \sum_{n=1}^{N} \frac{\exp(-3r^2/2nl^2)\sum_{m=-\infty}^{+\infty}(d - 2md - x)\exp[-3(d-2md-x)^2/2nl^2]}{n^2\sum_{m=-\infty}^{+\infty}\left[\exp(-6m^2d^2/nl^2 - \exp[-3(2m-1)^2d^2/2nl^2]\right]} \tag{17}$$

It will be convenient to express distances in units of $(Nl^2)^{1/2}$. We set $r = \gamma(Nl^2)^{1/2}$, $x = \beta(Nl^2)^{1/2}$, and $d = \delta(Nl^2)^{1/2}$. With these substitutions, the volume integrals of the type $\int(\rho_j)^2 dV$ in eq 12 may be written as

$$\int(\rho_j)^2 dV = 2\pi(Nl^2)^{3/2}\int_{\beta=0}^{\delta}\int_{\gamma=0}^{\infty}(\rho_j)^2\gamma\,d\gamma\,d\beta = \frac{3^4N^2}{2\pi(Nl^2)^{3/2}}B_{jj}(\delta) \tag{18}$$

where

$$B_{jj}(\delta) = \int_{\beta=0}^{\delta}\int_{\gamma=0}^{\infty}\left[\sum_{n=1}^{N}\frac{N}{n^2}\frac{\sum_{m=-\infty}^{+\infty}(\beta - 2m\delta)\exp[-3\{\gamma^2 + (\beta-2m\delta)^2\}N/2n]}{\sum_{m=-\infty}^{+\infty}\left[\exp(-6m^2\delta^2N/n) - \exp[-3(2m-1)^2\delta^2N/2n]\right]}\right]^2\gamma\,d\gamma\,d\beta \tag{19}$$

Correspondingly, the volume integrals of the type $\int \rho_j \rho_k dV$ may be written as

$$\int \rho_j \rho_k dV = 2\pi (Nl^2)^{3/2} \int_{\beta=0}^{\delta} \int_{\gamma=0}^{\infty} \rho_j \rho_k \gamma d\gamma d\beta = \frac{3^4 N^2}{2\pi (Nl^2)^{3/2}} B_{jk}(\delta) \tag{20}$$

where

$$B_{jk}(\delta) = \int_{\beta=0}^{\delta} \int_{\gamma=0}^{\infty} \left[\sum_{n=1}^{N} \frac{N}{n^2} \frac{\sum_{m=-\infty}^{+\infty} (\beta - 2m\delta) \exp[-3\{\gamma^2 + (\beta - 2m\delta)^2\} N/2n]}{\sum_{m=-\infty}^{+\infty} [\exp(-6m^2\delta^2 N/n) - \exp[-3(2m-1)^2\delta^2 N/2n]]} \right] \times$$

$$\left[\sum_{m=1}^{N} \frac{N}{n^2} \frac{\sum_{m=-\infty}^{+\infty} (\delta - 2m\delta - \beta) \exp[-3\{\gamma^2 + (\delta + 2m\delta - \beta)^2\} N/2n]}{\sum_{m=-\infty}^{+\infty} [\exp(-6m^2\delta^2 N/n - \exp[-3(2m-1)^2\delta^2 N/2n]]} \right] \gamma d\gamma d\beta \tag{21}$$

Equations 12, 18, and 20 give the change in the free energy of mixing as the separation distance is reduced from ∞ to δ $(=d/(Nl^2)^{1/2})$ as

$$\Delta f_M(\delta) = \frac{3^4 N^2 V_S^2 (1/2 - \chi_1) kT}{\pi (Nl^2)^{3/2} V_1} \{B_{jj}(\delta) + B_{jk}(\delta) - B_{jj}(\infty)\} \tag{22}$$

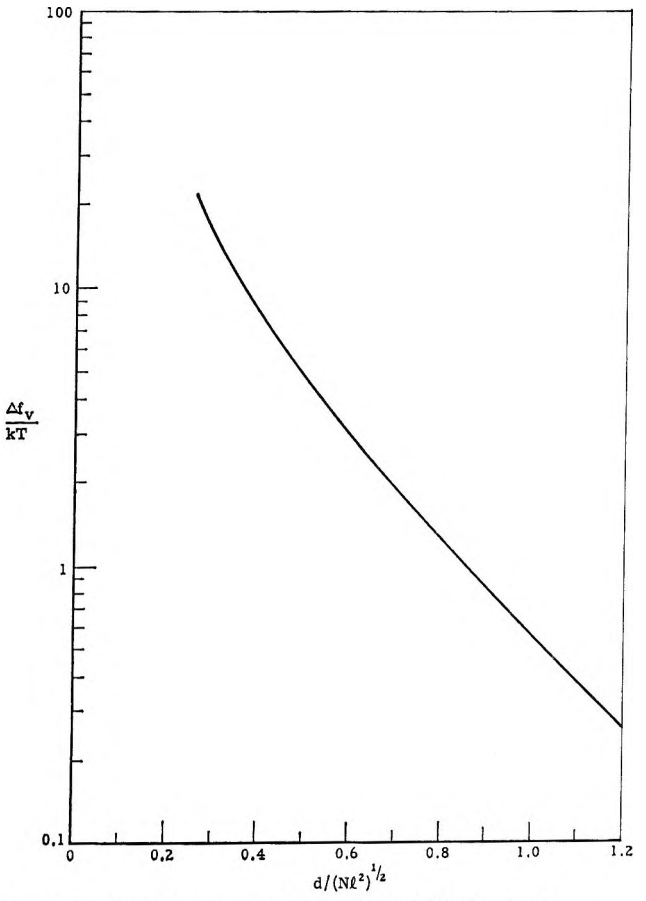

Figure 1. Free energy change due to restricted volume.

The relatively complex integrals represented by $B_{jj}(\delta)$ and $B_{jk}(\delta)$ have been evaluated with an IBM 7040 computer for values of δ ranging from 0.3 to 1.4 and for $\delta = \infty$. The results are shown in Table I.

Table I: Segment Density Functions $B_{jj}(\delta)$ and $B_{jk}(\delta)$

δ $(=d/(Nl^2)^{1/2})$	$B_{jj}(\delta)$	$B_{jk}(\delta)$
0.3	0.1755	0.174
0.4	0.1386	0.136
0.6	0.0932	0.0930
0.8	0.0757	0.0595
1.0	0.0679	0.0389
1.2	0.0642	0.0249
1.4	0.0626	0.0153
∞	0.0617	0.0000

We now express the polymer–solvent interaction parameter χ_1 in terms of the chain expansion parameter α $(=(Nl^2)^{1/2}/(Nl^2)_0^{1/2}$, *i.e.*, the ratio of perturbed to unperturbed end-to-end distances of the free chain). The difficult problem of relating α to χ_1 (or equivalently to $\psi_1[1 - (\theta/T)]$, a more general form of $(1/2 - \chi_1)$) has not been completely solved;[8,10,11] nevertheless, we shall use here Flory's[8] closed-form expression

$$\alpha^5 - \alpha^3 = \frac{27 N^2 V_S^2}{2^{3/2} \pi^{3/2} V_1 (Nl^2)_0^{3/2}} \psi_1 [1 - (\theta/T)] \tag{23}$$

Combining eq 22 and 23 gives

$$\Delta f_M(\delta) = 6(2\pi)^{1/2} (\alpha^2 - 1) kT \times \{B_{jj}(\delta) + B_{jk}(\delta) - B_{jj}(\infty)\} \tag{24}$$

Change in Free Energy of Mixing per Unit Area. Equation 24 gives the change in free energy of mixing

(10) M. Kurata, W. H. Stockmayer, and A. Roig, *J. Chem. Phys.*, **33**, 151 (1960).

(11) G. C. Berry, *ibid.*, **44**, 4550 (1966), and references cited therein.

per pair of chains which are directly opposite one another on the opposing surfaces. The free energy change per unit area is not obtained by merely multiplying by the number of chains per unit area since the probability that two chains are opposite one another must also be considered. This probability may be estimated to a sufficient degree of accuracy for present purposes by defining a distance ζ such that if the sites on which a pair of opposing molecules are adsorbed are offset by $r_2 > \zeta$ (the first molecule is adsorbed at $x = 0$, $r_1 = 0$ and the second on the surface at $x = d$, r_2 variable), the interaction is zero, while if $r_2 < \zeta$, the interaction is as if $r_2 = 0$; *i.e.*, the molecules are directly opposite. If η molecules are adsorbed per unit area and opposing molecules interact (overlap) if $r_2 < \zeta$, the number of such interactions will be $\eta^2\zeta^2$ per unit area. The change in the free energy of mixing per unit area $\Delta F_M(\delta)$ becomes from eq 24

$$\Delta F_M(\delta) = 6(2\pi)^{1/2}(\alpha^2 - 1)kT\eta \times \{B_{jj}(\delta) + \eta\zeta^2 B_{jk}(\delta) - B_{jj}(\infty)\} \quad (25)$$

ζ is an unevaluated parameter but is expected to be of the order of end-to-end chain distances.

In the event that only one surface has adsorbed polymer, $B_{jk}(\delta)$ is zero and

$$\Delta F_M(\delta) = 3(2\pi)^{1/2}(\alpha^2 - 1)kT\eta\{B_{jj}(\delta) - B_{jj}(\infty)\} \quad (26)$$

It is of interest to compare the changes in the free energy of mixing ΔF_M and free energy of restricted volume ΔF_V. Table II shows the ratio $\Delta F_M/\Delta F_V$ at various distances of separation δ for sparse surface coverage $\eta\zeta^2 \cong 0$ and for large coverage $\eta\zeta^2 = 1$. Since the free energy of mixing depends on the interaction parameter χ_1 (or, equivalently, on α), the data in Table II are calculated for a polymer in a "good" solvent, for which α has been taken as 1.5.

These data show that the free energies of mixing and restricted volume are similar *if* the surface coverage is large and the solvent is a good solvent for the polymer. As α decreases (poorer solvents), the change in the free energy of mixing decreases and will become negative in very poor solvents. In the latter case, there will be an additional attractive force between polymer-bearing surfaces which will tend to cause coagulation.

Table II: Comparison of Free Energies of Mixing ΔF_M and Restricted Volume ΔF_V ($\alpha = 1.5$)

$$\frac{\Delta F_M(\delta)}{\Delta F_V(\delta)} = -3(2\pi)^{1/2}(\alpha^2 - 1)\frac{\{\beta_{jj}(\delta) + \eta\zeta^2\beta_{jk}(\delta) - \beta_{jj}(\infty)\}}{\ln P_N(\delta)}$$

δ ($= d/(Nl^2)^{1/2}$)	$\Delta F_M/\Delta F_V$: Sparse coverage, $\eta\zeta^2 = 0$	$\Delta F_M/\Delta F_V$: Large coverage, $\eta\zeta^2 = 1$
0.4	0.075	0.228
0.8	0.102	0.535
1.0	0.100	0.728
1.2	0.089	1.03

Adsorption Required for Dispersancy. In order that a particulate system remain dispersed, it is necessary that the free energy per particle (including thermal energy kT) be positive at all distances of separation. For the infinite surfaces considered here, kT is negligible in comparison to the free energy of interaction of the surfaces; hence the criterion for stability is that the interaction free energy be positive. If we assume the attractive forces between surfaces to result from van der Waals–London type of interaction, the attractive free energy per unit area ΔF_A of planar parallel surfaces can be expressed[12] as $\Delta F_A(d) = -A/12\pi d^2$, where A is a numerical constant which is dependent on the nature of the surfaces. Since $\Delta F_M(\delta)$ is small compared to $\Delta F_V(\delta)$ at low surface coverages or when α is near unity (Table II), we neglect $\Delta F_M(\delta)$ and write the criterion for stability as $\Delta F_A + \Delta F_V > 0$. Using eq 8, this may be written as

$$-\eta(Nl^2)\delta^2 \ln P_N(\delta) > A/24\pi kT \quad (27)$$

where d is expressed in units of $(Nl^2)^{1/2}$, $d = \delta(Nl^2)^{1/2}$.

Since $Nl^2 = \alpha^2(Nl^2)_0 = \alpha^2K^2M$, where M is the molecular weight and K is an experimental constant, eq 27 may be rewritten as

$$-\eta K^2\alpha^2 M\delta^2 \ln P_N(\delta) > A/24\pi kT$$

By substituting $\omega = \eta M/N_A$, where ω is the weight of polymer adsorbed per unit area and N_A is Avogadro's number, we obtain

$$-\omega N_A K^2\alpha^2 \ln P_N(\delta) > A/24\pi kT \quad (28)$$

The minimum weight ω_{min} of adsorbed polymer required for stability is then

$$\omega_{min} = -A/24\pi kTN_A K^2\alpha^2\delta^2 \ln P_N(\delta) \quad (29)$$

As examples, with $A = 25kT$ (an average value given in ref 3), $\alpha = 1.0$, and $K = 0.8 \times 10^{-8}$,[3] we obtain the results shown in Table III for ω_{min} as a function of δ.

Unfortunately, there appear to be no experimental data in the literature with which to compare these predictions. The few data[13] which have been found concerning the stabilization of colloidal suspensions by nonionic polymers have not included the quantity of polymer adsorbed.

(12) J. H. de Boer, *Trans. Faraday Soc.*, **32**, 10 (1936).

(13) W. Heller and T. L. Pugh, *J. Polymer Sci.*, **47**, 203 (1960).

Table III: Weight of Adsorbed Polymer Required for Dispersancy[a]

δ $(=d/(Nl^2)^{1/2})$	$-\delta^2 \ln P_N(\delta)$	$10^8\omega_{min}$, g/cm²
0.4	1.33	0.640
0.8	0.825	1.03
1.2	0.378	2.25

[a] $A = 25kT$, $K = 0.8 \times 10^{-8}$, $\alpha = 1.0$.

The decreasing quantity of adsorbed polymer required at smaller distances shows that a system might be stable at particular distances of separation, provided the adsorption is in the range indicated in Table III. Also, these data show that less adsorption is required for higher molecular weight polymers. Referring to eq 29, we also see that less adsorption is required in "good" solvents ($\alpha > 1$), not only from the direct dependence of ω_{min} on α^{-2}, but also because of the effect of α on $-\delta^2 \ln P_N(\delta)$, which increases as α increases. Also, in "good" solvents, the neglected contribution of ΔF_M to the free energy of repulsion would tend to further decrease ω_{min}.

From the values of ω_{min} and the area per molecule, we may calculate the fraction φ of surface that must be covered with adsorbed polymer. The radius of the area occupied per molecule will be taken as the projected end-to-end distance on the surface, *i.e.*, to $(^2/_3Nl^2)^{1/2}$.

$$\varphi = {}^2/_3\pi\eta Nl^2 = \frac{2\pi}{3}\omega_{min}N_AK^2\alpha^2 \tag{30}$$

With $\omega_{min} = 10^{-8}$ g/cm², $K = 0.8 \times 10^{-8}$, and $\alpha = 1.0$, we obtain $\varphi = 0.78$; the surface will be well covered with adsorbed polymer.

Very Extensive Surface Coverage. In the preceding sections, the change in the free energy of mixing has been treated in terms of the statistics of "isolated" molecules. Although this treatment appears adequate for surface coverages for which each molecule more or less occupies an independent area on the surface, the treatment must be invalid when an appreciable overlap of segments from contiguous molecules occurs. In this section, a model applicable to very extensive surface coverage will be developed.

We shall assume that sufficient molecules are adsorbed such that the resulting overlap of neighboring molecules produces a constant density of segments parallel to the surface; *i.e.*, the segment density is a function only of the distance normal to the surface.

If η chains of n segments each are adsorbed per unit area on the jth surface at $x = 0$, the probable number $X_{nj}(x; 0; d)$ of free chain ends between x and $x + dx$ (per unit area) when reflective barriers are at $x = 0$ and $x = d$ is

$$X_{nj}(x; 0; d)dx = \frac{3\eta}{nl^2}\left[\frac{\sum_{m=-\infty}^{+\infty}(x - 2md)\exp[-3(2md - x^2)/2nl^2]}{\sum_{m=-\infty}^{+\infty}\left[\exp(-6m^2d^2/nl^2) - \exp[-3(2m-1)d^2/2nl^2]\right]}\right]dx \tag{31}$$

The density of segments $\rho_{Nj}(x; 0; d)$ from chains adsorbed on the jth surface placed at $x = 0$ becomes

$$\rho_{Nj}(x; 0; d) = \sum_{n=1}^{N}X_{nj}(x; 0; d) = \frac{3\eta(Nl^2)^{1/2}}{l^2}\sum_{n=1}^{N}\left[\frac{1}{n}\frac{\sum_{m=-\infty}^{+\infty}(\beta - 2m\delta)\exp\{-{}^3/_2(2m\delta - \beta)^2N/n\}}{\sum_{m=-\infty}^{+\infty}\exp(-6m^2\delta^2N/n) - \sum_{m=-\infty}^{+\infty}\exp\{-{}^3/_2(2m-1)^2\delta^2N/n\}}\right] \tag{32}$$

with distances expressed in units of $(Nl^2)^{1/2}$; *i.e.*, $x = \beta(Nl^2)^{1/2}$ and $d = \delta(Nl^2)^{1/2}$.

Correspondingly, the density of segments from chains adsorbed on the kth surface placed at $x = d$ is

$$\rho_{Nk}(x; 0; d) = \frac{3\eta(Nl^2)^{1/2}}{l^2}\sum_{n=1}^{N}\left[\frac{1}{n}\frac{\sum_{m=-\infty}^{+\infty}(\delta - 2m\delta - \beta)\exp\{{}^3/_2(\delta - 2m\delta - \beta)^2N/n\}}{\sum_{m=-\infty}^{+\infty}\exp(-6m^2\delta^2N/n) - \sum_{m=-\infty}^{+\infty}\exp\{-{}^3/_2(2m-1)^2\delta^2N/n\}}\right] \tag{33}$$

The change in the free energy of mixing per unit area $\Delta F_M(\delta)$ occurring as the opposing surfaces are brought from infinite separation to d is from eq 12, 23, 32, and 33

$$\Delta F_M(\delta) = \frac{2^{5/2}\pi^{3/2}}{3}(\alpha^2 - 1)kT(Nl^2)\eta^2[\Delta H(\delta)] \tag{34}$$

where $\Delta H(\delta) = H_{jj}(\delta) + H_{jk}(\delta) - H_{jj}(\infty)$ and

$$H_{jj}(\delta) = \int_{\beta=0}^{\delta} \left[\sum_{n=1}^{N} \frac{1}{n} \frac{\sum_{m=-\infty}^{+\infty} (\beta - 2m\delta) \exp[-3/2(2m\delta - \beta)^2 N/n]}{\sum_{m=-\infty}^{+\infty} \exp(-6m^2\delta^2 N/n) - \sum_{m=-\infty}^{+\infty} \exp[-3/2(2m-1)^2\delta^2 N/n]} \right]^2 d\beta \quad (35)$$

$$H_{jk}(\delta) = \int_{\beta=0}^{\delta} \left[\sum_{n=1}^{N} \frac{1}{n} \frac{\sum_{m=-\infty}^{+\infty} (\beta - 2m\delta) \exp[-3/2(2m\delta - \beta)^2 N/n]}{\sum_{m=-\infty}^{+\infty} \{\exp(-6m^2\delta^2 N/n) - \exp[-3/2(2m-1)^2\delta^2 N/n]\}} \right] \times$$

$$\left[\sum_{n=1}^{N} \frac{1}{n} \frac{\sum_{m=-\infty}^{+\infty} (\delta - \beta - 2m\delta) \exp[-3/2(\delta - \beta - 2m\delta)^2 N/n]}{\sum_{m=-\infty}^{+\infty} \{\exp(-6m^2\delta^2 N/n) - \exp[-3/2(2m-1)^2\delta^2 N/n]\}} \right] d\beta \quad (36)$$

Table IV: Segment Density Functions for Extensively Covered Surfaces

δ $(=d/Nl^2)$	$H_{jj}(\delta)$	$H_{jk}(\delta)$	$\Delta H(\delta)$
0.3	0.444	0.443	0.769
0.4	0.337	0.336	0.555
0.6	0.222	0.216	0.320
0.8	0.167	0.152	0.201
1.0	0.138	0.109	0.129
1.2	0.124	0.0763	0.082
1.4	0.118	0.0507	0.051
∞	0.118	0.000	0.000

$H_{jj}(\delta)$ and $H_{jk}(\delta)$ have been evaluated with an IBM 7040 computer with results shown in Table IV.

The ratio of the free energy changes due to mixing and to restricted volume is, using eq 8 and 34

$$\frac{\Delta F_M(\delta)}{\Delta F_V(\delta)} = -\frac{2^{3/2}\pi^{3/2}}{3} \frac{\Delta H(\delta)}{\ln P_N(\delta)} (\alpha^2 - 1)\eta(Nl^2) \quad (37)$$

The quantity

$$-\frac{2^{3/2}\pi^{3/2}}{3} \frac{\Delta H(\delta)}{\ln P_N(\delta)}$$

is shown in Table V.

Since $\eta(Nl^2)$ will be greater than 1.0 for extensively covered surfaces, eq 37 and the data in Table V show that, in good solvents, $\alpha > 1.3$–1.4, $\Delta F_M(\delta)$ will be comparable to $\Delta F_V(\delta)$ at small distances of separation and will be much larger at larger distances. We recall (Table II) that for sparsely covered surfaces $\Delta F_V(\delta)$

Table V: Comparison of Free Energy Change of Mixing and of Restricted Volume

δ $(=d/(Nl)^{1/2})$	$\frac{-2^{3/2}\pi^{3/2}\Delta H(\delta)}{3 \ln P_N(\delta)}$
0.4	0.350
0.6	0.560
0.8	0.815
1.0	1.16
1.2	1.63
1.4	2.38

was found to be much larger than $\Delta F_M(\delta)$ for any reasonable value of α. This change results from the dependence of ΔF_M on the square of surface coverage at large surface coverages while ΔF_V is proportional to only the first power of the surface coverage.

Heats of Mixing of Aqueous Electrolytes. IV. Potassium Salts of the Fluoride, Chloride, Bromide, and Acetate Ions[1]

by R. H. Wood and Henry L. Anderson[2]

University of Delaware, Newark, Delaware *(Received October 14, 1966)*

The heats of mixing of aqueous solutions of the potassium salts of fluoride, chloride, bromide, and acetate ions have been measured at 25° at 1 *m* constant total concentration. The sign of the heat of mixing has been correlated with the structure-making and structure-breaking properties of the ions. It has been shown that no such simple correlation exists on the basis of ion size.

Introduction

The heats of mixing of a wide variety of alkali metal[3-9] and alkaline earth[10] cation–common anion mixtures have been measured. However, only a relatively few anion–common cation mixtures have been studied.[4,8-10] The only anion–common cation mixings studied are those binary aqueous mixtures of the chloride, bromide, and nitrate anions. The heats of mixing of the halide anions were found to be approximately 1 cal/mole at 1 *m* and the heats of the halide–nitrate mixings about 3 cal/mole at 1 *m*. Thus, the magnitude of the anion heats of mixing have been considerably smaller than the cation heats of mixing (~ -50–$+30$ cal/mole at 1 *m*). It has been found that the cations can be classified into two groups,[3,8,10] (H^+, Li^+, Na^+, Mg^{2+}, Ca^{2+}, Sr^{2+}, and Ba^{2+}) and (K^+, Rb^+, and Cs^-). The common-ion heats of mixing between ions of the same group are endothermic and between opposite groups are exothermic, provided that salts of the same charge type are mixed. It has been suggested[8,10] that the classification of the ions may be a function of ion size and/or structural properties (structure making, structure breaking[11]) of the ions. Of the ions studied to date, no distinction can be made as to the nature of the classification, because the ions of the first group are all small, structure-making ions and the ions of the second group are all large, structure-breaking ions.

It was the purpose of the present work to measure the heats of mixing of some additional anions to see if the heat of mixing can be as large as the cation mixing. In addition, the binary heats of mixing of combinations of the acetate (a large, structure-making anion), fluoride (a small, structure-making anion), chloride, and bromide anions are the first mixings of ions which can no longer be classified according to both size and structure.

Experimental Section

Materials. All salts used in this work were analytical reagent grade materials. They were dissolved in deionized water and stored in polyethylene containers as approximately 4 *m* solutions.

The KBr and KCl stock solutions were standardized by the standard silver halide gravimetric procedure. The $KC_2H_3O_2$ and KF stock solutions were standardized by precipitating potassium tetraphenylborate as described by Flashka and Barnard.[12]

(1) Presented before the Division of Physical Chemistry, 152nd National Meeting of the American Chemical Society, New York, N. Y., Sept 11–16, 1966. This study was aided by a grant from the Office of Saline Water, U. S. Department of the Interior, Washington, D. C.

(2) To whom all correspondence should be addressed at The University of North Carolina at Greensboro, Greensboro, N. C. 27412.

(3) T. F. Young and M. B. Smith, *J. Phys. Chem.*, **58**, 716 (1954).

(4) T. F. Young, Y. C. Wu, and A. A. Krawetz, *Discussions Faraday Soc.*, **24**, 27, 77, 80 (1957).

(5) J. H. Stern and A. A. Passchier, *J. Phys. Chem.*, **67**, 2420 (1963).

(6) J. H. Stern and C. W. Anderson, *ibid.*, **68**, 2528 (1964).

(7) J. H. Stern, C. W. Anderson, and A. A. Passchier, *ibid.*, **69**, 207 (1965).

(8) Y. C. Wu, M. B. Smith, and T. F. Young, *ibid.*, **69**, 1868, 1873 (1965).

(9) R. H. Wood and R. W. Smith *ibid.*, **69**, 2974 (1965).

(10) R. H. Wood and H. L. Anderson, *ibid.*, **70**, 992 (1966).

(11) H. S. Frank and M. W. Evans, *J. Chem. Phys.*, **13**, 507 (1945).

(12) H. Flashka and A. J. Barnard, *Advan. Anal. Chem. Instr.*, **1**, 23 (1960).

Table I: Heats of Mixing at 25.00° and Unit Total Ionic Strength

Salt pair	RTh_0[b]	RTh_1[b]	N[c]	$\Delta H_{m,y=0.5}$[d]
KF–$KC_2H_3O_2$	+9.5 ± 0.3	+0.9 ± 0.4	6	+2.38 ± 0.08
KCl–KBr	+3.2[a]	...	...	+0.80
KF–KCl	−22.6 ± 0.2	−0.8 ± 0.3	18	−5.65 ± 0.05
KF–KBr	−16.7 ± 0.2	...	13	−4.18 ± 0.05
KCl–$KC_2H_3O_2$	−34.3 ± 0.3	+0.9 ± 0.4	11	−8.58 ± 0.08
KBr–$KC_2H_3C_2$	−32.4 ± 0.3	−1.5 ± 0.4	12	−8.10 ± 0.08

[a] See ref 8. [b] Units are cal/kg of solvent m^2. [c] N is the number of experiments. [d] Units are cal/kg of solvent.

The total cation impurities as found by flame photometric analysis[9] were found to be less than 0.1 mole % for the KCl and KBr stock solutions. The manufacturers, cation assays supplied with the KF and $KC_2H_3O_2$ were less than 0.1 mole % impurity. Thus, the stock solutions were assumed to be 99.9% pure.

Apparatus and Procedure. The heat of mixing experiments were performed as described before[9] with solutions diluted by weight from the stock solutions. To suppress hydrolysis, the pH of the solutions was adjusted to 8.0–10 by the addition of potassium hydroxide.

Results and Discussion

The experimental data were fitted by the method of least squares on an IBM 1620 II computer to the equation[13]

$$\Delta H_m \text{ (cal/kg of solvent)} = y(1 - y)I^2[RTh_0 + RTh_1(1 - 2y)]$$

where y is the mole fraction of the salt component with the highest molecular weight, I is the total ionic strength, R is the gas constant, T is the temperature, h_0 is the magnitude of the interaction, and h_1 is a measure of asymmetry of the interaction. The heats of mixing were determined for each mixture in the range 0–0.22 and 1–0.78 mole fraction. The results of the least-squares treatment are reported in Table I. Errors due to heats of concentration, dilution, and neutralization upon mixing in all experiments were negligible; thus, the uncertainty (95% confidence level) of RTh_0 and RTh_1 as reported in Table I is based only on the experimental precision.

The heats of mixing of the anions in the presence of the common potassium ion were found to range from +2.38 to −8.58 cal/mole at 1 m. These results include the largest heats of mixing observed for anion–common cation mixtures. This appears to be smaller than the cation–common anion heats of mixing (−50–+30 cal/mole), but when the very small ions, H^+ and Li^+, are left out of the cation comparison, the heats of mixing range from +2 to −12 cal/mole. If the heat of mixing is mainly influenced by the solvent sphere about an ion (to be expanded on later), it should not be unreasonable to find abnormally high interactions with the H^+ and Li^+ ions. Thus, the present results indicate that the anion heats of mixing can certainly be comparable in magnitude with those of the cation heats of mixing.

The results in Table I also show that the structural classification will correlate with the sign of the heats of mixing, whereas the size classification will not. Thus, for all common-ion heats of mixing that have been measured, the mixing of two structure breakers or two structure makers gives endothermic heats of mixing, while mixing a structure breaker with a structure maker gives an exothermic heat of mixing. The chloride and bromide ions are structure breakers, while the fluoride and acetate ions are structure makers.[11,14–16]

It is concluded that the detailed structure of the water around the ion is the most important factor in determining the heat of mixing. Of course, the detailed structure of the water around the ion is influenced by size as well as by the specific interactions of the solute with the water.

It is perhaps surprising that this simple classification will predict the sign of the heat of mixing when it is realized that the mechanism of structure making is probably quite different for the fluoride and acetate ions.[11,13] In the case of the fluoride ion, the structure is created by the high electric field while for the acetate ion the lack of specific interaction with the methyl group stabilizes a more highly hydrogen-bonded water structure around this part of the molecule. In addi-

(13) H. L. Friedman, *J. Chem. Phys.*, 32, 1134 (1960).

(14) T. Ackermann and F. Schreiner, *Z. Elektrochem.*, 62, 1143 (1958).

(15) J. N. Agar, *Advan. Electrochem. Electrochem. Eng.*, 3, 31 (1963).

(16) D. W. McCall and D. C. Douglas, *J. Phys. Chem.*, 69, 2001 (1965).

tion, there is probably a region near the oxygens where the high electric field creates structure, since Laurence and Wolfenden[17] have shown that the contribution of the acetate ion to the viscosity (B coefficient) is much greater than the contribution of acetic acid.

It is interesting to note that the arguments used in this work are analogous to those used by others to explain heats of dilution of strong electrolyte solutions. Frank and Robinson[18] have shown that the heats of dilution are mainly influenced by unlike-charged ion interactions and that deviations from the Debye–Hückel limiting slope can be interpreted in terms of the water structural properties of the two oppositely charged ions.

Summary

In previous communications[9,10] it has been shown that the heats of mixing are mainly influenced by pairwise interactions of like-charged ions. We concluded from this work that the heat of mixing is mainly influenced by the water structure about the like-charged ions. A general mixing rule has been given which states that for a common-ion mixture, upon mixing, the heat of mixing is endothermic for ions with like solvent structural properties and exothermic for ions with unlike solvent structural properties.

(17) C. D. Laurence and J. H. Wolfenden, *J. Chem. Soc.*, 1144 (1934).

(18) H. S. Frank and A. L. Robinson, *J. Chem. Phys.*, **8**, 933 (1940)

Heats of Mixing of Aqueous Electrolytes. V. Tetraalkylammonium Chlorides[1]

by R. H. Wood and Henry L. Anderson[2]

University of Delaware, Newark, Delaware *(Received October 14, 1966)*

The heats of mixing of aqueous solutions of the chloride salts of the tetramethylammonium, tetraethylammonium, tetrapropylammonium, lithium, potassium, and cesium ions have been measured at 0.5 total ionic strength and 25°. The results have been used to show the relative importance of solvent structure on the sign and magnitude of the heats of mixing. The tetrapropylammonium ion appears to be a strong hydrophobic structure maker, the tetramethylammonium ion appears to be a structure breaker, and the tetraethylammonium ion appears to be in a transition region between a structure breaker and a hydrophobic structure maker.

Introduction

The previous paper in this series[3] has shown that the detailed structure of water molecules around an ion is the most important factor in determining the heats of interaction of two like-charged ions. Ions can be roughly divided into three structural classes:[4] (1) structure breakers, which have a net effect of breaking the water structure around them, (2) electrostrictive structure makers, which order the water molecules by their high electric fields, and (3) hydrophobic structure makers, which induce more hydrogen bonding in the water near their nonpolar surface. The present investigation is concerned with the heats of interaction

(1) Presented before the Division of Physical Chemistry, 152nd National Meeting of the American Chemical Society, New York, N. Y., Sept 11–16, 1966. This study was aided by a grant from the Office of Saline Water, U. S. Department of the Interior, Washington, D. C.

(2) To whom all correspondence should be addressed at The University of North Carolina at Greensboro, Greensboro, N. C. 27412.

(3) R. H. Wood and H. L. Anderson, *J. Phys. Chem.*, **71**, 1869 (1967).

(4) H. S. Frank and M. W. Evans, *J. Chem. Phys.*, **13**, 507 (1945).

of a series of tetraalkylammonium chlorides with each other and with the chlorides of lithium, potassium, and cesium. The larger tetraalkylammonium ions are hydrophobic structure makers,[5] so that the results extend the measurements to this structural type.

Experimental Section

Materials. The tetramethylammonium chloride stock solution was prepared from Eastman tetramethylammonium chloride which had been precipitated from methanol and dried according to Unni, *et al.*[6] The chloride content determined gravimetrically as the silver salt was 99.95%. The amine content as determined by acid–base titration was less than 0.1 mole %. Thus, the tetramethylammonium chloride was assumed to be at least 99.9% pure. The tetraethylammonium chloride stock solution was prepared from the Eastman salt. Stock solution A was prepared from precipitated salt according to Unni, *et al.*,[6] and stock solution B was prepared directly from the bottle. The compounds were checked for chloride gravimetrically and yielded 99.78 and 100.14%, respectively, for A and B. The solutions were checked for amine content by acid–base titration and were found to contain less than 0.2 mole % amine. The tetrapropylammonium chloride was prepared from Eastman tetrapropylammonium iodide by passing the iodide through a Dowex 2-X4 anion-exchange column. The iodide ion content was checked by a color comparison starch–iodide test and indicated that the iodide concentration was less than 0.1 mole %. The tetrapropylammonium iodide was checked for halide content before passing through the column and was found to be 100.16% pure. The tripropylamine content was checked as above and found to be less than 0.1 mole %. The cesium chloride stock solution was made up from 99.7% salt from Penn Rare Metals, Inc. No attempt to purify the salt was made. However, a flame analysis was run for the sodium and potassium ions. The results gave a net impurity of 0.3 mole % sodium and 0.02 mole % potassium. The potassium chloride and lithium chloride stock solutions have been described previously.[7]

The concentrations of all of the stock solutions were determined *via* the standard silver halide gravimetric procedure. The tetraalkylammonium chloride stock solutions were also determined gravimetrically as the tetraalkylammonium tetraphenylborate. The procedure used was the same as the potassium tetraphenylborate alkaline procedure described by Flashka and Barnard.[8,9] The results agreed within 0.1% with the silver chloride analysis.

Procedure. The heats of mixing experiments were performed at 0.5 constant total molal ionic strength and at 25.00 ± 0.02° in the isothermal differential calorimeter (sensitivity 2×10^{-6}°) described in a previous communication.[7] For a description of the experimental procedure, see communication I.[7]

Treatment of Data and Results

The experimental data were fitted by the method of least squares on an IBM 1620 II computer to the equation[10]

$$\Delta H_m \text{ (cal/kg of solvent)} = RTI^2y(1 - y)[h_0 + (1 + 2y)h_1] \quad (1)$$

where R is the gas constant, T is the temperature, I is the molal ionic strength, y is the mole fraction of the salt component with the largest molecular weight, h_0 is the magnitude of the interaction, and h_1 is a measure of the asymmetry. The heats of mixing were determined for each mixture in the range 0–0.22 and 1–0.78 mole fraction. The results of the least-squares fit of eq 1 are recorded in Table I.

The heats of mixing were reasonably symmetrical with respect to mole fraction, where y of maximum ΔH_m ranged from 0.47 to 0.53. A comparison of the results in Table I with measurements on other systems[11,12] with a common anion shows that the tetraalkylammonium ions give somewhat larger heats of mixing ($RTh_0 = -700$–$+100$) than the alkali or alkaline earth metal ions ($RTh_0 = -200$–$+130$). Some theoretical calculations of the heats of mixing using Friedman's[10] model of hard, temperature independent spheres indicates that the large interactions cannot be explained by reasonable size parameters for the ions.[13] That is, it is an effect of the structure of the water around the ions even if only due to the way in which water structure influences the temperature dependence of the effective radius of the ions.

(5) H. S. Frank and W. Y. Wen, *Discussions Faraday Soc.*, 24, 133 (1957).

(6) A. K. R. Unni, L. Elias, and H. I. Schiff, *J. Phys. Chem.*, 67, 1216 (1963).

(7) R. H. Wood and R. W. Smith, *J. Phys. Chem.*, 69, 2974 (1965).

(8) H. Flashka and A. J. Barnard, *Advan. Anal. Chem. Instr.*, 1, 23 (1960).

(9) The precipitates were filtered in Selas crucibles. The tetramethylammonium and tetraethylammonium tetraphenylborate precipitates gave a little trouble in that some material passed through the filter initially, but recycling the filtrate through the filter proved to be quite satisfactory.

(10) H. L. Friedman, *J. Chem. Phys.*, 32, 1134 (1960).

(11) Y. C. Wu, M. B. Smith, and T. F. Yeung, *J. Phys. Chem.*, 69, 1868 (1965).

(12) R. H. Wood and H. L. Anderson, *ibid.*, 70, 992 (1966).

(13) R. H. Wood and H. L. Anderson, unpublished data.

Table I: Heat of Mixing at 25.00°

Salt pair	N^a	I^b	RTh_0^c	RTh_1^c	ΔH_m ($y = 0.5$)^d
LiCl–$(CH_3)_4NCl$	16	0.5	−160.8 ± 0.9	−7.8 ± 1.2	−40.2
KCl–$(CH_3)_4NCl$	15	0.5	118.9 ± 0.8	−2.2 ± 1.1	29.7
CsCl–$(CH_3)_4NCl$	16	0.5	82.0 ± 1.3	...	20.5
LiCl–$(C_2H_5)_4NCl$	15	0.5	−172.4 ± 1.0	−8.0 ± 1.4	−43.1
KCl–$(C_2H_5)_4NCl$	16	0.5	117.5 ± 0.9	...	29.4
CsCl–$(C_2H_5)_4NCl$	13	0.5	73.1 ± 1.3	−4.4 ± 1.8	18.4
LiCl–$(n\text{-}C_3H_7)_4NCl$	12	0.5	−693.3 ± 3.8	−33.0 ± 6.1	−173.3
KCl–$(n\text{-}C_3H_7)_4NCl$	12	0.5	−348 ± 4	−39.0 ± 5.9	−87.0
CsCl–$(n\text{-}C_3H_7)_4NCl$	14	0.5	−438.6 ± 1.5	12.7 ± 2.1	−109.6
$(CH_3)_4NCl$–$(C_2H_5)_4NCl$	13	0.5	−49.8 ± 0.7	1.3 ± 1.5	−12.5
$(CH_3)_4NCl$–$(n\text{-}C_3H_7)_4NCl$	12	0.5	−613.5 ± 2.3	−14.4 ± 3.8	−153.4
$(C_2H_5)_4NCl$–$(n\text{-}C_3H_7)_4NCl$	10	0.5	−308.4 ± 2.2	−8.3 ± 3.2	−77.1

[a] N is the number of experiments. [b] Molal ionic strength. [c] Units are cal/kg of solvent m^2. [d] Units are cal/kg of solvent.

Frank and Evans[4] proposed that the tetraalkylammonium ions should become hydrophobic structure makers as the size of the alkyl group increases. Measurements of heat capacity,[5] dielectric relaxation times,[14] viscosities,[15,16] soret coefficients,[17] partial molal volumes,[18] nmr relaxation times,[19] conductivities in D_2O,[20] and heats of dilution and solution,[21] indicate that indeed this is correct. The evidence is quite strong in indicating that the tetrapropylammonium ion is a strong hydrophobic structure maker. The evidence is not so conclusive about the tetramethylammonium and tetraethylammonium ions. From their partial molal volume measurements, Wen and Saito[18] pictured the tetramethylammonium ion as being a slight structure breaker and the tetraethylammonium ion as a slight structure maker. They visualized a competition between the charge effect and the hydrophobic effect, where the tetramethylammonium ion was just small enough so that the water structure around the ion was still under the influence of its charge, while the tetraethylammonium ion was just large enough that the effect of charge on the water structure was slightly overshadowed by the hydrophobic or clathrate effect.

Recent measurements of conductivities by Kay and Evans[22] and viscosities by Kay, Vituccio, Zawoyski, and Evans[23] indicate that the tetramethylammonium ion is a structure breaker but that the tetraethylammonium ion is in the transition region between a structure maker and a structure breaker.

For all of the common-ion heats of mixing that have been previously measured, the sign of the heats of mixing follows a simple rule. The mixing of two structure makers or two structure breakers gave endothermic heats of mixing, while a structure maker with a structure breaker gave an exothermic heat of mixing.[24]

With the uncertainty of classifying the ions it is not surprising to find that the simple correlation for the sign of the heat of mixing runs into some exceptions. Assuming the structural classification for determining the sign of the heat of mixing it is noted from the table that the tetramethylammonium ion acts as a structure breaker toward the alkali cations. Also note that the tetraethylammonium ion acts as a structure breaker. However, the tetramethylammonium and tetraethylammonium ion mixing is exothermic, indicating that they act as opposites when mixed with each other.

The results for the tetrapropylammonium ion show that all of the mixings of this ion with another ion give very large negative values for the heat of mixing (RTh_0 = −300 to −600). This suggests that the tetrapropylammonium ions are responsible and that the large interactions of two tetrapropylammonium ions

(14) G. H. Haggis, J. B. Hasted, and T. J. Buchanan, *J. Chem. Phys.*, **20**, 1452 (1952).

(15) E. Huckel and W. Schaaf, *Z. Physik. Chem.* (Frankfurt), **21**, 326 (1959).

(16) E. R. Nightingale, *J. Phys. Chem.*, **66**, 894 (1964).

(17) J. N. Agar, *Advan. Electrochem. Electrochem. Eng.*, **3**, 31 (1963).

(18) W. Y. Wen and S. Saito, *J. Phys. Chem.*, **68**, 2639 (1964).

(19) W. G. Hertz and M. O. Zeidler, *Ber. Bunsenges Physik. Chem.*, **68**, 821 (1964).

(20) R. L. Kay and D. F. Evans, *J. Phys. Chem.*, **69**, 4216 (1965).

(21) (a) S. Lindenbaum, *ibid.*, **70**, 814 (1966); (b) Y. C. Wu and H. L. Friedman, *ibid.*, **70**, 2030 (1966).

(22) R. L. Kay and D. F. Evans, *ibid.*, **70**, 2325 (1966).

(23) R. L. Kay, T. Vituccio, C. Zawoyski, and D. F. Evans, *ibid.*, **70**, 2336 (1966).

(24) For the rule to hold, Na^+ must be classified as a net structure maker. This ion is a borderline case, since, for instance, the entropy of solution data indicate that it is a net structure breaker,[4] while the viscosity coefficient indicates that it is a net structure maker (M. Kaminsky, *Z. Physik. Chem.* (Frankfurt), **8**, 173 (1956)). For a review of the evidence see J. L. Kavanau, "Water and Solute-Water Interactions," Holden-Day Inc., San Francisco, Calif., 1964, p 55 ff.

are masking other effects. In any common-ion heat of mixing, say MX with NX, there are three like-charged pair interactions to be considered: (1) the heat of diluting the M^+ ions and therefore the reduction in the overlap of the M^+ hydration sheaths with each other, (2) the dilution of the N^+ ions and the reduction of N^+–N^+ overlap, and (3) the formation of some M^+–N^+ overlap. It is expected that at any given concentration the tetrapropylammonium ions will have more hydration sphere overlap with neighbors because this is by far the largest ion represented in these experiments ($\bar{V}$ = 215).[18] The tetrapropylammonium ion is a strong hydrophobic structure maker and when the ion is mixed with another the overlap of the hydration sheaths of the tetrapropylammonium ions is reduced. For close contact both ions do not have their full hydration sphere so that on mixing (diluting the tetrapropylammonium ions) more structure is formed and heat is given out (RTh_0 is negative).[25] This interpretation is supported by the heat of dilution of the tetraalkylammonium halides measured by Lindenbaum.[21] The heats of dilution of the chloride and bromide of the tetrapropylammonium ion are much larger than the heats of dilution of the corresponding tetramethylammonium and tetraethylammonium ions. Heat is given out during dilution and the amount of heat given out is similar (±20) for the chloride and bromide. In fact, the entropies of dilution of the chlorides and bromides of the tetrapropylammonium and tetrabutylammonium ions are almost identical up to 1.5 *m*. Lindenbaum concludes that the larger entropy effect and most of the heat effect are due to the interactions of the tetrapropylammonium ions. This was supported by the earlier conclusions of Wen and Saito,[18] that the concentration dependence of the partial molal volumes could be explained by the effect of the overlap of the hydration sheaths of the tetraalkylammonium ions. If this is correct, both the heats of mixing and the heat of dilution are rough measures of the heat of interaction of two tetrapropylammonium ions. If the slope of the linear portion of the tetrapropylammonium chloride heat of dilution is taken as a measure of the interaction, a value of RTh_0 of −370 at 0.5 *m* is calculated for the heat of mixing of tetrapropylammonium chloride with other salts. Thus, the relative magnitudes of the heats of mixing and the heat of dilution are consistent with the idea that both are largely governed by overlap of the hydration sheaths of the large tetrapropylammonium ions. The agreement is expected to be only rough because the heat of dilution is affected by ionic strength changes and the negative ion. In addition, there may be a considerable contribution of triplet interactions to the heats of mixing. The interactions of the tetramethylammonium and tetraethylammonium ions are not large enough to mask these other effects in either the heats of dilution of the heats of mixing so the same kind of reasoning cannot be applied. However, the heat of dilution of tetrabutylammonium chloride could be used for a rough prediction of heats of mixing of tetrabutylammonium salts.

Summary

The present results quite clearly indicate the heat of mixing is strongly governed by the solvent structural properties of the ions. In the previous communication[3] it was shown that for small (electrostrictive structure-making and electrostrictive structure-breaking) ions, the sign of the heat of mixing can be accurately predicted. In the case of the very large hydrophobic structure-making ions, the effect of the overlap of the hydration spheres predominates in both the heat of mixing and the heat of dilution so that again the sign of the heat of mixing can be predicted. In addition, the present results support the previous claims that the tetramethylammonium ion is a structure breaker and that the tetraethylammonium ion is in a transition between a structure breaker and a structure maker.

(25) A discussion of this model in relation to previous theories and experimental results has been submitted for publication in this journal.

The Thermodynamic and Physical Properties of Beryllium Compounds. XI. The Heat of Formation and Entropy of Beryllium(I) Hydroxide(g)[1]

by H. C. Ko, M. A. Greenbaum, and M. Farber

Rocket Power, Inc., Pasadena, California *(Received November 1, 1966)*

An experimental study of the equilibrium BeO(c) + $^1/_2H_2$(g) = BeOH(g) in the temperature range of 2107–2368°K has been carried out employing the molecular flow effusion method. At an average temperature of 2235°K, second-law values of 88.3 ± 3.8 kcal for ΔH_r and 27.4 ± 1.7 cal/deg for ΔS_r were obtained. Employing available thermodynamic functions, values of −46.8 ± 3.8 kcal/mole and 54.0 ± 1.7 cal/deg mole were obtained for $\Delta H_{f,298}$ and $S°_{298}$ for the molecule BeOH(g). A corresponding third-law value for $\Delta H_{f,298}$ of BeOH(g) was found to be −48.2 ± 5 kcal/mole.

Introduction

Studies of the reaction between beryllium oxide and water vapor

$$BeO(c) + H_2O(g) = Be(OH)_2(g) \qquad (1)$$

to yield thermodynamic properties for beryllium hydroxide have been reported in the literature.[2,3] However, at the highest temperature studied, 1808°K, the formation of the subhydroxide BeOH has not been reported. Therefore, in an attempt to establish the formation of BeOH, a high-temperature study of the reaction between solid beryllium oxide and gaseous hydrogen was undertaken.

Experimental Section

Apparatus. A high-temperature carbon rod furnace was assembled in a high-vacuum system. The rods were supported vertically by tantalum sheets (five layers at the top and six layers at the bottom). Alumina caps were used to insulate the rods from the tantalum sheets. The carbon rods were shielded by five cylindrical layers of 5-mil tantalum separated by 0.25-in. graphite spacers. The inner and outer shields were 2.5 and 4.5 in. in diameter, respectively. Tantalum bolts and graphite spacers supported every shield. The entire assembly was supported from the brass plate base by three 0.25-in. diameter stainless steel rods attached to the outer shield. The leads for the carbon rod heating unit were extended through the five shields and attached to two copper rods, which were connected to the insulated feedthroughs attached to the brass plate. A detailed diagram of the apparatus is presented in Figure 1.

The reaction cell was a 2-in. long BeO tube closed at one end, with an o.d. of approximately 0.4 in. and an i.d. of approximately 0.3 in. A hole approximately 1 mm in diameter was drilled through the closed end of the tube. The exact dimensions of the cell hole diameter and thickness were measured with a traveling microscope. Two BeO cells with different hole dimensions (cell 1: 1.065-mm diameter, 1.27 mm deep; cell 2: 0.990-mm diameter, 2.0 mm deep) were employed for the series of experiments. The Clausing factors for cells 1 and 2 are 0.471 and 0.359, respectively. The cell was loosely covered with a rhenium cell with a 1.5-mm diameter hole drilled through the closed end. This rhenium cell in turn was covered with a tantalum cell with a 1.5-mm orifice at the center of the closed end. The entire unit was inserted tightly into a tantalum holder which was fitted to the end of the 0.25-in. o.d. tantalum flow tube (*cf.*, Figure 1). A rhenium foil insert with a 0.2-mm hole was placed over the tantalum tube inlet to prevent flow of species to the tantalum

(1) This work was sponsored by the Air Force Rocket Propulsion Laboratory, Research and Technology Division, Air Force Systems Command, U. S. Air Force, Edwards Air Force Base, Calif., under Contract No. AF 04(611)-10929.

(2) L. I. Grossweiner and R. L. Seifert, *J. Am. Chem. Soc.*, **74**, 2701 (1952).

(3) (a) W. A. Young, *J. Phys. Chem.*, **64**, 1003 (1960); (b) J. Blauer, M. A. Greenbaum, and M. Farber, *ibid.*, **70**, 973 (1966).

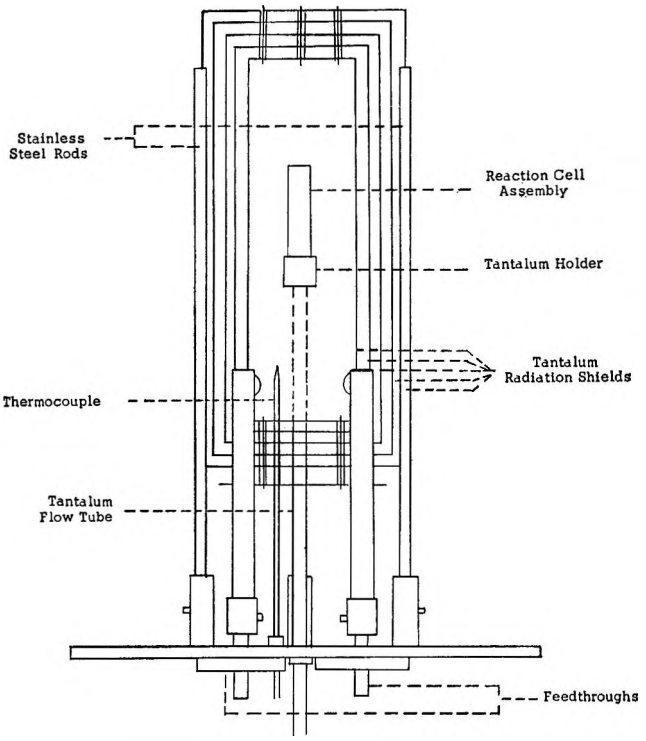

Figure 1. Schematic diagram of furnace assembly (side view) for BeOH studies.

tube. The flow tube penetrated the bottom tantalum sheets of the furnace and a thermocouple fabricated from tungsten, 5% rhenium–tungsten, 26% rhenium wires was used as the temperature-sensing element. This thermocouple was inserted approximately 1 in. inside the inner shield at the bottom of the furnace. The temperature of the cell was measured with an optical pyrometer through a window at the top of the furnace. This measurement was checked against a calibrated thermocouple which was placed inside the cell just below the effusion hole. This thermocouple was checked against a calibrated Pt—Pt–10% Rh thermocouple. The results showed that in the experimental temperature range the deviation was within 5° of the standard NBS values. Experiments were performed at 30° intervals for the total of more than 30 performed over the 300° temperature range. The 30° differential temperatures were reproducible to ±2°.

The entire furnace assembly was fitted into a 17-in. long stainless steel cross pipe with 10.5-in. diameter brass plates at the vertical ends and 4-in. diameter flanges at the side arms. One of the side arms was connected to the pumping system, the other to the ionization and thermocouple gauges. The temperature of the cell could also be measured with an optical pyrometer by viewing through a quartz plate fitted at the top end plate of the pipe. The pressure of the system was usually maintained in the region of 10^{-6} to 10^{-7} mm.

An 8-l. tank was filled with hydrogen (99.999% ultrapure grade) at the commencement of each H_2 experiment. A calibrated gauge was connected to the tank to permit calculation of the amount of hydrogen used during the run. A metering valve was connected to the line immediately prior to admitting hydrogen into the flow tube. Approximately the same valve reading was used for each run to ensure that the amount of hydrogen used would be fairly constant.

Procedure. In the temperature range of these experiments BeO has an appreciable weight loss due to vaporization. Therefore, a blank run in which no hydrogen was passed through was performed at each temperature to determine the weight loss of BeO due to vaporization alone. The BeO cell was weighed and the reaction assembly was placed in the system. The system was pumped down to the desired pressure, heating was commenced, and a constant temperature was maintained at a desired value. The blank or hydrogen experiment was then begun. Upon completion of the experiment, the system was allowed to cool down to near room temperature and the cell was removed and reweighed. Initial and final readings of the pressure in the hydrogen tank of calibrated volume were recorded. In this manner the number of moles of $H_2(g)$ used in each run was calculated.

Results and Discussion

After a considerable number of preliminary experiments were performed to establish that a reaction was indeed occurring between H_2 and BeO, a series of over 30 experiments was made with two effusion cells over a 300° temperature range. Experiments below 2100°K yielded weight losses too small from which to obtain accurate data. Consequently, the experimental temperature range was chosen as 2107–2338°K. The experiments were performed at 30° temperature intervals and in random fashion. Blank runs were made before and after each H_2–BeO reaction experiment. The data for these experiments are presented in Table I.

Although the two cells had different orifice dimensions, a further check for the establishment of equilibrium was made using BeO chips inside the BeO cell. The weight loss results for these experiments were essentially the same as those for the empty cells. Thus, within the experimental error, the surface area of several square centimeters of the cells was large enough (*i.e.*, reaction area to orifice area greater than 1000) to establish equilibrium with the hydrogen.

Having established that H_2 is reacting with the BeO,

Table I: Experimental and Calculated Data for the Reaction $BeO(c) + {}^1/_2H_2(g) = BeOH(g)$

Run no.	T, °K	Time, min	Total wt. loss of BeO, mg	Blank, mg	Total moles of $H_2 \times 10^2$	P_{Be}, atm $\times 10^6$	P_{BeOH}, atm $\times 10^5$	$K_2 \times 10^3$
29[b]	2107	290	6.1	0.2	3.567	1.94	2.269	0.707
5[b]	2139	230	7.0	0.5	2.459	2.36	3.232	1.086
30[b]	2139	230	7.2	0.5	2.840	2.55	3.302	1.029
6[b]	2171	230	8.9	1.2	2.344	2.99	3.821	1.322
7[b]	2171	230	9.0	1.2	2.524	3.12	3.856	1.283
8[b]	2171	230	8.7	1.2	2.944	3.38	3.644	1.120
9[b]	2203	110	5.8	1.0	1.372	4.30	4.949	1.546
10[b]	2203	230	12.1	2.6	2.745	4.19	4.665	1.495
11[b]	2235	110	8.5	2.5	1.487	5.71	6.188	1.867
12[b]	2235	110	8.0	2.0	1.372	5.46	6.224	1.957
13[b]	2235	230	18.4	5.0	2.613	5.18	6.761	2.239
14[b]	2235	230	17.0	5.0	2.548	5.11	5.974	2.005
15[b]	2268	110	11.9	4.3	1.425	7.09	7.929	2.466
17[a]	2268	110	13.3	2.2	1.487	5.72	7.825	2.981
18[a]	2268	110	11.4	2.2	1.434	5.61	6.342	2.453
19[a]	2268	110	12.0	2.2	1.449	5.64	6.969	2.691
16[b]	2301	110	14.6	5.2	1.349	8.63	9.913	3.213
20[a]	2301	110	21.1	4.3	1.420	6.94	12.24	4.857
21[a]	2301	110	20.9	4.3	1.420	6.94	12.08	4.794
22[a]	2301	110	19.8	4.3	1.482	7.12	11.17	4.329
23[a]	2335	110	25.8	6.8	1.430	8.67	13.82	5.573
24[a]	2335	110	27.6	6.8	1.415	8.59	15.27	6.195
25[a]	2368	110	31.8	8.5	1.372	10.27	17.14	7.232
26[a]	2368	110	30.0	8.5	1.377	10.32	15.67	6.584

[a] Cell 1. [b] Cell 2.

the treatment of the data involves a knowledge of the several equilibria that may be involved.

The primary reaction for the formation of BeOH employing H_2 is

$$BeO(c) + {}^1/_2H_2(g) = BeOH(g) \quad (2)$$

Also to be considered are the reactions

$$BeO(c) + H_2(g) = Be(g) + H_2O(g) \quad (3)$$

and

$$2BeO(c) + H_2(g) = Be_2O(g) + H_2O(g) \quad (4)$$

and the dissociation of hydrogen

$${}^1/_2H_2(g) = H(g) \quad (5)$$

Of secondary importance is the reaction to form the hydroxide from the water which is formed as a result of reaction 3

$$BeO(c) + H_2O(g) = Be(OH)_2(g) \quad (6)$$

The measured quantities for an experiment included the weight loss of BeO and the number of moles of elemental hydrogen employed in the reaction. The total number of moles of H_2, $n_{T(H_2)}$ entering the reaction zone is distributed over reactions 2–5 as

$$n_{T(H_2)} = {}^1/_2n_{BeOH} + n_{H_2O} + {}^1/_2n_H + n_{H_2} \quad (7)$$

After consideration for the weight loss of BeO due to vaporization, the remainder of the weight loss of BeO could be attributed to reactions 2, 3, 4, and 6. The weight loss that would be attributed to reaction 6 as a result of the water formed in reaction 3 was negligible in the temperature range studied.[3] Calculations based on free-energy values given in the JANAF tables also showed that the contribution due to reaction 4 is also negligible. The value reported for the vaporization of liquid beryllium (ΔH_v of Be = 75.38 at 298°K kcal/mole) in the JANAF tables[4] is based on an analysis of several recent measurements.[5-9] Employing this value,

(4) "JANAF Thermochemical Tables," The Dow Chemical Co., Midland, Mich.

(5) E. Baur and R. Brunner, *Helv. Chim. Acta*, **17**, 958 (1934).

(6) C. L. McCabe and C. E. Birchenali, *J. Metals*, **5**, 707 (1953).

(7) R. B. Holden, R. Speiser, and H. L. Johnston, *J. Am. Chem. Soc.*, **70**, 3897 (1948).

(8) E. A. Gulbransen and K. F. Andrew, *J. Electrochem. Soc.*, **97**, 383 (1950).

calculations were made for the weight loss of BeO resulting from reaction 3. The remaining weight loss of BeO was attributed to the formation of BeOH. In all experiments the total pressure inside the cell ranged from approximately 0.4 to 0.8 mm. Mean free path calculations in the experimental temperature range indicate that for the cell dimensions the flow for this pressure range is molecular. Therefore, all calculations were based on the modified Knudsen equation

$$P = \frac{17.14G}{W_0 A t}\sqrt{\frac{T}{M}} \qquad (8)$$

where P is pressure in mm for the species inside the cell, G is the weight in grams of the gas species escaping through the effusion hole, W_0 is the Clausing factor which was calculated from the effusion orifice dimensions as given in Dushman,[10] A is the area in cm^2 of the effusion hole, t is the total time of reaction in seconds, T is temperature in °K, and M is the molecular weight of the species.

The contribution to the weight loss due to reaction 3 was approximately 10%. Although the vaporization data for Be are quite definitive, it was decided to perform a further check to ascertain that the major reaction was not reaction 3. This check is based on the pronounced effect on reaction 3 which can be brought about by adding a small amount of water vapor to the H_2. A calculation showed that at 2235°K and a total pressure of 0.7 mm the addition of 3 mole % water would cause a 75% reduction in weight loss, if this weight loss were primarily due to reaction 3. Such a reduction would occur despite the simultaneous enhancement of reaction 6. This water percentage represents an optimum since at higher percentages the ascendancy of reaction 6 begins to outweigh the reduction in reaction 3.

Thus for a 110-min run at 2235°K and 0.7-mm total pressure, calculations based on available data[4] for the formation of Be and water as a result of the reaction of hydrogen and BeO would predict a weight loss of 0.74 mg of BeO, while the 3 mole % water and 97 mole % H_2 mixture experiment would predict a weight loss of 0.2 mg of BeO. Since the total weight loss in the pure hydrogen experiments at this temperature ranged between 8 and 9 mg, a reduction of 6–7 mg would be expected if Be were the chief product formed. However, if the data[4] for the Be correction were fairly accurate, a negligible change would be expected in the water experiments. Two water experiments (3 mole %) were performed. The weight losses were 9.6 and 10.1 mg, respectively, while the pure hydrogen experiments recorded weight losses of 8.1 and 8.8 mg, respectively. Although a decrease of ~0.5 mg was theoretically predicted, an actual increase of from 0.8 to 2 mg occurred. An examination of the 30 experiments performed in a 300° temperature range shows that this discrepancy between the actual change and the predicted change of weight losses due to the addition of H_2O is within the scatter of the pure hydrogen experiments, *i.e.*, 1–2 mg reproducibility at a given temperature.

The results of the water experiments indicated that use of the published value for the heat of vaporization of Be would be valid. Therefore, a weight loss of BeO was calculated for reaction 3 by means of the Knudsen equation (eq 8) and the JANAF tables.[4] The remaining weight loss of BeO was assumed to be due to the formation of BeOH. The partial pressure of BeOH(g) was then calculated and an equilibrium constant was obtained for eq 2. These data are presented in Table I. The experimental study was initiated with cell 1 but after fracturing was replaced with cell 2 of different orifice thickness. Since the experimental procedure was the same and Clausing factors were calculated

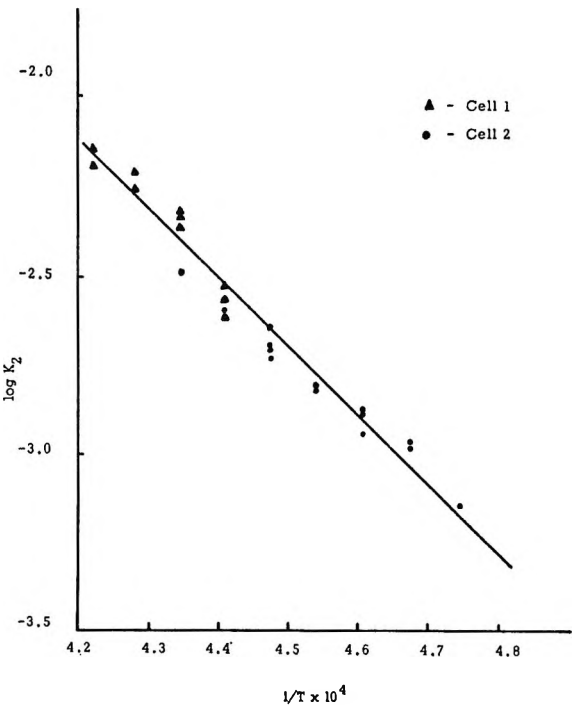

Figure 2. The log of the equilibrium constant for the reaction BeO(c) + $^1/_2H_2$(g) = Be(OH) (g) as a function of the reciprocal temperature.

(9) A. N. Nesmeyanov, "Vapor Pressure of the Chemical Elements," R. Gary, Ed., Elsevier Publishing Co., The Netherlands, 1963, p 172.

(10) S. Dushman, "Vacuum Technique," John Wiley and Sons, Inc., New York, N. Y., 1949.

Table II: Summary of Thermodynamic Data for the Reaction BeO(c) = $^1/_2H_2$(g) = BeOH(g)

	Second law	Third law
$\Delta H_r°_{2235°K}$	88.3 ± 3.8 kcal	87.2 ± 0.5 kcal
$\Delta H_r°_{298°K}$	96.3 ± 3.8 kcal	94.9 ± 0.5 kcal
$\Delta H_f°_{2235°K}$ BeOH(g)	−55.7 ± 3.8 kcal/mole	−56.7 ± 0.5 kcal/mole
$\Delta H_f°_{298°K}$ BeOH(g)	−46.8 ± 3.8 kcal/mole	−48.2 ± 0.5 kcal/mole
$\Delta S_r°_{2235°K}$	27.4 ± 1.7 cal/deg mole	
$S°_{2235°K}$ BeOH(g)	75.3 ± 1.7 cal/deg mole	
$S°_{298°K}$ BeOH(g)	54.0 ± 1.7 cal/deg mole	53.29 cal/deg mole[a]

[a] See ref 4.

for each cell, the data were treated as a single set for obtaining a least-squares analysis.

The plot of the experimental data in Table I in the form of log K_2 *vs.* $1/T$ is presented in Figure 2. A least-squares analysis of the data yields a value for the slope of the line which corresponds to 88.3 ± 3.8 kcal for ΔH_r at the average temperature of 2235°K. Similarly, a value for $\Delta S_{r,2235}$°K of 27.4 ± 1.7 cal/deg is obtained from the intercept of the curve. Employing the available thermodynamic values the thermal functions for BeO(c), H_2(g), and H(g) and thermal functions for BeOH(g),[4] the $\Delta H_f°_{298}$ and $S°_{298}$ for BeOH(g) are found to be −46.8 ± 3.81 kcal/mole and 54.0 ± 1.7 cal/deg mole, respectively. The corresponding average third-law value for the heat of reaction, $\Delta H_{r,2235°K}$, is 87.2 ± 0.5 kcal. The third-law $\Delta H_f°_{298}$ for BeOH(g) is calculated as −48.2 ± 0.5 kcal/mole. The only reported entropy value of BeOH(g)[4] is 53.29 cal/deg mole. The quoted uncertainties in the second and third-law values are the statistical uncertainties which do not include systematical ones and those involved in extrapolation from experimental temperatures to 298°K. In addition, they do not include the uncertainties of the other data used in the calculation. A summary of the thermodynamic functions for BeOH(g) is presented in Table II.

Summary

The excellent second- and third-law agreement, supported by the experiments performed employing a mixture of hydrogen and water, establish the validity of the reaction of BeO with H_2 to produce BeOH. The recommended values for heat of formation and entropy of BeOH(g) at 298°K are −47.0 ± 2 kcal/mole and 54.0 ± 1 cal/deg mole, respectively.

The Law of Corresponding States in Its Most General Form

by Reino W. Hakala

Department of Chemistry and Chemical Engineering and Department of Mathematics, Michigan Technological University, Houghton, Michigan 49931 *(Received November 15, 1966)*

It is shown that any two-body intermolecular potential function can be put into a dimensionless form involving only one energy parameter, e_0, and only one length parameter, r_0, in addition to any dimensionless intermolecular potential function-shape parameters C_1, C_2, ... and any dimensionless electrostatic parameters $\mu^2/e_0r_0^3$, $Q^2/e_0r_0^5$, ..., where μ, Q, ... are dipole, quadrupole, ... moments. Use is made of this result to derive the most general form of the law of corresponding states for PVT behavior at moderate densities by means of a completely general and systematic dimensional analysis procedure. The result, readily transferable to any equilibrium or transport bulk property in reduced form, is $Pv/nRT = f(v/r_0^3, kT/e_0, C_1, C_2, \ldots, \alpha/r_0^3, \mu^2/e_0r_0^3, Q^2/e_0r_0^5, \ldots, M, \Delta^*)$ where Δ^* is a new quantum-deviation parameter, combining into a single variable the quantum deviations from the classical law of corresponding states due to translation, rotation, vibration, and electronic transitions, the C_i's are intermolecular potential function-shape factors, and the other symbols have their usual meanings. Alternatively, $PV/RT = f[V/V_c, T/T_c, w_1, w_2, \ldots, \alpha N/V_c, \mu^2N/V_ckT_c, Q^2(N/V_c)^{5/3}/kT_c, \ldots, M, \Delta^{(c)}]$ where $\Delta^{(c)}$ is another general quantum-deviation parameter related to Δ^*, w_1, w_2, ... are molecular geometry parameters, and the other symbols are standard. Inclusion of the molecular weight, M, is considered here for the first time.

Introduction

The law of corresponding states has been extended considerably since it was introduced by van der Waals. Parameters are now included to account for molecular geometry and polarity and for a translational quantum effect. Because the law of corresponding states is an essentially universal relationship among dimensionless variables, it is natural to examine it from the viewpoint of dimensionless analysis. This has been done in the past, but not completely systematically and not including all of the important variables. We shall present a fully systematic dimensional analysis of PVT behavior accounting for all of the known variables. The results can readily be transferred to any bulk property.

General Form of the Intermolecular Potential Function

In order that our treatment be fundamental, we shall carry out the dimensional analysis in the light of the two-body intermolecular potential function. Other discussions of the law of corresponding states from the potential function point of view have been restricted to two-parameter, two-body intermolecular potential functions. This restriction to two-parameter functions is not necessary because any two-body intermolecular potential function, no matter how many parameters it contains, is reducible to a dimensionless form involving only one energy parameter, e_0, and only one length parameter, r_0, the remaining parameters all being dimensionless. This important fact, apparently not taken note of previously, will now be proved. (Multibody intermolecular potential functions can be treated the same way; more energy and length parameters will then be involved.)

According to the fundamental theorem of dimensional analysis,[1] a necessary and sufficient condition

(1) This is traditionally referred to as "Buckingham's theorem," though his statement of it (E. Buckingham, *Phys. Rev.*, 4, 354 (1914)) lacks generality. For completely general proofs, see H. L. Langhaar, *J. Franklin Inst.*, 242, 459 (1946); H. L. Langhaar, "Dimensional Analysis and the Theory of Models," John Wiley and Sons, Inc., New York, N. Y., 1951; E. R. Van Driest, *J. Appl. Mech.*, 13, A-34 (1946); G. Birkhoff, "Hydrodynamics," Princeton University Press, Princeton, N. J., 1950; R. W. Hakala, *J. Chem. Educ.*, 41, 380 (1964) (elementary proof).

that an equation be dimensionally homogeneous is that it be reducible to a relationship among dimensionless power products. Any intermolecular potential function is dimensionally homogeneous, since each term has the dimensions of energy. Dividing through by e_0 evidently renders each term dimensionless. According to the fundamental theorem, the resulting equation is such that, or it can be reduced further so that, the intermolecular separation, r, always occurs in the form of a dimensionless power product ar^b, where the power b is a positive or negative pure number and the factor a necessarily possesses the same dimensions as r^{-b}, in whatever types of terms (linear, exponential, etc.) r occurs. Let us now multiply a by r_0^b and divide r^b by r_0^b. The general result is $(ar_0^b)\cdot(r/r_0^b)$. The power product(s) ar_0^b is (are) evidently dimensionless. This completes the proof that only one energy parameter and only one length parameter are required in any intermolecular potential function. We shall now inquire into the general form of the intermolecular potential function.

In the nonelectrostatic part of the intermolecular potential function, the dimensionless power products ar_0^b are obviously related to the shape of the potential function. We shall therefore call the factors ar_0^b the "intermolecular potential function-shape parameters" and shall denote them by C_1, C_2, ... Each of the electrostatic terms, if any, of the original nonreduced potential function is of either of the two general forms

$$\{c[p^{(2n)}]^2/r^{2n+1}\}F$$

$$\{dp^{(2m)}p^{(2n)}/r^{m+n+1}\}G$$

where c, d, m, and n, are pure numbers, $p^{(2m)}$ and $p^{(2n)}$ are 2^m- and 2^n-pole moments, and F and G are the dimensionless angular dependences, including the signs, of the corresponding electrostatic interactions between two molecules. Reduction of these terms to dimensionless form is a simple matter. Proceeding as before, the results are

$$\{c[p^{(2n)}]^2/e_0r_0^{2n+1}\}(r_0/r)^{2n+1}F$$

and

$$\{dp^{(2m)}p^{(2n)}/e_0r_0^{m+n+1}\}(r_0/r)^{m+n+1}G$$

Thus, for the electrostatic part of the intermolecular potential function, the dimensionless factors ar_0^b are identified with

$$\{c[p^{(2n)}]^2/e_0r_0^{2n+1}\}F$$

and

$$\{dp^{(2m)}p^{(2n)}/e_0r_0^{m+n+1}\}G$$

Therefore, completely generally, the mutual potential energy of two molecules is given by the dimensionless expression

$$\Phi(r;\theta_A,\theta_B,\phi_A,\phi_B,\ldots)/e_0 = f\{r/r_0;C_1,C_2,\ldots;[p^{(2m)}]^2/e_0r_0^{2m+1},[p^{(2n)}]^2/e_0r_0^{2n+1},\ldots;\theta_A,\theta_B,\phi_A,\phi_B,\ldots\}$$

where θ_A, θ_B, ϕ_A, ϕ_B, ... are the angles involved in F, G, ... It is not necessary to include any multipole-moment-product parameters $p^{(2m)}p^{(2n)}/e_0r_0^{m+n+1}$ among the variables in the general form of the intermolecular potential function because they are the geometric means of the multipole-moment-square parameters $[p^{(2m)}]^2/e_0r_0^{2m+n+1}$ and $[p^{(2n)}]^2/e_0r_0^{2n+1}$ and are therefore not independent. It should be noted that the physical meanings of e_0 and r_0 (the depth of the potential well, the value of r for which $\Phi = 0$, etc.) will generally differ from one type of potential function to another.

By way of example, we shall superimpose point dipole–dipole, dipole–quadrupole, and quadrupole–quadrupole interaction terms on a Buckingham–Corner potential function. The resulting potential function can be written in the dimensionless form

$$\Phi(r;\theta_A,\theta_B,\phi_A,\phi_B)/e_0 = \exp(-C_1r/r_0) - [C_2(r_0/r)^6 + C_3(r_0/r)^8] \times \exp[-4(r_0/r-1)^3] - (\mu^2/e_0r_0^3)(r_0/r)^3F(\theta_A,\theta_B,\phi_A,\phi_B) + (3\mu Q/4e_0r_0^4)(r_0/r)^4G(\theta_A,\theta_B,\phi_A,\phi_B) + (3Q^2/16e_0r_0^5)(r_0/r)^5H(\theta_A,\theta_B,\phi_A,\phi_B)$$

Dimensional Analysis of PVT Behavior

Besides the parameters e_0, r_0, C_1, C_2, ..., and the various multipole moments (if not zero), other important molecular parameters that we shall take into account are the polarizability, α; the molecular mass, m; the moment of inertia, I, in the case of linear molecules, or, for nonlinear molecules, the product, ABC, of the principal moments of inertia; the various vibrational frequencies, ν_1, ν_2, ...; and the various electronic energy levels, ϵ_1, ϵ_2, ... Since translational, rotational, vibrational, and electronic energies are all quantized, Planck's constant, h, must also be included as a variable.

Although the law of corresponding states applies to any bulk property of the system, for both equilibrium and transport phenomena, we shall find it convenient to center our attention on PVT relationships. Thus, we shall also include among our variables the pressure, volume, and absolute temperature of the

system. As any one of these depends on the other two and on the quantity of material present in the system, the number of moles, n, likewise must be included. If we were to carry out a theoretical treatment of the problem, the temperature would enter solely as the product kT with Boltzmann's constant, and Avogadro's number, N, would be involved; these will therefore be included among our variables.

Denoting the dimensional variables mass, length, and time, as is customary, by the respective symbols, M, L, and T, the dimensional matrix of the variables we shall consider is

	P	v	kT	n	N	e_0	r_0	C	α	μ^2	Q^2	m	I	ν	ϵ	h
M	1	0	1	1	−1	1	0	0	0	1	1	1	1	0	1	1
L	−1	3	2	0	0	2	1	0	3	5	7	0	2	0	2	2
T	−2	0	−2	0	0	−2	0	0	0	−2	−2	0	0	−1	−2	−1

For simplicity, instead of listing C_1, C_2, ..., ν_1, ν_2, ..., and ϵ_1, ϵ_2, ..., only C, ν, and ϵ are given and I is used to represent either I or $(ABC)^{1/3}$, whichever applies. Each column of this matrix represents a dimensional equation, such as $[P] = ML^{-1}T^{-2}$ for the first column on the left.

It may be helpful to indicate how the dimensional formulas of certain ones of the variables were determined. One might think, offhand, that the number of moles of a substance is a dimensionless quantity, but further consideration shows that such is not the case. The number of moles is calculated by dividing the number of grams of a substance by its molecular weight, whence the dimensions of the number of moles are mass divided by the dimensions of molecular weight. The latter is a relative mass (currently, 12 times the mass of a given molecule divided by the mass of one carbon 12 atom) and is therefore dimensionless. As a consequence, we have the dimensional relationship $[n] = M$. Avogadro's number, the number of molecules per mole, then has the dimensions M^{-1}. (We might remark that molecular weight has *units*, grams per mole, although it has no *dimensions*. This seeming paradox, stemming from a confusion between units and dimensions, has caused much needless trouble in dimensional analysis.) The dimensions of the dipole and quadrupole moments depend on the dimensions of electric charge. The latter is usually taken to be a fundamental dimensional quantity but shall be regarded here as a derived physical quantity. According to Coulomb's law, assuming the proportionality constant to be dimensionless, the dimensions of electric charge are the dimensions of distance times the square root of the force or, in terms of the dimensional variables of the above matrix, $M^{1/2}L^{3/2}T^{-1}$. Therefore, $[\mu] = M^{1/2}L^{5/2}T^{-1}$, $[Q] = M^{1/2}L^{7/2}T^{-1}$, and similarly for higher multipole moments. The dimensional formulas of the remaining variables are all obvious.

A corollary of the fundamental theorem of dimensional analysis is that the number of independent dimensionless power products in a complete set is equal to the total number of variables (listed at the top of the dimensional matrix) minus the rank of the dimensional matrix.[2] The rank of a matrix is defined as the order of the greatest order nonzero determinant of a square submatrix obtained by deleting columns and, if necessary, rows from the matrix. The rank of the above dimensional matrix is 3 because, for example, the determinant of the second, third, and fourth columns does not vanish (even though those of the first and last three columns and of various other columns vanish). Therefore there are 12 independent dimensionless power products of the variables in a complete set, not counting C which is dimensionless to begin with. There are, of course, any number of complete sets from which we are to choose one particular complete set. This choice is best dictated by physical considerations. With as many variables as we have decided to relate to one another, it would be difficult to find a complete set of independent dimensionless power products without some kind of systematic procedure. The only fully systematic procedure in the previous literature appears to be that of Langhaar,[1,3] but it is not suitable in the present application. The simplest and most productive way to proceed is first to consider the smallest possible physically significant submatrix and then to increase the number of columns of the sub-

(2) H. L. Langhaar (see ref 1). We shall refer to this corollary as Langhaar's theorem. It is completely general whereas the corresponding much-quoted principle of Buckingham, which substitutes the number of dimensional variables involved for the rank of the dimensional matrix, lacks complete generality, as was first pointed out by P. W. Bridgman, "Dimensional Analysis," Yale University Press, New Haven, Conn., 1922.

(3) If the total number of variables is v and the rank of the dimensional matrix is r, then each of $(v - r)$ of the variables is combined into a dimensionless power product with the same remaining r variables. These $(v - r)$ power products are independent because the rank of the matrix of the solutions is necessarily equal to the number of rows in the matrix, which is $(v - r)$. Langhaar's procedure, for which he has developed an automatic numerical scheme, therefore always generates a complete set.

matrix, by one column each time, until all of the variables are accounted for.

The smallest physically significant submatrix consists of the first five columns of the dimensional matrix, which contain only general physical variables as opposed to molecular variables (except for Planck's constant which, however, we do not need to consider until we take into account the variables m, I, ν, and ϵ). Langhaar's theorem indicates that two independent dimensionless power products are related to one another. One of these is evidently nN, the total number of molecules in the system. Both kT and Pv have the dimensions of energy, whence Pv/kT is the other dimensionless power product that is sought. The combination NkT occurs in theoretical studies. Hence we shall form the combination $Pv/nNkT$. This is the same as PV/RT, the compressibility factor. Had we at the outset combined N and k to give R, there would have been only four variables and therefore only one possible dimensionless power product, PV/RT (or any power thereof), which must be equal to a universal constant if no other variables are important. We have thus derived the ideal gas law, except that the actual value of the universal constant (= 1) is not given by dimensional analysis.

According to statistical mechanics, the pressure of a system is given by

$$P = kT\left(\frac{\partial \ln Q_N}{\partial v}\right)_T$$

where Q_N is the total molar partition function. Assuming that

$$E = E_{tr} + E_{rot} + E_{vib} + E_{el} + E_{potential}$$

which is adequate at moderate densities, whence

$$Q_N = (Q_N)_{tr}(Q_N)_{rot}(Q_N)_{vib}(Q_N)_{el}(Q_N)_{potential}$$

we find that

$$\frac{PV}{RT} = 1 + \frac{V}{N}\left[\frac{\partial \ln (Q_N)_{potential}}{\partial v}\right]_T$$

since only the translational and potential partition functions depend on the volume. Consequently, deviations from the ideal gas law depend on the parameters of the intermolecular potential function. Hence we shall next consider combinations of P, v, and kT with these parameters. At first, we shall disregard any electrostatic interactions.

The only possible dimensionless combinations of e_0 and r_0 with P, v, and kT taken separately are Pr_0^3/e_0, v/r_0^3, and kT/e_0. Only two of these are independent, however, because the product of the first two divided by the third equals Pv/kT. A convenient pair to take for later discussion is v/r_0^3 and kT/e_0, although any two can be selected. The value of PV/RT will also depend on the values of any intermolecular potential function-shape factors, C_1, C_2, ... Thus far, we have derived the relationship[4] $PV/RT = f(v/r_0^3, kT/e_0, C_1, C_2, \ldots)$ which must be a universal function, according to dimensional analysis, if no other variables are important. If we omit C_1, C_2, ..., as is customary, then the result can apply only to substances whose potential functions are of the same type[5] and the same shape.

Since r_0^3 and e_0/k are proportional, respectively, to the critical molar volume, V_c, and the critical temperature, T_c, it is permissible to make these substitutions in the above relationship. As the proportionality constants depend on the molecular geometry, the latter is also a variable.[5] We can take it into account by replacing C_1, C_2, ... by the molecular shape factors $w_1, w_2, \ldots$. Thus, we have

$$PV/RT = f(V/V_c, T/T_c, w_1, w_2, \ldots)$$

In general, there will be *more than one* molecular shape factor. If the dependence of PV/RT on molecular geometry is neglected, this result retrogresses to the primitive form of the law of corresponding states.

Commonly, for experimental convenience, V/V_c is also replaced by P/P_c, in analogy to the permissible substitution of v/v_0^3 by Pr_0^3/e_0, but the analogy is not exact. The difficulty is that Pr_0^3/e_0 is directly proportional to PV_c/NkT_c, which is *not* directly proportional to P/P_c since P_cV_c/NkT_c is not a function of the molecular geometry alone. Thus, the fundamental critical constants in the law of corresponding states are T_c and V_c, not T_c and P_c, and the proper form for the reduced pressure is PV_c/RT_c, not P/P_c, an important feature of the law of corresponding states which appears to have been overlooked previously.

Since our study has thus far not taken into consideration any electrostatic interactions, it is necessarily restricted to substances of which the molecules possess identical values of the polarizability and their multipole moments in reduced form. There is no reason, however, to restrict the primitive form of the law of corresponding states to only nonpolar substances, as is often done. All that is required is that they be of equal, or nearly equal, reduced polarity, as well as of equal reduced polarizability. (The latter condition is more readily met.) We shall now find out how to compare substances of different polarizabilities and polarities.

(4) Omitting C_1, C_2, ..., this was first derived by J. de Boer, Doctoral Dissertation, University of Amsterdam, The Netherlands, 1940; *Physica*, **14**, 139 (1948)

(5) K. S. Pitzer, *J. Am. Chem. Soc.*, **77**, 3427 (1955), reached the same conclusion but in a different way.

We extend our submatrix further to include the α, μ^2, and Q^2 columns. Langhaar's theorem indicates that we should thereby obtain three new dimensionless power products, one for each new variable introduced. The most convenient combinations are with the intermolecular potential function parameters r_0 and e_0: α/r_0^3, $\mu^2/e_0r_0^3$, and $Q^2/e_0r_0^5$. As these are mathematically independent, our subset of dimensionless power products is complete. An infinite number of complete subsets is possible; we have selected the most convenient one, *e.g.*, we could have included the dipole–quadrupole interaction parameter $\mu Q/e_0r_0^4$ in place of either the dipole–dipole or quadrupole–quadrupole interaction parameter, but the last two are more convenient and inclusion of both in the subset also accounts for dipole–quadrupole interactions. The dimensionless power product $\mu^2/e_0r_0^3$ is well known as a correlation parameter for polar substances, whereas the quadrupole–quadrupole interaction parameter is not.

Higher multipole interactions can be included by inserting the corresponding higher multiple moment columns into the dimensional matrix. The corresponding dimensionless power products with r_0 and e_0 are very easy to obtain.

According to the statistical mechanical formula given earlier for the compressibility factor, we have completed our task. But quantum mechanical effects have not been accounted for because we have not yet considered Planck's constant as a variable. The variables m, I, ν, and ϵ are all related to h, as has already been indicated. We must therefore find dimensionless combinations of each of these variables with h wherever possible and e_0 and r_0 where required. These dimensionless power products are readily found to be[6] $h^2/me_0r_0^2$, h^2/Ie_0 (or $h^2/(ABC)^{1/3}e_0$), $h\nu/e_0$, and ϵ/e_0. It turns out that, even though electronic energy is quantized, h does not appear in the simplest possible dimensionless power product for ϵ. There will, of course, be a separate combination $h\nu/e_0$ and ϵ/e_0 for each vibrational and electronic energy level.

If we replace r_0 by $(V_c/N)^{1/3}$, which has the same dimensions as r_0, and e_0 by kT_c in the quantum-deviation parameters for the molecular mass and the moment(s) of inertia, we obtain parameters which are evidently directly related to the translational and rotational molecular partition functions at the critical point[7]

$$Q_{tr}^{(c)}/nN = (V_c/N)(2\pi mkT_c)^{3/2}/h^3$$

$$Q_{rot}^{(c)}(\text{linear}) = 8\pi^2IkT_c/\sigma h^2$$

$$Q_{rot}^{(c)}(\text{nonlinear}) = (8\pi^2kT_c)^{3/2}(\pi ABC)^{1/2}/\sigma h^3$$

The quantum-deviation parameter for vibration becomes $h\nu/kT_c$ which is the exponent in the vibrational molecular partition function at the critical point

$$Q_{vib}^{(c)}(\text{per mode of vibration}) = [1 - \exp(-h\nu/kT_c)]^{-1}$$

Finally, ϵ/e_0 becomes ϵ/kT_c which is the exponent in the electronic partition function at the critical point

$$Q_{el}^{(c)} = \sum g_i \exp(-\epsilon_i/kT_c)$$

Since all bulk properties of a given system are functions of its total partition function, which is the product of the partition functions corresponding to the various kinds of energy (assuming the energies to be additive), it follows that the various quantum-deviation parameters can be combined into a single quantum-deviation parameter

$$\Delta^{(c)} = nN/(Q_{tr}Q_{rot}Q_{el}\Pi Q_{vib})^c$$

where the product ΠQ_{vib} is over all modes of vibration. The reciprocal of the partition function product at the critical point is used, rather than the partition function product itself, because h then occurs in the numerator whence the smaller the quantum-deviation parameter, the smaller is the quantum effect. If the intermolecular potential function parameters r_0 and e_0 are used in place of $(V_c/N)^{1/3}$ and kT_c in $\Delta^{(c)}$, then, by analogy to de Boer's translational quantum-deviation parameter which is denoted by Λ^*, we shall employ the notation Δ^*.

We have found a total of eleven independent dimensionless power products (nN, Pv/kT, v/r_0^3, kT/e_0, α/r_0^3, $\mu^2/e_0r_0^3$, $Q^2/e_0r_0^5$, $h^2/me_0r_0^2$, h^2/Ie_0, $h\nu/e_0$, and ϵ/e_0) whereas Langhaar's theorem indicates that there must be altogether 12 (15 variables, not including C which is dimensionless to begin with, minus the rank, 3, of the dimensional matrix). In our systematic procedure for generating physically significant independent dimensionless power products, we divided the variables into four classes: P, v, kT, n, and N; e_0 and r_0;

(6) C. S. Wang Chang, Doctoral Dissertation, University of Michigan, 1944, showed that for linear rigid rotors there are quantum deviations from the second virial coefficient which depend upon h^2/m and h^2/I, in agreement with the above results. The complete translational parameter $h/(me_0)^{1/2}r_0$ was later found and was applied successfully by deBoer and his co-workers: J. deBoer and B. S. Blaisse, *Physica*, **14**, 149 (1948); J. deBoer and R. J. Lunbeck, *ibid.*, **14**, 520 (1948); R. J. Lunbeck, Doctoral Dissertation, University of Amsterdam, 1951. Pitzer[5] also obtained the complete translational parameter. The remaining two parameters have not been considered previously.

(7) The quantum-deviation parameter $h(N/V_c)^{1/3}/(mkT_c)^{1/2}$, which we see is equal to $(2\pi)^{1/2}[nN/Q_{tr}^{(c)}]^{1/3}$, was introduced, with the aid of dimensional analysis, by A. Byk, *Ann. Phys.*, **42**, 1417 (1913); **66**, 157 (1921); **69**, 161 (1922); *Physik. Z.*, **22**, 15 (1921); *Z. Physik. Chem.* (Leipzig), **110**, 291 (1924). Byk was the first author to consider quantum deviations from the classical law of corresponding states.

μ^2, Q^2, ...; and m, I, ν, ϵ, and h. We related the variables in the first class to one another and to those in the second class and those in the second class to those in the third and fourth classes, but we did not relate any of the variables in the first class to those in the third and fourth classes, whence this remains to be done. One such simple combination is Nm, the molecular weight. This has not been suggested previously as a parameter in the law of corresponding states. As it is independent of the other dimensionless power products, its inclusion completes the set.

We shall now check whether the twelve dimensionless power products we have found are indeed independent. We shall employ the theorem from the theory of equations according to which the number of independent equations in a system of linear equations is equal to the rank of the matrix of the coefficients. (Langhaar's theorem is also a corollary of this one.) In the present application, the rank of the dimensional matrix of the 12 dimensionless power products will be 12 if the power products are independent. The matrix of the set of dimensionless power products that we have chosen is

	P	v	kT	n	N	e_0	r_0	α	μ^2	Q^2	m	I	ν	ϵ	h
hN	0	0	0	1	1	0	0	0	0	0	0	0	0	0	0
Pv/kT	1	1	−1	0	0	0	0	0	0	0	0	0	0	0	0
v/r_0^3	0	1	0	0	0	0	−3	0	0	0	0	0	0	0	0
kT/e_0	0	0	1	0	0	−1	0	0	0	0	0	0	0	0	0
α/r_0^3	0	0	0	0	0	0	−3	1	0	0	0	0	0	0	0
$\mu^2/e_0r_0^3$	0	0	0	0	0	−1	−3	0	1	0	0	0	0	0	0
$Q^2/e_0r_0^5$	0	0	0	0	0	−1	−5	0	0	1	0	0	0	0	0
$h^2/me_0r_0^2$	0	0	0	0	0	−1	−2	0	0	0	−1	0	0	0	2
h^2/Ie_0	0	0	0	0	0	−1	0	0	0	0	0	−1	0	0	2
$h\nu/e_0$	0	0	0	0	0	−1	0	0	0	0	0	0	1	0	1
ϵ/e_0	0	0	0	0	0	−1	0	0	0	0	0	0	0	1	0
Nm	0	0	0	0	1	0	0	0	0	0	1	0	0	0	0

(It should be noted that the roles of the dependent and independent dimensional variables are reversed in the two matrices.) If a 12 × 12 submatrix with a nonvanishing determinant occurs in this matrix (which contains altogether 15!/12! 3!, or 455, different 12 × 12 submatrices), then the rank of the matrix is 12, whence each member of the chosen set of 12 dimensionless power products is independent and the set is complete. The sparsest 12 × 12 submatrix (obtained by deleting the e_0, r_0, and h colunns) can be partitioned into upper pseudo-triangular form, and the two subdeterminants lying along the principal diagonal of this submatrix are readily reduced to lower order and diagonal form by Laplace's development. In this way, the value of the determinant of the sparsest submatrix was very quickly found to equal unity, thereby proving that our set is complete.

Conclusion

We have found by means of dimensional analysis that the most general possible form of the law of corresponding states for PVT behavior at all moderate densities is

$$PV/RT = f(v/r_0^3, kT/e_0, kT/e_0, C_1, C_2, \ldots, \alpha/r_0^3, \mu^2/e_0r_0^3, Q^2/e_0r_0^5, \ldots, M, \Delta^*)$$

which includes several dimensionless power products not considered previously, including the molecular weight, M, and the new quantum-deviation parameter, Δ^*. The latter is obtained from the reciprocal of the total molecular partition function at the critical point by multiplying the reciprocal by nN, the product of the number of moles of substance present in the system and Avogadro's number, and then replacing $(V_c/N)^{1/3}$ and kT_c, respectively, by the intermolecular potential function parameters r_0 and e_0. The parameter Δ^* accounts for translational, rotational, vibrational, and electronic quantum effects; previous quantum-deviation parameters are special cases of this one.

In terms of the critical constants, this result can be written in the form

$$PV/RT = f[V/V_c, T/T_c, w_1, w_2, \ldots, \alpha N/V_c, \mu^2N/V_ckT_c, Q^2(N/V_c)^{5/3}/kT_c, \ldots, M, \Delta^{(c)}]$$

where w_1, w_2,... are molecular geometry parameters, of which there may be more than one, $\Delta^{(c)}$ is the quantum-deviation parameter Δ^* with r_0 and e_0 replaced by their dimensional equivalents $(V_c/N)^{1/3}$ and kT_c, and the other symbols have their usual meanings.

The parameter v/r_0^3 can be replaced by Pr_0^3/e_0 and correspondingly, V/V_c by PV_c/RT_c, but not, without some loss of accuracy, by P/P_c, contrary to current practice.

These results may be carried over readily to any bulk property which has been put into the appropriate reduced form.

Acknowledgment. The author is grateful to the Faculty Research Committee of Michigan Technological University for financial assistance.

Mean Activity Coefficient of Polyelectrolytes. V. Measurements of Polyvinyl Sulfates of Various Gegenions

by Norio Ise and Tsuneo Okubo

Department of Polymer Chemistry, Kyoto University, Kyoto, Japan (*Received November 17, 1966*)

The mean activity coefficients of various salts of polyvinyl sulfuric acid (PVAS) have been determined by the isopiestic vapor pressure measurements. It has been found that the logarithm of the mean activity coefficient decreases linearly with the cube root of polymer concentration up to 0.5 equiv/1000 g of water. The slopes of the cube-root plots are −0.60, −0.65, −0.97, −1.31, and −1.52 for lithium, sodium, potassium, calcium, and barium salts, respectively. This order of the slope is in accord with what is expected from Gurney's rule. The magnitude of the slope for the sodium salt is found to be smaller than that of sodium polycarboxylate. This is accounted for in terms of the difference in the structural effects of sulfate ion and carboxylate ion.

Introduction

In previous papers, the mean activity coefficients of polyelectrolytes have been determined by the emf measurements of a concentration cell with transference[1-3] and the isopiestic vapor pressure measurements.[4] The results showed that first, the logarithm of the mean activity coefficient decreased linearly with the cube root of polymer concentration ("cube-root" rule). The magnitude of the slope of the cube-root plot increased with increasing charge density and decreased with increasing degree of polymerization of macroion. This cube-root rule suggested the existence of a "linkage" between macroions through the intermediary of gegenions. Second, it was found that the mean activity coefficients of polyelectrolytes could not be equal to the single-ion activity coefficients of its gegenions and the discrepancy between the two coefficients could be small for the low molecular weight electrolytes.

In the present paper, experimental data are reported on various salts of a polyvinyl sulfuric acid (PVAS). The isopiestic vapor pressure measurements were carried out in order to determine the osmotic and mean activity coefficients in a comparatively concentrated region of polymer concentration. One purpose of the present research is to see whether the cube-root rule holds for the sulfates and to study the specific gegenion effects on the osmotic and mean activity coefficients. Gegenion effects are expected to arise

(1) N. Ise and T. Okubo, *J. Phys. Chem.*, 69, 4102 (1965).
(2) N. Ise and T. Okubo, *ibid.*, 70, 1930 (1966).
(3) N. Ise and T. Okubo, *ibid.*, 70, 2400 (1966).
(4) N. Ise and T. Okubo, *ibid.*, 71, 1287 (1967).

Table I: Isopiestic Measurements of Salts of PVAS (25°)

Sample[a]	Polyelectrolyte, *m*, equiv/1000 g	KCl, *m*	φ_z[b]	Log (γ^*/γ^*_0)
LiPVAS	0.182	0.0526	0.544	−0.333
	0.201	0.0591	0.551	−0.350
	0.238	0.0723	0.566	−0.376
	0.290	0.0935	0.597	−0.400
	0.369	0.122	0.612	−0.433
	0.461	0.165	0.655	−0.452
	0.706	0.286	0.734	−0.474
	1.59	0.961	1.08	−0.360
NaPVAS	0.111	0.0352	0.600	−0.298
	0.133	0.0422	0.602	−0.328
	0.188	0.0633	0.632	−0.373
	0.261	0.0916	0.651	−0.418
	0.340	0.122	0.662	−0.452
	0.431	0.161	0.685	−0.476
	0.535	0.203	0.692	−0.502
	0.780	0.319	0.741	−0.513
	0.806	0.342	0.767	−0.520
	0.894	0.381	0.769	−0.510
	1.19	0.558	0.846	−0.520
KVPAS	0.229	0.0581	0.475	−0.592
	0.278	0.0710	0.476	−0.635
	0.374	0.0966	0.479	−0.700
	0.459	0.121	0.487	−0.744
	0.939	0.257	0.499	−0.901
	1.74	0.491	0.507	−1.03
	2.17	0.658	0.543	−1.06
CaPVAS	0.228	0.0352	0.293	−0.793
	0.275	0.0426	0.293	−0.851
	0.350	0.0554	0.297	−0.922
	0.469	0.0736	0.293	−1.01
	0.563	0.0888	0.293	−1.07
	0.708	0.115	0.300	−1.14
	0.856	0.147	0.315	−1.19
	1.23	0.251	0.372	−1.27
	1.54	0.382	0.448	−1.29
BaPVAS	0.163	0.0260	0.304	−0.819
	0.184	0.0290	0.299	−0.859
	0.207	0.0328	0.300	−0.894
	0.231	0.0357	0.293	−0.930
	0.272	0.0425	0.295	−0.979
	0.312	0.0470	0.284	−1.03
	0.393	0.0580	0.277	−1.10
	0.536	0.0788	0.274	−1.20
	1.62	0.268	0.302	−1.55
	2.52	0.645	0.459	−1.60

[a] The degree of neutralization is 1.00 for all of the samples. [b] The φ_z values were obtained by using φ_{KCl} values which were taken from R. A. Robinson and R. H. Stokes, "Electrolyte Solutions," Butterworth and Co., Ltd., London, 1959, p 476, Table I and p 481, Table I.

mainly from nonelectrostatic, short-range forces rather than electrostatic, long-range forces which are predominant when macroions are highly charged. Therefore we used a PVAS having a low charge density (degree of esterification 0.227). Another purpose is to compare the mean activity coefficient data of a polycarboxylate with those of a polysulfate.

Experimental Section

The aqueous solutions of various salts of PVAS, such as Li, Na, K, Ca, and Ba salts, were prepared as follows. A solution of potassium polyvinyl sulfate (a product of the Seikc Chemical Co., Fukuoka, Japan) was passed through a column of cation- and anion-exchange resins to convert the polymer to the acid form.[5] Then, the solution was neutralized with an aqueous solution of reagent grade LiOH, NaOH, KOH, $Ca(OH)_2$, or $Ba(OH)_2$. The degree of polymerization of the parent polyvinyl alcohol was 1700 in viscometry. The degree of esterification was 0.227, determined by both a titration method and sulfur analysis.

Osmotic and activity coefficients were determined by the isopiestic vapor pressure method at 25 ± 0.005° with an apparatus employed by us earlier.[4] The experimental error of the isopiestic measurements was about 2% in the osmotic coefficient value at the highest.

Results

The measured concentrations of the solutions of PVAS salts and potassium chloride in isopiestic equilibria are listed in the second and third columns of Table I, respectively.

The practical osmotic coefficient of the polyelectrolyte (φ_z) was calculated by the equation

$$\varphi_z = \frac{2m_{KCl}}{(z+1)(m/z)}\varphi_{KCl} \qquad (1)$$

where m_{KCl} is the molality of the reference potassium chloride solution, m the concentration of the salts of PVAS (equiv/1000 g of water), z the stoichiometric valency of macroion, and φ_{KCl} the practical osmotic coefficient of potassium chloride solution. It should be noted here that the osmotic coefficient dealt with in the present paper is the one defined on the basis of the stoichiometric number of ions, not of the free ions.[6] The osmotic coefficient obtained was generally found to increase with increasing concentration as is clearly

(5) The polyvinyl sulfate was stable in passing through the ion-exchange column, which was ascertained by sulfur analysis.

(6) In ref 4, the osmotic coefficient of a polyacrylate was determined using $\varphi = 2m_{KCl}/[(\alpha + 1)(m/z)]\varphi_{KCl}$, where α is the effective valency of the macroion, instead of eq 1 in the present text.

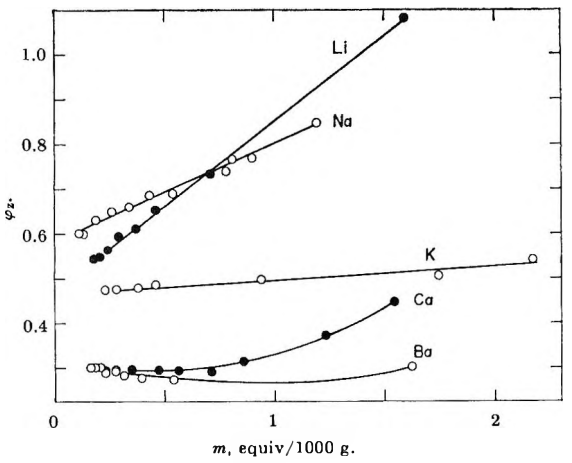

Figure 1. Osmotic coefficients of the aqueous solutions of various polyvinyl sulfates (25°).

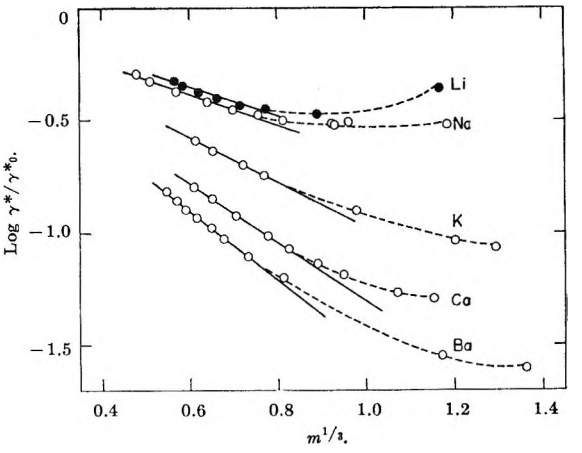

Figure 2. Cube-root plots of the mean activity coefficients of various polyvinyl sulfates in water (25°).

seen from the fourth column of Table I and Figure 1. This tendency is the same as found by Alexandrowicz[7] and us[4] for sodium polyacrylate and was earlier discussed in terms of the excluded volume effect by one of the present authors.[8] Figure 1 also demonstrates that the osmotic coefficient of the polyelectrolyte depends sharply on the gegenions. The order of the magnitude of the coefficient is

$$\text{Li} \approx \text{Na} > \text{K} > \text{Ca} > \text{Ba} \qquad \text{(A)}$$

This order for the polyelectrolytes is the same as that usually found for the salts of a low molecular weight strong acid.[9]

The mean activity coefficients (γ^*) were calculated using the rearranged Gibbs–Duhem relation, *i.e.*

$$\ln (\gamma_1^*/\gamma_2^*) = \varphi_{z1} - \varphi_{z2} + 2\int_{m_1}^{m_2} \frac{1-\varphi_z}{\sqrt{m}} d\sqrt{m} \qquad (2)$$

where the subscripts 1 and 2 correspond to m_1 and m_2, respectively. As previously mentioned,[1] the familiar assumption that the activity coefficient of electrolytes is unity at infinite dilution cannot generally be accepted for polyelectrolytes. This is due to the polyionic work, using Hayman's terminology.[10] It appears reasonable, however, to regard this work at infinite dilution as independent of the nature of the gegenions, since it is determined by the dielectric constant, electric charge, distance between ionized groups, and number of the groups. Thus, we may assume that the activity coefficients of the various salts of PVAS have the same value at infinite dilution, *i.e.*, γ^*_0. By assuming that the cube-root rule holds down to infinite dilution,[11] $\log \gamma^*/\gamma^*_0$ can be calculated for various salts and concentrations from the osmotic coefficient. The results are given in the fifth column of Table I and in Figure 2.

As is readily seen from the figure, the cube-root dependence holds for all salts studied except at higher concentrations. The slopes of the straight lines are −0.60, −0.65, −0.97, −1.31, and −1.52 for Li-, Na-, K-, Ca-, and BaPVAS, respectively. The magnitude of the slope is in the order

$$\text{Li} < \text{Na} < \text{K} < \text{Ca} < \text{Ba} \qquad \text{(B)}$$

Thus the nature of gegenions is seen to be an important factor influencing the solution property of polyelectrolytes.[12]

Discussion

In the above sections, the experimental data of the osmotic and mean activity coefficients of the PVAS salts were presented. These two coefficients are interrelated to each other so that our subsequent discussion will be limited to the mean activity coefficient.

In previous papers,[2-4] it was reported that the cube-root plot has long straight segments for the mean activity coefficients of some polyelectrolytes. Figure 2 shows that the rule also holds for the PVAS salts, up to about 0.5 equiv/1000 g of water. Again we notice that the upper limit of concentration, at which the

(7) Z. Alexandrowicz, *J. Polymer Sci.*, **56**, 115 (1962).

(8) N. Ise and M. Hosono, *ibid.*, **39**, 389 (1959).

(9) H. S. Harned and B. B. Owen, "The Physical Chemistry of Electrolytic Solutions," Reinhold Publishing Corp., New York, N. Y., 1958, Chapter 12.

(10) H. J. G. Hayman, *J. Chem. Phys.*, **22**, 1234 (1954).

(11) This is a rather crude assumption at present. There exists neither theoretical nor experimental support for this concentration dependence in *very* dilute regions.

(12) The degree of polymerization and charge density of the macroion are also influential factors as was clearly demonstrated in ref 2.

experimental data begin to deviate upward from the straight line, is much higher for the PVAS salts than for 1–1 type electrolytes.[13] Thus the previous interpretation, that the local regularity in ionic distribution can be more easily formed in polyelectrolyte solutions than in simple electrolyte solutions, proves to have obtained a new experimental support.

Discussion is now desirable on the relative order of the mean activity coefficients of the PVAS salts. For 1–1 type electrolytes, as is well known, Gurney found a rule that electrolytes composed of ions of dissimilar influence on the water structure have larger mean activity coefficients than those of ions of similar character.[14] In other words, the mean activity coefficient decreases most sharply with increasing concentration when the anion and cation are most similar in their structure effect, according to Frank and Thompson.[13] Since the entropy value, a measure of the structure effect, is not available for the macroions, we expediently use the value of HSO_3^- for ionized group of the polysulfates. The conventional partial molal entropy of this anion is reported as $+32.6 = 1.5$ eu on the scale of zero for proton, indicating the structure-breaking nature of the anion, and the values for Li^+, Na^+, and K^+ are $+4.7 \pm 1.0$, $+14.0 \pm 0.4$, and $+24.2. \pm 0.2$, respectively.[15] Therefore it is clear that the experimental data given in Figure 2 or inequality B can be accounted for by Gurney's rule, as far as monovalent gegenions are concerned. Furthermore, we note that the rule can be extended to Ca^{2+} and Ba^{2+}, since the molal entropy of the former is -11.4 ± 0.3 (strong structure former) and that of the latter is $+2.3 \pm 0.3$.[15]

The magnitude of the slope of the cube-root plot of the PVAS salts invites some comments. The values experimentally found (ranging from -0.6 to -1.5) are not far from those previously found for a sodium polyacrylate (-0.74) and for a polyethylenimine salt (-0.86),[16] but are much larger than those for 1–1 type electrolytes ($-0.2 \sim -0.3$).[13] Frank and Thompson, however, pointed out that the magnitude of the slope increases with rising valency and reported a value of -0.726 for $CaCl_2$ and -3.9 for $ZnSO_4$.[13] The authors have attributed these high values to ion-pair formation. Similarly it is possible that gegenion association by macroion is partly responsible for the large slope observed for the polysulfates.

Since the polysulfates under consideration are copolymeric polyelectrolytes of a low charge density, it is rather surprising to find that the constants of the cube-root plot for the PVAS salts (slope and upper limit) are fairly close to those found for homopolymeric polyelectrolytes of high charge densities such as the polyacrylates at the full degree of neutralization as mentioned in the preceding section. In the light of the difference in the charge density, such a comparison is not fully significant. In order to obtain information on the essential difference between the sulfate and carboxylate, therefore, it is necessary to compare NaPVAS with the sodium salt of a polyvinyl alcohol partially acetalized with glyoxylic acid (NaPVAG). Our experimental finding[2] has shown that the magnitude of the slope of the cube-root plot for NaPVAG (ranging from 1.6 to 3.2) decreases with increasing degree of polymerization and increases with increasing number of charges. If this finding also applies to the polysulfate, the magnitude of the slope of NaPVAS (degree of polymerization 1700, charge density 23/100 vinyl alcohol units) should be larger than 3.2, which was found for NaPVAG–N3 (degree of polymerization 1700, charge density 10.5). The value actually found for NaPVAS, however, is 0.65. In the light of the degree of polymerization dependence of the slope value mentioned above, it is difficult to escape the conclusion that NaPVAS molecules have a more highly stretched configuration than NaPVAG molecules. Correspondingly, the specific viscosity of a salt of PVAS was higher than that of PVAG with the same gegenion, when these polyelectrolytes have the same degree of polymerization and number of charges.[17]

Discussion can now be carried on further in terms of the influence of ions on water structure. The entropy value of acetate ion is not available so that we estimate it using the viscosity B coefficient of this ion ($+0.250$)[18] and the linear relation between the B coefficient and molal entropy.[19] The value thus obtained is about $+15$ eu on the scale of zero for the proton. If this estimate is correct, it is immediately clear that Na^+ and acetate ion are similar in their structure effect and a pair of Na^+ and HSO_3^- is rather dissimilar, since the molal entropy of Na^+ is about $+14.0$ eu and that

(13) For the detailed discussion of the cube-root formulation of various 1–1 type electrolytes in water, see H. S. Frank and P. T. Thompson, "The Structure of Electrolytic Solutions," W. J. Hamer, Ed., John Wiley and Sons, Inc., New York, N. Y., 1959, Chapter 8.

(14) R. W. Gurney, "Ionic Processes in Solution," McGraw-Hill Book Co., Inc., New York, N. Y., 1953, Chapter 16.

(15) W. M. Latimer, K. S. Pitzer, and W. V. Smith, *J. Am. Chem. Soc.*, **60**, 1829 (1938).

(16) These values were obtained by using the equation mentioned in ref 6. These slope values become somewhat large (for example, -1.4 for NaPAA) when use is made of eq 1. This change, which is completely due to a gegenion association phenomenon by macroions, will be discussed fully at a later date, but does not affect our discussion in the text.

(17) I. Sakurada and N. Ise, *Makromol. Chem.*, **40**, 126 (1960).

(18) See ref 14, p 169.

(19) It has been pointed out in ref 14 (p 174) that two straight lines can be obtained: the high-lying line is for the large molecular ions such as NO_3^-, ClO_3^-, and IO_3^-. In the present work, the acetate ion was assumed to fall on this line.

of HSO_3^- about +32.6 as was mentioned above. Thus, the fact that NaPVAG has a larger slope of the cube-root plot than NaPVAS can be accounted for by Gurney's rule.

We note that the foregoing discussion relies on the validity of the approximation by which the real ionized groups I and II have been replaced with acetate ion and HSO_3^-, respectively.

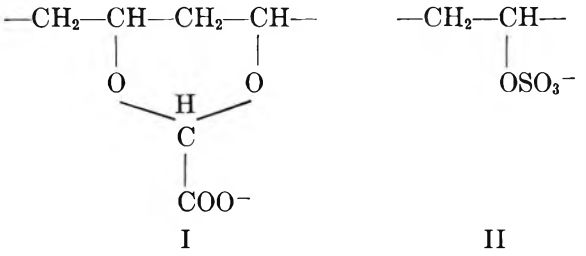

I II

It is therefore important to know the influence which the oxygen atom connecting COO^- or SO_3^- with the main polymer chain would exert on the water structure. According to existing data,[15] the conventional partial molal entropies of ClO^-, ClO_2^-, ClO_3^-, and ClO_4^- are 10.0 ± 2, 24.1 ± 0.5, 39.4 ± 0.5, and 43.6 ± 0.5 eu, respectively. It is seen from these data that oxygen has a structure-breaking effect and the effect of one oxygen atom becomes progressively small as the ion becomes more complex. This can be found in the pair of SO_3^{2-} and SO_4^{2-}, which have entropy values of 3 ± 3 and 4.4 ± 1.0 eu, respectively, and also in the case of NO_2^- and NO_3^-, the entropies of which are 29.9 ± 1.0 and 35.0 ± 0.2 eu, respectively. Thus, it seems possible to conclude that the structural influence of the oxygen under consideration in PVAG and PVAS is rather small.

Finally, we would like to comment on the magnitudes of the activity coefficients of NaPVAG and NaPVAS. As was mentioned in a previous paper,[1] the magnitude of the mean activity coefficients of polyelectrolytes cannot be determined, because it is not known how to estimate the polyionic work experimentally, which determines the mean activity coefficient at infinite dilution. Nevertheless, we know that the polyionic work should be determined by the distance between ionized groups and the number of the groups. Therefore it is expected that polyelectrolytes of the same (linear) charge density and degree of polymerization should have the same mean activity coefficient at infinite dilution. Then, the mean activity coefficient of NaPVAS should be larger than that of NaPVAG at finite concentrations, because the magnitude of the slope of the cube-root plot is smaller for the former than for the latter.

Acknowledgment. Sincere thanks are due to Professor I. Sakurada for his encouragement.

Temperature Effects on the Potential of Zero Charge of the Mercury Electrode

by Woon-kie Paik, Terrell N. Andersen, and Henry Eyring

Institute for the Study of Rate Processes, The University of Utah, Salt Lake City, Utah
(Received November 21, 1966)

The potential of a streaming mercury electrode was measured in aqueous 0.1 and 1.0 *N* KI, KBr, KCl, and NaF solutions from 0 to 60°. The resulting potentials of zero charge (pzc), measured with respect to a reference electrode held at 25°, increased approximately linearly with an increase in temperature, *T*. The increase in pzc with temperature for NaF is considered to be due to deorientation of solvent dipoles on the electrode surface with increasing temperature, while the increasing potentials of zero charge in the other solutions are due to a decrease of specific adsorption as well as to solvent deorientation. Using an adsorption isotherm, double-layer theory, and the results for NaF, calculations are made of the temperature dependence of the pzc for the Cl^-, Br^-, and I^- solutions. These results compare favorably with the experimental results.

Introduction

The effects of electrolyte concentration on the potential of zero charge (pzc) are widely used to provide information regarding adsorption onto electrodes and hence regarding the double-layer structure. Studies of temperature variation of the pzc, although valuable in providing additional insight into the double-layer structure, are sparse.

Anderson and Parsons obtained electrocapillary curves of Hg in KI solutions at various temperatures and from them calculated heats and entropies of specific adsorption of I^- ions onto Hg.[1] Koenig obtained electrocapillary curves of mercury in 1 *M* KNO_3 solutions between 9.3 and 55°[2] and Parry and Parsons made similar studies on aromatic sulfonate anions.[3] Grahame[4] measured the temperature coefficient of the pzc of mercury in NaF solutions from 0 to 85° by the capacity method. He also measured the pzc of a streaming mercury electrode in KCl solutions at different temperatures.[5] Similar measurements have been made on streaming Hg electrodes by Randles and Whiteley[6] in 0.1 *N* solutions of KCl, NaOH, and K_2SO_4 in the temperature range 15–35°; by Butler on Hg and Hg–In amalgam electrodes in 0.1 *N* $HClO_4$;[7] and by Hills and Payne on Hg in 0.1 *N* solutions of $NaNO_3$, NaF, Na_2SO_4, and NaCl at 20 and 30°.[8]

Minc and Jestrzebska[9] have measured the capacity minima in KF, KCl, and KBr solutions at very dilute concentrations. All of these workers, except Grahame kept their reference electrodes at the same temperature as the test solutions.

In the above zero charge potential determinations the structural aspects of the double layer were only somewhat delved into. Hills and Payne[8] considered changes in the concentration of adsorbed water on the electrode with variation in charge. Several of the above authors[6,7] noted that the temperature coefficient of the electrode potential at zero charge is larger for solutions containing more adsorbable anions and hence concluded that the pzc increases with temperature due to a decrease in specific adsorption (for solutions where such adsorption exists).

In the present work we have investigated the effect of temperature on the pzc from the standpoint of a

(1) W. Anderson and R. Parsons, *Proc. Intern. Congr. Surface Activity, 2nd, London*, 45 (1957).

(2) F. Koenig, *Z. Physik. Chem.* (Leipzig), **157**, 96 (1931).

(3) J. M. Parry and R. Parsons, *Trans. Faraday Soc.*, **59**, 241 (1963).

(4) D. C. Grahame, *J. Am. Chem. Soc.*, **79**, 2093 (1957).

(5) (a) D. C. Grahame, E. M. Coffin, J. I. Cummings, and M. A. Poth, *ibid.*, **74**, 1207 (1952); (b) D. C. Grahame, E. M. Coffin, and J. I. Cummings, Technical Report No. 2 to the Office of Naval Research, Aug 11, 1950.

(6) J. E. B. Randles and K. S. Whiteley, *Trans. Faraday Soc.*, **61**, 326 (1965).

(7) J. N. Butler, *J. Phys. Chem.*, **70**, 2312 (1966).

(8) G. J. Hills and R. Payne, *Trans. Faraday Soc.*, **61**, 326 (1965).

(9) S. Minc and J. Jastrzebska, *Electrochim. Acta*, **10**, 965 (1965).

variation in specific adsorption and a partial reorientation of water dipoles. The former contribution is calculated and the latter is estimated based on results for NaF and on calculations.

To provide an experimental test for our calculations, the pzc of a mercury electrode in various aqueous alkali halide solutions was measured in the temperature range 0–60°. The reference electrode was kept at a constant temperature in order to make the comparisons of the pzc at various temperatures more consistent for our double-layer studies and to avoid the somewhat inaccurate corrections for the entropy changes at the reference electrode. In return, possible thermal junction potentials were introduced and these are discussed later.

Experimental Section

The technique of the streaming mercury electrode[5,10] was employed in measuring the pzc. The cell, presaturator for N_2 gas, and a Pyrex coil which carried the mercury to the capillary were immersed in a bath in which the temperature was controlled to within ±0.02°. The solution was connected by means of a salt bridge of saturated KCl solution to the reference electrode, which was kept at 25°. A saturated calomel electrode served as the reference half-cell in most experiments, although a few experiments were repeated using an Ag–AgCl electrode. Solutions were made from reagent grade chemicals and water bidistilled from a basic permanganate solution.

The electrolytes studied were 0.1000 and 1.000 N (at 25°) solutions of NaF, KCl, KBr, KI, and 0.0100 N (at 25°) NaF.

The solution in the cell was flushed with purified (99.996%) nitrogen at least 15 hr prior to each experiment and during the measurements to prevent air oxidation of mercury and the anions. Then mercury was allowed to stream through the solution for a few minutes, before the potentiometer readings were recorded, to ensure a stable potential.[5]

The potential readings were made to 0.001 mv using a Leeds and Northrup K-3 potentiometer. The standard deviations of the readings were about 0.01 mv for 0.1 and 0.01 N solutions and a few hundredths of a millivolt for 1 N solutions. Although the actual potential values may not be this accurate (*e.g.*, owing to limits of chemical purity), this precision justifies the comparison of small differences in temperature coefficient of the pzc. Any set of readings that were not constant with time were discarded because such a shift of potential would be an indication of contamination of the solution either by impurities in the reagents or by oxidation of the mercury or anions.

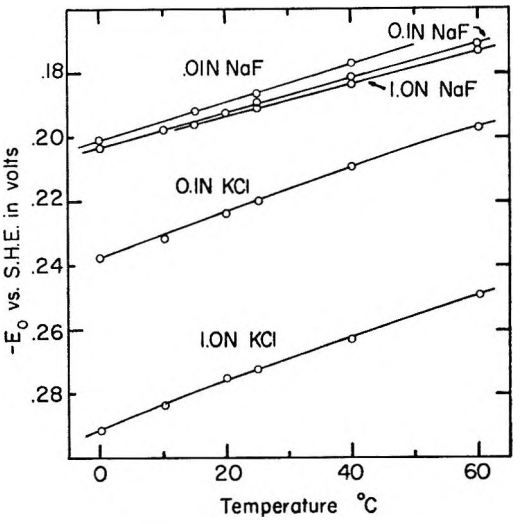

Figure 1a. Potential of zero charge, E_0 (corrected for liquid junction potential), *vs.* the standard hydrogen electrode as a function of temperature. Fluoride and chloride solutions.

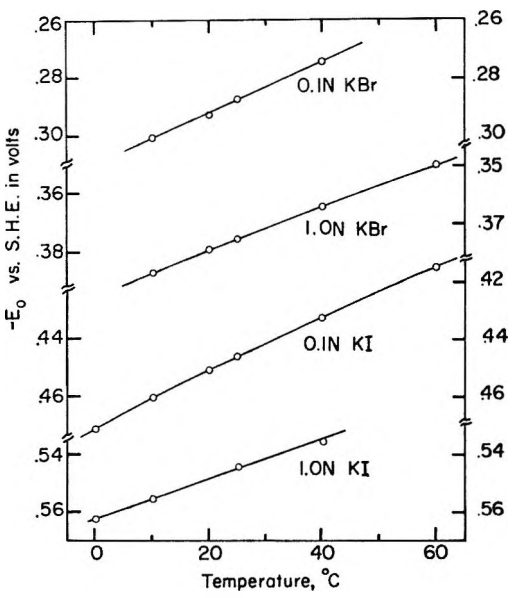

Figure 1b. Potential of zero charge, E_0, as a function of temperature for bromide and iodide solutions. E_0 measured *vs.* standard hydrogen electrode with correction made for liquid junction potential.

Results and Discussion

The experimental results are shown in Figures 1a and 1b. The recorded potentials of zero charge, E_0, in Figure 1 consist of the raw data with an estimated

(10) D. C. Grahame, R. P. Larsen, and M. A. Poth, *J. Am. Chem. Soc.*, 71, 2978 (1949).

Table I: Temperature Coefficient of Potential of Zero Charge, $d\phi_0/dT$, at 25° in Millivolt per Degree at Concentrations of 0.01, 0.1, and 1 N

Ref	NaF, N			KCl, N		KBr, N		KI, N	
	0.01	0.1	1	0.1	1	0.1	1	0.1	1
This work	0.593	0.528	0.507	0.673	0.697	0.870	0.742	0.925	0.675
Grahame		0.47[a]		0.586					
Randles and Whiteley (calcd)				0.67					
Hills and Payne		0.60[b]		0.64[b]					

[a] Independent of concentration within the limits of experimental error. [b] Calculated from the temperature coefficient data with reference electrode at the same temperature using the thermal temperature coefficient of potential of reference electrode.

correction added for the liquid junction potential between saturated KCl and the test solution at the cell temperature.[11]

The change of the pzc, E_0, with temperature is believed to be due to the change of inner potential difference, ϕ_0, across the double layer, because we maintained the reference electrode at constant temperature and the thermal junction potentials are believed to be negligible. There are two thermal junctions, one across the copper lead and one across the salt bridge. These can be neglected without any apparent serious error because the entropies of transfer of electrons and ions across these junctions are believed to be small. This point is supported by deBethune, Licht, and Swendeman.[12] Grahame also neglected the thermal junction potentials in his work.[4,5] Randles and Whiteley[6] and Butler[7] measured the pzc against reference electrodes at the same temperature as the test solutions as mentioned above. They then added the entropy changes accompanying the electrode reactions, $\Delta S/F$, to their measured dE_0/dT to get their temperature coefficient of the inner potential difference across the double layer. This procedure, however, is equivalent to keeping the reference electrode at constant temperature as was done in the present work. This is so because the entropy change at the reference electrode is nothing but the temperature coefficient of the potential of the reference electrode. Since there are uncertainties in the entropy values of ionic species in solution, those procedures may result in uncertain values of the temperature coefficient of the inner potential difference across the double layer.

In Table I the temperature coefficients of our pzc, $d\phi_0/dT$ ($= dE_0/dT$) at 25°, are listed together with other data obtained by previous workers. A positive value of the coefficient means that the mercury electrode with zero charge becomes more positive as the temperature is increased.

Because specific adsorption of anions makes the potential of zero charge more negative it is usually assumed that more specific adsorption of anions is accompanied by a larger temperature coefficient of the pzc. This is the case for 0.1 N solutions of the halide ions as seen by comparing Table I with the tendency for increasing specific adsorption, *i.e.*, $F^- < Cl^- < Br^- < I^-$.[13,14] This is, however, found to be not always true as seen from the data of 1 N solutions. The $d\phi_0/dT$ values for 1 N solutions of KBr and KI are smaller than their 0.1 N solutions, while there is more specific adsorption of anions from the more concentrated solutions. The value of 1 N KI is even smaller than that of 1 N KBr. The fluoride solutions of different concentrations were expected to have essentially the same temperature coefficients because F^- ions are only slightly specifically adsorbed. The data from 1 and 0.1 N solutions show the expected agreement, but $d\phi_0/dT$ for 0.01 N NaF is higher than the other two. The reason for this is unknown, but it may be due to uncertainties in the correction for the liquid junction potential.

(11) This correction was calculated using the Henderson equation. Ionic mobilities at the various temperatures could not be found for all the solutions in question. Therefore, mobilities at 25° were used for the KCl, KBr, and KI calculations. For NaF limiting ionic conductances at 25° were used. The above approximations removed any temperature dependence from the mobility terms in the Henderson equation. This approximation seems justified since the ionic mobilities increase proportionately with temperature for all the ions studied (*cf.* S. Glasstone, "Textook of Physical Chemistry," 2nd ed, D. Van Nostrand Co., Inc., New York, N. Y., p 895). The error from this approximation would be largest in the case of the most dilute solution, *i.e.*, 0.01 N NaF. Calculated liquid junction potentials did not exceed 3.2 mv and were proportional to the absolute temperature, according to our calculation.

(12) (a) A. J. deBethune, T. S. Licht, and N. Swendeman, *J. Electrochem. Soc.*, 106, 616 (1959); (b) A. J. deBethune and A. Swendeman, "Standard Aqueous Electrode Potentials and Temperature Coefficients at 25°C," Clifford A. Hampel, Publishers, Skokie, Ill., 1964.

(13) D. C. Grahame and B. A. Soderberg, *J. Chem. Phys.*, 22, 449 (1954).

(14) D. C. Grahame, *J. Am. Chem. Soc.*, 80, 4202 (1958).

Table II: Numerical Values Used in the Calculations

	N	r, Å	q_i, μcoulombs/cm²	q_s,[a] μcoulombs/cm²	a_0	Reference for q_i
Cl^-	0.1	1.81	2.3	122	0.0769	Averages taken from data of ref 18 and 19
	1		8.3		0.605	
Br^-	0.1	1.95	5.87	105	0.0771	13
	1		14.4		0.617	Computed from Γ^+ and Γ^- in ref 17
I^-	0.1	2.16	11.14	86	0.0776	14
	1		20.13		0.646	

[a] q_s is calculated as the amount of specific adsorption that will make a square array of ions in contact.

Table III: Calculated Values of W_0, dq_i/dT and $d\psi^0/dT$ at 25°

	KCl, N		KBr, N		KI, N	
	0.1	1	0.1	1	0.1	1
W_0, kcal mole^{-1}	−2.11		−3.90		−6.11	
dq_i/dT, μcoulombs/cm² deg	0.00946	0.0200	0.0244	0.0299	0.0394	0.0321
$d\psi^0/dT$, mv deg^{-1}	0.058	−0.008	0.039	−0.0285	−0.059	−0.080

Temperature Effects on Specific Adsorption of Ions

The portion of the metal–solution potential difference due to specifically adsorbed ions can be separated into a potential difference across the inner layer (metal to outer Helmholtz plane) ${}_{q_i}\psi^u$ and that across the diffuse layer, ψ^0. (The notation with respect to potentials used here follows that of Grahame.[15]) Therefore, the temperature coefficient of the pzc due to ionic specific adsorption, ${}_{q_i}(d\phi_0/dT)$, is given by

$$\left(\frac{d\phi_0}{dT}\right)_{q_i} = \left(\frac{d\psi^u}{dT}\right)_{q_i} + \frac{d\psi^0}{dT} \tag{1}$$

${}_{q_i}\psi^u$ is related to the amount of specific adsorption, q_i, according to the relation (*cf.* ref 16)

$${}_{q_i}\psi^u = \frac{4\pi\gamma q_i}{\epsilon} \tag{2}$$

where γ is the distance between the inner and outer Helmholtz planes and ϵ is the dielectric constant of the compact double layer. Assuming that temperature affects q_i much more than it does γ/ϵ we have

$$\left(\frac{d\psi^u}{dT}\right)_{q_i} = \frac{4\pi\gamma}{\epsilon}\frac{dq_i}{dT} \tag{3}$$

The effect of the temperature on specific adsorption, dq_i/dT, is calculated in this section from the temperature dependence of the adsorption isotherm. The isotherm we have used is a modified Langmuir isotherm analogous to Frumkin's and is given by

$$q_i = \frac{q_s - q_i}{q_s} 2re a_0 \exp\left(-\frac{W}{RT}\right) \tag{4}$$

where q_i is the charge of the specifically adsorbed ions per unit area, q_s is the value of q_i at saturation, r is the radius of the adsorbed ions, e is the electronic charge, a_0 is the activity of the ions in the bulk of the solution, and W is the electrochemical free energy of adsorption. Besides being of a fairly simple form for calculation purposes, this isotherm finds support in the work of Parry and Parsons.[3] Here $2r$ is introduced as the volume of the layer of adsorbed ions per unit area of the electrode surface.[17]

W can be split into electrostatic and nonelectrostatic terms

$$W = W_0 + zF(\psi^0 + \psi^A) \tag{5}$$

Here ψ^A is the potential difference from the outer to the inner Helmholtz plane. ψ^0, the Galvani potential of the outer Helmholtz plane with respect to the bulk

(15) D. C. Grahame, *Z. Elektrochem.*, 62, 264 (1958).

(16) P. Delahay, "Double Layer and Electrode Kinetics," Interscience Publishers, Inc., New York, N. Y., 1965, Chapter 4.

(17) D. C. Grahame, *Chem. Rev.*, 41, 441 (1947).

solution, is obtained from diffuse layer theory as

$$\psi^0 = \frac{2RT}{F}\sinh^{-1}\left(\frac{q_i}{A}\right) \quad (6)$$

at the pzc. $A = (\epsilon_d kTC_0/2\pi)^{1/2}$ where ϵ_d is the dielectric constant of the diffuse double layer and C_0 is the bulk concentration of ions. Differentiating eq 6 with respect to T and assuming ϵ_d to change very little with temperature, we have

$$\frac{d\psi^0}{dT} = \frac{\psi^0}{T} + \left(\frac{R}{F}\right)\left[1 + \left(\frac{2A}{q_i}\right)^2\right]^{-1/2} + \left(\frac{RT}{FA}\right)\left[\left(\frac{q_i}{2A}\right)^2 + 1\right]^{-1/2}\frac{dq_i}{dT} \quad (7)$$

From eq 4, 5, and 7 we get

$$\frac{dq_i}{dT} = \frac{\left(\frac{q_i}{T}\right)\left\{\frac{W}{RT} + \left[1 + \left(\frac{2A}{q_i}\right)^2\right]^{-1/2} + \frac{F\psi^0}{RT}\right\}}{\frac{q_s}{q_s - q_i} - \frac{F\psi^A}{RT} + 2\left[1 + \left(\frac{2A}{q_i}\right)^2\right]^{-1/2}} \quad (8)$$

For the calculation of dq_i/dT and hence ${}_{q_i}(d\psi^u/dT)$, values for W and ψ^A are required. W was obtained by substituting the known values for q_i, r, and a_0 into eq 4; q_s was calculated assuming complete coverage of the surface by the ions in a square-packed array. Table II[18,19] lists the values for q_i, q_s, r, and a_0. The calculated W values for 0.1 and 1.0 N values of a given salt were substituted into eq 5 to give two simultaneous equations with W_0, ψ^A (1 N) and ψ^A (0.1 N) as unknowns. It was then assumed that ψ^A for a given type of electrolyte is proportional to q_i, so that ψ^A (0.1 N) = ψ^A (1 N)(q_i (0.1 N)/q_i (1 N)). Thus, W_0 (independent of the bulk salt concentration for a given ion) and the ψ^A values were determined. With W and ψ^A known, dq_i/dT was readily calculated as was $d\psi^\circ/dT$ (*cf.* Table III).

For the calculation of ${}_{q_i}(d\psi^u/dT)$ from dq_i/dT, given by eq 3, the value of γ/ϵ is needed. These two constants are not yet accurately known. However, from the integral capacity data of the double layer, d/ϵ is estimated to be approximately 4×10^{-9} cm where d is the thickness of the inner layer.[16,17] In our calculations we assumed d = 4 A, ϵ = 10, and $\gamma = d - r$, where r is the radius of the anions. These values appear to be in agreement with the comparable values assumed by other workers in the field.[20] Errors in the dielectric constant should affect calculations for all ions to roughly the same extent since it is found that the inner layer dielectric constant depends on the field due to electrode charge, but not on that due to specifically adsorbed ions.[14,16]

Table III shows the $d\psi^\circ/dT$, dq_i/dT, and W_0 values calculated as outlined above. The total temperature coefficients of the zero charge potential at 25°, ${}_{q_i}(d\phi_0/dT)$, as calculated from eq 1 are shown in Figure 2 as dashed lines. This plot qualitatively shows $(d\phi_0/dT)$ as a function of adsorbability. The calculated ${}_{q_i}(d\phi_0/dT)$ values show certain aspects which are in agreement with experiment, *i.e.*, the tendency for $d\phi_0/dT$ for 1 N I^- to be less than that for 1 N Br^- or 0.1 N I^-. However, there are still significant differences between the experimental $(d\phi_0/dT)$ and the calculated ${}_{q_i}(d\phi_0/dT)$ values.

These differences are believed to come from the temperature variation of the orientation of the adsorbed solvent dipoles.

Temperature Effects on Orientation of Dipoles

The $d\phi_0/dT$ values for 0.1 and 1 N F^- solutions are considered to be due to the thermal deorientation of dipoles which cover the electrode surface with their negative end pointing preferentially toward the electrode.[21] The contribution to $d\phi_0/dT$ from this deorien-

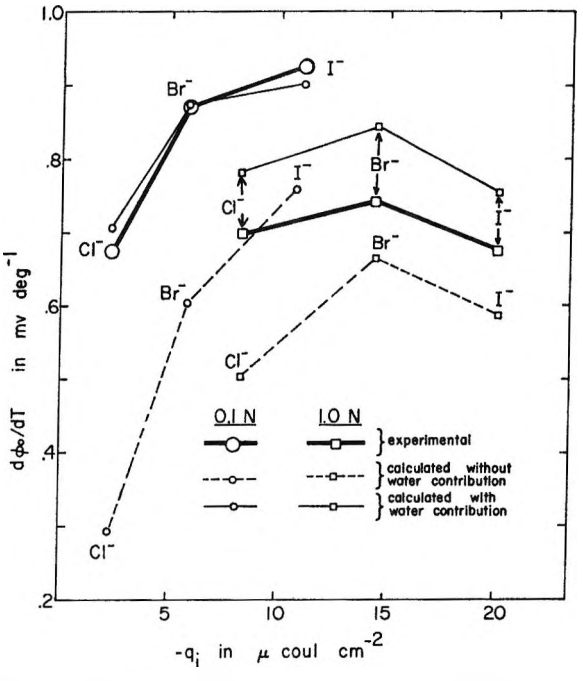

Figure 2. Experimental and calculated values of $d\phi_0/dT$ at 25° for the mercury–halide solution systems.

(18) D. C. Grahame and R. Parsons, *J. Am. Chem. Soc.*, **83**, 1291 (1961).

(19) H. Wroblowa, Z. Kovac, and J. O'M. Bockris, *Trans. Faraday Soc.*, **61**, 1523 (1965).

(20) J. R. Macdonald and C. A. Barlow, Jr., *Proc. Australian Conf. Electrochem., 1st, Sydney, Australia, 1963*, 199 (1965).

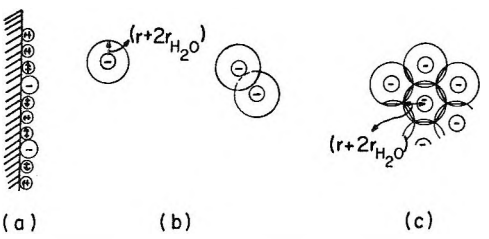

Figure 3. (a) Schematic diagram of adsorbed solvent dipoles and anions showing deorientation of dipoles adjacent to ion and orientation of dipoles nonadjacent to ion. (b) Projected area of adsorbed ion with its complement of nearest water neighbors when ions are separated by two or more water molecules (left) and when ions are separated by one water molecule (right). (c) Schematic diagram of surface layer of ions and water at which water dipole contribution to electrode potential is minimal.

tation, $d\chi/dT$, must be added to the above calculations, $q_i(d\phi_0/dT)$, to give the total $d\phi_0/dT$; $d\chi/dT$ for Cl^-, Br^-, and I^- will not be exactly the experimental value of $d\phi_0/dT$ found for fluoride, since there is a different electrode coverage by oriented dipoles for different anions. The coverage of the electrode by the oriented water dipoles will decrease with increasing q_i, since the adsorbed anions replace some water molecules and deorient some neighboring dipoles. The extent to which neighboring water molecules are deoriented depends on factors such as orientation forces between ions and dipoles, those between dipoles and the electrode, and mutual repulsion between oriented dipoles about the anion. No exact answer exists to the question of the dipole structure about an ion. However, such deorientation exists as pointed out by various workers[22,23] and by considerations of the strength of ion–dipole interactions *vs.* dipole–image or *vs.* hydrogen bond interactions. In this work we take the upper limit of such orientation of water dipoles with their negative ends pointing away from the anions and assume that a complete layer of water molecules about each anion deorients (*cf.* Figure 3a). The adsorbed anions at low coverage will accordingly decrease the oriented dipole coverage by the amount $(q_i/e)\pi(r + 2r_{H_2O})^2$, where e is the charge of the ion and r_{H_2O} is the radius of a water molecule, because $\pi(r + 2r_{H_2O})^2$ is the projected area of the anion with its deoriented neighboring water molecules around it.

This linearity of decreasing of the oriented water coverage, θ_w, with increasing q_i will not continue as the surface becomes crowded with anions because each ion does not then have an independent complement of nearest-neighbor solvent molecules (*cf.* Figure 3b). Therefore, in reality the θ_w *vs.* q_i relation may be a curved line as shown in Figure 4. The equation of the curve may be given by

$$\theta_w = 1 - \alpha + b\alpha^2 \tag{9}$$

where

$$\alpha = \left(\frac{q}{e}\right)\pi(r + 2r_{H_2O})^2 \tag{10}$$

The third term of eq 9 is quadratic in q_i because the probability of two ions getting together with the interaction energy E, as in Figure 3b, is $b'q_i^2 \exp(-E/RT)$. The constant b is chosen such as to give a minimum point of the curve (Figure 4) at $q_i = q_{i0}$, where q_{i0} is the amount of specific adsorption, such that there remain no water dipoles free of the direct influence of anions.[24] At such a coverage the average area that is covered by an anion is taken to be the combined area of the ion and its shell of nearest water neighbors. This is assumed to approximate the area of the hexagon shown in Figure 3c. Thus, values determined for q_{i0} in this way are 30.3, 28.4, and 26.1 μcoulomb cm^{-2} for Cl^-, Br^-, and I^-, respectively. Then the potential due to the dipoles is

$$\chi = \chi^0[1 - \alpha + b\alpha^2] \tag{11}$$

χ^0 is the dipolar potential of a full layer of water molecules and the part of the temperature coefficient that is due to the water dipoles is then

$$\frac{d\chi}{dT} = \frac{d\chi^0}{dT}[1 - \alpha + b\alpha^2] - \chi^0\frac{d\alpha}{dT}(1 - 2b\alpha) \tag{12}$$

where $d\alpha/dT = \pi/e(r + 2r_{H_2O})^2 dq_i/dT$; $d\chi^0/dT$

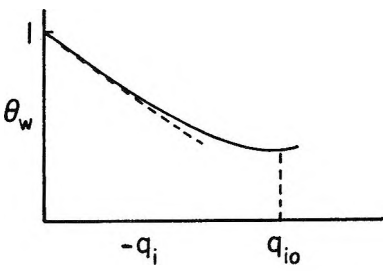

Figure 4. Fractional coverage of electrode with oriented water dipoles, θ_w, *vs.* amount of specific adsorption of anions.

(21) The field within the metal may contribute to the metal–solution potential, but should not contribute to the temperature variation of this potential difference (*cf.* R. J. Watts-Tobin, *Phil. Mag.*, 6, 133 (1961)).

(22) E. Shvarts, B. B. Damaskin, and A. N. Frumkin, *Russ. J. Phys. Chem.*, 36, 1311 (1962).

(23) T. N. Andersen and J. O'M. Bockris, *Electrochim. Acta*, 9, 347 (1964).

(24) At coverages of ions greater than q_{ic} the water dipole contribution to the potential can only remain unchanged or increase; the latter possibility is due to the fact that one water molecule sandwiched between two ions is not preferentially oriented toward either and may become aligned perpendicular to the surface.

must be equal to the $d\phi_0/dT$ values for F^- solutions since this ion does not adsorb on the electrode. The difference of $d\phi_0/dT$ between 0.01 N F^- solution and the other two (1 and 0.1 N) solutions is hard to explain at this stage as mentioned previously. The average value of 0.1 and 1.0 N NaF solutions (0.52 mv/deg) is used in our calculations for $d\chi^0/dT$ since the value is nearly the same for both concentrations and since the concentrations of other solutions studied in this work are 1 and 0.1 N.

If all water dipoles are assumed to face either toward or away from the electrode and if the energy of turning an oriented dipole to the opposite direction is ω, then[25]

$$\chi^0 = -\frac{4\pi N\mu}{\epsilon}\tanh\left(\frac{\omega}{2RT}\right) \qquad (13)$$

Here N is the number of dipoles covering unit area of electrode surface, μ is the dipole moment, and ϵ is the dielectric constant. ω is determined from the experimental value of $d\chi^0/dT$, where[26]

$$\frac{d\chi^0}{dT} = \frac{4\pi N\mu}{\epsilon}\frac{2W}{RT^2}\frac{\exp(\omega/RT)}{[\exp(\omega/RT)+1]^2} = 0.52 \qquad (14)$$

Taking $N = 10^{15}$, $\mu = 1.84$ D., and $\epsilon = 10$ gives $\omega = 0.28$ kcal/mole and $\chi^0 = -0.163$ v; a variation of ϵ affects ω but does not significantly change χ^0 as $\epsilon = 6$ gives $\omega = 0.16$ kcal/mole and $\chi^0 = -0.155$ v while $\epsilon = 1$ gives $\omega = 0.027$ kcal/mole and $\chi^0 = -0.160$ v. Hence the positive measured temperature coefficient of the pzc of F^- solutions is believed to be direct evidence that the solvent dipoles are preferentially pointed with the negative end toward the electrode.

Our final result of calculations including the above dipole considerations are given by

$$\frac{d\phi_0}{dT} = q_i\left(\frac{d\phi}{dT}\right) + \frac{d\chi}{dT} \qquad (15)$$

and are shown in Figure 2 by the thin lines.

Although there is a certain amount of arbitrariness in choosing some of the parameters used, it is seen that from adsorbed ion and water considerations (and using the results from F^-) (1) temperature coefficients of the potential of zero charge are calculated for Cl^-, Br^-, and I^- solutions which are of the same approximate magnitude as the experimental values; (2) the decrease in $d\phi_0/dT$ in going from certain solutions to other ones in which more specific adsorption occurs can be explained from a consideration of dq_i/dT, using an adsorption isotherm.

Reasonable variations in the parameters chosen would not appear to negate conclusions 1 and 2 above. As has been discussed, corrections to the inner layer dielectric constant would be expected to be similar for all the ions studied. It is doubtful that the average value of ϵ would differ from the chosen value of 10 by more than 40%, which would alter $_{q_i}(d\phi_0/dT)$ values by less than 0.3 mv/deg. It was shown that the value of ϵ used in the water dipolar contribution, χ^0, did not affect $d\chi/dT$. The distance from the metal to the outer Helmholtz plane d and hence γ might increase with specific adsorption[16] and hence with salt concentration. This would increase $_{q_i}(d\phi_0/dT)$ values for 1 N solutions with respect to those for 0.1 N solutions and could also increase $d\phi_0/dT$ for larger ions with respect to that for smaller ions.

Acknowledgment. The authors gratefully acknowledge the financial support of this work by the Atomic Energy Commission under Contract No. AT(11-1)-1144.

(25) N. F. Mott and R. J. Watts-Tobin, *Electrochim. Acta*, 4, 79 (1961).

(26) We assume that the concentration of adsorbed water molecules does not change with temperature except through variation in ion concentration.

On the Ionic Strength Dependence of Micelle Number. II[1,2]

by Marilyn F. Emerson and Alfred Holtzer

Department of Chemistry, Washington University, St. Louis, Missouri *(Received November 28, 1966)*

Measurements have been made of the cmc's and (light-scattering) molecular weights of sodium dodecyl sulfate (SDS) and of *n*-dodecyltrimethylammonium chloride, bromide, and nitrate in aqueous solvent containing varying concentration of NaCl, NaCl, NaBr, and $NaNO_3$, respectively. These experimental values are used with the theory developed earlier to calculate the hydrocarbon contribution to the standard free energy change for addition of one detergent molecule to a micelle of the most probable size (ΔG^{∞}_{HC}). For the cationic detergents, resulting values of ΔG^{∞}_{HC} are independent of ionic strength and roughly independent ($\sim 10\%$ spread) of supporting electrolyte. For SDS, a small, systematic dependence on ionic strength is observed. The value for SDS differs from that for the cationic detergents by $\sim 20\%$. Possible explanations of the observed differences are discussed.

Introduction

One of the most striking features of solutions of detergents in water is the existence of a critical micelle concentration (cmc). Since, furthermore, the cmc is a readily measurable property, many efforts have been directed toward obtaining a clear understanding of its physical significance. In an earlier paper[3] it was shown that the quantity RT ln (cmc) is equal to the standard free energy change ($\Delta G^{\infty}_{\hat{N}}$) for the addition of one more detergent monomer to a micelle which already contains that number of monomers most probable at the cmc ($\hat{N}$). This result is independent of assumptions about phase separation and does not require, for its derivation, a detailed statistical-mechanical analysis of micellar solutions. Such an analysis is, however, consistent with this conclusion.[4]

The standard free energy change in question can be divided, conceptually, into a hydrocarbon contribution and an electrostatic contribution. The latter can be expressed in terms of the magnitude of the electrostatic potential at the micellar surface (ψ_b). Thus

$$RT \ln (\text{cmc}) = \Delta G^{\infty}_{HC} + N_0 \epsilon \psi_b(b, a, \kappa, \hat{N}) \quad (1)$$

where N_0 is Avogadro's number and ϵ the magnitude of the protonic charge and it is emphasized that ψ_b depends on the micellar radius (b), the distance of the closest approach of small ions to the micelle (a), the ionic strength (through the Debye κ), and the most probable micelle number ($\hat{N}$).

The quantity ΔG^{∞}_{HC}, being a direct measure of the stability of the hydrophobic bond, is not only of interest in the theory of micelle formation, but may have implications for the theory of the stability of protein secondary, tertiary, and quaternary structure. As eq 1 makes clear, an experimental determination of the cmc, combined with an estimate of ψ_b, can be used to calculate this hydrocarbon part of the free energy change (ΔG^{∞}_{HC}).

The quantity κ is, of course, readily computed from the known ionic composition of the solution. The micellar radius can be estimated using a combination of the few available results of low-angle X-ray studies and some reasonable assumptions based upon the known dimensions of the monomer molecules.[3] The distance of closest approach can be calculated from b and existing tables of ionic radii.[3] The micelle number can be evaluated from results of any of the usual kinds of measurement of macromolecular weights, usually light scattering in the case of detergents. Thus, values

(1) This investigation was supported by Research Grant RG-5488 from the Division of General Medical Sciences, Public Health Service.

(2) Support for some of the computation was provided by National Science Foundation Grant G-22296 to the Washington University Computer Center.

(3) M. F. Emerson and A. Holtzer, *J. Phys. Chem.*, 69, 3718 (1965). This reference is paper number I.

(4) R. H. Aranow, *ibid.*, 67, 556 (1963). The authors are grateful to Dr. Aranow for pointing out to us the relevance of this reference in the present context.

are assigned to all the relevant parameters before the fact; none remains adjustable.

Given the values of these variables, the micellar surface potential can be estimated as the appropriate solution to the Poisson–Boltzmann equation. Because the surface potentials are quite high ($\epsilon\psi_b \sim 5kT$), the nonlinearized form of the Poisson–Boltzmann equation is required, necessitating numerical solution by electronic computation.

When this procedure was applied to data then extant for sodium dodecyl sulfate (SDS) in NaCl solutions and *n*-dodecyltrimethylammonium bromide (DTAB) in NaBr solutions, it was found that ΔG^{∞}_{HC} is roughly independent of detergent and ionic strength, although a small apparent difference exists between the values of ΔG^{∞}_{HC} obtained for the two detergents.[3]

While these results seemed promising, more detailed experimental evidence bearing on the validity of this approach was evidently needed. In this paper are presented results of measurements of the cmc (by light scattering and conductivity) and of $\hat{N}$ (by light scattering) for *n*-dodecyltrimethylammonium chloride (DTAC) in NaCl solutions and *n*-dodecyltrimethylammonium nitrate (DTAN) in $NaNO_3$ solutions, as well as for DTAB in NaBr solutions and SDS in NaCl solutions, from which ΔG^{∞}_{HC} for each of these systems is calculated. Thus, the effects on ΔG^{∞}_{HC} of changing the ionic strength, the supporting electrolyte, and the charged detergent head group are assessed.

Experimental Measurements and Treatment of Data

A. Materials. 1. General Reagents. All water used was first distilled in a commercial still, then passed through a charcoal filter (Culligan Water Conditioning Co.), and finally through two successive mixed-bed ion-exchange resin columns (Culligan Water Conditioning Co.). The water thus produced has a specific resistance greater than 1 megohm cm (0.1 ppm as NaCl).

The preparation of dust-free water for light scattering has been described previously.[5]

Unless otherwise specified, all chemicals were reagent grade and were used without further purification.

2. Sodium Dodecyl Sulfate (SDS). SDS was prepared by the reaction of 1-dodecanol (99.6% C_{12} and 0.4% C_{10}; obtained from the Givaudan–Delewanna Co., N. Y.) with chlorosulfonic acid, followed by neutralization with NaOH.[6-8]

The SDS was then extracted into hot 95% ethanol, recrystallized several times from 95% ethanol, and finally washed with spectranalyzed *n*-hexane (Fisher) for 12 hr in a Soxhlet extractor to remove trace amounts of 1-dodecanol.[9] The final product was dried over a Molecular Sieve (Fisher, Type 4A) in a vacuum desiccator.

The product was characterized by its conductance; values of the critical micelle concentration (cmc), the equivalent conductance at the cmc (Λ_{cmc}), and the equivalent conductance at infinite dilution (Λ_{∞}) of the sample in water at 25° are presented in Table I, along with the corresponding literature values.[10-12] The agreement is satisfactory.

Table I: Characterization of SDS and DTAB Samples by Conductance

	Cmc, moles/l.	Λ_{cmc}, cm²/ohm equiv	Λ_{∞}, cm²/ohm equiv
SDS	0.00800	67.0	74.3
SDS[a]	0.00813	66.8	71.7
DTAB	0.0148	93.0	101
DTAB[b]	0.0146	91.0	102

[a] See ref 10–12. [b] See ref 13.

3. n-Dodecyltrimethylammonium Bromide (DTAB). DTAB was prepared from *n*-dodecyl bromide (Eastman) by a method described elsewhere.[13,14] The salt was recrystallized several times from acetone–ether.[8] Values of the cmc, Λ_{cmc}, and Λ_{∞} of the product in water at 25° are presented in Table I along with the corresponding literature values.[13] Again, the agreement is satisfactory.

4. n-Dodecyltrimethylammonium Chloride (DTAC). DTAC was prepared by extensive dialysis of DTAB, first against NaCl solution (3 *M*) until no Br^- could be detected in the dialyzate (by oxidation with chlorine water and shaking with carbon tetrachloride), then against water.[8] At the high concentration of added

(5) T. M. Schuster, Ph.D. Thesis, Washington University, St. Louis, Mo., 1963.

(6) M. J. Schick, private communication.

(7) J. L. Kurz, private communication.

(8) M. F. Emerson, Ph.D. Thesis, Washington University, St. Louis, Mo., 1966.

(9) J. L. Kurz, private communication.

(10) R. J. Williams, J. N. Phillips, and K. J. Mysels, *Trans. Faraday Soc.*, **51**, 728 (1955).

(11) A. Wilson, M. Epstein, and J. Ross, *J. Colloid Sci.*, **12**, 345 (1957).

(12) P. Mukerjee, K. J. Mysels, and C. I. Dulin, *J. Phys. Chem.*, **62**, 1390 (1958).

(13) A. B. Scott and H. V. Tarter, *J. Am. Chem. Soc.*, **65**, 692 (1943).

(14) W. Bruning and A. Holtzer, *ibid.*, **83**, 4865 (1961).

electrolyte present during most of the dialysis, the detergent monomer concentration is very low, so that, although monomers can pass through the dialysis membrane,[15] they do so much more slowly than does the added electrolyte. Thus, small-ion equilibrium can be reached without significant over-all loss of detergent.

After dialysis, the water was removed from the sample by lyophilization. This detergent, unlike DTAB, is highly hygroscopic and was dried for several hours over P_2O_5 in a vacuum desiccator before use. The sample was then transferred in a drybox from the desiccator to weighed vials, which were then stoppered, removed from the drybox, and weighed again.

The total amount of chloride in a weighed sample of the detergent preparation was determined gravimetrically by precipitation of AgCl with $AgNO_3$ solution. Assuming that the major impurity is NaCl, the sample was found to be 99.38 wt % DTAC.

5. n-Dodecyltrimethylammonium Nitrate (DTAN). DTAN was prepared by reaction of a solution of DTAB with a stoichiometrically equivalent $AgNO_3$ solution.[8] After the precipitation of AgBr was complete, the mixture was heated to just below the boiling point (to coagulate the AgBr precipitate), cooled, and passed through a medium porosity, glass sinter (pore size 10–15 μ). The almost-clear filtrate was centrifuged at 20,000 rpm for 1 hr, the top two-thirds of the solution decanted, and one small portion of it tested for the presence of Ag^+ (with NaCl) and another for Br^- (with $AgNO_3$). Both tests were negative for all solutions of DTAN prepared in this manner. The DTAN was recovered from the solutions by lyophilization.

B. Preparation of Solutions and Expression of Concentrations. The solutions used in this study normally contained the detergent solute and a solvent that was itself an aqueous solution (*e.g.*, a typical solvent would be 0.2 *M* NaCl). A large batch of this solvent was prepared in advance and stock detergent solutions were made up by dissolving a weighed detergent sample in the desired aqueous solvent in a volumetric flask. Subsequent volumetric dilutions of these stock solutions with the same solvent thus provided a series of solutions of known molarity of detergent and constant (and known) *molality* of additive (*e.g.*, NaCl). The molarity of additive, of course, varies somewhat in such a series.

Detergent concentrations are therefore given as grams of detergent per milliliter of solution or formula weights of detergent per liter of solution. Concentrations of additive are expressed as molalities, although the solvent solutions were originally made up volumetrically. In all the cases involved, the difference between molarity and molality is small.

C. Refractometry. Specific refractive index increments were measured using a modified[16] Brice-Phoenix[17] differential refractometer (Phoenix Precision Instruments, Philadelphia, Pa.).

The instrument was calibrated using the data of Kruis[18] for KCl solutions, as interpolated by Stamm.[19] This calibration procedure has been described earlier.[5]

The procedure for calculating reliable molecular weights of charged detergent micelles in aqueous electrolyte solutions from the light-scattering data requires the values of the excess scattering and of the excess refractive index of a solution at detergent concentration c (grams per milliliter) over that of a solution at the cmc (c_0) but at constant molality of added salt (m_3).[20,21] Thus, the specific refractive index increment that must be used is $(n_c - n_{c_0})/(c - c_0) = (\Delta n/\Delta c)_{m_3}$, where n_c is the refractive index of a solution at concentration c. However, for systems in which the refractive index is a linear function of concentration above the cmc, $(\Delta n/\Delta c)_{m_3} = (n_{c_2} - n_{c_1})/(c_2 - c_1)$, where c_1 and c_2 are both greater than c_0.

Thus, differences in refractive index between pairs of solutions at different detergent concentrations above the cmc, but at constant molality of added electrolyte, were measured. In this manner, $(\Delta n/\Delta c)_{m_3}$ was determined for several different values of Δc in the concentration range used for light scattering and was, indeed, found to be constant within experimental error. Since the concentration of detergent monomers remains approximately constant in the concentration region of interest, *i.e.*, above the cmc,[20,22] the contribution of monomers to the refractive increment will cancel out and $(\Delta n/\Delta c)_{m_3}$ is that for the colloidal particle.

For cases involving mixed systems (DTAB in NaX), it was invariably true that $[X^-] >> [Br^-]$ so the solutions were considered to be mixtures of DTAX, NaX, and NaBr; the measured refractive index increments were corrected for differences in refractive index associated with differences in the concentrations of NaX and NaBr in the pair of solutions measured.[8,23]

(15) K. Mysels, P. Mukerjee, and M. Abu-Hamdiyyah, *J. Phys. Chem.*, **67**, 1943 (1963).

(16) A. Holtzer, R. Clark, and S. Lowey, *Biochemistry*, **4**, 2401 (1965).

(17) B. A. Brice and M. Halwer, *J. Opt. Soc. Am.*, **41**, 1033 (1951).

(18) A. Kruis, *Z. Physik. Chem.* (Frankfurt), **B34**, 13 (1936).

(19) R. F. Stamm, *J. Opt. Soc. Am.*, **40**, 788 (1950).

(20) P. J. Debye, *Ann. N. Y. Acad. Sci.*, **51**, 575 (1949).

(21) W. Prins and J. J. Hermans, *Koninkl. Ned. Akad. Wetenschap. Proc.*, **B59**, 162 (1956).

(22) P. J. Debye, *J. Phys. Colloid Chem.*, **53**, 1 (1949).

At some of the intermediate salt concentrations, the quantity $(\Delta n/\Delta c)_{m_3}$ was not measured directly, but was obtained from the empirical equation of Gladstone and Dale[24]

$$(\Delta n/\Delta c)_{m_3} = \bar{v}_2(n_2 - n_1) \quad (2)$$

where n_2 is the refractive index of the colloidal particle, n_1 the refractive index of the solvent medium, and $\bar{v}_2$ the partial specific volume of the colloidal particle.

If $\bar{v}_2$, n_1, and $(\Delta n/\Delta c)_{m_3}$ for the solution at one concentration of additive are known, n_2 can be obtained from eq 2. Then, assuming that n_2 and $\bar{v}_2$ remain constant, $(\Delta n/\Delta c)_{m_3}$ can be calculated, to a good approximation, at other concentrations of additive.

D. Light Scattering. 1. Experimental. a. Instrumentation. A commercial (Phoenix Precision Instrument Co., 1979-S series) light-scattering photometer, built according to the design of Brice, Halwer, and Speiser[25] and modified to improve the experimental precision,[5] was used for all light-scattering measurements. A description of the erlenmeyer cells used and of the instrument and cell calibration has been given by Schuster.[5]

b. Optical Clarification of Detergent Solutions. Detergent solutions were cleaned for light scattering by vacuum filtration through a clean, ultrafine (pore size, 0.9–1.4 μ), sintered-glass filter funnel directly into a clean, light-scattering cell. The filtration was carried out at a pressure differential sufficiently small to prevent the formation of bubbles in the filter stem and in the cell. The procedure for cleaning the cells and the filters and a detailed description of the filtration apparatus is given elsewhere.[5]

The cleanliness of the solutions was checked by placing the filled cell in the unfiltered beam of the light-scattering instrument and viewing it with a small hand mirror at the lowest possible angle ($\sim$5°) to the forward direction of the incident beam. In a completely darkened room, dust particles appear as small, bright spots moving about against a black background. Absolutely clean (by visual examination) solutions could be obtained in this manner, although some dust can be tolerated for measurement of the scattering at 90° to the incident beam.

The scattering from solutions of detergents in several aqueous electrolyte solvents was measured as a function of detergent concentration. All solutions were clarified individually because it was not possible to obtain clean solutions by dilution of a clean stock solution in the cell. The Rayleigh ratio of the scattering at 90° (R_{90}) to the incident beam was measured for all solutions and, for several of the solutions, the Rayleigh ratio at 45 (R_{45}) and 135° (R_{135}) to the incident beam was also determined. From these, the corresponding quantity for the same system at the cmc was subtracted to obtain the excess Rayleigh ratio ΔR_θ (see next section).

All solutions for which the Rayleigh ratio at 45 and 135° to the incident beam was measured had dissymmetries $(\Delta R_{45}/\Delta R_{135})$ which were within 1% of unity. The values of ΔR_{45}, ΔR_{135}, and ΔR_{90} agreed to within $\pm 1.5\%$.

2. Treatment of Data. To obtain the micellar molecular weight from light-scattering data it is necessary to measure the excess scattering of a series of solutions (all at concentrations above the cmc) over that of a solution at the cmc and to extrapolate a suitable plot of these data to the cmc.[20,26] The appropriate form for the extrapolation and the necessary relationship between the results and the molecular weight can be obtained from the discussion of Prins and Hermans,[21,27] who have applied the general theory of the scattering of light by a multicomponent system to the case of charged detergent micelles dissolved in solvents that may contain added salts.

If the Prins–Hermans expression (including nonideality) for the scattering at the cmc is subtracted from that at some higher concentration, the result is[28]

$$\frac{K(c - c_0)}{\Delta R_{90}} = \frac{q}{M}\left\{1 + \left[\frac{p^2 + p - qp}{2M(C_1 + C_3)} + \frac{8v_m N_0}{M}\right](c - c_0)\right\} \quad (3)$$

where ΔR_{90} is the Rayleigh ratio, at 90° to the incident beam, of a solution of concentration c (grams per milliliter) minus that of a solution of concentration c_0; C_1 is the molar concentration of detergent monomer and C_3 the molar concentration of added salt ions having the same charge as a monomer ion; p is the absolute value of the number of fundamental charges per micelle; q is defined by $q = (C_1 + C_3)^2/(C_1^2 d_1 + 2C_1C_3d_2 + C_3^2 d_3)$, with $d_1 = 1 - \alpha + \alpha^2/4 + \alpha/4N$, $d_2 = 1 - \alpha/2 - f\alpha/2 + f\alpha^2/4 + f\alpha/4N$, and $d_3 = 1 - f\alpha + f^2\alpha^2/4 + f^2\alpha/4N$ where α $(=p/N)$ is the effective degree of dissociation of the micelles, N the number of monomers per micelle, and $f = (dn/dm_3)_{m_1}/(dn/$

(23) E. W. Anacker and H. M. Ghose, *J. Phys. Chem.*, 67, 1713 (1963).

(24) P. Outer, C. I. Carr, and B. H. Zimm, *J. Chem. Phys.*, 18, 830 (1950).

(25) B. A. Brice, M. Halwer, and R. Speiser, *J. Opt. Soc. Am.*, 40, 768 (1950).

(26) L. H. Princen and K. J. Mysels, *J. Colloid Sci.*, 12, 594 (1957).

(27) W. Prins and J. J. Hermans, *Koninkl. Ned. Akad. Wetenschap. Proc.*, B59, 298 (1956).

(28) See eq 30 of ref 21.

$d m_1)_{m_3}$, with m_i the molality of the ith component; $8v_m$ is the excluded volume per micelle; and $K = 2\pi^2 \cdot n_0^2(dn/dc)_{m_3}^2/N_0\lambda^4$. Terms higher than the second in the virial expansion are assumed small.

According to eq 3, the intercept (I) and the limiting slope (S) of a plot of the experimental quantity $K(c - (c_0/\Delta R_{90}$ *vs.* $(c - c_0)$ are both functions of both the number of charges per micelle and the number of monomers per micelle. They are given explicitly by the expressions

$$I = q/M \tag{4}$$

and

$$S = \frac{q}{2M^2}\left[\frac{p^2 + p - qp}{C_1 + C_3} + 16v_mN_0\right] \tag{5}$$

Thus, the value of the micellar molecular weight obtained from eq 4 is q times that obtained simply from the reciprocal of the intercept. The numerical value of q is usually sufficiently close to unity[27] so that the molecular weights obtained by the two methods are not very different.

Equations 3 and 4 are not in a very useful form, since they do not give p and N explicitly in terms of the experimental quantities I and S. To utilize these simultaneous relationships, therefore, Anacker, *et al.*,[29] solved them, but only for the "ideal" case ($v_m = 0$). In the notation used here, their expressions for p and N are

$$p = \frac{\frac{M_0S'}{1000}(C_1 + fC_3) + \left[\frac{S'}{500}(C_1 + C_3)\right]^{1/2}}{I(1 - {}^1/_2M_0IE)} \tag{6}$$

$$N = {}^1/_2\left[pE + \frac{1}{IM_0}\right] + {}^1/_2\left[\left(pE + \frac{1}{IM_0}\right)^2 - (p^2 + p)E^2\right]^{1/2} \tag{7}$$

where S' is the slope if $v_m = 0$; $E = (C_1 + fC_3)/(C_1 + C_3)$; and M_0 is the formula weight of the detergent monomer.

Unfortunately, the approximation $v_m = 0$ is not always a good one. Nevertheless, these equations can still be used, because it is possible to estimate the contribution to the slope due to the excluded volume per micelle (*i.e.*, to estimate $16qv_mN_0/2M^2$) and then to calculate the value that the observed slope *would* have if the solution *were* ideal by subtracting the estimate from the observed slope. This value of S' can then be used in eq 6 and 7 to obtain p and N. The procedure is as follows.

The numerical value of q is close to unity,[27] so, defining an "ideal part" (S') of the slope (S), eq 5 can be written

$$S' = \frac{q}{2M^2}\left(\frac{p^2 + p - qp}{C_1 + C_3}\right) \cong S - 8v_mN_0I^2 \tag{8}$$

and S' can be calculated from the observed slope and intercept of the light-scattering plot and the excluded volume per micelle; the latter quantity is estimated from

$$8v_m = \frac{32\pi}{3}r^3 \tag{9}$$

where r is the micelle radius. We have assumed a micelle radius of 24 A, the experimental result for SDS micelles in pure water, including a layer of bound counterions.[30] The resulting S' is then substituted directly into eq 6 and p is calculated. Since the resulting value of p is rather insensitive to the value of S' used, this approximate way of obtaining S' is adequate. Once p is known, eq 7 can be used to obtain the value of N.

All the experimental data were thus plotted as $K(c - c_0)/\Delta R_{90}$ *vs.* $(c - c_0)$. When N and p are determined from eq 6 and 7 using the observed intercept, I, and a value for S' calculated as described above, the values of N determined by this more complex method do not differ significantly from those obtained directly from the reciprocal of the intercept (*i.e.*, q is, indeed, near unity). For this reason, the reciprocal of the intercept is essentially within experimental error of, and therefore may just as well be taken as, the molecular weight. Two examples of the results of the more elaborate computation are given in Table II.

E. Determinations of the Critical Micelle Concentration (Cmc). 1. Conductivity. The cmc's of the cationic detergents in dilute (≤ 0.05 M) electrolyte solutions are sufficiently high so that they can be determined with good precision by the conductivity method. Accordingly, these cmc's were measured using a Kohlrausch-type bridge equipped with a dipping electrode, calibrated using the data of Jones and Bradshaw for KCl solution.[31]

Conductance techniques used were conventional and a complete description is given elsewhere.[8] Values of Λ were plotted aganst $C^{1/2}$. A sharp break in the curve is observed at the cmc.

2. Light Scattering. The cmc's of SDS in 0.05

(29) E. W. Anacker, R. M. Rush, and J. S. Johnson, *J. Phys. Chem.*, **68**, 81 (1964).

(30) F. Reiss-Husson and V. Luzzati, *ibid.*, **68**, 3504 (1964).

(31) G. Jones and B. C. Bradshaw, *J. Am. Chem. Soc.*, **55**, 1780 (1933).

Table II: Light-Scattering Results

System	Molality of added salt	$10^5 I$, mole/g	$10^4 S$, mole ml/g²	$\frac{1}{M_0 I}$
SDS in NaCl solution	0.050	4.10	32.47[a]	84
	0.201	3.23	10.48	107
	0.506	2.75	−4.09	126
DTAB in NaBr solution	0.050	4.50	16.53[b]	72
	0.100	4.47	6.26	73
	0.508	3.70	1.51	88
DTAC in NaCl solution	0.050	6.71	12.60	57
	0.201	6.10	3.87	62
	0.506	5.60	−1.12	68
DTAN in $NaNO_3$ solution	0.050	5.48	13.90	63
	0.101	4.74	11.01	73
	0.253	4.32	1.25	80
	0.509	4.02	0.72	86

[a] Use of eq 6–9 gives $10^4 S' = 27.97$, $\alpha = 0.157$, and $N = 89.0$. [b] Use of eq 6–9 gives $10^4 S' = 11.14$, $\alpha = 0.130$, and $N = 76$.

Table III: Specific Refractive Index Increments

System	Molality of added salt	$10^3 c_1$, g/ml	$10^3 \Delta c$, g/ml	$(\Delta n/\Delta c)_{m_3}$, ml/g
SDS in NaCl solution	0.050	3.014	6.530	0.1199
	0.050	3.014	9.738	0.1195
	0.201	5.582	5.582	0.1166
	0.201	2.232	8.928	0.1158
	0.506	5.824	5.824	0.1114
	0.506	3.494	8.154	0.1115
	0.506	2.118	8.474	0.1115
DTAB in NaBr solution	0.050	5.550	5.550	0.1504
	0.050	2.024	8.096	0.1513
	0.050	2.220	8.880	0.1515
	0.100	5.388	5.388	0.1519
	0.100	2.155	8.621	0.1504
	0.100	2.307	9.229	0.1520
	0.100	...	...	0.1508[a]
	0.508	4.810	4.810	0.1459
	0.508	1.924	7.696	0.1451
	0.508	1.973	7.891	0.1459
	0.508	...	...	0.1456[a]
DTAC in NaCl solution	0.050	3.582	8.358	0.1588
	0.201	...	...	0.1574[b]
	0.506	...	...	0.1536[b]
DTAB in NaCl solution	0.506	1.800[c]	7.198[c]	0.1707
	0.506	...	...	0.1545[d]
DTAN in $NaNO_3$ solution	0.050	3.105	7.245	0.1408
	0.101	...	...	0.1403[e]
	0.253	3.090	7.210	0.1381
	0.253	...	...	0.1390[e]
	0.509	3.060	7.130	0.1363
	0.509	...	...	0.1367[e]
DTAB in $NaNO_3$ solution	0.509	1.807[f]	7.228[f]	0.1524
	0.509	...	...	0.1342[g]

[a] Calculated using the Gladstone–Dale equation with n_2 calculated from the measured value of $(\Delta n/\Delta c)_{m_3}$ of 0.05 M NaBr with $\bar{v}_2 = 0.956$[20] and n_1 for NaBr solutions computed from data of Anacker and Ghose.[23] [b] Calculated using the Gladstone–Dale equation with n_2 calculated from the measured value of $(\Delta n/\Delta c)_{m_3}$ of 0.05 M NaCl, with $\bar{v}_2 = 0.96$ and n_1 for NaCl solutions computed from the data of Kruis,[18] as interpolated by Stamm.[19] [c] Grams of DTAC/ml. [d] Calculated using data of Anacker and Ghose[23] for NaBr solutions and data of Kruis,[18] as interpolated by Stamm,[19] for NaCl solutions. [e] Calculated using the Gladstone–Dale equation with n_2 calculated from the measured value of $(\Delta n/\Delta c)_{m_3}$ of 0.05 M $NaNO_3$ with an assumed value of $\bar{v}_2 = 0.96$ and n_1 for $NaNO_3$ solutions computed from data of Anacker and Ghose.[23] [f] Grams of DTAN/ml. [g] Calculated using data of Anacker and Ghose[23] for NaBr and $NaNO_3$ solutions.

and 0.5 M NaCl and of all the cationic detergents in aqueous electrolyte solutions ($\gtrsim 0.05$ M) were determined by light scattering. Measurements of R_{90} for solutions at several different detergent concentrations above and below the cmc, but at constant molality of added electrolyte, were made and the results plotted against the detergent concentration. At the cmc, there is a sharp break in the curve, above which the solutions scatter much more strongly per unit weight concentration than below.

Experimental Results

In order to use eq 3 to obtain the micellar molecular weight, it is necessary to know the specific refractive index increment, the critical micelle concentration, and the scattering, the latter as a function of concentration of detergent at constant molality of added electrolyte. The results of each of these measurements will be discussed in turn.

A. Specific Refractive Index Increment. Values of the specific refractive index increments $(\Delta n/\Delta c)_{m_3}$ for the various detergents in aqueous electrolyte solutions are given in Table III. The measured values of $(\Delta n/\Delta c)_{m_3}$ at different Δc are constant within experimental error ($\pm 0.5\%$). Values of $(\Delta n/\Delta c)_{m_3}$ calculated from the Gladstone–Dale equation (eq 2) are also listed in the table and agree quite well with the corresponding measured values. At some of the intermediate concentrations of additive, the calculated values were used. For mixed systems (*e.g.*, those containing DTAB dissolved in NaX) a small correction must be and was applied.[8,23] These corrected values of $(\Delta n/\Delta c)_{m_3}$ for the mixed systems are also listed in the table.

B. Critical Micelle Concentration (Cmc). Since the values of the cmc's of detergents in aqueous salt solutions depend somewhat on the method of measurement,[8,10] the ones used in the light-scattering calcula-

tions were those either directly measured by light scattering or measured by conductivity—a method which has been shown to agree with light scattering.[8]

Because of its greater convenience and speed, conductivity is the method of choice wherever it can be employed without sacrifice in precision. Practically speaking, the method is not routinely useful for electrolyte concentrations $\gtrsim 0.1\ M$ because of the high solvent corrections that become necessary. Fortunately, the light-scattering method is *more* precise at higher concentrations of electrolyte because the micelle numbers are greater and there is a concomitantly larger increase in scattering upon micelle formation. The two methods are thus complementary. Of course, other methods have also been used.[8,32]

An example of a light-scattering determination of the cmc is given in Figure 1. The results are displayed (Figure 2) as $-\log C_0$ *vs.* $-\log (C_0 + C_3)$ because it is well known that such plots are linear. It is apparent from Figure 2 that conductivity and light-scattering results fall on the same line and that our data for SDS are in satisfactory agreement with those of Williams, *et al.*[10]

These results were fit to straight lines by the method of least squares. The resulting equations are

$$\log (C_0) = -0.666 \log (C_0 + C_3) - 3.491 \text{ for SDS in NaCl}$$

$$\log (C_0) = -0.621 \log (C_0 + C_3) - 3.021 \text{ for DTAB in NaBr}$$

$$\log (C_0) = -0.631 \log (C_0 + C_3) - 2.794 \text{ for DTAC in NaCl} \qquad (10)$$

$$\log (C_0) = -0.547 \log (C_0 + C_3) - 3.018 \text{ for DTAN in } NaNO_3$$

The cmc values used in the light-scattering calculations were obtained from these relationships.

C. Light Scattering. The light-scattering data were plotted as $K(c - c_0)/\Delta R_{90}$ *vs.* $(c - c_0)$; some typical plots are shown in Figure 3.

In all cases the data fall on straight lines within $\pm 1\%$. Values of the intercepts (I) and slopes (S) of these lines along with values of N calculated from the simple intercept ($N = 1/M_0 I$) are given in Table II. In the Table II footnotes are also given, for two of the solutions, values of S' calculated from eq 8 and 9, N from eq 7, and α ($=p/N$) from the value of p obtained from eq 6. As noted above, the differences between the results of the exact and approximate ($q = 1$) calculations of N are inappreciable.

The precision of the measurements of R_{90} is $\pm 1\%$ (probable error); however, the necessity of extrapolating the data to $(c - c_0) = 0$ produces an uncertainty in the intercept which is sometimes as large as $\pm 2.5\%$. The over-all precision of the light-scattering molecular weights is somewhat less than this, because of the dependence on other parameters. The measure-

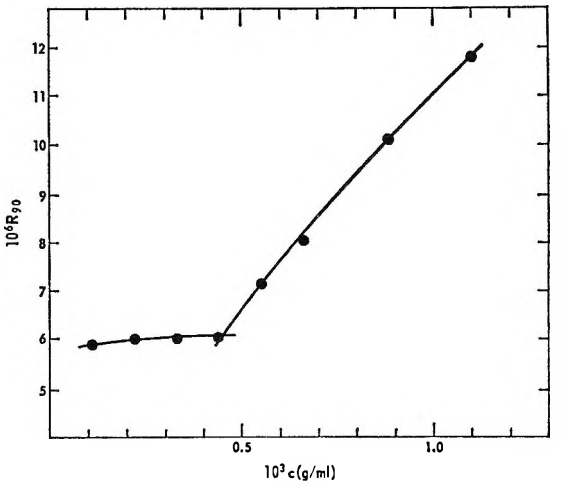

Figure 1. Light-scattering determination of the cmc of DTAB in 0.500 M NaBr.

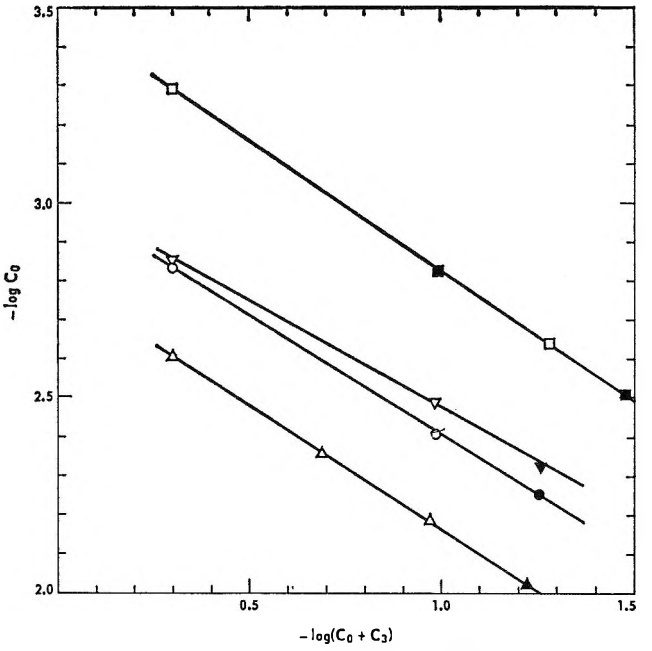

Figure 2. Plots of $-\log C_0$ *vs.* $-\log (C_0 + C_3)$ for detergents in aqueous salt solutions. SDS in NaCl: □, light-scattering values; ■, conductivity data of Williams, *et al.*[10]
DTAN in $NaNO_3$: ▽, light scattering; ▼, conductivity.
DTAB in NaBr: ○, light scattering; ●, conductivity.
DTAC in NaCl: △, light scattering; ▲, conductivity.

(32) M. L. Corrin and W. D. Harkins, *J. Chem. Phys.*, 14, 640 (1946).

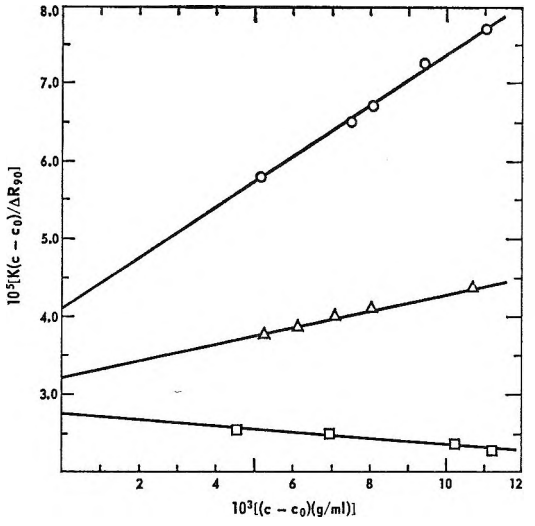

Figure 3. Light-scattering results for SDS in NaCl: O, 0.050 *m* NaCl; △, 0.201 *m* NaCl; □, 0.506 *m* NaCl.

ment of $(\Delta n/\Delta c)_{m_3}$ has been made to a precision of ±0.5%, but since it enters the light-scattering equation as the square, it contributes an additional probable error of ±1% to the molecular weight. The value of c is, of course, known quite accurately, but the imprecision of ±1% in c_0 produces a probable error which is sometimes as large as ±0.5% in $(c - c_0)$. Thus, the micellar molecular weights and therefore the micelle numbers determined by light scattering are sometimes precise only to about ±4%.

D. Comparison of Light-Scattering Results with Literature Values. The results obtained here for the micellar molecular weights may be compared with those of other investigations on SDS in NaCl solutions[33] and on DTAB in NaBr solutions.[29] There exist no comparable studies of DTAC or DTAN.

The values of the refractive index increments and the cmc's obtained here agree quite well with those obtained by Mysels and Princen[33] on SDS. On the other hand, the observed intercepts of the light-scattering plots differ by as much as 15%. However, most of their measurements were apparently made on solutions which produced scatterings less than five times that of solvent, so that the probable error involved in their determinations of ΔR_{90} would have to be as large as ±3% at low concentrations and the over-all error in the resulting molecular weights must be as great as ±8%. In addition, these earlier workers discarded "a very large number of measurements" for reasons such as "high dissymmetry, visible dust, or presence of impurities revealed upon further dilution to the cmc" as well as "a few stray values." No such difficulties were encountered here, possibly because of preliminary removal of dodecyl alcohol by extraction.

At first glance, it appears as though the results for DTAB in NaBr presented in Table II agree closely with those obtained by Anacker, *et al.*,[29] directly from the intercepts of their light-scattering plots. However, this is to some extent owing to a fortuitous cancellation of discrepancies, since the values of the refractive index increments, the cmc's, and therefore the scattered intensities obtained by them differ from those found here. Although many of their measurements were made on solutions which produced scatterings greater than five times that of background, their data points scatter about a smooth curve, falling as far as ±5% from it. This considerably higher probable error in the values ΔR_{90} must produce a correspondingly greater error in the molecular weights found by them.

For these reasons, but, more importantly, for the sake of internal consistency, we have used our own results in making comparisons with theory in all cases.

Theoretical Results

Values of ΔG^{∞}_{HC} were determined with the use of eq 1. The values of $\hat{N}$ determined by light-scattering experiments (Table II) on SDS, DTAB, DTAC, and DTAN solutions at various ionic strengths were used in the computations along with an assumed micelle radius of 19.7 A. This radius is an experimental result only for SDS micelles in pure water[30] and it is assumed that the same value is appropriate for all four detergents under all conditions considered. The use of this value for the radius has been discussed earlier.[3] The distance of closest approach (a) was than calculated as 19.7 + $r_{counterion}$; namely 21.8 A for SDS and 21.2 A for DTAB, DTAC, and DTAN. The values for the counterion radii used were those for the hydrated ions in aqueous solutions, as obtained from experimental data using the Debye–Hückel limiting law.[34] These two quantities, $\hat{N}$ and a, along with the ionic strength of the solution, were then used to calculate the boundary condition (*i.e.*, the electric field at the micelle surface) that applies and the appropriate computer solution was obtained from the computer tables by interpolation, as before.[3] Insertion of $\psi_{b,\hat{N}}$ and the experimental cmc (mole fraction basis[35]) into eq 1 allows computation of ΔG^{∞}_{HC} (infinitely dilute refer-

(33) K. J. Mysels and L. H. Princen, *J. Phys. Chem.*, 63, 1696 (1959).

(34) I. M. Klotz, "Chemical Thermodynamics," W. A. Benjamin, Inc., New York, N. Y., 1964, p 417.

(35) In an earlier paper (see ref 3), a molality basis was used. The mole fraction basis would seem, however, to be a better choice in that it is a more direct reflection of the cratic contribution and also is in more common use in the micelle literature.

ence state, mole fraction basis) as before.[3] Results of this computation for the four detergents at several ionic strengths are presented in Table IV.

Table IV: Computation of $-\Delta G^{\infty}_{HC}$

System	Molality of added salt[a]	10^3C_0, cmc in moles/l.	10^5X_0, cmc in mole fraction	$e\psi_a,\hat{N}/kT$	$-\Delta G^{\infty}_{HC}$, cal
SDS in NaCl	0.050	2.30	4.13	5.33	10,900
solution	0.201	0.94	1.69	4.48	11,400
	0.506	0.51	0.91	3.89	11,900
DTAB in NaBr	0.050	5.71	10.30	5.03	9,510
solution	0.100	3.88	6.98	4.47	9,460
	0.508	1.46	2.61	3.43	9,610
DTAC in NaCl	0.050	9.50	17.10	4.46	8,640
solution	0.201	4.36	7.83	3.52	8,630
	0.506	2.48	4.43	2.93	8,710
DTAN in $NaNO_3$	0.050	4.70	8.45	4.72	9,310
solution	0.101	3.32	5.97	4.46	9,510
	0.253	2.04	3.66	3.85	9,540
	0.509	1.40	2.50	3.39	9,590

[a] The micelles in these solutions exist in the presence of monomeric detergent ions of concentration equal to the cmc. Thus, the ionic strength used was the added electrolyte concentration plus C_0. This has no appreciable effect on the results.

As is clear from the table, ΔG^{∞}_{HC} for the cationic surfactants is roughly independent of the nature of the supporting electrolyte (~10% spread in all values) and essentially completely independent of ionic strength (~3% spread). For SDS, on the other hand, a small, but systematic dependence of ΔG^{∞}_{HC} on ionic strength is observed (~10% increase in going from 0.05 to 0.5 *M* NaCl). As reported earlier, an apparent difference (~20%) does indeed exist between the values of ΔG^{∞}_{HC} for SDS and those for the cationic detergents.

Discussion

First, it should be pointed out that eq 1 bears some resemblance to the empirical, linear log (C_0) *vs.* log ($C_0 + C_3$) relationship (eq 10). Both equations are of the form log cmc = constant + *f*(ionic strength). Thus, the constant term of the empirical equation is related to ΔG^{∞}_{HC} and the potential at the surface of the micelle must be approximately linear in log ($C_0 + C_3$).

The magnitude of ΔG^{∞}_{HC} obtained agrees quite well with two other experimental estimates of this quantity; namely Wishnia's[36] (from measurements of solubilities of gaseous hydrocarbons in detergent solutions), which gives between −7100 and −10,800 cal for a 12-carbon chain, and Corkill and co-workers'[37] (from cmc measurements on nonionic detergents[38]), which is −8600 cal for the same length hydrocarbon chain. Agreement is also manifest with the values previously calculated (from then extant data on SDS and DTAB), which fall between −9900 and −12,700 cal.[3]

The results of Table IV show, as before,[3] a slight increase of ΔG^{∞}_{HC} with increasing ionic strength. This change may be a result of increased "salting out" of the hydrocarbon chains or may be a result of a more fundamental variation of ΔG^{∞}_{HC} with $\hat{N}$, as suggested on theoretical grounds by Reich[39] and Ooshika.[40] However, the variation is small, even in the SDS case, and could merely be a result of the assumption that the micellar radius is independent of N.

The largest micelles of SDS, for example, might require some increase in radius because of crowding of hydrocarbon chains in its interior. An increase in radius of, say, 10% over the complete range of ionic strength would explain the apparent change in ΔG^{∞}_{HC} as computed here.

The differences in ΔG^{∞}_{HC} for the different detergents, especially those between SDS and the cationic detergents, may also be a result of small differences in radii of the micelles of the various detergents or it may reflect small, specific differences in the supporting electrolytes. It cannot, however, be explained by the difference in salting-out strengths of the various supporting electrolytes. Thus, NaCl salts out nonpolar substances more strongly than does NaBr or $NaNO_3$,[41] but the tendency for the DTAC hydrocarbon tails to enter the micelle from a medium containing NaCl is *not* as great as that for the DTAB and DTAN hydrocarbon chains from NaBr and $NaNO_3$, respectively.

Although small variations are encountered, this extension of the measurements to a wider range of detergents and supporting electrolytes has not altered the earlier suggestion[3] that the simple approach adopted here seems to be adequate as an approximate explanation of the ionic strength dependence of the micelle number; that is, that the micelle number is limited by electrostatic repulsions that may be estimated by numerical solution of the Poisson–Boltzmann equation. The approach appears to be particularly satis-

(36) A. Wishnia, *J. Phys. Chem.*, 67, 2079 (1963).

(37) J. M. Corkill, J. F. Goodman, and S. P. Harrold, *Trans. Faraday Soc.*, 60, 202 (1964).

(38) To eliminate the effect of the polar head groups the data of Corkill, *et al.*, for various sizes of head group have been extrapolated to zero head group.

(39) I. Reich, *J. Phys. Chem.*, 60, 257 (1956).

(40) Y. Ooshika, *J. Colloid Sci.*, 9, 254 (1954).

(41) H. S. Harned and B. B. Owen, "The Physical Chemistry of Electrolytic Solutions," Reinhold Publishing Corp., New York, N. Y., 1958, pp 531–534.

factory for cationic detergents. The crucial remaining question of the constancy of micellar radius can only be resolved by direct measurement of the quantity (by low-angle X-ray scattering) for solutions of the various detergents containing added salt. It would also be of interest, of course, to measure ΔG^{∞}_{HC} as a function of temperature in order to determine ΔH^{∞}_{HC} and ΔS^{∞}_{HC} under the various experimental conditions.

From a theoretical point of view, the next step would be to compare the experimental ΔG^{∞}_{HC} with a value predicted from, in essence, first principles. We do not believe that the present state of the statistical theory of aqueous solutions warrants such a comparison. Recent attempts in this direction are not promising.[42] Indeed, with the current range of adjustability of most theories, it is not unlikely that an embarrassment of riches would result, *i.e.*, that theories based on quite different physical models could *all* be made to yield an answer in agreement with experiment. As an example, we might cite the very simple approach of Aranow and Witten;[43] based on the increase in rotational freedom of a hydrocarbon chain inside, compared with outside, the micelle, this theory ignores all attendant alterations in the structure of water that most people feel is the very crux of the matter. Nevertheless, the Aranow and Witten theory provides a value of ΔG^{∞}_{HC} ($\sim -10{,}000$ cal) that is in rather good agreement with experiment.

Acknowledgment. The authors wish to thank Dr. Martin Schick of Lever Brothers for expert advice on the synthesis of SDS samples and Professor Joseph Kurz of Washington University for stimulating and informative discussions.

(42) D. C. Poland and H. A. Scheraga, *J. Colloid Interface Sci.*, **21**, 273 (1966).

(43) R. H. Aranow and L. Witten, *J. Phys. Chem.*, **64**, 1643 (1960)

Theory of Optically Active Compounds of High Latent Symmetry

by Dennis J. Caldwell

Department of Chemistry, The University of Utah, Salt Lake City, Utah 84112 *(Received November 29, 1966)*

The behavior of magnetic dipole transitions in different types of dissymmetric fields is discussed along with limitations of one-center models for optical rotation. The general properties of the angular wave functions are used in a second-order perturbation treatment to explain the qualitative features of the ORD of certain transition metal complexes.

I. Introduction

In a given dissymmetric field the sign of rotation for an optically active transition in a chromophore is determined by the general shape of the ground and excited orbitals. In most cases a detailed knowledge of the electron cloud is only necessary for quantitative work.

Since the basic mechanisms responsible for the phenomenon are still in contention, it is often advantageous to examine things from the simplest possible viewpoint. For example, possible intramolecular interactions leading to optical activity are coupled oscillator effects,[1,2] charge transfer,[3] and incomplete screening.[4] The appropriate theories of these separate

(1) J. G. Kirkwood, *J. Chem. Phys.*, **5**, 479 (1937).

(2) L. L. Jones, Ph.D. Thesis, University of Utah, Salt Lake City, Utah, 1961.

(3) S. F. Mason, *Nature*, **199**, 139 (1963).

(4) W. J. Kauzmann, J. E. Walter, and H. Eyring, *Chem. Rev.*, **26**, 339 (1940).

effects do not always predict the same sign for a transition, and since calculations of even relative magnitudes are often unreliable, experiment can exclude those effects which give the wrong sign.

With suitable interpretation the shapes and relative energies of the harmonic oscillator wave functions are in accord with much of what is known about the structure of actual atoms. Although the steep distance dependence of the Gaussian wave function cannot be expected to describe all of the subtle intramolecular interactions as accurately as the hydrogen-like functions, they should be capable of dealing with those effects which depend on inverse powers of distance such as the coupled oscillator effect and dipole and quadrupole terms. The fact that the oscillator model leads to the same expressions as are derived by general quantum mechanical methods in the polarizability theory of optical rotatory power and the theory of van der Waals forces is sufficiently encouraging to retain such approaches as a scaffolding until the general theory of optical rotatory power is on as firm a basis as, for example, nuclear magnetic resonance.

All solutions to the central force problem have identical angular functions. In addition the radial functions will all have the same number of nodes for a given orbital. Thus we expect that all solutions to the bound state central force problem should give rise to a series of functions similar in shape and relative energies.

Letting (000) be the ground state of the oscillator and $(n_1n_2n_3)$ the excited state with energy $h[(n_1 + {}^1/_2)\nu_1 + (n_2 + {}^1/_2)\nu_2 + (n_3 + {}^1/_2)\nu_3]$ one may make the following correspondence

Oscillator	Hydrogen-like
(000)	1s
(100), (010), (001)	2p
(200), (110), etc.	3s, 3d
(300), (111), etc.	4p, 4f

The 1s and 2p functions are except for the exponential function identical with the corresponding oscillator functions. In the next set the (110), (101), and (011) functions correspond to the $3d_{xy}$, $3d_{xz}$, and $3d_{yz}$ orbitals, the [2(002) − (020) − (200)] and [(200) − (020)] functions correspond to $3d_{3z^2-r^2}$ and $3d_{x^2-y^2}$, and [(002) + (020) + (200)] corresponds to the 3s orbital. The absence of the even or odd orbitals for a given level does not appear to present a serious obstacle, since they have the wrong symmetry for the mixing of electric and magnetic dipole transitions. For example, the major contribution from a 2p → 3s electric dipole transition comes from mixing with a 2p → 2p′ magnetic transition while a 3d → 3d′ magnetic transition mixes with a 3d → 4p or 3d → 4f electric transition. Owing to the same general symmetry characteristics, the behavior of a 3p → 4d transition may be inferred from that of 2p → 3d or 4p → 5d.

II. The Low-Symmetry Case

A general expression for the oscillator applicable to chromophores of low symmetry has been derived by Condon, *et al.*[5] The problem of a single electron in an arbitrary excited state was solved. A slightly different answer is obtained when all of the orbitals of lower energy are presumed filled; however, the essential qualitative features of the model remain intact. There are just nine possible transitions for a harmonic oscillator: three strong magnetic with frequencies $\nu_1 - \nu_2$, $\nu_1 - \nu_3$, and $\nu_2 - \nu_3$, three weak magnetic with frequencies $\nu_1 + \nu_2$, $\nu_1 + \nu_3$, and $\nu_2 + \nu_3$, and three strong electric with frequencies ν_1, ν_2, and ν_3. The rotation due to the three polarized along the x_1 direction for an electron initially in the $(n_1n_2n_3)$ state is

$$\theta = K\left\{\left(\frac{1}{\nu_2} - \frac{1}{\nu_3}\right)\frac{n_2 + n_3 + 1}{(\nu_2 + \nu_3)^2 - \nu_1^2} \times \left[-\frac{1}{\nu_1^2 - \nu_2} + \frac{1}{(\nu_2 + \nu_3)^2 - \nu^2}\right] + \left(\frac{1}{\nu_2} + \frac{1}{\nu_3}\right)\frac{n_2 - n_3}{(\nu_2 - \nu_3)^2 - \nu_1^2} \times \left[-\frac{1}{\nu_1^2 - \nu_2} + \frac{1}{(\nu_2 - \nu_3)^2 - \nu^2}\right]\right\} \quad (1)$$

Where K is a constant that depends on the surrounding field. The terms for the other six transitions are obtained by cyclic permutation.

Bearing in mind the correspondence in shapes and relative energies of oscillator and hydrogen-like functions, we may conclude from the above expression that the rotational strengths from the most common instances of degenerate transitions tend to cancel. In eq 1 the first term is somewhat smaller than the second and may be neglected unless $n_2 = n_3$. Taking into account the other terms obtained by permutation it is found that the sum of the $n_i - n_j$ terms is approximately zero. Since the coefficients of the linear combinations of functions satisfy the orthogonality conditions, this suggests that the sum of the rotational strengths of all degenerate transitions tends to zero. In fact, it should be possible to prove using the angular

(5) E. U. Condon, W. Altar, and H. Eyring, *J. Chem. Phys.*, 5, 753 (1937).

functions and unspecified radial functions that the sum of the rotational strengths of all degenerate bands in the perturbed central force problem tends to zero, provided certain conditions are satisfied.

One must not attempt to make this observation too general, for there are several other factors involved. The above discussion has indicated only that the sum tends to zero under the following conditions. (1) The major contribution to the rotation is due to the static charge and not the coupled oscillator effect. (2) The major term in the dissymmetric perturbing potential arises from pairwise interactions of the chromophore with individual neighboring groups. (3) Other types of degeneracy such as group degeneracy are not considered. The first condition is generally true for magnetic dipole transitions but is generally not satisfied for electric dipole transitions. The second condition is true for molecules whose vicinal groups do not lie on axes or planes of symmetry of the chromophore.

It will be shown below that when pairwise interactions are no longer responsible for optical activity and it becomes necessary to use second-order perturbation theory that the rotational strengths of a degenerate band do not necessarily sum to zero. In fact, they may all reinforce rather than cancel one another.

Before turning to the high-symmetry question, it is worthwhile to review the consequences of the low-symmetry theory. The coefficient K in eq 1 is proportional to $-Q\gamma_x\gamma_y\gamma_z$, where Q is positive for an attractive force (as is generally the case) and negative for a repulsive one, and γ_x, γ_y, and γ_z are the direction cosines of the perturbing group. The choice of axes is generally governed by the planes and axes of symmetry of the chromophore. The labeling is arbitrary, provided the system is right handed.

Consider the carbonyl chromophore (Figure 1). The product of the direction cosines of the vicinal group, which points upward, is negative. The lowest lying transition is n $\rightarrow \pi^*$ or (010) $\rightarrow$ (100) with frequency $(\nu_1 - \nu_2) < \nu_3$. This leads to a rotation proportional to $+Q$, or positive for an attractive potential, in agreement with experiment. The n $\rightarrow \sigma^*$ transition is (010) $\rightarrow$ (001) and gives the opposite sign provided $\nu_1 > (\nu_2 - \nu_3)$; *i.e.*, the electron cloud is not highly anisotropic.

For several reasons this model is suitable only for analyzing the features of magnetic dipole transitions. First, the coupled oscillator effect known to be important for electric dipole transitions is not included, and until such time as there are developed reliable methods for determining the relative magnitudes of these effects, one can never fully rely on a static field calculation for an electric dipole transition. Second, this is a one-center model and is unsuited for dealing with electric dipole transitions involving electron clouds equally attached to two or more nuclei in a highly anisotropic chromophore.

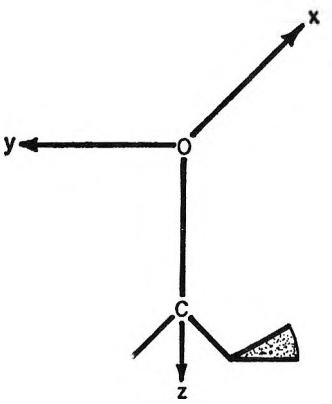

Figure 1. The carbonyl chromophore.

The situation with the magnetic dipole transition is somewhat different because in most cases the overlap between initial and final states is centered on one nucleus, which is qualitatively amenable to a one-center treatment.

III. High Symmetry

The first-order perturbation treatment of several degenerate systems such as the benzene chromophore[6] has led to the supposition that the rotational strengths of the component transitions of a degenerate band sum to zero. This work has been done on systems where the dissymmetric perturbations consisted of single groups whose centers were not located on planes or lines of symmetry of the chromophore. The rotation could be divided into partial contributions arising from pairwise interactions. Such molecules have C_1 symmetry. Any heuristic proofs of the sum rule tacitly invoke such pairwise interactions and rule out cases of high latent symmetry where three-way interactions are predominant and second-order pertubation theory is necessary to compute the rotatory power.

In this paper no attempt will be made to formulate and prove a theorem which covers all these cases; however, from what will be presented below on the transition metal octahedral complexes, it seems likely that the sum rule is still true for pairwise interactions but is not generally true for higher symmetry and three-way interactions. It is further emphasized that this discussion is confined to the static field effects of vicinal

(6) D. J. Caldwell and H. Eyring, *Ann. Rev. Phys. Chem.*, 15, 281 (1964).

groups, which will confine most of the general results to magnetic dipole transitions. The results will be true for electric dipole transitions only insofar as the static field effect is dominant.

Experimentally the behavior of the two cases may be distinguished. When the sum rule is satisfied, the circular dichroism and dispersion will appear as in Figure 2a. In intermediate cases where one component exhibits greater rotatory power than the other, the situation will be as in Figure 2b. Owing to the interference of other bands and background rotation, it is often difficult to make such distinctions in the ORD. The CD curves should prove to be more illuminating. When the components of the degenerate band are all of the same sign, the corresponding CD and ORD curves should be indistinguishable from the familiar nondegenerate case. This behavior is observed in the transition metal complexes of C_3 symmetry.[7]

In general the contribution to the dispersion outside the absorption band for a degenerate transition with frequency ν_0 may be written

$$\theta = \frac{a}{\nu_0^2 - \nu^2} + \frac{b}{(\nu_0^2 - \nu^2)^2} \qquad (2)$$

When $b >> a$, the behavior of Figure 2a is observed; the situation where $b \sim a$ is covered in Figure 2b; and when $a >> b$, one has normal dispersion (not shown).

IV. Transition Metal Complexes

As a preliminary problem in this method for treating molecules of high symmetry, the one-center formalism will be applied to diamagnetic octahedral complexes, the prototype of which will be $Co(en)_3^{3+}$ and its derivatives. A first-order perturbation treatment of this problem with a special form of potential function has been given by Moffitt[8] and by Piper and Karipides.[9] Even though the d orbitals may be involved in hybridization, the qualitative features of the system, which are of great interest, should be preserved.

Our model then consists of a system of six electrons constrained to move in a central force field. The radial oscillator functions are chosen because of the great simplification in the final formulas, which are only intended to illustrate the qualitative features of this system.

The configuration for the levorotatory form of the $Co(en)_3^{3+}$ ion is depicted in Figure 3. The cobalt atom has six paired d electrons. The perturbation of the system is split into two parts. First the coordinated nitrogen atoms effect a splitting of the degenerate d level into two levels consisting of three nonbonding orbitals of F_{2g} symmetry and two higher energy anti-

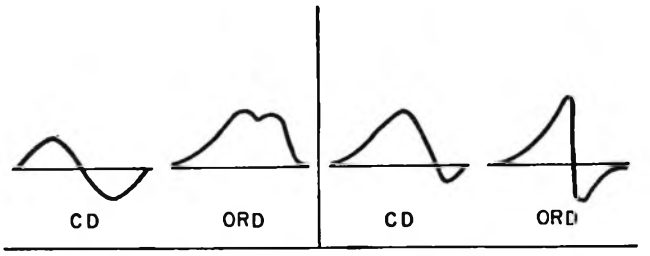

Figure 2. CD and ORD for degenerate transition.

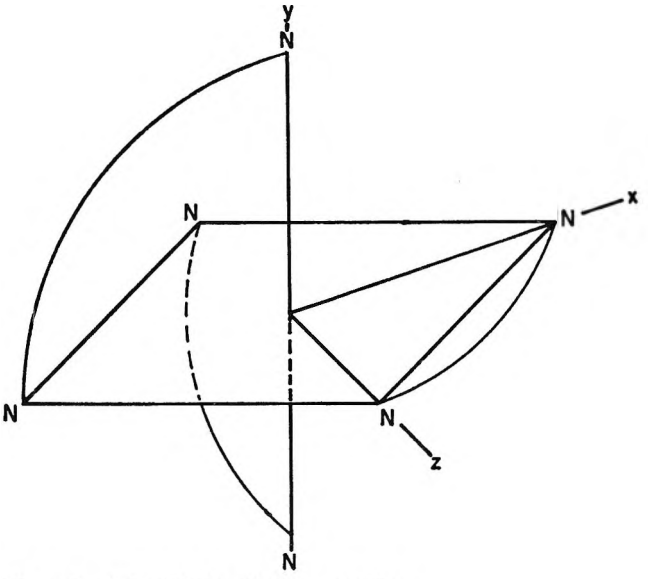

Figure 3. The ethylenediamine complex.

bonding orbitals of E_g symmetry. Second, the field of the bridge atoms slightly distorts the paths of the d electrons in their jump from the F_{2g} to the E_g orbitals making the transition optically active.

The starting point of the theory is the solution to the spherically symmetric central force problem. In harmonic oscillator notation the appropriate d functions are

$$\Phi_1 = (1/\sqrt{6})[2(002) - (020) - (200)] \qquad (3a)$$

$$\Phi_2 = (1/\sqrt{2})[(200) - (020)] \qquad (3b)$$

$$\Phi_{xy} = (110) \qquad (3c)$$

$$\Phi_{xz} = (101) \qquad (3d)$$

$$\Phi_{yz} = (011) \qquad (3e)$$

This is also the correct array of functions in the O_h field of the complex. Here the second set of orbitals

(7) J. G. Brushmiller, E. L. Amma, and B. E. Douglas, *J. Am. Chem. Soc.*, 84, 3227 (1962).

(8) W. Moffitt, *J. Chem. Phys.*, 25, 1189 (1956).

(9) T. S. Piper and A. Karipides, *Mol. Phys.*, 5, 475 (1962).

is lower in energy than the first, and the six d elections of the cobalt atom will be in these three orbitals. The determinantal wave function for the ground state is written

$$\theta_G = (1/\sqrt{6!})|\Phi_{xy}(1)\bar{\Phi}_{xy}(2)\Phi_{xz}(3)\bar{\Phi}_{xz}(4)\Phi_{yz}(5)\bar{\Phi}_{yz}(6)|$$
$$= |\Phi_{xy}^2\Phi_{xz}^2\Phi_{yz}^2| \quad (4)$$

The Φ_1 and Φ_2 functions span the E_g representation and the Φ_{xy}, Φ_{xz}, and Φ_{yz} functions belong to the F_{2g} representation. The ground state θ_G has, of course, A_{1g} symmetry.

The product rule $E_g \times F_{1g} = F_{1g} + F_{2g}$ indicates two classes of singly excited states. The F_{1g} will describe the triply degenerate magnetic dipole transition in question and the F_{2g} will be both electrically and magnetically forbidden. In the abbreviated notation the six excited-state wave functions are

$$\theta_{1a} = |\Phi_{xy}\ \Phi_1| \quad (5a)$$
$$\theta_{2a} = |\Phi_{xz}\ \Phi_1| \quad (5b)$$
$$\theta_{3a} = |\Phi_{yz}\ \Phi_1| \quad (5c)$$
$$\theta_{1b} = |\Phi_{xy}\ \Phi_2| \quad (5d)$$
$$\theta_{2b} = |\Phi_{xz}\ \Phi_2| \quad (5e)$$
$$\theta_{3b} = |\Phi_{yz}\ \Phi_2| \quad (5f)$$

The appropriate linear combination of functions for the F_{1g} state may be written

$$\theta_z = |(110)\ \Phi_a| \quad (6a)$$
$$\theta_y = |(101)\ \Phi_b| \quad (6b)$$
$$\theta_x = |(011)\ \Phi_c| \quad (6c)$$

and

$$\Phi_a = (1/\sqrt{2})[(200) - (020)] \quad (7a)$$
$$\Phi_b = (1/\sqrt{2})[(002) - (200)] \quad (7b)$$
$$\Phi_c = (1/\sqrt{2})[(020) - (002)] \quad (7c)$$

In this investigation we will neglect spin degeneracy and the perturbation of the ground state. The standard first-order perturbation treatment gives a zero result because by symmetry the pairwise interactions sum to zero. A three-body interaction and hence second-order perturbation theory must be invoked. The modified formula for the rotational strength of a transition is

$$R_{ab} = \sum_c{}' \sum_d{}' \frac{\langle c|V|d\rangle\langle d|V|b\rangle\langle a|\mathbf{R}|c\rangle\cdot\langle b|\mathbf{M}|a\rangle}{(E_b - E_c)(E_b - E_a)} \quad (8)$$

where $\langle b|\mathbf{M}|a|\rangle$ is the unperturbed magnetic moment of the transition and c and d are intermediate states.

The general expression for the potential of the perturbing field may be written

$$V = b_0 + b_i x_i + b_{ij}x_i x_j + b_{ijk}x_i x_j x_k + b_{ijkl}x_i x_j x_k x_l \quad (9)$$

where the summation convention is used and $x_1 = x$, $x_2 = y$, and $x_3 = z$.

In the octahedral field of the six identical coordinating atoms the lowest order nonvanishing terms are

$$V_0 = b_{11}(x^2 + y^2 + z^2) + b_{1111}(x^4 + y^4 + z^4) + b_{1122}(x^2y^2 + x^2z^2 + y^2z^2)$$

where b_0 has been set equal to zero.

The first term accounts for the spherically symmetric field of the central atom along with the spherically symmetrical component of the ligand field. The other terms represent the distinctively octahedral contribution that is responsible for splitting the degenerate levels of the central force system.

The influence of this field will be incorporated into the functions and energies of the zeroth-order set of states.

The potential function describing the influence of both bridge atoms and ligand substitution will have the form

$$V_D = b_1x + b_2y + b_3z + b_{12}xy + b_{13}xz + b_{23}yz + b_{112}x^2y + b_{113}x^2z + b_{122}xy^2 + b_{223}y^2z + b_{133}xz^2 + b_{233}yz^2 \quad (10)$$

Since all of the groups lie on planes or axes of symmetry of the chromophore, the $b_{123}xyz$ term is absent; but we are led to expect that the second-order treatment will lead to rotations proportional to such terms as b_1b_{23} or $b_{122}b_{23}$, which have the same symmetry as b_{123}. In the unsubstituted complex $Co(en)_3^{3+}$ $b_1 = b_2 = b_3 = 0$ and the lowest order contribution will be expected from the $b_{122}b_{23}$ terms. If one of the ethylenediamine groups is removed and replaced by two atoms such as in the complex ion $Co[(en)_2Cl_2]^+$ the b_1 terms are no longer all zero owing to the difference in electronegativity of chlorine and nitrogen, and a whole new set of terms must be computed.

The magnetic moments for the triply degenerate transition are

$$\langle\theta_z|\mathbf{M}|\theta_G\rangle = -2i(e\hbar/2mc)\mathbf{k} \quad (11a)$$
$$\langle\theta_y|\mathbf{M}|\theta_G\rangle = -2i(e\hbar/2mc)\mathbf{j} \quad (11b)$$
$$\langle\theta_x|\mathbf{M}|\theta_G\rangle = -2i(e\hbar/2mc)\mathbf{i} \quad (11c)$$

The calculation may be directed toward the $\theta_G \rightarrow \theta_z$ transition; the results for the other two will be ob-

tained by cyclic permutation. The appropriate electric dipole transition which may be mixed with the $\theta_G \rightarrow \theta_z$ transition involves the state $|(110)\ (111)|$. This leads to the evaluation in eq 8 of the sum

$$\sum_d{}' \frac{\langle((111)|V|d\rangle\langle d|V|\theta_a\rangle}{E_b - E_d} \qquad (12)$$

The lowest order nonvanishing terms will be supplied by those functions which are a linear combination of (210), (201), (120), and (021).

Were one to ignore the splitting of the excited states in the octahedral field and set the denominators, $E_b - E_d$, equal for these intermediate states, the above sum would vanish. The correct combination of functions leads to the following 4p and 4f prototypes

(111)	4f	A_{2u}
$\chi_1 = [(300) + (120) + (102)]/\sqrt{3}$		
$\chi_2 = [(210) + (030) + (012)]/\sqrt{3}$	4p	F_{1u}
$\chi_3 = [(201) + (021) + (003)]/\sqrt{3}$		
$\chi_4 = [(120) - (102)]/\sqrt{2}$		
$\chi_5 = [(012) - (210)]/\sqrt{2}$	4f	F_{2u}
$\chi_6 = [(201) - (021)]/\sqrt{2}$		
$\chi_7 = [(120) + (102) - 2(300)]/\sqrt{6}$		
$\chi_8 = [(210) + (012) - 2(030)]/\sqrt{6}$	4f	F_{1u}
$\chi_9 = [(201) + (021) - 2(003)]/\sqrt{6}$		

These orbitals will have the same shape, symmetry, and qualitative characteristics as any solution to the central force problem. The ten functions, together with the three ground-state orbitals (110), (101), (011), lead to the molecular functions which must be considered as intermediate states.

In eq 12 the matrix elements $\langle((111)|V|d\rangle$ will be zero for the wave functions involving the χ_4, χ_5, and χ_6 orbitals. This leaves 18 Slater functions—9 with the F_{1u} 4p orbitals and 9 with the F_{1u} 4f orbitals χ_7, χ_8, and χ_9. These sets of functions each lead to Slater functions of $F_{1g} \times F_{2u} = F_{1u} + F_{2u} + E_u + A_{2u}$ symmetry, or a total of 18.

The 4p functions are given along with their symmetry in eq 13. The obvious normalizing factors are omitted.

A_{2u}	$\|(011)\ \chi_1\| + \|(101)\ \chi_2\| + \|(110)\ \chi_3\|$	(13a)
E_u	$2\|(011)\ \chi_1\| - \|(101)\ \chi_2\| - \|(110)\ \chi_3\|$	(13b)
	$2\|(101)\ \chi_2\| - \|(011)\ \chi_1\| - \|(110)\ \chi_3\|$	(13c)
F_{1u}	$\|(110)\ \chi_1\| + \|(011)\ \chi_3\|$	(13d)
	$\|(110)\ \chi_2\| + \|(101)\ \chi_3\|$	(13e)
	$\|(101)\ \chi_1\| + \|(011)\ \chi_2\|$	(13f)
	$\|(101)\ \chi_3\| + \|(110)\ \chi_2\|$	(13g)
F_{2u}	$\|(110)\ \chi_1\| - \|(011)\ \chi_3\|$	(13h)
	$\|(011)\ \chi_2\| - \|(101)\ \chi_1\|$	(13i)

The 4f functions will not be written out in detail since they will give the same results as the 4p. For example, the appropriate A_{2u} function is $|(011)\ \chi_7| + |(101)\ \chi_8| + |(110)\ \chi_9|$ which by inspection is seen to give except for a numerical factor the same result as the function of (13a). The behavior of the functions (13a) will be duplicated by that of the 4f functions. A quantitative calculation would of course include configuration interaction between the sets of states with the same symmetry.

The A_{2u} and E_u states are linear combinations of one set of functions and the F_{1u} and F_{2u} are linear combinations of a second set. When the required matrix elements are calculated, these pairs of states should give equal and opposite contributions. A further guideline is obtained by observing that the F_{1u} functions of eq 13 will mix by configuration interaction with the $|(011)\ (111)|$ functions. The latter are expected to be lower in energy than any of the 4p or 4f functions for the same reason that the Φ_{xy} orbitals are lower in energy than the Φ_1. The sign of the rotation should then be determined by the behavior of the F_{1u} intermediate states.

For this problem the b_1, b_2, and b_3 terms in eq 10 are zero because the coordinates of the bridging atoms cancel in pairs. This will only be true, however, for those complexes with C_3 symmetry.

Assuming the sign to be governed by the F_{1u} intermediate state, the sum of eq 12 will consist of the three terms from the functions of eq 13d–f. The required matrix elements for the first term are

$$\langle|(110)\ (111)||V|(1/\sqrt{2})[|(110)\ \chi_1| + |(011)\ \chi_3|]\rangle = (2/\sqrt{12})b_{23}a^2 \qquad (14a)$$

$$\langle|(110)\ (111)||V|(1/\sqrt{2})[|(110)\ \chi_2| + |(101)\ \chi_3|]\rangle = (2/\sqrt{12})b_{13}a^2 \qquad (14b)$$

$$\langle|(110)\ (111)||V|(1/\sqrt{2})[|(101)\ \chi_1| + |(011)\ \chi_2|]\rangle = 0 \qquad (14c)$$

$$\langle(1/\sqrt{2})[|(110)\ \chi_1| + |(011)\ \chi_3|]|V||(110)\ \Phi_a|\rangle = (1/2\sqrt{3})[(1/2\sqrt{2})b_{133} - (3/2\sqrt{2})b_{122}]a^3 \qquad (14d)$$

$$\langle(1/\sqrt{2})[|(110)\ \chi_2| + |(101)\ \chi_3|]|V||(110)\ \Phi_a|\rangle = (1/2\sqrt{3})[(3/2\sqrt{2})b_{112} - (1/2\sqrt{2})b_{233}]a^3 \qquad (14e)$$

The calculation of the other necessary terms leads to the following result for the three components of the degenerate band.

$$R_z^{(I)} = [-(e\hbar/2mc)(ea^6/12)/(E_{200} - E_{111})(E_{200} - E_{210})] \times [(b_{133} - 3b_{122})b_{23} + (3b_{112} - b_{233})b_{13}] \quad (15a)$$

$$R_y^{(I)} = [-(e\hbar/2mc)(ea^6/12)/(E_{200} - E_{111})(E_{200} - E_{210})] \times [(3b_{223} - b_{113})b_{12} + (b_{112} - 3b_{233})b_{13}] \quad (15b)$$

$$R_x^{(I)} = [-(e\hbar/2mc)(ea^6/12)/(E_{200} - E_{111})(E_{200} - E_{210})] \times [(3b_{133} - b_{122})b_{23} + (b_{223} - 3b_{113})b_{12}] \quad (15c)$$

where E_{200} is the energy of the F_{1g} excited state for the transition in question, E_{111} is the energy of the F_{1u} state with the allowed electric dipole transition, and E_{210} is the energy of the intermediate state.

In view of the second-order nature of the problem, it is not necessary to know the sign of the potential function. The rotation will be of the same sign for both an attractive and a repulsive potential.

Assuming the applicability of a multipole expansion for the potential, it will happen that b_{133} will depend on the sign of XZ^2, where X and Z are the coordinates of the bridge in the XZ plane. Similarly the sign of b_{23} will depend on the product of the signs of the Y and Z coordinates of the ligand in the YZ plane. Referring to Figure 3 this leads to a positive value for the product $b_{133}b_{23}$. The other products all turn out to be of the same sign. In view of the symmetry involved, the rotational strengths of all three components are equal and are of negative sign in agreement with experiment for the indicated chirality.[10]

This equality in magnitude and sign is not surprising, since we are dealing with three mutually perpendicular transition moments along three entirely equivalent axes.

When the ligand atoms are substituted, b_1, b_2, and b_3 are all no longer zero and the lowest order terms must be calculated. The task is simplified in eq 12 by the fact that it is not necessary to take into account the octahedral splitting of the intermediate 4p and 4f states to obtain a nonzero result. Thus an average denominator may be used along with the six functions |(110) (210)|, |(110) (201)|, etc. The result is

$$R_z^{(A)} = -(e\hbar/2mc)(ea^4/2)(b_{13}b_2 - b_{23}b_1)/(E_{200} - E_{111})(E_{200} - E_{210}) \quad (16a)$$

$$R_y^{(A)} = -(e\hbar/2mc)(ea^4/2)(b_{23}b_1 - b_{12}b_3)/(E_{200} - E_{111})(E_{200} - E_{210}) \quad (16b)$$

$$R_x^{(A)} = -(e\hbar/2mc)(ea^4/2)(b_{12}b_3 - b_{13}b_2)/(E_{200} - E_{111})(E_{200} - E_{210}) \quad (16c)$$

Consider the case where the ligand in the XZ plane is replaced by two chlorine atoms. The difference between the electronegativities of chlorine and nitrogen will give appreciable values to b_1 and b_3; b_2 will remain zero, and now b_{13} will be zero. In addition, the octahedral field will be modified by a C_{2v} field sufficiently strong to split the degeneracy. The θ_y state is split from the θ_x and θ_z states, which remain accidentally degenerate. In view of the larger effect of the coordinated as opposed to the bridge atoms, we expect that the b_1 terms will predominate over the b_{122} terms. One obtains

$$R_y^{(A)} = A(b_{23}b_1 - b_{12}b_3) \quad (17a)$$

$$R_x^{(A)} + R_z^{(A)} = -A(b_{23}b_1 - b_{12}b_3) \quad (17b)$$

indicating opposite signed contributions from the two bands. Since the b_{122} terms, which are all of the same sign, must also be added, the magnitudes of the rotational strengths will not generally be equal.

When the ligand in the XZ plane is replaced with NH_3 and Cl, the field of the coordinated atoms has essentially C_{4v} symmetry, since NH_3 behaves nearly as the amino group. Again $b_{13} = 0$, and if the Cl atom lies on the Z axis, $b_1 = b_2 = 0$ with $b_3 \neq 0$. Now the θ_z transition is split in energy from the degenerate θ_x and θ_y transitions and $R_z^{(A)} = 0$, $R_y^{(A)} + R_x^{(A)} = 0$. The rotation is governed by the b_{122} terms which are all of the same sign. In this argument we have assumed that the effect of the bridge atoms on b_1 and b_2 is less than their contribution to the b_{122} terms.

V. Conclusion

The general picture may be summed up by saying that the rotational strength of a transition metal complex is made up of two sets of terms. The potentially larger set sums to zero in the absence of splitting, while the other set in general does not sum to zero. The latter terms are responsible for the normal Cotton effect of $Co(en)_3^{3+}$ while the former predominate when the energy of the band is split to give opposite signs to the two components of the $Co[(en)_2Cl_2]^+$ transition. In the $Co[(en)_2NH_3Cl]^{2+}$ type of complex the geometry of the situation leads to a canceling of the sizable effect of the electronegativity difference between Cl

(10) V. Saito, M. S. Nakatsu, and H. Kuroya, *Bull. Chem. Soc. Japan*, **30**, 795 (1957).

and N, and the rotation is evidently governed by the interaction of the bridge atoms with the d electrons in much the same way as that of the $Co(en)_3^{3+}$ complex. It is an interesting fact that the rotational strength of $Co[(en)_2(NH_3)_2]^{3+}$ is approximately one-third that of the $Co(en)_3^{3+}$ transition.[7] This is just the ratio of the number of three-way interactions of bridge atoms with the cobalt atom.

From this work, which is only intended to point the way toward a better qualitative understanding of transition metal complexes, have emerged several observations on the general behavior of degenerate transitions. The qualitative behavior of a chromophore in a dissymmetric molecule will depend on the type of dissymmetry. Confining our discussion to magnetic dipole transitions and those electric dipole transitions where the coupled oscillator effect is minimal, we may say that the rotational strengths of a degenerate transition sum to zero provided there is no dissymmetric array of atoms lying on centers or planes of symmetry of the chromophore. In general, when this condition is not satisfied, the sum rule will not apply. It would be interesting to see if the sum rule is satisfied for a complex such as $Co[(NH_3)_4(NH_2CHCH_3CH_2NH_2)]^{3+}$, in which a methyl group lies in one of the octants of the chromophoric coordinate system.

Radiation Chemistry of Aqueous Solutions of Ethanol[1]

by W. A. Seddon and A. O. Allen

Chemistry Department, Brookhaven National Laboratory, Upton, New York 11973 *(Received November 29, 1966)*

Hydrogen yields from γ rays on neutral solutions of ethanol and oxygen were determined over wide ranges of concentration. The results indicated a simple competition between O_2 and EtOH for an H atom, generated with a yield $G_H = 0.6$; the properties of this radical did not change at very low oxygen concentrations. In acid solutions, where H is generated with $G = 3.3$, the same competition was found. Oxygen-free solutions containing ethanol and hydrogen peroxide show a chain reaction under γ rays, the kinetics of which were found to be in agreement with the anticipated free-radical mechanism. The reaction was studied with intermittent X-rays ("rotating sector" method) and an absolute rate constant obtained for the reaction of ethanol radicals with H_2O_2. The results are all consistent with values for the primary radical yields of $G_{e^-} = G_{OH} = 2.25 \pm 0.05$. These values are significantly lower than those deduced from some other systems and the reasons for the discrepancies are not completely understood.

Solutions of alcohols have played an important role in the study of the occurrence and properties of OH and H radicals formed in water radiolysis. Here we present some new data on the reactions of radicals with ethanol and on the radiation-induced reaction between ethanol and hydrogen peroxide.

Experimental Section

Two ^{60}Co γ-ray sources were used, having intensities in the ratio 23.2:1; the more intense source gave about 60 μM Fe^{3+}/min in the Fricke dosimeter. Irradiations were all carried out in syringes at a temperature of 23°. Each G value quoted here is obtained by exposure of samples at four or more different doses.

Interrupted radiations were carried out using X-rays

(1) Research performed under the auspices of the U. S. Atomic Energy Commission.

generated at 1.95 Mev by a Van de Graaff electron accelerator, as described by Schwarz.[2] Two intensities were used, giving Fricke dosimeter responses of 24.0 and 4.8 μM Fe^{3+}/min, respectively. The ratio (time off/time on) was kept constant at 3.0, while the period was varied.

All oxygen-free samples were deaerated by bubbling with Ar for at least 30 min. The gas passed successively through a Dry Ice trap, through pure water, and finally through a solution of the same composition before reaching the actual solution to be irradiated. Syringes were rinsed several times with the deaerated solution before final filling. Oxygen concentrations were fixed by bubbling with O_2–N_2 mixtures made and analyzed by the Matheson Co., Inc.

Hydrogen was determined gas chromatographically by an adaptation of the method of Swinnerton, Linnenbom, and Cheek.[3] Samples of 10 ml were ejected *via* a hypodermic needle through a rubber cap into a bubbler containing water through which Ar carrier gas passed at 10 cc/min under 5 psig. Calibration was accomplished by injection of 0.200 ml of water saturated with hydrogen at atmospheric pressure. Three calibrations were run at the start of the day; thereafter a calibration run was made after each determination, though usually no change in the calibration occurred during any one day. A 6-ft column of Molecular Sieve 5A, 30–60 mesh, at room temperature was used in a Perkin-Elmer Model 154 vapor fractometer, with thermistor detector. Hydrogen elution time was about 1.5 min; oxygen appeared after a further 2 min and nitrogen after a further 5 min. Peak areas were determined with a planimeter; peak heights could not be used because of the finite injection times.

Acetaldehyde was determined by the method described by Hummel and Allen.[4] The correct extinction coefficient to use in this method is 19,100; it was wrongly quoted in the reference. The usual iodometric method for peroxide was used.

Results

Measured hydrogen yields, $G(H_2)$, from various solutions are shown in Table I. The molecular yield from water, G_{H_2}, is seen to be slightly lower in acid than in neutral solutions, as previously reported by Hayon.[5] The additional H_2 arising from ethanol is a measure of the independent yield of H atoms, which are formed in water and react with alcohol by eq 1

$$H + C_2H_5OH = H_2 + \cdot C_2H_4OH \qquad (1)$$

even when N_2O is present to scavenge all the solvated electrons. It is seen that this yield G_H increases with alcohol concentration, as reported by Scholes and Simic;[6] the increase presumably results from removal from the spurs at high alcohol concentrations of OH radicals, which normally react with H atoms or their precursors. In the phosphate solution, the solvated electrons react with the acid phosphate anions to form additional H atoms and the observed yield is the sum of G_{H_2}, G_H, and $G_{e_{aq}^-}$.

Table I: Some Measured Hydrogen Yields

Solution	$G(H_2)$
Neutral KBr (1.38 mM), air free	0.459 ± 0.017
Neutral KBr (1.5 mM), air saturated	0.431 ± 0.010
Neutral KBr (1.38 mM), with N_2O (0.32 mM)[a]	0.429 ± 0.013
$HClO_4$ (pH 1.69), KBr (1.53 mM), air free	0.419 ± 0.010
$HClO_4$ (pH 1.69), KBr (1.53 mM), air saturated	0.366 ± 0.010
Ethanol (10.5 mM), with N_2O (0.32 mM)[a]	1.051 ± 0.02
Ethanol (105 mM), with N_2O (0.32 mM)[a]	1.156 ± 0.02
Ethanol (10 mM), NaH_2PO_4 (0.1 M, pH 4.5)[b]	3.50 ± 0.07

[a] Saturated with Ar containing 1.26% N_2O. [b] Fifteen separate determinations, with several points taken in each determination.

When low concentrations of O_2 are present, reaction 2 competes with reaction 1. A simple competition should lead to a linear relation between the oxygen–

$$H + O_2 = HO_2 \qquad (2)$$

alcohol ratio and the reciprocal of the yield of H_2 in excess of the molecular

$$G(H_2) = G_{H_2} + G_H[1 + K(O_2)/(alc)]^{-1} \qquad (A)$$

where $K = k_2/k_1$, the ratio of rate constants for reactions 2 and 1. In this work G_{H_2} at the different oxygen concentrations is obtained by interpolation from the values of Table I, assuming that G_{H_2} is linear in the cube root of the oxygen concentration. The yield of hydrogen varies with total dose because consumption of the reactants alters their ratio. Integration of eq A, under the condition $x << 1$, where $x = (O_2)_0/(alc)_0$, gives

$$(H_2) = G_0D + \frac{D^2G_HG(-O_2)Kx}{2(1 + Kx)^2} + \frac{D^3G_HG(-O_2)^2K^2x^2}{3(1 + Kx)^3} + \ldots \qquad (B)$$

Each solution was run at four to seven different doses

(2) H. A. Schwarz, *J. Phys. Chem.*, **66**, 255 (1962).

(3) J. W. Swinnerton, V. J. Linnenbom, and C. H. Cheek, *Anal. Chem.*, **34**, 483, 1509 (1962).

(4) A. Hummel and A. O. Allen, *Radiation Res.*, **17**, 302 (1962).

(5) E. Hayon, *J. Phys. Chem.*, **65**, 1502 (1961).

(6) G. Scholes and M. Simic, *ibid.*, **68**, 1731 (1964).

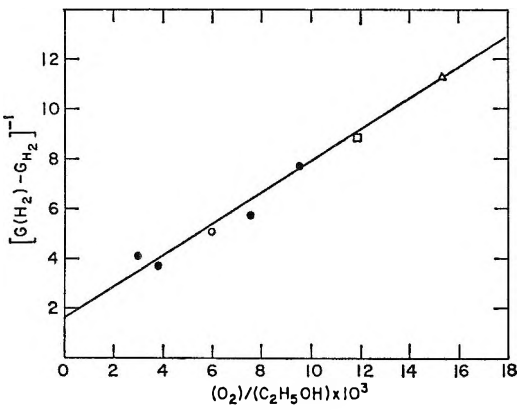

Figure 1. Hydrogen yields in neutral solutions containing ethanol and oxygen: ●, O_2 = 42.2 μM; ○, 65.8 μM; □, 13.1 μM; △, 270 μM.

and the yield at each dose was corrected using eq B with $G(-O_2)$ = 2.8, G_H = 0.62 in neutral or 3.4 in acid solution, and K = 380 or 400. The corrections in G amounted to only 1–5%. The results in neutral solution are shown in Figure 1. From the reciprocal of the intercept we find G_H = 0.62 and from the ratio of slope to intercept $K = k_{H+O_2}/k_{H+alc}$ = 390 ± 60, in good agreement with Willson and Scholes.[7] The reasonably good fit to a straight line shows that the entity being competed for does not appreciably change its properties over the range of concentrations studied and refutes Hayon's contention[8] that it acts like an H atom below about 60 μM (O_2) but like an electron at higher O_2 concentrations.

In acid solution, all e_{aq}^- are converted to H atoms, so that a much higher $G(H_2)$ is found. Again we find simple competition with oxygen (Figure 2). G_H = 3.3, in good agreement with the value expected[9] at the pH used; K = 447 ± 66, in agreement with the value found in neutral solution.

Hydrogen peroxide, in the absence of oxygen, also competes with alcohol for hydrogen atoms, as shown in Figure 3. Here the molecular yield G_{H_2} was estimated as a function of peroxide concentration by interpolation from the data of Ghormley and Hochanadel,[10] again assuming linearity of G_{H_2} with the cube root of the scavenger concentration. The ratio $k_{H+H_2O_2}/k_{H+C_2H_5OH}$ is 2.2 ± 1.0. Thus $k_{H+O_2}/k_{H+H_2O_2}$ is about 200; Thomas, in three different papers,[11] finds 175, 210, and 300; Hochanadel[12] finds 455.

During these irradiations, peroxide disappeared with a very high yield, evidently by a chain reaction with the alcohol. Such a chain would be expected from the reactions (R = $\cdot C_2H_4OH$)

$$H_2O = e_{aq}^-, H, OH, H_2, H_2O_2 \quad (3)$$

$$H + C_2H_5OH = H_2 + R \quad (4)$$

$$OH + C_2H_5OH = H_2O + R \quad (5)$$

$$e_{aq}^- + H_2O_2 = OH + OH^- \quad (6)$$

$$R + H_2O_2 = CH_3CHO + H_2O + OH \quad (7)$$

$$2R = R_2 \text{ or } CH_3CHO + C_2H_5OH \quad (8)$$

If it is assumed that $(C_2H_5OH) >> (H_2O_2)$, so that all H and OH react with the alcohol, the mechanism predicts

$$G(-H_2O_2) - G_{e_{aq}^-} + G_{H_2O_2} = [G_R^{1/2}I^{-1/2}k_7/(2k_8)^{1/2}](H_2O_2) \quad (C)$$

where $G_R = G_{OH} + G_{e_{aq}^-} + G_H$ and I is the radiation intensity or "dose rate" in units which may be described most conveniently as $(1/15.5)(d(Fe^{3+})/dt$ in Fricke dosimeter) (M/sec). Thus the yield of peroxide disappearance should rise linearly with the peroxide concentration and the reciprocal square root of the intensity and should be independent of the alcohol concentration. Figure 4 shows that these laws are accurately followed. The quantity plotted here is $G(-H_2O_2) + G_{H_2O_2}$, where we take $G_{H_2O_2}$ as 0.7.[9]

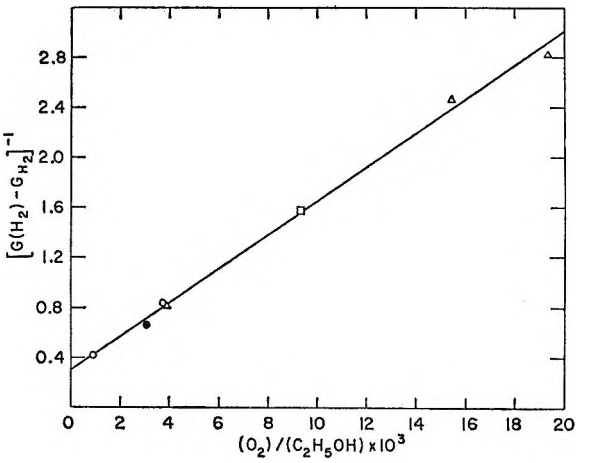

Figure 2. Hydrogen yields in solutions of ethanol and oxygen containing 0.0225 M $HClO_4$, pH 1.69. Meaning of symbols same as in Figure 1.

(7) G. Scholes, *Discussions Faraday Soc.*, **36**, 311 (1963).

(8) E. Hayon, *Trans. Faraday Soc.*, **60**, 1059 (1964).

(9) A. O. Allen, "The Radiation Chemistry of Water and Aqueous Solutions," D. Van Nostrand Co., Inc., Princeton, N. J., 1961.

(10) J. A. Ghormley and C. J. Hochanadel, *Radiation Res.*, **3**, 227 (1955).

(11) (a) J. K. Thomas, *J. Phys. Chem.*, **67**, 2593 (1963); (b) J. P. Sweet and J. K. Thomas, *ibid.*, **68**, 1363 (1964); (c) H. Fricke and J. K. Thomas, *Radiation Res., Suppl.*, **4**, 35 (1964).

(12) C. J. Hochanadel, *Radiation Res.*, **17**, 286 (1962).

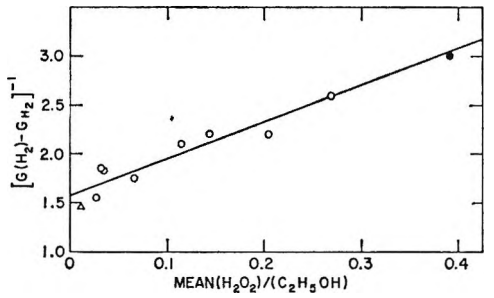

Figure 3. Hydrogen yields in neutral solutions containing hydrogen peroxide and ethanol but no oxygen: ●, 1.75 mM C_2H_5OH; ○, 3.5 mM; △, 10.5 mM.

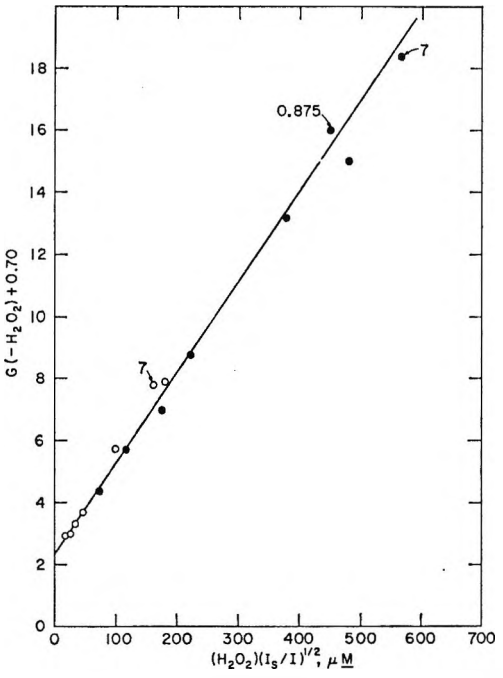

Figure 4. Peroxide destruction yields in solutions containing hydrogen peroxide and ethanol (3.5 mM except 0.875 and 7.0 mM where indicated): ○, high-intensity source; ●, low-intensity source; abscissa, peroxide concentration in μM multiplied by the square root of the ratio of the standard intensity (that of the high-intensity source on an arbitrary date) to the actual intensity.

The intercept should then be equal to $G_{e_{aq}^-}$; the value found is 2.3. From the slope, we find $k_7/(2k_8)^{1/2} = 3.30$.

At lower ratios of C_2H_5OH to H_2O_2, reaction 9 must be taken into account. Inclusion of reactions 9 and 10 in the scheme leads to a complicated expression which,

$$OH + H_2O_2 = H_2O + HO_2 \quad (9)$$

$$HO_2 + R = CH_3CHO + H_2O_2 \quad (10)$$

if $(C_2H_5OH) > (H_2O_2)$, can be approximated by

$$G(-H_2O_2) + G_{H_2O_2} - G_{e_{aq}^-} = G_0 - \frac{k_7^2 k_9 (H_2O_2)^3}{2k_8 k_5 (C_2H_5OH) I} \quad (D)$$

where G_0 is the expression on the right-hand side of eq C. Figure 5 gives data on yields at two different peroxide and three different alcohol concentrations, which vary with the concentrations according to eq D, although the intercepts (for infinite (C_2H_5OH)) are a little low. From the slopes of the two lines, we find $k_9/k_5 = 0.060$ and 0.058, respectively, but the uncertainty in the intercepts reduces one's confidence in the significance of the slopes. It is possible that a small quantity of oxygen is formed at the higher $(H_2O_2)/(C_2H_5OH)$ ratios, which tends to interrupt the chains. If we accept the above ratio, since $k_7 = 4.5 \times 10^7$,[2] we find $k_3 = 7.6 \times 10^8$, not very different from Adams' value[13] of about 10.5×10^8 and Thomas' value[14] of 7.2×10^8.

Measured aldehyde yields are shown in Table II. The missing compound in the material balance is R_2 (2,3-butanediol), presence of which was shown qualitatively by vapor-phase chromatography, using an F & M Model 300 with flame ionization detector. We also showed that isomeric diols are absent, or are at most 10% of the major isomer. If the product of chain-breaking reaction 6 were entirely diol, a yield of $G_R/2$ or about 2.6 would be expected. We conclude that disproportionation to aldehyde and alcohol occurs in about 30% of the reactions. Taub and Dorfman[15] estimate about 20%.

Table II: Material Balance in the Reaction of Ethanol (3.5 mM) with Hydrogen Peroxide

Source intensity	(H_2O_2), μM	$G(-H_2O_2)$	G(aldehyde)	$G(H_2)$	G(diol) = $G(-H_2O_2) + G(H_2) - G$(ald)
Low	99	14.3	13.5	1.0	1.8
High	99	5.05	4.4	1.0	1.65
High	160	7.2	6.7	1.0	1.5

To obtain absolute values of reaction rates of the alcohol radical R, we turned to the interrupted beam or "rotating sector" technique. The theoretical curve for this case, in which chains are terminated by a reac-

(13) G. E. Adams, J. W. Boag, and B. D. Michael, *Trans. Faraday Soc.*, **61**, 1417 (1965).

(14) J. K. Thomas, *ibid.*, **61**, 702 (1965).

(15) I. A. Taub and L. M. Dorfman, *J. Am. Chem. Soc.*, **84**, 4053 (1962).

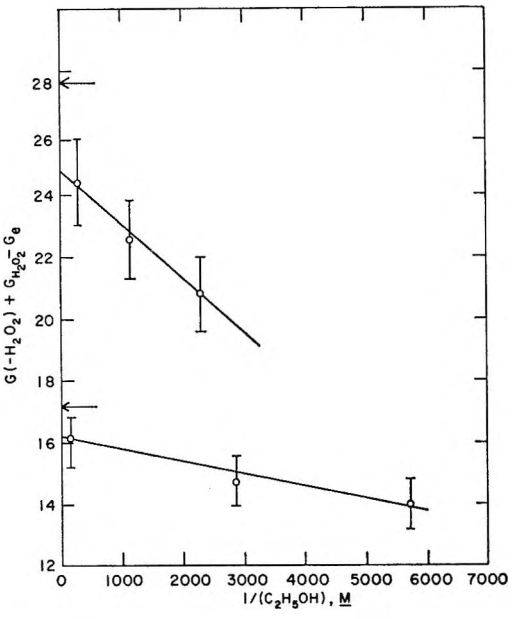

Figure 5. Effect of reduced alcohol concentration on the yield of peroxide destruction: upper line (H_2O_2) = 197 μM; lower line, 122 μM; arrows indicate intercepts calculated from the line of Figure 4; ratio of slopes, 4.35; ratio of $(H_2O_2)^3$, 4.2.

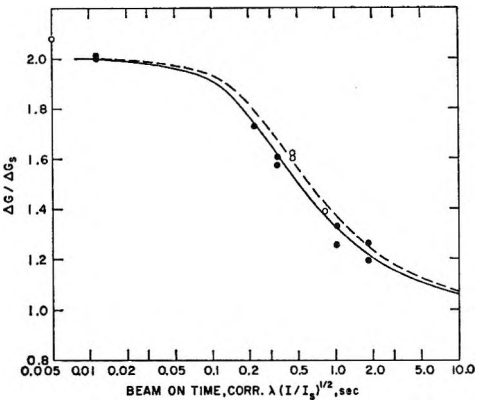

Figure 6. Pulsed-beam irradiation of ethanol–peroxide solutions: ordinate, ratio of the chain yield ΔG of peroxide destruction to that expected for steady-state irradiation under the same conditions of concentrations and radiation intensity (from Figure 4); abscissa, beam-on time λ, sec, multiplied by the square root of the ratio of intensity to standard intensity; ●, intensities near 2.6×10^{-8} M/sec/unit G value; ○, near 0.50×10^{-8}, in the same units. Curve is drawn with theoretical shape and may be fit to the data only by sliding horizontally. Solid curve shows the best fit; the dotted curve is expected from ref 17.

tion second order in the carriers, is given by Burnett.[16] With the beam on one-fourth of the time, the yield of the chain at very short on times should be twice that for steady irradiation. In Figure 6, the chain yield $\Delta G = G(-H_2O_2) - G_{e^-} + G_{H_2O_2}$ divided by its steady-state value is plotted against the on time (divided by $I^{1/2}$). The theoretical curve shown is fitted to the data by a single parameter, the value of which fixes $2k_8$ at $2.0 \pm 0.6 \times 10^9$ M^{-1} sec^{-1}. The value of Dorfman and Taub,[17] $1.4 \pm 0.4 \times 10^9$, is not really in disagreement, but the curve corresponding to 1.4×10^9, shown dotted in the figure, fits the data somewhat less well. From the ratio found in Figure 4, we find $k_7 = 1.5 \times 10^5$, which is rather smaller than might be expected.

Discussion

The data on the ethanol–peroxide chain reaction point toward a value of 2.3 for the yield of solvated electrons. This is lower than the value 2.85 of Czapski and Allen[18] and 2.6 of Hochanadel and Casey,[19] but agrees better with estimates by Hayon[20] (2.3) and by Head and Walker[21] (2.45).

The yield of peroxide in oxygenated ethanol solutions,[2] 3.2, should be equal to $G_{H_2O_2} + {}^1/_2(G_{OH} + G_H + G_{e^-})$. Since $G_{H_2O_2} = 0.7$,[12] $G_H = 0.6$ (present work), and $G_{OH} = 2.2$ (both by the difference in $G(H_2O_2)$ in the presence and absence of alcohol and by G(aldehyde) in the ethanol–oxygen solution), this gives $G_{e_{aq}^-} = 2.2$.

If OH, H, e_{aq}^-, H_2, and H_2O_2 are the only important oxidized and reduced species formed in radiolysis, then material balance requires that the above yield should be equal also to $G_{H_2} + G_H + G_{e_{aq}^-}$. This we measured as $G(H_2)$ in ethanol plus 0.1 M $H_2PO_4^-$ solutions and found it to be 3.5, 10% higher than the $G(H_2O_2)$ in oxygen. The difference, though outside experimental error, does not necessarily mean that other species are involved; it may be simply due to scavenging of radicals from the spur by the rather concentrated phosphate. It would be interesting to determine the effect of different phosphate concentrations on $G(H_2O_2)$ in oxygenated solutions.

The apparent inconsistencies in the measurement of radical yields, which have led to various proposals for the existence of additional transient species, are not yet all resolved. It is becoming clear, however, that radical yields may be increased by the presence of rather low concentrations of scavenger to a greater extent than was formerly realized.

(16) G. M. Burnett in "Mechanisms of Polymer Reactions," Vol. III, Interscience Publishers, Inc., New York, N. Y., 1954.

(17) L. M. Dorfman and I. A. Taub, *J. Am. Chem. Soc.*, **85**, 2370 (1963).

(18) G. Czapski and A. O. Allen, *J. Phys. Chem.*, **66**, 262 (1962).

(19) C. J. Hochanadel and R. Casey, *Radiation Res.*, **25**, 198 (1965).

(20) E. Hayon, *Trans. Faraday Soc.*, **61**, 723 (1965).

(21) D. Head and D. C. Walker, *Nature*, **207**, 517 (1965).

Pulse Radiolysis of Aqueous Solutions of Methyl Iodide and Methyl Bromide. The Reactions of Iodine Atoms and Methyl Radicals in Water[1]

by J. K. Thomas

Chemistry Division, Argonne National Laboratory, Argonne, Illinois *(Received December 19, 1966)*

The pulse radiolysis of aqueous solutions of methyl iodide and methyl bromide has been studied on the ANL linear accelerator. In the case of methyl iodide, methyl radicals and iodide atoms are produced: $e_{aq}^- + CH_3I \rightarrow CH_3 + I^-$ and $OH + CH_3I \xrightarrow{CH_3I} CH_3OH + I(CH_3I)$. With methyl bromide, methyl radicals are produced but no Br atoms could be detected. The absolute rates of several methyl radical reactions in water have been measured and these are discussed in terms of the corresponding H and OH radical reactions.

Introduction

In the past 5 years, the technique of pulsed radiolysis has provided extensive data on the nature of radiolytic processes in liquids and has elucidated many kinetic patterns of the radiolysis fragments. In water reliable rate data are available for reactions of H atoms, OH radicals, and hydrated electrons, e_{aq}^-.[2a] Previous work[2b] has shown that hydrated electrons react with rates that approach diffusion control with methyl iodide and with other alkyl halides. These reactions probably lead to bond breakage,[3] *e.g.*, e_{aq}^- — R(halide) → R + halide. Thus, these systems may be used as a convenient source of alkyl radicals in liquids where solvated electrons can be generated. The first part of the work uses the pulse radiolysis technique to study in detail the processes occurring in the radiolysis of aqueous solutions of methyl iodide. The second part describes the measurement of the rates of reaction of methyl radicals in water.

Experimental Section

Preparation of Solutions. Reagent grade methyl iodide from the Baker Chemical Co. is washed by shaking with triply distilled water. The mixture is allowed to settle and the supernatant water is poured away; the process is repeated three times. This treatment gives a water-saturated methyl iodide which is free of hydrogen iodide. A small quantity (~2 ml) of this purified methyl iodide is placed with 50 ml of triply distilled water in a 100-ml syringe, with no gas space. Pure argon gas (50 ml) is introduced into the syringe and the mixture is shaken vigorously for 3 min. The gas phase of air, methyl iodide, and argon is expelled and the whole procedure repeated four times. This gives a saturated solution of methyl iodide (0.1 *M*) in water, with less than 2×10^{-7} *M* oxygen. Dilute solutions of methyl iodide are then prepared by the syringe dilution technique.[4] Solutions of methyl bromide are prepared by bubbling CH_3Br through water for 15 min. This produces a saturated solution of CH_3Br in water which is free of oxygen. Dilute solutions are prepared by mixing the saturated solution with degassed water *via* the syringe technique.

Analysis. Iodine is determined by mixing the irradiated sample with an equal volume of 0.2 *M* potassium iodide and measuring the I_3^- at 350 mμ on a Cary spectrophotometer, the extinction coefficient of I_3^- at 350 mμ being 26,500.

Gases such as methane and oxygen are determined by stirring the irradiated solution in a Van Slyke apparatus and injecting the liberated gases into a gas chromatograph.[5]

(1) Based on work performed under the auspices of the U. S. Atomic Energy Commission.

(2) (a) M. Anbar and P. Neta, *Intern. J. Appl. Radiation Isotopes*, 16, 227 (1965); (b) A. Szutka, J. K. Thomas, S. Gordon, and E. J. Hart, *J. Phys. Chem.*, 69, 289 (1965).

(3) D. N. Skelly, R. G. Hayes, and W. H. Hamill, *J. Chem. Phys.*, 43, 2795 (1965).

(4) E. J. Hart, S. Gordon, and J. K. Thomas, *J. Phys. Chem.*, 68, 1271 (1964).

(5) J. K. Thomas and E. J. Hart, *Radiation Res.*, 17, 408 (1962).

Pulse Radiolysis Apparatus. This is described in detail elsewhere[6] and here it suffices to outline the procedure. The solutions are irradiated in a 4-cm quartz cell by 0.4- or 1.0-μsec pulses of 15-Mev electrons from an Arco linear accelerator. An analyzing light beam passes through the cell twice, giving a path length of 8 cm, and then after passing through a Bausch and Lomb monochromator, it is monitored with a 1P28 photomultiplier tube. The output of the tube is amplified and displayed on a Tektronix 545 A oscilloscope. The rise or response time of the whole apparatus is 80 nsec.

Dosimetry is carried out by direct observation of the e_{aq}^- in degassed water at 400 mμ where ϵ is 2720[7] or by direct observation of the I_2^- spectrum in 10^{-3} M potassium iodide where ϵ is 14,000 at 385 mμ.[8] The primary yields used in conjunction with the above dosimetry are $G(e_{aq}^-) = 2.40$, $G(OH) = 2.40$, and $G(H) = 0.60$.

Results

Rate of Appearance of I^-. Figure 1 shows the spectrum produced in a deoxygenated solution of 50 μM CH_3I–10^{-3} M C_2H_4. The spectrum grows in after the pulse to give a permanently absorbing product. The similarity of the spectrum to that given in the literature for iodide ion suggests that the observed product is indeed the stable iodide ion.

$$e_{aq}^- + CH_3I \longrightarrow CH_3 + I^-$$

$$\left.\begin{aligned} H + C_2H_4 &\longrightarrow C_2H_5 \\ OH + C_2H_4 &\longrightarrow C_2H_4OH \end{aligned}\right\} \text{removal of H + OH to give unreactive products}$$

The kinetics of decay of e_{aq}^-, measured at 600 mμ, and formation of I^-, measured at 230 mμ, in a solution of 25 μM CH_3I–10^{-3} M C_2H_4 are shown in Figure 2. The kinetics are apparently first order with $k_{(e_{aq} + CH_3I)} = 1.65 \pm 0.25 \times 10^{10}$ sec^{-1}. The plot of log $[e_{aq}^-]$ *vs.* log $([I^-]_0 - [I^-]_t)$ is linear with a slope of unity showing that e_{aq}^- immediately produces I^-.

Formation of Iodine Atoms. Figure 3 shows the spectrum obtained in the pulsed radiolysis of solutions of 2×10^{-2} M N_2O and 10^{-3} M CH_3I. The intensity of the spectrum is reduced by approximately half in the absence of N_2O and is completely removed by large concentrations of OH radical scavengers such as methanol and ethanol. Assuming that only OH radicals produce the spectrum, an absorption coefficient ϵ 5000 is measured at 310 mμ. The intensity of the spectrum is unaffected by oxygen and this spectrum is attributed to a complex of an iodine atom with a methyl iodide molecule, $I(CH_3I)$.

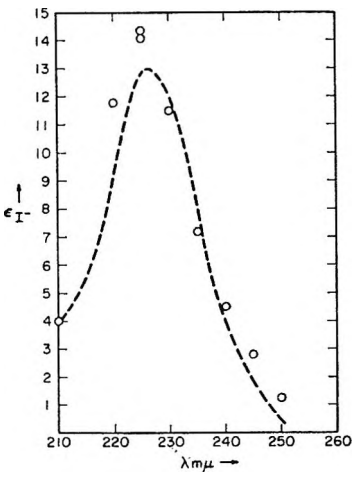

Figure 1. Spectrum of I^- in a solution of 50 μM CH_3I–10^{-3} M ethylene: – – – –, literature data for I^-.

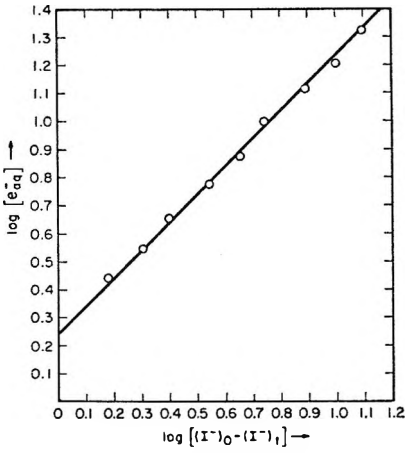

Figure 2. Kinetic plot of results in Figure 1, concentrations of e_{aq}^- and I^- expressed in arbitrary units.

Decay of the $I(CH_3I)$ Complex. In the presence of iodide ion the spectrum decays by a first-order process proportional to $[I^-]$ and produces directly the spectrum of I_2^-. The mean of ten measurements gives $k_{I(CH_3I)+I^-} = 6.0 \pm 0.5 \times 10^9$ sec^{-1}. The rate of decay of the spectrum is also increased by methyl and ethyl alcohols but not by sodium acetate and acetone. The rate of decay in the presence of alcohol is first order and directly proportional to [alcohol]: $k_{I(CH_3I)+CH_3OH} = 1.7 \pm 0.4 \times 10^9$ sec^{-1}.

The decay of the $I(CH_3I)$ complex in the absence of an added scavenger is first order at low intensities and

(6) J. K. Thomas, S. Gordon, and E. J. Hart, *J. Phys. Chem.*, **68**, 1524 (1964).

(7) E. J. Hart, private communication.

(8) J. K. Thomas, *Trans. Faraday Soc.*, **61**, 702 (1965).

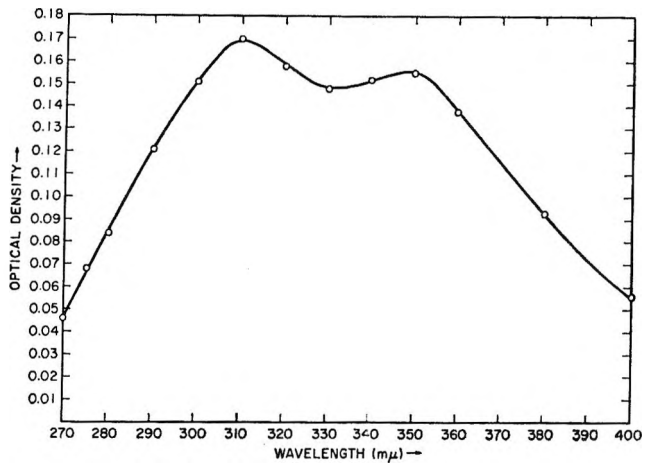

Figure 3. Spectrum of $I(CH_3I)$ in a solution of 2×10^{-2} M N_2O–10^{-3} M CH_3I.

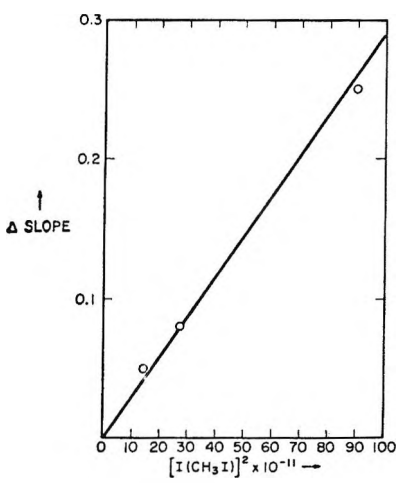

Figure 5. Plot of ΔS *vs.* $(I(CH_3I))^2$ from Figure 4; ΔS = (slope of curve − slope of curve at low intensity); $I(CH_3I)^2$ expressed in moles per liter.

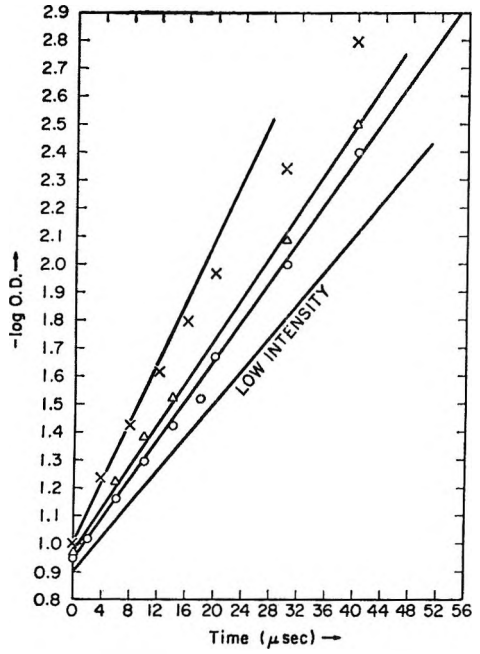

Figure 4. Decay of $I(CH_3I)$ expressed as −log (optical density $I(CH_3I)$ at 310 mμ) *vs.* time, μsec. The point at time zero is moved on the −log OD axis to a convenient position. The initial $[I(CH_3I)]$, expressed as optical density at 310 mμ, and the intensity, ev/l./pulse × 10^{19}, respectively, are, for low intensity, 0.008–0.041 and 0.25–1.29; ⊙, 0.148 and 4.65; △, 0.208 and 6.55; and ×, 0.38 and 12.0.

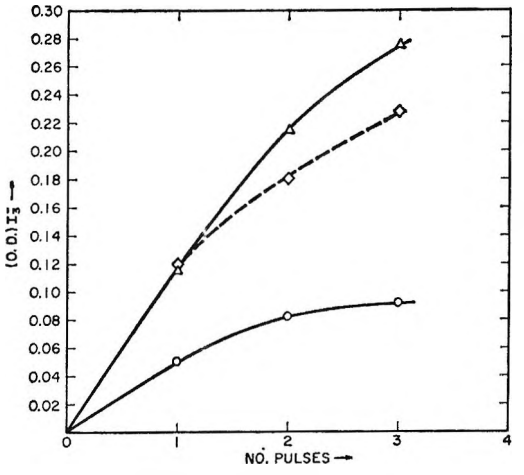

Figure 6. Yield of I_2 as optical density of I_3^- *vs.* dose expressed as number of pulses. The intensity, ev/l./pulse × 10^{19}, is for △, 1.32 (2×10^{-2} M N_2O–10^{-3} CH_3I) (1); ⊙, 1.82 (10^{-3} M CH_3I) (2); and ◇, 2.80 (2×10^{-2} M N_2O–10^{-3} M CH_3I–10^{-3} M methanol (3). (Because of the higher intensity the abscissa is plotted as number of pulses × 0.65.)

independent of intensity. At high intensities the rate of decay increases with intensity. The results are shown in Figures 4 and 5.

Iodine Yields. Figure 6 shows the yield of iodine I_2 (measured as I_3^-) *vs.* dose expressed as number of pulses in the pulse radiolysis of solutions of CH_3I with and without N_2O. In the CH_3I solutions alone the initial yield of iodine $G(I_2) = 1.10$ while in N_2O saturated solutions $G(I_2) = 2.50$, *i.e.*, $\frac{1}{2}(G(e_{aq}^-) + G(OH))$. There is no effect of millimolar concentrations of methanol and ethanol on these I_2 yields in spite of the fact that the decay of the $I(CH_3I)$ is more rapid in these solutions.

Radiolysis of Methyl Bromide. In many instances methyl bromide is a more suitable source of methyl radicals than methyl iodide (a) because the OH radical does not give a strongly absorbing species analogous to $I(CH_3I)$ and (b) the reaction product Br^- is more transparent than I^-.

The pulse radiolysis of deoxygenated solutions of CH_3Br shows a weak transient below 280 mμ with an absorption that increases with decreasing wavelength. In the presence of N_2O the intensity of the species is nearly doubled. In this system the OH radical abstracts an H atom from the CH_3 group of CH_3Br to give the radical CH_2Br, the yield of this radical being doubled in N_2O. There is no evidence that Br atoms are produced.

In the presence of oxygen a fairly strong absorption is observed in the ultraviolet region with a peak at 260 mμ (Figure 7). This spectrum is similar to the spectra of HO_2 and O_2^- and is attributed to the species CH_3O_2 and O_2CH_2Br. When nitrous oxide is added to the solution the electrons are captured by the N_2O yielding OH and subsequently CH_2Br is the only radical formed. The spectrum of CH_3O_2 may then be obtained as the difference between the spectra with and without N_2O in the solution.

Another approach used to obtain the spectrum of CH_3O_2 is to scavenge the OH radicals with potassium thiocyanate to give the radical CNS. The net result is that CNS is formed rapidly while CH_3O_2 is formed slowly. The difference in the rate of formation of CNS and CH_3O_2 is sufficiently great so that the spectrum of CH_3O_2 can be measured. The agreement between the two methods is good and is shown in Figure 7.

The oscilloscope tracing of the rate of production of CH_3O_2 at 260 mμ in a solution containing potassium thiocyanate, methyl bromide, and oxygen is shown in Figure 8. The first instantaneous rise of the trace is

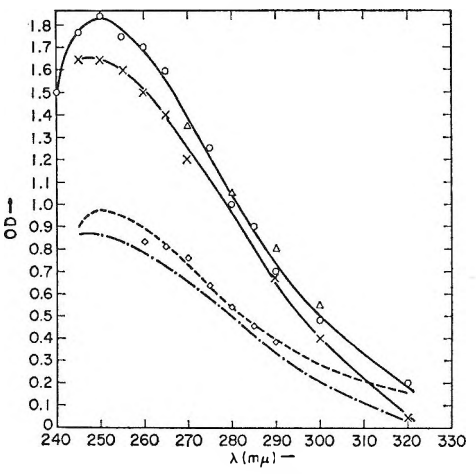

Figure 7. Spectra of O_2CH_2Br and CH_3O_2: ◇, 10^{-3} *M* CH_3Br–10^{-4} *M* O_2–10^{-2} *M* KCNS; ○, 10^{-3} *M* CH_3Br–10^{-4} *M* O_2; ×, 10^{-3} *M* CH_3Br–10^{-4} *M* O_2–saturated N_2O; – – – –, solution × divided by 1.92, *i.e.*, spectrum of O_2CH_2Br; —.—., difference between solution ○ and solution ×/1.92, *i.e.*, CH_3O_2.

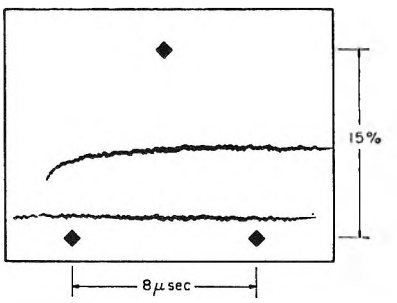

Figure 8. Oscilloscope trace of solution 10^{-3} *M* CH_3Br–10^{-2} *M* KCNS–5.25×10^{-5} *M* O_2.

due to the CNS radical, while the portion which grows to a plateau over many microseconds is due to CH_3O_2. This picture is read on the ANL reader CHLÖE and the digitalized information is fed into the ANL CDC 3600 computer. This machine calculates the optical density at time *t* and plots out the results in the desired form. Figure 9 shows the first-order plot from Figure 8. The computer calculates the least-square slope of the line and hence the rate constant of the reaction

$$CH_3 + O_2 \longrightarrow CH_3O_2 \qquad (1)$$

The mean of ten results gives $k_1 = 4.7 \pm 0.7 \times 10^9$ sec^{-1} at 23°; from the effect of temperature on the rate constant an activation energy $E = 3.5 \pm 0.3$ kcal is measured for reaction 1.

Production of Methane. In the low intensity Co^{60} γ radiolysis of aqueous solutions of 10^{-4} *M* CH_3I and alcohols, methane is produced with $G(CH_4) = 2.45 = 0.15$

$$CH_3 + RHOH \longrightarrow CH_4 + ROH \qquad (2)$$

The same result is obtained with solutions of methyl bromide and alcohol. The yield of methane is independent of alcohol concentration from 0.1 to 1.0 *M* and of CH_3Br from 10^{-4} to 10^{-3} *M*. With CH_3I, however, $G(CH_4)$ increases with CH_3I concentrations above 3×10^{-4} *M* reaching 10.9 at $[CH_3I] = 5 \times 10^{-3}$ *M*. This is due to a chain reaction

$$ROH + CH_3I \longrightarrow RIOH + CH_3$$

Oxygen lowers the yield of methane due to reaction 1 competing with reaction 2. This expression now holds

$$\frac{k_2[RHOH]}{k_1[O_2]} = \frac{G(CH_4)}{G^\circ(CH_4) - G(CH_4)}$$

where $G^\circ(CH_4)$ is the yield of methane in the absence of oxygen. A typical plot of the above equation is shown in Figure 10 for the competition between isopropyl alcohol and oxygen for CH_3 radicals. The slope

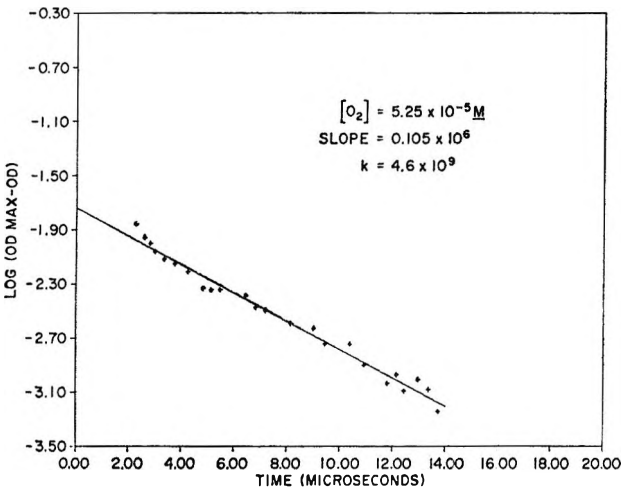

Figure 9. First-order plot of the results of Figure 8.

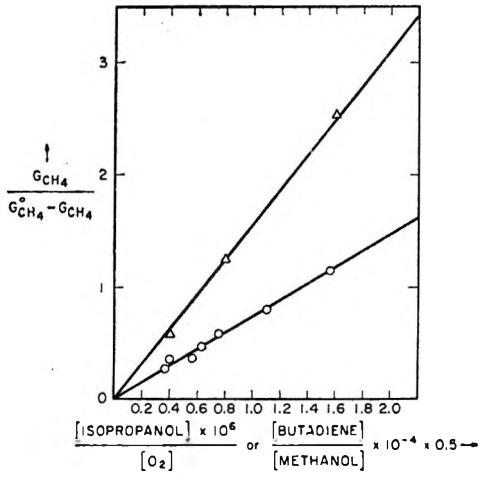

Figure 10. Competition plots for the reaction CH_3 + isopropyl alcohol *vs.* CH_3 + O_2: ⊙, [isopropyl alcohol] = 1.0 *M*; and CH_3 + methanol *vs.* CH_3 + butadiene: △, [methanol] = 0.95 *M*.

of the line gives the ratio k_2/k_1 and as $k_1 = 4.7 \times 10^9$ sec^{-1}, k_2 can be calculated. Some typical results are given in Table I together with the rates of addition of CH_3 radicals to unsaturated compounds, which are measured relative to k_2. A typical plot for the competition between methanol and butadiene is shown in Figure 10.

Discussion

Methyl Iodide Solutions. The results clearly demonstrate that three products are produced in the radiolysis of oxygen-free solutions of methyl iodide. The stable species in Figure 1 is the iodide ion produced from the reaction e_{aq}^- + CH_3I. The correlation between the rate of disappearance of e_{aq}^- and the appearance of I^- places a limit of less than 80 nsec on the lifetime of any negative ion intermediate. The fate of the H atom is not illustrated in these experiments; it probably reacts rapidly with CH_3I to produce CH_3 and HI.[9] The presence of the methyl radical is demonstrated by the production of methane gas in the low-intensity γ radiolysis of aqueous solutions of 10^{-4} *M* CH_3I and 1 *M* isopropyl alcohol. The methane yield $G(CH_4) = 2.45 \pm 0.15$[10] comes from the reaction

$$CH_3 + (CH_3)_2CHOH \longrightarrow (CH_3)_2COH + CH_4$$

The third short-lived species, Figure 3, is attributed to the complex of the iodine atom with CH_3I. This is in accord with the doubling of the intensity of the spectrum on addition of N_2O *via* reaction 3

$$N_2O + e_{aq}^- \xrightarrow{H^+} OH + N_2 \qquad (3)$$

and by the elimination of the spectrum by OH radical scavengers. The OH radical could react *via* reactions 4–6. The absence of any effect of oxygen on the spec-

$$OH + CH_3I \longrightarrow \begin{cases} CH_2I + H_2O & (4) \\ CH_3 + HOI & (5) \\ CH_3OH + I & (6) \end{cases}$$

trum rules out reaction 4 as the radical CH_2I would give O_2CH_2I with O_2 and alter the spectrum. Reaction 5 is unlikely as the spectrum of HOI is not that shown in Figure 4. This leaves reaction 6 as the most likely reaction path for the OH radical reaction with CH_3I. The yield of I_2, $G(I_2) = 2.5$ in N_2O–CH_3I solutions, and the direct decay of the spectrum with I^- to give I_2^- also support reaction 6. The exact nature of the spectrum is, however, less certain. In the gas phase iodine atoms show an absorption below 200 mμ;[11] no absorption has been reported above 300 mμ. However, many spectra of I atom complexes have been reported above 300 mμ.[12] In the present work a complex between I and water or CH_3I is possible.

A search was made for an absorption due to the I–H_2O complex in the pulse radiolysis of potassium iodide solutions. The conditions of the experiments are such that the OH radical concentration is in excess of the I^- concentration, *e.g.*, [OH] = 10 μ*M*, [I^-] = 5 μ*M*. Here the OH radical produces I *via* OH +

(9) T. J. Hardwick, *J. Phys. Chem.*, 66, 2246 (1962).

(10) J. K. Thomas, 3rd International Congress of Radiation Research, Cortina, Italy, 1966.

(11) R. J. Donovan and D. Husain, *Nature*, 206, 171 (1965).

(12) T. H. Glover and G. Porter, *Proc. Roy. Soc.* (London), 262, 476 (1961).

Table I: Rates of Reaction of Radicals and Atoms in the Gas Phase and in Water at 25°

Compound	$k_1 \times 10^{9}$ [a,b]	$k_2 \times 10^{9}$ [a,c]	$k_3 \times 10^{3}$ [a]	$k_4 \times 10^{3}$ [a]
Ethylene	4.1	3.2	4.9	2.0
Propylene	6.5	3.9	5.3	4.0
1-Butene	6.5	5.1	30.0	...
Isobutylene	5.0	10.0	39.0	...
Butadiene	6.5	10.0	1.25×10^{3}	1.18×10^{3}
Methanol	0.47	1.9×10^{-3}	0.22	0.05
Ethanol	0.72	1.6×10^{-2}	0.59	0.14
Isopropyl alcohol	1.74	5.0×10^{-2}	3.4	0.45
Oxygen	...	20	4.7×10^{6}	Diffusion controlled
Iodine	...	~10	6.0×10^{8}	Diffusion controlled

[a] k_1, OH radical rate; k_2, H atom rate; and k_3, CH_3 radical rate, all in water phase; k_4, CH_3 radical rate in gas phase. [b] Measured by I^- method, J. K. Thomas, *Trans. Faraday Soc.*, **61**, 702 (1965). [c] Measured *via* competition with methanol, ref 15.

$I^- \rightarrow I + OH^-$ and an $I\text{-}H_2O$ complex is formed. However, the only absorption observed is a weak I_2^- band. It is thus left to postulate that the observed spectrum is due to the $I(CH_3I)$ complex. The nature of iodine complexes has been discussed by Katzin,[13] who proposes that complexes showing an absorption with two peaks can be considered as perturbed iodide ion spectra. In the present case if a partial electron transfer occurred to the iodine atoms, then a complex of the form $I^{\delta-}(CH_3)^{\delta+}I^{\delta-}$ is formed. In the interpretation of ref 13 this should exhibit a perturbed iodide ion spectrum similar to that shown in Figure 3.

The first-order decay of $I(CH_3I)$ at low intensities in water and with alcohols is interpreted as a reaction of these solutes with the $I(CH_3I)$ to give complexes, which like the $I(H_2O)$ complex have no measurable absorption. The fact that $G(I_2)$ is not affected by the alcohols shows that the I atom does not undergo an irreversible chemical reaction in these systems. At high radiation intensities the I atom complexes recombine and increase the decay rate. This is illustrated in Figure 4; the increase in the reaction rate over that at low intensities is expressed by $k_8(I(CH_3I))^2$.

$$I(CH_3I) + H_2O \longrightarrow I\text{-}H_2O + CH_3I \qquad (7)$$

$$I(CH_3I) + I(CH_3I) \longrightarrow I_2 + 2CH_3I \qquad (8)$$

Figure 5 shows that the above relationship holds and gives $2k_8 = 3 \times 10^9$ l. M^{-1} sec^{-1}. The value for k_7 is given by the first-order decay at low intensity, *i.e.*, $k_7 = 3.0 \times 10^4$ sec^{-1}.

The Reaction of Methyl Radicals. In the gas phase the rate of reaction of methyl radicals with oxygen and iodine is very rapid and in the case of oxygen the activation energy is zero. In water the rates are again rapid and the activation energy for the oxygen reaction is 3.5 kcal/mole. In order for a species such as the CH_3 radical to diffuse, an adjacent water molecule has to move to create a vacant site. On this basis the activation energy for a diffusion-controlled reaction in water is the activation energy for viscosity change, which is 3.7 kcal/mole. As the measured activation energy of reaction 1 is in agreement with this value, the reaction of a methyl radical with oxygen is diffusion controlled in water as in the gas phase.

The comparison of the rates of CH_3 radical reactions in water and the gas phase shows that the same order of reactivity occurs in both phases. However, the rates in water are on the whole faster than those in the gas, a similar effect being noted with H atoms.[14,15] This may be due to the solvation of the solute by the water, *i.e.*, a change in reaction energy, or it may be due to the caging in of the reactants by the solvent. This would promote more encounters between the reactants resulting in an increased rate of reaction.

It is instructive to compare the rates of reaction of CH_3 radical reactions in water with the rates of H atoms and OH radicals. For abstraction reactions the same general increase in reactivity is noted for all radicals in going from methyl alcohol to isopropyl alcohol and shows that the same reaction mechanism holds for abstraction by all these radicals. For addition reactions to unsaturated hydrocarbons the CH_3 radical behaves in a similar fashion to the H atom, the rates following the atom-localization energy of the hydrocarbon.[16] The OH radical reactions show no dependence on the atom-localization energy, however, all the rates being similar and approaching diffusion control. The ab-

(13) L. I. Katzin, *J. Chem. Phys.*, **23**, 2055 (1955); L. I. Katzin and R. L. McBeth, *J. Phys. Chem.*, **62**, 253 (1958).

(14) H. Schwarz, *ibid.*, **67**, 2827 (1963).

(15) J. P. Sweet and J. K. Thomas, *ibid.*, **68**, 1363 (1964).

(16) S. Sato and R. J. Cvetanović, *J. Am. Chem. Soc.*, **81**, 3223 (1959).

solute value of the CH_3 radical rates is significantly less than the H atom rates. This is due to two factors: (a) the methyl radical is planar and an activation energy is required to reach the transition state which has the character of the tetrahedral methane molecule and (b) the preexponential or A factors for the methyl radical reactions are much smaller than the A factors for the H atom reactions. This is due to the significant amount of entropy lost by the CH_3 and the solute in forming the transition state of the reaction.[17]

The above data demonstrate the feasibility of using methyl iodide as a convenient source of methyl radicals in water and other solvents in which electrons are stabilized. For the particular case of water the methyl iodide is also a convenient source of iodine atoms and should provide valuable data on the various I atom complexes that may be formed.

Acknowledgment. I wish to thank Mr. B. E. Clift and Mr. E. Backstrom, who operated the Argonne linear accelerator. I also wish to extend special praise and thanks to Mr. A. Lent and Mr. J. Butler of the Applied Mathematics Division, who carried out all the programming on CHLOE and the 3600 computer, thereby enabling me to greatly improve the processing of my data.

(17) S. Benson, "The Foundations of Chemical Kinetics," McGraw-Hill Book Co., Inc., New York, N. Y., 1960, p 286.

NOTES

Phosphorus-31 Chemical Shifts of Phosphonate Anions

by Jean G. Riess,[1] John R. Van Wazer, and John H. Letcher

Central Research Department, Monsanto Company, St. Louis, Missouri *(Received August 15, 1966)*

In a publication from this laboratory[2] 10 years ago it was stated that the ^{31}P chemical shifts of "the phosphonic acids and the phosphonates offer a direct way to measure the relative electron-donating ability of organic radicals . . . [with] the stronger electron-donating groups cause[ing] the lesser shielding of the phosphorus nucleus." Recently the quantum mechanical theory of ^{31}P chemical shifts has been elucidated[3,4] for the entire range of phosphorus compounds and it is shown that the chemical shift of compounds in which phosphorus has four substituents is primarily sensitive to the polarity of the σ bonds and the total occupation of the d_π orbitals of the phosphorus. In view of this theoretical work, it seemed desirable to obtain the ^{31}P chemical shifts of a number of phosphonates under carefully controlled conditions. These data and the recently published[5] chemical shifts of quaternary triphenylphosphonium salts are compared with each other in light of the general theory and the problem of measuring electron-donating ability.

The ^{31}P chemical-shift measurements on the phosphonates were carried out at 40.5 Mc using a Varian HR-100 spectrograph on aqueous solutions in the range of 0.1–0.5 M in phosphorus, employing 85% H_3PO_4 in a capillary tube as the reference standard. In order to avoid complications due to hydrogen association and hydrogen bonding and to make the data comparable, solutions of the phosphonic acids were brought to pH 14 by addition of tetramethylammonium hydroxide. As long as the two hydrogens of the phosphonic acid are neutralized, it was found that the ^{31}P chemical shift is insensitive to rather large variations in alkalinity or dilution.[6] In the region of measurement, a severalfold change in either phosphorus or alkalinity concentration caused less than 0.2-ppm change in the chemical shift. The experimental data are presented in Table I.

(1) On leave from the University of Strasbourg, 1964–1966.

(2) J. R. Van Wazer, C. F. Callis, J. N. Shoolery, and R. C. Jones, *J. Am. Chem. Soc.*, **78**, 5715 (1956).

(3) J. H. Letcher and J. R. Van Wazer, *J. Chem. Phys.*, **44**, 815 (1966).

(4) J. H. Letcher and J. R. Van Wazer, *ibid.*, **45**, 2916, 2926 (1966).

(5) S. O. Grim, W. McFarlane, E. F. Davidoff, and T. J. Marks, *J. Phys. Chem.*, **70**, 581 (1966). Also see *Nature*, **208**, 995 (1965).

(6) Also see K. Moedritzer, submitted for publication.

Table I: ^{31}P Chemical Shifts[a] and Shift Differences[b] in Phosphonates

Organic group, R	Phosphonates, RPO_3^{2-} δ	Δδ	Organic group, R	Phosphonates, RPO_3^{2-} δ	Δδ
CH_3-	−20.12	0.0	$^-O(O)CCH_2-$	−13.3	+6.8
C_2H_5-	−24.1	−3.0	$^2-O_2P(O)CH_2-$	−15.4	+4.7
$c\text{-}C_6H_{11}$	−24.8	−4.8	$^2-O_2P(O)(CH_2)_2-$	−23.2	−3.1
C_6H_5-	−10.9	+9.9[c]	$^2-O_2P(O)(CH_2)_3-$	−22.4	−2.3
$CH_2{=}CHCH_2$	−18.6	+1.5	$N{\equiv}CCH_2-$	−13.1	+7.0
$ClCH_2$	−11.3	+8.8	C_6H_9-[d]	−17.6	+2.5
Cl_2CH-	−8.15	+12.0	$C_6H_5CH{=}CH-$	−10.4	+9.7
Cl_3C	−8.1	+12.0	$p\text{-}ClC_6H_5-$	−9.9	+10.9[c]
$HOCH_2-$	−15.5	+4.6	$p\text{-}IC_6H_5$	−10.1	+10.7[c]
$C_6H_5CH_2-$	−17.6	+2.5	$p\text{-}NH_2C_6H_5-$	−11.8	+9.0[c]
$(C_6H_5)_2CH-$	−16.5	+3.6	$m\text{-}BrC_6H_5-$	−8.8	+12.0[c]
$p\text{-}NH_2C_6H_5CH_2-$	−18.0	+2.1	$m\text{-}NH_2C_6H_5-$	−11.0	+9.8[c]
$CH_3C(O)CH_2-$	−9.6	+10.5			

[a] In ppm referenced to 85% H_3PO_4. [b] Δδ = (δ for R) − (δ for R = CH_3). [c] Corrected for the ring current in the phenyl group by adding 0.7 ppm to the Δδ value. [d] 1-Cyclohexenyl.

Table II: ^{31}P Chemical Shifts[a] and Shift Differences[b] in Various Phosphonium Cations

Organic group, R	Phosphonium cations: $RP(C_6H_5)_3^+$ δ	Δδ	$RP(n\text{-}C_4H_9)_3^+$ δ	Δδ	$RP(C_2H_5)_3^+$ δ	Δδ
CH_3-	−22.6	0.0	−32.3	0.0	−37.8	0.0
C_2H_5-	−26.2	−3.6	−35.5	−3.2	−40.5	−2.7
$n\text{-}C_4H_9-$	−24.0	−1.4	−33.9	−1.6		
$i\text{-}C_3H_7-$	−30.9	−8.3	−38.0	−7.7	−42.8	−5.0
$CH_2{=}CHCH_2-$	−21.4	+1.2	−32.4	−0.1		

[a] In ppm referenced to 85% H_3PO_4. [b] Δδ = (δ for R) − (δ for R = CH_3).

According to the theory for molecules of the type MPZ_3, the chemical shift, δ, in ppm is given by the expression

$$\delta = 11829 - 7940\zeta_1 - 147n_\pi \quad (1)$$

where n_π is the total number of electrons in the d_π orbitals of the phosphorus, and where in terms of the average amount of charge, h_M and h_Z, residing in the phosphorus atomic orbitals of the bonds to the M and Z substituents, respectively

$$\zeta_1 = 3[(h_Z^2/2) + h_M - h_M h_Z] + [1.5/\sin^2(\theta/2)](h_Z - h_Z^2 + h_M h_Z - h_M) \quad (2)$$

where θ is the usual ZPZ bond angle. Following Coulson,[7] we shall express the values of these charges in terms of the following equation, where χ is the Pauling electronegativity and A stands for either the M or Z substituent

$$h_A = 1.0 + 0.16(\chi_P - \chi_A) + 0.035(\chi_P - \chi_A)^2 \quad (3)$$

Employing values of $\chi_0 = 3.5$ and $\chi_C = 2.5$–2.8, the following quantum-mechanically based equations are obtained for the change, Δδ, in ppm of the ^{31}P chemical shift resulting from substituting one R group for another. For the phosphonate anions, RPO_3^{2-}

$$\Delta\delta = 100\Delta\chi_R - 4\Delta\theta_{OPO} - 147\Delta\pi_{P-O} \quad (4)$$

For the quaternary triphenyl- or trialkylphosphonium cations,[5] RPR'_3^+

$$\Delta\delta = 50\Delta\chi_R - \kappa\Delta\theta_{R'PR'} \quad (5)$$

with $-0.2 < \kappa < 0.5$, where $\Delta\chi_R$ is the difference in effective Pauling electronegativity (*i.e.*, electron-withdrawing power) between the two different R substituents, Δθ is the bond-angle change in degrees, and $\Delta\pi_{P-O}$ is the total change (electrons/P) in the amount of P–O π character upon substituting one R for another.

(7) C. A. Coulson, "Valence," corrected 2nd ed, Oxford University Press, London, 1963, p 141.

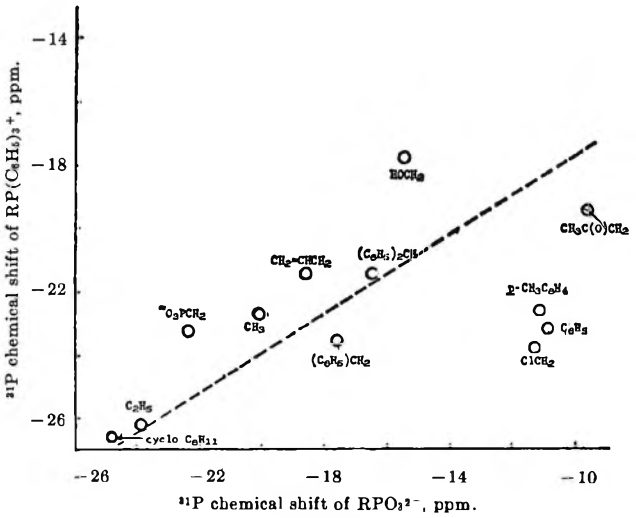

Figure 1. A plot of the ^{31}P chemical shifts of variously substituted phosphines *vs.* the chemical shifts of quaternary triphenylphosphonium compounds having the same substituent. The dotted line corresponds to the theoretical slope (see text).

If the P–O π bonding and the OPO bond angles in the phosphonates were not affected by changing the R substituent, a plot of ^{31}P chemical shifts of the phosphonate anions *vs.* those of the corresponding phosphonium cations, RPR'$_3^+$, should give a straight line of slope $^{100}/_{50}$. However, as shown in Figure 1, this is far from being the case, so that it appears that varying the R organic substituent does affect the P–O bond order to a small extent. In other words, the great sensitivity of the ^{31}P chemical shift to the occupation of the phosphorus d_π orbitals renders the phosphonates a poor tool for estimating the electron-donating ability of organic groups. Both bond-distance data[8] and the observed[3] ^{31}P chemical shifts of triphenylphosphine and the tetraphenylphosphonium ion indicate that there is little or no π character in the P–C bond between a phenyl group and a phosphorus atom. Therefore it seems reasonable to ascribe essentially all such π effects to the P–O bonds of the phosphonate anions. This is borne out by the rather good agreement of the $\Delta\delta$ values[5] between the various quaternary triphenyl- and trialkylphosphonium cations, shown in Table II. If there were much π bonding between the phenyl group and the phosphorus and if changing the R substituent affected this π bonding, these values of $\Delta\delta$ would be quite inconsistent.

(8) In the compound (C$_6$H$_5$)(CH$_3$)(S)PP(S)(CH$_3$)(C$_6$H$_5$), the P–C distances for the methyl groups are 1.82 A whereas they are 1.88 A for the phenyl groups, according to P. J. Wheatley, *J. Chem. Soc.*, 523 (1960). π bonding should shorten the bond. Other X-ray work has shown the P–C distance in (CH$_3$)$_3$P to be 1.84 A and in (C$_6$H$_5$)$_3$P to be 1.83 A.

Ionic and Partial Double-Bond Character of Carbon–Chlorine Bond in 1,1-Difluorovinyl Chloride

by Suresh Chandra

Physics Department, Allahabad University, Allahabad, India

Accepted and Transmitted by The Faraday Society (June 6, 1966)

The microwave spectrum of 1,1-difluorovinyl chloride has been studied by Jenkins and Sugden[1] and a structure for this molecule was given. A new and more probable structure for 1,1-difluorovinyl chloride has been proposed in order to get better and more probable molecular characteristics. From this structure a new value of the angle θ between the a axis and the C–Cl bond has been found. The principal quadrupole coupling constants, ionic and partial double-bond character of the carbon–chlorine bond, and percentage of s character of the chlorine bond orbital have also been evaluated.

The bond lengths and bond angles are intimately related to their bond environment. For a given bond environment they are remarkably constant in different molecules but vary systematically with the changes in the bond environment. However, small changes are observed when Cl, Br, and I atoms are adjacent to the bond.[2] So, for purposes of calculating approximate moments of inertia, structural parameters for 1,1-difluorovinyl chloride (CF_2=CHCl) are deduced from those molecules which have very nearly the same structure as CF_2=CHCl. The carbon–fluorine and carbon–carbon bond lengths and the corresponding angles (bond angles) are taken from the structure of the 1,1-difluoroethylene molecule ($C_2H_2F_2$)[3,4] and the carbon–chlorine and carbon–hydrogen bond lengths and the corresponding bond angles are taken from the structure of the vinyl chloride molecule (CH_2=CHCl).[5] In these calculations, the carbon–carbon bond distance was varied slightly in order to obtain better agreement between calculated and observed moments of inertia. The values of the structural parameters thus obtained

(1) D. R. Jenkins and T. M. Sugden, *Trans. Faraday Soc.*, **55**, 1473 (1959).

(2) A. S. Rajput and S. Chandra, *Bull. Chem. Soc. Japan*, **39**, 1854 (1966).

(3) J. Karle and I. L. Karle, *J. Chem. Phys.*, **18**, 163 (1950).

(4) A. Roberts and W. F. Edgell, *ibid.*, **17**, 742 (1950); *Phys. Rev.*, **76**, 178 (1950).

(5) D. Kivelson, E. B. Wilson, and D. R. Lide, *J. Chem. Phys.*, **32**, 205 (1960).

are quoted in Table I. The calculated and observed moments of inertia of CF_2=$CH^{35}Cl$ and CF_2=$CH^{37}Cl$ are also compared.

Table I: Structural Parameters of 1,1-Difluorovinyl Chloride

Bond length, A	Bond angle
C–F = 1.32	∠FCF = 110°
C–C = 1.30	∠CCH = 123° 49′
C–Cl = 1.726	∠CCCl = 122° 18′
C–H = 1.08	

Moments of inertia of CF_2=$CH^{35}Cl$

	Obsd	Calcd
I_a (amu A²)	47.20	46.93
I_b (amu A²)	220.09	220.52
I_c (amu A²)	267.45	267.45

Moments of inertia of CF_2=$CH^{37}Cl$

	Obsd	Calcd
I_a (amu A²)	47.20	46.94
I_b (amu A²)	226.41	226.94
I_c (amu A²)	273.76	273.88

The characteristic that the a axis passes through the chlorine nucleus was utilized for evaluating the angle θ between the a axis and the z axis (along the carbon–chlorine bond) which comes out to be 26° 10′ from the proposed structure of 1,1-difluorovinyl chloride. If it is assumed that the C–Cl bond coincides with the z principal axis of the quadrupole coupling dyadic, a transformation of axes may be used to find the components of the dyadic in its principal system.[1] The other two axes must lie in the plane of symmetry (x axis) and perpendicular to it (y axis). The values of the principal quadrupole coupling constants χ_{xx}, χ_{yy}, and χ_{zz} for CF_2=$CHC^{35}Cl$ obtained from the experimental values of χ_{aa}, χ_{bb}, and χ_{cc}[1] are listed in Table II. The value of χ_{zz} thus obtained may be compared with that of −70.16 mc/sec for vinyl chloride[5] and −74.77 Mc/sec for methyl chloride[6] and with many other analogous values for chloromethanes and chloroethylenes.

Following Goldstein,[7] an estimate of the partial double-bond character δ of the carbon–chlorine bond may be made from the relation

$$\delta = \frac{\chi_{xx} - \chi_{yy}}{-{}^3/_2 eQq_{(\text{atomic})}} \qquad (1)$$

where $-{}^3/_2 eQq_{(\text{atomic})}$ = 164.6 Mc/sec for ^{35}Cl. The result is 4.3% double bond character to the C–Cl bond, which is very close to the value 6% in vinyl chloride.[7] It may be mentioned here that eq 1 makes no allowance for the positive charge on chlorine in the structure.

Table II: Quadrupole Coupling Constants of CF_2=$CH^{35}Cl$

χ_{aa}	= −51.7 ± 1.3 Mc/sec
χ_{bb}	= 18.2 ± 1.0 Mc/sec
χ_{cc}	= 33.5 ± 0.8 Mc/sec
χ_{zz}	= −73.94 ± 1.5 Mc/sec
χ_{xx}	= 40.44 ± 1.0 Mc/sec
χ_{yy}	= 33.5 ± 0.8 Mc/sec
θ	= 26° 10′

The ionic character of a bond AB can be estimated from the electronegativity values (X_A and X_B) of the two atoms forming the bond. For a two-electron bond, the pair of electrons will divide themselves between the two atoms in the ratio of their relative electronegativities, such that a fraction $2X_A/(X_A + X_B)$ of electron atmosphere is on the atom A and a fraction $2X_B/(X_A + X_B)$ of electron atmosphere is on the atom B. The ionic character of the bond is then defined as[8]

$$\text{ionic character } \beta = \frac{|X_A - X_B|}{(X_A + X_B)} \qquad (2)$$

For polyatomic molecules, the values of group electronegativity[9] should be used. The group electronegativity value of the radical –$CHCF_2$ is 2.55,[9] and the electronegativity value of the chlorine atom is 3.00. Using these values, the ionic character of the carbon–chlorine bond in 1,1-difluorovinyl chloride is found to be 8%.

The values of the nuclear quadrupole coupling constants may be used for evaluating the hybridization of the atomic orbitals about the nucleus under consideration. The value of the fractional s character of the bonding orbital of chlorine, α^2, may be evaluated from the relation[10]

$$eQq_{zz} = (1 - \alpha^2 + d^2 - \beta - \delta)eQq_{\text{atomic}} \qquad (3)$$

where d^2 is the amount of the d hybridization of the bonding orbital of chlorine and eQq_{atomic} is the nuclear quadrupole coupling constant for the free atom. However, the d orbitals make only negligible contributions to the quadrupole coupling constant and its value

(6) J. Kraitchman and B. P. Dailey, *J. Chem. Phys.*, **22**, 1477 (1954)
(7) A. Goldstein, *ibid.*, **24**, 106 (1956).
(8) J. K. Wilmshurst, *ibid.*, **30**, 561 (1959).
(9) S. Chandra and S. Chandra, *Tetrahedron*, **22**, 3403 (1966).
(10) T. P. Das and E. L. Hahn, "Solid State Physics," Supplement 1, "Nuclear Quadrupole Resonance Spectroscopy," Academic Press Inc., New York, N. Y., 1958, p 138.

is predicted to be 5% or less. On the assumption of 5% d character and for the observed values of eQq_{zz} (−73.94 c/sec) and eQq_{atomic} (−109.74 Mc/sec), eq 3 shows that the s character of the chlorine bond orbital is nearly 25%.

Acknowledgment. The author expresses his gratitude and thanks to Professor Krishnaji for his kind supervision of the work.

Experimental Determination of the Electron Affinity of Several Aromatic Aldehydes and Ketones

by W. E. Wentworth and Edward Chen[1]

Department of Chemistry, University of Houston, Houston, Texas 77004 *(Received December 19, 1966)*

Recently, Wentworth, Chen, and Lovelock[2] have proposed a kinetic model for the processes occurring within the electron-capture detector operated in the pulse-sampling mode and have demonstrated its validity for several aromatic hydrocarbons. Earlier Wentworth and Becker[3] calculated the electron affinities of some aromatic hydrocarbons using the electron-capture detector data and correlated these electron affinities with their half-wave reduction potentials[3] and the energy of their 0–0 transition.[4] The experimental electron affinities were also compared with several theoretical calculations of the electron affinities.[4] However, thus far only aromatic hydrocarbons have been studied, although the technique for the calculation of the electron affinities originally given in ref 3 and later modified by the kinetic model[2] is applicable to any molecule which forms a stable negative ion. Therefore, the electron-capture detector response to a series of aromatic aldehydes and ketones has been studied as a function of temperature in order to test the validity of the interpretation for a different type of molecule which apparently forms a stable negative ion with respect to electron attachment.

For the kinetic model, the following expression can be derived for the response[2]

$$\frac{b - [e^-]}{[e^-]} = \frac{k_L k_1 a}{k_D(k_L + k_{-1})} = Ka \qquad (1)$$

where b is the electron concentration before the addition of the test molecule, AB, $[e^-]$ is the electron concentration in the presence of AB, a is the initial concentration of AB, k_D is a pseudo-first-order rate constant representing the loss of electrons due to processes other than attachment to AB, k_L is a pseudo-first-order rate constant representing the loss of AB^- due to all processes other than detachment or dissociation, k_1 is the rate constant for the attachment of electrons to AB, k_{-1} is the rate constant for the detachment of electrons from AB^-, and K is the electron-capture coefficient.

For some compounds, there is one region, designated β, at lower temperatures where $k_L \gg k_{-1}$, so that

$$K = k_1/k_D \qquad (2)$$

and K is relatively insensitive to temperature. In another region, designated α, $k_{-1} \gg k_L$ and, assuming the statistical thermodynamic expression for an ideal gas

$$K = \frac{k_1 k_L}{k_{-1} k_D} = K_{eq} k_L/k_D = A/T^{3/2} \exp(EA/kT) k_L/k_D \qquad (3)$$

A is a constant which can be calculated from fundamental parameters, EA is the electron affinity, and k is the Boltzmann constant. In the α region, the electron affinity can be obtained from the slope of a ln $KT^{3/2}$ *vs.* $1/T$ graph.

Experimental Section

The procedure and equipment used in this study have been described earlier.[2] The naphthaldehyde-1, benzaldehyde, and acetophenone were Eastman White Label. The phenanthrenealdehyde-9 and naphthaldehyde-2 were obtained from the Aldrich Chemical Co. The solvent used was Eastman's Spectroquality benzene.

Results and Discussion

The capture coefficients for the compounds studied are plotted in Figure 1 as ln $KT^{3/2}$ *vs.* $1/T$. All of the compounds except cinnamaldehyde exhibit an α region. Acetophenone and benzaldehyde do not have a β region. From the data in the α region, the electron affinities have been calculated from the slopes using an average intercept[2,5] and a variable intercept.

The average value for the intercept from the aromatic hydrocarbons and the compounds used in this study was used and is equal to 14.8. The average intercept

(1) This work was used for partial fulfillment of the requirements for the Ph.D. degree at the University of Houston, Houston, Texas.

(2) W. E. Wentworth, E. Chen, and J. E. Lovelock, *J. Phys. Chem.*, 70, 445 (1966).

(3) W. E. Wentworth and R. S. Becker, *J. Am. Chem. Soc.*, 84, 4263 (1962).

(4) R. S. Becker and W. E. Wentworth, *ibid.*, 85, 2210 (1963).

(5) W. E. Wentworth, W. Hirsch, and E. Chen, *J. Phys. Chem.*, 71, 218 (1967).

Table I: Electron Affinities and Half-Wave Reduction Potentials

Compound	Electron affinity, ev (variable intercept)	Intercept	Electron affinity, ev (common intercept)	$E_{1/2}$ (ref 7)
Acetophenone	0.334 ± 0.004	14.70 ± 0.15	0.334 ± 0.004	...
Benzaldehyde	0.421 ± 0.010	15.89 ± 0.30	0.448 ± 0.006	1.592
Naphthaldehyde-2	0.620 ± 0.040	14.46 ± 0.99	0.615 ± 0.014	1.505
Naphthaldehyde-1	0.745 ± 0.070	12.61 ± 1.60	0.669 ± 0.022	1.476
Phenanthrenealdehyde-9	0.655 ± 0.142	14.92 ± 3.34	0.712 ± 0.009	1.447
Cinnamaldehyde	...	...	0.823 ± 0.043	1.335
Anthracenealdehyde-9	...	...	(1.02)	1.207

Table II

Compound	k_1, l./mole sec	k_{-1}, sec^{-1}
Naphthaldehyde-2	$6.7 \pm 3.2 \times 10^{12}$	$2.7 \pm 1.2 \times 10^{7}T^{3/2} \exp(-0.615 \pm 0.014/kT)$
Naphthaldehyde-1	$5.7 \pm 3.4 \times 10^{12}$	$2.2 \pm 1.3 \times 10^{7}T^{3/2} \exp(-0.669 \pm 0.022/kT)$
Phenanthrenealdehyde-9	$3.7 \pm 2.3 \times 10^{13}$	$4.9 \pm 3.0 \times 10^{8}T^{3/2} \exp(-0.712 \pm 0.009/kT)$
Cinnamaldehyde	$3.4 \pm 2.2 \times 10^{12}$	$5.2 \pm 3.2 \times 10^{7}T^{3/2} \exp(-0.823 \pm 0.043/kT)$

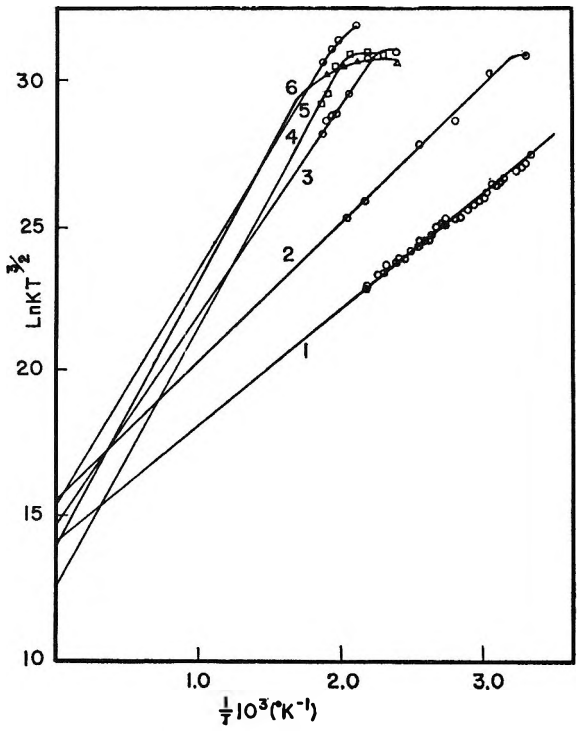

Figure 1. Ln $KT^{3/2}$ *vs.* $1/T$; 1, acetophenone; 2, benzaldehyde; 3, naphthaldehyde-2; 4, naphthaldehyde-1; 5, phenanthrenealdehyde-9; 6, cinnamaldehyde.

was used in two ways. For acetophenone and benzaldehyde, only the slope and hence the electron affinity using eq 3 was determined. For the other compounds, a least-squares fit to an equation expressing the temperature dependency in both the α and β regions was carried out. This is obtained by substituting eq 3 into eq 1 giving

$$K = \frac{k_L/k_D}{\frac{k_L}{k_1} + \frac{T^{3/2}}{A}\exp[-(EA/kT)]} \quad (4)$$

Three parameters, the electron affinity and the ratios of k_1/k_L and k_L/k_D, were determined using a nonlinear least-squares adjustment.[6] The average intercept was derived from the aromatic hydrocarbons[2,7] and the compounds in this study. The results of the least-squares data reduction procedure are given in Table I. The electron affinities are plotted against the half-wave reduction potentials[8] in Figure 2. There is a rather good linear correlation between the two, but the slope is greater than unity (approximately 1.5).

This is in contrast to the slope for the similar correlation for the aromatic hydrocarbons, which is less than unity.[2] Recently the correlation for the aromatic hydrocarbons has been reexamined with additional electron affinity data and the following equations have been obtained.

$$EA = 0.681 \pm 0.09E_{1/2} + 1.95 \pm 0.20, \quad \sigma_{ab} = -0.019 \quad (5)$$

(6) W. E. Wentworth, *J. Chem. Educ.*, **42**, 96, 162 (1965).

(7) R. S. Becker and E. Chen, *J. Chem. Phys.*, **45**, 2403 (1966).

(8) R. W. Schmidt and E. Heilbronner, *Helv. Chim. Acta*, **37**, 1453 (1954).

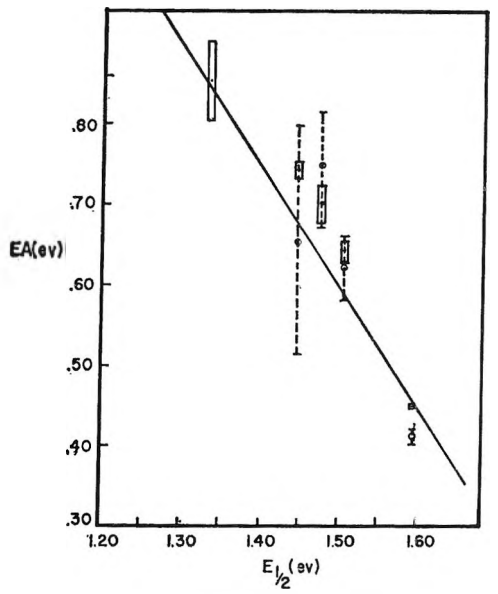

Figure 2. Electron affinity *vs.* half-wave reduction potential for the aromatic aldehydes. The compounds are, reading from left to right: cinnamaldehyde, phenanthrenealdehyde-9, naphthaldehyde-1, naphthaldehyde-2, and benzaldehyde. The values obtained from the average intercept are indicated by rectangles, the height at the rectangle being a measure of the standard error. The circles are the data obtained by using a variable intercept with the horizontal lines indicating the standard error limits.

for the polarographic data in dioxane and

$$EA = 0.705 \pm 0.10E_{1/2} + 1.67 \pm 0.17, \quad \sigma_{ab} = -0.018 \quad (6)$$

in 2-methoxyethanol. σ_{ab} is the covariance term associated with the two parameters shown in the linear equations, eq 5 and 6.

In ref 3 it was pointed out that the formation of a solvated charge-transfer complex could not be used to explain a slope which was less than unity. However, in the case of the aromatic aldehydes, the slope is greater than unity and would be in agreement with the postulate of complex formation.

The electron affinity of anthracenealdehyde-9 can be estimated from the plot in Figure 2 and is given in Table I in parentheses. From the least-squares estimate of k_1/k_L and a value for k_L, the rate constant, k_1, can be determined. The value for k_L can be determined from the average intercept and a value for k_D. The value of k_D is 2.4×10^3 sec^{-1} so that the value of k_L is 2.4×10^4 sec^{-1}. With these values and assuming a preexponential temperature dependency for k_{-1} of $T^{1/2}$, k_{-1} can be determined. The results of this analysis for the compounds exhibiting both an α and β region are given in Table II.

In conclusion, the results of the temperature study of the capture coefficients of the aromatic aldehydes and ketones are in agreement with the kinetic model proposed earlier.[2] The linear correlation of the electron affinities calculated using this model with the half-wave reduction potentials supports the interpretation of the electron-capture response in terms of the electron affinities for compounds which form stable negative ions. The absolute values of electron affinities for five aromatic aldehydes and acetophenone are given.

Acknowledgments. This work was financially supported by the Robert A. Welch Foundation. Edward Chen was also a NASA predoctoral fellow.

Carbon Monoxide Solubilities in Sea Water

by Everett Douglas

Scripps Institution of Oceanography, La Jolla, California[1,2]
(Received October 14, 1966)

Carbon monoxide was first reported in the brown alga *Nereocystis* in 1911.[3] Since then it has been observed in other algae,[4,5] some other plants,[6] and a few of the siphonophores such as the surface-floating *Physalia*,[7,8] a bathypelagic *Nanomia*,[9,10] and a benthic form.[11] The concentration of this gas in the siphonophore floats has been found to be as high as 93%[11] of the total gas while in the algae upward to 12% has been reported.[3]

With this rising interest in the occurrence and utilization of CO, generally considered toxic in biological systems, it has become desirable to measure some of the

(1) Contribution from the Scripps Institution of Oceanography, University of California, San Diego, Calif.

(2) This investigation was supported by Public Health Service Research Grant No. GM-10521 from the National Institutes of Health and was performed under contract for the United States Navy Electronics Laboratory, San Diego, Calif.

(3) S. E. Langdon, *J. Am. Chem. Soc.*, **39**, 149 (1917).

(4) M. W. Loewus and C. C. Delwicke, *Plant Physiol.*, **38**, No. 4, 371 (1963).

(5) D. J. Chapman and R. O. Tocher, *Can. J. Botany*, **44**, 1438 (1966).

(6) S. M. Siegel, G. Renwick, and L. A. Rosen, *Science*, **137**, 683 (1962).

(7) J. B. Wittenberg, *Biol. Bull.*, 115, 371 (1958).

(8) J. B. Wittenberg, *J. Exptl. Biol.*, **37**, 698 (1960).

(9) G. V. Pickwell, E. G. Barhan, and J. W. Wilton, *Science*, **144**, 860 (1964).

(10) G. V. Pickwell, U. S. Navy Electronics Laboratory, Report No. 1369, 1966.

(11) E. Douglas, unpublished data.

Table I: Experimental Solubility Coefficients of Carbon Monoxide

				Cl°/₀₀ = 15.38			
	1.50°	6.46°	10.00°	14.96°	19.86°	24.60°	30.00°
	0.02904	0.02606	0.02422	0.02216	0.02049	0.01913	0.01782
	0.02895	0.02590	0.02415	0.02225	0.02043	0.01920	0.01802
	0.02894	0.02597	0.02420	0.02217	0.02050	0.01910	0.01780
Av	0.02898	0.02598	0.02419	0.02219	0.02047	0.01914	0.01788
				Cl°/₀₀ = 18.60			
	2.20°	6.50°	10.14°	15.25°	20.08°	25.08°	30.70°
	0.02744	0.02485	0.02329	0.02127	0.01982	0.01832	0.01725
	0.02758	0.02488	0.02328	0.02125	0.01974	0.01829	0.01732
	0.02747	0.02512	0.02326	0.02129	0.01976	0.01826	0.01712
Av	0.02750	0.02495	0.02328	0.02127	0.01977	0.01829	0.01723
				Cl°/₀₀ = 20.99			
	0.88°	6.10°	10.04°	15.25°	19.86°	25.23°	30.05°
	0.02753	0.02452	0.02274	0.02085	0.01925	0.01775	0.01684
	0.02759	0.02440	0.02269	0.02075	0.01925	0.01779	0.01686
	0.02755	0.02440	0.02267	0.02060	0.01914	0.01783	0.01679
Av	0.02756	0.02445	0.02270	0.02073	0.01921	0.01779	0.01683

Table II: Carbon Monoxide Solubility in Sea Water[a]

Temp.	Chlorinity						
°C	15	16	17	18	19	20	21
	α, carbon monoxide						
−2	0.03162	0.03124	0.03084	0.03044	0.03004	0.02966	0.02926
−1	0.03090	0.03052	0.03014	0.02976	0.02938	0.02900	0.02862
0	0.03024	0.02986	0.02948	0.02910	0.02872	0.02835	0.02797
1	0.02949	0.02913	0.02878	0.02842	0.02807	0.02772	0.02736
2	0.02880	0.02846	0.02811	0.02776	0.02743	0.02709	0.02675
3	0.02812	0.02779	0.02746	0.02713	0.02680	0.02648	0.02614
4	0.02750	0.02717	0.02684	0.02652	0.02620	0.02588	0.02556
5	0.02686	0.02656	0.02625	0.02594	0.02564	0.02532	0.02501
6	0.02632	0.02602	0.02572	0.02541	0.02510	0.02480	0.02450
7	0.02578	0.02548	0.02519	0.02490	0.02460	0.02432	0.02402
8	0.02524	0.02496	0.02468	0.02440	0.02412	0.02384	0.02356
9	0.02475	0.02448	0.02421	0.02394	0.02366	0.02339	0.02312
10	0.02428	0.02402	0.02376	0.02350	0.02322	0.02296	0.02270
11	0.02385	0.02359	0.02334	0.02308	0.02282	0.02256	0.02230
12	0.02343	0.02318	0.02292	0.02267	0.02242	0.02216	0.02192
13	0.02302	0.02278	0.02252	0.02228	0.02202	0.02178	0.02153
14	0.02262	0.02238	0.02213	0.02188	0.02164	0.02140	0.02116
15	0.02224	0.02200	0.02176	0.02152	0.02128	0.02104	0.02080
16	0.02187	0.02164	0.02140	0.02116	0.02092	0.02070	0.02046
17	0.02152	0.02129	0.02106	0.02082	0.02059	0.02036	0.02014
18	0.02118	0.02094	0.02072	0.02048	0.02026	0.02002	0.01980
19	0.02084	0.02061	0.02038	0.02016	0.01994	0.01971	0.01949
20	0.02052	0.02030	0.02008	0.01985	0.01962	0.01940	0.01917
21	0.02022	0.02000	0.01978	0.01955	0.01932	0.01910	0.01888
22	0.01993	0.01971	0.01948	0.01926	0.01904	0.01882	0.01860
23	0.01965	0.01942	0.01920	0.01898	0.01876	0.01854	0.01832
24	0.01936	0.01915	0.01893	0.01872	0.01850	0.01828	0.01806
25	0.01912	0.01890	0.01868	0.01847	0.01825	0.01804	0.01782
26	0.01886	0.01864	0.01844	0.01822	0.01802	0.01780	0.01760
27	0.01862	0.01842	0.01822	0.01800	0.01780	0.01760	0.01740
28	0.01839	0.01820	0.01800	0.01780	0.01760	0.01740	0.01720
29	0.01819	0.01800	0.01780	0.01760	0.01741	0.01722	0.01702
30	0.01796	0.01778	0.01760	0.01742	0.01724	0.01706	0.01688

[a] Note that chlorinity is expressed in terms of grams of chlorine per kilogram of sea water while α is given as volume of gas (STPD) absorbed by a unit volume of water when the pressure of the gas equals 760 mm.

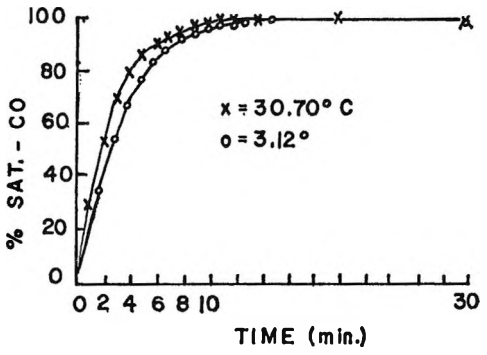

Figure 1.

physical properties of this gas. In this report one of these parameters, the solubility coefficients in three sea water chlorinities at seven temperatures per chlorinity, is given.

Experimental Section

The microgasometric method used has been described in detail earlier.[12,13a] The absorption chamber has been enlarged to employ 8 ml of water in order to maintain the same accuracy as obtained using distilled water.[13b] Figure 1 shows the rate of solution of CO in the absorption chamber, illustrating that 30 min is ample time for equilibration to occur.

The procedures used for obtaining gas-free sea water and the chlorinity determinations are detailed in an earlier work.[13a]

The purity of the CO was determined using a Scholander 0.5-cc gas analyzer[14] and microgasometric analyzer[15] showing the gas to be at least 99.7% pure. An independent method utilizing palladium chloride also gave a purity of greater than 99%.[5]

Results and Discussion

The experimental solubility coefficients are listed in Table I. Smooth curves were fitted on these points from which the values from −2 to 30° were taken. From these values the relations between solubility and chlorinity were graphed and the values from −2 to 30° in chlorinities ranging from 15–21‰ were obtained. These are given in Table II.

The only other solubility determinations of CO are those of Winkler for distilled water.[16,17]

(12) E. Douglas, *J. Phys. Chem.*, **68**, 169 (1964).

(13) (a) E. Douglas, *ibid.*, **69**, 2608 (1965); (b) for critical discussion of systematic errors refer to the original paper.[12]

(14) P. F. Scholander, *J. Biol. Chem.*, **167**, 235 (1947).

(15) P. F. Scholander, L. Van Dam, C. L. Claff, and J. W. Kanwisher, *Biol. Bull.*, **109**, 328 (1955).

(16) L. W. Winkler, *Z. Physik. Chem.* (Leipzig), **55**, 344 (1906).

(17) "Handbook of Chemistry and Physics," 39th ed, Chemical Rubber Publishing Co., Cleveland, Ohio, 1957.

Some Observations on the Kinetics of Hydrogen Iodide Addition to 1,3- and 1,4-Pentadiene[1]

by Kurt W. Egger and Sidney W. Benson

Department of Thermochemistry and Chemical Kinetics, Stanford Research Institute, Menlo Park, California 94025
(Received September 21, 1966)

We wish to report some quantitative kinetic information on the addition of HI to olefins, obtained complementary to reported studies of the iodine atom catalyzed isomerization[2a,b] and dimerization[2c] of *n*-pentadienes in the gas phase.

The rate of addition of HI to either 1,3- or 1,4-pentadiene was checked as a possible side reaction in these studies. We found that, during the isomerization of 1,4-pentadiene in the presence of iodine at temperatures between 420 and 515°K, 5–10% monoolefins had been produced, according to

$$\text{diolefin} + 2\text{HI} \rightleftarrows \text{olefin} + \text{I}_2$$

The mechanism of this over-all type of reaction has been shown to consist of[2d]

$$\text{diolefin} + \text{HI} \underset{-1}{\overset{1}{\rightleftarrows}} \text{RI} \quad \text{(slow)} \qquad \text{(A)}$$

and

$$\text{RI} + \text{HI} \underset{-2}{\overset{2}{\rightleftarrows}} \text{RH} + \text{I}_2 \quad \text{(fast)} \qquad \text{(B)}$$

with k_1 as the rate-controlling step. The intermediate alkyl iodide reacts rapidly and almost quantitatively with HI, forming the parent saturated compound, and in the case of diolefin as starting material, monoolefin is produced. Equation B was shown to be, in fact, a composite of

$$\text{RI} + \text{I} \rightleftarrows \text{R}\cdot + \text{I}_2 \qquad (\text{B}_1)$$

and

$$\text{R}\cdot + \text{HI} \rightleftarrows \text{RH} + \text{I} \qquad (\text{B}_2)$$

As both steps, B_1 and B_2, are fast compared to k_{-1}, they do not alter the simple second-order kinetics. Rate constants, k_1, were calculated from pressure measurements, as only the rate-controlling step A leads to a pressure change. The formulation given

(1) This work has been supported in part by Grant No. AP00353-01 from the Air Pollution Division of the U. S. Public Health Service.

(2) (a) K. W. Egger and S. W. Benson, *J. Am. Chem. Soc.*, **88**, 241 (1966); (b) K. W. Egger and S. W. Benson, *ibid.*, **87**, 3314 (1965); (c) K. W. Egger and S. W. Benson, unpublished data; (d) S. W. Benson, *J. Chem. Phys.*, **38**, 1945 (1963).

Table I: HI Addition to Olefins

Olefin	Vessel[a]	Temp, °K	$(Olefin)_0$,[b] torr	$(HI)_0$,[b] torr	Time, min	Δp,[c] torr	$(Olefin)_f$,[b] torr	$-\log k_1$,[d] $torr^{-1}$ sec^{-1}
2-Butene	2	461.2	96.8	97.5	170	2.5	94.3	8.04
1-Butene	1	483.6	52.9	134.1	36	3.0	49.9	6.44
1-Pentene	2	461.2	89.4	136.6	1067	31.1	58.3	7.45
1,4-Pentadiene	3	420.8	102.3	74.8	40	12.8	89.5	6.76
	3	424.1	136.0	80.6	31	15.1	120.9	6.85
	2	428.8	65.4	83.8	94	9.1	56.3	6.80
	2	461.2	53.3	84.8	42	20.0	33.3	5.75
1,3-Pentadiene	1	432.0	135.6	194.5	2	87.1	48.5	4.45

[a] 1, Unpacked "old" Pyrex glass reaction vessel used for a variety of reaction systems over a period of several months prior to use; 2, unpacked "new" Pyrex glass reaction vessels, Teflonized[2b] and coated with Dow Corning silicone oil 705; 3, aluminum vessel, covered with a 0.1-in. layer of Teflon, commercially applied. [b] Subscript 0 denotes initial, f final concentration. [c] Measured pressure difference. [d] Based on measured pressure differences (S. W. Benson and G. R. Haugen, *J. Am. Chem. Soc.*, **87**, 4036 (1965)).

in ref 3c was used to calculate k_1. The back reaction, the decomposition of the alkyl iodides, could be neglected as we were working at reasonably low conversions and in excess HI.[3c] (Furthermore, it was previously shown that the steady-state concentration of alkyl iodides in excess HI at temperatures between 480 and 600°K is very low.[3c]) Conversions ran between 11 and 38%.

The iodine buildup during the reaction, monitored spectrophotometrically, checks out within experimental error limits with the amount of saturated hydrocarbon or monoolefin, respectively (in the case of *n*-pentadiene), measured by gas–liquid chromatography.

The measured pressure changes are in reasonable agreement with the iodine produced. The method and experimental procedures used have been reported in detail earlier.[2a,4] The results are summarized in Table I. The use of coated reaction vessels was prompted by the finding that HI additions to olefins can be surface sensitive. Consistent results, using three different reaction vessels, indicate that the measured k_1 values probably represent homogeneous reaction rates.

The reliability of the rate constants measured for the *n*-pentadienes can be checked by comparison with the results obtained for 1- and 2-butene and 1-pentene. Careful studies of HI addition to ethylene,[3a] propylene,[3b] isobutene,[3c] vinyl chloride,[3c] and 2-butene[5] have been reported in the literature and for 1-butene good estimates are available.[5] The measured k_1 values for 1- and 2-butene are in good agreement with the literature data.

We cannot directly derive any meaningful Arrhenius parameters from such a limited number of experiments; therefore, activation energies have been calculated, using *estimated* A factors, based on an intrinsic A^* factor of $10^{7.4} \pm 0.7$ for all but 2-butene. This value has been arrived at on the basis of the reported log A values for HI, adding to ethylene (8.52),[3a] propylene (7.9),[3b] 1-butene (7.7),[5] isobutene (6.50),[3c] and 2-butene (6.3).[5c] It is further supported by consistent and reasonable A factors for the unimolecular back reaction, the elimination of HI from the corresponding iodides. These values, reported in Table II, are obtained

Table II: Activation Energies and Frequency Factors for the Addition of HI to Olefins and for the Back Reaction

$$HI + Olefin \underset{-1}{\overset{1}{\rightleftharpoons}} RI$$

Olefin	Log A_1, l./mole sec	E_1, kcal/mole	Log A_{-1},[b] sec^{-1}	E_{-1},[b] kcal/mole
trans-Butene-2	6.3[c]	(21.1)[c] 20.7	11.0	(37.5)[c]
1-Butene	7.7	(23.5)[c] 20.9	13.0	40.8
1-Pentene	7.7	22.0	13.0	42.0
1,4-Pentadiene[a]	8.0	19.3	13.6	39.3
1,3-Pentadiene ⇆ (4-iodopentene-2)	7.7	14.7	12.1	29.8

[a] Average value from all experiments, reported in Table I for 421–429°K. [b] ΔS and ΔH are computed for a mean temperature of 450°K, using the $\Delta C_p°$ shown in Table III. [c] See ref 5.

(3) (a) A. N. Bose and S. W. Benson, *J. Chem. Phys.*, **37**, 2935 (1962); (b) A. N. Bose and S. W. Benson, *ibid.*, **37**, 1081 (1962); (c) A. N. Bose and S. W. Benson, *ibid.*, **38**, 878 (1963).

(4) (a) D. M. Golden, K. W. Egger, and S. W. Benson, *J. Am. Chem. Soc.*, **86**, 5416 (1964); (b) K. W. Egger and S. W. Benson, *ibid.*, **88**, 236 (1966).

(5) P. S. Nangia and S. W. Benson, *J. Chem. Phys.*, **41**, 530 (1964).

Table III: Thermodynamic Data[a] Used for Calculating the Equilibrium Olefin + HI $\underset{2}{\overset{1}{\rightleftharpoons}}$ RI

Compounds	$C_p°$, cal/mole °K	S^c, cal/mole °K	$\Delta H_f°$, kcal/mole
HI	7.0	49 3	6.2
Butene-1	20.5	73 9	0.0
trans-Butene-2	21.0	70 9	−2.8
Pentene-1	27.4	83.1	−5.0
Pentadiene-1,4	25.1	79.7	25.2
Pentadiene-1,3	24.7	76.4	18.6
sec-Butyl iodide[b]	26.2	89.8	−14.4
2-Iodopentane[c]	31.7	99.2	−19.4
4-Iodopentene-1[c]	30.3	97.6	10.7
4-Iodopentene-2[d]	29.3	96.3	8.5

Reaction	$[\Delta C_p°]_{460}$	$[\Delta S°]_{460}$ $[\Delta S^{intr}]^e$	$[\Delta H_f°]_{460}$
sec-Butyl iodide → butene-1 + HI	1.8	33.4 32.6	20.6
→ *trans*-butene-2 + HI	0.8	30.4 33.2	17.8
2-Iodopentane → pentene-1 + HI	2.7	33.2 32.4	20.6
4-Iodopentene-1 → pentadiene-1,4 + HI	1.8	31.4 32.0	20.7
→ pentadiene-1,3 + HI	1.4	28.1 29.5	14.1
4-Iodopentene-2 → pentadiene-1,3 + HI	2.4	29.4 28.6	16.1

[a] Unless otherwise stated, values are taken from "JANAF Thermochemical Tables," Aug 1965, and API Tables. [b] See ref 5. [c] Estimated from group additivity properties and ref 5. [d] Estimated from group additivity properties and values for allyl iodide (A. S. Rodgers, D. M. Golden, and S. W. Benson, *J. Am. Chem. Soc.*, **88**, 3196 (1966)). [e] Intrinsic entropy difference, corrected for symmetry contributions.

from estimates of the equilibrium constants, $K_{2,1}$, in the systems, based on thermodynamic quantities, shown in Table III.

For 2-butene the literature value of 6.3 for log A_1 was used. From the narrow temperature range of 40° for the data of 1,4-pentadiene, E_1 is calculated as 22.2 ± 2 kcal and log A_1 (l./mole sec) as 9.4 ± 1. These rough values from limiting slopes in the Arrhenius plot are to be compared to the more reliable values of 19.3 and 8.1, respectively, based on the discussed estimate of the A factor. The disagreement is not significant, considering the scatter in the data and the narrow temperature range.

Table III shows all the data used in calculating the equilibrium constant, K_{-1}, for the reaction system A and the values of K_{-1} are incorporated in Table II. When combined with the measured rate constant, k_1, these data yield the Arrhenius parameters for the back reaction, k_{-1}, the elimination of HI from the iodides. Keeping in mind that all these values are based on few experiments at one temperature only, the values for E_{-1} and log A_{-1}, shown in Table II, are in good agreement with previous results reported in the literature. The log A_{-1} values are reasonable for unimolecular reactions (and are in line with the values for ethyl iodide [13.5],[3a] isopropyl iodide [13.0],[3b] isobutyl iodide [11.6],[3c] etc.). The activation energies for the HI elimination are consistent with the results in the series C_2H_5I (50 kcal), *i*-C_3H_7I (43.5), *t*-BuI (36.4), and *sec*-BuI (37.5).

While the activation energy for removing HI from 4-iodopentene-1 to form 1,4-pentadiene is about the same as for HI elimination from *sec*-butyl iodide, 1,3-pentadiene clearly shows significantly lower activation energies for both addition and elimination reactions. The difference of 11 kcal in E_2 between the nonconjugated 1,4-pentadiene and 1,3-pentadiene is taken up primarily by the extra conjugation energy in 1,3-pentadiene of about 7 kcal. The difference in activation energy of the forward reaction E_1 has to do with the lower barrier for the HI addition to a conjugated double bond as compared to an isolated double bond. In view of the recently proposed[6] detailed reaction mechanism of a four-center addition reaction, controlled by simple electrostatic dipole–dipole interactions, this difference would have to arise essentially from a much more facile polarizability of the conjugated double bond. In their calculation of H_2 addition to cyclopentadiene, Benson and Haugen assumed the longitudinal ground-state polarizability of the

(6) See Table I, footnote *d*.

conjugated bond to be the same as in 2-butene and obtained very good agreement with the observed values. No calculations have been carried out as of today for straight-chain conjugated systems.

A more careful and detailed study would have to give better experimental data for the HI addition to 1,3-pentadiene before any further conclusions can be drawn. There is no doubt, though, that HI adds much faster to the conjugated olefinic bond and we believe that this corresponds to the homogeneous reaction rate. However, more extensive studies are required to be certain of this point.

The Electrical Conductivity of Potassium Chloride in Heavy Water in the −2 to 12° Range

by R. A. Horne and D. S. Johnson

Arthur D. Little, Incorporated, Cambridge, Massachusetts
(Received September 22, 1966)

The structure D_2O is very similar to that of H_2O; however, the hydrogen bond is somewhat stronger in the former medium and, as a consequence, it is somewhat more highly structured.[1-3] This stabilization of the structured regions results in a displacement of the temperature of maximum density from 4 to 11°.[2] In order to determine if this greater structure is reflected in the energetics of transport processes[4] we have measured the temperature dependence of the electrical conductivity of solutions of KCl in D_2O in the −2 to 12° range.

The results of the measurements of equivalent conductances of 0.10 *M* KCl in H_2O and in D_2O and 1.0 *M* KCl in D_2O are shown in Table I. The apparatus and experimental procedures have been described previously;[5,6] however, the capillary cell used, unlike the high-pressure cell earlier described,[6] had widely separated filling and lead arms. General Dynamics Corp. 99.7% D_2O was used.

The present value for 0.10 *M* KCl in H_2O at 0° is in agreement with Jones and Bradshaw.[7] La Mer and Nachod[8] found that a 0.02 *M* KCl solution in H_2O is 1.28 and 1.20 times as conductive as in D_2O at 5 and 25°, respectively, which is to be compared with the present value of 1.21 times for 0.10 *M* KCl at 10°.

The Arrhenius activation energies of electrical conductance of aqueous alkali halide solutions, including sea water, exhibit maxima near the temperature of

Table I: The Equivalent Conductances of Solution of KCl in H_2O and D_2O

Temp, °C	Equiv condct, Λ, $cm^2\ ohm^{-1}\ equiv^{-1}$	Temp, °C	Equiv condct, Λ, $cm^2\ ohm^{-1}\ equiv^{-1}$
0.10 *M* KCl in H_2O			
−1.72 ± 0.06	67.85	+3.81 ± 0.03	79.49
−0.80 ± 0.04	69.79		79.45
+0.01 ± 0.04	71.52	+4.58 ± 0.02	81.06
+0.75 ± 0.05	72.99	+5.52 ± 0.03	83.05
	72.80	+6.41 ± 0.02	85.00
+1.50 ± 0.03	74.58	+7.20 ± 0.02	86.59
+2.29 ± 0.04	76.21	+7.83 ± 0.00	88.07
+3.00 ± 0.03	77.60	+8.39 ± 0.02	89.40
	77.53		
0.10 *M* KCl in D_2O			
−2.00 ± 0.05	54.60	+4.14 ± 0.04	66.09
−0.35 ± 0.04	57.35	+4.93 ± 0.03	67.60
	57.32		67.69
	57.10	+6.00 ± 0.02	69.71
+0.50 ± 0.05	59.09	+6.91 ± 0.03	71.53
	59.00	+7.58 ± 0.04	72.68
+1.00 ± 0.03	59.78	+8.00 ± 0.02	73.02
+1.39 ± 0.04	60.37		73.00
	60.21	+8.32 ± 0.03	74.04
+2.41 ± 0.04	62.53	+9.05 ± 0.02	75.29
	62.42		75.24
	64.44	+9.86 ± 0.03	76.73
+3.30 ± 0.03	64.38	+11.33 ± 0.02	79.50
	64.33		
1.00 *M* KCl in D_2O			
−1.70 ± 0.04	56.96	+5.00 ± 0.05	68.24
−0.81 ± 0.06	58.22		68.17
−0.01 ± 0.04	59.49	+5.73 ± 0.03	69.38
	59.47		69.30
+0.95 ± 0.04	61.00	+6.55 ± 0.04	71.11
+2.50 ± 0.03	63.56	+7.50 ± 0.02	73.02
	63.41	+9.07 ± 0.03	76.23
+3.44 ± 0.04	65.18	+9.89 ± 0.02	77.95
+4.02 ± 0.03	66.64	+11.52 ± 0.03	81.33

(1) J. L. Kavanau, "Water and Solute-Water Interactions," Holden-Day, Inc., San Francisco, Calif., 1964.

(2) I. Kirshenbaum, "Physical Properties and Analysis of Heavy Water," McGraw-Hill Book Co., Inc., New York, N. Y., 1951, pp 12–13.

(3) R. C. Bhandari and M. L. Sisodia, *Indian J. Pure Appl. Phys.*, 2, 266 (1964).

(4) R. A. Horne, R. A. Courant, and D. S. Johnson, *Electrochim. Acta*, 11, 987 (1966).

(5) R. A. Horne and R. A. Courant, *J. Phys. Chem.*, 68, 1258 (1964).

(6) R. A. Horne and G. R. Frysinger, *J. Geophys. Res.*, 68, 1967 (1963).

(7) G. Jones and B. C. Bradshaw, *J. Am. Chem. Soc.*, 55, 1780 (1933).

(8) V. K. La Mer and F. C. Nachod, *J. Chem. Phys.*, 9, 265 (1941).

maximum density.[5,9,10] The maxima occur in the cases of both water structure makers and breakers.[10] The temperatures at which the maxima occur appear to be related to the temperature of maximum density of the solutions and decrease with increasing concentration of electrolyte.[9,10]

The maximum in the activation energy for 0.10 *M* KCl in D_2O, calculated from the results in Table I, is higher (4.6 kcal/mole compared to 4.2 kcal/mole) than in H_2O and is displaced to a somewhat higher temperature (5° compared to 2.5°), as one might expect from the greater structure in D_2O. For 1.0 *M* KCl in D_2O a maximum of 4.2 kcal/mole appears at 3°.

Acknowledgment. This work was supported, in part, by the Office of Naval Research.

(9) R. A. Horne and R. A. Courant, *J. Geophys. Res.*, 69, 1152 (1964).

(10) R. A. Horne and D. S. Johnson, *J. Chem. Phys.*, 45, 21 (1966)

Surface Distortion in Face-Centered Cubic Solids

by J. J. Burton and George Jura

Inorganic Materials Research Division, Lawrence Radiation Laboratory, Department of Chemistry, University of California, Berkeley, California *(Received October 18, 1966)*

Until now, experimental values have not been obtained for the displacement of the surface layers from the bulk of semiinfinite crystals; such information will probably soon be available from low-energy electron diffraction (LEED) studies. It is desirable to have some theoretical estimation of the order of magnitude of the displacements.

Gazis and Wallis[1] have shown that a one-dimensional lattice with nearest and next-nearest neighbor interactions may exhibit a distortion of the lattice spacing at a free surface; the predicted distortion decreases exponentially with distance from the surface.

Shuttleworth[2] has calculated the displacement of the first layer of the (100) surface of argon and Alder, Vaisnys, and Jura[3] have calculated the displacements of the first five layers of the (100) surface of argon. Alder, *et al.*, found that the distortion decreased proportionally to the inverse cube of the distance from the surface.

The values of the coefficients in the Morse potential

$$\phi(r) = D[e^{-2\alpha(r-r_0)} - 2e^{-\alpha(r-r_0)}]$$

have been tabulated by Girifalco and Weizer[4] for six fcc metals, Ca, Ag, Al, Pb, Cu, and Ni (Table I). Girifalco's evaluation of the Morse potential parameters was based on experimental values of the solid inter-

Table I: Parameters of Morse Potential $\phi(r) = D[e^{-2\alpha(r-r_0)} - 2e^{-\alpha(r-r_0)}]$

Metal	α, A^{-1}	r_0, A	D, ev
Pb	1.1836	3.733	0.2348
Ag	1.3690	3.115	0.3323
Ni	1.4199	2.780	0.4205
Cu	1.3588	2.866	0.3429
Al	1.1646	3.253	0.2703
Ca	0.80535	4.569	0.1623

atomic distance, the heat of sublimation, and the solid compressibility. The Morse potentials obtained give good equations of state but poor elastic constants. We have calculated the displacements, δ_i (Figure 1), of the first two surface layers of these metals for the (100), (110), and (111) surfaces. For comparison purposes we have also calculated the same displacements for argon using a Lennard-Jones 6–12 potential.[5]

The expression for the surface energy of the (100) surface with the spacing of the first two planes perpendicular to the surface (z direction) allowed to change by δ_1 and δ_2 and the other planes fixed illustrates the method employed in these calculations, which is that employed by Alder, *et al.* We define $\theta(z + \delta_i)$ by

$$\theta(z + \delta_i) = \sum_{\substack{x,y=-\infty \\ x+y+z=\text{even}}}^{\infty} V(x, y, z + \delta_i)$$

where $V(x, y, z)$ is the potential between an atom at (0, 0, 0) and an atom at (x, y, z). Then the potential energy of an atom in the surface layer is given by

$$E(1) = \theta(0) + \theta(1 + \delta_1) + \sum_{z=2}^{\infty} \theta(z + \delta_1 + \delta_2)$$

with only the first and second layers relaxed. For an atom in the second layer the total energy is

$$E(2) = \theta(0) + \theta(1 + \delta_1) + \sum_{z=1}^{\infty} \theta(z + \delta_2)$$

(1) D. G. Gazis and R. F. Wallis, *Surface Sci.*, 3, 19 (1964).

(2) R. Shuttleworth, *Proc. Roy. Soc.* (London), A62, 167 (1949).

(3) B. J. Alder, J. R. Vaisnys, and G. Jura, *Phys. Chem. Solids*, 11, 182 (1959).

(4) L. A. Girifalco and V. G. Weizer, *Phys. Rev.*, 114, 687 (1959).

(5) T. Kihara, *J. Phys. Soc. Japan*, 3, 265 (1948).

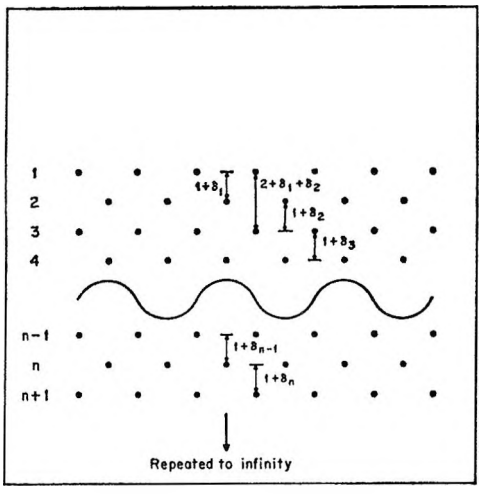

Figure 1. Schematic diagram of a semiinfinite crystal with displacements indicated.

For an atom in the Nth ($N > 2$) layer the total energy is

$$E(N) = \theta(0) + \theta(N - 1 + \delta_1 + \delta_2) + \theta(N - 2 + \delta_2) + \theta(N - 2) + \sum_{i=1}^{\infty} \theta(z)$$

Adding the energies of all of the atoms in all of the layers gives twice the total binding energy of the system

$$-2E_T = \sum_{N=1}^{\infty} E(N)$$

For a perfect infinite crystal the total binding energy, E^{∞}, is given by

$$-2E^{\infty} = \lim_{N \to \infty} 2N[\theta(0) + 2\sum_{z=1}^{\infty} \theta(z)]$$

The surface energy of a crystal is defined as one-half the energy required to split an infinite crystal into two semiinfinite crystals

$$E_s = {}^1/_2(E^{\infty} - 2E_T)$$

$$= {}^1/_2\sum_{z=1}^{\infty} z\theta(z) + \sum_{z=2}^{\infty} [\theta(z) - \theta(z + \delta_1 + \delta_2)] + \sum_{z=1}^{\infty} [\theta(z) - \theta(z + \delta_2)] + [\theta(1) - \theta(1 + \delta_1)]$$

Similar expressions may be developed for more relaxations and other crystal faces.

The surface energy, without allowing for distortion E_0, was calculated for each case considered by direct summation over a lattice of 2000 atoms. The surface energy was then minimized with respect to the displacements, δ_i, by direct summation of the energy over a lattice of 360 atoms on a CDC 6600 computer.

The surface energies without relaxation, E_0, the displacements, δ_i, and the changes in surface energy due to relaxation, ΔE, are tabulated in Tables II, III, and IV for the (100), (110), and (111) surfaces, respectively. This displacements, δ_i, are given in units of percentage of the normal bulk planar spacing and

Table II: The (100) Surface[a]

Solid	δ_1, %	δ_2, %	E_0, ev	ΔE, ev
Ca	12.504	3.587	0.99925	−0.06556
Ag	6.456	1.259	1.30302	−0.03755
Al	10.972	2.963	1.49150	−0.08410
Pb	5.542	0.978	0.85209	−0.02011
Cu	9.669	2.433	1.72345	−0.08319
Ni	9.121	2.232	2.02644	−0.09119
Ar	2.604	0.623	0.039021	−0.000355
Ar[b]	2.577	0.589	0.03951	−0.000349

[a] Relaxations, δ_i, are given as a percentage of the bulk (100) planar spacing; E is the unrelaxed (100) surface energy; ΔE is the change in surface energy due to relaxation. [b] Obtained by Alder, *et al.*[3]

Table III: The (110) Surface[a]

Solid	δ_1, %	δ_2, %	E_0, ev	ΔE, ev
Ca	9.621	2.628	1.45532	−0.08664
Ag	4.783	0.768	1.93619	−0.04494
Al	8.362	2.099	2.18216	−0.10898
Pb	4.075	0.559	1.27073	−0.02347
Cu	7.314	1.671	2.53181	−0.10587
Ni	6.872	1.507	2.98250	−0.11498
Ar	1.809	0.366	0.05779	−0.000394

[a] Relaxations, δ_i, are given as a percentage of the bulk (110) planar spacing; E_0 is the unrelaxed (110) surface energy; ΔE is the change in surface energy due to relaxation.

Table IV: The (111) Surface[a]

Solid	δ_1, %	δ_2, %	E_0, ev	ΔE, ev
Ca	4.297	0.899	0.87518	−0.02558
Ag	1.910	0.225	1.11727	−0.01087
Al	3.667	0.709	1.30167	−0.03111
Pb	1.580	0.159	0.72635	−0.00539
Cu	3.142	0.544	1.49844	−0.02913
Ni	2.927	0.490	1.75856	−0.03114
Ar	0.820	0.190	0.032520	−0.000113

[a] Relaxations, δ_i, are given as a percentage of the bulk (111) planar spacing; E_0 is the unrelaxed (111) surface energy; ΔE is the change in surface energy due to relaxation.

energies are in electron volts per surface atom. The results of Alder, *et al.*, are included in Table II.

The results of Alder, *et al.*,[3] are based on direct summation of the energy over a lattice of roughly 40,000 atoms and integration over the remainder of the lattice; our results are based on only 360 atoms. Comparison of Alder's results with ours shows that this small lattice yields good values of δ_1, δ_2, and ΔE. Alder's work shows that consideration of the relaxation of only two surface layers gives good values of the surface energy. It is not necessary to do calculations on large crystals to get reasonable values of the surface energy and surface distortion for solids with short-range potentials.

For all the materials considered, it was found that the (111) surface was the lowest energy surface and the (110) the highest; distortion was largest for the (100) surface and smallest for the (111) surface. Relaxations were found to alter the surface energy by at most 6% and only slightly affected the ratios of the surface energies of the various faces.

Acknowledgments. We are grateful to J. L. Strudel for suggesting these calculations. This work was done under the auspices of the United States Atomic Energy Commission.

Electron Impact Ionization Potentials of Methyl-Substituted Borazines

by P. M. Kuznesof, F. E. Stafford, and D. F. Shriver

Contribution from the Department of Chemistry and the Materials Research Center, Northwestern University, Evanston, Illinois 60201
(Received November 16, 1966)

There are relatively few quantitative data which are directly related to the electronic structure of borazine and the influence of substituents on this structure. Because of our general interest in this problem,[1] we have determined the ionization potentials of N-trimethylborazine, $(HBNCH_3)_3$, and hexamethylborazine, $(CH_3BNCH_3)_3$. In order to obtain an internally consistent set of data, we have reinvestigated the ionization potentials of borazine, $(HBNH)_3$, and B-trimethylborazine, $(CH_3BNH)_3$.[2]

Experimental Section

Preparations. Hexamethylborazine was prepared according to the method of Smalley and Stafiej;[3] mp 90–92° (lit. 99°). There was no attempt at further purification. The infrared spectrum agreed with the published spectrum.[4] B-Trimethylborazine was prepared according to the method of Haworth and Honstedt;[5] mp 30.0–31.0° (lit. 31.5°).[6] The mass spectrum showed diethyl ether to be a major impurity. N-Trimethylborazine was obtained from the Callery Chemical Co., Callery, Pa. The material was redistilled only once on a high-vacuum line, although repeated fractionation would have yielded a purer product; vapor pressure 20.3 mm at 37.0° (lit. 27 mm[7] and 28 mm[8]). Its infrared spectrum agreed with that given in the literature.[9] The mass spectrum of this sample was scanned from *m/e* 11 to 260. The absence of peaks above the parent ion (*m/e* 123) indicated the lack of volatile high molecular weight impurities. Borazine, previously prepared in this laboratory, was passed through a train of cold traps at −45, −95, and −195°. The material in the −95° trap was used; vapor pressure 84.8 mm at 0° (lit. 84.8 mm).[10] Reagent grade hexamethylbenzene and 1,3,5-trimethylbenzene were used without further purification. The thiophene-free benzene was treated with sulfuric acid, redistilled, and stored over sodium prior to use.

The inlet system consisted of the sample tubes connected through Teflon on glass needle valves (Fischer–Porter Co., Warminster, Pa.) to a glass manifold. The tubes containing liquid or solid samples were immersed in an appropriate constant-temperature bath: −78° for C_6H_6 and $(HBNH)_3$; 0° for $(CH_3BNH)_3$, $(HBNCH_3)_3$, $(CH_3BNCH_3)_3$, and $1,3,5\text{-}(CH_3)_3C_6H_3$; and *ca.* 22° for $C_6(CH_3)_6$. This provided a stable sample pressure in the ion source. The sample vapors were introduced from the manifold through a variable leak directly into the ionization chamber of the mass

(1) Quantitative phenyl substituent effects have been discussed by D. F. Shriver, P. Smith, and D. E. Smith, *J. Am. Chem. Soc.*, 86, 5153 (1964), and D. F. Shriver and P. M. Kuznesof, *Inorg. Chem.*, 4, 434 (1965).

(2) E. D. Loughran, C. I. Mader, and W. E. McQuistion, Los Alamos Scientific Laboratory, Report LA-2368, Jan 14, 1960.

(3) J. H. Smalley and S. F. Stafiej, *J. Am. Chem. Soc.*, 81, 582 (1959).

(4) H. Watanabe, M. Narisada, T. Nakagawa, and M. Kubo, *Spectrochim. Acta*, 16, 78 (1960).

(5) D. F. Haworth and L. F. Honstedt, *J. Am. Chem. Soc.*, 82, 3860 (1960).

(6) H. L. Schlesinger, L. Horvitz, and A. B. Burg, *ibid.*, 58, 409 (1936).

(7) H. L. Schlesinger, D. M. Ritter, and A. B. Burg, *ibid.*, 60, 1296 (1938).

(8) W. V. Hough, G. W. S. Schaeffer, M. Dzurus, and A. C. Steward, *ibid.*, 77, 864 (1955).

(9) R. I. Wagner and J. L. Bradford, *Inorg. Chem.*, 1, 93 (1962).

(10) A. Stock, "Hydrides of Boron and Silicon," Cornell University Press, Ithaca, N. Y., 1957, p 94.

spectrometer.[11] Argon, used for calibrating the ionizing electron voltage scale, was introduced into the ion source chamber through a separate leak.

Ionization efficiency curves were obtained with emission current regulated at 0.30 ma and repeller plates at zero voltage.[12] No source magnet was used. Source temperature was unregulated and estimated to be 150° (contact time with source *ca.* 10^{-2} sec). Typical operating conditions and sensitivity were: ionization chamber sample pressure, 10^{-6} mm; average trap current, 0.3 μa; multiplier gain, 5×10^5. The minimum signal conveniently detectable corresponded to 10^{-18} amp or about 10 ions/sec. The amounts of sample and calibrating gas simultaneously entering the ion source were adjusted to give signals of $\sim 2 \times 10^{-16}$ amp (full-scale deflection of the pen recorder) at electron energies 3.5 ev above the threshold voltage. The electron energy and ion current were displayed on the X and Y axes of an X–Y recorder, so that ionization efficiency curves were recorded directly.[13] Ionization potentials were extracted using the vanishing-current method. In preliminary runs the threshold voltage of hexamethylbenzene was found to decrease with increasing detection sensitivity. Measurements were made at a sensitivity such that no further decrease was observed.

Results

Table I presents the ionization potentials obtained in this laboratory compared with some literature values. It is not uncommon for electron impact determinations of ionization potentials to be as much as 0.5 ev higher than values obtained using photoionization methods. Preliminary measurements showed that the literature values for the ionization potentials of the analogous benzenes could be reproduced (Table I, footnote *e*). The ionization potentials for $(HBNH)_3$ and $(CH_3BNH)_3$ are significantly lower than those reported previously.[2] This discrepancy may be ascribed to the greater sensitivity used here. However, the internal consistency of Loughran, Mader, and McQuistion's data with ours is demonstrated by the difference between the ionization potentials for $(HBNH)_3$ *vs.* $(CH_3BNH)_3$ ($\sim$0.5 ev).[2]

The table shows that methyl substitution lowers the ionization potential of benzene more than that of borazine. It is also clear that methyl substitution on the three nitrogens of borazine has a greater effect than methyl substitution on the borons. Recently, Perkins and Wall have obtained a good agreement with the ultraviolet spectra of methylborazines using Pariser–Parr–Pople type SCF calculations in which they consider the methyl group as a heteroatom which contributes two electrons and one orbital to the π system.[14] The intervals between their calculated highest filled orbital energies are greater than the observed increments in ionization potentials but the calculated order $(HBNH)_3 > (CH_3BNH)_3 > (HBNCH_3)_3$ is correct.[15] Also, simple Hückel treatments based on either a heteroatom model or an inductive model reproduce the observed trends. We are currently investigating inductive as well as conjugative effects using semiempirical SCF procedures.

Table I: Ionization Potentials of Methylborazines

	I.P., ev[a,b]	Lit. I.P., ev[c,e]
$(HBNH)_3$	9.77	10.3 ± 0.1 (EI)[d]
$(CH_3BNH)_3$	9.30	9.8 ± 0.1 (EI)[d]
$(HBNCH_3)_3$	9.07	...
$(CH_3BNCH_3)_3$	8.77	...

[a] This work. [b] Each datum was subjected to the Q test for extraneous results: W. C. Pierce, E. L. Haenisch, and D. J. Sawyer, "Quantitative Analysis," 4th ed, John Wiley and Sons, Inc., New York, N. Y., 1958, p 135. The standard deviations are between 0.03 and 0.06 ev. Experience indicates that the accuracy of the absolute values is probably ±0.2–0.3 ev; the differences in I.P. in homologous series are estimated to be good to ±0.1 ev. [c] EI electron impact. [d] Reference 2. [e] In order to assess the reliability of the borazine values, ionization potentials were obtained for some benzenes and compared with literature values: C_6H_6, obsd 9.55, lit. 9.4–9.9 (several EI values have been reported in this range: R. W. Kiser, Tables of Ionization Potentials, TID-6142 (1960), U. S. Atomic Energy Commission); $1,3,5\text{-}(CH_3)_3C_6H_3$, obsd 8.58, lit. 8.5 ± 0.2 (H. Hartmann and M. B. Svendsen, *Z. Physik. Chem.* (Frankfurt), **11**, 16 (1957)); $C_6(CH_3)_6$, obsd 7.87, lit. 7.85 (photoionization, R. Bralsford, P. V. Harris, and W. C. Price, *Proc. Roy. Soc.* (London), **A258**, 459 (1960)).

Acknowledgments. We thank G. A. Pressley, Jr., for his assistance in the use of the mass spectrometer.

This investigation was supported by the Advanced Research Projects Agency of the Department of Defense through the Northwestern University Materials

(11) Nuclide, Inc., State College, Pa., Model 12-60 HT-8: 60° sector, 12-in. radius magnetic mass analyzer.

(12) Details and the $(HBNCH_3)_3$ mass spectrum appear in the Ph.D. dissertation of Paul M. Kuznesof, Northwestern University, 1967.

(13) R. J. Loyd and F. E. Stafford, Abstracts of Papers presented at the 152nd National Meeting of the American Chemical Society, New York, Sept 1966, p 132; to appear in Advances in Chemistry Series.

(14) P. G. Perkins and D. H. Wall, *J. Chem. Soc.*, 235 (1966).

(15) It is also possible that ionization occurs by loss of a σ electron because Hoffmann's extended Hückel calculations on borazine (R. Hoffmann, *J. Chem. Phys.*, **40**, 2474 (1964)) and our own unpublished SCF calculations for this molecule indicate the highest filled orbital has σ symmetry.

Research Center. The acquisition of the mass spectrometer was made possible by grants from the Materials Research Center, the U. S. Atomic Energy Commission, and Northwestern University. P. M. K. thanks the Public Health Service for a predoctoral fellowship from the National Institute of General Medical Sciences.

The Disproportionation of Hypoiodite

by O. Haimovich and A. Treinin

Department of Physical Chemistry, Hebrew University, Jerusalem, Israel *(Received December 5, 1966)*

The disproportionation of IO^-, as that of other hypohalites, is a second-order process

$$-\frac{d(IO^-)}{dt} = k_a(IO^-)^2$$

with $k_a = 4.0 \times 10^{-2}\ M^{-1}\ sec^{-1}$ at 25° in 4 M alkali solution.[1] The hitherto accepted mechanism[2] involves the rate-determining step

$$IO^- + IO^- \xrightarrow{k_1} IO_2^- + I^- \qquad (1)$$

where k_1 is defined by the relation $-d(IO^-)/dt = 2k_1(IO^-)^2$, followed by the fast reaction

$$\text{mechanism I:}\quad IO_2^- + IO^- \longrightarrow IO_3^- + I^- \qquad (2')$$

However, an alternative fast reaction should be considered

$$\text{mechanism II:}\quad IO_2^- + IO_2^- \xrightarrow{k_2} IO_3^- + IO^- \qquad (2)$$

where k_2 is defined by the relation $d(IO^-)/dt = k_2 \cdot (IO_2^-)^2$. An analogous reaction was proposed for BrO^- as a result of studying its radiation chemistry.[3] Both mechanisms account for the stoichiometry and kinetics of the decomposition. Hence the study of IO^- alone cannot distinguish between them. The ratio k_1/k_a derived by assuming a steady state for IO_2^- is $^1/_3$ and $^2/_3$ for mechanisms I and II, respectively. Here we report how the value of k_1 and thus the mechanism of the disproportionation can be determined. For this purpose the systems IO^-–IO_3^- and IO^-–ClO_3^- were investigated. Some previous results concerning these systems[4] are not reliable, since the solutions were relatively of low alkalinity and high (I^-) and so were chemically ill-defined. This could be shown by measuring the spectra of the solutions. Moreover, the formation of perhalate was overlooked.

Experimental Section

The systems investigated were prepared by rapidly dissolving I_2 in solutions containing 4 M NaOH and various concentrations of halates. The decay of IO^- with time at 25° was followed spectrophotometrically as described elsewhere.[1] The spectrum of IO^- above 300 mμ was found to be hardly affected by the halates. Most results were obtained at 365 mμ, where IO^- has its absorption peak; no variation of rate constant with λ was noticed in the range 300–400 mμ. The sum $(IO^-) + (IO_4^-)$ was measured by titration: a 2-ml sample was introduced into excess of 10^{-2} N arsenite and 4 g of $NaHCO_3$. Then 4 N H_2SO_4 was added with vigorous shaking until pH 8.3 was reached. Excess of KI (~0.2 M) was added and the mixture left in the dark for 1 hr. Under these conditions IO_4^- was found to be quantitatively reduced by I^- to IO_3^-. The excess of arsenite was titrated with 3×10^{-3} N I_2 solution.

Results and Discussion

The disproportionation is retarded by IO_3^- and ClO_3^- (Figure 1). The effect becomes apparent only when the halate concentration exceeds some threshold, above which the change induced is rather abrupt: the rate constant of the reaction, which is still second order, falls down to $(2.6 \pm 0.2) \times 10^{-2}\ M^{-1}\ sec^{-1}$. Further increase of (XO_3^-) has no effect. The threshold rises with an increase of (IO^-). Thus it happens that the disproportionation starts unretarded, but as the ratio $(XO_3^-)/(IO^-)$ increases there is a sudden drop of rate constant. This is clearly shown in curve a where IO_3^- is supplied only by the reaction.

The following results prove that the influence of the halates involves their conversion to perhalates. (a) A solution containing IO^- and excess of IO_3^- was left until effectively all the IO^- was consumed. Some precipitate was formed. It was analyzed by X-ray diffraction and found to consist mainly of $NaIO_4$. The sum $(IO^-) + (IO_4^-)$ was found to remain constant during the reaction (curve d). (b) A similar experiment was carried out with $KClO_3$ and KOH instead of KIO_3 and NaOH, respectively. At the end of the reaction $KClO_4$ was precipitated by acidifying the solution to pH 8 and adding ethanol. It was identified by gravimetric[5] and colorimetric[6] methods. $KClO_4$ (1 mole) was produced for each mole of IO^- consumed.

(1) O. Haimovich and A. Treinin, *Nature*, **207**, 185 (1965).
(2) C. H. Li and C. F. White, *J. Am. Chem. Soc.*, **65**, 335 (1943).
(3) C. H. Cheek and V. J. Linnenbom, *J. Phys. Chem.*, **67**, 1856 (1963).
(4) A. Rashid and E. Ali, *Anal. Chem.*, **36**, 1379 (1964).

Thus with excess of XO_3^- the reaction

$$XO_3^- + IO^- \longrightarrow XO_4^- + I^- \qquad (3)$$

occurs, which is *second* and *zero* order with respect to IO^- and XO_3^-, respectively. This indicates that it is rather a complex process which involves reaction 1 as its primary and slowest step. The subsequent step appears to involve the halate acting as efficient scavenger for IO_2^-

$$XO_3^- + IO_2^- \xrightarrow{k_4} XO_4^- + IO^- \qquad (4)$$

Reactions 1 and 4 constitute a full mechanism for reaction 3 with the rate law

$$-\frac{d(IO^-)}{dt} = k_a'(IO^-)^2 \qquad (5)$$

where $k_a' = k_1$. As further support to this mechanism we found that the activation energy of reaction 3 with ClO_3^- is nearly the same as that of the disproportionation—10 ± 1 kcal/mole. Now, the observed value of $k_a' = 2.6 \times 10^{-2}$ is nearly $^2/_3 k_a$, which proves that the disproportionation proceeds by mechanism II.

The effect of ClO_3^- and IO_3^- was also tested at 6 *M* OH^-, where k_a is lower, and then remains nearly constant up to 10 *M* NaOH.[1] Again it was found that the halates could reduce the rate constant to $^2/_3 k_a$. The effect of (OH^-) is not an ionic strength effect, since the addition of 2 *M* NaCl to 4 *M* NaOH does not affect the kinetics. It may be due to some HIO still present in solution at $(OH^-) \geq 4\ M$. The effect of I^- was also examined: at $(IO^-) \sim 10^{-2}\ M$ and $(I^-) \leq 8 \times 10^{-2}\ M$ no effect could be detected. This result is at variance with the kinetic law proposed by Li and White.[2] On further raising (I^-), k_a increased but the spectrum showed changes indicating the formation of I_3^-.

The general rate law for the IO^-–XO_3^- system derived from eq 1, 2, and 4 is

$$-d(IO^-)/dt = [^3/_2 + \beta - (\beta^2 + \beta)^{1/2}]k_1(IO^-)^2 \qquad (6)$$

where $\beta = k_4^2(8k_2k_1)^{-1}((XO_3^-)/(IO^-))^2$; eq 6 reduces to eq 5 for $(XO_3^-)/(IO^-) \gg k_4^{-1}(8k_2k_1)^{1/2}$. While the proposed mechanism accounts for the effect of the halate being a function of $(XO_3^-)/(IO^-)$, it does not explain the nature of this function. In particular, it appears that as soon as the halate starts to have a distinct effect, it acquires its full effect. Some kind of autocatalysis is probably involved. And indeed we observed that little IO_4^- or ClO_4^- largely enhances the effect of the corresponding halate. This is shown for ClO_4^-–ClO_3^- in Figure 1 (ClO_4^- alone has no effect on the reaction). Moreover, following

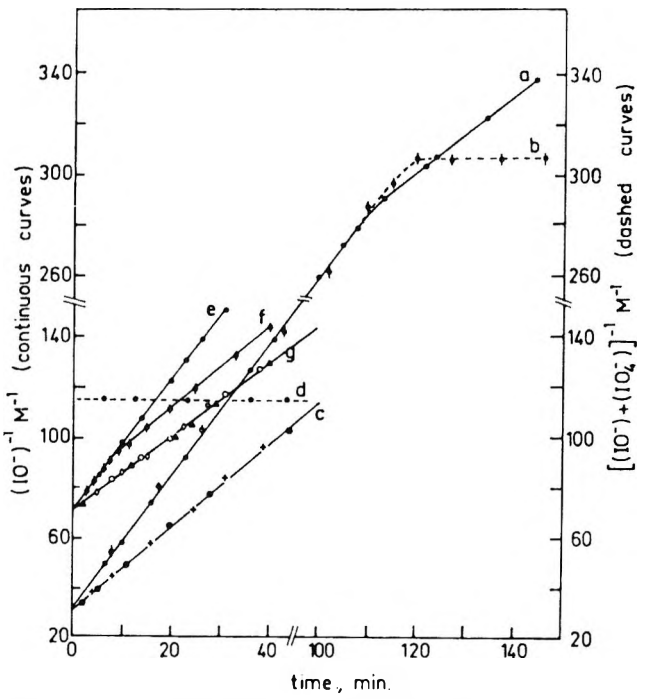

Figure 1. The effect of IO_3^- and ClO_3^- on the disproportionation of IO^-. Curves a and b, no halate initially added; curve c, $4.8 \times 10^{-2}\ M$ (●) and $8.6 \times 10^{-2}\ M$ (+) IO_3^-; curve d, $4.8 \times 10^{-2}\ M$ IO_3^-; curves e and f, $1.2 \times 10^{-2}\ M$ and $2.4 \times 10^{-2}\ M$ ClO_3^-, respectively; curve g, $4.2 \times 10^{-2}\ M$ (○) and $6.1 \times 10^{-2}\ M$ (▲) ClO_3^-, $2.0 \times 10^{-2}\ M$ ClO_3^- + $1.2 \times 10^{-3}\ M$ ClO_4^- (◇). (Continuous and dashed curves are second-order plots for IO^- and IO^- + IO_4^-, respectively.)

the disproportionation of IO^- alone by the arsenite method, we found that the abrupt drop of k_a occurs when IO_4^- could just be detected and from there on the sum (IO^-) + (IO_4^-) remained constant (curves a and b). (Before the drop the arsenite and spectrophotometric methods gave identical results. The same results were also obtained by the acetone method[4] with only a small excess of acetone and properly adjusted pH conditions.) The reason for the activation of halate by perhalate is still obscure. Some complex may be involved which is a very efficient scavenger for IO_2^-.

Finally, it is of interest to note that BrO_3^- has no retarding effect on the disproportionation. This is in accord with the nonexistence of the perbromate ion.

(5) F. P. Treadwell, "Analytical Chemistry," John Wiley and Sons, Inc., New York, N. Y., 1951, p 392.

(6) F. Feigl, "Spot Tests in Inorganic Analysis," Elsevier Publishing Co., Amsterdam, The Netherlands, p 300; L. Ben-Dor and E. Jungreis, *Mikrochim. Acta*, 1, 100 (1964).

Acknowledgment. We are indebted to Dr. I. Mayer from the Department of Inorganic and Analytical Chemistry for carrying out the X-ray analysis.

Small-Angle X-Ray Scattering from a Macroreticular Sulfonic Acid Cation-Exchange Resin—Amberlyst 15[1,2]

by B. Chu[3] and D. M. Tan Creti

Chemistry Department, The University of Kansas, Lawrence, Kansas 66044 *(Received September 30, 1966)*

Small-angle scattering of X-rays has been a rather powerful technique for characterizing the structure of noncrystalline substances. As part of a preliminary program of investigating the inhomogeneities in biological membranes which exhibit pore structures of appropriate dimensions suitable for studies using the small-angle scattering of X-rays, we have examined the angular distribution of the scattered intensity of a resin matrix which has an estimated specific surface area of tens of square meters per cubic centimeter.[4] It should be noted that small-angle scattering of X-rays, being an interference technique, is the only known method capable of directly examining the amorphous structure of substances immersed in a fluid. Such a technique should become a useful tool for studying the pore structures of some of the biological membranes in their natural environment.

Experimental Methods

The Amberlyst 15,[4] supplied in a toluene-saturated form, was converted to the water-saturated form, dried, and sieved. The fraction of resin beads from 0.35 to 0.85 mm in diameter was taken for the experiments. Deionized distilled water and reagent grade solvents were used.

The X-ray sample cell, 0.318 cm thick, had windows of 0.0025-cm thick mica held in place with Dow Corning (Q2-0046) aerospace sealant. A vial containing a small amount of the dry resin was filled with solvent *in vacuo*. Care was taken to avoid possible resin damage due to shock swelling. The solvent-saturated resin and excess solvent were then transferred to the cell with a syringe and needle. X-Ray measurements were performed with a Kratky camera[5] using Cu Kα radiation. The details have been described elsewhere.[6]

The observed scattered intensity was corrected for background scattering by subtracting from the measured intensity the product of the scattering from an empty cell and the sample transmission. The solvent-corrected points refer to those which have taken into account the scattering due to immersion solvents. Infinite slit-length collimation corrections were accomplished with the aid of an IBM 7040 computer.[7]

Results and Discussion

The scattering results have been summarized in Figure 1. Contributions made by scattering from the immersion fluid were estimated to be small except at relatively large angles, as shown by the solvent-corrected points in Figure 1 for Amberlyst 15 immersed in water and in methanol.

The small-angle X-ray scattering technique has been applied to catalysts,[8] porous glasses,[9] and synthetic zeolites.[10] For characterizing ionic species within the resin matrix, measurements in the angular range beyond 0.03 radian are important. There one may consider the ionic species as frozen-in suspensions of strong scatterers within the resin phase and the particle-scattering theory of Guinier[8] becomes appropriate. This part of the scattering curve has been deemphasized in the present investigation. Instead, we are concerned with the scattering at very small angles. As we have limited the macroscopic size of those spherical resin beads to approximately 0.35–0.85 mm in diameter, both the degree of compaction and the macroscopic size of the beads become unimportant. Only inhomogeneities in the resin matrix contribute substantially to the scattering within the angular range of our investigation. Here, the scattered intensity, I, for a random two-phase system may be represented by the relation[9]

$$I = V\langle\eta^2\rangle\int_0^\infty C(r)\frac{\sin ksr}{ksr}\mathrm{d}\tau \qquad (1)$$

where V is the scattering volume, k is $2\pi/\lambda$ with λ the X-ray wavelength, s is 2 sin $(\theta/2)$ with θ the scattering angle between the direction of propagation of the

(1) Courtesy of Rohm and Haas Co., Philadelphia, Pa.

(2) We wish to make acknowledgment to the donors of the Petroleum Research Fund, administered by the American Chemical Society, for partial support of this research.

(3) Alfred P. Sloan Research Fellow.

(4) R. Kunin, E. F. Meitzner, J. A. Oline, S. A. Fisher, and N. Frisch, *Ind. Eng. Chem. Prod. Res. Develop.*, **1**, 140 (1962).

(5) O. Kratky and Z. Skala, *Z. Elektrochem.*, **62**, 73 (1958).

(6) B. Chu, *J. Chem. Phys.*, **42**, 426 (1965).

(7) B. Chu and D. M. Tan Creti, *Acta Cryst.*, **18**, 1083 (1965).

(8) A. Guinier and G. Fournet, "Small-Angle Scattering of X-Rays," John Wiley and Sons, Inc., New York, N. Y., 1955.

(9) P. Debye and H. Brumberger, *J. Phys. Chem.*, **61**, 1623 (1957).

(10) P. A. Howell, *ibid.*, **64**, 364 (1960).

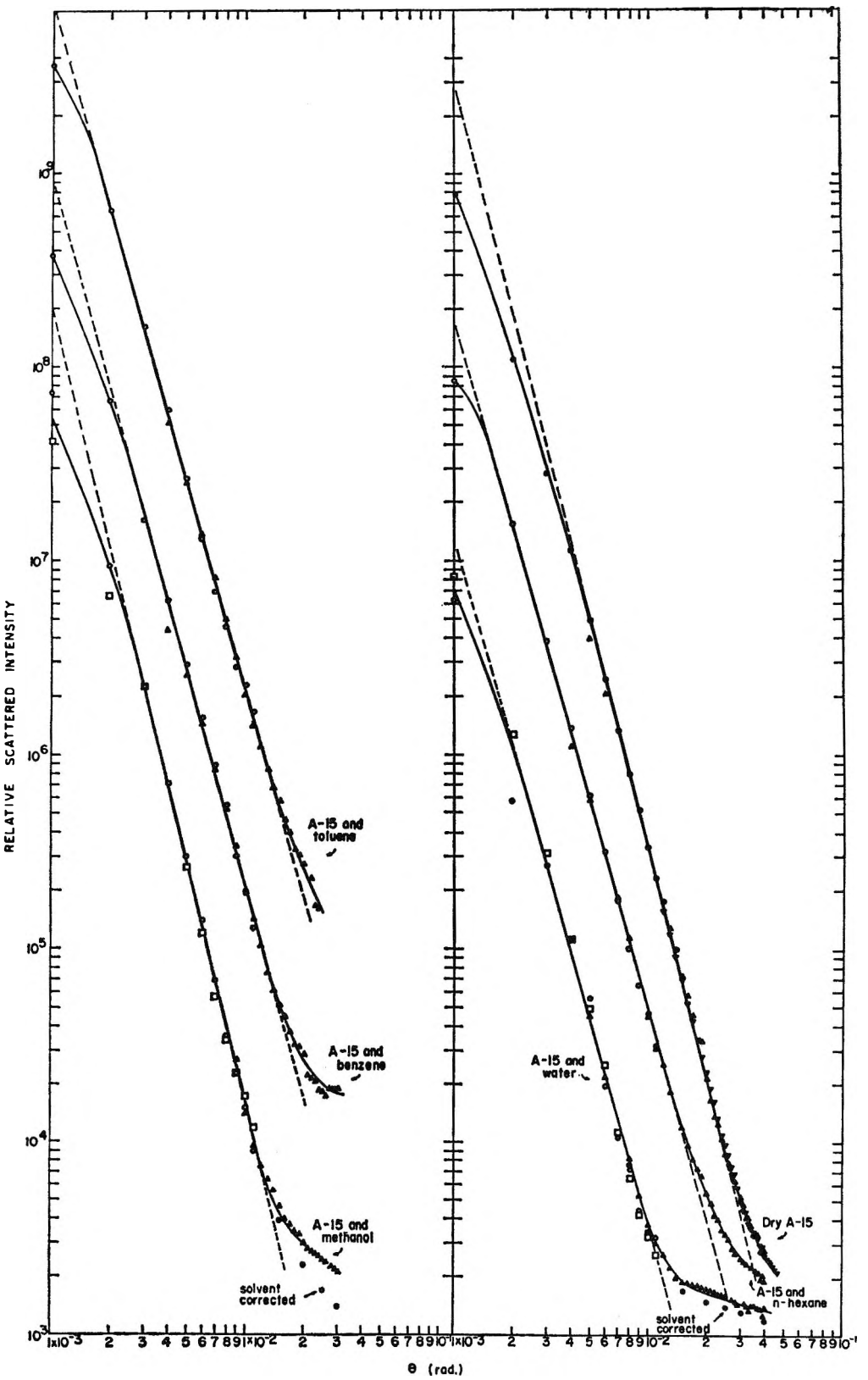

Figure 1. Plot of relative scattered intensity (after background and collimation corrections) *vs.* scattering angle θ.

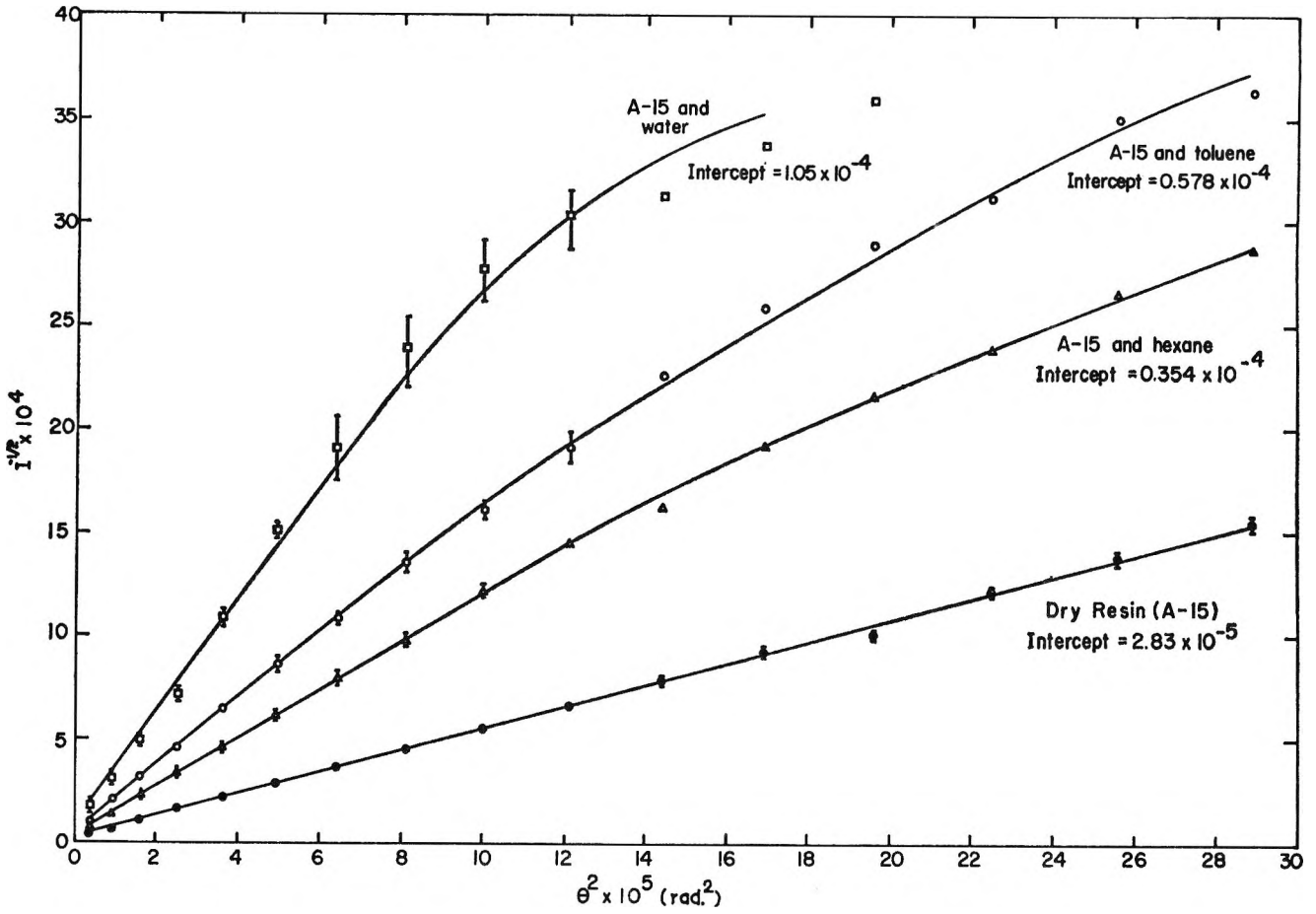

Figure 2. A typical plot of $I^{-1/2}$ *vs.* θ; I = relative scattered intensity after background, collimation, and sample transmission corrections.

Table I: Per Cent of Bulk Swelling and Characteristic Length a for Amberlyst 15 (A-15) Immersed in Various Solvents

System	A-15	A-15 and *n*-hexane	A-15 and toluene	A-15 and benzene	A-15 and methanol	A-15 and H_2O
BS[a]	0	0.026	0.036	0.047	0.455	0.458
a, A	1.3×10^2	1.5×10^2	1.3×10^2	1.4×10^2	(1.8×10^2)[b]	(1.5×10^2)[b]

[a] BS = $(h_{rf} - h_r)/h_r$, where BS is the bulk-swelling ratio and h_{rf} and h_r are, respectively, the apparent volume occupied by the solvent-saturated and the dry resins. [b] As the curvature in plots of $I^{-1/2}$ *vs.* θ^2 increases, the structure can no longer be represented by $C(r) = \exp(-r/a)$. So a for A-15–H_2O and A-15–methanol could be of doubtful value.

incident beam and the direction of observation of the secondary ray, $d\tau$ $(=4\pi r^2 dr)$ is a volume element, r being the distance between pairs of scattering centers A and B, and $C(r)$ is a correlation function, defined by

$$\langle \eta^2 \rangle C(r) = \langle \eta_A \eta_B \rangle \qquad (2)$$

η denoting fluctuations from an average electron density. It has been shown that, for a random distribution of inhomogeneities in the electron density, $C(r) = \exp(-r/a)$, where a is a correlation length characteristic of the substance. If this is so, the angular intensity distribution has the form

$$I = \frac{8\pi a^3 V \langle \eta^2 \rangle}{(1 + k^2 s^2 a^2)^2} \qquad (3)$$

whereby a plot of the reciprocal of the square root of the scattered intensity *vs.* s^2 should give a straight line with

$$a = \frac{1}{k}\left[\frac{\text{slope}}{\text{intercept}}\right]^{1/2} \qquad (4)$$

The dry Amberlyst 15 yields such a straight line over about a 20-fold angular change from 1.0×10^{-3} to 2.5×10^{-2} radian, as shown partially in Figure 2. Thus we have found, for the first time, a synthetic porous medium which has a truly random structure and obeys the correlation function $C(r) = \exp(-r/a)$. Estimates on a range around 1.3–1.5 $\times 10^2$ A, as shown in Table I. The extrapolated zero-angle scattered intensities were obtained from a plot of log I *vs.* θ^2. In order to test the reliability of a, we have also calculated the specific surface area, S_{sp}, from the expression

$$S_{sp} = \frac{-4\phi(1 - \phi)C'(0)}{\rho_b} \qquad (5)$$

where ϕ is the void fraction (porosity), $C'(0)$ is the derivative of the correlation function at $r = 0$, and ρ_b and ρ_s are, respectively, the bulk and the structural densities. With $\rho_b = 1.012$ g/cc and $\rho_s = 1.513$ g/cc, $\phi = 1 - (\rho_b/\rho_s) = 1 - (1.012/1.513) = 0.331$. If we take $a = 1.3 \times 10^2$ A, S_{sp} becomes about 69 m^2/g for the dry Amberlyst 15, which compares favorably with Kunin's BET value of 42.5 m^2/g in view of the difficulties encountered in obtaining the extrapolated zero-angle intensity.

In the case of immersed resins, we see that deviations in the linear behavior at relatively large scattering angles from a plot of $I^{-1/2}$ *vs.* θ^2 increase with increasing bulk-swelling ratio. We could propose three possible reasons for the curvatures in Figure 2: (1) inadequate solvent correction, (2) unfilled small holes, and (3) distortion of the resin matrix due to swelling.

It is apparent that the linear behavior for all the immersed resins would persist over a larger angular range than shown in Figure 2 if the background corrections were made to include the scattering due to solvents. This was demonstrated in Figure 1 for Amberlyst 15 immersed in water and in methanol. However, deviations from the linear behavior could not be accounted for in terms of only solvent corrections.

If a three-phase (resin–solvent–unfilled pores) system exists, then the calculated correlation length a would be of doubtful value except for the dry resin. On the other hand, a closer examination suggests that the amount of unfilled pores must be small or nonexistent, because the immersed resin (A-15 in *n*-hexane) shows a linear behavior in Figure 2 over an angular range from about 1×10^{-3} to 1×10^{-2} radian while deviations appear only in the larger angular range where the background corrections using an empty cell become inappropriate. The unfilled pores should contribute to relatively stronger scattering in the X-ray intensity because of larger electron density differences between holes and material. A distortion on the shape of the scattering curve is therefore to be expected. The absence of such a distortion for systems without appreciable swelling (A-15 in *n*-hexane) seems to confirm our conjecture that most of the pores are accessible by the solvent. Figure 1 appropriately illustrates the similarities of all the scattering curves. The linear dotted lines are for easier comparison of the scattering curves between the different systems. The solvent-saturated resins have tendencies to retain a random distribution of the form $C(r) = \exp(-r/a)$. We attribute the deviations from eq 3 in the larger angular range to the presence of distorted small inhomogeneities for the immersed Amberlyst 15 and not to unfilled holes. Such distortions from random distribution would therefore increase with increasing bulk-swelling ratio from *n*-hexane to water as shown in Figure 2. In summary, the small-angle scattering of X-rays has been observed for a macroreticular ion-exchange resin. The scattering data show that the resin matrix has a random distribution of inhomogeneities (or pores) with the correlation function $C(r) = \exp(-r/a)$ and a correlation length a of about 1.4×10^2 A. Most of the pores are accessible. Deviation away from random distribution of inhomogeneities (or pores) is appreciable whenever the bulk-swelling ratio becomes large. The distortion due to the presence of polar solvents, such as water and methanol, contributes more to the smaller holes as shown by deviations only in the larger angular range.

Dispersion Energies and Surface Tensions of Noble Metals

by Edmund Thelen

Chemistry Division, The Franklin Institute Laboratories, Philadelphia, Pennsylvania 19103 *(Received December 19, 1966)*

Erb[1] measured the contact angles of water drops on solid noble metal plates after 3650 hr of continual condensation of pure water. On his materials, no organic contamination was present and the vapor phase was virtually free of noncondensable gases. While his contact angles were measured at near the boiling point of water, according to Adam[2] they would not be significantly different at room temperature. Also as

(1) R. A. Erb, *J. Phys. Chem.*, 69, 1307 (1965).

(2) N. K. Adam, Advances in Chemistry Series, No. 43, American Chemical Society, Washington, D. C., 1964, Chapter 2.

Table I: Dispersion and Surface Energies of Noble Metals

	Ag	Au	Pd	Pt
Contact angle of water, θ	79.5	65.5	62.5	40.0
Dispersion energy, ergs/cm^2, γ_3^d	84.95	121.63	129.86	189.56
Energy of vaporization, kcal, ΔE_v	67.4	88.8	92.7	136.9
Atomic volume, cm^3, V	10.3	10.2	8.9	9.1
Atomic radius, A, R	1.44	1.44	1.37	1.38
Free surface energy, ergs/cm^2, γ_3	1195	1629	1871	2776
$\gamma_3^d/V^{1/3}$, ergs/cm^3	39.04	56.08	62.67	90.79
$\Delta E_v/V$, cal/cm^3	6544	8706	10416	15044

suggested by Adam, we averaged the advancing and receding angles for each metal, obtaining values from 40 to 79.5°.

Most metals have oxide coatings, and water spreads on them. The noble metals, under Erb's continuous condensation process, are continually washed, and from their apparent hydrophobicity, as shown by Erb's measurements, must be substantially free of oxide. Only the dispersion energies of the oxide-free metal surfaces can interact with water, and according to Fowkes[3]

$$\gamma_2 (1 + \cos\theta) = 2\sqrt{\gamma_2^d \gamma_3^d} \qquad (1)$$

if the spreading pressure is zero. For water at 20°, γ_2 is 72.8 ergs/cm^2 and γ_2^d, according to Fowkes, 21.8 ergs/cm^2.

Under the conditions of condensation of water from vapor, the spreading pressure would be significant if a monolayer or more of water molecules existed on the surface between the drops. Erb[4] shows, however, that drops form only at specific nucleating spots, especially under his conditions of a low supersaturation ratio ($p/p_0 < 1.13$); between these spots drops do not form. If vapor would condense in those areas, there would be a likelihood of drop formation in them; such is not the case. Furthermore, as Table I shows, γ_s^d for Ag as calculated by eq 1 is 84.95 ergs/cm^2. This compares with Fowkes' values[3] from heat of emersion data of 76 ergs/cm^2.

Erb's value for θ of water on Au of 65.5° compares with White's value[5] of 60 ± 5°.

Fowkes[6] discusses the calculation of γ_s^d from A_{12} values. From Reerink's[7] experimentally determined value for A_{12} of gold (1 to 6 × 10^{-13}), Fowkes calculates γ_s^d of 60 to 120 ergs/cm^2. This compares with the value in Table I of 121.6.

Relationships between surface energies and cohesive energy densities have been found by Hildebrand[8] and others for organic materials. We find that the dispersion energies of the noble metals, calculated from

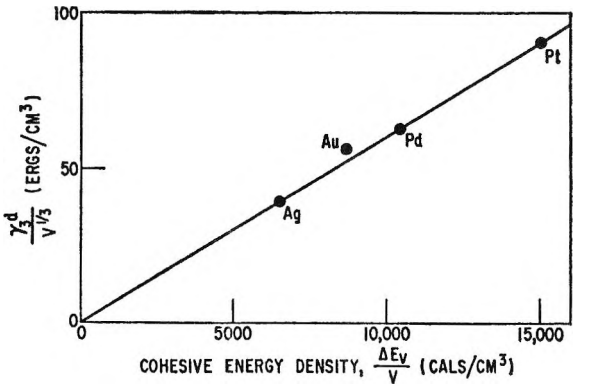

Figure 1.

contact angles with water, correlate with cohesive energy densities (Figure 1)

$$\text{cohesive energy density } \frac{\Delta E_v}{V} = \frac{166.7\gamma_3^d}{V^{1/3}} \qquad (2)$$

where ΔE_v is the energy of vaporization of a gram-atom in calories, V is the gram-atom volume in cubic centimeters, and γ_3^d is the surface dispersion energy and is in ergs per square centimeter. The ΔE_v values were calculated from Kelley's[9] recent data ($\Delta E = \Delta H - RT$).

Cottrell[10] offers an approximate equation for cal-

(3) F. M. Fowkes, Advances in Chemistry Series, No. 43, American Chemical Society, Washington, D. C., 1964, Chapter 6.

(4) R. A. Erb, Ph.D. Dissertation, Temple University, May 1965; University Microfilms No. 66-1403 (Ann Arbor, Mich.).

(5) M. L. White and J. Drobek, *J. Phys. Chem.*, **70**, 3432 (1966).

(6) F. M. Fowkes, *Ind. Eng. Chem.*, **56**, No. 12, 40 (1964).

(7) H. Reerink and J. Th. G. Overbeek, *Discussions Faraday Soc.*, **18**, 74 (1954).

(8) J. H. Hildebrand and R. L. Scott, "The Solubility of Nonelectrolytes," 3rd ed, Reinhold Publishing Corp., New York, N. Y., 1950.

(9) K. K. Kelley, U. S. Bureau of Mines Bulletin No. 584, U. S. Government Printing Office, Washington, D. C., 1960.

(10) A. H. Cottrell, "The Mechanical Properties of Matter," John Wiley and Sons, Inc., New York, N. Y., 1964, p 231.

culating total surface tensions from $\Delta E_v/V$, the cohesive energy density, and atomic radius (r) in angstroms

$$\gamma_S = \frac{r\Delta E_v}{3V} - TS \qquad (3)$$

The entropy of the surface (S) is taken by Cottrell as 0.4 erg/cm² °K, permitting γ_s values to be calculated as listed in Table I. These quantities cannot be confirmed by direct measurement, but are similar in magnitude to γ_s values quoted by Ehrlich,[11] from high-temperature measurements and corrected, through the entropy terms (TS), to 298°K.

Combining eq 2 and 3

$$\gamma = \frac{23.29\gamma_3^{d}r}{V^{1/3}} - TS = 15.29\gamma_3^{d} - 119 \qquad (4)$$

In conclusion, the dispersion energies calculated by Fowkes' method from the contact angles of water on noble metals are found to relate meaningfully to both the energies of vaporization of the noble metals and to their total surface tensions.

Acknowledgment. This work was supported in part by the Office of Saline Water, U. S. Department of the Interior, under Contract No. 14-01-0001-293. The thoughtful interest of Mr. E. A. Cadwallader of the Office of Saline Water and Dr. Robert A. Erb of The Franklin Institute Laboratories is acknowledged with appreciation.

(11) G. Ehrlich, "Metal Surfaces: Structure, Energetics and Kinetics," American Society for Metals, Metals Park, Ohio, 1963, Chapter 7.

A Nuclear Magnetic Resonance Solvent-Exchange Study of N,N-Dimethylformamide Complexes with Aluminum Chloride, Bromide, and Iodide

by Anthony Fratiello and Ronald Schuster

Department of Chemistry, California State College at Los Angeles, Los Angeles, California 90032 *(Received October 19, 1966)*

The technique of nuclear magnetic resonance (nmr) has been applied recently to kinetic studies of a variety of complexes in an attempt to determine rate constants, activation energies, and mechanisms for the solvent-exchange processes.[1-6] The nmr method is based on the fact that in certain cases, separate resonance signals can be observed for bulk and complexed solvent molecules.[1-8] When this occurs, the lifetime, τ, of a solvent molecule in either the bulk or complexed environment may be expressed as $1/\tau = (1/T_2') - (1/T_2)$, where the transverse relaxation time of a molecule is represented by T_2' when exchange is occurring and T_2 when exchange is negligible. Since $T_2 = 1/\pi\delta$, where δ is the resonance signal line width at half-height, τ values may be estimated from line-width measurements. For the solvent-exchange process, the first-order rate constant, k, may then be calculated at a particular temperature using the relationship $k = 1/\tau = \pi(\delta - \delta_0)$, where δ and δ_0 represent the line width in the presence and absence of exchange, respectively. In this study, T_2 was evaluated from the peak height, a quantity proportional to $2/\pi\delta$, rather than peak width. This choice was based on a greater reproducibility of the peak-height measurements.

The complexes to be described are those of N,N-dimethylformamide (DMF) with $AlCl_3$, $AlBr_3$, and

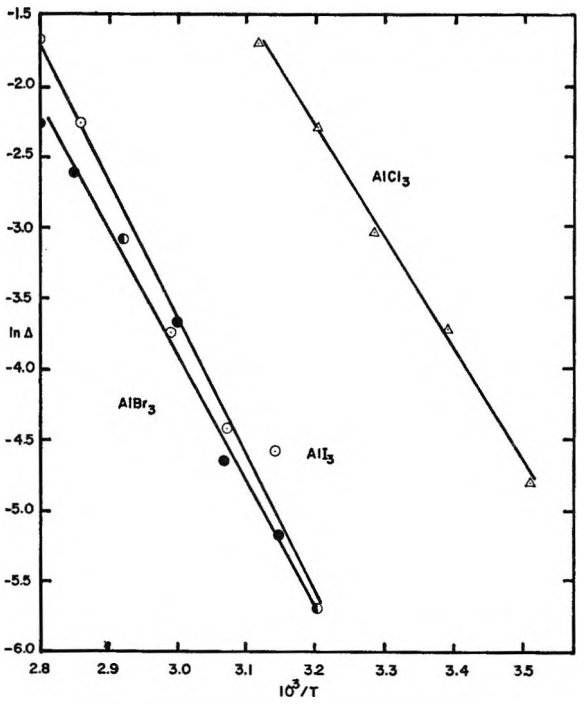

Figure 1. Typical plots of ln $(1/g - 1/g_0)$ as a function of $1/T$ for complexes of DMF with $AlCl_3$, $AlBr_3$, and AlI_3.

(1) A. Jackson, J. Lemons, and H. Taube, *J. Chem. Phys.*, **33**, 553 (1960).
(2) R. E. Connick and D. N. Fiat, *ibid.*, **39**, 1349 (1963).
(3) Z. Luz and S. Meiboom, *ibid.*, **40**, 1058, 1066 (1964).
(4) S. Thomas and W. L. Reynolds, *ibid.*, **44**, 3148 (1966).
(5) N. A. Matwiyoff, *Inorg. Chem.*, **5**, 788 (1966).
(6) A. Fratiello, D. P. Miller, and R. Schuster, *Mol. Phys*, in press.
(7) J. H. Swinehart and H. Taube, *J. Chem. Phys.*, **37**, 1579 (1962).
(8) A. Fratiello and D. P. Miller, *Mol. Phys.*, **11**, 37 (1966).

AlI_3. All salts were sublimed and samples prepared *in vacuo*. Although the exact composition of the complex in solution is unknown, it was determined, by direct integration, that the average number of DMF molecules coordinated per molecule of salt was about 5.7 ± 0.3 in each case. All measurements were made using a Varian A60 spectrometer equipped with a variable temperature accessory. The resonance signal studied as a function of temperature was that due to the formyl proton of the complexed DMF. The measurements were reversible, that is, the signal due to complexed DMF was reproducible at lower temperatures, after high-temperature studies were completed. The rate data are listed in Table I, where the symbol g represents the peak height and δ_0, the signal line width at an experimentally determined temperature corresponding to negligible exchange. The activation enthalpies, $\Delta H^{\ddagger}$, for the exchange process were calculated from ln k *vs.* $1/T$ plots such as those shown in Figure 1. For convenience, the logarithm of the difference between reciprocal peak heights, corresponding to a particular temperature, and the lowest temperature recorded in Table I for each system is plotted in the figure. This difference is proportional to the rate constant. For each system, no further peak-height change was noted at temperatures lower than those recorded in Table I.

Table I: Solvent-Exchange Rate Data for $AlCl_3$, $AlBr_3$, and AlI_3 Complexes with N,N-Dimethylformamide. The Data are Derived from the Formyl Proton Signal of Coordinated DMF

Compound	T, °K	g, cm	δ_0, cps	k, sec^{-1}	$\Delta H^{\ddagger}$, kcal
0.20 *M* $AlCl_3$	272	16.6	6.25		15.2
	281	14.7		2.51	
	294	11.5		8.70	
	302	9.7		13.9	
	307	8.7		17.8	
	314	5.3		41.9	
	321	3.2		83.8	
0.20 *M* $AlCl_3$	272	17.1	6.83		15.4
	285	14.5		3.81	
	295	12.1		8.82	
	305	9.4		17.7	
	312	6.2		37.6	
	321	3.8		76.3	
0.26 *M* $AlBr_3$	293	14.8	6.19		15.7
	314	13.6		1.90	
	325	12.2		4.23	
	332	10.5		8.04	
	339	8.9		13.0	
	345	7.0		21.8	
	350	7.2		20.7	
	354	5.2		36.5	
	359	4.8		40.8	
0.26 *M* $AlBr_3$	291	18.1	6.89		17.6
	312	17.0		1.25	
	318	16.4		2.22	
	326	15.4		3.82	
	334	12.3		10.1	
	343	9.9		18.0	
	351	7.7		29.2	
	357	6.3		40.4	
	362	4.6		63.0	
0.20 *M* AlI_3	293	15.7	6.38		16.5
	314	14.1		2.20	
	325	12.2		5.62	
	332	11.0		8.38	
	339	9.0		14.9	
	345	7.7		20.7	
	350	5.6		36.2	
0.20 *M* AlI_3	291	17.7	6.83		18.7
	312	16.7		1.24	
	318	14.9		3.91	
	326	14.5		4.59	
	334	12.4		9.14	
	343	9.7		17.6	
	351	6.1		40.5	
	357	4.1		70.2	

For the DMF complexes of $AlCl_3$, $AlBr_3$, and AlI_3, the activation enthalpies for solvent exchange are 15.3, 16.6, and 17.6 kcal, respectively. Since the measurements are precise to about 10%, one cannot conclusively state that the slight trend observed is real. Although not listed in the table the separation of the aldehydic proton resonance signals between bulk and complexed DMF are 53, 41, and 30 cps, respectively, for the $AlCl_3$, $AlBr_3$, and AlI_3 systems. The bulk DMF signals were not displaced by addition of salt, as indicated by internal TMS. Since many factors contribute to the chemical shift of a proton, a correlation of this signal separation and the strength of the complex may not be valid. However, if such a correlation does exist,[9-12] the $AlCl_3$ complex would be the strongest in this series and the AlI_3 complex the weakest. The $\Delta H^{\ddagger}$ values might then imply that the rate-determining step of the solvent exchange does not involve primarily the breaking of the Al(III)–DMF linkage in the complex. Rather, the ease with which a solvent molecule migrates from bulk solvent into the coordination shell of the central ion may be rate determining.

(9) T. D. Coyle and F. G A. Stone, *J. Am. Chem. Soc.*, **83**, 4138 (1961).

(10) R. A. Craig and R. E. Richards, *Trans. Faraday Soc.*, **59**, 1972 (1963).

(11) J. M. Miller and M. Onyszchuk, *Can. J. Chem.*, **42**, 1518 (1964).

(12) A. Fratiello, R. Schuster, and D. P. Miller, *Mol. Phys.*, **11**, 597 (1966).

To further elucidate the exchange mechanism, these DMF complexes are being studied in other solvents. Also complexes of these halides with other solvents are being investigated.

Acknowledgments. This research was supported in part by a grant from the National Institutes of Health.

Comparison of Hydrogen and Deuterium Solubility in Palladium-Rich Alloys. Gold-Palladium

by Arnulf Maeland and Ted B. Flanagan

Department of Chemistry, University of Vermont, Burlington, Vermont 05401 *(Received November 7, 1966)*

Recently, large differences in equilibrium isotopic solubilities were observed for hydrogen and deuterium in certain platinum–palladium alloys (25°, 1 atm of H_2 (or D_2)).[1,2] (It must be emphasized that these solubilities refer to the individual solubility of either pure hydrogen or pure deuterium in the alloy and not to their isotopic mixtures.[3]) These differences in isotopic solubility in certain platinum–palladium alloys result from the following empirical considerations. In platinum–palladium alloys, large solubility of hydrogen near room temperature obtains only if the second, β, phase is formed because the hydrogen content at the maximum α-phase boundary is small.[2] The heat of the reaction corresponding to absorption of hydrogen (1 atm) into the two-phase region becomes less exothermic as the platinum content of the alloy increases. The corresponding value of ΔS becomes somewhat less negative as the platinum content increases. At certain platinum contents, the value of ΔG becomes zero for the formation of the second phase and the hydrogen solubility is consequently small. The corresponding value of the heat of absorption of deuterium in the two-phase region of these same alloys is approximately 700 cal/mole of D_2 less exothermic than for the hydrogen. The magnitude of ΔS and its changes with added platinum metal are comparable to the values obtained for hydrogen. These considerations mean that there is a range of platinum contents, *e.g.*, ~9 to 11 atomic % (25°, 1 atm), where the free-energy change is negative for the formation of the β phase in the hydrogen system and zero or positive in the deuterium system.

By contrast, in the gold–palladium system, absorption of hydrogen (1 atm) into the two-phase region is characterized by an increase of exothermicity with added gold content. Since the accompanying change in entropy alters only slightly with gold content, the free energy for the formation of the second phase becomes increasingly negative with added gold. Reasoning from the arguments presented for the platinum–palladium system, a large difference in the solubilities of hydrogen and deuterium in certain gold–palladium alloys should not be expected, at least for those alloys which form two phases. The purpose of this note is to examine the absorption of deuterium by a series of gold–palladium alloys experimentally.

The experimental setup was identical with that previously employed.[4] Approximately 0.02 *N* DCl solutions were employed for the electrolyte through which deuterium gas was bubbled after having been purified by passing through a silver–palladium membrane. In some cases hydrogen–helium mixtures were employed to decrease the rate of the absorption reaction. The course of the absorption was followed by changes in the electrode potential of the specimen with respect to an Ag–AgCl reference electrode. The activity of the solution was determined by measuring the electrode potential of the Ag–AgCl electrode *vs.* a Pt–D_2 (1 atm) electrode in the same solution. The measured electrode potentials were corrected for the vapor pressure of D_2O which tended to reduce the deuterium pressure to values slightly below 1 atm.

Results and Discussion

Typical absorption data for deuterium, *e.g.*, plots of electrode potential *vs.* time where time can be taken as directly proportional to D/M, are similar to data obtained for hydrogen[4] except that the two-phase electrode potential is considerably reduced for deuterium as compared to hydrogen. When the specimen reaches an equilibrium deuterium content (1 atm of D_2, 25°) the electrode potential is zero with respect to the D_2 (1 atm)–Pt electrode. The equilibrium deuterium contents as determined by vacuum degassing are shown in Table I as compared to corresponding values for hydrogen.

It may be seen from Table I that there is very little difference in the equilibrium solubilities of the two isotopes even for alloys which do not form two phases, *i.e.*, Au $\geq$ 17 atomic %. This behavior is in marked contrast to the behavior of platinum–palladium alloys.

Several X-ray powder patterns were taken in the two-

(1) T. B. Flanagan, *J. Phys. Chem.*, **67**, 203 (1963).
(2) A. Maeland and T. B. Flanagan, *ibid.*, **68**, 1419 (1964).
(3) F. Botter, *ibid.*, **69**, 2487 (1965).
(4) A. Maeland and T. B. Flanagan, *ibid.*, **69**, 3575 (1965).

Table I: Equilibrium Solubilities (750 ± 10 mm, D_2 (H_2), 25°)

Atomic % Au	H/M	D/M
0	0.69[a]	0.65[a]
8.70	0.48[4]	0.49[b]
18.80	0.33[4]	0.32[b]
26.48	0.23[4]	0.22[b]
44.76	0.10[4]	0.08[b]
55.77	0.035[4]	0.024[b]
68.84	0[4]	0[b]

[a] T. B. Flanagan, *J. Phys. Chem.*, **65**, 280 (1961). [b] This work.

phase region of the D–Au–Pd system. The fcc lattice showed the presence of two phases and the lattice constants of α_{max} and β_{min} were very similar (±0.004 A) to those observed for the corresponding alloys containing hydrogen. This suggests that the compositions of α_{max} and β_{min} are comparable for the H–Au–Pd and D–Au–Pd alloys.

Thermodynamic quantities corresponding to the reaction

$$^1/_2D_2(1\text{ atm}) + xD_{\alpha_{max}}:y\text{Au}:z\text{Pd} \longrightarrow x'D_{\beta_{min}}:y\text{Au}:z\text{Pd}$$

where x and x' represent the number of D atoms characteristic of α_{max} and β_{min}, respectively, and y and z represent the number of atoms of Au and Pd in the alloy under consideration, were determined from the value of the two-phase electrode potential and its variation with temperature.[4,5] The two-phase potentials were very reproducible and stable, *i.e.*, 0.05 mv. Results for the values of ΔG, ΔS, and ΔH are shown in Table II. (These thermodynamic values refer unambiguously to the reaction given above; these quantities will henceforth not be referred to as standard values since the standard state of the H (or D) containing solid phase in analogous systems has been defined differently elsewhere.[6,7] These are not differential values since they represent a discontinuous change in the H (or D) content in going from the α phase to the β phase.)

Table II: Thermodynamic Parameters of the D–Au–Pd and H–Au–Pd Systems in the Two-Phase Region (25°, 1 atm)

Isotope	Atomic % Au	$-\Delta G$, cal/mole of D_2 (H_2)	$-\Delta S$, eu	$-\Delta H$, cal/mole of D_2 (H_2)	Ref
H_2	5.66	2464	23.6	9503	4
D_2	5.66	1513	24.2	8744	This work
H_2	8.70	2496	23.9	9634	4
D_2	8.70	1541	24.7	8896	This work
H_2	11.90	2565	24.4	9832	4
D_2	11.90	1601	25.5	9214	This work
H_2	15.26	2644	24.1	9852	4
D_2	15.26	1679	...	...	This work

It is seen from Table II that the free-energy and enthalpy changes corresponding to absorption in the two-phase region become more negative with increase of gold content for both hydrogen and deuterium.

There has been a great deal of interest recently in the absorption characteristics of hydrogen by palladium-rich alloys. From the data now available, these alloys can be grouped into two broad classes. Group I alloys (I = increase) will be designated as those in which the free energy for absorption into the two-phase region becomes more negative as the added metal content of the alloy is increased. Group I includes to date silver–palladium,[7,8] gold–palladium,[4] tin–palladium,[9] and lead–palladium.[9] The other group will be designated as group D alloys (D = decrease) and these are characterized by the opposite behavior; *i.e.*, the negative free energy decreases with added metal content. Group D includes: platinum–palladium,[10] rhodium–palladium,[11] nickel–palladium,[11,12] iridium–palladium,[13] and copper–palladium.[14] It can be predicted that for Group I alloys there will be no significant difference in the isotopic solubilities of pure hydrogen and pure deuterium. The absence of a marked difference between the solubilities of deuterium and hydrogen in gold–palladium alloys which do not form two phases (atomic % Au ≥ 17) suggests that the free energy for absorption increases with gold content for these alloys too, although in this work only thermodynamic parameters for the two-phase formation were

(5) R. J. Ratchford and G. W. Castellan, *J. Phys. Chem.*, **62**, 1123 (1958).

(6) E. Wicke and G. H. Nernst, *Z. Elektrochem.*, **68**, 224 (1964).

(7) H. Brodowsky and E. Poeschel, *Z. Physik. Chem.* (Frankfurt), **44**, 143 (1965).

(8) (a) F. A. Lewis and W. H. Schurter, *Naturwissenschaften*, **47**, 1477 (1960); (b) A. C. Makrides, *J. Phys. Chem.*, **68**, 2160 (1964); (c) Z. L. Vert and I. Tverdovski, *Russ. J. Phys. Chem.*, **28**, 317 (1954).

(9) H. Brodowsky and H. Husemann, *Ber. Bunsenges.*, **70**, 626 (1966).

(10) A. Carson, T. Flanagan, and F. Lewis, *Trans. Faraday Soc.*, **56**, 1311, 1324 (1960).

(11) (a) J. Barton, J. Green, and F. Lewis, *ibid.*, **62**, 960 (1966); (b) I. P. Tverdovski and A. I. Stetsenko, *Dokl. Akad. Nauk SSSR*, **84**, 997 (1952).

(12) I. P. Tverdovski and Z. L. Vert, *ibid.*, **88**, 305 (1953).

(13) M. LaPrade and T. B. Flanagan, to be published.

(14) (a) R. Karpova and I. Tverdovski, *Zh. Fiz. Khim.*, **33**, 1393 (1959); (b) D. Chisdes and T. Flanagan, unpublished results.

measured. For group D alloys there may be anticipated to be large differences in the solubilities at certain added metal contents. These predictions have been verified for only two alloy systems: the platinum–palladium[2] and the gold–palladium (ref 4 and this work).

Acknowledgments. This research was supported by the U. S. Atomic Energy Commission. The authors are most appreciative of this financial support. The authors are also indebted to Engelhard Industries, Inc., for the gold–palladium alloys used in this research.

Reactions of Diatomic Molecules. IV. Kinetics of Formation of Bromine Chloride

by Peter R. Walton and Richard M. Noyes

Department of Chemistry, University of Oregon, Eugene, Oregon 97403 *(Received December 5, 1966)*

Calculations described elsewhere[1] predict that all reactions of halogens with halogens will proceed by bimolecular mechanisms. For the formation of BrCl from the elements, the predicted activation energy is about 13 kcal/mole.

Previous studies of this reaction are mostly qualitative. Jost[2] and Brauer and Victor[3] found rapid reaction in gas phase, and Jost[2] even estimated an activation energy of 14 kcal/mole. These studies did not demonstrate homogeneity of the reaction, and surface effects are obviously hard to eliminate.

Although reactions in solution are more easily shown to be homogeneous, "inertness" of solvent can never be demonstrated unequivocally. Barratt and Stein[4] observed the reaction to be "instantaneous" in ether and chloroform but to have a time lag of several seconds in carbon tetrachloride. Dennis Forbess at the University of Oregon also observed a measurable rate in this solvent, but he could not get reproducible results. Our own qualitative observations indicated that the rate in carbon tetrachloride was strongly accelerated by traces of moisture as reported by Hildebrand[5] for the formation of ICl in this solvent.

This sensitivity to moisture suggested the use of pure sulfuric acid as a reaction medium. Visual examination indicated that the spectra of the halogens were the same in this solvent as in gas phase. Absorption spectra of bromine, chlorine, and a reacted mixture agreed well with those reported at wavelengths longer than 3100 A in carbon tetrachloride by Popov and Mannion,[6] and the position of equilibrium did not appear to be shifted from their observations. The rate of reaction was much slower than in organic solvents, was satisfactorily reproducible, and was not affected by the deliberate addition of small amounts of water. These facts offered enough evidence of "inertness" to justify the kinetic observations reported here.

Experimental Section

Materials. Reagent grade bromine was purified by shaking with concentrated sulfuric acid followed by distillation. Chlorine was purified by passing through concentrated sulfuric acid.

The solvent was 99.6% sulfuric acid prepared by adding reagent grade oleum to 98% acid. The composition was analyzed by electrical conductivity.

Solutions of the halogens were made up prior to each run. Since air-saturated solutions of chlorine were found to undergo photochemical deterioration when heated, the solvent used in preparing solutions had been saturated with dry nitrogen. The solutions were analyzed by diluting with ice water containing potassium iodide and then titrating with standardized thiosulfate.

Procedure. Mixtures of the desired composition were prepared directly in optical cells and thermostated to the desired temperature. Optical absorbance was then followed as a function of time with a Beckman spectrophotometer.

The observations could be fitted satisfactorily to the equation for a reversible bimolecular process, and a computer program with a variable infinite time absorbance was used to get the best fit and to compute the rate constant.

The calculations also required information as to the position of equilibrium. The equilibrium constant for the reaction

$$Br_2 + Cl_2 \rightleftharpoons 2BrCl \qquad (1)$$

has been estimated to be almost independent of temperature and to be about 7 in vapor phase[7] and in carbon tetrachloride.[6] Very rough measurements at 75.6° confirmed that the value in sulfuric acid is approximately the same or slightly less. Since uncertainties in this quantity have very little effect on

(1) R. M. Noyes, *J. Am. Chem. Soc.*, **88**, 4318 (1966).

(2) W. Jost, *Z. Physik. Chem.*, **B14**, 413 (1931).

(3) G. Brauer and E. Victor, *Z. Elektrochem.*, **41**, 508 (1935).

(4) S. Barratt and C. P. Stein, *Proc. Roy. Soc.* (London), **A122**, 582 (1929).

(5) J. H. Hildebrand, *J. Am. Chem. Soc.*, **68**, 915 (1946).

(6) A. I. Popov and J. J. Mannion, *ibid.*, **74**, 222 (1952).

(7) C. M. Beeson and D. M. Yost, *ibid.*, **61**, 1432 (1939).

rate constants measured when one reactant is in considerable excess, no attempt was made to measure the equilibrium constant more accurately.

Results

Since bromine absorbs much more strongly than chlorine at wavelengths of analytical interest, the absorbance change during a run was greatest when chlorine was the species in excess, and most runs were made for this condition. An extensive series of such runs at 75.6° supported the hypothesis that the rate was indeed first order in each reactant, and the same rate constant was computed for one run in which bromine was in twofold excess over chlorine.

For a series of runs at the same temperature in which chlorine and bromine were initially in equal (and stoichiometric) concentrations, the computed rate constants varied approximately inversely with initial concentration. Such behavior implies that the over-all order is little more than 1 instead of the anticipated value of 2. At several different temperatures, the rate constant for a solution 0.06 M in chlorine and 0.005 M in bromine was over twice that for a solution 0.04 M in each halogen.

We are unable to explain these kinetic anomalies or to derive a rate expression consistent with all of the observations. The runs in which one reactant was in excess definitely support the kinetics anticipated for a bimolecular mechanism, and the alternative atomic chain mechanism is at least as unsatisfactory with regard to kinetic consistency and is also untenable for reasons discussed below. The reported rate constants are therefore restricted to runs at unequal reactant concentrations.

Let k be the rate constant for reaction 1 from left to right. Estimated values of k are presented in Table I. The data can be fitted by the equation $\log k = 8.3 - 17.0/\theta$, where θ is $2.303RT$ in kilocalories per mole. Although the activation energy is probably uncertain by about 2 kcal/mole, these results are sufficiently precise to give the desired mechanistic information.

Table I: Rate Constants for Reaction 1

Temp, °C	10^4k, l./mole sec
50.1	7.5
59.8	15
67.4	24
75.6	45
84.7	100

Discussion

If the solvent is truly "inert," the reaction presumably proceeds either by a bimolecular mechanism or by an atomic chain initiated by dissociation of bromine.[8] If the atomic chain mechanism applies, the apparent activation energy can hardly be significantly less than $^1/_2D_0°(Br_2) + D_0°(Cl_2) - D_0°(BrCl) = 27.7$ kcal/mole. The very much smaller value observed makes the chain mechanism impossible.

Further support for this conclusion was provided by a run at 75.6° that was illuminated with a conventional incandescent lamp. The rate was not significantly increased, although the concentration of free bromine atoms must have been at least one order of magnitude greater than in the thermal runs.

Because of the compelling evidence against the atomic chain mechanism, we believe that even the crude kinetic measurements reported here are sufficient to demonstrate the bimolecular mechanism. The only alternative would seem to be the intervention of some ionic species in this highly polar medium, and we are not aware of any evidence for plausible concentrations of such species.

The observed activation energy of 17 kcal/mole is in gratifying agreement with the 13 kcal/mole predicted[1] for the gas phase; it is certainly very much less than the 52.9 kcal/mole predicted by Benson and Haugen[9] for the same reaction.

Acknowledgment. This work was supported in part by a grant from the U. S. Army Research Office (Durham).

(8) R. M. Noyes, *J. Am. Chem. Soc.*, 88, 4311 (1966).

(9) S. W. Benson and G. R. Haugen, *ibid.*, 87, 4036 (1965).

The Yield of Thermal Ethyl Radicals from the Radiolysis of Ethylene–Cyclohexane Solutions[1]

by J. L. McCrumb and Robert H. Schuler

Radiation Research Laboratories, Mellon Institute, Pittsburgh, Pennsylvania *(Received December 19, 1966)*

Recently, Holroyd[2] has used his ^{14}C-methyl radical sampling technique to look at the scavenging by ethylene of hydrogen atoms produced in the radiolysis of a number of hydrocarbons. From these studies he has

(1) Supported, in part, by the U. S. Atomic Energy Commission.

(2) R. A. Holroyd, *J. Phys Chem.*, 70, 1341 (1966).

concluded that for aliphatic hydrocarbons $G(H)$ is in the range 1.3–1.8 and that the ratio of rate constants for scavenging by ethylene to that for abstraction from the solvent is of the order of magnitude of 10^3. Only the relative yield of two radicals is, however, measured in these sampling experiments so that additional information is required to make the measurements absolute. We have carried out somewhat more direct studies in which dilute iodine is used to scavenge totally the product ethyl radicals and thus give a measure of the concentration dependence of the absolute yield for their formation. These studies are possible because of the high efficiency of iodine in the reaction[3]

$$R\cdot + I_2 \longrightarrow RI + I\cdot \qquad (1)$$

so that experiments can be carried out at sufficiently low concentrations that iodine will quantitatively scavenge the alkyl radicals and yet not interfere in either the abstraction[4] (eq 2) or addition (eq 3) reactions of the hydrogen atoms. The experiments in

$$H\cdot + RH \longrightarrow H_2 + R\cdot \qquad (2)$$

$$H\cdot + C_2H_4 \longrightarrow C_2H_5\cdot \qquad (3)$$

cyclohexane reported here completely confirm the rate constant ratio (k_2/k_3) found by Holroyd[2] though they do give a somewhat lower hydrogen atom yield than indicated in his work.

Experimental Section

Radioiodine (^{131}I) was used as the scavenger and the active ethyl iodide formed was separated gas chromatographically and examined in a manner very similar to that in the previous work on methyl radical formation.[3] Cyclohexane was Phillips Research grade and was chromatographed before use. Samples containing a known concentration of ethylene[5] and iodine ($\sim 10^{-4}$ M) of known relative specific activity were thoroughly outgassed and irradiated in a ^{60}Co source to a dose of 5×10^{17} ev/g. Approximately 25% of the iodine reacted during the irradiation. After irradiation 0.5 ml of the sample was chromatographed, the ethyl iodide fraction was collected, and the total activity in this fraction was determined. As commented on earlier[3] the radioiodine method is extremely sensitive and could be used to advantage here since the ethyl iodide content of the chromatographed sample was only 10^{-9} to 10^{-10} mole.

Results and Discussion

The ethylene concentration dependence of the ethyl iodide yield is given in Figure 1. A small correction has been made for the yield of 0.008 observed in the absence of ethylene. Presumably the ethyl iodide is formed by addition of thermal hydrogen atoms to the ethylene followed by the scavenging of the ethyl radicals produced. A plot of $1/G(C_2H_5I^*)$ *vs.* $1/[C_2H_4]$ shows an excellent linear relationship so that the data are at least in accord with a simple competition between eq 2 and 3 for a constant yield of hydrogen atoms, *i.e.*

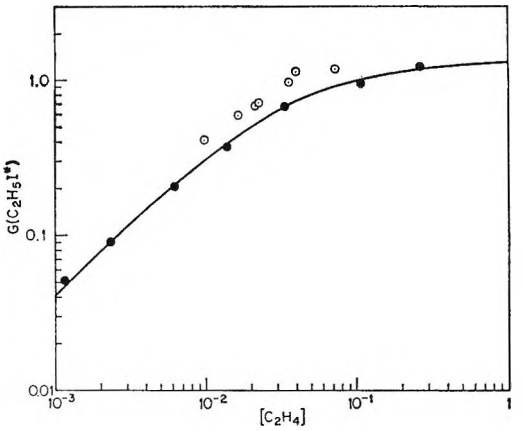

Figure 1. ●, Concentration dependence of ethyl iodide yield from ethylene–cyclohexane solutions; ———, calculated for simple competition between reactions 2 and 3 with $G(H) = 1.32$ and $k_2/k_1 = 0.00344$ (*cf.* eq I); ○, ethyl radical yields estimated from the work of Holroyd on the assumption that $G(C_2H_5) + G(c\text{-}C_6H_{11}) = 4$.

$$G(C_2H_5I^*) = G(C_2H_5I^*)_\infty\left(\frac{1}{1 + k_2[RH]/k_3[C_2H_4]}\right) \qquad (I)$$

As is seen in the figure, simple competition is observed over even a considerably wider range of ethylene concentrations than in the previous $^{14}CH_3$ study. Taking $[C_6H_{12}]$ as 9.3 M the parameters obtained from the best fit are $G(C_2H_5I^*)_\infty = 1.32$ and $k_2/k_3 = 0.0034$. The rate constant ratio is almost identical with that given by Holroyd (0.0037), but the limiting value is somewhat lower than his estimate of 1.8 for the hydrogen atom yield. For comparison purposes the yields of ethyl radicals calculated from the ratios of $G(c\text{-}C_6H_{11})$ to $G(C_2H_5)$, published by Holroyd on the assumption that $G(c\text{-}C_6H_{11}) + G(C_2H_5)$ equals the value of 4 measured for pure cyclohexane, are given by the open circles in

(3) R. H. Schuler and R. R. Kuntz, *J. Phys. Chem.*, **67**, 1004 (1963). In 2,2,4-trimethylpentane $k_{CH_3+I_2}/k_{CH_3+RH} \sim 10^7$ and scavenging of methyl radicals is essentially complete above 10^{-5} M I_2.

(4) The fact that iodine is effective in reducing the hydrogen yield only at concentrations greater than 10^{-3} M indicates that k_{H+I_2}/k_2 is similar to (or less than) the value of 2×10^3 observed for k_{H+HI}/k_2 by D. Perner and R. H. Schuler, *J. Phys. Chem.*, **70**, 317 (1966).

(5) From pressure–volume measurements. A small (and constant) correction was made for the ethylene in the vapor phase by assuming a solubility coefficient of 3.

Figure 1. These yields are consistently 35% higher and the reason for the discrepancy is not obvious at the moment. However, since methyl iodide is known to decompose with a $G \sim 0.5$ at the concentration used in the CH_3 experiment, the two systems are not completely identical and the difference could, in part, conceivably involve some effect of methyl iodide on the total yield with resultant inaccuracies in the intercomparison of the two sets of experiments.

The value of $G(C_2H_5I^*)_\infty$ obtained by extrapolation of the data to very high ethylene concentrations is quite dependent on the results of the experiments in the range of 0.1 M where various possible complications can occur.[6] The yield measured pertains, therefore, to that of hydrogen atoms from concentrated ethylene solutions and should not be completely identified with that from the pure solvent.[7] If, however, we multiply (as is done in Table I) the ethyl radical yield measured here by the ratios of $G(c\text{-}C_6H_{11})/G(C_2H_5)$ given in ref 2, we obtain an essentially constant total yield of C_2 and C_6 radicals. Hydrogen atom production cannot, therefore, be strongly dependent on ethylene concentration in this range.

Table I: Estimated Radical Yields

$[C_2H_4]$, mM	$G(C_2H_5)^a$	$G(c\text{-}C_6H_{11})/G(C_2H_5)^b$	$G(c\text{-}C_6H_{11})^c$	$G(c\text{-}C_6H_{11} + C_2H_4)^c$
71.7	0.91	2.36	2.15	3.06
39.7	0.73	2.53	1.85	2.58
36.3	0.70	3.10	2.17	2.87
22.6	0.54	4.62	2.50	3.04
21.6	0.53	4.79	2.54	3.07
15.7	0.43	5.72	2.49	2.92
9.85	0.31	8.64	2.68	2.99

[a] Interpolated from the data of Figure 1. [b] Measured by R. A. Holroyd.[2] [c] Calculated from columns 2 and 3. The cyclohexyl radical yield from pure cyclohexane has been measured to be ~4 (J. L. McCrumb and R. H. Schuler, unpublished results; see also G. A. Muccini and R. H. Schuler, *J. Phys. Chem.*, **64**, 1436 (1960)).

The rate constant ratio of 0.0034 given above for the competition between eq 2 and 3 is only a factor of 8 greater than the ratio between reaction 2 and that observed for the scavenging of hydrogen atoms by HI in hexane[4] where the latter is presumably a diffusion-controlled process. The absolute rate constant for eq 3 in solution is therefore estimated as $\sim 3 \times 10^8$ M^{-1} sec^{-1}. This value is comparable to recent determinations[8-11] in the gas phase. The activation energy is small (~2 kcal) so that in solution its rate will be in the transition region between being diffusion and activation controlled and is, in fact, expected to be fairly insensitive to the actual activation energy. The rate constant ratio appears, therefore, to be quite reasonable and gives a scavenging efficiency of 24% at 10 mM ethylene. At this concentration, where effects of ethylene on the hydrogen atom production should be small, both the ethyl radical yield measured here (0.31) and that estimated from the work of Holroyd (0.42) indicate thermal hydrogen atom production with a $G \sim 1.5$.[12] Though considerably smaller than estimates made from the effects of solutes in decreasing hydrogen production, it is believed that such a value does, in fact, represent a good approximation to the actual hydrogen atom production from cyclohexane itself.

(6) P. Ausloos, A. A. Scala, and S. G. Lias, *J. Am. Chem. Soc.*, 88, 1583 (1966), have, for example, observed transfer of H_2 to C_2D_4 at these concentrations.

(7) Taking k_{H+I_2}/k_2 as 2×10^3, only 2% of the hydrogen atoms will be scavenged by 10^{-4} M I_2 from cyclohexane itself and even less in the presence of ethylene.

(8) V. L. Tal'rose, V. P. Strunin, A. F. Dodonov, and G. K. Lavrovskaya, *Advan. Mass Spectrometry*, 3, 993 (1966).

(9) J. V. Michael and R. E. Weston, Jr., *J. Chem. Phys.*, in press.

(10) K. Yang, *J. Am. Chem. Soc.*, 84, 719 (1962).

(11) Very recently V. M. Brown, P. B. Coates, and B. A. Thrush, *Chem. Commun.*, 22, 843 (1966), claim to have measured a somewhat lower value (9×10^7 M^{-1} sec^{-1}) for the rate constant.

(12) This value must be regarded as a minimum, since in both experiments it neglects any ethyl radicals lost in hot reactions.

The Kinetics of the Periodate Oxidation of Substituted 2-Aminoethanols

by George Dahlgren[1] and Edith M. Rand

Department of Chemistry, University of Alaska, College, Alaska
(Received December 27, 1966)

In a recent paper on the periodate oxidation of dicarbonyl compounds Dahlgren and Reed[2] have suggested that the negative enthalpy of activation observed in the periodate oxidation of 2-aminoethanol[3] can be accounted for by considering $H_3IO_6^-$ as the reactive species instead of IO_4^- as proposed. They cite as evidence for this suggestion the nucleophilicity rate correlations for periodate species and the observed

(1) To whom all correspondence should be addressed at the Department of Chemistry, University of Cincinnati, Cincinnati, Ohio 45221.

(2) G. Dahlgren and K. L. Reed, *J. Am. Chem. Soc.*, 89, 1380 (1967).

(3) G. Dahlgren and J. M. Hodsdon, *J. Phys. Chem.*, 68, 416 (1964).

temperature coefficients of the rates in the periodate oxidation of glyoxal, pyruvaldehyde, and diacetyl.

We have investigated the effect of N-methyl and N,N-dimethyl substitution on the kinetics of the periodate oxidation of 2-aminoethanol considering both $H_4IO_6^-$ and $H_3IO_6^{2-}$ as the reactive periodate species.

Experimental Section

Materials. Commercially available amino alcohols were distilled in a 42-plate column. The boiling points and refractive indices ($n^{25}D$), respectively, of the fractions used in this work were: 2-aminoethanol, 86° at 24 mm, 1.4530; 2-(methylamino)ethanol, 68° at 26 mm, 1.4305; 2-(dimethylamino)ethanol, 50° at 29 mm, 1.4295. Inorganic materials were the best grade available.

Rate Determinations. The reactions were studied by the same procedure used in the rate studies previously noted,[3] with the exception that buffered solutions of the amino alcohols were added to buffered solutions of the periodate, instead of the reverse order. The least-squares linearity of a single run, determined on an IBM 1620 computer, was generally within 1% instead of 4% for the reverse addition, the difference probably being due to local excesses of periodate in the latter case. Acetate, phthalate, and formate buffers were used to maintain the pH at ±0.02 of the desired value. The ionic strength was held at 0.5 using sodium nitrate. The temperature was maintained at ±0.02° during the course of a run, except at 50.4°, where a variation of ±0.10 was observed.

pK_a Determination. The pK_a of 2-(methylamino)-ethanol was determined by titrating three different concentrations of the amino alcohol with dilute hydrochloric acid. The pH at one-half equivalence point was taken as the pK_a. Generally, the three determinations were within ±0.02 pH unit at each temperature.

Results and Discussion

In the cases of 2-aminoethanol and 2-(methylamino)-ethanol excellent pseudo-first-order plots were obtained when the amino alcohols were present in 5–25-fold molar excess over the periodate in the pH range 3–6. 2-(Dimethylamino)ethanol was not oxidized by periodate under these conditions nor at lower values of pH.

From a comparison of the stoichiometry studies of Maros and co-workers[4] on the periodate oxidation of amino alcohols and ethylenediamine and from the known behavior of periodate on glycols, the following stoichiometric expression is presented for the reaction of N-substituted amino alcohols with periodate.

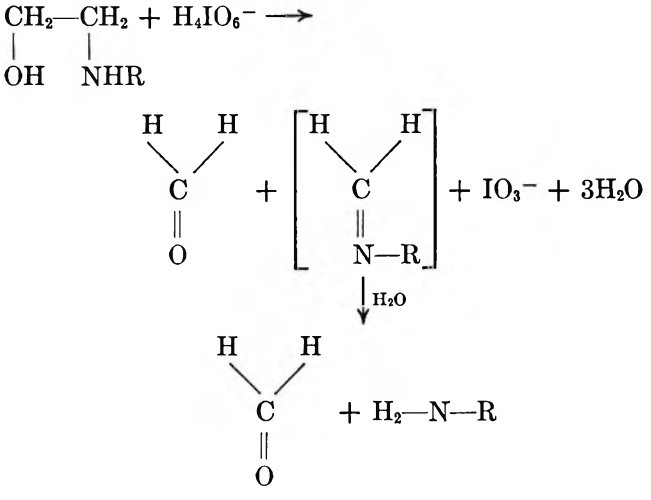

The amine products in the reactions of 2-aminoethanol and 2-(methylamino)ethanol are ammonia and methylamine, respectively. In the case of 2-(dimethylamino)-ethanol the iminelike intermediate cannot form because of the energetically unfavorable step of elimination of a methyl group and therefore this amine alcohol is not cleaved by periodate.

If we consider the reaction to be a second-order process represented by the scheme

$$AE + P \xrightarrow{k_2} \text{products}$$

where AE represents the amino alcohol or its protonated form and P the reactive periodate species, either $H_4IO_6^-$ or $H_3IO_6^{2-}$, the rate is given by

$$\frac{-d[P]_T}{dt} = k_2[P][AE]$$

where $[P]_T$ is the total concentration of periodate (H_5IO_6, $H_4IO_6^-$, IO_4^-, $H_3IO_6^{2-}$) in the acid pH range. Pseudo-first-order conditions (5–25-fold excess [AE]) lead to the expression $k_1' = k_2[AE]$. Table I gives the value of $k_1'/[AE]$ for both compounds over five temperatures. The constancy of this ratio is indicative of the second-order process (*i.e.*, no kinetically detectable intermediate).

The first-order dependence (increase in rate with increase in pH) of the rate on pH observed for 2-aminoethanol[3] was verified in pH-rate studies in the pH range 3–6.

If we limit our consideration of reactive species to $H_4IO_6^-$ and $H_3IO_6^{2-}$ for periodate and to protonated and unprotonated amino alcohols (AE and AEH^+) and if we further stipulate a single reaction path, then of the four possible reaction combinations only two,

(4) L. Maros, I. Molnar-Perl, and E. Schulek, *Acta Chim. Acad. Sci. Hung.*, **30**, 119 (1962).

Table I: Rate Constants and Equilibrium Constants for the Periodate Oxidation of 2-Aminoethanol (AE) and 2-(Methylamino)ethanol (MAE)

		Temperature, °C				
		0	11.8	25.0	36.0	50.4
$(k_1'/[AEH^+]) \times 10^3$, sec^{-1}	AE	5.77 ± 0.59	14.8 ± 0.60	25.8 ± 1.7	60.8 ± 3.5	88.7 ± 4.7
	MAE	11.7 ± 0.70	22.8 ± 1.1	...	45.4 ± 3.0	69.3 ± 5.3
pH		4.30 ± 0.03	4.20 ± 0.03	4.10 ± 0.03	4.20 ± 0.03	4.35 ± 0.03
$K_a \times 10^{11}$	AE[a]	5.06	12.5	31.8	65.8	154
	MAE[b]	3.12	6.21	12.8	22.1	42.5
K_D[c]		7.8	16.8	39.7	77.3	196
$K_2^o \times 10^7$		3.63	2.76	2.04	2.63	3.55
k_2[d] $\times 10^{-4}$, M^{-1} sec^{-1}	AE–$H_4IO_6^-$	5.06	13.3	26.2	45.7	50.8
	MAE–$H_4IO_6^-$	16.7	41.2	...	102	144
k_2,[d] M^{-1} sec^{-1}	AEH^+–$H_3IO_6^{2-}$	7.06	60.2	409	1140	2200
	$MAEH^+$–$H_3IO_6^-$	14.4	92.8	...	856	1720

[a] R. G. Bates and G. D. Pinching, *J. Res. Natl. Bur. Std.*, **46**, 349 (1951). [b] This work. [c] C. Crouthamel, A. Hayes, and D. S. Martin, *J. Am. Chem. Soc.*, **73**, 82 (1951). [d] Estimated error <±10%.

differing by a proton transfer, lead to the observed first-order dependence of the rate on the hydrogen ion concentration, *viz.*, AE–$H_4IO_6^-$ and AEH^+–$H_3IO_6^{2-}$. (The other two combinations lead to zero- and second-order dependence.)

The pseudo-first-order constant for the reaction pair AE–$H_4IO_6^-$ is given by $k_1' = k_2[\overline{AEH^+}]K_a/[H^+](1 + K_D)$, where $[\overline{AEH^+}]$ is the average concentration of amino alcohol during the course of a run, K_a is the ionization constant of the acid AEH^+, and K_D is the dehydration constant for $H_4IO_6^-$ to IO_4^-.[5] For the AEH^+–$H_3IO_6^{2-}$ reaction pair the pseudo-first-order constant is given by $k_1' = k_2[AEH^+]K_2/[H^+](K_D + 1)$, where K_2 is the ionization constant for $H_4IO_6^-$.

The values calculated for k_2 for each of these pairs are recorded in Table I along with the other data necessary for the calculations. The thermodynamic activation parameters for the two reaction paths are given in Table II.

The fact that we have not been able to demonstrate the presence of an intermediate as in the periodate oxidation of substituted ethylene glycols[6] is not sufficient to rule out its existence since we are forced to operate under the "limiting conditions" described in an earlier paper,[2] that is, on the "wrong" side of an equilibrium constant where the concentration of an intermediate complex necessarily would be small (given by an equilibrium constant expression) and not detectable by our methods.

While it is not possible to assign unequivocally either of the above possible paths to the reaction, the AE–$H_4IO_6^-$ path is preferred on the basis that glycols, in general, are not attacked by $H_3IO_6^{2-}$ under these same conditions. At least there is no evidence of such behavior in their pH–rate profiles at values of pH above 6, as has been observed with dicarbonyl compounds.[2]

The large values for the second-order rate constants for both compounds with either $H_4IO_6^-$ or $H_3IO_6^{2-}$ are quite surprising, since glycols which are oxidized by periodate in a simple second-order process[7] exhibit constants of the order of 20 or so at 25°. However, studies of oxygen-exchange rates in $H_4IO_6^-$ in aqueous solutions by nmr[8] and temperature-jump methods[9] yield rate constants of similar magnitude to those obtained here. By analogy to the two-step mechanism proposed for oxygen exchange by Kustin and Lieberman[9] we suggest that the actual mechanisms for perio-

Table II: Thermodynamic Functions of Activation for the Oxidation of 2-Aminoethanol and 2-(Methylamino)ethanol by the Periodate Species $H_4IO_6^-$ and $H_3IO_6^{2-}$

	2-Aminoethanol		2-(Methylamino)-ethanol	
	$H_4IO_6^-$	$H_3IO_6^{2-}$	$H_4IO_6^-$	$H_3IO_6^{2-}$
ΔH^*, kcal/mole[a]	+8.34	+26.0	+7.87	+17.4
ΔG^*, kcal/mole[b]	+10.1	+14.9	+9.42	+14.5
ΔS^*, eu[b]	−6.6	+4.1	−5.7	+1.1

[a] Estimated error <5%. [b] Calculated at 0° from data in Table I.

(5) For more details on the kinetic scheme see ref 2 and 3.

(6) F. R. Duke and V. C. Bulgrin, *J. Am. Chem. Soc.*, **76**, 3803 (1954).

(7) V. C. Bulgrin and G. Dahlgren, *ibid.*, **80**, 3833 (1958).

(8) I. Pecht and Z. Luz, *ibid.*, **87**, 4068 (1965).

(9) K. Kustin and E. C. Lieberman, *J. Phys. Chem.*, **68**, 3869 (1964).

date oxidations involve the short-lived intermediates $H_2IO_5^-$ and HIO_5^{2-} and not $H_4IO_6^-$ and $H_3IO_6^{2-}$.

It is interesting to note that at 25° the ratio of second-order constants (equimolar with $H_4IO_6^-$ reactant) for 2-(methylamino)ethanol to 2-aminoethanol (89.0/23.8) is almost identical with that reported for *trans*-2-(methylamino)cyclohexanol to *trans*-2-aminocyclohexanol (18/5.2),[10] whereas the *cis* isomers were quite different (0.77/1.6).[10] This behavior would suggest an *s-trans* configuration for 2-aminoethanols in aqueous solution in which the N-methyl substituent does not interfere with the periodate attack.

Lastly, it should be noted that a small increase in rate was observed due to general base catalysis by the buffer, as reported for the periodate oxidation of dicarbonyl compounds.[3] This rate enhancement may be similar in nature to the action of base on the exchange equilibria between oxygen and iodate in water solution observed by Anbar and Guttman.[11]

Acknowledgment. The authors gratefully acknowledge the financial assistance of the American Cancer Society through Grant No. P-272.

(10) J. Kovar, J. Jary, and K. Blaha, *Collection Czech. Chem. Commun.*, **28**, 2199 (1963).

(11) M. Anbar and S. Guttman, *J. Am. Chem. Soc.*, **83**, 781 (1961).

The Thermodynamics of Vaporization of Thallous Fluoride

by F. J. Keneshea and Daniel Cubicciotti

Stanford Research Institute, Menlo Park, California 94025
(Received December 27, 1966)

In our report of the thermodynamics of vaporization of thallous fluoride,[1] we derived the partial pressures of gaseous monomer (TlF) and dimer (Tl_2F_2) and their change with temperature in the saturated vapor from measurements of the total vapor pressure and transpiration pressure. By this "second-law" method we calculated the absolute entropy for the solid at 298°K to be 25.9 eu. Recently, Westrum[2] has determined this entropy calorimetrically and found 22.87 eu. Therefore, the second-law treatment of the data was inaccurate, presumably because it was based on second differences of experimental results.

We have recalculated the data by a third-law method using Westrum's entropy for the condensed phase and the molecular constant entropy for the gas phase for the monomer. At one temperature (800°K, where the pressure measurements by the two different methods were most reliable) the experimental pressure measurements were used to determine the partial pressure of monomer, which was then combined with the third-law entropy of vaporization to give the enthalpy of vaporization to the monomer. From this the vapor pressure equation for the monomer was calculated and from that equation and the measured pressures the partial pressure of dimer was calculated over the experimental range. The details of the calculations are given at the end of this note. The revised results for the experimental temperature range (690–965°K) are

$$\log P(\text{monomer, torr}) = \left[\frac{-7325}{T} - 3.62 \log T + 20.254\right] \pm 0.025 \quad (1)$$

$$\Delta H^\circ(\text{vaporization, monomer, kcal/mole}) = [33.5 - 7.2 \times 10^{-3}T] \pm 0.2 \quad (2)$$

$$\log P(\text{dimer, torr}) = -\frac{7143 \pm 20}{T} - 5.55 \log T + 25.881 \pm 0.026 \quad (3)$$

$$\Delta H^\circ(\text{vaporization, dimer, kcal/mole}) = [32.6 - 11 \times 10^{-3}T] \pm 0.2 \quad (4)$$

$$\log P(\text{total of monomer and dimer, torr}) = -\frac{7193 \pm 21}{T} - 4.78 \log T + 23.905 \pm 0.026 \quad (5)$$

$$\Delta H^\circ(\text{vaporization to equilibrium mixture, kcal/mole}) = [32.9 - 9.5 \times 10^{-3}T] \pm 0.2 \quad (6)$$

The uncertainties given for eq 1 and 2 are based on an estimate of 5% uncertainty in the pressure differences. The uncertainties for the other equations are standard errors obtained from the least-squares analysis of the data.

The enthalpy of sublimation to the monomer at 298°K was obtained by combining the third-law value for 800°K (see below) with enthalpy increment data from Cubicciotti and Eding.[3] This gives a third-law value for ΔH°_{298}(sublimation, monomer) of 34.1 kcal/mole. With this value the thermochemical dissocia-

(1) F. J. Keneshea and D. Cubicciotti, *J. Phys. Chem.*, **69**, 3910 (1965).

(2) E. F. Westrum, Jr., private communication.

(3) D. Cubicciotti and H. Eding, *J. Chem. Eng. Data*, **10**, 343 (1965).

tion energy of gaseous TlF at 298°K becomes 105 ± 3 kcal/mole (as compared with the value of 108 reported by Cubicciotti and Withers[4]). This revised value is within experimental error of that given by Murad, Hildenbrand, and Main[5] from mass spectrometric techniques, namely, 101 ± 3.5.

Extrapolation of the dimer and monomer pressures to the solid range (using the enthalpy of fusion given in ref 3) gives a dimer/monomer ratio over the solid which is essentially temperature independent and equal to 3.6 (80% dimer). The fact that the ratio is temperature independent indicates that the second-law enthalpy value obtained by Barrow, Jeffries, and Swinstead[6] from total pressures over the solid should agree with the monomer value. Their value of $\Delta H°_{298}$ (34.41 kcal/mole) is indeed in agreement with the third-law value we derived from our data over the liquid (34.1). We have further made a third-law calculation from the data of Barrow, *et al.*, assuming the monomer constituted 20% of the vapor in their measurements. The resulting value of $\Delta H°_{298}$ was 34.1 ± 0.1 kcal/mole, in excellent agreement with our results.

Thermodynamic quantities for the vaporization of the fluoride at 1000°K are shown in Table I while derived data for the dissociation of the gaseous dimer are given in Table II. Values for the other thallous halides, taken from ref 1, are also listed. The values for thallous fluoride are somewhat different from those obtained previously,[1] but the trends in comparison with the other halides are the same.

Using the dissociation entropy shown in Table II for thallous fluoride, a value of 30 eu is obtained for the "experimental" vibrational entropy for a square-planar dimer model. This is 6 eu greater than the value of 24 eu calculated from an estimate of the dimer frequencies.[1] This difference is not so large as the 13 eu obtained before[1] and perhaps is not great enough to rule out the square-planar geometry. Nevertheless, it is still large enough to suggest that the molecule may be more open than square planar. The existence of Tl_2^+ in the mass spectrum has been previously discussed as evidence for the presence of a Tl–Tl bond in the dimer.[1]

The details of the third-law treatment of the experimental data reported in ref 1 are as follows: at 800°K, where the original absolute pressure and transpiration data[1] are considered most reliable, the monomer pressure, p_M, and dimer pressure, p_D, calculated[7] from least-squares curves through the original data, are p_M = 3.88 torr and p_D = 6.81 torr. Using Westrum's value for $S°_{298}$ and thermal data previously cited,[3] the third-law entropy of vaporization for the monomer is calculated to be $\Delta S°_{800}(\text{vap}) = S°_{800}(\text{gas}) - S°_{800}$ (condensed) = 66.97 − 42.76 = 24.21 eu. This number, combined with the monomer partial pressure, gives for the enthalpy, $\Delta H°_{800}(\text{vap})$ = 27,758 cal/mole, which gives, in turn, a value for the integration constant in eq 2 of 33,518 cal/mole. The revised equations for the monomer pressure and enthalpy of vaporization over the liquid, derived from these third-law values, were given above as eq 1 and 2.

Table I: Thermodynamic Data for Vaporization of Liquid Tl Halides at 1000°K

Salt	$\Delta H°$ (monomer), kcal/mole	$\Delta H°$ (dimer), kcal/mole	$\Delta S°$ (monomer), cal/mole deg	$\Delta S°$ (dimer), cal/mole deg
TlF	26.3	21.6	22.6	17.3
TlCl	24.4	31.8	22.0	25.7
TlBr	24.3	50	22.0	42
TlI	25.2	...	23.8	...

Table II: Thermodynamic Quantities at 1000°K for the Reaction $Tl_2X_2(g) = 2TlX(g)$

Salt	$\Delta H°$, kcal/mole	$\Delta S°$, kcal/mole	Equil const, K_p, atm	Dimer/monomer ratio
TlF	31.0 ± 0.4	27.9 ± 0.5	0.21	1.05
TlCl	17.0 ± 0.8	18.3 ± 1.2	1.66	0.15
TlBr	−2 ± 5	2 ± 4	5	0.067

The monomer pressures given by eq 1 were checked for agreement with the experimental data over the whole temperature range in the following way. At temperatures from 800 to 1000°K, where total pressure measurements were more reliable than transpiration pressures, values of p_M from eq 1 were combined with least-squares values of the experimental total pressure, p_{tot}, yielding calculated values of transpiration pressure, p_{tr}. The greatest deviation of p_{tr}(calcd) from p_{tr}(exptl, least squares) was found to be 1% at 1000°K. Similarly, from 800 to 690°K, where transpiration measurements were more reproducible than absolute pressures, p_M from eq 1 was combined with p_{tr}(exptl) and values of p_{tot} calculated. The greatest deviation between p_{tot}(calcd) and p_{tot}(exptl, least squares) was 8% at 690°K. Since the scatter in the experi-

(4) D. Cubicciotti and G. L. Withers, *J. Phys. Chem.*, **69**, 4030 (1965).

(5) E. Murad, D. Hildenbrand, and R. Main, *ibid.*, **45**, 263 (1966).

(6) R. F. Barrow, E. A. Jeffries, and J. M. Swinstead, *Trans. Faraday Soc.*, **51**, 1950 (1955).

(7) The relationship used for the calculation is given by D. Cubicciotti, *J. Phys. Chem.*, **68**, 1528 (1964).

mental total pressures at 690°K amounted to 25%, the agreement within 8% is quite satisfactory. Thus, the monomer pressure equation (eq 1), derived by third-law considerations from the data at 800°K, is in good agreement with the original experimental data over the whole temperature range.

Using the corrected total and transpiration pressures obtained above by combining eq 1 with the data, we calculated revised equations by a least-squares Σ-plot treatment, for p_{tot} and for the dimer pressure, p_D. For the dimer ΔC_p was taken as -11 cal/mole deg,[1] while for the total pressure an average value of -9.5 cal/mole deg for ΔC_p was calculated over the temperature range 690–1000°K from the heat capacities of the monomer and dimer[1] and their relative amounts in the gas phase. The resulting equations were given above as eq 3–6.

Acknowledgment. This work was made possible by the support of the Research Division of the U. S. Atomic Energy Commission under Contract No. AT(04-3)-106.

COMMUNICATIONS TO THE EDITOR

The Elimination of HF from Vibrationally Excited 1,1,2-Trifluoroethane

Sir: We have extended our recent studies[1] on the elimination of HF from vibrationally excited fluoroethanes to the "hot" molecule CF_2HCFH_2*, formed *via* the cophotolysis of $(CF_2H)_2CO$ and $(CFH_2)_2CO$. Low pressures of the ketones (between 60 and 600 μ total pressure, in a roughly 1:1 mixture) were used in order to eliminate collisional quenching. At 20° the relative rate constants for formation of *cis*-1,2-, *trans*-1,2-, and 1,1-difluoroethylene are 6:3.8:1. The *cis* and *trans* isomers were distinguished by their infrared spectra.[2] We observe the *cis*:*trans* ratio to be constant at 1.55 ± 0.10 up to 350°, but $(k_{cis} + k_{trans})k_{1,1-}$ decreases monotonically from about 10:1 to 5:1 over this temperature range (see Figure 1).

Apparently the critical energies for *cis* and *trans* elimination are almost equal. The maximum difference between E_{cis}* and E_{trans}* that could be concealed by our experimental scatter in k_{cis}/k_{trans} is about 1 kcal mole^{-1}. This conclusion is based upon a crude RRK calculation[3] with E(298°K) = 85.4, E(650°K) = 96.5, E_{cis}* = 59 kcal mole^{-1}, and 13 effective oscillators. On the other hand the decrease in 1,1- product at lower temperatures may be attributed to a higher critical energy for this reaction. It is also consistent with previous observations that α halogenation promotes and β halogenation decreases the rate of dehydrohalogenation.[4] If we assume that E_{cis}* = E_{trans}*, then a second RRK calculation based on the parameters given above and the data in Figure 1 yields a value of $E_{1,1-}$* = 62.4 kcal mole^{-1}. This correlates well with the value of E* for CFH_2CFH_2*, which is in the range[1,3] 59–62 kcal mole^{-1}, and with Maccoll's prediction.[4]

Since $k_{cis}/k_{trans} \simeq 1.5$ is a ratio of small whole numbers,[5] it is tempting to try to rationalize this result on the basis of reaction path degeneracy. However, we have been unable to find any *consistent* model which reproduces the *cis*:*trans* ratio. In examining the various possibilities both the three-center α,α elimination as well as the usual four-center (α,β elimination) transition state were considered. Consideration of the former was prompted by the fact that in separate experiments[6] it was found that α,α elimination makes a significant contribution to the total elimination from "hot" CD_3CF_2H*, since d_3 as well as d_2 vinyl fluoride was formed.

Recently, Hassler and Setser[7] observed a *cis*:*trans* ratio of about 6 for the elimination of HCl from "hot" CCl_2HCClH_2*; at 25° the *cis*:*trans*:1,1- ratio was 25:4:1. These data[7] also argue against an explanation

(1) See G. O. Pritchard and R. L. Thommarson, *J. Phys. Chem.*, **71**, 1674 (1967), for a summary.

(2) H. G. Viehe, *Chem. Ber.*, **93**, 1697 (1960).

(3) See S. W. Benson and G. Haugen, *J. Phys. Chem.*, **69**, 3898 (1965), and ref 1 for definition and estimation of parameters.

(4) A. Maccoll, *Advan. Phys. Org. Chem.*, **3**, 91 (1965).

(5) In fact, in the high-temperature limit where activation energy differences are relatively unimportant all three products are formed in the ratio of small whole numbers (about 3:2:1).

(6) G. O. Pritchard and J. T. Bryant, submitted for publication.

(7) J. C. Hassler and D. W. Setser, *J. Chem. Phys.*, **45**, 3237 (1966).

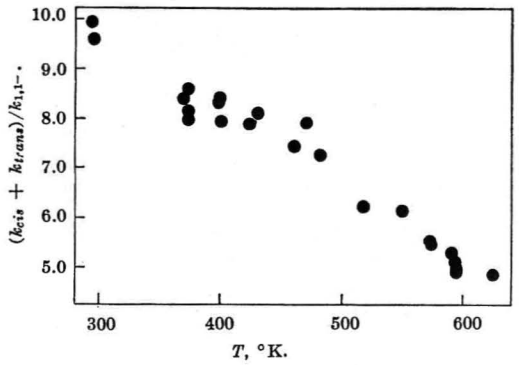

Figure 1. The variation with temperature of the rate of formation of 1,2-difluoroethylene to 1,1-difluoroethylene.

based on reaction path degeneracy alone. However, it should be pointed out that there are many more reaction possibilities in the chloro system and that the three isomeric chloroethylenes are also formed by a pathway not involving the "hot" trichloroethane intermediate.

A number of experimental and theoretical studies are now being undertaken to characterize the α,α and α,β transition states and to determine the relative significance of each elimination. In order to explain the proportion of 1,1- product it may very well be necessary to take into account the α,α elimination from $-CFH_2$ in CFH_2CF_2H*.

Acknowledgment. This work was supported by a grant from the National Science Foundation.

DEPARTMENT OF CHEMISTRY
UNIVERSITY OF CALIFORNIA
SANTA BARBARA, CALIFORNIA 93106

JAMES T. BRYANT
BERNARD KIRTMAN
GLYN O. PRITCHARD

RECEIVED FEBRUARY 10, 1967

Nucleophilic Micelles. I

Sir: The study of micelles has provided much of the basis for the understanding of lyophobic bonding, a factor of paramount importance in the stabilization of the tertiary structure of proteins.[1,2] The similarity in micelle and protein structure is seen from the X-ray determined tertiary structure of myoglobin[3] and lysozyme[4] from which it is evident that the nonpolar side chains are, in the main, located in the interior in lyophobic regions while the polar amino acid side chains are generally located at the periphery of the protein. Much the same information is obtained from chemical and physical studies of other proteins.[5] This resemblance between the structure of micelles and enzymes suggests the worthiness of investigations of the kinetics of reactions in or at the surfaces of micelles and the possible design of micelle catalysts. Though a few noteworthy contributions to the study of reactions in micelles have been made[6] the employment of an amphiphile as a nucleophile or general catalyst has yet to be investigated. To this end we have investigated in detail the reactions of esters of type I with micelle-forming agents of type II, III, and IV and with the nucleophilic agents V.

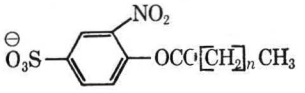

$(n = 0, 4, 6, 8)$ (I)[7]

(II)[8]

(III)[8]

(IV)[9]

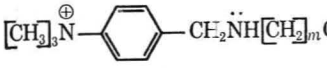

$(m = 3, 9)$ (V)[10]

The hydrolyses of esters I were followed spectrophotometrically at 410 mμ or autotitrimetrically. In the absence of agents II, III, IV, and V the hydrolyses of esters I were found to be first order in $[OH^-]$ and first order in ester between pH 8.0 and 10.5 ($\mu = 0.1$ and 0.5). The rate constants for alkaline hydrolysis at 30° and $\mu = 0.1$ (k_{OH} in liters per mole per minute) were 2651 (at 5×10^{-5} to 1.7×10^{-4} M) for $n = 0$; 1165 (at 5×10^{-5} to 1.7×10^{-5} M) for $n = 4$; 953 (at 2.08×10^{-5} to 8.33×10^{-4} M) for $n = 6$; and 340 (at 5×10^{-5} to 1.7×10^{-4} M) for $n = 8$. All the

(1) A. L. Berger and K. Linderstrøm-Lang, *Arch. Biochem. Biophys.*, **69**, 106 (1957).

(2) G. Némethy and H. A. Scheraga, *J. Phys. Chem.*, **66**, 1773 (1962).

(3) J. C. Kendrew, *et al.*, *Nature*, **185**, 422 (1960).

(4) D. C. Phillips, *Sci. Am.*, **215**, 78 (1966).

(5) G. G. Hammes and H. A. Scheraga, *Biochemistry*, **5**, 3690 (1966).

(6) E. F. J. Duynstee and E. Grunwald, *J. Am. Chem. Soc.*, **81**, 4540, 4542 (1959); J. L. Kurz, *J. Phys. Chem.*, **66**, 2239 (1962); D. G. Herries, W. Bishop, and F. M. Richards, *ibid.*, **68**, 1842 (1964); L. J. Winters and E. Grunwald, *J. Am. Chem. Soc.*, **87**, 4608 (1965); M. T. A. Behme, J. G. Fullington, R. Noel, and E. H. Cordes, *ibid.*, **87**, 266 (1965).

(7) For $n = 0$, *Anal.* Calcd for $C_3H_5NO_7NaS$: C, 33.93; H, 2.14; N, 4.95. Found: C, 33.81; H, 2.28; N, 4.93. For $n = 4$, *Anal.* Calcd for $C_{12}H_{14}NO_7SNa$: C, 42.50; H, 4.15; N, 4.13. Found: C, 42.11; H, 4.39; N, 4.32. For $n = 6$, *Anal.* Calcd for $C_{14}H_{18}NO_7SNa$: C, 45.77; H, 4.94; N, 3.81. Found: C, 45.50; H, 5.24; N, 3.74.

(8) City Chemical Corp.

(9) Courtesy of Professor E. H. Cordes (originally obtained from General Aniline and Film Corp.).

(10) For $n = 3$, *Anal.* Calcd for $C_{14}H_{26}N_2Cl_2$: C, 57.30; H, 8.94; N, 9.55. Found: C, 56.62; H, 9.14; N, 8.89. For $n = 9$, *Anal.* Calcd for $C_{20}H_{38}N_2Cl_2$: C, 63.66; H, 10.15; N, 7.43. Found: C, 63.01; H, 10.17; N, 7.42.

esters were found to provide Beer plots without change of slope across the range of concentrations for which the value of k_{OH} was found to be independent of ester concentration. Thus, no evidence exists for the formation of micelles in the concentration range of I employed in this study. Similar results were obtained at $\mu = 0.5$.

With 1.74×10^{-4} M anionic ester I ($n = 4$; $\mu = 0.5$) the value of k_{OH} remains unaffected on increase of the anionic amphiphile II to a concentration at which a precipitate is formed. When the anionic amphiphile II is replaced by the cationic III or neutral IV, however, the value of k_{OH} is found to decrease as the concentration of amphiphile is increased to the critical micelle concentration (cmc) of 10^{-4} M for III and 2×10^{-3} M for IV and then to reach a constant value above the cmc. The decrease in rate is 4.5–5.8-fold (independent of n) for III and 12.7-fold for IV ($n = 4$). It may be concluded, therefore, that I is incorporated into cationic and neutral micelles and thus protected from hydroxide ion catalyzed hydrolysis. That esters of type I are not incorporated into micelles of like charge is shown by the fact that the value of k_{OH} for VI is not affected by III until a concentration of amphi-

(VI)

phile is reached which is 10 times that of the cmc concentration and then the rate is only depressed by a factor of 1.7. That the values of k_{OH} are not reduced to zero, even when all ester must be incorporated into the micelles, indicates either that hydroxide ions can penetrate into the micelle or that the hydrolytic reactions occur only at the surface of the micelle. If I ($n = 6$) is allowed to react with V ($m = 3$) in the presence of III, above and below the cmc concentration of III, it is found that the incorporation of I into micelles of III almost or completely abolishes the second-order reaction of I and V.

To assess the feasibility of synthesizing micelle-forming reagents with catalytic groups the reaction of I with V was investigated. The reagents V were designed to attract I *via* both electrostatic and lyophobic bonding involving the oppositely charged head groups, the phenyl rings and the aliphatic chains, respectively, so that amine and ester would be juxtaposed for an aminolysis reaction within the micelle. When $n = 0$ or 6 and $m = 3$ the reactions of I and V were found to be second order (*i.e.*, first order in the basic form of V and first order in I; $k_0 = 15.8$ l. mole^{-1} min^{-1} and $k_6 = 2.4$ l. mole^{-1} min^{-1}). However, when $n = 0$, 4, 6 and $m = 9$, I was found to be incorporated into the micelles of V and its rate of disappearance at constant pH greatly enhanced. Thus, increase in the concentration of V (I at 5×10^{-5} M; $\mu = 0.1$) was accompanied by a rapid increase in the pseudo-first-order rate constant (k_{obsd}) for disappearance of I in the vicinity of the cmc (*ca.* 7×10^{-3} M), the value of k_{obsd} becoming invariant above the cmc. The increase in k_{obsd} in the vicinity of the cmc was found to be dependent on approximately the second power of the amphiphile. The best fit of the

$$k_{obsd} = k_{OH}[OH^-] + \frac{V_m[\text{amphiphile}]^2}{K + [\text{amphiphile}]^2} \quad (1)$$

kinetic data to eq 1 was at a pH (8.65) approximating the pK_a of the amphiphile where for $n = 0$, $V_m = 1.85$ min^{-1} and $K = 1.18 \times 10^{-4}$ M^2; $n = 4$, $V_m = 0.19$ min^{-1} and $K = 1.0 \times 10^{-4}$ M^2; and for $n = 6$, $V_m = 0.17$ min^{-1} and $K = 3.0 \times 10^{-5}$ M^2. The similarity of eq 1 and the Michaelis–Menten equation is obvious. From studies between pH 7.05 and 10.2 it was possible to show that the rate of the reactions was dependent on the mole fraction of V present as free amine and by the hydroxamate method[11] it could be shown that I plus V provided, in each case, an almost quantitative yield of acylated V.

These results point out the interesting possibility of preparing catalytic amphiphiles which are effective at very low concentrations. Studies of this nature are now in progress in this laboratory.

Acknowledgment. This work was supported by a grant from the National Institutes of Health.

(11) T. C. Bruice and F. H. Marquardt, *J. Am. Chem. Soc.*, **84**, 365 (1962).

DEPARTMENT OF CHEMISTRY
UNIVERSITY OF CALIFORNIA
AT SANTA BARBARA
SANTA BARBARA, CALIFORNIA

THOMAS C. BRUICE
J. KATZHENDLER
LEO R. FEDOR

RECEIVED MARCH 3, 1967

Revised Values of Integral Diffusion Coefficients of Potassium Chloride Solutions for the Calibration of Diaphragm Cells

Sir: The diaphragm cell method of determining diffusion coefficients is a relative one whose accuracy is largely determined by the precision of the calibration experiments used to obtain the cell constant. In 1951, Stokes[1] published integral diffusion coefficients $\bar{D}_c°$ for KCl for the calculation of diaphragm cell integral

(1) R. H. Stokes, *J. Am. Chem. Soc.*, **73**, 3527 (1951).

Table I: Integral Diffusion Coefficients for KCl at 25°

c, mole l.$^{-1}$	$\bar{D}^\circ \times 10^5$, cm^2 sec^{-1}	c, mole l.$^{-1}$	$\bar{D}^\circ \times 10^5$, cm^2 sec^{-1}	c, mole l.$^{-1}$	$\bar{D}^\circ \times 10^5$, cm^2 sec^{-1}	c, mole l.$^{-1}$	$\bar{D}^\circ \times 10^5$, cm^2 sec^{-1}
0.001	1.9734	0.008	1.9438	0.060	1.8904	0.400	1.8480
0.002	1.9660	0.009	1.9414	0.070	1.8856	0.500	1.8478
0.003	1.9607	0.010	1.9392	0.080	1.8815	0.600	1.8486
0.004	1.9563	0.020	1.9225	0.090	1.8778	0.700	1.8502
0.005	1.9526	0.030	1.9113	0.100	1.8746	0.800	1.8524
0.006	1.9494	0.040	1.9029	0.200	1.8565	0.900	1.8553
0.007	1.9465	0.050	1.8961	0.300	1.8501	1.000	1.8585

coefficients, $\bar{D}$, for these calibrations. Potassium chloride was chosen because precise optical[2] and conductometric[3] data were available for its diffusion coefficient D at 25°. There were, however, some gaps in the combined data and a much greater than average deviation between them near 0.1 M.

Since 1951, the limiting value of D for KCl at 25° has been slightly altered and additional precise optical data have been published.[4] Also improvements in diaphragm cell techniques in these and other laboratories have been made which make it desirable to use as precise $\bar{D}_c^\circ$ values as possible. Therefore, we have recalculated these coefficients. This was done by drawing a smooth curve through the combined D data from 0 to 1 M of ref 2–4 using the limiting value 1.993×10^{-5} cm^2 sec^{-1}; the root-mean-square deviation, rmsd, between the data and curve was 0.0019×10^{-5} cm^2 sec^{-1}. An IBM Series 360 computer was used to obtain an equation[5] for the curve of the form $D \times 10^5 = \sum_{i=0}^{8} A_i x^i$, where $x = C^{1/2}$ with an rmsd of 0.0008×10^{-5} cm^2 sec^{-1}. The equation thus obtained was integrated exactly and the computer then used to calculate and print in tabular form values of $\bar{D}_c^\circ$. Results obtained at round values of the concentration are given in Table I. The greatest deviations from Stokes' results[1] occur in the region 0.02–0.1 M and are of the order 0.2%.

A Simplified Calibration Procedure. It is common practice to express data for the concentration dependence of $\bar{D}_c^\circ$ in the form of a graph and obtain values by interpolation as required. The difficulties of constructing and using such graphs may be circumvented entirely by using a standardized calibration procedure. The initial concentration of KCl for the calibration experiment is chosen close to 0.5 M, the rule of Gordon[6] used to determine the length of the preliminary period, and the equation due to Robinson, *et al.*,[7] to fix the length of the experiment. As a general rule the value of $\bar{D}$ will then be $(1.840 \pm 0.001) \times 10^{-5}$ cm^2 sec^{-1}.

(2) L. J. Gosting, *J. Am. Chem. Soc.*, 72, 4418 (1950).

(3) H. S. Harned and R. L. Nuttall, *ibid.*, 69, 736 (1947); *ibid.*, 71, 1460 (1949).

(4) D. F. Akeley and L. J. Gosting, *ibid.*, 75, 5685 (1953); L. A. Woolf, D. G. Miller, and L. J. Gosting, *ibid.*, 84, 317 (1962).

(5) The coefficients A_i were: $A_0 = 1.993$, $A_1 = -1.002337601$, $A_2 = 3.235153497$, $A_3 = -9.780514174$, $A_4 = 24.34187091$, $A_5 = -35.81551219$, $A_6 = 26.75245668$, $A_7 = -7.833317444$, $A_8 = -1.989929326 \times 10^{-5}$.

(6) A. R. Gordon, *Ann. N. Y. Acad. Sci.*, 46, 285 (1945).

(7) R. L. Robinson, Jr., W. C. Edmister, and F. A. L. Dullien, *J. Phys. Chem.*, 69, 258 (1965).

DIFFUSION RESEARCH UNIT
RESEARCH SCHOOL OF PHYSICAL SCIENCES
AUSTRALIAN NATIONAL UNIVERSITY
CANBERRA, A. C. T., AUSTRALIA

L. A. WOOLF
J. F. TILLEY

RECEIVED JANUARY 6, 1967

Charge-Transfer Complexes of Polyenes

Sir: Lupinski has reported a band in a mixture of iodine and β-carotene which absorbs at 10,000 A.[1] By varying the concentrations and the solvent, he showed convincingly that the absorption is due to a molecular species β-carotene·I^+, which he considers may be a charge-transfer complex β-carotene·I^+. It appears that this new band might quite possibly be explained in terms of a shift in the absorption maximum of β-carotene rather than as a charge-transfer band.

The two classes of compounds, the symmetrical polymethines and the polyenes, have quite different absorption maxima although in each the absorption is due to a chain of CC=C bonds. This is because the polymethines have two or more possible bond configurations or resonance structures which are isoenergetic while the

(1) J. H. Lupinski, *J. Phys. Chem.*, 67, 2725 (1963).

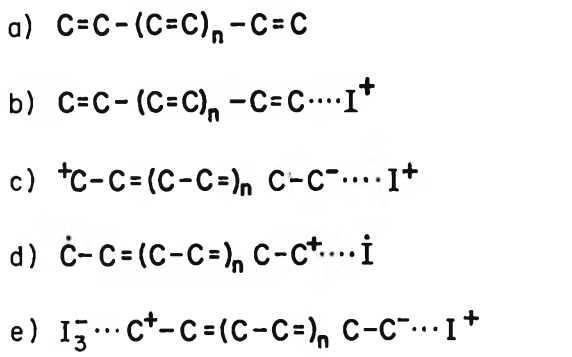

Figure 1. Possible charge-transfer complex of a polyene and I^+ and the approximate isoenergetic ground-state resonance structures that will tend to reduce bond alternation. β-Carotene is a diphenylpolyene with $n = 11$; (a) the principal ground-state resonance structure of the polyene; (b) the same state in the I^+ complex; (c) and (d) states whose contribution to the ground-state configuration will be much larger because of complex formation; (e) Platt's $D^+ \cdot cart \cdot A^-$ complex with I_3^- could strengthen structure c.

polyenes have only one principal resonance structure. Kuhn has derived a formula using the free-electron model for predicting the absorption peaks of polyenes as well as the symmetrical polymethines.[2] He introduces a Brillouin-type band splitting in the energy levels of the polyenes due to the unsymmetrical potential seen by the C atoms which causes the predicted wavelengths to be shifted to much shorter wavelengths than the corresponding polymethines. If β-carotene is treated as a polymethine, then the predicted λ_{max} is about 11,000 A, but if allowance is made for β-carotene to have a single resonance structure with alternating double bonds which dominates the ground state, then Kuhn finds good agreement between his calculation and the observed λ_{max} of 4510 A.

It may be possible to explain Lupinski's spectrum as being due to a charge-transfer effect rather than being a charge-transfer band of the usual donor–acceptor kind. The spectrum looks very much like what would be expected for β-carotene with a mixture of isoenergetic resonance structures to make the bonds nearly equal with no-bond alternation. If, due to the formation of a charge-transfer complex with iodine, several bond configurations are possible, then the absorption maximum of β-carotene would shift to much longer wavelengths. Previously, Platt has suggested a similar shift in β-carotene due to the formation of a donor–carotene–acceptor trimolecular complex, $D^+ \cdot cart \cdot A^-$, predicting also that this might absorb at wavelengths as great as 11,000 A.[3,4]

The interpretation of the Lupinski band as a "band shifted" β-carotene absorption is suggested not only by the close agreement with the predicted wavelength for no-bond alternation, but also by the narrow half-width of the band, only 2000 cm^{-1} (compared to that of β-carotene itself, about 4200 cm^{-1}) and by the shift in peak position by several hundred cm^{-1} with changing solvent polarity. The latter features are typical of the polarized conjugated-chain spectra (merocyanines) studied by Brooker and co-workers near their isoconjugate points,[5,6] and the narrowness has been shown theoretically to be a necessary consequence of the reduction of bond alternation.[3] True charge-transfer spectra, on the other hand, are commonly much broader than the spectra of the individual molecules.

In Figure 1 there are diagrams showing the β-carotene$\cdot I^+$ charge-transfer complex. This complex has several resonance structures for the β-carotene ground state that would equalize the bond length and shift the λ_{max} of β-carotene to longer wavelengths.

That the formation of a charge-transfer complex can cause large wavelength shifts in polyenes can be tested in several possible ways. One test is to try to form charge-transfer complexes with other polyenes and see if a band appears where the corresponding symmetrical polymethine would absorb. The band is predicted to move approximately 1000 A to longer wavelengths for every additional vinyl group in the chain.[7] Another possible test would be to see if charge-transfer complexes formed with β-carotene and another acceptor similar to iodine would also have a band at 10,000 A, since the λ_{max} of this band depends principally on the formation of a complex which would allow several isoenergetic bond structures and not on the particular properties of the acceptor.

Acknowledgments. I wish especially to thank Professor John R. Platt for his interest and advice. I also thank Professors R. S. Mulliken and W. B. Person for their criticism. This work was supported in part by Public Health Service Grant GM 14035-02 and a Public Health Service predoctoral fellowship to the author.

(2) H. Kuhn, *J. Chem. Phys.*, **17**, 1198 (1949).

(3) J. R. Platt, *ibid.*, **25**, 80 (1956).

(4) J. R. Platt, *Science*, **129**, 372 (1959).

(5) L. G. S. Brooker, G. H. Keyes, R. H. Sprague, R. H. VanDyke, E. VanLare, G. VanZandt, F. L. White, H. W. J. Cressman, and S. G. Dent, Jr., *J. Am. Chem. Soc.*, **73**, 5332 (1951).

(6) L. G. S. Brooker, G. H. Keyes, and D. W. Heseltine, *ibid.*, **73** 5350 (1951).

(7) L. G. Brooker and R. H. Sprague, *ibid.*, **63**, 3203 (1941).

(8) Mental Health Research Institute, University of Michigan, Ann Arbor, Mich. 48104.

DEPARTMENT OF PHYSICS
UNIVERSITY OF CHICAGO
CHICAGO, ILLINOIS 60637

THOMAS G. EBREY[8]

RECEIVED MARCH 9, 1967

Dispersal of Carbon Blacks to Individual Crystallites[1]

Sir: The detailed structure of carbon black has been the subject of theoretical and applied studies for many years. Surface area measurements and electron micrographs[2] show that carbon blacks consist of more or less spherical aggregates approximately 100–4000 A in diameter, depending on the method of manufacture. These aggregates are comprised of closely packed and tightly bonded crystallites. Warren, *et al.*,[3] have shown that these crystallites have a turbostratic, semigraphitic structure and range in size from 20 to 65 A across the *a* axis and from 12 to 40 A along the *c* axis.[2] Dark-field electron microscopy by Hall[4] suggested that the crystallites are arranged concentrically with their basal planes parallel to the surface in the outer layers of thermal and furnace blacks, but randomly in channel blacks; this interpretation is in agreement with recent oxidation experiments[5,6] where hollow spherical shells were obtained from furnace and thermal blacks. The two types of aggregate structures may be represented as shown in Figure 1.

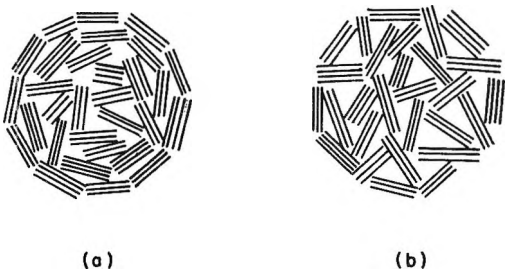

Figure 1. Idealized cross sections of two types of carbon black aggregate structures: (a) with the crystallites oriented concentrically in the outer layers and (b) with random arrangement of the crystallites.

For most carbon blacks, the crystallites are packed so closely together in the aggregates that N_2 cannot penetrate between the crystallites; *i.e.*, the aggregate diameter is the same as the particle size calculated from BET measurements. The only exceptions to this are the highly oxidized, highest surface area channel blacks, which are laced with open porosity; nevertheless, the crystallites are still bonded together into coherent aggregates except in the case of extreme oxidation (up to 90%), in which case separated crystallites may be observed. Preparation of carbon black sols by conventional methods yields a dispersion consisting of the preexistent aggregates suspended in the medium. Electron micrographs of such dispersions are shown in Figures 2a and 3a, which are, respectively, a thermal black with a specific surface area of 13 m^2/g (Cabot Corp.; Sterling FT-FF) and an oxidized porous channel black of 1400 m^2/g (Columbian Carbon Co.; Neo Spectra Mark I). These aggregates are immune to dispersal by any previously tried procedures; kinetic methods at best only split or spall off a large chunk,[5] while chemical methods preferentially attack only the exposed chemically active edges[2,7] of crystallites but not the basal planes or the bonds between crystallites.[5,6]

This communication reports preliminary studies of a dramatic dispersing effect observed when carbon blacks are blended with thoria sols, as shown in Figures 2b and 3b. In both instances, carbon blacks were blended

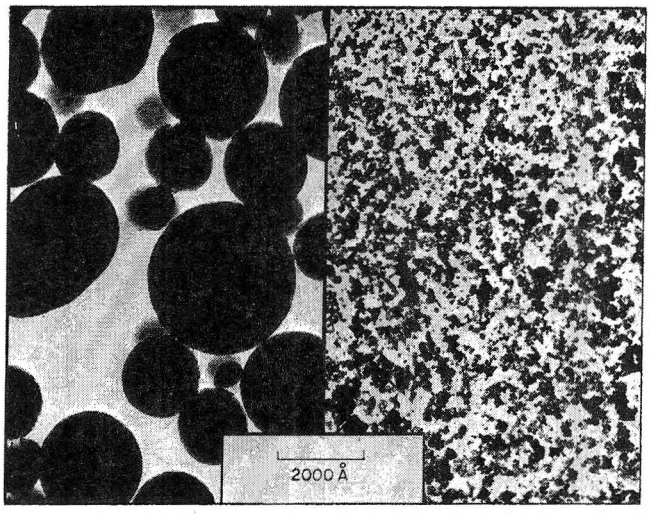

Figure 2. Sterling FT-FF carbon black dispersed (a, left) by itself and (b, right) with thoria sol.

with thoria sols in which the ThO_2 is present as hydrated, acid-stabilized, 70-A crystals.[8] Regardless of the blending method used, the action of the thoria sol is twofold; it disperses the carbon black aggregates to the individual crystallites and it stabilizes the carbon suspension. Many carbon blacks have been tested, covering a wide range of surface area and chemical

(1) Research sponsored by the U. S. Atomic Energy Commission under contract with the Union Carbide Corporation.

(2) W. R. Smith in "Encyclopedia of Chemical Technology," Vol. 4, 2nd ed, Interscience Publishers, Inc., New York, N. Y., 1964, p 243.

(3) (a) B. E. Warren, *J. Chem. Phys.*, **2**, 551 (1934); (b) J. Biscoe and B. E. Warren, *J. Appl. Phys.*, **13**, 364 (1942).

(4) C. E. Hall, *ibid.*, **19**, 271 (1948).

(5) W. A. Ladd and M. W. Ladd, *Rubber Chem. Tech.*, **34**, 697 (1961).

(6) F. A. Heckman and D. F. Harling, *ibid.*, **39**, 1 (1966).

(7) See, *e.g.*, J. V. Hallum and H. V. Drushel, *J. Phys. Chem.*, **62**, 110 (1958).

(8) P. A. Haas, S. D. Clinton, and A. T. Kleinsteuber, *Can. J. Chem. Eng.*, **44**, 348 (1966).

activity, and all are dispersed to individual crystallites by thoria sols. The carbon blacks shown in Figures 2 and 3 represent extremes in properties; the high surface area carbon is acidic (pH of aqueous suspension 3.0), while the low surface area carbon is basic (pH 9.0); the thermal black has concentrically ordered crystallites, thus exposing only basal planes, while the channel black consists of randomly oriented crystallites, thereby also exposing edges of crystallites.

In addition to the direct evidence described above, a number of other observations have been made. These deal with a loading or saturation limit, electrophoretic measurements, interactions with other oxides, and centrifugation experiments. Some of these are described briefly below. A detailed report on this work will be published later.

The blended sols from which the micrographs in Figures 2b and 3b were made contained carbon black–thoria at a mole ratio of 4:1, which is a volume ratio of approximately 1:1. The clumping and clustering evident in these photos may not be representative of the sol in its normal state, since sample preparation (for the electron microscope) involves dilution and drying. However, it is obvious that at least some individual particles exist in the sol and, further, that no regular micelle formation occurs. In other words, there is no visual evidence of a fixed interaction ratio, but "viscosity titrations" indicate that there is a limiting value beyond which a given thoria sol will not suspend any additional carbon black, and this value is a function of surface area.

As increasing amounts of carbon black are blended into a thoria sol, the viscosity increases slowly from a few centipoises to about 30–50 cp. Beyond that, additional carbon causes a very rapid rise into the hundreds of centipoises, thus providing an "end point." As the total available thoria surface area is varied, either by changing concentration or by using a thoria sol with a different particle size, the carbon capacity at the end point changes in direct proportion to the surface area of the thoria. Thoria concentrations of 250–500 g/l. were used for these viscosity titrations, and the carbon

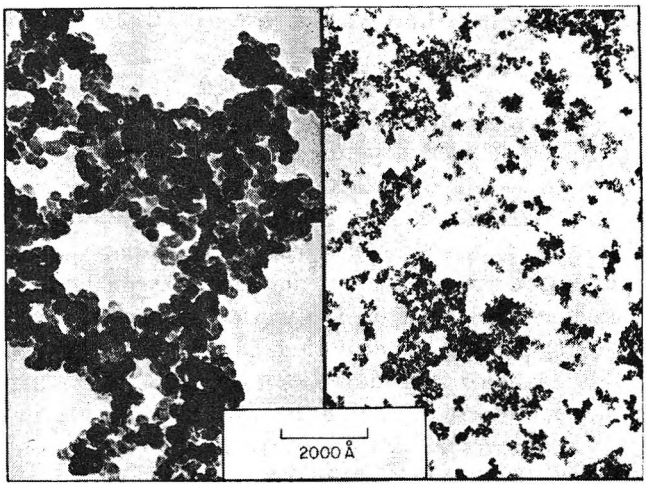

Figure 3. Neo Spectra Mark I carbon black dispersed (a, left) by itself and (b, right) with thoria sol.

content at the end point ran as high as 350 g/l., depending on the surface area relationships.

Other oxide sols, including silica, boehmite, and zirconia, do not disperse carbon black to the crystallites, but a urania sol does. Again, the same surface area:carbon loading ratio found for thoria also applies to urania. Other evidence of a carbon–thoria interaction is that the ζ potential of the mixed sol (55 mv) is about the same as that of pure thoria sol (67 mv), whereas conventional aqueous carbon sols have a negative potential. Finally, once carbon black and thoria have been combined to give a mixed sol, they come down together on centrifugation, despite the density differences, but any thoria that is not present as sol settles out *sans* carbon.

Acknowledgments. The excellent electron microscopy was performed by T. E. Willmarth and the electrophoretic data were provided by N. A. Krohn, both of ORNL. Helpful discussions were held with W. D. Bond, K. H. McCorkle, the late A. T. Kleinsteuber, J. Th. G. Overbeek, and P. H. Emmett.

OAK RIDGE NATIONAL LABORATORY K. J. NOTZ
OAK RIDGE, TENNESSEE

RECEIVED MARCH 9, 1967